

Vol. 22, No. 2, June, 2023

ISSN (Print): 0972-6268; ISSN (Online) : 2395-3454

NATURE ENVIRONMENT & POLLUTION TECHNOLOGY

*A Multidisciplinary, International Journal
on Diverse Aspects of Environment*



Technoscience Publications

website: www.neptjournal.com



Technoscience Publications

A-504, Bliss Avenue, Balewadi,
Opp. SKP Campus, Pune-411 045
Maharashtra, India

www.neptjournal.com

Nature Environment and Pollution Technology

(An International Quarterly Scientific Research Journal)

EDITORS

Dr. P. K. Goel (Chief Editor)

Former Head, Deptt. of Pollution Studies
Y. C. College of Science, Vidyanagar
Karad-415 124, Maharashtra, India

Dr. K. P. Sharma

Former Professor, Deptt. of Botany
University of Rajasthan
Jaipur-302 004, India

Managing Editor : Mrs. Apurva Goel Garg, C-102, Building No. 12, Swarna CGHS, Beverly Park, Kanakia, Mira Road (E) (Thane) Mumbai-401107, Maharashtra, India

Published by : Mrs. T. P. Goel, Technoscience Publications, A-504, Bliss Avenue, Balewadi, Pune-411 045, Maharashtra, India

E-mail : contact@neptjournal.com; operations@neptjournal.com

INSTRUCTIONS TO AUTHORS

Scope of the Journal

The Journal publishes original research/review papers covering almost all aspects of environment like monitoring, control and management of air, water, soil and noise pollution; solid waste management; industrial hygiene and occupational health hazards; biomedical aspects of pollution; conservation and management of resources; environmental laws and legal aspects of pollution; toxicology; radiation and recycling etc. Reports of important events, environmental news, environmental highlights and book reviews are also published in the journal.

Format of Manuscript

- The manuscript (*mss*) should be typed in double space leaving wide margins on both the sides.
- First page of *mss* should contain only the title of the paper, name(s) of author(s) and name and address of Organization(s) where the work has been carried out along with the affiliation of the authors.

Continued on back inner cover...

Nature Environment and Pollution Technology

Vol. 22, No. (2), June 2023

CONTENTS

1. **Ling He, Zhe Du, Jiabo Tian and Shuqi Chen**, Topographic Gradient Differentiation and Ecological Function Zoning Based on Ecosystem Services: A Case Study of Fuping County 541-552
2. **Sangram C. Patil and Milind R. Gidde**, RFID and IoT Enabled Framework to Make Pune City an Eco-friendly Smart City 553-563
3. **O.J. Oyeboode, F.O. Jimoh, S.M. Ajibade, S.A. Afolalu and F.A. Oyeboode**, Strategic Monitoring of Groundwater Quality Around Olusosun Landfill in Lagos State for Pollution Reduction and Environmental Sustainability 565-577
4. **S. Archana and P. Senthil Kumar**, A Survey on Deep Learning Based Crop Yield Prediction 579-592
5. **Tabassum-Abbasi, S. A. Abbasi, R. Rajalakshmi, Pratiksha Patnaik and Tasneem Abbasi**, Biomimetic Synthesis of Nanoparticles: State-of-the-Art 593-608
6. **L.R.S.D. Rathnayake, G. B. Sakura and N.A. Weerasekara**, Review of Outdoor Air Pollution in Sri Lanka Compared to the South Asian Region 609-621
7. **Tanya Srivastava and Nishchal Wanjari**, Boron Isotopic Systematics and Its Significance in Natural Processes: An Overview 623-637
8. **R. Shet and S. Mutnuri**, Removal of H₂S from Biogas Using Thiobacillus sp.: Batch and Continuous Studies 639-652
9. **O.J. Oyeboode, C.C. Okpala, S.M. Ajibade, N.M. Ogarekpe, S.A. Afolalu, A.O. Coker, S.G. Udeagbara, and A.T. Adeniyi**, Comparative Assessment of Medical Waste Management in Multi-System and Selected Teaching Hospitals in Ekiti State, Nigeria 653-669
10. **A. Zeb, I. U. Khan, S. Tripathi, M. R. Sahu and A. Kumar**, An Inappropriate Rise in NO₂ During the COVID-19 Pandemic in the Urban Area of Chhattisgarh, India 671-680
11. **L. Vidhya, S. Vinodha, S. J. Pradeeba, B. Jeyagowri, V. Nirmaladevi and N. Nithiya**, Adsorption and Kinetic Studies on Sequestering Effect of Porous Biodegradable Biochar Obtained from Pig-Bone on Hexavalent Chromium from Aqueous Solution 681-690
12. **A. Salauddin and C. Sandesh**, Heavy Metal Pollution of Soil and Crops in Rural Gujarat, Next to an Industrial Area: A Correlation Study 691-698
13. **M. S. Ogunshina, O. M. Abioye, K. A. Adeniran and D. A. Olasehinde**, *Moringa Oleifera* Coagulation Characteristics in Wastewater Treatment in a University Dormitory 699-707
14. **V. Hamsa Rekha and A. Shwetha**, Nesting Site Preferences of *Ratufa indica indica* in the Umbleyale Range Forest, Bhadravathi Division, Shimoga, Karnataka 709-719
15. **Sobha. P. and J. Prakash Arul Jose**, Investigating the Implications of Transit-Oriented Land Use Development for a Potential Node in an Urban Metro for Sustainability 721-730
16. **Phung Mai Lan and Nguyen Khac Minh**, Environmental Efficiency Evaluation in Vietnam Textile and Garment Industry: Super-SBM Model with Undesirable Output Approach 731-740
17. **Khadeejeh M. Hamasha**, Measurement of Black Carbon Absorption Coefficients Using an Aethalometer and Their Association with Visibility 741-753
18. **S. S. Deshpande and Y. A. Murkute**, Hydrogeochemical Characteristics and Suitability of Groundwater for Drinking and Irrigation from Shallow Aquifers of PG1 Watershed in Chandrapur District of Maharashtra 755-765
19. **A. Khatri and R. Bhaterra**, Efficacy of Nanofertilizers Over Chemical Fertilizers in Boosting Agronomic Production 767-776
20. **L. Ledheng and E. M. Y. Hano'e**, Analysis of Shoreline Change of North Central Timor Regency, Indonesia 777-787
21. **O. J. Oyeboode and F. Paul**, Flood Mitigation and Pollution Abatement in Kaduna Metropolis Through Engineering Assessment and Analytical Hierarchy Process Design 789-801
22. **S. Vinotha and A. Leema Rose**, Comparative Advanced Oxidation Decolorization of the Triphenylmethane Dye with Dimethyl Dioxirane and Hydrogen Peroxide 803-815
23. **N. P. Nisha and J. Prakash Arul Jose**, The Impact of High-Concentration Salt Solution on Morphological Changes in a Geosynthetic Clay Liner 817-824
24. **Kudrat-E-Khuda (Babu), Nazia Afroz Ananna and Arghyadeep Chakraborty**, Protection of the Environment Under Trade and Investment Agreements: An Analysis Based on Existing Legal Frameworks 825-833
25. **W. Budijastuti, R. Ambarwati, N. Ducha, F. Rachmadiarti, L. Lisdiana and K. Sahani**, Types and Distribution of Macroinvertebrates Stressed by Heavy Metals in Mangrove Forests 835-843
26. **A. Khan, A. A. Khan, S. Samreen and M. Irfan**, Assessment of Sodium Chloride (NaCl) Induced Salinity on the Growth and Yield Parameters of *Cichorium intybus* L. 845-852
27. **R. Sumathi and G. Sriram**, Comparison of Machine Learning Models in the Prediction of Accumulation of Heavy Metals in the Tree Species in Kanchipuram, Tamilnadu 853-860

28. **S. Balasubramanian, T. Bettin Thomas, D. Mathavan, R. Sathish Kumar, G. Uma, R. D. Stevens Jones and T. Citarasu**, Isolation and Screening of Probiotic Bacteria from the Gut of Polychaetes as a Probiotic Potential for Fish Aquaculture 861-868
29. **Poonam Sonwani and Sandhya Bharti**, Analyses of Polycyclic Aromatic Hydrocarbons (PAHs) in the Ganga River Water in Uttar Pradesh, India 869-877
30. **S. Padmanabhan, C. Joel, S. Mahalingam, J. R. Deepak, S. Baskar and M. Ruban**, Effects of Flex Fuel in Light Duty Power Generators on the Environment and Circular Bio-Economy 879-886
31. **Naina Gupta and Sewa Ram**, Effects of Traffic on Particulate Matter (PM_{2.5}) in Different Built Environments 887-894
32. **Y. Q. Li, L. J. Li, B. W. Zhao, Y. Zhao, X. Zhang and X. Dong**, Effects of Corn Straw Biochar, Soil Bulk Density and Soil Water Content on Thermal Properties of a Light Sierozem Soil 895-903
33. **Rana Hadi Hameed Al-Shammari, Shaimaa Satae M. Ali and Moayad Salih Hussin**, Efficient Copper Adsorption from Aqueous Solution by *Dictyuchus sterile* Pellets 905-912
34. **Anupama Mahato**, Comparative Assessment and Monitoring Changes in NDVI of Achanakmar Tiger Reserve (ATR) and its Buffer Zone, India 913-919
35. **Kerk Teck Seng, Lee Chia Shen, Ngo Sin Ling, Sim Pei Chin, Tan Jia Xin, Tan Kai En, Adnaan Ahmed Jama, Azian Hariri and Nurul Fitriah Nasir**, Comparative Study on the Indoor Air Quality in Critical Areas of Hospitals in Malaysia 921-927
36. **N. Y. Sudiar and M. I. Gautama**, Visitors Perceptions of the Climate Comfort at the Padang Coastal Tourism Area, Indonesia 929-935
37. **Abhishek Tyagi, Amitabh Raj Tripathi, Pratibha Naithani and M. K. Gupta**, Anaerobic Biodegradability Potential of RCF-Based Kraft Paper Mill Effluent 937-943
38. **Abhijit S. Jadhav and Ravindra Nalawade**, Tests for Evaluating the Efficacy of Phosphoric Acid Activated Charcoals from Two Biomasses 945-951
39. **Y. Hu, D. X. Qian, H. Zhu, L. F. Wang, B. Wang, Q. F. Ling and X. D. Xiao**, Purification Efficiency of Eutrophic Water by Three Submerged Plants 953-959
40. **Yuanbo Yao, Huixia Yang, Yunyun Wang, Jiajia Liang and Ling Yang**, Experimental Aeration Investigations on Supersaturated Total Dissolved Gas Dissipation 961-968
41. **Vijayant Panday and Ananda Babu K.**, The Potential of Phytoremediation to Treat Different Types of Wastewater - A Review 969-975
42. **Chinar Garg and Ananda Babu K.**, Extreme Flood Calibration and Simulation Using a 2D Hydrodynamic Model Under a Multipurpose Reservoir 977-983
43. **He Tao and Tihao Hou**, Study on the Temporal and Spatial Distribution of Air Pollutants in Typical Cities of China 985-990
44. **C. Fu, Y. He, C. Yang, J. He, L. Sun, K. Du, X. Zhang, G. Sheng, L. Li, L. Wang and W. Linghu**, Investigation of Adsorption of Nd(III) on Boron Nitride Nanosheets in Water 991-996
45. **Snehal Masurkar and Girish R. Pathade**, Microbial Consortia Preparation for Amylase, Protease, Gelatinase and Lipase Production from Isolates Obtained from Organic Kitchen Waste 997-1002
46. **M. B. Chakraborty, S. R. Patgiri, A. S. Rahman, A. Dasgupta and G. Pegu**, Denaturing Gradient Gel Electrophoresis (DGGE) Analysis Indicating Increased Microbial Diversity in Landfill Area Near Conserved Wetland 1003-1007
47. **Sulbha R. Kadam and Madhuri K. Pejaver**, Biodegradation and Kinetic Study of Hazardous Metribuzin Herbicide Using a Novel Soil Bacterial Isolate *Olivibacter oleidegradans* Strain SP01 in Aqueous Solution 1009-1015
48. **Suryanto Suryanto, Irwan Trinugroho, Fitri Susilowati, Jean Baptiste Aboyitungyi and Yuaninda Hapsari**, The Impact of Climate Change, Economic Growth, and Population Growth on Food Security in Central Java Indonesia 1017-1022
49. **Srinivasan Kumaraswamy, Vasantha-Srinivasan Prabhakaran and Radhakrishnan Narayanaswamy**, Molecular Docking Analysis of *Embelia ribes* for Selected Constituents as *Spodoptera frugiperda* (Fall Armyworm) Beta Glycosidase and Caspase-1 Inhibitors 1023-1028
50. **D. Quinto, D. Sanchez, M. Milla, M. Torres, B. Cayatopa, D. Jara and E. Morales**, Effect of Compliance with Environmental Regulations in the Construction of Public Civil Works, Cajamarca, Peru 1029-1033
51. **S. Karthikeyan**, Large Scale Cultivation and Pretreatment Optimization of Freshwater Microalgae Biomass for Bioethanol Production by Yeast Fermentation 1035-1040
52. **G. V. Patil and G. R. Pathade**, Stabilisation of Spent Wash by Polyhydroxybutyrate (PHB) Producing Microorganisms Isolated from Karad Region, Maharashtra 1041-1045
53. **Xu Meng, Chengzhi Song, Junfeng Yan, Yanyan Dong, Aiqin Hou, Kongliang Xie and Liping Liang**, A Review of Research on Materials for the Separation of Oil/Water Mixtures 1047-1062
54. **Maharshi Yadav, Govind Pandey and Pradeep Kumar**, Environmental Flow Assessment (EFA) of Tawi River Discharge at the Jammu Location Using the Global Environmental Flow Calculator (GEFC) 1063-1071
55. **C. C. Deocarís, M. C. Fernandez, A. R. Lee, S. L. A. Miao and J. B. P. Padolina**, Identification and Characterization of Microplastics on the Surface Water in Laguna de Bay, Philippines 1073-1080

The Journal
is
Currently
Abstracted
and
Indexed
in:

CAB Abstracts, U.K.

Ulrich's (Refereed) database

Zetoc

J-Gate

Centre for Research Libraries

Connect Journals (India)

Research Bible (Japan)

Elektronische
Zeitschriftenbibliothek (EZB)

CNKI Scholar (China National
Knowledge Infrastructure)

AGRIS (UN-FAO)

CNKI Scholar (China National Knowledge Infrastructure)

Scopus CiteScore (2021) 0.70

Scopus®, SJR (0.191) 2022

Index Copernicus (2021) = 111.68

Chemical Abstracts, U.S.A.

Indian Science Abstracts,
New Delhi, India

Pollution Abstracts, U.S.A.

Elsevier Bibliographic
Databases

Paryavaran Abstract,
New Delhi, India

Zoological Records

Electronic Social and Science
Citation Index (ESSCI)

Indian Citation Index (ICI)

CrossRef (DOI)

EBSCO: Environment Index™

Google Scholar

DOAJ

Environment Abstract, U.S.A.

ProQuest, U.K.

WorldCat (OCLC)

British Library

Indian Science

JournalSeek

SHERPA/RoMEO

Directory of Science

CSA: Environmental Sciences and Pollution Management

Access to Global Online Research in Agriculture (AGORA)

Present in UGC-CARE List (Group II)

UDL-EDGE (Malaysia) Products like *i*-Journals, *i*-Focus and *i*-Future

www.neptjournal.com

Nature Environment and Pollution Technology

EDITORS

Dr. P. K. Goel (Chief Editor)

Former Head, Deptt. of Pollution Studies
Yashwantrao Chavan College of Science
Vidyanagar, Karad-415 124
Maharashtra, India

Dr. K. P. Sharma

Former Professor, Ecology Lab, Deptt. of Botany
University of Rajasthan
Jaipur-302 004, India
Rajasthan, India

Managing Editor: Mrs. Apurva Goel Garg, C-102, Building No. 12, Swarna CGHS, Beverly Park, Kanakia, Mira Road (E) (Thane) Mumbai-401107, Maharashtra, India (**E-mail: operations@neptjournal.com**)

Business Manager: Mrs. Tara P. Goel, Technoscience Publications, A-504, Bliss Avenue, Balewadi, Pune-411 045, Maharashtra, India (**E-mail: contact@neptjournal.com**)

EDITORIAL ADVISORY BOARD

1. Dr. Saikat Kumar Basu, Deptt. of Biological Sciences, University of Lethbridge, Lethbridge AB, Alberta, Canada
2. Dr. Elsayed Elsayed Hafez, Plant Protection and Biomolecular Diagnosis Department, Arid Lands Cultivation Research Institute (ALCRI), Alexandria, Egypt
3. Dr. Tri Nguyen-Quang, Department of Engineering Agricultural Campus, Dalhousie University, Canada
4. Dr. Sang-Bing Tsai, Wuyi University Business School, Wuyishan, China
5. Dr. Zawawi Bin Daud, Faculty of Civil and Environmental Engg., Universiti Tun Hussein Onn Malaysia, Johor, Malaysia
6. Dr. B. Akbar John, School of Industrial Technology, Universiti Sains Malaysia (USM), Penang, Malaysia
7. Dr. C. Stella, School of Marine Sciences, Alagappa University, Thondi, Tamil Nadu, India
8. Dr. G.R. Pathade, Krishna Institute of Allied Scinces, Krishna Vishwa Vidyapeeth, Karad, Maharashtra, India
9. Prof. Riccardo Buccolieri, Deptt. of Atmospheric Physics, University of Salento, Dipartimento di Scienze e Tecnologie Biologiche ed Ambientali, Laboratory of Micrometeorology, Lecce, Italy
10. Dr. Amit Arora, Department of Chemical Engineering Shaheed Bhagat Singh State Technical Campus Ferozepur, Punjab, India
11. Dr. Tai-Shung Chung, Graduate Institute of Applied Science and Technology, National Taiwan University of Science and Technology, Taipei, Taiwan
12. Dr. Abdeltif Amrane, Technological Institute of Rennes, University of Rennes, France
13. Dr. Giuseppe Ciaburro, Dept. of Architecture and Industrial Design, Università degli Studi, Della Campania, Italy
14. Dr. A.B. Gupta, Dept. of Civil Engineering, MNIT, Jaipur, India
15. Claudio M. Amescua García, Department of Publications Centro de Ciencias de la Atmósfera, Universidad Nacional Autónoma de, México



Topographic Gradient Differentiation and Ecological Function Zoning Based on Ecosystem Services: A Case Study of Fuping County

Ling He^(**), Zhe Du^{*†}, Jiabo Tian^{*} and Shuqi Chen^{*}

^{*}College of Land Resources, Hebei Agricultural University, Baoding, Hebei, 071000, China

^{**}Cangzhou Field Research Station, Hebei-land Use of Circum Bohai Sea for the Ministry of Land and Resources, Cangzhou, Hebei, 061000, China

[†]Corresponding author: Zhe Du; ivypurple@163.com

Nat. Env. & Poll. Tech.
Website: www.neptjournal.com

Received: 06-07-2022

Revised: 22-08-2022

Accepted: 27-08-2022

Key Words:

Topographic gradient effect

K-means

Ecosystem services

PSO-SVM

Ecological function zone

ABSTRACT

Scientifically delineating ecological function zones is essential for national territory spatial planning and comprehensive management. In this study, we evaluated five ecosystem services, habitat quality, water yield, carbon sequestration, soil conservation, and food production, in Fuping County, China, and introduced the application of the topographic position index in exploring the topographic gradient effect of each service. We next applied the K-means clustering algorithm to identify the ecosystem services bundles and analyze the dominant type of ecosystem service in these bundles. A particle swarm optimization-support vector machine model was also constructed to identify the boundaries of ecological function zones and complete the ecological function zoning. The results are as follows: (1) In Fuping County, the high-value areas of habitat quality are distributed in the west, north, and southeast; those of soil conservation are in the northwest, northeast, and southwest; those of water yield are in the east and south; those of carbon sequestration are in the west, and those of food production is in the east. (2) The habitat quality first decreases and then increases with an increasing topographic gradient; food production and water yield decline with increasing topographic gradient; carbon sequestration and soil conservation increase with increasing topographic gradient. (3) Four types of ecosystem services bundles were identified. The dominant ecosystem functions of Type I, II, and III bundles are food production and water yield, carbon sequestration, and soil conservation, respectively. Type IV bundles generally have low levels of ecosystem services in the study area. (4) Four ecological function zones were delineated: food production zone, ecological conservation zone, potential restoration zone, and critical restoration zone. The research findings can provide a theoretical and practical basis for formulating and implementing ecological spatial management policies in the Taihang Mountains of China.

INTRODUCTION

According to the report to the 19th National Congress of the Communist Party of China, establishing a resource-conservative and environment-protective spatial pattern should be a priority in ecological civilization construction. Delineating ecological function zones is not only fundamental for developing natural resources, restoring ecological functions, and protecting the environment, but also for supporting socio-economic development and coordinating human-land relationships (Hong et al. 2019).

In recent years, ecological function zoning based on ecosystem services has gradually become mainstream in ecological zoning studies. Identifying ecosystem service bundles based on their service assessment and spatial

distribution is significant for exploring the regional ecological security pattern. The concept of an ecosystem service bundle, first proposed by Kareiva et al. (2007), refers to a combination of ecosystem services recurring in a specific region during a certain period and is a crucial criterion for delineating ecological zones (Raudsepp-Hearne et al. 2010). Scholars worldwide have mainly applied the K-means clustering algorithm (Peng et al. 2021), SOFM neural network (Yan et al. 2021), and PAM clustering algorithm (Pan et al. 2021) to identify and delineate the ecosystem service bundles at various scales, such as national (Turner et al. 2014) and regional scales (Crouzat et al. 2015). Such studies have also been combined with investigations in different fields, including urban spatial management (Riechers et al. 2018), land resource allocation (Balzan et al. 2018), and food security (Bommarco et al. 2013).

Identifying ecological function zone boundaries is the key to ecological function zoning. In previous studies, most scholars delineated the zones according to either the geographical locations of the boundaries between identified ecosystem services bundles and their research experience or by directly clustering the administrative and watershed units (Niu et al. 2020). Although this method can clarify the delineated zone boundaries, it is highly subjective, ignores the consistency of ecological functions within each zone, and does not follow any unified classification standard. To address this problem, a few scholars have standardized and automated ecological zoning in recent years by applying machine learning methods to delineate the ecological function zones. Mao et al. (2019) used the support vector machine (SVM) to mine grid data through machine training and employed the grid search algorithm to optimize the parameters and obtain the optimal classification plane that serves as the decision boundaries for ecological function zoning. This method can effectively eliminate subjectivity in ecological function zoning and quantitatively convert the classification to zoning. However, the SVM model based on the grid search optimization algorithm is not applicable to large-scale datasets, and its training efficiency and accuracy decline with expanding sample size (Xu 2014). In comparison, SVM combined with the particle swarm optimization (PSO) algorithm displays greater suitability for large-sample datasets because of its higher accuracy and steady operation (Xu 2014) and has been widely applied in geoscience research. Du et al. (2018) used the PSO-based SVM model to classify wetlands in remote sensing images and reported higher classification accuracy than the conventional SVM model. In ecological regionalization, the PSO-SVM model has not yet been applied to ecological function zoning studies.

Fuping County in Hebei Province, China, a region with typical topographic and geomorphological features of the Taihang Mountains, was selected as the study area. With the aim to provide technical reference for improving the eco-environmental quality of Fuping County and the Taihang Mountains, we first evaluated various ecosystem services of the county based on the InVEST model to explore their topographic gradient effect, used the K-means clustering algorithm to identify the ecosystem service bundles, and attempted to construct a PSO-SVM model on the MATLAB platform to obtain the optimal boundaries of the ecological function zones.

DATA AND METHODS

Study Area

Fuping County, covering an area of 2527.14 km², is situated in the middle of the Taihang Mountains and west of Hebei Province (Figs. 1 and 2). The geomorphological features of this county reflect those of the Taihang Mountains. The terrain is inclined from the northwest to southeast, with the highest and lowest elevations of 2282 m and 192 m in the northwest and southeast, respectively. The landform is dominated by mid- and low-altitude mountains and hills. Fuping County is in the warm temperate zone, with a semi-humid and semi-arid continental monsoon climate. The study area contains developed water systems and rich biological resources, making it a key ecological function zone.

Data Sources

The land use data were retrieved from the 2018 Land Change Survey Database of Fuping County; DEM data were

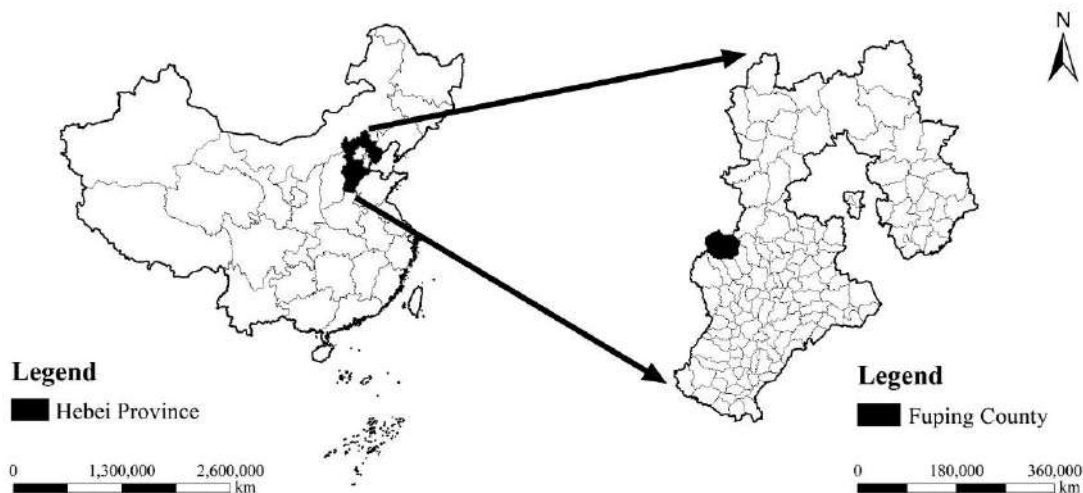


Fig. 1: Location of the study area.

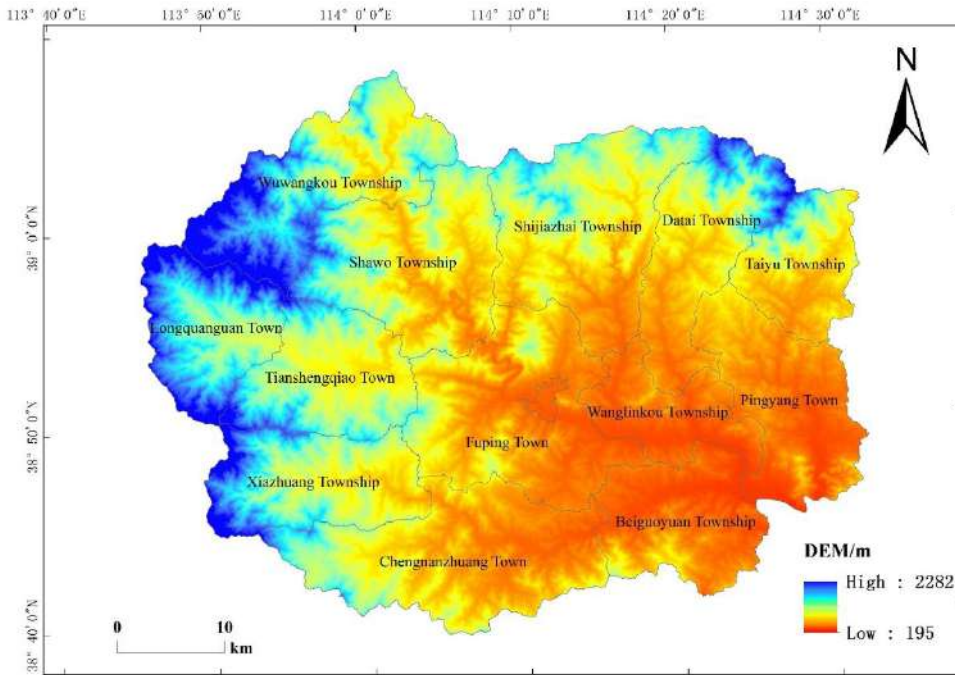


Fig. 2: Topographic map of the study area.

downloaded from the Geospatial Cloud (<http://ww.gscloud.cn/>) with a spatial resolution of 30 m; precipitation and meteorological data were obtained from the observations of 16 meteorological stations in Fuping County for the year 2018; soil data were collected from the China soil dataset of the Harmonised World Soil Database (HWSD); population and food production data were sourced from the 2018 Hebei Rural Statistical Yearbook.

Research Methods

Ecosystem Service Assessment

We used the InVEST model to evaluate five ecosystem services in Fuping County, including habitat quality, water yield, carbon sequestration, soil conservation, and food production (Table 1). The model parameters were obtained referring to the InVEST User’s Guide (Sharp et al. 2020)

Table 1: Calculation methods of ecosystem services.

Ecosystem service	Calculation formula	Variable interpretation
Habitat quality	$Q_{xj} = H_j \left[1 - \left(\frac{D_{xj}^z}{D_{xj}^z + K^z} \right) \right]$	Q_{xj} is the habitat quality of grid x of land-use type j ; H_j is the habitat suitability of land-use type j ; D_{xj} is the habitat stress suffered by grid x of land-use type j ; K is the half-saturation coefficient, usually half of the grid cell; z is a normalisation constant, generally considered as 2.5.
Water yield	$Y_i = \left(1 - \frac{AET_i}{P_i} \right) \times P_i$	Y_i , AET_i , and P_i are the annual water yield, evaporation, and precipitation on grid i , respectively, in mm.
Carbon sequestration	$C_{tot} = C_{above} + C_{below} + C_{soil} + C_{dead}$	C_{tot} is the supply of carbon sequestration service in t/hm^2 ; C_{above} and C_{below} are the carbon densities of aboveground and belowground biomass, respectively, in t/hm^2 ; C_{soil} and C_{dead} are the carbon densities of soil and dead organic matter, respectively, in t/hm^2 .
Soil conservation	$SC_i = RKLS_i - USLE_i$ $RKLS_i = R_i \times K_i \times LS_i$ $USLE_i = R_i \times K_i \times LS_i \times C_i \times P_i$	SC_i is the amount of soil conserved; $RKLS_i$ is the degree of potential erosion; $USLE_i$ is the amount of actual erosion; R_i is the rainfall erosivity factor; K_i is the soil erodibility factor; LS_i is the slope length factor; C_i is the vegetation cover and management factor; P_i is the soil and water conservation practice factor.
Food production	$G_{ij} = \frac{G_{agr}}{S_i} \times G$	G_{ij} is the food production capacity (t) of grid i in the j -th administrative unit; G_{agr} is the cultivated land area in grid i (hm^2) obtained by superimposing the grid map of each administrative unit onto the map of cultivated land; S_i is the total area of grid i (hm^2); G is the food production per unit area of cultivated land in the administrative unit (t/hm^2).

and available research results (Chen et al. 2019, Guo et al. 2008, Han et al. 2008, Liu et al. 2018, Liu et al. 2019, Liu et al. 2021, Wu et al. 2008, Zhao 2020, Zhu et al. 2019).

Topographic Gradient Classification

The topographic position index refers to the comprehensive elevation and slope gradient for a random point in a certain area and can reflect the terrain complexity comprehensively. It is calculated as:

$$T = \ln[(E/E_0 + 1) \times (S/S_0 + 1)] \quad \dots(1)$$

Here E and E₀ denote the elevation at the point and regional average elevation, respectively; S and S₀ represent the slope gradient at the point and regional average slope gradient, respectively.

Combined with the actual landform of Fuping County and an available study (Xu et al. 2020), we adopted the quantile method in ArcGIS to classify the topographic position index.

Identification of Ecosystem Service Bundles

In this study, we used the K-means clustering algorithm to identify the ecosystem service bundles in the study area based on the SPSS 26 platform. We set the five ecosystem services as variables and 500 m grids as evaluation units. The Z-scores of ecosystem services in each evaluation unit were standardized and clustered, and a total of six clustering results, each containing 2-7 types of clusters, were output for representing the actual situation of the study area. To avoid excessive subjectivity in the clustering process, we employed the Fragstats 4.2 software to calculate and analyze the contagion and patch cohesion indices of each clustering result and determine the optimal number of clusters based on the results (Peng et al. 2021).

Ecological Function Zoning Based on the PSO-SVM Model

1. **SVM:** SVM is a supervised learning algorithm first proposed by Boser (1992) with statistical theory. It can be used for classification, regression, and outlier detection. The classification is achieved by constructing an optimal hyperplane in the eigenspace. Theoretically, this model can optimally classify high-dimensional data. The SVM data processing steps are as follows.

Assume that the sensory feature data are of N dimensions, with total L sets, that is, $(x_1, y_1), \dots, (x_1, y_1) \in R^n$.

The decision plane can be expressed as:

$$f(x) = \varpi \cdot g(x) + b \quad \dots(2)$$

Here ϖ is the weight coefficient of the decision plane, $g(x)$ a nonlinear mapping function, and b the threshold.

The optimal classification hyperplane needs to fulfill the following condition:

$$y_i(\varpi \cdot g(x_i) + b) \geq 1 \quad \dots(3)$$

A non-negative slack variable ξ_i is introduced to restrict the classification error within a specified range, and the optimization problem is converted to:

$$\begin{cases} \min \frac{1}{2} \|\varpi\|^2 + c \sum_{i=1}^n \xi_i, c \geq 0 \\ \text{s.t. } y_i[(\varpi \cdot g(x_i) + b)] \geq 1 - \xi_i, \xi_i \geq 0 \end{cases} \quad \dots(4)$$

Here, c is a penalty factor that controls the complexity and generalisation ability of the model.

The Lagrangian algorithm is introduced to transform the optimisation problem into a dual problem:

$$\begin{cases} \min \frac{1}{2} \sum_{i=1}^n \sum_{j=1}^n y_i y_j a_i a_j K(x_i, x_j) - \sum_{i=1}^n a_i \\ \text{s.t. } \sum_{i=1}^n y_i a_i = 0, 0 \leq a_i \leq c \end{cases} \quad \dots(5)$$

Where,

$$K(x_i, x_j) = (g(x_i) \cdot g(x_j)) \quad \dots(6)$$

The RBF kernel is introduced as follows

$$K(x_i, x_j) = \exp(-g \|x_i - x_j\|)^2 \quad \dots(7)$$

Here g is the kernel function parameter that controls the range of the input space.

The above optimisation problem is converted into:

$$\begin{cases} \min \frac{1}{2} \sum_{i=1}^n \sum_{j=1}^n y_i y_j a_i a_j \exp(-g \|x_i - x_j\|)^2 - \sum_{i=1}^n a_i \\ \text{s.t. } \sum_{i=1}^n y_i a_i = 0, 0 \leq a_i \leq c \end{cases} \quad \dots(8)$$

2. **PSO Algorithm:** The PSO algorithm is a parallel search technique based on the evolution of swarm intelligence. It searches for the optimal solution by sharing information among different individuals in the swarm (Zhang 2005). First, m particles are assumed in the N-dimensional search space. The position and velocity of the i-th particle are defined as $X_k^i = (X_1^i, X_2^i, \dots, X_n^i)$ and $V_k^i = (V_1^i, V_2^i, \dots, V_m^i)$, respectively. Each particle is treated as a possible solution. Then, a fitness function is defined to calculate the fitness value corresponding to each particle. Finally, $P_k^i = (P_1^i, P_2^i, \dots, P_n^i)$ denotes the optimal solution found by each particle, that is, the individual extremum, and $P_k^g = (P_1^g, P_2^g, \dots, P_n^g)$ represents the global extremum of the entire particle swarm obtained from the optimal solutions. The velocity

and position of the particles are calculated using the following formulae.

$$V_{k+1}^i = \omega_k V_k^i + c_1 \phi_1 (P_k^i - \chi_k^i) + c_2 \phi_2 (P_k^g - \chi_k^i) \dots (9)$$

$$\chi_{k+1}^i = \chi_k^i + V_{k+1}^i \dots (10)$$

Here ω_k is the inertia factor, c_1 and c_2 are the learning factors, and ϕ_1 and ϕ_2 are random numbers between 0 and 1. The parameter values were determined referring to the relevant literature (Zhang 2005, Ding et al. 2011), and the parameters were optimised accordingly.

3. Ecological Function Zoning: The accuracy of the SVM model depends on two critical parameters, the penalty factor c and the kernel function parameter g . In this study, the PSO-SVM model was established on the MATLAB platform, and the optimal parameter combination was determined by integrating the PSO and SVM algorithms.

RESULTS

Spatial Distribution of Ecosystem Services

Each ecosystem service was evaluated based on the land use map of Fuping County (Fig. 3). The natural breaks classification method in ArcGIS was applied to classify the low value, relatively low value, relatively high value, and

high value areas of each ecosystem service and obtain their spatial distribution patterns (Fig. 4). The detailed analysis is as follows.

1. The habitat quality is high in the west, north, and southeast but low in the center. The landform in the west and north is dominated by mid-altitude mountains, with an elevation above 800 m. That region has high forest coverage and scarce cultivated land. In the southeast, the terrain is flat, with high grassland coverage, rich water sources, and high habitat quality. The low value areas are concentrated in central Fuping County, where the dominant land-use type is unused land, with low vegetation coverage.
2. The soil conservation level is high in the northwest, northeast, and southwest but low in the southeast. Woodland is the predominant land-use type in the high value and relatively high value areas of soil conservation, with high vegetation coverage. The southeast part of the study area has relatively low elevation and flat terrain, with low vegetation coverage and a large proportion of cultivated land. Intense erosion caused by rivers and rainfall results in weak soil conservation capacity.
3. The water yield level is high in the east and south and low in the north and west. The water yield service is mainly affected by precipitation, and its spatial

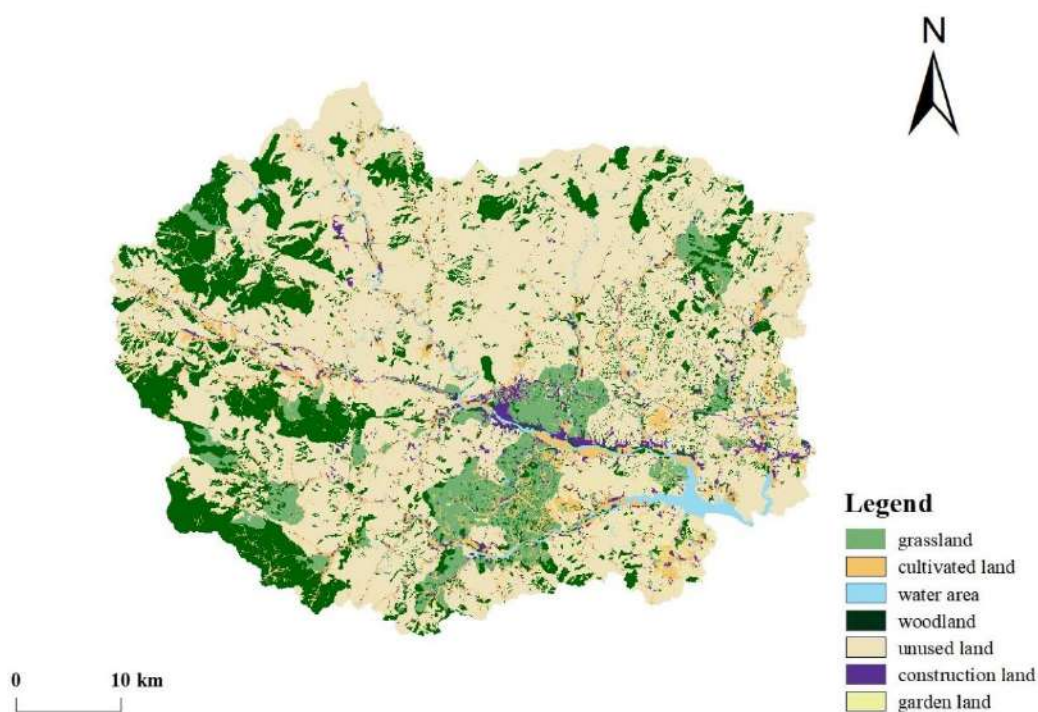


Fig. 3: Land use map of Fuping County.

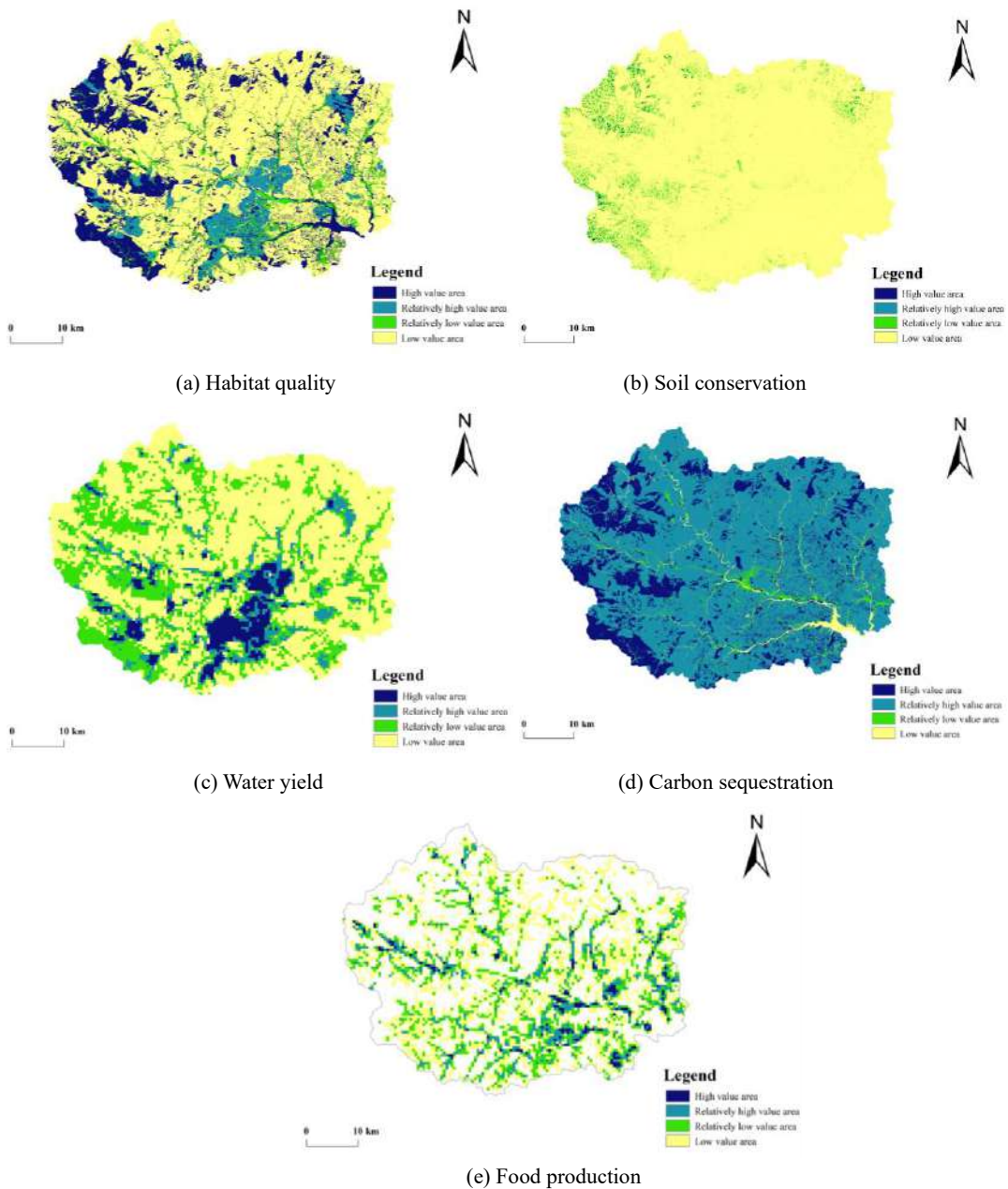


Fig. 4: Spatial distribution of ecosystem services.

distribution pattern is consistent with that of annual precipitation. Influenced by water areas and reservoirs in the county, the high value areas are concentrated in the central part, with a few scattered in the northwest and southeast.

4. The carbon sequestration capacity is high in most parts of the study area. The carbon sequestration service is mainly related to the area and coverage of woodland. The proportion of both woodland and vegetation
5. Food production service is restricted by the cultivated land area, with low overall production capacity. Generally, food production is high in regions with flat terrain, excellent irrigation conditions, and high

coverage is high in the western part of Fuping County, with correspondingly higher carbon sequestration ability. The eastern area has relatively abundant cultivated land resources, with several rural settlements and low vegetation coverage, and low carbon sequestration capacity.

quality cultivated land; conversely, it is low in areas with high elevation, steep slopes, and limited irrigation conditions.

Topographic Gradient Effect of Ecosystem Services

The topographic position indices of different locations in the study area were calculated using Eq. (1) and categorized into Classes I to V (Fig. 5). Class I is mainly distributed in the southeast of Fuping County; Classes II, III, and IV are found mostly in the central Fuping County; Class V is

concentrated in the western and northern parts of Fuping County. Combined with the distribution of land-use types, we can see that cultivated land, grassland, garden land, water areas, and construction land are dominant in Class I topographic positions, and their area decreases gradually with the increasing class number of topographic positions. Woodland is dominant in Class V topographic positions, and its area shrinks with decreasing class of topographic positions. Unused land is dominant in topographic positions of Classes II–IV (Fig. 6).

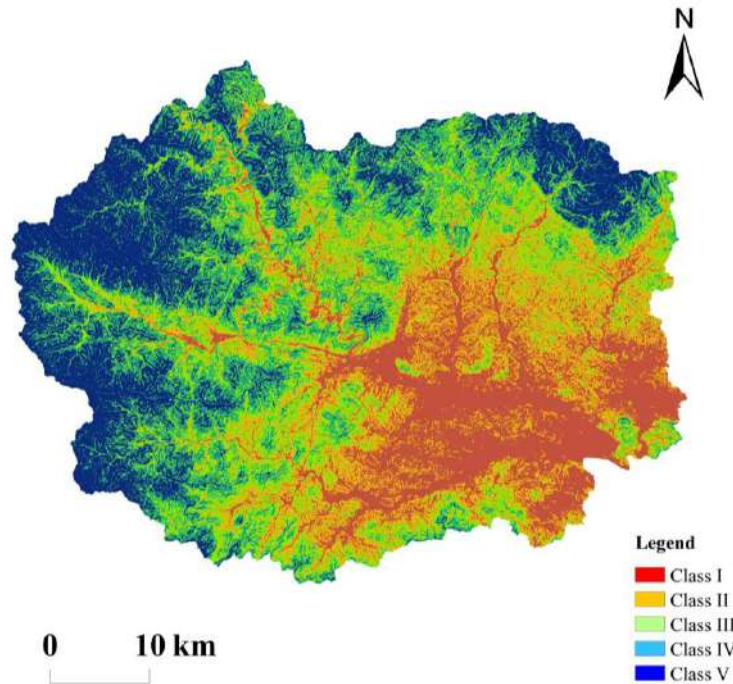


Fig. 5: Distribution of topographic position indices.

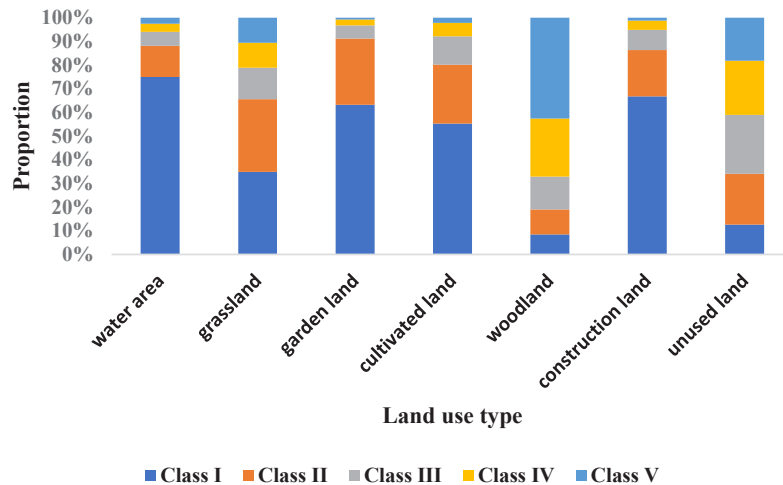


Fig. 6: Distribution of land-use types by topographic position classes.

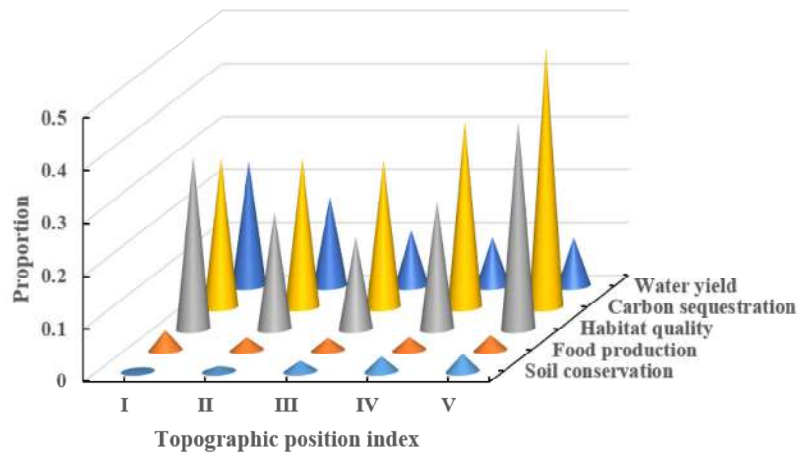


Fig. 7: Variation trends in ecosystem services with the topographic position index.

We analyzed the ecosystem service statistics according to the class of topographic positions (Fig. 7). We found that high value zones of average habitat quality are distributed in topographic positions of Classes I and V, and the level of habitat quality declines first and then increases with the increasing class number; high value areas of average carbon sequestration and soil conservation are distributed in Class V topographic positions, and service levels increase with the increasing class number; high value areas of average food production and water yield are distributed in Class I topographic positions, and service levels decrease with increasing class number.

Ecological Function Zoning

Identification of Ecosystem Service Bundles

We adopted the K-means algorithm to cluster the five

ecosystem service indicators, and the resulting cluster types were numbered 2, 3, 4, 5, 6, and 7, respectively. All these results passed the significance test. The Fragstats 4.2 software was applied to calculate the contagion index and the patch cohesion index for each clustering result, and four types of optimal ecosystem services bundles were determined according to the calculation results (Fig. 8).

Type I bundle is mainly distributed in the central and southern parts of Fuping County, with high capacities of water yield and food production; type II bundles are mostly distributed in the west and northeast of Fuping County, with high levels of habitat quality and carbon sequestration service; type III bundles are predominantly distributed in the northeast, northwest, and southwest, with a high soil conservation capacity; type IV bundles are mainly distributed in the central and eastern part of

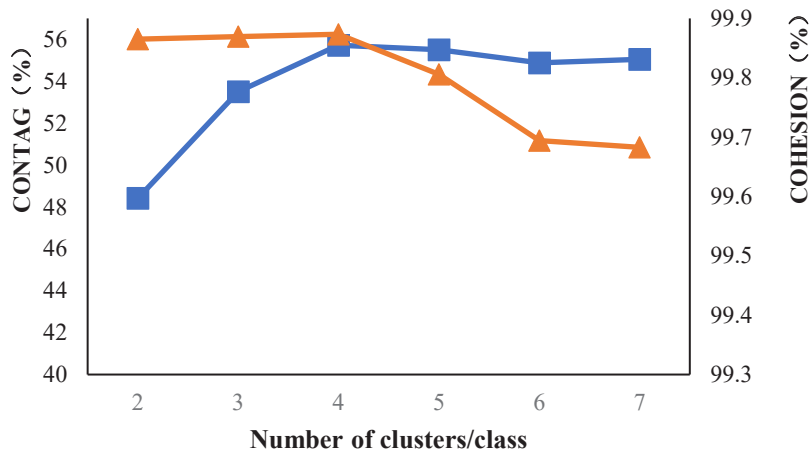


Fig. 8: Calculation results of the landscape index.

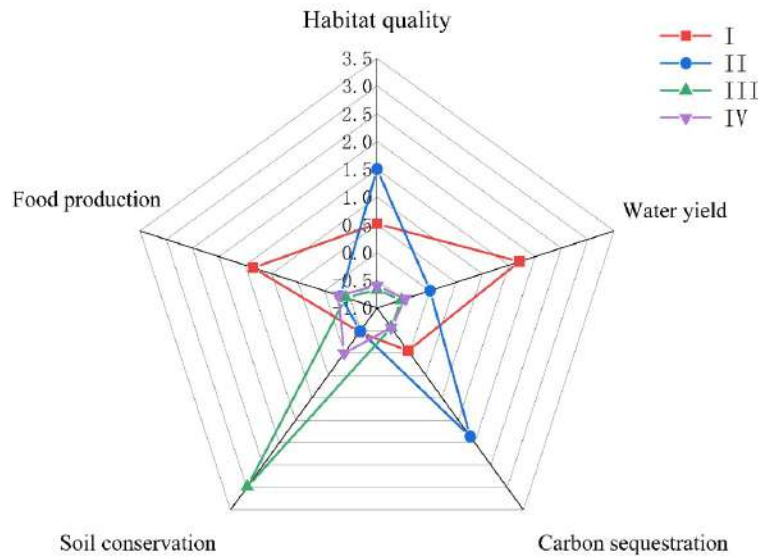


Fig. 9: Functional structures of the ecosystem services bundles.

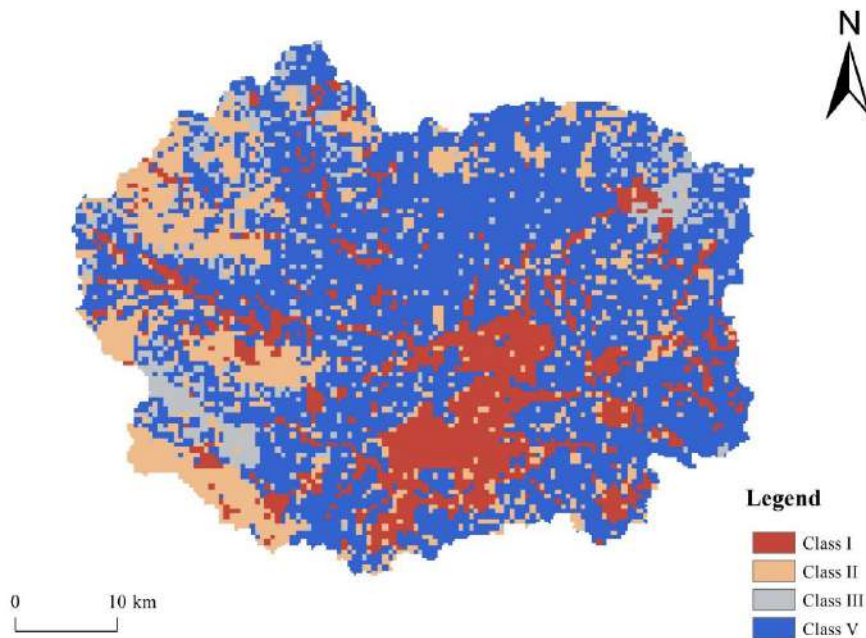


Fig. 10: Ecosystem services bundles in Fuping County.

Fuping County, with generally low ecosystem service levels (Figs. 9 and 10).

Identification of Ecological Function Zone Boundaries

We applied the PSO algorithm to explore the optimal solutions of the penalty factor *c* and the kernel function parameter *g* on the MATLAB platform (Fig. 11). The optimal parameters were then used to complete the SVM training and determine the subregion boundaries. The small patches

in the SVM training results were eliminated and smoothed in ArcGIS, and finally, Fuping County was divided into four ecological function zones (Fig. 12). These ecological function zones were superimposed on the map of topographic position classes to obtain the topographic position index of each zone (Fig. 13).

According to the characteristics of each type of ecosystem services bundle and the geographical location and ecological

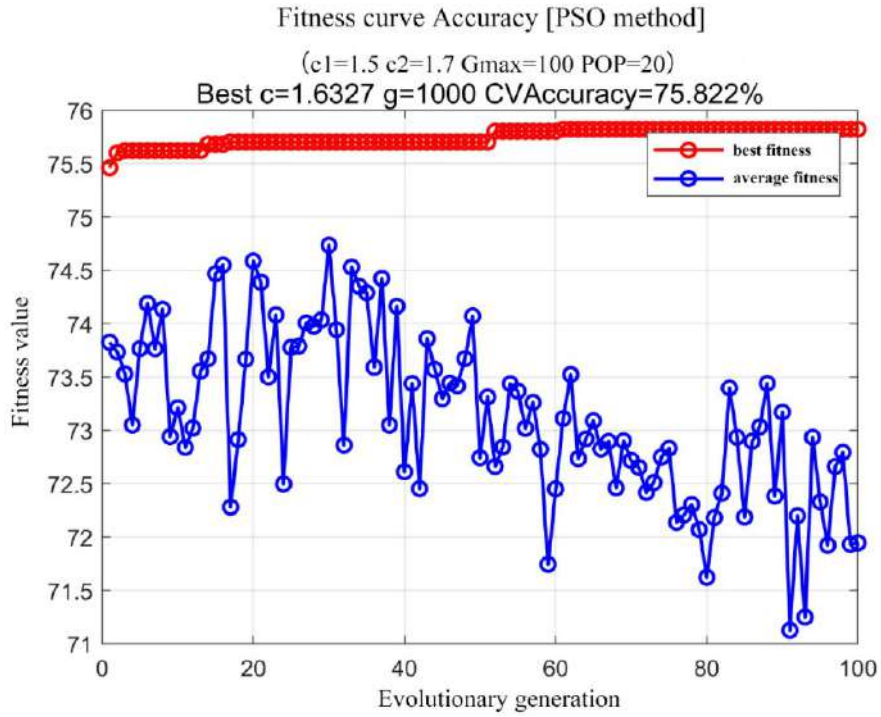


Fig. 11: PSO fitness curve.

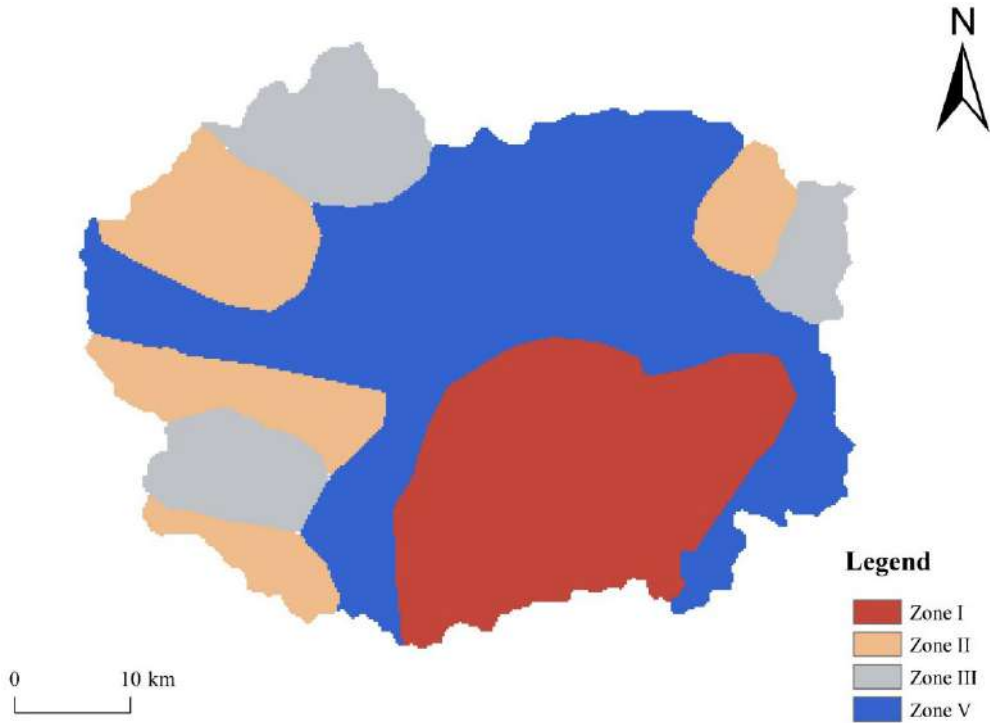


Fig. 12: Ecological function zoning in Fuping County.

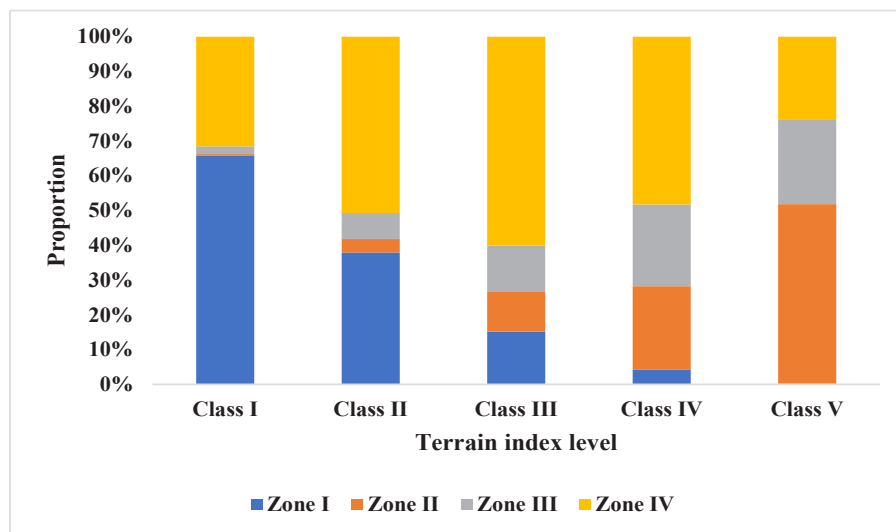


Fig. 13: Composition of topographic position index in each ecological function zone.

functions of each subregion, the ecological function zones are divided as follows.

1. Food production zone (I). It is located in the south-central part of Fuping County, accounting for 24.9% of the total area. The zone has high levels of water yield and food production services but low habitat quality and carbon sequestration capacity. This zone is mainly concentrated in the topographic positions of Class I, with a flat terrain and high average annual precipitation. It is surrounded by several water areas and reservoirs and is the main food production region in Fuping County.
2. Ecological conservation zone (II). It is located in the high-altitude regions in the west and northeast of Fuping County, accounting for 19.6% of the total area. Its habitat quality and carbon sequestration capacity are high, whereas the food production and soil conservation capacities are low. This zone is mainly distributed in the topographic positions of Class V, with high vegetation coverage and minor anthropogenic interference.
3. Potential restoration zone (III). It is located in the northwest, northeast, and southwest of Fuping County, accounting for 14% of the total area. Except for soil conservation service, the ecosystem services are of low levels. A single ecosystem service is provided. This zone is mainly distributed in the topographic positions of Classes IV and V, with generally low vegetation coverage and exhibiting the need for improving the regional ecological stability.
4. Critical restoration zone (IV). It is located in the central and eastern part of Fuping County, accounting for 41.5% of the total area, with all ecosystem services at a low

level. This zone is mainly distributed in the topographic positions of Classes II–IV, with a concentration of unused land. The vegetation coverage is low, and the ecological environment is severely damaged.

DISCUSSION AND CONCLUSION

In this study, we analyzed the ecological function zones in Fuping County using the PSO-SVM model based on the ecosystem services in the study area. First, the five ecosystem services of habitat quality, soil conservation, water yield, carbon sequestration, and food production were assessed using the InVEST model to clarify their spatial distribution patterns. Then, the topographic gradient effect of each ecosystem service was determined, and the K-means clustering algorithm was applied to identify the four types of ecosystem services bundles. Finally, the PSO-SVM model was applied to obtain the various ecological function zones, including the food production zone, ecological conservation zone, potential restoration zone, and critical restoration zone, in Fuping County.

Although this study has the advantages of simple operation and high repeatability, several limitations still remain. When evaluating the soil conservation service, the coefficient of rooting depth, plant available water capacity, and soil carbon density were obtained with reference to relevant literature or calculated from the available empirical equations. We did not conduct field sampling and measurements, which would have certainly affected the accuracy of the assessment results. We only assessed the ecosystem services and delineated the ecological function zones in Fuping County in 2018 and did not thoroughly

investigate the dynamic changes in the ecosystem services. Moreover, we automated the ecological function zoning by determining the ecological function zone boundaries using the SVM model. However, small patches were still observed in the zoning results owing to the number of sample points, and the results need to be further processed using ArcGIS tools. Therefore, revealing the spatiotemporal variation patterns of ecosystem services and further modifying the zoning method shall be the focus points of future studies.

Regardless of the limitations in this study, we have provided a new research idea for ecological function zoning. This study can help promote further application and exploration of the PSO-SVM model in ecological zoning studies. It can also facilitate the local government to improve the ecological environment and formulate relevant policies, in addition to providing a scientific basis for national territory spatial planning and the implementation of rural revitalisation strategy.

ACKNOWLEDGMENTS

This research was supported by S&T Program of Hebei (No.22554202D), and the Fundamental Research Funds for Hebei Provincial Universities (No. KY2021110).

REFERENCES

- Balzan, M.V., Caruana, J. and Zammit, A. 2018. Assessing the capacity and flow of ecosystem services in multifunctional landscapes: Evidence of a rural-urban gradient in a Mediterranean small island state. *Land Use Policy*, 146(75): 711-725.
- Bommarco, R., Kleijn, D. and Potts, S.G. 2013. Ecological intensification: Harnessing ecosystem services for food security. *Trends Ecol. Evol.*, 28(04): 230-238.
- Boser, B. (ed.) 1992. *A Training Algorithm for Optimal Margin Classifiers*. ACM Press, (0):144-152.
- Chen, J.Y., Wang, H.M., Liu, G. and Bai, Y. 2019. Evaluation of ecosystem services and its adaptive policies in the Hangjiahu region from the water-energy-food perspective. *J. Resources and Environment in the Yangtze Basin*, 28(3): 542-553.
- Crouzat, E., Mouchet, M., Urkelboom, F., Byczek, C., Meersmans, J., Berger, F., Verkerk, P.J. and Lavorel, S. 2015. Assessing bundles of ecosystem services from regional to landscape scale: Insights from the French Alps. *J. Appl. Ecol.*, 52(5): 1145-1155.
- Ding, S.F., Qi, B.J. and Tan, H.Y. 2011. A review of research on the support vector machine theory and algorithm. *Univ. Electron. Sci. Technol. China*, 40(1): 2-10.
- Du, K.L., Guan, Y.L., Pei, D.D., Xue, J. and Xu, L.L. 2018. Remote sensing classification of wetlands based on PSO parameter optimised support vector machine: A case study of some areas of Poyang Lake. *J. Jiangxi Sci.*, 36(1): 66-72+129.
- Guo, R., Wang, X.K., Lu, F., Duan, X.N. and OUYang, Z.Y. 2008. Soil carbon sequestration and its potential by grassland ecosystems in China. *J. Acta Ecol. Sin.*, 28(2): 862-867.
- Han, B., Wang, X.K., Lu, F., Duan, X.N. and Ouyang, Z.Y. 2008. Soil carbon sequestration and its potential by cropland ecosystems in China. *Acta Ecol. Sin.*, 28(2): 612-619.
- Hong, B.T., Ren, P., Yuan, Q.Z. and Wang, L. 2019. Ecological Function Regionalization in the Upper Yangtze River. *J. Ecol. Rural Environ.*, 35(8): 1009-1019.
- Kareiva, P., Watts, S., McDonald, R. and Boucher, T. 2007. Domesticated nature: Shaping landscapes and ecosystems for human welfare. *Science*, 316(5833): 1866-1869.
- Liu, H.Y., Xiao, W.F., Li, Q., Tian, Y., Zhang, Q.R. and Zhu, J.H. 2021. Spatiotemporal variations and trade-offs of ecosystem services in Beijing. *Chin. J. Ecol.*, 40(1): 209-219.
- Liu, J., Fu, B., Zhang, C.H., Hu, Z.P. and Wang, Y.K. 2019. Assessment of ecosystem water retention and its value in the upper reaches of Minjiang River Based on the InVEST model. *Resources and Environment in the Yangtze Basin*, 28(3): 577-585.
- Liu, J.H., Xu, H., Wang, Y., Li, H. and Shen, W.D. 2018. Evaluation of ecological risk and carbon fixation from land use change: A case study of Huanghua City, Hebei Province. *Chin. J. Eco-Agric.*, 26(8): 1217-1226.
- Mao, Q., Peng, J., Liu, Y.X., Wu, W., Zhao, M. and Wang, Y. 2019. An ecological function zoning method coupling SOFM and SVM: A case study in Ordos. *J. Acta Geogr. Sin.*, 74(3): 460-474.
- Niu, Z.P., Wang, X.F., Luo, G.X. and Yi, L.C. 2020. Ecological function zoning of Tibet Autonomous Region based on SOFM network at watershed scale. *J. Bull. Soil Water Conserv.*, 40(4): 116-123.
- Pan, Y., Zheng, H., Yi, Q.T. and Li, R.N. 2021. The change and driving factors of ecosystem service bundles: A case study of Daqing River Basin. *J. Acta Ecol. Sin.*, 41(13): 5204-5213.
- Peng, L., Deng, W., Huang, P. and Liu, Y. 2021. Evaluation of multiple ecosystem services landscape index and identification of ecosystem service bundles in Sichuan Basin. *Acta Ecol. Sin.*, 41(23): 1-13.
- Raudsepp-Hearne, C., Peterson, G.D. and Bennett, E.M. 2010. Ecosystem service bundles for analyzing tradeoffs in diverse landscapes. *Proc. Nat. Acad. Sci. U. S. A.*, 96(107): 5242-5247.
- Riechers, M., Barkmann, J. and Tschardtke, T. 2018. Diverging perceptions by social groups on cultural ecosystem services provided by urban green. *Landsc. Urban Plan.*, 33(175): 161-168.
- Sharp, R., Douglass, J., Wolny, S. 2020. InVEST 3.9.0 User's Guide [M/OL]. <https://storage.googleapis.com/releases.naturalcapitalproject.org/invest-userguide/latest/index.html>
- Turner, K.G., Odgaard, M.V., Bøcher, P.K., Dalgaard T. and Svenning, J. C. 2014. Bundling ecosystem services in Denmark: Trade-offs and synergies in a cultural landscape. *Landsc. Urban Plan.*, 29(125): 89-104.
- Wu, Q.B., Wang, X.K., Duan, X.N., Deng, L.B., Lu, F., Ouyang, Z.Y. and Feng, Z.W. 2008. Vegetation carbon sequestration and its potential by forest ecosystems in China. *Acta Ecol. Sin.*, 28(2): 517-524.
- Xu, C.X., Gong, J., Li, Y., Yan, L.L. and Gao, B.L. 2020. Spatial distribution characteristics of typical ecosystem services based on terrain gradients of the Bailongjiang Watershed in Gansu. *Acta Ecol. Sin.*, 40(13): 4291-4301.
- Xu, X.M. 2014. *SVM parameter optimisation and its application in classification*. Dalian: Dalian Maritime University.
- Yan, X., Huang, F.R., Li, Q., Zhou, H.F. and Li, L.H. 2021. Regionalisation of the matching degree of water, soil, and heat resources in Central Asia based on ecosystem services using PSO-SOFM neural network. *Chin. J. Eco-Agric.*, 29(2): 241-255.
- Zhang, L.P. 2005. *Theory and practices of the particle swarm optimisation algorithm*. Hangzhou: Zhejiang University.
- Zhao, N. 2020. Evaluation of carbon storage and habitat quality of the land system of Bohai Bay coast based on the InVEST model. Baoding: Hebei Agricultural University.
- Zhu, W.B., Zhang, J.J., Cui, Y.P., Zheng, H. and Zhu, L.Q. 2019. Assessment of the territorial ecosystem carbon storage based on land use change scenarios: A case study of the Qihe River Basin. *Acta. Geog. Sinica.*, 74(3): 446-459.



RFID and IoT Enabled Framework to Make Pune City an Eco-friendly Smart City

Sangram C. Patil*  and Milind R. Gidde 

*Bharati Vidyapeeth (Deemed to be University) College of Engineering, Pune, India

†Corresponding author: Sangram C. Patil; patil.sangram@bharativedyapeeth.edu

Nat. Env. & Poll. Tech.
Website: www.neptjournal.com

Received: 05-08-2022

Revised: 01-11-2022

Accepted: 02-11-2022

Key Words:

Eco-city

IoT application

Smart city

Solid waste management

RFID technology

ABSTRACT

The increasing volume and complexity of waste associated with the modern economy pose a serious risk to ecosystems and human health. Due to the intensive increase in computation, Machine learning is popular. Intelligent solid waste management motivates the Swachh Bharat mission to celebrate the 150th anniversary of the birth of Rastrapita Mahatma Gandhi. In the context of smart city development, an innovative means of implementing smart solid waste collection is to improve daily solid waste collection at the household level. An intelligent solid waste collection system will be implemented in the Smart City to improve solid waste collection. It is required to educate households about solid waste handling. Municipal Corporation can implement an innovative PPP model as part of an independent India campaign to motivate startup entrepreneurs, which will generate jobs in India. The city of Pune is in a phase of intelligent urban mobility development to improve citizens' living standards. Ensure safe traffic management, adequate water supply, smart amenities, and services such as the intelligent collection, transport, and processing of solid waste. RFID and IoT base IT solutions have the potential to develop sustainable, innovative technology to achieve 100% household collections and transportation and treatment of waste so that to minimize waste to send landfill side.

INTRODUCTION

Through a region-based development project, the Pune Smart City will implement the Zero Waste project at the ward level under the Swachh Bharat Assignment (Swachh Bharat 2014). The 90000 household data gathering process is ongoing. Collecting waste door-to-door and identifying the source of the waste is not sufficient information available in any place 100% collection. At the present PMC, the total footprint extends to 518 square kilometers (Times of India 2021). It is estimated that the amalgamation of 23 villages increased the town's population by more than 2 lakhs, according to the 2011 Census. In the current situation, it is not feasible to physically control and maintain a record of waste collection. Pune is among the fastest-growing cities, generating between 2100 and 2400 tons of solid waste daily.

Consequently, it is compulsory to ensure the proper collection and transport of waste in instruction to prevent the dumping of hazardous waste in the surroundings. The proposed work focuses on assessing the detailed process

for managing solid waste, for instance, collecting, storing, segregating, transporting, handling, and dumping consuming geospatial tools such as remote sensing, GIS (Anagal 2009, Municipal Corporation of Pune 2011, Khadke 2018) and GPS (Das & Bhattacharyya 2014, Jaybhaye et al. 2014, Hannan et al. 2011). It can potentially underwrite urban ecological surroundings in the city of Pune. The Municipal Corporation of Pune has issues like D2D (Hemalata 2011, Mundhe et al. 2014, Kumar et al. 2009), solid waste collection, segregation, control, monitoring, and disposal. The grouping of RFID (Kaushal et al. 2012, Mohan et al. 2016, Kumar & Agrawal 2020) and IoT computing solutions can achieve a 100% D2D collection of separate waste (Municipal Corporation of Pune 2011). Due to the continued growth in population density in urban areas, the Corporation of Municipalities does not achieve 100% of the home collection. As a result, the population density is increasing in the major city in the Maharashtra region, affecting 27 municipal corporations in Maharashtra and the existing municipal corporation waste collection infrastructure (Rahman et al. 2022).

Nevertheless, this region is one of the cities in Pune. Several municipal companies in India face this challenge

ORCID details of the authors:

Sangram C. Patil: <https://orcid.org/0000-0001-5431-2630>

Milind R. Gidde: <https://orcid.org/0000-0002-7213-6463>

to achieve 100% door-to-door (D2D) coverage and collect isolated municipal solid waste. Moreover, the population and rapid urbanization are increasingly difficult to health and environmental problems due to the huge amount of waste generated (Parhi 2018). However, the Municipal Corporation of Pune exerts significant additional pressure on infrastructure services by adding 23 new villages within the boundaries of the Municipal Corporation. India is experiencing significant urbanization, currently 31% based on the 2011 census (Mania & Singh 2016). From literature, surveys concluded in Maharashtra observe that most urban local bodies (ULBs) in Maharashtra are unable to achieve 100% D2D primary collection, segregation, secondary transportation, treasury treatment, and final disposal of municipal solid waste due to insufficient financial and institutional resources and integration of technology debilities. In addition, ULBs in Maharashtra rarely have resources such as technology infrastructure and appropriate innovative strategies to improve the solid waste collection process. Scientific collection of waste is separated from every household daily from its doors, apartment doors, and communal garbage. Technological differences between segregation methods, collection, transportation, and monitoring in this waste collection process f.2

ace major challenges (Anagal 2009). Its inadequate follow-up on waste collection and inappropriate disposal is a global environmental challenge that disrupts urban ecosystems. That is why 100% of the achievement of D2D collection of segregated municipal solid waste daily is the most important priority for the addition of new villages Municipal Corporations other than the negative effect on the local infrastructure of ULB (Kumar & Pandit 2013)

MATERIALS AND METHODS

Past Studies on the City of Pune

Pune is situated in the Deccan Plateau region at about latitude 18°32" N and longitude 73°51"E, height range between 550-565 m (average 1835-1845 ft) above the sea level. The topography of the city of Pune leans slightly westward and towards the natural flow east of the river banks Mula and Mutha. The town of Pune is the 6th largest computer industry center in India. The topography stretched the city limits of Pimpri Chinchwad and the out of seven three military cantonment boards in Pune cities, such as Pune, Dehu Road, and Khadki. The Pune Metropolitan Region (PMR) stands to the right and left of the Mula River, Mutha (Rode 2018)

Pune is India's first city to receive an "Easy Living" rating. The city is believed to be the cultural capital of Maharashtra. It is also known as "East Oxford" and is now in

the presence of several prominent academic institutions. The city has emerged as an important educational center recently, with nearly partial world students in the student country in Pune. Information technology, education, management, and training schools attract students and professionals from India and other countries (Kumar & Pandit 2013)

Growing Population in Pune

The population growth of Pune is growing steadily from 1901 to 2017 shown on the chart above. However, the simultaneous area of town also increases, and waste generation at the household level should be increased to affect the solid waste collection system and collection method. Moreover, out of 23 villages in the municipal Corporation, additional charges on its infrastructure and environmental problems have also increased (Mundhe et al. 2014)

Municipal Waste Challenges in Pune

The growth of waste generation as a by-product of economic development has given rise to different subordinate legislations. According to a report by IIT Kanpur (2006), it is possible to recover at least 15 percent or 15,000 tonnes of waste produced daily in the country. In addition, specific forms of waste are regulated separately and require distinct conformities, mostly like authorizations, maintenance of records, and adequate disposal mechanisms (Anagal 2009). According to the report, it could provide about half a million rag pickers employment opportunities (Anagal 2009). The report adds that despite the huge potential of large cities in the region, the involvement of associations or communities is limited. In Indian cities, people are not serious about the waste management rules 2016 for collecting household user fees and cooperating with waste collection workers.

Additionally, it should provide separate waste, such as wet and dry, daily. When biomedical waste is expected to be generated at the household level, it should be segregated and delivered separately to waste pickers. However, the reality on the ground shows that some people enjoy advantages such as inadequate monitoring of the waste collection process door to door and collection of user fees. So, it is the limits of the Municipal Corporation to keep a record of daily waste collection door-to-door in biological and home-to-home monitoring regularly is not possible in the ground situation. Therefore, that miss benefitted people disrupt municipal corporations surrounding the environment, like dumping waste at road site amenities, vacant land, barren government land, corners of the road, outskirts of road, crime spots, community bins, etc. This problem of Municipal Corporations at the primary stage of the waste collection process should be required based on RFID unique user identification with

the IT solution. To build the IT infrastructure at the primary stage and to track the collection, transport, processing, and disposal of waste, regular and timely measures will be taken to improve the waste collection process. It is a societal need to solve the problems caused by overflowing landfills, which are impossible to recover because of the disorderly way of immersion (Kumar et al. 2017)

Meanwhile, the amount of MSW-generated waste dumped on the outskirts road depends on many factors such as dietary habits, community living standards, level of commercial activity, and seasons. Determining quantity change and production is useful when planning collection, transportation, and disposal systems (Das & Bhattacharyya 2014). Moreover, the population and Prediction of MSW generation are directly proportional to municipal corporation waste collection infrastructure, so it plays an important role in waste management. The waste generation predictions depend on the implementation level of the municipal corporation effectively and efficiently of tracking waste collection, monitoring, awareness, and education are more speciously attributes affecting waste generation (Das & Bhattacharyya 2014) and untreated MSW become a factor in the spread of countless illnesses (Kumar et al. 2009).

Waste Segregation at the Household Level

Another option to effectively and efficiently manage solid waste is to separate its waste at source into categories such as recyclable waste, biodegradable waste, etc. More

than 60% of household waste is biodegradable (Fig. 1). Furthermore, the water content is too high for waste, requiring extra incineration fuel. If these wastes are insulated at the source, composting under natural conditions or in engineering reactors can be carried out efficiently and economically. This will make the overall system effective by using a biodegradable portion for composting and a non-biodegradable portion of the landfill (Kumar & Pandit 2013).

The PMC divides 5 zones for the administrative division of the area, which is under 15 ward offices; each zone has 3 ward offices and 76 subdivisions of wards for the Electoral. The five zones' primary collection waste was collected at the 07 transfer stations and then separated as wet, dry, and mixed waste (Hemalata 2011). Transporting waste from the transfer station to the recycling industry includes RDF, biogas, composting, waste at the energy plant, etc. The remaining residue, like debris, is sent to the landfill site for scientific disposal of waste at landfill sites. In that process, various types of waste should be collected at the primary stage by a waste picker properly at the household level daily to minimize waste sent to landfill sites.

Table 1 shows the amount of household and household waste collected in that information is 100% properties wise waste collection, and information on daily waste given to the waste picker is insufficient for the effect on the sounding environment and aesthetic view of the city. Moreover, waste collected from out courts of road and street

Table 1: Segregation of waste at household level.

Zone Name	Ward name	No. of HH.	Amount of waste (tons.day ⁻¹)	No. of HH, SWM is segregated.	% of HH SWM segregated
1	Nagar Road	77151	167	73293	95.00
	Yerwada Kalas Dhanori	72121	130	59860	83.00
	Dhole Patil	44357	98	34598	78.00
2	Aund Baner	69435	130	65963	95.00
	Shivajinagar Ghole road	40268	110	31409	78.00
	Kothrud Bawdhan	76935	135	64625	84.00
3	Dhankawadi Sahakarnagar	62667	120	58280	93.00
	Sinhagad road	96102	118	76882	80.00
	Warje Karvenagar	59906	117	58109	97.00
4	Hadapsar Mundhwa	79533	105	62831	79.00
	Wanawadi Ramtekadi	73481	148	51437	70.00
	Kondava-Yewalewadi	58870	100	51806	88.00
5	Kasaba Vishrambaug	53120	105	43027	81.00
	Bavanipeth	57985	110	37600	64.84
	Bibwewadi	44795	120	40763	91.00

(Source: PMC 2016-2017).

swiping is increasing continuously at the ward level (Parhi 2018).

Overview of Primary Collection Data of PMC Around a Municipal Corporation

Fig. 2 shows the primary collection data for the city of Pune and around the municipality of Pune.

Fig. 2 above shows a review of the city of Pune for the current state of primary solid waste collection by the munic-

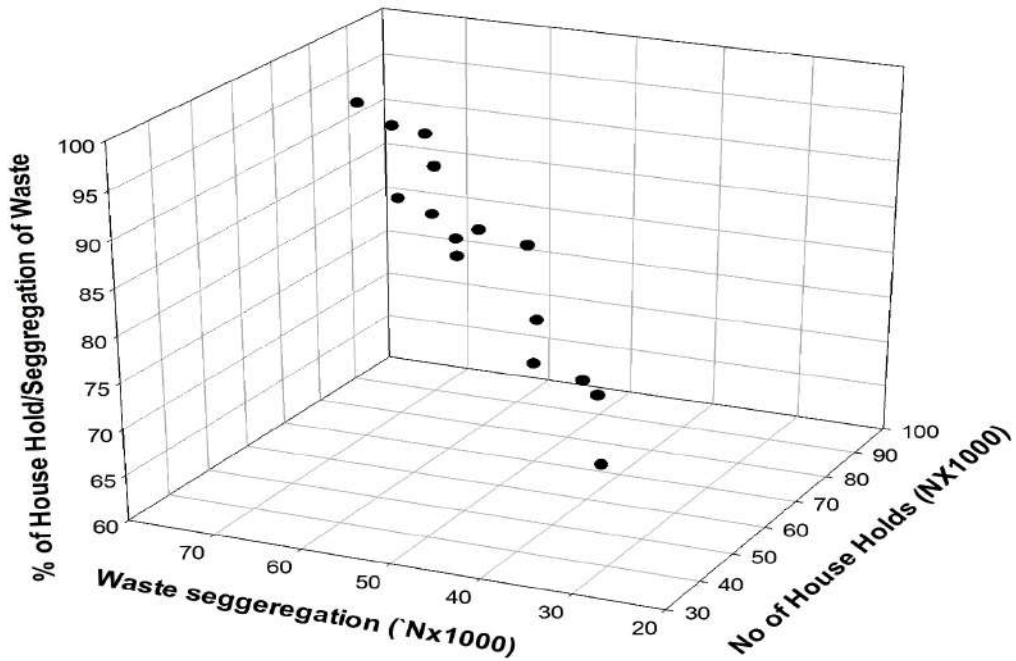


Fig. 1: PMC % of waste segregation in households.

Overview of Primary collection data around Pune Municipal Corporation

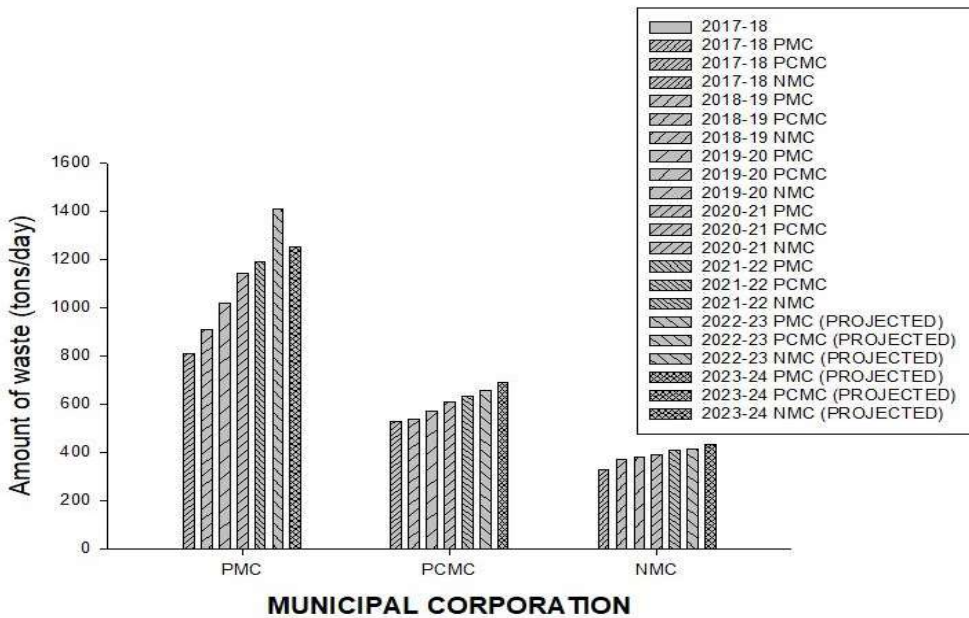


Fig. 2: Overview of primary collection data of PMC around Municipal Corporation.

ipality. The above literature survey reviews three municipal corporations around Pune city, Pimpri Chinchwad Municipal Corporation, and Nashik Municipal Corporation. When collecting all municipal data, take the waste collection data for the past three years and find the statistics for the next three projected years. It shows that waste collection should be continuously scaled up with all previous and projected municipal statistics.

Overview of Collection from Households Data of PMC Around Municipal Corporation

The chart below shows the collection of household data for the city of Pune and around the municipality of Pune.

Fig. 3 shows a review of the city of Pune and the city of Pune concerning the current state of household solid waste collection by the municipality. The above literature survey reviews three municipal corporations around Pune city, Pimpri Chinchwad Municipal Corporation, and Nashik Municipal Corporation. When collecting all municipal data, take the waste collection data for the past three years and find the statistics for the next three projected years. It shows

that waste collection should be continuously scaled up with all previous and projected municipal statistics.

Reason to Collect 100% of Separated Municipal Solid Waste at the Door

The following reason behind the 100% municipal solid waste collection at the door level in the collection of primary waste daily is timely waste collection and identifying the source of the waste collection.

Following reasons for unable to achieve 100% collected door-to-door solid waste

1. Waste is thrown at Chronic Sites daily.
2. Unevenness in waste user fee collection.
3. Daily waste is not given due to the Laziness of citizens.
4. Multi-storage building common collection not done properly.
5. Daily waste collection time and office time are different.
6. Waste is not segregated at the household level
7. Multiple days of waste to be stored in the plastic bag

Overview of Primary collection data around Pune Municipal Corporation

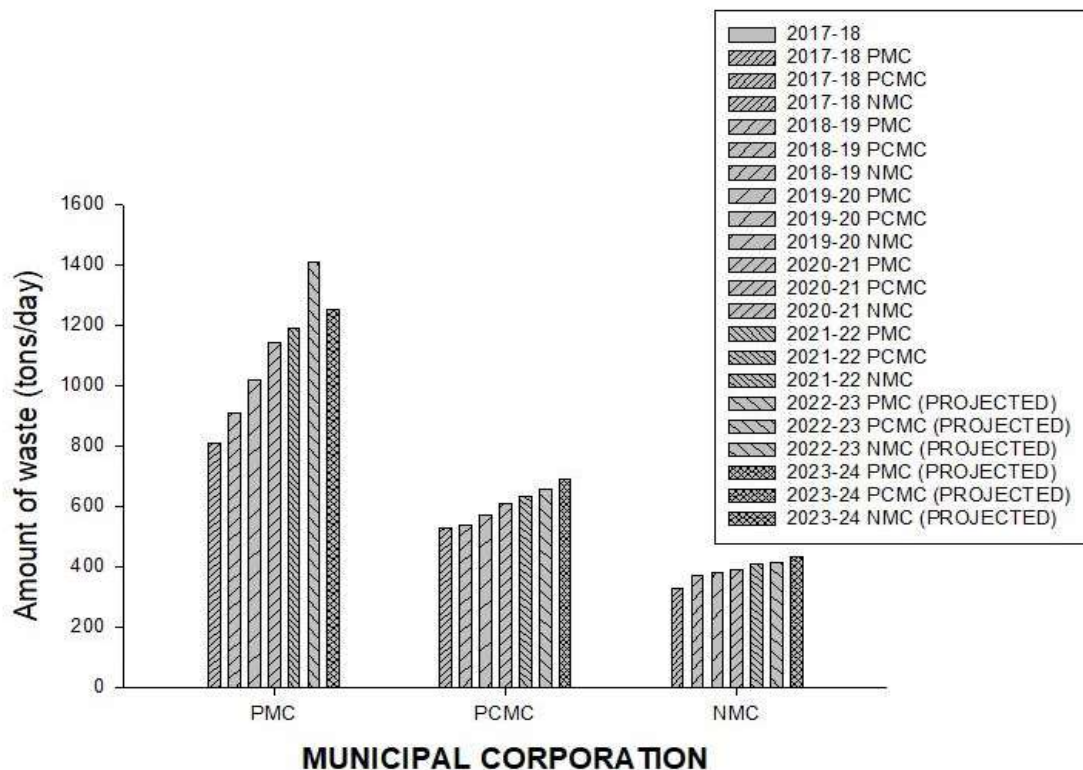


Fig. 3: Overview of collection from households data of PMC around Municipal Corporation.

Research Gap

1. Unscientific handling of MSW
2. Development of IT Solutions at the primary stage waste collection process
3. Insufficient waste monitoring and handling process
4. Development of an Eco-friendly, sustainable solution
5. Cleanness Training and Education of rag-pickers
6. Inadequate human resource management.
7. Development turnkey project BOT, PPP Mode

RESULTS AND DISCUSSION

To Collect 100% Door to Door collection of segregated waste by using dustbin tracking. The use of IT solutions in the door-to-door collection of Municipal solid waste management is needed now a day because the waste generation rate increases continuously in developing countries like India. Information technology in waste collection means integrating all technology available in modern electronic devices like RFID, GPS, GIS, ESP32 Wi-Fi Module, Web Portal, Data Center, Android application, etc.

Concept of D2D Collection of Municipal Solid Waste

This is the collection process of Municipal solid waste through waste pickers collecting waste from each household property daily rutting process is called the door-to-door (D2D) collection of urban solid waste. In those processes, waste pickers play an important role in waste collection. This is a regular process. Waste pickers' daily collected waste when reaching near the household property waste pickers announcing that time households are given to waste to the waste pickers. Those who are presented are given waste to the waste pickers, but those who are not present will be given the next day. This is an overall process of door-to-door (D2D) collection of urban solid waste (Municipal Corporation of Pune 2011).

Technologies Available for Achieving 100 % Door-To-Door (D2D) Collection of Solid Waste

To achieve 100% door-to-door collection by using technologies, it is possible to monitor and track the waste collection system. The technologies are available with us to meet this high demand for solid waste collection within the above limits. The use of High-tech communication technologies, solutions such as RFID for unique identification of households, ESP32 Wi-Fi Module for real-time information sent to sever, GPS for exact ground location, and GIS for geographic information that location must be used (Hannan et al. 2011) This research paper discusses available technology

for achieving municipal corporation 100% door-to-door (D2D) primary collection, segregation, and secondary transportation of solid waste. The use of, Radio frequency identification (RFID) with an IT solution has the potential to meet the municipal Corporation's objective. Consequently, the integration of RFID, ESP32 Wi-Fi Module, GPS, GIS, Android application and Web application, data center, etc. They are used for communication technologies to collect solid waste from households daily, segregation, and transport system. RFID, GPS, ESP32 Wi-Fi Module, GIS, and the camera have been incorporated and developed into the smart bin and smart solid waste garbage collection truck surveillance systems. This article shows the innovative, sustainable theoretical framework and interface logical algorithm between communication technologies, electronic devices, and logical software technologies interface reading graphically. All parameters used in this prototype, such as RFID passive tag, RFID long-range reader, ESP32 Wi-Fi Module connectivity, and GPS and GIS, were developed to implement the user-friendly prototype. The interface algorithm can control the server on the back end, analyze the trucks' location, estimate the waste's weight in the bin, and Co-relation between its surrounding area database GPS coordinator. In this way, the proposed system could address the problem raised by a sound solution.

The Function of GPS/GIS

GPS in the waste collection relates to the exact ground location with available GPS coordinates in a dataset. The GPS coordinator data set is used to create a new waste collection route and a map with the GIS position on the ground so that tracking is easy for the integrated waste collection process. The GPS is a set of US government satellites revolving around the Earth. It is used for navigational purposes. Satellites regularly transmit radio signals to GPS receivers before receiving the data system. Review 3 to 4 satellites at the ground station and then analyze and display the exact position, speed, and time. The GPS works precisely in any climate condition, terrain, day or night, 24 hours a day, and around the globe. The use of GPS in various applications for tracking the vehicle's position on an electronic chart, like to assist waste collection van drivers in setting and selecting a waste collection route with their tracking position. Modern systems use software to collect information automatically and send it to the data center for analysis. The logical interface creates a route and provides information on turn-by-turn directions to drivers in designated areas (Kumar & Moore 2002). The GPS is used for tracking waste collection, waste picker position, and its surrounding RFID tag validation its position. Simultaneously waste collection information sends to the data center and waste collection big van bin location (Hannan et al. 2011, Tongkaw 2017).

The GIS is an application for the user interface an integrated software and hardware to locate the exact size shown for the waste collection van position, storage of waste, waste collection, waste management, and mapping of waste collection route household. The data analysis is performed according to client requirements. This system shows the presentation of all required information in dedicated forms of geographic information in a computerized system. It also assists end users in visually analyzing data and examines trends, movements, and relations that are shown graphically. The even form data are associated with the spatial use of characteristics stored in a dedicated system that synchronizes the exact place on earth.

Function of RFID

The RFID passive tag and RFID long-range readers are designed to allow readers to read the information on a range

of 5m around a small waste collection by the waste picker, and the waste collection big van can read waste picker waste collection bin at a time waste bin empty on the big van automatically. When waste picker waste is collected from household waste bins, RFID passive tag information is read by RFID reader radio frequency and then transmitted to a computer system through a GSM/ GPRS/ Wi-Fi module network without any physical contactless connection between the radio frequency ranges. An RFID reader module consists of three main components: an antenna for data transfers and reading the data through radio frequency, a tag, and a reader. The passive label is loaded and activated when RFID transmits radio waves, forwarding information to the RFID reader. The RFID readers are available in different capacities; the frequency range depends on the use of contact. RFID readers are available with low frequency, contactless RFID readers with Ultra high frequency and High Frequency

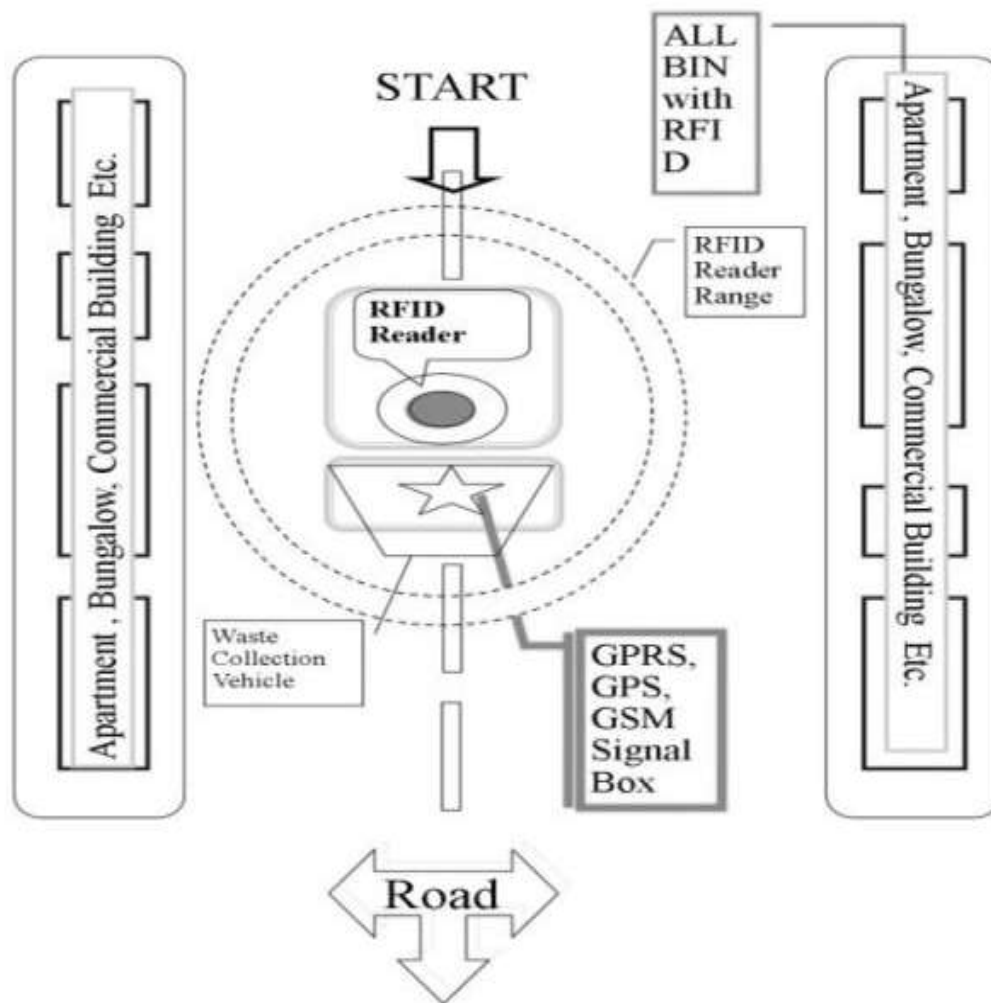


Fig. 4: Flow of information by using RFID technology.

depending on use up to 15 to 20 m long range. The integrated software gives real-time information to a user and servers to improve the entire waste collection process.

Function in ESP 32 Wi-Fi Module

The ESP32 WROOM 32D Wi-Fi Module uses for module transfer information remotely by using the 4GWi-Fi network to the data center through the internet. The mobile Wi-Fi network is provided to the ESP32 WROOM 32D module. The ESP32 Wi-Fi Module is a work-like wireless data transfer service between the device and the cloud server through the INTERNET. It provides a connection between data from users of the waste collection device to the data center over the wireless network and wireless broadband IP.

Working for RFID and IoT Solutions

The RFID tag is used for the waste collection process. The RFID tag is stuck on each household bin. In this process, when waste collection vehicles come from the waste collection before reaching the waste collection route, an alarm call is given to all households on this collection route (Fig. 4). When the empty dust tray is in the garbage collection vehicle at this time the RFID reader marks the presence, on the entry of the respective household in the database after completing the waste collection itinerary absent the property sends a message to the respective household.

1. Set RFID Tag on each household dustbin
2. Waste picker collection vehicle sets RFID Reader

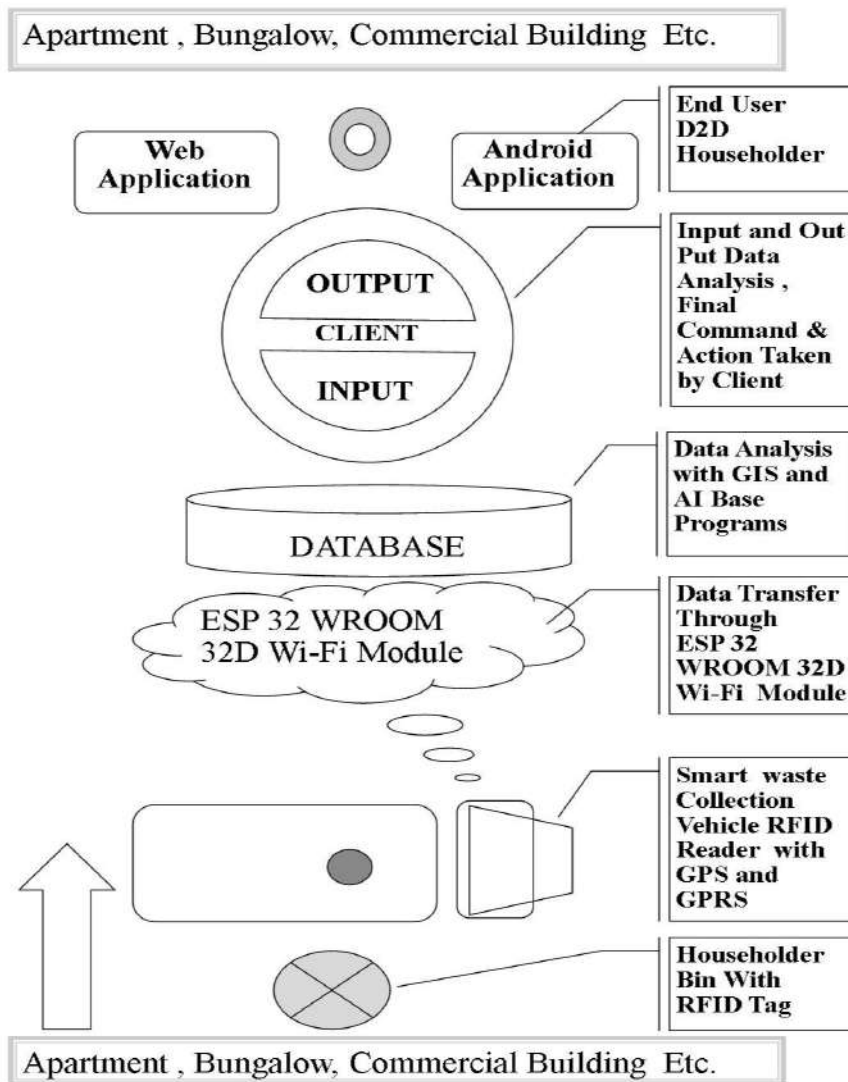


Fig. 5: Architecture of smart, solid waste management system.

3. RFID Reader sends all information through ESP 32 Wi-Fi module to the data center
4. All collected information is saved in the cloud at the data center
5. Datacenter analysis Input data as per the given command
6. All information is shown by the user interface Android and Web Application

Proposed System Architecture

The proposed method of the intelligent and environmentally responsible solid waste collection system is divided into two Infrastructure sections. Firstly, the hardware and software modules achieve 100% door-to-door (D2D) coverage of the separate solid waste collection. In the hardware module, using technologies such as GIS, GPS, RFID, and ESP 32 Wi-Fi module, the software module, covers two versions, one using Android Applications for home users, Waste Pickers, etc., and the other version will be a Web application for overall control of Administration.

Hardware Module of the System

The hardware module consists of ESP 32 WROOM 32D Wi-Fi module that connects with an RFID reader, an Ultrasonic sensor, GPS Module, a 5v DC power supply, and LCD.

The hardware module works on a Wi-Fi Internet network. The RFID reader is used to read and write waste bin RFID tags. When RFID passive tag contacts the RFID reader, the RFID reader reads all information with GPS coordinates that is sent to the data center through a Wi-Fi network.

Software Module of the System

The software module consists of two versions android application and a web application of a smart solid waste collection system. In that system android application is used for all user interfaces for easy communication and access all information at the user end, such as first user household, second Waste Picker, Driver, and Transfer station. Other user interfaces are web interfaces used as the administrative department and admin section (Wu et al. 2022)

Primary Waste Collection User Interface

The role of the waste picker is a collection of different types of waste. The waste picker roller plays a major role in the daily waste collection on time. However, the door-to-door collection is not carried out properly due to insufficient monitoring of the waste collection process. There is no way for the waste picker to monitor every household physically. This point of view is not achieved correctly. Collecting, sorting, and selling recyclable materials enhance the lives of waste pickers. They play a vital role in primary stage

sustainable solid waste management (Municipal Corporation of Pune 2011, Pal 2020, Dhawale et al. 2022).

1. Wet waste
2. Dry waste
3. Mix waste
4. Biomedical waste
5. Construction and demolition waste
6. Garden waste
7. Hazardous waste
8. E-waste

Secondary waste collection from a small waste picker collection is empty in a large van.

SOC Analysis of Its Base Waste Technology and Discussion

Strength

1. 100% Door to door waste collection Properly
2. User fees will be collection done properly
3. Waste collection regularly on time
4. Waste collection record maintains proper
5. No need to keep a record physically 100 % of waste should be segregated at the source
6. Decentralize waste

Opportunities

1. Awareness of the scientific handling of MSW
2. Development of IT solutions for 100% door-to-door collection
3. Decentralize waste management at the ward level
4. Development of integrated solid waste management
5. Management of Rag-Pickers daily on time
6. Uniformity in User fee collection of weight
7. Reliability of collection vehicle in terms of breakdowns, timing, and of route

Challenges

1. The primary collection of data
2. Registration of each Householder
3. Analysis of data
4. Taking action on householders
5. Proper execution
6. Health issues of rag-picker Training and Education of rag-pickers management at the ward level

Scope of Work

1. Decentralized process of solid waste management at wards
2. Zero waste generation at the ward
3. 100% Coverage of Household door to door
4. Smart Collection, segregation
5. MSW Separation
6. Scientific Disposal
7. MSW Recovery
8. Cost Recovery
9. User charges collection Efficiency
10. Complaint Redressed

CONCLUSION

The Smart City agenda entails improving the citizens' quality of life and strengthening and diversifying the economy while prioritizing environmental sustainability by adopting smart solutions.

Collection can be enhanced by implementing soft computing tools for the collection and a different methodology for waste segregation and providing a processing plant at the ward level. The study reflects the current stage and future scope of methodologies. Encourage citizen participation in the waste management system.

The study was covered over one year and included field visits to 7 transfer stations and 15 ward officers' interviews with various factors involved in 100% Door to door coverage and collection of segregated Municipal solid waste current challenges and sustainable solutions to solve the above problem.

This paper reviews the modern waste collection technology available in some countries and cities to collect door-to-door solid waste effectively and optimize the process of handling waste from primary to secondary transportation.

Solving the above problem by using RFID and IoT base IT solution has the potential to achieve 100% door-to-door waste collection of municipal solid waste.

REFERENCES

- Anagal, V. 2009. Sustainable urban solid waste management: A case study of Pune. 10th National Conference on Technological Trends (NCTT09), Thiruvananthapuram, Kerala, 6-7 Nov 2009, College of Engineering, Thiruvananthapuram, pp. 241-248.
- Das, S. and Bhattacharyya, B.K. 2014. Estimation of municipal solid waste generation and future trends in greater metropolitan regions of Kolkata, India. *J. Indus. Eng. Manag. Innov.*, 1(1): 31.
- Dhawale, N., Mohite, N., Nalawade, A. and Sinha, S. 2022. Geo-mapping trees planted in the college campus premises using smartphone-based GPS. *Int. J. Innov. Res. Sci. Eng. Technol.*, 11(5): 5896-5906.
- Hannan, M.A., Areby, M., Begum, R.A. and Basri, H. 2011. Radiofrequency identification (RFID) and communication technologies for the solid waste bin and truck monitoring system. *Waste Manag.*, 31(12): 2406-2413.
- Hemalata, H.N. 2011. The existing situation of solid waste management in Pune City, India. *Res. J. Sci.*, 1: 348-351.
- IIT Kanpur 2006. Blog, Solid Waste Management. <http://home.iitk.ac.in/~askumar/404.html>
- Jaybhaye, R., Mundhe, N. and Dorik, B. 2014. Site suitability for urban solid waste disposal using geoinformatics: A case study of Pune municipal corporation, Maharashtra, India. *Int. J. Adv. Remote Sens. GIS*, 3(1): 769-783.
- Kaushal, R.K., Chabukdhara, M. and Varghese, G.K. 2012. Municipal solid waste management in India: Current state and future challenges: A review. *Int. J. Eng. Sci. Technol.*, 4(4): 1474-1489.
- Khadke, P.M. 2018. To study willingness to pay for improved solid waste management for Pune city. *Int. Res. J. Multidisc. Stud.*, 4(1): 1-10.
- Kumar, A. and Agrawal, A. 2020. Recent trends in solid waste management status, challenges, and potential for the future Indian cities: A review. *Curr. Res. Environ. Sustain.*, 2: 100011.
- Kumar, S. and Moore, K.B. 2002. The evolution of global positioning system (GPS) technology. *J. Sci. Edu. Technol.*, 11(1): 59-80.
- Kumar, S., Bhattacharyya, J.K., Vaidya, A.N., Chakrabathi, T., Devotta, S. and Akolkar, A.B. 2009. Assessment of the status of municipal solid waste management in metro cities, state capitals, class I cities, and class II towns in India: An insight. *Waste Manag.*, 29(2): 883-895.
- Kumar, S., Smith, S.R., Fowler, Velis, C., Kumar, S.J., Arya, S., Kuamr, R.K. and Cheeseman, C. 2017. Challenges and opportunities associated with waste management in India. *Royal Soc. Open Sci.*, 4(3): 160764.
- Kumar, V. and Pandit, R.K. 2013. Problems of solid waste management in Indian cities. *Int. J. Sci. Res. Publ.*, 3(1): 2250-3153.
- Mani, S. and Singh, S. 2016. Sustainable municipal solid waste management in India : A policy agenda. *Procedia Environ. Sci.*, 35: 150-157.
- Ministry of Housing and Urban Affairs. (2017). Swachh Bharat Mission (Urban). Ministry of Housing and Urban Affairs Government of India, October, 1-68.
- Mohan, G., Sinha, U.K. and Lal, M. 2016. Managing solid waste through a public-private partnership model. *Proceed. Environmental Sciences*, 35, pp. 158-168.
- Mundhe, N., Jaybhaye, R. and Dorik, B. 2014. Assessment of municipal solid waste management of Pune city using geospatial tools. *Int. J. Comp. Appl.*, 100(10): 24-32.
- Municipal Corporation of Pune. 2011. Involving Waste-Pickers to Improve Door-To-Door Collection. <https://swachhcoop.com/pdf/wastepickerstoimprovedoor-to-doorcollection.pdf>
- Municipal Corporation of Pune. 2015. What is Pune Municipal Corporation CARE ? <https://www.pmc.gov.in/en/pmc-care-1>
- Pal, S. 2020. Application of GIS in road information system: An experience with state highways of West Bengal. In: Prisco, M.P., Chen, S.H., Vayas, I., Shukla, S.K., Sharma, Kumar, N., Wang, C.M. (eds), *Lecture Notes in Civil Engineering*. Springer, Singapore, pp. 413-421.
- Parhi, S. 2018. Solid Waste Management : A Study of Pune Municipal Corporation. Pune, SIOM, pp. 1-17.
- Rahman, M.W., Islam, R., Hasan, R., Bithi, N.I., Hasan, M.M. and Rahman, M.M. 2022. Intelligent waste management system using deep learning with IoT. *J. King Saud Univ. Comp. Inform. Sci.*, 34(5): 2072-2087.
- Rode, S. 2018. An integrated approach to solid waste management in Pune city. *Af. J. Environ. Waste Manag.*, 5(7): 1-6.

- Swachh Bharat Abhiyan 2014. Swachh Bharat Mission – Urban Guidelines. http://swachhbharaturban.gov.in/writereaddata/SBM_GUIDELINE.pdf
- Times of India 2021. With inclusion of 23 villages, PMC becomes state's largest civic body. <https://timesofindia.indiatimes.com/city/pune/with-inclusion-of-23-villages-pmc-becomes-states-largest-civic-body/articleshow/84006954.cms>
- Tongkaw, S. 2017. GIS application management for disabled people. IOP Conference Series: Materials Science and Engineering, 226(1). <https://doi.org/10.1088/1757-899X/226/1/012112>
- Wu, W., Liu, Y. and Hu, M. 2022. Geo-information technology and its applications. ISPRS International Journal of Geo-Information, 11(6). <https://doi.org/10.3390/ijgi11060347>



Strategic Monitoring of Groundwater Quality Around Olusosun Landfill in Lagos State for Pollution Reduction and Environmental Sustainability

O.J. Oyeboade*†, F.O. Jimoh*, S.M. Ajibade**, S.A. Afolalu*** and F.A. Oyeboade****

*Civil and Environmental Engineering Department, Afe Babalola University, Ado-Ekiti, Ekiti State, Nigeria

**Department of Computer Engineering, Istanbul Ticaret Universitesi, Istanbul, Turkey

***Mechanical and mechatronics Engineering Department, Afe Babalola University Ado-Ekiti (ABUAD), Ado-Ekiti, Ekiti State, Nigeria

****Ondo State Rural Water Supply and Sanitation Agency Alagbaka, Akure, Ondo State, Nigeria

†Corresponding author: O.J. Oyeboade; oyeboadedare@yahoo.com

Nat. Env. & Poll. Tech.
Website: www.neptjournal.com

Received: 02-12-2022

Revised: 02-01-2023

Accepted: 05-01-2023

Key Words:

Landfill
Solid waste
Groundwater
Pollution
Solid Waste Management

ABSTRACT

As urbanization and population increase in the megacity, there is a need for engineering intervention and strategic monitoring of groundwater around landfills for environmental sustainability, pollution reduction and public health. This study evaluated water's physical and chemical parameters in wells and boreholes near the Olusosun landfill in Lagos State to determine how they impact groundwater quality. An Atomic Absorption Spectrometer (AAS) was used to evaluate groundwater samples obtained from five locations within the dump site. Some water parameters, such as dissolved oxygen (DO), iron (Fe), lead (Pb), manganese (Mn), and magnesium (Mg), had concentrations that were higher than the WHO, NESREA, and Nigerian Standard for Drinking Water Quality (NSDWQ) standard limits in some sampling sites, with mean concentrations of 0.33 mg.L⁻¹, 0.04 mg.L⁻¹, 0.74 mg.L⁻¹, and 0.74 mg.L⁻¹, respectively. A small amount of lead was identified in the groundwater of the study area. A major source of air and groundwater pollution, the Olusosun landfill has a detrimental impact on the health of those who live there. Solid waste, groundwater interactions, and contaminated migration into the nearby neighbourhood were studied. It was observed that the degradation of waste products in dump sites releases harmful leachate into the groundwater. Even though some heavy metal concentrations in the study area are still within WHO, NESREA, and NSDWQ standard limits, investigations and further monitoring should be conducted regularly to assess the concentrations of heavy metals in groundwater.

INTRODUCTION

The open dump disposal system is the most popular technique of solid waste disposal in Lagos and the rest of the country. This disposal strategy, like the landfilling waste management system, is most common in developing nations worldwide due to the related cheap costs. According to (Longe & Balogun 2010), landfills dispose of practically all solid waste created in low and middle-income nations due to abundant land and low operational costs. On the other hand, landfills and dump sites have health and environmental problems. While "poor operation and management of municipal solid waste (MSW) dump present a substantial threat to the environment, particularly "surface water, and groundwater," this is the case. Uncontrollable waste disposal, a lack of liners

and leachate treatment and disposal facilities, insufficient compaction, inappropriate site design, the presence of scavengers, and low operational control are all features of open dumps.

In many places around the world, groundwater provides a significant source of fresh water for drinking. With many benefits over surface water, it is a significant renewable resource. Because of its superior capacity for self-cleansing and simplicity of treatment, groundwater is usually less polluted than surface water. As the population increases, so does the worry about trash disposal. A lack of waste disposal options causes this. Most urban dwellers must use open landfills to dispose of their trash. Degradation of these waste products releases harmful leachate into the groundwater. Due to insufficient water delivery by the Lagos State Water Corporation in these regions, groundwater is an important water source near the many dumpsites in Lagos. Current waste management procedures in Lagos represent a threat to

ORCID details of the authors:

O.J. Oyeboade: <https://orcid.org/0000-0003-2792-146X>

the quality of surrounding groundwater to landfills, given the rising dependency on water for irrigation purposes and the fact that, in the majority of instances, little or no treatment is conducted on the water before consumption. Lagos has no truly sanitary landfills, and trash disposal facilities can only be regulated dumps. Controlled landfills are inspected and monitored, and they maintain track of incoming wastes, waste compaction, and soil cover application. A sanitary landfill, unlike a controlled dump, is well maintained. As illustrated in Fig. 1, the facility is strategically positioned and fitted with liner and leachate collecting systems, which prevent leachate from penetrating groundwater. Fig. 1 illustrates the state of major landfills.

PAST STUDIES

Rivers and lakes account for 0.32 percent of total moisture, with atmospheric moisture accounting for 0.03 percent and soil moisture accounting for 0.05 percent (Gleick 1996). The subsequent groundwater contamination by discharged leachate is the most serious environmental issue surrounding landfill (Afolayan et al. 2012). Landfills have long been the final destination for all types of waste, including municipal solid, industrial, and hazardous waste. Liners at the bottom of modern landfills act as hindrances to leachate migration. However, it is widely recognized that such liners degrade over time and eventually fail to prevent leachate from contaminating groundwater (Jagloo 2002). Natural processes (like precipitation rate, weathering processes, and soil erosion) and anthropogenic effects (like urban, industrial, and agricultural activities, as well as human exploitation of

water resources) influence the quality of surface water in a region. Heavy metals are good indicators of contamination in urban soils and street dust, according to (Kholoud et al. 2009). In the context of the periodic table, heavy metals have atomic weights ranging from 63.546 to 200.590 with specific gravities greater than 4 (Kennish 1992). Polluted water with high amounts of nitrates can induce methemoglobinemia (cyanosis) in infants and gastrointestinal problems in adults (Kumar et al. 2006). Environmental engineers and other stakeholders must act quickly to protect the environment and improve public health against environmental dangers, climate change difficulties, ecological challenges, and unsanitary behaviours (Oyeboade 2022). The Nigerian government should establish and enforce regulations banning municipal and medical garbage disposal in dumpsites, making some dumpsites available, and offering barriers to keep scavengers away (Oyeboade & Otoko 2022). An essential prerequisite for human existence is public health. Waste has a direct relationship with human development, both technologically and socially. Once properly recovered, some waste components have economic value and can be repurposed (Oyeboade 2013).

According to Taylor & Allen (2006), landfills are most associated with groundwater contamination by waste-derived liquids in terms of situation assessment. Any location where waste is concentrated, processed, and stored, even for a short time, could be a point source of groundwater contamination. According to Lee & Jones (1991), about 75% of the projected 75,000 waste disposal pollutes nearby groundwater with leachate. Depending on the types of waste deposited,

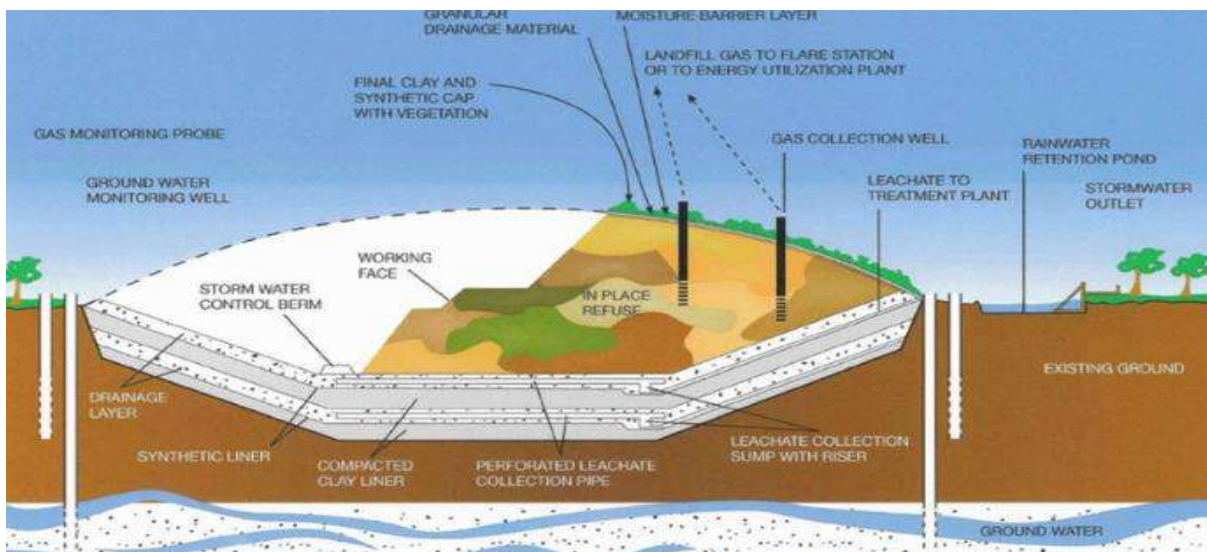


Fig. 1: Diagram of a modern engineered landfill.

leachate produced from waste deposits can contain a wide range of contaminants. Groundwater contamination poses a significant risk to local resource users and the natural environment (Taylor & Allen 2006).

Characteristics of Leachate on groundwater quality

According to Longe & Balogun (2010), the greatest threat to groundwater contamination comes from the leachate produced by the waste material, which mostly contains toxic substances, especially when industrial wastes are landfilled. However, it's widely reported that leachates from non-hazardous waste landfills may contain complex organic compounds, chlorinated hydrocarbons, and metals at levels that endanger surface and groundwater.

Any polluted liquid that results from water percolating through a solid waste disposal site, picking up impurities, and flowing into subterranean regions is referred to as leachate. High moisture levels in some discharged wastes are a second source of leachate. Inadequate solid waste disposal facilities are one of Nigeria's biggest environmental and public health problems today (Oyebode 2019). Organic and inorganic compositions are common in the leachate produced. Furthermore, as time passes, the leachate produced makes its way into ground systems, changing groundwater's physical and chemical properties (Vasanthi et al. 2008). When it comes to time and age, the condition of a landfill can change from aerobic to anaerobic, allowing for different chemical reactions to occur (Taylor & Allen 2006). General geology, the degree of chemical weathering of distinct rock formations, the condition of recharge water, and materials from sources other than rock contact all impact groundwater chemistry. As a result of these elements and their interplay, water quality is complicated (Aghazadeh & Mogaddam 2010). Several extensive investigations of leachate plumes have discovered that they seldom extend more than a few hundred kilometers from the landfill. Still, a few of the most persistent toxins are entirely suppressed (Christensen et al. 1994, Robinson et al. 1999). The most prevalent natural solvent in the world is water. As a result, it dissolves minerals as it flows through the earth. These minerals make up the Total Dissolved Solids (TDS) in water. Because the water in a shallow aquifer moves a smaller distance through the ground, it has less mineralization. In contrast, deeper aquifers are more susceptible to pollution by local land use activities, such as nitrate and microbiological degradation (McLeod et al. 2005).

Analysis of water quality

Water quality may be assessed in a variety of ways. Instead of creating a cost-effective scheme for assessing

groundwater quality by collecting samples from boreholes and acquiring usable data, Yeh et al. (2008) attempted to use approaches that cannot properly distinguish the various water contaminants. Using the Water Quality Index approach, a mathematical expression obtained cumulatively and specifying a certain level of water quality may be presented to the public. Because the Water Quality Index incorporates data from numerous water quality measures, it offers a numerical number to the water's overall health (Yogedra & Puttaiah 2008). Combustion produces methane, which may ignite flames, explode, and generate leachate that pollutes groundwater and surface water (Oyelola et al. 2009).

For many years, landfills have served as the dumping area for all types of waste, including municipal solid waste, industrial sewage, and hazardous waste. Physical, chemical, and biological processes all interact simultaneously to decompose waste. Leachate is one of the byproducts of this mechanism. It is produced from rainwater, assisting bacteria in the decomposition process. Leachate typically comprises dissolved organic matter, inorganic macro components (like chlorides, iron, aluminium, zinc, and ammonia), and heavy metals. Other chemicals, such as pesticides and solvents, may also be present. Leachates are a type of hazardous waste that can be found in landfills.

Landfills and dump sites continue to be a source of public health and environmental concern worldwide. This is because of the negative consequences for public health, groundwater and surface water quality, air quality, the greenhouse effect, and global warming. Several uncertainties surround the short and long-term impact of LAWMA-operated dumpsites on the environment and its resources near these dumpsites. On the other hand, residents rely on untreated groundwater, frequently from shallow wells and boreholes, putting them at risk of ingesting any toxic material or compounds in groundwater due to leachate contamination. Landfills have been connected to illnesses, including nervous system damage, ocular and upper respiratory irritation, arrhythmias, and dizziness in humans. Long-term ingestion of hydrogen sulfide (H_2S) and volatile organic compounds like benzene has been linked to cancer development. In a neighbourhood in the United States, liver disease has been related to groundwater pollution leachate produces (Bundschuh et al. 2021).

Furthermore, groundwater surrounding dumpsites is a danger of pollution, especially in light of the observed leachate ponds Fig. 1, which form around dumpsites during the wet season. Leachate ponds are formed when water flowing through an unlined landfill or dumpsite above an aquifer is top-dressed; the increased hydraulic head causes leachate to flow downhill and out of the dumpsite. Leachate

springs, which are the consequence of outward flow, show that leachate has not only been formed but is also running within the subsurface, providing a public health danger. The lack of environmental protection measures such as artificial sealing liners, upstream diversion, and leachate collecting wells or control facilities near dumpsites exacerbates the threat to groundwater quality. Furthermore, these dumpsites were not discovered using hydrogeological criteria. No hydro-geological investigations were undertaken before sanitary landfill operations to determine the probable link between groundwater flow and dumping sites and the potential consequences of this relationship on groundwater quality inside and around the dumpsites. These dumpsites were once laterite burrow pits where garbage was dumped to help the soil restore itself. Finally, the landfill gases (LFG) created by these dumps harm the environment and public health. Due to the unmistakable stench of hydrogen sulfide and other gases, landfill gases are the leading source of air quality degradation. Greenhouse gases, especially methane and carbon dioxide affect global warming. Fig. 2 presents Water Table Mounding and Leachate Spring at the Periphery of Waste Deposited at a Dumpsite.

Landfill System in the Developing Countries

It has been said that landfills provide the “ultimate means of survival” for the poor in developing nations worldwide, especially in Africa. It also acts as an additional source of raw material for recycling, putting into effect the proverb “one man’s food is another man’s poison.” They view garbage as both a source of wealth and a method of sustenance.

Scavengers compete to make “payments” to the dumpsite manager to gain access to the dumpsite for scavenging, especially in Lagos dumpsites. There are various landfill systems throughout the world. In most African nations, open dumps are still the predominant method of trash disposal. Fig. 2 presents a cross-section of an Engineered Sanitary Landfill.

Typically, the first step in a nation’s effort to rehabilitate its landfills is establishing a managed or semi-controlled landfill. Controlled dumpsites do some incoming waste inspection and documentation, employ considerable waste compaction, and regulate the tipping front and application of soil to cover the waste.

The surrounding hydrological system instantly absorbs landfill waste. Rainfall, snowmelt, and groundwater, as well as liquids generated by the waste through condensation reactions and solubilization procedures prompted by a series of complex biochemical reactions during the degradation of organic wastes, percolate through the deposit and mobilize other waste components, with the resulting leachate migrating offsite either through direct infiltration on-site or through leachate-laden runoff infiltration. Various factors determine the content of leachate and the degree of contamination it causes, including the age of the landfill, the type of trash it includes and the hydrological characteristics of the landfill (Bidhendi et al. 2010).

Difference between Landfills and Dumpsites

A sanitary landfill is a designed system, while a dumpsite

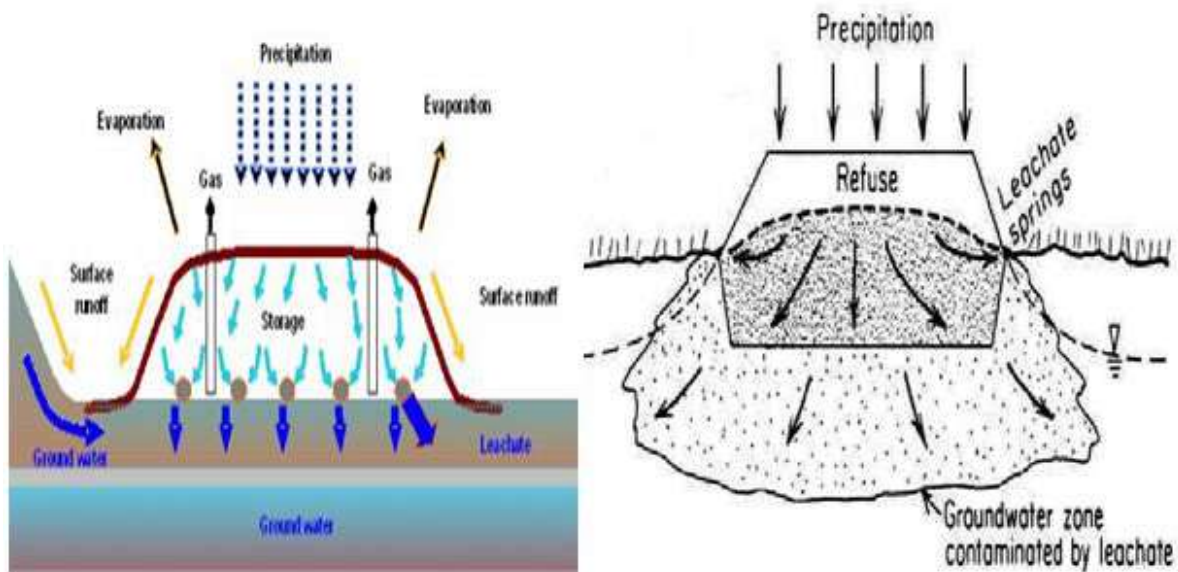
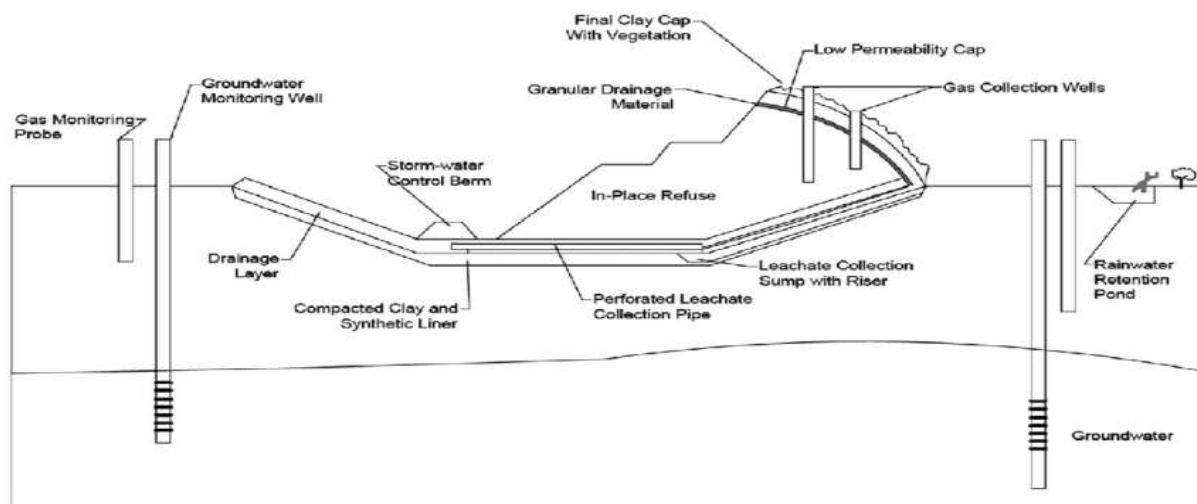


Fig. 2: Water table mounding and leachate spring at the periphery of waste deposited at a dumpsite.



(Source: Zume et al. 2006)

Fig. 3: Cross section of an engineered sanitary landfill.

is an arbitrary location for solid waste disposal. Generally, sanitary landfills are constructed where groundwater and runoff are not an issue. Local governments and residents must be taken into account. Dumpsites are excavated areas of ground where residents dispose of their solid waste. Most families, especially in rural areas, have waste landfills, whereas urban populations share a single dump. The authorities do not regulate solid waste, and there is no oversight over their processing. They can be found practically anywhere and may or may not be covered by soil. They are also unmonitored, which increases the likelihood that solid waste leachate will enter the water supply. Open dumpsites attract flies and rats and generate unpleasant odours that harm humans. The ideal is a landfill confined to a limited area and covered with earthen layers.

Sustainability of Water Development

The water cycle connects the world's fresh water and oceans. Water is roughly 70% of the human body and 60-70% of plant cells. The ocean contains 97 percent of the world's water, providing almost all that falls as rain and snow. About 2/3 of the remaining freshwater is groundwater, with only 0.3 percent in accessible surface waters. Water contamination, whether endogenous or exogenous, is a major issue, particularly in developing countries. Water, particularly groundwater, can become contaminated and remain so without treatment. In its liquid state, water is the substance that allows life to exist on Earth. Every living organism comprises cells constituting at least 60% of water because water is the foundation of life. Access to water resources is a critical component of any area's overall development.

MATERIALS AND METHODS

This section examines the study region from a geological, climatic, vegetation, and topographical aspect. In this section, we will take a quick look at the research process and the heavy metal parameters we'll be looking at.

Study Area

The Olusosun landfill in Lagos State, Nigeria, has been used since 1992 and is located in the city of Oregun. Approximately 10 km south of the Ikeja Local Government Area, Lagos Waste Management Authority (2011) estimates the landfill's area to be 42.7 hectares. (Eludoyin & Oyeku 2010). The Olusosun dumpsite is situated between latitudes 2°42' E and 3°42' E and longitudes 6°23' N and 6°41' N in the Ojota neighborhood of Lagos. Due to urbanization, the site, which was formerly outside of the city, is now inside of it. The dump facility, which is the biggest in Lagos State, gathers more than 50 percent of the waste produced. In the dumpsite, a sizable number of scavengers reside and earn a living (Aboyeji and Eigbokhan 2016).

The landfill is expected to be operational for around 20 years. Fig. 5 shows that the settlements of Ojota, Ketu, and Oregun bound the landfill. Fig. 4 presents a map showing the study area.

Due to a lack of public water, most residents in the neighbourhoods surrounding the landfill rely on private wells as a water source. Lagos State is home to over 19 million people and is growing at a 3.2 percent annual rate. The state generates much waste daily due to its large population. Approximately 40% of all waste deposits are deposited at the Olusosun Landfill site (LAWMA 2010). The Lagos



Fig. 4: Map showing the study area.

Waste Management Authority (LAWMA) manages the landfill, which accepts all types of waste in its natural state, from inorganic to organic, hazardous to non-hazardous. The landfill lacks a protective bottom liner to prevent leachate from entering groundwater. Most trash collected in Lagos is disposed of at the Lagos State Waste Management Authority's waste dumpsites (LAWMA 2010). The Olusun Dumpsite near Ojota, the Abule-Egba Dumpsite along the Lagos-Abeokuta Expressway, and the Solous Dumpsites along the LASU Isheri Expressway are among these dumpsites. Fig. 4 presented Leachate Spring at Olusun Dumpsite Environment, while Fig. 6 presented the map of the Lagos urban centre showing the major landfill sites.

The Olusun dumpsite is situated between latitudes $2^{\circ}42' E$ and $3^{\circ}42' E$ and longitudes $6^{\circ}23' N$ and $6^{\circ}41' N$ in the Ojota neighborhood of Lagos. Due to urbanization, the site, which was formerly outside of the city, is now inside of it. The dump facility, which is the biggest in Lagos State and measures 42 hectares, gathers more than 50 percent of the waste produced. In the dumpsite, a sizable number of scavengers reside and earn a living (Aboyeji and Eigbokhan, 2016). The Open dump is the default option for municipal solid waste management, featuring uncontrolled trash disposal and low operational restrictions, including the environmental effects of landfills. Fig. 7 indicates scavengers sorting solid waste in the study area.



Fig. 5: Leachate spring at olusosun dumpsite environment.



Fig. 6: Map of the Lagos urban centre showing the major landfill sites.



Fig. 7: Scavengers sorting solid waste in the study area.

Fig. 8 presented an overview of the environmental pollution and health effects associated with waste landfilling and open dumping while Fig. 9 presented the location Map of Olushosun Dumpsite in Ojota.

Climatic Condition of Study Area

There are two separate rainy seasons in the study area: one from April to July and the other from October to November.

Most days in Lagos during the rainy season are cloudy or overcast. When it rains less than two days per month in August, September, December, and March, Lagos has a dry season, preceded by the Harmattan winds from the Sahara, which is greatest in December and early February. This is followed by the rainy season in April and May. The temperature ranges from 33 to 21 degrees Celsius. At an average of 32°C, the warmest month is March, while the coldest is August, at 25°C daily.

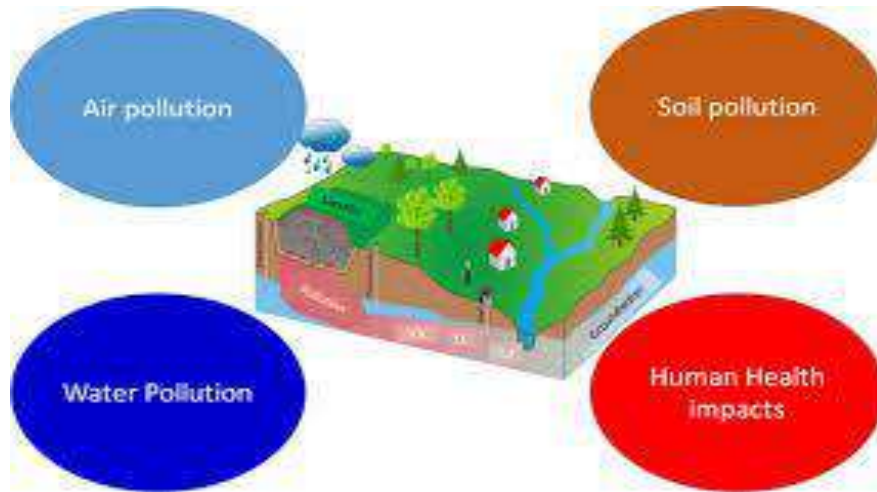


Fig. 8: An overview of the environmental pollution and health effects associated with waste land filling and open dumping.

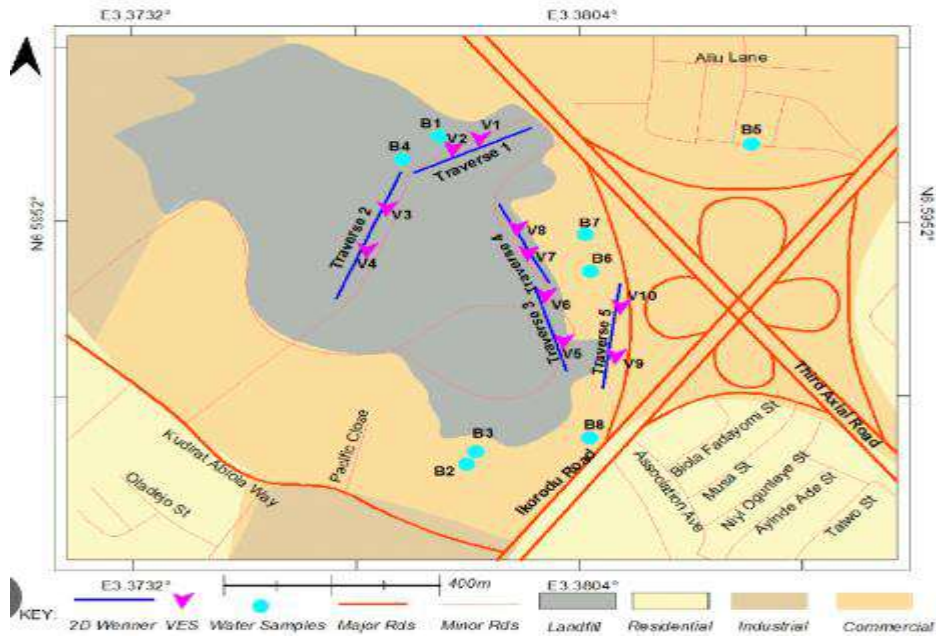


Fig. 9: Location map of olusosun dumpsite in Ojota.

Vegetation and Drainage of Study Area

For much of the territory, the state’s twofold rainfall pattern creates a wetland habitat dominated by freshwater tropical rainforest and mangrove swamp forest. Extremely dry times of the year are from November to March, while rainy times are from April to September. A network of canals and waterways in the Study region covers approximately 22% of the State’s geographical area.

Data Source

A combination of primary and secondary sources provided

the data for this project. Direct field surveys were used to gather primary data. The information was obtained from wells close to Lagos State’s biggest dumpsite, Olusosun, in Ojota, Lagos State. The research area’s wells and boreholes provided the study’s groundwater samples. For physicochemical characteristics and heavy metals analysis, the samples were numbered from Bh1 to Bh5 and sent to the University of Lagos. Laboratory professionals performed the tests, and the findings were gathered and analyzed. Table 1 contains information about the data points. Secondary data included information gleaned from publications such as books, papers, and journal articles. Secondary data sources

include the NESREA (National Environmental Standards and Regulations Enforcement Agency), WHO, the Nigerian Standard for Drinking Water Quality (NSDWQ), and maps of Lagos State.

Collection of Samples

Over three months, groundwater samples were gathered from five unique locations, with three collected from each. The plastic bottle, which had been well-cleaned and labeled Bh1 through Bh5, was used to collect and store the samples for further analysis. After that, the samples were transferred to the University of Lagos' chemistry laboratory for assessment.

Data Analysis

All analytical techniques fulfilled the 2005 APHA standard guideline for drinkable and wastewater parameters. I tested each sample against various physical, chemical, and heavy metals criteria.

Onsite data analysis

The pH, temperature, electrical properties, and dissolved oxygen values were gathered. Dissolved oxygen concentrations were determined with a Dissolved Oxygen Meter (DOM). The pH of the sample was determined using a pH meter. The temperature was measured using a thermometer. Additionally, a conductivity/EC meter was used to assess electrical conductivity.

Offsite data analysis

An Atomic Absorption Spectrometer was used to check for metals in groundwater samples sent to the chemistry department at the University of Lagos (UNILAG) (AAS). Analyzed samples were heated and tested within six (six) days following collection. Aqua regia was used to dry the combination of water in a fume cupboard to analyze heavy metals in the water sample. For atomic absorption spectrometer (AAS) metal analysis, 25 mL of distilled water was poured and filtered through a funnel and filter paper. In addition to copper, lead, iron, calcium, chromium,

manganese, magnesium, and zinc, the metals investigated were copper, lead, iron, calcium, chromium, manganese, magnesium, and zinc (Zn).

Data Evaluation

Average mean, standard deviation, tables, and various data were all part of the statistical analysis utilized to analyze the information. Each well's characteristics were compared against the distances from the landfill and the concentrations in mg.L^{-1} in a table. Each parameter's average value was obtained utilizing equation (1). The equation was used to calculate the range (2)

$$M(x) = (x_1 + x_2 + x_3 + \dots + x_n) / n \quad \dots(1)$$

$$\text{Range (R)} = \text{Highest parameter value} - \text{Lowest parameter value} \quad \dots(2)$$

The results are then compared to the groundwater quality of nearby environments such as Oregun, Ketu, and Ojota, as reported by Olaniyan et al. (2015) as well as the W.H.O standard and NSDWQ water quality guidelines (Oseke et al. 2021). Heavy metal poisoning of the environment and groundwater supplies, particularly in developing nations, has become a growing ecological and public health concern in recent years (Zacchaeus et al. 2020). Due to the hazardous and greenhouse gas (GHG) emissions from the direct combustion and/or decay of trash, open dumping practices significantly endanger the environment and human health (Pujara et al. 2019).

Due to a lack of infrastructure at these dumpsites, there is a high risk of leachate contaminating the groundwater within the dumpsites, especially during the rainy season. The quality, volume, and sensitivity of the groundwater that receives the leachate, as well as the leachate's concentration and flow, the landfill's hydrogeological setting, the level of protection provided by the landfill, and the quality, quantity, and sensitivity of the groundwater that receives the leachate all play a role in how polluted the leachate can be. Because of the vast spectrum of chemical compounds that may be present in landfill leachate, groundwater within the dumpsites may be unfit for drinking and other household purposes. Several common contaminants can be discovered

Table 1: Site description of sample locations.

S/n	Sample code	Street name	Distance [m]	Source of sample	North	East
1.	Bh ₁	Moshalasi Street	610m	well	06°35'27.69"	003°22'19.48"
2.	Bh ₂	Anisere Close	500m	well	06°35'23.13"	003°22'21.75"
3.	Bh ₃	Kudirat Abiola Way	300m	Borehole	06°35'23.86"	003°22'30.67"
4.	Bh ₄	Ayinde Street	875m	Borehole	06°35'26.12"	003°23'26.79"
5.	Bh ₅	Niyi Ogunleye Street	378m	Borehole	06°35'19.26"	003°23'24.76"

Source: Fieldwork 2022

in municipal solid waste (MSW). Because groundwater may be affected, particularly regarding how garbage is disposed of at LAWMA dumpsites, various studies have been conducted to see how these dumpsites influence groundwater quality in the surrounding areas. Flows into lakes and base flows into rivers from groundwater, as part of the hydrologic cycle, help maintain surface water systems by supporting inflow needs for surface water. Maintaining sensitive ecosystems' biodiversity and habitats often depends on these flows (Tharme 2003). Groundwater contamination can be transferred to surface water via the hydrologic cycle, impacting aquatic organisms' health and quality.

the area's groundwater quality. Tables and figures are used to displaying the information clearly and concisely.

Physical Parameters

Each sampling point's physical and chemical properties were found to comply with World Health Organization (WHO) standards in terms of appearance, odour, and turbidity. There was evidence of pathogens, such as active microorganisms, with temperatures ranging from 25.7 to 26.4°C below the recommended range of 35-40°C (Akinbile & Yusoff 2011, Jaji et al. 2007). Table 2 presented the physical parameters of water in the study area.

Chemical Parameters

According to W.H.O, NESREA, and NSDWQ standards,

RESULTS AND DISCUSSION

Water samples were used to assess the landfill's impact on

Table 2: Physical Parameters of Water in Study Area.

Physical Parameter	Temperature [°C]	Appearance	Electrical Conductivity	Total Dissolve Solid	Odour	Turbidity (NTU)
W.H.O Standard	35 – 40	Colourless	1000	500	Odourless	5NTU
Bh1	26.4	Colourless	110.6	70.3	Odourless	Clear
Bh2	26.3	Colourless	119.3	92.3	Odourless	Clear
Bh3	25.7	Colourless	205.6	96.6	Odourless	Clear
Bh4	25.9	Colourless	150.6	63.3	Odourless	Clear
Bh5	25.6	Colourless	118.6	71.6	Odourless	Clear

Table 3: Chemical parameters in the study area.

	pH	Total Hardness [mg.L ⁻¹]	Chloride [mg.L ⁻¹]	Nitrates [mg.L ⁻¹]	Phosphate [mg.L ⁻¹]	Sulfates [mg.L ⁻¹]	Dissolved Oxygen [mg.L ⁻¹]
NSDWQ	6.5 - 8.5	Not Stated	250	50	Not Stated	100	5.0
W.H.O Standard	6.5 - 8.5	100	250	10	5	250	Not Stated
NESREA	6.5 – 8.5	150	200	50	Not Stated	100	Not Stated
Bh ₁	5.61	32.3	64.2	1.83	1.40	3.68	4.69
Bh ₂	6.36	52.6	70.7	1.04	0.44	0.74	5.01
Bh ₃	6.30	51.3	23.1	4.86	0.33	12.63	8.46
Bh ₄	6.91	103.6	45.8	2.09	0.12	0.22	3.21
Bh ₅	6.48	93.3	65.4	0.07	0.40	2.03	4.61

Table 4: Heavy metal concentration in the study area.

Parameters	Chromium [mg.L ⁻¹]	Copper [mg.L ⁻¹]	Iron [mg.L ⁻¹]	Lead [mg.L ⁻¹]	Manganese [mg.L ⁻¹]	Magnesium [mg.L ⁻¹]	Chloride [mg.L ⁻¹]	Zinc [mg.L ⁻¹]
NSDWQ	0.05	1	0.3	0.01	0.2	0.2	0.25	3.0
W.H.O Standard	0.05	2	0.1	0.01	0.4	0.4	1.5	Not Stated
NESREA	Not Stated	0.5	0.6	0.01	0.2	0.05	200	3
Bh₁	0	0	0.03	0.04	0.12	2.66	64.2	0.09
Bh₂	0	0	0.79	0.04	1.77	12.62	70.7	0.09
Bh₃	0	0	0.24	0.04	0.72	14.12	23.1	0.07
Bh₄	0	0	0	0.03	0	0.64	45.76	0.20
Bh₅	0.01	0.05	0.61	0.04	1.08	3.59	65.36	0.13

Table 5: Descriptive Statistics of water parameters in the study area.

S/N	PARAMETERS	MEAN	RANGE	STANDARD DEVIATION
1.	Calcium (Ca)	72.38	144.51	56.954
2.	Copper (Cu)	0.01	0.05	0.018
3.	Chromium(Cr)	0	0.04	0.010
4.	Manganese (Mn)	0.74	1.97	0.651
5.	Magnesium (Mg)	6.73	14.18	5.340
6.	Lead (Pb)	0.04	0.01	0.005
7.	Iron(Fe)	0.33	0.79	0.316
8.	Zinc (Zn)	0.12	0.13	0.045
9.	pH	6.33	1.76	3.116
10.	Total Dissolved Solids (TDS)	78.82	36	52.362
11.	Hardness	70.63	76	27.542
12.	Nitrates	2.46	4.81	1.636
13.	Dissolve Oxygen (DO)	5.20	5.25	6.753
14.	Sodium	1.98	3.13	1.041
15.	Potassium	21.072	73.266	26.228

the average concentration of chemical parameters is shown in Table 3. Samples of groundwater containing heavy metal concentration are shown in Table 4. Table 5 also presents descriptive statistics of water parameters in the study area.

pH: The groundwater's pH was somewhat acidic because of low amounts of metal pollutants (below 7). pH is one of the environmental parameters that influence the movement of pollutants. Toxic metals and nutrients can be released into the groundwater when acidity (low pH) is present in the water. When acidity is reduced (raising pH), some nutrients become insoluble and inaccessible to plants. In soil with a pH > 7.5, calcium binds phosphorus, making it less accessible to plants (Lake et al. 2000). WHO and NSDWQ recommend a pH range of 6.5–8.5 for drinking water. An acidity level that is slightly below normal indicates that water is not safe to consume. The pH of the lowest sample was found at Bh1, where it was 5.6.

Dissolved Oxygen: Water quality is closely tied to the concentration of dissolved oxygen (DO). According to the NSDWQ, the oxygen levels in groundwater samples from selected locations Bh1, Bh4, and Bh5 were within the acceptable limit of 5.0 mg.L⁻¹; however, samples from Bh2 and Bh3 exceeded this threshold. Drinking water quality is not regulated in DO. When DO levels fall below 5 mg.L⁻¹, aquatic organisms are under stress, causing them to die.

Total Dissolved Solids: Table 4 shows that TDS levels in the samples were below the WHO recommendation of 500 mg.L⁻¹ and the NSDWQ allowable limit of 1000 mg.L⁻¹. According to the data, metals had been dissolved in the groundwater by dissolved chemical components.

Chromium: There were no significant differences in Chromium (Cr) concentrations between the sampling locations, as indicated in Table 4. Mean Cr concentrations are within the acceptable range of 0.05 mg.L⁻¹. Chromium compounds are classified as harmful or non-toxic depending on the metal's oxidized state. Even though chromium (III) is an important element that can be hazardous in large amounts, chromium (VI) compounds have been related to lung cancer. Chromium aids insulin in its role in blood sugar regulation. Diabetes, infertility, and heart disease have been related to a shortage of this metal (Al Osman 2019).

Nitrates: According to the WHO, NESREA, and NSDWQ, nitrate concentrations in groundwater samples were below the maximum allowed levels of 50 mg.L⁻¹ and 10 mg.L⁻¹, respectively. The high nitrate concentration of groundwater in landfills can be transferred to surface water, resulting in eutrophication. In addition, human red blood cells' capacity to carry oxygen can be hampered by water with high nitrate concentrations.

Lead: All of the samples had Lead levels that were over the acceptable limit. In each case, the WHO and NSDWQ allowable limit of 0.01 mg.L⁻¹ were exceeded by an average of 0.004 mg.L⁻¹. Children are particularly at risk from Lead's potentially detrimental effects on their health (Payne 2008). In the samples, lead concentrations weren't high enough to represent a significant health hazard.

Copper: All groundwater samples from the five locations analyzed were within the WHO and NSDWQ standards. Despite this, it has persisted and is completely safe to consume. The liver and kidneys can be damaged by copper

toxicity, resulting in death. It can induce dizziness, nausea, vomiting, and diarrhoea, among other symptoms.

Iron: It was found that the concentrations of Bh2 and Bh5 were greater than the WHO limit of 0.3 mg.L^{-1} at 0.79 mg.L^{-1} and 0.61 mg.L^{-1} . Table 4 shows the average iron content to be 33 micrograms per litre. Discolouration and staining are possible when washing textiles in water with high iron content.

Comparison of Present Results with Previous Studies

Table 6 shows that the metal pollutants reported in samples by Olaniyan et al. (2015) were likewise discovered in this research. Nitrogen, Zinc, and Chromium levels were greater in his research, though. These metal pollutants were reported to have 26.0, 0.15, and 0.03 mg.L^{-1} values, respectively, whereas this research revealed amounts of 2.46, 0.12, and 0 mg.L^{-1} . Because of this, seasonality significantly affects how groundwater is polluted, as shown by the results. A shallow water table during the rainy season can contribute to groundwater pollution, whereas a deep-water table is more common during the dry season. Although Olaniyan et al. (2015) results were more accurate, the trash created by paint and plastic firms in Ojota, Ketu, and Oregun communities impacts groundwater pollution more than those identified in this study.

CONCLUSIONS

During a visit to the study area, it was discovered that there were insufficient facilities and that the waste disposal method employed was open dumping, which does not necessitate special oversight. Residents in this neighborhood have to rely on sachet water for their drinking water, while water for domestic use is provided by water trucks. A lot of pollution comes from the dump, making the environment unpleasant. According to the presence of leachate ponds, the landfill is responsible for this region's groundwater pollution. Residents in this area cannot breathe clean air because of the landfill, which contributes to air pollution.

In Lagos city, where adequately constructed waste

Table 6: Descriptive statistical analysis of water quality parameters in previous research.

Parameters [mg.L^{-1}]	Current Study		Olaniyan et al. (2015)	
	Mean	Range	Mean	Range
pH	6.33	1.76	5.63	0.38
DO	5.20	5.25	0.59	0.21
Nitrates (NO_3)	2.46	4.81	26.0	56.75
Iron (Fe)	0.33	0.79	0.56	2.34
Zinc (Zn)	0.12	0.13	0.15	0.22
Chromium (Cr)	0	0.04	0.03	0.09
Manganese (Mn)	0.74	1.97	0.27	0.30

facilities are lacking, insufficient solid waste management is a significant environmental issue. Leachates from municipal solid waste dumps are a major contributor to groundwater contamination in urban areas. The pH values of the groundwater samples taken near the dumpsite were generally low, with 84.58 percent falling below the World Health Organization recommended range of 6.5 to 8.5 for drinking water.

According to the results of this study, the concentrations of various water parameters, such as dissolved oxygen (DO), iron (Fe), lead (Pb), manganese (Mn), and magnesium (Mg), were slightly higher than the WHO, NESREA, and NSDWQ permitted levels of 5.02 mg.L^{-1} , 0.33 mg.L^{-1} , 0.04 mg.L^{-1} , 0.74 mg.L^{-1} , and 6.73 mg.L^{-1} .

RECOMMENDATIONS

- i. Based on the result obtained from this study, groundwater quality monitoring should be encouraged as a continuous process.
- ii. Because seasons (dry and rainy) play a major role in the contamination level of water parameters, proper and appropriate treatment should be done according to seasonal variation.
- iii. Even though some heavy metal concentrations in the study area are still within WHO, NESREA, and NSDWQ standard limits, investigations and further monitoring should be conducted regularly to assess the concentrations of heavy metals in groundwater.
- iv. People should be educated about the negative impact of heavy metal concentrations on humans and plants.
- v. The government should provide adequate and functional disposal facilities for appropriate refuse collection and disposal.
- vi. Soil should be used to cover the daily waste collected to reduce air pollution in the study area.
- vii. Proper remediation techniques should be utilized to prevent leachates from landfill and dump sites from further contaminating the groundwater.

ACKNOWLEDGMENTS

We appreciate the management of Afe Babalola University for its special drive towards quality research output.

REFERENCES

- Aboyeji, O.S. and Eigbokhan, S.F., 2016. Evaluations of groundwater contamination by leachates around Olusosun open dumpsite in Lagos metropolis, southwest Nigeria. *Journal of Environmental Management*, 183, pp. 333-341.

- Afolayan, O.S., Ogundele, F.O. and Odewumi, S.G. 2012. The hydrological implication of solid waste disposal on groundwater quality in urbanized areas of Lagos State, Nigeria. *Int. J. Pure Appl. Technol.*, 2(5): 74.
- Al Osman, M., Yang, F., and Massey, I. Y. 2019. Exposure routes and health effects of heavy metals on children. *Biometals*, 32: 563-573.
- Bidhendi, M.E., Karbassi, A.R., Baghvand, A., Saeedi, M. and Pejman, A.H. 2010. The potential of natural bed soil in adsorption of heavy metals in an industrial waste landfill. *Int. J. Sci. Technol.*, 7(3): 545-552.
- Bundschuh, J., Schneider, J., Alam, M. A., Niazi, N. K., Herath, I., Parvez, F. and Mukherjee, A. 2021. Seven potential sources of arsenic pollution in Latin America and their environmental and health impacts. *Science of the Total Environment*, 780: 146274.
- Christensen, T. H., Kjeldsen, P., Albrechtsen, H. J., Heron, G., Bjerg, P.L. and Holm, P. 1994. Attenuation of landfill leachate pollution in aquifers. *Crit. Rev. Environ. Sci. Technol.*, 24: 119- 202.
- Eludoyin, A.O. and Oyeku, O.T. 2010. Heavy metal contamination of groundwater resources in a Nigerian urban settlement. *Afr. J. Environ. Sci. Technol.*, 4(4): 201-214.
- Gleick, P.H. 1996. Water Resources. In Schneider, S.H. (ed), *Encyclopedia of Climate and Weather*, Oxford University Press, New York, pp. 817-823.
- Jagloo, K. 2002. Groundwater Risk Analysis in the Vicinity of a Landfill: A Case Study in Mauritius. M.Sc. Thesis, Royal Institute of Technology, Stockholm.
- Jaji, M.O., Bamgbose, O., Odukoya, O.O. and Arowolo, T.A. 2007. Water quality assessment of Ogun River, southwest Nigeria. *Environ. Monit. Assess.*, 133: 473-482.
- Kennish, L. 1992. Toxicity of heavy metals: Effects of Chromium and Selenium on human health. *J. Indian Pub. Health Edu.*, 2: 36-64.
- Kholoud, M., Al-qinna, M. and Yahya, A. 2009. Spatial distribution and environmental implications of lead and zinc in urban soils and street dust samples in Al-Hashimeyeh Municipality. *Jordan J. Mech. Indust. Eng.*, 3(2): 141-150.
- Kumar, S., Saha, M., Takada, H., Bhattacharya, A., Mishra, P. and Bhattacharya, B. 2006. Water quality management in the lower stretch of the river Ganges, east coast of India: An approach through environmental education. *J. Clean. Prod.*, 15(16): 1559-1567.
- Lake, P. S., Palmer, M. A., Biro, P., Cole, J., Covich, A. P., Dahm, C. and Verhoeven, J. O. S. 2000. Global Change and the Biodiversity of Freshwater Ecosystems: Impacts on Linkages between Above-Sediment and Sediment Biota: All forms of anthropogenic disturbance—changes in land use, biogeochemical processes, or biotic addition or loss—not only damage the biota of freshwater sediments but also disrupt the linkages between above-sediment and sediment-dwelling biota. *BioScience*, 50(12): 1099-1107.
- LAWMA 2010. Statistical analysis of landfill reports by various Agencies. Lagos State Waste Management Authority Report.
- Lee, G.F. and Jones-Lee, A. 1991. Groundwater pollution by municipal landfills: Leachate composition, detection, and water quality significance. *Int. Waste Manag. Landfill Symp.*, 441: 1093-1103.
- Longe, E.O. and Balogun, M.R. 2010. Groundwater quality assessment near a municipal landfill, Lagos, Nigeria. *Res. J. Appl. Sci. Eng. Technol.*, 2(1): 39-44.
- McLeod M., Close M. and Collins R. 2005. Relative Risk Indices for Microbial Transport from Land to Water Bodies. Landcare Research Contract Report LCR0405/165, Ministry of Agriculture and Forestry, Wellington.
- Olaniyan, O. S., Ojoawo, S. O., Olaoye, R. A., Akolade, A. S., Olawoore, B. K. and Oyediran, E. R. 2015. Modeling the environmental impacts of landfilling and incineration waste management scenarios with Gabi6 tool. *International Journal of Research in Engineering and Technology*, 4(7): 259-266.
- Oseke, F. I., Anornu, G. K., Adjei, K. A. and Eduvie, M. O. 2021. Assessment of water quality using GIS techniques and water quality index in reservoirs affected by water diversion. *Water-Energy Nexus*, 4: 25-34.
- Oyebode, O.J. 2013. Solid waste management for sustainable development and public health: A case study of Lagos State in Nigeria. *Univ. J. Pub. Health.*, 12: 65-73.
- Oyebode, O.J., 2019. Design of engineered sanitary landfill for efficient solid waste management in Ado-Ekiti, South-Western Nigeria. *Journal of Multidisciplinary Engineering Science Studies*.
- Oyebode, O.J. 2022. Adoption of environmental engineering strategies for public health and sustainable development. In Ayeni, A.O., Oladokun, O. and Orodu, O.D. (eds), *Advanced Manufacturing in Biological, Petroleum, and Nanotechnology Processing*, Springer, Cham, pp. 197-209.
- Oyebode, O.J. and Otoko A.J. 2022. Medical waste management and design of a low-cost incinerator for reduction of environmental pollution in a multi-system hospital. *Nature Environ. Pollut. Technol. Int. Quart. Sci. J.*, 16: 555
- Oyebode, O.J., Coker, A.O., Sridhar, M.K.C. and Ogarekpe, N.M., 2022. Biomedical Waste Management Practices in Sub-Saharan Africa: Insights of Its Impacts and Strategies for Its Mitigation. In *Advanced Manufacturing in Biological, Petroleum, and Nanotechnology Processing: Application Tools for Design, Operation, Cost Management, and Environmental Remediation* (pp. 256-249). Cham: Springer International Publishing.
- Oyelola, O.T., Babatunde, A.I. and Odunlade, A.K. 2009. Health implication of solid waste disposal: A case study of Olusosun dumpsite, Lagos State. *Int. J. Pure Appl. Sci.*, 3(2):1-8.
- Pujara, Y., Pathak, P., Sharma, A. and Govani, J. 2019. Review on Indian Municipal Solid Waste Management practices for reduction of environmental impacts to achieve sustainable development goals. *Journal of environmental management*, 248: 109238.
- Vasanthi, P., Kaliappan, S. and Srinivasaraghavan, R. 2008. Impact of poor solid waste management on groundwater. *Environmental Monitoring Assessment*, 143(1-3): 227-238.
- Yeh, M.S., Shaun, H.Y., Chang, L.C. and Lin, Y.P. 2008. Establishing index wells for monitoring groundwater quality using multivariate geostatistics. *J. Chin. Instit. Civ. Hydraul. Eng.*, 20(3): 315-330.
- Yogedra, K. and Puttaiah, E.T. 2008. Determination of water quality index and suitability of an urban waterbody in Shimoga town. In Sengupta, M.K. and Dalwani, R. (eds.), *Proceedings of Taal 2007: The World Lake Conference, ILEC, Jaipur, Rajasthan*, pp. 342-346.
- Zacchaeus, O. O., Adeyemi, M. B., Adedeji, A. A., Adegoke, K. A., Anumah, A. O., Taiwo, A. M. and Ganiyu, S. A. 2020. Effects of industrialization on groundwater quality in Shagamu and Ota industrial areas of Ogun state, Nigeria. *Heliyon*, 6(7): e04353.
- Zume, J.T., Tarhule, A. and Christenson, S., 2006. Subsurface imaging of an abandoned solid waste landfill site in Norman, Oklahoma. *Groundwater Monitoring & Remediation*, 26(2), pp.62-69.



A Survey on Deep Learning Based Crop Yield Prediction

S. Archana and P. Senthil Kumar[†]

School of Information Technology and Engineering, Vellore Institute of Technology, Vellore-632014, Tamil Nadu, India

[†]Corresponding author: P. Senthil Kumar; psenthilkumar@vit.ac.in

Nat. Env. & Poll. Tech.
Website: www.neptjournal.com

Received: 08-08-2022

Revised: 03-11-2022

Accepted: 10-11-2022

Key Words:

Yield estimation

Convolutional neural networks

Recurrent neural networks

Long short term memory network

Multilayer perceptron

ABSTRACT

Agriculture is the most important sector and the backbone of a developing country's economy. Accurate crop yield prediction models can provide decision-making tools for farmers to make better decisions. Crop yield prediction has challenged researchers due to dynamic, noisy, non-stationary, non-linear features and complex data. The factors that influence crop yield are changes in temperature and rainfall, plant disease, pests, fertilizer, and soil quality. The paper discusses the factors affecting crop yield, explores the features utilized, and analysis deep learning methodologies and performance metrics utilized in crop yield prediction.

INTRODUCTION

The most important sector in growing nations like India is agriculture. In addition to food, agriculture provides raw materials for many industries, like textiles, jute, sugar, tobacco, and vegetable oil. The importance of agriculture can be understood from the fact that almost 60% of the employment in India is related to agriculture, contributing to 17% of the gross domestic product in India. Crop growth monitoring and yield estimates are essential for a country's economic success. It immediately influences international and national economies and plays a significant role in food security and management. Farmers need an effective crop yield prediction method to determine what crop to grow in a particular field and when to grow that crop. Yield prediction used to be done by considering a farmer's previous experience with a specific field and crop (Nevavuori et al. 2019). When making decisions about agricultural risk management and predicting the future, it is essential to have precise knowledge about crop production history. Many factors influence crop yield, including plant diseases, environmental factors, soil quality, genotype, insect infestations, water quality and availability, and harvest activity planning (Elavarasan & Vincent 2020). Plant diseases are a worldwide hazard to food security and management, but they can be incredibly destructive to small-scale farmers who rely on healthy crops for their income (Chu & Yu 2020). When these factors are not adequately monitored and managed, they can pose a

substantial risk to farmers (Saravi et al. 2019). The main aim of predicting the yield of crops is to increase crop production. Many well-developed models are used to attain this goal (Cao et al. 2021a). Recent developments include crop yield prediction models that use deep learning and machine learning techniques to increase crop productivity. As a part of artificial intelligence, machine learning algorithms, and deep learning algorithms appear to have improved yield prediction and the ability to evaluate large amounts of data.

Machine learning algorithms are a subset of AI programs that give more accurate results in software applications without being specifically designed to do it (Rashid et al. 2021). An ML model is established with a few parameters and learning. Learning is executing a program to optimize the model's parameters using training data or prior experience (Paudel et al. 2021). The model could be predictive to make future predictions, descriptive to learn from data, or both. Due to their efficiency and prediction accuracy, many ML algorithms have been used to handle complex problems such as forecasting, fault detection, resource management, pattern recognition, and robotics in these highly dynamic times. Reinforcement learning, unsupervised ML, supervised ML, and semi-supervised ML are the four main approaches of ML algorithms. ML algorithms can discover knowledge from datasets by identifying patterns and correlations for improving crop yield predictions (Van Klompenburg et al. 2020). Decision support tools are essential for crop yield

prediction to decide which crops to cultivate and what to do with them while growing. Recently, ML approaches such as decision trees, stepwise multiple linear regression, multivariate regression, applied decision trees, and weighted histogram regression have been used in yield prediction (Abbas et al. 2020). ML's significant limitations are difficulty finding optimal features, limited learning from data, and low prediction efficiency of crop yield. So, DL (deep learning) algorithms are used to estimate the yield.

A deep learning algorithm is part of an ML algorithm used to perform complex computations on large volumes of data in sophisticated ways (Muruganatham et al. 2022). A neural network is made up of artificial neurons called nodes. Nodes are arranged as input, hidden, and output layers. Each node receives information in the form of inputs from data. The inputs are multiplied with random weights, adding a bias to the results. Finally, activation functions are used to decide which neuron should fire. DL algorithms can automatically learn hidden patterns from the data and construct more efficient decision rules. In DL, a model learns to perform tasks directly from sound, text, or pictures and can achieve remarkable precision. The DL process consists of two main steps: testing and training. The training phase can be used to label large volumes of data and identify their similar features. As a result, the model extracts the features and contributes to increasing the accuracy of the results. The model uses its gathered knowledge to render unexposed data and labels during testing. DL algorithms produce more accurate predictions than traditional ML algorithms (Elavarasan & Vincent 2021). DL is used in various applications like crop yield prediction, natural language processing, fraud detection, visual recognition, entertainment, news aggregation and fraud news detection, self-driving cars, virtual assistants, and healthcare. Due to many complex factors, crop yield prediction has been challenging for researchers. For example, environmental factors like weather data have nonlinear and non-stationary data, which is difficult to estimate.

The DL algorithms handle the spatiotemporal dependency in a dataset in an effective manner (Tian et al. 2021a). Many studies have used DL methods such as RNN, CNN, LSTM, MLP, and autoencoders to predict crop yield. The DL algorithms can identify the important features of data without the need for handcrafting input data. The vanishing gradient problem may occur in deeper networks, which can be addressed by a Long Short Term Memory network (Liu et al. 2022). Other techniques like stochastic gradient descent, dropout, and batch normalization have been created to increase the performance and accuracy of DL models. DL algorithms can improve performance, but there is a lack of literature on the issues of applying DL techniques to estimate

crop yields. Crop yield prediction depends on the data source, crop type, and DL algorithm.

MATERIALS AND METHODS

There are two steps to the bibliographic analysis in crop yield prediction: (a) to collect papers related to crop yield prediction and (b) to analyze and review the papers in detail. The resources for this study were collected from IEEE Xplore, Science Direct, Springer, MDPI, Wiley, and IOP scientific databases. The following query ["deep learning"] AND ["yield prediction"] OR ["yield estimation"] is used as a search keyword to filter out papers referring to deep learning and the agricultural domain. From this effort, a total of 48 documents were found for analysis and review. The entire process of this review is based on the research questions. The significant role of research questions is to analyze and explore all the dimensions of the studies. The following 5 research questions are listed in this study.

- RQ1: What are the features used for crop yield prediction?
- RQ2: What are the data sources used to predict crop yield?
- RQ3: What kinds of crops are used in yield prediction using deep learning algorithms?
- RQ4: What deep learning approaches have been applied to predict crop yield?
- RQ5: What are approaches used to evaluate the performances of deep learning algorithms?

Factors Affecting Crop Yield Prediction

Crop yield is influenced by multiple factors like soil fertility, water availability, climatic conditions, plant diseases, and pests are the most critical factors influencing crop productivity. When these factors are not monitored and handled correctly, they can cause considerable risk to farmers. Soil fertility is soil's ability to supply nutrients necessary for a crop's optimal growth (Elavarasan & Vincent 2020). A total of 17 nutrients are required for healthy crop growth. Each nutrient is equally necessary to the plant's development but in varying proportions. Due to these variations, the critical elements have been grouped as key sources of micronutrients such as Mo, Cl, Fe, Mn, B, Ni, Cu, and Zn and macronutrients like O, P, C, N, K, S, H, Mg, and Ca (Elavarasan & Vincent 2021). Plant nutrients include root, leaf, fruit development, chlorophyll, protein and hormone production, and photosynthesis. Because soil fertility is a primary source of these nutrients for plants, nutrient content in soil can significantly impact crop yield. Any one of these nutrient deficiencies can reduce crop production by affecting

the growth factor of the crop. The amount of water and crop yield is strongly interrelated.

Water significantly impacts crop productivity and is considered the world’s most important agricultural input. Throughout a plant’s lifespan, it requires large volumes of water to perform processes like photosynthesis, translocation, utilization of mineral nutrients, respiration, cell division, and absorption. Both excessive and insufficient water has a significant impact on yield quantity and quality. When too much water is on a farm, the roots can decay, and the crops will not get sufficient oxygen from the soil. When there is insufficient water on a farm, the plant does not receive the necessary nutrients. As a result, both water scarcity and excess water on fields can equally impact crop growth and development, yield, and quality. Solar radiation and temperature are other essential elements affecting crop growth, development, and yield. All plants have maximum, optimum, and minimum temperature limits (Jeong et al. 2022). High temperatures influence plant growth in a variety of ways. When the temperature rises, the activities of photosynthesis and respiration increase. When temperatures rise above a certain threshold, the two processes become

imbalanced, affecting mineral nutrition, pollen formation, and shoot growth, resulting in a reduced yield. Low temperatures impact crop growth characteristics, including cell division, water transport, survival, photosynthesis, growth, and yield.

When an organism infects a plant, it disturbs its normal growth tendencies. Symptoms might range from minor discoloration of plants to the plant’s death. Common plant diseases include blight, gall, canker, leaf curl, root rot, chlorosis, leaf spot, stunting, wilt, and powdery mildew. Microorganisms that can damage and cause plant diseases include bacteria, fungi, and viruses. Crop yield is also influenced by several soil-borne and above-ground insect pests. Pathogens negatively impact crop yield and soil quality and can harm plants in various ways (Lee et al. 2019). Aside from causing direct damage to crops, pests can also harm plants in other ways, such as by destroying plant roots, which affects the plant’s ability to absorb water and nutrients.

Classification of Features Used in Crop Yield Prediction

The features employed with the DL approaches used in the

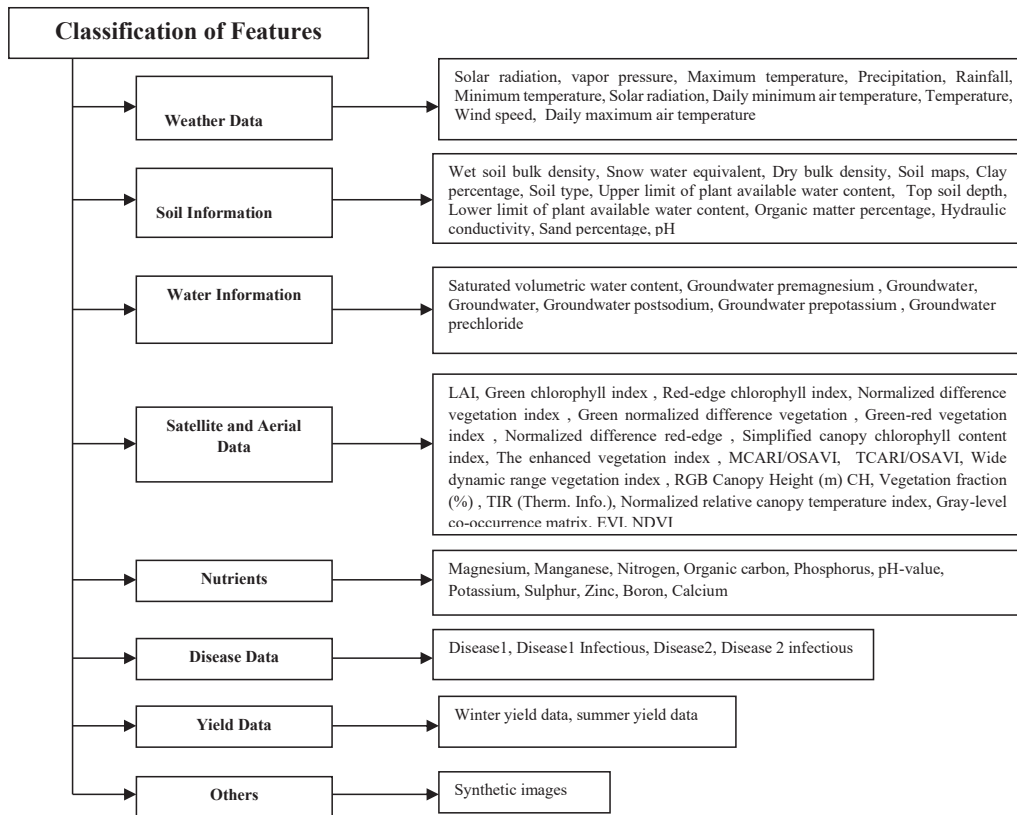


Fig. 1: Features categorization for crop yield prediction.

articles were analyzed and presented to answer research question one (RQ1). The massive amount of data features employed in yield estimation better understanding of the features. The features were grouped into six categories: weather data, soil information, water information, satellite and aerial data, nutrients, crop disease data, yield data, and others. The categorization of features is shown in Fig. 1.

For example, all data features related to satellite and aerial data were grouped, and data features like saturated volumetric water content, groundwater magnesium, groundwater sodium, groundwater potassium, and groundwater chloride were placed in a group with water information. Soil-related features like wet soil bulk density, snow water equivalent, clay percentage, dry bulk density, the lower limit of plant-available water content, an upper limit of plant-available water content, organic matter percentage, hydraulic conductivity, soil maps, pH, soil type,

and topsoil depth were grouped with soil data in one category. Weather-related features like maximum temperature, solar radiation, minimum temperature, vapor pressure, rain, solar radiation, temperature, wind speed, precipitation, daily maximum air temperature, and daily minimum air temperature were grouped with weather data. Disease data, yield data, and synthetic images were placed under one group with the name of others. Features and datasets used in the articles to predict crop yields to answer research question two (RQ2) are displayed in Table 1.

The distribution of the data features of the group in the reviewed articles is shown in Fig. 2. The data features related to satellite and aerial data and weather conditions were commonly used in most articles. Satellite images are less expensive and more accessible. It is easy to scale across a large area (Petersen 2018). The MODIS

Table 1: Summary of features utilized in reviewed articles.

Authors	Data Set	Weather Data	Satellite and Aerial Data	Soil Information	Water Information	Yield Data	Nutrients	Disease Data	Synthetic Image
Alibabaei et al. (2021)	Climate data from the agricultural weather station in Portugal, Fadagosa dataset.	✓				✓			
Bhojani & Bhatt (2020)	wheat yield data from the Directorate of Agriculture, Gandhi nagar, weather datasets from the Agro meteorology Department, Gujarat	✓				✓			
Cao et al. (2021a)	MODIS dataset, TerraClimate dataset	✓	✓	✓					
Cao et al. (2021b)	Agricultural Statistical Yearbook, ChinaCropPhen dataset, CSIF dataset, TerraClimate datasets, Soil particle-size distribution dataset	✓	✓	✓		✓			
Chu & Yu (2020)	Rice yield data, meteorology data in the Guangxi Zhuang Autonomous Region, China	✓				✓			
Elavarasan & Vincent (2020)	Climatic data from the Indian meteorological department using the METdata tool.	✓		✓	✓			✓	
Elavarasan & Vincent (2021)	Meteorological data were collected using the METdata tool from the website of the Indian Meteorological Department.	✓		✓	✓			✓	
Gao et al. (2020)	MODIS Dataset, climate data from the Daily Surface Weather and Climatological Summaries (DAYMET) databases, and soybean and maize yields from the USDA Quick Statistic Database.	✓	✓			✓			
Jeong et al. (2022)	MODIS, COMS MI, RDAPS, IRRI Paddy Map	✓	✓			✓			
Jiang et al. (2020)	MODIS Dataset	✓	✓	✓					
Khaki & Archontoulis (2020)	USDA-NASS, Daymet, Gridded Soil Survey Geographic Database	✓		✓	✓	✓			
Khaki & Wang (2019)	Syngenta Crop Challenge dataset in the US and Canada spanning 8 years of data.	✓		✓		✓			
Khaki et al. (2021a)	yield performance dataset between 2004 and 2018 in US Corn Belt, Satellite data- MODIS(MOD09A1 and MYD11A2) crop-specific land cover data- USDA-NASS cropland data layers	✓	✓	✓		✓			
Lee et al. (2019)	PlantVillage dataset	✓			✓			✓	
Liu et al. (2022)	satellite-based SIF Dataset, MODIS Dataset, TerraClimate Dataset	✓	✓			✓			

Table Cont....

Authors	Data Set	Weather Data	Satellite and Aerial Data	Soil Information	Water Information	Yield Data	Nutrients	Disease Data	Synthetic Image
Ma et al. (2021)	MODIS Dataset, Parameter elevation Regressions on Independent Slopes Model dataset, Soil Survey Geographic Database	✓	✓	✓		✓			
Nevavuori et al. (2019)	Temperature data from the Finnish meteorological department, Sentinel – 2A Data, UAV images.	✓	✓			✓			
Nevavuori et al. (2020)	Meteorological data from the Finnish meteorological institute for the Pori area, UAV images	✓	✓			✓			
Qiao et al. (2021)	Satellite data- MODIS(MOD09A1 and MYD11), Yield data collected from Agricultural statistic yearbook		✓			✓			
Rahneemofar & Sheppard (2017)	Synthetic Image								✓
Sagan et al. (2021)	WorldView-3 and PlanetScope satellite data	✓	✓						
Saravi et al. (2019)	DSSAT weather file	✓			✓	✓			
Schwalbert et al. (2020)	MODIS dataset, soybean yield data from IBGE	✓	✓			✓			
Shahhosseini et al. (2021)	corn yields data from USDA National Agricultural Statistics Service	✓		✓		✓			
Sun et al. (2019)	MODIS SR data MODIS LST data Daymet Weather Data	✓	✓						
Teodoro et al. (2021)	multitemporal–multispectral dataset		✓						
Tian et al. (2020)	MODIS Dataset.		✓			✓			
Tian et al. (2021a)	MODIS products (d60-d152), wheat yield data from the Shaanxi Rural Yearbooks data, meteorological data from the China Meteorological Administration website	✓	✓			✓			
Yang et al. (2019)	BBCH65 Dataset		✓						
Zhou et al. (2021)	At late vegetation, early reproductive and late reproductive growth stages of RGB and multispectral images		✓			✓			

(Moderate Resolution Imaging Spectroradiometer) dataset contains satellite and aerial data used in most reviewed articles for crop yield prediction. Low-resolution MODIS pixels decrease the quantity of data that needs to be processed, making the system less expensive and more efficient.

Crop Used in Yield Prediction Using Deep Learning Approaches

DL techniques are used to estimate crop yield for many different crops. The crops employed in the deep learning approaches used in the articles were analyzed and presented

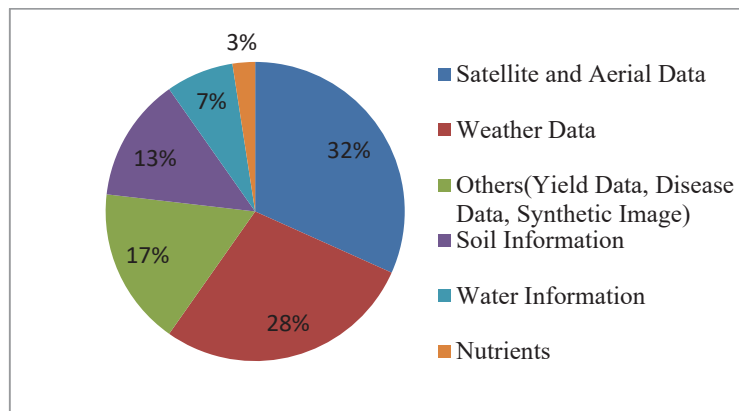


Fig. 2: Distribution of Data features group in the reviewed articles.

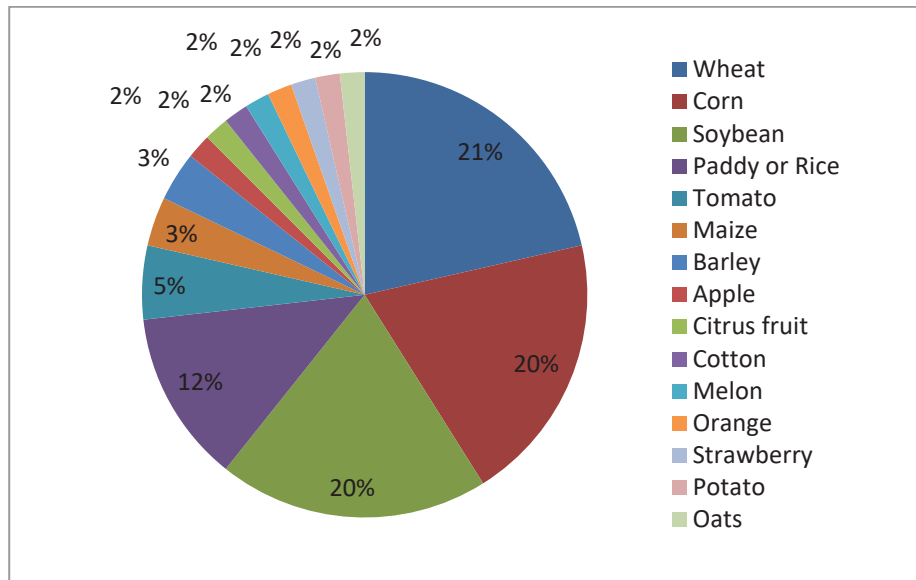


Fig. 3: Distribution of different kinds of crops used in reviewed articles.

to answer research question three (RQ3). Different crops such as Wheat, Corn, Soybean, Paddy or Rice, Tomato, Maize, Barley, Apple, Citrus fruit, Cotton, Melon, Orange, Strawberry, Potato, and Oats were investigated in the reviewed papers. The distribution of different types of crops used in the reviewed articles is displayed in Fig. 3. The yield of crops such as soybean, rice, wheat, and corn was predicted using a DL algorithm. Corn is the most common crop whose yield can be predicted widely using DL techniques.

Deep Learning Algorithms in Crop Yield Prediction

The deep learning algorithm plays a very important role in crop yield prediction. The DL approaches like CNN, RNN, LSTM, and Autoencoder were investigated in the review

paper. The advantages of these algorithms were listed to answer the research question (RQ4).

Convolutional Neural Network (CNN)

A CNN is made up of many artificial neurons stacked on layers. CNN has multiple layers like the pooling layer, convolution layer, and fully connected layer (Fig. 4). The dataset is processed, and features are extracted using the Layers of CNN (Wang et al. 2020). The convolution layer uses many filters to perform the convolution operation and create a feature map. The Rectified Linear Unit layer performs the operations of a feature map on elements. The pooling layer down-samples the rectified feature map derived from the convolution layer to minimize its dimensions and smoothens the resulting two-dimensional arrays into a

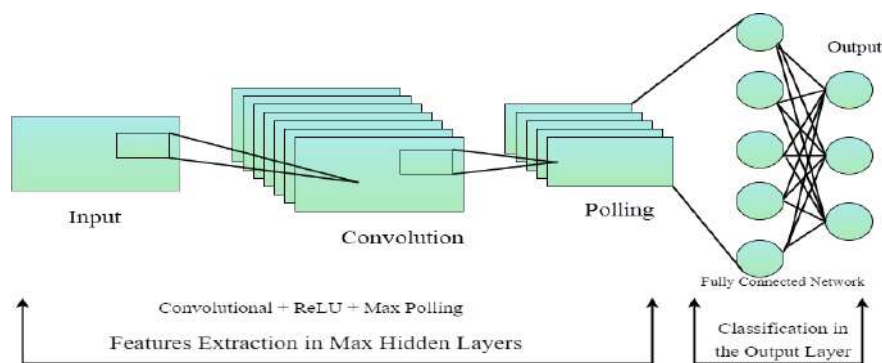


Fig. 4: Architecture of CNN.

continuous, long, single-linear vector. The fully connected layer classifies and identifies the images using the flattened matrix from the pooling layer. The filter counts, size of filters, type of padding, and stride are the design parameters for CNN. A filter is a weighted matrix to perform convolution operations on data. Padding is a technique for preserving the input dimension by adding zeroes. The stride refers to how much the filter is moved. Lenet, Alexnet, Googlenet or Inception, and VGGNet are CNN variants. CNNs are widely used for identifying satellite images, processing medical images, forecasting time series, detecting anomalies, and predicting crop yield. CNN can analyze data in various array formats, including one-dimensional, two-dimensional, and three-dimensional data. The CNN captures and explores time and spatial dependencies in weather and soil data (Wang et al. 2020). It efficiently finds salient features within data compared to traditional feedforward neural networks.

The different variants of CNN are 3D-CNN, Deep CNN, RCNN, VGGNet, and YOLO. In 3D-CNN architecture, the kernels move over three dimensions, height, length, and depth, to produce three-dimensional activation maps. In 3D CNN, convolutional layers perform 3D convolution operations (Nevavuori et al. 2020). Deep CNN is another type of CNN widely used in images and videos for pattern identification. Deep CNNs have evolved from ANN, using a three-dimensional neural pattern inspired by the visual cortex of animals. Deep CNN networks are mainly used in recommendation systems, natural language processing, image classification, and object detection. The R-CNN is a type of CNN architecture created primarily for object detection problems (Chen et al. 2019). To give a better solution to the detection problem, RCNN forms a bounding box over the object present in the image and then recognizes which object is present in the image. R-CNN has several variations, including Fast R-CNN, Mask R-CNN, and Faster R-CNN. An RPN is added to Faster R-CNN to interpret features retrieved from CNN. Researchers from the Visual Graphics Group at Oxford introduced the VGG Network.

The pyramidal structure of this network is defined by huge bottom layers closer to the images and deep top layers. It was created using a 16-layer deep CNN architecture. In the VGG, convolutional layers are followed by pooling layers. The narrowing of the layers is the responsibility of the pooling layers. It achieves its performance by using 3x3 convolutions and training on four GPUs for over two weeks. Excellent architecture for benchmarking on a specific activity and VGG pre-trained networks are frequently used for a range of applications because they are freely available on the internet are the advantages of VGG (Khaki et al. 2021b). The YOLO algorithm is used to detect objects in real-time.

It divides the image into defined bounding boxes and uses a parallel recognition algorithm to determine which object class each box belongs to. After detecting these classes, it automatically merges these boxes to build an optimal bounding box around the objects. The advantages of YOLO are accuracy and speed (Lu et al. 2022).

Nevavuori et al. (2019) created a model using deep CNN to detect crop and weed, evaluate biomass, and predict wheat and barley crops yield using multispectral data. The Convolutional Neural Network algorithm produces outstanding results in object detection and image classification tasks. The results show that CNN models can estimate yields with greater accuracy when using RGB images. Nevavuori et al. (2020) discussed their research to perform intra-field yield prediction using spatial and temporal base 3D-CNN architectures with time-series and multi-temporal data. 3D CNN can be used to handle spatial and temporal data. The prediction accuracy of the 3D CNN model is high when compared to other models. Khaki et al. (2021a) created a VGG-16 model to predict the yield of corn. In addition to image classification, the VGG-16 network performs other vision tasks like object detection and counting and efficiently learns more fine-grained patterns. The model can be applied to quickly count multiple ears of corn to speed up the yield prediction. Lu et al. (2022) created a soybean yield prediction model using the YOLOv3 DL algorithm. YOLOv3 has only half of the parameters used in ResNet101, but the performance is near. The model effectively predicts the yield of the crop. Zhou et al. (2021) presented a paper that examined the possibility of using UAV multispectral imagery to estimate soybean yields from many breeding lines under drought stress using CNN. The model can accurately predict soybean yields under drought stress. Sagan et al. (2021) presented a study to create a DL-based model for field-scale yield prediction.

The model is built using DL approaches like 2-D CNN and 3-D CNN to integrate temporal, spatial, and spectral data in satellite images of the WorldView-3 and 25 PlanetScope datasets. It avoids the vanishing gradient problem by incorporating identity skip connections. Imagery deep learning-based algorithm modeling outperforms the other model. Tedesco-Oliveira et al. (2020) made a cotton yield prediction model using the CNN DL algorithm. CNN is adept in image classification and object detection. According to the testing results, the model can be used in real-time on low-cost devices. Yang et al. (2019) created an efficient CNN model for extracting key features of rice yield from low-altitude remotely sensed images. The outcomes demonstrate that the CNN model trained with RGB and multispectral datasets outperforms VI-based regression models. Khaki et

al. (2021) developed a model using recurrent 3D CNN with a Transfer learning technique to predict the yield of corn and soybean. 3D-CNN captures the temporal and spatial effects in remote sensing data. Before harvest, the model can accurately estimate the yield of corn and soybean. Yang et al. (2021) designed a corn yield prediction model using the 2D-CNN DL algorithm. 2D-CNN is more suitable for classification and feature extraction. According to the findings, an integrated CNN model is better than 1D-CNN and 2D-CNN.

Mirhaji et al. (2021) developed a model using YOLOv4 to predict oranges yield. The “Bag of Freebies” and “Bag of Specials” can improve the YOLO v4 model’s efficiency and accuracy. The YOLO model is a simple and efficient method for predicting orange fruits yield. Danilevicz et al. (2021) presented a multimodal DL model using ResNet18 to estimate Maize yield. The self-attention mechanism used in ResNet aids in identifying the region’s most essential to the forecasting. The model can use as a decision-support tool. Apolo et al. (2020b) created a model using RegionCNN to estimate the yield of apples. The model will help to maximize production by optimizing orchard management.

Recurrent Neural Network (RNN)

RNN is derived from the feedforward network where the current step’s input depends on the previous step’s output (Chu & Yu 2020) (Fig. 5). A hidden state of an RNN preserves some information about an input sequence. So RNNs can handle any length of the input. The computation considers historical data, and the model size does not grow in proportion to the input size. RNNs are used in handwriting recognition, image captioning, natural-language processing, computer translation, crop yield prediction, and time-series analysis. A type of recurrent neural network called an IndRNN, widely used in crop yield prediction, has been developed to address gradient decay over layers problems, where neurons present in the same layer are independent and remain interconnected between the layers. It can be trained effectively using non-saturated activation functions like ReLu.

Chu and Yu (2020) developed a novel IndRNN-based model for accurate rice yield prediction. The IndRNN learns temporal features effectively in meteorology data. The model can predict rice yield in the summer and winter seasons.

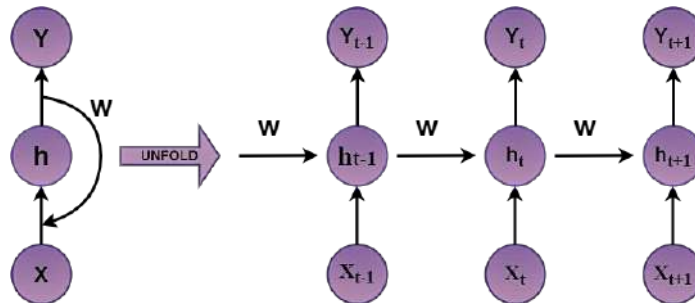


Fig. 5: Architecture of RNN.

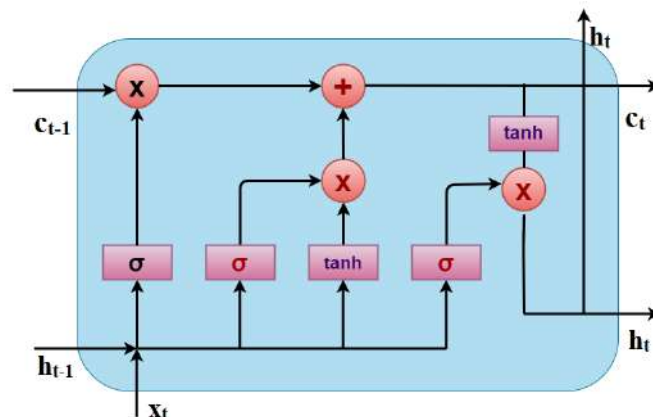


Fig. 6: Architecture of LSTM.

Long Short-Term Memory Network (LSTM)

LSTM is an RNN variant that can handle long-term dependencies and store and recall information from the past (Tian et al. 2021b). The LSTM was developed to address the drawbacks that occur during the training of traditional RNNs, such as the vanishing gradient problem and the exploding gradient problem. LSTM is effective in time-series prediction because it remembers past inputs. An LSTM unit comprises a cell (Fig. 6). An input gate, an output gate, and a forget gate are the three gates in the cell. All the gates control the data flow in the cell, and the cell stores values for an indefinite period. LSTMs are widely used in pharmaceutical growth, speech recognition, music composition, and time-series predictions. LSTM can identify the phonological characteristics and help to learn the temporal features present in the data. It has shown good ability in transfer learning and generates high accuracy yield estimation results (Wang et al. 2020).

Elavarasan and Vincent (2020) built a framework based on a deep recurrent Q-learning network using 38 features to predict the yield of crops. The Q-learning algorithm strengthens yield forecasting efficiency with the best rewards compared to other models. Tian et al. (2021a) designed a model for yield estimation in the Guanzhong Plain using an LSTM model by combining meteorological data and VTCI and LAI indices. The LSTM can detect and capture complex and nonlinear relationships in the data over long intervals. The outcomes show that the model is a robust, promising method for predicting yields. Yuanyuan Liu et al. (2022) created an LSTM-based model to forecast wheat yield across the Indo-Gangetic plains. LSTM can solve the problem in high-dimensional data and is effectively used in time-series

data. With limited data, the approach can accurately predict the yield of wheat. Schwalbert et al. (2020). presented a novel LSTM-based model to estimate soybean yield in southern Brazil with four steps: data access, data wrangling, modeling, and yield prediction. The LSTM model produces better results when compared to multivariate OLS and random forest models. Shook et al. (2020) designed a framework using stacked LSTM with a temporal attention mechanism to protect crop production against climatic changes such as irregular rainfall and temperature variations. The stacked LSTM model with a temporal attention mechanism overcomes the backflow problem. Soybean yield prediction with LSTM and Temporal Attention model is reliable and accurate. Cao et al. (2021b) built a model to predict rice yield by incorporating SIF and EVI, climate variables, and soil parameters. Three models were developed using Least Absolute Shrinkage and Selection Operator regression, Random Forest, and Long Short-Term Memory Network model. The LSTM model produces accurate results when compared to Machine learning models.

Tian et al. (2021) designed a model using LSTM with an attention mechanism to forecast wheat yield with remotely sensed biophysical indices. Time-series data can be processed efficiently by LSTM, and the attention mechanism is employed to extract essential information from the input sequence data. The ALSTM (attention-based LSTM) model can give reliable crop yield estimation. Cho et al. (2021) used an attention-based LSTM network to estimate tomato yields using environmental variables. LSTM can handle long-term dependencies in data. The outcomes demonstrate that the method predicts the value more accurately. Alibabaei et al. (2021) created a bidirectional LSTM-based model to analyze time-series data in agricultural datasets to predict the yield

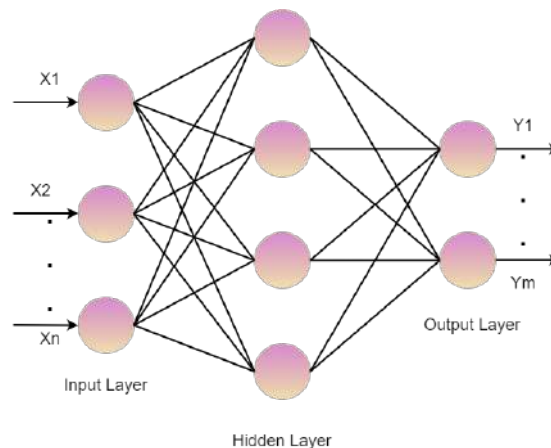


Fig. 7: Architecture of MLP.

of tomatoes and potatoes. The model accurately identifies nonlinear relationships in the data. The results demonstrate the effectiveness of the LSTM model for yield prediction. Jiang et al. (2020) created an LSTM model by integrating meteorology, remote sensing data, and crop phenology to predict the yield of corn. To avoid over-fitting, regularization techniques are used in LSTM. The model outperformed under extreme weather.

Multilayer Perceptron (MLP)

An MLP is a part of feed-forward neural networks with numerous perceptron layers and activation functions (Saravi et al. 2019) (Fig. 7). It computes the input using the weights shared by the input and hidden layers. ReLUs, tanks, and sigmoids are the activation functions that MLP uses to determine which nodes to fire (Bhojani & Bhatt 2020). It uses a training dataset to train the model to identify the correlation and learn the dependencies between the independent and target variables. It may be used to create applications for speech recognition, machine translation, image recognition, and crop yield prediction.

Saravi et al. (2019) created an agrotechnology Transfer agricultural system using the MLP deep learning algorithm, which acts as a Decision Support System to predict crop yield. Principle component analysis is added to the dataset to reduce input which speeds up the training and computing of the model. The outcomes demonstrate the MLP model is effective in predicting crop yields. Bhojani and Bhatt (2020) discussed developing a Multilayer Perceptron based model with a new activation function called DharaSig for crop yield estimation in their research. The MLP algorithm with the DharaSig activation function outperforms the original MLP algorithm for yield forecasting with a lower error rate.

Hybrid Deep Learning Approaches

Cao et al. (2021a) created a hybrid DNN+1D CNN+LSTM model for crop yield prediction. Four models were built using Convolutional Neural Networks, Random Forests, and Long Short-Term Memory networks. 1D-CNNs are used in applications like fault detection in high-power engines, structural damage detection systems, and electrocardiogram beat classification. The model can efficiently predict crop yield at field and county levels. Jeong et al. (2022) developed a model by combining LSTM and 1D-CNN to predict the yield of a rice crop. LSTM added a batch normalization layer after activation layers to speed convergence and prevent vanishing gradient problems. The approach successfully predicts the yield of rice in inaccessible locations. Lee et al. (2019) created a platform that estimates the yield of a crop by integrating crop disease data, climate change data and form status information using CNN and ANN algorithms.

CNN effectively perform object detection and classification task. The model is more effective and accurate at predicting farm yields. Wang et al. (2020) built a CNN-LSTM DL model to estimate wheat yield in China's major planting area. LSTM is adept at processing time-series data in climatic data. The model has much potential for use in other varieties of crops and agricultural landscapes worldwide. Chen et al. (2019) designed a system that automatically detects strawberry flowers to predict yield using the Faster R-CNN DL algorithm. Faster R-CNN effectively handles the degradation problem using a deep residual learning framework. The model gives accurate counts of strawberry flowers and forecasts future yields. Sun et al. (2019) formed a model to predict the yield of soybeans at the country level using deep CNN and LSTM.

CNN explores spatial features, and LSTM reveals phenological properties of the MODIS dataset. The outcomes reveal the CNN-LSTM model is efficient in soybean yield prediction. Khaki and Archontoulis (2020) presented a paper to accurately predict the yield of corn and soybean using CNN and RNN with a back propagation method. RNN, with the backpropagation method, supports time-dependent data, and CNN captures the temporal and spatial dependency in the dataset. The dataset contained four different types of dataset: weather, yield performance, management-related information, and soil. The CNN-RNN model gives better prediction results when compared to other models. Qiao et al. (2021) designed a novel spatial-spectral-temporal neural network using recurrent 3D-CNN to predict the yield of wheat and corn. 3D-CNN exploits spectral information from 3D data. The model outperforms better prediction performance when compared to other models. Apolo et al. (2020a) designed a model to identify and estimate the yield and size of citrus fruits using Faster R-CNN + LSTM. The Faster-R-CNN model can utilize Inception, Atrous, and ResNet architectures to improve accuracy and efficiency. The results show that the model can estimate the yield of all types of fruit. Shahhosseini et al. (2021) created a model by combining CNN and DNN DL algorithms to predict the yield of corn. CNN captures the temporal and spatial dependencies in data. The model was designed to predict corn yield and assist agronomic decision-makers.

RESULTS AND DISCUSSION

Performance Evaluation Metrics

Different evaluation metrics utilized to measure the performance of DL in crop yield prediction are given in Table 2. A total of 18 different evaluation metrics such as RMSE, R2, MAE, MAPE, MSE, F1 Score, Recall, MedAE, mAP, Accuracy, Average Precision, Kappa coefficient,

Table 2: Performance metrics used in crop yield prediction.

Performance Metrics	Formula	Description
Root Mean Square Error (RMSE)	$RMSE = \sqrt{\frac{1}{n} \sum_{j=1}^n (y_j - \hat{y}_j)^2}$	y_j - Actual value \hat{y}_j - Forecast value n - no. of observation
Mean Square Error (MSE)	$MSE = \frac{1}{n} \sum_{j=1}^n (y_j - \hat{y}_j)^2$	
Mean Absolute Error (MAE)	$MAE = \frac{1}{n} \sum_{j=1}^n y_j - \hat{y}_j $	
Mean Absolute Percentage Error (MAPE)	$MAPE = \frac{1}{n} \sum_{j=1}^n \left \frac{y_j - \hat{y}_j}{y_j} \right $	
Coefficient of determination (R^2)	$R^2 = 1 - \frac{RSS}{TSS}$	RSS - Sum of square of residuals TSS - Total sum of square
Precision	$P = \frac{TP}{TP + FP}$	TP - True positive FP - False positive
Recall	$R = \frac{TP}{TP + FN}$	TP - True positive FN - False negative
F1 Score	$F1 = 2 * \frac{precision * recall}{precision + recall}$	

Table 3: Overview of different deep learning algorithms, crop utilized, and evaluation metrics used in crop yield prediction.

Authors	Deep Learning Algorithms	Crops	Performance Evaluation Metrics
Alibabaei et al. (2021)	Bidirectional LSTM	Tomato, Potato	MSE, R^2
Apolo et al. (2020b)	R-CNN	Apple	R^2 , MAE, RMSE
Apolo et al. (2020)	Faster R-CNN +LSTM	Citrus fruit	Precision, Recall, F1 Score
Bhojani and Bhatt (2020)	MLP	Wheat	MAE, RMSE, MAPE, MSE, RAE, RRSE
Bi and Hu (2021)	Genetic algorithm-assisted DNN	Crop	RMSE
Cao et al. (2021a)	DNN+1D CNN+LSTM	Wheat	RMSE, R^2
Cao et al. (2021b)	LSTM	Rice	RMSE, R^2
Chen et al. (2019)	Faster R-CNN	Strawberry	Mean Average Precision
Cho et al. (2021)	Attention-based LSTM +ARMA	Tomato	MSE, RMSE
Chu and Yu (2020)	IndRNN	Rice	MAE, RMSE
Danilevicz et al. (2021)	Spectral deep neural network (ResNet18)	Maize	RMSE, relative RMSE, R^2 score
Elavarasan and Vincent (2020)	Deep RNN +Q Learning	Paddy	MAE, MSE, RMSE, R^2 , MedAE, MAPE
Elavarasan and Vincent (2021)	DBN+FNN	Paddy	MSLE, RMSE, MSE, MAE, R^2 , MedAE, MSLE
Gao et al. (2020)	DNN	Corn and Soybean	R^2 , MAE, MAPE
Jeong et al. (2022).	LSTM+1D-CNN	Rice	R^2 , RMSE, NSE
Jiang et al. (2020)	LSTM	Corn	RMSE, R^2
Kalantar et al. (2020)	RetinaNet deep CNN, Transfer learning	Melon	Average precision score, F1 score, MAPE.
Khaki and Archontoulis (2020)	CNN-RNN	Corn	RMSE

Authors	Deep Learning Algorithms	Crops	Performance Evaluation Metrics
Khaki and Wang (2019)	DNN	Maize	RMSE
Khaki et al. (2021a)	CNN with Transfer Learning	Corn and Soybean	MAE
Khaki et al. (2021b)	VGG-16	Corn	MAE, RMSE
Liu et al. (2022)	LSTM	Wheat	R ² , RMSE
Lu et al. (2022)	YOLOv3+RCNN+SSD+FPN	Soybean	Accuracy, Precision, Recall, F1 value, MAP
Ma et al. (2021)	Bayesian Neural Network	Corn	R ² , RMSE, MAPE
Maimaitijiang et al. (2020).	DNN	Soybean	R ² , RMSE
Mirhaji et al. (2021)	YOLO-V4	Orange	MAP, Precision, F1-score, Recall
Moghimi et al. (2020)	MLP	Wheat	RMSE, R ²
Nevavuori et al. (2019)	Deep CNN	Wheat and barley	MAE, MAPE
Nevavuori et al. (2020)	3D CNN	Wheat, Barley, Oats	MAE, MAPE
Qiao et al. (2021)	Recurrent 3D-CNN	Wheat and Corn	RMSE, R ² , MAPE
Sagan et al. (2021)	ResNet-18	Soybean, Corn	R ² , RMSE
Saravi et al. (2019)	MLP	Maize	RMSE
Schwalbert et al. (2020)	LSTM	Soybean	MAE, MSE, RMSE
Shahhosseini et al. (2021)	CNN-DNN	Corn	RMSE, RMSE
Shook et al. (2020)	LSTM and Temporal Attention	Soybean	RMSE
Sun et al. (2019)	Deep CNN+LSTM	Soybean	RMSE, R ²
Teodoro et al. (2021)	DL Model	Soybean	MAE, RMSE, Pearson's correlation coefficient
Tian et al. (2020)	BPNN with PSO algorithm	Wheat	R ²
Tian et al. (2021a)	LSTM with an attention mechanism	Wheat	R ² , MAPE, RMSE, NRMSE
Tian et al. (2021b).	LSTM	Wheat	R ² , RMSE
Wang et al. (2020).	LSTM+CNN	Wheat	R ² , RMSE
Yang et al. (2019)	Deep CNN	Rice	RMSE, R ² , MAPE
Yang et al. (2021)	2D- CNN	Corn	Kappa coefficient, Accuracy
Zhou et al. (2021)	CNN	Soybean	RMSE

MSLE, RAE, RRSE, NSE, Precision, and Relative RMSE were investigated in the reviewed papers. The DL algorithms and different evaluation approaches used in the articles were analyzed and presented in Table 3 to answer the research question (RQ5)

CONCLUSION

The paper analyzes the study of a deep learning algorithm based on crop yield prediction. The survey categorizes existing strategies based on the crop used, the methodologies employed, the datasets used, and the performance metrics used. CNN, RNN, LSTM, and MLP are some of the DL algorithms used to predict crop yield. The CNN algorithm produces outstanding results in object detection and image classification tasks. The LSTM can detect and capture complex and nonlinear relationships in the data over long intervals. Two main DL algorithms for accurately estimating

crop yields are CNN and LSTM. These techniques can successfully estimate and forecast various crops' yields. Transfer learning and Data augmentation were used to solve the large dataset training in DL models. The RMSE was the most frequently used evaluation metric in the reviewed articles, followed by MAPE, R², MSE, and MAE. In the future, the factors like plant disease, temperature and rainfall, pests, fertilizer, and soil quality can be considered for improving the performance of crop yield prediction using DL approaches.

REFERENCES

- Abbas, F., Afzaal, H., Farooque, A.A. and Tang, S. 2020. Crop yield prediction through proximal sensing and machine learning algorithms. *Agronomy*, 10(7): 1046.
- Alibabaei, K., Gaspar, P.D. and Lima, T.M. 2021. Crop yield estimation using deep learning based on climate big data and irrigation scheduling. *Energies*, 14(11): 3004.

- Apolo, O.E.A., Guanter, J.M., Cegarra, G.E., Raja, P. and Ruiz, M.P. 2020. Deep learning techniques for estimation of the yield and size of citrus fruits using a UAV. *Europ. J. Agron.*, 115(4): 183-194.
- Apolo, O.E.A., Ruiz, M.P., Guanter, J.M. and Valente, J. 2020a. A cloud-based environment for generating yield estimation maps from apple orchards using UAV imagery and a deep learning technique. *Front. Plant Sci.*, 1086.
- Bhojani, S.H. and Bhatt, N. 2020. Wheat crop yield prediction using new activation functions in neural network. *Neural Comp. Appl.*, 5: 1-11.
- Bi, L. and Hu, G. 2021. A genetic algorithm-assisted deep learning approach for crop yield prediction. *Soft Comp.*, 25(16): 10617-10628.
- Cao, J., Zhang, Z., Luo, Y., Zhang, L., Zhang, J., Li, Z. and Tao, F. 2021a. Wheat yield predictions at a county and field scale with deep learning, machine learning, and the google earth engine. *European J. Agron.*, 123: 126204.
- Cao, J., Zhang, Z., Tao, F., Zhang, L., Luo, Y., Zhang, J. and Xie, J. 2021b. Integrating multi-source data for rice yield prediction across china using machine learning and deep learning approaches. *Agric. Forest Meteorol.*, 297: 108275.
- Chen, Y., Lee, W.S., Gan, H., Peres, N., Fraisse, C., Zhang, Y. and He, Y. 2019. Strawberry yield prediction based on a deep neural network using high-resolution aerial orthoimages. *Remote Sens.*, 11(13): 1584.
- Cho, W., Kim, S., Na, M. and Na, I. 2021. Forecasting of tomato yields using attention-based LSTM network and ARMA model. *Electronics*, 10(13): 1576.
- Chu, Z. and Yu, J. 2020. An end-to-end model for rice yield prediction using deep learning fusion. *Comp. Electr. Agric.*, 174, 105471.
- Danilevicz, M.F., Bayer, P.E., Boussaid, F., Bennamoun, M. and Edwards, D. 2021. Maize yield prediction at an early developmental stage using multispectral images and genotype data for preliminary hybrid selection. *Remote Sens.*, 13(19): 3976.
- Elavarasan, D. and Vincent, P.D. 2020. Crop yield prediction using deep reinforcement learning model for sustainable agrarian applications. *IEEE Access*, 8: 86886-86901.
- Elavarasan, D. and Vincent, P.D. 2021. Fuzzy deep learning-based crop yield prediction model for sustainable agronomical frameworks. *Neural Comp. Appl.*, 33(20): 13205-13224.
- Gao, Y., Wang, S., Guan, K., Wolanin, A., You, L., Ju, W. and Zhang, Y. 2020. The ability of sun-induced chlorophyll fluorescence from OCO-2 and MODIS-EVI to monitor spatial variations of soybean and maize yields in the Midwestern USA. *Remote Sens.*, 12(7): 1111.
- Jeong, S., Ko, J. and Yeom, J.M. 2022. Predicting rice yield at pixel scale through synthetic use of crop and deep learning models with satellite data in South and North Korea. *Sci. Tot. Environ.*, 802: 149726.
- Jiang, H., Hu, H., Zhong, R., Xu, J., Xu, J., Huang, J. and Lin, T. 2020. A deep learning approach to conflating heterogeneous geospatial data for corn yield estimation: A case study of the US Corn Belt at the county level. *Glob. Change Biol.*, 26(3): 1754-1766.
- Kalantar, A., Edan, Y., Gur, A. and Klapp, I. 2020. A deep learning system for single and overall weight estimation of melons using unmanned aerial vehicle images. *Comp. Electr. Agric.*, 178, 105748.
- Khaki, S. & Archontoulis, S.V. 2020. A CNN-RNN framework for crop yield prediction. *Front. Plant Sci.*, 10: 1750.
- Khaki, S. and Wang, L. 2019. Crop yield prediction using deep neural networks. *Front. Plant Sci.*, 10: 621.
- Khaki, S., Pham, H. and Wang, L. 2021a. Simultaneous corn and soybean yield prediction from remote sensing data using deep transfer learning. *Sci. Rep.*, 11(1): 1-14.
- Khaki, S., Pham, H., Han, Y., Kuhl, A., Kent, W. and Wang, L. 2021b. Deepcorn: A semi-supervised deep learning method for high-throughput image-based corn kernel counting and yield estimation. *Knowl. Based Syst.*, 218: 106874.
- Lee, S., Jeong, Y., Son, S. and Lee, B. 2019. A self-predictable crop yield platform (SCYP) based on crop diseases using deep learning. *Sustainability*, 11(13): 3637.
- Liu, Y., Wang, S., Wang, X., Chen, B., Chen, J., Wang, J. and Zhu, K. 2022. Exploring the superiority of solar-induced chlorophyll fluorescence data in predicting wheat yield using machine learning and deep learning methods. *Comp. Electr. Agric.*, 192: 106612.
- Lu, W., Du, R., Niu, P., Xing, G., Luo, H., Deng, Y. and Shu, L. 2022. Soybean yield preharvest prediction based on bean pods and leaves image recognition using deep learning neural network combined with GRNN. *Front. Plant Sci.*, 12: 791256.
- Ma, Y., Zhang, Z., Kang, Y. and Özdoğan, M. 2021. Corn yield prediction and uncertainty analysis based on remotely sensed variables using a Bayesian neural network approach. *Remote Sens. Environ.*, 259: 112408.
- Maimaitijiang, M., Sagan, V., Sidike, P., Hartling, S., Esposito, F. and Fritschi, F.B. 2020. Soybean yield prediction from UAV using multimodal data fusion and deep learning. *Remote Sens. Environ.*, 237: 111599.
- Mirhaji, H., Soleymani, M., Asakereh, A. and Mehdizadeh, S.A. 2021. Fruit detection and load estimation of an orange orchard using the YOLO models through simple approaches in different imaging and illumination conditions. *Comp. Electr. Agric.*, 191: 106533.
- Moghimi, A., Yang, C. and Anderson, J.A. 2020. Aerial hyperspectral imagery and deep neural networks for high-throughput yield phenotyping in wheat. *Comp. Electr. Agric.*, 172: 105299.
- Muruganantham, P., Wibowo, S., Grandhi, S., Samrat, N.H. and Islam, N. 2022. A systematic literature review on crop yield prediction with deep learning and remote sensing. *Remote Sens.*, 14(9): 1990.
- Nevavuori, P., Narra, N. and Lipping, T. 2019. Crop yield prediction with deep convolutional neural networks. *Comp. Electr. Agric.*, 163: 104859.
- Nevavuori, P., Narra, N., Linna, P. and Lipping, T. 2020. Crop yield prediction using multitemporal UAV data and spatio-temporal deep learning models. *Remote Sens.*, 12(23): 4000.
- Paudel, D., Boogaard, H., de Wit, A., Janssen, S., Osinga, S., Pylaniadis, C. and Athanasiadis, I.N. 2021. Machine learning for large-scale crop yield forecasting. *Agric. Syst.*, 187: 103016.
- Petersen, L.K. 2018. Real-time prediction of crop yields from MODIS relative vegetation health: A continent-wide analysis of Africa. *Remote Sens.*, 10(11): 1726.
- Qiao, M., He, X., Cheng, X., Li, P., Luo, H., Zhang, L. and Tian, Z. 2021. Crop yield prediction from multi-spectral, multi-temporal remotely sensed imagery using recurrent 3D convolutional neural networks. *Int. J. Appl. Earth Observ. Geoinform.*, 102: 102436.
- Rahnemoonfar, M. and Sheppard, C. 2017. Deep count: fruit counting based on deep simulated learning. *Sensors*, 17(4): 905.
- Rashid, M., Bari, B.S., Yusup, Y., Kamaruddin, M.A. and Khan, N. 2021. A comprehensive review of crop yield prediction using machine learning approaches with special emphasis on palm oil yield prediction. *IEEE Access*, 9: 63406-63439.
- Sagan, V., Maimaitijiang, M., Bhadra, S., Maimaitiyiming, M., Brown, D.R., Sidike, P. and Fritschi, F.B. 2021. Field-scale crop yield prediction using multi-temporal WorldView-3 and PlanetScope satellite data and deep learning. *ISPRS J. Photogramm. Remote Sens.*, 174: 265-281.
- Saravi, B., Nejdhashemi, A.P. and Tang, B. 2019. Quantitative model of irrigation effect on maize yield by the deep neural network. *Neural Comp. Appl.*, 7: 1-14.
- Schwalbert, R.A., Amado, T., Corassa, G., Pott, L.P., Prasad, P.V. and Ciampitti, I.A. 2020. Satellite-based soybean yield forecast: Integrating machine learning and weather data for improving crop yield prediction in southern Brazil. *Agric. Forest Meteorol.*, 284: 107886.
- Shahhosseini, M., Hu, G., Khaki, S. and Archontoulis, S.V. 2021. Corn yield prediction with ensemble CNN-DNN. *Frontiers in Plant Science*, 12.

- Shook, J., Gangopadhyay, T., Wu, L., Ganapathysubramanian, B., Sarkar, S. and Singh, A.K. 2020. Crop yield prediction integrating genotype and weather variables using deep learning. *ArXiv* 6: 13847.
- Sun, J., Di, L., Sun, Z., Shen, Y. and Lai, Z. 2019. County-level soybean yield prediction using deep CNN-LSTM model. *Sensors*, 19(20): 4363.
- Tedesco-Oliveira, D., da Silva, R.P., Maldonado, W. and Zerbato, C. 2020. Convolutional neural networks in predicting cotton yield from images of commercial fields. *Comp. Electr. Agric.*, 171: 105307.
- Teodoro, P.E., Teodoro, L.P.R., Baio, F.H.R., da Silva Junior, C.A., dos Santos, R.G., Ramos, A.P.M. and Shiratsuchi, L.S. 2021. Predicting days to maturity, plant height, and grain yield in soybean: a machine and deep learning approach using multispectral data. *Remote Sens.*, 13(22): 4632.
- Tian, H., Wang, P., Tansey, K., Han, D., Zhang, J., Zhang, S. and Li, H. 2021a. A deep learning framework under attention mechanism for wheat yield estimation using remotely sensed indices in the Guanzhong Plain, PR China. *Int. J. Appl. Earth Observ. Geoinform.*, 102: 102375.
- Tian, H., Wang, P., Tansey, K., Zhang, J., Zhang, S. and Li, H. 2021b. An LSTM neural network for improving wheat yield estimates by integrating remote sensing data and meteorological data in the Guanzhong Plain, PR China. *Agric. Forest Meteorol.*, 310: 108629.
- Tian, H., Wang, P., Tansey, K., Zhang, S., Zhang, J. and Li, H. 2020. An IPSO-BP neural network for estimating wheat yield using two remotely sensed variables in the Guanzhong Plain, PR China. *Comp. Electr. Agric.*, 169: 105180.
- Van Klompenburg, T., Kassahun, A. and Catal, C. 2020. Crop yield prediction using machine learning: A systematic literature review. *Comp. Electr. Agric.*, 177: 105709.
- Wang, X., Huang, J., Feng, Q. and Yin, D. 2020. Winter wheat yield prediction at the county level and uncertainty analysis in main Wheat-Producing regions of China with deep learning approaches. *Remote Sens.*, 12(11): 1744.
- Wolanin, A., Mateo-García, G., Camps-Valls, G., Gómez-Chova, L., Meroni, M., Duveiller, G. and Guanter, L. 2020. Estimating and understanding crop yields with explainable deep learning in the Indian Wheat Belt. *Environ. Res. Lett.*, 15(2): 024019.
- Yang, Q., Shi, L., Han, J., Zha, Y. and Zhu, P. 2019. Deep convolutional neural networks for rice grain yield estimation at the ripening stage using UAV-based remotely sensed images. *Field Crops Res.*, 235: 142-153.
- Yang, W., Nigon, T., Hao, Z., Paiao, G.D., Fernández, F.G., Mulla, D. and Yang, C. 2021. Estimation of corn yield based on hyperspectral imagery and convolutional neural network. *Comp. Electr. Agric.*, 184: 106092.
- Zhou, J., Zhou, J., Ye, H., Ali, M.L., Chen, P. and Nguyen, H.T. 2021. Yield estimation of soybean breeding lines under drought stress using unmanned aerial vehicle-based imagery and convolutional neural network. *Biosyst. Eng.*, 204: 90-103.



Biomimetic Synthesis of Nanoparticles: State-of-the-Art

Tabassum-Abbasi*, S. A. Abbasi†**, R. Rajalakshmi**, Pratiksha Patnaik** and Tasneem Abbasi**

*School of Engineering, University of Petroleum and Energy Studies, Dehradun-248 007, India

**Centre for Pollution Control and Environmental Engineering, Pondicherry University, Chinakalpet, Puducherry-605 014, India

†Corresponding author: S. A. Abbasi; abbasi.cpee@gmail.com

Nat. Env. & Poll. Tech.
Website: www.neptjournal.com

Received: 14-07-2022

Revised: 02-11-2022

Accepted: 03-11-2022

Key Words:

Biomimetics
Nanoparticles
Plant extracts
Energy generation
Microbial fuel cells

ABSTRACT

A state-of-the-art review of biomimetic nanoparticle synthesis is presented. The technique's origin has been traced to the studies, started over 150 years ago, on the hyperaccumulation of certain metals by different species of plants. How the initial intracellular method of nanoparticle synthesis evolved into the now widely used extracellular route has been described. The review then covers the gist of all the studies reported on the biomimetic synthesis of nanoparticles of different metals using extracts of different botanical species (plants). The synthesis mechanism is discussed, and the factors influencing the nanoparticles' extent, shapes, and sizes are identified.

INTRODUCTION

Barring some exceptions – such as the reactions in the atmosphere due to lightning – most chemical reactions occur in nature under very benign conditions of ambient temperatures and pressures (Huang et al. 2015, Bao et al. 2021). The natural synthesis routes are also almost always free from harmful emissions. Additionally, they are exceedingly efficient in terms of energy and material inputs (Jabbari et al. 2014, Ngo 2015, Miyauchi & Shimomura 2023).

These characteristics of biosynthesis in nature extend from the formation of simple products like carbon dioxide to very complicated and large biomolecules (Prescott et al. 2018, Kim 2020, Primrose 2020).

The science of biomimetics has emerged in recent decades in appreciation of the 'simplicity in complexity' of nature, especially in the astonishing manner in which organisms have been designed by nature to achieve multiple tasks in the most space-efficient, energy-efficient, and material-efficient manner - with little or no accompanying pollution (Gebeshuber 2022). What little pollution that does get generated-such as animal excreta and dead zoomass-is immediately worked upon by a wide variety of scavengers and is totally recycled. Biomimetics aims to mimic nature by synthesizing chemicals, designing systems, and problem-solving in the 'easy' and 'natural' way it occurs in nature.

BIOMIMETIC NANOPARTICLE SYNTHESIS

Biomimetic nanoparticle (BMNP) synthesis is one of the many branches of biomimetics. It mimics how living plants and other organisms convert ions of different elements, especially metals, into nanoparticles (Fig. 1). The focus of this paper is on plant-based synthesis because it is a simpler, cleaner, faster, and more versatile route than the ones based on other organisms (Ganaie et al. 2014, 2015, 2016, 2021). 'Plant' refers to vascular botanical species which form the largest component of the plant kingdom.

Plant-based BMNP synthesis constitutes one of the 'bottom-up' approaches to nanoparticle (NP) synthesis wherein one begins with elements or molecules and induces their aggregation into nanoparticles (Anuradha et al. 2009, Khandel et al. 2018). It contrasts with the 'top down' approaches in which one begins with bulks of elements or molecules and gradually disaggregates them to the nanoscale (Fig. 2). But if we put aside the biomimetic option, all other routes to NP synthesis, be it 'top down' or 'bottom-up,' are besieged with serious disadvantages.

The top-down approaches usually need expensive instruments and consume a lot of power, which leads to high operating costs and a proportionately large ecological footprint. On the other hand, the bottom-up approach often involves using toxic chemicals and generating problematic

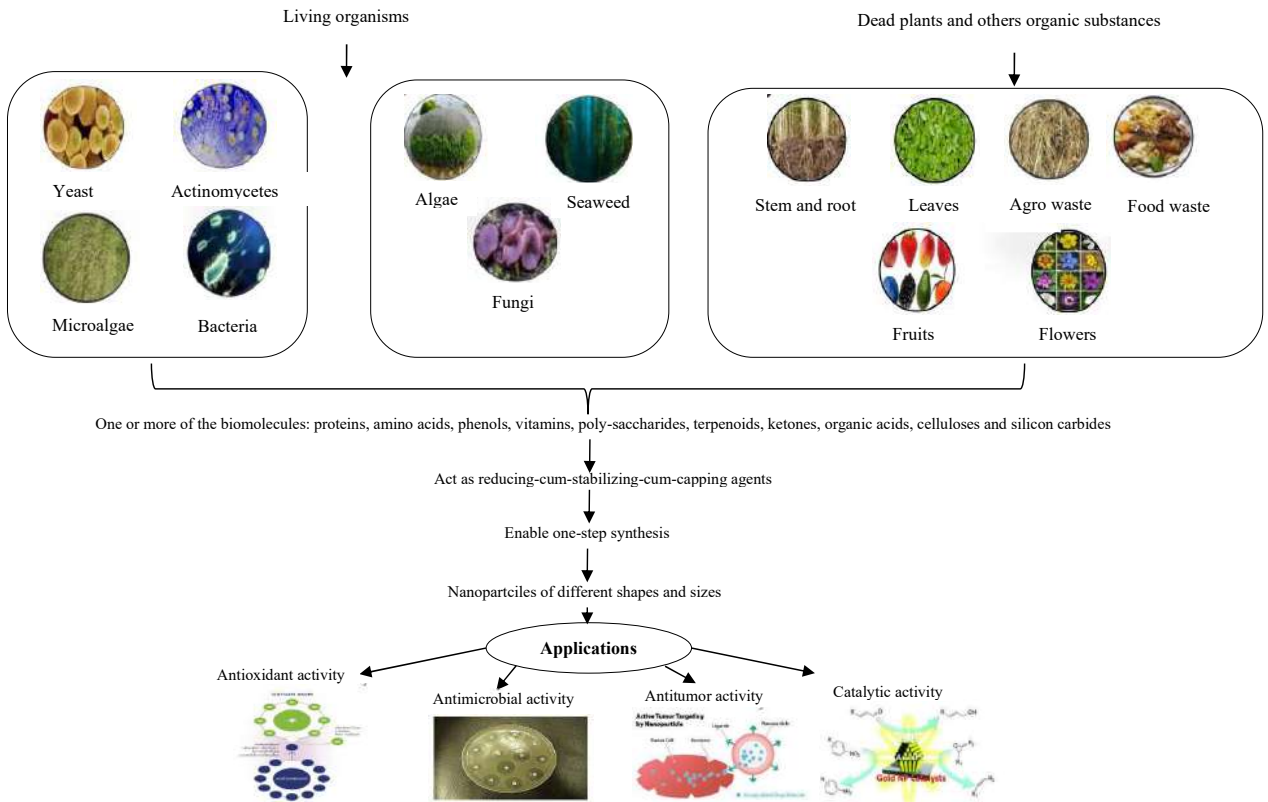


Fig. 1: An overview of the biomimetic synthesis of nanoparticles and their applications.

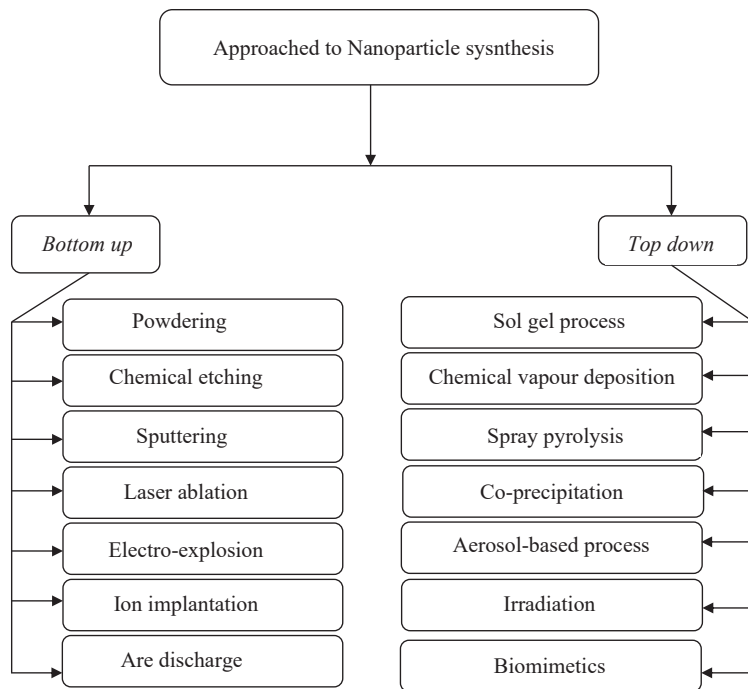


Fig. 2: The bottom-up and top-down routes of nanoparticle synthesis.

emissions. Moreover, NPs thus generated are likely to carry toxic moieties. There is also a significant requirement for energy which may not be as great as necessitated in the top-down methods, yet is nevertheless substantial (Abbasi et al. 2015, Shah et al. 2015, Siddiqi et al. 2018).

The biological entities explored for BMNP synthesis are broadly of two types. One comprises unicellular organisms such as viruses, bacteria, yeast, etc., and the other comprises multicellular organisms such as algae, fungi, plants, and their parts (Fig. 2). Of all these, the synthesis based on vascular plants is found to be quicker and simpler than the synthesis employing unicellular and the other multicellular organisms (Ganaie et al. 2018a, 2018b). This paper surveys and analyzes past work on BMNP synthesis using plants.

A BRIEF HISTORY OF THE EVENTS LEADING TO THE EXTRACELLULAR NP SYNTHESIS ROUTE

The Discovery That Plants Can Hyperaccumulate Metals

A hyperaccumulator plant can grow in soil or water containing abnormally high concentrations of certain chemicals, absorbing those chemicals through its roots and storing them in its tissues to an abnormal extent without suffering from phytotoxicity (Reeves et al. 2017). Studies related to the bioaccumulation of nickel, copper, zinc, cobalt, lead, and manganese by various species of plants have been reported since the mid-nineteenth century (Abbasi 1988, 1989, Abbasi & Sharma 1981). Besides providing a means to bioremediate soils by extracting metal ions from them, hyperaccumulator plants also serve as a means for prospecting □ as indicators of the contents of the soils on which they grow (Abbasi 1982, Hussain et al. 2022).

As noted by Reeves and Baker (Reeves 2000), the maiden *in vitro* study on hyperaccumulation of metal was reported by Braun in 1855 (Barun 1855). Later, Gautheret (1935) observed that silver ions were reduced to metal and were bioaccumulated in the tissues of the hydroponically cultured carrot. But the products could not be characterized because the equipment required to do so did not exist at that time. Now, with the advent of analytical instruments such as Fourier transform infrared (FTIR) spectroscopy, X-ray absorption spectroscopy (XAS), proton-induced X-ray emission (PIXE), energy dispersive X-ray spectroscopy (EDX), and transmission electron microscopy (TEM), it has become possible to study the formation and distribution of metal NPs within plant cells. The instruments can also determine the size of the metal NPs accumulated inside the cytosol of the plant cells. It is now well-established that hyperaccumulating plants have an enhanced rate of metal

uptake, a faster rest-to-shoot translation, and a greater ability to sequester the accumulated metals. It is also believed that hyperaccumulator species so behave to defend themselves against grazers and other natural enemies. And that the heavy metals support and enhance the effect of organic defensive compounds (Sytar et al. 2021, Skuza et al. 2022).

Anderson et al. (1998) were the first to record that gold ions were hyper-accumulated in Indian mustard (*Brassica juncea*) when the latter was grown in containers filled with different gold compounds mixed with ammonium thiocyanate. They characterized the products using XAS and stated that ammonium thiocyanate had acted as a chelating agent and had induced the gold ions to accumulate in the leaf tissues.

The Discovery that NP Formation Drives Hyperaccumulation of Metals by Plants

Gardea-Torresdey et al. (2002, 2003) were among the first to report that gold and silver metals are stored inside the living plant cells of alfalfa (*Medicago sativa*) as NPs. They characterized the products using XAS and TEM and showed that the plant's roots were key in absorbing the metal ions. They observed that the absorbed metal ions accumulate inside the plant tissues. They also noted that the accumulated metal ions undergo aggregation at the nanoscale, which causes the formation of the NPs.

Attempts at Using Intracellular Synthesis to Obtain NPs

After the early work described above, several authors have shown that the storage of metals inside the cytoplasm of plant cells occurs as NPs. Yates et al. (2005) reported the formation of silver, cobalt, titanium, gold, zinc, and chromium NPs inside the living plants of the morning glory (*Ipomoea lacunosa*) and alfalfa (*Medicago sativa*).

Haverkamp et al. (2007) reported that AuNPs, AgNPs, and CuNPs were formed in the tissues of the *Brassica juncea* plants grown in an Au-Ag-Cu enriched soil culture over a period of 9 weeks. EDX analysis of the products confirmed the presence of all three elements, and the results indicated that it is possible to produce alloys of NPs.

Over the years, numerous reports have appeared on the formation of NPs in different plant species encompassing herbs, shrubs, and trees (Sytar et al. 2020). These include food plants, medicinals, and ornamentals of a very wide variety, representing diverse regions and genotypes (Armendariz et al. 2004, Rai et al. 2004, Gardea-Torresdey et al. 2005, Lopez et al. 2005, Beattie & Haverkamp 2011, Sharma et al. 2007, Huang et al. 2007, Manceau et al. 2008,

Łukaszewicz et al. 2009, Mishra et al. 2010, Cyganiuk et al. 2010, Cai et al. 2010, Anuradha et al. 2015, Roy et al. 2012, Tamuly et al. 2014, Marchiol et al. 2014). Many aquatic, amphibious, and terrestrial weeds have also been explored (Rai et al. 2004, Manceau et al. 2008, Kumar et al. 2015, Ganaie et al. 2017, 2021).

Difficulties Associated with the Use of Intracellular Synthesis for Manufacturing NPs.

The intracellular route has several major constraints. It requires steps like cell lysis/cracking through ultra-sonication to extract formed NPs from the plant biomass (Gürsoy et al. 2021). This makes the process highly cumbersome and can also cause changes in the shapes of the NPs. Moreover, enzymes or detergents may have to be used to separate NPs from unwanted cellulosic materials.

Special Attributes of Extracellular BMNP Synthesis Using Plants

In the first decade of this century, attempts were made to synthesize NPs extracellularly by employing plant extracts to get around the complications associated with retrieving the intracellularly synthesized NPs. It was also expected that extracellular synthesis of NPs may be more suitable for the large-scale manufacture of the NPs. As reviewed by these authors and others (Abbasi et al. 2012, Singh et al. 2016, Pareek et al. 2017, Gondwal & Joshi 2018, Khandel & Shahi 2018, Wei et al. 2018, Ahmed et al. 2021), there is a rapidly

rising interest in the field of plant-based NP synthesis through extracellular route, due to the non-toxic, non-hazardous, and eco-friendly nature of this route. Further analysis by these authors has revealed that India is presently leading the world in the number of papers published in this field (Fig. 3), and the Indian scientists happen to have pioneered the plant-based extracellular NP synthesis.

In contrast to other organisms used for extracellular NP synthesis—notably algae, fungi, and bacteria—plants have a special advantage. The phytochemicals available in most plant extracts reduce metal ions much faster than other organisms (Jha et al. 2009). Phytochemicals also serve as stabilizing agents, facilitating the synthesis even further. Additionally, harvesting and using plants is much easier than other organisms requiring much greater care and effort to maintain and use (Malik et al. 2014).

SUMMARY OF PRIOR ART ON THE EXTRACELLULAR BMNPS SYNTHESIS USING PLANTS

Based on a very extensive prior art search using *Web of Science*, *Science Direct*, *Google Scholar*, and *Research Gate*, we have compiled most of the reports, which are close to 1500, that have appeared so far on this subject. We have prepared the gist of their contents, which are discussed in this and subsequent sections.

It is seen that 97.7% of all the reports are based on the use of aqueous extracts of the plant parts in synthesizing the

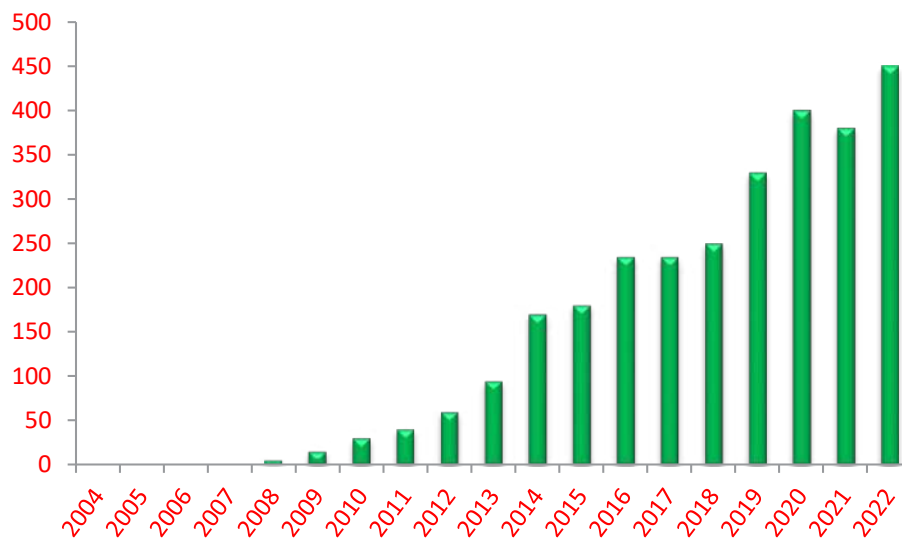


Fig. 3: Number of papers published on the bioinspired synthesis of nanoparticles using various plant parts.

NPs. In each case, those aqueous extracts were prepared by boiling a known quantity of a plant part — mostly leaves and flowers, in a few cases fruits — in water for a few minutes. Then the extract was mixed with one or more metal ion solutions, with or without some pH adjustment and/or heating/stirring, to generate mono-metallic or multi-metallic NPs.

The remaining 2.3% of the reports use organic solvents, principally methanol and ethanol, instead of water to extract biomolecules from the plants.

Most (85.5%) of the studies are on synthesizing AgNPs and AuNPs. Of the rest, 7.5%, 3.2 %, and 2.4% of the studies have been on PdNPs, CuNPs, and PtNPs, respectively. The remaining 1.4% of the reports are on other metals and metal oxides. The focus on AgNPs and AuNPs stems from both possessing low cytotoxicity, high surface area-to-volume ratio, and stability. These attributes make them particularly preferred for immunotherapy and chemotherapy (Wei et al. 2019). AuNPs have also been found to be excellent contrasting agents in X-ray and CT scans. Additionally, they have gained prominence as radio sensitizers for early cancer detection and as antitumor agents (Sindhu et al. 2011, Daraee et al. 2016, Panahi et al. 2017). AgNPs have similar virtues and much less expensive parent metal than AuNPs (Mousavi et al. 2018).

First Attempts at Using Extracellular Synthesis to Obtain NPs

The first breakthrough in achieving an extracellular synthesis of NPs was achieved by Sastry and co-workers (Shankar et al. 2003). They employed a broth of geranium (*Pelargonium graveolens*) to synthesize gold NPs extracellularly. After this pioneering work, Sastry and co-workers demonstrated using the extracts of neem, lemon grass, gooseberry, and other species for synthesizing gold and silver NPs (Shankar et al. 2004a, 2004b, 2004c). Their work has been followed by a fast-increasing number of studies being carried out worldwide (Fig. 3).

The gist of the prior art on different categories of plants is given in the following sections. Of all the categories of plants, the ones with recognized medical properties—medicinal plants—have been the most widely studied. Food plants and ornamental plants, respectively, follow them.

BMNP Synthesis Using Medicinal Plants

More than 300 medicinal plants have been employed for generating NPs of silver, gold, palladium, platinum, cobalt, copper, and zinc oxide (Priya et al. 2022, Shahid et al. 2022, Singh et al. 2022, Johnson et al. 2022).

Of all the medicinal plants, neem (*Azadirachta indica*), tulsi (*Ocimum tenuiflorum*), and aloe vera (*Aloe vera*) are

the most extensively explored. Most (90%) of the authors have used leaf extracts of medicinal plants for synthesizing the NPs. The rest have used seeds, fruits/pods, or roots. TEM and SEM studies have revealed that the formed NPs were mostly spherical. Triangular, hexagonal, and rod-like shapes are also encountered but to a much lesser extent.

With the aid of FTIR, it has been seen that, in general, the leaf extracts of medicinal plants contain flavonoids, terpenoids, proteins, alkaloids, and polyols, which could have been involved in the formation of the NPs. The AuNPs and AgNPs formed using medicinal plants have been mostly explored for their antimicrobial, catalytic, and free-radical scavenging properties, besides their use in the early diagnosis and treatment of cancer, as detailed in Section 4.

Gist of the Reports on NP Synthesis Using Food Plants

Close to 275 food plants have been used for synthesizing NPs of Au, Ag, Pt, Pd, Cu, Co, and ZnO (Eze et al. 2022, Veeramani et al. 2022, Indira et al. 2022). Grapes, pomegranate, turmeric, onion, and garlic have been the most often explored. Interestingly 80% of the researchers have used the edible parts of these plants, while a much lesser number have used the leaves.

As was seen in medicinal plants, TEM and SEM studies reveal that the formed NPs are mostly spherical, and only a few plants generated cubical, triangular, rod-like, and hexagonal shapes. Polysaccharides, flavonoids, proteins, and terpenoids have been identified as the biomolecules most often associated with forming the NPs by food plants. The resulting NPs have been mainly explored as agents in antimicrobial, catalytic, and antioxidant applications.

BMNP Synthesis Using Ornamental Plants

More than 150 ornamental plants have been utilized to synthesize various NPs. Henna and rose have been the most explored. In 85% of the studies, plant leaves have been used to prepare extracts, while stem or bark have been used in the rest of the reports.

As revealed by TEM, the NPs synthesized using these plants have had triangular, polygonal, rod-like, spherical, and cubical shapes. As revealed by FTIR, the biomolecules involved have been terpenoids, flavonoids, alkaloids, proteins, and polyols. As in the case of NPs synthesized with other plants, the NPs of ornamentals have been mostly explored for their antimicrobial, catalytic, and antioxidant scavenging properties.

BMNP Synthesis Using Weeds

These authors have been among the first to utilize terrestrial,

aquatic, and amphibious weeds for nanoparticle synthesis (Ganaie et al. 2014, 2015, 2016, 2017, 2021, Anuradha et al. 2015, Abbasi et al. 2012). The following considerations prompted the choice of weeds:

- i) Unlike medicinal, feed, food, or ornamental plants, the weeds have no competing use. Hence their utilization for NP synthesis does not infringe upon other demands.
- ii) For this reason, coupled with abundant availability that too free of cost, the use of weeds helps bring down the cost of production of the NPs.
- iii) As weeds harm biodiversity and stress the environment in multiple other ways, their large-scale utilization can potentially reduce the harm they cause.
- iv) The biomass from weed-infested tracts of land and water runs into billions of tonnes. Hence it can support very large-scale NP manufacture.

Several common weeds have been explored to manufacture gold, silver, palladium, platinum, copper oxide, and zinc oxide NPs. All other weeds studied so far have been terrestrial except for five aquatic weeds and 1 amphibious weed. These authors (Ganaie et al. 2014, 2015, Abbasi et al. 2015) have utilized whole plants for synthesizing gold, silver, and bimetallic Au-Ag NPs, while Saikia et al. (2018) have used only the stem. All other authors have used leaves for the synthesis.

Concerning the shape of the NPs, associated biomolecules, and application of the NPs, the findings with the weeds have been broadly similar to those with other plants.

MECHANISM OF NANOPARTICLE FORMATION WITH PLANT EXTRACT

The Accepted Mechanism

The initial work on the mechanism of plant-based NP synthesis was with reference to intracellular NP formation. Gardea-Torresdey et al. (1999), while studying the accumulation of gold in the desert willow *Chilopsis linearis*, hypothesized that the ionic form of the metal is evidently getting taken up by the membrane of the plant root. It then gets translocated in the plant, eventually converted to a zerovalent form, and aggregated into nano-sized particles. A decade later, Haverkamp and Marshall (2009) advanced this hypothesis, proposing a five-step mechanism:-

- i) The elements are in their ionic forms when absorbed by plants via their roots.
- ii) The absorbed ions are transported across the root membranes.
- iii) The ions are reduced to zerovalent forms by the biomolecules available in the cytosol of the plant cells.

- iv) There is an aggregation of zerovalent atoms inside the plant cells at nanosize through biomolecules in the plant cells.
- v) The NPs thus formed diffuse into other compartments of the plant cells, and their deposition/storage occurs therein.

The mechanism suggested that biomolecules are occurring in the plant cells' cytoplasm, which plays a key role in reducing and agglomerating metal ions to form NPs inside the living plant cells. When the first successful attempt to extracellularly synthesize the NPs was reported by Shanker et al. (2003), they also suggested that a mechanism similar to this is operative. According to them, the gold ions were reduced to gold atoms by reducing agents such as terpenoids in the geranium extract. The essential steps of the mechanism are depicted in Fig. 4.

About two decades have passed since this mechanism of NP formation by extracts of plants was proposed. It now stands almost universally accepted because no other plausible suggestion has emerged. (Singh et al. 2018, El Shafey, 2020)

How Different Biomolecules Act?

In the intervening years, several authors have identified the biomolecules that reduce metal ions into their atoms and/or facilitate the stabilization of the aggregating atoms at a nano size. For example, Shahverdi et al. (2007) reported that *Cinnamom zeylanicum* extract contains eugenol (a terpenoid), which causes the reduction of silver and gold ions. Through FTIR analysis, the authors found that the presence of -OH groups in eugenol causes tautomeric transformation, forming a compound that probably acts as a reducing agent.

Li et al. (2007), explaining Ag NP formation from chili extract, suggested that in the first step, the silver ions attach to the proteins contained in the plant extract through electrostatic attraction. This reduces the silver ions to zerovalent silver, followed by Ag NP formation. According to Tan et al. (2010a), if metal ions are sequestered into the peptides present in a plant extract, it may cause an inhibition in the reduction step.

Rajani et al. (2010) opined that a repulsive force must be available to stabilize the NPs in a reaction medium to overcome the attractive Van der Waals force, which causes coagulation. They proposed that carboxylate groups present in proteins may act as surfactants. Those groups may attach to the active sites of NPs, providing a repulsive force to prevent aggregation beyond nano-size and then stabilizing the formed NPs.

Lukman et al.(2011) gave the NP formation a 3-phase interpretation (Fig. 4): induction phase – where metal ions

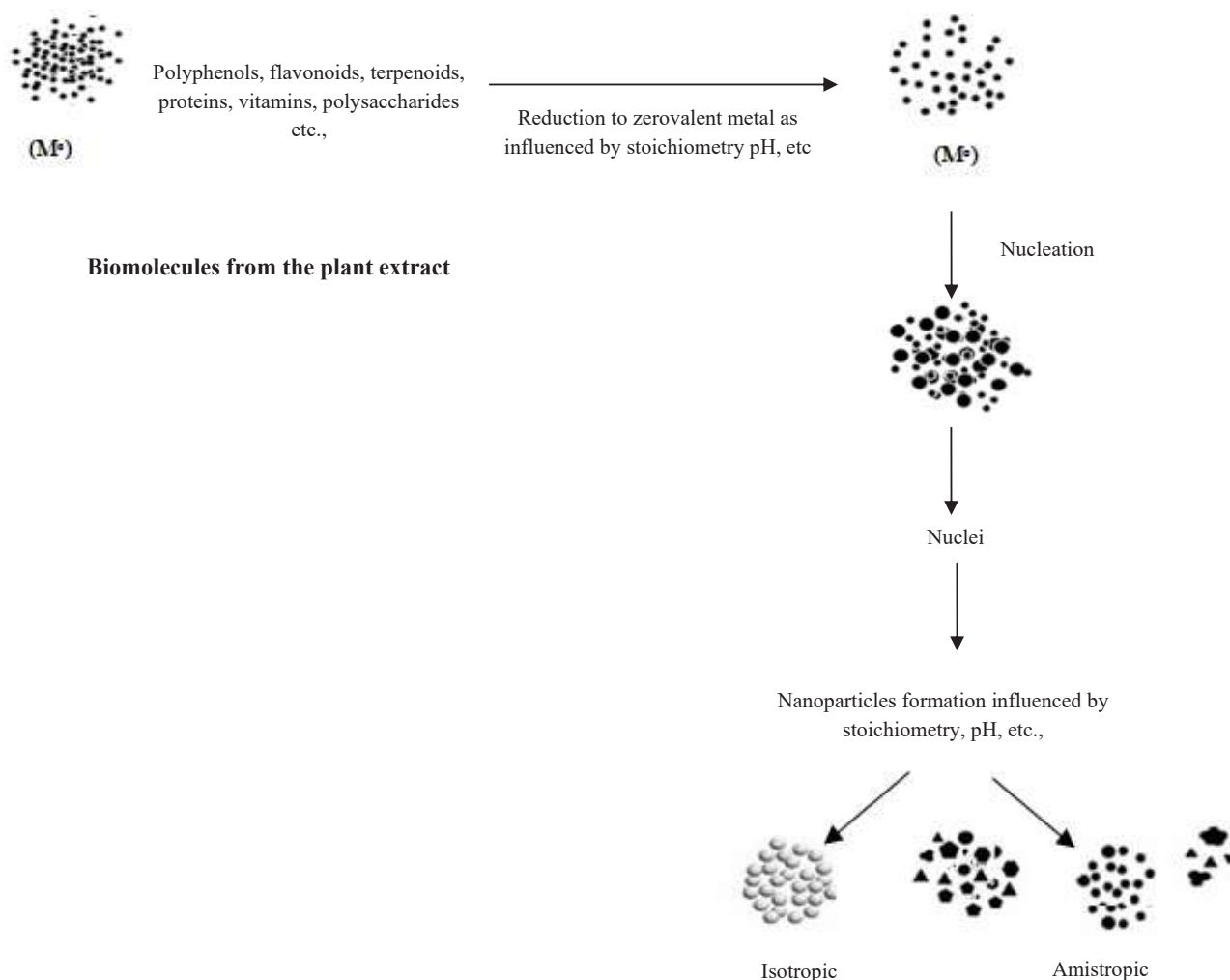


Fig. 4: The generally accepted mechanism of plant-based biomimetic NP synthesis.

interact with the bioagents and undergo reduction, which then leads to nucleation, growth phase—where the nuclei aggregates with each other forming nanostructures, and termination phase—where the rate of reduction controls the formation of NPs. They also suggested that the reduction rate may determine whether the nuclei are homogenous or heterogeneous.

Dumur et al. (2011) state that the stabilization of NPs may occur via two basic modes. The interaction of metal particles with the biomolecules may be causing repulsive electrostatic forces, providing the particle surfaces with a charged coating. Non-ionic surfactants may generate steric repulsions between the particles and biomolecules, forming a coating around the surface of the NPs. Either mode may be preventing aggregation of the metal particles beyond nano size.

It is generally agreed that the NPs continue to grow until the stabilizing agents occupy the active sites of NPs. For this

reason, the capping/stabilizing agents appear to play a crucial role in regulating the growth of the NPs.

Postulating the mechanism of AgNP formation, Ahmad et al. (2011) assumed that the secondary metabolites in the plant extracts cause a reduction of the Ag ion in the reaction medium. The energy released during glycolysis could transform the monovalent Ag ion to elemental Ag. The ascorbates in the plant extract may also be reacting with oxygen species present in the reaction medium, reducing them to form ascorbate radicals and free electrons. The free electrons may interact with Ag^+ ions to reduce them to Ag^0 NPs.

Gan & Li (2012) have attributed the formation of NPs of multiple shapes to Ostwald ripening. They suggest that during Ostwald ripening, the smaller particles may migrate and feed the adjacent particles, aggregating to larger particles of isotropic and anisotropic shapes.

Others, including Mittal et al. (2013) and Castillo-Lopez & Pal (2014), have given a mechanism of NP formation that essentially confirms the deductions made by Gardea-Torresdey et al. (1999) and Haverkamp & Marshall (2009). To wit, secondary metabolites or some other biomolecules found in the plant extracts cause the reduction of the metal ions. They also play the role of stabilizing agents. As for the shapes and sizes of the NPs, they are controlled by pH, temperature, metal-extract stoichiometry, and other conditions such as reaction duration, illumination, and stirring. These aspects are addressed below.

FACTORS WHICH INFLUENCE THE FORMATION AND THE MORPHOLOGY OF THE NPs

In all approaches to NP synthesis-chemical, physical, or biological-the main thrust is towards tailoring the process to obtain NPs of premeditated sizes and shapes. The same concern dominates the route of NP synthesis using plant extracts. Accordingly, several authors have studied the influence of numerous factors likely to regulate the synthesis. These most extensively explored parameters are temperature, pH, metal-extract stoichiometry, stirring, illumination, and reaction time.

Nature and Concentration of Phytochemicals

The composition and relative concentration of different phytochemicals can strongly influence the kinetics of NP formation and the shapes, sizes, and concentrations of the resulting NPs (Li et al. 2011, Mukunthan & Balaji 2012). The phytochemicals influencing NP formation in plants include flavones, terpenoids, sugars, ketones, aldehydes, carboxylic acids, and amides (Prathna et al. 2010).

The functional groups contained by flavonoids have a particularly marked ability to reduce metal ions. During NP synthesis, reactive hydrogen atoms are released due to tautomeric transformations in flavonoids converting enol-forms into the keto-form. The reduction of metal ions achieves this process into metal nanoparticles. For example, enol- to keto-transformation is the key factor in synthesizing biogenic silver nanoparticles from sweet basil (*Ocimum basilicum*) (Ahmad et al. 2010, 2021).

Glucose and fructose can also be responsible for forming metallic nanoparticles. Whereas glucose drives the formation of polydisperse nanoparticles, fructose-mediated gold, and silver nanoparticles are predominantly monodisperse (Panigrahi et al. 2004).

Nascent nanoparticles have repeatedly been found to be associated with proteins (Zayed et al. 2012). Amino acids cysteine, arginine, lysine, and methionine are proficient in

binding with silver ions (Gruen, 1975) and gold ions (Tan et al. 2010b).

In summary, the types and the relative concentrations of phytochemicals present in a plant extract play a key role in the first and the third steps of nanoparticle synthesis, which occur in these three phases : (1) the activation phase (bio-reduction of metal ions/salts and nucleation process of the reduced metal ions), mediated by phytochemicals, (2) the growth phase (combination of smaller particles into larger ones) via a process acknowledged as Ostwald ripening, and (3) the termination phase which finalizes the shapes and the sizes of the NPs and in which phytochemicals cause stabilization of the formed NPs (Si & Mandal, 2007, Shah et al. 2015).

Effect of pH

In their study on intracellular NP formation, Gardea-Torresdey et al. (1999) observed that the pH had exerted a significant influence on the formation of the NPs.

A decade later, Sathishkumar et al. (2009) became the first to report that pH plays a major role in extracellular NP formation. They observed this while synthesizing AgNPs extracellularly with the aid of bark extracts of Cinnamon (*Cinnamomum zeylanicum*). They reported that the pH of the reaction medium had a decisive effect on the reduction of the metal ions.

Dubey et al. (2010) have reported that when the reaction medium's pH increases above 7 units, the zeta potential value of the formed NPs tends to increase. On the other hand, a decrease in the pH below 7 causes the zeta potential value of the formed NPs to decrease. Philip (2010) reported that an increase in the pH of the reaction medium induces an increase in the reduction rate of metal ions, thereby facilitating NP formation. Veerasamy et al. (2011) have shown that acidic conditions in the reaction mixture suppress the formation of NPs even as alkaline pH facilitates it. Edison & Sethuraman (2012) also found that NP formation occurred more rapidly at neutral or alkaline than at acidic pH. They have linked it to the ionization of the phenolic groups occurring in the plant extract, which is suppressed at acidic pH due to the common ion effect. According to these authors, slower NP formation at acidic pH may also be due to the electrostatic repulsion of the anions occurring in the acidic pH range.

The sizes and size ranges are also strongly influenced by pH (Gontijo et al. 2020). Yang et al. (2019) found that the SPR peaks of the AgNPs became sharper at elevated pH values and attributed it to the decrease in the size of the NPs. They observed that the particles' shape was irregular at acidic pH, and the particles tended to aggregate. The decrease in

the size of the NPs was attributed to the deprotonation of the functional groups carrying negative charges. The functional groups seemed to bind with the formed NPs, enhancing their stability as the electrostatic repulsion prevented aggregation. Dauthal & Mukhopadhyay (2013) also believed that the shift in the SPR peak of the formed NPs is due to their surface charges at different pH levels.

The studies of Tripathi et al. (2013), Sadeghi & Gholamhoseinpour (2015), and others (Ganaie et al. 2017, 2018b, Yazdani et al. 2021) have led to similar conclusions.

In summary, the pH of the reaction medium exerts a major influence in controlling the morphology, average size, size range, and stability of NPs during biomimetic extracellular synthesis.

Effect of Temperature

Several authors have shown that the kinetics of the reduction of metal ions and the shape and size of the formed NPs are strongly influenced by the temperature of the reaction medium. Chen et al. (2008) were the first to study the influence of temperature while synthesizing AgNPs extracellularly with the extracts of onion (*Allium cepa*) peels. They report that when the temperature of the reaction medium was increased, the size of the formed NPs tended to decrease. Similarly, in their work on AuNPs, Song & Kim (2008) have reported that as the reaction medium's temperature increases, smaller-sized NPs are formed in larger concentrations, as compared to larger NPs of smaller concentrations forming at lower temperatures.

In another study, Song et al. (2009) reported that when the reaction temperature was increased from 25°C to 95°C the rate of formation of AgNPs from Ag(i) by the leaf extracts of mokreyon (*Magnolia kobus*) and Japanese persimmon (*Diospyros kaki*) went up. There was a simultaneous decrease in the circumference of the NPs from 50 nm to 16 nm. The authors inferred that elevated temperatures might be suppressing the secondary nucleation process. This might be the reason for forming smaller-sized NPs of more consistent morphology. Chauhan & Upadhyay (2012) observed that an increase in the temperature of the reaction mixture was seen to cause a rapid depletion of the reactants, leading to the formation of smaller-sized NPs. A similar effect has been recorded by White et al. (2012), who report that an increase in the temperature of the reaction medium resulted in a reduction in the size of the formed NPs. It was attributed to the variation in the nucleation process and the growth rate of the NPs during the synthesis.

Interestingly Sun et al. (2014) found no significant change in the NP formation while investigating the effect of 25, 40, and 55°C temperatures. The possible reason, as

suggested by the authors, was that almost complete (99.7%) NP formation had occurred at 25°C itself, which had left little scope for further increase in the NP formation. One of the exceptions is the report of Paarakh and Jose (2020), which claims an increase in the size of the *Murraya Koenig*-derived AgNPs formation as the temperature was increased from room temperature to 55°C and 75°C.

Even as higher temperature favors greater NP formation, this benefit is countered by the lower stability of the NPs. Due to this reason, it is deemed preferable to synthesize NPs at ambient temperatures. Moreover, the concentration of the metal ion precursor can influence both the nucleation and growth kinetics as the reaction temperature changes (Li et al. 2020).

Effect of Metal Ion-Extract Stoichiometry on the NP Formation

Shankar et al. (2005) were the first to explore the impact of changes in the metal-extract concentration ratio on NP formation while synthesizing AuNPs extracellularly with the aid of leaf extracts of cochineal grass (*Cymbopogon flexuosus*). The authors reported that the change in the concentration of the extract relative to the metal ion concentration led to a change in the size of the NPs. They also observed that when the extract concentration was raised with respect to metal ion concentration, the size of the formed NPs decreased, and the ratio of the number of spherical NPs to the NPs of different shapes increased. The reported studies seem to support the hypothesis proposed by Dumur et al. (2011), according to which the formation of NPs occurs only when the precursor concentration is within a range suitable for nucleation. However, this range is seen to vary from species to species of the plants and the other physics-chemical conditions associated with the synthesis process.

According to Vilchis-Nestor et al. (2008), an increase in the extract concentration relative to the metal ion concentration caused the formed NPs to exhibit anisotropy. It was attributed to the faster reduction of metal ions in the NPs formation. Bar et al. (2009) also reported that NPs tended to aggregate more when the concentration of the plant extract was increased while keeping the metal ion concentration constant.

It was found by Vidhu et al. (2011) that sharpness in the SPR peaks of the NPs increased in proportion to the extract concentration relative to the metal ion concentration. The NP formation also occurred more rapidly. In contrast, with a lower concentration of the extract relative to the metal ion, the SPR peaks of the NPs were seen to be broader, and the reduction of the metal ions occurred more slowly. Khan et al. (2012) and Daniel et al. (2012) reported similar variations

accompanying an increase in the concentration of the plant extract relative to the metal ion solution.

In their work on AgNPs, Khalil et al. (2013) reported that at lower extract concentrations relative to the metal ion solution, quasi-spherical NPs were formed with an average size of 24-36 nm. In contrast, most of the formed NPs were in the 8-15 nm range at higher extract concentrations relative to the metal ion solution. It was attributed to the insufficient availability of biomolecules in the extracts. Their concentration was inadequate to reduce the metal ions or protect the formed NPs from aggregating.

According to Bindhu & Umadevi (2013), as the concentration of the extract increased, the full width at half maximum (FWHM) values of the spectral peaks of the formed NPs decreased. Concomitantly, the sharpness of the SPR peaks increased, and a blue shift of the peak was observed. This indicates a decrease in the mean diameter of the formed NPs. The blue shift and the greater sharpness in the peak indicated the formation of spherical NPs and the homogeneous distribution of the NPs.

Broadening of the SPR peaks was observed, along with the formation of larger-sized NPs, by Yang et al. (2019) when the concentration of the plant extract was increased relative to the concentration of the metal ion. The authors felt that reducing agents bound to the surface of the preformed nuclei might have intensified the subsequent reduction of the metal ions and would have enhanced bridging among the formed NPs, leading to the aggregation of the NPs. On the other hand, Yang et al. (2019) reported that with an increase in the metal ion concentration with respect to the extract concentration, an increase in the polydispersity of the formed NPs was seen owing to the occurrence of secondary particle growth by aggregation, coalescence, and Ostwald ripening. In several other studies by Anuradha et al. (2015), Abbasi et al. (2015), and Ganaie et al. (2015, 2017, 2018a), it has been shown that by controlling the metal-extract stoichiometry, it is possible to manipulate the rate of reaction, and the shapes and sizes of the NPs to suit the objective of the synthesis.

In general, smaller particles of spherical shape are obtained at higher extract: metal ion ratios. When the ratio decreases, anisotropic nanostructures form a mix of triangular, hexagonal, polygonal, rod-shaped, and cubical NPs. The concentrations of the plant extracts necessary for obtaining isotropic or anisotropic particles differ for different plant species. This is because plants' nature and concentration of biomolecules vary from species to species, even from variety to variety.

Effect of Reaction Duration

Li et al. (2016) were the first to report on the influence of

reaction time while synthesizing AgNPs extracellularly with fruit extracts of capsicum (*Capsicum annum*). According to them, the optical density values of the metal-plant extract mixtures increased with time, reflecting a rising trend in forming NPs. They also noted that NP formation started after 5 hours of mixing the reactants and was almost completed by the 11th hour, as indicated by the gradual rise and then flattening of the optical density values of the SPR peaks.

The work of Li et al. (2016) was followed by Vilchis-Nestor et al. (2008) and Wang et al. (2009), who all noted that an increase in NP formation was observed with an increase in reaction duration. Dubey et al. (2010) opined that an increase in reaction duration was responsible for sharpening the SPR peaks of the formed NPs.

Several subsequent reports have shown that the contact time of the reactants plays a major role in NP synthesis.

Effect of Other Factors on the NP Formation

Apart from pH, metal-extract stoichiometry, temperature, and contact time, several other factors also play a role in determining the dimensions, shape, and longevity of the NPs. The investigations of Haverkamp & Marshall (2009) were among the first on the role of a source of metal ion solution while studying AgNP formation inside a living plant mustard (*Brassica juncea*). According to them, the plants supplied with AgNO₃ as a source of Ag (i) produced AgNPs of 10-35 nm. But the plants which were supplied with complex ions such as Ag (NH₃)²⁺ and Ag(S₂O₃)²⁺ as an Ag (i) source produced much smaller AgNPs of 2-3 nm.

Rai et al. (2007) have reported on the influence of halide ions while synthesizing AuNPs extracellularly with leaf extracts of lemon grass. They observed that the halide ions could transform triangular AuNPs to circular disk-like shapes and that iodide ions were more effective than other halide ions. The addition of iodide ions distorted the nanotriangles into spherical AuNPs.

Several authors (Saxena et al. 2010, Ali et al. 2011, Shen et al. 2011, Prathna et al. 2011, Abdelrasoul et al. 2014, Raut et al. 2014) have reported the influence of duration of exposure to electromagnetic waves on NP formation. They also noted that when the reaction mixtures were kept for shaking, NPs of different sizes and shapes were formed as a function of the duration and intensity of shaking. According to Abdelrasoul et al. (2014), the irradiation of reaction mixtures by visible and UV light influenced the sizes and shapes of the formed NPs. A reckoner is presented in Fig. 5.

ENERGY EFFICIENCY OF BMNPS

In most cases, BMNPs are synthesized at ambient

temperatures and pressures, without hazardous chemicals, and they have lower ecological carbon footprints than NPs synthesized by other routes. This imparts life-cycle energy efficiency to all those applications in which BMNPs are utilized. This aspect is illustrated below with a specific example of the role of BMNPs in enhancing the efficiency of microbial fuel cells (MFCs).

In recent decades, enormous effort has been made to develop microbial fuel cells (MFCs) with which energy can be generated with concomitant waste treatment (Yang et al. 2019, Goel 2018, Mian et al. 2019). However, as elucidated by us recently (Tabassum-Abbasi & Abbasi 2019), MFCs are both cost-ineffective and leave large ecological footprints. Hence there is no net energy gain and/or pollution control advantage from MFCs. This has made it imperative to remedy this situation.

One dimension of the MFCs that BMNPs can contribute is to catalyze the redox reactions occurring in the MFCs. So far, the other catalysts used for the purpose are either expensive and susceptible to poisoning – such as those based on platinum group metals – or are low in efficacy (Palanisamy et al. 2019, Noori et al. 2020). Moreover, making these catalysts itself leaves a significantly large carbon footprint. In contrast, BMNPs entail very little energy use and generate negligible emissions. The use of such catalysts can contribute towards reducing the ecological as well as monetary costs of MFCs. However, a very extensive survey has revealed that other than the work of these authors, only a solitary report by Harshiny et al. (2017) is available on the use of BMNPs

in MFCs. Harshiny et al. (2017) generated iron oxide NPs using amaranthus (*Amaranthus dubius*) leaf extract and carbon-coated papers as electrodes in MFCs. They found that coating of the NPs led to a 31% enhancement in the accruable power density, attaining $145.5 \text{ mW} \cdot \text{m}^{-2}$. The NP coating also enabled 68.5% COD removal efficiency compared to 63.1% achieved with the bare electrode, even as the NPs decreased anodic charge transfer resistance.

Available reports on the use of NPs synthesized with chemical or physical methods in the MFCs (Noori et al. 2020, Rajalakshmi 2019) show that NPs help in increasing MFC performance by reducing the biofouling caused by fungi such as *Cladasporium* spp. and *Aspergillus* spp., thereby reducing ohmic over potential and proportionately enhancing the MFC's energy output. They also enhance the oxygen reduction reaction (ORR), a major step in the MFC functioning (Li et al. 2016), thus serving as efficient electrochemical catalysts.

Recently those authors (Abbasi et al. 2021) have studied the role of AgNPs, and AuNPs derived from several weedy plant species in MFCs, to find that the NCs boost energy yield compared to substrates not spiked by them.

Besides stand-alone single-element NPs like AgNPs, the NPs of silver, gold, manganese oxide, titanium oxide, vanadium pentoxide, etc., either coated upon or, in general, modified with carbon paper or nanotubes, have been explored in enhancing the waste reduction and energy generation capabilities of MFCs (Naruse et al. 2011, Alatraktchi et al. 2012, Kalathil et al. 2013, Noori et al. 2016, Zakaria et al. 2018).

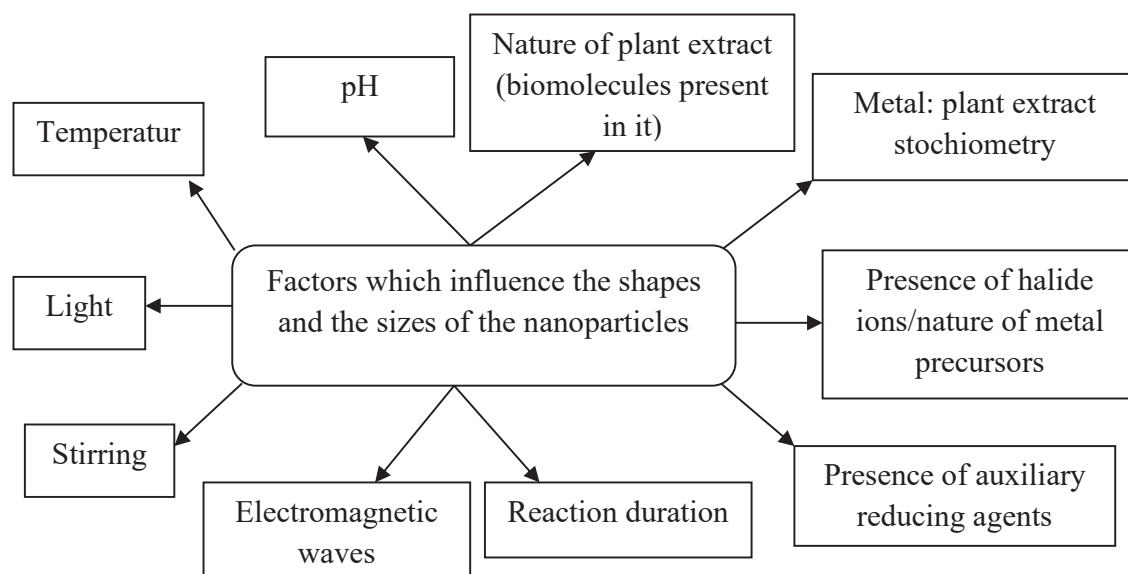


Fig. 5: A reckoner of the factors that influence the shapes and sizes of the nanoparticles.

From the foregoing, it appears clear that nanoparticles have the potential to enhance the performance of MFCs. If instead of the NPs generated using chemical or physical methods as in the studies quoted above, BMNPs are used (as pioneered by Harshini & Preeti (2017), it would reduce monetary and ecological costs. Future efforts ought to be oriented in that direction.

SUMMARY

1. Studies on the hyperaccumulation of metals by various species of plants have been carried out for more than 150 years. *In vitro* studies on metal accumulation gave the first clue that NPs can be formed intracellularly. Later, attempts were made to obtain intracellularly synthesized NPs, but several difficulties have prompted efforts toward an extracellular synthesis of the NPs. Sastry, Ahmed, and co-workers from the National Chemical Laboratory, Pune, India, were the first to successfully use a plant broth, that of geranium (*Pelargonium graveolens*), for synthesizing gold NPs extracellularly. Following that work, several reports have been published on synthesizing NPs of various metals using many different plant species. The non-toxic, non-hazardous, and simple nature of this synthetic route makes it particularly attractive.
2. Most reported studies on extracellular NP synthesis based on plant extracts have covered medicinal plants, food, and ornamental plants. In more recent years, there has been an increasing emphasis on the synthesis of NPs by utilizing weeds because weeds are freely and abundantly available and have no economically viable use at present.
3. The metals explored so far have largely been gold and silver. Palladium, copper, and platinum have been studied to a lesser extent in that order. Hence, many elements and their compounds have not been explored so far.
4. The NPs formed by the biomimetic route have been mostly explored for their antimicrobial, catalytic, and free radical scavenging properties.
5. The reaction medium's pH strongly influences the reduction of metal ions to their zerovalent forms. The NP formation occurred more rapidly at neutral and alkaline pH than at acidic pH. The NPs formed at elevated temperatures were generally smaller in size and larger in number than the NPs formed at ambient temperature. However, the former tended to lose stability and agglomerated much faster. Hence synthesizing NPs at ambient temperature appears preferable.

6. Studies on the effect of the metal-extract concentration ratio on NP formation reveal that the concentrations which favor the formation of isotropic or anisotropic particles vary with the plant species, in turn, with the type and the concentration of biomolecules present in the extract of a given plant. The contact time of reaction mixtures has also been found to play a key role in NP synthesis. The extent of this impact varied with the plant species.

ACKNOWLEDGMENT

SAA is thankful to the Indian National Science Academy (INSA), New Delhi, for providing him with an Emeritus Scientist grant (21(1034)/16/EMR-II). T-A thanks the University of Petroleum and Energy Studies authorities for facilitating her work.

REFERENCES

- Abbasi, S.A. 1982. Trace analysis of titanium in environmental samples using Np-Methoxyphenyl-2-furohydroxamic acid for separation and colorimetric determination. *Int. J. Environ. Anal. Chem.*, 11(1): 1-7.
- Abbasi, S.A. 1988. Niobium in the environment and a new method for its trace analysis using molecular or atomic absorption spectrometry. *Int. J. Environ. Anal. Chem.*, 33(1): 43-57.
- Abbasi, S.A. 1989. Synergistic spectrophotometric and atomic absorption spectrometric analysis of zinc in alloys and environmental samples with Np-methoxyphenyl-2-furylacrylohydroxamic acid and pyridylazo reagents. *Int. J. Environ. Anal. Chem.*, 36(3): 173-184.
- Abbasi, S.A. and Sharma, R.K. 1981. Copper salicylates: occurrence of linear free energy relationships. *J. Inorg. Nucl. Chem.*, 43(3): 625-627.
- Abbasi, S.A., Abbasi, T. and Anuradha, J. 2012. A process for the synthesis of metal nanoparticles from aquatic weeds. *Offl. J Patent Off.*, 6184.
- Abbasi, T., Anuradha, J., Ganaie, S.U. and Abbasi, S.A. 2015. Biomimetic synthesis of nanoparticles using aqueous extracts of plants (botanical species). *J. Nano Res.*, 31: 138-202.
- Abbasi, S.A., Tabassum-Abbasi and Patnaik, P. 2021. Biomimetically generated nanoparticles in boosting the performance of microbial fuel cells. *Nature Environ. Pollut. Technol.*, 20(5): 1881-1886, DOI:10.46488/NEPT.2021.v20i05.003.
- Abdelrasoul, G.N., Cingolani, R., Diaspro, A., Athanassiou, A. and Pignatelli, F. 2014. Photochemical synthesis: Effect of UV irradiation on gold nanorods morphology. *J. Photochem. Photobiol., A*, 275: 7-11.
- Ahmad, N., Sharma, S., Singh, V.N., Shamsi, S.F., Fatma, A. and Mehta, B.R. 2011. Biosynthesis of silver nanoparticles from *Desmodium triflorum*: A novel approach towards weed utilization. *Biotechnol. Res. Int.*, 2011.
- Ahmad, N., Sharma, S. and Alam, M.K. 2010. Rapid synthesis of silver nanoparticles using dried medicinal plant of basil. *Colloids Surf. B Biointerfaces*, 81: 81-6. <https://doi.org/10.1016/j.colsurfb.2010.06.029>.
- Ahmad, T., Iqbal, J., Bustam, M.A., Irfan, M., Asghar, H.M.A. 2021. A critical review on phytosynthesis of gold nanoparticles: Issues, challenges, and future perspectives. *J. Clean. Prod.*, 309: 127460.
- Alatraktchi, F.A.A., Zhang, Y., Noori, J.S. and Angelidaki, I. 2012. Surface area expansion of electrodes with grass-like nanostructures and gold nanoparticles to enhance electricity generation in microbial fuel cells. *Bioresour. Technol.*, 123: 177-183.
- Ali, M.D., Thajuddin, N., Jeganathan, K. and Gunasekaran, M. 2011. Plant

- extract mediated synthesis of silver and gold nanoparticles and its antibacterial activity against clinically isolated pathogens. *Colloids Surf., B*, 85: 360-365.
- Anderson, C.W., Brooks, R.R., Stewart, R.B. and Simcock, R. 1998. Harvesting a crop of gold in plants. *Nature*, 395(6702): 553-554.
- Anuradha, J., Abbasi, T. and Abbasi, S.A. 2009. Nanotechnology and its potential in revolutionizing the pollution control scenario. *J. Institut. Pub. Health Eng.*, 10(2): 5-12.
- Anuradha, J., Tasneem, A. and Abbasi, S.A. 2015. Rapid and green synthesis of gold nanoparticles by the use of an otherwise worthless weed, *Lantana (Lantana camara L.)*. *J. Environ. Sci. Eng.*, 57(3): 203-213.
- Armendariz, V., Herrera, I., Jose-yacaman, M., Troiani, H., Santiago, P. and Gardea-Torresdey, J.L. 2004. Size controlled gold nanoparticle formation by *Avena sativa* biomass: Use of plants in nanobiotechnology. *J. Nanopart. Res.*, 6(4): 377-382.
- Bao, R., Zhang, H. and Tang, Y. 2021. Biomimetic synthesis of natural products: A journey to learn, to mimic, and to be better. *Acc. Chem. Res.*, 54(19): 3720-3733. doi:10.1021/acs.accounts.1c00459
- Bar, H., Bhui, D.K., Sahoo, G.P., Sarkar, P., De, S.P. and Misra, A. 2009. Green synthesis of silver nanoparticles using latex of *Jatropha curcas*. *Colloids Surf., A*, 339: 134-139.
- Beattie, I.R. and Haverkamp, R.G. 2011. Silver and gold nanoparticles in plants: Sites for the reduction to metal. *Metallomics*, 3(6): 628-632.
- Bindhu, M.R. and Umadevi, M. 2013. Synthesis of monodispersed silver nanoparticles using *Hibiscus cannabinus* leaf extract and its antimicrobial activity. *Spectrochim. Acta Part A*, 101: 184-190.
- Braun, A. 1855. *New and Less Known Genera of Unicellular Algae with Preliminary Observations on the Genus Unicellular Algae*. Kessinger Publishing, Whitefish, Montana, US, pp. 114
- Cai, Y.L., Zhang, J.J., Zhang, S., Venkatraman, S.S., Zeng, X.T., Du, H.J. and Mondal, D. 2010. Osteoblastic cell response on fluoridated hydroxyapatite coatings: The effect of magnesium incorporation. *Biomed. Mater.*, 5(5): 054114.
- Castillo-López, D.N. and Pal, U. 2014. Green synthesis of Au nanoparticles using potato extract: Stability and growth mechanism. *J. Nanopart. Res.*, 16(8): 45
- Chauhan, S. and Upadhyay, M.K. 2012. Fruit-based synthesis of silver nanoparticles-an effect of temperature on the size of particles. *Rec. Res. Sci. Technol.*, 4(5): 65.
- Chen, P., Wu, Q.S., Ding, Y.P. 2008. Facile synthesis of monodisperse silver nanoparticles by bio-template of *Squama* inner coat of onion. *J. Nanopart. Res.*, 10: 207-213.
- Cygniuk, A., Klimkiewicz, R., Olejniczak, A. and Lukaszewicz, J.P. 2010. Biotechnological fabrication of LaMnO_3 -carbon catalyst for n-butanol conversion to ketones. *Carbon*, 48(1): 99-106.
- Daniel, K.S.C.G., Nehru, K. and Sivakumar, M. 2012. Rapid biosynthesis of silver nanoparticles using *Eichornia crassipes* and its antibacterial activity. *Curr. Nanosci.*, 8: 125-129.
- Daraee, H., Eatemadi, A., Abbasi, E., Fekri Aval, S., Kouhi, M. and Akbarzadeh, A. 2016. Application of gold nanoparticles in biomedical and drug delivery. *Artif. Cells Nanomed. Biotechnol.*, 44: 410-422.
- Dauthal, P. and Mukhopadhyay, M. 2013. In-vitro free radical scavenging activity of biosynthesized gold and silver nanoparticles using *Prunus armeniaca* (apricot) fruit extract. *J. Nanopart. Res.*, 15(1): 1366.
- Dubey, S.P., Lahtinen, M. and Sillanpää, M. 2010. Green synthesis and characterizations of silver and gold nanoparticles using leaf extract of *Rosa rugosa*. *Colloids Surf., A*, 364(1-3): 34-41.
- Dumur, F., Guerlin, A., Dumas, E., Bertin, D., Gignes, D. and Mayer, C.R. 2011. Controlled spontaneous generation of gold nanoparticles assisted by dual reducing and capping agents. *Gold Bull.*, 44(2): 119-137.
- Edison, T.J.I. and Sethuraman, M.G. 2012. Instant green synthesis of silver nanoparticles using *Terminalia chebula* fruit extract and evaluation of their catalytic activity on reduction of methylene blue. *Process Biochem.*, 47(9): 1351-1357.
- El Shafey, A.M. 2020. Green synthesis of metal and metal oxide nanoparticles from plant leaf extracts and their applications: A review. *Green Process. Synth.*, 9(1): 304-339.
- Eze, F.N., Ovatlarnporn, C., Nalinbenjapun, S. and Sripetthong, S. 2022. Ultra-fast sustainable synthesis, optimization, and characterization of guava phenolic extract functionalized nanosilver with enhanced biomimetic attributes. *Arab. J. Chem.*, 15(10): 104167.
- Gan, P.P. and Li, SFY 2012. Potential of the plant as a biological factory to synthesize gold and silver nanoparticles and their applications. *Rev. Environ. Sci. Biotechnol.*, 11(2): 169-206.
- Ganaie, S.U., Abbasi, T. and Abbasi, S.A. 2016. Low-cost, environment-friendly synthesis of palladium nanoparticles by utilizing a terrestrial weed *Antigonon leptopus*. *Part. Sci. Technol.*, 34(2): 201-208.
- Ganaie, S.U., Abbasi, T. and Abbasi, S.A. 2018a. Biomimetic synthesis of platinum nanoparticles utilizing a terrestrial weed *Antigonon leptopus*. *Part. Sci. Technol.*, 36(6): 681-688.
- Ganaie, S.U., Abbasi, T., Anuradha, J. and Abbasi, S.A. 2014. Biomimetic synthesis of silver nanoparticles using the amphibious weed *Ipomoea* and their application in pollution control. *J. King Saud Univ. Sci.*, 26(3): 222-229.
- Ganaie, S.U., Rajalakshmi, R., Abbasi, T. and Abbasi, S.A. 2017. Clean green synthesis of silver nanoparticles with shape/size control using aquatic weed *Pistia stratiotes* and their antioxidant, antibacterial and catalytic activity. *J. Indian Chem. Soc.*, 94(11): 1203-1212.
- Ganaie, S.U., Rajalakshmi, R., Abbasi, T. and Abbasi, S.A. 2018b. Green synthesis of silver nanoparticles by coral vine and assessment of their properties. *Bioinsp. Biomim. Nanobio.*, 8(2): 115-129.
- Ganaie, S.U., Ravindran, S., Abbasi, T. and Abbasi, S.A. 2015. Rapid and clean biomimetic synthesis of bimetallic Au-Ag nanoparticles using an otherwise worthless and noxious weed, *Ipomoea carnea*. *J. Nano Res.*, 31: 1-14.
- Ganaie, S. U., Abbasi T., Tabassum-Abbasi, Rajalakshmi, R. and Abbasi, S.A. 2021. Development of process parameters for the clean synthesis of silver nanoparticles using the pernicious aquatic weed *Eichhornia crassipes* and an assessment of their properties. *Indian J. Environ. Protect.*, 41(7): 762-771. ISSN: 0253-7141.
- Gardea-Torresdey, J.L., Dokken, K., Tiemann, K.J., Parsons, J.G., Ramos, J., Pingitore, N.E. and Gamez, G. 2002. Infrared and X-ray absorption spectroscopic studies on the mechanism of chromium (III) binding to alfalfa biomass. *Microchem. J.*, 71(2-3): 157-166.
- Gardea-Torresdey, J.L., Gomez, E., Peralta-Videa, J.R., Parsons, J.G., Troiani, H. and Jose-Yacaman, M. 2003. Alfalfa sprouts: A natural source for the synthesis of silver nanoparticles. *Langmuir*, 19(4): 1357-1361.
- Gardea-Torresdey, J.L., Rodriguez, E., Parsons, J.G., Peralta-Videa, J.R., Meitzner, G. and Cruz-Jimenez, G. 2005. Use ICP and XAS to determine the enhancement of gold phytoextraction by *Chilopsis linearis* using thiocyanate as a complexing agent. *Anal. Bioanal. Chem.*, 382(2): 347-352.
- Gardea-Torresdey, J.L., Tiemann, K.J., Gamez, G., Dokken, K., Tehuacanero, S. and Jose-Yacaman, M. 1999. Gold nanoparticles obtained by bio-precipitation from gold (III) solutions. *J. Nanopart. Res.*, 1(3): 397-404.
- Gautheret, R.J. 1935. The formation of chlorophyll in roots and the reduction of silver salts by chloroplasts. *Rev. Gen. Bot.*, 47: 401-421.
- Gebeshuber, I.C. 2022. Biomimetic nanotechnology. *Biomimetics*, 7(1): 16. <https://doi.org/10.3390/biomimetics7010016>
- Goel, S. 2018. From waste to watts in micro-devices: Review on development of membraned and membraneless microfluidic microbial fuel cell. *Appl. Mater. Today*
- Gondwal, M. and Joshi, N.Pant, G. 2018. Synthesis and catalytic and biological activities of silver and copper nanoparticles using *Cassia occidentalis*. *Int. J. Biomater.*, 2: 8.
- Gontijo, L.A.P., Raphael, E., Ferrari, D.P.S., Ferrari, J.L., Lyon, J.P.

- and Schiavon, M.A. 2020. pH effect on the synthesis of different size silver nanoparticles evaluated by DLS and their size-dependent antimicrobial activity. *Matéria*, 25(04): 145 <https://doi.org/10.1590/S1517-707620200004.1145>.
- Gruen, L.C. 1975. Interaction of amino acids with silver(I) ions. *BBA Protein Struct.*, 38(6): 270–274. [https://doi.org/10.1016/0005-2795\(75\)90268-8](https://doi.org/10.1016/0005-2795(75)90268-8).
- Gürsoy, N., Yılmaz Öztürk, B. and Dağ, İ. 2021. Synthesis of intracellular and extracellular gold nanoparticles with a green machine and its antifungal activity. *Turk. J. Biol.*, 45(2): 196-213. doi: 10.3906/biy-2010-64.
- Harshini, M. and Preeti, K. 2017. Autism behavioural interventional research in low-resource settings: Overcoming prevailing challenges an Asian perspective. *Asian J. Psychiatry*, 25: 224-227.
- Harshiny, M., Samsudeen, N., Kameswara, R.J. and Matheswaran, M. 2017. Biosynthesized FeO nanoparticles coated carbon anode for improving the performance of microbial fuel cell. *Int. J. Hydrogen Energy*, 42(42): 26488-26495.
- Haverkamp, R.G. and Marshall, A.T. 2009. The mechanism of metal nanoparticle formation in plants: limits on accumulation. *J. Nanopart. Res.*, 11(6): 1453-1463.
- Haverkamp, R.G., Marshall, A.T. and van Agterveld, D. 2007. Pick your carats: Nanoparticles of gold–silver–copper alloy produced in vivo. *J. Nanopart. Res.*, 9(4): 697-700.
- Huang, J., Li, Q., Sun, D., Lu, Y., Su, Y., Yang, X., Wang, H., Wang, Y., Shao, W., He, N. and Hong, J. 2007. Biosynthesis of silver and gold nanoparticles by novel sundried *Cinnamomum camphora* leaf. *Nanotechnology*, 18(10): 105104.
- Hussain, N., Patnaik, P., Tabassum-Abbasi, Khamrang, C., Abbasi, S.A. and Abbasi, T. 2022. Role of different earthworm species in nullifying the toxicity of *Ipomea carnea* and enhancing its utility as a phytoremediator. *Int. J. Phytomed.*, 24(13): 1385-1394. <https://doi.org/10.1080/15226514.2022.2031864>
- Huang, J., Jeong, Y., Park, J.M., Lee, K.H., Hong, J.W. and Choi, J. 2015. Biomimetics: Forecasting the future of science, engineering, and medicine. *International Journal of Nanomedicine*, 10, 5701-5713. doi:10.2147/IJN.S83642.
- Indhira, D., Krishnamoorthy, M., Ameen, F., Bhat, S.A., Arumugam, K., Ramalingam, S., Priyan, S.R. and Kumar, G.S. 2022. Biomimetic facile synthesis of zinc oxide and copper oxide nanoparticles from *Elaeagnus indica* for enhanced photocatalytic activity 2022. *Environ. Res.*, 212: 113323.
- Jabbari, E., Kim, D.H. and Lee, L.P. (eds.) 2014. *Handbook of Biomimetics and Bioinspiration: Biologically-Driven Engineering of Materials, Processes, Devices, and Systems*. World Scientific, Singapore.
- Jha, A.K., Prasad, K., Kumar, V. and Prasad, K. 2009. Biosynthesis of silver nanoparticles using eclipta leaf. *Biotechnol Prog.*, 25: 1476-1479. <https://doi.org/10.1002/btpr.233>.
- Johnson, A.P., Sabu, C., Nivitha, K.P., Sankar, R., Ameena Shirin, V.K., Henna, T.K., Rapphey, V.R., Gangadharappa, H.V., Kotta, S. and Pramod, K. 2022. Bioinspired and biomimetic micro- and nanostructures in biomedicine. *J. Control. Release*, 343: 724-754.
- Kalathil, S., Khan, M.M., Lee, J. and Cho, M.H. 2013. Production of bioelectricity, bio-hydrogen, high-value chemicals, and bioinspired nanomaterials by electrochemically active biofilms. *Biotechnol. Adv.*, 31(6): 915-924.
- Khalil, M.M.H., Ismail, E.H., El-Baghady, K.Z. and Mohamed, D. 2013. Green synthesis of silver nanoparticles using olive leaf extract and its antibacterial activity. *Arab. J. Chem.*, 2: 18.
- Khan, Z., Bashir, O., Hussain, J. I., Kumar, S. and Ahmad, R. 2012. Effects of ionic surfactants on the morphology of silver nanoparticles using Paa (*Piper betel*) leaf petiole extract. *Colloids Surf., B*, 98: 85-90.
- Khandel, P. and Shahi, S.K. 2018. Mycogenic nanoparticles and their bio-prospective applications: current status and future challenges. *J. Nanostruct. Chem.*, 8(4): 369-391.
- Khandel, P., Yadav, R.K., Soni, D.K., Kanwar, L. and Shahi, S.K. 2018. Biogenesis of metal nanoparticles and their pharmacological applications: Present status and application prospects. *J. Nanostruct. Chem.*, 8(3): 217-254. doi:10.1007/s40097-018-0267-4
- Kim, H.J. (ed.) 2020. *Biomimetic Microengineering*. CRC Press, Boca Raton, Florida.
- Kumar, M.R., Tauseef, S.M., Abbasi, T. and Abbasi, S.A. 2015. Control of amphibious weed ipomea (*Ipomea carnea*) by utilizing it for the extraction of volatile fatty acids as energy precursors. *J. Adv. Res.*, 6(1): 73-78.
- Li, S., Shen, Y., Xie, A., Yu, X., Qui, L., Zhang, L. and Zhang, Q. 2007. Green synthesis of silver nanoparticles using *Capsicum annum* L. extract. *Green Chem.*, 9: 852-858.
- Li, X., Wang, X., Zhao, Q., Wan, L., Li, Y. and Zhou, Q. 2016. Carbon fiber enhanced bioelectricity generation in soil microbial fuel cells. *Biosens. Bioelectron.*, 85: 135-141.
- Li, X., Xu, H., Chen, Z.S. and Chen, G. 2011. Biosynthesis of nanoparticles by micro-organisms and their applications. *J. Nanomater.*, 7: 478. <https://doi.org/10.1155/2011/270974>
- Li, P.J., Liang, J.Y., Su, D.L., Huang, Y., Pan, J.J., Peng, M.F., Li, G.Y. and Shan, Y. 2020. Green and efficient biosynthesis of pectin-based copper nanoparticles and their antimicrobial activities. *Bioprocess. Biosyst. Eng.*, 43(11): 2017-2026. doi: 10.1007/s00449-020-02390-w.
- Lopez, M.L., Parsons, J.G., Videa, J.P. and Gardea-Torresdey, J.L. 2005. An XAS study of the binding and reduction of Au (III) by hop biomass. *Microchem. J.*, 81(1): 50-56.
- Łukaszewicz, J.P., Wesolowski, R.P. and Cyganiuk, A. 2009. Enrichment of *Salix viminalis* wood in metal ions by means phytoextraction. *Pol. J. Environ. Stud.*, 18: 507-511.
- Lukman, A.I., Gong, B., Marjo, C.E., Roessner, U. and Harris, A.T. 2011. Facile synthesis, stabilization, and antibacterial performance of discrete Ag nanoparticles using *Medicago sativa* seed exudates. *J. Colloid Interface Sci.*, 353(2): 433-444.
- Malik, P., Shankar, R. and Malik, V. 2014. Green chemistry-based benign routes for nanoparticle synthesis. *J. Nanopart.*, 4: 1-14. <https://doi.org/10.1155/2014/302429>.
- Manceau, A., Nagy, K.L., Marcus, M.A., Lanson, M., Geoffroy, N., Jacquet, T. and Kirpichtchikova, T. 2008. Formation of metallic copper nanoparticles at the soil-root interface. *Environ. Sci. Technol.*, 42(5): 1766-1772.
- Marchiol, L., Mattiello, A., Pošćić, F., Giordano, C. and Musetti, R. 2014. In vivo synthesis of nanomaterials in plants: Location of silver nanoparticles and plant metabolism. *Nanoscale Res. Lett.*, 9(1): 1-11.
- Mian, M.M., Liu, G. and Fu, B. 2019. Conversion of sewage sludge into environmental catalyst and microbial fuel cell electrode material: A review. *Sci. Total Environ.*, 666: 525-539.
- Mishra, A.N., Bhadauria, S., Gaur, M.S., Pasricha, R. and Kushwah, B.S. 2010. Synthesis of gold nanoparticles by leaves of zero-calorie sweetener herb (*Stevia rebaudiana*) and their nanoscopic characterization by spectroscopy and microscopy. *Int. J. Green Nanotechnol. Phys. Chem.*, 1(2): P118-P124.
- Mittal, A.K., Chisti, Y. and Banerjee, U.C. 2013. Synthesis of metallic nanoparticles using plant extracts. *Biotechnol. Adv.*, 31: 346-356.
- Miyauchi, A. and Shimomura, M. 2023. *Biomimetics: Connecting Ecology and Engineering by Informatics*. Jenny Stanford Publishing, Dubai.
- Mousavi, S.M., Hashemi, S.A., Ghasemi, Y., Atapour, A., Amani, A.M., Savar Dashtaki, A., Babapoor, A. and Arjmand, O. 2018. Green synthesis of silver nanoparticles toward bio and medical applications: Review study. *Artif. Cells Nanomed. Biotechnol.*, 2018, 46, S855–S872.
- Mukunthan, K.S. and Balaji, S. 2012. Cashew apple juice (*Anacardium occidentale* L.) speeds up the synthesis of silver nanoparticles. *Int. J. Green Nanotechnol.*, 4: 71-9. <https://doi.org/10.1080/19430892.2012.676900>.

- Naruse, J., Sugano, Y., Ikeuchi, T., Yoshikawa, H., Saito, M. and Tamiya, E. 2011. Development of biofuel cells based on gold nanoparticle decorated multi-walled carbon nanotubes. *Biosens. Bioelectron.*, 30(1): 204-210.
- Ngo, T.D. (ed.) 2015. *Biomimetic Technologies: Principles and Applications*. Woodhead Publishing, Swaston, Cambridge.
- Noori, M.T., Bhowmick, G.D., Tiwari, B.R., Das, I., Ghangrekar, M.M. and Mukherjee, C.K. 2020. Utilisation of waste medicine wrappers as an efficient, low-cost electrode material for the microbial fuel cell. *Environ. Technol.*, 41(10): 1209-1218.
- Noori, M.T., Jain, S.C., Ghangrekar, M.M. and Mukherjee, C.K. 2016. Biofouling inhibition and enhancing the performance of microbial fuel cell using silver nanoparticles as fungicide and cathode catalyst. *Bioresour. Technol.*, 220: 183-189.
- Palanisamy, G., Jung, H.Y., Sadhasivam, T., Kurkuri, M.D., Kim, S.C. and Roh, S.H. 2019. A comprehensive review on microbial fuel cell technologies: Processes, utilization, and advanced developments in electrodes and membranes. *J. Clean. Prod.*, 221: 598-621.
- Panigrahi, S., Kundu, S. and Ghosh, S. 2004. General method of synthesis for metal nanoparticles. *J. Nanoparticle Res.* 6: 411-4. <https://doi.org/10.1007/s11051-004-6575-2>.
- Paarakh, M.P. and Jose, P.A. 2020. Effect of temperature on green synthesis of silver nanoparticle synthesized from *Murraya Koenigii* Linn and *Punica Granatum* Linn. *J. Res. Pharmacog. Natural Med. Prod.*, 2(1), 1-17. <https://doi.org/10.5281/zenodo.3763153>.
- Pareek, V., Bhargava, A., Gupta, R., Jain, N. and Panwar, J. 2017. Synthesis and applications of noble metal nanoparticles: a review. *Adv. Sci. Eng. Sci.* 9(7): 527-544.
- Philip, D. 2010. Green synthesis of gold and silver nanoparticles using *Hibiscus rosa sinensis*. *Physica E.*, 42(5): 1417-1424.
- Prathna, T.C., Mathew, L. and Chandrasekaran, N. 2010. Biomimetic synthesis of nanoparticles: science, technology, and applicability. *Biomimet. Learn Nat.*, 8: 776. <https://doi.org/10.5772/8776>.
- Prathna, T.C., Chandrasekaran, N., Raichur, A.M. and Mukherjee, A. 2011. Biomimetic synthesis of silver nanoparticles by *Citrus limon* (lemon) aqueous extract and theoretical prediction of particle size. *Colloids Surf., B*, 82: 152-159.
- Prescott, T.J., Lepora, N. and Verschure, P.F.J. (eds.), 2018. *Living Machines: A Handbook of Research in Biomimetics and Biohybrid Systems*. Oxford University Press.
- Primrose, S.B. 2020. *Biomimetics: Nature-Inspired Design and Innovation*. Wiley-Blackwell, NJ.
- Priya, K., Das, D., Singh, S. and Rai, G. 2022. Green synthesis of silver nanoparticles using *Musa balbisiana* and their cytotoxic effect on HL-60 and SiHa cancer cells through clathrin-mediated endocytosis. *BioNanoScience*, 12(2): 582-600.
- Panahi, Y., Mohammadhosseini, M., Nejati-Koshki, K., Abadi, A.J., Moafi, H.F., Akbarzadeh, A. and Farshbaf, M. 2017. Preparation, surface properties, and therapeutic applications of gold nanoparticles in biomedicine. *Drug Res.*, 67: 77-87.
- Rai, A., Chaudhary, M., Ahmad, A., Bhargava, S. and Sastry, M. 2007. Synthesis of triangular Au core-Ag shell nanoparticles. *Mater. Res. Bull.*, 42(7): 1212-1220.
- Rai, U.N., Pandey, K., Sinha, S., Singh, A., Saxena, R. and Gupta, D.K. 2004. Revegetating fly ash landfills with *Prosopis juliflora* L.: Impact of different amendments and Rhizobium inoculation. *Environ. Int.*, 30(3): 293-300.
- Rajalakshmi, R. 2019. An approach towards energy conservation and process simplification in the biomimetic synthesis of nanoparticles. Doctoral Thesis, Pondicherry University, pp. 1-310.
- Rajani, P., SriSindhura, K., Prasad, T.N., Hussain, O.M., Sudhakar, P., Latha, P., Balakrishna, M., Kambala, V. and Reddy, K.R. 2010. Fabrication of biogenic silver nanoparticles using agricultural crop plant leaf extracts. *AIP Conf. Proceed.*, 1276(1): 148-153.
- Raut, R.W., Mendhulkar, V.D., Kashid, S.B. 2014. Photosensitized synthesis of silver nanoparticles using *Withania somnifera* leaf powder and silver nitrate. *J. Photochem. Photobiol., B.*, 132: 45-55.
- Reeves, R.D. 2000. Metal-Accumulating Plants. *Phytoremediation of Toxic Metals: Using Plants to Clean up the Environment*.
- Reeves, R.D., Baker, A.J.M., Jaffré, T., Erskine, P.D., Echevarria, G. and van der Ent, A. 2018. A global database for plants that hyperaccumulate metal and metalloid trace elements. *New Phytologist*, 218(2): 407-411. doi:10.1111/nph.14907
- Roy, N., Alam, M.N., Mondal, S., Sk, I., Laskar, R.A., Das, S., Mandal, D. and Begum, N.A. 2012. Exploring Indian rosewood as a promising biogenic tool for the synthesis of metal nanoparticles with tailor-made morphologies. *Process Biochem.*, 47(9): 1371-1380.
- Sadeghi, B. and Gholamhoseinpour, F. 2015. A study on the stability and green synthesis of silver nanoparticles using *Ziziphora tenuior* (Zt) extract at room temperature. *Spectrochim. Acta, Part A.*, 134: 310-315.
- Saikia, N., Johnson, F., Waters, K. and Pandey, R. 2018. Dynamics of self-assembled cytosine nucleobases on graphene. *Nanotechnology*, 29(19): 195601.
- Sathishkumar, M., Sneha, K., Won, S.W., Cho, C.W., Kim, S. and Yun, Y.S. 2009. *Cinnamon zeylanicum* bark extract and powder mediated green synthesis of nano-crystalline silver particles and its bactericidal activity. *Colloids Surf., B.*, 73(2): 332-338.
- Saxena, A., Tripathi, R.M. and Singh, R.P. 2010. Biological synthesis of silver nanoparticles by using onion (*Allium cepa*) extract and their antibacterial activity. *Dig. J. Nanomater. Biostruct.*, 5: 427-432.
- Shah, R.R., Davis, T.P., Glover, A.L., Nikles, D.E. and Brazel, C.S. 2015. Impact of magnetic field parameters and iron oxide nanoparticle properties on heat generation for use in magnetic hyperthermia. *J. Magn. Magn. Mater.*, 387: 96-106.
- Shahid, S., Ejaz, A., Javed, M., Mansoor, S., Iqbal, S., Elkaeed, E.B., Alzhirani, R.M., Alsaab, H.O., Awwad, N.S., Ibrahim, H.A., Fatima, U., Zaman, S. and Nazim Sarwar, M. 2022. The anti-inflammatory and free radical scavenging activities of bio-inspired nano magnesium oxide. *Front. Mater.*, 9: 875163.
- Shahverdi, A.R., Fakhimi, A., Shahverdi, H.R. and Minaian, S. 2007. Synthesis and effect of silver nanoparticles on the antibacterial activity of different antibiotics against *Staphylococcus aureus* and *Escherichia coli*. *Nanomed. Nanotechnol. Biol. Med.*, 3(2): 168-171.
- Shankar, S.S., Ahmad, A., Pasricha, R. and Sastry, M. 2003. Bioreduction of chloroaurate ions by geranium leaves and its endophytic fungus yields gold nanoparticles of different shapes. *J. Mater. Chem.*, 13(7): 1822-1826.
- Shankar, S.S., Ahmad, A., Pasricha, R., Khan, M.I., Kumar, R. and Sastry, M. 2004a. Immobilization of biogenic gold nanoparticles in thermally evaporated fatty acid and amine thin films. *J. Colloid Interface Sci.*, 274(1): 69-75.
- Shankar, S.S., Rai, A., Ahmad, A. and Sastry, M. 2004b. Rapid synthesis of Au, Ag, and bimetallic Au core-Ag shell nanoparticles using *Neem (Azadirachta indica)* leaf broth. *J. Colloid Interface Sci.*, 275(2): 496-502.
- Shankar, S.S., Rai, A., Ahmad, A. and Sastry, M. 2005. Controlling the optical properties of lemongrass extract synthesized gold nanotriangles and potential application in infrared-absorbing optical coatings. *Chem. Mater.*, 17: 566-572.
- Shankar, S.S., Rai, A., Ankamwar, B., Singh, A., Ahmad, A. and Sastry, M. 2004c. Biological synthesis of triangular gold nanoprisms. *Nat. Mater.*, 3(7): 482-488.
- Sharma, N.C., Sahi, S.V., Nath, S., Parsons, J.G., Gardea-Torresde, J.L. and Pal, T. 2007. Synthesis of plant-mediated gold nanoparticles and catalytic role of biomatrix-embedded nanomaterials. *Environ. Sci. Technol.*, 41(14): 5137-5142.
- Sheny, D.S., Mathew, J. and Philip, D. 2011. Phytosynthesis of Au, Ag, and Au-Ag bimetallic nanoparticles using aqueous extract and dried leaf



- of *Anacardium occidentale*. *Spectrochim. Acta, Part A*, 79: 254-262.
- Si, S. and Mandal, T.K. 2007. Tryptophan-based peptides to synthesize gold and silver nanoparticles: A mechanistic and kinetic study. *Chem. A. Eur. J.* 13: 3160-3168. <https://doi.org/10.1002/chem.200601492>.
- Siddiqi, K.S., Husen, A. and Rao, R.A., 2018. A review on the biosynthesis of silver nanoparticles and their biocidal properties. *J. Nanobiotechnol.*, 16(1): 1-28.
- Sindhu, K., Indra, R., Rajaram, A., Sreeram, K.J. and Rajaram, R. 2011. Investigations on the interaction of gold-curcumin nanoparticles with human peripheral blood lymphocytes. *J. Biomed. Nanotechnol.*, 7: 56
- Singh, P., Kim, Y.J., Wang, C., Mathiyalagan, R. and Yang, D.C. 2016. The development of a green approach for the biosynthesis of silver and gold nanoparticles by using *Panax ginseng* root extract and their biological applications. *Artif. Cells Nanomed. Biotechnol.*, 44(4): 1150-1157.
- Singh, J., Dutta, T., Kim, K., Rawat, M., Samddar, P. and Kumar, P. 2018. 'Green' synthesis of metals and their oxide nanoparticles: Applications for environmental remediation. *J. Nanobiotechnol.*, 16(1): 408. doi:10.1186/s12951-018-0408-4
- Singh, A., Dar, M.Y., Nagar, D.P., Tomar, R.S., Shrivastava, S. and Shukla, S. 2022. Biomimetic synthesis of silver nanoparticles for treatment of N-Nitrosodihyamine-induced hepatotoxicity. *J. Biochem. Mol. Toxicol.*, 3 (3): e22968.
- Shah, M., Fawcett, D. and Sharma, S. 2015. Green synthesis of metallic nanoparticles via biological entities. *Materials (Basel)*, 8: 278-308.
- Skuza, L., Szućko-Kociuba, I., Filip, E., & Bożek, I. 2022. Natural molecular mechanisms of plant hyperaccumulation and hypertolerance towards heavy metals. *International Journal of Molecular Sciences*, 23(16) doi:10.3390/ijms23169335
- Song, J. and Kim, B. 2008. Biological synthesis of bimetallic Au/Ag nanoparticles using Persimmon (*Diopyros kaki*) leaf extract. *Korean J. Chem. Eng.*, 25: 808-811.
- Song, J.Y., Jang, H.K. and Kim, B.S. 2009. Biological synthesis of gold nanoparticles using *Magnolia kobus* and *Diopyros kaki* leaf extracts. *Process Biochem.*, 44(10): 1133-1138.
- Sun, D., Zhang, G., Huang, J., Wang, H. and Li, Q. 2014. Plant-mediated fabrication and surface enhanced raman property of flower-like Au@Pd nanoparticles. *Materials*, 7(2): 1360-1369.
- Sytar, O., Ghosh, S., Malinska, H., Zivcak, M. and Brestic, M. 2021. Physiological and molecular mechanisms of metal accumulation in hyperaccumulator plants. *Physiologia Plantarum*, 173(1): 148-166. doi:10.1111/ppl.13285
- Sytar, O., Ghosh, S., Malinska, H., Zivcak, M. and Brestic, M. 2020. Physiological and molecular mechanisms of metal accumulation in hyperaccumulator plants. *Physiol. Plant.*, 173(1): 148-166. doi: 10.1111/ppl.13285.
- Tabassum-Abbasi and Abbasi, S.A. 2019. Microbial fuel cells as source of clean energy-potential and pitfalls. *Nature Nat. Environ. Pollut. Technol.*, 18(3): 789-797.
- Tamuly, C., Hazarika, M., Bordoloi, M., Bhattacharyya, P.K. and Kar, R. 2014. Biosynthesis of Ag nanoparticles using pedicellamide and its photocatalytic activity: An eco-friendly approach. *Spectrochim. Acta, Part A*, 132: 687-691.
- Tan, M.L., Choong, P.F. and Dass, C.R. 2010a. Recent developments in liposomes, microparticles, and nanoparticles for protein and peptide drug delivery. *Pept.*, 31(1): 184-193.
- Tan, Y.N., Lee, J.Y. and Wang, D.I.C. 2010b. Uncovering the design rules for peptide synthesis of metal nanoparticles. *J. Am. Chem. Soc.* 132: 5677-86. <https://doi.org/10.1021/Ja907454f>.
- Tripathi, R.M., Kumar, N., Shrivastav, A., Singh, P. and Shrivastav, B.R. 2013. Catalytic activity of biogenic silver nanoparticles synthesized by *Ficus panda* leaf extract. *J. Mol. Catal. B. Enzym.*, 96: 75-80.
- Veerasingh, R., Xin, T.Z., Gunasagaran, S., Xiang, T.F.W., Yang, E.F.C., Jeyakumar, N. and Dhanaraj, S.A. 2011. Biosynthesis of silver nanoparticles using mangosteen leaf extract and evaluation of their antimicrobial activities. *J. Saudi Chem. Soc.*, 15: 113-120.
- Vidhu, V.K., Aromal, S.A. and Philip, D. 2011. Green synthesis of silver nanoparticles using *Macrotyloma uniflorum*. *Spectrochim. Acta, Part A*, 83: 392-397.
- Vilchis-Nestor, A.R., Sanchez-Mendieta, V., Camacho-Lopez, M.A., Gomez-Espinosa, R.M., Camacho-Lopez, M.A. and Arenas Alatorre, J.A. 2008. Solventless synthesis and optical properties of Au and Ag nanoparticles using *Camellia sinensis* extract. *Mater. Lett.*, 62: 3103-3105.
- Veeramani, C., El Newehy, A.S., Alsaif, M.A. and Al-Numair, K.S. 2022. Cassia fistula nutrition-rich flower tea derived biotic nanoparticles synthesis, characterization, and their antioxidant and anti-hyperglycaemic properties. *Afr. Health Sci.*, 22(1): 384-394.
- Wang, X., Cheng, S., Feng, Y., Merrill, M.D., Saito, T. and Logan, B.E. 2009. Use of carbon mesh anodes and the effect of different pretreatment methods on power production in microbial fuel cells. *Environ. Sci. Technol.*, 43(17): 6870-6874.
- Wei, Q., Yang, Q., Wang, Q., Sun, C., Zhu, Y., Niu, Y., Yu, J. and Xu, X. 2018. Formulation, characterization, and pharmacokinetic studies of 6-gingerol-Loaded nanostructured lipid carriers. *AAPS Pharm. Sci. Tech.*, 19: 3661-3669.
- Wei, Q.Y., He, K.M., Chen, J.L., Xu, Y.M. and Lau, A.T.Y. 2019. Phytofabrication of nanoparticles as novel drugs for anticancer applications
- White, G.V., Kerscher, P., Brown, R.M., Morella, J.D., Allister, W.M., Dean, D. and Kitchens, C. L. 2012. Green synthesis of robust, biocompatible silver nanoparticles using garlic extract. *J. Nanomater.*, 2012: 12.
- Yang, E., Chae, K.J., Choi, M.J., He, Z. and Kim, I.S. 2019. Critical review of bioelectrochemical systems integrated with membrane-based technologies for desalination, energy self-sufficiency, and high-efficiency water and wastewater treatment. *Desalination*, 452: 40-67.
- Yates, B.J., Myre, E., Breetz, D. and Dionysiou, D.D. 2005. Biotemplating of nanoparticles for environmental applications using phytomining techniques. *J. Am. Chem. Soc.*, 230: U1593-U1593.
- Yazdani, S., Daneshkhal, A., Diwate, A., Patel, H., Smith, J., Reul, O., Cheng, R., Izadian, A. and Hajrasouliha, A.R. 2021. Model for gold nanoparticle synthesis: Effect of pH and reaction time. *ACS Omega*, 6(26): 16847-16853.
- Zakaria, B.S., Barua, S., Sharaf, A., Liu, Y. and Dhar, B.R. 2018. Impact of antimicrobial silver nanoparticles on anode respiring bacteria in a microbial electrolysis cell. *Chemosphere*, 213: 259-267.
- Zayed, M.F., Eisa, W.H. and Shabaka, A.A. 2012. *Malva parviflora* extract assisted green synthesis of silver nanoparticles. *Spectrochim. Acta Part A Mol. Biomol. Spectrosc.*, 98: 423-428. <https://doi.org/10.1016/j.saa.2012.08.072>.



Review of Outdoor Air Pollution in Sri Lanka Compared to the South Asian Region

L.R.S.D. Rathnayake , G.B. Sakura†  and N.A. Weerasekara 

Department of Civil and Environmental Technology, Faculty of Technology, University of Sri Jayewardenepura, Dampe, Pitipana Rd, Homagama, Sri Lanka

†Corresponding author: G. B. Sakura; sakurabogoda@sjp.ac.lk

Nat. Env. & Poll. Tech.
Website: www.neptjournal.com

Received: 09-01-2022

Revised: 22-08-2022

Accepted: 27-08-2022

Key Words:

Indoor air pollution
Outdoor air pollution
Ambient air quality standards

ABSTRACT

Air pollution is a significant issue that affects almost all the countries in the world while predominating in South Asian Regional countries due to poverty, less attention, and less awareness towards the implementation and obeying of air quality guidelines in public. As a developing country, Sri Lanka stands at an optimum state of national air quality compared to other SARC because it is an island with a minor population compared to India, Pakistan, Bangladesh, etc. Maldives and Bhutan lie straightforwardly in owing mild air quality in SARC. However, SARC is far behind the world in maintaining optimistic air quality nationwide. Ambient air pollution-attributable deaths have become interim in past decades, a severe burden to the sustainable existence of SARC. A well-established systematic epidemiological, empirical studies and revisions regarding air pollution, strategic planning for mitigating air pollution, and frequent Spatio-temporal pollution monitoring nodes are necessary for Sri Lanka to achieve the sustainable goal. Other South Asian countries: India, Bangladesh, Pakistan, Afghanistan, Nepal, Bhutan, and Maldives, also should pay attention to minimizing outdoor air pollution nationwide for the betterment of future existence.

INTRODUCTION

Substances in the atmosphere that are harmful to living creatures and cause damage to climate are generally considered “Air Pollutants,” which release into the air through anthropogenic activities and natural phenomena (Saxena & Sonwani 2019). Following this definition, particulate matter (PMs), ground-level ozone (O₃), carbon monoxide (CO), sulfur oxides (SO_x), nitrogen oxides (NO_x), and lead (Pb) (Table 1a & 1b) are identified as the primary air pollutants (EPA 2020). Air Pollution imbalances the whole environment making it a more perilous risk; it kills millions of human beings and meanwhile affects trees, animals, and inanimate objects (Senarath 2005). Air pollution affects public health, the economy, and aesthetics in a country, and it resulted in much concern raised among policymakers, clinicians, public health experts, and the general public in recent years (Ileperuma 2020, Nandasena et al. 2012)

Air pollution is not manageable like other pollution, such as water, soil, and solid pollution, also predominantly associated with environmental health problems (Jacquemin et al. 2012, Karunasekara 2012). It is confirmed that nine out of ten people breathe air containing a high level of pollutants, and 91% of the world’s population lives in polluted atmospheres that predominantly exceed the WHO air quality permissible levels (WHO 2021). Asian Environment has considerably become polluted and a significant threat to both the life quality of people and the economic prospects in Asia, indicating that 13 mostly polluted cities lie in out of the world’s most polluted 15 cities (Ileperuma & Oliver 2010). Rapid urbanization, industrialization, and no proper attention to air pollutants aggravated air pollution worldwide, especially in SAR (Kumar et al. 2018). South Asia undergoes the worst air pollution in the world, which is maximal in India (Hasnat et al. 2018). In recent years, a phenomenon called “Brown Cloud” caused by air pollution due to Carbon aerosols (atmospheric haze) over the SAR was captured by satellite images (Begum 2017).

This review describes Air Quality Guidelines (AAQS) of SAR, AQI parameters, health outcomes due to OAP, and mitigation policies of OAP, respectively.

ORCID details of the authors:

L.R.S.D. Rathnayake: <https://orcid.org/0000-0002-7405-7785>

G.B. Sakura: <https://orcid.org/0000-0003-0533-9380>

N.A. Weerasekara: <https://orcid.org/0000-0001-6809-8778>

AQI Value	Color	Description
0-50	Green	Good
51-100	Yellow	Moderate
101-150	Orange	Unhealthy for Sensitive Group
151-200	Red	Unhealthy
201-300	Violet	Very Unhealthy
301-Higher	Maroon	Hazardous

Fig. 1: Color-coded AQI values (USEPA, 2021).

AMBIENT AIR QUALITY STANDARDS (AAQS)

A comparison of WHO guidelines with local and SAR national AAQS is shown in Tables 2a & 2b. The guideline values recommended by WHO acknowledge the heterogeneity and, in particular, should be recognized when formulating policy targets. Governments (each country) should consider their local circumstances carefully before adopting the guidelines directly as legally based standards (WHO 2005).

Generally, AAQS vary from a 1-hour maximum to 8 hours or 24-hour mean annual averages. Short-term

averaging values protect from peak concentrations that can cause adverse health risks, while long-term averaging values protect from chronic health effects (WHO 2005). AAQS plays a crucial role in maintaining the air quality of a country, supporting its legislation, and regulating criteria for its self-sustainability.

AIR QUALITY INDEX (AQI)

AQI is an index (ranging from 0-500, no units) introduced by the US EPA, regulated by the “Clean-Air Act” (Ileperuma

Table 1a: Major Air Pollutants, Origination, Risk Effects, and Health Effects.

Air Pollutant	Origination/Formation	Risk Effect	Health effects
PMs	<ul style="list-style-type: none"> Emits directly from motor vehicles, and power plants (HEI 2004) Forms by reactions with gaseous emissions in the atmosphere (e.g.: [NO_x, SO_x] react to form nitrates and sulfates) (HEI 2004) 	<ul style="list-style-type: none"> PM₁₀ get deep into the lungs (EPA 2020) PM_{2.5} get into the bloodstream pose, reduce visibility (haze) (EPA 2020) Particles can be conveyed long distances by wind and settle on ground or water, resulting in lakes and streams being acidic, changing the nutrient, depleting the nutrients in the soil, damaging sensitive forests, and farm crops, affecting the diversity of ecosystems, and contributing to acid rain (EPA 2020) 	<ul style="list-style-type: none"> Aggravates heart and lung conditions (Senarath 2005, WHO 2014b) Smaller particles (<PM_{2.5}) can pass through the lungs, causing inflammation and scarring to lung tissue (Senarath 2005, WHO 2014b) Irritates nose and throat (Senarath, 2005) (WHO 2014b)
Ground Level O ₃	<ul style="list-style-type: none"> Created by chemical reactions between NO_x and volatile organic compounds (Pollutants emitted by cars, power plants, industrial boilers, refineries, chemical plants, and other sources chemically react in sunlight). (EPA 2020). 	<ul style="list-style-type: none"> Ground Level O₃ affects human health, echo systems (forests, parks, wildlife refuges, wilderness areas), and water bodies. (EPA 2020) Threatens and harms sensitive vegetation during the growing season (EPA 2020) 	<ul style="list-style-type: none"> Asthma attacks (Senarath 2005) Loss of lung function (Senarath 2005) Breathing and respiratory problems (Senarath 2005)
CO	<ul style="list-style-type: none"> Emissions of vehicles (cars, trucks, etc.). (EPA 2020) Machinery that burns fossil fuels. (EPA 2020). Household appliances: unvented kerosene, gas-space heaters, leaking chimneys and furnaces, and gas stoves (WHO 2014a). 	<ul style="list-style-type: none"> Harmful when inhaled in large amounts (EPA 2020) Long-term exposure to low concentrations affects health (HEI 2004). Affects indoor air quality (HEI 2004). 	<ul style="list-style-type: none"> CO poisoning: Dizziness, Headache, General fatigue (Senarath 2005, WHO 2014b) Blocks the uptake of oxygen by blood by forming carboxyhemoglobin. Respiration, Brain, and heart functioning are affected (Senarath 2005)

Table 1b: Major Air Pollutants, Origination, Risk Effects, and Health Effects.

Air Pollutant	Origination/Formation	Risk Effect	Health effects
SO ₂	<ul style="list-style-type: none"> Burning fossil fuels (coal, oil) (HEI 2004) Smelting of mineral ores containing Sulphur (HEI 2004) 	<ul style="list-style-type: none"> Poisonous substance (EPA 2020) Forms harmful acids (EPA 2020). Affects both human health and the environment (EPA 2020). Forms fine particles that reduce visibility (haze). (EPA 2020). 	<ul style="list-style-type: none"> Irritation of the mucous membrane (Senarath 2005) Aggravate existing conditions- bronchitis (Senarath 2005) Cause wheezing, shortness of breath, and coughing (Senarath 2005)
NO ₂	<ul style="list-style-type: none"> Power generation, industrial and traffic sources (HEI 2004). 	<ul style="list-style-type: none"> Severe threat to human health (HEI 2004) Form acid rains (HEI 2004). Harms sensitive eco systems (HEI 2004). 	<ul style="list-style-type: none"> Irritates mucous lining of nose and throat, coughing, choking, headache, and lung inflammation such as bronchitis or pneumonia (Senarath 2005)
Pb	<ul style="list-style-type: none"> Ore and metals processing. (EPA 2020) Piston-engine aircraft operate on leaded aviation fuel. (EPA 2020) Waste incinerators, utilities. (EPA 2020) Lead-acid battery manufacturing process. (EPA 2020) 	<ul style="list-style-type: none"> Decreases growth and reproductive rates of plants (EPA 2020). Neurological effects in vertebrates (EPA 2020). 	<ul style="list-style-type: none"> Anemia (Senarath 2005) Weakness (Senarath 2005, WHO 2014b) Kidney and brain damage (Senarath 2005) High exposure can cause death (Senarath 2005)

Table 2a: WHO and SAR countries' AAQS.

Pollutant	Averaging-Time	Maximum Concentration (Ambient air)												
		WHO	Sri Lanka	Nepal	Bangladesh	India	Pakistan	Bhutan	Afghanistan					
		[µg.m ⁻³]	[µg.m ⁻³]	ppm	[µg.m ⁻³]	ppm	Industrial Area, Residential, Rural & Other Areas [µg.m ⁻³]	Ecologically Sensitive Area (Notified by Central Govt) [µg.m ⁻³]	[µg.m ⁻³]	Industrial Area [µg.m ⁻³]	Mixed Area ¹ [µg.m ⁻³]	Sensitive Area ² [µg.m ⁻³]	[µg.m ⁻³]	
NO ₂	Annual	40	-	40	100	0.053	40.0	30.0	40	-	-	-	40	
	24hrs	-	100	0.05	80	-	80.0	80.0	80	-	-	-	80	
	8hrs	-	150	0.08	-	-	-	-	-	-	-	-	-	
	1hr	200	250	0.13	-	-	-	-	-	-	-	-	-	
SO ₂	Annual	-	-	50	80	0.33	50.0	20.0	80	80	60	15	50	
	24hrs	20	80	0.03	70	365	0.14	80.0	80.0	120	120	80	30	
	1hr	-	200	0.08	-	-	-	-	-	-	-	-	-	
	10 min	500	-	-	-	-	-	-	-	-	-	-	-	
O ₃	24hrs	-	-	-	-	-	60.0	60.0	-	-	-	-	-	
	8hrs	100	-	-	-	-	100.0	100.0	-	-	-	-	100	
	1hr	-	200	0.10	-	-	180.0	180.0	130	-	-	-	-	
CO	8hrs	-	10,000	9.00	10,000	157	0.08	-	-	5000	5000	2000	1000	30
	1hr	-	30,000	26.00	-	235	0.12	4000.0	4000.0	10,000	10,000	4000	2000	10
	30 min	-	-	-	-	-	-	-	-	-	-	-	-	60
	15 min	-	-	-	100,000	-	-	-	-	-	-	-	-	-
	Any Time	-	58,000	50.00	-	-	-	-	-	-	-	-	-	-

¹ Residential, Commercial areas

² Areas such as hospitals, schools, sensitive ecosystems

Table 2b: WHO and SAR countries' AAQS.

Pollutant	Averaging Time	Maximum Concentration in Ambient air												
		WHO	Sri Lanka	Nepal	Bangladesh	India	Pakistan	Bhutan	Afghanistan					
		[$\mu\text{g.m}^{-3}$]	[$\mu\text{g.m}^{-3}$]	ppm	[$\mu\text{g.m}^{-3}$]	[$\mu\text{g.m}^{-3}$]	ppm	Industrial Area, Residential, Rural & Other Areas [$\mu\text{g.m}^{-3}$]	Ecologically Sensitive Area (Notified by Central Govt) [$\mu\text{g.m}^{-3}$]	[$\mu\text{g.m}^{-3}$]	Industrial Area [$\mu\text{g.m}^{-3}$]	Mixed Area [$\mu\text{g.m}^{-3}$]	Sensitive Area [$\mu\text{g.m}^{-3}$]	[$\mu\text{g.m}^{-3}$]
NOx	Annual	-	-	-	-	-	-	-	-	40	80	60	15	-
	24hrs	-	-	-	-	-	-	-	-	40	120	80	30	-
PM ₁₀	Annual	20	50	-	50	-	60.0	60.0	60.0	120	120	60	50	70
	24hr	50	100	-	120	150	100.0	100.0	100.0	150	200	100	75	150
PM _{2.5}	Annual	10	25	-	15	-	40.0	40.0	40.0	15	-	-	-	35
	24hr	25	50	-	65	-	60.0	60.0	60.0	35	-	-	-	75
TSP ³	Annual	-	-	-	-	-	-	-	-	360	360	140	70	300
	24hr	-	-	230	-	-	-	-	-	500	500	200	100	-
Lead	Annual	-	-	0.5	0.5	-	0.50	0.50	0.50	1	-	-	-	0.5
	24hrs	-	-	-	-	-	1.0	1.0	1.0	1.5	-	-	-	-
Benzene	Annual	-	-	20	-	-	-	-	-	-	-	-	-	-
	24hrs	-	-	-	-	-	-	-	-	-	-	-	-	-

³ Total Suspended Particulates

Sources Table 2a, 2b: (CPCB 2009, Government of Pakistan 2010, Government of the People's Republic of Bangladesh 2013, Ministry of Environment 2003, National Environment Commission 2010, Sri Lanka Government 2008, Torabi & Nogami 2016, WHO 2005)

2020), to indicate the air quality status and its relation to health effects due to air pollutants. All national governments use a color-coded AQI (Fig. 1) to effectively circulate air quality measurements to the general public (CEA 2021a, USEPA 2021). AQI values are generally based on PM_{2.5} (Ileperuma 2020).

OAP in SAR

WHO 2021 reported that about 4.2 million premature deaths would cause worldwide (2016) due to OAP by inhaling PM₁₀ and PM_{2.5} particles. PM_{2.5} is the 5th ranking global mortality risk factor and reported 7.6% of global mortality in 2015 (Saud & Paudel 2018). Most low and middle-income countries experience the burden of ambient air pollution, specifically South-Asia and Western Pacific Regions (WHO 2021). The sources of the significant ambient air pollutants are a massive range of stationary (industries, household sources, open burning of domestic and agricultural waste and mobile (road vehicles, trains, ships) (Nandasena et al. 2012, Thishan et al. 2008).

In Sri Lanka, 40- 50% of power is generated by burning fossil fuels (NCSD 2009). Seneviratne et al. (2017) concluded that aged sea salt, soil, traffic, biomass burning, and industrial

sources distinguished as the general air pollution sources in the city, Kandy while reporting the familiar sources of particulate pollution in metropolitan Colombo is motor vehicles, road dust, and biomass. Gunathilaka et al. (2011) investigated that the atmospheric Pb and Zn amounts are more highly perceived in Colombo than that in Kurunegala, a rural city, highlighting the increased traffic in Colombo would be the reason for the OAP. The industrial sector accounts for nearly half of the total emission of SO₂ in Sri Lanka; the primary reason is the improper release of air pollutants into the atmosphere (Senarath 2005).

The reported PM₁₀ concentration variation at Colombo-Fort Air Quality Monitoring Station (AQMS) during 1998-2016 had remained relatively stable between 72-82 $\mu\text{g.m}^{-3}$ while it ranged from 55-100 $\mu\text{g.m}^{-3}$ with an increasing proving the exceedance in the annual air quality standard of 50 $\mu\text{g.m}^{-3}$ in Sri Lanka (Ileperuma 2020). In 2007, the Colombo-Fort AQMS data analysis in a day indicated a peak in CO, NO₂, and SO₂ during traffic congestion (office and school traffic) at around 8.00 am, while the O₃ showcases a steady rise with increasing the solar-intensity at noon and an increase of NO₂, SO₂ levels were reported. Dharshana et al. (2008) reported that PM₁₀ is the prominent air pollutant

in the Colombo atmosphere using the data monitored from the Colombo-Fort AQMS.

In 2016 (January - May), National Building Research Organization (NBRO) monitored exposure levels due to vehicular emissions in the country, focusing on several major cities (Colombo, Gampaha, Kalutara, Horana, Kurunegala, Ratnapura, Galle, Kurunegala, Kandy, Anuradhapura) using passive-sampling technology, according to wet-analysis methods and showcased an exceedance in average SO₂ levels in 24-hours. Recent annual air-quality (2019, 2020) measurements-reports of AQMS in Battaramulla and Kandy, Sri Lanka (Table 3), show PM levels exceed WHO acceptable limits. Further, analysis for PM_{2.5} and PM₁₀ at the same AQMS indicates a frequent exceedance in the relevant Sri Lanka standards in 2018-2019 (Ileperuma O. A. 2020), while the yearly summary in 2020 reveals a specific control in PM_{2.5} and PM₁₀ at the same AQMS (Fig. 2, 3) because of the enacted curfew and travel restrictions due to the corona pandemic situation in the country. Yet, there was a sudden unexpected increase of PM_{2.5} levels at the end of October 2020 in most of the urban cities of Sri Lanka (Jaffna, Vavuniya, Puttalam, Kegalle, Kurunegala, Anuradhapura, Kandy, Colombo, Rathnepura, Nuwara-Eliya) according to the NBRO (2020) air-quality measuring data, indicated US-AQI values in between 100-150, alerting the sensitive groups about their health while confessing the reason of this higher increase would be the prevailed wind pattern around the island and the high amount of air pollutants found at in Indian peninsular which was reported in Air Visual website within the due time period. Coarse particulates (windblown dust from deforested and eroded areas), soot, and vapor from combustion vehicles and open burnings such as agricultural and domestic waste are highly contributable to PMs (Thishan et al. 2008).

AQI values measured at Battaramulla AQMS (December 2020 - May 2021) show a satisfactory trend in lying in

good (0-50) and (51-100) moderate AQI categories (Fig. 4). But more significant than that in March-June, 2020 as being regular the human life after the 2nd wave of Covid-19 outbreak in Sri Lanka. Recently (2021), the prominent pollutants were PM_{2.5} and O₃ in Battaramulla and Kandy, Sri Lanka (CEA 2021a).

Though the OAP in Sri Lanka causes primarily due by commercial energy combustion (soot and condensed vapor highly contributed to PM_{2.5} (Thishan et al. 2008), the most significant contributor is the increased vehicle population (Senarath 2005) and traffic congestion (Ileperuma 2020). As per the updated statistics on vehicle population in Sri Lanka, the newly registered total vehicle population (Fig. 5) in 2015 is the maximum throughout the past 5 years (2015-2019) (MoT 2021a). Further, the total new registration of vehicles dramatically reduced in 2019 to 367,303 (in 2018, it was 479,340) due to government taxes and some measures taken to limit vehicle importation to Sri Lanka (MoT 2021b, NTC 2017). Overall vehicle registration from 1997 to 2019 devoted 50% in Western Province, Sri Lanka (Ileperuma 2020). Meanwhile, private vehicles have a higher rate of registering than that public vehicles and tend to increase outdoor air pollution due to the formation of higher traffic congestion (dust stirring), uncomfortable road conditions as well as low priority for vehicle maintenance and fuel efficiency, mainly in Colombo city (Senarath 2005). However, the total vehicle population has been increasing each year respectively, making considerable weight into ambient air pollution in the country.

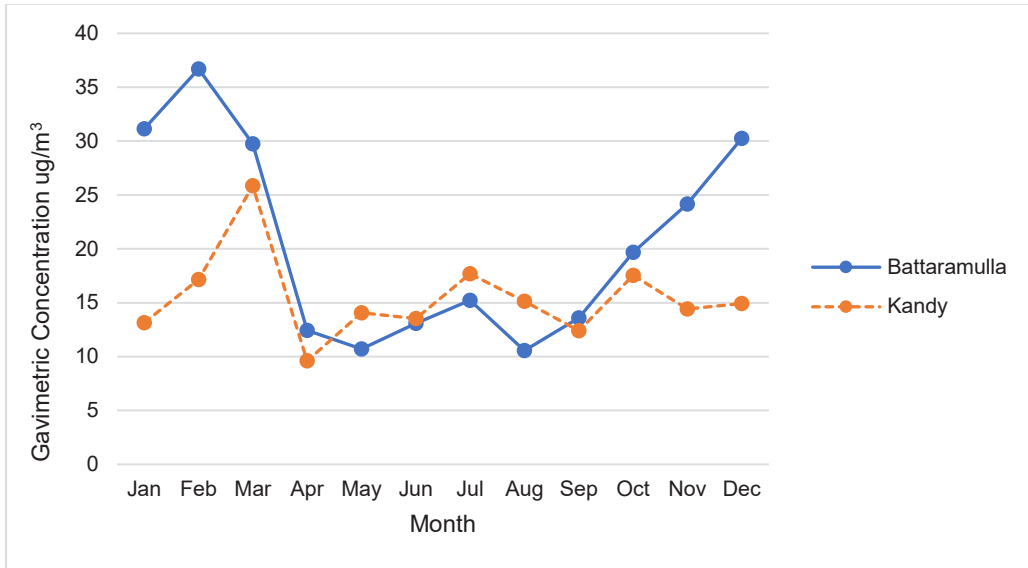
Further, improper economic and planning policies have become the parent cause of the problems relating to ambient air pollution in Colombo by today; the use of low-quality fuels, incoherent traffic management policies, poor land-use planning, and use of reconditioned vehicles and engines are some of the examples that contribute to the OAP problem (Thishan et al. 2008, Torabi & Nogami 2016).

Table 3: Annual Air Pollutant Averages in Sri Lanka 2019, 2020 (Central Environment Authority AQMS) (CEA 2021b).

Pollutant	Mean Concentration ^{4,5}			
	2019		2020	
	Battaramulla AQMS	Kandy AQMS	Battaramulla AQMS	Kandy AQMS
O ₃	13.68	11.74	15.72	15.71
CO	629	673	237	912
NO ₂	11.41	13.36	11.18	8.72
SO ₂	5.77	1.65	6.87	1.17
PM _{2.5}	21.36	16.49	21.18	15.10
PM ₁₀	40.35	42.68	35.66	38.66

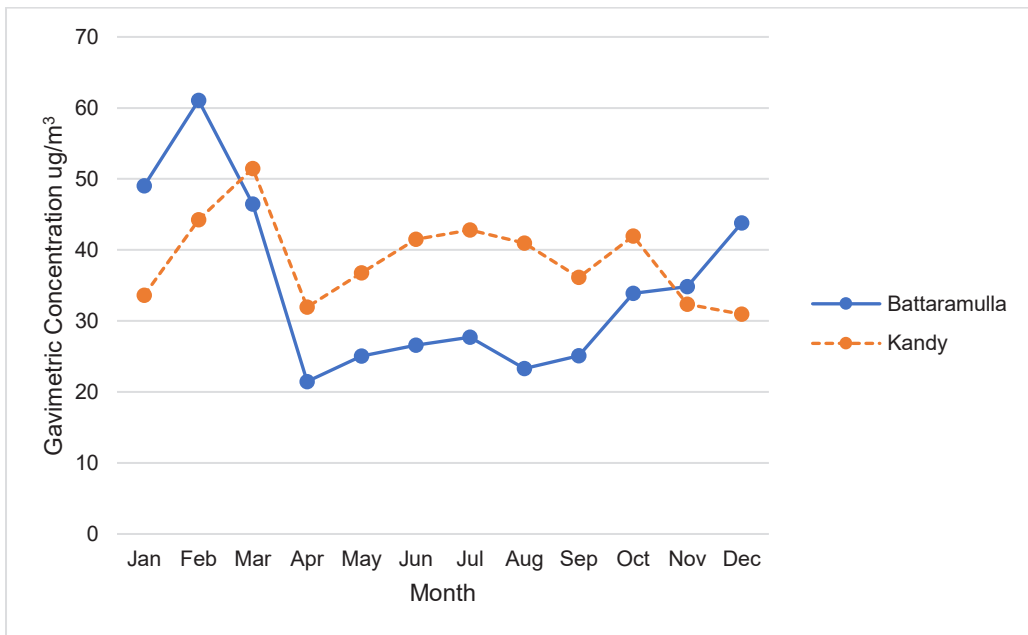
⁴ Gas concentrations in 'ppb' and Particulates in 'µg.m⁻³'

⁵ Averaging Method: Averages of 1hr (Hourly) Concentrations



[Source: Central Environmental Authority, Sri Lanka]

Fig. 2: PM_{2.5} by Month (Diurnal) Battaramulla and Kandy in 2020 (From 01-01-2020 to 01-01-2021) PM_{2.5} Concentration 1-month Average (ug.m⁻³).

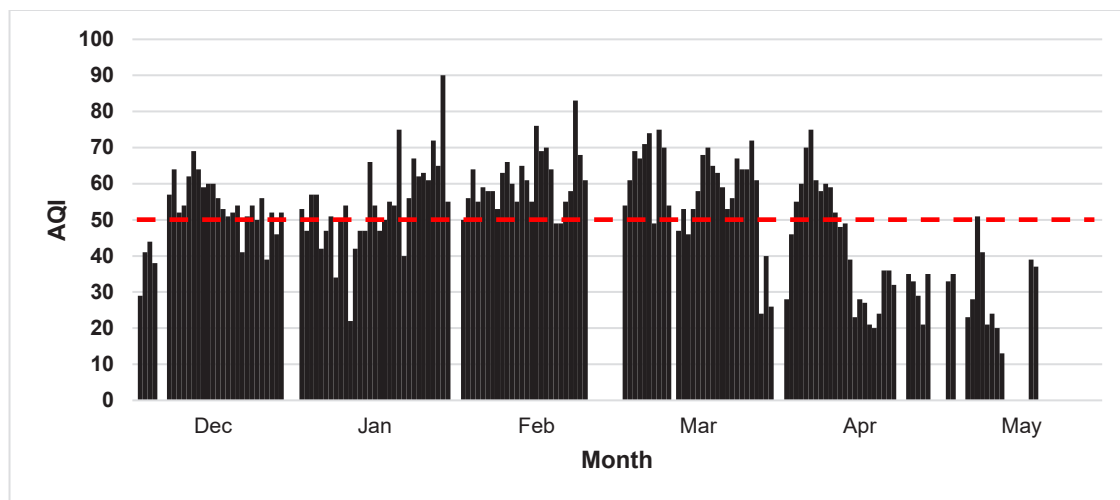


[Source: Central Environmental Authority, Sri Lanka]

Fig. 3: PM₁₀ by Month (Diurnal) Battaramulla and Kandy in 2020 (From 01-01-2020 to 31-12-2020) PM₁₀ Concentration 1-month Average (ug.m⁻³).

Liu et al. (2013) reported that the primary reasons for outdoor air pollution in Kanpur, India are industries and vehicle emissions. The dense population and the higher usage of motor vehicles significantly contribute to OAP in Pakistan and Bangladesh (Hopke et al. 2008). Pakistan Environmental Protection Agency (PEPA) reports that air

pollution levels in major cities of Pakistan delineated seven times higher than the WHO permissible levels (Purohit et al. 2013). Kathmandu (Nepal) possessed 4.78% population growth in 2011 amidst the country’s rapid urbanization. The registered number of vehicles has been more than 32 times within the last 1.5 decades (~ 2000–2016), susceptible to in-



[Source: Central Environmental Authority, Sri Lanka; Some AQI values are missing due to the power failure of AQMS, Battaramulla]

Fig. 4: Ambient AQI at Battaramulla AQMS (From Dec 2020 to May 2021).

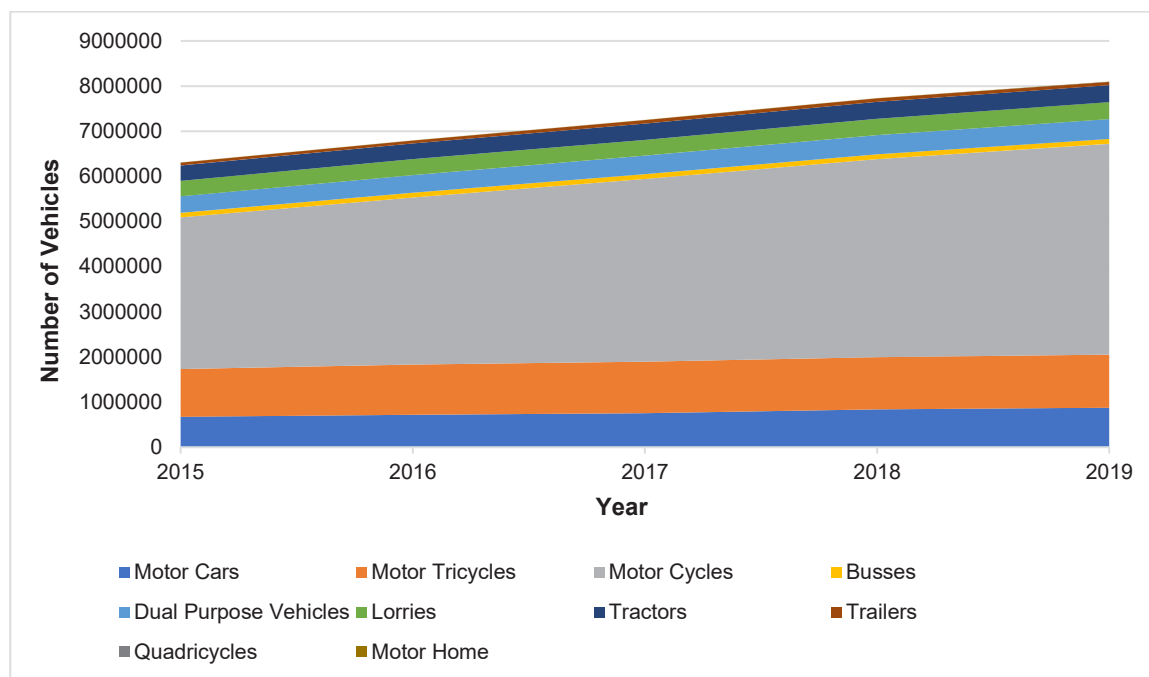


Fig. 5: Total vehicle population in Sri Lanka 2015-2019 (MoT, 2021b; NTC, 2017).

crease air pollution in Nepal (Saud & Paudel 2018). The key factors are the ongoing industrial activities without proper air pollution control, inefficient energy usage, higher numbers of motor vehicle usage, and open burning of solid waste and plastics (Purohit et al. 2013, Saud & Paudel 2018). In Afghanistan, massive traffic congestion due to limited road capacity, poorly maintained timeworn vehicle usage, using electric generators, combustion processes, using poor fuel

quality, and population growth are the significant reasons for OAP (Mehrad 2020, Torabi & Nogami 2016). Thereby it accounts for about 75% of OAP in Afghanistan by 2020, and been reported that old and smoky cars are the primary source of O₃ concentration in Kabul and in 2019, NO₂ (305 µg/m³ – 1-hour average) and SO₂ (63.7 µg/m³ – 1hours average) expose a significant exceedance in that of WHO permissible concentration level in Kabul ensuring the failure

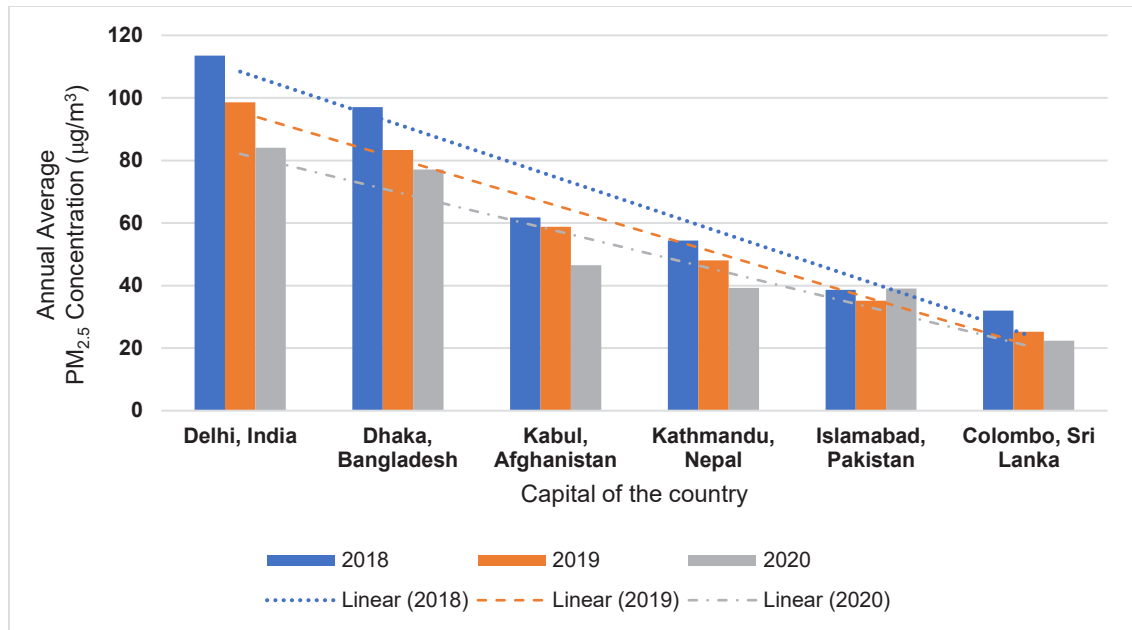


Fig.6: Annual average $PM_{2.5}$ concentration of the SAR (Visual, 2018, 2019, 2020).

of adapting to an efficient air quality plan in the country (Mehrad 2020). Also, the higher NO_2 concentration is why the frequently occurring smog in Kabul (Mehrad 2020). Begum 2017 reveals that cars, trucks, and industrial activities are the primary reason for the highest emissions of black carbon in SAR. Pollutant exposures have increased considerably due to improper management of waste, construction, and energy derived from dirty fuels in developing countries in SAR (Brauer et al. 2016).

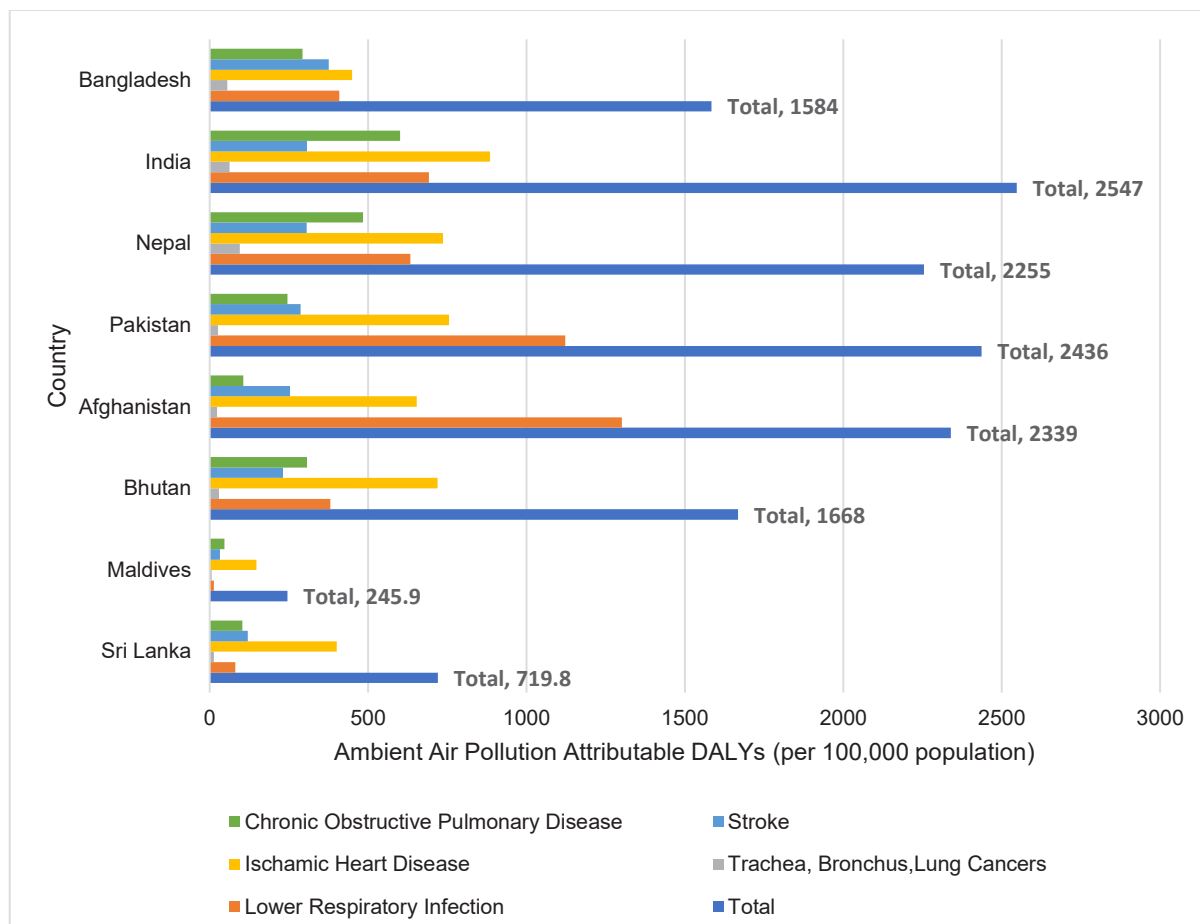
PM levels in SAR report alarming levels owing to more air pollution in most cities (Fig. 6). The overall impact of $PM_{2.5}$ in SAR has been reduced linearly from 2018 to 2019. Limiting traveling and transportation due to the Covid-19 pandemic would be the reason, along with the weather (rain and tropical cyclones occurred during the period). In 2019, about 32% of the days were reported as unhealthy, with AQI values between 101-300 in Kabul, Afghanistan (Mehrad 2020). In 2018 and 2019, Delhi (India), Dhaka (Bangladesh), and Kabul (Afghanistan) were reported as the most polluted cities in the world (Mehrad 2020). Generally, the PM disperses readily in India, Nepal, Bangladesh, and Pakistan due to lower humidity-level and increased wind speeds in the summer. Yet, it traps PMs on the ground surface in winter, increasing PM air pollution, and PM concentration tends to decrease as it settles down with rainfall in the monsoon season (Junaid et al. 2018). In 2019, $PM_{2.5}$ and PM_{10} concentrations indicated an alarming level in Kabul, Afghanistan exceeding the WHO permissible levels (Mehrad 2020). Qiu et al. (2021), studied the air pollution levels in major cities in

Bangladesh using multi-sensor readings and investigated a significant reduction of PM_{10} , $PM_{2.5}$, and gaseous pollutants except for O_3 during the strict and partial lockdown in 2020 when compared to that in 2019 and reported that the reason for reducing of O_3 concentration might be the prevailed sunny weather during the strict lockdown period (2020) in Bangladesh.

Economic aspects indicate that the possible economic loss is estimated to be about USD 7.0 million due to OAP (due to $PM_{2.5}$) in Colombo. An undertaken case study in Kanpur, India, estimated that the annual economic benefit of approximately 3.96 million US dollars could be achieved by uplifting air quality to safe levels per 2.7 million population (Nandasena et al. 2012). Pakistan's government undergoes about US\$ 250 to US\$ 350 million in economic losses alone due to deaths attributable to vehicular emission air pollution (Purohit et al. 2013). Thus, there is a burden on economic status in SAR due to prevailing health outcomes that are directly attributable to IAP and OAP.

OAP AND HEALTH IN SAR

Ghaffar et al. (2004) stated that the primary reason for chronic respiratory diseases in SAR is the effect of chronic obstructive airway diseases (emphysema and chronic bronchitis) and asthma due to OAP and IAP exposures. Cohen et al. (2017) concluded that exposure to $PM_{2.5}$ is directly attributable to mortality from cardiovascular disease (IHD and cerebrovascular disease) and DALYs globally with



[Source: WHO Country Health Statistics-2016 (WHO 2016).

Fig. 7: Ambient Air Pollution attributable DALYs values (per 100,000 population) in SAR.

respect to OAP.

PM_{2.5} is more perilous compared to PM₁₀ because of its properties, such as deep penetration into the alveolar sacs, high adsorption capacity, and large surface area (Xing et al. 2016). Dharshana et al. (2018) revealed that PM₁₀ is significantly related to three types of respiratory diseases (bronchitis, emphysema, and chronic obstructive pulmonary diseases) among children (Tables 1a, 1b). A high prevalence of obstructive airway disease is directly associated with industrial pollution in Sri Lanka (Premaratna et al. 2002). Researchers observed that there would be a high tendency of increased asthma with exposure to dust at home for children of 11 years of age (Karunasekera et al. 2009). Cardiovascular mortality is convincing solid evidence for the OAP, and pre-existing cardiovascular diseases and smoking predisposes cause adverse exposure to air pollution (Nandasena et al. 2012).

Senanayake et al. (2004) reported that Lead exists for 50 days in soft tissue while having a half-life of 25 days in the

bloodstream, causing terrible health problems to almost all humans with no age limits. In Sri Lanka, studies have proved that the most people living in and adjacent to traffic-congested areas, traffic police officers approach the interim toxic levels of blood lead concentrations (Senanayake et al. 2004). Higher abdominal discomfort, tremor, and hypertension levels were more common among traffic police officers than non-traffic police officers, although the differences were insignificant. The exposure misclassification would be led to non-traffic police officers being duty-bound to control traffic during busy hours. Nandasena et al. (2012) suggested through their study that the respiratory health status of school children living in urban areas is much poorer than that of children from semi-urban areas due to poor outdoor air quality. Senanayake et al. (2009) reported that the highest recorded SO₂ and oxides of Nitrogen levels in Colombo correlate with hospital attendance rate that was primarily correlated with the air pollution in Colombo and investigated that there exists an association between air pollution and drastic

wheezy occurrence in children in Colombo by analyzing the correlation between daily rates of nebulization and ambient air pollutant levels.

About 2500 people die due to air pollution combined with vehicular emissions every year in Pakistan (Purohit et al. 2013). Lahore, the most polluted city in Pakistan (2018), afflicted with heavy smog due to industrialization and urbanization, lacks a proper air quality action plan and results in more perilous health issues that cause premature deaths by cardiac pathologies and exacerbation of asthma allergies, respiratory tract infections, and eye infections. Liu et al. (2013) reported a higher correlation between OAP and cardiopulmonary diseases in Kanpur, India, indicating an alarming situation in 2006. Non-communicable diseases such as lung cancer, chronic obstructive pulmonary disease (COPD), heart diseases, strokes, allergies, eye infections, respiratory illness, etc., have become more alarming in Nepal today (Saud & Paudel 2018).

The Sri Lankan Disability Adjusted Life Years (DALYs) value for OAP is somewhat less, unlike other SAR countries. At the same time, the Maldives is the neap (Fig. 7). India indicates the highest rate of DALYs value attributable to OAP, proving the country's poor outdoor air quality among other countries in the SAR. Generally, SAR is far behind the world in outdoor air quality. The primary reason would be less consideration and advocacy towards air quality management (WHO 2005).

Maldives' ambient air quality is generally said to be in a pristine state because the sea breezes flush the air masses over the islands by keeping air over the islands fresh to some extent through transboundary air pollution (generally,

90% of PM_{2.5} results from transboundary sources in Male, Maldives) (Hameed et al. 2019, SACEP 2001). IAMAT 2020 states that Maldives is considered to possess safe air quality in accordance with WHO guidelines the recent data indicate that the annual mean concentration of PM_{2.5} (8.0 µg.m⁻³) is prevailing below the WHO permissible maximum value and frequently has low levels of SO₂ (µg.m⁻³) compared to other SAR countries throughout the year (Hameed. et al. 2019).

Better immunization coverage, better nutrition indicators, widely accessible and well-established public health system would help mitigate adverse health problems in the presence of OAP exposures (Nandasena et al. 2012). Unlike India, Pakistan, Bangladesh, etc., Sri Lanka possesses an excellent public health profile that OAP causes, albeit far from the world.

MINIMIZE OAP EFFECTS

WHO (2018) published a set of successful policies assisting policymakers in mitigating air pollution to secure public health in the world by considering several categories (Table 4).

The air quality of a country can be enhanced through favorable policies in the long run by minimizing polluting sources and exposed population, also encouraging a city structure that would minimize pollution emissions (World Bank 2016). Unfortunately, urban regulations in SAR have historically contributed to the misallocation of land use and the growth of urban shapes that are not necessarily conducive to air quality improvement and economic development (World Bank Group 2002). Existing political platforms, such as the South Asian Association for Regional Cooperation,

Table 4: Successful Policies Proposed by WHO to Mitigate Air Pollution (WHO 2018).

Category	Description
Industry	<ul style="list-style-type: none"> • Use clean technologies that demote flue (E.g., biogas) • Optimistic waste management
Energy	<ul style="list-style-type: none"> • Use clean, affordable fuel for household cooking, heating, lighting
Transport	<ul style="list-style-type: none"> • Develop walking, and cycling networks • Develop public transportation • Shifting to clean fuel (including less sulfur content), low-emissions vehicles • Maintain the quality of vehicles
Urban Planning	<ul style="list-style-type: none"> • Improve the energy-efficient means/ ways of building • Make greenish cities
Power Generation	<ul style="list-style-type: none"> • Augment the use of renewable combustion-accessible power sources (hydropower, wind, solar energy) • Limit the usage of high-emissions fuels • Co-generation of heat and power • Implement distributed energy generation (Rooftop solar grids, mini-grids)
Municipal and Agricultural Waste Management	<ul style="list-style-type: none"> • Implement strategic plans for waste reduction, waste separation, recycling, waste reprocessing (E.g., Feasible, Low-cost, Environmental friendly biological waste management (Produce biogas; anaerobic waste digestion))

should be authorized and leveraged to perform action plans to improve air quality (Begum 2017).

Sri Lanka has taken many actions such as the Clean-Air 2000 Action Plan, standards revisions in 2007 and 2015 for fuel quality (reducing Sulphur in fuel from 0.5% to 0.25%) and vehicle importation, banning of leaded-petrol, controlling of importing two-stroke vehicles and introducing Vehicle Emission-maintenance Testing (VET) programs since 1992. Still, most of these have been limited to papers due to political and socio-economic issues (Ileperuma 2020, Thishan et al. 2008). In Sri Lanka (2002), tetraethyl lead was removed from the petrol initiative to the “Clean-Air Action Plan-2000.” Drastically it realizes a significant reduction in lead in blood being positive in reducing the risk of environmental lead exposure and also reported a reduction in atmospheric lead in Colombo one year after introducing the free lead petrol in Sri Lanka (Ileperuma & Oliver 2010, Senanayake et al. 2004).

India has standardized a National AAQS of annual 40 $\mu\text{g}/\text{m}^3$ $\text{PM}_{2.5}$ concentrations to improve the country's air quality and enhance both economic and social development by introducing the “2018 legislation” emission scenario accessing the effective additional policy interventions, including all emission control measures, standards, regulations (Purohit et al. 2019). In 2017, “Harith Diwali” and “Swasth Diwali” campaigns were launched involving about 2000 schools in Delhi and over two lakh schools in the country by the Indian government as an advocacy for mitigating air pollution (MoEFCC 2020).

In Bhutan, the National Environment Protection Act -2007 regulates the legal framework for environmental protection and management and aims to broaden green space and reduce dust through the act. National Human Settlements Strategy-2017 and finer public transport system promoting electric vehicles are some strategies that aim to uplift the ambient air quality in the country Bhutan (NEC 2020).

Municipal solid waste, non-ferrous metal smelting, and galvanizing activities result in emitting Zinc and contribute to a fine fraction as well as two-stroke emissions consequentially contribute to the urban dust; coarse fraction and literature explained that regulating such activities in Bangladesh could be able to witness a substantial decrease in PM levels together with reported a decreased value of one third from the previous airborne particulate matter concentration as a result of the introduction of unleaded gasoline in 1999 (Hopke et al. 2008).

Air quality monitoring is a confident manner of an effective air quality management system. Almost all the SAR countries maintain ambient air-quality monitoring systems nationally. In 1997, automated air quality monitoring

stations, Peak and Background stations, were authorized at Colombo Fort and Baudhdhaloka Mawatha (Ileperuma O. A. 2020). NBRO is maintaining a mobile AQMS at Colombo Municipal Council, Sri Lanka. The Indian government is executing a national program: The “National Air Quality Monitoring Program” (NAMP), for ambient air-quality monitoring (MoEFCC 2020). “CLEAN” laboratory; Pakistan regularly monitors the air in Islamabad, Pakistan (PEPA 2021). In Bhutan, automatic stations to monitor air quality are being installed to track whether the industries comply with the national environmental standards (NEC 2020).

Thus, Bhutan, Maldives, and Sri Lanka own optimistic air quality nationwide, unlike other countries in SAR, and should be empowered with public awareness programs through social interventions. Optimum policies in consuming clean fuels, managing pollutant exposures and emissions, and establishing efficient infrastructures would help to mitigate OAP.

CONCLUSION

Sri Lanka prevails in an optimum stage in air pollution compared to other countries in SAR. The available data sources indicate that the air quality of Maldives is outstanding among other countries in SAR. Higher population and less public awareness of air quality guidelines and health effects have uplifted countries like India, Bangladesh, and Nepal toward polluted air, specifically among other SAR Countries. Consuming efficient energy means clean fuels, obey to air quality guidelines, often air quality monitoring and a colossal public awareness of air pollution and its mitigating techniques make a country with magnificent national air quality. Most of the countries in SAR suffer a huge loss of GDP due to the health effects of air pollution. Quantitative and qualitative research studies should be performed to mitigate air pollution. The rules and regulations should be updated regularly while continuing regular monitoring of air pollution in a country to achieve good air quality.

ACKNOWLEDGEMENTS

This study is supported by the University Research Grant, Faculty of Technology, University of Sri Jayewardenepura, Sri Lanka (Grant No: ASP/01/RE/FOT/2017/76).

REFERENCES

- Begum, B. 2017. Tackling the health burden of air pollution in South Asia. 2017. *Brit. Med. J.*, 359: j5209. doi: 10.1136/bmj.j5209, 359. doi:10.1136/bmj.j5209
- Brauer, M., Freedman, G., Frostad, J., van Donkelaar, A., Martin, R.V., Dentener, F. and Cohen, A. 2016. Ambient air pollution exposure estimation for the global burden of disease 2013. *Environ. Sci. Technol.*, 50(1): 79-88. doi:10.1021/acs.est.5b03709

- CEA. 2020. Air Quality Monitoring. Retrieved from <http://www.cea.lk/web/en/air-quality> (accessed 28-06-2020)
- CEA. 2021a. Ambient Air Quality Monitoring. Retrieved from <http://203.115.26.10/2020/Air%20Quality%20Web/Scaffold/index.html> (accessed 06-03-2021)
- CEA. 2021b. CEA AQMS Annual Air Pollutant Averages in Sri Lanka for 2019, 2020 (Data Retrieved from Air Quality Department of CEA, Colombo on 27-03-2021).
- Cohen, A.J., Brauer, M., Burnett, R., Anderson, H.R., Frostad, J., Estep, K. and Forouzanfar, M.H. 2017. Estimates and 25-year trends of the global burden of disease attributable to ambient air pollution: an analysis of data from the global burden of diseases study. 2015. *Lancet*, 389(10082): 1907-1918. doi:10.1016/s0140-6736(17)30505-6
- CPCB. 2009. National Ambient Air Quality Standards, India. Retrieved from https://www.jspcb.nic.in/upload/uploadfiles/files/National_Ambient_Air_Quality_Standards.pdf (accessed 28-05-2020)
- EPA. 2020. Criteria Air Pollutants. Retrieved from <https://www.epa.gov/criteria-air-pollutants> (accessed 28-05-2020)
- Ghaffar, A., Reddy, K.S. and Singhi, M. 2004. Burden of non-communicable diseases in South Asia. *Brit. Med. J.*, 328(7443): 807-810. doi:10.1136/bmj.328.7443.807
- Government of Pakistan. 2010. The Gazette of Pakistan. Ministry of Environment, Government of Pakistan. Retrieved from <http://environment.gov.pk/images/rules/SRO2010NEQSAirWaterNoise.pdf> (accessed 28-06-2020)
- Government of the People's Republic of Bangladesh. 2013. Monthly Air Quality Monitoring Report. Retrieved from http://case.doe.gov.bd/file_zone/reports_publications/monthly_reports/Monthly-Report_March_2013_REV1.0.pdf (accessed 28-06-2020)
- Gunathilaka, H.N., Ranundeniya, R.M.N.S, Najim, M.M.M. and Seneviratne, S. 2011. A determination of air pollution in Colombo and Kurunegala, Sri Lanka, using energy dispersive X-ray fluorescence spectrometry on *Heterodermia speciosa*. *Turk. J. Bot.*, 35: 439-446. doi:10.3906/bot-1006-15
- Hameed, M.A., Ajmal, I. and Malley, C. 2019. National Action Plan on Air Pollutants. Republic of Maldives. Retrieved from <https://www.environment.gov.mv/v2/wp-content/files/publications/20160920-pub-national-action-plan-on-air-pollutants.pdf> (accessed 29-06-2020)
- Hasnat, T., Kabir, G.N., Alamgir, M.D., Hossain, M. and Akhter, M.D. 2018. Major environmental issues and problems of South Asia, particularly Bangladesh. In Hussain, C.M. (ed), *Handbook of Environmental Materials Management*, Springer, Cham, pp. 1-40.
- HEI 2004. Health Effects of Outdoor Air Pollution in Developing Countries of Asia: A Literature Review. Retrieved from Boston MA: <https://www.healtheffects.org/system/files/SpecialReport15.pdf> (accessed 06-07-2020)
- Hopke, P.K., Cohen, D.D., Begum, B.A., Biswas, S.K., Ni, B., Pandit, G.G. and Markowicz, A. 2008. Urban air quality in the Asian region. *Science of The Total Environment*, 404(1), 103-112. doi:<https://doi.org/10.1016/j.scitotenv.2008.05.039>
- IAMAT. 2020. Maldives General Health Risks: Air Pollution. Retrieved from <https://www.iamat.org/country/maldives/risk/air-pollution> (accessed 19-06-2020)
- Ileperuma, O.A. 2010. Environmental pollution in Sri Lanka: A review. *J. Nat. Sci. Found. Sri Lanka*, 28: 2644. doi:10.4038/jnsfsr.v28i4.2644
- Ileperuma O. A. 2020. Review of air pollution studies in Sri Lanka. *Ceylon Journal of Science*, 49(3), 225-238. doi:<http://doi.org/10.4038/cjs.v49i3.7773>
- Jacquemin, B., Kauffmann, F., Pin, I., Le Moual, N., Bousquet, J., Gormand, F. and Siroux, V. 2012. Air pollution and asthma control in the Epidemiological study on the Genetics and Environment of Asthma. *J. Epidemiol. Comm. Health*, 66(9): 796-802. doi:10.1136/jech.2010.130229
- Junaid, M., Syed, J.H., Abbasi, N.A., Hashmi, M.Z., Malik, R.N. and Pei, D.S. 2018. Status of indoor air pollution (IAP) through particulate matter (PM) emissions and associated health concerns in South Asia. *Chemosphere*, 191: 651-663. doi:10.1016/j.chemosphere.2017.10.097
- Karunasekera, K.A.W., Perera, K.P.J., Perera, T. and Abeynarayana, J. 2009. Genetic and environmental risk for asthma in children aged 5-11 years. *Sri Lanka J. Child Health*, 34: doi:10.4038/sljch.v34i3.398
- Kumar, R., Barth, M. C., Pfister, G. G., Delle Monache, L., Lamarque, J. F., Archer-Nicholls, S., Walters, S. 2018. How Will Air Quality Change in South Asia by 2050? *123(3): 1840-1864*. doi:<https://doi.org/10.1002/2017JD027357>
- Liu, H.Y., Bartonova, A., Schindler, M., Sharma, M., Behera, S.N., Katiyar, K. and Dikshit, O. 2013. Respiratory disease in relation to outdoor air pollution in Kanpur, India. *Arch. Environ. Occup. Health*, 68(4): 204-217. doi:10.1080/19338244.2012.701246
- Mehrad, A. 2020. Causes of air pollution in Kabul and its effects on health. *Indian J. Ecol.*, 47: 997-1002.
- Ministry of Environment 2003. Annex 7.1 National Ambient Air Quality Standards for Nepal, 2003. Retrieved from <https://www.bpc.com.np/uploads/file/eia/annexes/Annex-7.pdf> (accessed 19-06-2020).
- MoEFCC. 2020. Pollution. Retrieved from <http://moef.gov.in/environment/pollution/> (accessed 23-12-2020).
- MoT. 2021a. New Registration. Retrieved from <https://www.transport.gov.lk/web/index.php?> (accessed 01-02-2021).
- MoT. 2021b. Vehicle Population. Retrieved from <https://www.transport.gov.lk/web/index.php?> (accessed 01-02-2021).
- Nandasena, S., Wickremasinghe, A.R. and Sathiakumar, N. 2012. Respiratory health status of children from two different air pollution exposure settings of Sri Lanka: a cross-sectional study. *Am. J. Ind. Med.*, 55(12): 1137-1145. doi:10.1002/ajim.22020
- Nandasena, S., Wickremasinghe, A.R. and Sathiakumar, N. 2012. Air pollution and public health in developing countries: Is Sri Lanka different? *J. Coll. Comm. Phys. Sri.*, 17: 4932. doi:10.4038/jccpsl.v17i1.4932
- National Environment Commission. 2010. Environmental Standards. Retrieved from nec.gov.bt/necs/wp-content/uploads/2020/10/Environmental-Standards-2010.pdf (accessed 22-06-2020).
- NCSD. 2009. National Action Plan for Haritha Lanka Program, Mission No-01, Clean Air Everywhere. Retrieved from <https://policy.asiapacificenergy.org/sites/default/files/National%20Action%20Plan%20for%20Haritha%20Programme.pdf> (accessed 01-07-2020).
- NEC 2020. National Environment Strategy 2020. Retrieved from http://www.nec.gov.bt/necs/wp-content/uploads/2020/10/NES-English_web.pdf (accessed 10-01-2021)
- NTC 2017. National Transport Statistics - 2017. Retrieved from Colombo 5: <https://www.ntc.gov.lk/corporate/pdf/NTCEnglishReport2017.pdf> (accessed 10-01-2021).
- PEPA 2021. CLEAN Laboratory. Retrieved from http://environment.gov.pk/desc.php?page=clean_lab (accessed 25-03-2021)
- Premaratna, R., Pathmeswaran, A., Chandrasekara, B., Dissanayake, A. S., & de Silva, H. J. 2002. Effects of pollution on health of residents in an industrial area in Sri Lanka. *Arch Environ Health*, 57(6): 579-583. doi:10.1080/00039890209602091
- Purohit, P., Amann, M., Kiesewetter, G., Rafaj, P., Chaturvedi, V., Dholakia, H.H. and Sander, R. 2019. Mitigation pathways towards national ambient air quality standards in India. *Environ. Int.*, 133: 105147. doi:<https://doi.org/10.1016/j.envint.2019.105147>
- Purohit, P., Munir, T. and Rafaj, P. 2013. 10 Scenario analysis of strategies to control air pollution in Pakistan. *J. Integr. Environ. Sci.*, 10(2): 77-91. doi:10.1080/1943815X.2013.782877
- Qiu, Z., Ali, M.A., Nichol, J.E., Bilal, M., Tiwari, P., Habtemicheal, B.A. and Rahman, M.A. 2021. Spatiotemporal investigations of multi-sensor air pollution data over Bangladesh during Covid-19 lockdown. *Remote Sens.*, 13(5): 877.
- SACEP. 2001. Environmental Legislation and Institutions in the Maldives.

- Retrieved from <http://www.sacep.org/pdf/Reports-Technical/2001-UNEP-SACEP-Law-Handbook%20-Maldives.pdf> (accessed 10-01-2021).
- Saud, B. and Paudel, G. 2018. The threat of ambient air pollution in Kathmandu, Nepal. *J. Environ. Public Health*, 20: 1504591. doi:10.1155/2018/1504591
- Saxena, P. and Sonwani, S. 2019. Primary Criteria Air Pollutants: Environmental Health Effects. In Saxena, P. and & Sonwani, S. (eds), *Criteria Air Pollutants and their Impact on Environmental Health* (pp. 49-82). Singapore: Springer Singapore.
- Senanayake, M., Samarakkody, R., Sumanasena, S., Kudalugodaarachchi, J., Jasinghe, S. and Hettiarachchi, A. 2009. A relational analysis of acute wheezing and air pollution. *Sri Lanka J. Child Health*, 30: 847. doi:10.4038/sljch.v30i3.847
- Senanayake, M.P, Rodrigo, M.D. and Malkanthi, R. 2004. Blood lead levels of children before and after introduction of unleaded petrol. *Ceylon Med. J.*, 49(2): 60-61. doi:10.4038/cmj.v49i2.3264
- Senarath, C. 2005. An overview of air pollution and respiratory illnesses in Sri Lanka. <https://www.osti.gov/etdweb/biblio/20604576>.
- Seneviratne, S., Handagiriathira, L., Sanjeevani, S., Madusha, D., Waduge, V., Attanayake, T. and Hopke, P. 2017. Identification of sources of fine particulate matter in Kandy, Sri Lanka. *Aerosol Air Qual. Res.*, 17: 0123. doi:10.4209/aaqr.2016.03.0123
- Sri Lanka Government. 2008. The National Environmental Act, No. 47 of 1980. Authority Retrieved from http://www.cea.lk/web/images/pdf/airquality/1562_22E%20Ambient%20air%20quality%20-%20english.pdf (accessed 10-01-2021).
- Thishan, D., Coowanitwong K.G. and Nowarat, M. 2008. Ambient PM10 and respiratory illnesses in Colombo City, Sri Lanka. *J. Environ. Sci. Health, Part A*, 43(9): 1064-1070. doi:10.1080/10934520802060035
- Torabi E. and Nogami A. 2016. Environmental Assessment of Suspended Particulate Matter over the Kabul City, Afghanistan.
- USEPA 2021. Air Quality Index (AQI) Basics. Retrieved from <https://www.airnow.gov/aqi/aqi-basics/> (accessed 10-02-2021).
- Visual. 2018. 2018 World Air Quality Report Retrieved from <https://www.iqair.com/world-most-polluted-cities/world-air-quality-report-2018-en.pdf> (accessed 10-03-2021).
- Visual. 2019. 2019 World Air Quality Report Retrieved from <https://www.iqair.com/world-most-polluted-cities/world-air-quality-report-2019-en.pdf> (accessed 10-03-2021).
- Visual. 2020. 2020 World Air Quality Report. Retrieved from <https://www.iqair.com/world-most-polluted-cities/world-air-quality-report-2020-en.pdf> (accessed 10-03-2021).
- World Health Organization (WHO). (2005). *Air Quality Guidelines For Particulate Matter, Ozone, Nitrogen Dioxide and Sulfur Dioxide, Global update 2005*. Retrieved from https://apps.who.int/iris/bitstream/handle/10665/69477/WHO_SDE_PHE_OEH_06.02_eng.pdf (accessed 22-05-2020).
- World Health Organization (WHO). 2014a. *WHO Guidelines For Indoor Air Quality: Household Fuel Combustion*. WHO, Geneva (accessed 23-01-2021).
- World Health Organization (WHO). 2014b. *WHO Indoor Air Quality Guidelines: Household Fuel Combustion*. Retrieved from https://apps.who.int/iris/bitstream/handle/10665/141496/9789241548885_eng.pdf? (accessed 23-01-2021).
- World Health Organization (WHO). 2016. *Ambient Air Pollution Attributable DALYs (per 100,000 population)*. Retrieved from [https://www.who.int/data/gho/data/indicators/indicator-details/GHO/ambient-air-pollution-attributable-dalys-\(per-100-000-population\)](https://www.who.int/data/gho/data/indicators/indicator-details/GHO/ambient-air-pollution-attributable-dalys-(per-100-000-population)) (accessed 23-01-2021).
- World Health Organization (WHO). 2018. *Ambient (Outdoor) Air Pollution*. Retrieved from [https://www.who.int/news-room/fact-sheets/detail/ambient-\(outdoor\)-air-quality-and-health](https://www.who.int/news-room/fact-sheets/detail/ambient-(outdoor)-air-quality-and-health) (accessed 28-05-2020).
- World Health Organization (WHO). 2021. *Air Pollution*. Retrieved from <https://www.who.int/health-topics/air-pollution> (accessed 28-05-2020).
- World Bank. 2016. *The Cost of Air Pollution: Strengthening the Economic Case for Action*. Retrieved from <https://openknowledge.worldbank.org/bitstream/handle/10986/25013/108141.pdf> (accessed 28-05-2021).
- World Bank Group. 2002. *Urban planning and air quality (English)*. Retrieved from <http://documents1.worldbank.org/curated/en/515081468101343461/pdf/multi0page.pdf> (accessed 28-05-2020).
- Xing, Y.F., Xu, Y.H., Shi, M.H. and Lian, Y.X. 2016. The impact of PM2.5 on the human respiratory system. *J. Thoracic Dis.*, 8(1): E69-E74. doi:10.3978/j.issn.2072-1439.2016.01.19



Boron Isotopic Systematics and Its Significance in Natural Processes: An Overview

Tanya Srivastava*† and Nishchal Wanjari*

*Department of Geology, Sikkim University, Gangtok, Sikkim, India

†Corresponding author: Tanya Srivastava; tanya.srivastava1711@gmail.com

Nat. Env. & Poll. Tech.
Website: www.neptjournal.com

Received: 23-09-2022

Revised: 10-11-2022

Accepted: 14-11-2022

Key Words:

Isotopes

Boron

Himalayas

Groundwater pollution

Natural processes

ABSTRACT

In recent years, interest in boron has expanded from microscopic to macroscopic levels, and several studies have contributed to understanding the role of boron in earth and natural processes. The boron isotopic composition provides a unique perspective into the crystallization process in granites, pegmatites, and temperature variations. Boron isotopic studies have been used as a tracer to understand geothermal systems, rivers, rock processes, reconstruction of pH and pCO₂, groundwater pollution, and further help in understanding the changes which have occurred in oceans through geological time. Furthermore, boron isotopes have also been utilized to understand the genesis of ores and understanding subduction processes and as a tracer in groundwater pollution. In plants, it acts as a micronutrient. However, its deficiency and the excessive amount may inhibit the growth of plants, bacteria, and fungi and may also affect the soil and aquatic microflora. Boron maintains and regulates several metabolic pathways, and its quantity above a certain level may prove detrimental to the environment. This overview explains boron isotope variations and their implications in earth sciences and natural processes.

INTRODUCTION

Radiogenic and stable isotopes have been extensively utilized for understanding various phenomena, such as earth systems, paleoclimate, ecology, the hydrologic cycle, biology, and forensic investigations. Over the past few decades, the application of stable isotopes has grown considerably, each with its unique potential for illuminating particular processes (Rasbury & Hemming 2017). Stable isotopes of carbon (¹²C and ¹³C), nitrogen (¹⁴N and ¹⁵N), and oxygen (¹⁶O, ¹⁷O, ¹⁸O) are valuable for retracing oceanic changes and past climatic conditions (Tiwari et al. 2015). Sulfur has four stable isotopes (32S, 33S, 34S, 36S), which are found in rivers, the atmosphere, lakes, and groundwater. The sulfur compounds have been tracked using stable isotopes of sulfate. To understand the sulfur cycle of marine sediments in both the present and past, stable isotopes are a crucial tool (Thode 1963, Jørgensen 2021). Silicon has three stable isotopes (²⁸Si, ²⁹Si, ³⁰Si) and silicon isotope ratios can be used to derive paleoenvironmental information, and in phytoliths may be used in archaeological studies (Leng et al. 2009).

In 1808, Joseph Louis Gay-Lussac, Humphry Davy, and Louis Jacques Thénard were the first to isolate boron by heating boron oxide with potassium metal (Davy 1808, Gay-Lussac & Thénard 1808). However, the first measurements of boron isotopes in natural materials were made in 1961 (McMullen et al. 1961). Boron with atomic number 5 has an extremely high affinity for oxygen (Lemarchand & Gaillardet 2005). When combined with oxygen, boron invariably forms trigonal and tetrahedral complexes, and boron is primarily found in weakly alkaline as the trigonal B(OH)₃ complex but in strongly alkaline conditions as the tetragonal B(OH)₄ (Baes & Mesmer 1976). Over the past years, many investigations have been conducted to determine whether boron isotopes in carbonates may be used as a proxy for paleo-ocean pH. However, for such usage of boron isotopes, both as sources or as a process proxy, it is necessary to thoroughly characterize the physicochemical processes that govern boron incorporation in carbonates and to quantify the corresponding chemical and isotopic fractionation (Hemming & Hanson 1992, Lemarchand et al. 2002, Lemarchand & Gaillardet 2005). Material science, energy research, and electronics boron have a wide range of applications in chemistry. In medical chemistry, boron is either used as an atom or cluster and in recent days, boron has been used in antibacterial, antifungal, and antiseptic

ORCID details of the authors:

Tanya Srivastava: <https://orcid.org/0000-0001-7700-1616>

Nishchal Wanjari: <https://orcid.org/0000-0002-8145-3575>

treatments (Leśniowski 2016). Boron compounds are employed in nuclear technology, rocket engines as fuel, the manufacture of heat-resistant materials, and high-resistant polymers (Yilmaz et al. 2008). Apart from this, boron isotopes have been used as a geochemical tracer, and their major applications are in the field of ore genesis, sedimentary environments, crustal mantle evolution, subduction-related processes, and cosmochemistry (Foster et al. 2018, Liu & Chaussidon 2018, Marschall & Foster 2018). Boron is important for the assimilation of nitrogen in plants and the growth of roots in nitrogen-fixing plants (Bolaños et al. 1994, Camacho-Cristóbal et al. 2005), boron isotopic composition provides a better understanding of the rate of ocean acidification during periods of warming events (Penman et al. 2014). In this study, we present a short review of the application and significance of boron isotopic systematics for understanding its importance in natural processes.

BORON GEOCHEMISTRY AND GEOCHEMICAL CYCLE

Since 1961, when the boron isotopes were first measured, several research articles have been published on boron isotope geochemistry and its analytical techniques (Spivack & Edmond 1987, Barth 1993, Aggarwal & Palmer 1995, Marschall 2018, Trumbull & Slack 2018, Wang et al. 2019). Boron is a lithophile element having two stable isotopes ^{10}B and ^{11}B , with an abundance of ~20% and ~80%, respectively (Kakihana et al. 1977, Barth 1993, Palmer & Swihart 1996, Foster et al. 2018). The boron isotopes are generally expressed as $\delta^{11}\text{B}$ as,

$$\delta^{11}\text{B}(\text{‰}) = \left[\frac{(^{11}\text{B}/^{10}\text{B})_{\text{sample}} - (^{11}\text{B}/^{10}\text{B})_{\text{standard}}}{(^{11}\text{B}/^{10}\text{B})_{\text{standard}}} - 1 \right] \times 10^3$$

And the $^{11}\text{B}/^{10}\text{B}_{\text{standard}}$ is the boron isotopic composition of the National Institute of Standards and Technology (NIST) Standard Reference Material (SRM) 951 boric acid, which is used in most of the studies, and the value of $(^{11}\text{B}/^{10}\text{B})_{\text{standard}} = 4.04367$ (Catanzaro 1970). Other isotopic reference materials for the isotope ratio of boron are NIST-SRM-952, IAEA-B1, IAEA-B2, and IAEA-B4 (Aggarwal & You 2016). There are over 250 known minerals that contain boron, the most prevalent of which are calcium, sodium, and magnesium salts (Helvacı 2017). Commercially important minerals with boron contents are represented in (Fig. 1). Boron is also found in skarns, calcareous sediments, metasediments, metamorphic minerals, mafic and ultramafic igneous rocks and minerals (Henry & Dutrow 1996). The concentration of boron (ppm) in different rocks is represented in Fig. 2 (a-c).

A significant flux of gaseous B drives the atmospheric component of the global B cycle in the form of boric acid (H_3BO_3) derived from sea salt aerosols (Park & Schlesinger 2002). Exchanges primarily determine the oceanic boron fluxes with the atmosphere; influx and outflux occur mostly due to direct precipitation, dry deposition, and gaseous absorption and outflux through seawater aerosol production (Carrano et al. 2009). By delivering boron from natural and anthropogenic sources via riverine transport, the hydrosphere is the second largest flux to the oceans (Carrano et al. 2009).

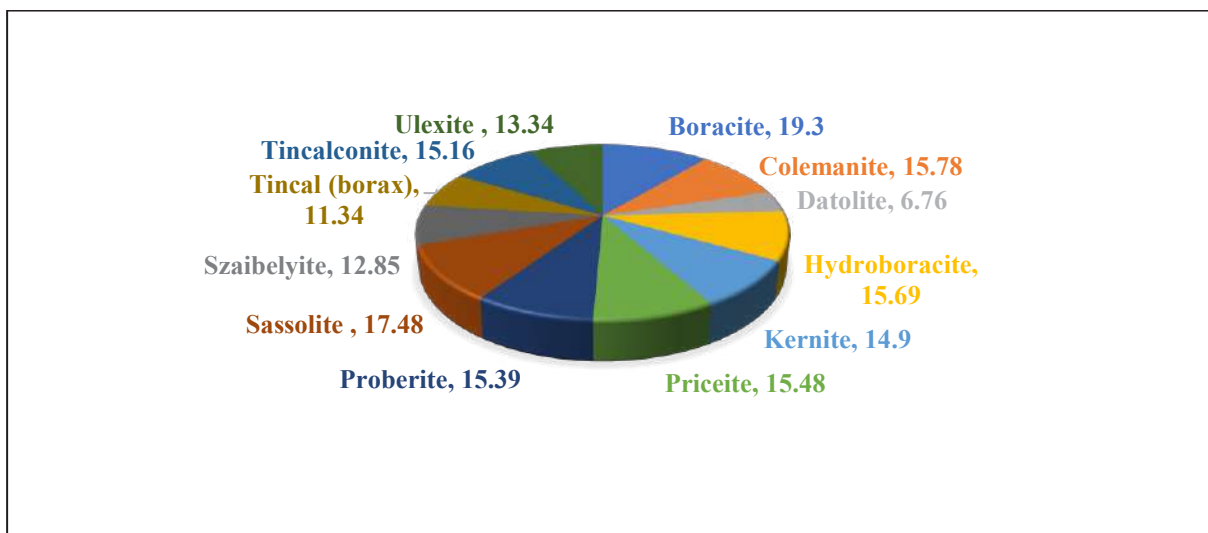
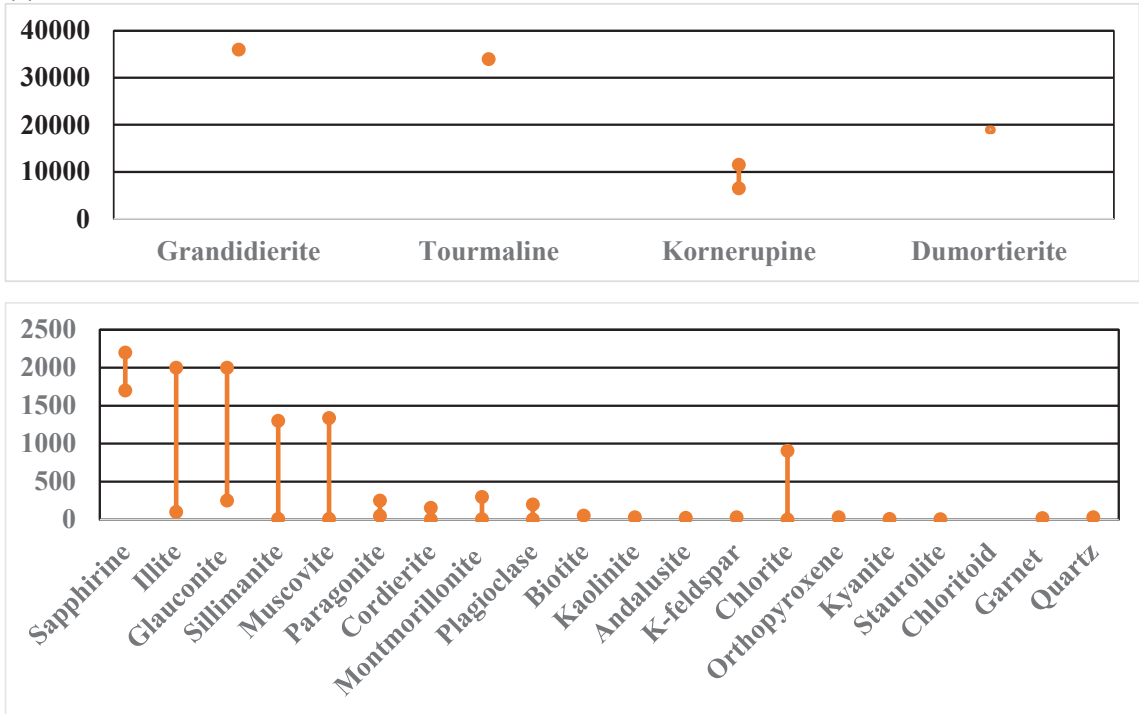


Fig. 1: Percentage of boron in commercially important boron-containing minerals Data source: Lyday (2000).

(a)



(b)

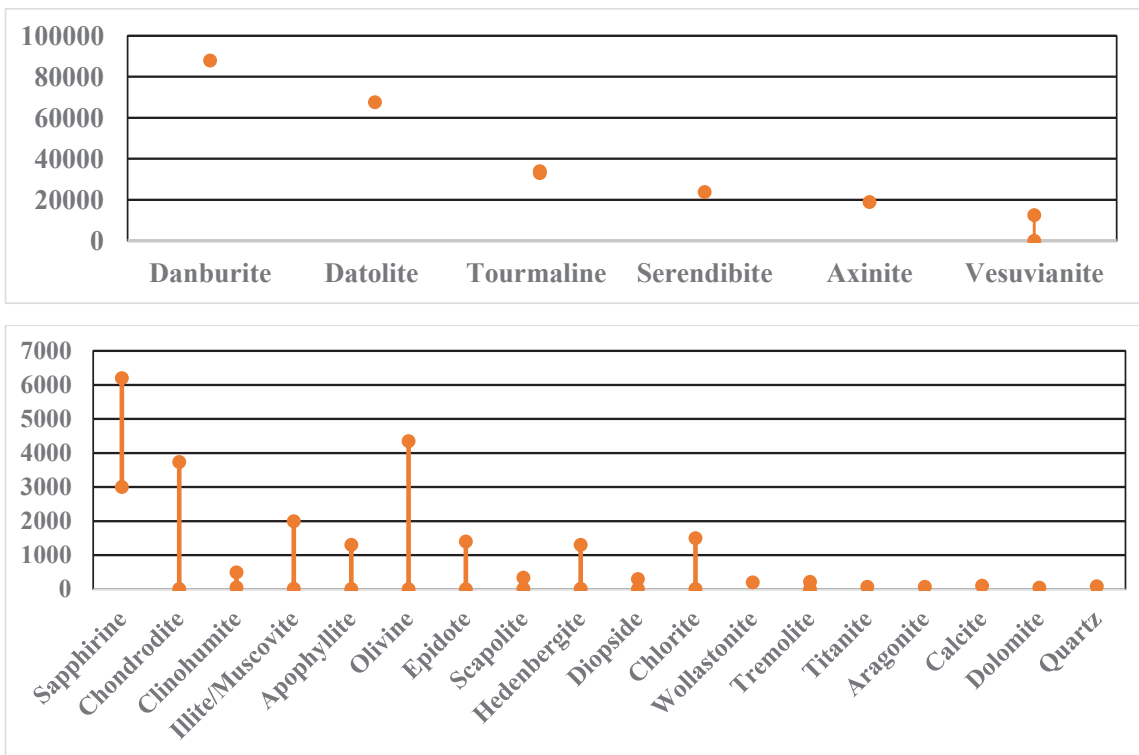


Fig. Cont....

(c)

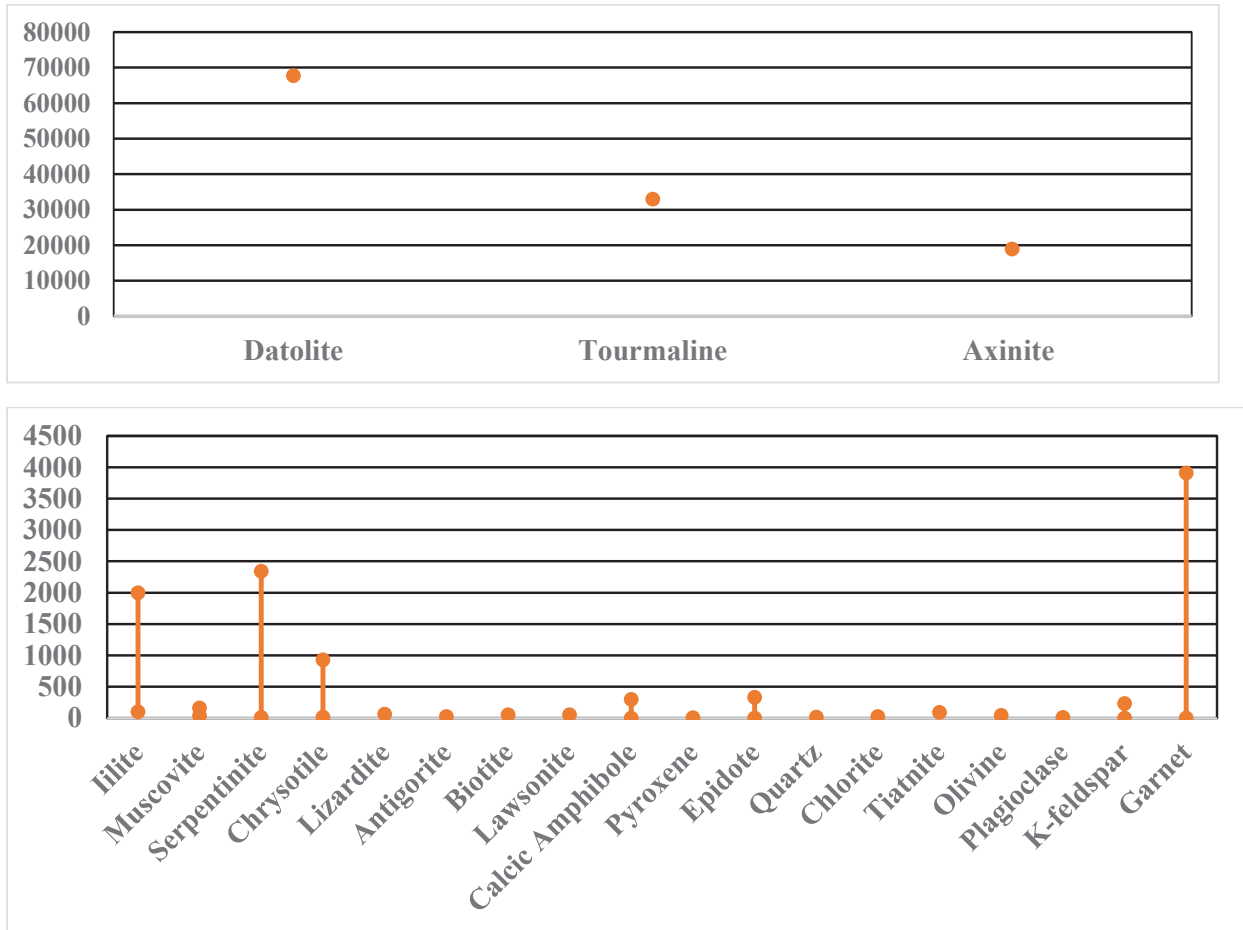


Fig. 2: Range of boron (ppm) in minerals (a) pelitic and psammitic sedimentary and metasedimentary rocks (b) calcareous sediments, metasediments and skarns (c) mafic and ultramafic igneous and metamorphic rocks. Data sources: Henry & Dutrow (1996).

METHODS FOR BORON ISOTOPE DETERMINATION

Mass spectrometry is one of the best analytical techniques that possess unparalleled sensitivity, detecting range, speed, and a plethora of uses, and it also has played a decisive role in understanding the geological processes in the past decades (Jocelyn Paré & Yaylayan 1997, Hoffmann & Stroobant 2007, Joshi et al. 2021, Banerji et al. 2022).

For boron isotope analysis, mass spectrometry is used in various ways, which include: Multi-collector and Inductively coupled Plasma Mass spectrometry (MC-ICPMS) which is relatively fast with high precision and requires a small sample size. However, it is a bit expensive (Aggarwal et al. 2003). Thermal ionization mass spectrometry (TIMS), including negative ion thermal ionization (N-TIMS), has

a higher analytical speed and requires minimal sample preparation. However, limited precision is the disadvantage of this technique (Hemming & Hanson 1994). The advantage of using Positive ionization mass spectrometry (P-TIMS) is that it has a high level of accuracy, whereas the drawback is that the sample should be pure (Aggarwal & Palmer 1995). Secondary-ion mass spectrometry (SIMS) is used in the micro-analysis of boron in various solid rock samples and does not require sample preparation (Chaussidon et al. 1997). Laser Ablation Inductively Coupled Mass Spectrometry (LA-ICPMS) has the benefit of high spatial resolution (Fietzke et al. 2010). A Triple quadrupole-based ICP system (ICP-QQQ) has the advantage of high abundance sensitivity and elimination of interferences (Fernández et al. 2015). High-resolution inductively coupled plasma mass spectrometry (HR-ICPMS) is responsible for fast analysis (Gäbler & Bahr 1999).

BORON ISOTOPES IN THE HIMALAYAN REGION

Geothermal Systems and Rivers

In the Himalayas, Steller et al. (2019) analyzed the boron isotopic and elemental concentrations from diatom-rich sediments of the Puga geothermal system in India and reported $\delta^{11}\text{B} = -41.0\text{‰}$. In Tibetan, geothermal areas $\delta^{11}\text{B}$ values vary from (-16.0 to 13.1‰) and indicate non-marine origin, whereas, in Tengchong geothermal areas in Yunnan province, $\delta^{11}\text{B}$ varies from (-11.8 to 4.2‰) (Lü et al. 2014). The boron isotopic variations in the geothermal system are plotted in Fig. 3.

In the Himalayas, the isotopic composition of the rivers varies greatly up to $\sim 35 \delta^{11}\text{B} \text{‰}$. The huge difference seen in the boron isotopic composition of Brahmaputra and Ganga may be due to the variation in the chemical composition of bedrock and silicate alteration (Rose-Koga et al. 2000). The $\delta^{11}\text{B} \text{‰}$ concentrations in Himalayan rivers are highly variable. Range from -7‰ to 29.4‰ (Rose-Koga et al. 2000) with variable major ion concentrations have differing inputs from various weathered lithologies, including evaporites, carbonates, and silicates. The boron isotopic variation of different river systems is mentioned in Fig. 4.

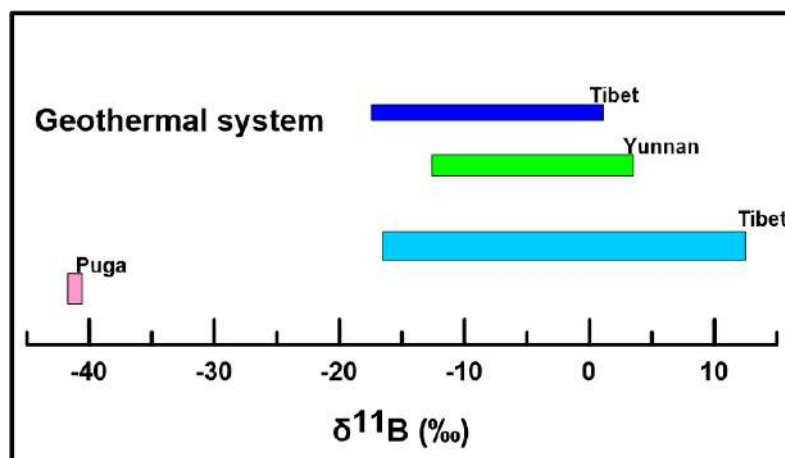


Fig. 3: Boron isotopic compositions in the geothermal system. Data sources Steller et al. (2019), Lü et al. (2014), Zhang et al. (2015).

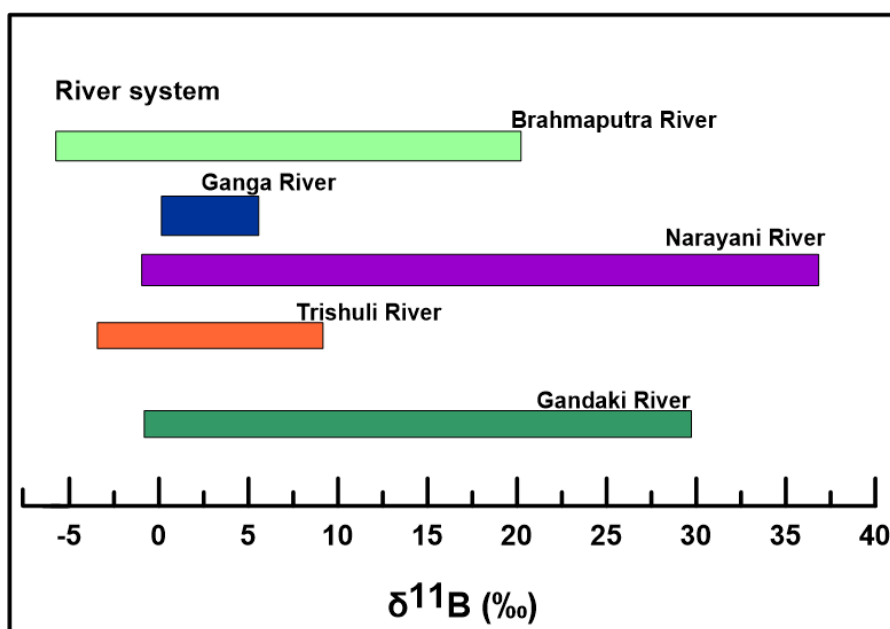


Fig. 4: Boron isotopic compositions of the river system. Data sources (Rose-Koga et al. 2000).

Igneous and Metamorphic Rocks

In the Himalayas, numerous studies on tourmaline boron isotopic and chemical compositions have been used to elucidate the genesis of leucogranite or pegmatites (Yang et al. 2015, Gou et al. 2017, Hu et al. 2018, Zhou et al. 2019, Cheng et al. 2021, Srivastava et al. 2022). In igneous petrology, boron plays an important role as a flux for silicate melts, where it lowers the solidus and liquidus temperatures and the viscosity of the melts (Dingwell 1992, London et al. 2018). In peraluminous granites, boron isotopic composition is determined by the isotopic nature of their source composition (Trumbull et al. 2008). Tourmaline is the most common borosilicate mineral in crustal rocks

analyzed for boron isotopic composition (Samson & Sinclair 1992, Trumbull et al. 2008, Marschall & Jiang 2011, Yang & Jiang 2012). Tourmaline is ubiquitous in igneous and metamorphic rocks in the Himalayas (Henry & Guidotti 1985, Henry & Dutrow 2018), and as it crystallizes at the late stage of magmatic evolution and its abundance in leucogranites makes it an appropriate tracer of source rocks and its genesis (London 1996, Kasemann et al. 2000, Van Hinsberg et al. 2011).

Some researchers inferred that tourmaline-bearing leucogranites are generated by dehydration melting of metasedimentary rocks having either muscovite, biotite, or both (Le Fort et al. 1987, Harris & Massey 1994, Harris et

Table 1: Boron isotopic compositions in the Himalayan region in different systems.

Area	Sample Description	$\delta^{11}\text{B}$ (‰)	References
Puga	Geothermal system	-41.0‰	Steller et al. (2019)
Tibet	Geothermal system	-16.0 to 13.1‰	Lü et al. (2014)
Yunnan	Tengchong Geothermal	-11.8 to 4.2‰	
Tibet	Geothermal waters	-16.57 to 0.52‰	Zhang et al. (2015)
Gandaki River Basin	Riverine	-1.7 to 29.8‰	Rose et al. (2000)
Trishuli River Basin	Riverine	-3.1 to 8.5‰	
Narayani River Basin	Riverine	-1.6 to 36.9‰	
Ganga	Riverine	0.1 to 5.1‰	
Brahmaputra	Riverine	-5.7 to 21.0‰	
Nyalam	Leucogranites (mineral: tourmaline)	-15.1‰ to -14.4‰	Yang et al. (2015)
Conadong, South Tibet	Leucogranites (mineral: tourmaline)	-9.78 to -8.53‰	Zhou et al. (2019)
	Pegmatite	-14.02 to -11.83‰	
LHS, Central Himalayas	Chlorite schist (mineral: tourmaline)	-17.8‰ to -13.9‰	Liu et al. (2022)
Main Central Thrust Zone, Central Himalayas	Quartz tourmaline (mineral: tourmaline)	-18.3 to -12.8‰	
GHS, Central Himalayas	Leucogranites (mineral: tourmaline)	-17.2 to -8.2‰	
GHS, Central Himalayas	Leucosomes (mineral: tourmaline)	-11.8 to -10.7‰	
GHS, Central Himalayas	Garnet Amphibolite (mineral: tourmaline)	-16.9 to -13.6‰	
GHS, Central Himalayas	Mica Schist (mineral: muscovite)	-22.4 to -15.4‰	
GHS, Central Himalayas	Leucogranites (mineral: muscovite)	-23.3 to -17.2‰	
Himalayas	Leucogranites (mineral: tourmaline)	-7 to -13‰	Cheng et al. (2021)
Sikkim Himalayas	Pegmatite (mineral: tourmaline)	-13.83 to -12.78‰	Srivastava et al. (2022)
Ama Drime gneiss	Ama Drime Gneiss (mineral: tourmaline)	-17.6 to -14.3‰	Hu et al. (2018)
Majba	Leucogranite (mineral: tourmaline)	-18.9 to -17.4‰	
Quedang	Metapelite (mineral: tourmaline)	-15.3 to -12.5‰	
Malaysian	Leucogranite (mineral: tourmaline)	-16.2 to -8.0‰	
Yardo	Leucogranite (mineral: tourmaline)	-8.4 to -5.4‰	
Conadong Leucogranite	Two-mica granites,	-15.80 to -13.25‰	Fan et al. (2021)
	Muscovite Leucogranite, Biotite -rich granite	-15.38 to -11.90‰	
	Biotite-rich granite (whole rock)	-11.97 to -9.00‰	

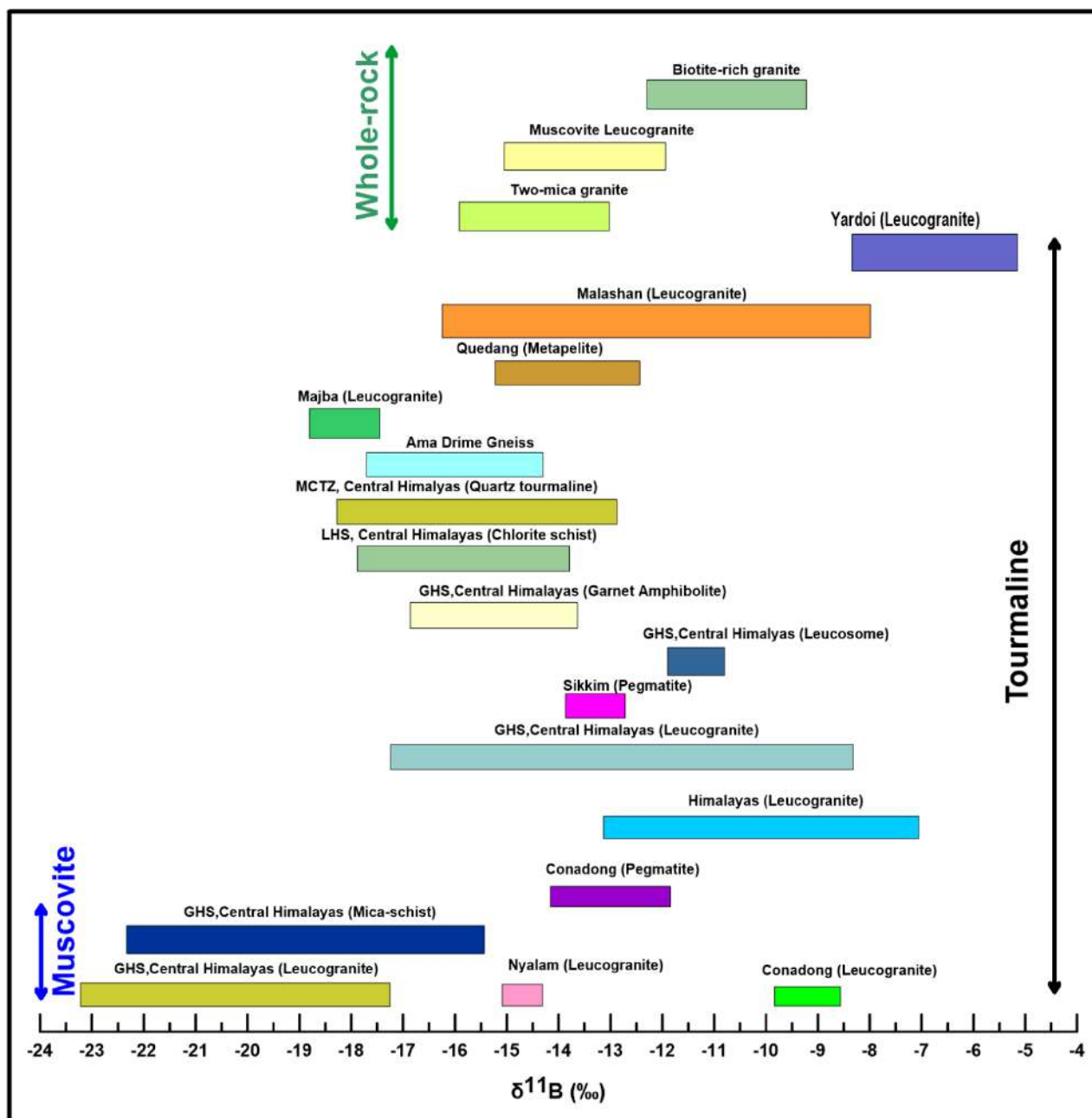


Fig. 5: Boron isotopic composition of tourmaline, muscovite, and whole rock boron isotopic composition in Igneous and metamorphic rocks from the Himalayan region. Data Sources Yang et al. (2015), Zhou et al. (2019), Liu et al. (2022), Cheng et al. (2021), Srivastava et al. (2022), Hu et al. (2018) Fan et al. (2021).

al. 1995, Guo & Wilson 2012) while a few researchers have suggested that Himalayan leucogranites are crystallized from highly fractionated magma (Wu et al. 2015, Zheng et al. 2016). Besides tourmaline, muscovite is also a major boron-bearing mineral in metasedimentary rocks and granites (Nakano & Nakamura 2001, Cheng et al. 2021, Liu et al. 2022). The

boron isotopic compositions of tourmaline and muscovite are represented in Fig. 5. Fan et al. (2021) performed whole rock-boron isotopic compositions for two-mica granite, muscovite leucogranite and biotite granite from the Conadong region represented in Fig. 5. The boron isotopic composition of the Himalayan region in different systems is compiled in Table 1.

BORON ISOTOPES IN EARTH SCIENCES AND BIOLOGICAL PROCESSES

Understanding Subduction Zone Processes

In magmatic processes, boron behaves as an incompatible trace element and is a highly fluid mobile; thus, it acts as a perfect tracer for the role and motion of water during subduction (Palmer 2017). In high-pressure metamorphic rocks, like mantle wedge peridotites boron isotope concentrations have been employed as markers for mass fluxes, mass transfer between the slab and overlying mantle, and element recycling during subduction (Palmer & Helvacı 1997, Peacock & Hervig 1999, Tonarini et al. 2001, Savov et al. 2007, Pabst et al. 2011). The abundance of boron and the isotopic compositions of fluids and lavas from subduction zone environments offer a great deal of information for understanding the mass flux along the present-day convergent boundaries of the earth (Bebout & Nakamura 2003). During serpentinization, boron is readily taken up into serpentine phyllosilicates (Pabst et al. 2011). The abyssal peridotites react with hydrothermal fluids and become serpentinized, due to which serpentine, amphibole, magnesite, and talc are formed due to the reaction of pyroxenes and olivine which are found along spreading ridges and transform faults (De Hoog & Savov 2018). Boron is significantly enriched and isotopically fractionated in subducted sediments, altered oceanic crust, and serpentinized mantle. These materials are among the most effective tools for studying fluid-mediated processes at subduction zones, and the partitioning of boron is independent of melt composition between hydrous fluids and melts (Hervig et al. 2001, De Hoog & Savov 2018). The boron from micas is either purged from the subduction-zone rocks beneath forearcs. Volcanic arcs by metamorphic fluids or is sequestered by developing tourmaline, where the boron can be entrained to even greater depths (Bebout & Nakamura 2003). The deep mantle may recycle a small amount of subducted boron even if ninety percent of subducted boron is recycled back to the surface, and boron has also been used as a tracer to probe into crustal carbonate degassing in volcanic arcs (Savov et al. 2007, Deegan et al. 2016, De Hoog & Savov 2018). In arc-related and granitic magmas, the isotope ratios of boron are sensitive indicators of subduction slab components and fluid-mediated mass transfer during subduction (Palmer 1991, Scambelluri & Tonarini 2012). The amount of boron and its isotopic composition in the altered oceanic crust are greatly influenced by the temperature and water-to-rock ratio at the time of alteration (Ishikawa & Nakamura 1992).

Mineralization

The boron sources and the fluids involved in bentonitization

in marine and non-marine environments are better understood because of the mineralogical, chemical, and isotopic analyses of smectites with variable interlayer cation occupancies from bentonite deposits in different depositional environments (Köster et al. 2019). It is seen that the boron isotope geochemistry of smectites can be used to shed light on the fluids responsible for the development of clay mineral deposits. It also offers a lot of potential for tracing fluids in other environments with authigenic clay minerals, like sedimentary basins and surfaces of crystalline rocks, as well as in artificial settings, like storage facilities for radioactive waste that is very active (Köster et al. 2019). The boron isotopes in tourmaline are useful in depicting sources (Spivack & Edmond 1987) and explicating the fluid processes (Palmer & Swihart 1996; Marschall et al. 2008). The ore-forming processes of tourmaline have been better constrained by mineralogical, chemical, and boron isotopic analyses and provide important insights on petrologic, fluid or magma origin, the evolution of genesis of ore deposits (Marschall & Jiang 2011, Trumbull et al. 2011, Yang & Jiang 2012). The composition of the boron sources mostly determines the $\delta^{11}\text{B}$ value of boron (Palmer & Slack 1989) and the variation in boron isotopes of tourmaline from large sulfide sources also depends on the composition of parent rocks (Jiang 2001). The boron isotopic fingerprints of fluids originating from magmatic-hydrothermal and basin evaporitic sources are very different, and tourmaline in hydrothermal deposits is a great recorder of fluid sources due to its refractory properties. Hence tourmaline boron isotopes can be used as the sources of fluids in iron-oxide copper gold (IOCG) (Xavier et al. 2008, Pal et al. 2010, Van Hinsberg et al. 2011). The use of boron isotopes in investigating mineral resources is a relatively new advancement, and tourmaline is the major mineral studied, particularly in large sulfide deposits and hydrothermal W-Sn associated with granites (Slack 1996).

Erosion and Weathering

The rivers are the main source of boron input into the ocean, while clay minerals are the principal boron sink, and this makes boron, in addition to its ability to trace the pH and ancient seawater, a particularly strong tracer of the weathering/erosion balance of terrestrial surfaces (Gaillardet & Lemarchand 2018). The partitioning of boron into the soluble and solid phases occurs when water and rock interact and can be included in secondary phases like clay minerals and amorphous iron oxyhydroxides, which are liberated into the hydrosphere by the dissolution of primary minerals (Ercolani et al. 2019). It has been suggested that isotopic fractionations occurring during the adsorption of riverine-dissolved boron onto detrital clays are the causes of this

significant $\delta^{11}\text{B}$ enrichment of saltwater relative to ordinary continental crust (Palmer et al. 1987).

Depositional Environment

Depositional environment and secondary enrichments affect the B content of coals from sedimentary basins, and boron has been utilized to estimate the paleoenvironments of coal reserves (Williams & Hervig 2004). Using marine and non-marine evaporite minerals, boron isotopes are useful geochemical tracers to distinguish depositional environments (Bassett 1990). The mineralogy of borates, as well as the pH of the brine borate precipitation, affect the $\delta^{11}\text{B}$ values of borates in the same depositional environment, and the minerals with the same geologic origin are observed to have decreasing $^{11}\text{B}/^{10}\text{B}$ values in the following order Na borates, Na/Ca borate and Ca borates (Oi et al. 1989, Palmer & Helvacı 1997). Apart from this, loess and paleosols also contain clay minerals, and these minerals adsorb boron resulting in boron fractionation (Zhao et al. 2003)

Paleo pH, Paleo Salinity and Paleo CO_2

It is crucial to understand the ranges of pH variations at various time scales to properly comprehend the severity of the environmental issues posed by ocean acidification, and this information is necessary to determine the pH ranges at which marine creatures may survive and further our understanding of how the oceans are absorbing atmospheric CO_2 through its many mechanisms (Pelejero & Calvo 2008). The boron isotope fractionation is a function of pH (Hemming & Hanson 1992, Sanyal et al. 1995, Lécuyer et al. 2002), and the boron isotope ratio of marine biogenic carbonates can be used to reconstruct pH and pCO_2 of seawater, as well as atmospheric CO_2 concentration (Spivack et al. 1993, Palmer et al. 1998, Zeebe & Wolf-Gladrow 2001, Kubota et al. 2015, Martínez-Boti & Marino 2015), it is also used for the reconstruction of pH variations for glacial cycles (Hönisch & Hemming 2005). Foraminifers and tropical corals' boron isotope ratio ($\delta^{11}\text{B}$) has been suggested as a way to measure the pH of seawater, and the long-term climate variability has been constructed using the ($\delta^{11}\text{B}$) pH proxy (Pelejero & Calvo 2008, Anagnostou et al. 2012). Boron isotope measurements have been widely employed as proxies for surface oceanic pH or pCO_2 in foraminiferal calcite and tropical coral aragonite (Hönisch & Hemming 2005, Douville et al. 2006). The surface ocean pH often decreases during increasing atmospheric CO_2 due to CO_2 uptake (Hönisch & Hemming 2005). Borate $\text{B}(\text{OH})_4$ and boric acid $\text{B}(\text{OH})_3$ are the two main dissolved forms of boron in seawater, and relative quantities of each form depend on the pH of the environment, $\text{B}(\text{OH})_3$ and $\text{B}(\text{OH})_4$ are predominant form

under low and high pH respectively (Klochko et al. 2006, Pelejero & Calvo 2008), and contrast to borate, which prefers the lighter isotope ^{10}B , boric acid prefers the heavier isotope ^{11}B and the boron isotope composition of marine carbonate fossils records ancient ocean pH by incorporating only borate in carbonate shells (Rasbury & Hemming 2017). Since boron has ~14-20 million years of residence time in seawater (Lemarchand et al. 2000), most boron research focuses on pre-Quaternary times, however, due to temporal changes of $\delta^{11}\text{B}$ in seawater for these ages, the inferences can be wide-ranging (Lemarchand et al. 2000, Pelejero & Calvo 2008).

The extreme sensitivity of seawater isotope $\delta^{11}\text{B}$ to global weathering and denudation (via rivers) and the significance of boron isotopes in carbonates for reconstructing atmospheric and oceanic CO_2 levels (Gaillardet & Lemarchand 2018). Due to its generally warmer climate, protracted volcanism, and CO_2 emissions, quick ocean acidification events, and other abrupt carbon cycle alterations that occurred in the early Cenozoic of utmost relevance for researching climate sensitivity to carbon system perturbation under greenhouse conditions (Zachos et al. 2008) estimate paleo- CO_2 concentrations for periods older than those accessible from ice cores and to reconstruct surface pH fluctuations on glacial/interglacial, marine carbonate boron isotopic compositions have been used (Sanyal et al. 2000, Palmer & Pearson 2003, Hönisch & Hemming 2005). Due to the proven correlation between pH and partial pressure of atmospheric CO_2 , the boron isotope composition of calcium carbonate shells of marine organisms has the unique potential to record the surface ocean pH and enable the calculation of atmospheric pCO_2 (Rasbury & Hemming 2017).

One of the most pervasive processes that lower water quality and put future water use at risk is salinization. The drinkable freshwater supply is often constrained by groundwater salinization, especially in arid and semiarid regions (Vengosh et al. 1999). The geochemical properties of boron isotopes are used extensively to evaluate a variety of geological processes, including the interaction of water and rock, the sedimentary environment, the genesis of salt lakes and groundwater, wastewater recharging, and the causes of anthropogenic pollution (Vengosh et al. 1994, Widory et al. 2005, Pennisi et al. 2006, Wei et al. 2014, Musashi et al. 2015).

The chemical weathering of evaporites and silicates, along with their mixing with seawater, regulates the amount of dissolved boron in groundwater; however, as a trace element or minor ion, boron is typically present in groundwater in extremely low amounts (Morell et al. 2008). For Mesozoic and Cenozoic clayey strata, the presence of boron is a sign of paleo salinity. However, clay diagenesis affects the boron

content of deeply buried Paleozoic and Ediacaran sediments (Retallack et al. 2020). As marine waters have a larger boron level of 20-50 ppm than freshwater, which has a boron content of only 2 ppm, boron in clays has been employed as a paleo salinity proxy (Walker & Price 1963, Couch 1971). The boron concentration of known marine fossils, such as Ediacaran stromatolites and algae, is substantially higher than that of Ediacaran vendobionts, which is indistinguishable from that of fossil plants and paleosols (Retallack et al. 2020)

Groundwater Contamination

An understanding of hydrogeological processes can be gained by identifying the composition and concentration of boron isotopes, and these isotopes further reveal that evaporite dissolution had an impact on salinization (Vengosh et al. 1994, Bassett et al. 1995, Gómez-Alday et al. 2022). Boron is a useful natural isotopic tracer for identifying the sources of pollution in groundwater systems due to the wide range in the isotopic composition of the boron sources in water resources, both natural (such as seawater, fossil brines, and hydrothermal fluids) and anthropogenic (sewage effluent, boron fertilizers, fly ash leachate, and landfill effluents) (Vengosh et al. 1994, Vengosh et al. 1998). In most river waters, the amount of boron is below 40 µg/L, while high levels of boron are present in rivers draining evaporites due to weathering (Lemarchand et al. 2002, Lemarchand & Gaillardet 2006). As nitrate transformation processes do not affect it, the boron isotope can discriminate between sewage and manure sources (Vengosh et al. 1994, Barth 1998). The investigations have demonstrated a clear difference in $\delta^{11}\text{B}$ values between seawater and terrestrial water (Barth 1993). The ocean water, groundwater, geothermal water and brines have a similar range of $\delta^{11}\text{B}$ (Bassett et al. 1995). Water-rock interactions and the biological cycle of B are the major causes of B isotopic fractionation in regolith and groundwater, whereas adsorption on sediments affects B isotopic fractionation in rivers slightly (Mao et al. 2019). Urban wastewater can be detected in surface water using boron isotopes, and also the source of boron in solution and the origin of the water are determined using the boron isotope composition of the groundwater (Petelet-Giraud et al. 2003, Nigro et al. 2018).

Biological Processes

Boron is an essential plant micronutrient in their metabolic activities (Blevins & Lukaszewski 1998, Pereira et al. 2021). In addition to facilitating vegetative growth and tissue differentiation, boron affects phenolic metabolism, cell wall synthesis, membrane integrity, RNA metabolism, indole acetic acid metabolism, and carbohydrate metabolism (Blevins & Lukaszewski 1998, Camacho-Cristóbal et al.

2005, 2008). The plants absorb boron as boric acid, and its deficiency prevents root growth and leaves expansion (Tanaka & Fujiwara 2008). When plants are deficient in boron, carbohydrates accumulate in the chloroplasts, increasing the rate of pentose phosphate cycle activity and decreasing the Krebs cycle activity (Goldbach 1997). In plants, the research on the first vascular plant, *Zosterophyllum shengfengense*, revealed that boron is primordial, originated in the root system in the terrestrial environment, and is also associated with the biosynthesis of lignin and differentiation of xylem (Lewis 1980, Pereira et al. 2021). The bacteria and fungi strains are affected by boron and boron-containing compounds (Gerretsen & Hoop 1957, Baker et al. 2009, Hunt et al. 2012). As boron protects plants from fungal decay, it is used in the timber industry as a termite and fungus repellent (Kartal et al. 2004) and also prevents infection in white fir *Abir concolor* by *Fomes Annosus* (Smith 1970). Boron further regulates the metabolism of numerous minerals, such as calcium, magnesium, phosphorus, and molybdenum (Wilson & Ruszler 1996). A positive correlation between boron and *Azotobacter* has also been reported (Gerloff 2006).

In cows, treatment of fatty liver (hepatic lipidosis) disease is costly, and researchers believe that borax (sodium borate $\text{Na}_2\text{B}_4\text{O}_7$) helps to prevent fatty liver disease because it helps in significant reductions in serum triglyceride (TG) and very low-density lipoprotein (VLDL) levels (Basoglu et al. 2002, Bobe et al. 2004). When either vitamin D or magnesium nutrition was disrupted in chicks and rats, it was claimed that lack of boron increased the amount of insulin required to maintain plasma glucose concentrations, and boron deficiency has been linked to hyperinsulinemia in vitamin D-deficient mice (Hunt & Herbel 1991, Bakken & Hunt 2003).

Ocean Acidification

The growth of coral skeletons is susceptible to environmental changes and may be adversely affected by ocean acidification (Gagnon et al. 2021). The analysis of boron elemental and isotopic composition of coral aragonite can uncover important information about coral skeletal calcification strategies (Chalk et al. 2021), also evaporites and brines can be traced using boron isotope geochemistry (Palmer & Slack 1989, Vengosh et al. 1991). As alkalinity and total inorganic carbon concentration control the pH of the surface ocean, so does atmospheric CO_2 partial pressure (Spivack et al. 1993, Bröcker & Franz 1998), and the boron isotopic composition of foraminiferal tests may also be affected by pH and isotopic composition (Bröcker & Franz 1998). The speciation process between the borate ion and boric acid pH dependent and isotopically unique, boron isotope variations in biogenic carbonates can be used to determine the pH of

the calcifying medium (Blamart et al. 2007, Rollion-Bard et al. 2011).

CONCLUSIONS AND FUTURE SCOPE

This work includes a short compilation of boron isotopes in various processes, boron-containing minerals, the latest instrumental techniques involved in the measurement of boron, its distribution and applications in nature. In addition to this, it includes a review of boron isotopic variation in the Himalayas in different systems. In conclusion, boron is a highly mobile element with large fractionation between its two isotopes due to their significant mass differences. Compared to other stable isotopes, it is considered the specific geochemical tracer. In the ocean, boron occurs in abundance, is appraised as an essential trace element, and proves extremely beneficial for paleoclimatic studies. In subduction zones, it acts as powerful means of reconnoitering fluid-mediated processes. The role of boron in cell wall stability may have an impact on how well plants and algae resist infection. Altogether, the current level of understanding about the significance of boron has widened some interesting prospects for more scientific and applied research. In the future, boron, due to its highly incompatible nature and reactive nature, can further provide a special tool to test comprehension across various timescales. In plants and agroecosystems, the role of the boron cycle can be sufficiently evaluated as the research in this area is scarce. As per the literature review study in laboratory experiments, calibrated equations are not available for many coral species, and there is a scarcity of knowledge on boron incorporation, which can be further elaborated.

ACKNOWLEDGEMENTS

The authors are thankful to the Head, Department of Geology, Sikkim University, Gangtok, Sikkim and acknowledge Dr. Kumar Batuk Joshi, National Centre for Earth Science Studies, Thiruvananthapuram, Kerala, for his suggestions in the manuscript preparation.

REFERENCES

Aggarwal, J., Sheppard, D., Mezger, K. and Pernicka, E. 2003. Precise and accurate determination of boron isotope ratios by multiple collectors ICP-MS: Origin of boron in the Ngawha geothermal system, New Zealand. *Chem Geol.*, 199: 331-342. [https://doi.org/10.1016/S0009-2541\(03\)00127-X](https://doi.org/10.1016/S0009-2541(03)00127-X).

Aggarwal, J.K. and Palmer, M.R. 1995. Boron isotope analysis. *Analyst*, 120: 1301-1307. <https://doi.org/10.1039/AN952001301>.

Aggarwal, S. and You, C.F. 2016. A review on the determination of isotope ratios of boron with mass spectrometry. *Mass Spectrom Rev.*, 9: 199. <https://doi.org/10.1002/mas.21490>.

Anagnostou, E., Huang, K.F., You, C.F., Sikes, E.L. and Sherrell, R.M. 2012. Evaluation of boron isotope ratio as a pH proxy in the deep

sea coral *Desmophyllum dianthus*: Evidence of physiological pH adjustment. *Earth Planet. Sci. Lett.*, 349-350: 251-260. <https://doi.org/10.1016/j.epsl.2012.07.006>.

Baes, C.F. and Mesmer, R.E. 1976. *The Hydrolysis of Cations*. Wiley, New York, pp. 267-274.

Baker, S.J., Ding, C.Z., Akama, T., Zhang, Y.K., Hernandez, V. and Xia, Y. 2009. Therapeutic potential of boron-containing compounds. *Future Med. Chem.*, 11: 1275-1288. <https://doi.org/10.4155/fmc.09.71>.

Bakken, N. and Hunt, C. 2003. Dietary boron decreases peak pancreatic in situ insulin release in chicks and plasma insulin concentrations in rats regardless of vitamin D or magnesium status. *J. Nutri.*, 133: 3577-3583. <https://doi.org/10.1093/jn/133.11.3577>.

Banerji, U.S., Goswami, V. and Joshi, K.B. 2022. Quaternary dating and instrumental development: An overview. *J. Asian Earth Sci.*, 7: 100091. <https://doi.org/https://doi.org/10.1016/j.jaesx.2022.100091>.

Bartelink, E. 2016. *Stable Isotopes*. John Wiley, NY. <https://doi.org/10.1093/obo/9780199766567-0153>.

Barth, S. 1993. Boron isotope variations in nature: A synthesis. *Geol. Rundsch.*, 82: 640-651. <https://doi.org/10.1007/BF00191491>.

Barth, S. 1998. Application of boron isotopes for tracing sources of anthropogenic contamination in groundwater. *Water Res.*, 32: 685-690.

Basoglu, A., Sevinc, M., Birdane, F.M. and Boydak, M. 2002. Efficacy of sodium borate in the prevention of fatty liver in dairy cows. *J. Veter. Int. Med.*, 16: 732-735. <https://doi.org/10.1111/j.1939-1676.2002.tb02416.x>.

Bassett, R., Buszka, P., Davidson, G. and Chong-Diaz, D. 1995. Identification of groundwater solute sources using boron isotopic composition. *Environ. Sci. Technol.*, 29: 2915-2922. <https://doi.org/10.1021/es00012a005>.

Bassett, R.L. 1990. A critical evaluation of the available measurements for the stable isotopes of boron. *Appl. Geochem.*, 5: 541-554. [https://doi.org/10.1016/0883-2927\(90\)90054-9](https://doi.org/10.1016/0883-2927(90)90054-9).

Bebout, G. and Nakamura, E. 2003. Record in metamorphic tourmalines of subduction-zone devolatilization and boron cycling. *Geology*, 31: 0407. [https://doi.org/10.1130/0091-7613\(2003\)031<0407:RIMTOS>2.0.CO;2](https://doi.org/10.1130/0091-7613(2003)031<0407:RIMTOS>2.0.CO;2).

Blamart, D., Rollion-Bard, C., Meibom, A., Cuif, J.-P., Juillet-Leclerc, A. and Dauphin, Y. 2007. Boron isotopic composition correlates with ultra-structure in a deep-sea coral *Lophelia pertusa*: Implications for biomineralization and paleo-pH. *Geochem. Geophys. Geosyst.*, 8: 1686. <https://doi.org/10.1029/2007GC001686>.

Blevins, D.G. and Lukaszewski, K.M. 1998. Boron in plant structure and function. *Annual Rev. Plant Biol.*, 49: 481-500. <https://doi.org/10.1146/annurev.arplant.49.1.481>.

Bobe, G., Young, J.W. and Beitz, D. 2004. Invited review: Pathology, etiology, prevention, and treatment of fatty liver in dairy cows. *J. Dairy Sci.*, 87: 3105-3124. [https://doi.org/10.3168/jds.S0022-0302\(04\)73446-3](https://doi.org/10.3168/jds.S0022-0302(04)73446-3).

Bolaños, L., Esteban, E., de Lorenzo, C., Fernández-Pascual, M., Felipe, M., Garate, A. and Bonilla, I. 1994. Essentiality of boron for symbiotic nitrogen fixation in pea (*Pisum sativum*) rhizobium nodules. *Plant Physiol.*, 104: 85-90. <https://doi.org/10.1104/pp.104.1.85>.

Bröcker, M. and Franz, L. 1998. Rb-Sr isotope studies on Tinos Island (Cyclades, Greece): Additional time constraints for metamorphism, the extent of infiltration-controlled overprinting and deformational activity. *Geol. Mag.*, 135: 369-382. <https://doi.org/10.1017/S0016756898008681>.

Camacho-Cristóbal, J., Maldonado, J. and González-Fontes, A. 2005. Boron deficiency increases putrescine levels in tobacco plants. *J. Plant Physiol.*, 162: 921-928. <https://doi.org/10.1016/j.jplph.2004.09.016>.

Camacho-cristóbal, J.J., Rexach, J. and González-Fontes, A. 2008. Boron in plants: Deficiency and toxicity. *J. Integr. Plant Biol.*, 50: 1247-1255. <https://doi.org/10.1111/j.1744-7909.2008.00742.x>.

Carrano, C.J., Schellenberg, S., Amin, S.A., Green, D.H. and Küpper, F.C.

2009. Boron and marine life: A new look at an enigmatic bioelement. *Marine Biotechnol.*, 11: 431-440. <https://doi.org/10.1007/s10126-009-9191-4>.
- Catanzaro, E.J. 1970. *Boric Acid: Isotopic and Assay Standard Reference Materials*. Elsevier, Amsterdam
- Chalk, T.B., Standish, C.D., D'Angelo, C., Castillo, K.D., Milton, J.A. and Foster, G.L. 2021. Mapping coral calcification strategies from in situ boron isotope and trace element measurements of the tropical *Siderastrea siderea*. *Sci. Rep.*, 11: 1-13. <https://doi.org/10.1038/s41598-020-78778-1>.
- Chaussidon, M., Robert, F., Mangin, D., Hanon, P. and Rose-Koga, E. 1997. Analytical procedures for the measurement of boron isotope compositions by ion microprobe in meteorites and mantle rocks. *Geostand. Newslett.*, 21: 7-17. <https://doi.org/10.1111/j.1751-908X.1997.tb00527.x>.
- Cheng, L., Zhang, C. et al. 2021. Significant boron isotopic fractionation in the magmatic evolution of Himalayan leucogranite recorded in multiple generations of tourmaline. *Chem. Geol.*, 571: 120194. <https://doi.org/10.1016/j.chemgeo.2021.120194>.
- Chesson, L.A., Tipple, B.J., Howa, J.D., Bowen, G.J., Barnette, J.E., Cerling, T.E. and Ehleringer, J.R. 2014. Stable Isotopes in Forensics Applications. In: Holland, H. D. and Turekian, K. K. (eds) *Emerald Pub*, Bingley, pp. 285-317. <https://doi.org/https://doi.org/10.1016/B978-0-08-095975-7.01224-9>.
- Couch, E. 1971. Calculation of Paleosalinities from Boron and Clay Mineral Data. *AAPG Bull.*, 55: 1865. <https://doi.org/10.1306/819A3DAC-16C5-11D7-8645000102C1865D>.
- Davy, H. 1808. Electro-Chemical research on the decomposition of the earths with Observations on the metals obtained from the alkaline earths and on the amalgam procured from ammonia. *Royal Soci. Lond. Proceed. Ser. I*, 1: 313-314. <https://doi.org/10.1098/rstl.1808.0023>.
- De Hoog, J.C.M. and Savov, I.P. 2018. Boron Isotopes as a Tracer of Subduction Zone Processes. Springer, NY. https://doi.org/10.1007/978-3-319-64666-4_9.
- Deegan, F.M., Troll, V.R., Whitehouse, M.J., Jolis, EM and Freda, C. 2016. Boron isotope fractionation in magma via crustal carbonate dissolution. *Sci. Rep.*, 6: 1-7. <https://doi.org/10.1038/srep30774>.
- Diez-Fernández, S., Encinar, J., Sanz-Medel, A., Isensee, K. and Heather, S. 2015. Determination of low B/Ca ratios in carbonates using ICP-QQQ. *Geochem., Geophys. Geosyst.*, 16: 581. <https://doi.org/10.1002/2015GC005817>.
- Dingwell, F.H. 1992. Experimental studies of Boron in Granitic melts. Sage, NJ, p. 710.
- Douville, E., Paterne, M., et al. 2006. Abrupt pH Changes of sea Surface Waters in the sub-Equatorial Pacific Ocean at the end of the Younger Dryas (YD): MC-ICPMS Analysis of Boron Isotopes in Reef Corals. AGU Fall Meeting Abstracts.
- Ercolani, C., Lemarchand, D. and Dosseto, A. 2019. Insights on catchment-wide weathering regimes from boron isotopes in riverine material. *Geochim. Cosmochim. Acta*, 261, 35-55. <https://doi.org/10.1016/j.gca.2019.07.002>.
- Fan, J.-J., Wang, Q. et al. 2021. Boron and molybdenum isotopic fractionation during crustal anatexis: Constraints from the Conadong leucogranites in the Himalayan Block, South Tibet. *Geochim. Cosmochim. Acta*, 297: 120-142. <https://doi.org/https://doi.org/10.1016/j.gca.2021.01.005>.
- Fietzke, J., Heinemann, A., Taubner, I., Böhm, F., Erez, J. and Eisenhauer, A. 2010. Boron isotope ratio determination in carbonates via LA-MC-ICP-MS using soda-lime glass standards as reference material. *J. Anal. At. Spectrom.*, 25, 1953-1957. <https://doi.org/10.1039/C0JA00036A>.
- Foster, G.L., Marschall, H.R., Palmer, M.R., Palmer, Á.M.R. and Marschall, H.R. 2018. Boron isotope analysis of geological materials analytical methods: A sample digestion á sample purification. *Boron Isotopes, Adv. Geochem.*, 4: 13-32.
- Gäbler, H.E. and Bahr, A. 1999. Boron isotope ratio measurements with a double-focusing magnetic sector ICP mass spectrometer for tracing anthropogenic input into surface and groundwater. *Chem. Geol.*, 156: 323-330. [https://doi.org/10.1016/S0009-2541\(98\)00181-8](https://doi.org/10.1016/S0009-2541(98)00181-8).
- Gagnon, A.C., Gothmann, A.M., Branson, O., Rae, J.W.B. and Stewart, J.A. 2021. Controls on boron isotopes in a cold-water coral and the cost of resilience to ocean acidification. *Earth Planet. Sci. Lett.*, 554: 116662. <https://doi.org/https://doi.org/10.1016/j.epsl.2020.116662>.
- Gaillardet, J. and Lemarchand, D. 2018. Boron in the weathering environment. *Adv. Isotop. Geochem.*, 4: 163-188. https://doi.org/10.1007/978-3-319-64666-4_7.
- Gay-Lussac, T. n.d. Sur la décomposition et la recombinaison de l'acide boracique. *Ann. Chim. Phys.*, 68: 167-174.
- Gerloff, G. 2006. The comparative boron nutrition of several green and blue-green algae. *Physiol. Plant.*, 21: 369-377. <https://doi.org/10.1111/j.1399-3054.1968.tb07260.x>.
- Gerretsen, F. and Hoop, H. 1957. Nitrogen losses during nitrification in acid sandy soil. *Can. J. Microbiol.*, 3: 040. <https://doi.org/10.1139/m57-040>.
- Goldbach, H. 1997. A critical review on current hypotheses concerning the role of boron in higher plants: Suggestions for further research and methodological requirements. *J. Trace Microprobe Tech.*, 15: 51-91.
- Gómez-Alday, J.J., Hussein, S., Arman, H., Alshamsi, D., Murad, A., Elhaj, K. and Aldahan, A. 2022. A multi-isotopic evaluation of groundwater in a rapidly developing area and implications for water management in hyper-arid regions. *Sci. Tot. Environ.*, 805: 150245. <https://doi.org/10.1016/j.scitotenv.2021.150245>.
- Gou, G.N., Wang, Q., Wyman, D.A., Xia, X.P., Wei, G.J. and Guo, H.F. 2017. In situ boron isotopic analyses of tourmalines from Neogene magmatic rocks in the northern and southern margins of Tibet: Evidence for melting of continental crust and sediment recycling. *Solid Earth Sci.*, 2: 43-54. <https://doi.org/10.1016/j.sesci.2017.03.003>.
- Guo, Z. and Wilson, M. 2012. The Himalayan leucogranites: Constraints on the nature of their crustal source region and geodynamic setting. *Gondwana Res.*, 22: 360-376. <https://doi.org/10.1016/j.gr.2011.07.027>.
- Harris, N. and Massey, J. 1994. Decompression and anatexis of Himalayan metapelites. *Tectonics*, 13: 1537-1546. <https://doi.org/10.1029/94TC01611>.
- Harris, N., Ayres, M. and Massey, J. 1995. Geochemistry of granitic melts produced during the incongruent melting of muscovite: implications for the extraction of Himalayan leucogranite magmas. *J. Geophys. Res.*, 1: 100. <https://doi.org/10.1029/94jb02623>.
- Helvaci, C. 2017. Borate deposits: An overview and future forecast with regard to mineral deposits. *J. Boron*, 7: 59-70.
- Hemming, N.G. and Hanson, G.N. 1992. Boron isotopic composition and concentration in modern marine carbonates. *Geochim. Cosmochim. Acta*, 56: 537-543. [https://doi.org/10.1016/0016-7037\(92\)90151-8](https://doi.org/10.1016/0016-7037(92)90151-8).
- Hemming, N.G. and Hanson, G.N. 1994. A procedure for the isotopic analysis of boron by negative thermal ionization mass spectrometry. *Chem. Geol.*, 114: 147-156. [https://doi.org/https://doi.org/10.1016/0009-2541\(94\)90048-5](https://doi.org/https://doi.org/10.1016/0009-2541(94)90048-5).
- Henry, D.J. and Dutrow, B. 1996. Metamorphic tourmaline and its petrologic applications. In: Grew, ES and Anovitz, L.M. (eds.), *Boron: Mineralogy, Petrology and Geochemistry: Reviews in Mineralogy*, Elsevier, Amsterdam, pp. 503-557.
- Henry, D.J. and Dutrow, B.L. 2018. Tourmaline studies through time: Contributions to scientific advancements. *J. Geosci.*, 63: 77-98. <https://doi.org/10.3190/jgeosci.255>.
- Henry, D.J. and Guidotti, C. V. 1985. Tourmaline as a petrogenetic indicator mineral: an example from the staurolite-grade metapelites of NW Maine. *Am. Mineral.*, 70: 1-15.
- Hervig, R., Moore, G., Holloway, J. and Williams, L. 2001. *Isotopic and Elemental Partitioning of Boron Between Hydrous Fluid and Melt*. Elsevier, Amsterdam.
- Hoefs, J. 2021. *Stable Isotope Geochemistry*. CRC Press, Boca Raton, Florida. <https://doi.org/10.1007/978-3-030-77692-3>.

- Hoffmann, E. and Stroobant, V. 2007. *Mass Spectrometry: Principles and Applications*. McGraw Hill, NY.
- Hönisch, B. and Hemming, N. 2005. Surface ocean pH response to variations in pCO₂ through two full glacial cycles. *Earth and Planetary Science Letters*, 236, 305-314. <https://doi.org/10.1016/j.epsl.2005.04.027>.
- Hu, G., Zeng, L., Gao, L.-E., Liu, Q., Chen, H. and Guo, Y. 2018. Diverse magma sources for the Himalayan leucogranites: Evidence from B-Sr-Nd isotopes. *Lithos*, 314-315: 88-99. <https://doi.org/10.1016/j.lithos.2018.05.022>.
- Hunt, A.C., Parkinson, I.J., Harris, N.B.W., Barry, T.L., Rogers, N.W. and Yondon, M. 2012. Cenozoic volcanism on the Hangai Dome, Central Mongolia: Geochemical evidence for changing melt sources and implications for melting mechanisms. *J. Petrol.*, 53: 1913-1942. <https://doi.org/10.1093/petrology/egs038>.
- Hunt, C. and Herbel, J. 1991. Boron affects energy metabolism in the streptozotocin-injected, vitamin D3-deprived rat. *Magnes. Trace Elem.*, 10: 374-386.
- Ishikawa, T. and Nakamura, E. 1992. Boron isotope geochemistry of the oceanic crust from DSDP/ODP Hole 504B. *Geochim. Cosmochim. Acta*, 56: 1633-1639. [https://doi.org/10.1016/0016-7037\(92\)90230-G](https://doi.org/10.1016/0016-7037(92)90230-G).
- Jiang, S.Y. 2001. Boron isotope geochemistry of hydrothermal ore deposits in China: A preliminary study. *Phys. Chem. Earth, Part A Solid Earth Geodesy.*, 26: 851-858. [https://doi.org/10.1016/S1464-1895\(01\)00132-6](https://doi.org/10.1016/S1464-1895(01)00132-6).
- Jocelyn Paré, J.R. and Yaylayan, V. 1997. *Mass Spectrometry: Principles and Applications*. In: Paré, J.R.J. and Bélanger, J.M.R. (eds), *Instrumental Methods in Food Analysis*, Springer, Cham, pp. 239-266.. [https://doi.org/10.1016/S0167-9244\(97\)80016-9](https://doi.org/10.1016/S0167-9244(97)80016-9).
- Jørgensen, B.B. 2021. Stable sulfur isotopes. *Geochem. Perspect.*, 10: 251-267.
- Joshi, K.B., Goswami, V., Banerji, U. and Shankar, R. 2021. Recent Developments in Instrumentation and its Application in Absolute Dating: Historical Perspective and Overview. *J. Asian Earth Sci.*, 211: 104690. <https://doi.org/10.1016/j.jseas.2021.104690>.
- Kakihana, H., Kotaka, M., Satoh, S., Nomura, M. and Okamoto, M. 1977. Fundamental Studies on the Ion-Exchange Separation of Boron Isotopes. *Bull. Chem. Soc. Japan*, 50: 158-163. <https://doi.org/10.1246/bcsj.50.158>.
- Kartal, S., Yoshimura, T. and Imamura, Y. 2004. Decay and termite resistance of boron-treated and chemically modified wood by in situ co-polymerization of allyl glycidyl ether (AGE) with methyl methacrylate (MMA). *Int. Biodeterior. Biodegrad.*, 53: 111-117. <https://doi.org/10.1016/j.ibiod.2003.09.004>.
- Kasemann, S., Erzinger, J. and Franz, G. 2000. Boron recycling in the continental crust of the Central Andes from the Palaeozoic to Mesozoic, NW Argentina. *Contrib. Mineral. Petrol.*, 140: 328-343. <https://doi.org/10.1007/s004100000189>.
- Klochko, K., Kaufman, A.J., Yao, W., Byrne, R.H. and Tossell, J.A. 2006. Experimental measurement of boron isotope fractionation in seawater. *Earth Planet. Sci. Lett.*, 248: 276-285. <https://doi.org/10.1016/j.epsl.2006.05.034>.
- Köster, M.H., Williams, L.B., Kudejova, P. and Gilg, H.A. 2019. The boron isotope geochemistry of smectites from sodium, magnesium and calcium bentonite deposits. *Chem. Geol.*, 510: 166-187. <https://doi.org/10.1016/j.chemgeo.2018.12.035>.
- Kubota, K., Yokoyama, Y., Ishikawa, T. and Suzuki, A. 2015. A new method for calibrating a boron isotope paleo-pH proxy using massive Porites corals. *Geochem. Geophys. Geosyst.* 16: 3333-3342. <https://doi.org/10.1002/2015GC005975>.
- Le Fort, P., Cuney, M., Deniel, C., France-Lanord, C., Sheppard, S.M.F., Upreti, B.N. and Vidal, P. 1987. Crustal generation of the Himalayan leucogranites. *Tectonophysics*, 134: 39-57. [https://doi.org/10.1016/0040-1951\(87\)90248-4](https://doi.org/10.1016/0040-1951(87)90248-4).
- Lécuyer, C., Grandjean, P., Reynard, B., Albarède, F. and Telouk, P. 2002. 11B/10B analysis of geological materials by ICP-MS Plasma 54: Application to the boron fractionation between brachiopod calcite and seawater. *Chem. Geol.*, 186: 45-55. [https://doi.org/10.1016/S0009-2541\(01\)00425-9](https://doi.org/10.1016/S0009-2541(01)00425-9).
- Lemarchand, D. and Gaillardet, J. 2006. Transient features of the erosion of shales in the Mackenzie River Basin (Canada), evidence from boron isotopes. *Earth Planet. Sci. Lett.*, 245: 174-189. <https://doi.org/10.1016/j.epsl.2006.01.056>.
- Lemarchand, D., Gaillardet, J., Lewin, E. and Allègre, C. 2000. The influence of rivers on marine boron isotopes and implications for reconstructing past ocean pH. *Nature*, 408: 951-954. <https://doi.org/10.1038/35050058>.
- Lemarchand, D., Gaillardet, J., Lewin, A. and Allègre, C.J. 2002. Boron isotope systematics in large rivers: Implications for the marine boron budget and paleo-pH reconstruction over the Cenozoic. *Chem. Geol.*, 190: 123-140. [https://doi.org/10.1016/S0009-2541\(02\)00114-6](https://doi.org/10.1016/S0009-2541(02)00114-6).
- Lemarchand, E. and Gaillardet, J. 2005. Boron isotopic fractionation related to boron sorption on humic acid and the structure of surface complexes formed. *Geochim. Cosmochim. Acta*, 69: 3519-3533. <https://doi.org/10.1016/j.gca.2005.02.024>.
- Leng, M.J., Swann, G.E.A., Hodson, M.J., Tyler, J.J., Patwardhan, S. V and Sloane, H.J. 2009. The Potential use of silicon isotope composition of biogenic silica as a proxy for environmental change. *Silicon*, 1: 65-77. <https://doi.org/10.1007/s12633-009-9014-2>.
- Leśnikowski, Z.J. 2016. Challenges and opportunities for the application of boron clusters in drug design. *J. Med. Chem.*, 59: 7738-7758. <https://doi.org/10.1021/acs.jmedchem.5b01932>.
- Lewis, BYDH 1980. Boron, Lignification and the origin of vascular plants-a unified hypothesis. *CABI Direct*, 84(2): 209-229.
- Liu, M.C. and Chaussidon, M. 2018. The Cosmochemistry of Boron Isotopes. In Marschall, H. and Foster, G. (eds), *Boron Isotopes: The Fifth Element*, Springer, Cham, 273-289. https://doi.org/10.1007/978-3-319-64666-4_11.
- Liu, S., Zhang, G.-B., Zhang, L., Liu, Z. and Xu, J. 2022. Boron isotopes of tourmalines from the central Himalaya: Implications for fluid activity and anatexis in the Himalayan orogen. *Chem. Geol.*, 12: 800 <https://doi.org/10.1016/j.chemgeo.2022.120800>.
- London, D. 1996. Granitic pegmatites. Special Paper of the Geological Society of America. GSAA, Boulder, Colorado, pp. 315, 305-319. <https://doi.org/10.1130/0-8137-2315-9.305>.
- London, D., Morgan, G.B. and Wolf, M.B. 2018. Chapter 7. Boron in Granitic rocks and their contact aureoles. *Boron*, 56: 299-330. <https://doi.org/10.1515/9781501509223-009>.
- Lü, Y.Y., Zheng, M.P., Zhao, P. and Xu, R.H. 2014. Geochemical processes and origin of boron isotopes in geothermal water in the Yunnan-Tibet geothermal zone. *Science China Earth Sciences*, 57, 2934-2944. <https://doi.org/10.1007/s11430-014-4940-2>.
- Lyday, P.A. 2000. Boron. US Geological Survey, Washington DC.
- Mao, H.R., Liu, C.Q. and Zhao, Z.Q. 2019. Source and evolution of dissolved boron in rivers: Insights from boron isotope signatures of end-members and model of boron isotopes during weathering processes. *Earth-Science Rev.*, 190: 439-459. <https://doi.org/10.1016/j.earscirev.2019.01.016>.
- Marschall, H.R. 2018. Boron Isotopes in the ocean floor realm and the mantle. *Adv. Isotop. Geochem.*, 189-215. https://doi.org/10.1007/978-3-319-64666-4_8.
- Marschall, H.R. and Foster, G.L. 2018. Boron isotopes in the earth and planetary sciences-a short history and introduction. *Adv. Isotop. Geochem.*, 6: 1-11. https://doi.org/10.1007/978-3-319-64666-4_1.
- Marschall, H.R. and Jiang, S.Y. 2011. Tourmaline isotopes: No element left behind. *Elements*, 7: 313-319. <https://doi.org/10.2113/gselements.7.5.313>.
- Marschall, H.R., Altherr, R., Kalt, A. and Ludwig, T. 2008. Detrital, metamorphic and metasomatic tourmaline in high-pressure

- metasediments from Syros (Greece): Intra-grain boron isotope patterns determined by secondary ion mass spectrometry. *Contrib. Mineral. Petrol.*, 155: 703-717. <https://doi.org/10.1007/s00410-007-0266-9>.
- Martinez-Boti, M. and Marino, G. 2015. Boron isotope evidence for oceanic carbon dioxide leakage during the last deglaciation. *Nature*, 518: 219-222. <https://doi.org/10.1038/nature14155>.
- McMullen, C.C., Cragg, C.B. and Thode, H.G. 1961. Absolute ratio of $^{11}\text{B}/^{10}\text{B}$ in Searles Lake borax. *Geochim. Cosmochim. Acta*, 23: 147-149.
- Miller, J., Mackin, G. and Miller, S. 2015. *Radiogenic Isotopes*. Elsevier, Amsterdam, pp. 89-116. https://doi.org/10.1007/978-3-319-13221-1_4.
- Morell, I., Pulido, A., et al. 2008. Characterization of the Salinisation Processes in Aquifers Using Boron Isotopes; Application to South-Eastern Spain. *Water Air Soil Pollut.*, 187: 65-80. <https://doi.org/10.1007/s11270-007-9497-7>.
- Musashi, M., Oi, T. and Kreulen, R. 2015. Chlorine isotopic compositions of deep saline fluids in Ibusuki coastal geothermal region, Japan: using B-Cl isotopes to interpret fluid sources. *Isotop. Environ. Health Stud.*, 51: 1-15. <https://doi.org/10.1080/10256016.2015.997722>.
- Nakano, T. and Nakamura, E. 2001. Boron isotope geochemistry of metasedimentary rocks and tourmalines in a subduction zone metamorphic suite. *Phys. Earth Planet. Interiors*, 127: 233-252. [https://doi.org/10.1016/S0031-9201\(01\)00230-8](https://doi.org/10.1016/S0031-9201(01)00230-8).
- Nigro, A., Sappa, G. and Barbieri, M. 2018. Boron isotopes and rare earth elements in the groundwater of a landfill site. *J. Geochem. Explor.*, 190: 200-206. <https://doi.org/10.1016/j.gexplo.2018.02.019>.
- Oi, T., Nomura, M., Musashi, M., Osaka, T., Okamoto, M. and Kakihana, H. 1989. Boron isotopic compositions of some boron minerals. *Geochim. Cosmochim. Acta*, 53: 3189-3195. [https://doi.org/10.1016/0016-7037\(89\)90099-9](https://doi.org/10.1016/0016-7037(89)90099-9).
- Pabst, S., Zack, T., Savov, I., Ludwig, T., Rost, D. and Vicenzi, E. 2011. Evidence for boron incorporation into the serpentine crystal structure. *Am. Mineral.*, 96: 1112-1119. <https://doi.org/10.2138/am.2011.3709>.
- Pal, D., Trumbull, R. and Wiedenbeck, M. 2010. Chemical and boron isotope compositions of tourmaline from the Jaduguda U (-Cu-Fe) deposit, Singhbhum shear zone, India: Implications for the sources and evolution of mineralizing fluids. *Chem. Geol.*, 277: 245-260. <https://doi.org/10.1016/j.chemgeo.2010.08.008>.
- Palmer, M. 2017. Boron cycling in subduction zones. *Elements*, 13: 237-242. <https://doi.org/10.2138/gselements.13.4.237>.
- Palmer, M., Spivack, A.J. and Edmond, J.M. 1987. Temperature and pH control over isotopic fractionation during adsorption of boron on marine clay. *Geochim. Cosmochim. Acta*, 51: 2319-2323. [https://doi.org/10.1016/0016-7037\(87\)90285-7](https://doi.org/10.1016/0016-7037(87)90285-7).
- Palmer, M.R. 1991. Boron-isotope systematics of Halmahera Arc (Indonesia) lavas: evidence for involvement of the subducted slab. *Geology*, 19: 215-217. [https://doi.org/10.1130/0091-7613\(1991\)019<0215:BISOHA>2.3.CO;2](https://doi.org/10.1130/0091-7613(1991)019<0215:BISOHA>2.3.CO;2).
- Palmer, M.R. and Helvacı, C. 1997. The boron isotope geochemistry of the neogene borate deposits of western Turkey. *Geochim. Cosmochim. Acta*, 61: 3161-3169. [https://doi.org/10.1016/S0016-7037\(97\)00135-X](https://doi.org/10.1016/S0016-7037(97)00135-X).
- Palmer, M.R. and Pearson, P.N. 2003. A 23,000-year record of surface water pH and PCO_2 in the western equatorial Pacific ocean. *Science*, 300: 480-482. <https://doi.org/10.1126/science.1080796>.
- Palmer, M.R. and Slack, J.F. 1989. Boron isotopic composition of tourmaline from massive sulfide deposits and tourmalinites. *Contrib. Mineral. Petrol.*, 103: 434-451. <https://doi.org/10.1007/BF01041751>.
- Palmer, M.R. and Swihart, G.H. 1996. Boron isotope geochemistry: An overview. *Boron*, 150: 709-744. <https://doi.org/10.1515/9781501509223-015>.
- Palmer, M.R., Pearson, P.N. and Cobb, S.J. 1998. Reconstructing past ocean pH-depth profiles. *Science*, 282, 1468-1471. <https://doi.org/10.1126/science.282.5393.1468>.
- Park, H. and Schlesinger, W.H. 2002. Global biogeochemical cycle of boron. *Glob. Biogeochem. Cycles*, 16: 1766. <https://doi.org/10.1029/2001gb001766>.
- Peacock, S.M. and Hervig, R.L. 1999. Boron isotopic composition of subduction-zone metamorphic rocks. *Chem. Geol.*, 160(4): 281-290.
- Pelejero, C. and Calvo, E. 2008. Reconstructing past seawater pH from boron isotopes in carbonates. *Contr. Sci.*, 3(3): 385-394.
- Penman, D., Hönlisch, B., Zeebe, R., Thomas, E. and Zachos, J.C. 2014. Rapid and sustained surface ocean acidification during the Paleocene-Eocene thermal maximum. *Paleoceanography*, 29: 2621. <https://doi.org/10.1002/2014PA002621>.
- Pennisi, M., Bianchini, G., Muti, A., Kloppmann, W. and Gonfiantini, R. 2006. The behavior of boron and strontium isotopes in groundwater-aquifer interactions in the Cornia Plain (Tuscany, Italy). *Appl. Geochem.*, 21: 1169-1183. <https://doi.org/10.1016/j.apgeochem.2006.03.001>.
- Pereira, G.L., Siqueira, J.A. and Batista-silva, W. 2021. Boron : More Than an Essential Element for Land Plants ? *Front. Plant Sci.*, 11: 307. <https://doi.org/10.3389/fpls.2020.610307>.
- Petelet-Giraud, E., Négrel, P. and Casanova, J. 2003. Variability of $^{87}\text{Sr}/^{86}\text{Sr}$ in water-draining granite was revealed after a double correction for atmospheric and anthropogenic inputs. *Hydrol. Sci. J.*, 48: 729-742. <https://doi.org/10.1623/hysj.48.5.729.51448>.
- Rasbury, E.T. and Hemming, N.G. 2017. Boron isotopes: A 'paleo-ph meter' for tracking ancient atmospheric CO_2 . *Elements*, 13: 243-248. <https://doi.org/10.2138/gselements.13.4.243>.
- Retallack, G., Gates, N., York, N. and Feldshuhorn, M. 2020. Boron paleosalinity proxy for deeply buried Paleozoic and Ediacaran fossils. *Palaeogeogr. Palaeoclimat. Palaeoecol.*, 540: 109536. <https://doi.org/10.1016/j.palaeo.2019.109536>.
- Rollion-Bard, C., Blamart, D., Trebosc, J., Tricot, G., Mussi, A. and Cuif, J.P. 2011. Boron isotopes as pH proxy: A new look at boron speciation in deep-sea corals using ^{11}B MAS NMR and EELS. *Geochim. Cosmochim. Acta*, 75: 1003-1012. <https://doi.org/10.1016/j.gca.2010.11.023>.
- Rose-Koga, E., Chaussidon, M. and France-Lanord, C. 2000. Fractionation of boron isotopes during erosion processes: The example of Himalayan rivers. *Geochim. Cosmochim. Acta*, 64: 397-408. [https://doi.org/10.1016/S0016-7037\(99\)00117-9](https://doi.org/10.1016/S0016-7037(99)00117-9).
- Samson, I.M. and Sinclair, W.D. 1992. Magmatic hydrothermal fluids and the origin of quartz-tourmaline orbicules in the Seagull Batholith, Yukon Territory. *Canad. Mineral.*, 30: 937-954.
- Sanyal, A., Hemming, N.G., Broecker, W.S. and Hansont, G.N. 1995. Evidence for a higher pH in the glacial ocean from boron isotopes in foraminifera. *Nature*, 373, 234-236. <https://doi.org/10.1038/373234a0>.
- Sanyal, A., Nugent, M., Reeder, R.J. and Bijma, J. 2000. Seawater pH control on the boron isotopic composition of calcite: Evidence from inorganic calcite precipitation experiments. *Geochim. Cosmochim. Acta*, 64: 1551-1555. [https://doi.org/10.1016/S0016-7037\(99\)00437-8](https://doi.org/10.1016/S0016-7037(99)00437-8).
- Savov, I., Ryan, J., D'Antonio, M. and Fryer, P. 2007. Shallow Slab Fluid Release Across and Along the Mariana Arc-Basin System: Insights from Geochemistry of Serpentinized Peridotites from the Mariana Fore Arc. *J. Geophys. Res.*, 112: 4749. <https://doi.org/10.1029/2006JB004749>.
- Scambelluri, M. and Tonarini, S. 2012. Boron isotope evidence for shallow fluid transfer across subduction zones by the serpentinized mantle. *Geology*, 40(10): 907-910. <https://doi.org/10.1130/G33233.1>.
- Slack, J.F. 1996. Tourmaline associations with hydrothermal ore deposits. *Rev. Mineral.*, 33: 558-643.
- Smith, R. 1970. Borax to control Fomes annosus infection of white fir stumps. *Plant Dis. Rep.*, 54: 872-875.
- Spivack, A.J. and Edmond, J.M. 1987. Boron isotope exchange between seawater and oceanic crust. *Geochim. Cosmochim. Acta*, 51: 1033-1043. [https://doi.org/10.1016/0016-7037\(87\)90198-0](https://doi.org/10.1016/0016-7037(87)90198-0).
- Spivack, A.J., You, C.F. and Smith, H.J. 1993. Foraminiferal boron isotope

- ratios as a proxy for surface ocean pH over the past 21 Myr. *Nature*, 363: 149-151. <https://doi.org/10.1038/363149a0>.
- Srivastava, T., Joshi, K.B. and Wanjari, N. 2022. Boron isotopic composition of pegmatitic tourmaline from Yumthang Valley, North Sikkim. *Geochem. Treas. Petrogen. Process*, 10: 782. https://doi.org/10.1007/978-981-19-4782-7_8.
- Steller, L.H., Nakamura, E., Ota, T., Sakaguchi, C., Sharma, M. and Van Kranendonk, M.J. 2019. Boron isotopes in the puga geothermal system, India, and their implications for the habitat of early life. *Astrobiology*, 19: 1459-473. <https://doi.org/10.1089/ast.2018.1966>.
- Tanaka, M. and Fujiwara, T. 2008. Physiological roles and transport mechanisms of boron: Perspectives from plants. *Pflügers Archiv : Europ. J. Physiol.*, 456: 671-677. <https://doi.org/10.1007/s00424-007-0370-8>.
- Thode, H.G. 1963. Sulphur isotope geochemistry. *Stud. Anal. Geochem.*, 1: 25-41.
- Tiwari, M., Singh, A.K. and Sinha, D.K. 2015. Stable Isotopes: Tools for Understanding Past Climatic Conditions and Their Applications in Chemostratigraphy. In: Ramkumar, M. B. T.C. (eds), *Chemostratigraphy*, Elsevier, Amsterdam, pp. 65-92. <https://doi.org/10.1016/B978-0-12-419968-2.00003-0>.
- Tonari, S., Armienti, P., D'Orazio, M. and Innocenti, F. 2001. Subduction-like fluids in the genesis of Mt. Etna magmas: evidence from boron isotopes and fluid mobile elements. *Earth Planet. Sci. Lett.*, 192: 471-483. [https://doi.org/10.1016/S0012-821X\(01\)00487-3](https://doi.org/10.1016/S0012-821X(01)00487-3).
- Trumbull, R.B. and Slack, J.F. 2018. Boron Isotopes in the continental crust: Granites, pegmatites, felsic volcanic rocks, and related ore deposits. In: Marschall, H. and Foster, G. (eds), *Boron Isotopes: The Fifth Element*, Springer, Cham, pp. 249-272. https://doi.org/10.1007/978-3-319-64666-4_10.
- Trumbull, R.B., Krienitz, M.S., Gottesmann, B. and Wiedenbeck, M. 2008. Chemical and boron-isotope variations in tourmalines from an S-type granite and its source rocks: The Erongo granite and tourmalinites in the Damara Belt, Namibia. *Contrib. Mineral. Petrol.*, 155: 1-18. <https://doi.org/10.1007/s00410-007-0227-3>.
- Trumbull, R.B., Slack, J.F., Krienitz, M.S., Belkin, H.E. and Wiedenbeck, M. 2011. Fluid sources and metallogenesis in the Blackbird Co-Cu-Au-Bi-Y-REE district, Idaho, USA: Insights from major-element and boron isotopic compositions of tourmaline. *Canad. Mineral.*, 49: 225-244. <https://doi.org/10.3749/canmin.49.1.225>.
- Van Hinsberg, V.J., Henry, D.J. and Marschall, H.R. 2011. Tourmaline: An ideal indicator of its host environment. *Canadian Mineralogist*, 49: 1-16. <https://doi.org/10.3749/canmin.49.1.1>.
- Vengosh, A., Starinsky, A., Kolodny, Y. and Chivas, A.R. 1991. Boron isotope geochemistry as a tracer for the evolution of brines and associated hot springs from the Dead Sea, Israel. *Geochim. Cosmochim. Acta*, 55: 1689-1695. [https://doi.org/10.1016/0016-7037\(91\)90139-V](https://doi.org/10.1016/0016-7037(91)90139-V).
- Vengosh, A., Starinsky, A. and Kolodny, Y. 1994. Boron isotope geochemistry of thermal springs from the northern Rift Valley, Israel. *J. Hydrol.*, 162: 155-169. [https://doi.org/10.1016/0022-1694\(94\)90009-4](https://doi.org/10.1016/0022-1694(94)90009-4).
- Vengosh, A., Kolodny, Y. and Spivack, A.J. 1998. Groundwater Pollution Determined By Boron Isotope Systematics. Application of Isotope Techniques to Investigate Groundwater Pollution. IAEA, Vienna, Austria, pp. 17-37.
- Vengosh, A., Spivack, A.J., Artzi, Y. and Ayalon, A. 1999. Geochemical and boron, strontium, and oxygen isotopic constraints on the origin of the salinity in groundwater from the Mediterranean Coast of Israel. *Water Resour. Res.*, 35: 1877-1894.
- Walker, C.T. and Price, N.B. 1963. Departure curves for computing paleosalinity from boron in illites and shales. *AAPG*, 47: 833-841.
- Wang, Z., Chen, B. and Yan, X. 2019. Geochemistry and boron isotopic compositions of tourmaline from the Paleoproterozoic amphibolites, NE China: Implications for the origin of borate deposit. *Precamb. Res.*, 326: 258-271. <https://doi.org/10.1016/j.precamres.2018.01.006>.
- Wei, H.-Z., Jiang, S.Y., Tan, H.-B., Zhang, W.J., Li, B.K. and Yang, T.L. 2014. Boron isotope geochemistry of salt sediments from the Dongtai salt lake in Qaidam Basin: Boron budget and sources. *Chem. Geol.*, 380: 74-83. <https://doi.org/10.1016/j.chemgeo.2014.04.026>.
- Widory, D., Petelet-Giraud, E., Négrel, P. and Ladouche, B. 2005. Tracking the Sources of Nitrate in Groundwater Using Coupled Nitrogen and Boron Isotopes: A Synthesis. *Environ. Sci. Technol.*, 39: 539-548. <https://doi.org/10.1021/es0493897>.
- Williams, L.B. and Hervig, R.L. 2004. Boron isotope composition of coals: A potential tracer of organic contaminated fluids. *Editorial handling by R.S. Harmon. Appl. Geochem.*, 19: 1625-1636. <https://doi.org/10.1016/j.apgeochem.2004.02.007>.
- Wilson, J. and Ruzsler, P. 1996. Effects of dietary boron supplementation on laying hens. *Brit. Poul. Sci.*, 37: 723-729. <https://doi.org/10.1080/00071669608417902>.
- Wu, F.Y., Liu, Z.C., Liu, X.C. and Ji, W.Q. 2015. Himalayan leucogranite: Petrogenesis and implications to orogenesis and plateau uplift. *Acta Petrol. Sin.*, 31: 1-36.
- Xavier, R., Wiedenbeck, M., Trumbull, R., Dreher, A., Monteiro, L., Rhede, D., Ganade, C., Torresi, I. 2008. Tourmaline B-isotopes fingerprint marine evaporites as the source of high-salinity ore fluids in iron oxide copper-gold deposits, Carajás Mineral Province (Brazil). *Geology*, 36: 743-746. <https://doi.org/10.1130/G24841A.1>.
- Yang, S.Y. and Jiang, S.Y. 2012. Chemical and boron isotopic composition of tourmaline in the Xiangshan volcanic-intrusive complex, Southeast China: Evidence for boron mobilization and infiltration during magmatic-hydrothermal processes. *Chem. Geol.*, 312-313: 177-189. <https://doi.org/10.1016/j.chemgeo.2012.04.026>.
- Yang, S.Y., Jiang, S.Y. and Palmer, M.R. 2015. Chemical and boron isotopic compositions of tourmaline from the Nyalam leucogranites, South Tibetan Himalaya: Implication for their formation from B-rich melt to hydrothermal fluids. *Chem. Geol.*, 419: 102-113. <https://doi.org/10.1016/j.chemgeo.2015.10.026>.
- Yilmaz, A.E., Boncukcuoğlu, R., Kocakerem, M.M. and Kocadağistan, E. 2008. An empirical model for the kinetics of boron removal from boron containing wastewaters by the electrocoagulation method in a batch reactor. *Desalination*, 230: 288-297. <https://doi.org/10.1016/j.desal.2007.11.031>.
- Zachos, J.C., Dickens, G.R. and Zeebe, R.E. 2008. An early Cenozoic perspective on greenhouse warming and carbon-cycle dynamics. *Nature*, 451: 279-283. <https://doi.org/10.1038/nature06588>.
- Zeebe, R. and Wolf-Gladrow, D. 2001. CO₂ in Seawater: Equilibrium, Kinetics, Isotopes. Elsevier, Amsterdam.
- Zhang, W., Tan, H., Zhang, Y., Wei, H. and Dong, T. 2015. Boron geochemistry from some typical Tibetan hydrothermal systems: Origin and isotopic fractionation. *Appl. Geochem.*, 63: 436-445. <https://doi.org/10.1016/j.apgeochem.2015.10.006>.
- Zhao, Z., Liu, C., Xiao, Y. and Lang, Y. 2003. Geochemical study of boron isotopes in the process of loess weathering. *Sci. China Ser. D-Earth Sci.*, 46: 106-116. <https://doi.org/10.1360/03yd9010>.
- Zheng, Y., Chuan, Hou, Z., Qian, Fu, Q., Zhu, D.C., Liang, W. and Xu, P. 2016. Mantle inputs to Himalayan anatexis: Insights from petrogenesis of the Miocene Langkazi leucogranite and its dioritic enclaves. *Lithos*, 264: 125-140. <https://doi.org/10.1016/j.lithos.2016.08.019>.
- Zhou, Q., Li, W., Wang, G., Liu, Z., Lai, Y., Huang, J., Yan, G., Zhang, Q. 2019. Chemical and boron isotopic composition of tourmaline from the Conadong leucogranite-pegmatite system in South Tibet. *Lithos*, 326-327: 529-539. <https://doi.org/10.1016/j.lithos.2019.01.003>.



Removal of H₂S from Biogas Using *Thiobacillus* sp.: Batch and Continuous Studies

R. Shet and S. Mutnuri†

Applied Environmental Biotechnology Laboratory, BITS Pilani, K.K. Birla Goa Campus, Zuarinagar, Goa-403726, India

†Corresponding author: S. Mutnuri; srikanth@goa.bits-pilani.ac.in

Nat. Env. & Poll. Tech.
Website: www.neptjournal.com

Received: 10-10-2022

Revised: 06-12-2022

Accepted: 22-12-2022

Key Words:

Thiobacillus sp.

H₂S removal

Anaerobic co-digestion

Adsorption kinetics

Adsorption isotherms

ABSTRACT

Anaerobic digestion produces biogas which usually contains 60-70% of methane (CH₄), 30-40% of carbon-di-oxide (CO₂), and 10-2,000 ppm hydrogen sulfide (H₂S). The concentration of H₂S depends upon the type of substrate. H₂S tends to corrode pipes and machines carrying them. The high concentrations of H₂S present in biogas may adversely affect electricity generation. Hence, the removal of H₂S and enrichment of biogas with CH₄ is an essential step towards higher energy production. In the present study, the biological method of removing H₂S using *Thiobacillus* sp. was demonstrated for a one cu.m anaerobic co-digestion (ACD) unit running on an organic fraction of municipal solid waste (OFMSW) and septage sludge. Initial lab scale studies were conducted by collecting the biogas generated from 1 cu.m digesters, and continuous experiments were optimized for the process parameters such as flow rate, the volume of medium with culture, time, the height of the column, column composition, etc. The raw biogas was purged in a liquid medium (LM) with a culture containing *Thiobacillus* sp. The studies with the LM containing *Thiobacillus* sp. culture showed a 68% removal of H₂S in the first 8 min, and the saturation occurred at 75 min when the time-dependent experiment was studied. The smaller flow rate (0.48 L.min⁻¹) and highest volume of culture (500 mL) showed better results than other parameters. The highest and average oxidation rates of sulfate were recorded as 39 and 40.3 ppm.sec⁻¹, respectively, for 0.48 L.min⁻¹ flow rate and 500 mL of the culture volume. In the column studies, a column containing cocopeat (CP) was studied for its efficiency in removing H₂S. At a flow rate of 0.9 L.min⁻¹, 25% adsorption was encountered and reached saturation at 90 min. The bed height of 9 inches with CP and plastic support (PS) showed a 20% H₂S removal. The filling ratio of CP and PS (1:1) was the best ratio for proper gas passage with optimal time for adsorption/absorption. The kinetic, isotherm, and continuous models helped to understand the capacity of the adsorbent. Freundlich, Yoon-Nelson, and BDST model were best fit for the present study. A pilot scale setup for one cu.m biogas reactor showed an average of 50% removal of H₂S for LM with culture, and an additional 20% removal was possible by the introduction of a column along with the liquid bed in series. An overall efficiency of 70-75% of H₂S removal was achieved. No significant CH₄ loss was encountered during the study.

INTRODUCTION

The anaerobic reduction of sulfur by the sulfur-reducing bacteria in the presence of hydrogen produced during the hydrolysis and fermentation process produces hydrogen sulfide (H₂S) gas. Sulfurs are present in organic compounds such as amino acids, enzymes, proteins, fats, etc. inorganic sulfur does not functionally interfere with any biological pathways; instead, it serves as a precursor for the synthesis of organic compounds (Jensen & Webb 1995). The biogas contains concentrations of H₂S varying between 500 ppm to 20,000 ppm depending on the type and nature of substrates (Pokorna & Zabranska 2015). The biogas generated from

different substrates contains different concentrations of H₂S. For example, the biogas from organic waste contains 10-2,000 ppm of H₂S, and with sewage sludge as the substrate, it varies from 10-20,000 ppm of H₂S respectively (Aslam et al. 2019, Dumont 2015, Monteleone et al. 2011).

Inhaling high concentrations of H₂S can adversely affect humans, causing severe toxic sensory problems (Díaz et al. 2011). It is also harmful to cement and steel structures, such as old heritage monuments, where they can deteriorate the binding capacity of the cement and can accelerate rusting (de Oliveira et al. 2019). The biogas plants handling high amounts of liquids and gases containing H₂S also affect the

steel structures like pipes and pumps, causing corrosion (Zhang et al. 2008). The flaring/burning of the biogas containing high H₂S will lead to higher emissions of SO_x into the environment. H₂S is an airborne pollutant causing acute and chronic health problems depending on the exposure time and toxicant concentration (Aslam et al. 2019). Hence, it is important to remove the H₂S content before utilizing the biogas without hampering the process of anaerobic co-digestion (ACD).

Different removal methods are available, applied, and studied over time, including physical such as scrubbing through water, carbon, etc. Moreover, chemical methods include adding NaOH (Bagreev et al. 2000) and using iron filling (Andriani et al. 2020, Ho et al. 2013) to oxidize H₂S. However, these methods are reliant on resources that are either expensive or require frequent regeneration. Micro aeration is another process of reducing H₂S in biogas where limited oxygen will be supplied to the reactors at the outlet to oxidize the H₂S. However these method is extremely sensitive and may result in decreased reactor efficiency if not monitored (Pokorna & Zabranska 2015).

Several studies have explored the application of biological methods of H₂S removal. *Thiobacillus* is one such species of microorganism that has the potential to oxidize sulfur compounds. Other organisms include *Acidophile*, *AcidiThiobacillus*, *Thiooxidans*, *Thiobacillus*, *Thioparus*, and *Pseudomonas* (Ramírez-Aldaba et al. 2016, Zicari 2003). These microbes have the potential to withstand high concentrations of H₂S, and they do not diminish quickly and can be sustained for a longer span of time (Lin et al. 2013). The use of *Thiobacillus* sp. to enrich biogas evokes a redox reaction, producing elemental sulfur (Zhao et al. 2010).

Adsorption is another method that can be implemented to remove H₂S. Many studies have been conducted to investigate column behavior toward adsorption. Different compounds have been used for the adsorption study, including activated carbon (de Oliveira et al. 2019), zeolites, and AD fibers (Ayiania et al. 2019, Kulkarni & Ghanegaonkar 2019, Shah et al. 2017), oil fly ash (Aslam et al. 2019), biochar (Sethupathi et al. 2017), cow manure compost (Zicari 2003), sugarcane bagasse (Pantoja et al. 2010) and use of molecular sieves (Georgiadis et al. 2021). Few studies have used cocopeat (CP) as an adsorbent to remove H₂S (De Silva et al. 2019, Pantoja et al. 2010). Only a few studies have been reported using column and microbial culture broth (Dumont 2015). Kumari & Dey (2019) used CP as an adsorbent to remove malachite green dye from wastewater.

The present study aimed to remove H₂S from the biogas obtained from ACD of OFMSW and septage using reactors containing liquid medium (LM) with *Thiobacillus* culture.

The study aims to use a continuous column containing CP, plastic support (PS), and culture for H₂S removal. Further, both these approaches were combined, and the combination of the two systems in series was implemented at 1 cu.m reactor ACD reactors to study the H₂S removal efficiency.

MATERIALS AND METHODS

Primary Requirements

The raw biogas required for this study was collected from the existing 1 cu.m biogas digesters (R1 and R2). The *Thiobacillus* culture was prepared by dissolving the salts listed and represented in Table 1 using sterile distilled water (Pokorna & Zabranska 2015). The primary culture was prepared using 5% (v/v) domestic wastewater/sewage as inoculum, and it was subcultured to obtain concentrated *Thiobacillus* sp. culture. The inoculated media was incubated for nine days at room temperature under anaerobic conditions. The media showed a white, turbid, and denser texture as the incubation period passes, indicating *Thiobacillus* sp. proliferation. This culture was used for liquid bed (LM) studies and column experiments. The CP and PS for the column experiments were procured from the local vendors used as the adsorbent medium. The composition of biogas was analysed using Geotech BIOGAS 5000 portable biogas analyser.

Liquid Bed Experiments

The raw biogas from digesters R1 and R2 were stored in 1.5 m³ capacity biogas balloons. The liquid bed experiments began with purging raw biogas (mixture of CH₄, CO₂, and H₂S) into borosilicate bottles (500 mL capacity) containing LM with culture through the inlet port (Zhu et al. 2020). The outlet port was connected to a portable biogas analyzer, and the CO₂, H₂S, and CH₄ concentrations were measured at different intervals. The effect of different parameters such as flow rate, time, and amount of LM with culture on absorption was studied individually, keeping other parameters constant. The initial and final methane concentration (CH₄) through

Table 1: Chemical composition of the *Thiobacillus* sp. specific broth.

Chemical salts	Quantity [g.L ⁻¹]
Ammonium sulfate	0.4
Mono-potassium phosphate	4
Calcium chloride	0.25
Ferrous sulfate	0.1
Magnesium sulfate	0.5
Sodium thiosulfate	5
Agar	20

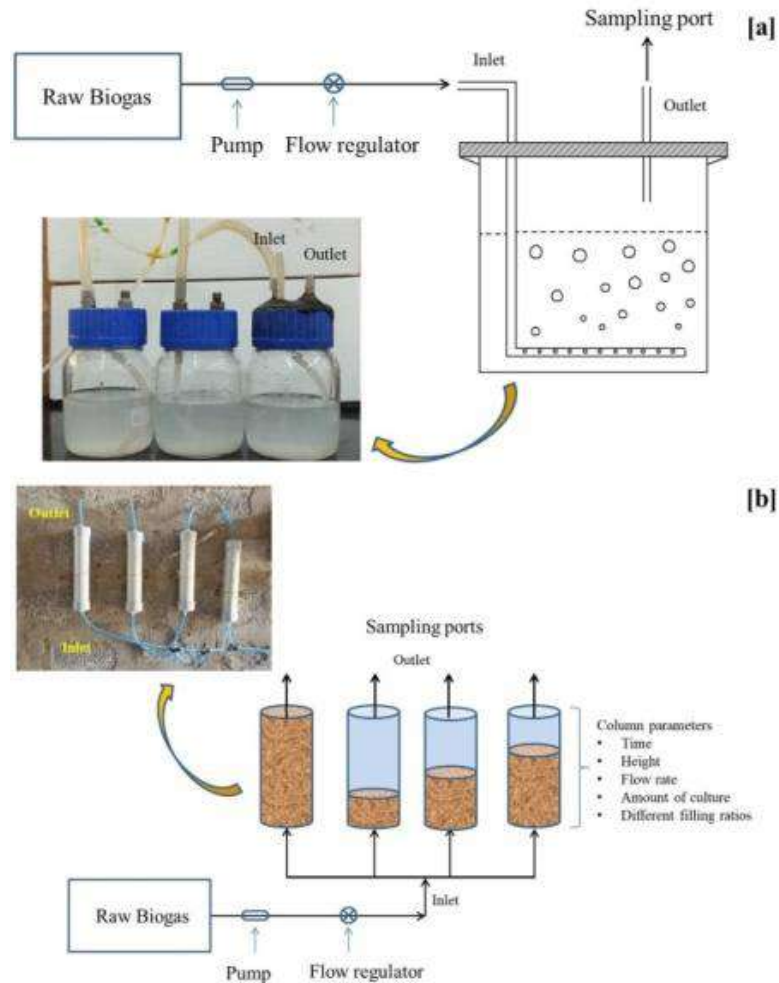


Fig. 1: H₂S removal set up [a] liquid bed and [b] continuous column experiment.

LM with culture was recorded at varying times (0, 5, 10, 15, 20-200 min). Different flow rates of biogas, such as 0.48, 0.66, and 1.2 L.min⁻¹, and amounts of culture as 100, 200, and 500 mL, were selected. Fig. 1[a] represents the setup and the real-time picture of the liquid bed filled with the culture.

Continuous Column Experiments: Microorganism Cultivation and Immobilization

The continuous column experiments were set up using PVC pipes (diameter 5.03 cm). For this study, different column parameters such as time, the height of the bed (3, 6, and 9 inches), amount of culture (0, 20, and 50 mL), the flow rate of the biogas (0.48, 0.66, and 1.2 mL.min⁻¹) and filling ratios of PS and CP (100% PS, 50:50 PS: CP and 20:80 PS: CP) were selected. The column was filled with different ratios of PS and CP, and the raw biogas was passed from the bottom using a 0.15 HP pump. The CP as a packing material offered a

higher surface area for adsorption and microbes to proliferate.

To promote a uniform gas distribution through the column, the porosity of the packing material is crucial. The packing material should also have water absorption capacity so microorganisms can grow onto them (Fischer 2010). While a particular parameter was varied and studied, other parameters were kept constant for each experiment. The outlet was provided at the top, where biogas compositions were monitored using a portable biogas meter. Different flow rates were fixed using a gas flow meter at room temperature. The columns were provided with a headspace of 3 inches. The experiments were conducted until the saturation points were reached. The breakthrough curves were plotted between normalized concentration (C/C_0) and time (Aslam et al. 2019, Ayiania et al. 2019). The breakthrough curve gives an understanding of the system's capacity to adsorb the particular gaseous component, in this case, the adsorption

Table 2: Mathematical forms of the kinetics and its parameters (Kumari & Dey 2019, Zulkefli et al. 2017).

Models	Equation	Parameters
Adsorption kinetics		
Pseudo first order	$\ln(q_e - qt) = \ln q_e - K_1 t$	q_e = adsorption capacity at equilibrium (mL.g^{-1}) qt = adsorption capacity at time t (mL.g^{-1}) K_1 = equilibrium constant for pseudo-first-order (min^{-1}) t = time (min)
Pseudo second order	$\frac{t}{qt} = \frac{1}{K_2 q_e^2} + \frac{t}{q_e}$	K_2 = equilibrium constant for pseudo-second-order (min^{-1})
Elovich model	$qt = \frac{1}{\beta} \ln(\alpha\beta) + \frac{1}{\beta} \ln t$	β = fraction of surface coverage (g.mL^{-1}) α = initial adsorption rate ($\text{mL.(g.min}^{-1})$)
Adsorption isotherms		
Langmuir isotherm	$\frac{C_e}{q_m} = \frac{1}{q_m b} + \frac{C_e}{q_m}$	C_e = concentration at equilibrium (ppm) q_m = maximum adsorption capacity (mg.mL^{-1}) b = Langmuir constant (L.mg^{-1})
Freundlich isotherm	$\log q_e = \log k_f + \frac{1}{n} \log C_e$	k_f = adsorption capacity parameter (mg.mL^{-1}) n = Freundlich index
Continuous column study models		
Thomas model	$\ln \frac{C_o}{C_e} - 1 = \frac{kth q_{max} M}{Q} - kth C_o t$	C_o = inlet concentration C_e = outlet concentration kth = Thomas constant ($\text{L.mg}^{-1}.\text{h}^{-1}$) M = mass of adsorbent (g) t = time (h)
Yoon–Nelson model	$\ln \frac{C_e}{C_o} = k_{YN} t - J k_{YN}$	k_{YN} = rate constant (min^{-1}) J = time required for 50% adsorbate breakthrough (min)
Adams–Bohart model	$\ln \frac{C_e}{C_o} = k_{AB} C_o t - k_{AB} N_o \left(\frac{Z}{U_o}\right)$	k_{AB} = kinetic constant ($\text{L.mg}^{-1}.\text{min}^{-1}$) N_o = saturation concentration (mL.kg^{-1}) Z = bed depth of the fixed-bed column (cm) U_o = superficial velocity (cm.min^{-1})

capacity of H_2S . The breakthrough point, which shows the adsorbent's maximum capacity, is responsible for knowing the highest bed volume (BV) (Sunzini et al. 2020, Zulkefli et al. 2017).

Fig. 1[b] shows the liquid bed and column experiment setups. To understand the column behavior of the adsorbent, several models such as BDST, Thomas model, Yoon–Nelson

model, and Adams–Bohart model were studied and are expressed in the mathematical forms in Table 2.

Performance of Optimized Condition for H_2S Scrubbing at Pilot Scale

The pilot scale H_2S scrubbing system was set up with the combination of liquid bed and the column considering the

optimized conditions from lab-scale experiments to evaluate the system's performance for a 1cu.m digester. The liquid bed setup was set up in a 35 L HDPE barrel with a provision for the inlet and outlet on the top. The inlet pipe was extended in an "L" shape inside the barrel at the bottom, and 2 mm perforations were provided for uniform diffusion of the inflowing gas. The outlet is provided as represented in Fig. 2. The barrel was filled with 30 L of *Thiobacillus* culture. The column setup was fabricated using PVC pipe with an 11 cm diameter and height of 1.5 m with 1 m working volume and 0.5 m head space. The column was filled with equal volumes of PS and CP. Before the experiment began, the column was added with 1 L of the culture. The biogas inflow was given at the rate of 1.5 cu.m.hr⁻¹ with a provision to regulate the flow rate. The setup was connected in series such that the outlet of the liquid bed was connected to the inlet of the column. The outlet at the top of the column was connected to the biogas meter to record the H₂S concentrations. Fig. 2 shows the flow diagram representing the setup and the real-time picture of the setup.

RESULTS AND DISCUSSION

Effect of Different Parameters on Absorption in Liquid Bed Studies

The effect of time on the absorption represents the capacity of the LM to the extent to which the particular molecule

will be absorbed. Fig. 3 [a] represents the effect of time on absorption. As time increases, it was observed that the absorption of the H₂S gradually increases, attaining saturation. In the initial 8 min, the H₂S concentration reached 287 ppm from 147 ppm. Further, from 287 ppm, the saturation concentration, i.e., 467 ppm, was reached at 75 min. The total time observed for the culture to saturate was 75 min keeping other parameters such as flow rate, amount of culture, and initial concentrations constant at 1 L.min⁻¹, 250 mL, and 467 ppm, respectively.

The study on the amount of culture was found to be a significant parameter affecting the process of absorption (Fig. 3 [b]). Three different volumes were considered for the study, and it was evident that the highest volume was more efficient than the rest. For the experiment with 500 mL LM, it was observed that in the first 20 min, the concentration of H₂S was reduced to 34 ppm from 467 ppm, and in the 25th min, the concentration reached 134 ppm. The concentration gradually increased with time till 60th min and was observed to attain saturation. A similar trend was seen with 100 and 200 mL of LM. For 100 mL, the saturation was achieved at the 5th and 200 mL at the 45th min, respectively.

When the flow rate was studied (Fig. 3 [c]), the highest flow rate, 1.2 L.min⁻¹, was the least effective, while the lowest flow rate showed better results. The saturation for 1.2 L.min⁻¹ was reached in no time (<1 min) whereas, at

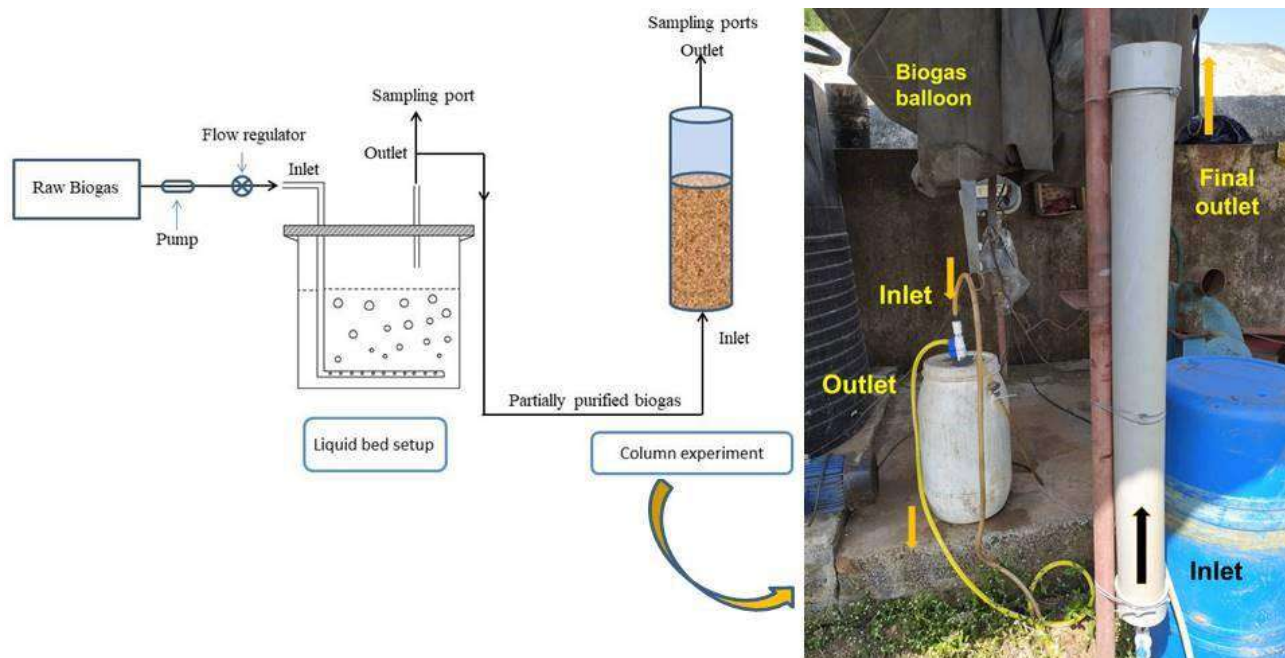


Fig. 2: Set up illustrating the combination of liquid bed and continuous column at pilot scale.

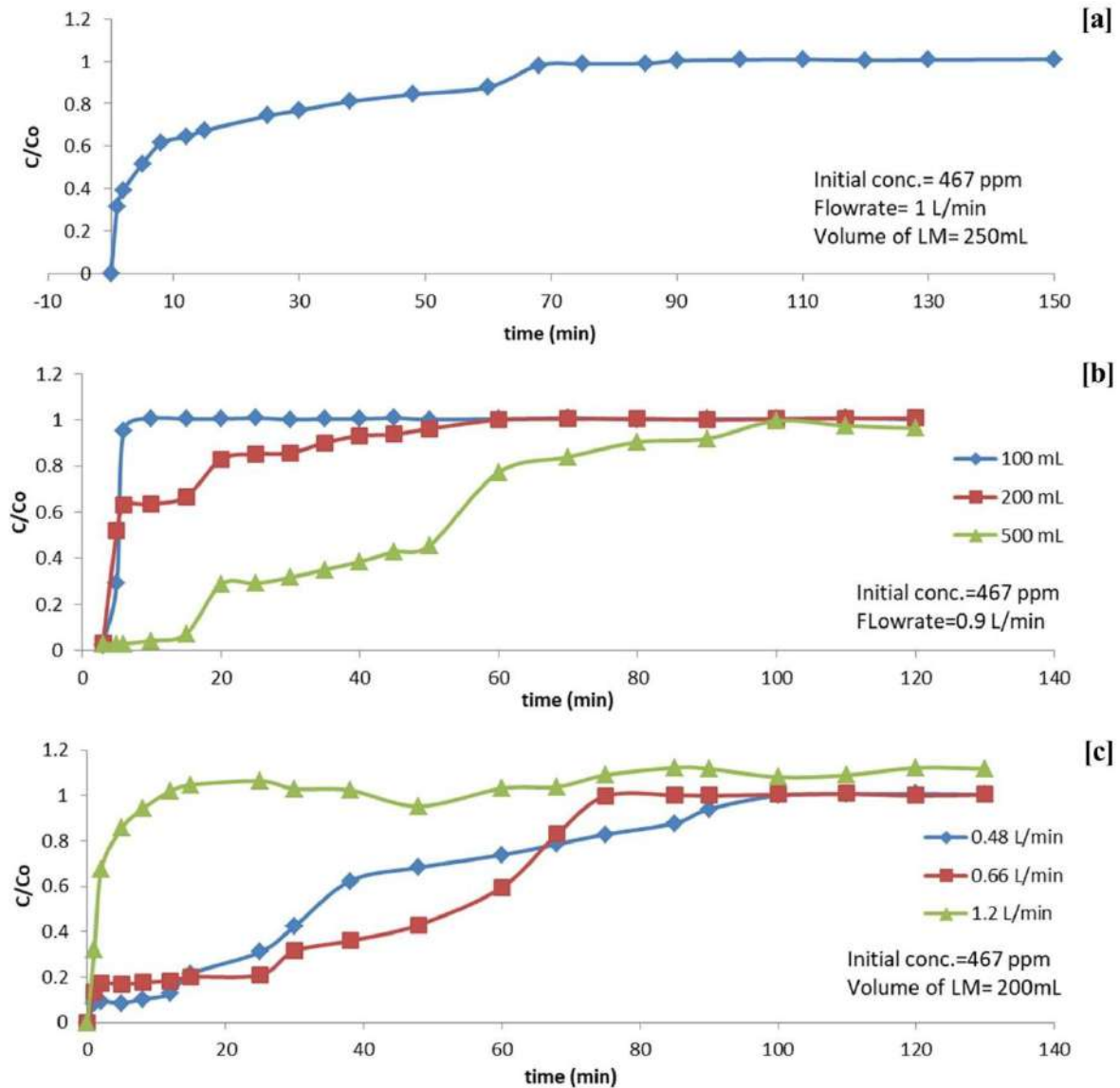


Fig. 3: Graphical representation of plot between time and C/C_o for [a] time, [b] volume of culture, and [c] flow rate for liquid bed experiments.

0.66 $L \cdot min^{-1}$ flow rate, the saturation reached at 75th min with an increase in H_2S concentration from 78 ppm to >467 ppm. The best flow rate found to be 0.48 $L \cdot min^{-1}$ showed a maximum H_2S removal until the 12th min with 98 ppm and a linear increase until the 38th min to 291 ppm, followed by a gradual increase to achieve saturation at the 90th min.

The absorption of H_2S in the LM can be studied with reference to the oxidation rate of sulfur. The gas retention time (GRT) and loading rate were calculated before calculating the biological oxidation rate. The formulae for the above parameters are as follows,

$$GRT = \frac{V}{Q} \quad \dots(1)$$

Where GRT is the gas retention time (min), V is the volume of absorbers (L), and Q is the gas flow rate ($L \cdot min^{-1}$).

$$H_2S \text{ loading} = \frac{(QXC)}{V} \quad \dots(2)$$

Where H_2S loading is in $g \cdot m^{-3} \cdot h^{-1}$, and C is the inlet concentration (g-S/L).

$$\text{Oxidation rate} = \frac{(C_o - C_i) \cdot Q}{V} \quad \dots(3)$$

Where C_o is the H₂S concentration of the medium leaving the LM (g.L⁻¹), and C_i is the H₂S concentration of the medium flow into the LM (g.L⁻¹) (Lin et al. 2013).

As anticipated, the GRT of the three different volumes of culture increased as the volume increased. The highest volume was chosen, i.e., 500 mL showed the highest GRT as 0.555 min. Seemingly the H₂S loading rate showed a maximum for the lowest volume of 100 mL as 4.20 g.m⁻³.h⁻¹, and a decrease was observed as the volume increased. Similarly, for other parameters, flow rate, the GRT, and H₂S loading rates were found maximum for the highest flow rate set (i.e., 1.2 L.min⁻¹) as 0.833 min and 5.60 g.m⁻³.h⁻¹, respectively, concluding that the parameters were well within the experiment. All the other values for every parameter are listed in Table 3. Fig. 4 and Table 3 represent the variation in the oxidization rate at every step. As can be observed from the Fig. 4 [b], the lowest volume of culture showed the highest oxidation rate occurring but for a substantially minimal time. However, as the volume increases, the time taken for the oxidation also increases but at a lower oxidation rate when compared to 100 mL volume.

Similarly, for different flow rates, 0.48, 0.66, and 1.2 L.min⁻¹, the highest oxidation rates recorded were 70.5, 35.01, and 13.6 ppm.sec⁻¹, respectively. After several minutes of operation, the oxidation rate expressed a negative

value, showing that sulfur oxidation has stopped and no further conversion is possible. The average oxidation rate was calculated considering all the positive values of oxidation rates, which were found to be in decreasing order and are reported in Table 3 and can be observed in Fig. 4.

Effect of Parameters on Adsorption in Column Experiments

The column studies allowed us to investigate more parameters than the liquid bed study with five different parameters: time, bed height, culture volume, flow rate, and filling ratio. From the literature, it was found that the increase in dissolved oxygen (DO) decreases the elemental sulfur (Doungprasopsuk & Suwanvitaya 2017). However, in the current study, DO was not considered, as the raw biogas had no DO present. The adsorption is a time-dependent process. Hence, the other parameters were fixed, and the time parameter was studied. Fig. 5 [a] represents the effect of time on the adsorption of H₂S. With the initial concentration of 467 ppm and flow rate of 0.9 L.min⁻¹, the adsorption was achieved up to 25%. At the 90th min, saturation occurs, and no changes were observed between the inlet and outlet concentration of H₂S.

Furthermore, the bed height showed a significant difference in the result. All three heights selected showed

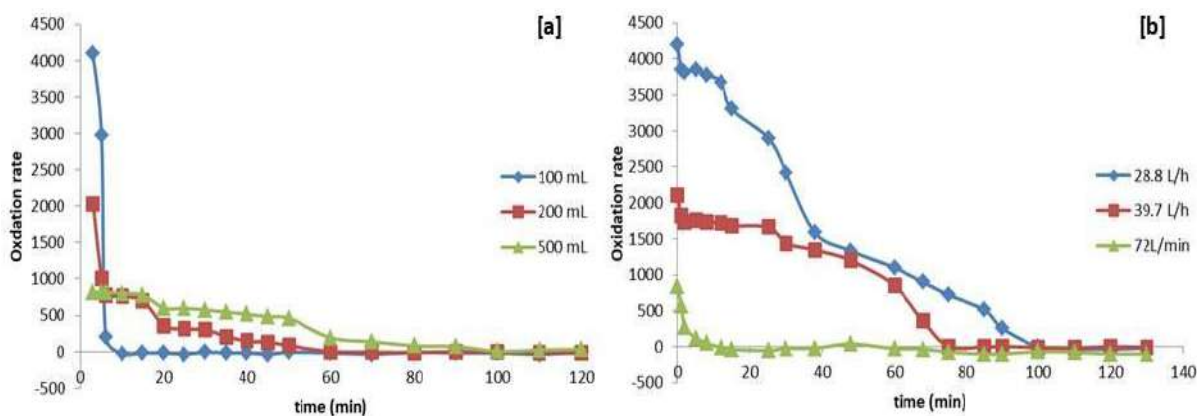


Fig. 4: Graphical representation of oxidation rate for [a] volume of LM and [b] flow rate for liquid bed experiments.

Table 3: The parameters related to absorption of H₂S.

		GRT (min)	H ₂ S loading [g.m ⁻³ .h ⁻¹]	Max. oxidation rate [ppm.min ⁻¹]	Avg. oxidation rate [ppm.min ⁻¹]
Volume	100 mL	0.111	4.203	4095	2421
	200 mL	0.222	2.101	2034	568.1
	500 mL	0.555	0.840	817.2	438.6
Flow rate	0.48 L.min ⁻¹	0.208	2.24	4203	2386.1
	0.66 L.min ⁻¹	0.151	3.08	2101.5	1385.3
	1.2 L.min ⁻¹	0.833	5.60	840.6	370.8

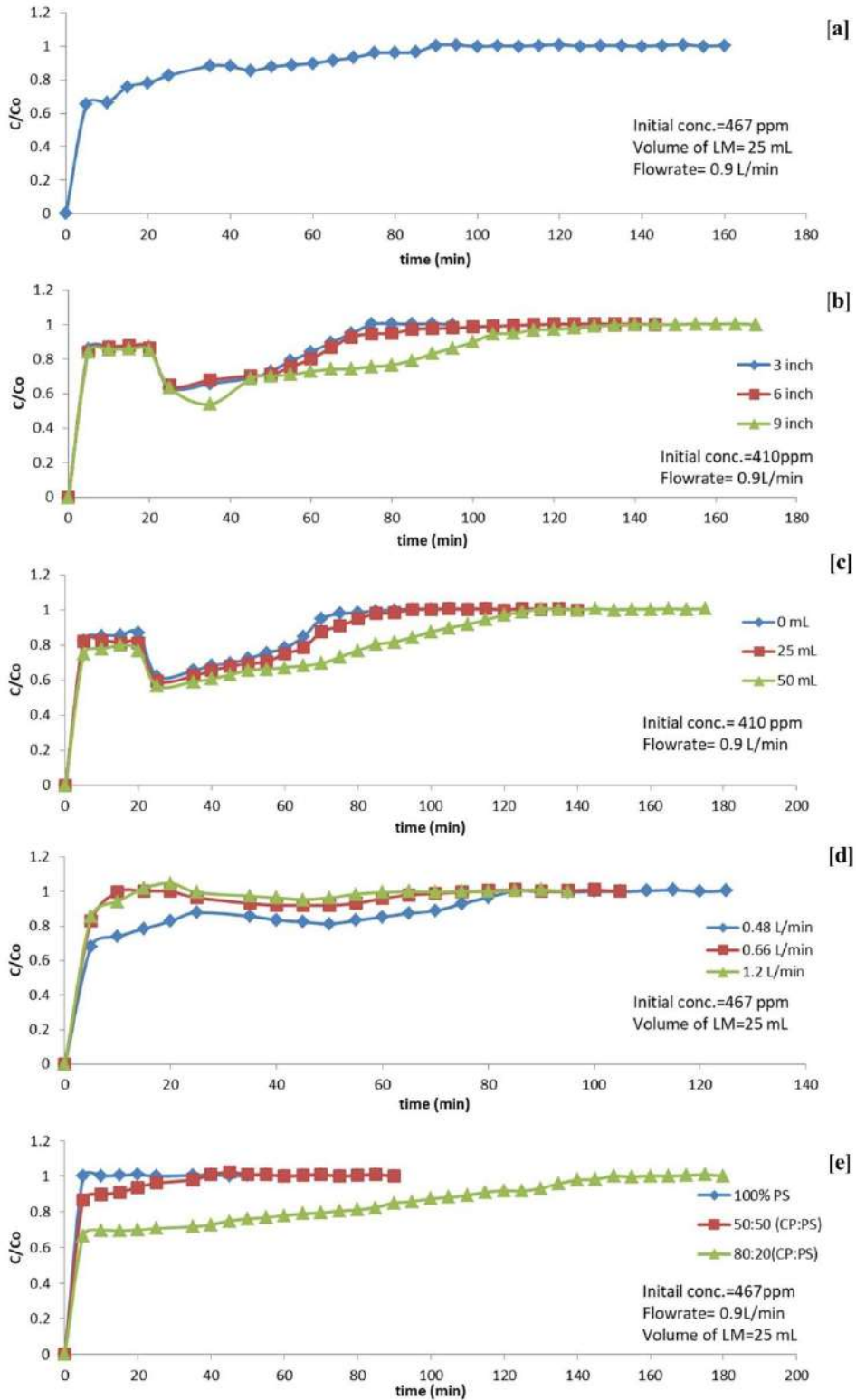


Fig. 5: Graphical representation of plot between time and normalized concentration for [a] time, [b] bed height, [c] volume of culture, [d] flow rate, and [e] filling ratio of the column for continuous column experiments.

around 20% adsorption for the first 20 min. However, this trend changed at the 26th min, and a sudden drop in efficiency was seen. This peculiar behavior can be inferred as single-layer adsorption taking place as biogas enters the column and the efficiency reduces. As the biogas adsorption enters the multi-layer regime, the performance increases; hence a steep decrease in the concentration can be seen. Similar behavior was seen for all the parameters studied. The highest bed height of 9 inches showed better results than the other two, with a saturation time of 110 min of continuous operation. The three and 6-inch bed height columns saturated at 70th and 90th min, respectively.

The column with CP and PS without LM showed adsorption of about 20% at the initial time of operation. The 50 mL LM selected showed similar results as the controls initially. The trend changed at 30 min as the peak gradually increased towards saturation than the control. The flow rate affected the column performance as expected. The higher flow rate, 1.2 mL.min⁻¹, showed rapid saturation at 15 min, whereas the lowest selected flow rate, 0.48 mL.min⁻¹, showed complete saturation at 80 min with 25 mL of culture and an initial H₂S concentration of 467 ppm.

The filling ratio of the column is essential when two or more adsorbents are used. The combination of CP and PS was studied as CP acts as an adsorbent along with LM, and the PS provides porosity in the column. The CP was used in many of these studies as an adsorbent to remove ammonia from the waste stream (Baquerizo et al. 2009). It has been used to remove various types of dyes from wastewater (Chong & Tam 2020).

The 100% CP was used to study the efficiency of the column toward the adsorption of H₂S. However, it was found not feasible as the addition of LM increased the moisture in the system, and the goo-like texture did not allow the air/biogas to pass through the column due to decreased medium porosity (Guo et al. 2007). Hence, an optimized ratio of these two will be necessary for large-scale implementation. The first column was selected with only PS, which reported no adsorption and allowed the biogas to pass through and reach the saturation levels at the first minute. The second column, selected with a 50:50 ratio of CP and PS, showed better results than the previous column. The third column, selected with an 80:20 ratio of CP and PS, showed the best results in removing the H₂S from biogas. However, it had the disadvantage of not allowing the gas to pass through the column easily. The column output was significantly less, and most of the biogas either leaked due to back pressure or could not enter the column. Hence, this setup and the first column with 100% PS were forsaken. The literature suggested that the presence of higher concentrations of H₂S (>500 ppm) in

the inlet might lead to a decrease in a breakpoint, as it was also encountered in the present study (Georgiadis et al. 2021).

As this study mainly focused on the enrichment of biogas, the concentration of CH₄ is important in the further advancement of the experiments. The studies involving the removal of H₂S might also affect the CH₄ concentration adversely. In these studies, the concentration of CH₄ and CO₂ along with H₂S, was recorded. Table 4 represents the amount of CH₄ and CO₂ at different optimized and selected conditions for the study. From the raw biogas, the reduction of CH₄ was assessed to be around 20%. With this representation of each condition set, it can be summarized that the CH₄ loss is minimal when the reduction of H₂S is about 70% on average in the absorption study. From the literature, it was found that a CO₂ concentration of more than 200 ppm affects the H₂S removal through the column (Georgiadis et al. 2021). In the present study, the concentration of CO₂ was around 25 ppm. CO₂ is a recalcitrant gas, which reduces the calorific value and density of the biogas (Aita et al. 2016). In the column studies, the H₂S removal was found to be around 25%, and the CH₄ loss was around 22%. At the saturation point of H₂S, minimal removal of CH₄ of around 5% was noted, and most of the saturation levels showed no removal of CH₄. The variations in CH₄ are believed to be not from the adsorption through column constituents or due to the microbial culture. The study by Aita et al. (2016) and Montebello et al. (2013) state that CH₄ has a lower solubility in the liquid phase. Other literature by Salehi and Chairapat (2019) reveals that the methanogens present can take up CH₄. However, there are high chances of variations in pH which do not allow methanogens to proliferate (Aita et al. 2016).

Iron filings or iron oxide are also being used for H₂S scrubbing. When hydrogen sulfide reacts with iron oxide, it produces iron sulfide, an iron sponge (Andriani et al. 2020). However, the disposal of this is the main issue when it comes to the use of iron sponges. The study conducted by Bagreev et al. (2000) used activated carbon which also oxidizes H₂S to elemental sulfur (Bagreev et al. 2000). These procedures either increases the cost of the process or may become difficult to dispose of or regenerate the used column constituents after saturation.

Adsorption Kinetics, Isotherms, and Models for Continuous Column Studies

The validation of any adsorption process can be done by the study of adsorption kinetics and adsorption isotherms. Kinetics studies the relationship between the retention time of the adsorbent in any media interface and the ion removal rate (Guo et al. 2007). Kinetics is an important validation step to determine the adsorption rate (Habeeb et al. 2016).

Table 4: Comparison of CH₄ and CO₂ removal in pilot scale study along with H₂S.

	Raw biogas conc.			Intermediate conc.			Saturation conc. at n th min		
	CH ₄	CO ₂	H ₂ S	CH ₄	CO ₂	H ₂ S	CH ₄	CO ₂	H ₂ S
Absorption studies									
Amount of culture	53.5	25.6	467	42.2	22.3	137	48.6	23.7	469
Flow rate	53.5	25.6	467	48	13.8	150	48.1	23	470
Adsorption studies									
Time	55.9	26.9	410	43.6	24.3	346	53.9	25.7	411
Bed height	55.9	26.9	410	43.4	26.2	307	54.3	25.3	412
Amount of culture	55.9	26.9	410	45.3	26.5	304	53.6	25.4	412
Flow rate	53.5	25.6	467	42.5	22.1	298	52.6	25.8	469
Filling ratio	53.5	25.6	467	49.5	22.5	295	52.4	25.2	470

Hence, three requisite models were considered for the study: pseudo-first order, pseudo-second order, and Elovich model. The adsorption isotherm is a transit for understanding the relationship among the active sites of adsorbent and the adsorbate at constant temperature (Guo et al. 2007). Off the adsorption isotherms, Langmuir isotherm and Freundlich isotherms were studied (Ayiania et al. 2019, Shah et al. 2017). The following two formulas were used to calculate the adsorbents' adsorption capacity and efficiency.

$$R (\%) = \left(\frac{C_o - C_e}{C_o} \right) \times 100 \quad \dots(4)$$

$$qe = \left(\frac{C_o - C_e}{m} \right) \times V \quad \dots(5)$$

Where C_o and C_e are the initial and equilibrium concentrations of H₂S, respectively; V is the volume of the solution (L); m is the amount of adsorbent (g); ' q_e ' is the adsorption capacity (mL.g⁻¹) and $R\%$ is the adsorption percentage.

The ' q_e ' determines the extent of the occurrence of adsorption. The logarithmic curve between the time and ' q_e ' represents the adsorption capacity of the individual adsorbent. Fig. 6 shows a plot between the same and the logarithmic curve observed until the 60th min. Later the decrement path was observed. The adsorption kinetics study evaluates the rate-controlling steps involved in the process (Georgiadis et al. 2021). The pseudo-second-order

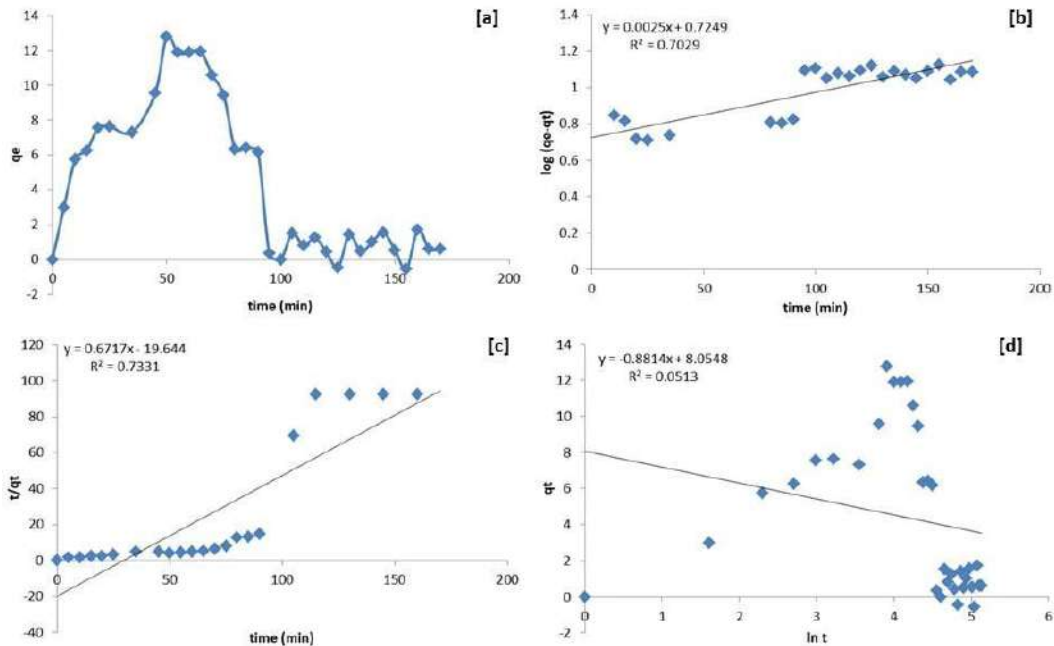


Fig. 6: Plots depicting [a] adsorption capacity of adsorbent, [b] pseudo-first-order, [c] pseudo-second-order, and [d] Elovich, model.

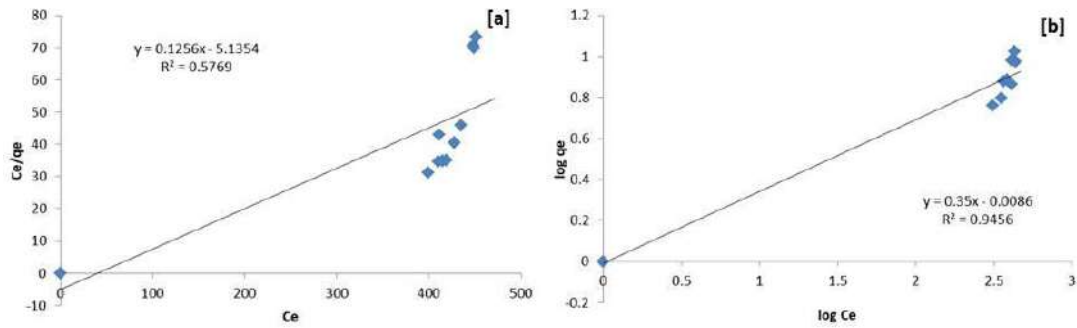


Fig. 7: Plots depicting [a] Langmuir and [b] Freundlich isotherm.

model was the best-fitted kinetic model for the present study, with $R^2 = 0.7331$. The pseudo-second-order kinetics provides the best correlation for the experimental data, and the adsorption mechanism is a chemically rate-controlling step in the adsorption. The other models, i.e., pseudo-first-order and Elovich models, showed $R^2 = 0.7029$ and 0.0513 , respectively. This resulted in the limelight on the non-fitting models (Fig. 6). The Elovich model brings an understanding of whether the reaction is chemical in nature or not.

Although this model did not fit the current study, the other isotherm studies proved the process. When the adsorption isotherms were studied, it was found that the process followed the Freundlich model with $R^2 = 0.9456$. Correspondingly, it made us understand that adsorption occurs on heterogenous surfaces (multilayer adsorption)

(Bagreev et al. 2005). The 'n' value from the linear equation is important because it described the quality of the adsorption taking place and was found to be 0.35 for the present study. The R^2 value for Langmuir isotherm was 0.5769, which did not follow the adsorption conditions. Fig. 7 represents linear equations for each model studied, and Table 5 shows the parameters of the studied models.

In the present study, four continuous column-based models were studied. Every model describes conditions for fulfilling the adsorption process being valid. The Thomas model gives an understanding of the dynamics of the process (Sunzini et al. 2020). The plot for the Thomas model is presented as Fig. 8. The R^2 and kth values were found to be 0.7889 and -0.7819. Other models, such as the Yoon-Nelson model and BDST, showed R^2 as 0.9301 and 0.9911, where the BDST model was

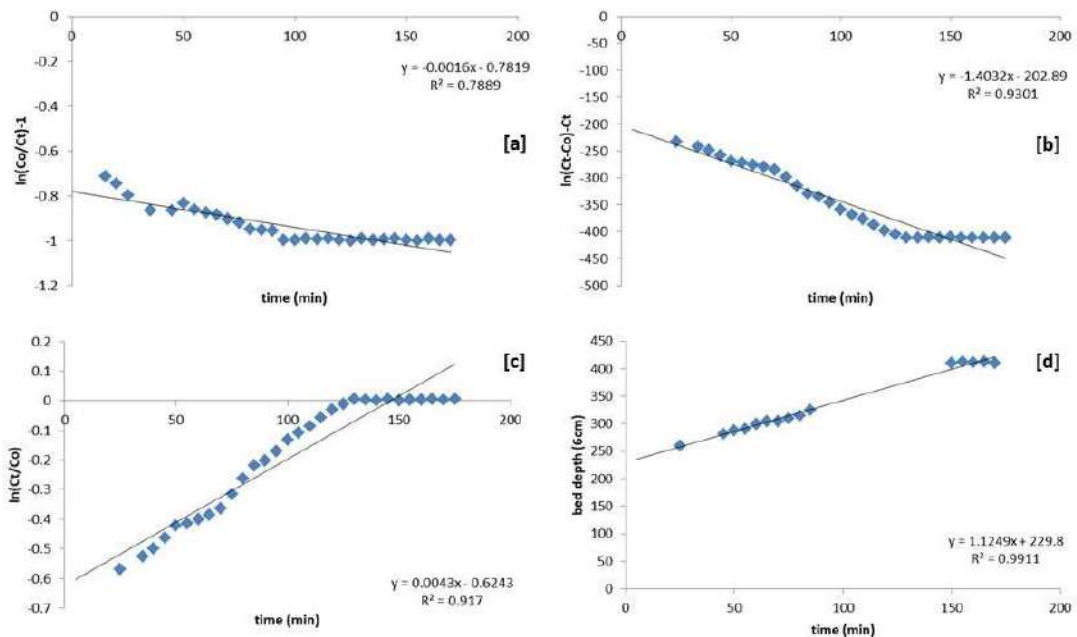


Fig. 8: Plots depicting [a] Thomas model, [b] Yoon-Nelson model, [c] Adams-Bohart model, and [d] BDST model.

Table 5: Parameters of kinetics and isotherms for adsorption.

Models	Parameters		Models	Parameters	
Adsorption kinetics			Continuous column experiments		
Pseudo first order	q_e	0.7249	Thomas model	k_{th}	-0.7819
	k_1	0.0025		R^2	0.7889
	R^2	0.7029	Yoon-Nelson model	k_{YN}	-1.403
Pseudo second order	q_e	-19.64		τ	-202.89
	k_1	0.6717	R^2	0.9301	
	R^2	0.7331	Adams-Bohart model	k_{AB}	0.0043
Elovich model	α	8.054		N_o	-0.6243
	β	-0.8814	R^2	0.917	
	R^2	0.0513	BDST	N_o	1.12
Adsorption isotherms				k_a	229.8
Langmuir isotherm	q_m	0.125	R^2	0.9911	
	b	- 5.13			
	R^2	0.5739			
Freundlich isotherm	n	0.35			
	k_f	-0.0086			
	R^2	0.9456			

the best fit. The equation constants for each model were $k_{YN} = -1.403$, $k_{AB} = 0.0043$, and $k_a = 229.8$, respectively.

The Yoon-Nelson model explains the 50% of the time required for the adsorbate breakthrough (Zulkefli et al. 2017). The rationale of the BDST model is that equilibrium is not immediate in the bed. Therefore, the rate of the sorption process is directly proportional to the fraction of sorption capacity remaining on the media (Aslam et al. 2019). All the parameters associated with the kinetic and isotherm study are presented in Table 5.

Performance of Pilot-scale H₂S Scrubbing System

The optimized conditions from the lab-scale experiments were selected to operate the setup at a larger scale. At a large scale, liquid bed and column setup were combined with increasing the system's overall efficiency. The optimized conditions, such as a filling ratio of 50% of CP and 50% of PS, were uptaken. The column height was 1.5 m with 1 m of the working volume and 0.5 m headspace. The flow rate was fixed as $0.9 \text{ m}^3 \cdot \text{h}^{-1}$, and liquid beds were prepared in a 35 L HDPE tank with 30 L of LM with *Thiobacillus*

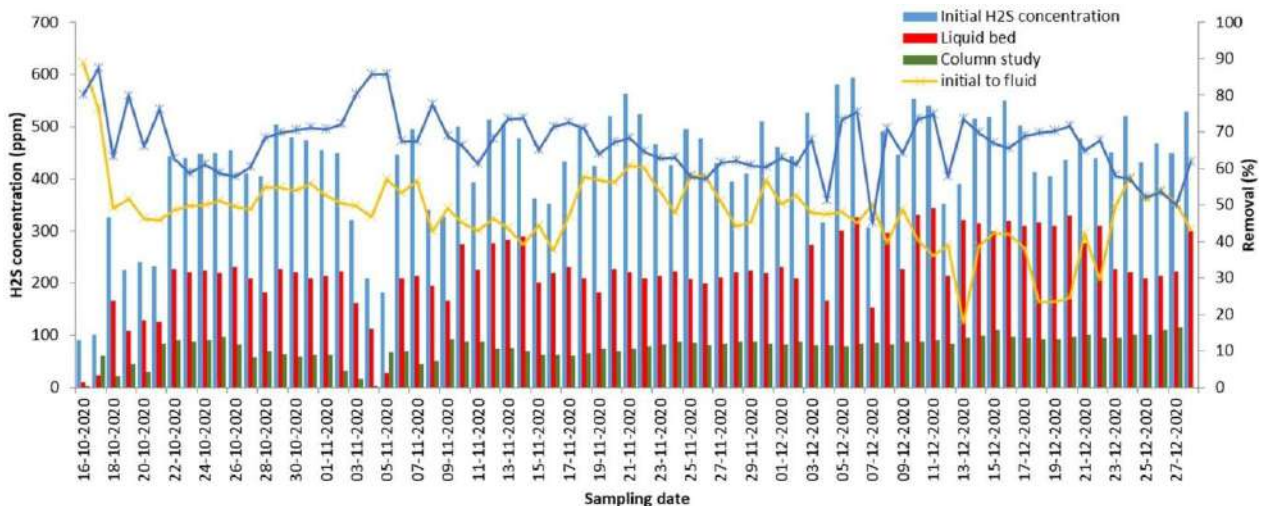


Fig. 9: Graphical illustration of removal of H₂S from biogas at every stage for the pilot scale setup.

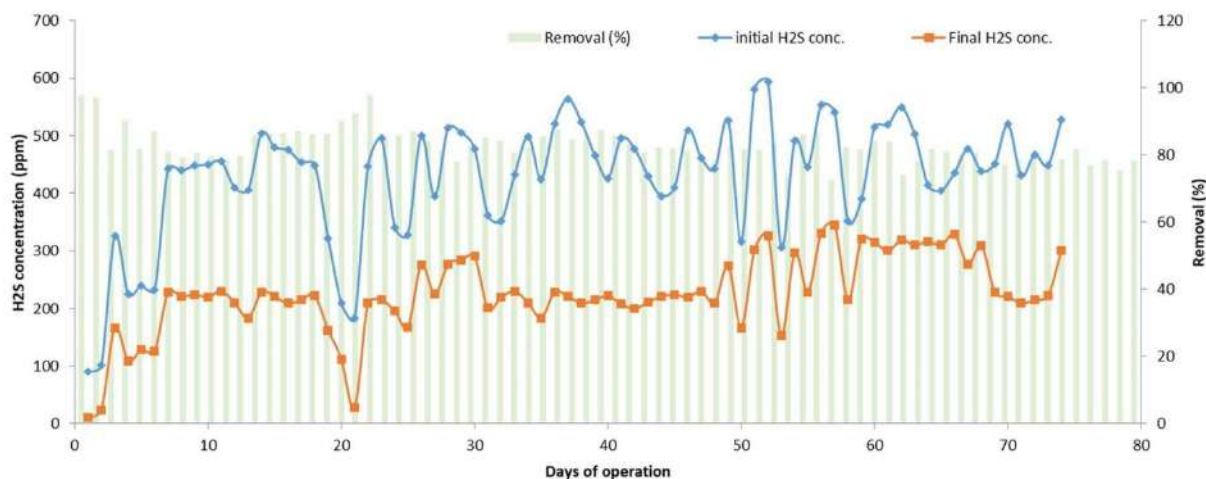


Fig. 10: Graphical representation of overall removal of H₂S from biogas and efficiency at pilot scale setup.

sp. culture added. The outlet concentration from the liquid bed and the column were recorded periodically along with the inlet concentrations. Every day around 1.5 m³ of biogas was passed through the setup. The column and the liquid bed did not attain complete saturation even after 2 months of continuous operation. A small decrease in efficiency was observed after purging 1.5 m³ of raw biogas. However, this did not affect the next day's performance which showed better efficiency in removing H₂S. The addition of LM was done when the moisture in the column decreased, and this was done 4 times during the entire operation. The liquid bed was never refilled or replenished with the new culture.

Fig. 9 shows the variations in the concentrations of H₂S. As can be observed from the graphical representation, an average of 50% removal of H₂S was seen with the liquid bed. 20% more removal was possible by introducing a column in series with the liquid bed. An average of 70-75% of H₂S removal was recorded. The study conducted by Pantoja et al. (2010) encountered above 99% removal of H₂S with CP (Pantoja et al. 2010). This was possible due to the particle size of CP. As the size of the particles is reduced, higher adsorption is achieved (Cherosky 2012). The average inlet concentration was 500 ppm of H₂S and 65% CH₄. At the end of the combined treatment, the H₂S concentration was less than 50 ppm, with 55-60% CH₄ in the biogas. Fig. 10 explains the overall treatment of the system from initial to final concentration. Another study by Habeeb et al. (2016) removed liquid sulfide from wastewater using CP. It was evident that the use of CP adsorbed high concentrations of H₂S. In addition, the LM boosted the efficiency to a higher level.

CONCLUSIONS

The study began with a focus on enriching the biogas with

CH₄ and evaluating its relevance for commercial application. The in-depth study of the adsorption and absorption of H₂S helped to set up the pilot-scale treatment system. By evaluating the laboratory scale study, it was found that the H₂S concentration could be minimized using the combination of LM containing *Thiobacillus sp.* culture with the column containing CP and PS with the LM. These setups were studied individually to know the adsorption, absorption, and microbial conversion. The evaluation study aided in understanding the extent of adsorption in the system. The treatment becomes effective when both the systems are combined, i.e., passing the H₂S-rich biogas through the LM containing *Thiobacillus sp.* culture than through the column. The present study showed that passing biogas through the LM with culture was more efficient than using a column. Since the efficiency needed to be maximized, combining the two was necessary. The combined pilot scale setup successfully reduced the H₂S concentration to 75% with only 5-8% of CH₄ loss, which can be undervalued as the reduction in the H₂S concentration was observed from 500 ppm to less than 50 ppm. The experimental setup successfully ran for over 8 weeks without replenishing the LM with fresh culture. However, the column was added with fresh culture to balance the moisture. The setup was successful in both laboratory and pilot scales and treated 1.5 m³ of raw biogas daily.

ACKNOWLEDGMENTS

The authors thank the BITS Pilani K.K. Birla Goa Campus for providing facilities to conduct the experiments and construct the pilot scale reactors at the Sewage treatment plant (STP).

REFERENCES

- Aita, B.C., Mayer, F.D., Muratt, D.T., Brondani, M., Pujol, S.B., Denardi, L.B. and Da Silveira, D.D. 2016. Biofiltration of H₂S-rich biogas using *Acidithiobacillus thiooxidans*. *Clean Technol. Environ. Policy*, 18(3): 689-703.
- Andriani, D., Rajani, A., Santosa, A., Saepudin, A., Wresta, A. and Atmaja, T. 2020. A review on biogas purification through hydrogen sulphide removal. *IOP Conf. Ser. Earth Environ. Sci.*, 16: 545-563.
- Aslam, Z., Hussein, I.A., Shawabkeh, R.A., Parvez, M.A., Ahmad, W. and Ihsanullah, M. 2019. Adsorption kinetics and modeling of H₂S by treated waste oil fly ash. *J. Air Waste Manag. Assoc.*, 69(2): 246-257.
- Ayiania, M., Carbajal-Gamarrá, F.M., Garcia-Perez, T., Frear, C., Suliman, W. and Garcia-Perez, M.J.B. 2019. Production and characterization of H₂S and PO₄³⁻-carbonaceous adsorbents from anaerobic digested fibers. *Biomass Bioenergy*, 120: 339-349.
- Bagreev, A., Rahman, H. and Bandosz, T. 2000. Study of H₂S adsorption and water regeneration of spent coconut-based activated carbon. *Environ. Sci. Technol.*, 34(21): 4587-4592.
- Bagreev, A.A., Kuang, W. and Bandosz, T.J. 2005. Predictions of H₂S breakthrough capacity of activated carbons at low concentrations of hydrogen sulfide. *Adsorption*, 11(1): 461-466.
- Baquerizo, G., Maestre, J.P., Machado, V.C., Gamisans, X. and Gabriel, D. 2009. Long-term ammonia removal in a coconut fiber-packed biofilter: Analysis of N fractionation and reactor performance under steady-state and transient conditions. *Water Res.*, 43(8): 2293-2301.
- Cherosky, P.B. 2012. Anaerobic Digestion of Yard Waste and Biogas Purification by Removal of Hydrogen Sulfide. The Ohio State University, Ohio.
- Chong, M.Y. and Tam, Y.J. 2020. Bioremediation of dyes using coconut parts via adsorption: A review. *SN Appl. Sci.*, 2(2): 1-16.
- de Oliveira, L.H., Meneguim, J.G., Pereira, M.V., da Silva, E.A., Grava, W.M., do Nascimento, J.F. and Arroyo, P.A. 2019. H₂S adsorption on NaY zeolite. *Micropor. Mesopor. Mater.*, 284: 247-257.
- De Silvaa, J.A., Karunaratne, A. and Sumanasinghea, V. 2019. Wastewater treatment using attached growth microbial biofilms on coconut fiber: A short review. *J. Agric. Value Add.*, 2(1): 61-70.
- Díaz, I., Pérez, S., Ferrero, E. and Fdz-Polanco, M. 2011. Effect of oxygen dosing point and mixing on the microaerobic removal of hydrogen sulphide in sludge digesters. *Bioresour. Technol.*, 102(4): 3768-3775.
- Doungprasopsuk, W. and Suwanvitaya, P. 2017. Effect of oxygen on sulfur products from H₂S removal by *Thiobacillus* in a biotrickling filter column. *Eng. Appl. Sci. Res.*, 44(4): 214-221.
- Dumont, E. (2015). H₂S removal from biogas using bioreactors: a review. *Int. J. Energy Environ.*, 6(5): 479-498.
- Fischer, M.E. 2010. Biogas Purification: H₂S removal Using Biofiltration. The University of Waterloo.
- Georgiadis, A.G., Charisiou, N.D., Gaber, S., Polychronopoulou, K., Yentekakis, I.V. and Goula, M.A. 2021. Adsorption of hydrogen sulfide at low temperatures using an industrial molecular sieve: An experimental and theoretical study. *Acs Omega*, 6(23): 14774-14787.
- Guo, J., Luo, Y., Lua, A.C., Chi, R.A., Chen, Y.L., Bao, X.T. and Xiang, S.X. 2007. Adsorption of hydrogen sulphide (H₂S) by activated carbons derived from oil-palm shell. *Carbon*, 45(2): 330-336.
- Habeeb, O., Ramesh, K., Ali, G.A., Yunus, R., Thanusha, T. and Olalere, O. 2016. Modeling and optimization for H₂S adsorption from wastewater using coconut shell-based activated carbon. *Aust. J. Basic Appl. Sci.*, 10(17): 136-147.
- Ho, K.L., Lin, W.C., Chung, Y.C., Chen, Y.P. and Tseng, C.P. 2013. Elimination of high concentration hydrogen sulfide and biogas purification by chemical-biological process. *Chemosphere*, 92(10): 1396-1401.
- Jensen, A.B. and Webb, C. 1995. Treatment of H₂S-containing gases: A review of microbiological alternatives. *Enzy. Microb. Technol.*, 17(1): 2-10.
- Kulkarni, M. and Ghanegaonkar, P. 2019. Hydrogen sulfide removal from biogas using chemical absorption technique in packed column reactors. *Glob. J. Environ. Sci. Manag.*, 5(2): 155-166.
- Kumari, R. and Dey, S. 2019. A breakthrough column study for removal of malachite green using coco-peat. *Int. J. Phytoremed.*, 21(12): 1263-1271.
- Lin, W.C., Chen, Y.P. and Tseng, C.P. 2013. Pilot-scale chemical-biological system for efficient H₂S removal from biogas. *Bioresour. Technol.*, 135: 283-291.
- Montebello, A.M., Bezerra, T., Rovira, R., Rago, L., Lafuente, J., Gamisans, X. and Gabriel, D. 2013. Operational aspects, pH transition and microbial shifts of an H₂S desulfurizing biotrickling filter with random packing material. *Chemosphere*, 93(11): 2675-2682.
- Monteleone, G., De Francesco, M., Galli, S., Marchetti, M. and Naticchioni, V. 2011. Deep H₂S removal from biogas for molten carbonate fuel cell (MCFC) systems. *Chem. Eng.*, 173(2): 407-414.
- Pantoja, J.L.R., Sader, L.T., Damianovic, M.H.R.Z., Foresti, E. and Silva, E.L. 2010. Performance evaluation of packing materials in the removal of hydrogen sulphide in gas-phase biofilters: polyurethane foam, sugarcane bagasse, and coconut fibre. *Chem. Eng.*, 158(3): 441-450.
- Pokorna, D. and Zabranska, J. 2015. Sulfur-oxidizing bacteria in environmental technology. *Biotechnol. Adv.*, 33(6): 1246-1259.
- Ramírez-Aldaba, H., Valles, O.P., Vazquez-Arenas, J., Rojas-Contreras, J.A., Valdez-Pérez, D., Ruiz-Baca, E. and Lara, R.H. 2016. Chemical and surface analysis during the evolution of arsenopyrite oxidation by *Acidithiobacillus thiooxidans* in the presence and absence of supplementary arsenic. *Sci. Total Environ.*, 566: 1106-1119.
- Salehi, R. and Chairapat, S. 2019. Single-/triple-stage biotrickling filter treating an H₂S-rich biogas stream: statistical analysis of the effect of empty bed retention time and liquid recirculation velocity. *J. Air Waste Manag. Assoc.*, 69(12): 1429-1437.
- Sethupathi, S., Zhang, M., Rajapaksha, A.U., Lee, S.R., Mohamad Nor, N., Mohamed, A.R. and Ok, Y.S. 2017. Biochars as potential adsorbents of CH₄, CO₂, and H₂S. *Sustainability*, 9(1): 121.
- Shah, M.S., Tsapatsis, M. and Siepmann, J.I. 2017. Hydrogen sulfide capture: From absorption in polar liquids to oxide, zeolite, and metal-organic framework adsorbents and membranes. *Chem. Rev.*, 117(14): 9755-9803.
- Sunzini, F., De Stefano, S., Chimenti, M.S. and Melino, S. 2020. Hydrogen sulfide as potential regulatory gasotransmitter in arthritic diseases. *Int. J. Mol. Sci.*, 21(4): 1180.
- Zhang, L., De Schryver, P., De Gussem, B., De Mynck, W., Boon, N. and Verstraete, W. 2008. Chemical and biological technologies for hydrogen sulfide emission control in sewer systems: A review. *Water Res.*, 42(1-2): 1-12.
- Zhao, Q., Leonhardt, E., MacConnell, C., Frear, C. and Chen, S. 2010. Purification technologies for biogas generated by anaerobic digestion. *Compr. Biometh.*, 24: 625.
- Zhu, H.L., Papurello, D., Gandiglio, M., Lanzini, A., Akpınar, I., Shearing, P.R. and Zhang, Y.S. 2020. Study of H₂S removal capability from simulated biogas by using waste-derived adsorbent materials. *Processes*, 8(9): 1030.
- Zicari, S.M. 2003. Removal of hydrogen sulfide from biogas using cow-manure compost. *Citeseer*, 11: 22-36.
- Zulkefli, N.N., Masdar, M.S., Isahak, W., Jahim, J., Majlan, E., Rejab, S. and Lye, C. 2017. Mathematical modeling and simulation on the adsorption of Hydrogen Sulfide (H₂S) gas. *IOP Conf. Ser. Mater. Sci. Eng.*, 1603: 150411.



Comparative Assessment of Medical Waste Management in Multi-System and Selected Teaching Hospitals in Ekiti State, Nigeria

O.J. Oyeboade* , C.C. Okpala*, S.M. Ajibade** , N.M. Ogarekpe*** , S.A. Afolalu**** , A.O. Coker*****, S.G. Udeagbara***** and A.T. Adeniyi*****

*Civil and Environmental Engineering Department, Afe Babalola University, Ado-Ekiti, Ekiti State, Nigeria

**Department of Computer Engineering, Istanbul Ticaret Universitesi, Istanbul, Turkey

***Department of Civil Engineering, Cross River University of Technology, Calabar, Nigeria

****Mechanical and Mechatronics Engineering Department, Afe Babalola University Ado-Ekiti (ABUAD), Ado-Ekiti, Ekiti State, Nigeria

*****Civil Engineering Department, Faculty of Technology, University of Ibadan, Ibadan, Nigeria

*****Chemical and Petroleum Engineering Department, Afe Babalola University Ado-Ekiti (ABUAD), Ado-Ekiti, Ekiti State, Nigeria

†Corresponding author: O.J. Oyeboade; oyeboadedare@yahoo.com, ojoyeboade@abuad.edu.ng

Nat. Env. & Poll. Tech.

Website: www.neptjournal.com

Received: 15-09-2022

Revised: 18-10-2022

Accepted: 19-10-2022

Key Words:

Medical waste

Effective management

Multi-system hospitals

Public health

ABSTRACT

Medical facilities, such as hospitals, clinics, and locations where diagnosis and treatment are administered, create dangerous waste that predisposes individuals to deadly infections. Medical waste management aims to improve health and prevent public health and environmental threats. Questionnaires, interviews, site visitations, and observations were utilized to determine the management strategies implemented in the three hospitals and evaluate the efficacy of waste management. The hospitals under review are Afe Babalola University Multi-system Hospital (AMSH), Ekiti State University Teaching Hospital (EKSUTH), and Federal Teaching Hospital Ido-Ekiti (FETHI). Statistical Package for the Social Sciences (SPSS) was utilized for the statistical analysis of the questionnaires, and the mean assessment was utilized to compute the waste per bed each day. The results revealed that the three hospitals' sharp, infectious, and pharmaceutical waste is the most sorted. All hospitals burn their medical waste in incinerators but dispose of the ashes in dumpsites. The mean evaluation of all hospitals' medical waste was weighed to establish the overall amount generated. The total amount of medical waste created at AMSH, EKSUTH, and FETHI is 31.5 kg, 53.6 kg, and 135.1 kg, respectively. The medical waste generated per bed per day in AMSH, EKSUTH, and FETHI is 0.61 kg, 0.74 kg, and 0.73 kg, respectively. It was determined that the proper management and disposal of waste is a critical obligation of healthcare facilities. There should be a provision for educating personnel about the consequences of inappropriately disposing of medical waste.

INTRODUCTION

There are several ways to ensure health, restore patients' health, and save lives through healthcare activities. However, they also generate waste, 20% hazardous to health, damage, or exposure to synthetic or radioactive materials. Waste management is a serious problem that affects everyone, from healthcare workers to patients and their families, and

the general public is no exception. It's also possible that improper treatment or disposal of such waste could result in environmental contamination or desecration. There are several easy and effective ways to limit the dangers associated with hazardous medical waste.

The current method of waste management in our current circumstances has been causing worry in recent years. Litters of solid waste and wastewater pollute diverse ecosystems and the environment. Businesses and industries in our society have a history of dumping waste into rivers and farmlands without first treating it, endangering the natural environment in the process. The possibility of contamination of the water resources of Calabar due to poor waste management and the

ORCID details of the authors:

O. J. Oyeboade: <https://orcid.org/0000-0003-2792-146X>

N. M. Ogarekpe: <https://orcid.org/0000-0001-5436-9434>

S. M. Ajibade: <https://orcid.org/0000-0002-3452-1889>

S. A. Afolalu: <https://orcid.org/0000-0002-1186-001X>

potential human health risk to the residents of the metropolis has been reported (Ogarekpe et al. 2023). The effects of poor waste management are enormous, hence, unacceptable. Hospitals and other medical care facilities are not exempt from this rude protest. Municipal wastes (MW) are distinct from other waste because of their destructive properties. It has received minimal attention compared to managing other forms of solid waste in Nigeria (Agunwamba et al. 2013). The strategic and holistic management of biomedical waste in sub-Saharan Africa cannot be overemphasized. Healthcare Waste Management (HCWM) ensures that medical wastes are handled correctly and disposed of safely. The entire waste management process, from planning to disposal, which is covered by HCWM (Oyeboade et al. 2022, Oyeboade 2022a). According to (Adu et al. 2010), healthcare workers should get regular in-service training on proper source segregation of MW to aid in the efficient and secure handling, transportation, treatment, and disposal of waste from healthcare Institutions. The transmission of infectious organisms can be greatly reduced by separating hospital waste at the site of its creation. The most important natural resources are land and water since they are essential to all life (Verma et al. 2022, Oyeboade 2022b). The lack of water treatment technology has led to severe pollution in developing and growing countries, worsening the water crisis (Abdelfattah et al. 2022). A large amount of solid garbage is produced by human activity (Sharma 2008).

PAST STUDIES

During production and consumption, waste might be anything that is no longer needed. The definition of waste is everything the owner discards pursues, or is forced to discard (EU 2013). Waste is everything that will be disposed of, has been designated for disposal, or must be disposed of by national legislation as specified by the Basel Convention. Unwanted resources are what we mean when we talk about waste. Debris from our homes, offices, schools, and other

public institutions (domestic waste), as well as industrial waste (industrial waste from corporations and industries), are all examples of garbage (industrial waste).

Nigeria's waste-generating situation has been a source of global and local concern. Cities in Nigeria, which are among the world's fastest expanding, are confronted with the challenge of SWG. The implications are substantial when a country's population rapidly increases, and waste is not adequately handled (Babayemi & Dauda 2009). SWG and management in cities in developing countries have emerged as important issues. Waste products are created in considerable numbers due to the rapid turnover of things manufactured, sold, and acquired. A wide range of factors, including population expansion, changes in lifestyle, increased use of throwaway materials, excessive packaging of goods, and consumer habits, all contribute to incremental change. Depending on the location, Nigerian municipal trash densities typically range from 250 to 370 kg.m⁻³. About 25 million tons of garbage are produced yearly in impoverished countries at daily rates of 0.44 to 0.6 kilos per capita per day, whereas in wealthy nations, the rate is 0.7 to 1.2 kilograms per hour per day (Olukanni & Mnenga 2015).

Wastes produced from different sources are classified as follows. Fig. 1 shows different sources of waste.

- I. Urban or Municipal wastes
- II. Industrial wastes
- III. Commercial wastes
- IV. Agricultural wastes

Medical Waste

When it comes to the waste created during medical or diagnostic treatments, it is known as medical waste (or HCW). MW comes from hospitals, doctors' offices, dentists' offices, blood banks, veterinary hospitals and clinics, and



Source: (Almuneef & Memish 2003)

Fig. 1: Sources of waste.

medical research institutes and labs. Hospitals, physicians' offices, dental offices, blood banks, veterinary hospitals and clinics, and medical research institutes and labs generate medical waste. Medical discharge, or "controlled hospital waste," contains blood, bodily fluids, or other infectious agents (EU 2013).

In Nigeria and throughout the world, MW is a major source of concern since it has the potential to spread disease or cause damage. Care workers and employees who deal with medical waste, patients and their families, and the broader community, are all in danger from improper waste management. In addition, incorrect waste disposal or treatment might lead to environmental pollution or contamination. Among the many types of hazardous waste are sharps (of which infected ones are a subcategory), medical waste, radioactive waste, industrial by-products, and infectious waste. Other types of hazardous waste include pharmaceutical waste and containers under pressure. When it comes to medical waste management (MWM), each organization takes a different approach, but it must be evaluated as a whole. Fig. 2 presents the different types of medical waste.

Medical Waste Management and Treatment

The MWM literature is dense with studies examining and explaining various management techniques and methodologies for achieving effective, responsive, and long-term processes. Managing waste in health facilities is complicated, and everyone involved in the industry, from floor cleaners to senior managers, must understand and address it to be effective.

It's a global challenge when it comes to MWM. If waste is not adequately handled in the healthcare business, it can harm the environment, the local people, and both domestic and wild animals. Waste disposal capacity decreases as the number of HCI grows, and the population increases, putting people and natural resources in danger (Kwikiriza et al. 2019).

Medical Waste Segregation

Everyone on the team is affected by the importance of segregation in waste management. Training, regular information, and frequent checks are all important for maintaining the long-term viability of the system already in place. Disposal and management costs can be reduced by segregating the many types of waste produced simultaneously. Most MWM begins with segregation (Arivarasu et al. 2020).

Sharps

A "sharp" instrument has a point or edge that may pierce or cut through the flesh. Sharps can be used at home, at work, and on the road to treat the medical needs of humans and their pets. Examples of sharps include needles, syringes, lancets, auto injectors, infusion sets, and connection needles/sets.

Around the world, 66,000 cases of hepatitis B, 16,000 cases of hepatitis C, and 200-5,000 cases of HIV infection were linked to sharps injuries reported by the World Health Organization (WHO 2013).

Sharp waste must be carefully handled and disposed of. The goal of sharps waste management is to keep all things safe until they can be disposed of in an environmentally-



Source: (Puška et al. 2021)

Fig. 2: Medical waste.

friendly manner. The autoclave is the last step in the sharps waste disposal process. Only chemotherapeutic sharp waste is normally burned, making it a less prevalent alternative. Safety measures must be adopted to minimize harm from sharps while increasing the amount of waste that can be disposed of. The best and safest way to manage sharps waste is to follow hospital guidelines and government regulations, instructing healthcare providers on properly disposing of the waste.

Pharmaceutical Waste

Examples of pharmaceutical waste include drugs that are outdated or contaminated with other substances. Most pharmaceutical waste comprises expired, unused, spilled, and harmful pharmaceuticals, medications, and immunizations. Discarded bottles, vials, and connecting tubing used in handling pharmaceuticals are also included in this category. Healthcare facilities should only deal with small amounts of pharmaceutical waste.

Pathological Waste

Waste considered pathological comprises organs, tissues, and body parts or fluids such as blood. Pathological waste is made up of identifiable body parts and infected animal corpses. Even though these pathological wastes may include nutritional and physiological components, they must be handled as infectious wastes for safety purposes (Nwachukwu et al. 2013). When performing research at veterinary facilities, researchers must use various animal feces exposed to infectious organisms.

Infectious Waste

According to (NESREA 2020), biomedical research lab waste, pathological waste, and standard disposable tools and equipment contaminated with infectious pathogens are all included in the definition of infectious waste. Infectious waste includes blood, synovial fluid, spermatozoa, cervical mucus, nausea, fecal matter, and urinalysis samples.

Infectious waste infections can put people's health in danger, causing a global disaster and causing problems in health, economics, and other aspects of human activity. To minimize the source of infection, waste management is crucial, and preventing waste from ever becoming infectious would necessitate a difficult and specialized treatment and management system. Waste containment, transportation, treatment, and disposal systems will be strained as infectious MW rises (Ali et al. 2021).

Chemical Waste

To fulfill safety, health, and regulatory standards, chemical waste is typically segregated on-site into designated waste carboys and transported by a professional contractor. It is possible to flush sodium chloride solutions and other watery

waste. Some chemicals require a lot of water to be flushed away. An example of a drying agent is an acid or alkaline solution that contains soluble salts, such as soluble inorganic salts or alcohols that include salts. Toxic chemicals are segregated in watery waste. Chlorinated waste and non-chlorinated waste are the two categories of organic solvent waste. To avoid the formation of dioxins, chlorinated solvent waste is frequently incinerated at high temperatures (Shibamoto et al. 2007).

Radioactive Waste

Radioisotopes are commonly used in tertiary care centers for diagnosis and treatment. MWM includes the proper disposal of radioactive waste. One of the primary goals of radioactive waste management is to safeguard the public, medical professionals, and patients from exposure to harmful radiation. Using radioisotopes for diagnostic or therapeutic reasons necessitates keeping radiation levels at tolerable ranges. To evaluate radiation safety, regular hospital and radiation staff monitoring is required. You should keep track of the types and quantities of radioactive waste you produce and how you dispose of it. During waste disposal, a radiation safety officer must be present (Khan et al. 2010).

Medical Waste Disposal and Treatment

In underdeveloped countries, the most prevalent means of disposing of MW are incineration or landfilling on a limited scale. Microwave irradiation, electromagnetic treatment, high-temperature sterilization, chemical hydrolysis, and ionized combustion are some non-thermal treatments that have gained favor recently (Zafar 2022).

Individuals who come into contact with hazardous healthcare waste are in danger of becoming hurt or contaminated. It has been claimed that certain health institutions dispose of syringes in pit latrines. Patients and communities can become infected when syringes are not properly disposed of, such as by burning (destructive incineration) or burying them. Practitioners' understanding of proper disposal techniques for spent syringes is limited, which may be traced back to a lack of curriculum in medical schools (Manyele & Lyasenga 2013).

Incineration of Waste

Human and veterinary healthcare facilities, academic hospitals, and medical research facilities should practice ecologically responsible waste disposal. This category also includes non-infectious household garbage. From 1800 to 2000 degrees Fahrenheit, garbage is combusted in this process (982 to 1093 degrees Celsius). On the other hand, on-site burning has the advantage of being quick and easy, but it has issues with emissions. Incineration minimizes the waste that

must be disposed of, even if landfill cannot be completely substituted. Compressors are commonly integrated inside garbage trucks to limit the amount of waste delivered to the incinerator. Before 1997, infectious medical waste, including body parts and tissues, could only be disposed of by burning. As more information on incineration safety becomes available, certain governments and municipalities will continue promoting it as a treatment option.

In the burning of medical waste, there are three primary types of incinerators. They include;

1. Controlled-Air incinerator
2. Excess-Air incinerator
3. Rotary Kiln incinerator

Autoclaves

Autoclaving, or steam sterilization, is the most commonly used alternative to incineration. It's less expensive and poses no known health risks. This procedure is used to sterilize or disinfect waste before landfilling. Thermal breakdown of waste occurs in a pressure and temperature-controlled

chamber. This method will destroy bacteria. Most medical waste, especially microbiological waste, may be autoclaved. As a result, autoclaving is not an option for hazardous chemical wastes like pathology and cytotoxicity. Steam sterilizes bio-hazardous waste. After sterilization, waste can be disposed of in landfills or burnt under less strict conditions. Fig. 3 is a picture of an autoclave.

Microwave

Waste can also be disinfected with the use of microwave technology. Computerized controls guarantee that the minimal conditions for disinfection and appropriate equipment performance are satisfied. Approximately 90% of MW may be handled using this method, similar to autoclaving. According to reports, shredding reduces volume and uses less energy than an incinerator. Due to the size of the autoclave and the amount of material, temperatures can vary from 250 to 325 degrees Fahrenheit, and pressures can range from 40 to 80 PSI. For 20 to 30 minutes, waste is normally held at a high temperature and pressure. When the cycle is over, the steam is removed from the autoclave, the



Source: (Bondtech 1997)

Fig. 3: Autoclave.



Source: (Pascoe et al. 2020)

Fig. 4: Microwave.

pressure is relieved, and the autoclave is ready to be opened. Fig. 4 below shows a microwave used to treat medical waste.

Chemical Disinfection

Chlorine and other chemical disinfectants are employed in this method. When dealing with liquid waste, chemical disinfection is the way to go. Microbes in waste, contamination level, disinfectant concentration and quantity, contact duration, and mixing requirements all play a role in determining the efficacy of disinfection. Alternatively, MW might be ground up and disinfected using a liquid solution. Earth's waste is more evenly dispersed, making it easy to dispose of any remaining debris. Sewage and landfills are used to dispose of liquids and solids. Reactive chemicals can be used to make some chemical waste inert. Most chemical waste is disposed of in this way.

Irradiation

The waste must be sterilized using a cobalt source. Gamma radiation from cobalt destroys all microorganisms in sewage. Cobalt's pricing and operational costs have prevented commercial waste management organizations from adopting this technology. Also, there are concerns about the radiation-based cleaning method. Autoclaving and microwave procedures should still be used to dispose of pathological waste.

Sanitary Landfill

The most ecologically responsible method of disposing of MW is to use a sanitary landfill. Waste is buried in the earth, where microorganisms slowly convert it into harmless molecules. Many toxic chemicals, bacteria, radioactive substances, and other hazardous materials will seep into the soil if anti-seepage measures aren't implemented at the MW dump system. The anti-seepage layer should be made using clay, high-density polyethylene, and other materials to ensure the sanitary landfill is adequately selected. Installation of landfill gas collection and distribution pipelines is also necessary. According to (Oyeboade 2019), decomposable waste is created more than non-decomposable waste, particularly in Ado Ekiti. In his research, he designed a sanitary landfill, which included evaluating the landfill's lifespan, locating a suitable site, determining the cost analysis, and shaping the landfill's building timeline.

Best Practice for Medical Waste Handling

Most MW issues may be avoided if healthcare providers follow simple best practices. Employees should be aware of the guidelines and then sort and segregate all waste into the proper, color-coded waste containers based on the kind of waste. It is imperative that all containers of waste be properly labelled and that they are accompanied by the proper paperwork while being transported. A professional

Table 1: Standard colour coding recommendations.

Type of waste	Color coding	Type of container
Household refuse	Black	Plastic bag
Waste entails a risk of contamination	Yellow	Plastic bag or container
Anatomical waste	Yellow	Plastic bag or container
Infectious waste	Yellow marked "highly infectious."	Plastic bag or container which can be autoclaved
Sharps	Yellow	Sharps container
Chemical and pharmaceutical waste	Brown, marked with a suitable symbol	Plastic bag, container

Source: (ISWA 2017)

MW disposal company may help a hospital achieve these best practices. Table 1 presents the standard color coding system recommended by the International Solid Waste Association (ISWA) for collecting and disposing of medical waste.

Medical Waste Management Practices in Ekiti State

According to Nigeria's constitution, local governments must deal with waste. In Ekiti State, there is no need for the EKSWMB to act as the sole governmental entity responsible for waste management. As a result of the local government authority's inability to handle the waste management profession, the Ekiti State Waste Management Board was established. When it started, waste management in Ado-Ekiti was also disorganized and embarrassing for most of the city's residents.

Medical Waste Management Practices in Nigeria

Poor countries produce much thicker, wetter, and more harmful types of garbage than wealthy nations, so affluent countries' waste disposal methods don't work there. There are also many unplanned slum areas in underdeveloped nations, making it difficult for collecting vehicles to navigate the densely populated areas. According to Awosusi (2010), underdeveloped countries like Nigeria, where a wide range of health issues compete for limited resources, tend to provide less attention and importance to waste management in the healthcare industry. A lack of practical information and studies on the public health repercussions of poor waste management in the healthcare sector is a problem. A lack of reliable records and effective waste management practices in many poor nations means that hundreds of tons of healthcare waste are thrown in waste dumps and other areas of the environment, frequently with non-hazardous waste. According to other surveys (Offorma 2017), MW disposal systems are almost nonexistent in Nigeria.

MATERIALS AND METHODS

Southern Nigeria's Ekiti State is bordered by four states: Kwara State in the north; Kogi State in the northeast; Ondo State in the south and southeast; and Osun State in the west. Ado-Ekiti is the capital of Ekiti State, which was created in 1996 from a section of Ondo State. Most of the state's population is from the Ekiti tribe, a subset of the Yoruba people. Nigeria's tiniest state, Ekiti, is the country's 30th-largest and 31st-most populous, with an estimated population of 3.3 million in 2016. The state borders Nigeria's lowland forests in the south and Guinea's forest-savanna mosaic in the north. The Ekiti State map is seen in Fig. 5.

Ekiti State's economy is partly built on agriculture, including yams, rice, cocoa, and cassava. Logging and tourism are two important small businesses. Ekiti has the country's joint-thirteenth highest Human Development Index and is considered the core of the Ekiti people's motherland.

Research Methodology

Surveys were used as part of the study's research design. Each hospital was asked to complete a short survey based on best practices for the safe disposal of medical waste. Interviewees included healthcare managers, nurses, nursing assistants, and trash handlers within and outside institutions. There was a questionnaire about MW creation and the key elements of its collection, transportation, treatment, and final

disposal. The data collected will be utilized to examine the profile of the MWM program implemented by the hospitals. To gather primary data on MWM procedures, we conducted site visits. MW generation per patient per day was calculated for each facility.

Data Collection and Method of Analysis

The information was gathered throughout March and April in the year 2022. A mix of primary and secondary sources provided the research data, and they include:

- I. Weighing scales were used to calculate the daily waste created per bed in each hospital.
- II. The same strategy was utilized in the design of the questionnaires to gather data on the management of waste created in the selected hospitals. Also included were questions on possible factors that might affect waste development and management practices (Wafula et al. 2019, Awodele et al. 2016)
- III. Literature includes journals, textbooks, conference proceedings, dissertations, and online publications.

RESULTS AND DISCUSSION

Quantity of Medical Waste Generated in the Hospitals

The quantity of waste generated in the three hospitals under study could not be calculated in terms of waste category



Fig. 5: Map of Ekiti State.

because not all the MW in the three hospitals was sorted. Hence, the quantity of the daily waste generated was determined according to the departments/units/wards where the waste was generated. Table 2 presents the quantity of MW generated in FETHI.

Quantity of Waste Generated at Federal Teaching Hospital Ido Ekiti

From Plate 1 (Fig. 7), the total quantity of MW generated at FETHI is 135.1 kg per day. There are 450 beds in this teaching hospital. There is a total of 185 beds in use. The quantity of MW per bed per day is 0.73 kg. Table 2 further presents the Environmental Department generates the highest quantity of waste (42.3 kg). The table shows that the renal department generates the least MW (6.3 kg). Fig. 6 presents the distribution of the MW in percentages.



Fig. 7: Plate 1- Medical waste being weighed in FETHI.

Table 2: Quantity of Medical Waste Generated at FETHI.

S/N	Department/Unit/Ward	Weight [kg]
1.	Male Medical Ward	10
2.	Female Medical Ward	7
3.	Radiology Department	29.5
4.	Theatre Department	6.5
5.	Mortuary Department	18.2
6.	Environmental Department	42.3
7.	Renal Department	6.3
8.	Emergency Department	15.3
	TOTAL	135.1

Source: (Fieldwork 2022)

As shown in Fig. 6, the units with the leading proportion are Environmental Department (31.31%), Radiology Department with (21.84%), Mortuary Department with (13.47%), Emergency Department (11.33%), Male Medical Ward (7.40%), Female Medical Ward with (5.18%), Theatre Department with (4.81%) and Renal Department with (4.66%). Table 3 presents the quantity of MW generated in EKSUTH.

Quantity of Medical Waste Generated at Ekiti State University Teaching Hospital Ado Ekiti

Table 4 gives the total quantity of MW generated at EKSUTH as 53.6kg per day. There are 238 beds in EKSUTH and 72 beds in use, so the quantity of MW per bed per day is 0.74 kg. In this hospital, the unit that generates the highest quantity of waste is the Radiology Department (14 kg), and the unit that generates the least amount of waste is the Emergency Department (3.5 kg). Fig. 8 presents the distribution of MW in percentages.

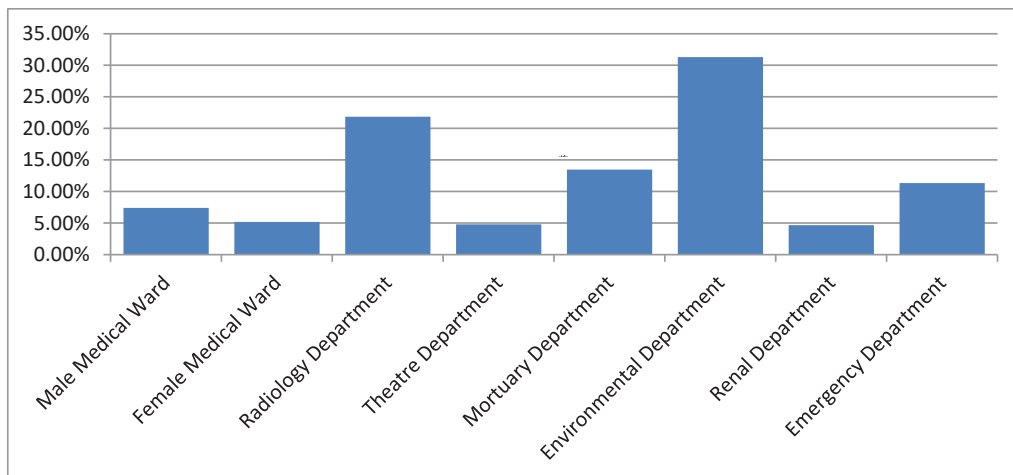


Fig. 6: Proportion of the percentage of medical waste in Federal Teaching Hospital Ido Ekiti.

Table 3: Quantity of medical waste generated at EKSUTH.

S/N	Department/Unit/Ward	Weight [kg]
1.	Male Medical Ward	11
2.	Female Medical Ward	4.9
3.	Radiology Department	14
4.	Theatre Department	10.5
5.	Laboratory Department	3.8
6.	Emergency Department	3.5
7.	GENERAL OUTPATIENT DEPARTMENT	5.9
	TOTAL	53.6

Source: (Fieldwork 2022)

The proportion of MW generated in the different units of the teaching hospital is shown in plate 2 (Fig. 9). The locations with leading proportions are Radiology Department (26.12%), Male Medical Ward (20.52%), Theatre Department

(19.59%), General Outpatient Department (11%), Female Medical Ward (9.14%), Laboratory Department (7.09%) and Emergency Department with (6.53%). Table 4 presents the quantity of medical waste generated at AMSH.

Quantity of Medical Waste Generated at Afe Babalola University Multi-System Hospital Ado Ekiti

Table 4 gives the total quantity of waste generated at AMSH is 31.2kg. There are 400 beds in this teaching hospital, and the total number of beds in use is 51.

The quantity of MW generated per bed per day is 0.61kg. Table 4 presents that the male medical ward generates the most waste (7.5kg). The Pediatrics Ward generates the lowest quantity of waste (3.9kg). Fig. 10 presents the distribution of MW in percentages.

The proportion of the MW generated in the different units of the teaching hospital is shown in plate 3 (Fig. 11). The

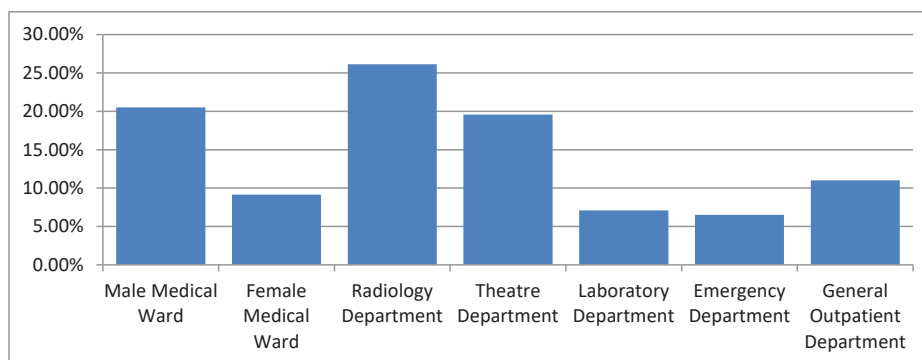


Fig. 8: Proportion of the percentage of medical waste in Ekiti State University teaching hospital.



Fig. 9: Medical waste being measured in EKSUTH.

Table 4: Quantity of medical waste generated at AMSH.

S/N	Department/unit/ward	Weight [kg]
1.	Male Medical Ward	7.5
2.	Female Medical Ward	6
3.	Emergency Department	4.3
4.	Renal Department	4
5.	Pediatrics Ward	3.9
6.	Obstetrics and Gynecology Department	5.5
	TOTAL	31.2

Source: (Fieldwork 2022)

units with the highest proportions are the Male Medical Ward (24.04%), Female Medical Ward (19.23%), Obstetrics and Gynecology Department (17.63%), Emergency Department (13.78%), Renal Department (12.82%), and Pediatrics Ward (12.5%).

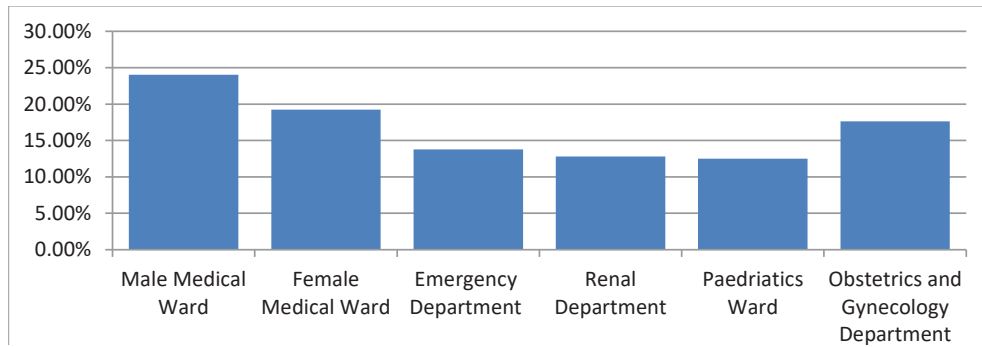


Fig. 10: Proportion of the percentage of medical waste in Afe Babalola University Teaching Hospital Ado Ekiti.



Fig 11: Plate 3 - Medical waste being measured in AMSH.

Medical Waste Sorting in the Hospitals

The questionnaires administered to the health workers were used to determine the frequency of waste generated in the teaching hospitals. There were 54 respondents; 22 from Afe Babalola University Multi-System Hospital, 17 respondents from Federal Teaching Hospital Ido Ekiti, and 15 respondents from Ekiti State University Teaching Hospital. Table 5 presents all respondents' responses to MW sorting.

From Table 5, sharps are the most segregated MW in the hospitals, with 88.9% and 48 respondents segregating sharp waste in the teaching hospitals. This table also presents sharp, infectious, and pharmaceutical waste, which are the most segregated in teaching hospitals. Fig. 11 presents the graphical representations of the waste frequencies of MW sorted out in all the hospitals and Table 6 presents the frequency of medical waste sorted out in AMSH.

Table 5: Frequency of medical waste sorted in all the Teaching Hospitals.

		Responses		Percent of Cases
		N	Percent	
The type of waste is sorted out	Sharps	48	22.5%	88.9%
	Infectious waste	44	20.7%	81.5%
	Pathological waste	32	15.0%	59.3%
	Pharmaceutical waste	40	18.8%	74.1%
	Chemical waste	26	12.2%	48.1%
	Radioactive waste	23	10.8%	42.6%
Total		213	100%	394.4%

Source: (Fieldwork 2022)

Medical Waste Sorted Out in Afe Babalola University Multi-System Hospital.

From Table 6, it is clear that in AMSH Sharps, infectious and chemical wastes are the most sorted wastes in teaching hospitals. The least sorted-out waste in AMSH is a pharmaceutical waste. Table 7 presents the frequency of medical waste sorted out in EKSUTH.

Medical Waste Sorted out in Ekiti State University Teaching Hospital

Table 8 presents that sharps, infectious waste, and pharmaceutical waste are the most segregated waste in EKSUTH. The least segregated waste is chemical waste and radioactive waste. Table 8 presents the frequency of

Table 6: Frequency of medical waste sorted out in AMSH.

The type of waste is sorted out	Sharps	Count	19
		% within the Hospital of Respondent	86.4%
	Infectious waste	Count	16
		% within the Hospital of Respondent	72.7%
	Pathological waste	Count	14
		% within the Hospital of Respondent	63.6%
	Pharmaceutical waste	Count	13
		% within the Hospital of Respondent	59.1%
	Chemical waste	Count	16
		% within the Hospital of Respondent	72.7%
	Radioactive waste	Count	14
		% within the Hospital of Respondent	63.6%
Total		Count	22

Source: (Fieldwork 2022)

medical waste sorted out in FETHI. The tables presented that sharps, infectious waste, and pharmaceuticals are the most segregated waste in FETHI. However, it further says that infectious waste is the most segregated waste in the hospital, and radioactive waste is the least segregated waste in FETHI.

Medical Waste Sorted Out in Federal Teaching Hospital Ido Ekiti

Methods of Medical Waste Management

The questionnaire administered to the health professionals and workers examined MW awareness, collection, treatment, and disposal. Table 9 presents the respondents' awareness of the risk of poor MWM.

Table 10 shows that 94.4% of respondents know the risk of poor MWM, while a few are unaware. All respondents in EKSUTH, FETHI, and about 19 in AMSH know the risk of improper MWM. This indicates that most healthcare professionals and workers in these teaching hospitals know the risks of poor MWM. Table 9 presents the number of respondents that have been to training on MWM.

Table 10 presents that 22 respondents have attended training in MWM, and 31 respondents have not been to any training or offered courses on MWM. Most respondents in AMSH and EKSUTH have not attended any training on MWM. Table 11 presents the waste management methods practiced in the hospital.

Table 7: Frequency of medical waste sorted out in EKSUTH.

Type of wastes sorted out	Sharps	Count	16
		% within the Hospital of Respondent	94.1%
	Infectious waste	Count	14
		% within the Hospital of Respondent	82.4%
	Pathological waste	Count	9
		% within the Hospital of Respondent	52.9%
	Pharmaceutical waste	Count	14
		% within the Hospital of Respondent	82.4%
	Chemical waste	Count	5
		% within the Hospital of Respondent	29.4%
	Radioactive waste	Count	5
		% within the Hospital of Respondent	29.4%
Total		Count	17

Source: (Fieldwork 2022)

Table 8: Frequency of medical waste sorted out in FETHI.

The type of waste is sorted out	Sharps	Count	13
		% within the Hospital of Respondent	86.7%
Infectious waste		Count	14
		% within the Hospital of Respondent	93.3%
Pathological waste		Count	9
		% within the Hospital of Respondent	60.0%
Pharmaceutical waste		Count	13
		% within the Hospital of Respondent	86.7%
Chemical waste		Count	5
		% within the Hospital of Respondent	33.3%
Radioactive waste		Count	4
		% within the Hospital of Respondent	26.7%
Total		Count	15

Source: (Fieldwork 2022)

From plate 4 (Fig. 13), incineration is widely used in hospitals in Ekiti State. 15 respondents from AMSH and FETHI indicated that incineration is the waste management method in their hospitals, while 16 respondents from EKSUTH agreed with this same waste management method. Incineration is one of the best methods for MWM, and these hospitals practice such a method. Fig. 12 presents the graphical representation of this frequency, and Table 12 presents the location of medical waste segregation.

Table 12 presented that 50% of the respondents believe that MW should be segregated at the source of generation. Eight respondents in AMSH and EKSUTH are of the opinion that MW should be sorted at the source of generation, while 11 respondents in FETHI also agree with this. The table further shows that 18 respondents do not know where MW

Table 9: Are you aware of the risk of poor medical waste management?

	Frequency	Percent	Valid Percent
Yes	51	94.4	94.4
No	1	1.9	1.9
Maybe	2	3.7	3.7
Total	54	100.0	100.0

Source: (Fieldwork 2022)

Table 10: Have you attended any training in medical waste management?

	Frequency	Percent	Valid Percent	Cumulative Percent
Yes	22	40.7	40.7	40.7
No	31	57.4	57.4	98.1
Maybe	1	1.9	1.9	100.0
Total	54	100.0	100.0	

Source: (Fieldwork 2022)

should be segregated; 11 are from AMSH, and 6 are from EKSUTH. Fig. 14 indicates the graphical representation of this frequency. Table 13 presents the frequency of the procedures for collecting and handling waste.

Table 14 presents that the majority of the respondents have procedures for the collection and handling of waste in hospitals. 16 respondents in AMSH, 13 from EKSUTH, and 14 from FETHI have procedures for collecting and handling waste. Table 14 presents the type of containers for sharps.

98% of respondents consent to the safety boxes as the preferred container for sharps. All respondents in EKSUTH, FETHI, and 21 respondents in AMSH are aware of the

Table 11: Which waste management method is practiced in your hospital?

	Frequency	Percent	Valid Percent	Cumulative Percent
Open burning	4	7.4	7.4	7.4
Incineration	46	85.2	85.2	92.6
Landfills	1	1.9	1.9	94.4
Open dumping	3	5.6	5.6	100.0
Total	54	100.0	100.0	

Source: (Fieldwork 2022)

Table 12: Location of medical waste segregation.

	Frequency	Percent	Valid Percent	Cumulative Percent
Source of generation	27	50.0	50.0	50.0
Outside the bin	9	16.7	16.7	66.7
I don't know	18	33.3	33.3	100.0
Total	54	100.0	100.0	

Source: (Fieldwork 2022)



Fig. 12: Graphical representation of waste management methods practiced in hospitals.



Fig. 13: Plate 4: A preceding incinerator in EKSUTH.

presence of safety boxes for sharps in their hospitals. These sharps include needles, syringes with needles, broken glass ampoules, scalpels, blades, infusion sets, etc. Table 15 presents the frequency of color coding for MW disposal.

Table 15 shows that more than 50% of the respondents color code their waste for disposal, and more than 30% do not color-code their waste. 15 respondents in AMSH, 6 respondents in EKSUTH, and 8 respondents in FETHI

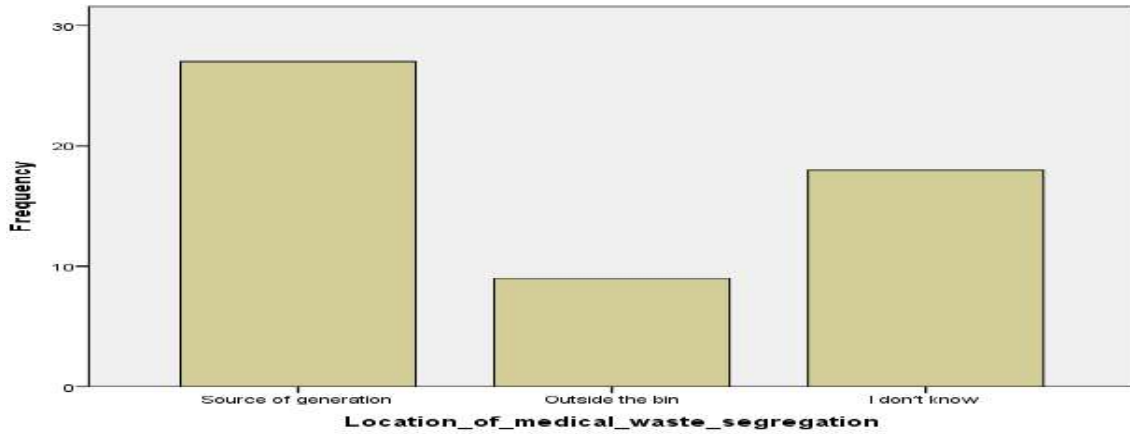


Fig. 14: Graphical representation of the location of medical waste segregation.

believe that they color-code their waste for disposal, but 8 respondents from EKSUTH, 3 respondents from AMSH, and 7 respondents from FETHI do not agree. Fig. 15 below presents the graphical representation of this frequency. Table 16 presents the waste disposal frequency in hospitals. Plate 5 (Fig. 15) presented Colour coded waste for disposal in EKSUTH (Fig. 11).

Table 16 presents 37 respondents who consent to waste disposal daily, and 13 respondents dispose of waste when storage is full. 14 respondents in AMSH, 13 in EKSUTH, and 10 in FETHI dispose of their MW daily, while 5 from AMSH, 4 from EKSUTH, and FETHI disposes of their waste when full.

CONCLUSIONS

MWM is critical in any country to safeguard the general public’s health. Healthcare workers need to be aware of the

Table 13: Do you have procedures for the collection and handling of waste?

	Frequency	Percent	Valid Percent	Cumulative Percent
Yes	43	79.6	79.6	79.6
No	4	7.4	7.4	87.0
Maybe	7	13.0	13.0	100.0
Total	54	100.0	100.0	

Source: (Fieldwork 2022)

Table 14: Types of container for sharps.

	Frequency	Percent	Valid Percent	Cumulative Percent
Nylon bags	1	1.9	1.9	1.9
Safety boxes	53	98.1	98.1	100.0
Total	54	100.0	100.0	

Source: (Fieldwork 2022)

dangers of inappropriate MW disposal. Patients, medical workers, and waste handlers can all die due to improper handling of MW. The government should establish fundamental rules for MWM in the health sector. In the course of our investigation, there have been challenges, problems, and positives. The results of this study, which included AMSH, EKSUTH, and FETHI, led to the following conclusions.

1. The wastes that get the most attention in the three hospitals are sharps. Sharps are stored in red and white boxes by AMSH, EKSUTH, and brown boxes by FETHI. Boxes are located in key locations in each hospital and may only be accessed by healthcare staff.
2. Before the waste was taken away to be thrown away, it was collected at the three hospitals in bins next to

Table 15: Do you color code your medical waste for disposal?

	Frequency	Percent	Valid Percent	Cumulative Percent
Yes	29	53.7	53.7	53.7
No	18	33.3	33.3	87.0
Maybe	7	13.0	13.0	100.0
Total	54	100.0	100.0	

Source: (Fieldwork 2022)

Table 16: Waste disposal frequency.

	Frequency	Percent	Valid Percent	Cumulative Percent
Daily	37	68.5	68.5	68.5
Weekly	4	7.4	7.4	75.9
When storage is full	13	24.1	24.1	100.0
Total	54	100.0	100.0	

Source: (Fieldwork 2022)



Fig. 15: Plate 5 - Colour-coded waste for disposal in EKSUTH.

patients' beds and other places inside and outside of the different units/wards.

3. The most sorted out wastes in the three hospitals are Sharps, Infectious waste, and Pharmaceutical waste, with a percentage frequency of 88.9%, 81.5%, and 74.1%, respectively.
4. The total medical waste generated at AMSH, EKSUTH, and FETHI is 0.61kg, 0.74 kg, and 0.73 kg, respectively.
5. AMSH and EKSUTH use appropriate color codes for their waste, while FETHI use the same color code for all their waste.
6. All hospitals have similar waste management methods.
7. MW treatment is practiced in all hospitals. The sharp wastes are sterilized using an autoclave before final disposal.
8. Incineration is the waste management method used in all hospitals. The type of MWI technology used is the controlled-air incinerator. It is also known as a starved air incinerator or modular combustion. But after being burned, all hospitals dump their MW out in the open with their other general waste.
9. There is no current dumpsite near any of the hospitals or any existing environment in any of the hospitals studied.
10. While most hospital employees know the dangers of improper MW disposal, they get little to no training.
11. FETHI and EKSUTH are secondary care level hospitals, while AMSH is a tertiary care level hospital.

Recommendations

The following are the most important suggestions that came out of the evaluation that was conducted.

1. Educating the public about the dangers of MW and the best methods to follow.
2. Segregation should always take place at the source of generation.
3. As part of the treatment process, contaminated sharps need to be transported in a safe, secure way.
4. Hazardous material waste minimization should be a priority.
5. More MW recycling firms should be put up to use recyclable medical waste.
6. The correct management and disposal of waste is a vital responsibility of healthcare establishments.
7. Educate employees on the dangers of improperly disposing of MW by providing them with educational opportunities.
8. For a Health Care Facilities (HCF) to be registered, it should be required to adhere to correct waste disposal rules and laws.
9. All hospitals utilized the incinerator to dispose of medical waste. The following factors should be taken into account and implemented to ensure the appropriate application of this technique:
 - i. They ensure that only the right kinds of waste are burnt through effective waste reduction and segregation measures.

- ii. This incinerator must be constructed in a location far away from people. As a result, there will be less exposure and danger.
 - iii. A qualified person should be in charge of the operation. To achieve the necessary combustion conditions and emission levels, this is essential.
 - iv. Protective gear should always keep workers safe, and suitable temperatures must be used.
 - v. Defective components should be replaced or repaired regularly.
10. It is necessary to dispose of MW through incineration properly. The residues are disposed of in a uniquely engineered landfill or used as building aggregate. The following considerations must be made before MW may be disposed of in landfills:
- i. The landfill must be built and operated appropriately, with all the necessary environmental regulations.
 - ii. We must verify that disposal mechanisms are safe to avoid harm to waste operators.
 - iii. Humans and animals should not come close to MW until it has been disposed of.
 - iv. Waste personnel should be informed when MW is carried to the site for disposal so that they can take further measures if necessary.
 - v. The wastes should be unloaded as close as possible to where they will be dumped and then dumped immediately.
 - vi. When HCW is dumped, it should be covered with soil.
 - vii. The landfill should be isolated, and a security fence should be placed.

REFERENCES

Abdelfattah, I., Abdelwahab, W. and El-Shamy, A.M. 2022. Environmental remediation of contaminated wastewater with ammonium using clay-based adsorbents. *Nature Environ. Pollut. Technol.*, 21(4): 641.

Adu, R.O., Gyasi, S.F., Esumang, D.K. and Otobil, K.B. 2020. Medical waste-sorting and management practices in five hospitals in Ghana. *J. Environ. Pub. Health*, 20: 6-17.

Agunwamba, J.C., Emenike, P.C. and Tenebe, I.T. 2013. Comparative analysis of hospital waste management in Calabar metropolis and developed countries. *Int. J. Struct. Civ. Eng. Res.*, 2(4): 154-167.

Ali, M. B., Kyari, D.M.Z. and Lamini, M. 2021. Practices and challenges of infectious medical waste management: A qualitative approach to infectious waste management in Maiduguri, Borno State Nigeria. *Int. J. Pure Appl. Sci. Res.*, 12(2): 96-107.

Almuneef, M. and Memish, Z.A. 2003. Effective medical waste management: It can be done. *Am. J. Infec. Contr.*, 31(3): 188-192.

Arivarasu, L. 2020. Segregation of medical waste and disposal management: A survey. *Europ. J. Mol. Clin. Med.*, 7(1): 2197-2209.

Awodele, O., Adewoye, A.A. and Oparah, A.C. 2016. Assessment of medical waste management in seven hospitals in Lagos, Nigeria. *BMC Pub. Health*, 16(1): 1-11.

Awosusi, A.O. 2010. Assessment of environmental problems and methods of waste management in Ado-Ekiti, Nigeria. *Afr. Res. Rev.*, 4(3): 171.

Babayemi, J.O. and Dauda, K.T. 2009. Evaluation of solid waste generation, categories and disposal options in developing countries: A case study of Nigeria. *J. Appl. Sci. Environ. Manag.*, 13(3): 54-69.

European Union (EU). 2013. Decision No 1386/2013/EU of the European Parliament and of the Council of 20 November 2013 on a General Union Environment Action Programme to 2020 'Living well, within the limits of our planet', Annex A, paragraph 43(d) (OJ L 354, 28.12.2013, p. 171-200).

Khan, S., Syed, A.T., Ahmad, R., Rather, T.A., Ajaz, M. and Jan, F.A. 2010. Radioactive waste management in a hospital. *Int. J. Health Sci.*, 4(1): 39.

Kwikiriza, S., Stewart, A. G., Mutahunga, B., Dobson, A. E. and Wilkinson, E. (2019). Whole systems approach to hospital waste management in rural Uganda. *Front. Pub. Health*, 7: 136.

Manyele, S. and Lyasenga, T. 2013. Factors affecting medical waste management in low-level health facilities in Tanzania. *Afr. J. Environ. Waste Manag.*, 1: 42-55.

National Environmental Standards and Regulations Enforcement Agency (NESREA). 2020. Guidelines for Handling Infectious Waste within the Context of Coronavirus (COVID-19). <https://www.nesrea.gov.ng/handling-infectious-waste-guidelines>

Nwachukwu, N.C., Orji, F.A. and Ugbogu, O.C. 2013. Healthcare waste management—public health benefits, and the need for effective environmental regulatory surveillance in the Federal Republic of Nigeria. *Curr. Top Pub. Health*, 2, 149-178.

Offorma, I.M. 2017. Comparative Assessment Of Healthcare Waste Management In Public and Private Specialist Healthcare Facilities In Port Harcourt, Rivers State, Nigeria. Public Health. Dissertation, National Postgraduate Medical College of Nigeria (NPMCN), Nigeria.

Ogareke, N.M., Nnaji, C.C., Oyeboade, O.J., Ekpenyong, M.G., Ofem, O.I., Tenebe, I.T. and Asitok, A.D. 2023. Groundwater quality index and potential human health risk assessment of heavy metals in water: a case study of Calabar metropolis, Nigeria. *Environ. Nanotechnol. Monit. Manag.*, 100: 780.

Olukanni, D.O. and Mnenga, M.U. 2015. Municipal solid waste generation and characterization: A case study of Ota, Nigeria. *Int. J. Environ. Sci. Toxicol. Res.*, 3(1): 1-8.

Oyeboade, O.J. 2019. Design of engineered sanitary landfill for efficient solid waste management in Ado-Ekiti, South-Western Nigeria. *J. Multidiscip. Eng. Sci. Stud.*, 41: 521-539.

Oyeboade, O.J. 2022. Adoption of Environmental Engineering Strategies for Public Health and Sustainable Development. In Ayeni, O., Oladokun, O. and Orodu, O.D. (eds), *Advanced Manufacturing in Biological, Petroleum, and Nanotechnology Processing*. Springer, Cham, pp. 197-209.

Oyeboade, O.J. 2022. Sustainable Waste Management Towards Circular Economy in Nigerian Context: Challenges, Prospects and Way Forward. In Ayeni, O., Oladokun, O. and Orodu, O.D. (eds), *Advanced Manufacturing in Biological, Petroleum, and Nanotechnology Processing*. Springer, Cham, pp. 237-248.

Oyeboade, O. J. and Otoko, J.A. 2022. Medical waste management and design of a low-cost incinerator for reduction of environmental pollution in a multi-system hospital. *Nature Environ. Pollut. Technol.*, 21(4): 389.

Oyeboade, O. J., Coker, A. O., Sridhar, M. K. C., & Ogareke, N. M. (2022). Biomedical Waste Management Practices in Sub-Saharan Africa: Insights of Its Impacts and Strategies for Its Mitigation. In *Advanced Manufacturing in Biological, Petroleum, and Nanotechnology Processing* (pp. 256-249). Springer, Cham.

- Pascoe, M.J., Robertson, A., Crayford, A., Durand, E., Steer, J., Castelli, A. and Maillard, J.Y. 2020. Dry heat and microwave-generated steam protocols for the rapid decontamination of respiratory personal protective equipment in response to COVID-19-related shortages. *J. Hosp. Infec.*, 106(1): 10-19.
- Puška, A., Stević, Ž. and Pamučar, D. 2021. Evaluation and selection of healthcare waste incinerators using extended sustainability criteria and multi-criteria analysis methods. *Environ. Dev. Sustain.*, 17: 1-31.
- Sharma, R. 2008. Municipal solid waste management in Ajmer City, Rajasthan: An overview. *Nature Environ. Pollut. Technol.*, 8(4): 741-744.
- Shibamoto, T., Yasuhara, A. and Katami, T. 2007. Dioxin formation from waste incineration. *Rev. Environ. Contam. Toxicol.*, 57: 419.
- Bondtech. 1997. Medical Waste Autoclaves. Retrieved from <https://bondtech.com/autoclaves/medical-waste-autoclaves> (Accessed 12 December 2022)
- Verma, S.K., Prasad, A.D. and Verma, M.K. 2022. An assessment of ongoing developments in water resources management incorporating SWAT model: Overview and perspectives. *Nature Environ. Pollut. Technol.*, 21(4): 162.
- Wafula, S.T., Musiime, J. and Oporia, F. 2019. Healthcare waste management among health workers and associated factors in primary healthcare facilities in Kampala City, Uganda: A cross-sectional study. *BMC Pub. Health*, 19(1): 1-10.
- World Health Organization (WHO). 2013. *Safe Management of Wastes From Healthcare Activities*, Second Edition. WHO, Washington DC.
- Zafar, S. 2022. Medical waste management in developing countries. Bioenergy consult. Retrieved from <https://www.bioenergyconsult.com/medical-waste-management>. (Accessed 12 December 2022)



An Inappropriate Rise in NO₂ During the COVID-19 Pandemic in the Urban Area of Chhattisgarh, India

A. Zeb*, I. U. Khan*, S. Tripathi**, M. R. Sahu*** and A. Kumar****† 

*Department of Mathematics, COMSATS University, Islamabad, Abbottabad Campus, Pakistan

**Department of Science and Technology, Government of India, India

***Department of Biotechnology, Government V.Y.T. P.G. Autonomous College, Durg, India

†Corresponding author: A. Kumar; anilkumardurg1996@gmail.com

Nat. Env. & Poll. Tech.
Website: www.neptjournal.com

Received: 14-08-2022

Revised: 06-10-2022

Accepted: 19-10-2022

Key Words:

Air quality index
COVID-19
Lockdown
Urban area

ABSTRACT

The COVID-19 first case was reported in India on January 30, 2020, and in Chhattisgarh on March 19, 2020, and since then a sharp surge has been noticed. The government of India imposed a nationwide lockdown on March 25, 2020, a complete suspension of human activities, viz., industry, construction, transport, academic institutions, etc., which resulted in an improvement in air quality (a decrease in PM_{2.5} and PM₁₀, alteration in NO₂ and an increase in O₃). But the rate of cases of COVID-19 has increased sharply, and eventually, under economic pressure, the lockdown was withdrawn on June 1, 2020, which further accelerated the exponential growth of COVID-19 cases. We noticed that in the Chhattisgarh State of India, the alteration in the air quality index during the lockdown period is continuing even after the restoration of anthropogenic activities. Among PM_{2.5}, PM₁₀, NO₂, and O₃, the behavior of NO₂ was found to be different than others; it was found to increase during the lockdown period but further decreased with the resumption of anthropogenic activities. We conclude that the air quality index has an insignificant impact on COVID-19 infection.

INTRODUCTION

The world has been facing a serious problem with the COVID-19 pandemic since December 2019, and therefore, the problem has threatened human life, not only by its pathogenic impact (Bai et al. 2020, Sohrab et al. 2020), but also by its economic impact (Bai et al. 2020) to a greater extent. Initially, it was reported in Wuhan, a city in the Republic of China, and gradually spread to more than 200 countries through human-to-human transmission. Only in July 2020 did the scientific community recognize that it spreads not only through human-to-human contact but also through the air; the WHO later validated the concept. On July 23, the total number of confirmed COVID-19 cases in India reached 1,238,798 with a death toll of 29,865.

There is no specific treatment known to the scientific community for SARS-CoV-2 infection; therefore, the world was compelled to go under a state of lockdown to prevent human-to-human transmission of the virus, which resulted in the suspension of human movement, vehicular movement, and industrial activities to a greater extent. Environmentalists

have predicted a large reduction in greenhouse gas (GHG) emissions to the environment; some of them have predicted the biggest reduction of greenhouse gases after World War II (Global Carbon Project 2020). In several parts of the world, the total lockdown led to a significant reduction in nitrogen dioxide (NO₂), particulate matter, and GHG from the environment, especially in France, Germany, Italy, and Spain (European Space Agency 2020).

More than 91% of the world's population lives in polluted air, which has contributed to adverse impacts on human health, and it is supposed that nearly 8% of total deaths in the world, especially in Asia, Africa, and Europe, are caused by air pollution (World Health Organization, 2016). According to several authors, air pollution causes death through cardiovascular failure regardless of age (Peng et al. 2009, Wong et al. 1999) and respiratory failure (Katanoda et al. 2011, Nakao et al. 2018, Spix et al. 1998). Zhu et al. (2020) have predicted a positive correlation between higher concentrations of air pollution and a higher risk of SARS-CoV-2 infection.

In several studies, it's been predicted that anthropogenic activities are the main contributor to air pollution, viz., industrial emissions, mining, vehicular emissions, and real

ORCID details of the authors:

A. Kumar: <https://orcid.org/0000-0002-1667-4419>

estate activities. In India, a total lockdown was imposed on March 25 to inhibit SARS-CoV-2 transmission, which resulted in the suspension of all anthropogenic activities and probably the emission of air pollutants. Although the COVID-19 spread wasn't controlled even after the lockdown, India witnessed the world's largest migration of laborers in the meantime. The COVID-19 infection surge was not reduced after 70 days of lockdown, but it caused severe economic strain, forcing the Government of India to lift the lockdown on June 1, 2020. In 2013, Tamrius et al. (2013) reported on the transmission and survival of viruses (influenza and SARS viruses) under the influence of environmental factors. Rahman and MacNee (2000) have concluded that air pollutants create toxicity in the respiratory and cardiovascular systems of people and that some pollutants, viz., ozone, oxides of nitrogen, and suspended particulates, act as potent oxidants by acting directly on lipid or protein or indirectly on intracellular oxidant pathways. Glencross (2020) established a link between environmental pollutants and the immune system, which explains the acceleration of respiratory disorders in the presence of novel coronavirus infection. They have also concluded that the air pollutant can affect different immune cell types such as particle-clearing macrophages, inflammatory neutrophils, and dendritic cells that create adaptive immune responses. Thus, it becomes essential to evaluate the air quality index, particularly particulate matter, ozone, and oxides of nitrogen,

to understand the pathogenic impact of the novel coronavirus. In the Indian state of Chhattisgarh, there is Asia's largest steel plant, as well as many thermal power plants and coal mines, which continuously pour particulate matter and oxides of nitrogen, and accelerate O_3 in the atmosphere. In this COVID-19 pandemic, the evolution of the air quality index to understand the pathogenicity of novel coronaviruses is essential and may be helpful for future planning.

In the present paper, we have tried to address the air quality index of the state of Chhattisgarh considering major cities with industrial activities, viz. Bhilai, Durg, Raipur, Bilaspur, Korba, and Raigarh. The air quality index was comparatively examined during the pre-lockdown period, post-lockdown period, and a brief unlocking period. We have also examined the correlation between air quality and a surge of COVID-19 infection in the state of Chhattisgarh, India, to understand the behavior of the air quality index and the infectious nature of SARS-CoV-2.

MATERIALS AND METHODS

Research Settings

The present study has been carried out in cities with major business and industrial activities in the state of Chhattisgarh, India, and for this study, we selected Bhilai (21.1938°N, 81.3509°E), Durg (21.1623°N, 81.4279°E), Raipur

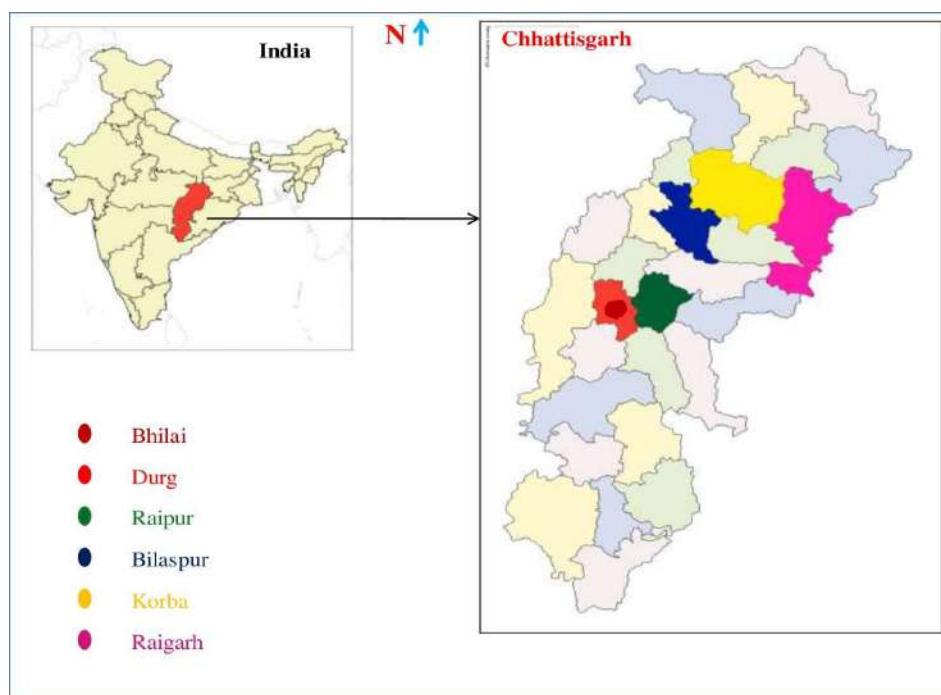


Fig. 1: Selected major cities of Chhattisgarh state of India for the study of Air Quality Index, during COVID-19 pandemic.

(21.2514°N, 81.6296°E), Bilaspur (22.0797°N, 82.1409°E), Korba (22.3595°N, 82.7501°E) and Raigarh (22.0078°N, 83.3362°E) (Fig. 1).

Measures of Variables

For the air quality index study, we considered PM_{2.5}, PM₁₀, NO₂, and O₃ right from January 1, 2020, to July 15, 2020, with data collected at an interval of every 15 days. The source of the data was Copernicus Atmospheric Monitoring Service South America Model: GMAI/CPTEC/INDP, through Plume Labs. The cases of COVID-19 infection for the retrospective data were collected from the government site. To perform a comparative study, the data were segmented into three blocks: first, the pre-lockdown period; second, the lockdown period; and third, the unlocking period.

Data Analysis

For each parameter of air quality (PM_{2.5}, PM₁₀, NO₂, O₃), a one-way analysis of variance was calculated to test the level of significance. The correlation coefficient of Karl Pearson was calculated to determine the relationship between the air quality index and an increase in COVID-19 infections.

RESULTS AND DISCUSSION

The average air quality index of six cities in Chhattisgarh (Bhilai, Durg, Raipur, Bilaspur, Korba, and Raigarh) was measured for the pre-lockdown period (Jan 1, 2020, to March 15, 2020), the lockdown period (April 1, 2020, to July 1, 2020), and the post-lockdown period (June 15 to July 15, 2020). It was found that during the pre-lockdown period, the average AQI was reported as maximum (111.67 ± 24.83 µg.m⁻³) in Bhilai followed by Durg (107.67 ±

20.68 µg.m⁻³), Raipur (107.83 ± 20.16 µg.m⁻³), Korba (86.33 ± 17.35 µg.m⁻³), Bilaspur (86.17 ± 24.14 µg.m⁻³) and minimum in Raigarh (85.17 ± 22.81 µg.m⁻³). During the lockdown period, the maximum AQI was again reported in Bhilai (97.17 ± 52.17 µg.m⁻³), followed by Raigarh (73.6 ± 14.53 µg.m⁻³), Raipur (71.2 ± 27.98 µg.m⁻³), Korba (71.00 ± 7.61 µg.m⁻³), Bilaspur (67.25 ± 7.08 µg.m⁻³) and the minimum in Durg (47.25 ± 20.78 µg.m⁻³). The AQI was found further improved even after revocation of the lockdown under economic pressure and during this period it was recorded maximum in Bilaspur (40.00 ± 12.12 µg.m⁻³) followed by Korba (39.00 ± 12.53 µg.m⁻³), Raipur (38.00 ± 3.46 µg.m⁻³), Raigarh (33.00 ± 11.53 µg.m⁻³) and minimum in Durg (31.67 ± 4.93 µg.m⁻³) (Fig. 2).

In our study, we found that the AQI of all the cities improved during the lockdown period and even during the restoration of all anthropogenic activities (post-lockdown period). In Bhilai, where the maximum AQI was reported, it has further improved by 14.5 µg.m⁻³ during the lockdown period and 61.17 µg.m⁻³ during the post-lockdown period. In Durg, it was improved by 60.47 µg.m⁻³ during the lockdown period and by 15.53 µg.m⁻³ during the post-lockdown period. In Raipur, it improved by 36.63 µg.m⁻³ during the lockdown period and 33.2 µg.m⁻³ during the post-lockdown period. In Bilaspur, it was improved by 18.97 µg.m⁻³ during the lockdown period and by 27.2 µg.m⁻³ during the post-lockdown period. In Korba, it was improved by 15.33 µg.m⁻³ during the lockdown period and by 32.00 µg.m⁻³ during the post-lockdown period, and similarly, it was found to improve during the lockdown period by 11.57 µg.m⁻³ and the post-lockdown period by 40.6 µg.m⁻³ in Raigarh. The maximum improvement in the air quality index was reported in Durg (60.47 µg.m⁻³) during the lockdown period and in

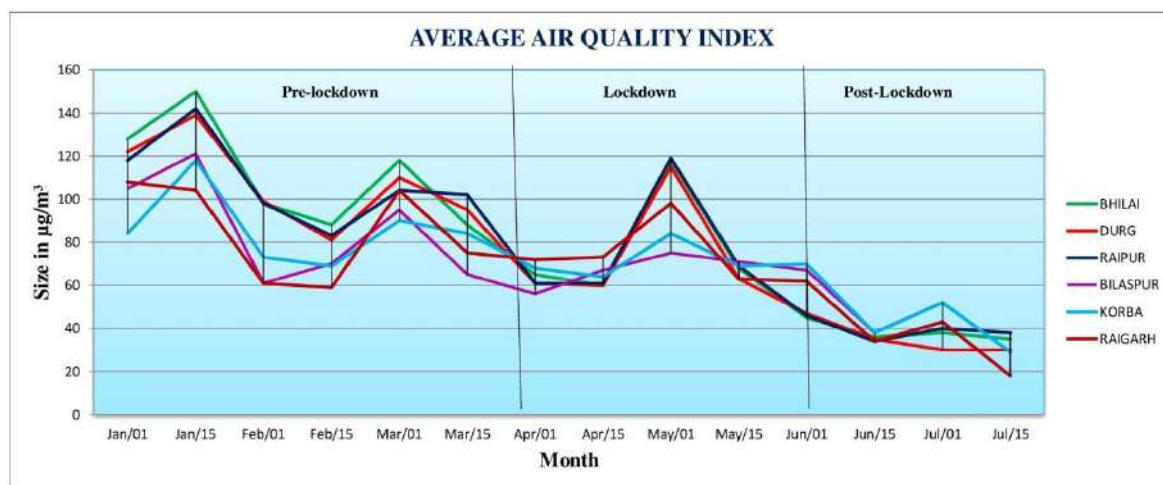


Fig. 2: Average Air Quality Index of the major cities of Chhattisgarh, India.

Table 1: Average Air Quality Index of various cities of Chhattisgarh, India (in $\mu\text{g.m}^{-3}$ from January 1, 2020 to July 15, 2020).

Cities	Pre-lockdown Period						Pre-lockdown Period				Post-lockdown Period			
	Jan 01	Jan 15	Feb 01	Feb 15	March 01	March 15	April 01	April 15	May 01	May 15	June 01	June 15	July 01	July 15
Bhilai	128	150	98	88	118	88	65	160	118	68	45	36	39	33
Durg	122	139	97	81	110	95	61	60	65	31	19	35	34	26
Raipur	118	142	98	83	104	102	61	61	119	69	46	34	40	40
Bilaspur	105	121	61	70	95	65	56	67	75	71	67	38	53	29
Korba	84	118	73	69	90	84	68	64	84	69	70	38	52	27
Raigarh	108	104	61	59	104	75	72	73	98	63	62	34	44	21

Bhilai ($61.17 \mu\text{g.m}^{-3}$) during the revocation of the lockdown. Out of six cities considered for the study, we found better improvement in AQI in four cities, i.e., Bhilai ($61.17 \mu\text{g.m}^{-3}$), Bilaspur ($27.2 \mu\text{g.m}^{-3}$), Korba ($32.00 \mu\text{g.m}^{-3}$), and Raigarh ($40.6 \mu\text{g.m}^{-3}$) when the lockdown was revoked and anthropogenic activities were restored. Our findings establish that the AQI improvement during lockdown was not helpful; it occurred in the natural course of the phenomenon (Table 1).

Out of six cities, $\text{PM}_{2.5}$ was reported maximum in Raipur ($60.5 \pm 17.63 \mu\text{g.m}^{-3}$) and minimum in Korba ($41.83 \pm 13.19 \mu\text{g.m}^{-3}$) during the pre-lockdown period, and during the lockdown period, it was recorded maximum in Raipur ($36.8 \pm 18.63 \mu\text{g.m}^{-3}$) and minimum in Bilaspur ($32.8 \pm 3.49 \mu\text{g.m}^{-3}$) but during the post-lockdown period, it was reported maximum in Bhilai ($24.6 \pm 3.60 \mu\text{g.m}^{-3}$) and minimum in Durg ($9.66 \pm 4.61 \mu\text{g.m}^{-3}$). During the lockdown and post-lockdown periods, we found a significant improvement in $\text{PM}_{2.5}$ in all six cities. In Bhilai, an improvement in $\text{PM}_{2.5}$ was reported by $22.4 \mu\text{g.m}^{-3}$ and $11.00 \mu\text{g.m}^{-3}$ ($F = P 0.5 < 7.4945$); in Durg by $24.33 \mu\text{g.m}^{-3}$ and $25.34 \mu\text{g.m}^{-3}$ ($F = P 0.5 < 10.06$); in Raipur by $23.7 \mu\text{g.m}^{-3}$ and $25.14 \mu\text{g.m}^{-3}$ ($F = P 0.5 < 9.1819$); in Bilaspur by $13.36 \mu\text{g.m}^{-3}$ and $15.14 \mu\text{g.m}^{-3}$ ($F = P 0.5 < 7.2875$); in Korba by $6.63 \mu\text{g.m}^{-3}$ and $17.87 \mu\text{g.m}^{-3}$ ($F = P 0.5 < 6.1733$) and in Raigarh by $7.76 \mu\text{g.m}^{-3}$ and $20.4 \mu\text{g.m}^{-3}$ ($F = P 0.5 < 7.8896$) during the lockdown and post-lockdown period respectively.

PM_{10} was reported maximum in Raipur ($89.5 \pm 25.05 \mu\text{g.m}^{-3}$) and minimum in Raigarh ($70.16 \pm 16.59 \mu\text{g.m}^{-3}$) during the pre-lockdown period, and during the lockdown period, it was reported maximum in Korba ($59.60 \pm 5.17 \mu\text{g.m}^{-3}$) minimum in Durg ($55.81 \pm 26.81 \mu\text{g.m}^{-3}$). After the lockdown was lifted, it was found to be highest in Bilaspur ($26.66 \pm 14.84 \mu\text{g.m}^{-3}$) and lowest in Durg ($13.66 \pm 7.23 \mu\text{g.m}^{-3}$). The status of PM_{10} in the air was also found to improve during the lockdown and the post-lockdown period compared to the pre-lockdown period. The concentration of PM_{10} was found to improve in Bhilai by $29.43 \mu\text{g.m}^{-3}$ and $39.4 \mu\text{g.m}^{-3}$ ($F = P 0.5 < 7.477$); in Durg $32.19 \mu\text{g.m}^{-3}$ & $42.15 \mu\text{g.m}^{-3}$ ($F = P 0.5 < 10.1913$); in Raipur $31.3 \mu\text{g.m}^{-3}$

and $40.20 \mu\text{g.m}^{-3}$ ($F = P 0.5 < 8.9965$); in Bilaspur $14.53 \mu\text{g.m}^{-3}$ and $30.14 \mu\text{g.m}^{-3}$ ($F = P 0.5 < 8.7204$); in Korba $14.56 \mu\text{g.m}^{-3}$ and $33.27 \mu\text{g.m}^{-3}$ ($F = P 0.5 < 12.961$) and in Raigarh $11.36 \mu\text{g.m}^{-3}$ and $33.8 \mu\text{g.m}^{-3}$ ($F = P 0.5 < 11.1529$) during the lockdown and post-lockdown period respectively.

The concentration of NO_2 in the air was also found to be altered during the lockdown and post-lockdown periods in comparison to the pre-lockdown period. It was found maximum in Raipur ($89.5 \pm 25.05 \mu\text{g.m}^{-3}$) and the minimum in Korba ($59.33 \pm 7.96 \mu\text{g.m}^{-3}$) during a pre-lockdown period, and during the lockdown period, it was reported maximum in Raipur ($95.6 \pm 16.14 \mu\text{g.m}^{-3}$) and the minimum in Bilaspur ($74.20 \pm 10.08 \mu\text{g.m}^{-3}$). In the post-lockdown period, it was reported at its maximum in Bhilai ($66.33 \pm 4.72 \mu\text{g.m}^{-3}$) and at its minimum in Raigarh ($39.33 \pm 7.50 \mu\text{g.m}^{-3}$). The NO_2 concentration was found to increase in the air during the lockdown period more than during the pre-lockdown period and to further decrease during the post-lockdown period in all cities except Durg. It was found to increase by $9.17 \mu\text{g.m}^{-3}$ and decreased by $27.64 \mu\text{g.m}^{-3}$ ($F = P 0.5 < 7.1266$) in Bhilai; increased by $23.44 \mu\text{g.m}^{-3}$ and decreased by $33.27 \mu\text{g.m}^{-3}$ ($F = P 0.5 < 5.7595$) in Raipur; increased by $3.37 \mu\text{g.m}^{-3}$ and decreased by $13.2 \mu\text{g.m}^{-3}$ ($F = P 0.5 < 0.9213$) in Bilaspur; increased by $17.67 \mu\text{g.m}^{-3}$ and decreased by $20.67 \mu\text{g.m}^{-3}$ ($F = P 0.25 < 10.4317$) in Korba; increased by $11.9 \mu\text{g.m}^{-3}$ and decreased by $41.07 \mu\text{g.m}^{-3}$ during the lockdown and the post-lockdown respectively, but in Durg it was found to decrease by $1.9 \mu\text{g.m}^{-3}$ and $22.6 \mu\text{g.m}^{-3}$ ($F = P 0.5 < 6.7149$) during the lockdown and the post-lockdown period consecutively. The behavior of NO_2 was found to be quite different from that of other pollutants; it was found to increase in the air when anthropogenic activities were almost suspended and to decrease further with the resumption of anthropogenic activities.

The O_3 in the air was also recorded, and it was found that it increased consecutively from the pre-lockdown to the lockdown to the post-lockdown period. The rise of O_3 during this period was reported significantly only in Durg ($F = P 0.5 < 6.5815$) and in the rest all, viz. Bhilai ($F = P 0.5$

> 6.5815), Raipur (F = P 0.5 > 6.5815), Bilaspur (F = P 0.5 > 6.5815) it was found to increase at non-significant level (Figs. 3, 4, 5, 6 & Table 2).
> 6.5815), Korba (F = P 0.5 > 6.5815) and in Raigarh (F = P 0.5 > 6.5815) it was found to increase at non-significant level (Figs. 3, 4, 5, 6 & Table 2).

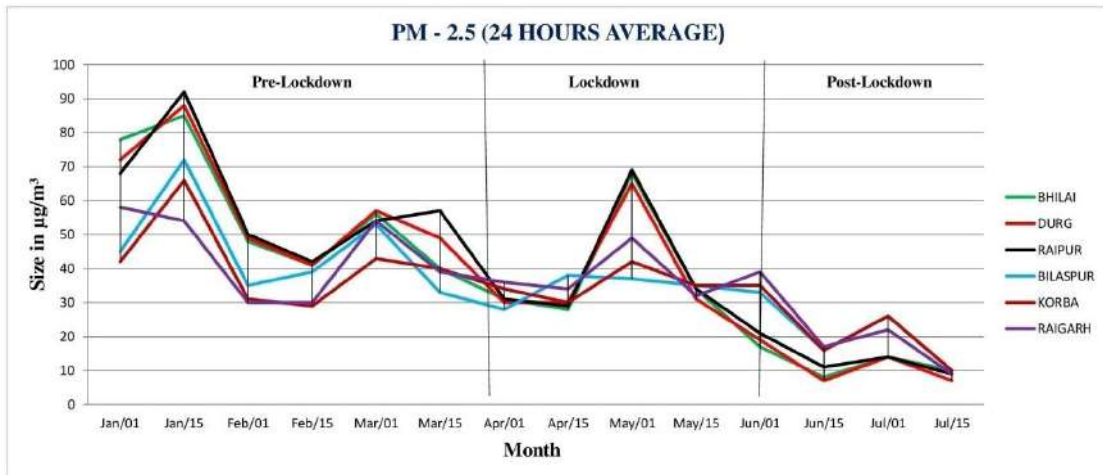


Fig. 3: Level of PM_{2.5} during the pre-lockdown, lockdown, and post-lockdown period.

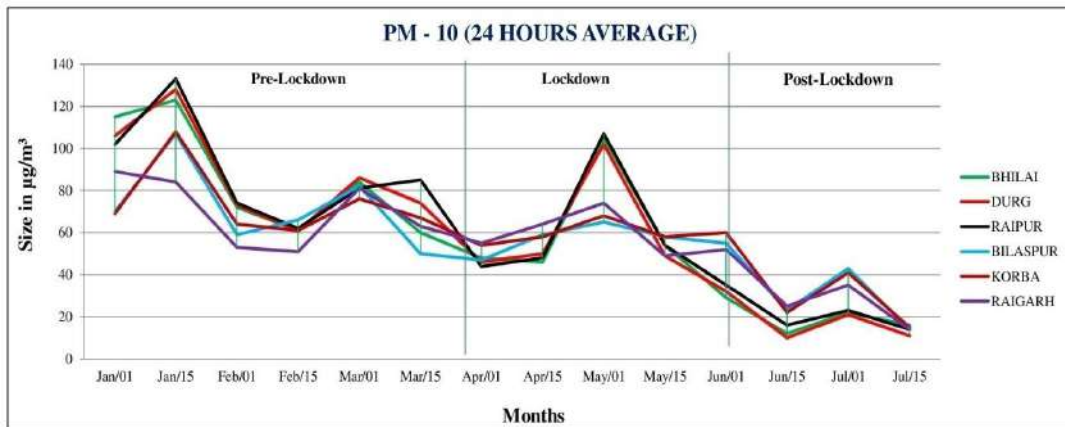


Fig. 4: Level of PM₁₀ during the pre-lockdown, lockdown, and post-lockdown period.

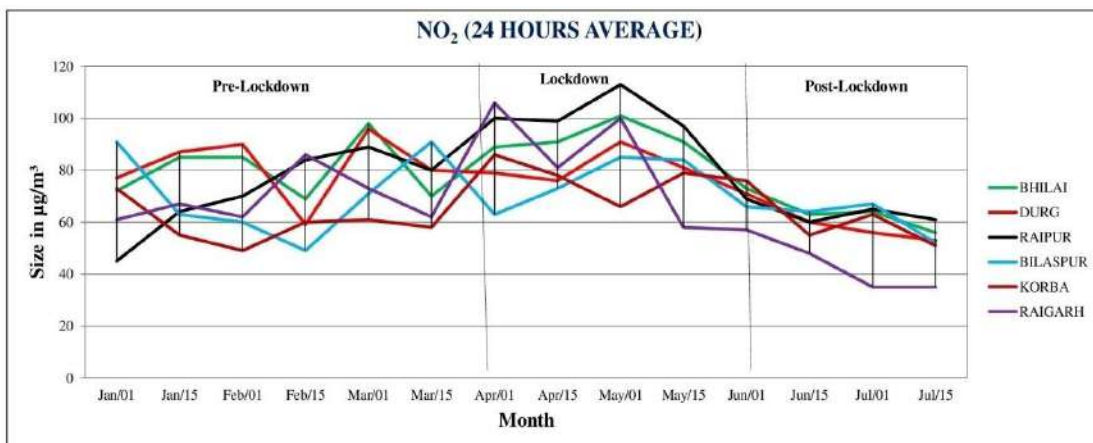


Fig. 5: NO₂ concentration during the pre-lockdown, lockdown and the post-lockdown period.

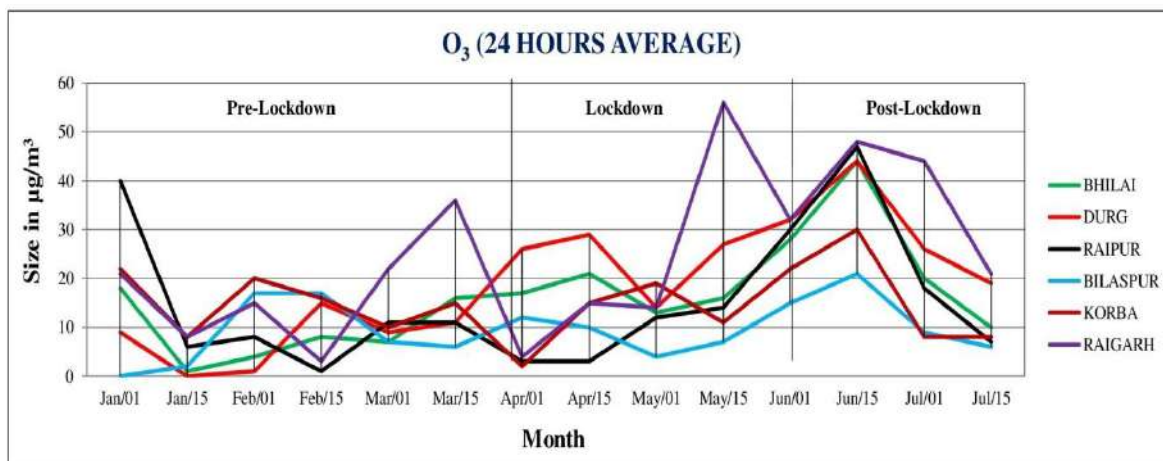


Fig. 6: O₃ concentration during the pre-lockdown, lockdown and the post-lockdown period.

Table 2: Alteration in PM_{2.5}, PM₁₀, NO₂, and O₃ during the Pre-lockdown, Lockdown, and Post-lockdown periods.

Cities	Bhilai		Durg		Raipur		Bilaspur		Korba		Raigarh													
	PM 2.5	PM 10	NO ₂	O ₃	PM 2.5	PM 10	NO ₂	O ₃	PM 2.5	PM 10	NO ₂	O ₃												
Pre-lockdown period	58.00±19.21	85.83±27.27	79.83±11.47	9.00±6.99	59.33±17.53	88.00±24.81	81.5±12.97	6.66±5.28	60.5±17.63	89.5±25.05	72.16±16.19	12.83±13.81	46.16±14.59	71.33±20.08	70.83±17.13	8.00±7.48	41.83±13.19	74.16±17.13	59.33±7.96	15.16±5.45	44.16±12.75	70.16±16.59	68.5±9.69	17.5±11.67
Lockdown period	35.6±21	56.4±28.71	89.00±10.09	19.00±5.78	35.00±17.47	55.81±26.81	79.6±7.40	25.6±6.87	36.8±18.63	58.2±28.13	95.6±16.14	12.40±11.05	32.8±3.49	56.8±6.57	74.20±10.08	9.6±4.27	35.20±4.32	59.60±5.17	77.00±7.21	13.8±7.79	36.4±7.30	58.8±10.18	80.4±22.85	24.2±12.42
Post-lockdown period	24.6±3.60	17.00±5.56	61.33±4.72	24.66±17.47	9.66±4.61	13.66±7.23	57.00±3.60	30.00±12.76	11.66±3.05	18.00±5.29	62.33±3.21	19.00±14.33	17.66±8.62	26.66±14.84	61.00±7.93	12.00±7.93	17.33±8.08	26.33±13.45	56.33±6.11	15.33±12.70	16.00±6.55	25.00±11.00	39.33±7.50	37.66±14.57
F @ < 0.5	7.4945	7.47701	7.1266	3.2038	10.16	10.1913	6.7149	6.5815	9.1819	8.9965	5.7595	0.2008	7.2875	8.7204	0.9213	0.3600	6.1733	12.961	10.4317	0.0505	7.8896	11.1529	6.5969	1.6121

India's first novel coronavirus patient, a student studying at Wuhan University, was reported in Kerala's Thrissur district at a time when more than 7,500 cases were reported in 20 countries around the world. In Chhattisgarh state, the first confirmed case of coronavirus was reported on March 19, 2020, in Raipur, where a girl who returned from London via Mumbai Airport tested positive. Cases of novel coronavirus infection were later reported to be increasing day by day. In the present study, we have summarized the data of novel coronavirus infection in Chhattisgarh as 8 on April 1, 33 on

April 15, 40 on May 1, 60 on May 15, 498 on June 1, 1715 on June 15, 2860 on July 1, and 4379 on July 15. Further, it was increased to 5407 on July 20 and 5968 on July 23. In our study (Fig. 7), the air quality index and the increasing trend of COVID-19 cases were found to be negatively correlated ($r = -0.7688$, $p = 0.0258$).

In less than five months, the COVID-19 outbreak in India has spread to all states and union territories, infecting more than 1,238,798 people, and nearly 29,861 people have lost their lives as of the date of this paper, July 23, 2020. There



Fig. 7: Negative correlation between average air quality index and increasing cases of COVID-19 (From 1 April to 15 July).

is no sign of a reduction in COVID-19 cases, but we are witnessing that the doubling time of infection was reduced very rapidly. Some of the authors have reported a positive correlation between the air quality index and COVID-19 cases. Zhu et al. (2020) have reported a significant relationship between air pollution and COVID-19 infection and a positive association of PM_{2.5}, PM₁₀, CO₂, NO₂, and O₃ with COVID-19 confirmed cases; however, a negative association between SO₂ and COVID-19 cases in China was also reported. Fattorini et al. (2020) have also expressed the view that there is a significant correlation between atmospheric pollution and the SARS-CoV-2 outbreak in Italy. It was also reported that high NO₂ concentrations in the atmosphere contribute to fatalities caused by COVID-19, especially in cases such as those observed in Italy, Spain, France, and Germany (Ogen 2020).

In our study, we found that gradually the air quality index from January to the 15th of July improved, but simultaneously the COVID-19 cases also increased during the period. In a systematic study of PM_{2.5}, PM₁₀, NO₂, and O₃ for Bhilai, Durg, Raipur, Bilaspur, Korba, and Raigarh, we found a remarkable decrease in PM_{2.5} and PM₁₀ during the lockdown and post-lockdown periods, a rise in NO₂ during the lockdown period and a decrease in the post-lockdown period, and a non-significant rise in O₃ during the lockdown and post-lockdown periods consecutively.

The accumulation of NO_x in the air and water can cause serious environmental pollution. NO and NO₂ may react with other chemicals to form acid rain, which harms

the ecosystem (Akimoto 2003). Nitrogen dioxide (NO₂) is regarded as an indicator of nitrogen oxide and is used to assess environmental pollution levels. The WHO has listed NO₂ as one of the six typical air pollutants (Brunekreef & Holgate 2002). Breathing air containing a high concentration of NO₂ may stimulate the body's respiratory system, but this toxic gas may corrode the body's lung tissue. Short-term exposure to a high concentration of NO₂ can cause respiratory symptoms (e.g., coughing, wheezing, or difficulty in breathing) and aggravate respiratory disease. NO₂ comes from the combustion of oil, coal, natural gas, and other fuels and the exhaust of urban vehicles. It is estimated that anthropogenic pollution worldwide emits approximately 53 million tons of nitrogen oxide per year.

In China, the NO₂ in the atmosphere was measured by the European Space Agency from December 19, 2019, to March 15, 2020, during the lockdown period, and it was reported that during this period, the NO₂ in China was found to be significantly lower than the previous period. The Chinese government resumed industrial activities on February 10, and after that, the NO₂ concentration in the atmosphere increased. Guo et al. (2020) and Mehta et al. (2020) reported that cytokine storm, also known as hypercytokinemia, is one of the major causes of COVID-19 patients due to an uncontrolled release of proinflammatory cytokines (Tisoncik et al. 2012). It is a severe reaction of the immune system, leading to a chain of destructive processes in the body that can end in death, and it has been reported by several authors that the cytokine storm syndrome can be caused by long exposure

to air pollutants, especially NO₂. Furthermore, elevated NO₂ exposure has been linked to hypertension (Saeha et al. 2020), heart and cardiovascular disease (Mann et al. 2002, Arden et al. 2004), chronic obstructive pulmonary disease (Abbey et al. 1993), significant deficits in lung function growth in children (Avol et al. 2001), poor lung function in adults, or injury (Bowatte et al. 2017). It has been reported that NO₂ exposure may induce an inflammatory response in the airway by inducing the synthesis of proinflammatory cytokines from pulmonary epithelia (Persinger et al. 2017). Khoder (2002) has reported that high NO₂ concentrations may generate some harmful secondary pollutants, such as nitric acid (HNO₃) and ozone (O₃). WHO (World Health Organization 2016) has warned that NO₂ and its secondary products are the main health issues and that the population should be protected from these pollutants.

Muhammad (2020) has reported that during the COVID-19 lockdown period, NO₂ emission to the atmosphere was reduced by up to 30% in China, Spain, France, Italy (European Space Agency 2016), and the USA (National Aeronautics and Space Administration 2020). As NO₂ is a free radical, it has the potential to deplete tissue antioxidants and cause injury and inflammation. It has also been reported that uric acid and ascorbic acid deplete in bronchoalveolar lavage (BAL) fluid even at low concentrations of antioxidant defenses (Kelly & Tetley 1997). Olker et al. (2004) reported that the release of superoxide radicals from BAL cells decreases under the influence of NO₂ and results in the inhibition of NADPH oxidase and complex III of the respiratory chain and a mild increase in scavenging by enhanced glutathione peroxidase and CuZn-superoxide dismutase mRNA expression and enzyme activities. In cultured human bronchial epithelial cells, NO₂-induced cell membrane damage and increased membrane permeability have been reported by Devalia et al. (1993).

The immunofluorescence studies confirmed that the NO₂ exposed cell increases the level of nitrite, IL-8, IL-β, and TNF-α which further stimulates inflammatory conditions of the bronchial epithelium, leading to asthma and other hyperactive airway diseases. It has also been reported that during the early post-NO₂ period, the cells initiate apoptosis, while necrotic cell death was found to be more prevalent at later time intervals. The NO₂-exposed cell has exhibited increased expression of heme oxygenase-1 (OH-1), a redox-sensitive stress protein, and increased adhesion to neutrophils, which resulted in increased normal human bronchial cell death (Ayyagari et al. 2007). Some structural changes in respiratory cells under the influence of long-term exposure to nitrogen dioxide have also been reported, viz. emphysema-like structural changes, thickening

of the alveolar-capillary membrane, loss of the ciliated epithelium, and an increase in lung collagen (EPA Report-No. EPA/600/8-91/049af-cf) (Jarvis et al. 2010).

Miller et al. (1987) discovered that NO₂ exposure affected pulmonary functions such as end-expiratory volume, vital capacity, and respiratory system compliance. Hussain et al. (2004) reported that even short-term exposure to NO₂ causes enhanced epithelial damage, reduced mucin expression, and increased baseline smooth muscle tone. Garn et al. (2003) investigated the inflammatory response to NO₂ and discovered an increase in the number of inflammatory cells, total protein concentration, and decreased TNF- in bronchoalveolar lavage (BAL), but elevated IL-10, IL-6, and suppressor of cytokine signaling-3 protein. In vitro lipopolysaccharide stimulation of BAL cells reduced TNF- and IL- production while increasing transcription and protein release of IL-10. Besides the above, an elevated level of IL-6, scavenger receptor B, and suppression of cytokine signaling-3 mRNA were also detected in BAL cells of NO₂-exposed animals.

Based on statistics, we discovered a negative correlation between the air quality index and cases of COVID-19 in our study, implying that the air quality index is unrelated to novel coronavirus infection in humans. Our findings disagree with the findings of Zhu et al. (2020) in the context of the scenario of Chhattisgarh, India. The decrease in PM_{2.5} and PM₁₀, and the alteration with NO₂ might be due to the restriction of human activity under fear or precautionary steps against coronavirus.

The rise in the O₃ level in the air was found as a normal course of seasonal changes and might be contributed to the NO₂ increase. NO₂ has been recognized as the most dangerous pollutant, especially for lung damage and dysfunction. SARS-CoV-2 attacks the pulmonary system after entry through the ACE-2 receptor and causes serious, irreversible damage to the pulmonary system. In our study, we found that during the lockdown period, the NO₂ concentration was markedly increased in the state of Chhattisgarh, which has contributed a lot to enhance the pathogenicity of the disease and has created a serious lethal impact on infected persons. Although it is unclear why NO₂ concentrations increased in the atmosphere during the lockdown period, emissions from the Bhilai Steel Plant (one of Steel Authority of India Limited's largest units), the Steel Plant in Raigarh, and the Coal-based Thermal Power Plant in Korba are likely to have contributed because these units were operating at full capacity even during the lockdown period. Based on this study, it is suggested that during such a respiratory problem-based pandemic, the emissions from similar types of industrial units should be under control and evaluated consistently.

CONCLUSION

The first case of novel coronavirus was reported in the Indian state of Chhattisgarh by a migrant from London, and despite all efforts of the government, it has increased exponentially and spread to every corner of the state, prompting a lockdown as per national policy. In our study, we found that the air quality index considering PM_{2.5}, PM₁₀, NO₂, and O₃ improved during the lockdown period and continued to improve even during the post-lockdown period. We did not find the effect of the restoration of anthropogenic activities on the air quality index during the post-lockdown period. Our study revealed that the change in air quality was largely influenced by its natural course instead of an absolute anthropogenic impact. We also discovered that the rise in novel Coronavirus infection was not directly related to the air quality index, as previously reported by several authors from around the world. The behavior of NO₂ during the lockdown period in Chhattisgarh was reported quite differently, probably due to the continuation of specified industrial activities, and it has contributed to pulmonary dysfunction in the infected persons. Except for a few cases of cytokine storm-related organ dysfunction, the majority of infected patients reported severe pulmonary dysfunctions, and both symptoms were likely exacerbated by increased NO₂ in the air. The outcome of the study is that there is a need for NO₂ management not only during novel coronavirus infections but for epidemics related to lung dysfunctions. The findings of the present study may help authorities with NO₂ management during the concerned epidemic period by enforcing steel plants, thermal power plants, and coal-fired units to minimize adverse pulmonary pathogenicity in the future.

ACKNOWLEDGEMENTS

The authors are grateful to Copernicus Atmospheric Monitoring Service Information 2020, the South America Model: GMAI/LPTEC/INDP, and Plum Lab. We are also thankful to Prof. Somali Gupta for her valuable suggestions.

REFERENCES

Abbey, D.E. Colome, S.D. Mills, P.K. Burchette, R. Beeson, W.L. and Tian, Y. 1993. Chronic disease is associated with long-term concentrations of nitrogen dioxide. *Journal of Exposure Analysis and Environmental Epidemiology*, 3: 181-202.

Akimoto, H. 2003. Global air quality and pollution. *Science*, 302: 1716-1719.

Arden, P.C. Burnett, R.T. Thurston, G.D. Thun, M.J. Calle, E.E. Krewski, D. and Godleski, J.J. 2004. Cardiovascular mortality and long-term exposure to particulate air pollution. *Circulation*, 109: 71-77.

Avol, E.L. Gauderman, W.J. Tan, S.M. London, S.J. and Peters, J.M. 2001. Respiratory effects of relocating to areas of differing air pollution levels. *American Journal of Respiratory and Critical Care Medicine*, 164: 2067-2072.

Ayyagari, V.N. Januszkiewicz, A. and Nath, J. 2007. Effects of nitrogen dioxide on the expression of intercellular adhesion molecule-1, neutrophil adhesion, and cytotoxicity: studies in human bronchial epithelial cells. *Inhalation Toxicology*, 19: 181-94.

Bai, Y. Yao, L. Wei, T. Tian, F. Jin, D.Y. Chen, L. and Wang, M. 2020. Presumed asymptomatic carrier transmission of COVID-19. *Journal of the American Medical Association*, 323: 1406-1407.

Bowatte, G. Erbas, B. Lodge, C.J. Knibbs, L.D. Gurrin, L.C. Marks, G.B. Thomas, P.S. Johns, D.P. Giles, G.G. and Hui, J. 2017. Traffic-related air pollution exposure over a 5-year period is associated with an increased risk of asthma and poor lung function in middle age. *European Respiratory Journal*, 50: 1602357. doi: 10.1183/13993003.02357-2016.

Brunekreef, B. and Holgate, S.T. 2002. Air pollution and health. *Lancet*, 360: 1233-1242.

Devalia, J.L. Campbell, A.M. Sapsford, R.J. Rusznak, C. Quint, D. Godard, P. Bousquet, J. and Davies, R.J. 1993. Effect of nitrogen dioxide on a synthesis of inflammatory cytokines expressed by human bronchial epithelial cells in vitro. *American Journal of Respiratory Cell and Molecular Biology*, 9: 271-278.

European Space Agency. 2020. Available online at: http://www.esa.int/Applications/Observing_the_Earth/Copernicus/Sentinel5P/Coronavirus_lockdown_leading_todrop_in_Pollution_across_Europe (accessed: 4 April 2020).

Fattorini, D. and Regoli, F. 2020. Role of the atmospheric pollution in the Covid-19 outbreak risk in Italy. *Environmental Pollution*, 264: 114732.

Garn, H. A. Siese, A. Stumpf, S. Barth, P.J. Muller, B. and Gemsa, D. 2003. Shift toward an alternatively activated macrophage response in lungs of NO₂-exposed rats. *American Journal of Respiratory Cell and Molecular Biology*, 28: 386-396.

Glencross, D.A. HO, T.R. Camina, N. Catherine, M. Hawrylowicz, C.M. and Pfeffer, P.E. 2020. Air pollution and its effects on the immune system. *Free Radical Biology and Medicine*, 151: 56-68.

Global Carbon Project. Available online at <http://www.globalcarbonproject.org/carbonbudget/index.html>. (accessed date: 4 April 2020).

Guo, Y.R. Cao, Q.D. Hong, Z.S. Tan, Y.Y. Chen, S.D. Jin, H.J. Tan, K.S. Wang, D.Y. and Yan, Y. 2020. The origin, transmission and clinical therapies on coronavirus disease 2019 (COVID-19) outbreak- an update on the status. *Military Medical Research*, 7: 11.

Hussain, I. Jain, V.V. O'Shaughnessy, P. Thomas R. Businga, T.R. and Kline, J. 2004. Effect of nitrogen dioxide exposure on allergic asthma in a murine model. *Laboratory and Animal Investigations*, 126: 198-204.

Jarvis, D.J. Adamkiewicz, G., Heroux, M.E., Rapp, R., Frank, J. and Kelly, F.J. 2010. WHO Guidelines for indoor air quality: selected pollutants. Copenhagen: World Health Organization, Regional Office at Europe, pp. 201-248.

Katanoda, K. Sobue, T. Satoh, H. Tajima, K. Suzuki, T. and Tominaga, S. 2011. An association between long-term exposure to ambient air pollution and mortality from lung cancer and respiratory diseases in Japan. *Journal of Epidemiology*, 21: 132-143.

Kelly, F. and Tetley, D.T. 1997. Nitrogen dioxide depletes uric acid and ascorbic acid but not glutathione from lung lining fluid. *Biochemical Journal*, 325: 95-99.

Khoder, M.I. 2002. Atmospheric conversion of sulfur dioxide to particulate sulfate and nitrogen dioxide to particulate nitrate and gaseous nitric acid in an urban area. *Chemosphere*, 49: 675-684.

Mann, J.K. Tager, I.B. Lurmann, F. Segal, M. Quesenberry, C.P. Lugg, M.M. Shan, J. and Eden, S.K.V.D. 2002. Air pollution and hospital admissions for ischemic heart disease in persons with congestive heart failure or arrhythmia. *Environmental Health Perspectives*, 110: 1247-1252.

Mehta, P. McAuley, D.F. Brown, M. Sanchez, E. Tattersall, R.S. and Manson, J.J. 2020. COVID-19: consider cytokine storm syndromes and immunosuppression. *Lancet*, 395: 1033-1034.

- Miller, K.G. Janecek, T.R. Katz, M.E. and Keil, D.J. 1987. Stable carbon and oxygen isotope record of benthic foraminifera from Paleocene-Eocene sediments. *Pangaea*, doi:10.1594/Pangaea.726768.
- Muhammad, S. Long, X. and Salman, M. 2020. COVID-19 pandemic and environmental pollution: A blessing in Disguise. *Science of the Total Environment*, 728: 138820.
- Nakao, M. Ishihara, Y. Kim C.H. and Hyun, I.G. 2018. The impact of air pollution, including asian sand dust, on respiratory symptoms and health-related quality of life in outpatients with chronic respiratory disease in Korea: A panel study. *Journal of Preventive Medicine & Public Health*, 51: 130-130.
- National Aeronautics and Space Administration. 2020. Available online at https://neo.sci.gsfc.nasa.gov/view.php?datasetId=AURA_NO2. (accessed date: 5 May 2020).
- Ogen, Y. 2020. Assessing nitrogen dioxide (NO₂) levels as a contributing factor to coronavirus (COVID-19) fatality. *Science of the Total Environment*, 726: 138605.
- Olker, C. Siese, A. Stumpf, S. Müller, B. Gamsa, D. and Garn, H. 2004. Impaired superoxide radical production by bronchoalveolar lavage cells from NO₂-exposed rats. *Free Radical Biology and Medicine*, 37: 977-987.
- Peng, R.D. Bell, M.L. Geyh, A.S. McDermott, A. Zeger, S.L. Samet, J.M. and Dominici, F. 2009. Emergency admissions for cardiovascular and respiratory diseases and the chemical composition of fine particle air pollution. *Environmental Health Perspectives*, 117: 957-963.
- Persinger, R.L. Poynter, M.E. Ckless, K. and Janssen-Heininger, Y.M.W. 2002. Molecular mechanisms of nitrogen dioxide induced epithelial injury in the lung. *Molecular and Cell Biochemistry*, 234: 71-80.
- Rahman, I. and MacNee, W. 2000. Oxidative stress and regulation of glutathione in lung inflammation. *European Respiratory Journal*, 16: 534-554.
- Saaha, S. Bai, Li. Oiamo, T.H. Brunet. R.T. Scott, W. Jerrett, M. Kwong, J.C. Goldber. M.S. Copes, R. Kopp, A. and Chen, H. 2020. Association between road traffic noise and incidence of diabetes mellitus and hypertension in Toronto, Canada: a population-based cohort study. *Journal of the American Heart Association*, 9: 013021.
- Sohrab, C. Alsaf, Z. O'Neill, N. Khan, M. Kerwan, A. Al-Jabir, A. Iosifidis, C. and Agha, R. 2020. World Health Organization declares global emergency: A review of the 2019 novel coronavirus (COVID-19). *International Journal of Surgery*, 76: 71-76.
- Spix, C. Anderson, H.R. Schwartz, J. Vigotti, M.A. Leterttre, A. Vank, J.M. Touloumi, G. Balducci, F. Piekarski, T. and Bacharova, L. 1998. Short-term effects of air pollution on hospital admissions of respiratory diseases in Europe. *Archives of Environmental Health*, 53: 54-64.
- Tamrius, J.D. Shaman, J. Alonso, W.J. Bloom Feshbach, K. Uejio, C.K. Comrie, A. and Vibond, C. 2013. Environmental predictors of seasonal influenza epidemics across the temperate and tropical climates. *PLoS Pathology*, 9: 1003194.
- Tisoncik, J.R. Korth, M.J. Simmons, C.P. Farrar, J. Martin, T.R. and Katze, M.G. 2012. Into the eye of the cytokine storm. *Microbiology and Molecular Biology Reviews*, 76: 16-32.
- Wong, T.W. Lau, T.S. Yu, T.S. Neller, A. Wong, S.L. Tam, W. and Pang, S.W. 1999. Air pollution and hospital admissions for respiratory and cardiovascular diseases in Hong Kong. *Occupational Environmental Medicine*, 56: 679-683.
- World Health Organization. 2016. Available online at: http://www.who.int/health-topic/air-pollution#tab=tab_1 (accessed: 5 April 2020).
- Zhu, Y. Xie, J. Huang, F. and Cao, L. 2020. Association between short-term exposure to air pollution and COVID-19 infection: Evidence from China. *Science of the Total Environment*, 727: 138704.



Adsorption and Kinetic Studies on Sequestering Effect of Porous Biodegradable Biochar Obtained from Pig-Bone on Hexavalent Chromium from Aqueous Solution

L. Vidhya*^{ID}, S. Vinodha**, S. J. Pradeeba*[†]^{ID}, B. Jeyagowri*^{ID}, V. Nirmaladevi*^{ID} and N. Nithiya***^{ID}

*Department of Chemistry, Hindustan College of Engineering and Technology, Coimbatore-641032, Tamil Nadu, India

**Department of Chemical Engineering, Jayaraj Annabackiam CSI College of Engineering, Thoothukudi-628617, Tamil Nadu, India

***Department of Physics, Hindustan College of Engineering and Technology, Coimbatore-641032, Tamil Nadu, India

[†]Corresponding author: S. J. Pradeeba; pradeebasj@gmail.com

Nat. Env. & Poll. Tech.
Website: www.neptjournal.com

Received: 19-08-2022

Revised: 18-10-2022

Accepted: 24-12-2022

Key Words:

Chromium
Pig-bone biochar
Biosorbent
Kinetic studies
Isotherms

ABSTRACT

In the current research work, the authors proposed a list of tactics to eliminate Cr (VI) with the help of pig bone biochar. The Cr (VI) was adsorbed in batches onto pig bone biochar to scrutinize the adsorption data. The studies determine the impact of adsorption dose, pH, and concentration. From the results, it was inferred that the optimum pH level was 7 for the removal of metal. The study calculated the adsorption isotherms in terms of affinity and adsorption capacity by leveraging Temkin, Langmuir and Freundlich equations. According to the reports, the Langmuir model is suitable for the adsorption data, followed by Temkin and Freundlich equations. In this model, rapid adsorption kinetic rates were observed, whereas the equilibrium state was achieved after two hours. There seems to be a perfect collation between the kinetic adsorption data and the pseudo-second-order equation. The researchers determined both Lagergren and Ho's constants. When biochar was characterized with SEM (Scanning Electron Microscope), EDX (Energy Dispersive X-ray spectrometer), and FTIR (Fourier Transform Infrared spectrometer), it was revealed that the Cr (VI) ions interacted with the isolated aggregates formed on the biosorbent surface. From the results, it can be understood that the pig bone biochar can be effectively used to eliminate chromium ions from an aqueous solution.

INTRODUCTION

There is a tremendous increase observed in the utilization and discharge of chemicals due to rapid industrialization. Industrial effluents generally possess a huge quantity of heavy metals in them. These heavy metals get transported to other members of the ecosystem and exhibit toxicity, while they accumulate in human beings through food chain contamination. Chromium, Lead, Nickel, and Cadmium are the common toxic heavy metals that remain non-biodegradable and threaten environmental flora and fauna despite fewer concentrations (Shamaa Shroff & Varsha Vaidya 2011, Pradeeba & Sampath 2019). Having been identified as carcinogenic and mutagenic agents, these heavy metals bring imbalance in the environment. Various

industries such as paints and pigments, galvanization, metal plating, smelting and mining, textile dyeing, and leather tanning use chromium compounds in their daily purposes. So removing chromium (VI) from wastewater remains crucial before discharge. Wastewater treatment is a critical process due to various challenges associated with it, such as strict discharge regulations, cozy methods of wastewater discharge, and scarce water resources. Few methods are traditionally followed in the isolation of metal ions, such as electrolysis, ion exchange, reverse osmosis, solvent extraction, precipitation, adsorption and electrochemical precipitation, and electrochemical treatment. Of these methods, the biosorption process is found to be cost-efficient and eco-friendly when it comes to metal ions isolation from contamination solution since it uses bioadsorbents (Nessim et al. 2011). The activated carbon adsorption method is deemed one of the most viable solutions to eliminate contaminants from the polluted medium. The method is also effective at low concentrations with a large surface area and high porosity (Ayaliew et al. 2014). The present study is aimed at reviewing the pig bone biochar (activated carbon) on its

ORCID details of the authors:

L. Vidhya: <https://orcid.org/0000-0001-6161-1786>

S. J. Pradeeba: <https://orcid.org/0000-0002-3737-8440>

B. Jeyagowri: <https://orcid.org/0000-0002-4252-2785>

V. Nirmaladevi: <https://orcid.org/0000-0001-8463-6185>

N. Nithiya: <https://orcid.org/0000-0003-3545-1955>

adsorption ability of Chromium (VI) ions from aqueous simulated solutions.

The study objectives are as follows; (i) amalgamate and distinguish biochar from pig bone, (ii) assess the possibility of pig bone biochar (PBBC) for the removal of Cr, (VI) from aqueous solution, (iii) evaluate the control of experimental variables on Cr (VI) adsorption onto PBBC and (iv) investigate adsorption kinetic and isotherms to identify with the mechanism of Cr (VI) removal.

MATERIALS AND METHODS

Preparation of Pig-Bone Biochar Adsorbent

The researcher collected the pig bones from a slaughterhouse at Navakarai village of Coimbatore, Tamil Nadu, India. After washing the pig bones extensively with deionized water, it was dried in an oven at 60°C for 24 h. Biochar was produced from these dried bones using a small-scale biochar-producing plant (Safire Scientific Company, Tamil Nadu Agriculture University, Coimbatore, Tamil Nadu, India). After crushing and drying the bones in the sun, the samples were dried in a hot air oven at 100°C for 24 h. The dehydrated material was then compressed and fed into the pyrolysis stove. The biochar sample was collected, sieved (<0.25 mm), and their notable features were determined before investigations.

Characterization of Pig Bone Biochar

As per the literature (Shenbagavalli & Mahimairaja 2012), the sieved pig bone biochar samples were evaluated for their water-holding capacity, particle size, and zeta potential following standard methods. Further, the pig bone biochar adsorbent was also assessed for its characteristics. A particle size analyzer Horiba, SZ-100 (Japan), was used to measure the size of the pig bone biochar particles and zeta potential. As per the regulations from the American Society for Testing and Materials (ASTM 1977), the proximate and ultimate factors, for instance, ash content, volatile matter, fixed carbon content, and moisture content of the PBBC, were determined. The biochar's morphological features and elemental composition before and after Cr (VI) adsorption were determined using SEM-EDS (Scanning Electron Microscopy - Energy Dispersive Spectroscopy; Quanta FEI250, Czechoslovakia). Likewise, the biochar spectra (of Fourier transform infrared spectroscopy, FTIR) before and post-Cr (VI) adsorption were obtained using a spectrometer (Shimadzu, Model 8400S) in a diffuse reflectance moderate resolution of 8cm in KBr pellets. The researcher performed the scanning in the range of 400 to 4000 cm^{-1} .

Stock Solutions and Standards

The researcher prepared the standard stock solution using 2.828 g of $\text{K}_2\text{Cr}_2\text{O}_7 \cdot \text{H}_2\text{O}$ (bought from Hi Media Laboratories India, (Molecular weight 294.18, 99.9% Assay) in double distilled water. The stock solution was diluted per the working concentration requirements (50–250 $\text{mg} \cdot \text{L}^{-1}$). All the solutions' pH values were adjusted with the help of 0.1 N HCl or 0.1 N NaOH solutions (Mohanty et al. 2014). The study used chemicals only of analytical grade.

Analysis of Cr (VI)

Before and after the Cr (VI) got adsorbed over biochar, the Hexavalent chromium present in the solution was determined spectrophotometrically by diphenyl carbazide (Thamilarasu et al. 2011). At 540 nm, the absorbance was measured for Cr(VI) (Rajoriya & Kaur 2014) using a Shimadzu spectrophotometer. The sample concentrations were calculated with the help of a calibration graph.

Adsorption Studies

The researcher carried out the batch adsorption experiment as given herewith. Pigbone biochar weight 0.05 g was separately placed in an Erlenmeyer flask (250 mL) (Deveci & Kar 2013). The PBBC (0.05 g) was agitated along with 25 mL of metal solution individually at $32 \pm 10^\circ\text{C}$ briefly. After this, the solution was kept in a rotary shaker (VRN-480, GEMMY Orbit Shaker, Taiwan) to ensure a smooth blend. This was then allowed to equilibrate for two hours. Throughout the analysis, the shaking speed was maintained at 100 rpm. The samples were collected at specified time intervals, whereas the metal solution was isolated from the adsorbent by centrifuging the samples at 6,000 rpm for 5 min. At 540 nm, the supernatant was visually analyzed for residual chromium concentration using UV-Vis spectrophotometer (UV-1800 Shimadzu, Japan) once complexed with 1,5diphenylcarbazide. The study considered the following variables for the experiment (i) pH effect on adsorption capacities, (ii) dosage of PBBC (0.01 to 0.05 g), (iii) initial chromium concentration (50 to 250 $\text{mg} \cdot \text{L}^{-1}$) (Yang et al. 2013).

Data Evaluation

The samples were filtered and analyzed to prevent any possible intrusion of carbon fines with the analysis. The absorbance of the supernatant solution was calculated to determine the standard solutions' residual hexavalent Cr concentration. The hexavalent chrome removal percentage (R%) was determined for every run. The experiments were conducted in triplicates, while the mean values were reported to prevent any redundancies in experimental results.

The controls for metal solutions were maintained for all the experiments. The researcher calculated the adsorption capacity at equilibrium q_e . As given herewith, the removal percentage (R %) of hexavalent chromium was determined for every run.

$$R (\%) = \frac{C_o - C_e}{C_o} * 100$$

The expression below determined the adsorption capacity for every Cr (VI) concentration at equilibrium.

$$\text{Adsorption capacity} = q_e \frac{(mg)}{(g)} = \frac{C_o - C_e}{m} * V$$

Here V denotes the volume of solution in terms of liters, whereas 'm' denotes the mass of the adsorbent utilized in grams (Hossain et al. 2012).

Optimum Analysis of Adsorption of Cr(VI) over PBBC

According to the literature by Deveci and Kar (2013), the authors conducted batch experiments. The variables measured in the experiments were (i) pH effect on the adsorption capacities, (ii) adsorbent dosage of PBBC (0.01 to 0.05 g), and (iii) initial concentration of Cr (50 to 250 mg.L⁻¹).

Data Modeling

To decode the relationship between the amount of Cr (VI) ions adsorbed (C_e) on the adsorbent surface and the equilibrium adsorption capacity (q_e), the adsorption isotherm studies were conducted at equilibrium conditions. The researcher plotted Langmuir (equation 1), Freundlich (equation 2), and Temkin (equation 3) isotherms with the help of standard straight-line equations. While the two corresponding parameters of hexavalent chromium ions, C_e and Q_e , were determined based on the relevant graphs. According to Langmuir isotherm, monolayer sorption occurs on a homogeneous surface without interacting with the sorbed species. There seems to be a specific number of binding sites homogeneously distributed over the biosorbent surface, and it is with this theory the Langmuir isotherm equation is applied (Inyang et al. 2010). As per this theory, no interaction is found between the adsorbate and adsorbent.

Following is the linear form of the Langmuir equation.

$$\frac{C_e}{Q_e} = \frac{C_e}{Q} + \frac{1}{Qb} \quad \dots(1)$$

Where Q_e denotes the sorbent's equilibrium adsorption capacity in mg/g, C_e in mg.L⁻¹ at equilibrium indicates the concentration of metal ions. Q denotes the maximum capacity of the metal monolayer in mg.g⁻¹, whereas b denotes the adsorption equilibrium constant in L.mg⁻¹.

Freundlich isotherm elucidates the heavy metal adsorption by biosorbent since it is held accountable for various binding sites. Following is the notion for the adsorption isotherm model, which considers the heterogeneous adsorption on the adsorbent surface (Sukumar et al. 2014).

$$\ln q_e = \ln K_f + \frac{1}{n} \ln C_e \quad \dots(2)$$

Here, C_e denotes the equilibrium concentration of metal ion (mg.L⁻¹), the amount of metal ion adsorbed at equilibrium (mg.g⁻¹) is denoted by q_e (Cheng et al. 2016), n denotes the heterogeneity factor, and K_f is the Freundlich constant that is related to sorption capacity (mg.g⁻¹). Determining K_f and n from a linear plot of log q_e against log C_e is possible.

Temkin isotherm is provided herewith as a linear equation. This model considers that the heat of adsorption (function of temperature) of almost all the molecules present in the layer gets reduced in linear relatively than logarithmic with coverage.

$$q_e = B \ln KT + B \ln C_e \quad \dots(3)$$

Where B_T denotes the Temkin constant correlated with the heat of sorption, mathematically, $B_T = RT/b_T$ (J.mol⁻¹) where R denotes the gas constant (8.314 J.mol⁻¹.K⁻¹), b_T denotes the Temkin isotherm constant, and T denotes the absolute temperature (K). C_e denotes the equilibrium concentration of a metal in solution (mg.L⁻¹), q_e denotes the amount of Ni(II) ions sorbed onto the PBBC (mg.g⁻¹), and K_T (L.g⁻¹) denotes the equilibrium potential corresponding to the maximum binding energy. The researcher conducted blank experiments excluding PBBC to ensure that the sorption of Cr (VI) on the flasks' walls was negligible.

RESULTS AND DISCUSSION

Characterization of Biochar

Table 1 shows the results of the proximate analysis. The PBBC pH value was alkaline (7.1), like biochar from anaerobic-digested sugarcane bagasse (Janaki et al. 2013, 2014). This might be a tribute to the presence of alkali metals such as magnesium and calcium from pig bone. The PBBC moisture content was 2.20%, whereas this low moisture content denotes that the PBBC has good adsorptive capacity. The PBBC had a fixed carbon content of 60%. This denotes a high carbonization process, whereas the chances of metals getting adsorbed onto PBBC are high. The PBBC had an ash content of 29%. Zeta potential study is nothing but a measure of charge stability, and it keeps all the particle-particle interaction under control within a suspension. In Table 1, one can observe that the zeta potential of biochar

Table 1: Physio-chemical characteristics of PBBC.

S.No.	Characteristics	PBBC
Proximate characteristics		
1	Moisture content [%]	0.27
2	Volatile content [%]	18
3	Fixed carbon content [%]	61
4	Ash Content [%]/	16
Electrochemical properties		
1	pH	7.7
2	EC [ds ⁻¹]	2.87
3	Zeta potential [mV]	-26.3
Physical property		
1	Water holding capacity [%]	193

was 3.9V denoting that PBBC carries a positive charge on its surface. The presence of relatively high zeta potentials

in high cation-containing biochar is due to the amount of sorbed cations, for instance, K^+ and Ca^{2+} (Gonen & Onalan 2016). The biochar's stability behavior is determined to be fast coagulation or flocculation. Zeta potential is the potential difference between a stationary layer of fluid attached to the dispersed particle and that of the dispersion medium. The PBBC particle size ratio was found to be 1.00.

Scanning Electron Micrographs and Energy Dispersive X-Ray Spectroscopy

The surface morphologies and adsorption of the Cr (VI) ions PBBC samples were studied by SEM analysis. The adsorbent surface has flake-like structures with an uneven size distribution,

Figs. 2(a) and 2(b) show the EDAX mapping of a blank and a PBBC with adsorbed Cr (VI) ions, respectively. The SEM images are in good match with EDAX.

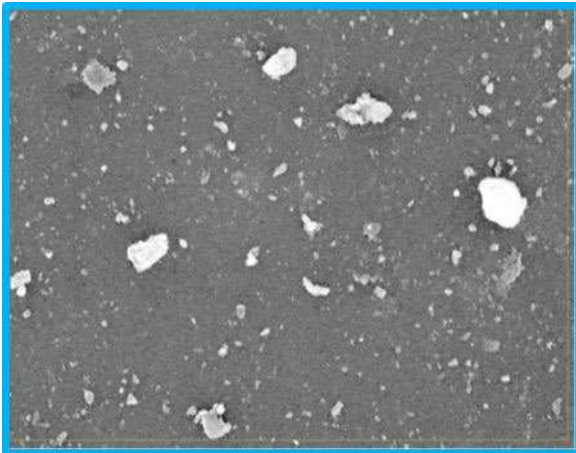


Fig.1(a): SEM image of blank PBBC.

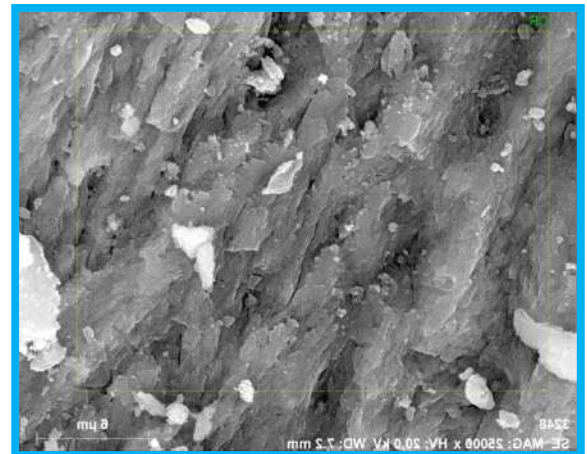


Fig.1(b): SEM image of Cr(VI) adsorbed PBBC.

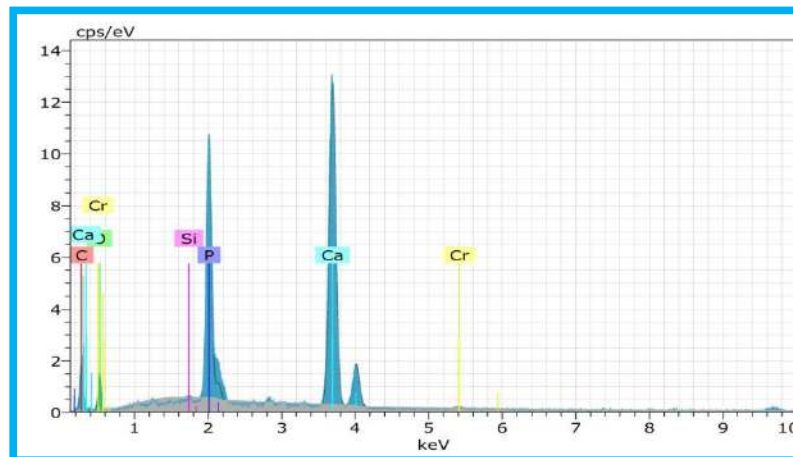


Fig. 2(a): EDAX spectra of blank pig bone biochar.

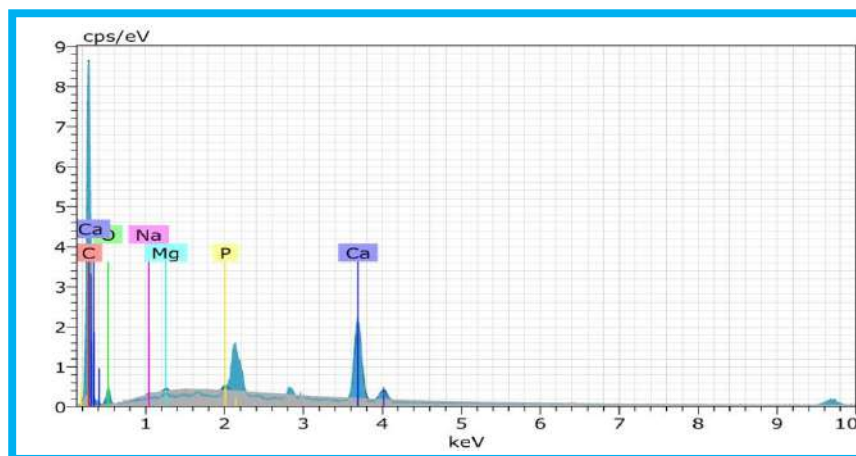


Fig. 2(b): EDAX spectra of Cr (VI) adsorbed pig bone.

The functional parameters like concentration, dosage, and pH are optimized by carrying out the trial experiments. Initial experiments are conducted with the concentration varied, and the dosage and pH kept constant. The next step is that dosage varies with concentration, keeping pH constant. Lastly, pH values are changed with concentration and dosage made constant.

FT-IR Analysis

Several functional groups, such as sulfhydryl, alkyl, hydroxyl, aryl, carboxyl, keto, phosphate sulphonate, and amide groups, contribute to the adsorption of metal ions in biochar. Therefore, to realize the functional groups concerned

with the adsorption of Cr (VI) ions in PBBC, Fourier-transform infrared (FTIR) analysis was conducted, and the results are shown in Fig. 3(a) & 3(b). The spectra were plotted using the same scale on the transmittance axis for PBBC before and after adsorption. The FTIR spectra of the PB-BC exhibit the number of adsorption peaks, representing the composite nature. The essential changes observed in the spectrum before and after Cr (adsorption VI) onto PBBC indicated the control of various functional groups' adsorption process. The wave number 2927.27 cm^{-1} to 2923.09 cm^{-1} was shifted and identified as C–H stretch aldehyde groups. The transform in the peak from 1417.15 cm^{-1} to 1412.32 cm^{-1} depicts the presence of C–C aromatics. The peak from

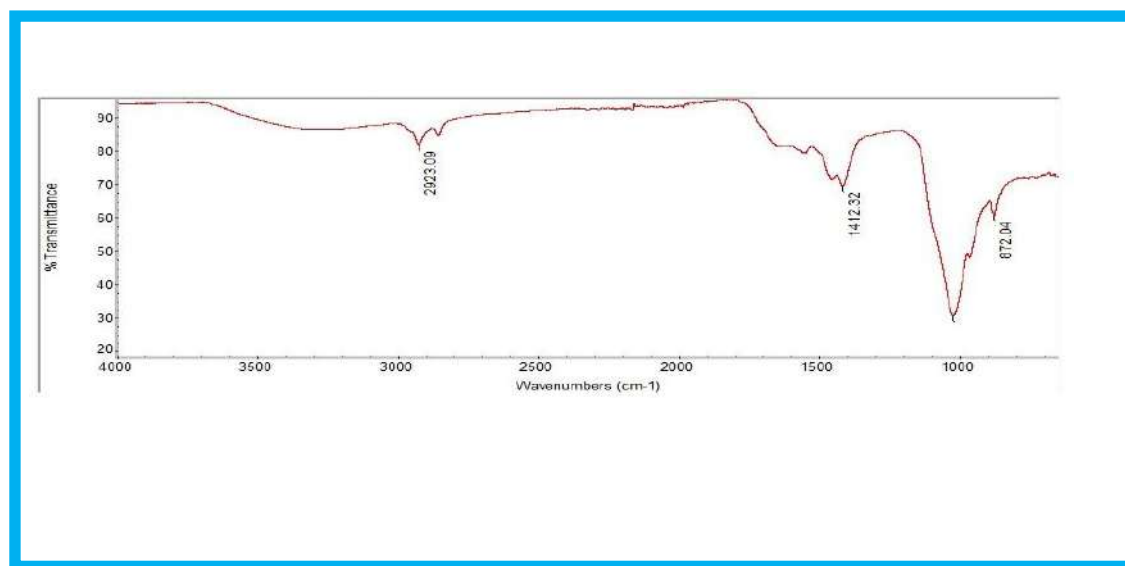


Fig. 3(a): FT-IR Spectra of blank pig bone biochar.

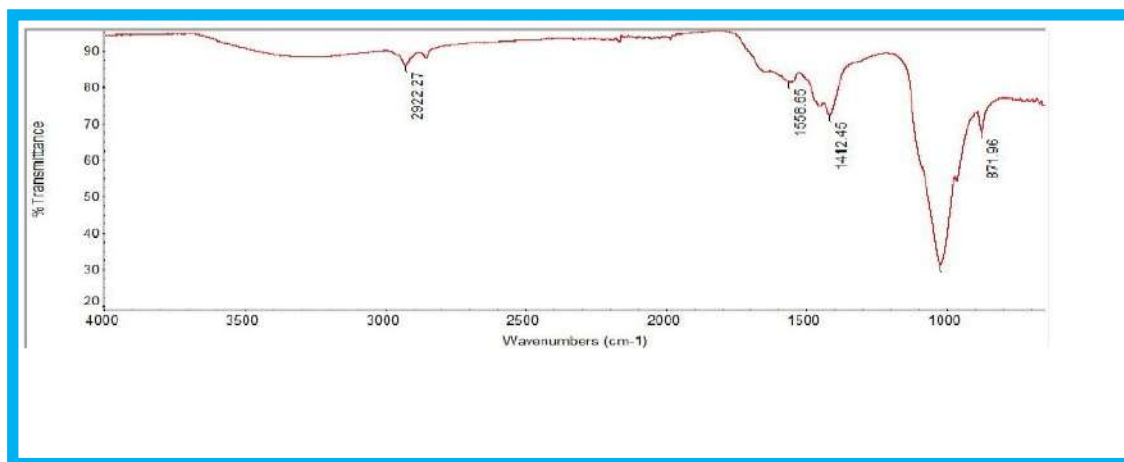


Fig. 3(b): FT-IR Spectra of Cr (VI) adsorbed pig bone biochar.

8781.96 cm^{-1} to 872.04 cm^{-1} depicts the bonding of C–H bending, thereby indicating the presence of an alkyl group in the adsorption process.

Effect of Cr (VI) Concentration

Dosage is a significant factor in the effective adsorption process. It creates a Driving force that removes all mass transfer resistance of metal ions between the aqueous phase and the solid (Shanmugapriya et al. 2013). The effect of initial Cr (VI) concentration (50 to 250 mg.L^{-1}) with the optimized parameters (0.05 g of biochar, pH 7.0) was investigated. Fig. 4(a) shows the results. There was a slight decrease observed (0.4–2%) in the removal percentage when the Cr (VI) (50 to 250 mg.L^{-1}) concentration was increased. The increased sorption at lower concentrations might be attributed to easy access to enough active sites present in biochar. At later stages, when these active sites got saturated, the sorption process slowed due to steric repulsion between solute molecules, thus reducing the removal capacity. Cadmium adsorption was also investigated in an earlier study (Mao et al. 2011) on peanut husk biochar by Cheng et al. (2016).

Effect of Adsorbent Dosage

Dosage is the main parameter in the sorption process since it evaluates the system's adsorbent-adsorbate equilibrium (Kumar et al. 2013). So the optimum dosage was finalized through experimentation with different doses (0.01–0.05 g) of PBBC, and the results of such experiments are showcased in Fig. 4(b) respectively. The figure shows no significant change in the removal capacity of Cr (VI) because of PBBC dosage since more than 99% removal was observed in almost all the dosages. The presence of more active sites and adsorptive surfaces present in the PBBC led to high

adsorption. The experiment results can be relied on since the literature (Arivoli et al. 2012) cited an increase in the level of Cr (VI) adsorption onto biochar prepared from oily seeds of *Pistacia terebinthus* L.

Effect of pH

As per Fig. 4(c), there seems to be a change in the percent removal of metal ions in the entire range of pH values from the experiments conducted. The pH of the solution remains an important parameter since it influences the interface between adsorbate and adsorbent by altering the surface charge (Pandian et al. 2014). Further, the degree of ionization of materials in the solution is also influenced by pH value. So, PBBC measuring 0.05 g was added to 100 mL of Cr (VI) (100 mg.L^{-1}) at different pH values (2–8), while Fig. 4(c) showcases the results of this experiment. One can understand that Cr and Ni get sorbed at all pH ranges (2–8) with a removal capacity of <88%. In the case of chromium, the adsorption at neutral pH (7) was found to be 99.75%, while in the case of Ni, it was 99.88%. As per the study conducted earlier (Zavvar & Seyedi 2011), the maximum adsorption at pH 7 might be attributed to the negative charge on the surface in an alkaline medium. Further, the protonation of amine and carboxyl functional groups in the PBBC adsorbent might have played an important role here. Altogether this resulted in strong electrostatic attraction between chromate ions and PBBC in chromium solution.

Further, nickelate ions and PBBC also got a similar attraction in nickel solutions. According to Janaki et al. (2014), the rivalry between OH^- ion and the chromate or nickelate ions threatens the neutral pH. This threat results in high consumption of chromium or nickel. So, the next sets of experiments were conducted at pH 7. In other

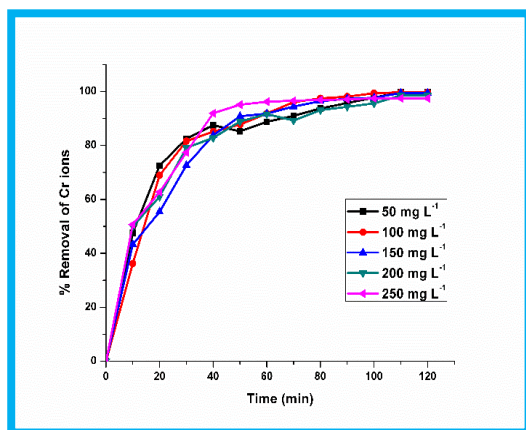


Fig. 4(a): Effect of Concentration.

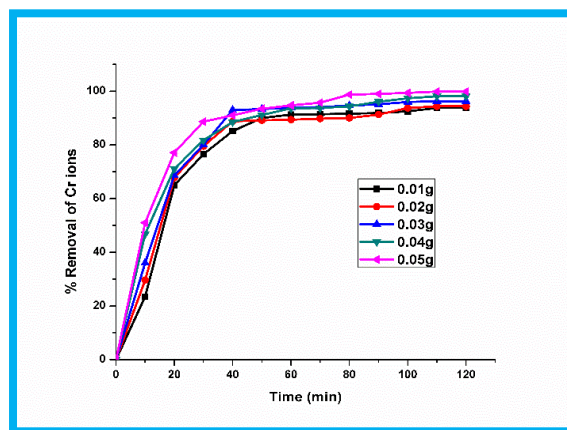


Fig. 4(b): Effect of Adsorbent Dosage.

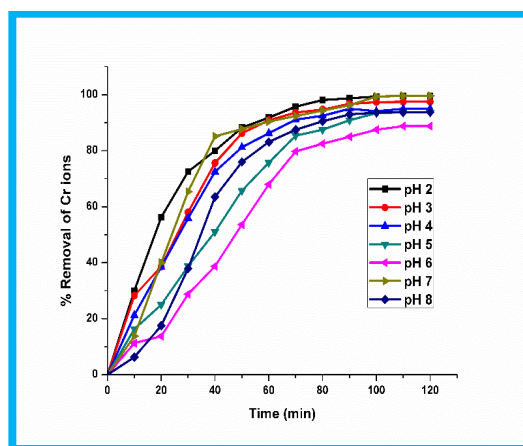


Fig. 4(C): Effect of pH.

terms, the deprotonation of the carboxylic group in acidic pH (3-6) would have mildly reduced the adsorption of Cr (VI) onto PBBC. In line with this, scenarios like increased concentration of OH^- ion in pH8, competition between OH^- ion and chromate ions or nickelate ions or in alkaline solutions may hinder the interface between PBBC and Cr (VI) ions.

The results infer that Cr (VI) adsorption may be adapted to a pH value prism dependent on PBBC features. The biochar contains cellulose, lignin, tannins, and polysaccharides which may enter into a binding reaction with Cr (VI) ions (Soheil et al. 2016) and reported similar results for cadmium adsorption onto peanut husk biochar.

Data Modeling of Isotherms

The Langmuir isotherm denotes the development of monolayer coverage of adsorbate on the adsorbent surface. Further, one can also observe the constant nature of sorption

energy. The sites seem energetically equal without any interface between adsorbed molecules on adjacent sites (Dada et al. 2012). According to the results, an appropriate fitness is found in the case of linear equations that assess the adsorption of Cr (VI) ions onto PBBC, compared with the Langmuir equation (Pradeeba et al. 2022). Further, the maximum adsorption capacity (Q_e) of PBBC for Chromium (VI) was found to be $259.55 \text{ mg} \cdot \text{g}^{-1}$. The study mentioned that the adsorbent with a high Q_e value is accepted in wastewater treatment. The relationship is more linear because the correlation coefficient value R^2 is closer to 1 (Chromium $R^2 = 0.9936$). So, the adsorption of Cr (VI) onto PBBC is found to have been suitable with the Langmuir isotherm equation (Fig. 5). The biochar adsorption capacity has few differences due to structural, functional differences and also due to the presence of polysaccharides in raw materials, preparation conditions, and proximate characteristics. To ensure the favorability of the adsorption process, it is possible

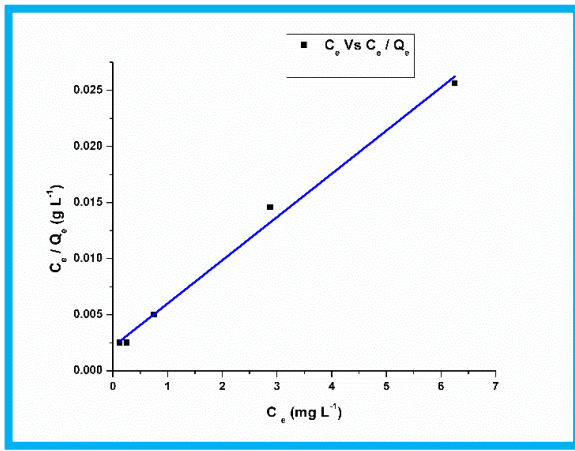


Fig. 5: Langmuir isotherm of concentration.

to explain the equilibrium parameter, R_L , and the separation factor. The following equation was used to calculate it (Dada et al. 2012).

$$R_L = 1 / (1 + bC_0)$$

Table 2: Isotherm model constants for Cr (VI)ion adsorption onto PBBC.

Isotherm models	Parameters	PBBC
Langmuir model	$q_m(\text{mg.g}^{-1})$	259.55
	$K_L(\text{L.mg}^{-1})$	1.788
	R^2	0.99
Freundlich model	$K_f(\text{mg.g}^{-1})(\text{L.mg}^{-1})^{1/n}$	137.41
	N	2.72
	R^2	0.91
Temkin model	K_T	28.177
	B_T	46.74
	R^2	0.98

Where $C_0(\text{mg.L}^{-1})$ denotes the initial concentration of metal ions, R_L value denotes either the isotherm shape is unfavorable ($R_L > 1$), linear ($R_L = 1$), favorable ($0 < R_L < 1$), or reversible ($R_L = 0$). In the current research, the R_L values (0.009-0.005) for chromium ions and (0.005-0.001) for nickel ions inferred that the adsorption of ions upon PBBC is favorable when the values lie in the range of 0 and 1. The R_L

Table 3: Adsorption kinetic model constants for Cr (VI) adsorption onto PBBC.

Kinetic models	Parameters	Initial concentration [mg.L^{-1}]				
		PBBC				
		50	100	150	200	250
PPseudo first order	$q_e(\text{exp})(\text{mg.g}^{-1})$	49.8750	99.7500	149.2500	197.1250	243.7500
	$q_e(\text{calc})(\text{mg.g}^{-1})$	31.7062	82.8083	136.7362	169.7926	145.8930
	$K_1(\text{min}^{-1})$	-0.0311	-0.0430	-0.0419	-0.0393	-0.0503
	R^2	0.9545	0.9403	0.9909	0.9306	0.9158
PPseudo second order	$q_e(\text{exp})(\text{mg.g}^{-1})$	49.8750	99.7500	149.2500	197.1250	243.7500
	$q_e(\text{max})(\text{mg.g}^{-1})$	52.3836	108.8068	163.5461	208.5315	260.4999
	$k_2(\text{g mg}^{-1} \text{min}^{-1})$	0.0023	0.0009	0.0005	0.0005	0.0006
	R^2	0.9934	0.9886	0.9878	0.9928	0.9930
	H	0.1221	0.0967	0.0875	0.1131	0.1443

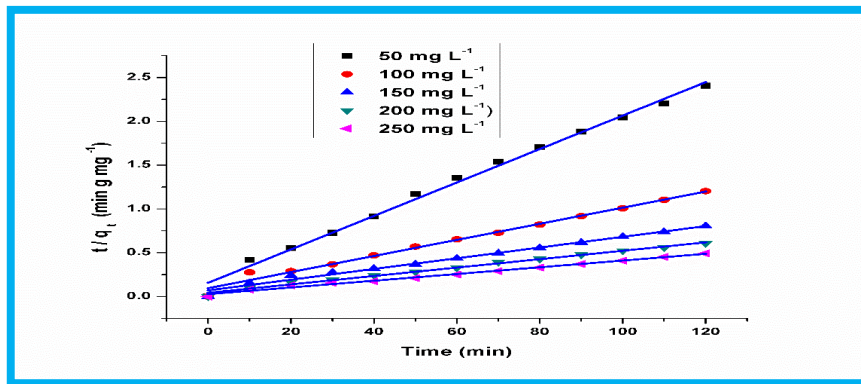


Fig. 6: Pseudo II order kinetic model for concentration.

is near 0 and is grateful to the pore diffusion sorption effect. The R_L values attained were in the range of 0 and 1. This assured the proceedings of a favorable adsorption process (Pradeeba et al. 2022).

Freundlich adsorption isotherm was attained by drawing a plot $\ln C_e$ versus $\ln Q_e$ in the adsorption of Ni (II) and Cr (VI) ions on PBBC. The K_f and n values were determined from the intercept and slope of the plot of $\log C_e$ vs. $\log Q_e$ and are shown in Table 2.

As per Table 2, the K_f values generally denote the control in adsorption capacity. The value of $n > 1$ (or) $1/n$ in the range of 1 and 10 infers the adsorption condition to be favorable. High adsorption co-efficient K_f values were found for Chromium (137.4072) and Nickel (144.649) on PBBC. Higher values of K_f denote that the saturation time for the adsorption of Ni and Cr ions was attained rapidly. It's a gratitude to the high affinity of PBBC towards adsorbate. In the case of Nickel ions, the values of $1/n$ were around $3.081 \text{ (mg.L}^{-1}\text{)}$, and in the case of Chromium ions. It was $2.728 \text{ (mg.L}^{-1}\text{)}$. Based on the values attained for K_f and $1/n$, one can infer that PBBC is highly efficient in removing Ni or Cr ions. For Cr, the correlation coefficient value was 0.9084, and for Ni, it was 0.8206. The Tempkin isotherm evaluated the adsorption potentials of the sorbent for Cr(VI) adsorption onto the PBBC plot for sorbate. The sorption heat of molecules in the layer reduces linearly mainly because of sorbate and sorbent contacts. Table 2 shows the results along with correlation coefficients (R^2). For Chromium (V), the correlated coefficient value was ($R^2=0.988537$). The Tempkin isotherm model seemed to have good fitness for the data (Pradeeba & Sampath 2022). But of the three adsorption isotherm models under investigation, i.e., Langmuir, Freundlich, and Temkin isotherms, the Langmuir model seems appropriate for sorption data. In contrast, the value was high and remained the best fit.

Adsorption Kinetic Models

The kinetic models are generally utilized to detail the efficacy of adsorption, associated mechanisms, and adsorbate effectiveness. So, the study used equilibrium data and investigated two kinetic models to scrutinize the adsorption mechanisms of Ni and Cr, as given herewith. Lagergren proposed a pseudo-first-order kinetic model. The adsorption rate constants and their correlation coefficients (R^2) were determined from the curves. Table 3 shows the summary of this analysis.

From the experimental kinetic data, a low correlation coefficient was observed for the pseudo-first-order kinetic model. Fig. 6 showcases the second-order model for Chromium (VI). This proves to be a not-so-good fit

for the model. In other terms, the correlation coefficient value of the pseudo-second-order model ($R^2=0.99$) was close to unity. This denotes that the pseudo-second-order model was the best fit than the pseudo-first-order model. Adding to the above, the q_e theoretical values calculated from the pseudo-second-order model were close to that of the experimental values of q_e . These outcomes denote the kinetic analysis results, i.e., the chemisorption processes control the adsorption rate (Pradeeba & Sampath 2022). The results align with earlier studies investigating the adsorption of Ni (II) and Zn (II) onto chitosan following pseudo-second-order kinetics. The pseudo-second-order kinetic equation seems to be the best-fit model in the current study.

CONCLUSION

There was an effective removal of (>99%) of Cr (VI) observed in an aqueous solution by PBBC. The removal of Cr (VI) was heavily influenced by pH, i.e., at pH7, the maximum removal was noted. There was an increase in the adsorption of Cr (VI) on PBBC with an increase in the dose and contact time of the adsorbent. There was a decrease in the adsorption efficiency of Cr (VI) on PBBC when the initial Cr (VI) concentration was increased. Based on the kinetic studies, it can be established that the adsorption of Cr (VI) ions followed the pseudo-second-order model. At the same time, the equilibrium data had the best fit with the Langmuir isotherm. The results infer that PBBC is an efficient and cost-effective adsorbent that can remove Cr (VI) from an aqueous solution. Further, PBBC can be recycled to reduce contamination and environmental pollution.

REFERENCES

- American Society for Testing and Materials (ASTM), USA., 1977.
- Arivoli, S., Marimuthu, V., Ravichandran, T. and Hema, M. 2012. Kinetic, equilibrium, and mechanistic studies of nickel adsorption on a low-cost activated referncalcite powder. *Indian J. Sci. Res. Tech.*, 1: 41-49.
- Ayaliew, A.W., Nigus, G.H. and Hayelom, D.B. 2014. Removal of hexavalent chromium from tannery wastewater using activated carbon primed from sugarcane bagasse: adsorption/desorption studies. *Am. J. Appl. Chem.*, 2(6): 128-135.
- Cheng, Q., Huang, Q., Khan, S., Liu, Y., Liao, Z. and Ligy, Y.S. 2016. Adsorption of Cd by peanut husks and peanut husk biochar from aqueous solution. *Ecol. Eng.*, 87: 240-245.
- Dada, A.O., Olalekan, A.P., Olatunya, A.M. and Dada, O. 2012. Langmuir, Freundlich, Temkin, and Dubinin-Radushkevich isotherm studies of equilibrium sorption of Zn^{2+} onto phosphoric acid modified rice husk. *IOSR J. Appl. Chem.*, 3(1): 38-45.
- Deveci, H. and Kar, Y. 2013. Adsorption of hexavalent chromium from aqueous solutions by bio-chars obtained during biomass pyrolysis. *J. Ind. Eng. Chem.*, 19(1): 190-196.
- Gonen, F. and Onalan, F. 2016. Adsorptive removal behaviour of procion MX-R dye from SRDW by chitosan. *Appl. Ecol. Environ. Res.*, 14(1): 77-98.

- Hossain, M.A., Hao Ngo, H., Guo, W.S. and Nguyen, T.V. 2012. Removal of copper from water by adsorption onto banana peel as bioadsorbent. *Int. J. Geomate.*, 2(2): 227-234.
- Inyang, M., Gao, B., Pullammanappalli, P., Ding, W. and Zimmerman, A.R. 2010. Biochar from anaerobically digested sugarcane bagasse. *Bioresour. Technol.*, 101(22): 8868-8872.
- Janaki, V., Shin, M.N., Kim, S.H., Lee, K.J., Cho, M., Ramasamy, A.K., Oh, B.T. and Kamala Kannan, S. 2014. Application of polyaniline / bacterial extracellular polysaccharide nanocomposite for removal and detoxification of Cr(VI). *Cellulose*, 21: 463-472.
- Janaki, V., Oh, B.T., Shanthi, K., Lee, K.J., Ramasamy, A.K. and Kamala Kannan, S. 2013. Polyaniline/chitosan composite: An eco-friendly polymer for enhanced removal of dyes from aqueous solution. *Synth. Met.*, 162(11): 974-980.
- Kumar, M., Pal, A., Singh, J., Shashank, G., Madhu, B., Ashis, V., Pal, Y.K. and Pachouri, U.C. 2013. Removal of chromium from water effluent by adsorption onto *Vetiveria zizanioides* and *Anabaena* species. *Nat. Sci.*, 5(3): 341-348.
- Mao, J., Won, S.W., Vijayaraghavan, K. and Yun, Y.S. 2010. Immobilized citric acid-treated bacterial biosorbents for the removal of cationic pollutants. *Chem. Eng. J.*, 162(2): 662-668.
- Mohanty, S. Bal, B. and Das. A.P. 2014. Adsorption of hexavalent chromium onto activated carbon. *Austin J. Biotechnol. Bioeng.*, 1(2): 5.
- Nessim, R.B., Ahmad Bassiouny, R., Hermine Zaki, R., Madelyn Moawad, N. and Kamal Kandeel, M. 2011. Biosorption of lead and cadmium using marine algae, *Chem. Biol.*, 27(6): 579-594.
- Pandian, P., Arivoli, S., Marimuthu, V. and Peter, P.R.A. 2014. Kinetic, equilibrium and mechanistic studies of nickel adsorption on acid-activated *Ipomoea carnea* leaves. *Sch. J. Eng. Tech.*, 2: 60-67.
- Prabakaran, R. and Arivoli, S. 2012. Adsorption kinetics, equilibrium and thermodynamic studies of nickel adsorption onto *Thespesia populnea* bark as biosorbent from aqueous solutions. *Euro. J. App. Eng. Sci. Res.*, 1(4): 134-142.
- Pradeeba, S.J. and Sampath, K. 2019. Synthesis and characterization of poly(azomethine)/ZnO nanocomposite towards photocatalytic degradation of methylene blue, malachite green, and bismarck brown., *J. Dyn. Syst. Meas. Contr.*, 1: 41.
- Pradeeba, S.J. and Sampath, K. 2022. Photodegradation, a thermodynamic and kinetic study of cationic and anionic dyes from effluents using polyazomethine/ZnO and polyazomethine/TiO₂ nanocomposites. *J. Optoelectr. Biomed. Mater.*, 14(3): 89-105.
- Pradeeba, S.J., Sampath, K. and Jeyagowri, B. 2022. Kinetic and adsorption isotherm modeling of photodegradation of anionic dyes using polyazomethine/titanium dioxide and polyazomethine/zinc oxide nanocomposite. *Desal. Water Treat.*, 262: 266-282.
- Rajoriya, S. and Kaur, B. 2014. Adsorptive removal of zinc from wastewater by natural biosorbents. *Int. J. Engg. Sci. Inv.*, 3(6): 60-80.
- Shamaa Shroff, K. and Varsha Vaidya, K. 2011. Effect of pre-treatments on biosorption of Ni (II) by dead biomass of *Mucor hiemalis*. *Bionano. Front.*, 11(6): 588-597.
- Shanmugapriya, A., Hemalatha, M., Scholastica, B. and Augustine, A.P.T. 2013. Adsorption studies of lead (II) and nickel (II) ions on chitosan-G-polyacrylonitrile. *Der. Pharma. Chemica.*, 5(3): 141-155.
- Shenbagavalli, S. and Mahimairaja, S. 2012. Production and characterization of biochar from different biological wastes. *Int. J. Plant Agric. Sci.*, 2: 2231-4490.
- Soheil, S.D., Raziye, Z.M. and Javad, M. 2016. Removal of Ni (II) and Zn (II) from aqueous solutions using chitosan. *Arch. Hyg. Sci.*, 5: 47-55.
- Sukumar, C., Gowthami, G., Nitya, R. Janaki, V., KamalaKannan, S. and Shanthi, K. 2014. Significance of co-immobilized activated carbon and *Bacillus subtilis* on the removal of Cr (VI) from aqueous solutions. *Environ. Earth Sci.*, 72: 839-847.
- Thamilarasu, P., Sivakumar, P. and Karunakaran, K. 2011. Removal of Ni (II) from aqueous solutions by adsorption onto *Cajanus cajan* L. Milsp seed shell-activated carbons. *Indian J. Chem. Technol.*, 18: 414-420.
- Yang, Z.H., Xiong, S., Wang, B., Li, Q. and Yang, W.C. 2013. Cr (III) adsorption by sugarcane pulp residue and biochar. *J. Cent. South Univ.*, 20: 1319-1325.
- Zavvar, M.H. and Seyedi, S.R. 2011. Nettle ash is a low-cost adsorbent for the removal of nickel and cadmium from wastewater. *Int. J. Environ. Sci. Tech.*, 8: 195-202.



Heavy Metal Pollution of Soil and Crops in Rural Gujarat, Next to an Industrial Area: A Correlation Study

A. Salauddin*¹ and C. Sandesh**

*Department of Chemistry, Rai University, Saroda, Ahmedabad-382260, Gujarat, India

**Department of Biotechnology, Mehsana Urban Institute of Sciences, Faculty of Science, Ganpat University-Kherva-384012, India

†Corresponding author: A. Salauddin; ansariasalauddin2008@yahoo.co.in

Nat. Env. & Poll. Tech.
Website: www.neptjournal.com

Received: 08-11-2022
Revised: 17-01-2023
Accepted: 18-01-2023

Key Words:

Industrial area
Heavy metals
Soil
Crops
Rural Gujarat

ABSTRACT

Heavy metal contamination is one of the significant concerns of environmental pollution. The present study was conducted to find out the correlation between soil and crop/food matrices grown at the exact location for Al, As, Ca, Cd, Cr, Cu, Fe, Hg, K, Mg, Mn, Ni, Na, P, Zn, and Pb elements near the industrial areas of Narol, Changodar, Vatva, Makarpura, Nandesari, and Ankleshwar in Gujarat, India. Soil samples were collected from 64 sampling sites in an industrial area. Twenty of these sites contained crop/food matrices used for the correlation study. The ranges of concentration of Cr (17-74.4 mg.kg⁻¹), Cu (9.6-82.4 mg.kg⁻¹), Ni (10.6-55.9 mg.kg⁻¹), Pb (4.5- 20.7 mg.kg⁻¹), Zn (21.5-112.4 mg.kg⁻¹), and Al (7075-44557.5 mg.kg⁻¹) for Soil and for crop Cr (0.3-0.6 mg.kg⁻¹), Cu (0.3-8.6 mg.kg⁻¹), Zn (1.1-43.5 mg.kg⁻¹), Fe (12.6-69.4 mg.kg⁻¹), and Al (5.8-102.2 mg.kg⁻¹). According to the study, there is a strong correlation between the soil and crop/food matrices at the different locations, like 0.97 for Fe and Ni, 0.94 for Mg, 0.95 for Mn, and 0.55 for Pb and Zn, and very little correlation between K, P, and Ca, while a negative correlation between Al, Cr, Cu, and Na. The DTPA extractable method was used for the elemental analysis, and analysis was done using the ICP-OES instrument following microwave-assisted digestion. The results show that metal contamination transforms from soil to crop/food matrices, which represents a serious concern and requires action to address the metal contamination by industrialization.

INTRODUCTION

The two most important natural resources on the Earth's surface are soil and water, affecting all terrestrial life. Modern technology development and rapid industrialization aggravate environmental pollution. Heavy metals, one of the most prevalent environmental pollutants, pose long-term health concerns to both people and the ecosystem (Lin et al. 2007, Antli & Canli 2008, Manyin & Rowe 2009, Perianez 2009). Regularly using heavy metal-contaminated water in agricultural regions leads to soil contamination and heavy metal enrichment (Lokhande & Kelkar 1999). Soil pollutants like heavy metals can leak into underlying groundwater with enough surface water infiltration. Depending on the kind of soil, heavy metals can affect groundwater in various ways (Kumar et al. 2013). The toxicity of heavy metals in animals varies depending on the animal type, the metal, the concentration, the chemical form, the composition of

the groundwater, and the period of exposure. Heavy metals such as cadmium (Cd), lead (Pb), arsenic (As), and mercury (Hg) are highly toxic to metal-sensitive enzymes, resulting in organism death and growth suppression (Huang et al. 2012, Li & Zhang 2012, Matache et al. 2009). Heavy metals, including Pb, Hg, and nickel (Ni), are trace elements that are not needed. These are very hazardous elements because they are persistent, bioaccumulative, and challenging to break down or metabolize in the environment. Heavy metals, including Pb, Hg, and Ni, accumulate in the ecological food chain after being taken up by primary producers and consumed by consumers (Lenoble et al. 2013, Dupler 2001). Heavy metals can enter the human body through food, water, air, and skin absorption in modern agriculture, industrial, and residential environments. Humans are exposed to heavy metals such as Cd, Pb, and As. Heavy metals are also known to cause cancer. Arsenic poisoning is caused by contaminated drinking water. Heavy metal vapors, such as Cd, Pb, and As, mix with water in the atmosphere to generate aerosols, which can cause health issues (Bruins et al. 2000, Zenglu 1992,

ORCID details of the authors:

A. Salauddin: <https://orcid.org/0000-0002-0040-5548>

Burkat et al. 1999). Some heavy metals, such as Hg and Pb, can cause autoimmunity, a condition in which a person's immune system destroys their cells. Heavy metals are among the contaminants introduced into soils by industrial processes such as moving scrap metal and raw materials, forging metal, producing alkaline batteries, and creating synthetic organic compounds (Lokeshwari & Chandrappa 2006).

Gujarat is India's metropolis and the center of many multinational industries. Industries have come up in the last three decades around the cities of Gujarat. Ankleshwar, Makarpura, Vatva, Nandesari, Changodar, and Narol GIDC (Gujarat Industrial Development Corporation) area was selected for the study to cover the majority of industries of Gujarat. Sample extraction was performed using DTPA (diethylenetriaminepentaacetic acid) metal extraction method. For quantification, Inductively Coupled Plasma Optical Emission Spectroscopy (ICP-OES) technique was used to achieve a lower detection level. Pearson's correlation was used to determine the correlation between soil and crop/food matrices. ICP-OES provides an advanced technique for very low-level metal detection following the advanced micro-assisted digestion system. This study's primary objectives were to assess the soil's quality and determine the levels of heavy metals present in the soil and the association between those levels and the crop/food matrices planted nearby.

MATERIALS AND METHODS

Study Area

In this study, samples were obtained from nearby farming areas of all possible directions with increasing distances of 100 m, 200 m, 400 m, and 800 m of the industrial areas of Ahmedabad, Vadodara, and Ankleshwar in Gujarat. 64 soil samples were obtained, with 20 containing crop/food samples used in correlation analysis. These locations were selected based on the total industrial area, the total number of industries, and the types of manufacturing. Numerous industrial operations in this area serve as the primary source of hazardous waste, which includes medicines, medications, metal, paint, packaging, machinery, and chemicals.

Sampling

Soil Sample Collection

For soil sample collection, the zigzag approach was used. To avoid unwanted interference, the surface was properly cleaned by removing herbs, and samples were collected after identifying the collection point from a farming region (Table 1). Samples were gathered from 4-5 zigzag points using a hand auger from 15 cm deep on both sides of the wall and combined into a single composite sample. Approximately 1

kg of the sample was collected from each zigzag point, and around 2 kg of samples were prepared for the study. Each sample was carefully sealed in a plastic bag after being collected, and a specific identification number was used to identify each sample.

Crop/Food Sample Collection

Crop/food samples were gathered from all four sides of a designated industrial region at distances of 100 m, 200 m, 400 m, and 800 m depending upon availability. Crop samples such as wheat, pearl millet, rice, pulses, and fodder crops were collected from various locations, as were food samples such as brinjal, bottle gourd, and cauliflower. All crop/food samples were collected according to their type, such as 2-3 whole pieces of bottled gourd and cauliflower collected from the same place in vegetable samples and 10-12 bunch of grain of different points collected from the same site in crop samples. Every sample was defined by its location, sides, distance, and industrial sector.

Sample Preparation

Soil samples were dried in the shade for two to three days before being conserved after passing through a 2 mm sieve. The samples were then crushed to pass through a 0.25 mm filter for heavy metal analysis. 4 mL HNO₃, 1 mL HCl, and 0.5 mL H₂O₂ were added to a 0.2 gm sample in a micro oven vessel for analysis, and the samples were digested in a micro oven digestion machine. After digestion, the samples were made up to 50 mL with type-1 water and analyzed using an ICP-OES instrument (Kebata-Pendias 2000). To avoid contamination, vegetable plant samples were cleaned (dirt removed) using shaking and a dry pre-cleaned vinyl brush. The entire vegetable plant body was then separated into distinct segments, and non-edible components were removed in accordance with standard home norms. To eliminate airborne contaminants, the edible sections of the vegetable samples were rinsed multiple times with tap water before being immersed in 0.01 N HCl acid for 5 minutes and thoroughly washed in distilled and deionized water. Crop/food samples were crushed and homogenized in a stone mortar pistol to avoid metal contamination. 1 g of samples were taken for analysis in a micro oven vessel, and 5 mL

Table 1: Sampling location.

Name of Industrial area	City area	Location
Narol GIDC	Ahmedabad	23.0906° N, 72.6714° E
Vatva GIDC	Ahmedabad	22.9738° N, 72.6479° E
Changodar GIDC	Ahmedabad	22.9272° N, 72.4484° E
Makarpura GIDC	Vadodara	22.2503° N, 73.1895° E
Nandesari GIDC	Vadodara	22.4130° N, 73.0951° E
Ankleshwar GIDC	Ankleshwar	21.6174° N, 73.0283° E

HNO₃, 1 mL HCl and 0.5 mL H₂O₂ were added, and samples were digested in a micro oven digestion machine. After digestion, the samples were made up to 50 mL with type-1 water and analyzed by an ICP-OES system.

Chemicals

Sigma-Aldrich in the United States provided the entire Standard. Merck, USA, provided laboratory-grade nitric acid (HNO₃), hydrochloric acid (HCl), and Hydrogen peroxide (H₂O₂). Type-1 water was obtained from the Elga water purification system.

Analysis and Determination of the Heavy Metal Concentrations in Samples

The soil sample digests were analyzed for Aluminium (Al), As, Calcium (Ca), Cd, Chromium (Cr), Copper (Cu), Iron (Fe), Hg, Potassium (K), Manganese (Mg), Magnesium (Mn), Nickel (Ni), Sodium (Na), Phosphorous (P), Zinc (Zn) and Pb using the Inductively coupled plasma optical emission spectroscopy (ICP-OES) equipment (Agilent Technology, Model 5110). For each metal, calibration curves were created by running different concentrations of standard solutions. To adjust for reagent impurities and other sources of errors from the environment, a blank reagent sample was taken through the technique, evaluated, and subtracted from the samples. Each determination was based on the average of three replicates.

RESULTS AND DISCUSSION

Heavy Metal Concentrations in Soil

The data showing the distribution of selected heavy metals in terms of concentration, along with statistical parameters, is presented in Table 2. From Table 2, Al and Fe contents of the soil samples were very high, in the majority of the location ranging from 7075 mg.kg⁻¹ to 44558 mg.kg⁻¹ for Al with a median value of 15279 mg.kg⁻¹ and Fe range from 8128 mg.kg⁻¹ to 40320 mg.kg⁻¹ with median value 16300 mg.kg⁻¹. Heavy metals like As higher at Ankleshwar and Makarpura locations was 5.7 mg.kg⁻¹, and Pb higher at Vatva and Makarpura locations were 20 mg.kg⁻¹ and 20.7 mg.kg⁻¹, respectively. Chromium slightly to moderately higher at Changodar, Ankleshwar, and Makarpura locations from were 48.6 mg.kg⁻¹ to 74.4 mg.kg⁻¹, which shows the level of contamination of heavy metal in these areas, and Cu was present in the range from 9.6 mg.kg⁻¹ to 82.4 mg.kg⁻¹ with median value 24.3 mg.kg⁻¹. Heavy metals like Ni at a higher level at Vatva and Ankleshwar locations were 49.2 mg.kg⁻¹, 55.9 mg.kg⁻¹, respectively, and metals like Cd and Hg were absent at most locations except Hg at the Vatva location at 4.9 mg.kg⁻¹. Other analytes like Ca, K, Mg, Mn, Na, and

P were present in the range from 2118 mg.kg⁻¹ to 43033 mg.kg⁻¹g with median value 4156 mg.kg⁻¹, 1246 mg.kg⁻¹ to 6323 mg.kg⁻¹ with median value 1883 mg.kg⁻¹, 1892 to 8844 mg.kg⁻¹ with median 4391 mg.kg⁻¹, 156 mg.kg⁻¹ to 879 mg.kg⁻¹ with median 280 mg.kg⁻¹, 285 mg.kg⁻¹ to 1452 mg.kg⁻¹ with median 625 mg.kg⁻¹, and 866 mg.kg⁻¹ to 6423 mg.kg⁻¹ with median 1564 mg.kg⁻¹ respectively. Zinc (Zn) present in a soil sample ranged from 22 mg.kg⁻¹ to 112 mg.kg⁻¹ with a median value of 51 mg.kg⁻¹, and the highest concentration was observed at Naroda and Makarpura industrial areas. The order of metals present in the soil in decreasing order was as Fe> Al> Ca> Mg> K> P> Na> Mn> Zn> Cr> Cu> Ni> Pb> As> Hg> Cd.

Heavy Metal Concentrations in Crop/Food Matrices

DTPA-extractable Al, As, Ca, Cd, Cr, Cu, Fe, Hg, K, Mg, Mn, Ni, Na, P, Zn, and Pb contents in crop/food samples are presented in Table 3. The highest concentration of Al was found at Naroda, Vatva, and Changodar in crop/food matrix was 102.2 mg.kg⁻¹, 46.3 mg.kg⁻¹, and 57.6 mg.kg⁻¹ respectively, with the range from 5.8 mg.kg⁻¹ to 102.2 mg.kg⁻¹ and 25.3 mg.kg⁻¹ median value. Copper was found at the highest level at Makarpura and Nandesari locations, 8.6 mg.kg⁻¹ and 8.0 mg.kg⁻¹, respectively, with a range from 0.3 mg.kg⁻¹ to 8.6 mg.kg⁻¹ and a median value of 2.8 mg.kg⁻¹ and Iron found higher side from 69.4 mg.kg⁻¹ to 49.3 mg.kg⁻¹ at Changodar and Nandesari location respectively with range 13 mg.kg⁻¹ to 69 mg.kg⁻¹ and median value 32 mg.kg⁻¹ showing the contamination level of the soil of farming area nearby the industrial areas. Heavy metals like As, Cd, and Hg were absent in all the locations, and Pb was present at a few locations at a very low level. Other metals like Ca, Cr, Cu, K, Mg, Mn, Na, Ni, P, and Zn highest concentrations were 1632, 0.6, 8.6, 2670, 1496, 30, 962, 1.8, 3995, and 44 mg.kg⁻¹ respectively with the range 136 to 1632, 0.2 to 0.6, 0.3 to 8.6, 421 to 2670, 71 to 1496, 0.7 to 30, 92 to 962, 0 to 1.8, 212 to 3995 and 1.1 to 44 mg.kg⁻¹ respectively. The median values for Ca, Cr, Cu, K, Mg, Mn, Na, Ni, P, and Zn were 376, 2.8, 32, 1039, 345, 3.5, 130, 0.3, 750, and 7.6 mg.kg⁻¹, respectively. The order of metals present in crop/food matrices in decreasing order was as P> Mg> Ca> Na> Fe> Al> Zn> Mn> Cu> Ni> Cr> Pb.

From Table 3, Al was found at Muthiya of Naroda, Changodar gam of Changodar and Vinzol of Vatva location very high and Fe very high at Vinzol of Vatva, respectively Changodar gam of Changodar and Koili of Nandesari location. The contamination levels of Al, Fe, Zn, and Cu in crop/food were above the level suggested by WHO, showing the quality of cop/food gowned in the metal-contaminated soil and not healthy for human consumption.

Table 2: Determination of soil samples from different villages in surrounding areas of Naroda, Vatva, Changodar, Ankleshwar, Makarpura, and Nandedari GIDC.

Industrial Area	Village (location)	Distance (meter)	Al	As	Ca	Cd	Cr	Cu	Fe	Hg	K	Mg	Mn	Na	Ni	P	Pb	Zn
Naroda	Ranasan (northeast)	800	14637.8	2.1	2854.9	ND	32.2	14.0	14352.9	0.6	1700.4	3531.3	252.2	784.1	20.2	944.4	6.3	30.6
	Muthiya (east)	100	17563.3	2.0	5887.3	ND	39.9	29.6	13553.9	2.5	2513.9	4458.8	251.9	735.5	20.8	2613.6	11.5	111.2
	Ranasan (north east)	400	10049.3	1.4	2360.6	ND	26.7	9.9	10000.4	0.6	1245.7	2339.6	201.9	414.4	13.7	866.3	4.5	23.2
Vatva	Nana chioda (west)	800	10101.0	1.9	2439.3	ND	24.2	9.6	10144.0	0.5	1454.0	2360.3	184.9	468.9	13.0	872.4	4.6	21.5
	Vinzol (south east)	200	44557.5	6.4	4444.9	0.3	74.0	36.3	40320.2	0.0	6322.7	8011.1	491.9	1069.1	49.2	1122.0	20.0	80.8
	Vinzol (south west)	400	9153.9	1.4	3957.9	ND	25.0	10.1	9541.0	0.5	1319.5	2887.3	189.2	1095.3	13.6	972.2	6.0	26.8
Changodar	Vinzol (north east)	400	7075.0	0.9	2849.9	ND	17.0	12.5	8127.7	4.9	1386.1	1891.5	155.8	285.3	10.6	1815.9	6.7	29.0
	Changodar gam	400	10454.2	2.7	2117.7	ND	22.7	14.2	10723.1	1.5	2720.2	2850.5	170.2	686.5	12.2	1850.5	7.6	42.6
	Changodar (Northwest)	400	30812.9	5.7	6934.2	ND	48.6	32.0	25973.0	1.9	4694.4	7124.1	410.6	1451.7	35.9	1558.7	14.7	63.2
Ankleshwar	Changodar gam	400	27352.0	4.1	6182.0	0.1	50.9	24.5	21862.2	ND	3044.9	6725.7	297.5	1105.8	28.6	1309.8	10.4	50.3
	Changodar (Northeast)	400	12812.5	3.1	2312.3	ND	27.9	24.0	14677.2	0.7	1638.7	4323.9	230.2	640.6	18.7	3103.3	9.6	51.6
	Changodar (Southeast)	400	42298.3	4.6	6443.7	ND	74.4	60.4	35623.6	ND	1638.1	7799.8	879.2	431.5	55.9	947.8	9.6	46.1
Makarpura	Jitali (east)	200	38283.6	4.9	12231.0	0.3	69.8	71.3	35307.4	ND	1911.6	8844.4	724.3	458.3	55.0	1457.3	11.7	53.8
	Jitali (east)	400	36975.3	4.9	11350.4	ND	65.9	65.6	33617.0	ND	1904.3	8687.3	777.8	552.7	53.7	1568.7	11.9	51.1
	Omkar chokadi (North)	400	12812.5	3.1	2312.3	ND	27.9	24.0	14677.2	0.7	1638.7	4323.9	230.2	640.6	18.7	3103.3	9.6	51.6
Nandedari	Omkar chokadi (North)	800	16931.1	3.2	4353.6	0.1	35.4	34.1	18158.5	ND	2240.5	6767.3	335.0	895.9	23.9	6422.8	13.9	78.7
	Talodara (west)	100	28922.1	5.7	6386.3	0.5	70.5	82.4	30213.2	0.6	2758.8	6693.8	468.5	604.9	46.2	2226.6	20.7	112.4
	Talodara (west)	400	24989.0	4.3	43033.1	ND	45.0	47.9	27022.3	ND	2616.0	7496.3	508.8	610.2	39.3	2139.5	10.6	52.1
Nandedari	Dashrath (Karachiya)	400	14147.5	2.3	3381.6	0.2	34.7	22.3	15617.9	ND	1658.1	3780.3	212.6	594.3	19.9	1929.9	7.3	47.3
	Koili (southwest)	400	15279.1	2.9	3942.2	0.2	34.4	23.6	16273.6	ND	1861.7	4157.7	263.0	667.7	20.7	1987.9	8.5	50.3
	Koili (north west)	400	13793.1	2.7	2805.9	0.2	35.2	21.9	16326.8	ND	1552.0	3872.3	296.1	530.1	21.8	1534.9	6.8	54.5

All the above results are in mg.kg⁻¹, ND- Not detected

Table 3: Determination of crop/Food samples from different villages in the surrounding area of Naroda, Vatva, Changodar, Ankleshwar, Makarpura, and Nandedari GIDC.

Industrial Area	Village (location)	Distance (meter)	Al	As	Ca	Cd	Cr	Cu	Fe	Hg	K	Mg	Mn	Na	Ni	P	Pb	Zn
Naroda	Ranasan (northeast)	800	15.8	ND	182.1	ND	0.3	0.8	19.0	ND	494.5	121.2	1.3	208.0	ND	289.9	0.2	1.9
	Muthiya (east)	100	102.2	ND	166.2	ND	0.6	1.0	62.5	ND	893.5	148.8	1.4	143.5	0.0	315.0	0.2	3.2
	Ranasan (north east)	400	9.2	ND	164.4	ND	0.2	0.9	12.6	ND	961.8	181.6	1.6	104.0	ND	344.0	0.1	2.3
Vatva	Nana chiloda (west)	800	29.4	ND	230.0	ND	0.4	0.9	32.3	ND	447.3	91.5	1.3	110.7	0.1	245.3	0.3	2.5
	Vinzol (south east)	200	29.6	ND	444.2	ND	0.4	4.6	55.4	ND	1694.6	1052.4	29.5	503.0	0.1	3109.6	0.1	23.4
	Vinzol (south west)	400	29.3	ND	373.8	ND	0.3	4.0	50.0	ND	1381.5	946.1	26.4	275.5	0.1	2698.1	0.1	17.4
Changodar	Vinzol (north east)	400	46.3	ND	540.4	ND	0.5	4.4	66.2	ND	1847.0	1091.6	24.6	962.0	0.1	2755.0	0.2	26.8
	Changodar gam (northwest)	400	31.5	ND	370.4	ND	0.6	5.0	33.2	ND	1945.1	314.5	3.4	133.5	1.5	1378.5	ND	12.7
	Changodar gam (northeast)	400	24.1	ND	457.8	ND	0.3	1.7	28.1	ND	1023.2	297.7	2.8	104.1	0.4	604.5	ND	4.9
Ankleshwar	Changodar gam (southeast)	200	57.6	ND	407.0	ND	0.3	4.9	69.4	ND	1240.6	764.4	22.4	170.3	0.1	1674.7	0.1	43.5
	Ankleshwar gam (west)	100	18.0	ND	162.9	ND	0.3	0.6	20.1	ND	420.5	70.6	0.7	93.3	0.0	211.8	0.2	1.9
	Jitali (east)	200	11.4	ND	378.4	ND	0.4	2.8	17.2	ND	1054.7	375.9	3.8	116.7	0.3	812.6	ND	8.5
Makarpura	Jitali (east)	400	14.0	ND	450.7	ND	0.2	2.7	17.4	ND	922.9	398.7	3.6	92.1	0.3	687.0	ND	6.6
	Omkar chokadi (north)	400	11.9	ND	147.9	ND	0.3	0.8	12.7	ND	666.1	124.7	0.9	115.2	ND	248.7	ND	1.1
	Omkar chokadi (north)	800	12.0	ND	159.5	ND	0.2	0.3	13.8	ND	906.0	153.9	1.2	498.9	ND	382.7	ND	4.5
Nandedari	Talodara (west)	100	26.7	ND	640.2	ND	0.3	4.2	30.8	ND	1875.3	424.9	4.6	151.4	0.6	1022.9	0.2	12.3
	Talodara (west)	400	26.6	ND	1631.5	ND	0.3	8.6	42.2	ND	1620.6	1356.3	12.0	211.3	1.2	3443.5	ND	39.7
	Dashrath (Karachiya)	400	13.2	ND	136.4	ND	0.3	0.9	15.0	ND	791.6	141.6	1.3	96.6	ND	321.7	ND	1.7
	Koili (southwest)	400	32.1	ND	1469.3	ND	0.2	8.0	37.1	ND	1763.4	1490.9	9.4	111.9	1.8	3973.3	ND	33.3
	Koili (north west)	400	5.8	ND	1497.7	ND	0.3	6.5	49.3	ND	2670.3	1496.3	12.4	126.7	1.2	3994.6	ND	37.0

All the above results are in mg.kg⁻¹, ND- Not detected

Correlation Between Soil and Crop/Food Sample

The result of Table 4 was obtained by applying the correlation formula between soil and crop/food matrices data of industrial area for individual metals. Table 4 represents the correlation of metal between soil and crop/food matrices for particular industrial areas, shown in Table 4 as metal correlation at different industrial areas and correlation between the metal. The two variables for particular metal were a concentration in soil and the other was a concentration in crop/food

matrices, obtained results of Table 2 and Table 3 and the correlation between parallel metal concentrations. From the correlation Table 4 Al at Naroda, Ankleshwar, Makarpura, and Nandesari showing the negative correlation between soil and crop/food sample were -0.46; for Cr showing negative correlation values were seen as -0.22, -0.05 and -0.53. Further, Mg, Mn, and Ni showing the highest correlation with respect to Al were 0.94, 0.95, and 0.97, respectively. P has a negative correlation with most elements, except for K and Na, and Fe has a high correlation of 0.97 with Al. Other

Table 4: Correlation between metal concentrations in soil vs. metal concentration in crop/food sample.

	Al	Ca	Cr	Cu	Fe	K	Mg	Mn	Na	Ni	P	Pb	Zn
Soil vs. Crop	-0.46	0.01	-0.22	-0.23	-0.48	0.43	-0.33	-0.31	0.28	-0.20	0.01	0.01	0.02
Al	-	-0.31	-0.05	-0.21	0.97	0.04	0.94	0.95	-0.20	0.97	-0.13	0.51	0.04
Ca	-	-	-0.53	-0.14	-0.63	-0.27	-0.32	-0.37	-0.13	0.08	-0.35	0.55	-0.27
Cr	-	-	-	-0.23	-0.55	-0.38	-0.31	-0.23	-0.21	-0.22	-0.35	0.41	-0.35
Cu	-	-	-	-	-0.73	-0.40	-0.34	-0.40	-0.28	-0.04	-0.39	0.59	-0.39
Fe	-	-	-	-	-	-0.27	-0.21	-0.14	-0.12	-0.17	-0.25	0.35	-0.23
K	-	-	-	-	-	-	0.20	0.61	0.47	-0.15	0.24	-0.93	0.53
Mg	-	-	-	-	-	-	-	-0.27	-0.24	-0.08	-0.36	0.31	-0.25
Mn	-	-	-	-	-	-	-	-	-0.27	-0.23	-0.40	0.51	-0.44
Na	-	-	-	-	-	-	-	-	-	0.02	0.21	-0.96	0.55
Ni	-	-	-	-	-	-	-	-	-	-	-0.35	0.45	-0.36
P	-	-	-	-	-	-	-	-	-	-	-	0.29	0.12
Pb	-	-	-	-	-	-	-	-	-	-	-	-	0.16
Zn	-	-	-	-	-	-	-	-	-	-	-	-	-

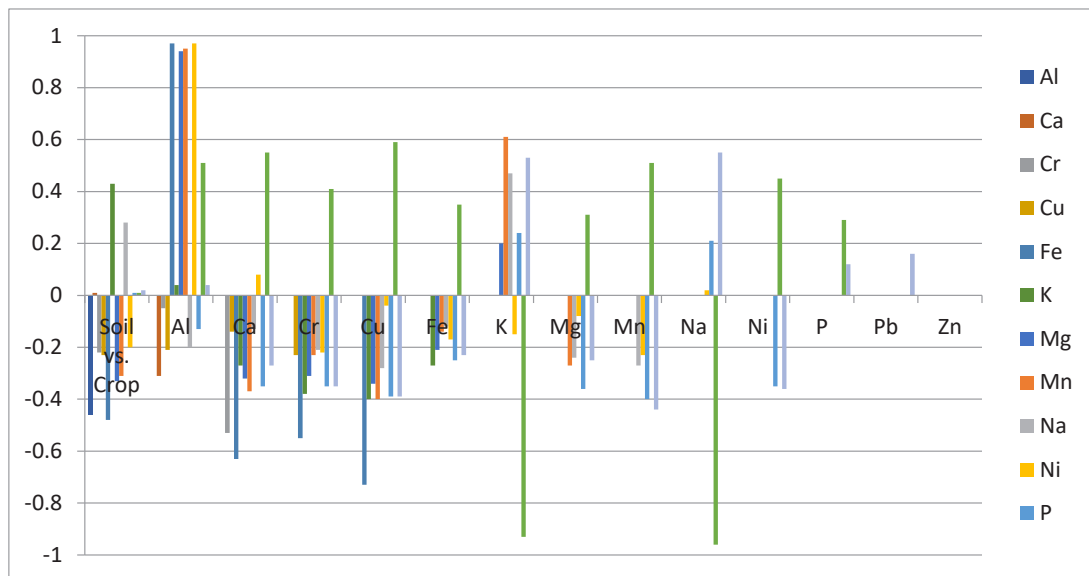


Fig. 1: Correlation chart of metal contamination for soil and crop/food matrices.

elements, such as Mg and Mn, view negative correlation with all elements except with respect to Al ranging value from -0.20 to -0.34 and -0.14 to -0.4, respectively. Some elements have a weak to strong positive correlation, like Zn and Pb, with the range 0.02 to 0.16 and 0.01 to 0.24 with different elements, respectively. P shows a negative correlation with the remaining elements. Pb exhibits a strongly negative correlation with K and Na of -0.93 and -0.96, respectively. The nutrients like Ca, P, K, and Na showed low to moderately negative correlations ranging from 0.01 to -0.31, 0.01 to -0.4, 0.04 to -0.4, and 0.47 to -0.27. Data showed that metals like Fe, Mg, Mn, Ni, Pb, and Zn changed from the soil to the matrix of crops and foods. From Table 4, results observed that the correlation at Ankleshwar and Makarpura industrial places was very high for most metals.

The statistical parameters for the elements, as given in Table 4, have high skewness and kurtosis. Pearson's correlation analysis for DTPA extractable metal Al, As, Ca, Cd, Cr, Cu, Fe, Hg, K, Mg, Mn, Ni, Na, P, Zn, and Pb were performed between all variables of soil sample and crop/food sample. Fig. 1 represents the correlation of metal contamination between soil and crop/food matrices and metal. Table 4 shows that all elements are significant at the p 0.01 level. The presence of high and significant correlations between these samples suggests that contaminants also move from soil to crop/food matrices. From the above-presented correlation matrix, we observe a high correlation between soil and crop/food matrix for Al, Fe, Mg, Mn, and Ni exhibit four different places and Ca, Cu, and Na showing moderate correlation with respect to other metals and for Cr, Cu, Na, and P showing negative correlation with respect to other metals. Between soil and crop/food matrices, Na and Pb show a very modest association, but Cr, Ni, and K show a little high correlation. Table 2 and Table 3 showed that higher contamination of Fe, Ni, and Pb transformed through the soil into a crop grown at the same place, and high contamination of Fe in soil was transforming into a crop which represents that metal contamination was transferring from soil to crop. The study shows a strong correlation between the soil and crop/food matrices at the different locations, and metals like Fe, Mg, Mn, and Ni show high correlations of 0.97, 0.94, 0.95, and 0.97 with respect to Al. Cr and Cu show very little correlation with most metals, and P shows a negative correlation with most elements.

CONCLUSION

According to the findings, heavy metal content is introduced through various sources and human activities, including industrial operations. Heavy metal contamination in soil may be caused primarily by atmospheric deposition of

contaminated dust and industrial discharge. Heavy metals in the field were also present in significant concentrations in the form of Al, Fe, Mg, Mn, and Ni in soil, and the same was transferred into crop/food matrices through its natural process resulting in negative impacts on the soil. The results of correlation research for metal between soil and crop/food matrices cultivated in the same location show a substantial connection between them. It is indicated that increased heavy metal concentration in the soil may damage soil quality and study locations, which is unsuitable for soil health. Crops and food commodities that grow in polluted accessible soil are likewise exposed due to their growth mechanisms, as evidenced by correlation research between soil and crop/food matrices.

ACKNOWLEDGEMENT

For his encouragement and approval to publish this research, Dr. C. Sandesh, Professor at Rai University in Saroda, Gujarat, is gratefully acknowledged by the authors. This study details a fundamental research effort in the Analytical Laboratory, Department of Chemistry, Rai University, Saroda, to gather information on heavy metals in the soil and water close to a particular industrial region.

REFERENCES

- Atli, G. and Canli, M. 2008. Responses of metallothionein and reduced glutathione in a freshwater fish *Oreochromis niloticus* following metal exposures. *Environ. Toxicol. Pharm.*, 25: 33-38.
- Bruins, M.R., Kapil, S. and Oehme, F.W. 2000. Microbial resistance to metals in the environment. *Ecotox. Environ. Safe*, 45: 198-207.
- Burkat, M.R., Kolpin, D.W., Jaquis, R.J. and Cole, K.J. 1999. First agrichemicals in groundwater of the Midwestern USA: Relations to soil characteristics. *J. Environ. Qual.*, 26: 1908-1915.
- Dupler, D. 2001. Heavy Metal Poisoning. In: Longe, J.L. (ed), *Gale Encyclopedia of Alternative Medicine*, Gale Group, Farmington Hills, pp. 2054-2057.
- Huang, Y.L., Zhu, W.B., Le, M.H. and Lu, X.X. 2012. Temporal and spatial variations of heavy metals in urban riverine sediment: An example of Shenzhen River, Pearl River Delta, China. *Quatern. Int.*, 282: 145-151.
- Kebata-Pendias, A. 2000. *Trace Elements in Soils and Plants*. Third Edition. CRC Press, Boca Raton, Florida, p. 413.
- Kumar, R.N., Solanki, R. and Kumar, J.I.N. 2013. Seasonal variation in heavy metal contamination in water and sediments of river Sabarmati and Kharicut canal at Ahmedabad, Gujarat. *Environ. Monit. Assess.*, 185: 359-368.
- Lenoble, V., Omanovic, D., Garnier, C., Mounier, S., Donlagic, N., Le Poupon, C. and Pizeta, I. 2013. Distribution and chemical speciation of arsenic and heavy metals in highly contaminated water used for health care purposes. Srebrenica, Bosnia, and Herzegovina. *Sci. Total Environ.*, 443: 420-428.
- Li, S.Y. and Zhang, Q.F. 2010. Risk assessment and seasonal variations of dissolved trace elements and heavy metals in the Upper Han River, China. *J. Hazard. Mater.*, 181: 1051-1058.
- Lin, K.C., Lee, Y.L. and Chen, C.Y. 2007. Metal toxicity to *Chlorella pyrenoidosa* was assessed by a short-term continuous test. *J. Hazard. Mater.*, 142: 236-241.

- Lokeshwari, H. and Chandrappa, G.T. 2006. Impact of heavy metal contamination of Bellandur Lake on soil and cultivated vegetation. *Curr Sci.*, 91(5): 584.
- Lokhande, R.S and Kelkar, N. 1999. Studies on heavy metals in water of Vasai Creek, Maharashtra. *Indian J. Environ. Protect.*, 19: 664-668.
- Manyin, T. and Rowe, C.L. 2009. Bioenergetic effects of aqueous copper and cadmium on the grass shrimp, *Palaemonetes pugio*. *Comp. Biochem. Phys.*, 150: 65-71.
- Matache, M.L., David, I.G., Matache, M. and Ropota, M. 2009. Seasonal variation in trace metals concentrations in the Ialomita River, Romania. *Environ. Monit. Assess.*, 153: 273-279.
- Perianez, R. 2009. Environmental modeling in the Gulf of Cadiz: Heavy metal distributions in water and sediments. *Sci. Total. Environ.*, 407: 3392-3406.
- Zenglu, X. 1992. *Soil Environmental Capacity of China*. Earthquake Publishing.



Moringa Oleifera Coagulation Characteristics in Wastewater Treatment in a University Dormitory

M. S. Ogunshina*, O. M. Abioye**† , K. A. Adeniran* and D. A. Olasehinde***

*Department of Agricultural Engineering, University of Ilorin, PMB 1515, Ilorin, Kwara State, Nigeria

**Department of Agricultural and Biosystems Engineering, Landmark University, PMB 1001, Omu-Aran, Kwara State, Nigeria

***Landmark University SDG 6 (Clean Water and Sanitation Research Group), Nigeria

†Corresponding authors: O. M. Abioye; abioye.oluwaseyi@lmu.edu.ng

Nat. Env. & Poll. Tech.
Website: www.neptjournal.com

Received: 07-06-2022

Revised: 27-07-2022

Accepted: 30-07-2022

Key Words:

Cake residue

Coagulation

Jar test experiment

Moringa oleifera seed

Turbidity

Wastewater

ABSTRACT

Wastewater treatment necessitates the use of an appropriate method to achieve satisfactory results. The conventional method of Alum addition has been widely used for years, but it is prohibitively expensive. This study uses *Moringa oleifera*, an inexpensive and readily available plant, as a natural coagulant to treat wastewater collected from university dormitories. Physicochemical parameters such as pH, Turbidity, Electrical Conductivity (EC), Total Dissolved Solids (TDS), Biochemical Oxygen Demand (BOD), Chemical Oxygen Demand (COD), and Dissolved Oxygen (DO) were examined based on appropriate standards. Wastewater treatment with varied coagulant dosages of 50, 100, and 150 mg.L⁻¹ was monitored using a standard jar test device with an initial wastewater perturbation at 100 rpm for 5 min was reduced to 50 rpm in 10 minutes with a rest time of 30 min. The results showed that the quality of the physicochemical properties of the water improved. The percentage increase in the water quality is; BOD (92%), COD (92%), and TDS (52-64%), with an increase in *Moringa* coagulant achieving a reduction of 96% of Turbidity. While the DO improved (79%), the pH remained below acceptable limits (6.73-7.56) for effluent disposal. The treated water showed clarity (colorless) and no odor compared to the wastewater. Hence, *Moringa oleifera* seeds cake residue can be an effective coagulant for wastewater treatment.

INTRODUCTION

The quality of surface and groundwater bodies in the immediate area is jeopardized by improper wastewater discharge (Kharake & Raut 2012). Untreated wastewater can have long-term negative consequences on the environment. Water bodies in developing countries, such as Nigeria, where wastewater treatment infrastructure is limited, are the most vulnerable to its detrimental effects. This has numerous negative effects on human health since it contains diseases that contribute to the emergence of bacteria and chemicals damaging the ecology (Iheukwumere et al. 2018). Traditionally, wastewater is classified as either black water or greywater. Blackwater is considered more hazardous, especially when in contact with human waste.

On the other hand, greywater is non-hazardous water without contact with human waste, discharged from various water facilities on a property. Wastewater considered in this

study tends to be greywater. In reality, the composition of wastewater generated in many Nigerian Universities is a hybrid of greywater and blackwater that requires proper treatment. Most learning institutions cannot treat their wastewater before discharging it due to the high cost of chemicals and improper infrastructure. In water treatment processes, coagulants are classified according to their chemical characteristics (Vijayaraghavan et al. 2011). Chemical coagulants such as aluminum sulfate and iron salts have been traditionally used in wastewater treatment. For many developing countries, the cost of chemical coagulants, the side effects of high sludge volumes, and a decrease in pH value make this treatment process difficult and endanger aquatic life (Egbuikwem & Sangodoyin 2013). Polyaluminium chloride and alum are currently used for wastewater treatment with numerous disadvantages, such as epichlorine. This is a poisonous impurity and can cause Alzheimer's disease. Coagulation is one of the stages of water treatment. It is an essential physicochemical process for reducing suspended and colloidal materials causing turbidity in wastewater.

ORCID details of the authors:

O. M. Abioye: <https://orcid.org/0000-0002-1108-4970>

In contrast, as described by Doerr (2005), the typical household water treatment method recommends settling the particles and contaminants for one to two hours at the tank's base. Lilliehöök (2005) uses sand filtration with *Moringa oleifera* and a settling time of 30 minutes to two hours for low, medium, and high turbidity water. For clean water, Hsu et al. (2006) specified that *Moringa oleifera* seed powder mixed with water should be kept for hours without specifying the amount of time. In developing countries, natural coagulants are preferred due to their efficiency, availability, low price, and biodegradability (Betatache et al. 2014, Antov et al. 2012). Subramaniam et al. (2011) explored using *C. Obtusifolia* seed gum in undiluted pulp and paper mill effluents. In textile wastewater, *Ocimum basilicum* has been used as a coagulant (Shamsnejati et al. 2015). The defatted cake is the seed waste remaining after oil extraction, which can be utilized as fertilizer and animal feed ingredients (Ganatra et al. 2012). It is also cost-effective and commonly employed in water treatment and purification (Marquetotti et al. 2010, Beltran et al. 2011, Pandey et al. 2011). Processed *Moringa oleifera* seed is a good example of these coagulants. *Moringa oleifera* seed has excellent antimicrobial qualities and decent coagulating capabilities and is also less expensive than artificial coagulants such as aluminum sulfate (Alo et al. 2012, Egbuikwem et al. 2013). *Moringa oleifera* powder can reduce

high and low surface water turbidity levels (Bina et al. 2010). Various settling times for *Moringa oleifera* water treatment have been used, and a one-hour settling time has been advocated for softening hard water with *Moringa oleifera* seed powder (Thakur & Choubey 2014). By the literature review, for the past 30 years, researchers have reported many uses of *Moringa oleifera*, especially in developing countries. Muyibi & Evison (1995) use *Moringa oleifera* seed powder in treating low and high-turbid surface water. Hsu et al. (2006) used the powdery form of *Moringa oleifera*. Thakur & Choubey (2014) used the seeds of *Moringa oleifera* ground into powder to treat turbid water. Also, López-Ramírez et al. (2022) use *Moringa oleifera* seeds powder for treating urban wastewater. This research used the defatted seed of *Moringa oleifera* to treat turbid water due to its inexpensive and environmental benefits in wastewater treatment. The current study aims to purify low-turbid wastewater by using *Moringa oleifera* seed cake residue to replace existing chemical-based coagulants with natural coagulants.

MATERIALS AND METHODS

Description of the Study Area

The study area in the present work is an educational institution in the ancient city of Ilorin (University of Ilorin),

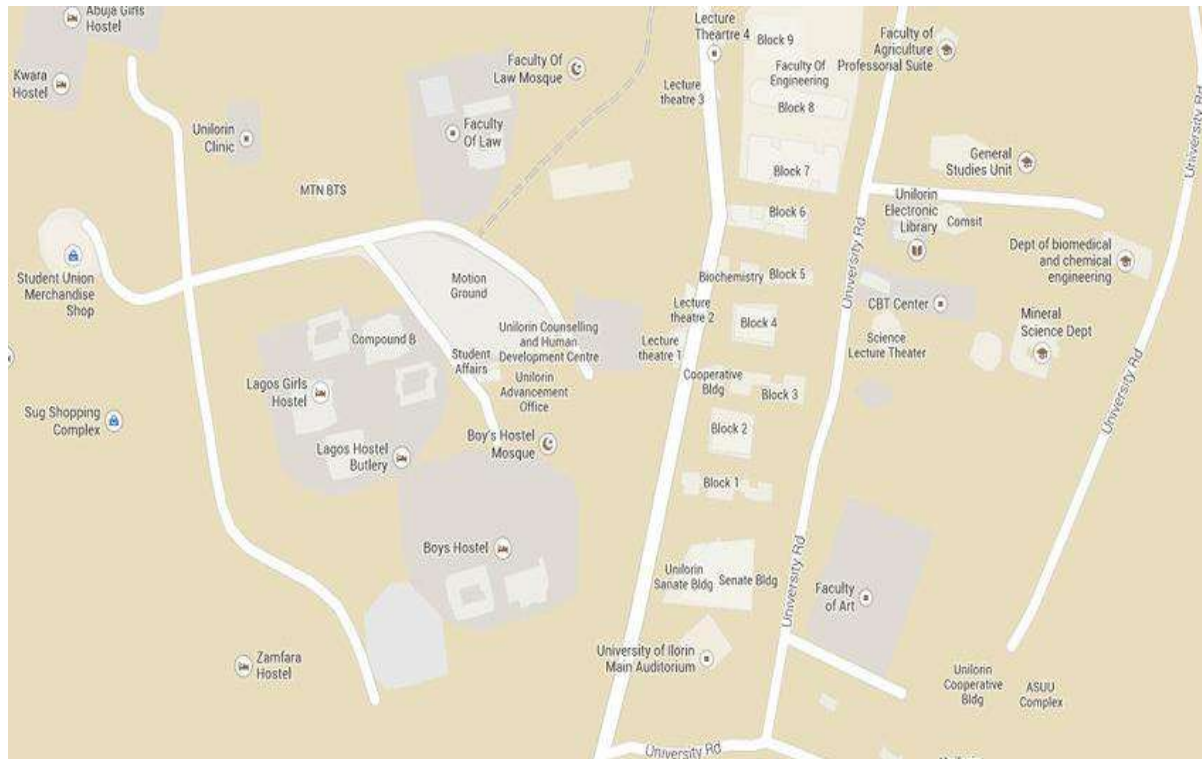


Fig. 1: University of Ilorin hostel map showing the study area.

with available bed spaces in the hostel on campus of about 5000 with the private hostels contributing about 2150-bed spaces for accommodation. Approximately 30 % of these students are residents on campus (Agava et al. 2018). The university has a land area of about 5000 hectares; the part covered by this work is approximately located between longitude 4°39'36" E to 4°41'19" E and latitude 8°27'54" N to 8°28'09" N (Alade et al. 2020). Fig. 1 shows the location of the study.

Sample Collection for Wastewater

Grab sampling was used to collect samples from the study area in a sterilized 25 L gallon container. The wastewater sample from the dormitory, including the toilet, was transported to the laboratory at 25°C and analyzed for physicochemical parameters such as pH, turbidity, Electrical Conductivity (EC), Total Dissolved Solid (TDS), Bacteriological Oxygen Demand (BOD), and Chemical Oxygen Demand (COD) following the American Public Health Association's Standard (APHA 2008). Dried *Moringa oleifera* pods (2 kg) were obtained from the Kwara State Ministry of Agriculture, Ilorin, Nigeria (Fig. 2a). To maintain a steady seed weight, the shells were removed (Fig. 2b) and air-dried at 40°C for two days. The seeds were crushed into a powdery form (Fig. 2c) using an electric grinder (Eurosonic Model ES-242) and screened with a 0.5 mm mesh sieve size to obtain a dried cake.

Experimental Work

The coagulation properties of wastewater were tested using sedimentation jars in the laboratory. Coagulation was performed as described by Ndabigengesere et al. (1995). Control bottles were used, as well as bottles with various

coagulant doses. Raw wastewater samples collected in jars from the dormitory were tested. In the 1-liter capacity container, the addition of the coagulant doses of 0, 50, 100, and 150 mg.L⁻¹ of the *Moringa oleifera* seeds cake was done. The doses were chosen based on the safety threshold of less than 200 mg.L⁻¹. The samples were subjected to a rapid mixing at 100 rpm for 5 minutes and a slow mixing step at 50 rpm for 10 min. The stirrer was switched off, and the floc was allowed to settle for 30 minutes. The evaluation was in triplicate. The ability of the *Moringa oleifera* as a coagulant was assessed by the physicochemical analysis of untreated and treated wastewater samples in terms of color, pH, turbidity, TDS, BOD, and COD. After treatment, the color and odor of the wastewater were observed. The pH of the untreated and treated wastewater was measured using an Inolab pH meter (Model: pH 7310), while turbidity was measured using a 2100 Q turbidity meter (HACH Instrument). A benchtop EC meter (EC 214) was used for conductivity measurement, while a TDS meter was used to measure total dissolved solids (TDS). $BOD_n = DF \cdot OC - (DF - 1) \cdot OC_{DW}$, where DF = Dilution Factor ($V_{\text{diluted sample}} / V_{\text{sample before dilution}}$), OC = the difference in oxygen concentration (mgO₂.L⁻¹), OC_{DW} = oxygen consumption of the blank, and n = several days for organic biochemical degradation at 20°C. The COD analyses were performed using the dichromate open reflux method using the COD apparatus (5101 Instrument). Biochemical oxygen demand (BOD₅) and chemical oxygen demand (COD) were determined by conventional methods according to the Association of Official Analytical Chemists (AOAC 2002). The physicochemical parameters were calculated as % removal = $(C_i - C_r) / C_i \times 100$, where C_i and C_r are the initial and residual concentration of examined parameters, respectively. Fig. 3 shows the process involved in the use of *Moringa oleifera* in the treatment of wastewater.

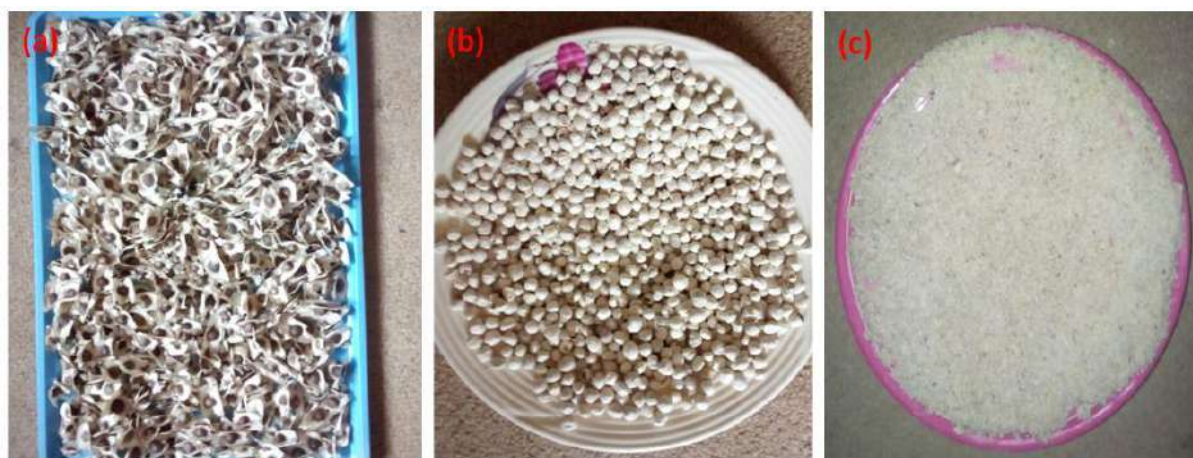


Fig. 2: (a) Matured *Moringa oleifera* pods (b) *Moringa oleifera* removed from the pod (c) *Moringa oleifera* cake.



Fig. 3: The general overview of the procedure utilized.



Fig. 4: (a) Untreated wastewater sample (b) Treated wastewater

RESULTS AND DISCUSSION

Color and Odor of the Water Sample

The color of the untreated and treated wastewater is shown in Fig. 4a and 4b. Using *Moringa oleifera* seeds cake residue, the wastewater sample's dark greyish color was removed entirely. It can be observed that the more the *Moringa oleifera* seeds cake residue dosage in the wastewater, the cleaner the treated water sample was. According to Wilson and Andrews (2011), *Moringa oleifera* seeds reduced discoloration in effluent and improved clarity. Mangale et al. (2012) demonstrated that *Moringa oleifera* seeds could absorb liquids. *Moringa oleifera* seeds have been reported to contain between 37 and 27 percent protein. This property is attributed to cellulose bonded to lignin in proteins, fatty acids, and carbohydrates (Ndibewu et al. 2011). As a coagulant, *Moringa oleifera* seed powder binds

contaminants and improves the color purity of wastewater (Madrona et al. 2012).

The pH of the Wastewater Sample

Fig. 5 compares the pH of wastewater with different coagulant dosages and several benchmarks. With an increased dose, wastewater treated with *Moringa oleifera* seed cake residues has a higher pH. SON (2007) suggested a pH limit of 6.5 to 8.5 for surface water. The pH range of the wastewater (6.73 - 7.56) in this study was within the WHO (2006), and the National Environmental Standards and Regulations Enforcement Agency (2009) suggested an acceptable effluent limit. However, Ubuoh et al. (2013) reported no difference in pH values before and after treatments at different mixture ratios when the leaves of *Moringa oleifera* were used. According to Garcia-Fayos et al. (2010), the result observed

could be attributed to the existence of a small amount of oil content remaining after extraction, as well as the release of CO_2 during aerobic degradation of organic matter, which could produce a slight increase in pH value (Hagman & Lansen 2007). The results, however, are consistent with Arnoldsson et al. (2008), Amagloh & Benang (2009), Suhartini et al. (2013), and Eman et al. (2014), who found a modest change in the pH of treated water after adding *Moringa oleifera* seed. According to Suhartini et al. (2013), natural coagulant does not require pH modification, and there is no need to modify the pH value of wastewater following treatment.

Turbidity of the Wastewater

The turbidity of the wastewater was 76.75 NTU, which is higher than the 5 NTU recommended for effluent limitation standards by the Nigerian Standards Organization and National Environmental Standards and Regulations Enforcement Agency and the World Health Organization (NESREA 2009, SON 2007, WHO 2006). Wastewater having a turbidity of more than 5 NTU is deemed detrimental to the environment and should not be let into receiving water bodies or utilized for irrigation. The WHO and NESREA standards and SON requirements of 5 NTU for residual

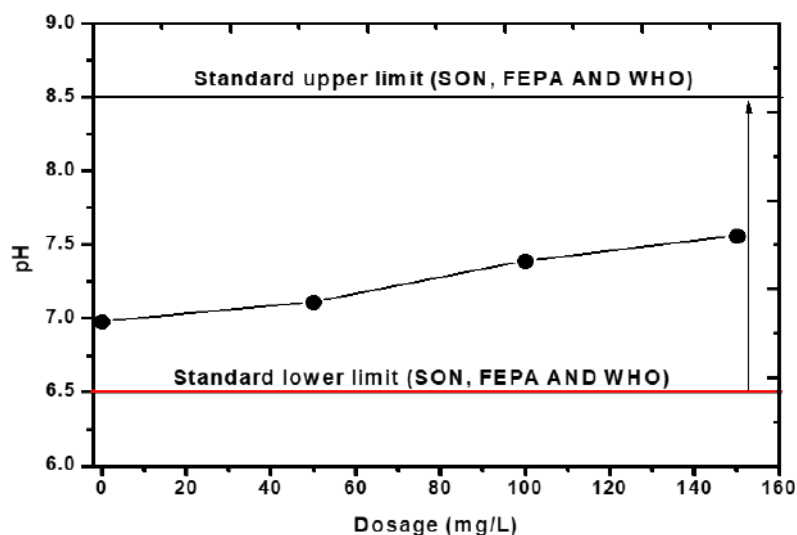


Fig. 5: The effect of coagulant dosage on the pH of the wastewater compared with some standards.

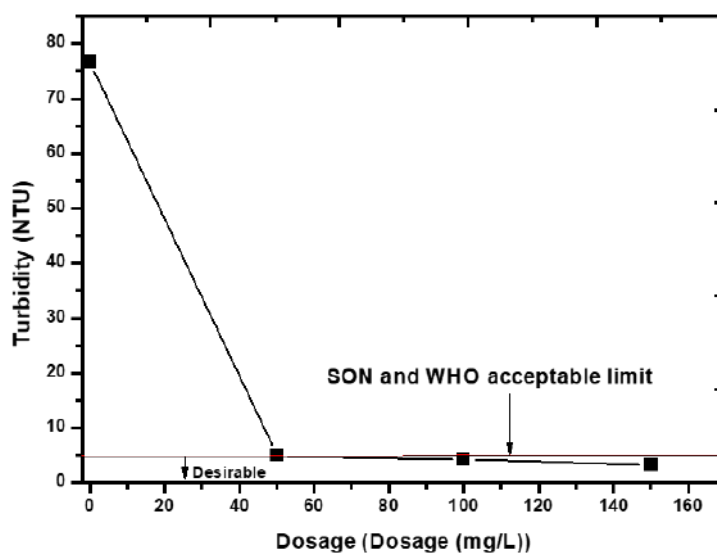


Fig. 6: The effect of coagulant dosage on the turbidity of the wastewater compared with some standards.

turbidity were substantially exceeded (WHO 2006, NESREA 2009, SON 2007). The lower the turbidity of the wastewater, the higher the dosage of *Moringa oleifera* seed cake residue, implying better coagulation characteristics (Jadhav & Mahajan 2014). As indicated in Fig. 6, *Moringa oleifera* seed cake residue successfully eliminated 93 percent to 96 percent turbidity from wastewater. According to Muyibi & Evison (1995) and Katayon et al. (2006), *Moringa oleifera* is ineffective in treating low turbid water, but the current investigation proves otherwise. This could be because the oil from the *Moringa oleifera* seed was removed, and the *Moringa oleifera* seed cake was used instead of the powdered form in this study. Nwaiwu & Bello (2011) also found that by employing *Moringa oleifera* seed powder and a 24-h settling time, excellent efficiency (up to 96.3 percent) may be achieved while treating low turbid wastewater.

Conductivity and Total Dissolved Solids (TDS)

Fig. 7 compares the effect of coagulant dosage on wastewater conductivity to specific industry norms. Before treatment, the effluent had a conductivity of 401.07 mS/cm. After treatment, the conductivity value was found to have increased to 1000 mS/cm. This could be due to dissolved ions in the water, which allows it to conduct electricity, which is essential for living organisms. It can indicate other water quality issues due to its ease of measurement. As demonstrated in Fig. 8, the initial TDS ($630 \text{ mg}\cdot\text{L}^{-1}$) was over WHO-acceptable limits. After treatment with *Moringa oleifera* seed cake residue, the total dissolved solids were reduced. The residual total dissolved solids range between 225 and 309 $\text{mg}\cdot\text{L}^{-1}$, which are still below safe limits (NESREA 2009, SON 2007, WHO 2006). This is well-supported by Chonde & Raut (2017), as TDS decreases with increased dosage concentration.

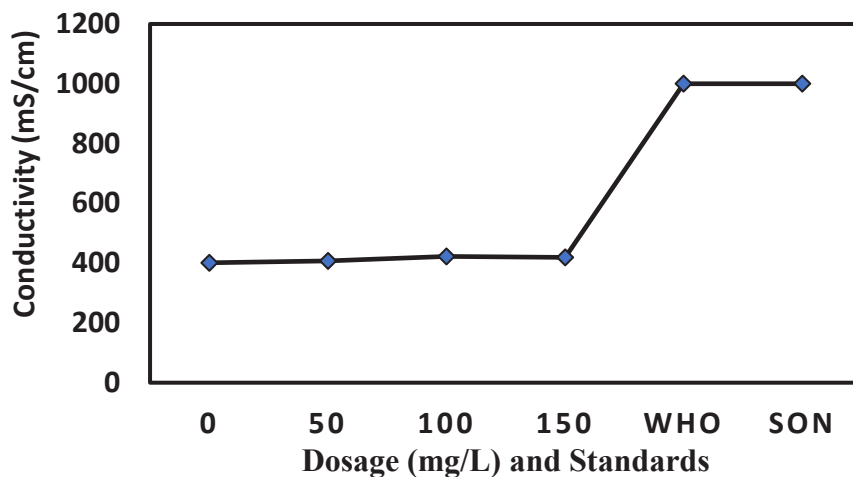


Fig. 7: The effect of coagulant dosage on the conductivity of the wastewater compared with some standards.

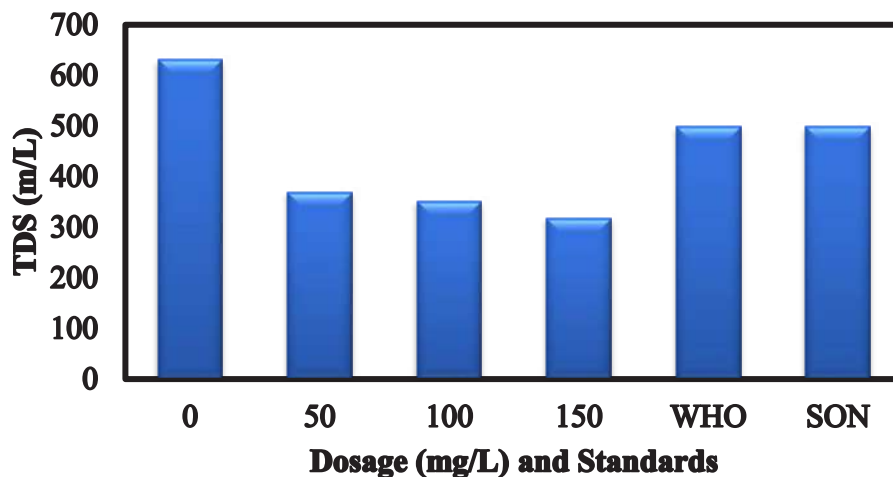


Fig. 8: The TDS of the wastewater compared with some standards.

Moringa oleifera has a natural cationic polyelectrolyte and flocculant chemical composition comprising essential polypeptides with molecular weights ranging between 6000 and 1600 dalton and six amino acids, the majority of which are glutamic acid, arginine, and methionine (Muyibi & Evison 1995).

Chemical Oxygen Demand, Biochemical Oxygen Demand, and Dissolved Oxygen

After directly applying *Moringa oleifera* seeds cake residue into wastewater, the initial chemical oxygen demand (COD) decreased. The COD was reduced by 92 percent when the *Moringa oleifera* seeds cake residue dosage was 150 mg.L⁻¹. The reduction was wide-ranging from 953.45 mg/l before treatment to 79.5 mg/l after treatment with 150 mg.L⁻¹ *Moringa oleifera* seeds cake residue. This implies that *Moringa oleifera* is a suitable coagulant for COD reduction because it reduces solids, organics, and nutrients, especially when de-oiled. *Moringa oleifera*, according to Suhartini et al. (2013) and Patel & Vashi (2013), lowered the chemical oxygen demand (COD) of wastewater. Fig. 9 demonstrates that as the dosage of *Moringa oleifera* was increased, the BOD values decreased. Studies have demonstrated that dumping wastewater with high BOD levels into a stream or river accelerates bacterial growth and depletes oxygen levels in the river (Kumar & Chopra 2012). Folhard & Sutherland (2001) and Suhartini et al. (2013) found a similar pattern in the reduction of BOD after varied therapy doses. This is also in line with the findings of Adeniran et al.

(2017), who found that a greater concentration of *Moringa oleifera* is needed to eliminate BOD. However, this finding contrasted with that of Eman et al. (2014), who found that BOD increased as *Moringa oleifera* seed dose was raised following treatment, probably due to the presence of natural and organic compounds in *Moringa oleifera* seed cake as reported by (Tan et al. 2017). BOD value decreased with an increase in the *Moringa oleifera* seed cake residue dose from 550-50 mg.L⁻¹. This could result from the use of *Moringa oleifera* alone without the mixture of Alum and the solvent used to extract the oil from *Moringa oleifera* seeds. The dissolved oxygen (DO) value significantly increased after the treatment (1.98 to 7.39 mg.L⁻¹), as shown in Fig. 9. The DO obtained for the 150 mg.L⁻¹ doses was better than 50 and 100 mg.L⁻¹. This implied that a higher *Moringa oleifera* seed cake residue dosage resulted in better coagulation properties. An increase in DO can lead to aerobic conditions, which pose no danger to higher aquatic life forms. Eman et al. (2014) reported a similar finding of DO in wastewater of 5- 7 mg.L⁻¹. Besides this, the *Moringa oleifera* seed cake residue dosage is directly proportional to the DO value. Hence, using *Moringa oleifera* seed cake residue to improve the DO value is strongly recommended. The improvement of DO in the water sample after treatment is traceable to extracted oil from *Moringa oleifera* seeds.

CONCLUSION

The coagulation potentials of *Moringa oleifera* in wastewater treatment were evaluated in this study. *Moringa oleifera*

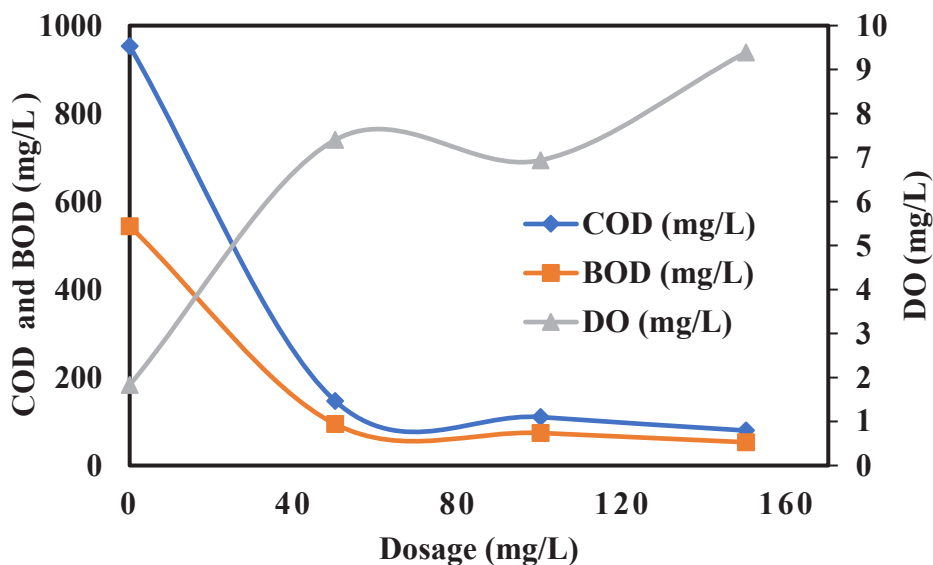


Fig. 9: The variations in chemical oxygen demand, biochemical oxygen demand, and dissolved oxygen with the dosage of *Moringa oleifera* cake residue

seeds cake residue successfully removed turbidity up to 96% after treatment. The turbidity of the wastewater sample after treatment with all three doses from the *Moringa oleifera* seed cake residue reduced the turbidity of the water sample below the acceptable limit. Treated wastewater became aesthetically cleared and odorless. *Moringa oleifera* cake is easy to use as an alternative to conventional treatment. The wastewater treated can be used for other activities within the dormitory and the institution. The results obtained from this work compare favorably well with WHO, SON, and NESREA standards.

ACKNOWLEDGEMENT

The authors would like to acknowledge Engineer Ezekiel Ariyo and Mrs. Umu Zeinat of the State Ministry of Agriculture for supplying *Moringa oleifera* seeds. Department of Chemistry Laboratory Technology, University of Ilorin, Ilorin, Nigeria support in water quality assessment is also acknowledged for this study.

REFERENCES

- Adeniran, K.A., Akpenpuun, T.D., Akinyemi, B.A. and Wasiu, R.A. 2017. Effectiveness of *Moringa oleifera* Seed as a Coagulant in domestic wastewater treatment. Afr. J. Sci. Technol. Innov. Dev., 16: 1-6.
- Agava, Y.H., Bello, N.A., Abdurraheem, M.O. and Gombwer, N.W. 2018. Implications of mass off-campus student housing at the University of Ilorin, Nigeria. Ife Res. Publ. Geogr., 16(1): 75-86.
- Alade, A.K., Abdulyekeen, A.O., Ahmadu, H.A., Yusuf, A. and Amoo, A.K. 2020. 3D Reconstruction of the University of Ilorin Campus using High-Resolution Satellite Imagery and Conventional Survey, FIG Working Week 2020. Smart Surveyors for Land and Water Management, Amsterdam, the Netherlands.
- Alo, M.N., Anyim, C. and Elom, M. 2012. Coagulation and Antimicrobial Activities of *Moringa oleifera* Seed Storage at 3°C Temperature in Turbid Water. Adv. Appl. Sci. Res., 3: 887-894.
- Amagloh, F.K. and Benang, A. 2009. Effectiveness of *Moringa oleifera* Seed as Coagulant for Water Purification. African Journal of Agricultural Research 4: 119-123.
- Antov, M., Sciban, M. and Prodanovic, J. 2012. Evaluation of the efficiency of natural coagulant obtained by ultrafiltration of common bean seed extract in water turbidity removal. Ecol. Eng., 49: 48-52.
- AOAC. 2002 Official Method of Analysis. Sixteenth Edition, Association of Official Analytical, Washington DC.
- APHA. 2008. Standard Methods for the Examination of Water and Wastewater. Twentieth edition. American Public Health and American Water Works Association and Water Environment Association.
- Arnoldsson, E., Bergman, M., Matsinhe, N. and Persson, M.K. 2008. Assessment of drinking water treatment by using *Moringa oleifera* natural coagulant. Vatten, 64: 137-150.
- Aswathy, V G., Arun, O S., Gobinath R., Arun, P. C., Vijayakumar, S., Shanmugam, T. and Nagaraj, C. 2013. Studies on the Efficiency of Polyelectrolyte as Coagulant Aid. Universal J. Environ. Res. Technol., 3(4): 458-464.
- Ayotunde, E.O., Fagbenro, O.A. and Adebayo O.T. 2011. Toxicity of aqueous extract of *Moringa oleifera* seed powder to Nile tilapia *Oreochromis niloticus* (LINNE I779) fingerlings. Int. Res. J. Agric. Sci. Soil Sci., 1(4): 142-150.
- Beltran-Heredia, J., Sanchez-Martin, J. and Barrado-Moreno, M. 2011. Removal of anionic surfactants in aqueous solutions with *Moringa oleifera* seed extract coagulant. Sustainability, 5: 1 -20.
- Betatache, H., Aouabed, A., Drouiche, N. and Lounici, H. 2014. Conditioning of sewage sludge by prickly pear cactus (*Opuntia ficus Indica*) Juice. Ecol. Eng., 70: 465-469.
- Bina, M.H. Mehdinejad, G., Dalhammer, G., Rajarao, M., Nikaee, H. and Movahedi, A. 2010. Effectiveness of *Moringa oleifera* coagulant protein as a natural coagulant aid in the removal of turbidity and bacteria from turbid waters. World Acad. Sci. Eng. Technol., 67: 617-620.
- Chonde, S. and Raut, P.D. 2017. Treatment of dairy wastewater by *Moringa oleifera* seeds. World J. Pharm. Res., 6(8): 1484-1493.
- Doerr, B. 2005. *Moringa* Water Treatment: An ECHO technical note, ECHO, USA.
- Egbuikwem, P.N. and Sangodoyin, A.Y. 2003. Coagulation Efficacy of *Moringa oleifera* Seed Extract Compared to Alum for Removal of Turbidity and E. coli in Three Different Water Sources. Europ. Int. J. Sci. Technol., 2: 13-20.
- Eman, N.A., Tan, C.S. and Makky, E.A. 2014. Impact of *Moringa oleifera* cake residue application on wastewater treatment: A case study. J. Water Resour. Prot., 6: 677-687.
- Folhard, G. and Sutherland, T. 2001. The Use of *Moringa oleifera* Seed as a natural coagulant for water and wastewater treatment. Department of Engineering, University of Leicester, The UK.
- Ganatra, T.H., Joshi, U.H., Bhalodia, P.N., Desai, T.R. and Tirgar, P.R. 2012. Review article therapeutic and prophylactic values of *Moringa oleifera*. Int. Res. J. Pharm., 3: 1-7.
- García-Fayos, B., Arnal, J.M., Verdu, G. and Sauri, A. 2010. Study of *Moringa oleifera* Oil extraction and its influence in primary coagulant activity for drinking water treatment. Int. Conf. Food. Innov., 16: 4561.
- Hagman, M.F. and Larsen, J.C. 2007. Oxygen uptake rate measurements for application at wastewater treatment plants. Vatten, 63: 131-138.
- Iheukwumere, S.O., Nwabudike, P.C., Nkwocha, K.F. and Phil-Eze, O.P. 2018. Domestic Wastewater Treatment and Reuse in Awka Urban, Anambra State, Nigeria. IIARD. Int. J. Geogr. Environ. Manag., 4(2): 16-24.
- Jadhav, M.V. and Mahajan, Y.S. 2014. Assessment of the feasibility of natural coagulants in turbidity removal and modeling of the coagulation process. Desal. Water Treat., 52(31-33): 5812 -5821.
- Kharake, A.C. and Raut, V.S. 2021. An assessment of water quality index of Godavari River water in Nashik city, Maharashtra. Appl. Water Sci., 11: 101.
- Kumar, V. and Chopra, A. K. 2012. Monitoring of Physicochemical and Microbiological Characteristics of Municipal Wastewater at Treatment Plant, Haridwar City (Uttarakhand) India. J. Environ. Sci. Technol., 5(2): 109-118.
- Lilliehöök, H. 2005. Use Of Sand Filtration On River Water Flocculated With *Moringa oleifera*, Division Of Sanitary Engineering, Department Of Civil And Environmental Engineering, Luleå University of Technology, Sweden.
- López-Ramírez, M.A., Argüelles-López, C., Aguilar-Rodríguez, M.R., Barragán-Díaz, J., Castellanos-Onorio, O.P. and Lango-Reynoso, F. 2022. The effect of *Moringa oleifera* as a primary treatment in urban wastewater in Martínez De La Torre, Veracruz. Nature Environment & Pollution Technology, 21(1): 241-246.
- Madrona, G.S., Branco, I.G., Seolin, V.J., Bdaa, F., Fagundes-Klen, M.R. and Bergamasco, R. 2012. Valuation of extracts of *Moringa oleifera* Lam Seeds obtained with NaCl and their effects on water treatment. Acta Sci. Technol., 34: 289-293.
- Mangale S.M., Chonde S.G., Jadhav A.S. and Raut, P.D. 2012. Study of *Moringa oleifera* (Drumstick) Seed as Natural Absorbent and Antimicrobial Agent for River Water Treatment. J. Nat. Prod. Plant Resour., 2: 89-100.

- Marquetotti, A., Vieira, S., Vieira, M.F., Silva, G.F., Araujo, A.A., Fagundes-Klen, M.R. and Veit, M.T. 2010. Use of *Moringa oleifera* Seed as a Natural Adsorbent for Wastewater Treatment. *Water Air Soil Pollution* 206: 273-281.
- Mataka, L.M., Henry, E.M.T., Masamba, W.R.L. and Sajidu S.M. 2006. Lead remediation of contaminated water using *Moringa stenopetala* and *Moringa oleifera* seed powder. *Int. J. Environ. Sci. Tech.*, 3(2): 131-139.
- Muyibi, S.A. and Evison, L.M. 1995. *Moringa oleifera* seeds for softening hard water. *Water Resources*, 29(4):1099-1105.
- Ndabigengesere, A., Narasiah, K.S. and Talbot, B.G. 1995. Active agents and mechanism of coagulant of turbid waters using *Moringa oleifera*. *Water Res.*, 29(2): 703-710.
- Ndibewu, P.P., Mnisi, R.L., Mokgalaka, S.N. and Mccrindle, R.I. 2011. Heavy metal removal in aqueous systems using *Moringa oleifera*: A review. *J. Mater. Sci. Eng.*, 1: 843-853.
- NESREA 2009. National Environmental Standards and Regulations Enforcement Agency. Effluents Limitations Standards for Food, Beverages and Tobacco Sector Regulations, 96(65): B1211-1248.
- Nwaiwu, N.E. and Bello, A.A. 2011. Effect of *Moringa oleifera*- alum ratios on surface water treatment in North-East Nigeria. *Res. J. Appl. Sci. Eng. Technol.*, 3(6): 505-512.
- Pandey, A., Pradheep, K., Gupta, R., Nayar, E.R. and Bhandari, D. 2011. Drumstick tree (*Moringa oleifera* Lam): A potential multipurpose species in India. *Gene. Resour. Crop Evol.*, 58: 453-460.
- Pardede, A., Budihardjo, M.A. and Purwono, S. 2018. The removal of turbidity and TSS of the domestic wastewater by coagulation: Flocculation process involving oyster mushroom as bio coagulant. *E3S Web Conf.*, 31: 05007-05011.
- Patel, H. and Vashi, R.T. 2013. Comparison of naturally prepared coagulants for removal of COD and colour from textile wastewater global. *NEST J.*, 15(4): 522-528.
- Shamsnejati, S., Chaibakhsh, N., Pendashteh, A.R. and Hayeripour, S. 2015. Mucilaginous Seed of *Ocimum basilicum* as a natural coagulant for textile wastewater treatment. *Ind. Crop. Prod.*, 69: 40-47.
- SON 2007. Standards Organisation of Nigeria. Nigeria Standards for Drinking Water Quality: Nigerian Industrial Standard (NIS 554): 15-20.
- Subramaniam, S., Vikashini, N., Matakite, M. and Kanayathu, K. 2011. *Moringa oleifera* and other local seeds in water purification in developing countries. *Res. J. Chem. Environ.*, 15: 135-138.
- Suhartini, S., Hidayat, N. and Rosaliana, E. 2013. Influence of powdered *Moringa oleifera* seeds and natural filter media on the characteristics of tapioca starch wastewater. *Int. J. Recycl. Org. Waste Agric.*, 2: 1-11.
- Tan, C.S., Manaf, A.M., Essam, A.M. and Eman, N.A. 2017. The use of *Moringa oleifera* seed as a natural coagulant for wastewater treatment and heavy metals removal. *Appl. Water Sci.*, 7: 1369 -1376.
- Tat, W.K., Idris, A., Noor, M.J.M.M., Mohamed, T.A., Ghazali, A.H. and Muyibi, S.A. 2010. Optimization Study on Sewage Sludge Conditioning Using *Moringa oleifera* Seeds. *Desal. Water Treat.*, 16: 402-410.
- Ubuoh, E. A. Akhionbare, S. M. O. and Onifade A. O. 2013. Potential of *Moringa oleifera* seed powder as a coagulation agent for Refinery wastewater treatment in Warri, Delta State, Nigeria. *Int. J. Adv. Biol. Res.*, 3(1): 17-20.
- WHO. 2006. Guidelines for Drinking-Water Quality. Third Edition, World Health Organization, Geneva, Switzerland.
- Wilson, S.A. and Andrews, S.A. 2011. Impact of a natural coagulant pretreatment for colour removal on solar water disinfection (SODIS). *J. Wash. Dev.*, 1: 57-67.



Nesting Site Preferences of *Ratufa indica indica* in the Umblebyle Range Forest, Bhadravathi Division, Shimoga, Karnataka

V. Hamsa Rekha[†] and A. Shwetha

Department of P.G. Studies and Research in Applied Zoology, Kuvempu University, Shankarghatta-577451
Shimoga, Karnataka, India

[†]Corresponding author: V. Hamsa Rekha; hamsarekhanaik@gmail.com

Nat. Env. & Poll. Tech.
Website: www.neptjournal.com

Received: 02-09-2022

Revised: 20-10-2022

Accepted: 03-11-2022

Key Words:

Ratufa indica indica

Dreys

Umblebyle range

Nest tree preferences

Nest tree selection

ABSTRACT

Malabar Giant Squirrel (*Ratufa indica indica*) is one of the four subspecies endemic to India (Abdulali 1952), common to northern and central Western Ghats among species *Ratufa indica* belonging to Subfamily Ratuinae. The study was designed to analyze the nest tree preferences of animals in the dry deciduous forests of the Umblebyle range, Shimoga, Karnataka (South India) during February, March, and April 2021, surveying 20 transects covering a distance of 47.7 km. Nest tree preferences were assessed by observing 406 dreys (nests) on 385 trees covering an area of 8350.89 ha. The nest trees came from 20 families and 41 species, with 12 tree species in the Family Fabaceae and 84 trees in the *Terminalia paniculata* having the highest preference. The Squirrels showed the highest preference for deciduous trees over semi-evergreen and evergreen trees. The most preferred tree height and nest height ranged between 11-20m, including 87.53% of nesting trees and 83.89% of nests, respectively. The average nest height was estimated to be 14.73 (± 3.311) m, with a minimum and maximum height of 7 m and 28 m, respectively. The difference between average tree height and average nest height was 1.512m.

INTRODUCTION

Ratufa indica indica, also referred to as Malabar Giant Squirrel (MGS) from the sub-family Ratuinae, is a cat-sized diurnal (Nowak 1999), arboreal, upper canopy dwelling species rarely moving to the ground (Baskaran et al. 2011), found in northern and central Western Ghats, at an elevation of 180-2300m from Mumbai to Karnataka inhabiting deciduous, mixed deciduous and moist evergreen forests (Prater 1980, Aparajita & Goyal 1996). The animal is listed in Appendix II of CITES, 2005, Least Concern category of the IUCN red list, Schedule II of Wildlife (Protection) Act, 1972. It is an upper canopy dwelling species (Ramachandran 1988) active in the early morning and evening hours, resting during mid-day (Basantha & Ajay 2015), locally known as Kendalilu. They construct more than one drey within a single breeding season (Pradhan et al. 2017), usually in high canopies using leaves and twigs in profusely branched tall trees (Basantha & Ajay 2015).

In the past, similar studies have been made on the nesting of *Ratufa indica* in places like Mudumalai Tiger

Reserve (Nagarajan et al. 2011), Karalpat Wildlife Sanctuary (Pradhan et al. 2017), Dalma wildlife sanctuary (Mishra et al. 2011), Sitanadi wildlife Sanctuary (Ravi 2008) Kuldihya wildlife sanctuary (Basantha & Ajay 2015). As nesting and feeding are two vital aspects of animal ecology and no previous study has been conducted so far in the Umblebyle range forest, in the present study, we documented nest tree preferences of the animal in the study area.

STUDY AREA

The Umblebyle Range Forest (Fig. 1) is located in the foothills of Western Ghats, situated in the southwestern part of the Bhadravathi division forest, Shimoga district, Karnataka, within the geographic coordinates of 14°30'0" to 13°43'0" N and 75°30'0" to 75°47'30" E. The area enjoys a tropical climate for the whole of the year. The annual average rainfall is around 769.4 mm, with minimum and maximum temperatures of 20°C and 31°C, respectively. The main watershed systems covering the area include Tunga and Bhadra rivers draining the (South-South-East) SSE part and are the main seasonal river. The location's topography is undulating hills and hillocks with a dry deciduous forest. The area's relief varies between 500 and 1520 m above (Mean Sea Level) MSL. The area comprises 20 villages

ORCID details of the authors:

Hamsa Rekha V: <https://orcid.org/0000-0003-2236-0755>

Shwetha A: <https://orcid.org/0000-0003-0213-9922>

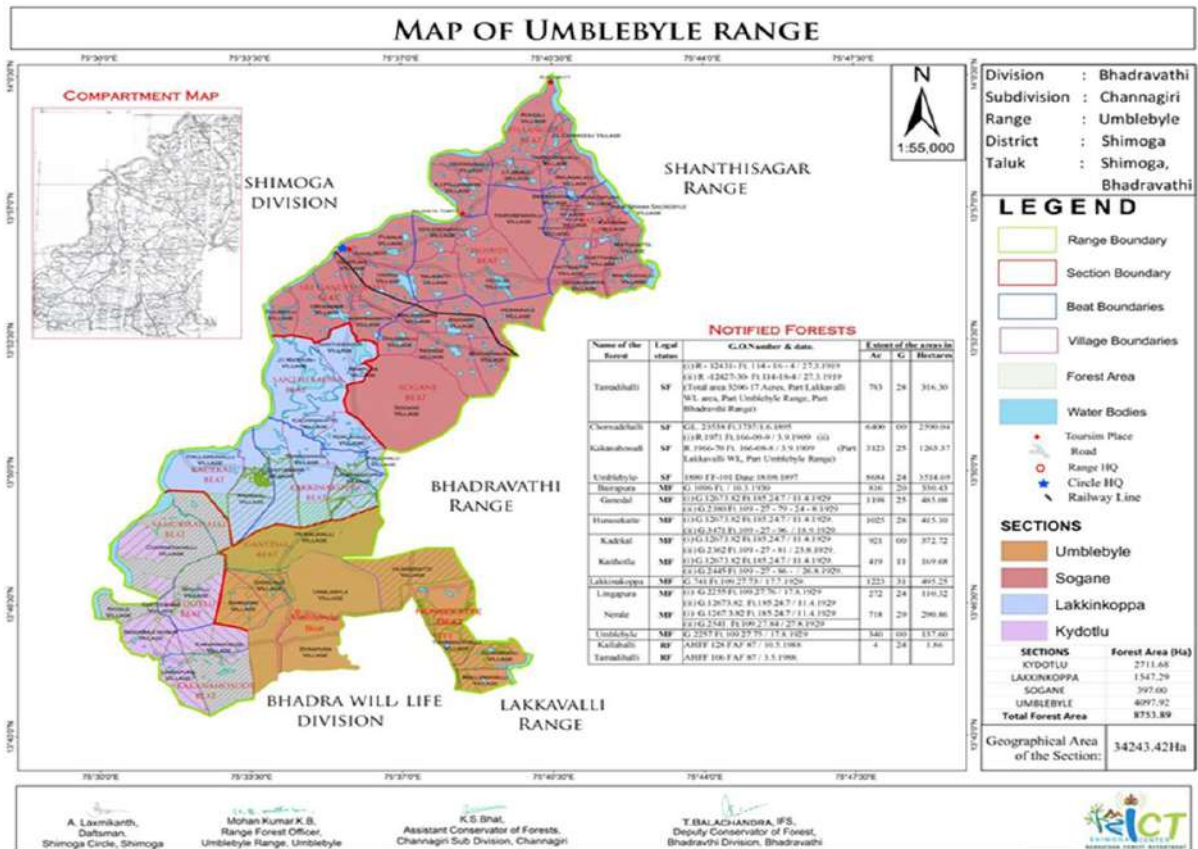


Fig. 1: Map of Umbleyle Range.

and four beats, namely Umbleyle, Kydotlu, Lakkinkoppa, and Sogane beats, among which three comprised forest cover, namely Umbleyle, Kydotlu, and Lakkinkoppa beats. Prominent trees include *Terminalia paniculata*, *Terminalia tomentosa* and *Tectona grandis*.

MATERIALS AND METHODS

The survey was carried out using the Line transect method (Altmann 1975, Buckland et al. 1993, Devcharan 2008). The nesting behavior documentation was done from February 2021 to April 2021, walking in line transects laid using Arc Gis Software to cover the entire study area, keeping the transects equidistant, covering a distance of 47.7 km walking over 20 transects ranging from 2-3 km each. The transects were walked during the morning 06:00 am – 10:00 am as the animal is active during this period (Pradhan 2017). The number of nests and nesting trees species were documented considering different parameters like tree species, the height of the tree (Girth at Breast Height) GBH, number of nests, the height of the nest from the ground, age of the nest, and (Global Positioning System) GPS location of the nest

(Basantha & Ajay 2015). An Olympus 10 × 50 binocular was used to observe the nests and the species. The common names of the tree species were recorded with the aid of the local personnel, and their scientific names were ascertained from the book Endemic Woody Plants of the Western Ghats (Navendu 2017).

RESULTS

A total of 406 dreys were observed on 385 nesting trees that included 41 different species belonging to 20 families (Tables 1, 2, and 3; Fig. 2, 3 and 4). Among the 20 families recorded, the animal preferred tree species of certain families over others. Based on the variety of tree preference for nesting, Family Fabaceae (29.26%) was the most preferred including 12 tree species namely *Acacia auriculiformis*, *Albizia odoratissima*, *Albizia procera*, *Bahunia malabarica*, *Butea monosperma*, *Cassia siamea*, *Dalbergia latifolia*, *Dalbergia paniculata*, *Pterocarpus marsupium*, *Pongamia pinnata*, *Tamrindus indica* and *Xylocarpus xylocarpa* followed by Family Combretaceae (12.19%) including 5 tree species namely *Anogeissus latifolia*, *Terminalia arjuna*, *Terminalia*

bellerica, *Terminalia paniculata* and *Terminalia tomentosa*, Families Malvaceae and Rubiaceae with equally 14.63% each having 3 species each *Bombax ceiba*, *Grewia tillifolia*, *Kydia calycina* and *Adina cordifolia*, *Hymenodictyon excelsum* and *Mitragina parviflora* respectively. These are followed by Families Lamiaceae and Moraceae contributing 9.75% each having 2 tree species *Gmelina arborea*, *Tectona grandis* and *Ficus bengalensis* and *Ficus tsiela* respectively, and 14 families contributing 34.14% that included 1 tree species each namely *Semecarpus anacardium* from Family Anacardiaceae, *Saccopetalum tomentosum* from Family Annonaceae, *Sterospermum xylocarpus* from Family Bignoniaceae, *Cordia macleodii* from Family Boraginaceae, *Garuga pinnata* from Family Burseraceae, *Dillenia pentagyna* from Family Dilleniaceae, *Diospyros monata* from Family Ebenaceae, *Careya arborea* from Family Lecythidaceae, *Strychnos nux-vomica* from Family Loganiaceae, *Lagerstroemia lanceolata* from Family Lythraceae, *Syzigium cumini* from Family Myrthaceae, *Chloroxylon swietenia* from Family Rutaceae, *Schleichera trijunga* from Family Sapindaceae and *Bassia latifolia* from Family Sapotaceae.

Among the total 41 tree species recorded (Tables 1, 2 & 3), the nesting of the animal indicated preferences for some species more than others. *Terminalia pinaculata* (84 trees, 21.81%) was the most preferred tree species followed by *Terminalia tomentosa* (45 trees, 11.68%), *Schleichera trijunga* (41 trees, 10.64%), *Pterocarpus marsupium* (34 trees, 8.83%), *Tectona grandis* (28 trees, 7.27%), *Dillenia pentagyna* (20 trees, 5.19), *Terminalia bellerica* and *Anogeissus latifolia* (14 trees each, 7.27%), *Dalbergia latifolia* (12 trees, 3.11%), *Adina cordifolia* (11 trees, 2.85%), *Kydia calycina* (9 trees, 2.33%), *Xylia xylocarpa* and *Lagerstroemia lanceolata* (7 trees each, 3.63%), *Albizia odoratissima* and *Grewia tillifolia* (6 trees each, 3.11%), *Garuga pinnata* and *Bahunia malabarica* (4 trees each, 2.07%), *Ficus benghalensis*, *Hymenodictyon excelsum*, *Semecarpus anacardium*, *Dalbergia paniculata* and *Saccopetalum tomentosum* (3 trees each, 3.89%), *Tamrindus indica*, *Cardia macleodii*, *Sterospermum xylocarpus* and *Chloroxylon swietenia* (2 trees each, 2.07%), *Acacia auriculiformis*, *Ficus tsiela*, *Mitragina parviflora*, *Albizia procera*, *Bombax ceiba*, *Terminalia arjuna*, *Pongamia pinnata*, *Diospyros montana*, *Strychnos nux-vomica*, *Careya arborea*, *Butea monosperma*, *Cassia siamea*, *Gmelina arborea*, *Bassia latifolia* and *Syzigium cumini* (1 tree each, 4.15%).

During this study, 92.36% (375 number) of dreys were new, and 7.63% (31 number) were old. The animal preferred deciduous over evergreen and semi-evergreen trees (Tables

1, 2 & 3). Among 41 nesting tree species, 32 were deciduous, contributing 78.04%; 5 were evergreen, contributing 12.19% and 4 were semi-evergreen, contributing 9.75%. Tree species that showed multiple nesting include *Dillenia pentagyna*, *Garuga pinnata*, *Pterocarpus marsupium*, *Schleichera trijunga*, *Tamrindus indica*, and *Terminalia pinaculata*. (Figs. 5, 6, 7).

Among 41 tree species recorded in all the study sites, Umblebyle beat (Table 1), was found to have highest nesting tree species diversity with 28 tree species namely *Adina cordifolia*, *Anogeissus latifolia*, *Bahunia malabarica*, *Bassia latifolia*, *Bombax ceiba*, *Butea monosperma*, *Cassia siamea*, *Chloroxylon swietenia*, *Cordia macleodii*, *Dalbergia paniculata*, *Dalbergia latifolia*, *Dillenia pentagyna*, *Diospyros monata*, *Ficus bengalensis*, *Ficus tsiela*, *Garuga pinnata*, *Hymenodictyon excelsum*, *Lagerstroemia lanceolata*, *Pongamia glabra*, *Pterocarpus marsupium*, *Schleichera trijunga*, *Tamrindus indica*, *Tectona grandis*, *Terminalia arjuna*, *Terminalia bellerica*, *Terminalia paniculata*, *Terminalia tomentosa* and *Xylia xylocarpa* followed by Lakkinkoppa beat (Table 2) with 25 tree species namely *Acacia auriculiformis*, *Adina cordifolia*, *Albizia odoratissima*, *Albizia procera*, *Anogeissus latifolia*, *Bahunia malabarica*, *Careya arborea*, *Chloroxylon swietenia*, *Cordia macleodii*, *Dalbergia latifolia*, *Ficus bengalensis*, *Garuga pinnata*, *Kydia calycina*, *Lagerstroemia lanceolata*, *Mitragina parviflora*, *Pterocarpus marsupium*, *Saccopetalum tomentosum*, *Schleichera trijunga*, *Sterospermum xylocarpus*, *Strychnos nux-vomica*, *Syzigium cumini*, *Tectona grandis*, *Terminalia bellerica*, *Terminalia paniculata* and *Terminalia tomentosa* while Kydotlu beat (Table 3) had least tree species diversity with 13 tree species namely *Grewia tillifolia*, *Dalbergia latifolia*, *Dillenia pentagyna*, *Gmelina arborea*, *Kydia calycina*, *Lagerstroemia lanceolata*, *Pterocarpus marsupium*, *Schleichera trijunga*, *Semecarpus anacardium*, *Tectona grandis*, *Terminalia paniculata*, *Terminalia tomentosa* and *Xylia xylocarpa*.

Dalbergia latifolia, *Pterocarpus marsupium*, *Terminalia pinaculata*, *Schleichera trijunga*, *Terminalia tomentosa*, *Lagerstroemia lanceolata*, and *Tectona grandis* tree species were common to all the three beats. *Kydia calycina* was the only tree species common to Lakkinkoppa and Kydotlu beats. Similarly, *Xylia xylocarpa* and *Dillenia pentagyna* were common to Umblebyle and Kydotlu beats. Also, *Cordia macleodii*, *Ficus benghalensis*, *Bahunia malabarica*, *Anogeissus latifolia*, *Garuga pinnata*, *Chloroxylon swietenia*, *Terminalia bellerica*, and *Adina cordifolia* were tree species common to Lakkinkoppa and Umblebyle beats. There were tree species endemic to specific beats, *Gmelina arborea*, *Grewia tillifolia* and *Semecarpus anacardium*

were endemic to Kydotlu beat, while *Mitragina perviflora*, *Acacia auriculiformis*, *Albizia procera*, *Steropermum xylocarpus*, *Strychnos nux-vomica*, *Careya arborea*, *Syzigium cumini*, and *Saccopetalum tomentosum* were endemic to Lakkinkoppa beat. The tree species *Ficus tsiela*, *Bombax ceiba*, *Hymenodictyon excelsum*, *Terminalia arjuna*, *Pongamia pinnata*, *Tamrindus indica*, *Diospyros montana*, *Terminalia tomentosa*, *Butea monosperma*,

Dalbergia paniculata, *Cassia siamea* and *Bassia latifolia* were endemic to Umbleble beat.

In all three beats, the average tree height was estimated to be 16.18 (\pm 3.430) m, with minimum and maximum tree heights of 8m and 30m, respectively. The most preferred tree height for nesting was 11-20m, which supported 87.53%. Trees less than 11m supported 8.57%, and trees more than 20m supported 3.89%. The average nest height was estimated

Table 1: Tree Species, Tree height, Nest height, and GBH in Umbleble beat.

Sl. No.	Family	Scientific names	Habitat	Tree Height Avg (m)Z	Nest height Avg (m)	GBH Avg (m)	No of trees	RA Nest tree %	No of nest	RA of nest %
1.	Boraginaceae	<i>Cardia macleodii</i>	D	22	20	1.3	1	0.61	1	0.58
2.	Burseraceae	<i>Garuga pinnata</i>	D	12	11	0.8	1	0.61	1	2.33
3.	Combretaceae	<i>Anogeissus latifolia</i>	D	16.5 \pm 2.121	15 \pm 1.414	0.75 \pm 0.070	2	1.22	2	0.58
4.	Combretaceae	<i>Terminalia arjuna</i>	E	15	14	1	1	0.61	1	0.58
5.	Combretaceae	<i>Terminalia paniculata</i>	D	15.8 \pm 4.507	14 \pm 4.305	0.8 \pm 0.159	51	31.28	57	1.16
6.	Combretaceae	<i>Terminalia tomentosa</i>	D	14.7 \pm 3.283	13.3 \pm 2.887	0.7 \pm 0.135	23	13.49	23	1.75
7.	Combretaceae	<i>Terminalia bellerica</i>	SE	13 \pm 3.605	11.3 \pm 3.214	0.8 \pm 0.173	3	1.84	3	0.58
8.	Dilleniaceae	<i>Dillenia pentagyna</i>	D	17.3 \pm 2.081	16 \pm 1.732	0.95	3	1.84	3	0.58
9.	Ebenaceae	<i>Diospyros monata</i>	D	10	9	0.7	1	0.61	1	8.77
10.	Fabaceae	<i>Tamrindus indica</i>	E	16	14.5 \pm 0.707	1.1	2	1.22	2	0.58
11.	Fabaceae	<i>Bahunia malabarica</i>	SE	14.5 \pm 7.778	13.75 \pm 7.424	0.7 \pm 0.141	2	1.22	2	33.33
12.	Fabaceae	<i>Dalbergia latifolia</i>	D	13.25 \pm 2.753	12 \pm 2.44	0.8 \pm 0.15	4	2	4	2.33
13.	Fabaceae	<i>Pongamia pinnata</i>	D	16	14	0.7	1	0.61	1	0.58
14.	Fabaceae	<i>Pterocarpus marsupium</i>	D	15.6 \pm 3.352	14 \pm 3.070	0.8 \pm 0.148	15	9.2	15	0.58
15.	Fabaceae	<i>Xylia xylocarpa</i>	D	15	14	0.6	1	0.61	1	1.75
16.	Fabaceae	<i>Butea monosperma</i>	D	10	9	0.7	1	0.61	1	12.86
17.	Fabaceae	<i>Dalbergia paniculata</i>	D	17	20 \pm 18.666	1 \pm 0.2	3	1.84	3	0.58
18.	Fabaceae	<i>Cassia siamea</i>	E	10	9	0.6	1	0.61	1	12.86
19.	Lamiaceae	<i>Tectona grandis</i>	D	13.7 \pm 3.683	12.2 \pm 3.860	0.914 \pm 0.110	7	4.29	7	0.58
20.	Lythraceae	<i>Syzigium cumini</i>	E	17 \pm 1.414	16.2 \pm 1.767	0.85 \pm 0.070	2	1.22	2	1.16
21.	Malvaceae	<i>Bombax ceiba</i>	D	15	13	0.8	1	0.61	2	1.16
22.	Moraceae	<i>Ficus bengalensis</i>	E	13 \pm 4.242	11.5 \pm 3.535	1	2	1.22	2	1.16
23.	Moraceae	<i>Ficus tsiela</i>	D	25	21	1.3	1	0.61	1	1.75
24.	Rubiaceae	<i>Hymenodictyon excelsum</i>	D	16.6 \pm 3.055	14.3 \pm 3.214	0.76 \pm 0.144	3	1.84	3	0.58
25.	Rubiaceae	<i>Adina cordifolia</i>	D	16 \pm 3.464	14.1 \pm 3.184	1 \pm 0.343	7	4.29	7	1.75
26.	Rutaceae	<i>Chloroxylon sweetenia</i>	D	10	9	0.6	1	0.61	1	4.09
27.	Sapindaceae	<i>Schleichera trijunga</i>	D	12 \pm 1.732	11 \pm 1.732	0.9 \pm 0.264	22	13.49	22	4.09
28.	Sapotaceae	<i>Bassia latifolia</i>	D	10	9	0.7	1	0.61	1	0.58
							163		170	

RA- Relative Abundance, D- Deciduous, E- Evergreen, SE- Semi-evergreen.

to be 14.73 (± 3.311) m, with minimum and maximum nest heights of 7m and 28m, respectively. The most preferred nest height was 11-20m, which supported 83.89%. Trees with a height of less than 11m supported 12.20%, and trees with more than 20m supported 3.89%. The average GBH was estimated to be 0.912 (± 0.373) m, with minimum and

maximum GBH of 0.2m and 3m, respectively. The most preferred GBH was from 0.6-1.5m, which supported 87.27% of the nest. Trees with GBH of less than 0.5m supported 9.09%, and trees with more than 1.5m supported 3.37% of the nest. The difference between average tree height and average nesting height was estimated at 1.512 m.

Table 2: Tree Species, Tree height, Nest height, and GBH in Lakkinkoppa beat.

Sl. No.	Family	Species	Habitat	Tree Height Avg (m)	Nest height Avg (m)	GBH Avg (m)	No of trees	RA Nest tree %	No of nest	RA of nest %
1.	Bignoniaceae	<i>Sterospermum xylocarpus</i>	D	13 \pm 1.414	11 \pm 1.414	0.5	2	1.4	2	1.36
2.	Boraginaceae	<i>Cardia macleodii</i>	D	12	11	0.4	1	0.7	1	0.68
3.	Burseraceae	<i>Garuga pinnata</i>	D	13 \pm 1.73	11.3 \pm 2.309	0.83 \pm 0.057	3	2.11	5	3.42
4.	Combretaceae	<i>Anogeissus latifolia</i>	D	16.5 \pm 2.314	15.16 \pm 2.367	0.85 \pm 0.305	12	8.4	12	8.21
5.	Combretaceae	<i>Terminalia paniculata</i>	D	16 \pm 2.190	14 \pm 2.182	0.75 \pm 0.439	16	11.2	16	10.95
6.	Combretaceae	<i>Treminalia toman-tosa</i>	D	15.6 \pm 3.089	14.166 \pm 3.451	0.66 \pm 0.250	18	12.67	18	12.32
7.	Combretaceae	<i>Terminalia bell-erica</i>	SE	17.363 \pm 3.139	16 \pm 3.0331	1.03 \pm 0.382	11	7.74	11	7.53
8.	Fabaceae	<i>Acacia auriculi-formis</i>	E	15	14	0.4	1	0.7	1	0.68
9.	Fabaceae	<i>Bahunia mala-barica</i>	SE	15 \pm 1.414	14 \pm 1.414	0.95 \pm 0.070	2	1.4	2	1.36
10.	Fabaceae	<i>Dalbergia latifolia</i>	D	16.28 \pm 2.429	15.28 \pm 2.429	0.957 \pm 0.427	7	4.92	7	4.79
11.	Fabaceae	<i>Albizia odoratis-sima</i>	D	22 \pm 3.651	20 \pm 3.670	1.7 \pm 0.730	7	4.92	7	4.79
12.	Fabaceae	<i>Albizia procera</i>	D	20	18	0.7	1	0.7	1	0.68
13.	Fabaceae	<i>Pterocarpus mar-supium</i>	D	17.2 \pm 3.192	15.3 \pm 3.122	0.94 \pm 0.287	9	6.33	9	6.16
14.	Lamiaceae	<i>Tectona grandis</i>	D	17.85 \pm 2.497	16.4 \pm 2.542	0.86 \pm 0.178	20	14.08	20	13.69
15.	Lecythidaceae	<i>Careya arborea</i>	D	19	18	0.7	1	0.7	1	0.68
16.	Loganiaceae	<i>Strychnos nux-vomica</i>	D	13	12	0.8	1	0.7	1	0.68
17.	Lyrtaeae	<i>Lagerstroemia lanceolata</i>	D	16 \pm 1.732	15 \pm 1.732	0.9 \pm 0.173	3	2.11	3	2.05
18.	Malvaceae	<i>Kydia calycina</i>	D	15.87 \pm 2.356	14 \pm 2.203	0.91 \pm 0.295	8	5.63	8	5.4
19.	Moraceae	<i>Ficus bengalensis</i>	SE	20	18	3	1	0.7	1	0.68
20.	Mythraceae	<i>Syzigium cumini</i>	E	15	14	2	1	0.7	1	0.68
21.	Rubiaceae	<i>Mitragina pervi-flora</i>	D	15	14	0.7	1	0.7	1	0.68
22.	Rubiaceae	<i>Saccopetalum tomentosum</i>	D	18 \pm 2	16 \pm 1.527	0.966 \pm 0.057	3	2.11	3	2.05
23.	Rubiaceae	<i>Adina cordifolia</i>	D	17.75 \pm 2.629	16.75 \pm 2.629	1 \pm 0.687	4	2.81	4	2.73
24.	Rutaceae	<i>Chloroxylon sweitenia</i>	D	18	17	1	1	0.7	1	0.68
25.	Sapindaceae	<i>Schleichera trijunga</i>	D	19.1 \pm 4.648	17.7 \pm 4.465	1.4 \pm 0.787	9	6.33	11	7.53
							142		146	

RA- Relative Abundance, D- Deciduous, E- Evergreen, SE- Semi-evergreen.

Table 3: Tree Species, Tree height, Nest height, and GBH in Kydotlu beat.

Sl. No.	Family	Scientific names	Habitat	Tree Height Avg (m)	Nest height Avg (m)	GBH Avg (m)	No of trees	RA Nest tree %	No of nest	RA of nest %
1.	Anacardiaceae	<i>Semecarpus anacardium</i>	D	13	12	0.7 ± 1.359	3	3.75	3	3.37
2.	Combretaceae	<i>Terminalia paniculata</i>	D	17.529 ± 2.095	16.1 ± 2.007	0.9 ± 0.560	17	21.25	17	19.1
3.	Combretaceae	<i>Terminalia tomentosa</i>	D	17.4 ± 2.509	16 ± 2.345	0.79 ± 0.300	5	6.25	5	5.61
4.	Dilleniaceae	<i>Dillenia pentagyna</i>	D	15.3 ± 2.089	14.4 ± 2.034	0.8 ± 0.134	17	21.25	21	23.59
5.	Fabaceae	<i>Dalbergia latifolia</i>	D	15	14	0.7	1	1.25	1	1.12
6.	Fabaceae	<i>Pterocarpus marsupium</i>	D	17 ± 1.247	18.5 ± 1.354	0.92 ± 0.091	10	12.5	13	14.6
7.	Fabaceae	<i>Xylocarpus xylocarpa</i>	D	17.833 ± 2.401	16.3 ± 1.861	0.8 ± 0.040	6	7.5	6	6.74
8.	Lamiaceae	<i>Gmelina arborea</i>	D	20	18	0.8	1	1.25	1	1.12
9.	Lamiaceae	<i>Tectona grandis</i>	D	15	14	0.8	1	1.25	1	1.12
10.	Lythraceae	<i>Lagerstroemia lanceolata</i>	D	18 ± 2.828	16 ± 4.242	1.15 ± 0.494	2	2.5	2	2.24
11.	Malvaceae	<i>Kydia calycina</i>	D	10	9	0.4	1	1.25	1	1.12
12.	Malvaceae	<i>Grewia tillifolia</i>	D	16 ± 2.683	14.5 ± 2.258	0.9 ± 0.109	6	7.5	6	6.74
13.	Sapindaceae	<i>Schleichera trijunga</i>	SE	16.4 ± 2.547	15.2 ± 2.573	1.2 ± 0.385	10	12.25	12	13.48
							80		89	

RA- Relative Abundance, D- Deciduous, E- Evergreen, SE- Semi-evergreen.

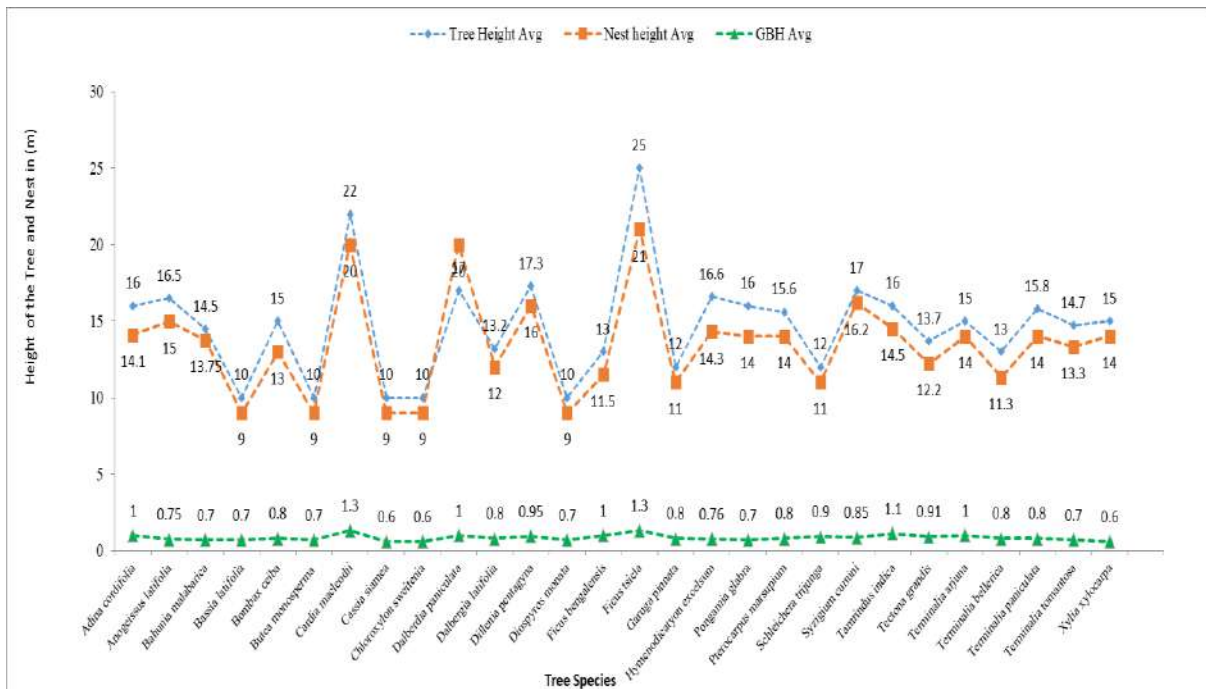


Fig. 2: Tree height, Nest height, and GBH of trees in Umbleybeat.

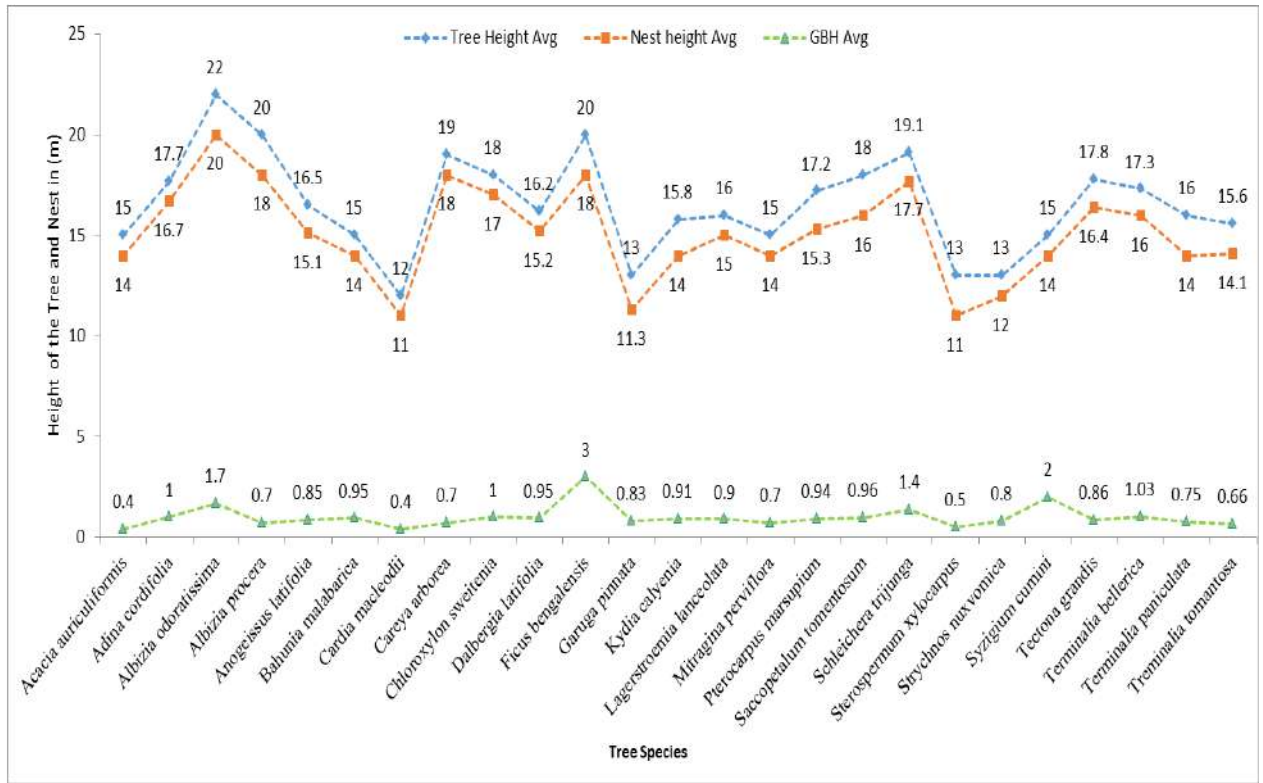


Fig. 3: Tree height, Nest height, and GBH of trees in Lakkinkoppa beat.

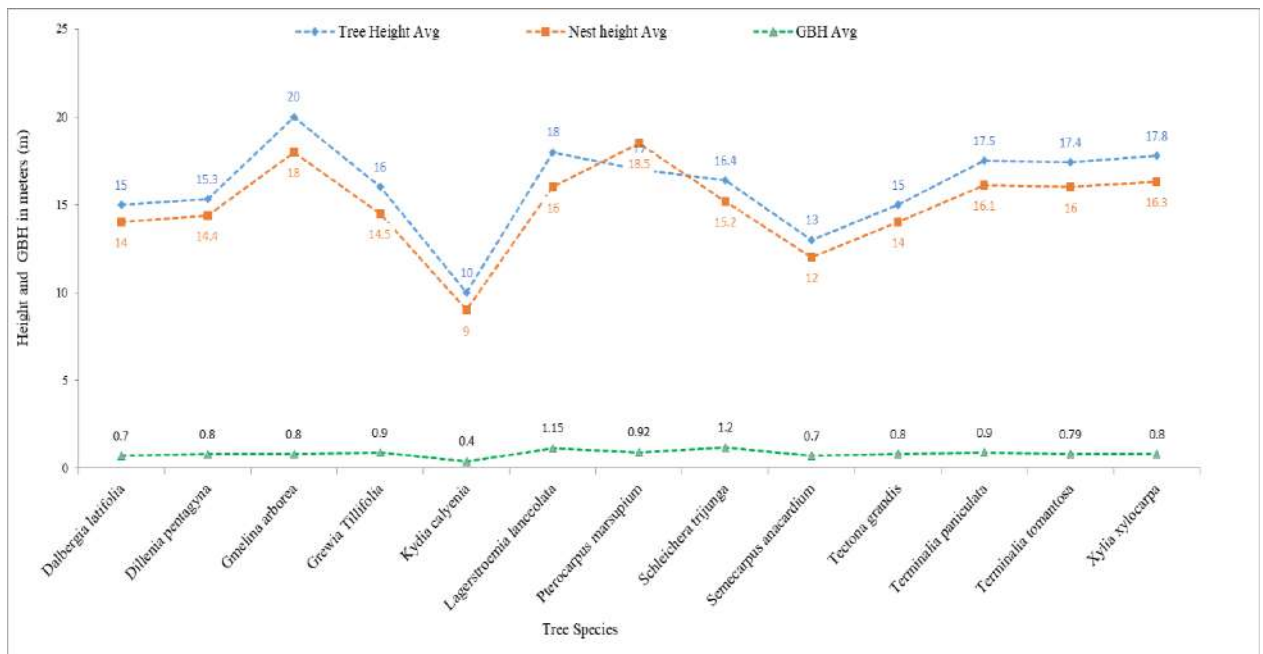


Fig. 4: Tree height, Nest height, and GBH of trees in Kydotlu beat.

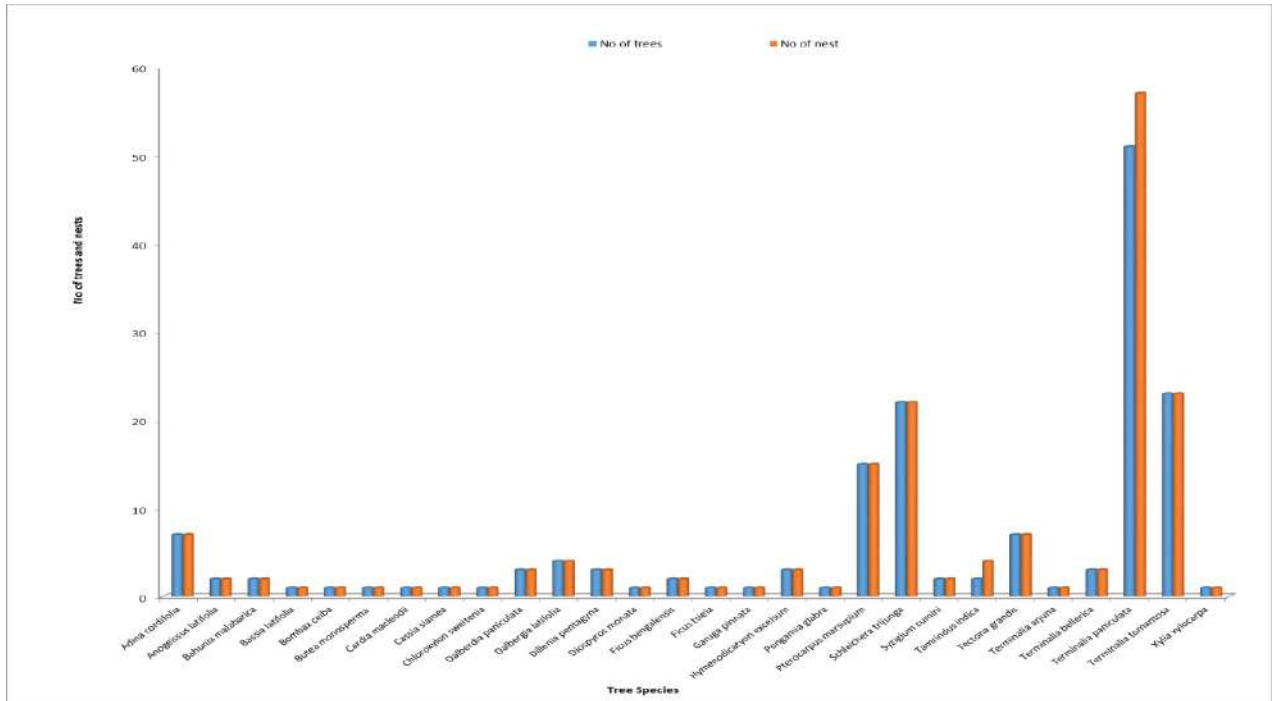


Fig. 5: Number of trees v/s number of dreys in Umbley beat.

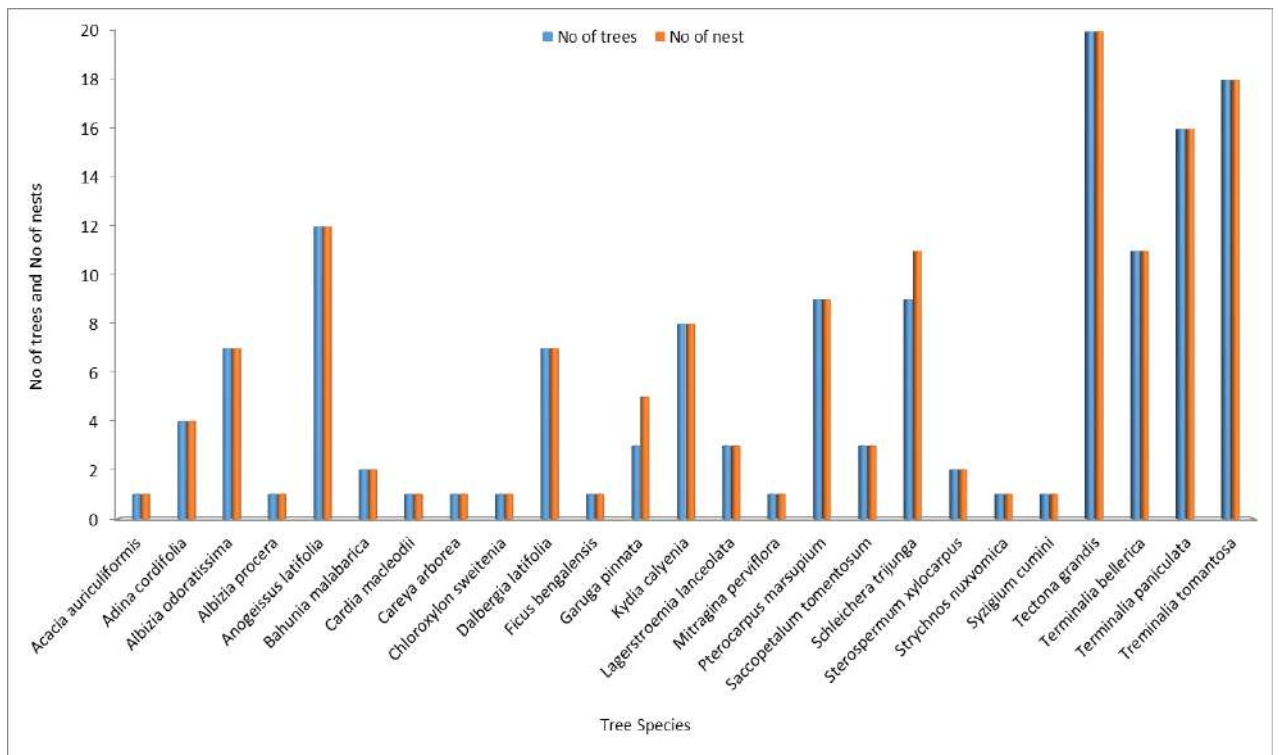


Fig. 6: Number of trees v/s number of dreys in Lakkinkoppa beat.

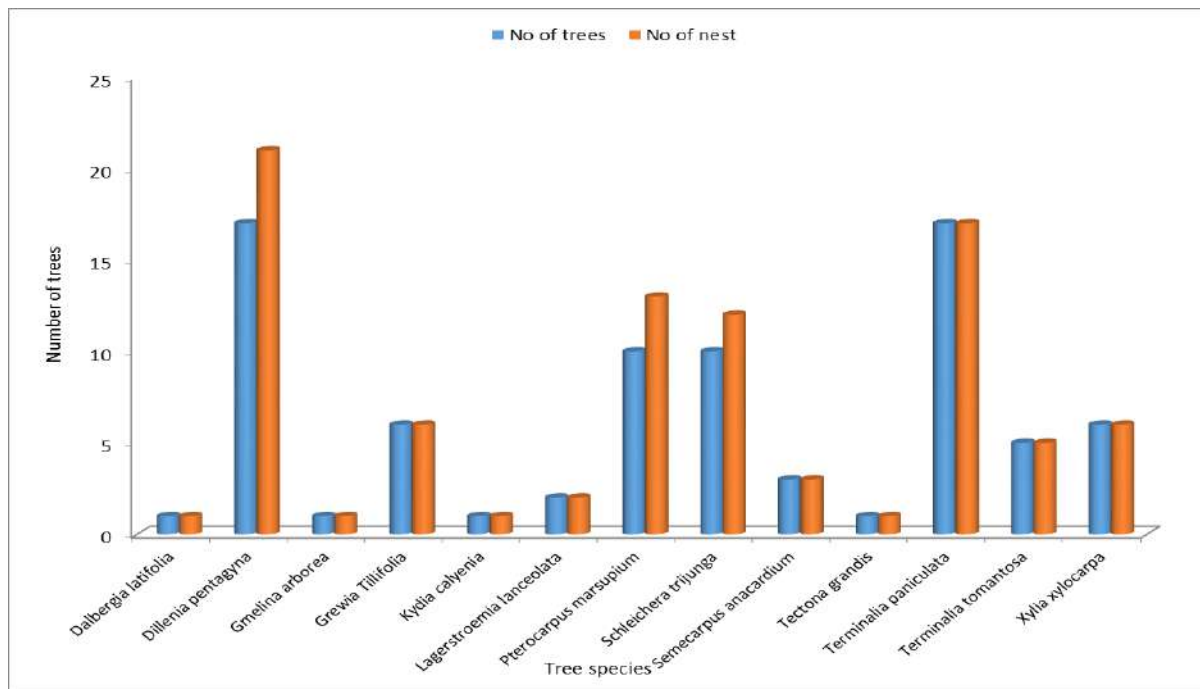


Fig. 7: Number of trees v/s number of dreys in Kydotlu beat.

DISCUSSION

In the above study, the nest tree preferences of *Ratufa indica indica* were analyzed in the Umblebyle Range Forest of Bhadravathi division, Shimoga, Karnataka, which comprised four beats. Among the study beats, only three comprised forest cover: Umblebyle beat, Kydotlu beat, and Lakkinkoppa beat.

Ratufa indica indica used a large variety of tree species for nesting ($n = 41$) in the study area, which is similar to previous records from Dalma wildlife sanctuary ($n = 59$), Mudumalai Tiger Reserve ($n = 19$), Karalpat Wildlife Sanctuary ($n = 37$), Kuldiha Wildlife Sanctuary ($n = 27$) and Sitanadi Wildlife Sanctuary ($n = 30$). The animal was found to have a preference for some tree species. *Terminalia paniculata* (21.81%) was the most preferred tree species, followed by *Terminalia tomentosa* (11.68%), *Schleicheria trijunga* (10.64%), *Pterocarpus marsupium* (8.83%) and *Tectona grandis* (7.27%). However, these trees were common to all three beats. The number of dreys varied with every beat. The animal constructed more dreys in forests around the human-disturbed area, i.e., Umblebyle and Lakkinkoppa beats, as they provided both shelter and easy access to food both from the forest and agricultural fields, least number of dreys were recorded in Kydotlu beat that had fairly undisturbed forest with an abundance of water

from Tunga backwaters indicating the dependency of animal on agricultural products. Similar nesting tree preference from Karalpat wildlife sanctuary showed preferences for *Terminalia alata* (11.03%) and *Anogeissus latifolia* (8.82%), Sitanadi wildlife sanctuary showed a preference for *Terminalia tomentosa* (14.73%), and *Schleicheria oleosa* (13.39%), Mudumalai wildlife sanctuary showed a preference for *Terminalia arjuna* (10%), *Spondias mangifera* (9%) and *Syzygium cumini* (7%), Dalma Wildlife Sanctuary showed a preference for *Terminalia tomentosa* (23.97%) and *Anogeissus latifolia* (9.37%), Kuldiha Wildlife Sanctuary showed a preference for *Shorea robusta* (20%), *Schleicheria oleosa* (17.5%) and *Terminalia tomentosa* (15%).

Ratufa indica, a top canopy-dwelling species, rarely visits the ground (Ramachandran 1992, Borges, 1989, Borges et al. 1992) and prefers tall trees with greater GBH, canopy contiguity, and height for construction of dreys (Basantha & Ajay 2015). In the study area, 83.89% of dreys were found in trees with a height of 11-20m. Similar preferences were observed in Karalpat Wildlife Sanctuary, with a preference for tall trees with a mean height of 11.08 (± 2.11 SD) m, and Dalma Wildlife Sanctuary, with a preference for 12m to 21m, accommodating 86.15% of dreys. This preference provides easy access for movement in the home range and helps avoid and escape predators (Basantha & Ajay 2015, Mishra et al. 2011).

The animal preferred deciduous (78.04%) over evergreen (12.19%) and semi-evergreen (9.75%) trees. Similar preferences for deciduous trees were observed in Kuldiha Wildlife Sanctuary with deciduous (80%) and evergreen (20%) trees, in Dalma Wildlife Sanctuary with deciduous (83.26%), evergreen (13.02%) and semi-deciduous (3.72%) trees, in Karalpat Wildlife Sanctuary with dry deciduous (61.07%), semi-evergreen (30.15%) and moist deciduous (8.83%) trees, and in Sitanadi Wildlife Sanctuary with deciduous (77.68%) and evergreen (22.32%) trees.

Tree species selected for multiple nesting in the study area include *Dillenia pentagyna*, *Garuga pinnata*, *Pterocarpus marsupium*, *Schleichera trijunga*, *Tamrindus indica* and *Terminalia pinaculata*. Similar preferences were observed in the Dalma wildlife sanctuary, where multiple nests were found on *Lannea grandis*, *Anogeissus latifolia*, *Terminalia bellirica*, *Terminalia chebula*, *Terminalia tomentosa*, *Bombax ceiba*, *Dillenia pentagyna*, *Dillenia indica*, *Lagestroemia parviflora*, *Artocarpus lakoocha*, *Syzygium cumini* and *Sterculia urens*, Mudumali Tiger Reserve that included *Terminalia arjuna*, *Spondias Mangifera* and *Syzgium cumini* and Sitanadi Wildlife Sanctuary that included *Pterocarpus marsupium*, *Stereospermum chelonoides*, *Bridelia squamosal*, *Terminalia arjuna*, *Mangifera indica*, and *Schleichera oleosa*.

The nesting preference of *Ratufa indica* showed old and new nests along the transects (Mishra 2011). Among the dreys, 92.36% (375 number) were new, and 7.63% (31 number) were old, similar to observations from Dalma Wildlife Sanctuary, where 73.35 percent dreys were new, and 26.65 percent were old.

CONCLUSION

Ratufa indica indica, a potential pollinator and a good indicator of forest health, becomes an important species to be conserved to conserve the forests as the importance of the animal in seed dispersal can not be ruled out. To reduce human-animal conflicts and the chances of animals being hunted outside the forest area, increasing the food source in the forest area is essential. Further, there is a need to create awareness among the people to reduce hunting. The animal population was good as we recorded 406 nests indicating the animal's survivability despite hunting and human disturbances. The study provides information on the nesting preference of the animal in Umbley Range Forest, which remains unexplored and can help conserve the animal in its habitat.

ACKNOWLEDGMENT

The authors are thankful to the Principal Chief Conservator of Forest, PCCF (Wildlife), Karnataka, for granting permission to conduct the research. They would also thank the staff of Umbley Range Forest for providing the necessary support.

REFERENCES

- Abdulali, H. and Daniel, J.C. 1952. Race of the Indian giant squirrel (*Ratufa indica*). J. Bom. Natural Hist. Soc., 50: 469-474.
- Altmann, J. 1974. Observational study of the behavior sampling method. Behavior, 49: 227-265.
- Aparajita, D. and Goyal S.P. 1996. Comparison of forest structure and use by the Indian giant squirrel (*Ratufa indica*) in two riverine forests of Central India. Biotropica, 28(3): 394-399.
- Basantha, K.N. and Ajay, K.P. 2015. Feeding and nesting ecology of Indian giant squirrel (*Ratufa indica*) (Erxleben 1777) in Kuldiha wildlife sanctuary, Balasore, Odisha, India, and its conservation. Int. J. Bioass., 4(03): 3741-3746.
- Baskaran, N., Venkatesan, S., Mani, J., Srivastava, S.K. and Desai, A.A. 2011. Some aspects of the ecology of the Indian Giant Squirrel *Ratufa indica* (Erxleben 1777) in the tropical forests of Mudumalai Wildlife Sanctuary, southern India and their conservation implications. Journal of Threatened Taxa, 3(7): 1899-1908.
- Borges, R. 1989. Resource Heterogeneity and the Foraging Ecology of the Malabar Giant Squirrel (*Ratufa indica*). Ph.D. Thesis, University of Miami, Florida.
- Borges, R., Mali R.S. and Somanathan, H. 1998. The Status, Ecology and Conservation of the Malabar Giant Squirrel *Ratufa indica*. Final Report, Wildlife Institute of India, New Delhi.
- Buckland, S.T., Anderson, D.R., Burnham, K.P. and Laake J.L. 1993. Distance Sampling: Estimating Abundance of Biological Populations. Chapman & Hall, London.
- Devcharan, J.N., Samba, K. and Ullas K.K. 2008. Measuring Indian giant squirrel (*Ratufa indica*) abundance in southern India using distance sampling: Special editing: Arboreal squirrel. Curr. Sci., 95(7): 885-888.
- Keystone Foundation. 2015. Forests Plants of the Nilgiris Southern Nilgiri Biosphere Reserve: A Pictorial Field Guide. Keystone Foundation, Tamil Nadu, p. 365.
- Mishra, A.T., Kazmi, S.E.H. and Satya, P. 2011. Nesting and feeding behavior of Indian giant squirrel (*Ratufa indica*) in Dalma wildlife sanctuary, Jamshedpur (Jharkhand). Indian Forest., 137(10): 1155-1159.
- Nagarajan, B., Venkatesan, S., Mani, J., Sanjay, K.S. and Ajay A.D. 2011. Some aspects of the ecology of the Indian giant squirrel *Ratufa indica* (Erxleben, 1777) in the tropical forests of Mudumalai wildlife sanctuary, southern India, and their conservation implications. J. Threat. Taxa., 3(7): 1899-1908.
- Navendu, Page 2017. Endemic Woody Plants of the Western Ghats. Trail Blazer Printers and Publishers, Bangalore, p. 207.
- Nowak, R.M. and Walker, E.P. 1999. Walker's Mammals of the World, Vol. 1, JHU press.
- Pradhan, A.K., Shrotriya, S., Rout, S.D. and Dash, P.K. 2017. Nesting and feeding habits of the Indian giant squirrel (*Ratufa indica*) in Karalpat wildlife sanctuary, India. Animal Biodiv. Conserv., 40(1): 63-69.
- Prater, S.H. 1980. The Book of Indian Animals. Bombay Natural History Society, Mumbai, p. 348.
- Ramachandran, K.K. 1988. Ecology and Behavior of Malabar Giant Squirrel, *Ratufa indica maxima* (Schreber) 1788. Report of the Project Wild 04/83. Division of Wildlife Biology, Kerala Forest Research Institute, Peechi, Kerala, p. 47.

- Ramachandran, K.K. 1992. Certain Aspects of Ecology and Behaviour of Malabar Giant Squirrel *Ratufa indica* (Schreber). PhD Thesis. Department of Zoology, University of Kerala, p. 191.
- Ravi, S.K. 2008. Nesting sites of Indian giant squirrels in Sitanadi wildlife sanctuary, India. *Curr. Sci.*, 95(7): 882-884.
- Samson, A. 2020. Nesting behavior of (*Ratufa indica* Erxleben 1777) in Mudumalai tiger reserve, Western Ghats, Southern India. *J. Threat. Taxa.*, 3(7): 1899-1908.
- Satya, P., Anil, K.M. and Mohammad, R. 2011. Studies on the nesting habits of Indian giant squirrel *Ratufa indica centralis* (Ryley 1913) in Dalma Wildlife Sanctuary, Jharkhand, India. *Columb. J. Life Sci.*, 12(1&2): 9-18.



Investigating the Implications of Transit-Oriented Land Use Development for a Potential Node in an Urban Metro for Sustainability

Sobha. P. and J. Prakash Arul Jose†

Department of Civil Engineering, Noorul Islam Centre for Higher Education, Thuckalay, Kanyakumari, Tamilnadu, India

†Corresponding author: J. Prakash Arul Jose; joseprakash1430@gmail.com

Nat. Env. & Poll. Tech.
Website: www.neptjournal.com

Received: 08-09-2022

Revised: 03-11-2022

Accepted: 04-11-2022

Key Words:

Transit-oriented development

Trip generation

Land use

Smart growth

Sustainable development

ABSTRACT

Urbanization is intrinsically connected to economic progress. India's rapid economic and population growth has increased its carbon footprint and traffic congestion. A long-term strategy is essential to preserve the balance and alleviate the issues arising from the expansion. Integrating land use and transportation planning has been acknowledged as a means to achieve sustainable urban development worldwide. Transit Oriented Development (TOD) is one such strategy. TOD is a planning and design strategy for promoting urban development by clustering jobs, housing, services, and amenities around public transport stations. This strategy can help achieve sustainable communities and improve the quality of life. This research paper assessed the land use characteristics of an urban fringe area in Trivandrum city and completed a land suitability analysis using GIS software tools. A potential node for re-development was identified by looking at various traffic, demographic, and land use parameters. Detailed TOD recommendations for the area surrounding the transit node were proposed based on its development potential.

INTRODUCTION

Man's activities on land are referred to as land usage. The land pattern of a place is the result of natural and socioeconomic forces, as well as man's use of them over time and space. Due to massive agricultural and demographic pressures, land is becoming increasingly scarce. As a result, information on land use is critical for selecting, planning, and implementing land use plans to fulfill rising demands for fundamental human requirements and well-being. Transportation planners and engineers must improve the quality of transportation facilities for all citizens.

Transit Oriented Development (TOD) creates vibrant, sustainable communities worldwide (Cervero et al. 2004). It is a powerful strategy for developing compact, high-density, walkable communities around public transport stations. This reduces the heavy reliance on private modes of transportation for mobility needs. Eboli analyzed the quality of transit service from the passengers' perspective (Eboli & Mazzulla 2011). The quality of public transit services can be improved using shared autonomous vehicles. They can provide inexpensive mobility-on-demand services and facilitate dynamic ride-sharing (Krueger et al. 2016, Vakayil et al. 2017, Yap et al. 2016). A simulation analysis evaluated TOD's land development impacts across all Chinese cities

expected to have metro systems by 2020. Results show that China's second and third-class cities will have more potential for TOD implementation than the first-class cities in the next five years (Xu et al. 2017). Many studies have provided strong evidence of residents' support for the characteristics of transit-oriented development (TOD) neighborhoods.

For over two decades, planners have urged changing from mobility-centered to accessibility-focused land use and transportation planning. The ease with which any land use activity can be reached from a given place utilizing a specific transportation system is known as accessibility (Burns & Golob 1976). In planning, accessibility is seen as a reliable, clear, and communicated metric (Bertolini et al. 2005, Hansen 1959). An elasticity-based metric of accessibility that can enable project-level evaluation of land-development projects as an accessibility-based alternative to traffic-impact analysis was proposed by Levine (Levine et al. 2017). TOD improves access by offering many transportation linkages and dense, mixed-use, cycling, and pedestrian-friendly land use around transit stations (Calthorpe et al. 2014, Curtis et al. 2009). How TOD components are related to the accessibility of metro station areas at the one-hour travel time catchment level was studied in Beijing (Guowei et al. 2019). TOD is a prominent accessibility-focused planning method that is

gradually gaining popularity. Identifying and measuring specific TOD components related to accessibility in station areas is also studied (Shiliang et al. 2020). The advantages of TOD include increased transit ridership, reduced roadway expansions due to decreased private vehicle usage, and increased mobility choices, including walking and cycling (Handy 2002, Papa & Bertolini 2015, Yeung et al. 2015). Construction and other commercial products are expensive due to the excessive cost of transportation from natural sources (Alex et al. 2022a). This results in reduced household transportation costs, improved access to shopping, services, and the ability to live, work and shop within the same neighborhood. According to Cervero, people and places matter, not transportation (Cervero 1997).

One of the first assumptions in the research is that TOD is a strategy for sustainable development. According to Newman and Kenworthy, sustainable development is any development with social, economic, and environmental benefits. The TOD communities are also designed to promote non-motorized transport and use transit to travel larger distances. TOD aims to increase the accessibility to work and other activities so that people have more choices and can benefit economically. Sustainable urban mobility plays an important part in the competition, as several topic areas are directly or indirectly linked to transport (sustainable urban mobility, air quality, noise, climate mitigation, energy performance). European Green Capital Award (EGCA) rewards environmentally friendly cities through a competitive application, evaluation, and ranking (Müller & Reutter 2020).

In Curitiba and Bogota, TOD has been implemented successfully. In Curitiba, a transit-first policy is aggressively pursued by focusing development along the transit axes. The success element of Bogota focuses on pedestrians and bicycles as an access mode to the BRT. But in Bogota, changes were not made to the cityscape, unlike Curitiba. Thus Bogota focuses on access to the BRT, and Curitiba focuses on accessibility. Both projects are land use and transport integration, which promote public transit use. Thus in principle, they are both TOD (Rajakumari 2008, Straatemeier & Bertolini 2020, Alex et al. 2016). Most land use theories considered the transportation system as having a definite effect on the location of activities. Transport and land use largely remained in separate compartments, and the transport variables that go into the land use model were restricted to the concept of 'distance to the center (Wegener 2020).

This research paper aims to apply the TOD concepts and guidelines for the overall development of a transit node in Trivandrum city. The guidelines must be effectively

considered within the transport planning process (Turnheim et al. 2020, Alex et al. 2022b). One of the first assumptions in the research is that TOD is a strategy for sustainable development. According to Newman and Kenworthy, sustainable development is any development with social, economic, and environmental benefits. The TOD communities are also designed to promote non-motorized transport and use transit to travel larger distances. TOD aims to increase the accessibility to work and other activities so that people have more choices and can benefit economically.

This research paper aims to apply the TOD concepts and guidelines for the overall development of a transit node. The guidelines must be effectively considered within the transport planning process.

NEED FOR TOD IN TRIVANDRUM CITY

Demographic Aspects

Kerala State covers barely 1% of India's total land area but has 3% of the country's population. The population density of the state is 859 persons/km² (3x the national average). The population density of Trivandrum City is 4,454/km² (3x that of Trivandrum District). The Trivandrum Metropolitan Area (TMA) comprises Trivandrum City and its satellite towns.

Land Use

Urbanization has resulted in significant changes in land use. The urbanization trend is more in urban fringe areas adjoining the corporation area. Parks and open spaces occupy only 7.8% of the city area.

Economy

The first IT Park-Technopark was established in 1991 and situated at Kazhakuttom. Technopark spans over 300 acres and has a 4 million square feet built-up area. Since the formation of Technopark, the city has seen significant expansion and growth. Additional jobs are getting created, and this is bringing in migrant workers into the city, thereby increasing the need for infrastructure development as well as the construction of roads and buildings.

Growth of Automobiles

The population of Trivandrum district only grew by 2% in 10 years (from 32.34 lakhs in 2001 to 33.01 lakhs in 2011). This trend is not expected to change much, even during the 2021 census (awaited). Meanwhile, vehicle registrations in the Trivandrum district have grown by an average of 11% yearly. This disproportionate increase in private vehicles puts an enormous strain on the roads, results in accidents and traffic congestion, and necessitates a renewed focus on

Table 1: The percentage share of trips for different transport modes.

Year	2021		2031		2041	
	Trips	% share	Trips	% share	Trips	% share
Two wheeler	32195	28%	35954	27%	36976	24%
Car	16933	15%	23469	17%	29567	19%
Three wheeler	11006	9%	15307	11%	23527	15%
Public Transport System	55939	48%	60772	45%	66947	43%
Total	116073	100%	135502	100%	157017	100%

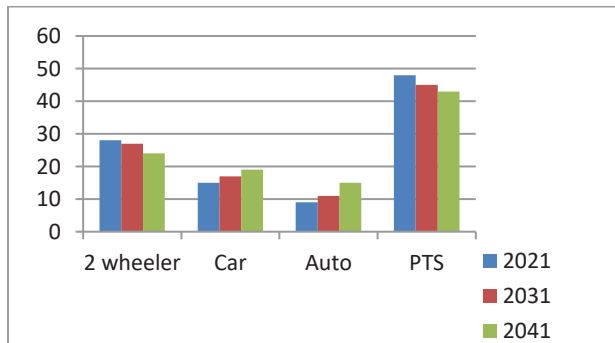


Fig. 1: Chart showing the decadal growth of automobiles.

public transport systems. The TOD areas will be served by high-quality public transit systems, thereby encouraging more people to use the public transportation systems, causing a reduction in private car use. The percentage share of trips for all modes of transport is projected until the horizon year 2041, as shown in Table 1. The data is indicated as a bar chart in Fig. 1.

MATERIALS AND METHODS

Research Area Identification

The different criteria considered for research area identification include:

1. Connectivity– National Highway (NH 66) passing through the settlements, and proximity to International Airport and railway stations
2. Residential and Commercial development projects
3. Employment Opportunities in the area
4. Land Value considerations
5. Urbanization trends

Connectivity

Traffic volume and passenger volume data were analyzed along the NH corridor. It was found that the traffic volume was relatively high in the transit nodes along the corridor.

Residential and Commercial Development Projects

More than 20 real estate projects in and around Kazhakuttom are present. Major players are Heera, SFS, Skyline, Confident, and Oceanus. One of the largest shopping malls (Lulu mall) is in close proximity.

Employment Opportunities in the Area

Kazhakuttom is developing into a major self-contained and prominent township. The increase in employment opportunities will significantly increase traffic volume from the rest of the city. Housing demand increases due to migration owing to an increase in employment.

Land Value Considerations

Owing to an increase in employment, the housing demand increases. People tend to migrate and settle close to their place of employment. This results in an increase in land value.

Urbanization Trend

The Urbanization trend is more in the fringe areas surrounding Trivandrum Corporation, along the NH Corridor and Railway line. The Census data indicate that the population growth rate pattern is the highest along the traffic corridor. These adjacent fringe areas are estimated to attain an urban state in the next 10yrs.

Settlements Selected for the Research

Based on the various criteria adopted, the following five



Fig. 2: Location of research zones.

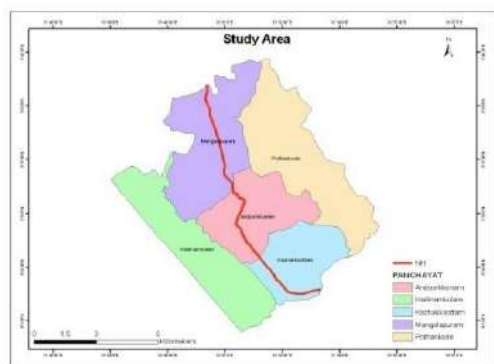


Fig. 3: Delineation of zones in the research area.

settlements were selected for land use and traffic analysis (Fig. 2 and 3). Andoorkonam, Kadinamkulam, Kazhakuttom, Mangalapuram and Pothencode.

Data Collection

Started the data collection exercise with a land use map of the research area. Various land use categories were identified and delineated as agricultural, built-up, mixed built-up, wastelands, water bodies, etc. The purpose of the trip, mode of travel, and socioeconomic characteristics of the trip maker were all identified in the travel survey. These are

Table 2: The percentage of land use distribution in the research zones.

Type of Land use	Andoorkonam		Kadinamkulam		Kazhakuttom		Mangalapuram		Pothencode	
	sq.km	%	sq.km	%	sq.km	%	sq.km	%	sq.km	%
Residential	0.42	3.0	0.88	5.0	1.75	9.0	0.87	4.0	1.04	5.0
Water Body	0.14	1.0	2.12	12.0	0.19	1.0	0.43	2.0	0.21	1.0
Waste Land	0.28	2.0	1.77	10.0	0.39	2.0	0.22	1.0	0.42	2.0
Forest	0.0		0.0		0.0		0.0		0.21	1.0
Agricultural	8.93	64.0	9.02	51.0	12.85	66.0	17.76	82.0	17.10	82.0
Mixed Built up	4.19	30.0	3.89	22.0	4.28	22.0	2.38	11.0	1.88	9.0
TOTAL	13.96	100	17.68	100	19.47	100	21.66	100	20.85	100

the elements that make up a location's travel characteristics. Travel characteristics are significant resources that provide vital information on people's travel behavior across time and throughout the population.

Primary surveys with questionnaires were employed to obtain data on the area's demographic and socioeconomic parameters. A sample size of nearly 0.2% of the research area population is considered for the survey. Data was collected from 250 households and was grouped into three categories. i.e., Data from the household, personal data, and travel data. Data were analysed using category analysis by classifying households based on the size of households, their income, and vehicle ownership.

RESULTS AND DISCUSSION

This section used Arc GIS software to analyze the five zones' land use and suitability analysis. The weighted Overlay technique is adopted to find the land suitable for development. For the identified zones, the daily trip generation is calculated using TransCAD software. This exercise intends to identify the zone with the maximum number of daily trips. A transit node in that identified zone will be selected for transit-oriented land use development.

Land Use Analysis

The collected land use map was imported into ArcGIS (Version 9.3), and by selecting different attributes, the area of different land uses was calculated. The distribution of land in the zones calculated from ArcGIS is shown in Table 2.

The data analysis shows that more than 50% of the area in all the zones is agricultural. Forest areas constitute only 1%. By considering the total area, the percentage-wise distribution of various land use types is given in Fig. 4.

Categories of Land

The land is categorized based on land use characteristics as follows:

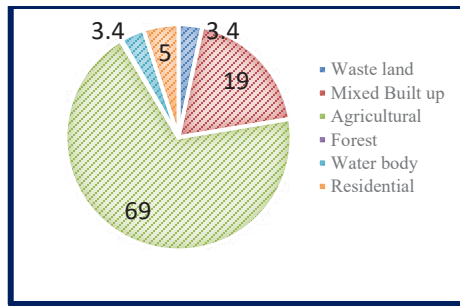


Fig. 4: Land use distribution of research area.

Built-up Land: Built-up land is defined as a habitable area that has been established as a result of non-agricultural use and includes buildings, transportation networks, and communication utilities, as well as vegetation, water bodies, and unoccupied areas.

Agricultural Land: The area is predominantly agricultural. The principal crops grown are coconut, paddy, rubber,

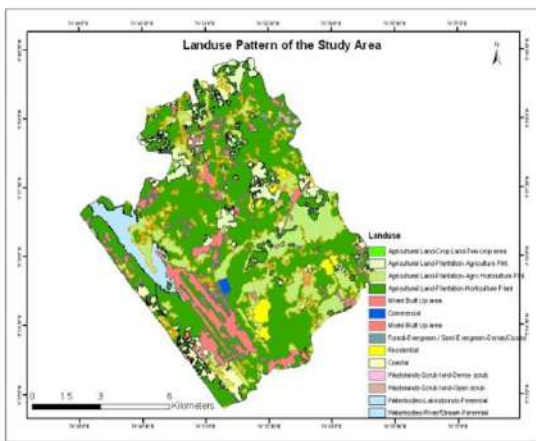


Fig. 5: Land use pattern of the research area.

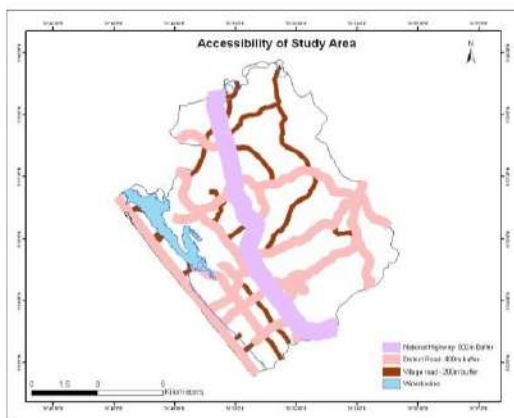


Fig. 6: Accessibility of the research area.

cashew, and garden crops like bananas. The percentage of the agricultural area is 69%.

Waste Lands: They are degraded lands that, with reasonable effort, can be restored to vegetative cover and are now underutilized and deteriorating, either owing to poor management or natural reasons. About 3.4% of the total area is a wasteland.

Water Bodies: Water bodies are any significant accumulation of water by natural or artificial means. This constitutes 3.4% of the total area.

Land Suitability Analysis

Land suitability analysis aims to determine future land use patterns by looking at the specific requirements, preferences, or predictors of a particular activity. Changes in transportation affect the location of land investment, which affects the demand for travel to and from an area. Urban transport has a high impact on land value. Over time, transportation networks and the spatial patterns of land use they serve influence each other. Different land uses different trip generation characteristics. Fig. 5 shows the different land use patterns in the research area.

The existing road network map was used as the base map for preparing the land value layer and accessibility layer. Buffers were drawn at suitable intervals to zone the map to different levels of accessibility. Buffers were created 80m for NH, 40m for district roads, and 20m for village roads. The accessibility of the research area is shown in Fig. 6.

The land value variations in the area were also found (Fig. 7). It was observed that the land surrounding the national highway has high land value.

The slope details of the region in the area were analyzed. Gentle slope (0-5 percent), moderately sloping (5-15

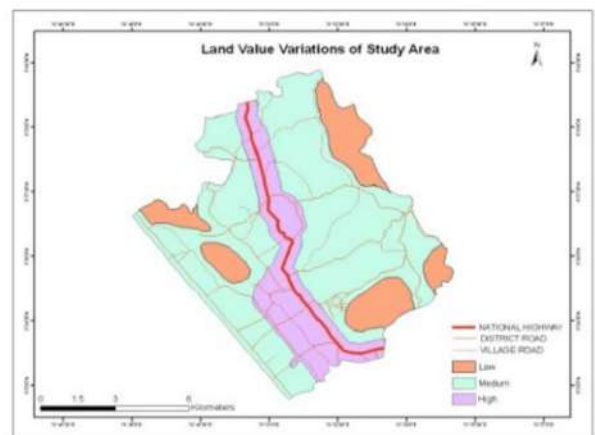


Fig. 7: Land Value variations in the research area.

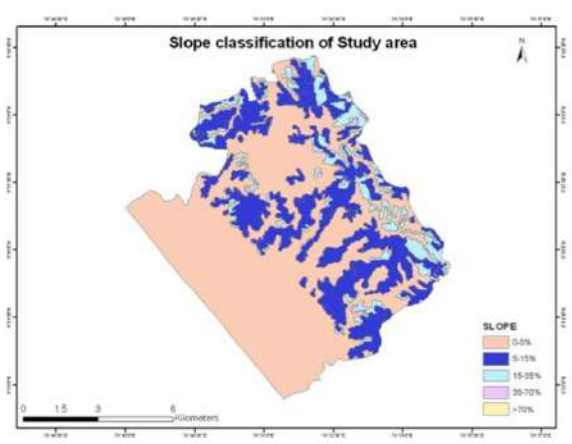


Fig. 8: Slope classification in the research area.

percent), strongly sloping (15-35 percent), moderate to steep slope (35-70 percent), and steep slope (>70 percent) were used to classify the slope (Fig. 8).

Weighted Overlay for Land Suitability Analysis

The weighted overlay is a technique for creating an integrated analysis by applying a single measurement scale of values to various and dissimilar inputs. This data is stored in many raster layers with varying value scales. It evaluates the relative influence of input rasters in a decision-making process. Within a single raster layer, values were prioritized. For example, 1 represents slopes of 0 to 5 degrees, and 2 represents 5 to 10 degrees. Steps for running overlay analysis are given in Table 3.

The overlay of the coverages was done so that the attributes of both coverages were present in the final output. The land value, slope condition, and accessibility maps were overlaid to get the composite map. This can be used as a reference for the proposed activities in the area. The results were assigned four suitability classes such as high, moderate,

Table 3: Weighted overlay method procedure.

Steps	Procedure I	Procedure II
1	Selecting an evaluation scale	Raster's Reclassified (1 most suitable and 5 least)
2	Adding Raster's	Raster added to weighted overlay table
3	Set scale values	The value assigned based on which land use is more suitable (Ex. Forest=Restricted)
4	Assign weights to input raster's	Assign influence percentage based on its importance
5	Execute the weighted overlay model	Cell value of each raster by influence percentage

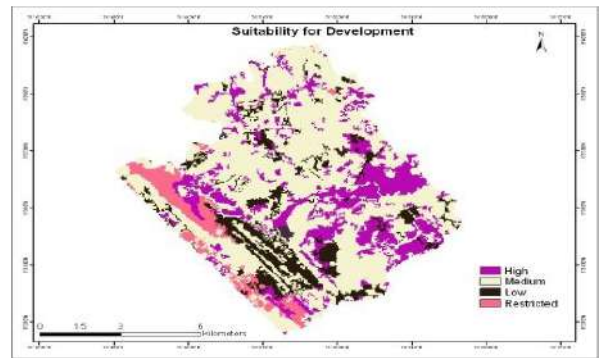


Fig. 9: Land suitable for development.

Table 4: Area of different classes of suitability.

Suitability Class	Area in Sq.km
Restricted	6.35
Highly suitable	20.43
Medium	58.55
Least	14.67

low, and restricted. The map showing the suitability of land parcels for development is displayed (Fig. 9).

Nearly 20 Sq.km of the area is highly suitable for any development. About 7% of the total area comes under the restricted category. And more than half of the total area is moderately suitable for development, as shown in Table 4.

Estimation of Trip Generation and Transit Node Identification

For each identified zone, the daily number of trips generated is computed.

This is achieved as follows:

1. Do a Category Analysis using the zonal characteristics data points (e.g., number of persons in the household, income per household, number of vehicles) as inputs.
2. Zones and the road network are digitized in ArcGIS and imported into TransCAD.
3. Generate a Trip Rate table using TransCAD software. The Trip Rate table illustrates the number of trips by household and income for various vehicle ownership levels (Table 5).
4. Calculation of the daily trips produced for each zone.

Steps for Creating a Trip Rate Table

1. A table containing disaggregate data was opened
2. 'Planning'-Planning Utilities'-Build Cross Classifi-

ation Table’ was chosen to display the Build Cross Classification Table dialogue box

3. The classification variables selected:
 - a) Number of persons per household
 - b) Income per household
 - c) Number of vehicles per household
4. The classification variables were given ranges, and Cross Classification table was prepared.

The zonal characteristics were calculated for the year 2022 (Table 6). The income growth was derived from the previous data on per capita income. The increase in the income rate of the people is found to be 8.76%. The number of employed persons per household and vehicle ownership had an increasing trend.

By giving the zonal characteristics as input, the trips produced daily for the year 2022 were calculated (Table 7). The bar chart showing the trip generation is shown in Fig. 10.

The highest number of trips generated was in Kazhakuttom.

TOD Design for the Transit Node

The research shows that the trip generation of Kazhakuttom is highest when compared with the other zones. A transit

Steps for Analysis

The first step for the analysis was activating the zone layer and opening the trip rate table in that layer. The generation of trips in each zone was calculated by category analysis.

Table 5: Trip rate table.

Vehicle Ownership = 0					
Income (Rs)	Household Size				
	<=2	3	4	5	>5
<10000	1.05	1.1	2.08	2.07	2.6
10000-20000	1.12	1.38	2.12	2.55	2.65
20000-30000	1.4	1.4	2.47	2.6	2.78
>30000	1.75	1.88	2.6	3.2	3.55
Vehicle Ownership = 1					
Income (Rs)	Household Size				
	<=2	3	4	5	>5
<10000	1.36	1.3	2.38	2.47	2.8
10000-20000	1.5	1.6	2.5	2.65	2.85
20000-30000	1.7	1.8	2.7	2.9	2.98
>30000	1.99	2.1	3.1	3.6	3.75
Vehicle Ownership = 2					
Income (Rs)	Household Size				
	<=2	3	4	5	>5
<10000	1.66	1.6	2.68	2.77	3.1
10000-20000	1.8	1.9	2.8	2.95	3.15
20000-30000	2.0	2.1	3.0	3.2	3.28
>30000	2.29	2.4	3.4	3.9	4.05

Table 6: Zonal Characteristics for 2022.

Zone	Name of the settlement	Number of Households	Number of employed persons/HH	Income/HH	Number of vehicles owned/HH
1	Kadinamkulam	16441	2.6	41331	0.83
2	Mangalapuram	13744	2.8	43645	0.98
3	Kazhakuttom	14935	2.6	59989	3.66
4	Andoorkonam	9989	2.8	55213	1.64
5	Pothencode	10674	2.4	45957	1.39

Table 7: Daily trips generated for 2022.

Zone	Name of Settlement	Number of trips produced
1	Andoorkonam	168659
2	Kadinamkulam	230652
3	Kazhakuttom	250754
4	Mangalapuram	177209
5	Pothencode	135657

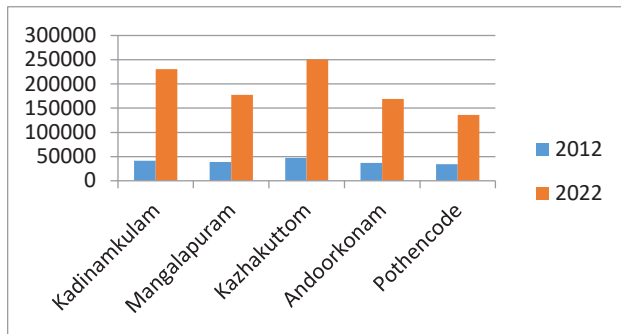


Fig. 10: Chart showing Trip Generation.

station for the proposed MRTS in Kazhakuttom was identified as a node for Transit Oriented Development based on its development potential (Fig. 11).

General TOD Guidelines

The TOD Guidelines provide a framework for anticipating transit and land use integration around the transit stops. They act as a catalyst for infrastructure investments, private development, formulation of public policies and regulations, and encourage transit-oriented development by:

1. Promoting city transportation infrastructure investment, concentrating higher density residential, retail, and job expansion near transit centers
2. Major trip generators (office buildings, commercial malls, schools, and entertainment venues) should be located near public transportation
3. Promoting a station-specific land use mix to provide people accessibility for their work, life, and mobility needs
4. Fostering the development of high-quality projects
5. Providing facilities that allow passengers to shift between modes of transportation in a timely, safe, and convenient manner
6. Create a system that connects destinations that is pedestrian and bicycle friendly, direct, safe, and convenient, and caters to all modes of transportation
7. Planning for the development of a beautiful, green city

Design of TOD for Transit Node

Based on the development potential of the node, the TOD design was formulated considering the key TOD components (Fig. 12).

Hectic zone – Zone of high-intensity conflict (First 100m from the transit stop): The first zone is 100m from the transit stop. There would be heavy traffic flow and pedestrian movements. A subway, two bus bays, and bicycle parking spaces were proposed. Bus bays are provided at least 15m from either side of the transit stop. Segregated bicycle lanes could ease smoother traffic flow and minimize conflicts. Continuous footpaths (1.5 m) on either side of the carriage-way are proposed. Shopping facilities were provided close to parking areas. Existing shops can be developed into shopping complexes, malls, etc.

The key benefit of this zone is that it minimizes vehicular and pedestrian conflicts. Subways and bus bays improve the traffic flow by reducing congestion along the main road. It ensures safe and smooth connections for pedestrians and cyclists.

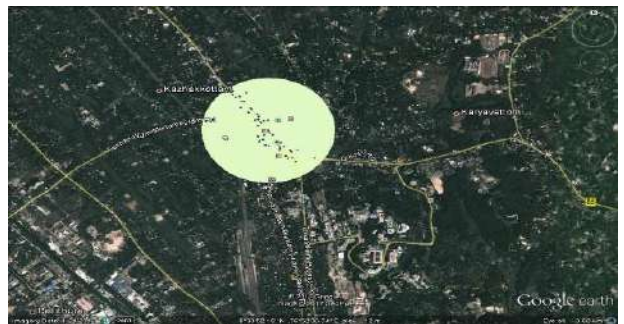


Fig. 11: Transit Node and Buffer Zones (A bird's Eye View).

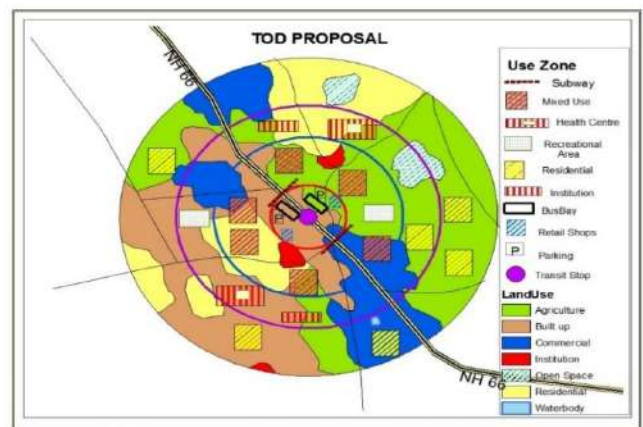


Fig. 12: TOD Design for Transit Node.

Mixed use zone (250m from the transit stop): Mixed uses are provided in the second zone, i.e., 250m from the transit stop. These include high-intensity uses like residential, retail, employment centers, institutions, etc. In addition to these uses, recreational areas and multilevel parking structures are also provided.

The benefits include high residential density with supporting activities, enabling residents to access various services and amenities. It also encourages people to walk instead of taking a car. Furthermore, it enables the formation of a close-knit neighborhood and a sense of community.

Public/semi-public zone (350m from the transit stop): In the third zone, medical and institutional activities are proposed, and provision for open spaces and recreational facilities are considered. There are many advantages, such as the best access for residents to all facilities and the availability of public services in the area.

Residential zone (500m from the transit stop): Plotted housing options are provided in this tranquil zone. This becomes the primary residential area. The advantages are people with a higher income can enjoy the benefits of open spaces and larger homes/villas. Also, the residents are protected from traffic noise and other negative effects. Public spaces for recreation, such as parks and playgrounds, are also proposed.

Preliminary Study

The exponential increase in private vehicles has many ill effects on Trivandrum city. To reduce these issues, some long-term strategy has to be looked into. Considering the growth potential of the city, it was found that transit-oriented development plans are ideal. Various criteria were considered, and the area suitable for TOD was delineated (Fig. 3). Demographic and socio-economic data were collected by conducting household surveys using questionnaires. Around 250 households were selected for the survey.

Land Use/Land Suitability Analysis

Various Land use categories like built-up areas, agricultural areas, residential areas, etc., were identified from the land use map by importing it into GIS software. The next step was to determine the percentage-wise area distribution of these land categories (Table 2). It was inferred that more than 50% of the area in all the zones was used for agricultural purposes (Fig. 4). Land use pattern of the five zones was generated using ArcGIS software (Fig. 5). Road network map was overlaid into the land use map and the accessibility of the zones were found out. Similarly, the land value variations, as well as the slope classifications, were noted. The weighted Overlay technique was adopted to find the land suitable for

development (Fig. 9). The result showed that around 20 sq. km of the area is suitable for any development.

Estimation of Trip Generation

The number of daily trips generated in each of the five zones was calculated using TransCAD software. A transit node for TOD was identified in the Kazhakuttom zone, where the number of daily trips was maximum.

TOD Design for the Transit Node

A transit stop along the National Highway (NH 66) in Kazhakuttom was selected as the potential node for TOD. The area surrounding the node was chosen for TOD design. The area was divided into concentric circles, i.e., the first 100m was considered a high-intensity conflict zone. Next zone would be 250m from the node, the third zone 350m, and the last zone 500m. The TOD plans for each zone were overlaid on the land use map with the help of GIS software (Fig. 12). The plans were given according to the standard TOD guidelines mentioned earlier.

Environmental Benefits

With the help of the above TOD design, optimum land use allocation can be achieved, thereby maximizing the public transit ridership. The high residential density close to the transit stop increases the ridership on public transportation systems. This reduces the number of people driving single-occupancy vehicles, decreasing air pollution and fuel conservation, thereby reducing the region's carbon footprint. The travel time can also be reduced considerably due to decreased traffic congestion.

CONCLUSION

The transportation challenges developing countries face, especially emerging economies, are manifold. Rapid population explosion, lack of infrastructure, and significant growth in the number of vehicles imply that radical approaches are needed in transportation planning. Transit Oriented Land use Development provides solutions to solve these issues. Benefits include improved safety, accessibility, convenience, and comfort in using public transport services and reducing carbon footprint.

The above research looked at five key settlements in Trivandrum city with growth potential from land use, traffic characteristics, and demographic perspective. The findings helped identify a transit node. The research shows that the trip generation of Kazhakuttom is highest when compared with the other zones. A transit station for the proposed MRTS was identified as a node for Transit Oriented Development based on its development potential. A detailed Transit Oriented

Development design adhering to the key TOD components and guidelines was formulated for the region surrounding the transit node.

The scope of this research was limited to providing the TOD design for one identified node. The same approach can be extended to other transit nodes along the corridor for holistic, integrated land use and traffic planning for the urban metro (Trivandrum).

Data Availability Statement

The datasets generated and analyzed during the current study are available from the corresponding author upon reasonable request.

ACKNOWLEDGMENT

The author sincerely thank Kerala State Remote Sensing and Environment Centre for providing the necessary research data. I extend my gratitude to the scientists of NATPAC for giving valuable input during the research work.

REFERENCES

- Alex, A.G., Basker, R. and Chettiyar, G. 2016. Effect of micro and nanoparticles in m-sand cement mortar. *Int. J. Civ. Struct. Res.*, 1(1): 67-76.
- Alex, A.G., Gebrehiwet Teweale, T., Kemal, Z. and Subramanian, R.B. 2022b. Flexural behavior of low calcium fly ash based geopolymer reinforced concrete beam. *Int. J. Concr. Struct. Mater.*, 16(1): 1-11.
- Alex, A.G., Gebrehiwet, T. and Kemal, Z. 2022a. Structural performance of low-calcium fly ash geo-polymer reinforced concrete beam. *Iran. J. Sci. Technol. Trans. Civ. Eng.*, 46(1): 1-12. <https://doi.org/10.1007/s40996-022-00832-x>.
- Bertolini, L., Le Clercq, F. and Kapoen, L. 2005. Sustainable accessibility: A conceptual fram integrated transport and land use plan-making: Two test applications in the Netherlands and flection on the way forward. *Transp. Policy*, 12(3): 207-220. doi: <https://doi.org/10.1016/j.tranpol.2005.01.006>.
- Burns, L.D. and Golob, T.F. 1976. The role of accessibility in basic transportation choice behavior. *Transportation*, 5(2): 175-198. doi: <https://doi.org/10.1007/BF00167272>
- Calthorpe, P., Yang, B. and Zhang, Q. 2014. *Transit-Oriented Development in China: A Manual of Land use and Transportation for Low Carbon Cities*. China Architecture and Building Press, Beijing.
- Cervero, R. 1997. Paradigm shift: from automobility to accessibility planning. *Urban Futures*, 22: 9.
- Cervero, R., Murphy, S., Ferrell, C., Goguts, N., Tsai, Y.H., Arrington, G.B.B. and Witenstein, N. 2004. *Transit-oriented development in the United States: Experiences, challenges, and prospects*. Washington, DC: Transportation Research Board of the National Academies.
- Curtis, C., Renne, J. and Bertolini, L. 2009. *Transit-oriented development: making it happen*. Farnham: Ashgate.
- Eboli, L. and Mazzulla, G. 2011. A methodology for evaluating transit service quality based on subjective and objective measures from the passenger's point of view. *Transp. Policy*, 18: 172-181. <https://doi.org/10.1016/j.tranpol.2010.07.007>
- Guowei, L., Luca, B. and Karin, P. 2020. How does transit-oriented development contribute to station area accessibility? A study in Beijing. *Int. J. Sustain. Transp.*, 14:7, 533-543. DOI: <https://doi.org/10.1080/15568318.2019.1578841>
- Handy, S.L. 2002. Accessibility- vs. mobility-enhancing strategies for addressing automobile dependence in the US. *Inst. Transp. Stud.*, 34: 645.
- Hansen, W.G. 1959. How accessibility shapes land use. *J. Am. Inst. Plan.*, 25(2): 73-76. doi: <https://doi.org/10.1080/01944365908978307>
- Krueger, R., Rashidi, T.H. and Rose, J.M. 2016. Preferences for shared autonomous vehicles. *Transp. Res. Part C Emerg. Technol.*, 69: 343-355.
- Levine, J., Merlin, L. and Grengs, J. 2017. Project-level accessibility analysis for land use planning. *Transp. Policy*, 53: 107-119. doi: <https://doi.org/10.1016/j.tranpol.2016.09.005>
- Müller, M. and Reutter, O. 2020. Benchmark: Climate and environmentally friendly urban passenger transport: The concepts of the European Green Capitals 2020-2010. *World Transp. Policy Pract.*, 26(2): 21-43.
- Papa, E. and Bertolini, L. 2015. Accessibility and transit-oriented development in European metropolitan areas. *J. Transp. Geogr.*, 47: 70-83. doi: <https://doi.org/10.1016/j.jtrangeo.2015.07.003>
- Rajakumari, M. 2008. *Integration of Land Use with Transportation Planning for a Sustainable City-Approach through Transit Oriented Development*. Proceedings of International Conference on Best Practices to Relieve Congestion on Mixed-Traffic Urban streets in Developing Countries, 12-14 September 2008, IIT Madras, Chennai, pp. 15-36.
- Shiliang, S., Hui, Z., Miao, W., Min, W. and Mengjun, K. 2020. Transit-oriented development typologies around metro station areas in urban china: A comparative analysis of five typical megacities for planning implications. *J. Transp. Geogr.*, 2: 39. <https://doi.org/10.1016/j.jtrangeo.2020.102939>.
- Sraatemeier, T. and Bertolini, L. 2020. How can planning for accessibility lead to more integrated transport and land use strategies? Two examples from the Netherlands. *Euro. Plan. Stud.*, 28(9): 1713-1734. DOI: <https://doi.org/10.1080/09654313.2019.1612326>
- Turnheim, B., Asquith, M. and Geels, F.W. 2020. Making sustainability transitions research policy-relevant: Challenges at the science-policy interface. *Environ. Innov. Soc. Trans.*, 34: 116-120. <https://doi.org/10.1016/j.eist.2019.12.009>
- Vakayil, A., Gruel, W. and Samaranyake, S. 2017. *Integrating Shared-Vehicle Mobility-On-Demand Systems with Public Transit*. Transportation Research Board, US.
- Wegener, M. 2020. Are Urban Land use Transport Interaction Models Planning Support Systems? In Geertman, S. and Stillwell, J. (eds.), *Handbook of Planning Support Science*, Edward Elgar Publishing, Cheltenham, UK, pp. 153-160. <https://doi.org/10.4337/9781788971089.00017>
- Xu, W.A., Guthrie, A., Fan, Y. and Li, Y. 2017. Transit-oriented development: Literature review and evaluation of TOD potential across 50 Chinese cities. *J. Transp. Land Use*, 10(1): 743-762. doi: <https://doi.org/10.5198/jtlu.2017.1217>.
- Yap, M.D., Correia, G. and van Arem, B. 2016. Preferences of travellers for using automated vehicles as the last mile public transport of multimodal train trips. *Transp. Res. Part A Policy Pract.* 94, 1-16.
- Yeung, J.S., Wong, Y.D. and Secadiningrat, J.R. 2015. Lane-harmonized passenger car equivalents for heterogeneous expressway traffic. *Transp. Res. Part A Policy Pract.*, 78: 270-361.



Environmental Efficiency Evaluation in Vietnam Textile and Garment Industry: Super-SBM Model with Undesirable Output Approach

Phung Mai Lan*† and Nguyen Khac Minh**

*Thuyloi University, 175 Tay Son, Dong Da, Hanoi, Vietnam

**IMAS, Thang Long University, Nghiem Xuan Yem, Dai Kim, Hoang Mai, Hanoi, Vietnam

†Correspondence author: Phung Mai Lan; lanpm@tlu.edu.vn

Nat. Env. & Poll. Tech.
Website: www.neptjournal.com

Received: 06-10-2022

Revised: 11-12-2022

Accepted: 14-12-2022

Key Words:

Environmental efficiency
Super-SBM DEA model
Undesirable output
Textile and garment industry

ABSTRACT

The purpose of the paper is to estimate the environmental efficiency of the Vietnamese textile and garment industry and evaluate the impact of the factors on environmental efficiency. The study uses firm-level panel data from the Vietnam annual enterprise survey data for the 2012–2018 period in the Vietnam textile and garment industry to evaluate the environmental efficiency by using the Super-SBM DEA model with undesirable output and applies the Tobit regression model to measure the impact of the factors on the environmental efficiency. This study evaluates environmental efficiency and assesses the impact of some core factors, including the origin of imported machinery and equipment, the origin of imported materials, the management of industrial zones, and the presence of FDI firms, on environmental efficiency at the firm level. The results indicate that the average score for environmental efficiency is 0.233. Some factors, such as income per employee, machined goods imported from developed countries, industrial zones, firm improvement processes, and the presence of FDI, have a positive impact on a firm's environmental efficiency, whereas materials made in Vietnam have a negative impact.

INTRODUCTION

After 35 years of implementing an economic renovation policy (known as *Doi Moi*), launched in 1986, Vietnam has made notable economic achievements. Vietnam's GDP grew from \$6.472 billion in 1990 to \$343 billion in 2020. Vietnam's economic structure is shifting toward modernization, with agriculture contributing less and industrial and service production contributing more. Exports have frequently experienced rapid growth, especially in manufactured goods such as textile and garment products, food products, footwear, electrical machinery, and equipment. However, with the high growth of Vietnam's industry, the country is facing high energy consumption and high carbon dioxide emissions, which have resulted in environmental pollution and climate change. The textile and garment industry plays an important role in Vietnam's economic growth, contributing 10% of industrial production value, supporting nearly 3 million jobs in Vietnam, and ranking third worldwide in exports with a value of about \$36 billion in 2020. However, for various textile manufacturing processes, this industry relies on the use of a large amount of water, energy, and toxic chemicals, resulting in a variety of waste streams, including gaseous, liquid, and solid forms. Vietnam has about 180 firms operating in the field of dyeing and finishing textiles: 70

floral print lines, 200 dyeing lines, 750 dyeing machines, and about 100 yarn dyeing machines. However, the technology level in the dyeing industry is about 15–20 years lower in comparison with other countries in the area. In Vietnam, the amount of chemicals used in textile and dyeing firms ranges between 500 and 2,000 kg per ton of product. Therefore, the textile and garment industry has become one of the most polluted industries in Vietnam. To sustain economic growth in conditions of environmental protection for the industry, evaluation of the environmental pollution effects, analysis of the factors that influence environmental efficiency, and provision of the scientific basis for environmental efficiency improvement are required.

Under consideration for environmental efficiency measurement, there are two main methods used in previous literature: parametric Stochastic Frontier Analysis (SFA) and non-parametric Data Envelopment Analysis (DEA). The DEA method, developed by Charnes et al. (1978), is better suited for efficiency evaluation because it does not require prior assumptions about the production function and can handle multiple inputs and outputs at the same time (Cooper et al. 2007, Asmild et al. 2004, Pulina et al. 2010). Standard DEA models provide a radial input-oriented or output-oriented efficiency measurement. When some undesirable

inputs or outputs (e.g., pollutants, emissions, or wastes) occur in the model, the undesirable outputs or undesirable inputs should be adjusted to improve efficiency. As a result, evaluating efficiency becomes a difficult problem when environmental pollutants are present in the model, especially when these pollutants do not have the same proportions of increase or decrease with inputs or outputs. Based on DEA models, there are a number of methods being developed to handle undesirable outputs, such as the BCC (Banker, Charnes, and Cooper) model (Fare et al. 1989, Seiford & Zhu 2002), the SBM (slack-based measure) (Chu et al. 2018, Tone 2002, Zhang & Kim 2014), the additive DEA model (Charnes et al. 1985) and the super-SBM efficiency model (Tone 2004, Li et al. 2013). Fare et al. (1989) made two modifications to the standard Farrell approach, which allows the expansion of good outputs and the contraction of bad outputs using a single scalar to make the measure nonlinear. However, this study does not consider the positive effects of decreasing the environmental pollution. Hailu & Veeman (2001) applied non-parametric analysis as extended by the Chavas-Cox approach to calculate environmental efficiency. They treat undesirable outputs as input variables and handle the issue to decrease the undesirable outputs and maximize desirable outputs. Based on the standard linear BCC DEA model of Banker et al. (1984), Seiford & Zhu (2002) evaluated the environmental efficiency by converting the undesirable output's negative number into a positive input through vector transformation. Fare et al. (2003) proposed an output-oriented distance function to estimate energy efficiency by using output and input forms, but the problem of the slack variables was not explained. Tone (2002) proposed a non-oriented efficiency evaluation model called the Slack-Based Model (SBM). Tone (2002) can deal with the slack variables, but this study does not consider the undesirable outputs. Tone (2004) and Li et al. (2013) then propose the super-SBM model to evaluate environmental efficiency. The super-SBM has an advantage due to its higher discriminating ability when dealing with slack variables and undesirable outputs. These studies mainly focus on measuring environmental efficiency, and some of them initially evaluate factors affecting environmental efficiency at the macro level (Li et al. 2013, Honma 2015, Grigoroudis & Petridis 2018). While many core factors at the firm level, including the origin of imported machinery and equipment, the origin of imported materials, the management of industrial zones, and the presence of FDI firms, are not discussed.

As mentioned above, the textile and garment industries are one of the most polluted industries in Vietnam. Support policies for exporting textile and garment products may increase exports and economic growth while increasing pollution in the industry if no other environmental policies are in place. Previous studies have only focused on factors

that affect pure efficiency, leaving out environmental efficiency, which is critical for the long-term development of the Vietnam textile and garment industry. To investigate the impact of these factors on environmental efficiency at the firm level, in this paper, the Super-SBM model with undesirable outputs is used to calculate environmental efficiency in Vietnam's textile and garment industry, and then the Tobit regression model is applied to evaluate the factors affecting environmental efficiency based on Vietnam-specific conditions. To examine whether the efficiency scores vary among different groups (firm scales, regions), the Kruskal-Wallis rank test is used. This paper is believed to provide support for the government's issuing appropriate policies relating to environmental protection in the sustainable development of Vietnam's textile and garment industry.

MATERIALS AND METHODS

Super-SBM Model for Efficiency Evaluation

Each firm in the textile and garment industry is called a decision-making unit (*DMU*). Suppose having n decision-making units (n *DMUs*). There are three factors in each unit: input, desired outputs, and undesirable outputs (environmental pollution, CO₂, ...), defined by three vectors $x \in R^m$, $y^g \in R^{s_1}$, $y^b \in R^{s_2}$, respectively. The matrices X , Y^g , and Y^b are defined as follows:

$$X = [x_1, x_2, \dots, x_n] \in R^{m \times n}$$

$$Y^g = [y_1^g, y_2^g, \dots, y_n^g] \in R^{s_1 \times n},$$

$$Y^b = [y_1^b, y_2^b, \dots, y_n^b] \in R^{s_2 \times n},$$

It is assumed that $X > 0$, $Y^g > 0$, and $Y^b > 0$. According to Banker et al. (1984), the production possibility set is defined as:

$$P = \{(x, y^g, y^b) \mid x \geq X \lambda, y^g \leq Y^g \lambda, y^b \geq Y^b \lambda, \lambda \geq 0, e\lambda = 1\},$$

Where, $\lambda \in R^n$ and e is a row vector with all elements equal to 1.

The SBM model with undesired outputs to evaluate the *DMU* (x_0, y_0^g, y_0^b) is as follows (Tone 2004):

[SBM -Undesirable]

$$\rho^* = \min_{s^-, s^b, s^g, \lambda} \left\{ \frac{1 - \frac{1}{m} \sum_{i=1}^m \frac{s_i^-}{x_{i0}}}{1 + \frac{1}{s_1 + s_2} \left(\sum_{r=1}^{s_1} \frac{s_r^g}{y_{r0}^g} + \sum_{r=1}^{s_2} \frac{s_r^b}{y_{r0}^b} \right)} \right\} \dots (1)$$

Subject to. $x_0 = X \lambda + s^- \dots (2)$

$y_0^g = Y^g \lambda - s^g \dots (3)$

$y_0^b = Y^b \lambda + s^g \dots (4)$

$s^- \geq 0, s^g \geq 0, s^b \geq 0, \lambda \geq 0, e\lambda=1 \dots (5)$

Where s^- and s^b correspond to excesses in inputs and undesirable outputs, respectively, while s^g indicates shortages in desirable outputs, λ is the intensity vector. The target function value of ρ^* is the environmental efficiency value (EE*) of DMU (x_0, y_0^g, y_0^b) .

The equation (1) - (5) is a nonlinear programming problem with the nonlinear objective function in s^-, s^g, s^b and with the constraints of the linear presented in (2) - (5). The minimum value of the objective value function satisfies $0 < \rho^* < 1$. DMU (x_0, y_0^g, y_0^b) is SBM efficiency with undesirable outputs if and only if $\rho^* = 1$, that is, $s^- = 0, s^g = 0, s^b = 0$. If $\rho^* < 1$, that means the DMU is inefficient.

Problem (1) - (5) is a nonlinear programming problem. By using the Charnes-Cooper transform (Charnes 1952), it can be transformed into a linear programming problem. An equivalent linear programming problem in t, v, s^-, s^g and s^b is constructed as follows:

$[LP] \theta^* = \min_{s^-, s^g, s^b, t, v} \left\{ t - \frac{1}{m} \sum_{i=1}^m \frac{S_i^-}{x_{i0}} \right\} \dots (6)$

Subject to $1 = t + \frac{1}{s_1 + s_2} \left[\sum_{r=1}^{s_1} \frac{S_r^g}{y_{r0}^g} + \sum_{r=1}^{s_2} \frac{S_r^b}{y_{r0}^b} \right] \dots (7)$

$x_0 t = X v + s^- \dots (8)$

$y_0^g t = Y^g v - s^g \dots (9)$

$y_0^b t = Y^b v + s^g \dots (10)$

$s^- \geq 0, s^g \geq 0, s^b \geq 0, v \geq 0, t > 0 \dots (11)$

As shown by Cooper et al. (2007), since $(t^*, v^*, s^-, s^g, s^b)$ is the optimal solution of the equation (6)-(11) the optimal solution of [SBM-Undesirable] as defined by

$\rho^* = \theta^*, \lambda^* = v^* / t^*, s^{-*} = S^{-*} / t^*, s^{g*} = S^{g*} / t^*, s^{b*} = S^{b*} / t^*$

Kruskal-Wallis Rank Test to Examine the Difference of the Environmental Scores Among Groups

To test this stability hypothesis, the study uses the Kruskal-Wallis non-parametric ANOVA test (Brockett & Levine 1984). There are simultaneously N "overall" (firms) under consideration and the original hypothesis (Ho) is that all N

totals have the same score distribution. Firstly, ranking the set of $N.k$ points in ascending order (equal positions are also taken in the middle-rank position) and the symbol R_j is the sum of the rank positions corresponding to the DMU (bank). Then, the Kruskal-Wallis test is calculated as follows:

$H = \frac{12}{N \cdot k \cdot (N \cdot k + 1)} \cdot \left(\frac{R_1^2}{k} + \frac{R_2^2}{k} + \dots + \frac{R_N^2}{k} \right) - 3 \cdot (N \cdot k + 1) \dots (12)$

$H \sim \chi_{N-1}^2$ with $N-1$ degrees of freedom. If χ_{N-1}^2 larger than χ_{N-1}^2 at the desired significance level, the null hypothesis of the distribution of efficiency ratings similar to all DMUs is rejected at given the significance level.

Tobit Regression Model for Evaluating Factors Affecting the Environmental Efficiency

After estimating environmental efficiency from the Super-SBM model, the study explores factors affecting on environmental efficiency, especially factors restricting efficiency. Traditional OLS methods may have the problem of asymmetry or inconsistency when dealing with censored or truncated data as environmental efficiency. To solve problems with limited dependent variables and investigates the determinants of truncated variables such as environmental efficiency, the study applies the Tobit model proposed by Tobin (1958). The standard model is as follows:

$y_i^* = \beta X_i + \mu_i; \mu_i \sim N(0, \sigma^2), i = 1, 2, \dots, n, \dots (13)$

Where n is the number of observations, i is the i^{th} DMU, y_i^* is a latent variable, X_i is a $K \times 1$ matrix of independent variables, μ_i is an independently-distributed error, which is assumed $N(0, \sigma^2)$ distribution. β is a vector of unknown coefficients. The limited sample value y_i is:

$y_i = \begin{cases} y_i^*, & y_i^* > 0 \\ 0, & y_i^* \leq 0 \end{cases} \dots (14)$

DATA AND ESTIMATED RESULTS

Data

The data used in the study are collected from two surveys: the Annual Enterprise Survey and the technology survey conducted by the General Statistics Office (GSO) which was obtained from 2012 to 2018 (The most updated data in the present). These two sets of data are grouped together into a set of survey data which included both firm technology activities and general information about firm characteristics, financial accounts, and energy consumption. The firms which don't report energy consumption, total wages, assets, number of workers, and revenue are not positive or in the case of

incomplete replies are also dropped. Variables in monetary values are calculated in VND millions and adjusted for various years using annual inflation rates. After removing the firms in other industries and generating balanced datasets of Vietnam's textile and garment industry, the database includes 324 firms in Vietnam's textile and garment sector (2.268 observations in total over the 2012-2018 period).

Environmental Efficiency in Vietnam Textile and Garment Industry

Inputs and outputs used for the Super-SBM model: Capital and labor are the most important production inputs in terms of input variables. In most studies, real capital stock (K), as measured by total fixed assets - depreciation (Mil. VND), is a desirable indicator for capital investment. The number of firm employees at the end of each year is used as an indicator of labor input (L) (Person). Each firm must use one or more sources of energy (such as coal, oil, gasoline, ...) to meet production needs. Each category of used energy has different technical parameters, making it difficult to assess a firm's total energy consumption. To solve the above problem, the unit "Ton Oil Equivalent - TOE (Ton Oil Conversion)" was counted as the common standard for various energy category evaluations. The TOE unit was used in the research referred to in document No. 3505/BCT-KHCN, April 19, 2011. The consumption quantity of the four major energy sources of firms is converted into a unified unit

of TOE, including coal, oil, natural gas, and gasoline. The measurement unit of energy input is set as "tons of standard TOE". In the paper, TOE is used as an energy input variable for the Super-SBM model.

For the output indicators, value-added (VA), desirable output, is defined as the value of gross output subtract from intermediate inputs. Based on the factor income approach, in this study, value-added is determined by the incomes of labor and capital separately in which, capital income is defined as the sum of firm depreciation and total profit. CO₂ emission (*Emis*) is considered an undesirable output. In fact, there is less detailed data on CO₂ emissions for each firm in Vietnam. Therefore, the calculation of CO₂ emissions from firm energy consumption is based on the IPCC reference approach (IPCC 2006) and Chen et al. (2010). Firm CO₂ emission from energy consumption (coal, oil, natural gas, gasoline) is constructed as follows:

$$CO_{2t} = Emis_t = \sum_{i=1}^4 Emis_{i,t} = \sum_{i=1}^4 Eng_{i,t} * NCV_i * CEF_i * COF_i * \left(\frac{44}{12}\right) \quad \dots(15)$$

Where, $CO_{2t} = Emis_t$ = flow of carbon dioxide with the unit of tons, NCV_i (TJ/Gg) = net calorific value provided by 2006 National Greenhouse Gas Inventories in IPCC (2006), CEF_i (ton/GJ) = carbon oxidization factor provided by IPCC (2006), COF_i is the carbon oxidization factor set to be 1 in this study. (44/12) is the molecular weight ratio of CO₂ to carbon. Therefore, based on equation (15), the calculated

Table 1: Descriptive statistics of some input and output variables from 2012 to 2018.

Variables	Input variables			Output variables	
	K (capital) (Mil. VND)	L (labor) (Persons)	TOE (Ton Oil Equivalent) (tons)	VA (Value -added) (Mil. VND)	CO ₂ (CO ₂ emissions) (tons)
	x_1	x_2	x_3	y^g	y^b
Mean	102496.1	844.827	2467.79	15871.1	5318.004
Std.Dev.	689659.5	1348.126	34672.92	40385.24	67600.43
Maximum	2.18e+07	10656	1061269	782315.6	2.40e+09
Minimum	93.278	4	0.0102	55.32	32.672
Skewness	26.44	2.943	26.605	10.076	28.444

Source: the author estimates from annual surveys of GSO.

Table 2: Pearson correlation of input and output variables.

Correlation	K	L	TOE	VA	CO ₂
K	1.0000				
L	0.1988***	1.0000			
TOE	0.8221***	0.1121***	1.0000		
VA	0.7638***	0.6360***	0.7556***	1.0000	
CO ₂	0.9110***	0.1211***	0.9519***	0.7391***	1.0000

*** p<0.01. Source: the author estimates from annual surveys of GSO.

CO₂ emission for coal is 2.259 (ton CO₂/ton coal), for oil 3.153 (ton CO₂/ton oil), for natural gas 2.983 (ton CO₂/1000 m³ natural gas) and for gasoline 3.069 (ton CO₂/1000 liter).

Table 1 reports summary statistics for Vietnam's Textile and garment industry in the period 2012-2018. In general, the value of variables increases over the years. Especially, the growth rates of value-added are higher than those of capital and labor variables (an increase of 159% in 7 years). However, TOE consumption and CO₂ emission are at a very high growth rate (334% and 298% in 7 years, respectively).

Table 2 shows the correlation between input and output variables. The Pearson coefficient results show that there is a positive correlation between inputs and outputs. There is a high correlation between energy input TOE and desirable outputs (VA), and undesirable outputs (CO₂), reaching 0.7556, and 0.9519, respectively. Therefore, the measurement of efficiency using the Super-SBM model is quite reliable in the sample of Vietnam textile and garment industry

Evaluating environment efficiency of textile and garment firms: The efficiency result calculated from the Super-SBM model is used as independent variables to measure the impact of factors on environmental efficiency by using the Tobit regression model. Table 3 provides a summary statistics of

environmental efficiency in Vietnam's textile and garment sector.

The estimation results show a slight decrease in average efficiency over time, with a value of 0.233 on average. In this case, FDI firms' environmental efficiency is 27.9%. The results are lower than the findings of Duong (2016) in Vietnam's textile industry that the technology efficiency without undesirable outputs estimated by Stochastic Frontier Analysis (SFA) is 63.4% for export FDI firms and 47.4% for non-export FDI firms from 2009 to 2013. The results are also lower than the environmental efficiencies estimated by Hongqi et al. (2013) in China's manufacturing industry from 2002 to 2009, with an efficiency score of 0.298. In recent years, although Vietnam has issued some regulations relating to restructuring industrial, protecting the environment, and decreasing the emissions, such as Vietnam's National Energy Development Strategy, the Revised National Power Development Plan (PDP) for 2011-2020, the Law on Environmental Protection, and the National Action Programme on Reduction of GHG Emissions, its enforcement capacity is still weak. Therefore, environmental efficiency has not improved. Being one of the leading export industries with a high growth rate, the entrants of much more textile and garment firms can tend toward higher levels of TOE consumption and CO₂ emission.

Table 3: Environmental efficiency of Vietnam's textile and garment sector.

Variables	2012-2018	2012	2014	2016	2018
Environmental Efficiency (EE)					
Mean	0.233	0.346	0.283	0.230	0.215
Std.Dev.	0.258	0.326	0.205	0.267	0.258
Skewness	1.694	0.972	1.757	1.427	1.740
Observations	2,268	324	324	324	324
Environmental Efficiency (EE) by scales					
Micro and small-sized firms	0.170	0.302	0.259	0.139	0.136
Medium-sized firms	0.121	0.264	0.175	0.059	0.104
Large-sized firms	0.255	0.384	0.313	0.298	0.271
Environmental Efficiency (EE) by ownership					
FDI firms	0.279	0.385	0.323	0.294	0.269
Domestic firms	0.189	0.308	0.242	0.166	0.163

Source: the author estimates from annual surveys of GSO.

Table 4: Environmental efficiency by the origin of imported technology.

Type of firms	EE	CO ₂ (Ton)	TOE (Ton)	CO ₂ /TOE
Firms with main technology imported from developed countries	0.252	6030.853	2938.23	2.05
Firms with main technology imported from developing countries	0.189	1736.189	717.27	2.42
Total sample	0.233	5318.004	2467.79	2.15

Source: the author calculates from annual surveys of GSO.

In general, average environmental efficiency for all scales decreases dramatically over the same time period, particularly for micro and small-sized businesses in which, the efficiency of large-sized firms is always higher than the industry's average level (25.5%). Larger firms are both energy and emission-intensive compared to medium-sized firms. The result is similar to the analysis by Lee & Yu (2019), and Sabtosh & Deepanjali (2019). Large-sized firms with more sophisticated technology can organize production activities more rationally to decrease CO₂ emissions and gain higher environmental efficiency.

Table 4 shows environmental efficiency by the origin of imported technology. Of the total firms under consideration, firms with main technology imported from developed countries accounted for 58.3% (The ratio of FDI firms is over 77%) and gain environmental efficiency much larger by 133% than the others.

Equipment imported from developed countries with a larger scale has used a larger number of TOE and emitted much more CO₂ than equipment imported from developing countries. However, the level of CO₂ emission per TOE unit (2.05) of the firms with a main machine imported from developed countries is lower than those imported from developing countries (2.42), machines imported from developed countries tend to be more environmental efficiency due to better environmental standards and regulations.

Evaluating the Impact of Factors on Textile and Garment Firms' Environmental Efficiency

The Suggestion of Experimental Model Based on the Tobit Regression Model

The theoretical model mentioned above (model 13) is expressed in the following econometric model:

$$EE_{it}^* = \beta_1 * \ln KL_{it} + \beta_2 * \ln LC_{it} + \beta_3 * \ln Trade_{it} + \beta_4 * Machine_dep_{it} + \beta_5 * Mater_dep_{it} + \beta_6 * Mater_VN_{it} + \beta_7 * FDI_{it} + \beta_8 * Improve_{it} + \beta_9 * Industry_zone_{it} + \beta_{10} * North_i + \beta_{11} * South_i + i.Scale_{it} + i.Year + \mu_i \quad \dots(16)$$

Dependent Variables:

EE_{it}^* : Environmental Efficiency of firm i in the year t , which is estimated from Super-SBM model with undesirable outputs.

Independent Variables:

$\ln KL_{it}$: The log of capital intensity, measured by capital stock per employee of the i^{th} firm in the year t . An increase in capital intensity is assumed to increase the labor productivity since more capital per employee is available.

$\ln LC_{it}$: The log of human capital, measured by total wages and training costs per employee of the i^{th} firm in the year

t . An increase in human capital increases production scale and increases the capability of firms' entering the industry or stay in the industry.

$\ln Trade_{it}$: The log of trade openness, trade openness is measured by the total of exports and imports value of the i^{th} firm. Trade openness reflects the engagement of the i^{th} firm in the global trading system in the year t . The net effect of high trade intensity in the world can tend to generate a positive effect on emissions from developing countries as found by Managi et al. (2009).

$Machine_dep_{it}$: Dummy variable having a value of 1 if the most important machine of the i^{th} firm i , in the year t is imported from developed countries and has a value of 0 if otherwise. Due to better environmental standards and regulations, machines imported from developed countries tend to be more environmental efficiency. This can reduce pollution in developing countries (Perkins & Neumayer 2009). Therefore, an increase in $machine_dep_{it}$ is expected to reduce undesirable outputs and improve the firm's environmental efficiency.

$Mater_dep_{it}$: Dummy variable having a value of 1 if the most important materials of the i^{th} firm, in the year t , are imported from developing countries and having a value of 0 if otherwise. $Mater_VN_{it}$: Dummy variable having a value of 1 if the most important materials of the firm i , in the year t , are produced in Vietnam and having a value of 0 if otherwise. Using materials from developing countries with a higher level of emission may affect negatively on environmental efficiency (Perkins & Neumayer 2009).

FDI_{it} : Dummy variable having a value of 1 if the i^{th} firm, in the year t , is a foreign-owned firm, having a value of 0 if otherwise. Some research finds that the presence of FDI firms that bring new and advanced technologies into developing countries can improve environmental efficiency while some other studies have suggested that FDI firms can produce higher levels of pollution in developing countries.

$Improve_{it}$: Dummy variable having a value of 1 if the firm i , in the year t , implements activities for manufacturing process improvement, having a value of 0 if otherwise.

$Industry_zone_{it}$: Dummy variable having a value of 1 if the firm i , in the year t , is in an industrial zone, having a value of 0 if otherwise.

$North_i$: Dummy variable having a value of 1 if the firm i , in the year t , is in the North of Vietnam, having a value of 0 if otherwise.

$South_i$: Dummy variable having a value of 1 if the firm i , in the year t , is in the South of Vietnam, having a value of 0 if otherwise.

Scale_{it}: Scale represents for firm's size. The scale has a value of 1 if firm *i*, in the year *t*, is a micro-sized enterprise (less than 10 people employed), having a value of 2 if firm *i* is a small-sized enterprise (less than 100 persons employed), having a value of 3 if the firm *i* is a medium-sized enterprise (less than 200 people employed), having a value of 4 if the firm *i* is large – sized enterprise (200 or more person employed). According to Klepper (2002), larger entrants have higher survival rates. As such, the firms generate higher profits, allocate more resources to research and development, and grow faster.

Table 5 shows the estimation results of influence factors on environmental efficiency by using the Tobit regression model. Evaluating the impact of variables characterized by firms can show that the *lnLC* variable is positive. When income per employee increases by an average of 1%, the environmental efficiency of the firms increases by 0.0304%. Raising employee incomes is an important factor in improving the quality of labor and improving the productivity of the labor force as well as the firm's environmental efficiency. The estimated coefficient of *lnKL* (capital intensity) is negative and statistically significant. This indicates that firms' capital intensity is inefficient. An increase of capital intensity at 1% will cause a decrease of 0.0559% in the enterprises' environmental efficiency. The capital-intensity is always expected to have a positive effect on environmental efficiency, but the negative sign of this variable indicates that capital intensity has not reached the expected results. The cause behind it may be that although the level of capital per worker increased but the capital intensity does not increase accordingly. Combined with an evaluation of the origin of imported machines, it appears that high-tech equipment imported may not be fully exploited. The cause of this phenomenon is that the management level has not fully responded to modern technology or equipment is not synchronous. *Ln_trade* variable is not statistically significant in the model. Trade openness has no significant influence on environmental efficiency.

The estimated coefficient of *Machine_deped* is positive and statistically significant. That means more machines imported from developed countries will increase the efficiency level of this sector. The result is similar to the findings of Perkins & Neumayer (2009), Li et al. (2013). Machine imported from developed countries tends to be more environmental efficiency due to better environmental standards and regulations. Therefore, using technology imported from developed countries can reduce undesirable outputs and improve a firm's environmental efficiency compared to technology imported from developing countries. This level of CO₂ emission per TOE unit (2.05) is lower than machines imported from developing countries (2.42). In fact,

the Vietnam government issues many related preferential policies of environmental protection in order to reduce CO₂ emissions from the firm's production process.

From the results estimated in Table 4., the coefficient of *Mater_deping* is negative but not statistically significant, while the coefficient of *Mater_VN* is also negative but statistically significant at 1%. Using materials from developing countries with a higher level of emission may affect negatively environmental efficiency. Therefore, firms' consciousness of environmental protection needs to be improved, especially in the process of importing equipment and materials.

The sign of the FDI variable is positive and statistically significant. The presence of FDI firms with updated technology can bring benefits to this sector, such as a decrease in CO₂ emission, and stimulating competition

Table 5: The estimation results of the Tobit regression model (Model 15).

Dependent variable: Environmental Efficiency			
VARIABLES	Tobit model	VARIABLES	Tobit model
lnKL	-0.0559*** (0.00747)	2. Scale	-0.337*** (0.0346)
lnLC	0.0304*** (0.00750)	3. Scale	-0.357*** (0.0427)
ln_trade	-9.24e-05 (0.00168)	4. Scale	-0.297*** (0.0468)
Machine_deped	0.0208* (0.0120)	13. year	-0.190*** (0.0140)
Mater_deping	-0.00254 (0.0155)	14. year	-0.0704*** (0.0142)
Mater_VN	-0.0401*** (0.0150)	15. year	-0.187*** (0.0143)
FDI	0.0575** (0.0232)	16. year	-0.125*** (0.0164)
Improve	0.0251** (0.00990)	17. year	-0.0331 (0.0214)
Industry_zone	0.0350** (0.0142)	18. year	-0.136*** (0.0217)
North	-0.0137 (0.0386)	Constant	0.981*** (0.0688)
South	-0.0233 (0.0406)	sigma_u	0.167*** (0.00880)
Constant	0.981*** (0.0688)	sigma_e	0.177*** (0.00300)
Observations	2,268	rho	0.472

Standard errors in parentheses *** p<0.01, ** p<0.05, * p<0.1
Source: the author estimates from annual surveys of GSO.

within the industry. This high competitiveness will force domestic firms to either apply updated technology, and new management method or employ the existing resources more efficiently, which increase firms' environmental efficiency in this industry. The result is similar to the findings by Marques & Caetano (2020), and Demena & Afesorghor (2020) which show that FDI significantly reduces environmental emissions and improves energy usage efficiency.

The relationship between firm process improvement and environmental efficiency is a positive correlation, which means firm regulation and process renovation can increase efficiency. The Vietnam government has issued many regulations and policies to promote environmental protection technology innovation. These bring more advantages to the firm's process improvement to save the cost of materials and reduce TOE consumptions. Firm environmental efficiency, therefore, is improved.

With more than 325 industrial zones in Vietnam, the industrial zone's influence on environmental efficiency (*Industry_zone*) is positive and statistically significant for the whole country. By 2013, 173 industrial zones had been established, with an average of 90 firms in each zone, the Vietnam government passed basic environmental legislation but regulation and enforcement capacity for implementation was weak. The fast-paced economic development in the industrial zone depended on the high consumption of natural gas, oil, and especially coal, resulting in a rapid increase in CO₂ emissions. As a result, approximately 70% of firms in industrial zones have a high level of CO₂ emissions. Since 2013, the United National Industrial Development Organization (UNIDO) and Vietnam Ministry of Planning and Investment, with support from many international organizations such as Global Environmental Facility (GEF), The U.S. Agency for International Development (USAID), Vietnam tends to implement an eco-industrial park for sustainable industrial zones in Vietnam with many projects such as increasing the transfer, development, and innovation of clean and low-carbon technologies, improving production process for the minimization of CO₂ emission, managing the chemicals as well as raised firm awareness on making optimum use of materials, minimizing environmental pollution. Therefore, the textile and garment firms located in industrial zones can improve environmental efficiency more than other firms.

The region variables (*North*, *South*) have no significant influence on environmental efficiency. The government should focus on regulations to promote environmental protection and develop a sustainable economy oriented by regions.

Compared with micro-scale firms, the others with a larger scale of production tend to impact more negatively

on environmental efficiency. In which, large-scale firms tend to be more efficient than small-scale and medium-scale firms. Large-scale firms applying advanced technology and developing actionable solutions to effectively reduce CO₂ emissions and improve firms' environmental efficiency.

Remarkably, the coefficients of time control variables are all taking negative signs with statistical significance (except for the years of 2017). The government policies to control CO₂ emissions from the textile and garment industry are still weak. As a result, they have no significant influence on environmental efficiency.

Kruskal-Wallis Rank Test to Examine the Differences of Environmental Efficiency Among Sizes and Regions

Table 6 shows the results of the Kruskal-Wallis rank test by size. From the above analysis, it can be seen that the environmental efficiency was different among sizes: Micro-sized firms (n=68); Small-sized firms (n=576); Medium-sized firms (n=224); Large-sized firms (n=1380). The Kruskal-Wallis non-parametric test is used to verify the results of this empirical analysis.

Kruskal-Wallis H test shows that there was a statistically significant difference in environmental efficiency between four scale groups, $\chi_3^2 = 205.685$, Pvalue = 0.0001, allowing rejecting the H₀ hypothesis about the distribution of the same environmental efficiency ranking of four scale groups. Similarly, there was a statistically significant difference in environmental efficiency between the three regions, $\chi_2^2 = 14.921$, Pvalue = 0.0006.

Sensitivity Analysis

Sensitivity analysis is a very important aspect of the super-SBM DEA model to evaluate the robustness of the results. Since super-SBM DEA results can depend on user input and output sets and the results can be changed by any error in the dataset. Sensitivity analysis is examined to see how environmental efficiency through the super-SBM DEA model changes when using different input and output options.

The original model used the super-SBM DEA model, where three inputs and two outputs were selected and called

Table 6: The results of the Kruskal-Wallis rank test by sizes.

Scale of firms	Observation 2012-2018	Rank sum 2012-2018
Micro-sized firms	68	88354
Small-sized firms	576	504300.50
Medium-sized firms	244	211143.50
Large-sized firms	1,380	1.77e+06

Source: the author estimates from annual surveys of GSO.

Table 7: Environmental efficiency value analysis of different indicator combinations.

Overall efficiency	Model M_0	Model M_1
Environmental Efficiency	0.233	0.226

the M_0 model, comprising the three inputs: X_1 : capital, X_2 : labor and X_3 : TOE and two outputs: Y_1 : VA; Y_2 : CO_2 . The other model to be compared to M_0 model was called the M_1 model, comprising the three inputs: X_1 : capital, X_2 : labor, and X_3 : TOE and two outputs: Y_1 : GO; Y_2 : CO_2 . Table 7 shows the environmental efficiency results estimated M_0 model and M_1 model.

Fig. 1 shows changes in environmental efficiency during the study period. The environmental efficiencies in the two models are quite similar.

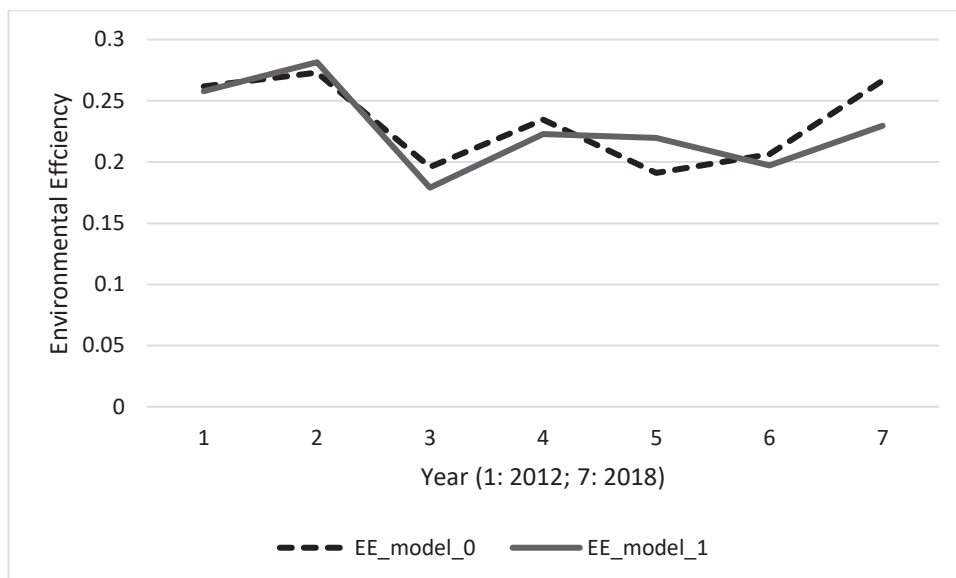
CONCLUSION

This study applied the Super-SBM DEA model, considering undesirable outputs, to estimate the environmental efficiency of the Vietnam textile and garment industry in the period 2012-2018. Then, the Tobit regression model is used to measure the impact of factors on environmental efficiency and test the stability of environmental efficiency rankings by using the Kruskal-Wallis H test. The empirical results show that (i) there has been a slight decrease in environmental efficiency over the years, at an average of 23.3%. (ii) Some factors, such as income per employee, machined imports from developed countries, industrial zones, firm

improvement processes, and the presence of FDI, have positive effects on a firm's environmental efficiency, while materials made in Vietnam have a negative influence. (iii) There are great differences in environmental efficiency between the four scale groups. In which large-scale firms tend to be more efficient than small- and medium-scale firms. (iv) The government's policies to control CO_2 emissions from the textile and garment industry are still weak.

In conclusion, some suggestions for increasing environmental efficiency in the textile and garment industry are given as follows:

- (i) Increase the attractiveness of industrial parks and economic zones in attracting investment and firm participation, develop eco-industrial parks, and transition traditional to ecological ones through preferential policies and incentives, because industrial parks, particularly eco-industrial parks, can help reduce CO_2 emissions for sustainable development in this industry. Some support policies that can be applied are tax exemption, reduction, land rent, and priority in credit loans for firms operating in eco-industrial parks.
- (ii) Promote the development of technology imported from developed countries, encourage firms to access environmentally friendly technology, and prevent the import of technology harmful to the environment. The government strengthens the standards for importing used machinery by regulating the age of all used machinery to not exceed 10 years, improving national technical



Source: the author estimates from annual surveys of GSO.

Fig 1: Changes in environmental efficiency trend of two models.

regulations on safety, energy savings, and environmental protection to be on a par with global standards, and supporting or guaranteeing loans for imported advanced machinery from developed countries.

- (iii) Regarding foreign investment, it is necessary to choose investors with a sustainable and environmentally friendly investment history to ensure environmental protection.
- (iv) Encourage firms to regularly implement innovation and improvement processes to increase the quality of their products and apply advanced processes and tools in their production. Some solutions that can be applied are efficiency improvements in the internal cooperation process, increased receptive capabilities, and promotion of cooperation with other firms and institutions, especially FDI firms, via conferences, seminars, training courses, and consultations.
- (v) Strengthen the environmental control by making CO₂ emission reduction policies such as environmental tax policies, managing chemicals and energy, raising firm awareness on using optimal materials, and increasing the enforcement capacity for implementing regulations of environmental protection.

REFERENCES

- Asmild, M., Paradi, J.C., Aggarwall, V. and Schaffnit, C. 2004. Combining DEA window analysis with the Malmquist index approach in a study of the Canadian banking industry. *Journal of Productivity Analysis*, 21(1): 67-89.
- Banker, R. D, Charnes, A. and Cooper, W. W. 1984. Some models for estimating technical and scale inefficiencies in data envelopment analysis. *Management Science*, 1092-1078 :(9) 30.
- Brockett, P. L. and Levine, A. 1984. *Statistics, Probability and Their Applications*. W. B. Saunders Publishing Co.
- Charnes, A. 1952. Optimality and degeneracy in linear programming. *Econometrica*, 20: 135-159.
- Charnes, A., Clark, T., Cooper, W.W. and Golany, B.1985. A developmental study of data envelopment analysis in measuring the efficiency of maintenance units in U. S. Air Forces. *Annals of Operational Research*, 2: 95-112.
- Charnes, A., Cooper, W.W. and Rhodes, E. 1978. Measuring the efficiency of decision-making units. *European Journal of Operational Research*, 2(6): 429-444.
- Chen, J., Song, M. and Xu, L. 2010. Evaluation of environmental efficiency in China using data envelopment analysis. *Ecological Indicators*, 52: 577-583.
- Chu, J.F., Wu, J. and Song, M.L. 2018. An SBM-DEA model with parallel computing design for environmental efficiency evaluation in the big data context: a transportation system application. *Annals of Operations Research*, Springer, 270(1): 105-124.
- Cooper, W., Seiford, L.M., Tone and K. 2007. *Data Envelopment Analysis: A Comprehensive Text with Models Applications*. Springer Science, pp. 21.
- Demena, B.A. and Afesorgbor, S.K. 2020. The effect of FDI on environmental emissions: Evidence from a meta-analysis, *Energy Policy*, 138, (C).
- Duong, V.H. 2016. Technical efficiency of FDI firms in the Vietnamese manufacturing sector, review of economic perspectives. 16(3): 205-230, DOI: 10.1515/revcep-2016-0013
- Fare, R. Grosskopf, S., Lovell C.A.K. and Pasurka C. 1989. Multilateral productivity comparisons when some outputs are undesirable: a nonparametric approach. *The Review of Economics and Statistics*, 71(1): 90-98
- Fare, R., Grosskopf, S. and Zaim, O. 2003. An environmental Kuznets curve for the OECD countries. In: *New Directions: Efficiency and Productivity*. Kluwer Academic Publishers, The Kingdom of the Netherlands, 79-90.
- Grigoroudis, E. and Petridis, K. (ed) 2019. Evaluation of national environmental efficiency under uncertainty using data envelopment analysis. In: Doukas H., Flamos A., Lieu J. (ed.) *Understanding Risks and Uncertainties in Energy and Climate Policy*. Springer, Cham. https://doi.org/10.1007/978-3-030-03152-7_7
- Hailu, A. and Veeman, T. S. 2001 Non-parametric productivity analysis with undesirable outputs: an application to the Canadian pulp and paper industry. *Am. J. Agric. Econ.*, 83: 605-616.
- Hongqi, W., Xueyuan, W. and Yuqi, W. 2013. Transverse and longitudinal analysis of the environmental efficiency of Chinese industries. *Mathematical and Computer Modelling*, 58(5-6): 961-970.
- Honma, S. 2015. Does international trade improve environmental efficiency? An application of a super slacks-based measure of efficiency. *Journal of Economic Structures*, Springer; Pan-Pacific Association of Input-Output Studies (PAPAIOS), 4(1): 1-12.
- IPCC. 2006. *IPCC Guidelines for National Greenhouse Gas Inventories*, <https://www.ipcc-nggip.iges.or.jp/public/2006gl/>
- Klepper, S. 2002. The capabilities of new firms and the evolution of the US automobile industry, *Industrial and Corporate Change*, 11 (4): 645-666.
- Lee, J. and Yu, J. 2019. Heterogeneous energy consumption behavior by firm size: evidence from Korean environmental regulations. *Sustainability*, 11: 3226. doi:10.3390/su11113226.
- Li, H., Fang, K., Yang, W., Wang, D. and Hong, X. 2013. Regional environmental efficiency evaluation in China: Analysis based on the Super-SBM model with undesirable outputs. *Mathematical and Computer Modelling*, 58(5-6): 1018-1031.
- Managi, S., Hibiki, A. and Tsurumi, T. 2009. Does trade openness improve environmental quality? *Journal of Environmental Economics and Management*, 58(3): 346-363.
- Marques, A. and Caetano, R. 2020. The impact of foreign direct investment on emission reduction targets: Evidence from high- and middle-income countries. *Structural Change and Economic Dynamics*, 55(C): 107-118.
- Perkins, R. and Neumayer, E. 2009. Transnational linkages and the spillover of environment-efficiency into developing countries. *Global Environmental Change*, 19(3): 375-383.
- Pulina, M., Detotto, C. and Paba, A. 2010. An investigation into the relationship between size and efficiency of the Italian hospitality sector: A window DEA approach. *European Journal of Operational Research*, 204(3): 613-620.
- Sabtoosh, K. S. and Deepanjali, M. 2019. Determinants of energy and CO₂ emission intensities: a study of manufacturing firms in India. *The Singapore Economic Review*, 63(2): 389-407.
- Seiford, L. and Zhu, J. 2002. Modeling undesirable factors in efficiency evaluation. *European Journal of Operational Research*, 142(1): 16-20.
- Tobin, J. 1958. Estimation of Relationships for Limited Dependent Variables. *Econometrica*. 26(1): 24-36. doi:10.2307/1907382.
- Tone, K. 2002. A slacks-based measure of super-efficiency in data envelopment analysis. *European Journal of Operational Research*, 143(2002): 32-41.
- Tone, K. 2004. Dealing with undesirable outputs in DEA: as lacks-based measure (SBM) approach, Presentation at NAPWIII, Toronto.
- Zhang, N. and Kim, J.D. 2014. Measuring sustainability by energy efficiency analysis for Korean power companies: a sequential slacks-based efficiency measure. *Sustainability*, 6: 1414-1426. <https://doi.org/10.3390/su6031414>



Measurement of Black Carbon Absorption Coefficients Using an Aethalometer and Their Association with Visibility

Khadeejeh M. Hamasha*†

*Department of Physics, Yarmouk University, Jordan

†Corresponding author: Khadeejeh M. Hamasha; khamasha@yu.edu.jo

Nat. Env. & Poll. Tech.
Website: www.neptjournal.com

Received: 07-11-2022

Revised: 16-12-2022

Accepted: 05-01-2023

Key Words:

Black carbon
Absorption coefficient
Fossil fuel
biomass burning
Visibility

ABSTRACT

Black carbon (BC) is a pollutant aerosol affecting climate and human health. Light absorption coefficients of black carbon (B_{abs}) were measured using an aethalometer model AE33 at wavelengths 370, 470, 520, 660, 880, and 950 nm. B_{abs} for the seven wavelengths at seven sites in Jordan fluctuated with time and peaked at rush hours. The daily average values for all sites were inversely proportional to the wavelength. The average daily visibility values in the seven Jordan sites varied between 72 km and 211 km. In the Irbid site, the daily average visibility values for 7-13 Nov. 2021 varied between 43 km and 107 km. BC varied from hour to hour and from day to day. The daily average values of BC in Irbid for the period of 7 -13 Nov. 2021 varied between $2.24 \mu\text{g}\cdot\text{m}^{-3}$ and $4.66 \mu\text{g}\cdot\text{m}^{-3}$. BC peaked at the rush hour and had the lowest values on Friday. About 90% of the measured BC was from fossil fuel sources and 10% from biomass-burning sources.

INTRODUCTION

Light-absorbing carbon particles are the most abundant and efficient light-absorbing component in the atmosphere in the visible spectrum (Liu et al. 2020, Ziyong et al. 2022). It typically depends inversely on wavelength. Organic carbon is strongly wavelength dependent, with increased absorption for UV and short wavelength visible radiation, but hardly at all at 870 nm. Black carbon is very likely to dominate at 870 nm. Black carbon, the main constituent of soot, is almost exclusively responsible for aerosol light absorption at long-wavelength visible radiation and near-infrared wavelengths. This type of pollution is sometimes referred to as black carbon pollution. Air pollution caused by black carbon particles has been a major problem since the beginning of the industrial revolution and the development of the internal combustion engine. Scientific publications dealt with soot and smoke analysis as early as 1896. Mankind has become so dependent on burning fossil fuels (petroleum products, coal, and natural gas) that all combustion-related emissions now constitute a serious and widespread problem for human health and the entire global environment. The absorption of solar radiation by black carbon is expected to lead to the heating of the atmosphere since the light energy is converted into thermal energy. This heating effect would be expected to be most important in polluted urban areas. Black carbon aerosol light absorption reduces the amount of sunlight

available at the surface to drive atmospheric circulation and boundary layer development. Even burning wood and charcoal in fireplaces and barbecues can release significant soot into the air. Some of these pollutants can be created by indoor activities such as smoking and cooking.

An aethalometer usually measures black Carbon concentrations. Aethalometer is an instrument that uses the filter-based technique to measure the aerosol absorption coefficients (B_{abs}) at a specific wavelength (Drinovec et al. 2017, Olson et al. 2015, Wang et al. 2011, Sandradewi 2008). B_{abs} is proportional to the concentration of the black carbon. A new generation of aethalometer, model AE33 (Magee Scientific Corp. 2015), uses the DualSpot technology. In this technology, simultaneous analysis of the absorption of light by the aerosol collected on two parallel points on the filter tape at different loading rates. The two results are combined to eliminate changes in response due to load effects during the measurement (Drinovec et al. 2015).

MATERIALS AND METHODS

In this study, the B_{abs} of black carbon were measured using the aethalometer for seven different wavelengths at different sites in Jordan. Measurement sites were Irbid, Amman, Zarqa, Mafraq, Ajloun, North Shuna, and Tapqat Fahel. Measurement in each site was for one day except in Irbid city, which was for a week. The measurement site in Irbid

was chosen to be in Yarmouk University at the location of the Science Building. This building is next to the university's northern gate on the city's most crowded street.

Aethalometer model AE33 (Magee Scientific, USA) was used to measure the absorption coefficients in this study. Aethalometer AE33 is an instrument used to measure the black carbon concentration in real-time by measuring the light absorption on an aerosol-loaded filter. Using dual-spot technology and multi-seven-wavelength optical analysis, the AE33 provides accurate data on a time scale as rapid as 1 minute. An external pump is used to draw the air sample at a flow rate of 5 liters per minute through the inlet port of the aethalometer. The sample that enters the optical chamber is deposited on two spots on the filter tape at different loading rates. The instrument then performs an optical analysis of the sample by measuring the transmission of light emitted by the optical source at seven wavelengths; 370, 470, 520, 590, 660, 880, and 950 nm through the two spots containing the sample compared to the transmission of the unloaded portion of the filter tape, which acts as a reference region. Because the instrument is characterized by cumulative deposition of the sample on the filter, it depends on the change of the light attenuation every minute to calculate the concentration of black carbon.

RESULTS AND DISCUSSION

In this study, aethalometer AE33 was used to measure the light absorption coefficients at seven wavelengths in seven sites in Jordan in 2021. Diurnal measurements were performed at seven sites (Table 1), and a one-week-long

Table 1: Site names and dates for AE33 measurements in Jordan in 2021.

Site	Site Name	Date of Measurement
1	Mafrag	9/9/2021
2	North Shuna	13/9/2021
3	Tabqat Fahl	15/9/2021
4	Ajloun	20/9/2021
5	Amman	4/10/2021
6	Zarqa	6/10/2021
7	Irbid	7/11/2021

measurement at site seven. Black carbon concentrations (BC) were calculated from the absorption coefficients at a wavelength of 880 nm (Sandradewi 2008, Yang et al. 2009). Also, absorption coefficients at pairs of wavelengths assessed the component apportionment of the BC from fossil fuel (BCff) and biomass-burning (BCbb) sources.

Table 2 shows the average values of B_{abs} and BC with their sources for the seven wavelengths at the study sites. These measurements were taken by AE33 during the day for one day at each site. B_{abs} is inversely proportional to the wavelength of all sites, as shown in Fig. 1. Irbid (site 7) had the highest values for B_{abs} , while Tabqat fahl (site 3) had the lowest. Irbid is a crowded city in northern Jordan, close to the border with Syria. About 90% of the measured BC was from fossil fuel sources.

Fig. 2 shows B_{abs} for seven wavelengths in Mafrag city on 9 Sep 2021. It's clear from the figure that B_{abs} is inversely proportional to the wavelength. The average values of B_{abs} for the seven wavelengths ranged between 10.6 Mm^{-1} for the

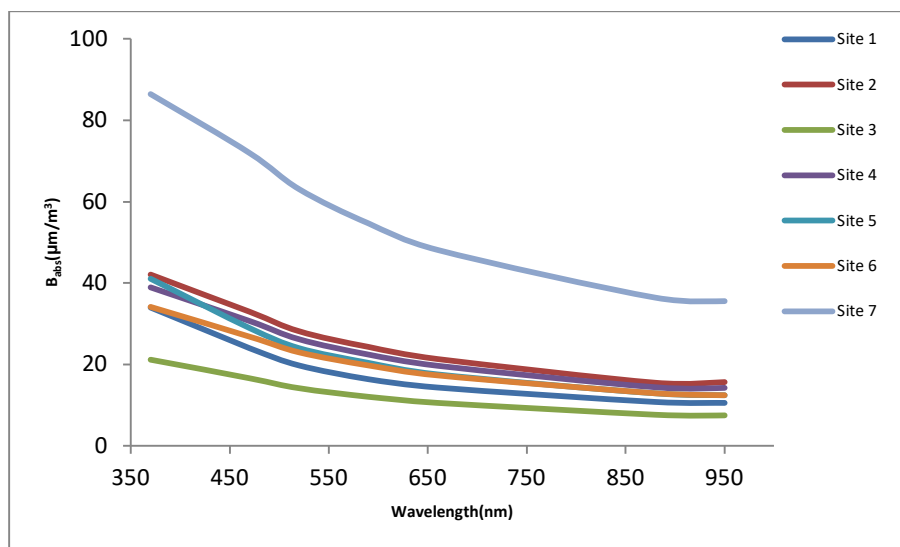


Fig. 1: Average values of light absorption coefficients at seven sites from Jordan for wavelengths 370, 470, 520, 590, 660, 880, and 950 nm.

Table 2: Diurnal average values of the absorption coefficients for the seven sites in Jordan.

Site	$\bar{B}_{abs}(Mm^{-1})$ (370 nm)	$\bar{B}_{abs}(Mm^{-1})$ (470 nm)	$\bar{B}_{abs}(Mm^{-1})$ (520 nm)	$\bar{B}_{abs}(Mm^{-1})$ (590 nm)	$\bar{B}_{abs}(Mm^{-1})$ (660 nm)	$\bar{B}_{abs}(Mm^{-1})$ (880 nm)	$\bar{B}_{abs}(Mm^{-1})$ (950 nm)	BC ($\mu g \cdot m^{-3}$)	BC _{bb} ($\mu g \cdot m^{-3}$)	BC _{ff} ($\mu g \cdot m^{-3}$)
1	33.99 ± 8.90	24.02 ± 6.09	19.77 ± 5.06	16.37 ± 4.07	14.30 ± 3.39	10.74 ± 2.62	10.56 ± 2.44	1.382 ± 0.337	0.172 ± 0.075	1.210 ± 0.262
2	42.06 ± 5.43	32.94 ± 3.85	28.13 ± 3.19	24.29 ± 2.38	21.34 ± 2.18	15.48 ± 1.35	15.64 ± 1.08	1.773 ± 1.298	0.102 ± 0.534	1.671 ± 1.196
3	21.17 ± 3.38	16.58 ± 2.69	14.13 ± 2.48	12.06 ± 2.13	10.53 ± 1.79	7.62 ± 1.20	7.44 ± 1.06	0.981 ± 0.483	0.104 ± 0.163	0.876 ± 0.442
4	38.95 ± 9.81	30.69 ± 7.34	26.18 ± 6.21	22.43 ± 5.52	19.68 ± 4.60	14.35 ± 3.72	14.24 ± 3.49	1.846 ± 1.810	0.142 ± 0.132	1.704 ± 1.811
5	41.07 ± 5.09	28.95 ± 2.90	24.01 ± 2.38	20.35 ± 2.31	17.54 ± 1.79	12.86 ± 1.33	12.45 ± 1.31	1.654 ± 0.171	0.245 ± 0.014	1.409 ± 0.156
6	34.09 ± 21.51	26.85 ± 8.41	22.96 ± 5.63	19.77 ± 4.55	17.27 ± 3.54	12.92 ± 2.04	12.46 ± 2.21	1.663 ± 0.499	0.115 ± 0.160	1.547 ± 0.459
7	86.47 ± 42.17	71.96 ± 35.88	63.07 ± 31.30	54.64 ± 26.70	48.13 ± 2.64	36.38 ± 17.03	33.54 ± 15.20	5.152 ± 3.197	0.446 ± 0.502	4.706 ± 3.083

wavelength of 950 nm and 33.9 Mm⁻¹ for the wavelength of 370 nm. For all wavelengths, B_{abs} values fluctuate with two peaks, one at 11:31 am and the other at 12:30 pm. Using the B_{abs} data for pairs of wavelengths, it was found that 12% of the BC was from biomass-burning sources and 88% from the fossil fuel source.

Fig. 3 shows B_{abs} for seven wavelengths in North Shuna city on 13 September 2021. It's clear from the figure that B_{abs} is inversely proportional to the wavelength. The average values of B_{abs} for the seven wavelengths ranged between 15.6Mm⁻¹ for the wavelength of 950 nm and 42.1 Mm⁻¹ for the wavelength of 370 nm. For all wavelengths, B_{abs} values fluctuate with time. Using the B_{abs} data for pairs of wavelengths, it was found that 6% of the BC was from biomass-burning sources and 94% from the fossil fuel source.

Fig. 4 shows B_{abs} for seven wavelengths in Tabqat Fahel city on 15 September 2021. It's clear from the figure that B_{abs} is inversely proportional to the wavelength. The average values of B_{abs} for the seven wavelengths ranged between 7.4 Mm⁻¹ for the wavelength of 950 nm and 21.2 Mm⁻¹ for the wavelength of 370 nm. For all wavelengths, B_{abs} values fluctuate with time. Using the B_{abs} data for pairs of wavelengths, it was found that 11% of the BC was from biomass-burning sources and 89% from the fossil fuel source.

Fig. 5 shows B_{abs} for seven wavelengths in Ajloun city on 20 September 2021. It's clear from the figure that B_{abs} is inversely proportional to the wavelength. The average values of B_{abs} for the seven wavelengths ranged between 14.2 Mm⁻¹ for the wavelength of 950 nm and 38.9 Mm⁻¹ for the wavelength of 370 nm. For all wavelengths, B_{abs} values fluctuate with time. Using the B_{abs} data for pairs of wavelengths, it was found that 8% of the BC was from biomass burning and 92% from fossil fuel sources.

Fig. 6 shows B_{abs} for seven wavelengths in Amman city on 4 October 2021. It's clear from the figure that B_{abs} is inversely proportional to the wavelength. The average values of B_{abs} for the seven wavelengths ranged between 12.5 Mm⁻¹ for the wavelength of 950 nm and 41.1 Mm⁻¹ for the wavelength of 370 nm. For all wavelengths, B_{abs} values fluctuate with time. Using the B_{abs} data for pairs of wavelengths, it was found that 15% of the BC was from biomass-burning sources and 85% from the fossil fuel source.

Fig. 7 shows B_{abs} for seven wavelengths in Zarqa city on 6 October 2021. It's clear from the figure that B_{abs} is inversely proportional to the wavelength. The average values of B_{abs} for the seven wavelengths ranged between 12.5 Mm⁻¹ for the wavelength of 950 nm and 34.1 Mm⁻¹

for the wavelength of 370 nm. For all wavelengths, B_{abs} values fluctuate with time. Using the B_{abs} data for pairs of wavelengths, it was found that 7% of the BC was from biomass-burning sources and 93% from the fossil fuel source.

Fig. 8 shows B_{abs} for seven wavelengths in Irbid city on 7 November 2021. It's clear from the figure that B_{abs} is inversely proportional to the wavelength. The average values of B_{abs} for the seven wavelengths ranged between

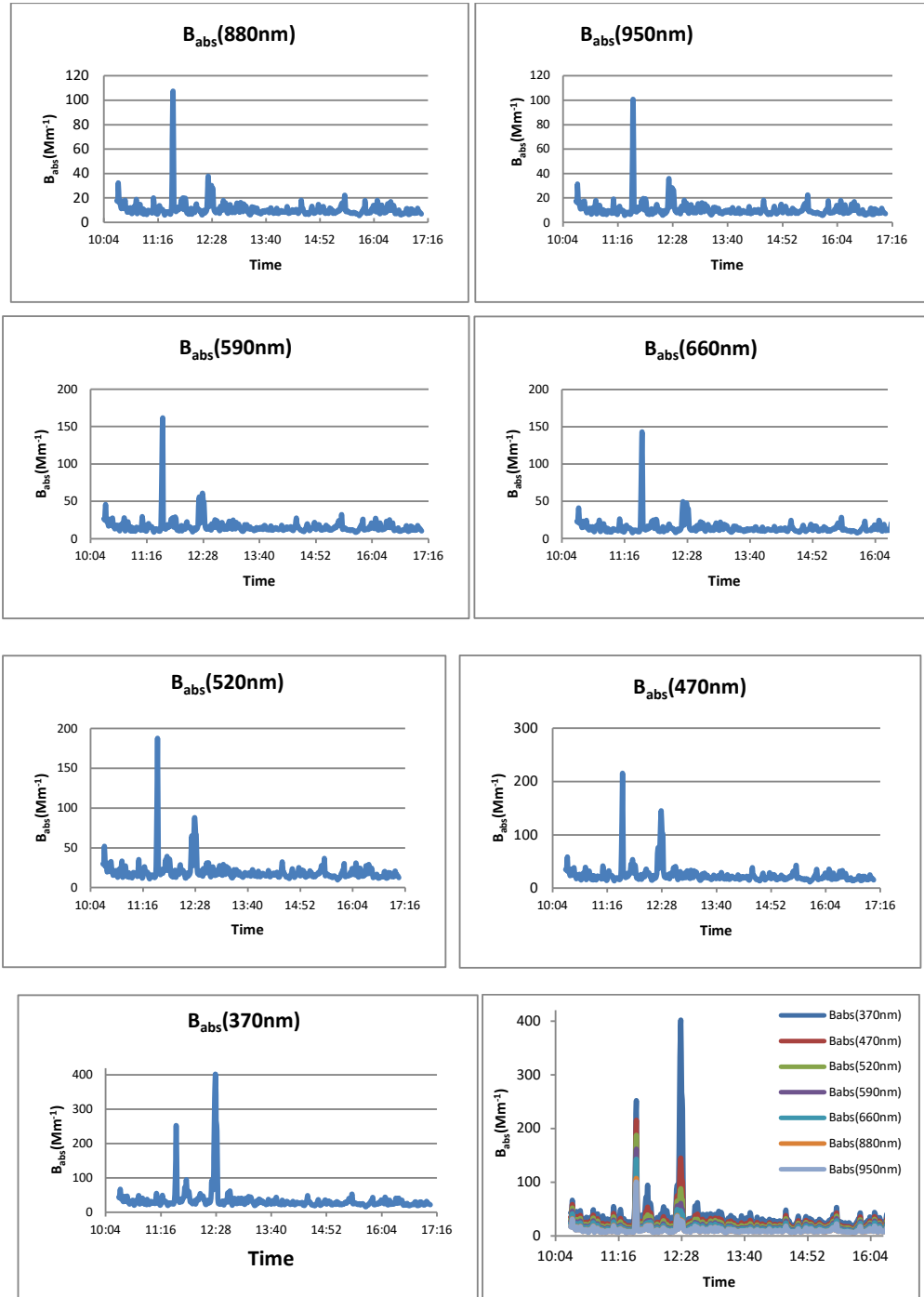


Fig. 2: Diurnal time series of B_{abs} in Mafrqa city on 9 September 2021 for the wavelengths 370, 470, 520, 590, 660, 880, and 950nm.

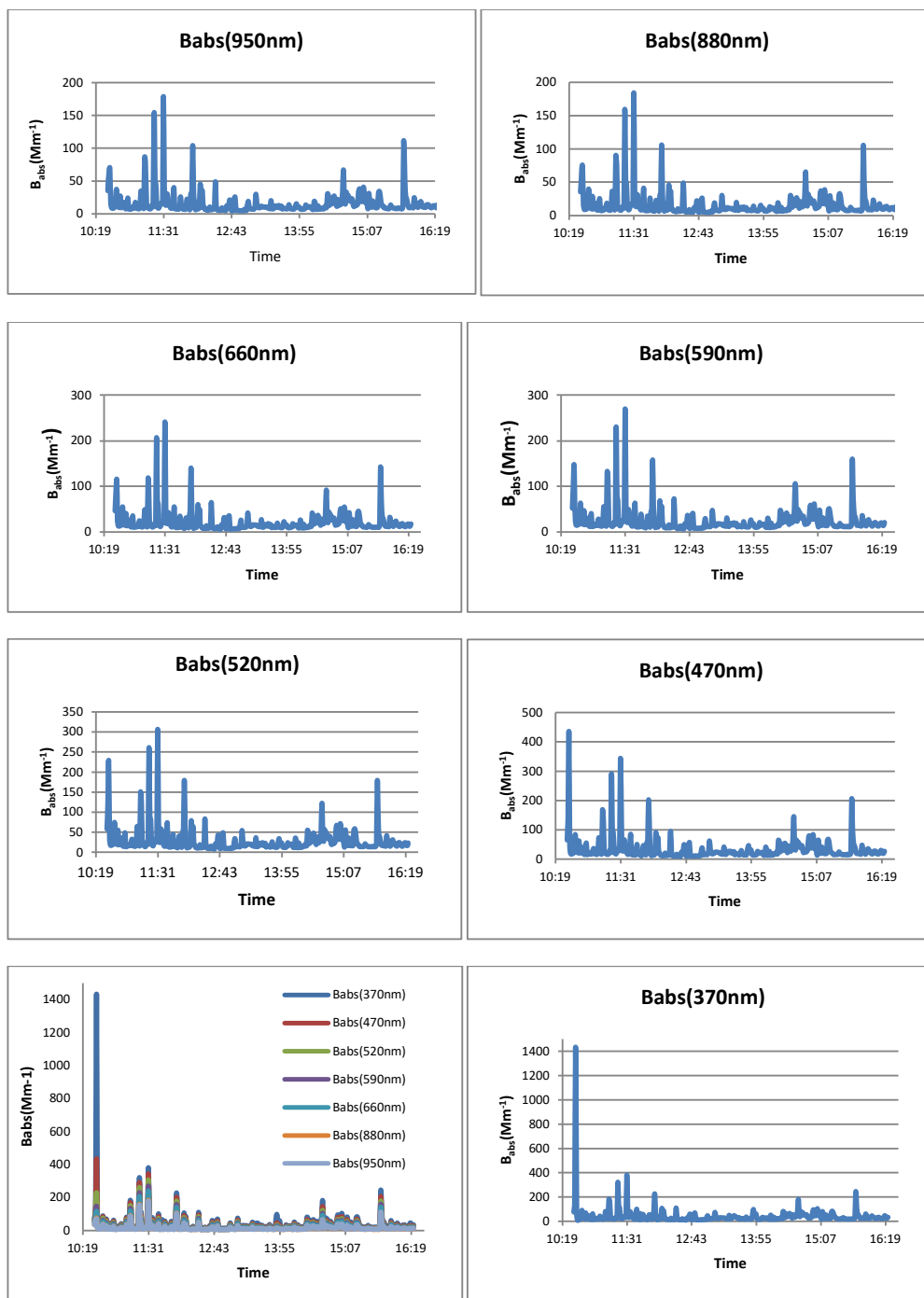


Fig. 3: Diurnal time series of B_{abs} in North Shuna city on 13 September 2021 for the wavelengths 370, 470, 520, 590, 660, 880, and 950nm.

33.5 Mm^{-1} for the wavelength of 950 nm and 86.5 Mm^{-1} for the wavelength of 370 nm. For all wavelengths, B_{abs} values fluctuate with time. Using the B_{abs} data for pairs of wavelengths, it was found that 9% of the BC was from biomass-burning sources and 91% from the fossil fuel source.

Visibility can be calculated from the absorption coefficients at the wavelength of 520nm using the Koschmieder equation (Middleton 1952); $Vis = \frac{3.912}{B_{ATN}}$, where B_{ATN} is the attenuation coefficient of the light due to

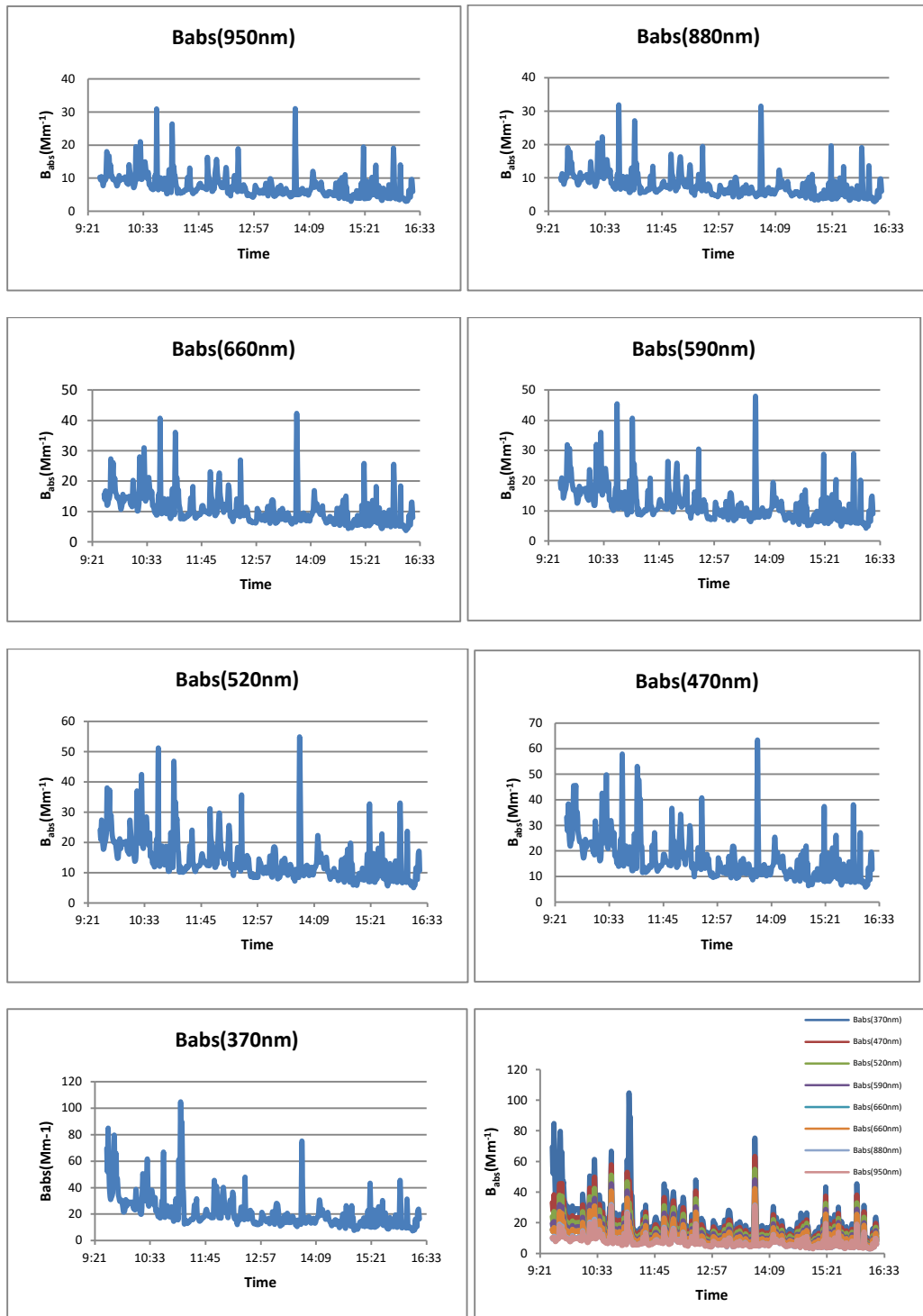


Fig. 4: Diurnal time series of B_{abs} in Tabqat Fabel city on 15 September 2021 for the wavelengths 370, 470, 520, 590, 660, 880, and 950nm.

scattering and atmospheric absorption by particles and gases. For the AE33 instrument, B_{ATN} can be calculated from B_{abs} by $B_{ATN} = 1.57 B_{abs}$.

Fig. 9 shows the visibility variation during the daytime of the seven sites in Jordan. As seen from the figure, Visibility varies with time and depends on the amount of pollutant

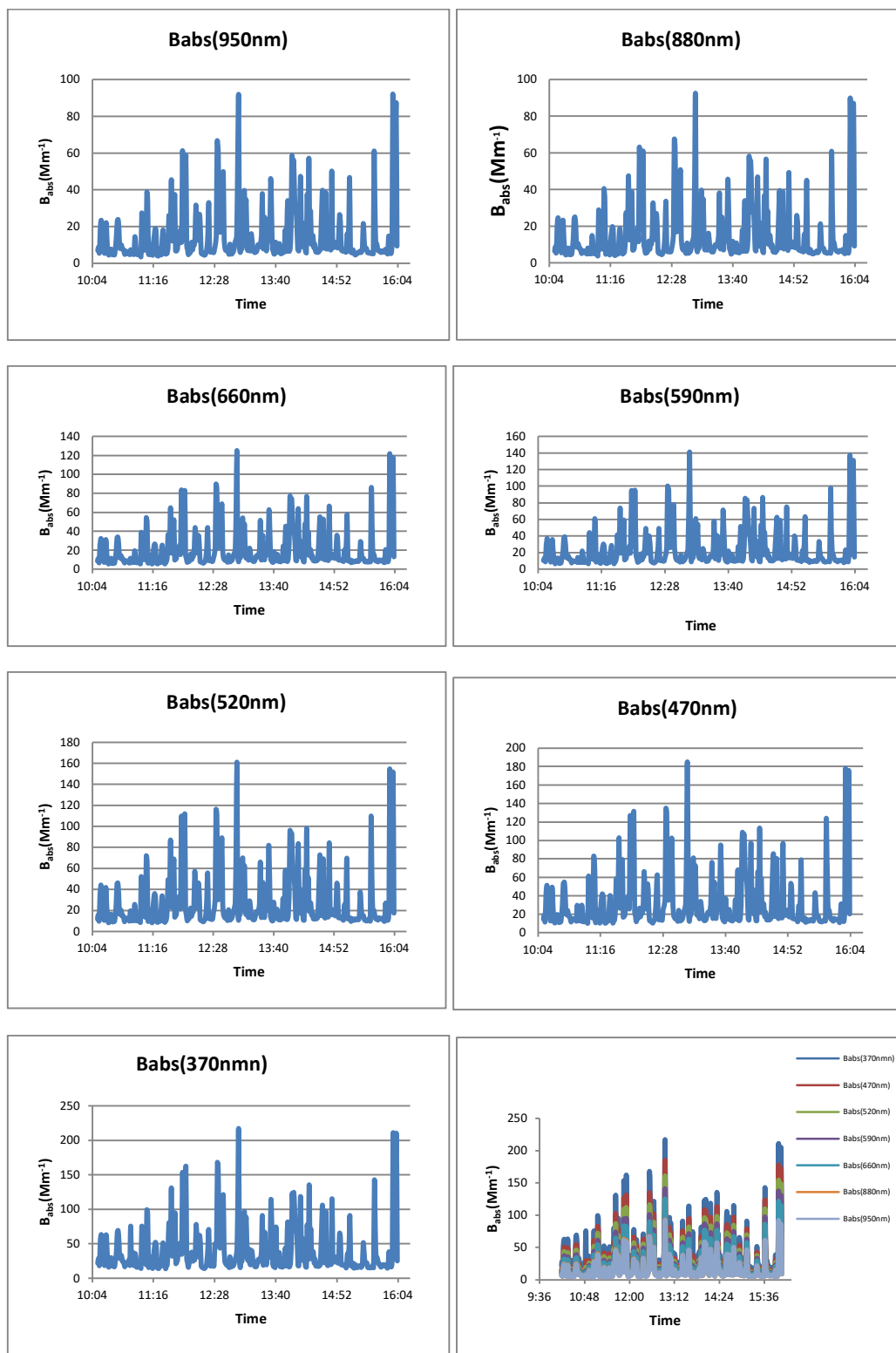


Fig. 5: Diurnal time series of B_{abs} in Ajloun city on 20 September 2021 for the wavelengths 370, 470, 520, 590, 660, 880, and 950nm.

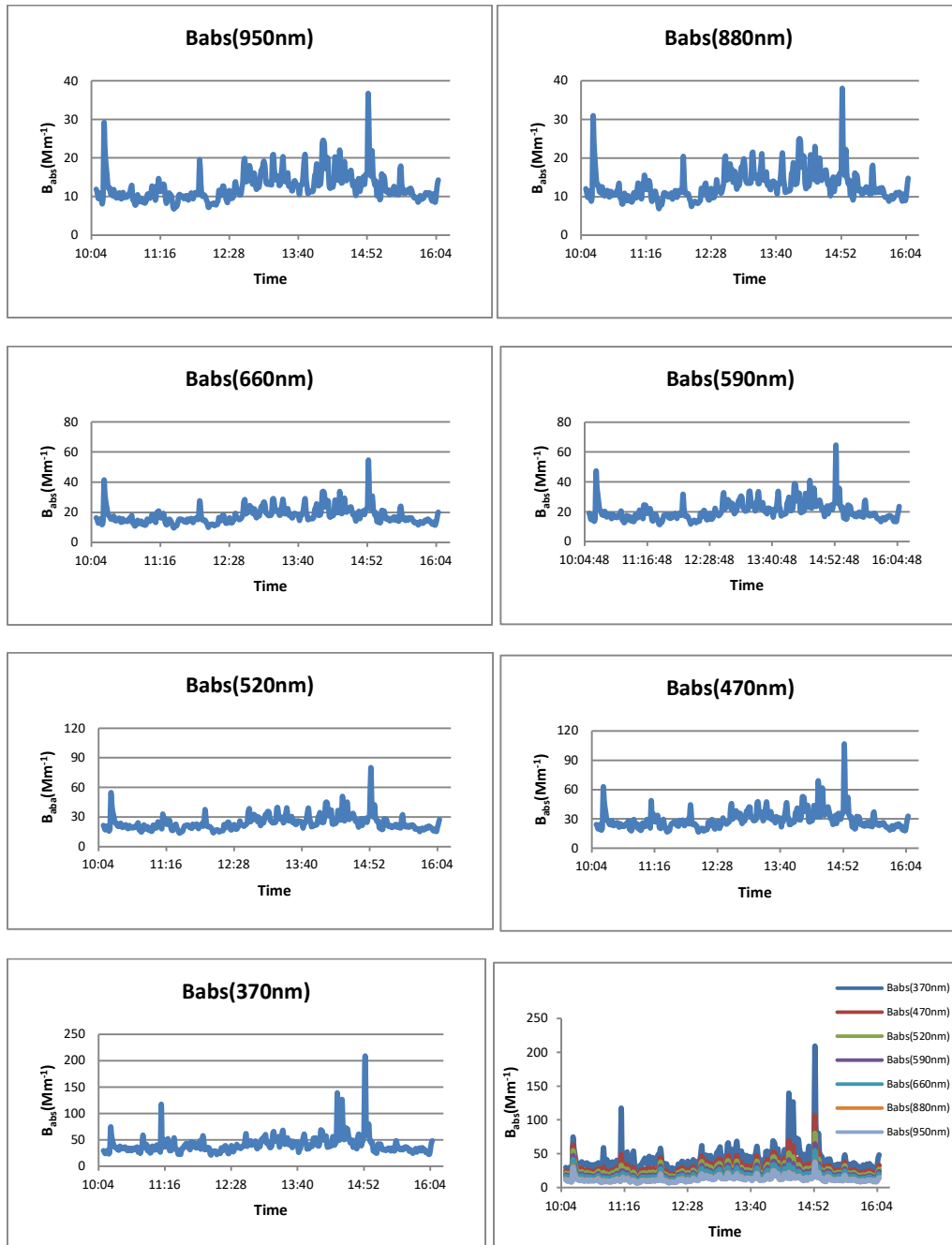


Fig. 6: Diurnal time series of B_{abs} in Amman city on 4 October 2021 for the wavelengths 370, 470, 520, 590, 660, 880, and 950nm.

particles that scatter or absorb lights on the sight path. Visibility decreases with increasing pollutants. The daily average visibility values varied between 72 km at Irbid city and 211 km at Tabqat Fahel. The daily average visibility values showed that the most polluted site by aerosols from the study areas was Irbid, followed by Zarqa, then Amman. Even for one area, the average visibility changes from day

to day according to the clearness of the sky from pollutants. Fig. 10 shows a chart of the daily visibility variation for the Irbid site during 7-13 October 2021.

As site seven had the lowest visibility, we studied the black carbon concentration for this site for one week. Fig. 11 shows the variation of BC in Irbid city during the period (7-13) Nov 2021. BC concentrations fluctuated between 0

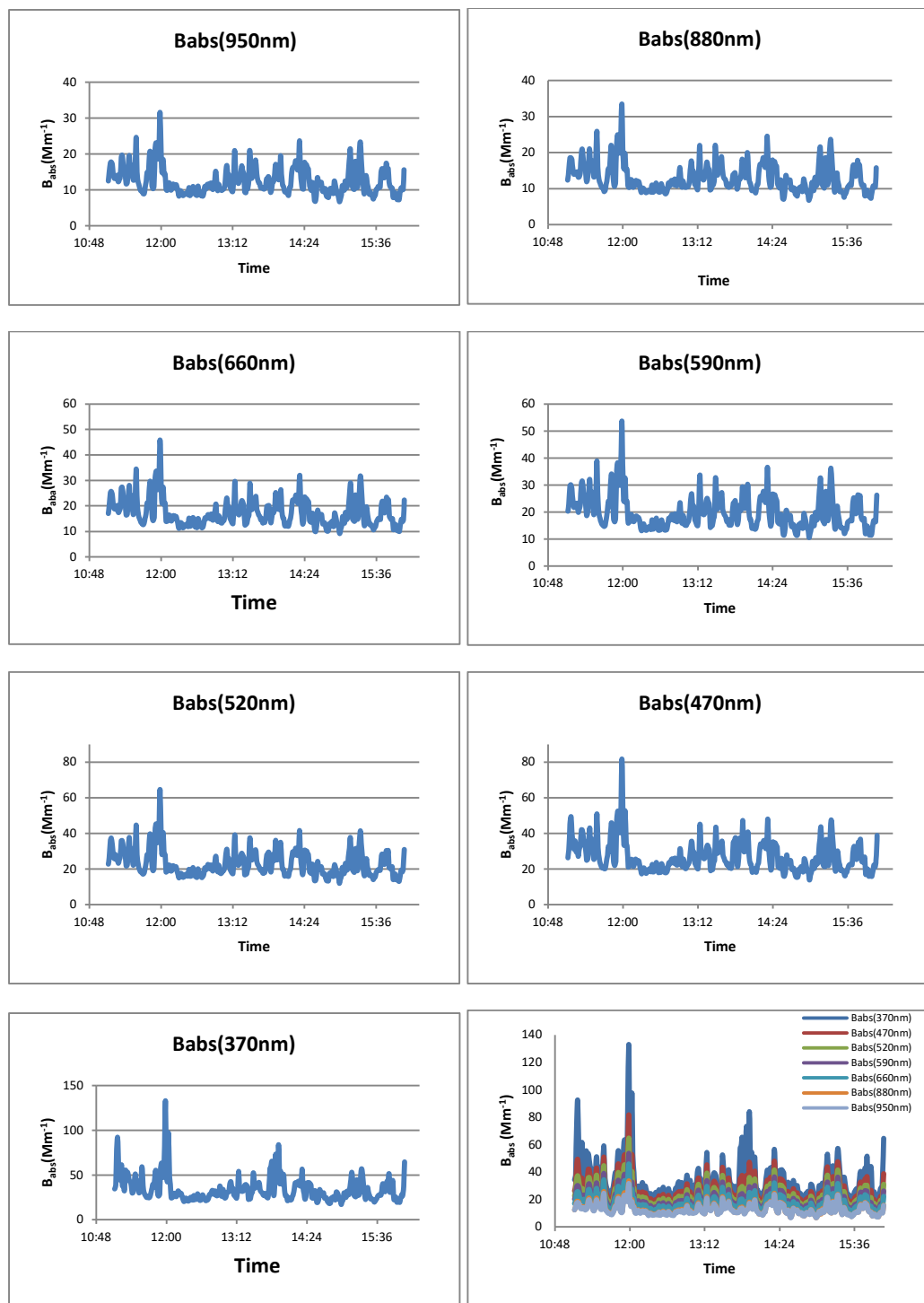


Fig. 7: Diurnal time series of B_{abs} in Zarqa city on 6 October 2021 for the wavelengths 370, 470, 520, 590, 660, 880, and 950nm.

and $10,000 \text{ ng}\cdot\text{m}^{-3}$ and peaked around rush hours. Irbid is a city that is very crowded with means of transportation. Irbid has a population of about one million people and

has many restaurants, cafes, and factories scattered around it, besides Yarmouk University, which has 40,000 students. Also, Irbid is close to the Syrian and Palestinian

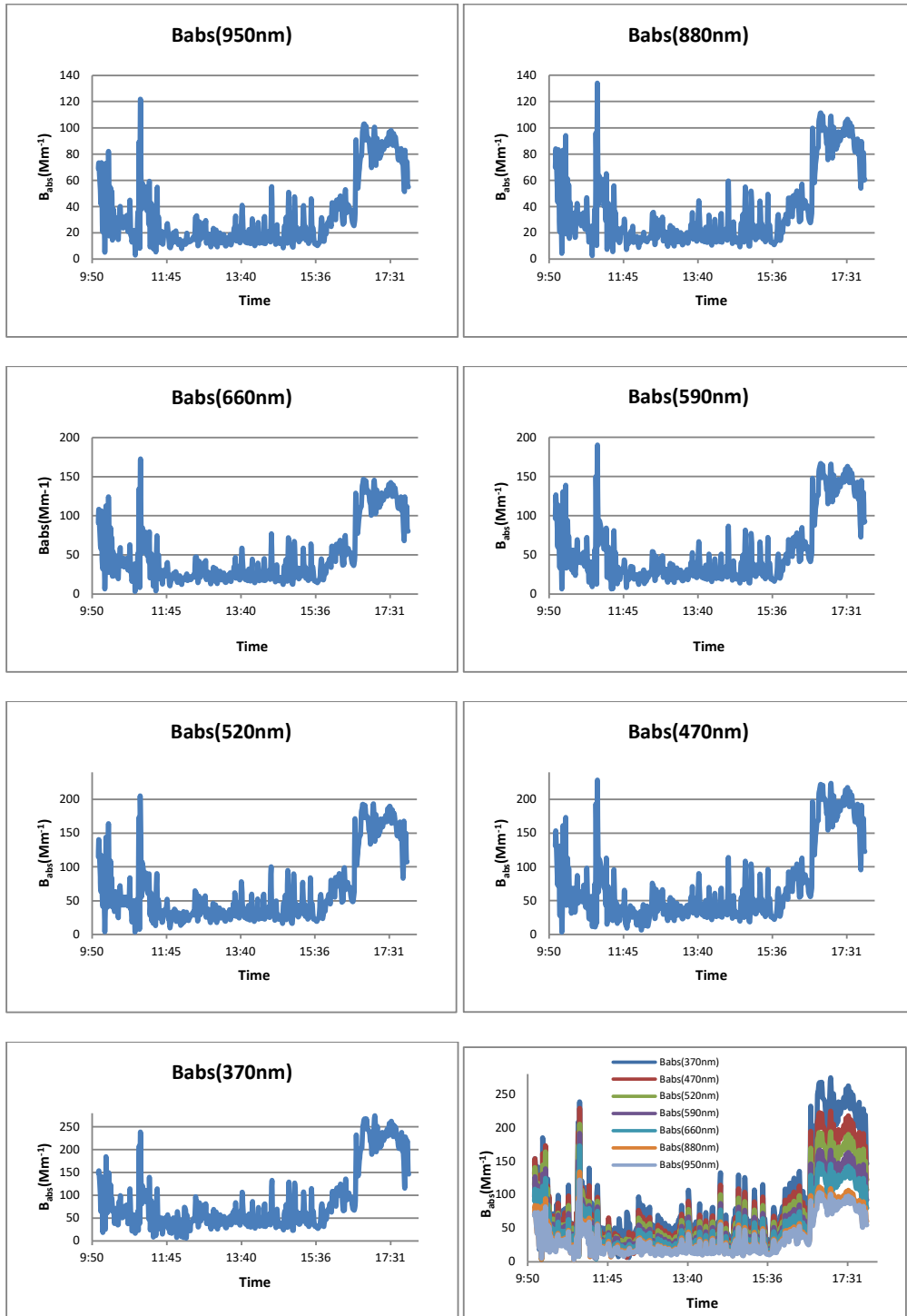


Fig. 8: Diurnal time series of B_{abs} in Irbid city on 7 November 2021 for the wavelengths 370, 470, 520, 590, 660, 880, and 950nm.

borders, increasing the black carbon pollution sources. The daily average values of BC were different from day to day, and Friday had the lowest value of BC, as seen in Fig. 12.

CONCLUSION

B_{abs} in Jordan fluctuated with time and peaked at rush hours. The daily average values of B_{abs} are inversely proportional

to the wavelengths. The daily average visibility values are inversely proportional to the values of BC. BC varied from hour to hour and from day to day. BC peaked during the

rush hours and had the lowest values on Friday. Most of the measured BC in Jordan is from fossil fuel sources. The Irbid city has the highest values of aerosols in Jordan.

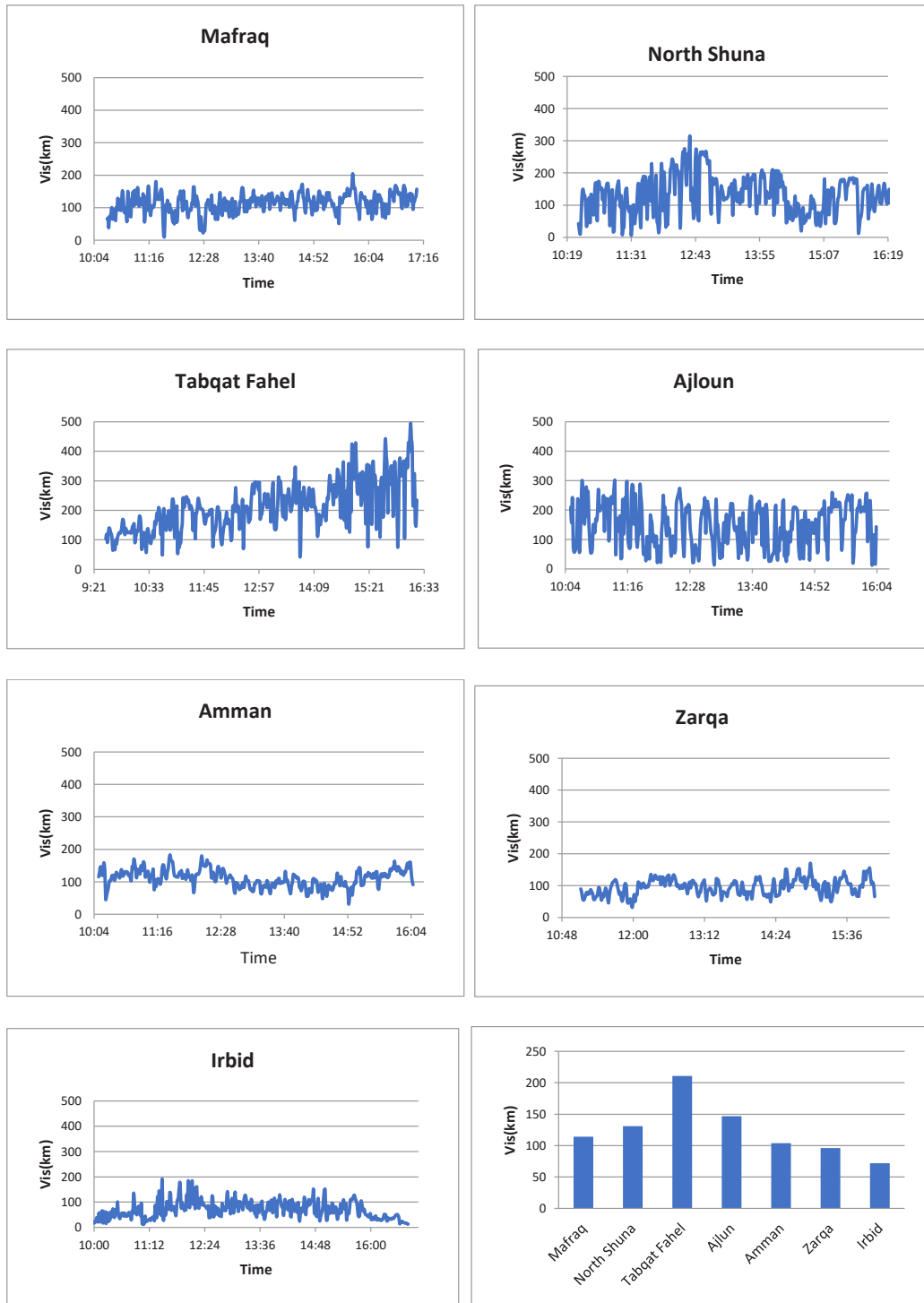


Fig. 9: Diurnal visibility variation in the seven sites in Jordan.

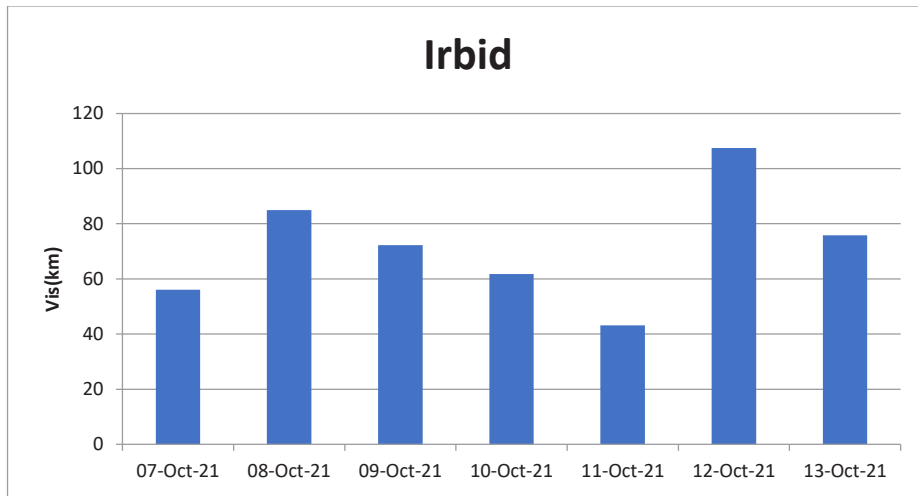


Fig. 10: Daily average visibility values in site 7 during 7-13 October 2021.

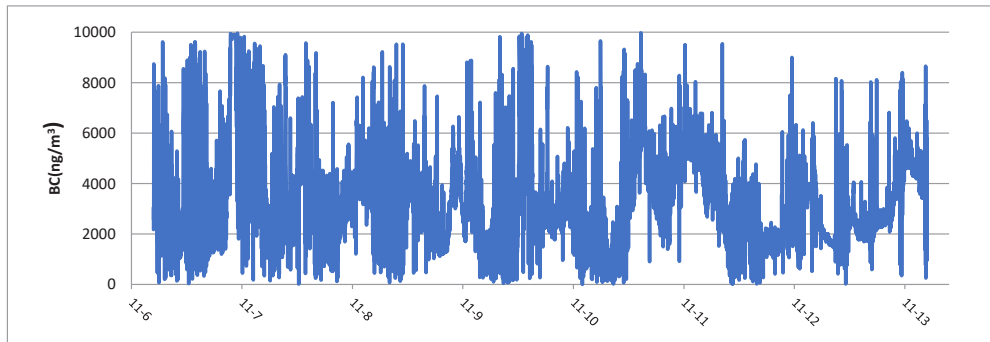


Fig. 11: Time series of BC in Irbid city during the period of 7-13 November 2021.

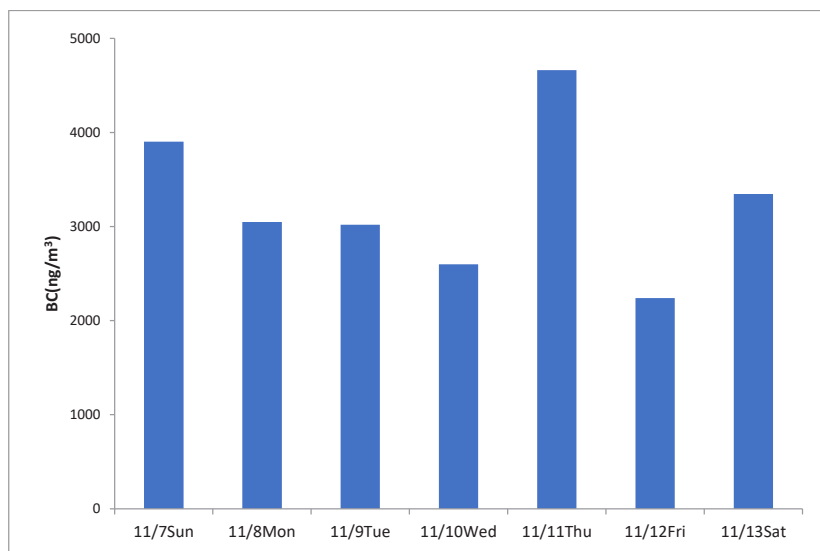


Fig. 12: The daily average value of BC concentrations during the period of 7-13 November 2021 in Irbid city.

ACKNOWLEDGMENT

We thank Scientific Research and Graduate Studies Deanship at Yarmouk University for supporting this work with Grant No. 18/2019.

REFERENCES

- Drinovec, L., Močnik, G., Zotter, P., Prévôt, A., Ruckstuhl, C., Coz, E., Rupakheti, M., Sciare, J., Müller, T. and Wiedensohler, A. 2015. The dual-spot aethalometer: an improved measurement of aerosol black carbon with real-time loading compensation. *Atmos. Meas. Tech.*, 8: 1965-1979. <https://doi.org/10.5194/amt-8-1965-2015>.
- Drinovec, L., Gregoric, A., Zotter P., Wolf R., Bruns E.A., Prevot A., Jean-Eudes Petit J., Favez O., Sciare J., Arnold I., Chakrabarty R., Moosmüller H., Filep A. and Mocnik, G. 2017. The filter-loading effect by ambient aerosols in filter absorption photometers depends on the coating of the sampled particles. *Atmos. Meas. Tech.*, 10: 1043-1059. <https://doi.org/10.5194/amt-10-1043-2017>.
- Liu, D., He, C. and Schwarz, J.P. 2020. Lifecycle of light-absorbing carbonaceous aerosols in the atmosphere. *Clim. Atmos. Sci.*, 3: 40. <https://doi.org/10.1038/s41612-020-00145-8>.
- Middleton, W.E.K. 1952. *Vision through the Atmosphere*. The University of Toronto Press, Toronto.
- Olson, M.R., Victoria Garcia, M., Robinson, M.A., Van Rooy, P., Diitenberger, M.A., Bergin, M. and Schauer, J.J. 2015. Investigation of black and brown carbon multiple-wavelength-dependent light absorption from biomass and fossil fuel combustion source emissions. *J. Geophys. Res. Atmos.*, 120: 6682-6697. <https://doi.org/10.1002/2014JD022970>.
- Sandradewi, J. 2008. Using aerosol light absorption measurements for the quantitative determination of wood burning and traffic emission contributions to particulate. [^]
- Wang, Y., Hopke, P.K., Rattigan, O.V., Xia, X., Chalupa D.C. and Mark J. 2011. Characterization of residential wood combustion particles using the two-wavelength aethalometer. *Environ. Sci. Technol.*, 45: 7387-7393.
- Yang, M., Howell, S.G., Zhuang, J. and Huebert, B.J. 2009. Attribution of aerosol light absorption to black carbon, brown carbon, and dust in China – interpretations of atmospheric measurements during EAST AIRE. *Atmos. Chem. Phys.*, 9: 2035-2050. <https://doi.org/10.5194/acp-9-2035-2009>.
- Ziyong, G., Yuxiang, Y., Xiaodong, H., Xiacong, P., Yuzhen, F., Wei Sun, G., Zhang, D.C., Xinhui, B., Xinming, W. and Ping, P. 2022. The optical properties and in-situ observational evidence for the formation of brown carbon in clouds. *Atmos. Chem. Phys.*, 22(7): 4827-4839.





Hydrogeochemical Characteristics and Suitability of Groundwater for Drinking and Irrigation from Shallow Aquifers of PG1 Watershed in Chandrapur District of Maharashtra

S. S. Deshpande and Y. A. Murkute†

Postgraduate Department of Geology, Nagpur University, Law College Square, Nagpur-44000, India

†Corresponding author: Y. A. Murkute; yogmurkute@rediffmail.com

Nat. Env. & Poll. Tech.
Website: www.neptjournal.com

Received: 16-09-2022

Revised: 05-11-2022

Accepted: 12-11-2022

Key Words:

Hydrogeochemical characteristics
Rock-water interaction
Groundwater suitability
PG1 watershed

ABSTRACT

An endeavor has been made to understand the hydrogeochemical characteristics of groundwater from shallow aquifers of the PG1 watershed (latitudes 19°38'30" to 19°50'30" N and longitudes 79°04'00" to 79°11'00" E). The appropriateness of groundwater has also been checked for various purposes. The groundwater from the study area is alkaline and slightly saline. The $\text{Ca}^{2+} > \text{Mg}^{2+} > \text{Na}^+ > \text{K}^+$ and $\text{HCO}_3^- > \text{SO}_4^{2-} > \text{Cl}^- > \text{NO}_3^-$ was the ascendancy of cations and anions. The earth metals (Ca + Mg) exceeded the alkali metals (Na + K). The positive correlation interpreted from the interrelationship of Na^+ vs Cl^- exhibited a silicate weathering process for the liberation of ions in groundwater at the rock-water interface. In addition to the non-lithological source, anthropogenic inputs were inferred, indicating the agricultural fertilizers and domestic wastewater. All the groundwater samples from the study area are suitable for drinking and domestic use. The groundwater from the study area is also suitable for irrigation with negligible exceptions.

INTRODUCTION

Water is an indispensable commodity of every life that sustains on planet earth. Rainfall is the source of water and has two phases, *viz.*, surface water and another is groundwater. Every year, after the spells of monsoon, groundwater gets replenished beneath the earth's surface. This groundwater source is often contaminated because of the geogenic contaminants present at the rock-soil interface (Subba Rao 2002, Si et al. 2009, Murkute 2014). As the residence time increases, the interaction of water with rock minerals gets pronounced, and the concentrations of contaminants increase in many folds. The groundwater sources at shallow aquifers are more susceptible to swift contamination, while the deeper sources are less vulnerable. However, the groundwater positioned at a deeper depth may get contaminated quickly if a zone of mineralization occurs at that depth. In addition to geogenic sources, anthropogenic inputs may also deteriorate the quality of groundwater situated at shallow or even deeper depths. Groundwater contamination and its threat to human health have now been a major concern at a global level (Jalali 2006, Bhardwaj et al. 2010, Brindha & Elango 2013, Wu et al. 2015, Herojeet et al. 2015, Thilagavathi et al. 2015, Xu et al. 2018, Li et al. 2012, 2018, Duraisamy et al. 2018, Sreedevi et al. 2018, Adimalla & Qian 2019, Singh et al. 2019, Wang et al. 2019, Eyankware et al. 2020).

In the present paper, an attempt has been made to understand the rock-water interaction at the shallow aquifer depths since there was a lack of database information on the geochemical behavior of groundwater from this area. The PG1 watershed lies on the southwestern boundary of Chandrapur district, Maharashtra, covering 17 villages. This endeavor will also enable us to understand the suitability of groundwater quality for various purposes.

STUDY AREA

The study area is located in the southwestern part of Chandrapur district in Maharashtra. It is bounded by latitudes 19°38'30" to 19°50'30"N and longitudes 79°04'00" to 79°11'00"E (Fig. 1), covering 314 km² area. The study area experiences semi-arid climatic conditions, where the temperature rises to 48°C in the summer (middle March-middle June), while the temperature drops down gradually up to 8°C in December and January. The rainy season starts mid-June and extends to September, with an average annual rainfall of 1132.21 mm. The dendritic drainage pattern drains the entire area from the south towards the north direction, where run-off merges into the Penganga River in the watershed's northern part.

Geology and Hydrogeology

The Penganga Group of rocks (limestone-shale and limestone

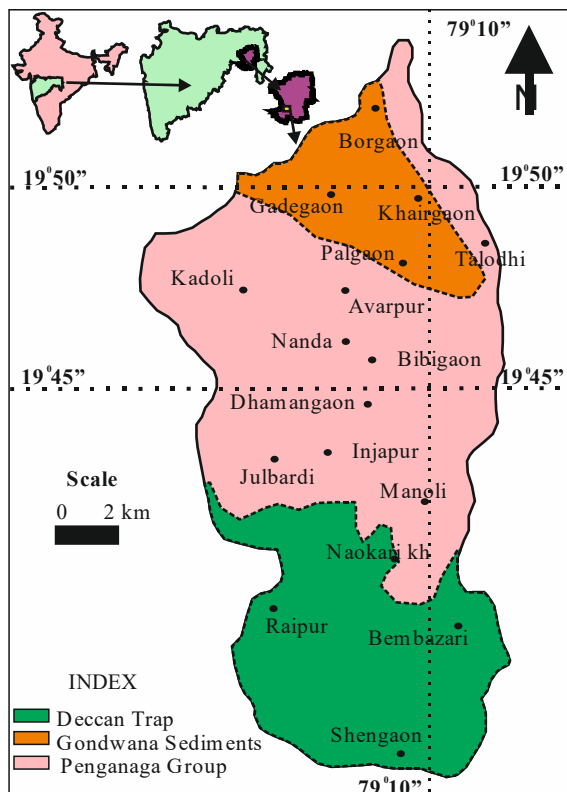


Fig. 1: Location and geological map of the study area with groundwater sampling sites.

sequences belonging to the Penganga Group of Godavari valley) located at a whole central-northern part of the watershed forms the base for the upper geological formations. The rocks of the Lower Gondwana Group (Talchir, Barakar and Kamthi formations) crop out at the northeastern boundary, while Deccan Trap Basalts cover the entire southern part of the study area. Local patches of alluvium, soil, and laterite are also discernible (not seen in Fig. 1).

The wells pierced in Penganga limestone have a groundwater discharge of 50 to 300 $\text{m}^3 \cdot \text{day}^{-1}$; these wells generally have a depth between 7 to 18 meters below ground level (mbgl) and diameters ranging from 2.5 to 5.5 m (GSDA 2009, 2015). The Gondwana formations have enhanced capacities of groundwater discharge to the tune of 100 to 350 $\text{m}^3 \cdot \text{day}^{-1}$ to the dug wells. These wells have a normal diameter of up to 5m and depth ranges from 10 to 15 mbgl (GSDA 2009, 2015). The wells penetrated in Deccan basaltic disposing of deep weathering, and well-developed joints have depths between 5 to 15 mbgl with diameters from 4 to 5.5 m and yield from 75 to 100 $\text{m}^3 \cdot \text{day}^{-1}$ (GSDA 2009, 2015).

MATERIALS AND METHODS

Seventeen groundwater samples were collected in

polyethylene bottles of 1000 mL capacity from villages of the PG1 watershed. The guiding principles of WHO (2011) and BIS (2012) were followed in the standard analytical procedures (Table 1). The customary measures prescribed by American Public Health Association (APHA 2005) were followed for the various laboratory analyses. The Gibbs (1970) variation diagrams and the Piper (1953) trilinear diagram were depicted to understand the mechanism of rock-water interaction.

RESULTS AND DISCUSSION

Physical Properties and Ion Concentrations

The field temperature recorded from each groundwater sample ranges from 23 to 28°C. The groundwater is dominantly alkaline in nature, showing pH values varying from 7.7 to 8.4 (Table 1). The electrical conductivity (EC) values grade from 456.8 to 3413.7 $\mu\text{s} \cdot \text{cm}^{-1}$, while total dissolved solids (TDS) values range between 292.4 to 2184.8 $\text{mg} \cdot \text{L}^{-1}$. As per US Geological Surveys (2000), if TDS values grade up to 1000 $\text{mg} \cdot \text{L}^{-1}$, then the water is referred to as freshwater; between 1000 to 3000 $\text{mg} \cdot \text{L}^{-1}$ is slightly saline water, and between 3000 to 10000 $\text{mg} \cdot \text{L}^{-1}$ is moderately saline. This classification shows that 29% of groundwater

Table 1: Analytical data of cations and anions with physical and computed parameters from the PG2 watershed.

Sr. no	Village	Sample No	pH	EC	TDS	TA	TH	Ca ²⁺	Mg ²⁺	Na ⁺	K ⁺	HCO ₃ ⁻	Cl ⁻	SO ₄ ²⁻	NO ₃ ⁻	CA-I	CA-II	Gibbs Cations	Gibbs Anions)
1.	Kadoli	DW1	7.8	781.2	500.0	350	353.5	54.8	52.8	44.7	8.1	352.8	71.8	23.8	14.5	0.49	0.09	0.49	0.17
2.	Dhamamgaon	DW2	7.7	526.7	337.1	223	284.4	50.8	38.4	23.8	1.2	223.6	35.7	17.2	12.7	0.37	0.05	0.33	0.14
3.	Bibigaon	DW3	8.2	899.6	575.7	311	474.9	63.2	77.3	29.1	1.4	312.5	103.2	38.6	10.8	0.73	0.21	0.33	0.25
4.	Nanda phata	DW4	8.2	945.9	605.4	387	434.1	63.6	67.1	32.8	1.3	383.5	77.9	42.7	22.4	0.60	0.10	0.35	0.17
5.	Palgaon	DW5	7.7	2208.5	1413.4	254	517.3	65.4	86.3	93.7	42.3	259.8	369.4	94.2	44.8	0.86	0.80	0.68	0.59
6.	Awarpur	DW6	7.9	2912.6	1864.1	443	427.4	79.6	55.7	209.4	3.3	439.6	294.4	170.9	1.3	0.30	0.14	0.73	0.40
7.	Gadegaon	DW7	8.3	878.4	562.2	369	333.1	38.6	57.7	88.2	1.2	362.4	75.3	44.8	9.1	-0.16	-0.03	0.70	0.17
8.	Talodhi	DW8	8.4	2756.5	1764.2	567	514.4	78.5	77.6	215.6	103.4	549.2	440.3	98.2	44.7	0.75	0.47	0.80	0.44
9.	Khairgaon	DW9	7.9	3413.7	2184.8	429	470.6	81.3	65.2	93.8	2.7	299.7	423.4	92.7	43.8	0.78	0.76	0.54	0.59
10.	Injapur	DW10	7.9	609.4	390.0	233	307.6	61.7	37.4	25.1	1.3	274.3	51.2	19.9	38.5	0.54	0.08	0.30	0.16
11.	Bembazari	DW11	7.7	857.7	548.9	342	330.3	62.4	42.5	22.8	2.3	342.7	35.7	13.8	5.7	0.43	0.04	0.29	0.09
12.	Naokari Kh.	DW12	8.3	511.3	327.2	167	257.9	48.7	33.2	17.9	4.8	163.2	41.8	42.3	2.2	0.69	0.14	0.32	0.20
13.	Shengaoon	DW13	8.2	818.7	524.0	289	373.2	56.3	56.7	19.2	1.2	183.8	21.5	1.3	1.1	0.16	0.02	0.27	0.10
14.	Borgaon	DW14	7.8	608.5	389.4	279	249.7	68.4	19.2	14.9	1.1	279.7	37.2	6.5	1.3	0.63	0.08	0.19	0.12
15.	Raipur	DW15	8.1	1167.9	747.5	326	479.6	98.7	56.8	39.2	1.4	325.6	155.8	34.2	13.7	0.76	0.32	0.29	0.32
16.	Manoli Kh.	DW16	8.3	456.8	292.4	233	237.5	51.7	26.4	18.9	1.3	227.2	27.7	4.9	1.3	0.36	0.04	0.28	0.11
17.	Julbardi	DW17	7.9	867.4	555.1	212	374.4	86.3	38.7	16.3	1.2	210.3	79.6	27.8	18.9	0.81	0.25	0.17	0.27
		Min	7.7	456.8	292.4	167	237.5	38.60	19.20	14.90	1.10	163.20	21.50	1.30	1.10	-0.16	-0.03	0.17	0.09
		Max	8.4	3413.7	2184.8	567	517.3	98.70	86.30	215.60	103.40	549.20	440.30	170.90	44.80	0.86	0.80	0.80	0.59
		Avg	8.0	1248.3	798.9	318	377.6	65.29	52.29	59.14	10.56	305.29	137.76	45.52	16.87	0.53	0.21	0.41	0.25
		SD	0.2	942.7	603.4	101	93.9	15.42	18.90	63.71	25.88	97.30	146.06	44.49	16.26	0.27	0.25	0.20	0.16
		CV	3.0	75.5	75.5	32	24.9	23.62	36.14	107.72	245.07	31.87	106.02	97.73	96.36	50.21	117.32	48.42	63.94

Gibbs Cations: (Na+K)/(Na+K+Ca), Gibbs Anions: (Cl/(Cl+HCO₃)), cation and anion values are presented in mg.L⁻¹.

samples are fresh, while the rest are slightly saline. The samples' average total alkalinity (TA) is 318 mg.L⁻¹, while total hardness (TH) values range from 237.5 to 517.3 mg.L⁻¹. Table 1 also exhibits that in 75% of samples, TH values are more than TA values, indicating noncarbonate hardness that cannot be removed easily (Chow 1964).

The dominance sequence of cations for groundwater samples from the study area is Ca²⁺ > Mg²⁺ > Na⁺ > K⁺. The Ca²⁺ values range between 38.6 to 98.7 mg.L⁻¹, and Mg²⁺ values vary from 19.2 to 86.3 mg.L⁻¹. Though the Ca²⁺ concentration is dominant amongst the cations, in 3 groundwater samples, Mg²⁺ values exceed it. The Na⁺ content ranges between 14.9 to 215.6 mg.L⁻¹, and K⁺ values fluctuate between 1.1 to 103.4 mg.L⁻¹.

The geogenic processes are mostly responsible for the calcium enrichment in the groundwater. However, loss of carbon dioxide, ion exchange processes, and calcium precipitation at the aquifer interface also causes the variation of calcium content in groundwater (Karanth 1987, Jain et al. 2010, Ahada & Suthar 2018). Similarly, the leaching of magnesium-bearing minerals and ion exchange processes at the rock-water interface is liable for the behavioral change in magnesium content (Thivya et al. 2018). The sodium and potassium concentration within the permissible limits represents the geogenic interface, while the increase in their concentration beyond the permissible limits as prescribed

by WHO (2011) and BIS (2012), certainly reflects human interventions and may be a threat to the human body (Mor et al. 2006, Murkute 2022).

The dominance sequence of anions is HCO₃⁻ > SO₄²⁻ > Cl⁻ > NO₃⁻; where in HCO₃⁻ and SO₄²⁻ contents vary from 163.2 to 549.2 mg.L⁻¹ and 1.30 to 170.9 mg.L⁻¹ respectively. Though the higher concentration of HCO₃⁻ primarily corresponds to geogenic contamination, the elevated values of SO₄²⁻ content certainly divulges anthropogenic contamination through the oxidation of supplementary sulfide-rich minerals supplied in fertilizers (Min et al. 2003, Chae et al. 2004). The Cl⁻ concentration varies between 21.5 to 440.3 mg.L⁻¹, and 40% of samples exceed the prescribed limit of 250 mg.L⁻¹ (WHO 2011, BIS 2012). This excess of Cl⁻ concentration indicates groundwater contamination (Loizidou & Kapetanos 1993). The average NO₃⁻ content in groundwater is 17.64 mg.L⁻¹, and all the samples have a concentration less than the prescribed limit of 45 mg.L⁻¹ (BIS 2012).

Hydrogeochemical Facies

Piper's trilinear diagram (Piper 1953) depicts cations and anions, which divulges the combination of water types. The trilinear diagram (Fig. 2), prepared for the present study, reveals that the earth metals (Ca + Mg) exceeded the alkali metals (Na + K); however, in seldom, alkalis (Na + K) also

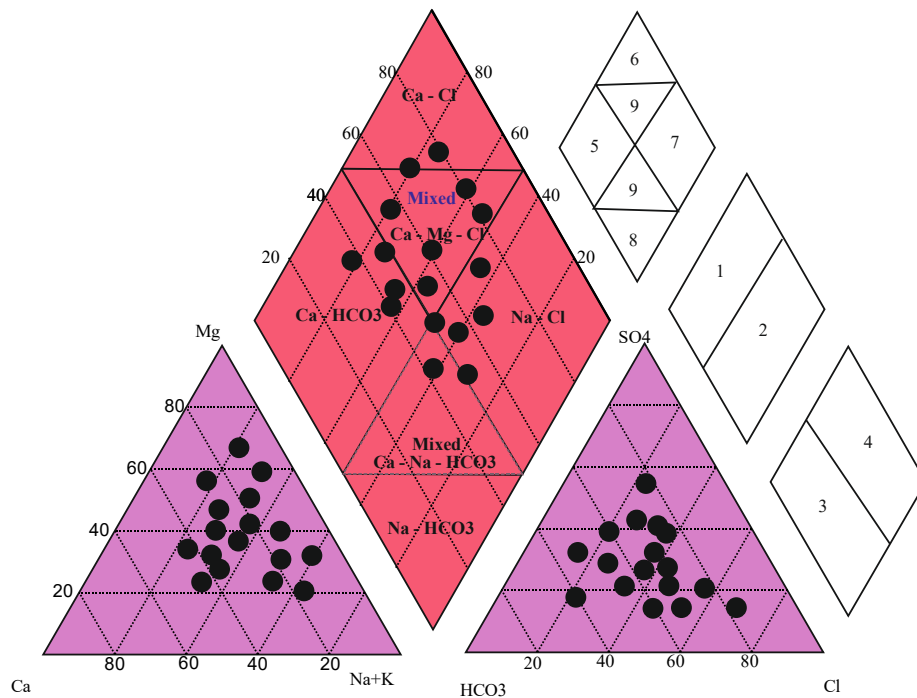


Fig. 2: Piper trilinear diagram for groundwater samples of the study area.

exceeded the alkaline earth (Ca + Mg). The weak acid ($\text{CO}_3 + \text{HCO}_3$) (35%) surpassed the combination of strong acids ($\text{SO}_4 + \text{Cl}$). In addition, 27% of mixed sectional (Ca-Mg-Cl and Ca-Na- HCO_3) and 46% of combinational hydrochemical facies (Ca-Mg- HCO_3 -Cl and Ca-Na- HCO_3 -Cl) have been noticed.

Rock-Water Interaction

The cations and anions have distinct behavior at the rock-water interface where certain reactions occur. In the present investigation, when the data points of HCO_3^- and Ca^{++} are plotted in terms of scatter diagram (Fig. 3a), a negative correlation has been observed; conversely, the scatter diagram of Na^+ vs Cl^- (Fig. 3b) exhibits a positive correlation, which divulges the reaction of silicate weathering, liberating calcium and bicarbonate in groundwater at rock-water interface (Lakshmanan et al. 2003). The minerals, namely feldspars, pyroxenes, and amphiboles from igneous and metamorphic rocks, while the calcite and clay minerals from sedimentary rocks are the primary sources of Ca^{2+} in groundwater samples (Todd 1995, Murkute & Badhan 2011). The points above the equiline in the scatter diagram of Na^+ vs Cl^- also suggest interventions by human activities (domestic waste, animal waste, septic tanks, etc.) in the groundwater domain (Murkute & Badhan 2011). In the $\text{Ca}^{2+} + \text{Mg}^{2+}$ and

$\text{SO}_4^{2-} + \text{HCO}_3^-$ interrelationship diagram of (Fig. 3c), all points fall above the equiline. In addition, the dominance of $\text{SO}_4^{2-} + \text{HCO}_3^-$ suggests a silicate weathering process for solute generation (Ramesh & Elango 2011).

The cations like Ca^{2+} , Mg^{2+} , Na^+ and HCO_3^- , Cl^- and SO_4^{2-} anions are released in groundwater after irrigation return flow (Karanth 1987). The negative correlation of NO_3^- and HCO_3^- contents in a scatter diagram reveals anthropogenic interventions. Contrary, in the present investigation, the scatter diagram of NO_3^- and HCO_3^- contents (Fig. 3d) points out a positive correlation, which suggests the different sources for the release of these ions, where NO_3^- is liberated due to anthropogenic input while lithological inputs are attributed to a derivation of HCO_3^- in groundwater (Subba Rao & Chaudhary 2019).

Hydrogeochemistry Controlling Mechanism

The interrelationship diagrams above explain the liberation of various cations and anions at the rock-water interface. Hence, all such processes worked out at the rock-water interface are called rock dominance (Gibbs 1970). In addition, precipitation and evaporation are other processes that liberate various cations and anions. The Gibb's diagrams, wherein the plotting of TDS against both the dominant cations [$(\text{Na}+\text{K}) / (\text{Na}+\text{K}+\text{Ca})$] (Fig. 4A), as well as dominant

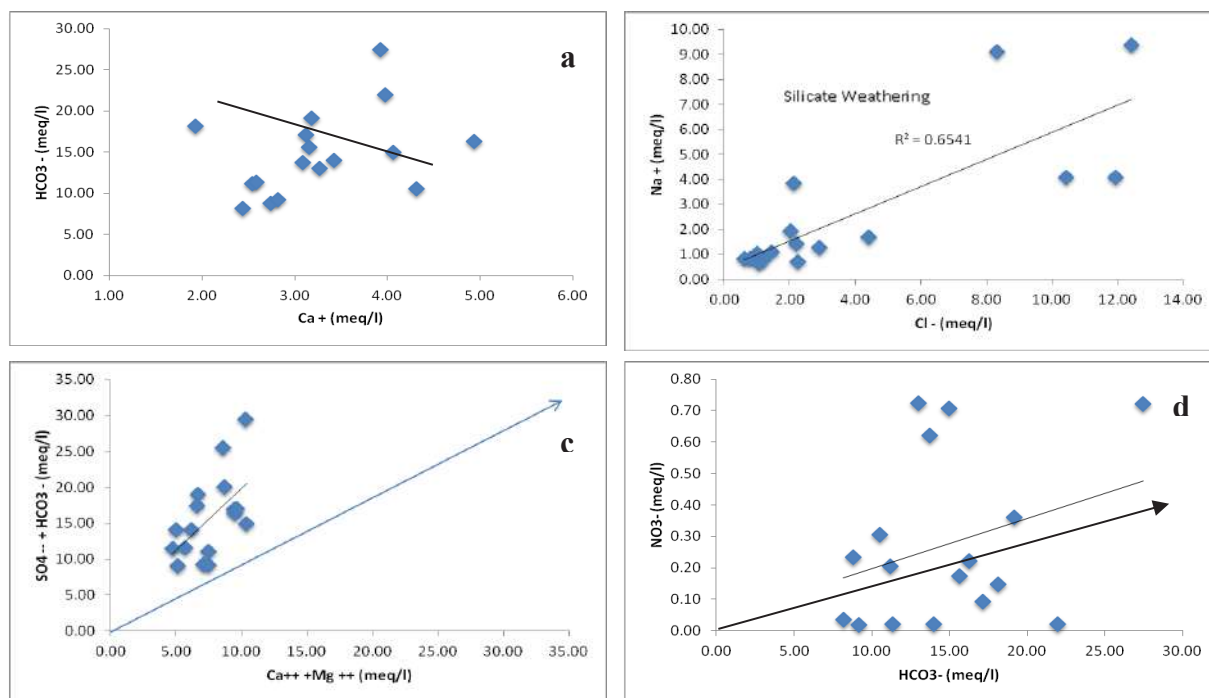


Fig. 3: Inter-ionic relationship between ions. a) scatter diagram of HCO_3^- and Ca^{2+} , b) scatter diagram of Na^+ vs Cl^- and c) scatter diagram of $\text{Ca}^{2+} + \text{Mg}^{2+}$ and $\text{SO}_4^{2-} + \text{HCO}_3^-$, d) scatter diagram of NO_3^- vs HCO_3^- .

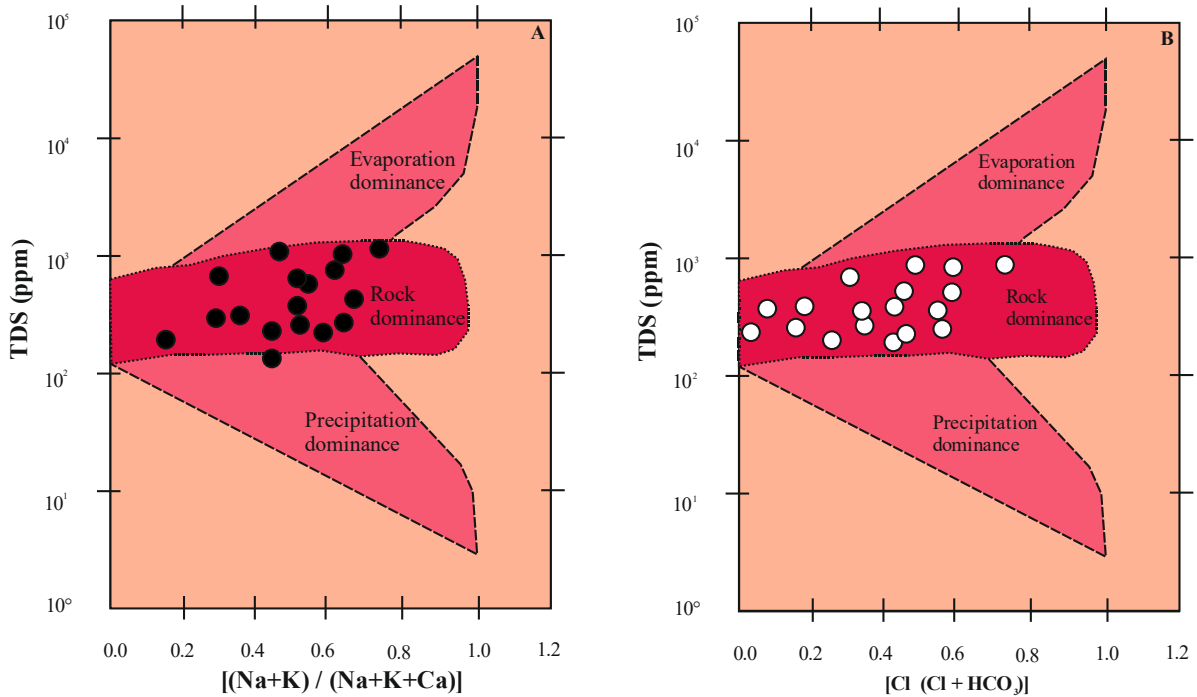


Fig. 4: Gibbs diagram (A) TDS with $[(Na+K)/(Na+K+Ca)]$, (B) TDS with $[(Cl/Cl+HCO_3)]$.

anions $[(Cl/Cl+HCO_3)]$ (Fig. 4B), is carried out to confirm the hydrogeochemical controlling mechanism of dissolved cations and anions with the precipitation dominance, rock dominance, and evaporation dominance (Gibbs 1970). The Gibbs diagrams plotted for the groundwater samples from the study area point out that some anthropogenic activities also influence rock dominance as the main hydrogeochemical controlling mechanism (Gibbs 1970, Ravikumar et al. 2010).

Hydrogeochemical Correlation

The correlation matrix has been computed for pH, EC, TDS, TH, Ca^{2+} , Mg^{2+} , Na^+ , K^+ , HCO_3^- , NO_3^- , SO_4^{2-} and Cl^- (Table 2). The positive correlation between TDS with TH, Ca^{2+} , Na^+ , NO_3^- , SO_4^{2-} and Cl^- suggests the association of hydrochemical processes responsible for rock-water interaction, concomitantly with anthropogenic interventions (Tay et al. 2017, Murkute 2022). The correlation matrix

Table 2: Correlation matrix of hydrochemical parameters from the study area.

	pH	EC	TDS	TH	Ca^{2+}	Mg^{2+}	Na^+	K^+	NO_3^-	HCO_3^-	SO_4^{2-}	Cl^-
pH	1.00											
EC	-0.23	1.00										
TDS	-0.41	1.00	1.00									
TH	-0.28	0.73	0.66	1.00								
Ca^{2+}	-0.41	0.67	0.73	0.94	1.00							
Mg^{2+}	-0.26	0.38	0.42	0.93	0.65	1.00						
Na^+	-0.17	0.73	0.73	-0.32	0.38	0.21	1.00					
K^+	-0.25	0.46	0.74	-0.35	0.41	0.33	0.43	1.00				
NO_3^-	0.31	0.68	0.79	-0.18	0.65	0.37	0.54	0.23	1.00			
HCO_3^-	0.66	0.32	0.32	-0.29	0.22	-0.28	0.39	0.45	-0.19	1.00		
SO_4^{2-}	-0.13	0.69	0.75	0.83	0.77	0.53	0.77	0.33	0.33	0.73	1.00	
Cl^-	-0.43	0.79	0.77	0.31	0.69	0.29	0.84	0.52	0.75	0.31	0.45	1.00

also indicates a low correlation between K^+ with NO_3^- and SO_4^{2-} suggesting the non-lithological source, indicating the agricultural fertilizers and domestic wastewaters (Chacha et al. 2018). Na^+ has a strong positive correlation with both Cl^- and SO_4^{2-} , which indicates the presence of pollution in the groundwater of the study area (Barzegar et al. 2017). The HCO_3^- having a negative correlation with NO_3^- also points out the non-geogenic sources for NO_3^- content (Wu & Sun 2016).

Groundwater Suitability

Drinking and Domestic Use

The groundwater suitability has been checked with desirable and permissible limits suggested by WHO (2011) and BIS (2012) (Table 3). The WHO (2011) has suggested a permissible limit of 1500 mg.L^{-1} for EC, which is also a measure of salinity hazard. All the groundwater samples from the study area have EC values less than the prescribed permissible limit indicating their suitability for drinking purposes (Table 3). The BIS (2012) has a permissible limit of 2000 mg.L^{-1} for TDS; considering this as the upper limit, all the groundwater samples are suitable for drinking except one (Khairgaon). Generally, the concentration of TH content is used as the parameter to decide the utility of groundwater for domestic use (Karanth 1987, Todd 1995). The BIS (2012) has suggested a permissible limit of 600 mg.L^{-1} for TH. Hence, all the study area’s groundwater samples can be used for domestic purposes without hesitation.

Irrigation Use

The irrigation suitability of groundwater samples was ensured through the parameters, evolved through the mathematical expressions in equations 1 to 8, and results are presented in Table 4.

Sodium Absorption Ratio (SAR); $SAR = Na^+ / \sqrt{[(Ca^{2+} + Mg^{2+})/2]}$... (1)

Percent Sodium (%Na); $\% Na = Na^+ + K^+ / (Ca^{2+} + Mg^{2+} + Na^+ + K^+) \times 100$... (2)

Residual Sodium Carbonate (RSC); $RSC = (HCO_3^- + CO_3^{2-}) - (Ca^{2+} + Mg^{2+})$... (3)

Residual Sodium Bicarbonate (RSBC); $RSBC = HCO_3^- - Ca^{2+}$... (4)

Soluble Sodium Percentage (SSP); $SSP = [(Na^+ + K^+) / (Ca^{2+} + Mg^{2+} + Na^+ + K^+)] \times 100$... (5)

Corrosivity Ratio (CR); $CR = [(Cl^- / 35.5) + 2 (SO_4^{2-} / 96)] / 2 (HCO_3^- + CO_3^{2-} / 100)$... (6)

Kelley’s Ratio (KR); $KR = Na^+ / (Ca^{2+} + Mg^{2+})$... (7)

Synthetic Harmful Coefficient (K); $K = 12.4\text{ TDS} + SAR$... (8)

SAR: It measures soil permeability with respect to cations. The SAR values from the study area range from 0.4 -4.4 meq.L^{-1} , inferring the excellent quality of groundwater for irrigation purposes. The US Salinity Laboratory’s diagram (US Salinity Laboratory Staff 1954) uses SAR values and compares with the salinity hazard (Fig.5). The plots of the groundwater samples have been noted to cluster in C_3-S_2 (41%) and C_3-S_1 (47%) types, except one plot. The C_3-S_2 type represents the high salinity - medium sodium type,

Table 3: Range of cations and anions with desirable and permissible limits.

Parameter	Min	Average	Max	WHO (2011)		BIS (2012) IS: 10500		SD	CV
				Desirable (DL)	Permissible (PL)	Desirable (DL)	Permissible (PL)		
pH	7.7	8.0	8.4	7.0-8.5	6.5-9.2	6.5-8.5	8.5-9.2	0.2	3.0
EC	456.8	1248.3	3413.7	750	1500	-	-	942.7	75.5
TDS	292.4	798.9	2184.8	500	1500	500	2000	603.4	75.5
TA	167.0	318.5	567.0	100	500	200	600	100.9	31.7
TH	237.5	377.6	517.3	100	500	300	600	93.9	24.9
Ca ⁺⁺	38.6	65.3	98.7	75	200	75	200	15.4	23.6
Mg ⁺⁺	19.2	52.3	86.3	30	150	30	100	18.9	36.1
Na ⁺	14.9	59.1	215.6	50	200	-	-	63.7	107.7
K ⁺	1.1	10.6	103.4	100	200	-	-	25.9	245.1
HCO ₃ ⁻	163.2	305.3	549.2	200	600	200	600	97.3	31.9
Cl ⁻	21.5	137.8	440.3	250	600	250	1000	146.1	106.0
SO ₄ ⁻	1.3	45.5	170.9	200	600	200	400	44.5	97.7
NO ₃ ⁻	1.1	17.6	56.8	-	50	45	100	17.8	101.1

Cation and anion values are presented in mg.L^{-1} . SD – standard deviation, CV – covariance.

Table 4: Irrigation suitability indices for groundwater of study area.

Sr.No	Village	Sample No	SAR	% Na	RSC	RSBC	SSP	CR	KR	<i>K</i>
1.	Kadoli	DW1	1.0	29.0	0.2	-2.1	23.8	0.1	0.3	3.9
2.	Dhamamgaon	DW2	0.6	8.3	0.7	1.0	15.8	0.1	0.2	4.4
3.	Bibigaon	DW3	0.6	12.5	0.8	3.0	12.0	0.1	0.1	7.9
4.	Nanda phata	DW4	0.7	11.7	1.3	6.5	14.4	0.1	0.2	7.1
5.	Palgaon	DW5	1.8	123.7	0.3	-0.1	35.6	0.5	0.4	6.3
6.	Awarpur	DW6	4.4	31.3	1.7	6.1	52.0	0.4	1.1	3.4
7.	Gadegaon	DW7	2.1	15.5	1.4	10.4	36.7	0.1	0.6	2.1
8.	Talodhi	DW8	4.1	290.2	2.1	11.8	61.0	0.4	0.9	3.4
9.	Khairgaon	DW9	1.9	20.4	0.7	-1.3	30.7	0.5	0.4	9.3
10.	Injapur	DW10	0.6	8.6	0.9	1.4	15.5	0.1	0.2	5.0
11.	Bombezari	DW11	0.5	11.4	1.3	4.7	13.8	0.0	0.1	8.1
12.	Naokari Kh.	DW12	0.5	16.6	0.4	-1.6	15.1	0.1	0.2	5.4
13.	Guwariguda	DW13	0.4	9.4	0.2	-2.1	10.4	0.0	0.1	9.7
14.	Belampur	DW14	0.4	5.7	1.1	0.3	11.9	0.0	0.1	7.6
15.	Gadchandur	DW15	0.8	11.7	0.8	-3.5	15.4	0.2	0.2	7.7
16.	Manoli kh	DW16	0.5	7.2	0.8	1.0	15.3	0.0	0.2	4.4
17.	Nagrala	DW17	0.4	7.7	0.4	-6.7	9.0	0.1	0.1	12.1
Min			0.4	5.7	0.2	-6.7	9.0	0.0	0.1	2.1
Max			4.4	290.2	2.1	11.8	61.0	0.5	1.1	12.1
Average			1.3	36.5	0.9	1.7	22.8	0.2	0.3	6.3
SD			1.26	70.95	0.545	4.883	15.28	0.16	0.29	2.672
CV			99.8	194.3	60.76	289.5	66.92	91.	92.1	42.13

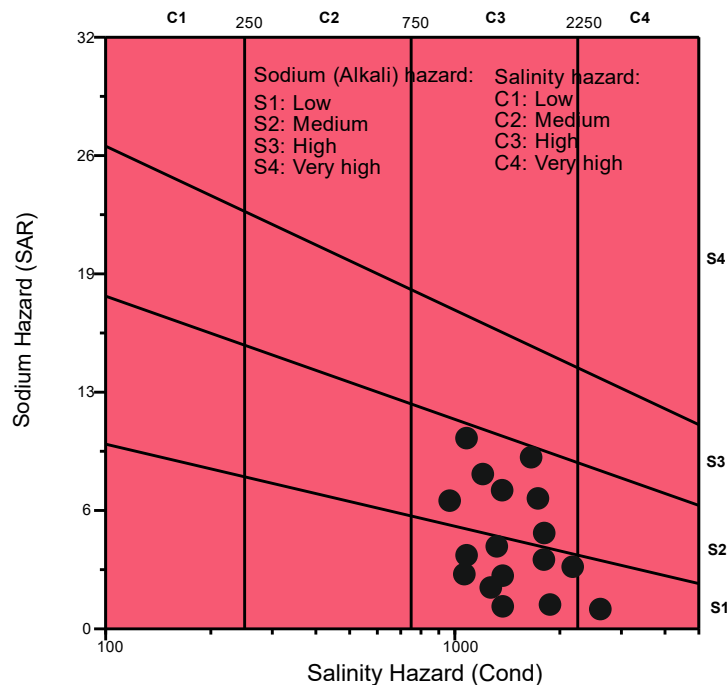


Fig. 5: US Salinity diagram for groundwater samples from the PG1 watershed.

while the C₃-S₁ type represents the medium salinity - medium sodium characters. These two categories reveal that the groundwater from the study area may pose a slight threat of exchangeable sodium, but even then can be utilized for irrigation purposes.

%Na: The %Na in higher concentration in water causes the obliterating of inner drainage, and hence such water is not appropriate for irrigation for a longer duration (Simsek & Gunduz 2007, Murkute 2014, Chacha et al. 2018). Almost all values of %Na in the study area are less than 20 meq.L⁻¹ (except two samples), suggesting their suitability for irrigation purposes.

RSC: The RSC values exceeding 2.5 meq.L⁻¹ indicate its harmful nature to the growth of plants. Generally, RSC values are categorized as RSC < 1.25, as good; 1.25 to 2.5 as doubtful and > 2.5 as unsuitable. As per this scheme, all the samples (except one) are good and can be used for irrigation.

RSBC: The high RSC content in water poses carbonate deposition in soil and deteriorates its fertility (Agoubi et al. 2011). RSBC value above 10 meq.L⁻¹ is unsuitable for irrigation. Except for one sample, all the samples from the study area are suitable for irrigation (Table 4).

SSP: The higher SSP values lower the soil permeability. The SSP values should be less than 50 meq.L⁻¹. The groundwater samples of the study area (except one sample) have SSP values less than 50 meq.L⁻¹, hence suitable for irrigation purposes.

CR: The water with CR values < 1 is suitable for irrigation without the threat of corrosiveness; hence, all the groundwater samples from the study area are suitable for irrigation (table 4), and water can be transported to longer distances for irrigation activity.

KR: The water with KR values < 1 is suitable for irrigation. Except for one, groundwater from the study area is suitable for irrigation.

K: The high *K* value evaluated for irrigation-use of water represents the high salt presence and alkali hazards (Xu et al. 2018, Zhou et al. 2020). The *K* value exceeding 36 meq/l corresponds to the fact that water is not suitable for irrigation purposes. The maximum *K* value obtained for groundwater samples from the study area is 12.1 meq.L⁻¹, suggesting the suitability of water for irrigation use (Table 4).

CONCLUSIONS

The present study was to understand the hydrogeochemical characteristics and to evaluate the suitability of groundwater from shallow aquifers of the PG1 watershed. Based upon the various investigations carried out, the conclusions made

are as follows:

- i) The maximum electrical conductivity (EC) and TDS values are 3413.7 and 2184.8 mg.L⁻¹, respectively, which suggest that 29% of groundwater samples from the study area are fresh, while the rests of the sample are slightly saline in nature. The dominant sequence of cations and anions for groundwater samples from the study area is Ca²⁺ > Mg²⁺ > Na⁺ > K⁺ and HCO₃⁻ > SO₄²⁻ > Cl⁻ > NO₃⁻ respectively.
- ii) The trilinear diagram prepared for the present study reveals that the earth metals (Ca + Mg) exceeded the alkali metals (Na + K); however, in some cases, alkalis (Na + K) also exceeded the alkaline earth (Ca + Mg). 27% of mixed sectional water types (Ca - Mg - Cl and Ca - Na - HCO₃) and 46% of combinational hydrochemical facies (Ca - Mg - HCO₃ - Cl and Ca - Na - HCO₃ - Cl) have been noticed from the study area.
- iii) The interrelationship of Na⁺ vs Cl⁻ exhibits a positive correlation, divulging the reaction of silicate weathering, allowing the liberation of calcium and bicarbonate ions in groundwater at the rock-water interface. In the Ca²⁺+Mg²⁺ and SO₄²⁻+HCO₃⁻ interrelationship diagram, all the points fall above the equiline, suggesting the dominance of SO₄²⁻+HCO₃⁻ and, therefore, indicate silicate weathering process for a solute generation. The positive correlation of NO₃⁻ and HCO₃⁻ suggests the different sources for releasing these ions, where NO₃⁻ is liberated due to anthropogenic input, while lithological inputs are attributed to the derivation of HCO₃⁻ in groundwater.
- iv) The Gibbs diagrams for study area point out the rock dominance as the main hydrogeochemical controlling mechanism along with some inputs of anthropogenic activities observed through NO₃⁻. The correlation matrix shows a low correlation between K⁺ with NO₃⁻ and SO₄²⁻ suggesting the non-lithological source, indicating the agricultural fertilizers and domestic wastewater. While, Na⁺ has a strong positive correlation with both Cl⁻ and SO₄²⁻, which also indicates the presence of pollution in the groundwater of the study area, which may be a non-geogenic source.
- v) All the groundwater samples from the study area have EC values less than the prescribed permissible limit indicating their suitability for drinking purposes. The suitable TH values indicate that groundwater samples from the study area are appropriate for domestic purposes without hesitation. The 8 parameters involved in the present study for inferring the suitability of groundwater for irrigation purposes are: SAR, %Na, RSC, RSBC, SSP, CR, KR, *K*. The values computed

for these parameters point out that groundwater from the study area is also suitable for irrigation purpose with negligible exceptions.

ACKNOWLEDGEMENTS

The authors thank Dr. A.P. Dharashivkar and Dr. V.V. Solanki, Groundwater Survey and Development Agency (GSDA), for their technical support during fieldwork and valuable suggestions. The authors gratefully acknowledge the anonymous reviewer for constructive suggestions and comments in the manuscript.

REFERENCES

- Adimalla, N. and Qian, H. 2019. Groundwater quality evaluation using water quality index (WQI) for drinking purposes and human health risk (HHR) assessment in an agricultural region of Nanganur, south India. *Ecotoxicol. Environ. Saf.*, 176: 153-161.
- Agoubi, B., Kharroubi, A. and Abida, H. 2011. Hydrochemistry of groundwater and its assessment for irrigation purpose in coastal Jeffara aquifer, southeastern Tunisia. *Arab. J. Geosci.*, 6: 1163-1172.
- Ahada, C.P.S. and Suthar, S. 2018. Assessing groundwater hydrochemistry of Malwa Punjab, India. *Arab. J. Geosci.*, 11: 17.
- American Public Health Association (APHA) 2005. Standard Methods for the Examination of Water and Wastewater. American Public Health Association, Water Pollution Control Federation, American Water Works Association, Water Environment Federation, Washington DC.
- Barzegar, R., Moghaddam, A.A., Tziritis, E., Fakhri, M.S. and Soltani, S. 2017. Identification of hydrogeochemical processes and pollution sources of groundwater resources in the Marand Plain, northwest of Iran. *Environ. Earth. Sci.*, 76: 297.
- Bhardwaj, V., Singh, D.S. and Singh, A.K. 2010. Water quality of the Chhoti Gandak River using principal component analysis, Ganga plain. *J. Earth Syst. Sci.*, 119(1): 117-127.
- BIS (2012). Indian Standard Drinking Water Specifications. IS: 10500. Bureau of Indian Standards, New Delhi.
- Brindha, K. and Elango, L. 2013. Geochemistry of fluoride rich groundwater in a weathered granitic rock region, Southern India. *Water Qua. Expo. Health*, 5(3): 127-138.
- Chacha, N., Njau, K.N., Lugomela, G.V. and Muzuka, A.N.N. 2018. Hydrogeochemical characteristics and spatial distribution of groundwater quality in Arusha well fields, northern Tanzania. *Appl. Water Sci.*, 8: 1-23.
- Chae, G.T., Kim, K., Yun, S.T., Kim, K.H., Kim, S.O., Choi, B.Y., Kim, H.S. and Rhee, C.W. 2004. Hydrogeochemistry of alluvial groundwaters in an agricultural area, an implication for groundwater contamination susceptibility. *Chemosphere*, 55: 369-378.
- Chow, V.T. 1964. *Handbook of Applied Hydrology*. McGraw-Hill, New York.
- Duraisamy, S., Govindhaswamy, V., Duraisamy, K., Krishinaraj, S., Balasubramanian, A. and Thirumalaisamy, S. 2018. Hydrogeochemical characterization and evaluation of groundwater quality in Kangayam taluk, Tirupur district, Tamil Nadu, India, using GIS tech. *Environ. Geochem. Health*, 16: 183 <https://doi.org/10.1007/s10653-018-0183-z>.
- Eyankware, M.O., Aleke, C.G., Selemo, A.O.I. and Nnabo, P.N. 2020. Groundwater for sustainable development hydrogeochemical studies and suitability assessment of groundwater quality for irrigation at Warri and environs, Niger delta basin, Nigeria. *Ground. Sustain. Dev.*, 10: 100293.
- Gibbs, R.J. 1970. Mechanism of controlling world water chemistry. *Science*, 17: 1088-1090.
- GSDA. 2009. Dynamic Groundwater Resources of Maharashtra Detailed Report (as of 2007-08). Groundwater Surveys and Development Agency, Water Supply and Sanitation Department, Government of Maharashtra and Central Ground Water Board, Central Region, Nagpur, 228p.
- GSDA. 2015. Report on Dynamic Groundwater Resources of Maharashtra Detailed Report (as of 2007-08). Groundwater Surveys and Development Agency, Water Supply and Sanitation Department, Government of Maharashtra and Central Ground Water Board, Central Region, Nagpur, 732p.
- Herojeet, R., Rishi, M.S. and Kishore, N. 2015. Integrated approach of heavy metal pollution indices and complexity quantification using chemometric models in the Sirsa Basin, Nalagarh valley, Himachal Pradesh, India. *Chin. J. Geochem.*, 34: 620-633.
- Jain, C.K., Bandyopadhyay, A. and Bhadra, A. 2010. Assessment of ground water quality for drinking purpose, District Nainital, Uttarakhand, India. *Environ. Monit. Assess.*, 166: 663-676.
- Jalali, M. 2009. Geochemistry characterization of groundwater in an agriculture area of Razan, Hamadan, Iran. *Environ. Geol.*, 56: 1479-1488.
- Karant, K.R. 1987. *Groundwater Assessment Development and Management*. Tata McGraw Hill Publishing Company Ltd, New Delhi, p. 468.
- Lakshmanan, E., Kannan, R. and Senthilkumar, M. 2003. Major ion chemistry and identification of hydrogeochemical processes of groundwater in a part of Kancheepuram District, Tamil Nadu, India. *Environ. Geosci.*, 10(4): 157-166.
- Li, P., Wu, J. and Qian, H. 2012. Groundwater quality assessment based on rough sets attribute reduction and TOPSIS method in a semi-arid area, China. *Environ. Monit. Assess.*, 184: 4841-4854.
- Li, P., Wu, J., Tian, R., He, S., He, X., Xue, C. and Zhang, K. 2018. Geochemistry, hydraulic connectivity and quality appraisal of multilayered groundwater in the Hongdunzi coal mine, Northwest China. *Mine Water Environ.*, 37: 222-237.
- Loizidou, M. and Kapetanios, E.G. 1993. Effect of leachate from landfills on underground water quality. *Sci. Tot. Environ.*, 128: 69-81.
- Min, J.H., Yun, S.T., Kim, K., Kim, H.S. and Kim, D.J. 2003. Geologic controls on the chemical behavior of nitrate in riverside alluvial aquifers, Korea. *Hydrol. Process*, 17: 1197-1211.
- Mor, S.K., Ravindra, R.P., Dahiya and Chandra, A. 2006. Leachate characterization and assessment of groundwater pollution near municipal solid waste landfill site. *Environ. Monit. Assess.*, 118: 435-456.
- Murkute, Y.A. 2014. Hydrogeochemical characterization and quality assessment of groundwater around Umrer Coal Mine area, Nagpur District, Maharashtra, India. *Environ. Earth Sci.*, 72: 4059-4073.
- Murkute, Y.A. 2022. Major ion chemistry and assessment of groundwater quality around Gangpur Village, Nagpur District, Maharashtra, India. *J. Geosci. Res.*, 7(1): 112-120.
- Murkute, Y.A. and Badhan, P.P. 2011. Fluoride contamination in groundwater from Bhadravati Tehsil, Chandrapur District, Maharashtra. *Nature Environ. Pollut. Technol.*, 10(2): 255-260.
- Piper, A.M. 1953. A graphical procedure in the Geochemical Interpretation of water analyses. *Am. Geophy. Union Trans.*, 25: 914-923.
- Ramesh, K. and Elango, L. 2011. Groundwater quality and suitability for domestic and agricultural use in the Tondiar river basin, Tamil Nadu, India. *Environ. Monit. Assess.*, 184: 3887-3899.
- Ravikumar, P., Venkatesharaju, K., Prakash, K.L. and Somashekar, R.K. 2010. Geochemistry of groundwater and groundwater prospects evaluation, Anekal Taluk, Bangalore urban district, Karnataka, India. *Environ. Monit. Assess.*, 16: 721. <https://doi.org/10.1007/s10661-010-1721-z>.

- Si, J., Feng, Q., Wen, X., Su, Y., Xi, H. and Chang, Z. 2009. Major ion chemistry of groundwater in the extremely arid region of northwest China. *Environ. Geol.*, 57: 1079-1087.
- Simsek, C. and Gunduz, O. 2007. IWQ Index: A GIS-integrated technique to assess irrigation water quality. *Environ. Monit. Assess.*, 128: 277-300.
- Singh, G., Rishi, M.S., Herojeet, R., Kaur, L. and Sharma, K. 2019. Evaluation of groundwater quality and human health risks from fluoride and nitrate in the semi-arid region of northern India. *Environ. Geochem. Health*, 6: 449. <https://doi.org/10.1007/s10653-019-00449-6>
- Sreedevi, P.D., Sreekanth, P.D., Ahmed, S. and Reddy, D.V. 2018. Appraisal of groundwater quality in a crystalline aquifer: A chemometric approach. *Arab. J. Geosci.*, 12: 517. <https://doi.org/10.1007/s12517-018-3480-z>.
- Subba Rao, N. 2002. Geochemistry of groundwater in parts of Guntur district, Andhra Pradesh, India. *Environ. Geol.*, 41: 552-562.
- Subba Rao, N. and Chaudhary, M. 2019. Hydrogeochemical processes regulating the spatial distribution of groundwater contamination, using pollution index of groundwater (PIG) and hierarchical cluster analysis (HCA): A case study. *Ground. Sustain. Dev.*, 10: 238. <https://doi.org/10.1016/j.gsd.2019.100238>.
- Tay, C.K., Hayford, E.K. and Hodgson, I.O.A. 2017. Application of multivariate statistical technique for hydrogeochemical assessment of groundwater within the Lower Pra Basin, Ghana. *Appl. Water Sci.*, 7: 1131-11150.
- Thilagavathi, N., Subramani, T., Suresh, M. and Karunanidhi, D. 2015. Mapping of groundwater potential zones in Salem Chalk Hills, Tamil Nadu, India, using remote sensing and GIS techniques. *Environ. Monit. Assess.*, 43: 1514. <https://doi.org/10.1007/s10661-015-4376-y>.
- Thivya, C., Chidambaram, S., Thilagavathi, R., Venkatraman, Ganesh, N., Panda, B. and Prasanna, M.V. 2018. Short-term periodic observation of the relationship of climate variables to groundwater quality along the KT boundary. *J. Clim. Chang.*, 4: 77-86.
- Todd, D.K. 1995. *Groundwater Hydrology*. John Wiley and Sons, NY.
- US Geological Survey. 2000. *Classification of Natural Ponds and Lakes*. US Department of the Interior, US Geological Survey, Washington, DC
- US Salinity Laboratory Staff. 1954. *Diagnosis and Improvements of Saline and Alkali soils*. US Department of Agriculture Handbook, USDA, p. 160
- Wang, L., Mei, Y., Yu, K., Li, M. and Hu, X. 2019. Anthropogenic effects on the hydrogeochemical characterization of the shallow groundwater in an arid irrigated plain in northwestern China. *Water (Switzerland)*, 11: 11. <https://doi.org/10.3390/w11112247>
- WHO. 2011. *Guidelines for Drinking-Water Quality 216*. World Health Organization, Geneva, Switzerland, pp. 303-304.
- Wu, J. and Sun, Z. 2016. Evaluation of shallow groundwater contamination and associated human health risk in an alluvial plain impacted by agricultural and industrial activities, mid-west China. *Expo Health*, 8(3): 311-329.
- Wu, J., Li, P. and Qian, H. 2015. Hydrochemical characterization of drinking groundwater with special reference to fluoride in an arid area of China and the control of aquifer leakage on its concentrations. *Environ. Earth Sci.*, 73: 8575-8588.
- Xu, Y., Dai, S., Meng, K., Wang, Y., Ren, W., Zhao, L., Christie, P. and Teng, Y. 2018. Occurrence and risk assessment of potentially toxic elements and typical organic pollutants in contaminated rural soils. *Sci. Tot. Environ.*, 30: 618-629.
- Zhou, Y., Li, P., Xue, L., Dong, Z. and Li, D. 2020. Solute geochemistry and groundwater quality for drinking and irrigation purposes: A case study in Xinle City, North China. *Geochemistry*, 20: 1256. <https://doi.org/10.1016/j.chemer.2020.125609>.



Efficacy of Nanofertilizers Over Chemical Fertilizers in Boosting Agronomic Production

A. Khatri and R. Bhatia†

Department of Environmental Science, Maharshi Dayanand University, Rohtak-125001, Haryana, India

†Corresponding author: R. Bhatia; bioremediationlab.mdu@gmail.com

Nat. Env. & Poll. Tech.
Website: www.neptjournal.com

Received: 20-10-2022

Revised: 12-12-2022

Accepted: 24-12-2022

Key Words:

Nanofertilizers

Micronutrients

Macronutrients

Environmental stress

Disease resistance

ABSTRACT

Global agricultural production cannot catch the increasing population's exigency. At different times, the world has faced food crises of varying intensity. Many steps have been taken after that to encounter the rising concerns. Nowadays, nanofertilizers are being experimented with as an alternative to conventional fertilizers. Nanofertilizers can be classified as macronutrients and micronutrients nanofertilizers. Synthesis of macronutrient nanofertilizers (nitrogen, phosphorus, potassium, calcium, magnesium, etc.) and micronutrient nanofertilizers (iron, boron, zinc, copper, silicon, etc.) can be done using chemical and green synthesis methods, which involves reducing agents, capping agents, dendrimers, microbial synthesis, solvents, and others. Composition of the nanofertilizers can be done using top-down and bottom-up approaches incorporating hydrocarbon polymer, dendrimers, microbes, etc., which decides their usage in various crops depending upon the requirement of the plant. Engineered nanofertilizers can improve crop yield by mitigating environmental pollution, environmental stress, and plant diseases. However, the unsystematic use of nanofertilizers can be a hurdle in its utilization. This article discusses various types of nanofertilizers with their unique properties and applications. Each category of nanofertilizers is explained considering their composition, particle size, concentrations applied, benefited plant species, and plant-growth enhancement aspects.

INTRODUCTION

The rapidly growing population has been causing food scarcity worldwide. Many factors, such as land degradation, climate change, and expanding population, threaten the food supply. The Food and Agriculture Organization (FAO) reported that about 670 million people in the world, constituting about 8 % of the world population, would be facing hunger in 2030, the same as in 2015 when the 2030 Agenda was launched (FAO et al. 2022). These statistics can increase to 840 million by 2030 if the present mode extends. As per the report, the factors responsible for worldwide famine are industrial decline and the uttermost meteorological phenomena. The UNO notified the need to improve global nutrition systems otherwise, zero hunger by 2030 cannot be achieved. The FAO's instructional global mapping facilitates readers to envisage hunger patterns.

In the present scenario, chemical fertilizers are becoming a threat in one way or another. Different factors are responsible for the same, but growing demand has resulted in excessive utilization of chemical fertilizers. These factors include limited cultivable lands, water scarcity, growing population, etc. (Shuqin & Fang 2018). Earlier, these factors

oriented us toward the usage of chemical fertilizers. Although conventional supplements began to enhance crop growth and productivity, the intensive usage of these for a long time resulted in unimagined and devastating environmental impacts worldwide, such as groundwater contamination, water eutrophication, soil quality degradation, and air pollution.

Many approaches have been used to enhance fertilizer efficiency. Some of these involve the development of chemical fertilizers, changes in irrigation systems, crop hybrids, etc. Initially, when chemical fertilizers were used, an upsurge in production was noticed. However, in the long run, it resulted in various problems like soil pollution, water contamination, health issues, and many more. The application of nanotechnology for synthesizing fertilizers can be seen as a new step toward sustainable agriculture. It can be considered a promising option for dealing with the menace of food scarcity and bringing sustainability during climate change (Qureshi et al. 2018). Nanomaterials are particles whose size ranges between 1 and 100 nanometers (nm) (Hussain et al. 2016). Specified fertilization or localized supply can be done using nanofertilizers. Nanofertilizers can accelerate crop productivity by releasing the desired nutrient

(Al-Juthery et al. 2018a, 2018b). Applying the nanofertilizers correctly and systematically can bring requisite progress in crop productivity while keeping a check on the various environmental hazards caused by them. These benefits include fertilizer use efficiency, minimized volatilization, leaching, and lowering of environmental hazards.

Nanofertilizer can improve crop productivity by preventing various environmental problems and providing the nutrient at a site where it is required (Mehta & Bharat 2019). The technique of spraying liquid fertilizer is quite effective, whether micronutrients or macronutrients (Popko et al. 2018). Many agricultural specialists have been interested in generating and utilizing nanofertilizers (Khot et al. 2012). However, the highly specified research is inadequate. Besides, there is a perturbation that using nanofertilizers over the years might diminish soil fertility if nutrients are not used cautiously. Although, absolute soil analysis after crop harvesting can help overall soil fertility management and improve crop yield. The major objective of this review is to give an insight into various types of nanofertilizers to emphasize their efficiency in countering incoming challenges of food scarcity.

FERTILIZERS AND THEIR TYPES

Fertilizers are crucial for maintaining soil fertility and the productivity of crops in different environmental conditions. Rejuvenating the soil with fertilizers is indispensable to meet the deficiency of any nutrients in the soil. The dose of nutrients needs to be highly precise to ensure that neither the deficiency nor the accumulation of nutrients occurs in the soil. The deficiency of nutrients can hinder plant productivity, whereas the excess nutrients left in the soil may cause eutrophication or bioaccumulation into the

aquatic environment (Subramanian et al. 2015). In this situation, nanofertilizers with high nutrient use efficiency can be exploited. Nanotechnology enables atom-by-atom manipulation such that precise and desired particles can be made compared to conventional methods. The most promising factor of nanofertilizers over chemical fertilizers is their excellent nutrient distribution (Liu & Lal 2015).

Chemical Fertilizers

Chemical fertilizers provide nutrients for plants' optimal growth. There are different types of fertilizers like nitrogen fertilizers (ammonium nitrate, calcium ammonium nitrate, ammonium sulfate, etc.), phosphate fertilizers (single superphosphate, monoammonium phosphate, diammonium phosphate, triple superphosphate, etc.), and potassium fertilizer (potassium chloride, potassium sulfate, potassium nitrate, etc.). Some other essential secondary plant nutrients include calcium, magnesium, and sulfur, which are not applied directly; instead, these are used in combination with primary nutrients (NPK), e.g., sulfur added to ammonium nitrate or urea or single superphosphate. Other micronutrient fertilizers comprises iron, manganese, boron, zinc, copper, etc.

Nanofertilizers

Particle dimensions and surface layering are significant factors that decide the effectiveness of nanoparticles and their usage. Characteristics such as organic matter content, soil fabrication, and soil pH also decide its usage (El-Ramady et al. 2018). There are different mechanisms for the absorption of nanofertilizers. Fig.1 represents efficient nutrient delivery systems and bio- interaction of nanofertilizers. These can be taken via plant roots or leaves in crops, so



(Source: Al-Mamun et al. 2021).

Fig. 1: Types of nanofertilizers and their smart nutrient delivery system in plants.

Table 1: Macronutrient nanofertilizers and their effect on different crops.

Macronutrients	Test plant/ soil type	Applied form of micronutrient	Output	Additional effect
Nitrogen (N)	Sugarcane	Urea and Nano- Nitrogen Chelate (NNC)	Improved sugarproduction (Alimohammadi et al. 2020)	Prevented leaching
Phosphorus (P)	In clay and loamy soil	Hydroxyapatite ($\text{Ca}_{10}(\text{PO}_4)_6(\text{OH})_2$)	Doubled the efficiency of nutrient delivery from 23.44% (Calcium phosphorus) to 46.21% (Nanophosphorus fertilizers) (Tang & Fei 2021).	Hamper eutrophication
Potassium (K)	Peanut	Potassium nanofertilizers	Highly significant increase in plantparameters, with thehighest increase in the chlorophyll content (Afify et al. 2019).	Overall biomass increased
Magnesium(Mg)	Green gram , Groundnut	Magnesium oxide nanoparticles synthesized frombrown algae	Antioxidants are released to enhance chlorophyll production (Anand et al. 2020).	Stabilizes chloroplast (Cai et al. 2018)
Sulfur (S)	Groundnut	Sulfate-loaded surface-modifiednano-zeolite	Improved productivity in terms of root, shoot, kernel, and shell growth (Thirunavukkarasu et al. 2018).	Improved seed germination Seed germination

their absorption mechanism decides their bioavailability. Using these nanoparticles, two types of fertilizers can be made (i) nanoparticles that directly supply the nutrients (micronutrients or macronutrients) or (ii) nanoparticles that enhance the activity of the conventional fertilizer. The former is termed nanofertilizers, and the latter is called nanomaterial-enhanced fertilizers. Nanofertilizers can be categorized as macronutrient and micronutrient nanofertilizers.

Macronutrient Nanofertilizers

Macronutrients are responsible for the optimum growth of plants. These include nitrogen, phosphorus, potassium, calcium, sulfur, magnesium, carbon, oxygen, and hydrogen. Fig. 2 illustrates the availability of primary, secondary, and non-mineral nutrients to plants in their ionic forms. Nitrogen is the most important element for plant physiology. It forms chlorophyll molecules, imparting green color to plants which act as a site for photosynthesis. Deficiency of nitrogen results in chlorosis (yellowing of leaves) in plants. Nitrogen is a primary nutrient for plant growth, like potassium and phosphorus. An experiment was performed to determine the outcomes of Urea and Nano-Nitrogen Chelate (NNC) fertilizers on sugarcane production (*Saccharum Officinarum*) and nitrate drainage from the soil. It showed that the height of the sugarcane stems increased at the same rate in case of both fertilizers. However, the sugar content was found to be different. This study emphasized that nano nitrogen fertilizer (NNC) not only improved sugar production in sugarcane but also prevented nitrate leaching (Alimohammadi et al. 2020).

Potassium is a significant nutrient as it helps in the synthesize of biomolecules and activation of enzymes (Gosavi et al. 2017). Nano-potassium also enhances the absorption of other nutrients, such as nitrogen, calcium,

magnesium, and phosphorus, along with root and shoot growth. However, it is usually more effective in the root region (Ajirloo et al. 2015). Highly enhanced chlorophyll content was observed when monopotassium was applied foliarly to peanuts (Afify et al. 2019). Saleem et al. (2021) coated diammonium phosphate(DAP) with nanoparticles (NPs) of potassium ferrite (KFeO_2 NPs). Calcium phosphate-derived phosphorus fertilizers rocks-based study emphasized that the solubility of hydroxyapatite ($\text{Ca}_{10}(\text{PO}_4)_6(\text{OH})_2$) depends upon various factors such as pH ionic strength, Ca / P ratio, NPs size, etc. (Tang & Fei 2021). Its application almost doubled the nutrient delivery efficiency from 23.44% (Calcium phosphorus) to 46.21% (Nanophosphorus fertilizers).

Many studies have been conducted to evaluate the effect of magnesium nanofertilizers in crops such as legumes, horse grams, etc. Anand et al. (2020) studied magnesium oxide (MgO) nanoparticles to improve seed germination of mung beans (*Vigna radiata L.*). For this, MgO nanoparticles were synthesized from marine brown alga, *Turbinaria ornata*, using the co-precipitation method. When mung bean seeds nano-primed with MgO (100 mg L^{-1}) were used, it improved seed germination (%) compared to conventional hydropriming methods. MgO oxide nanoparticles were reported to have enhanced chlorophyll production by releasing free radicles. The antioxidant enzyme can counter the free radical to stabilize the chloroplast membrane (Cai et al. 2018).

Sulfur penetration via sulfate nanoparticles (Sulphate packed surface modified nano- zeolite), as well as ordinary sulfur, boosted the consumption of sulfur, thus improving the productivity in terms of the root, shoot, kernel, and shell growth in groundnut. Sulfur uptake was observed to be 0.76,

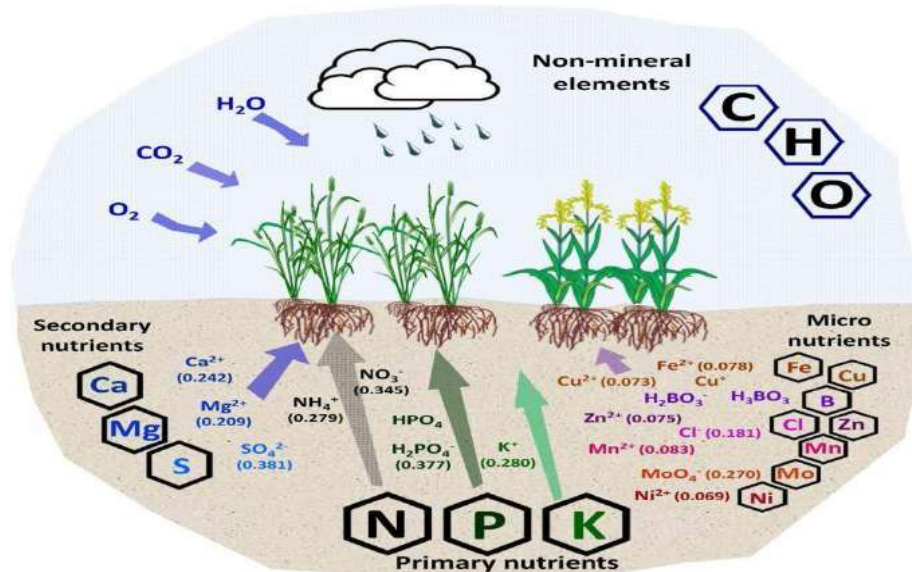


Fig. 2: Various types of nutrients available to plants. (Numbers in brackets refer to the hydrated radius (nm) of plant-available ionic species) (Bhardwaj et al. 2022).

40.5, 14.9, and 3.09 mg plant⁻¹ when sulfur NFs were applied, whereas when conventional sulfur was applied, its uptake was found to be 0.43, 30.6, 8.37, and 2.15 mg plant⁻¹ by the root, shoot, kernel, and shell, respectively (Thirunavukkarasu et al. 2018). When applied to a specific crop the various macronutrient application differs in terms of test plant or medium, applied concentration, and ionic form used. Table 1 represents the effect of macronutrients such as nitrogen, potassium, phosphorus, magnesium, and sulfur. Each nutrient has a distinct impact in terms of the growth of plants and other additional effects.

Micronutrients Nanofertilizers

Micronutrients are required in small quantities, but they can potentially disrupt plant physiology when deficient. These include iron, boron, chlorine, manganese, zinc, copper, etc. Table 2 illustrates the effect of different micronutrients on specific crops. Iron is considered a special nutrient for the plant as it promotes RNA synthesis, enzyme activity, photosynthesis, etc. (Mushtaq et al. 2020). Iron is a notably abundant element present on earth. However, its accessibility to plants is limited because of its dependency on soil pH (Alidoust & Isoda 2013). Iron deficiency can result in poor growth, lesser leaves, and lowered chlorophyll content. The distribution, accumulation, and metabolism of iron nanofertilizers have attracted various researcher's attention. However, the focus should be on maintaining an optimized concentration of nanofertilizers to avoid any toxicity to the plant and the surrounding.

The lowering of cadmium and lead accumulation in coriander plants was observed after using iron oxide (Fe₃O₄) nanofertilizer. It acted as a proliferator and antimicrobial agent (Fahad et al. 2014). Hasan (2015) compared the effect of chemical and biologically synthesized iron oxide NRs (Nanorods) on *Zea mays*' morphological and biochemical specification. It was noticed that biologically synthesized nanomaterials at low and medium concentrations showed optimum growth, whereas chemically synthesized nanomaterials reduced the growth when applied at a medium dose. As per the studies, the negative impact of a high concentration of NFs can be attributed to their accumulation around the root (Izadiyan et al. 2020).

Zinc is considered indispensable for development in humans, animals, and plants. It exhibits remarkable antimicrobial properties. Awan et al. (2021) synthesized zinc oxide nanofertilizer (ZnO-NFs) from zinc sulfate solution and seed extract of black seeds (*Nigella sativa* L.). It showed that ZnO-NPs application to the Broccoli resulted in increased seed germination, root length, shoot length, the weight of seedlings, leaf count, plant height, and leaf surface.

Boron (B), as a micronutrient promotes plant growth by developing cell walls, pollen grains, and tube elongation. It brings the translocation from leaves to the involved location, thus improving flower growth and fruit yield (Davaranah et al. 2016). Ibrahim & Farttoosi (2019) studied the response of boron nanoparticles by spraying them on mung bean (*vigna radiata* L.). The finding of the study

Table 2: Micronutrient nanofertilizers and their effect on various crops.

Micronutrient	Test plant/Soil Type	Applied form of Micronutrient	Output	Additional effect
Iron (Fe)	Maize	Iron oxide nanorods	At low and medium concentrations showed optimum growth (Izadiyan et al. 2020).	Acted as a growth regulator and antimicrobial agent (Fahad et al. 2014).
Zinc (Zn)	Broccoli	Zinc oxide nanoparticles (ZnO-NPs) Using Zinc sulfate solution	Increased seed germination, root length, shoot length, the weight of seedlings, the count of leaves, plant height, and leaf surface (Awan et al. 2021).	Antimicrobial property
Boron (B)	Mung bean	Boron nanoparticles	Improved plant height, pods per plant, and total seed growth (Ibrahim & Fartooosi 2019).	N/A
Silicon (Si)	Maize	Chitosen-Silicon nanofertilizer	Improved plant growth and yield (Kumaraswamy et al. 2021)	Antioxidant- defense enzymes activities
Copper (Cu)	Maize	Copper oxide nanofertilizer	Positively regulates drought stress responses (Van Nguyen et al. 2022)	Disease management

suggested that the spraying stages of boron nanoparticles improved plant height, pods per plant, and total seed productivity.

Silicon (Si) is also a notable nutrient for plant growth. It is the most abundant element in the earth's crust after oxygen. In many studies, silicon nanostructures have also proven to be an excellent inhibitors of biotic and abiotic stresses. Chitosan-Silicon nanofertilizer showed a steady release of silicon to improve plant growth and productivity in maize crops. Its foliar sprinkling provides antioxidant-defense enzymes to equilibrate biological redox homeostasis by balancing O₂ and H₂O₂ content in leaves (Kumaraswamy et al. 2021). Tereshchenko et al. (2017) conducted a small plot experiment to study the impact of the solution of silicon dioxide nanoparticles on the monocotyledons and dicotyledons viz., hullless oat (*Avena sativa* L.) and lucerne (*Medicago sativa* L. Subsp. *varia* (Martyn) Arcang.). Various findings showed higher resistance in these plants.

Copper nanoparticles showed improved nutrient efficiency when compared to the bulk copper material. It is an essential micronutrient comprising many proteins and enzymes contributing to plant growth. Van Nguyen et al. (2022) emphasized that copper nanoparticle priming manages drought stress response in maize. Additionally, histochemical depicted that the accumulation of reactive oxygen species (ROS) in plants was lowered as a mark of intensification of ROS scavenging enzyme actions in aridity. Kasana et al. (2017) suggested that biosynthesized copper nanoparticles showed appreciable results against plant pathogens, but their application for boosting yield in the field needs thorough study.

SYNTHESIS AND CHARACTERIZATION OF NANOFERTILIZERS

Physical (top-down) and chemical (bottom-up) approaches synthesize nanofertilizers intended to provide plant nutrients. There are cationic nutrients (NH₄⁺, K⁺, Ca²⁺, Mg²⁺) and anionic nutrients (NO₃⁻, PO₄²⁻, SO₄²⁻) to meet different nutrient deficiencies (Subramanian et al. 2015). The top-down approach is considered when a sizeable material is fragmented into nanosized entities. This process is complex, expensive, and requires high energy consumption. It operates in specific conditions of pressure and temperature. In the case of the bottom-up approach, nanostructures are synthesized by integrating the atomic or molecular species. This is based on wet chemical synthesis. Wet chemical processes had better nanostructure than the top-to-bottom approach. Various capping agents are used in colloidal synthesis, including heteroatom-operationalized long-chain hydrocarbons. One of them is oleic acid (OA), oleylamine (OAm), trioctylphosphine (TOP), dodecanethiol, etc., polymers that provide stability to nanoparticles (Kumar & Kumbhat 2016). Dendrimers macromolecules can also be used to develop and maintain nanoparticles as these are highly split (Duan et al. 2015). Yamamoto et al. (2019) synthesized quantum-sized titanium oxide nanoparticles using phenyl azomethine dendrimers (DPA) G4 as the capping template. Various attempts have been made for the green synthesis of nanoparticles following the fundamentals of green chemistry with a sustainable or green approach. It permits using water as the solvent in nanoparticle synthesis instead of relatively toxic solvents (Parveen et al. 2016). Biomolecules can be employed as capping agents for nanoparticle synthesis (Nasrollahzadeh et al. 2021). Biological methods include

synthesizing nanofertilizers using proteins and/or peptides (Duan et al. 2015).

Characterization of nanofertilizers has become essential to evaluate the size and explore their properties so that these can be utilized as per the peculiarity. With the help of characterization techniques, safety issues regarding nanofertilizers can also be resolved before their application (Lin et al. 2014). Reduced silver nanoparticles in colloidal solution were observed by using a UV-vis spectrophotometer and absorption spectra of the supernatant (Elamawi et al. 2018)

Fourier transform infrared (FT-IR) spectroscopy characterized zeolite/Fe₂O₃ nanocomposites in which the FT-IR spectra were indicated within the range of 400–4000 cm⁻¹ and 100–700 cm⁻¹ (Jahangirian et al. 2020). Transmission Electron Microscopy and Scanning Electron Microscopy analysis depicted the surface characteristics and dimensions of the resultant NPs (Hodoroaba et al. 2014). A Field Emission Scanning Electron Microscope uses a zig-zag pattern instead of light. Shimadzu XRD- 600 with Cu K α radiation ($k = 0.15405$ nm) was used to find out the crystal structure of the nanoparticles (XRD) (Deng et al. 2018).

Other techniques, such as Energy Dispersive Spectroscopy, Dynamic Light Scattering, Atomic Force Microscopy, Raman Spectroscopy, X-Ray Photoelectron Spectroscopy, etc., are also effective for characterizing nanofertilizers. Characterization is important as it helps in the controlled synthesis of nanofertilizers and their application

for different crops. The development of faster, simpler, more efficient, and newer techniques for their characterization has now become an area of research. Different techniques can be integrated to understand these fertilizers and their characteristics in a better way.

UTILIZATION OF NANOFERTILIZERS

Applications of nanofertilizer in agriculture can bring sustainability by raising global food production since there is immense pressure on food production to fulfill the nutritional demand of the human population. Enriching the soil with more nutrients can counter the problem of low fertility (Cornelis et al. 2014). Various studies have analyzed the mode of interaction of nanofertilizers with different crops. Table 3 demonstrates the effect of a different supplied nutrient on various crops. These studies focus on the effect of different nanofertilizers in crops, viz. gain in fresh weight, increase in carotenoid concentration, improvement in leaf peroxidase activity over control or rise in density and fibrosity of plant parts, etc., which depicts the beneficial impact of nanofertilizers on plants.

Nanofertilizers for Boosting Growth and Yield of Crops

Various nanofertilizers have a definite impact on the development of plants. When nitrogen in its Chelated nanofertilizers form was applied to *Solanum tuberosum* (potato), improvement in their yield was observed (Al-Juthery & Al-Shami 2019). Potassium nanofertilizer with

Table 3: Major applications of different nutrients (micronutrients and macronutrients).

S.No.	Applications	Elements	Effect
1.	Enhance growth and yield of crop	Nitrogen, Potassium, Phosphorus, Silver, Zinc, and Iron.	NPK (nitrogen, phosphorous, potassium) nanofertilizers on <i>Coffea arabica</i> enhanced the chlorophyll amount and net photosynthesis rate (Ha et al. 2019). Silver nanoparticles accelerated seed growth rate in rice crops (<i>Oryza sativa</i>) by improving α -amylase function (Kumar & Nagesh 2019). Zinc oxide nanoparticles improved the sprouting of peanuts (<i>Arachis hypogaea</i>) (Seleiman et al. 2020). Iron nanoparticles significantly enhanced the root growth in peanut plants (Rui et al. 2016).
2.	Mitigate environmental stresses		
	(a) Abiotic stress	Nitric oxide	Antistressor (Nabi et al. 2019)
	(b) Biotic stress	Rhizobacteria (PGPR)	Antistressor (Khan et al. 2020)
		Nano silica	Effectiveness against insects, bringing a 100% mortality rate (El-Naggar et al. 2020).
		Silicon oxide, Zinc Oxide, Selenium, and graphene.	Elsheery et al. (2020) observed that SiO ₂ , ZnO, Se, and graphene nanoparticles lowered the unfavorable consequences of freezing injury in sugarcane by conserving the photochemical efficiency of photosystem II (PSII), photoxidizable photosystem I (PSI) and photosynthetic gas exchange.
3.	To combat plant diseases	Copper, Titanium	Copper is very effective in lowering the symptoms of Turcicum leaf blight disease (Tamez et al. 2019). Fabricated TiO ₂ also improved the yield and disease resistance in <i>Capsicum annuum</i> (Prakashraj et al. 2021).

foliar application showed an improved biomechanical and biochemical response in *Cucurbita pepo* (squash) (Gerdini 2016). Silver nanoparticles accelerated the seed growth rate in rice (*Oryza sativa*) by improving α -amylase activity (Kumar & Nagesh 2019). NPK (nitrogen, phosphorous, potassium) nanofertilizers on *Coffea arabica* (coffee plant) enhanced the chlorophyll content as well as the net photosynthesis rate (Ha et al. 2019).

Nanofertilizers for Mitigating Environmental Stress

Nanofertilizers can mitigate different environmental stress to improve crop productivity. In general, two types of stress are there, i.e., abiotic (50–70%) and biotic (40–60%) which results in the decline of crop productivity (Tiwari et al. 2022). Abiotic stress comprises heat stress, flooding, drought, and salinity, whereas biotic stress consists of bacteria, viruses, fungi, etc. Such stress can be controlled in plants by using various types of anti stressors viz. nitric oxide (Nabi et al. 2019), rhizobacteria (PGPR) (Khan et al. 2020), and strigolactones (Hussain et al. 2017). In maize plants, nanosilica increased the metabolic balance of chlorophyll, proteins, and cell wall transporters, thereby damping off stress-responsive enzyme activities. These also reflected effectiveness against insects by bringing a 100% mortality rate (El-Naggar et al. 2020).

Nanoparticles use can ameliorate the stress resistance in plants as it helps in alleviating reactive oxygen species (ROS) which are responsible for stress in crops. These PNCs (polyacrylic acid nanoceria) decline leaves ROS levels but improve the photosynthetic pace in *Arabidopsis thaliana* (Wu et al. 2017). When *Moringa* plants were sprayed with Hoagland (mixture of ZnO and Fe₃O₄) nanoparticles, a significant reduction in sodium and chloride concentration was observed. However, it enhanced nitrogen, potassium, phosphorus, magnesium, manganese, iron, and zinc content. (Amira et al. 2015). Zinc oxide nanoparticles improved the maturation of peanut seeds (*Arachis hypogaea*) (Seleiman et al. 2021). Iron nanoparticles significantly enhanced root growth in peanut plants (Rui et al. 2016). Some studies showed that nanoparticles stimulated proteobacteria while suppressing acid bacteria. Nitrogen and carbon cycles were affected by the nanofertilizers in a positive way (Kalwani et al. 2022). In addition, compounds secreted via root exudates and rhizospheric microorganisms combine with metallic species, influencing their assessment of plants and microorganisms (Faizan et al. 2021).

In drought-prone regions, plant water requirement is an ultimatum for subsequent decades. It was observed that utilization of the nano-fertilizers not only upgraded wheat grain yield by improving plant height, spike length, and the

number of grains per spike but also mitigated the negative effects of water scarcity by enhancing the superoxide dismutase (SOD) activity (Ahmadian et al. 2021). Elsheery et al. (2020) observed that nanofertilizers (SiO₂, ZnO, Se, and graphene) reduced the harmful outcomes of freezing injury in sugarcane by conserving the photochemical effectiveness of photosystem II (PSII), photoxidizable photosystem I (PSI) and photosynthetic gas exchange. When iron nanoparticles were applied in water scarcity, it reduced the hydrogen peroxide levels, thereby lowering lipid peroxidation in *Brassica napus* (Rapeseed) (Palmqvist et al. 2017). Silicon-based nanofertilizers raised heavy metal resistance in rice (Wang et al. 2016).

Nanofertilizers for Disease Control in Plants

Copper nanoparticles showed improvement in plant growth and productivity. In addition, it was very effective in lowering the symptoms of Turicum leaf blight disease (Tamez et al. 2019). Fabricated titanium oxide also improved the yield and disease resistance in *Capsicum annuum* (Prakashraj et al. 2021). Silver, Copper, and Zinc nanofertilizers regulate host defense by suppressing disease. They lower the active metals entering the environment when applied for disease management or antimicrobial activity (Elmer & White 2018). Antimicrobial functions of zinc NFs against bacteria have also been observed (Graham et al. 2016). Some intrinsic factors, such as particle size and surface coatings, and extrinsic factors, like soil texture or pH, decide these potentials (El-Ramady et al. 2018). Besides this, the application method significantly determined the utilization of nanofertilizers in crops (Prasad et al. 2017).

Nanofertilizers have great potential to enhance nutrient use efficiency. The nutrient delivery system of nanofertilizer is one of the significant reasons for orientation towards it (Liu & Lal 2015). This slow delivery system of nutrients because of the attachment of these with the nanoparticles (Solanki et al. 2015) provides nutrients for the long term. Moreover, nanofertilizers can be synthesized as per the crop's specified nutrient demand (Kah et al. 2018). Nutrient uptake of nano fertilizers is more compared to conventional fertilizers as it takes 40–50 days to slowly release nutrients using the former, whereas 4–10 days in the case of the latter (Solanki et al. 2015). In conventional nutrient management systems, there is more loss of nutrients due to leaching, making soil deficient of nutrients or accumulation around roots inhibiting growth and causing toxicity in the plant. In addition, using small quantities prevents soil from overloading with salts, as generally seen in the case of conventional fertilizer's over-application (León-Silva et al. 2018). A boost to nanofertilizer efficiency has been provided by fertilizer

with biosensor, which exhibits control over the delivery of the nutrients considering the soil nutrient level. Making the specific micronutrient available promotes plant growth (López-Valdez et al. 2018) which conventional fertilizer systems cannot achieve. Large surface area, reactivity, and nano size are the characteristics of nanofertilizers responsible for excellent diffusion of nutrients (Feregrino-Perez et al. 2018). Providing excellent nutrition nanofertilizers enhances plant's potential to combat biotic and abiotic stress.

LIMITATIONS OF NANOFERTILIZERS

The advantages of nanofertilizers are creating new ventures in the direction of sustainable agriculture. However, its drawbacks should also be examined before the market distribution (Zulfiqar et al. 2019). The large scale discharge of nanomaterials into the environment and the food chain is risky for human health (Gopalakrishnan Nair 2018). Nanofertilizers show excellent penetration power, which provides them with brilliant absorption efficiency. This factor can be harmful when nanofertilizers are in excess or when it gets to the wrong target. There are cases in which plants activate their defense system against NFs, especially in the case of metallic oxide-based nanofertilizers as in these parent nanomaterials, as well as the metal ions nanofertilizers, give aggravated impact (White & Gardea-Torresdey 2018). The excessive intake and assimilation in the plant parts can adversely affect human health. Transformation of nanoparticles is also a threat while applying them in the field, as these are highly reactive. When nanofertilizers are applied, being reactive, these tend to interact with the environment bringing change in their physicochemical properties. Nanofertilizer phytotoxicity can also exist as specific plants interact differently with these at particular doses (Ashkavand et al. 2018). As the nanofertilizers are highly reactive with their miniature size and small area (Konate et al. 2018), this raises a question about the suitability of their use by farm workers (Gopalakrishnan Nair 2018). There is a need to consider both the benefits and adverse effects before using these in the field. Risk assessment and hazard recognition of the nanofertilizers using their life cycle analysis are crucial, along with establishing advances for toxicological research (Ebbs et al. 2016).

CONCLUSION

The growing population and various other environmental issues have threatened food security. This makes it inevitable to look for some alternative approach to sustainable development. In this direction, efforts have been made from time to time. The most essential hindering factor regarding the usage of chemical fertilizers is their low nutrient

efficiency which poses an obstacle in achieving sustainability of crop production. Moreover, as these are required in large quantities, it does not remain economically efficient. The high release rate of these chemical fertilizers does not correspond to their absorption by the plants, or the bioavailability of plants is relatively insignificant. Thus it brings the need to develop an alternative to chemical fertilizers that can cope with the challenges arising from their usage. Many studies have clearly emphasized that the nanofertilizers can increase a plant's productivity via various means, e.g., improved seed germination, photosynthesis improvement, increased nutrient metabolism and synthesis efficiency, and promoting the capacity to tolerate various kinds of stress bringing stability in growth. The potential of nanofertilizers as growth and yield enhancer in combating environmental stresses and pathogen resistance has been discussed in many studies. Another advantage is the smaller quantity applied, thus resolving the pollution problem and promoting the specified nutrient supply. However, the fact cannot be ignored that nanofertilizers usage needs to be highly systematic and supervised, prohibiting their free availability in the market and usage in the field. If judicious use of nanofertilizer is not done, phytotoxicity, high reactivity, and biotransformation are the most prevalent phenomenon that can be seen. Hence, the focus of the concern should not be restricted to their benefits but also be extended to their negative aspects as well. Before its application, a proper risk assessment of the nanofertilizer life cycle is critical.

REFERENCES

- Affify, R.R., El-Nwehy, S.S., Bakry, A.B. and Abd El-Aziz, M.E. 2019. Response of peanut (*Arachis hypogaea L.*) crop grown on newly reclaimed sandy soil to foliar application of potassium nanofertilizer. Middle East J. Appl. Sci., 9(1): 78-85.
- Ahmadian, K., Jalilian, J. and Pirzad, A. 2021. Nano-fertilizers improved drought tolerance in wheat under deficit irrigation. Agric. Water Manag., 244: 106544.
- Ajirloo, A.R., Shaaban, M. and Motlagh, Z.R. 2015. Effect of K nanofertilizer and N bio-fertilizer on yield and yield components of tomato (*Lycopersicon esculentum L.*). Int. J. Adv. Biol. Biom. Res., 3(1): 138-143.
- Alidoust, D. and Isoda, A. 2013. Effect of $\gamma\text{Fe}_2\text{O}_3$ nanoparticles on photosynthetic characteristic of soybean (*Glycine max (L.) Merr.*): foliar spray versus soil amendment. Acta Physiol. Plant., 35(12): 3365-3375.
- Alimohammadi, M., Panahpour, E. and Naseri, A. 2020. Assessing the effects of urea and nano-nitrogen chelate fertilizers on sugarcane yield and dynamic of nitrate in the soil. Soil Sci. Plant Nutr., 66(2): 352-359.
- Al-Juthery, H.W.A., Ali, N.S., Al-Taey, D. K.A. and Ali, E.A.H. M. 2018. The impact of foliar application of nanofertilizer, seaweed, and hypertonic on yield of potato. Plant Arch., 18(2): 2207-2212.
- Al-Juthery, H.W., Habeeb, K.H., Altaee, F.J. K., Al-Taey, D.K. and Al-Tawaha, A.R.M. 2018. Effect of foliar application of different sources of nano-fertilizers on growth and yield of wheat. Biosci. Res., 4: 3976-3985.
- Al-Mamun, M.R., Hasan, M.R., Ahommed, M.S., Bacchu, M.S., Ali, M.R., and Khan, M.Z.H. 2021. Nanofertilizers towards sustainable agriculture and environment. Environ. Technol. Innov., 23: 101658.

- Al-Juthery, H.W. and Al-Shami, Q.M. 2019. Impact of fertigation of nano NPK fertilizers, nutrient use and distribution in the soil of potato (*Solanum tuberosum* L.). *Plant Arch.*, 19: 1087-1096.
- Amira, S.S., Souad, A.E.F. and Essam, D. 2015. Alleviation of salt stress on *Moringa peregrina* using the foliar application of nanofertilizers. *J. Hortic. For.*, 7(2): 36-47.
- Anand, K.V., Anugraga, A.R., Kannan, M., Singaravelu, G. and Govindaraju, K. 2020. Bio-engineered magnesium oxide nanoparticles as nano-priming agent for enhancing green gram seed germination and seedling vigor (*Vigna radiate* L.). *Mater. Lett.*, 271: 127792.
- Ashkavan, P., Zarafshar, M., Tabari, M., Mirzaie, J., Nikpour, A., Bordbar, S.K. and Striker, G.G. 2018. Application of SiO₂ nanoparticles as pretreatment alleviates the impact of drought on the physiological performance of *Prunus mahaleb* (Rosaceae). *Bol. Soc. Argent. Bot.*, 53(2): 207-219.
- Awan, S., Shahzadi, K., Javad, S., Tariq, A., Ahmad, A. and Ilyas, S. 2021. A preliminary study of the influence of zinc oxide nanoparticles on growth parameters of *Brassica oleracea* var *italica*. *J. Saudi Soc. Agric. Sci.*, 20(1): 18-24.
- Bhardwaj, A.K., Arya, G., Kumar, R., Hamed, L., Pirasteh-Anosheh, H., Jasrotia, P. and Singh, G.P. 2022. Switching to nano nutrients for sustaining agroecosystems and environment: the challenges and benefits of moving from ionic to particle feeding. *J. Nanobiotechnol.*, 20(1): 1-28.
- Cai, L., Chen, J., Liu, Z., Wang, H., Yang, H. and Ding, W. 2018. Magnesium oxide nanoparticles: effective agricultural antibacterial agent against *Ralstonia solanacearum*. *Front. Microbiol.*, 9, 790.
- Cornelis, G., Hund-Rinke, K., Kuhlbusch, T., Van den Brink, N. and Nickel, C. 2014. Fate and bioavailability of engineered nanoparticles in soils: A review. *Crit. Rev. Environ. Sci. Technol.*, 44(24): 2720-2764.
- Davarpanah, S., Tehranifar, A., Davarynejad, G., Abadía, J. and Khorasani, R. 2016. Effects of foliar applications of zinc and boron nano-fertilizers on pomegranate (*Punica granatum* cv. *Ardestani*) fruit yield and quality. *Sci. Hortic.*, 210: 57-64.
- Deng, L., Mohan, T., Chang, T.Z., Gonzalez, G.X., Wang, Y., Kwon, Y.M. and Wang, B.Z. 2018. Double-layered protein nanoparticles induce broad protection against divergent influenza A viruses. *Nat. Commun.*, 9(1): 1-12.
- Duan, H., Wang, D. and Li, Y. 2015. Green chemistry for nanoparticle synthesis. *Chem. Soc. Rev.*, 44(16): 5778-5792.
- Ebbs, S.D., Bradfield, S.J., Kumar, P., White, J.C., Musante, C. and Ma, X. 2016. Accumulation of zinc, copper, or cerium in carrot (*Daucus carota*) exposed to metal oxide nanoparticles and metal ions. *Environ. Sci. Nano.*, 3(1): 114-12.
- Elamawi, R.M., Al-Harbi, R.E. and Hendi, A.A. 2018. Biosynthesis and characterization of silver nanoparticles using *Trichoderma longibrachiatum* and their effect on phytopathogenic fungi. *Egypt. J. Biol. Pest. Control.*, 28(1): 1-11.
- Elmer, W. and White, J.C. 2018. The future of nanotechnology in plant pathology. *Annu. Rev. Phytopathol.*, 56: 111-133.
- El-Naggar, M.E., Abdelsalam, N.R., Fouda, M.M., Mackled, M.I., Al-Jaddadi, M.A., Ali, H.M. and Kandil, E.E. 2020. Soil application of nano silica on maize yield and its insecticidal activity against some stored insects after the post-harvest. *Nanomaterials*, 10(4): 739.
- El-Ramady, H., Abdalla, N., Alshaal, T., El-Henawy, A., Elmahrouk, M., Bayoumi, Y. and Schnug, E. 2018. Plant Nano-Nutrition: Perspectives and Challenges. In Gothandam, K.M., Ranjan, S., Dasgupta, N., Ramalingam, C. and Lichtfouse, E. (eds), *Nanotechnology, Food Security and Water Treatment*, Springer, Cham., pp. 129-161.
- Elsheery, N.I., Sunoj, V.S.J., Wen, Y., Zhu, J.J., Muralidharan, G. and Cao, K.F. 2020. Foliar application of nanoparticles mitigates the chilling effect on photosynthesis and photoprotection in sugarcane. *Plant Physiol. Biochem.*, 149: 50-60.
- Fahad, S., Ahmad, M., Akbar Anjum, M. and Hussain, S. 2014. The effect of micronutrients (B, Zn, and Fe) foliar application on the growth, flowering, and corm production of gladiolus (*Gladiolus grandiflorus* L.) in calcareous soils. *J. Agric. Sci. Technol.*, 16(7): 1671-1682.
- Faizan, M., Bhat, J.A., Hessini, K., Yu, F. and Ahmad, P. 2021. Zinc oxide nanoparticles alleviate the adverse effects of cadmium stress on *Oryza sativa* via modulation of the photosynthesis and antioxidant defense system. *Ecotoxicol. Environ. Saf.*, 220: 112401.
- FAO, IFAD, UNICEF, WFP and WHO. 2022. Repurposing Food and Agricultural Policies to Make Healthy Diets More Affordable. The State of Food Security and Nutrition in the World 2022, FAO, Rome.
- Feregrino-Perez, A.A., Magaña-López, E., Guzmán, C. and Esquivel, K. 2018. A general overview of the benefits and possible negative effects of nanotechnology in horticulture. *Sci. Hortic.*, 238: 126-137.
- Gerdini, F.S. 2016. Effect of nano potassium fertilizer on some parchment pumpkin (*Cucurbita pepo*) morphological and physiological characteristics under drought conditions. *Int. J. Farm. Allied Sci.*, 11: 367-371.
- Gopalakrishnan Nair, P.M. 2018. Toxicological Impact of Carbon Nanomaterials on Plants. In Gothandam, K.M., Ranjan, S., Dasgupta, N., Ramalingam, C. and Lichtfouse, E. (eds), *Nanotechnology, Food Security and Water Treatment*, Springer, Cham., pp. 163-183.
- Gosavi, A.B., Deshpande, A.N. and Maity, A. 2017. Identifying nutrient imbalances in pomegranate (Cv. Bhagwa) at different phenological stages by the diagnosis and recommendation integrated system. *J. Plant Nutr.*, 40(13): 1868-1876.
- Graham, J.H., Johnson, E.G., Myers, M.E., Young, M., Rajasekaran, P., Das, S. and Santra, S. 2016. Potential of nano-formulated zinc oxide for control of citrus canker on grapefruit trees. *Plant Dis.*, 100(12): 2442-2447.
- Ha, N.M.C., Nguyen, T.H., Wang, S.L. and Nguyen, A.D. 2019. Preparation of NPK nanofertilizer based on chitosan nanoparticles and its effect on biophysical characteristics and growth of coffee in green house. *Res. Chem. Intermed.*, 45(1): 51-63.
- Hasan, S. 2015. A review on nanoparticles: Their synthesis and types. *Res. J. Recent Sci.*, 22: 2502.
- Hodoroaba, V.D., Motzkus, C., Macé, T. and Vaslin-Reimann, S. 2014. Performance of high-resolution SEM/EDX systems equipped with transmission mode (TSEM) for imaging and measurement of size and size distribution of spherical nanoparticles. *Microsc. Microanal.*, 20(2): 602-612.
- Hussain, I., Singh, N.B., Singh, A., Singh, H. and Singh, S.C. 2016. Green synthesis of nanoparticles and its potential application. *Biotechnol. Lett.*, 38(4): 545-560.
- Hussain, I., Singh, N.B., Singh, A., Singh, H., Singh, S. C. and Yadav, V. 2017. Exogenous application of phytosynthesized nanoceria to alleviate ferulic acid stress in *Solanum lycopersicum*. *Sci. Hortic.*, 214: 158-164.
- Ibrahim, N.K. and Al Fartoosi, H.A.K. 2019. Response of mung bean to boron nanoparticles and spraying stages (*Vigna Radiata* L.). *Plant Arch.*, 19(2): 712-715.
- Izadiyan, Z., Shamel, K., Miyake, M., Hara, H., Mohamad, S.E.B., Kalantari, K. and Rasouli, E. 2020. Cytotoxicity assay of plant-mediated synthesized iron oxide nanoparticles using *Juglans regia* green husk extract. *Arab. J. Chem.*, 13(1): 2011-2023.
- Jahangirian, H., Rafiee-Moghaddam, R., Jahangirian, N., Nikpey, B., Jahangirian, S., Bassou, N. and Webster, T.J. 2020. Green synthesis of zeolite/Fe₂O₃ nanocomposites: toxicity and cell proliferation assays and application as a smart iron nanofertilizer. *Int. J. Nanomed.*, 15: 1005.
- Kah, M., Kookana, R.S., Gogos, A. and Bucheli, T.D. 2018. A critical evaluation of nanopesticides and nanofertilizer against their conventional analogues. *Nat. Nanotechnol.*, 13(8): 677-684.
- Kalwani, M., Chakdar, H., Srivastava, A., Pabbi, S. and Shukla, P. 2022. Effects of nanofertilizers on soil and plant-associated microbial communities: Emerging trends and perspectives. *Chemosphere*, 287: 132107.

- Kasana, R.C., Panwar, N.R., Kaul, R.K. and Kumar, P. 2017. Biosynthesis and effects of copper nanoparticles on plants. *Environ. Chem. Lett.*, 15(2): 233-240.
- Khan, N., Ali, S., Tariq, H., Latif, S., Yasmin, H., Mehmood, A. and Shahid, M.A. 2020. Water conservation and plant survival strategies of rhizobacteria under drought stress. *Agronomy*, 10(11): 1683.
- Khot, L.R., Sankaran, S., Maja, J.M., Ehsani, R. and Schuster, E.W. 2012. Applications of nanomaterials in agricultural production and crop protection: A review. *Crop Prot.*, 35: 64-70.
- Konate, A., Wang, Y., He, X., Adeel, M., Zhang, P., Ma, Y. and Zhang, Z. 2018. Comparative effects of nano and bulk-Fe₃O₄ on the growth of cucumber (*Cucumis sativus*). *Ecotoxicol. Environ. Saf.*, 165: 547-554.
- Kumar, A. and Nagesh, B. 2019. Foliar application of nanofertilizers in agricultural crops: A review. *J. Farm. Sci.*, 32: 239-249.
- Kumar, N. and Kumbhat, S. 2016. *Essentials in Nanoscience and Nanotechnology*. John Wiley and Sons, NY, pp. 30-75
- Kumaraswamy, R., Saharan, V., Kumari, S., Choudhary, R.C., Pal, A., Sharma, S.S., Rakshit, S., Raliya, R. and Biswas P. 2021. Chitosan-silicon nanofertilizer to enhance plant growth and yield in maize (*Zea mays* L.). *Plant Physiol. Biochem.*, 159: 53-66
- León-Silva, S., Arrieta-Cortes, R., Fernández-Luqueño, F. and López-Valdez, F. 2018. Design and production of nanofertilizers. In: Ghosh, S., Thongmee, S. and Kumar, A (eds), *Agricultural Nanobiotechnology*, Woodhead Publishing, UK, pp. 17-31.
- Lin, X., Li, J., Ma, S., Liu, G., Yang, K., Tong, M. and Lin, D. 2014. Toxicity of TiO₂ nanoparticles to *Escherichia coli*: Effects of particle size, crystal phase and water chemistry. *PLoS One*, 9(10): e110247.
- Liu, R. and Lal, R. 2015. Potentials of engineered nanoparticles as fertilizers for increasing agronomic productions. *Sci. Total Environ.*, 514: 131-139.
- López-Valdez, F., Miranda-Arámula, M., Ríos-Cortés, A.M., Fernández-Luqueño, F. and de-la-Luz, V. 2018. Nanofertilizers and their controlled delivery of nutrients. In Ghosh, S., Thongmee, S. and Kumar, A (eds), *Agricultural Nanobiotechnology*, Woodhead Publishing, UK, pp. 35-48.
- Mehta, S. and Bharat, R. 2019. Effect of integrated use of nano and non-nano fertilizers on nutrient use efficiency of wheat (*Triticum aestivum* L.) in irrigated subtropics of Jammu. *J. Pharmacogn. Phytochem.*, 8(6): 2156-2158.
- Mushtaq, T., Shah, A.A., Akram, W. and Yasin, N.A. 2020. Synergistic ameliorative effect of iron oxide nanoparticles and *Bacillus subtilis* S4 against arsenic toxicity in *Cucurbita moschata*: polyamines, antioxidants, and physicochemical studies. *Int. J. Phytoremed.*, 46: 1408-1419.
- Nabi, R.B.S., Tayade, R., Hussain, A., Kulkarni, K.P., Imran, Q.M., Mun, B.G. and Yun, B.W. 2019. Nitric oxide regulates plant responses to drought, salinity, and heavy metal stress. *Environ. Exp. Bot.*, 161: 120-133.
- Nasrollahzadeh, M., Shafiei, N. and Nezafat, Z. 2021. Synthesis of biopolymer-based metal nanoparticles. *Biopolym. Metal Nanopart. Chem. Sustain. Appl.*, 1: 255.
- Palmqvist, N.G., Seisenbaeva, G.A., Svedlindh, P. and Kessler, V.G. 2017. Maghemite nanoparticles acts as nanozymes, improving growth and abiotic stress tolerance in *Brassica napus*. *Nanoscale Res. Lett.*, 12(1): 1-9.
- Parveen, K., Banse, V. and Ledwani, L. 2016. Green synthesis of nanoparticles: Their advantages and disadvantages. *AIP Conf. Proceed.*, 1724: 020048.
- Popko, M., Michalak, I., Wilk, R., Gramza, M., Chojnacka, K. and Górecki, H. 2018. Effect of the new plant growth biostimulants based on amino acids on yield and grain quality of winter wheat. *Molecules*, 23(2): 470.
- Prakashraj, R., Vijayakumar, S., Punitha, V.N., Vidhya, E., Nilavukkarasi, M. and Praseetha, P.K. 2021. Fabricated TiO₂ nanofertilizers for foliar assimilation to enhance yield and disease resistance in *Capsicum annuum* L. *J. Plant Growth Regul.*, 1: 1-8.
- Prasad, R., Bhattacharyya, A. and Nguyen, Q.D. 2017. Nanotechnology in sustainable agriculture: recent developments, challenges, and perspectives. *Front. Microbiol.*, 8: 1014.
- Qureshi, A., Singh, D.K. and Dwivedi, S. 2018. Nano-fertilizers: A novel way for enhancing nutrient use efficiency and crop productivity. *Int. J. Curr. Microbiol. App. Sci.*, 7(2): 3325-3335.
- Rui, M., Ma, C., Hao, Y., Guo, J., Rui, Y., Tang, X. and Zhu, S. 2016. Iron oxide nanoparticles as a potential iron fertilizer for peanut (*Arachis hypogaea*). *Front. Plant Sci.*, 7: 815.
- Saleem, I., Maqsood, M.A., Rehman, M.Z., Aziz, T., Bhatti, I.A. and Ali, S. 2021. Potassium ferrite nanoparticles on DAP to formulate slow-release fertilizer with auxiliary nutrients. *Ecotoxicol. Environ. Saf.*, 215: 112148.
- Seleiman, M.F., Almutairi, K.F., Alotaibi, M., Shami, A., Alhammad, B.A. and Battaglia, M.L. 2020. Nano-fertilization as an emerging fertilization technique: Why can modern agriculture benefit from its use? *Plants*, 10(1): 654.
- Shuqin, J. and Fang, Z. 2018. Zero growth of chemical fertilizer and pesticide use: China's objectives, progress and challenges *J. Resour. Ecol.*, 9(1): 50-58.
- Solanki, P., Bhargava, A., Chhipa, H., Jain, N. and Panwar, J. 2015. Nano-Fertilizers and Their Smart Delivery System. In Rai, M., Ribeiro, C., Mattoso, L. and Duran, N. (eds), *Nanotechnologies in Food and Agriculture*, Springer, Cham., pp. 81-101.
- Subramanian, K.S., Manikandan, A., Thirunavukkarasu, M. and Rahale, C.S. 2015. Nano-Fertilizers for Balanced Crop Nutrition. In Rai, M., Ribeiro, C., Mattoso, L. and Duran, N. (eds), *Nanotechnologies in Food and Agriculture*, Springer, Cham., pp. 69-80.
- Tamez, C., Morelius, E. W., Hernandez-Viezcas, J. A., Peralta-Videa, J. R. and Gardea-Torresdey, J. 2019. Biochemical and physiological effects of copper compounds/nanoparticles on sugarcane (*Saccharum officinarum*). *Sci. Total Environ.*, 649: 554-562.
- Tang, S. and Fei, X. 2021. Refractory Calcium phosphate-derived phosphorus fertilizer based on hydroxyapatite nanoparticles for nutrient delivery. *ACS Appl. Nano Mater.*, 4(2): 1364-1376.
- Tereshchenko, N., Zmeeva, O., Makarov, B., Kravets, A., Svetlichny, V., Lapin, I. and Yunusova, T. 2017. The influence of silicon oxide nanoparticles on morphometric parameters of monocotyledons and dicotyledons in soil and climatic conditions of western Siberia, as well as on microbiological soil properties. *Bionanoscience*, 7(4): 703-711.
- Thirunavukkarasu, M., Subramanian, K.S., Kannan, P. and Balaji, T. 2018. Response of nano-sulphur to the groundnut. *Int. J. Conserv. Sci.*, 6(3): 2067-2072.
- Tiwari, K., Kumar, Y., Singh, T. and Nayak, R. 2022. Nano technology-based P fertilizers for higher efficiency and agriculture sustainability. *Ann. Plant Soil Res.*, 24(2): 198-207.
- Van Nguyen, D., Nguyen, H.M., Le, N.T., Nguyen, K.H., Nguyen, H.T., Le, H.M. and Van Ha, C. 2022. Copper nanoparticle application enhances plant growth and grain yield in maize under drought-stress conditions. *Plant Growth Regul.*, 41(1): 364-375.
- Wang, S., Wang, F., Gao, S. and Wang, X. 2016. Heavy metal accumulation in different rice cultivars as influenced by foliar application of nano-silicon. *Water Air Soil Pollut.*, 227(7): 1-13.
- White, J.C. and Gardea-Torresdey, J. 2018. Achieving food security through the very small. *Nat. Nanotechnol.*, 13(8): 627-629.
- Wu, H., Tito, N. and Giraldo, J.P. 2017. Anionic cerium oxide nanoparticles protect plant photosynthesis from abiotic stress by scavenging reactive oxygen species. *ACS Nano*, 11(11): 11283-11297.
- Yamamoto, K., Imaoka, T., Tanabe, M. and Kambe, T. 2019. New horizon of nanoparticle and cluster catalysis with dendrimers. *Chem. Rev.*, 120(2): 1397-1437.
- Zulfiqar, F., Navarro, M., Ashraf, M., Akram, N.A. and Munné-Bosch, S. 2019. Nanofertilizer use for sustainable agriculture: Advantages and limitations. *Plant Sci.*, 289: 110270.



Analysis of Shoreline Change of North Central Timor Regency, Indonesia

L. Ledheng*†  and E. M. Y. Hano'e*

*Biology Education Study Program, Faculty of Educational Sciences, Timor University, Indonesia

†Corresponding author: L. Ledheng; ludgardisledheng12@gmail.com

Nat. Env. & Poll. Tech.
Website: www.neptjournal.com

Received: 02-12-2022

Revised: 23-01-2023

Accepted: 01-02-2023

Key Words:

Abrasion
Accretion
Landsat images
Shoreline change

ABSTRACT

Shoreline change is a process that occurs due to the impact of natural factors and human activities. Geographically, the coastal area of North Central Timor Regency (NCT) is in the northern part of the island of Timor, East Nusa Tenggara Province (ENT). Physically, the area is affected by the oceanographic dynamics of the Sawu Sea waters and aquaculture activities, which impact the damage to coastal ecosystems. This study aims to analyze shoreline change in the northern coastal area of NCT Regency. The data used are Landsat 8 images from 2015-20221 to describe current conditions. Meanwhile, Landsat 5 imagery data from 1990 - 2000 was used to describe the initial conditions. The satellite imagery is analyzed to map shoreline changes that experience accretion or abrasion. The results show that the shoreline of the study area has experienced changes in accretion and abrasion. Based on the area of change in the northern coastal area of NCT Regency, the dominant accretion area was 1108.07 m² with a rate of change of 20.19 m.year⁻¹, as long as 1021 meters, while the abrasion was 845.43 m² at a rate of 12.65 m.year⁻¹ as long as 36520 meters. The average shoreline change distance in accretion conditions was 11.3 meters, while the abrasion was 7.93 meters. The shoreline shift due to the highest abrasion in Ponu was -16.08, while accretion in North Oepuah was 35.63 meters. The results of this research will contribute to planning the management of the coastal area of NCT Regency.

INTRODUCTION

The Indonesian archipelago is the largest, with the second longest coastline in the world. Such conditions cause most of Indonesia's territory to border the sea (Kurniawan & Marfa'i 2020). The area that borders the sea with land ecosystems is called the coastal area (Dahuri et al. 2013). The characteristics of the sea and land always influence coastal areas. The characteristics of the sea that affect the land include tides, wind, and sea waves.

In contrast, the characteristics of the land that affect the sea are sedimentation and human activities, which cause deforestation and pollution (Winarso et al. 2001). Geomorphological processes in coastal areas can be divided into destructive and constructive. Destructive processes tend to damage or change existing coastal landforms, while constructive processes can produce new ones (Sugiarta 2018). The occurrence of geomorphological processes causes the coastline to shift. Change in the coastline can be positive due to the sedimentation process, which results in coastal areas having additional land. However, coastline

changes can also cause abrasion or land erosion (Winarso et al. 2001).

The coastal area of NCT Regency is in the northern part of the island of Timor, ENT Province, which is directly opposite the Sawu Sea. Physically, this area is affected by oceanographic dynamics (such as tides, waves, and currents) from the waters of the Sawu Sea and the flow of small rivers upstream that changes every season. In general, sea waves in the waters of NCT Regency in the West monsoon propagate from the northwest, west, and southwest, while in the East monsoon originate from the south and southeast. In addition, the utilization and development of the northern coastal area of NCT Regency tend to increase every year, for example, as an aquaculture area (Ledheng et al. 2012).

Utilization of the area for aquaculture has caused the population of mangrove species on the north coast of NCT Regency to decrease or even become extinct. A study of mangrove vegetation in 2009 found that there were as many as 24 types of mangroves (Ledheng et al. 2012), then in 2020, it was only 4 species (Ledheng et al. 2020). The reduced population of the species indicates that there has been damage and disturbance in the coastal area, which has caused abrasion. The loss of most of the vegetation in the northern coastal area of NCT Regency led this area

ORCID details of the authors:

L. Ledheng: <https://orcid.org/0000-0003-0086-6261>

to be designated as abrasion-prone by the NCT Regency Government (Timor Tengah Utara Regency 2021). The impacts faced by the northern coastal communities of NCT Regency include damage to settlements, pond areas, and highway infrastructure. One of the causes of damage is tidal flooding. The phenomenon encourages people to open new pond areas (Ledheng et al. 2012). It caused the coastline to shift towards the mainland and salty water to inundate once-dry land. Therefore, studying shoreline changes is an important step to understanding the dynamism and evolution of coastal areas; thus, stakeholders can do better to reduce the risk of coastal abrasion disasters to minimize physical and economic losses (Fuad & Fais 2017).

According to Williams (2013), the study of coastlines plays an important role in coastal management, climate change, and sea level rise. The study of shoreline change on the north coast of NCT Regency applied an *overlay* technique with the help of a *Geographic Information System* (GIS) with ArcGIS software (Nassar et al. 2019). Statistical analysis was performed using the *Digital Shoreline Analysis System* (DSAS). DSAS analysis is useful for knowing the

value of *Net Shoreline Movement* (NSM) and *End Point Rate* (EPR) as reports of shoreline changes (Jonah et al. 2016). This study aims to analyze shoreline change along the north coast of NCT Regency over the past 9 years: 1990, 2000, 2015, 2016, 2017, 2018, 2019, 2020, and 2021. The results of this study can be used for the formulation of mitigation and regulatory policies as well as giving contribution to the research literature.

MATERIALS AND METHODS

Research Site

The research was conducted on the north coast of NCT Regency, ENT Province. The number of transects at the research location was 4696. They spread across 9 coastal villages divided into 3 sub-districts with 10-meter distances per transect. There were 1354 transects along the coast of the Insana Utara sub-district (Wini and Oekolo Villages), 1112 in Biboki Moenleu sub-district (Oepuah Utara and Oepuah Villages), and 2228 in Biboki Anleu sub-district (Oemanu, Ponu, Tuamese, Nonotbatan, and Motadik villages), as

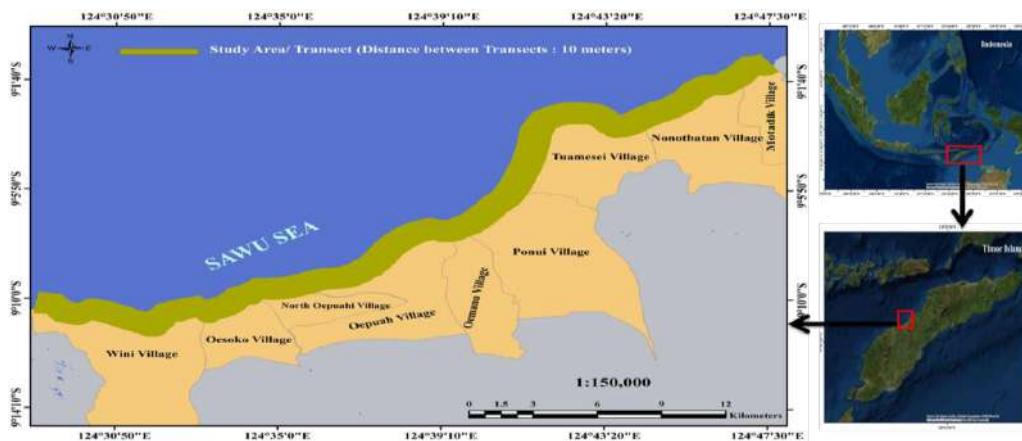


Fig. 1: The research site.

Table 1: Satellite imagery data used in the research.

Satellite Imagery	Resolution	Radiometric	Path/Row	Date
Landsat 5 TM	30	8 bit	110/066	3/31/1990
Landsat 5 TM	30	8 bit	110/066	7/16/2000
Landsat 8 OLI	30	12 bit	110/066	9/28/2015
Landsat 8 OLI	30	12 bit	110/066	8/13/2016
Landsat 8 OLI	30	12 bit	110/066	8/16/2017
Landsat 8 OLI	30	12 bit	110/066	8/19/2018
Landsat 8 OLI	30	12 bit	110/066	7/21/2019
Landsat 8 OLI	30	12 bit	110/066	7/23/2020
Landsat 8 OLI	30	12 bit	110/066	8/11/2021

shown in Fig. 1. The choice of research site, was based on the consideration that the North coast of NCT Regency has a very low mangrove population level which triggers tidal floods that damage settlements, aquaculture areas and roads (Ledheng et al. 2020).

Image Data

The data used in this study are Landsat 5 TM image data for 1990 and 2000 and Landsat 8 OLI from 2015 to 2021, which were compiled from the *United States Geological Survey* (USGS) at <https://glovis.usgs.gov/app?fullscreen=0>. The satellite images used meet the criteria of less than 10% cloud cover Table 1. Supporting data for this research are tidal prediction from MIKE 21 software and slope data measured from the field.

Data Analysis

Data processing includes several stages, such as image correction and cropping. Image processing is done using the ArcGIS program. The stages of image data processing consist of geometric correction, image cropping, image analysis for shoreline change, and shoreline correction for tides. A geometric correction was carried out on Landsat 5 TM to correct the spatial distortion of objects in the image. Thus, the position of the recorded object matches the coordinates in the field. This action was done because Landsat 5 TM raster data is generally displayed as unprocessed data (raw) and has geometric errors that must be corrected geometrically into the earth's coordinate system.

Image data cutting is done to limit the images to only the research area. Image cropping can be done based on the coordinates, number of pixels, or area magnification results. Image band sharpening uses a *Red-Green-Blue* (RGB) 123 band composite. This band is used because they are the most suitable for detecting shoreline change. After sharpening the image, digitizing the image is also done to get the accuracy of the coastline. Correction of tides is very important to eliminate standing water due to the effect of tides on image recording. Shoreline correction to tides is done by determining the beach bottom's slope and the image

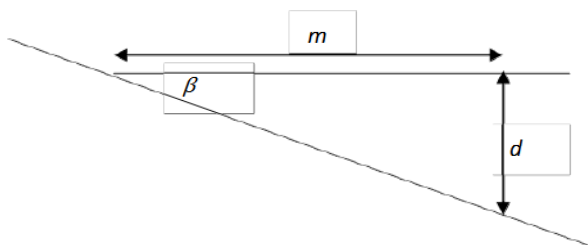


Fig. 2: Scheme for calculating the slope of the coast.

shoreline correction to the mean sea level (MSL). The slope of the seabed is obtained by knowing the depth (d) and horizontal distance (m) from the shoreline to depth Fig. 2.

Based on Fig. 2, the beach bottom slope equation is obtained:

$$\tan \beta = \frac{d}{m} \quad \dots(1)$$

Correction of the imaged coastline to mean sea level (MSL) is carried out by defining the difference in the position of the water level (η) when recording the image to MSL Fig. 3. The MSL is obtained from the tidal constants from the MIKE 21 prediction; therefore the distance to the shoreline shift (r) is obtained through the equation:

$$r = \frac{\eta}{\tan \beta} \quad \dots(2)$$

If the image recording is done during high tide, the coastline is shifted seaward as far as r . Conversely, when the sea water recedes, the coastline is shifted inland as far as r . The last process is overlapping, which is carried out to see shoreline change at the research site by calculating the values of abrasion and accretion. To see changes in the shoreline clearly, the site was divided into 9 locations representing each coastal village in NCT Regency. If the shoreline in 1990 shifted further out to sea compared to one in 2021, then the location is determined to have occurred with abrasion or, vice versa, accretion occurred.

RESULTS AND DISCUSSION

Shoreline Extraction

Satellite images obtained from radiometric and atmospheric corrections are used for the shoreline extraction stage. The shoreline extraction process is preceded by transferring band colors to separate land and water colors. Using the Short Wave Infrared 1 (SWIR 1) color band for the Landsat 8 OLI and Near Infrared for the Landsat 5 TM produces the color reflection presented in Fig. 4.

Based on image analysis using ENVI 5.3, the infrared reflectance reflected by the land has a high value compared to the reflectance value from the sea, which is close to zero. According to Alesheikh et al. (2007), the sea absorbs

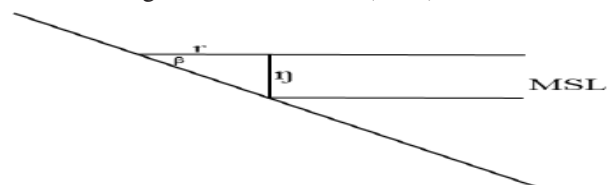


Fig. 3: Schematic drawing of the sea level position at the time of satellite image acquisition.

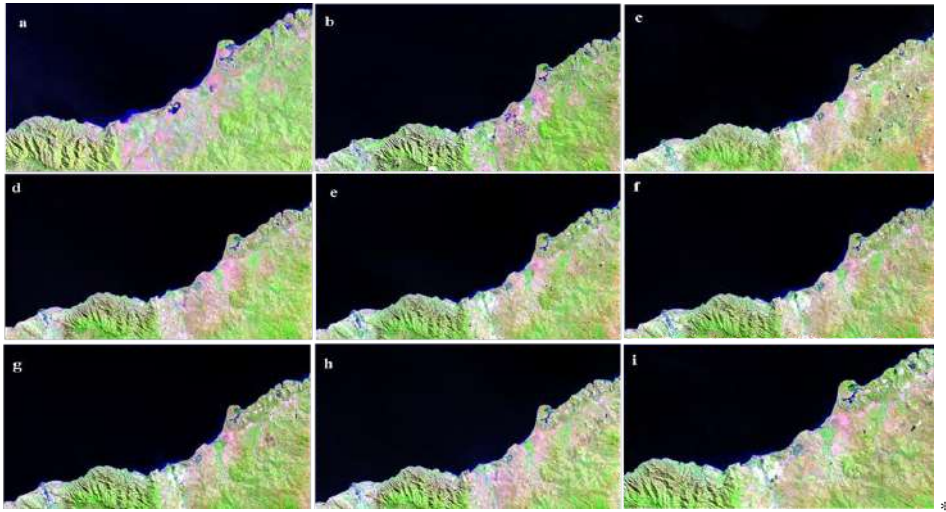


Fig. 4: Land and sea thresholds using Near Infrared for Landsat 5 TM: (a) 1990; (b) 2000, and using SWIR 1 for Landsat 8 OLI: (c) 2015, (d) 2016, (e) 2017, (f) 2018, (g) 2019, (h) 2020 dan (i) 2021.

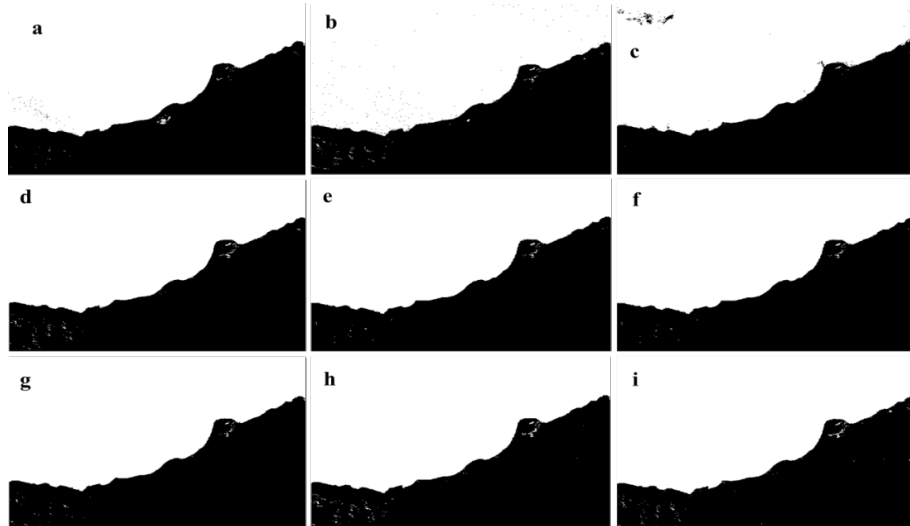


Fig. 5: The results of threshold and band ratio approaches combination images of the year: (a) 1990; (b) 2000, (c) 2015, (d) 2016, (e) 2017, (f) 2018, (g) 2019, (h) 2020 dan (i) 2021.

Table 2. Coastal Slope Calculation Results, Tidal Analysis, and Shoreline Correction Distance to Tide on the North Coast of TTU Regency.

Image Recording Time	MSL [m]	β [°]	N [m]	Condition	X [m]
3/31/1990 8:00 WITA	2.87	0.8	2.87	Tide	4.25
7/16/2000 8:00 WITA	2.59	0.8	1.85	Recede	2.25
9/28/2015 8:00 WITA	2.68	0.8	1.94	Recede	2.36
8/13/2016 8:00 WITA	2.33	0.8	2.03	Recede	2.46
8/16/2017 8:00 WITA	2.38	0.8	2.38	Tide	2.9
8/19/2018 8:00 WITA	2.33	0.8	2.45	Tide	2.97
7/21/2019 8:00 WITA	2.57	0.8	2.83	Tide	3.43
7/23/2020 8:00 WITA	2.44	0.8	2.45	Tide	2.97
8/11/2021 8:00 WITA	2.72	0.8	1.82	Recede	2.21

Note: Slope classification: < 1 (even), 3-6 (sloping), 9-25 (steep), > 140 (very steep) (Portal Geograf 01 November 2018)

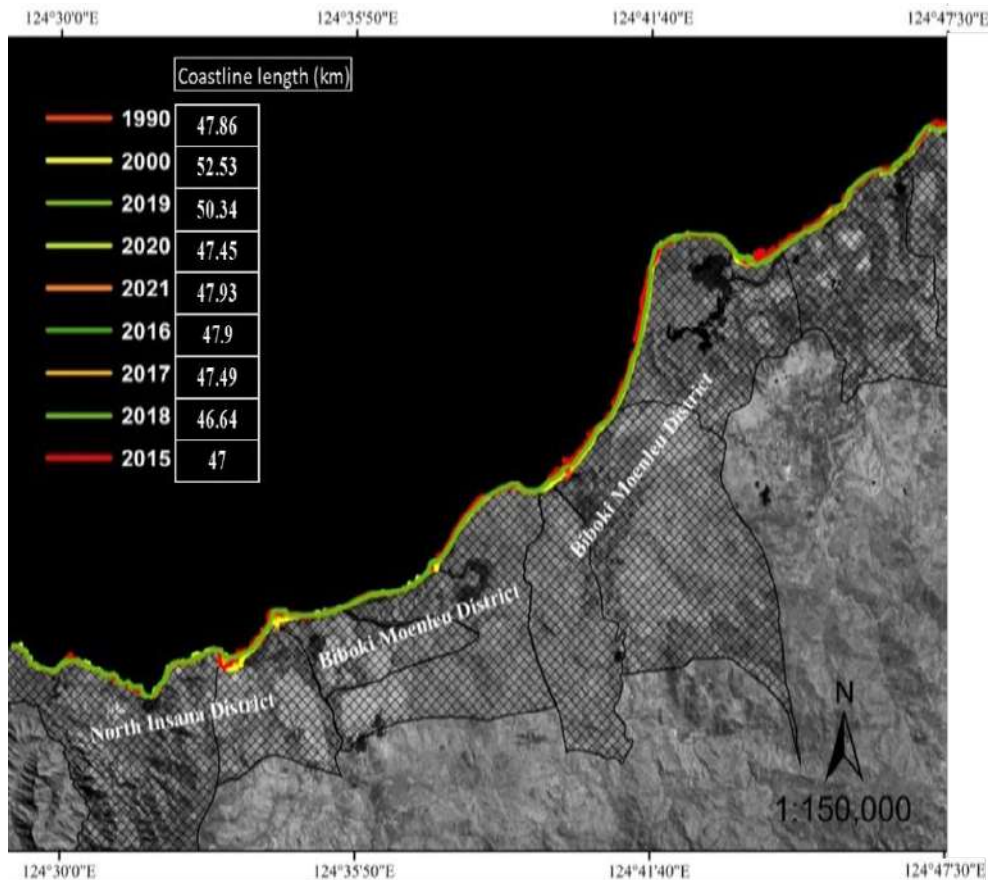


Fig. 6: Landsat imagery from 1990 to 2021 after shoreline correction for tides.

the infrared reflectance value; thus, it is not reflected. In addition, the band ratio used for Landsat 8 is Band 3/6 and Band 3/5. Meanwhile, Landsat 5 uses Band 2/5 and Band 2/4. Combining the threshold and band ratio approaches produces an image converted to a coastline. The results of the band ratio and the combination of the two approaches are shown in Fig. 5.

The combined binary image of the threshold and band ratio is classified between water and land. The results of this classification are vectors, which are conversions from rasters to polygon shapefile formats. The polygon vector is converted into points and then into UTM coordinates for shoreline corrections for tides. Correcting the UTM coordinate value using the line shift (x) obtained from observing the beach slope and tidal analysis using MIKE 21 Table 2.

Landsat 5 imagery recorded on March 31, 1990, was obtained at a sea level elevation of 2.87 m or during high tide conditions. While the recording date of 16 July 2000 was obtained at a sea level elevation of 1.85 m at low tide. Landsat 8 imagery recording dates 28 September 2015, 13 August

2016, 16 August 2017, 19 August 2018, 21 July 2019, 23 July 2020, and 11 August 2021 obtained at elevation altitudes respectively: 1.94 m, 2.03 m, 2.38, 2.33 m, 2.57 m, 2.44 m, and 2.72 m. Based on the elevation value, it is known that the change in coastline distance to the normal position from 1990 to 2021 is successive: 4.25 m, 2.25 m, 2.36 m, 2.46 m, 2.9 m, 2.97 m, 3.43 m, 2.97 m, and 2.21 m. The condition of the coastline of NCT Regency in the landscape images from 1990 to 2021 after correction for tides produces the length of the coastline as shown in Fig. 6.

Shoreline Change Analysis

Based on the analysis of shoreline change in NCT Regency from satellite imagery observations in 1990, 2000, 2015 to 2021, the shoreline has experienced both abrasion and accretion. The average abrasion area is 845.43 m², as long as 36520 meters, while accretion is 10621 m long with an area of 1108.07 m². The accretion area is larger than the abrasion, which may be due to a very large supply of sedimentation occurring in the estuary on the north coast of NCT Regency, causing sedimentation to move faster. According to Muryani

Table 3: Analysis of shoreline change of North Central Timor Regency in 2021.

Beach Conditions	Change in coastline			
	The rate of shoreline change [m.tahun ⁻¹]	Area [m ²]	Length [m]	Percentage [%]
Abrasion	12.65	845.43	36520	77.47
Accretion	20.19	1108.07	10620	22.53
Total			47140	100

(2010), coastal areas near river mouths experience relatively rapid sedimentation, thus forming new land or increasing the existing land area. The analysis results using the *End Point Rate* (EPR) method show an accretion rate of 20.19 m.year⁻¹, higher than the abrasion rate of 12.65 m.year⁻¹. The average change in the northern coastline of NCT Regency from 1990-2021 is presented in Table 3.

Change in the shoreline in 2000 caused abrasion of 211.35 m² with an average change distance of 44.68 m, while accretion covered an area of 218.51 m² and a change distance of 43.29 m. Then in 2015, there was an additional abrasion area of 282.16 m² and 328.88 m² of accretion; thus, the abrasion area reached 493.51 m² and 547.39 m² of accretion with the distance of changes in abrasion and accretion 22.53 m and 105.75 m respectively. In 2016, the area of abrasion and accretion decreased by 44.28 m² and 237.51 m² with a distance of 72.7 m abrasion change and 11.75 accretions. The abrasion area from 2000 continued to decrease until 2017 to 186.27 m² while accretion became 224.33 m². The area of abrasion and accretion increased again in 2018, with 4963.26 m² of abrasion and 7101.99 m² of accretion, with a change in abrasion of 13.73 m while accretion was 18.91 m. Then, there will be a decrease in abrasion and accretion until 2021. They are the abrasion and accretion of 106 m²,

Table 5: Changes in abrasion and accretion in 2017-2018.

Village	Abrasion			Accretion		
	Area [m ²]	NSM [m]	EPR [m]	Area [m ²]	NSM [m]	EPR [m]
Wini	1144.90	-7.17	-7.11	1159.57	8.16	8.09
Oesoko	2439.78	-19.64	-19.48	2477.8495	7.78	7.71
Oepuah Utara	10001.85	-15.23	-15.10	9300.83	24.20	31.17
Oepuah	2666.75	-4.98	-4.94	2636.81	11.51	11.41
Oemanu	2517.42	-18.86	-18.71	299.80	23.92	23.73
Ponu	9778.69	-27.56	-27.33	31315.61	31.43	24
Tuamese	9035.79	-11.19	-11.10	9165.41	22.08	21.90
Nonatbatan	2703.56	-9.70	-9.62	2764.91	14.28	14.16
Motadik	4380.63	-9.26	-9.19	4797.10	26.82	26.60

Table 4: The extent and distance of changes in abrasion and accretion in 1990-2021.

Tahun	Width (m ²)		NSM (m)	
	Abrasion	Accretion	Abrasion	Accretion
1990 - 2000	211.35	218.51	-44.68	43.29
2000 - 2015	493.51	547.39	-22.53	105.75
2015 - 2016	449.23	309.88	-72.67	11.75
2016 - 2017	186.27	224.33	-9.60	32.81
2017 - 2018	4963.26	7101.99	-13.73	18.91
2018 - 2019	163.41	143.22	-19.12	8.54
2019 - 2020	189.50	212.61	-24.40	8.35
2020 - 2021	106.90	106.59	-7.93	11.07
Average	845.43	1108.07	-26.83	30.06

each with a distance of 7.93 m of abrasion change and 11.1 m of accretion.

Based on the slope level, the north coast of NCT Regency is included in the flat category so that it impacts sea level rise. It is known that the tides in this research area are double-inclined, which can affect shoreline change. The bottom sediments on the north coast of NCT Regency are predominantly very fine to sandy (Ledheng et al. 2012). According to Tarigan (2010), flat beach conditions with a fine sediment substrate will easily experience abrasion when the waves come. The dynamics of changes in line shift distance and beach area due to abrasion and accretion on the north coast of NCT Regency are presented in Table 4.

Based on the observation, the dominant abrasion occurred in 2017 - 2018 on the North Oepuah coast, covering an area of 10001.85 m² along 8090 m with an average shoreline shift of 15.23 m. Ponu beach covers an area of 9778.69 m² along 8090 m with an average shoreline shift of 27.56 m.



Fig. 7: The condition of North Oepuah beach and Ponu photos from 2017-2018.

Meanwhile, accretion on the North Oepuah coast is still dominant, which is 31315.61 m² and 1110 m long with an average shoreline shift of 24 m, followed by Ponu beach with an area of 31315.61 m² and 790 m long with an average shift of 31.43 m. Ponu Beach has the highest average abrasion rate of 27 m·year⁻¹, followed by Oesoko beach at 19.64 m·year⁻¹. Meanwhile, the highest accretion rate was on Ponu beach, which was 31 m/ year, followed by North Oepuah beach, which was 24 m·year⁻¹ (Table) 5.

River mouths still influence the two coastal areas with muddy beach conditions. The condition of accretion on the coast of North Oepuah and Ponu Beach is thought to be related to the geomorphological shape of the beach in the form of a bulge along the coast area; thus, the sea waves crash more intensively in the west monsoon period. Based on data from the Central Bureau of Statistics for NCT Regency in 2018, there was a very high rain intensity of 148 mm/ day (Statistics of Timor Tengah Utara Regency 2018). This causes the coastal areas, especially the North Oepuah and Ponu areas, to receive floods that carry large particles (Fig. 7).

The accretion that occurred in 2018 is thought to have been caused by particles carried along with the floods due to the low-lying areas of the coastal part of the island of Timor, which always experience floods from upstream that come unexpectedly due to differences in high rainfall upstream. Based on data from the Central Bureau of Statistics for NCT Regency in 2018, there was rain with a high intensity of 148 mm/day (Statistics of Timor Tengah Utara Regency 2018). According to Diposaptono et al. (2009), particle deposition is caused by current energy generated from tides

and waves. River currents that enter seawater during high tide conditions will experience a slowdown resulting in reduced material transportability so that the material settles. On the other hand, during low tide, sediment from the river will be carried out to sea. Rising sea levels also cause changes in sedimentation patterns and siltation in river mouths which can interfere with access to and from boats used by fishermen to go to sea. The flat slope and waters that tend to be shallow cause material resuspension which is influenced by wind, waves, and tides, as well as causing expansion and changes in land use that occur in the research site. Hammar-Klose et al. (2003) explained that beaches that are sloping to flat are more susceptible to the movement of sediment particles as the main component forming the beach profile compared to steeper beaches. The dynamics of changes in the coastline from 1990 – 2021 are presented in Table 6 and Fig. 8.

The changes in an abrasion on Nonotbatan and Motadik beaches are 580.73 m² along 5350 m and 877.84 m² along 1620 m, respectively. Meanwhile, the accretion reaches an area of 587.82 m² along 530 m and 877.84 m² along 160 m, respectively. The condition of Nonotbatan beach is dominated by mixed and sandy beaches with settlements in this area, so it is prone to abrasion. The Motadik coastal area includes a flat tidal area with muddy beach conditions; thus, many mangrove plants grow as a coastline. This condition differs from the Tanjung Bastian area on Oesoko beach, which was damaged by abrasion.

The research by Ledheng et al. (2020) showed that the mangrove vegetation in the Bastian Cape area has become extinct. According to Soraya et al. (2012), mangrove damage affects shoreline change. Based on the NSM method, there

Table 6: Changes in the coastline from 1990-2021.

Village	Transect number	Transect length [m]		Total	NSM [m]		Width [m ²]		Total
		Abrasi	Akresi		Abrasion	Accretion	Abrasion	Accretion	
Wini	1 - 975	9720	40	9760	-14.06	9.84	248	253.4	501.4
Oesoko	976 - 1354	130	3680	3810	-7.48	16.23	399.05	406.22	805.27
Oepuah Utara	1355 - 1581	8090	790	8880	-7.86	35.63	1536.44	4713.03	3203.89
Oepuah	1582 - 2467	1380	910	2290	-3.87	6.59	530.88	525.47	1056.35
Oemanu	2468 - 2522		570	570	-2.11	2.28	711.38	399.49	1110.87
Ponu	2523 - 2950	1110	3200	4310	-16.08	9.59	1642.77	1561.12	6249.46
Tuamese	2951 - 3934	9120	740	9860	-7.73	8.47	1268.46	1265.2	2533.66
Nonotbatan	3935 - 4520	5350	530	5880	-6.09	4.49	580.73	587.82	1168.55
Motadik	4521 - 4696	1620	160	1780	-6.06	6.49	846.51	877.84	1724.35
Total		36520	10620	47140			7764.24	10589.57	18353.81
Average					-7.93	11.07			

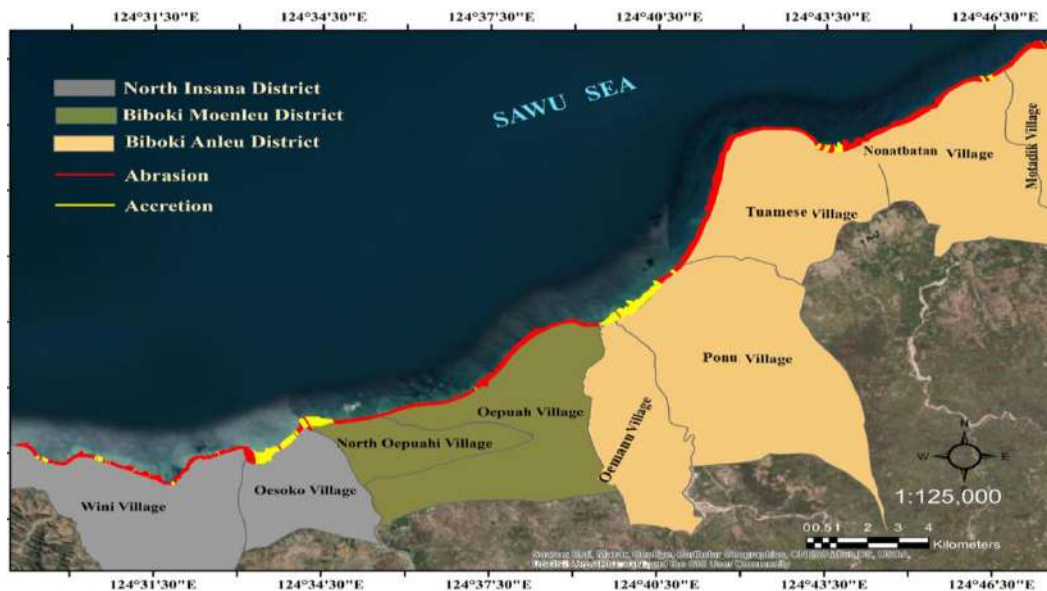


Fig. 8: Conditions of abrasion and accretion on the north coast of TTU Regency in 1990-2021.

was a line shift of 549.97 meters from 1990 to 2021 at Tanjung Bastian at the transect number 2996 Fig. 9. The dynamics of changes in the coastline causing accretion and abrasion in 2021 are also the impact of tropical cyclone storms which cause tidal waves and floods.

Three coastal villages were significantly affected by the tidal wave and flooding: Wini, Oesoko, Oepuah Utara, Motadik, and Ponu (Timor Tengah Utara Regency 2021). Sediment from erosion in the Tanjung Bastian, which has experienced the impact of abrasion, is distributed towards the coast of North Oepuah. Sediment runoff from the watershed on the coast of Oesoko is then driven by a similar current

heading east towards North Oepuah at a speed of 3.60 to 11.10 m.s^{-1} . This condition was confirmed by windrose from recording results at the BMKG database from January to December 2021 on the north coast of Timor Island Fig. 10. Sediments carried by tidal waves accumulated with those sent by floods from land during tropical cyclone storms so that around the estuary of North Oepuah village there was a shift of the long coastline towards the sea. On transect number 3976, there was the highest change in distance, 467 meters Fig. 11.

According to Darmiati et al. (2020), coastal accretion occurs due to transporting sediment from other areas that

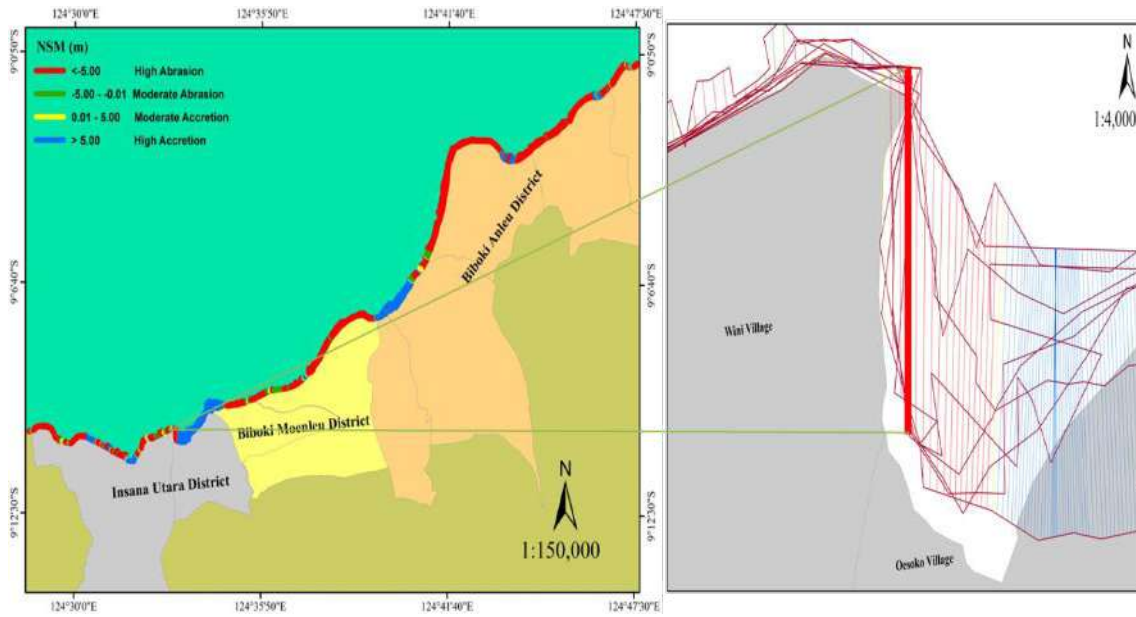


Fig. 9: Changes in the maximum abrasion distance in the Tanjung Bastian area of Oesoko Village.

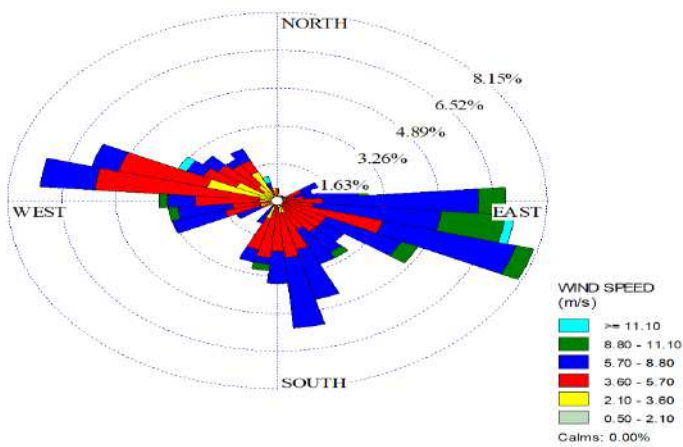


Fig. 10: Windrose area on the north coast of Timor Island.

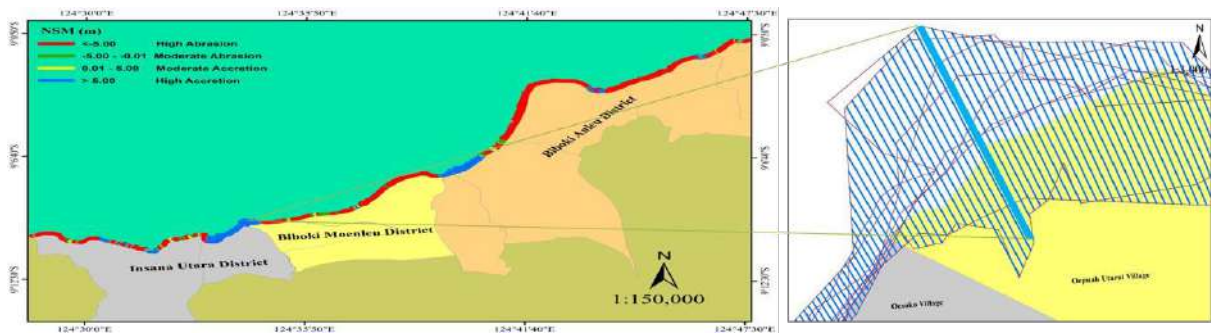


Fig. 11: Changes in the maximum distance of accretion on the coast of North Oepuah.

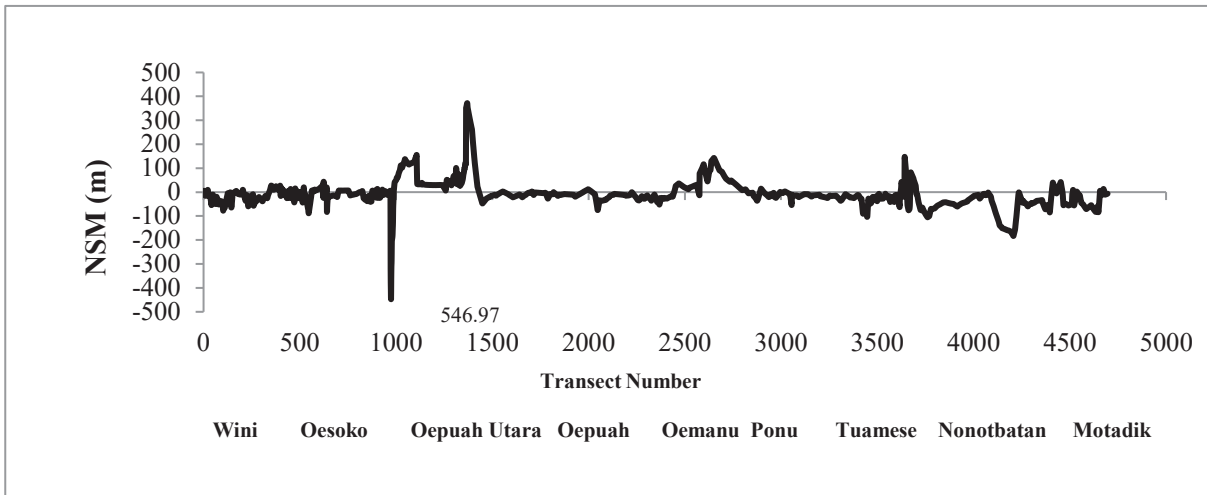


Fig. 12: Dynamics of change in shoreline distance observation 1990-2021.

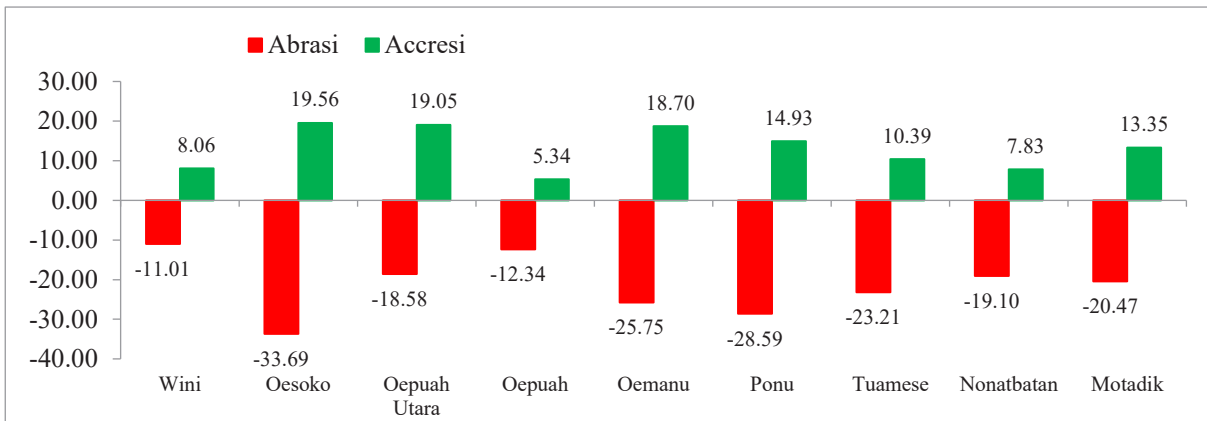


Fig. 13: Average rate of change for 1990-2021.

experience abrasion, which allows sediment to enter due to the force of currents generated from tides and waves. The dynamics of changes in shoreline distance using the NSM method are presented in Fig. 12.

The shoreline distance due to abrasion on the coast of Oesoko underwent a very extreme change of 546.97 meters (Fig. 8). This is due to the high rate of change at that location. The EPR method analysis shows that the maximum average rate of abrasion changes occurs on the Oesoko coast, which is 33.69 m/year, followed by the Ponu coast, 28.59 m/year⁻¹ Fig. 13.

CONCLUSION

Based on the observations of satellite imagery during 1990 - 2021, the north coast of NCT Regency generally experiences the dynamics of change, both abrasion and accretion. The average area of accretion is 1108.07 m² with a rate of change

of 20.19 m.year⁻¹ occurring along 1021 m, while the average abrasion area is 845.43 m² with a rate of change of 12.65 m.year⁻¹ occurring along 36520 m. The average distance of the shoreline change in accretion conditions is 11.3 m, while abrasion is 7.93 m. The distance to the shoreline changed due to the highest abrasion that occurred in Ponu, namely -16.08 m resulting in an area of 1642.77 m² with a rate of change of 27.33 m.year⁻¹, while the shift in distance due to abrasion of 35.63 m resulted in an area of 4713.3 m² with a rate of change of 31.17 m.year⁻¹.

In general, the area that experienced the greatest change in abrasion distance was Oesoko Beach, especially in the Bastian Cape area, with a shift reaching 549.97 m. The maximum accretion shift of 467 m was found on the North Oepuah beach. This research indicates that the north coast of NCT Regency has experienced a significant increase in land area in the estuary. However, there is still the potential

for an increase in abrasion area as, in general, the overall flat topography of the North Coast still influences it. The results of the research will contribute to decision-making for coastal management planning for NCT Regency.

REFERENCES

- Alesheikh, A.A., Ghorbanali, A. and Nouri, N. 2007. Coastline change detection using remote sensing. *J. Environ.*, 4(1): 61- 66
- Dahuri, R., Rais, J., Ginting, P., S. and Sitepu M. 2013. *Pengelolaan Sumber Daya Pesisir Secara Terpadu* (Jakarta: PT. Balai Pustaka) 201
- Darmiati, N.I., Nunisthi, W. and Atmadipoera, A.S. 2020. Analysis of shoreline change in west coast area of Tanah Laut District South Kalimantan. *J. Teknol. Kel. Tropis*, 12(1): 211-222. <https://doi.org/10.29244/jitkt.v12i1.22815>
- Diposaptono, S., Budiman, M. and Agung., F. 2009. *Dealing with Climate Change in Coastal Areas and Small Islands*. Popular Scientific Books, Bogor, p. 359.
- Fuad, M.A.Z. and Fais, D.A.M.F. 2017. Automatic detection of decadal shoreline change on the northern coast of Gresik, East Java – Indonesia. *IOP Conf. Ser. Earth Environ. Sci.*, 98: 012001. doi:10.1088/1755-1315/98/ 1/012001
- Hammar-Klose, M., Erika, S., Pendleton, E.A., Thieler, E.R., Williams, S.J. and Norton, G.A. 2003. Coastal vulnerability Assessment of Cape Cod National Seashore (CACO) to Sea-level Rise. USGS Report, p. 23.
- Jonah, F.E., Boateng, I., Osman, A., Shimba, M.J., Mensah, E.A., Adu-Boahen, K., Chuku, E.O. and Effah, E. 2016. Shoreline change analysis using point rate and net shoreline movement statistics: an application to Elmina Cape coast and more sections of Ghana's coast. *Reg. Stud. Marine Sci.*, 7: 19 – 31. <https://doi.org/10.1016/j.rsma.2016.05.003>
- Kurniawan, I.A. and Marfai, M.A. 2020. Shoreline changes the analysis of Kendal Coastal Area. *IOP Conf. Ser. Earth Environ. Sci.*, 451: 012056. doi:10.1088/1755-1315/451/1/012056
- Ledheng, L., Ardhana, I., and Sundra, I. K. 2012. Komposisi dan Struktur Vegetasi Mangrove di Pantai Tanjung Bastian Kabupaten Timor Tengah Utara Provinsi Nusa Tenggara Timur. *Ecotrophic: Jurnal Ilmu Lingkungan*, 4(2): 80-85.
- Ledheng, L., Naisumu, Y.G., and Binsasi, R. 2020. Study of biomass and carbon stocks in the north coast mangrove forest of North Central Timor District, East Nusa Tenggara Province. *Multidiscip. Inertia Sci. Technol.*, 3(1): 217-229.
- Muryani, C. 2010. Analysis of coastline changes using GIS and its impact on the community's life around Rejoso river estuary Pasuruan district. *J. Forum Geografi.*, 24(2): 173-182. <http://doi.org/10.23917/forgeo.v24i2.5024>
- Nassar, K., Mahmud, W.E., Fath, H., Masria, A., Nadaoka, K. and Negm, A. 2019. Shoreline change detection using DSAS technique: The case of North Sinai coast, Egypt. *Marine Georesour. Geotechnol.*, 37(1): 81-95. doi:10.1080/ 1064119X.2018.1448912
- Portal Geografi. 2018. Morfometri: Pembagian Kemiringan Lereng. Blog Portal Geografi. <http://portalgeograf.blogspot.com/2018/11/morfometri.html>
- Soraya, D., Djunaedi, O.S. and Taofiqurohman, A. 2012. Shoreline changes due to mangrove forests damage in the Sub-District Blanakan and Legonkulon Subang. *J. Perik. Kel.*, 3(4):355-364.
- Statistics of Timor Tengah Utara Regency, 2018. North Central Timor Regency in Figures. Statistics of North Central Timor Regency. Kefamenanu.
- Sugiarta, E. 2018. Analysis of Shoreline Change Using Satellite Imagery on Lemukutan Island, Bengkayang Regency, West Kalimantan. Bogor Agricultural Institute, Bogor, Indonesia.
- Tarigan, M.S. 2010. Changes in the coastline in the coastal area of Cisadane waters, Banten Province. *Makara. J. Sci.*, 11(1): 49-55.
- Timor Tengah Utara Regency, 2021. Keputusan Bupati Timor Tengah Utara Nomor 209 Tahun 2021 tentang Status Tanggap Darurat Penanganan Bencana Angin Sklon Tropis, Banjir, Tanah Longsor, Gelombang Pasang dan Abrasi di Kabupaten Timor Tengah Utara. Pemerintah Kabupaten Timor Tengah Utara: Kefamenanu. file:///C:/Users/A%20C%20E%20R/Downloads/status%20tanggap%20darurat%20TTU%20NTT01%20Gelombang%20pasang%20dan%20Abrasi.pdf
- Williams, S.J. 2013. Sea-level rise implications for coastal regions. *J. Coast. Res.*, 63: 184-196. doi:10.2112/SI63-015.1.
- Winarso, G., Judijanto, M. and Budhiman, S. 2001. The Potential Application Remote Sensing Data For Coastal Study. 22nd Asian Conference on Remote Sensing, 5-9 November 2001, Singapore.



Flood Mitigation and Pollution Abatement in Kaduna Metropolis Through Engineering Assessment and Analytical Hierarchy Process Design

O. J. Oyebode† and F. Paul

Civil and Environmental Engineering Department, Afe Babalola University, Ado-Ekiti, Ekiti State, Nigeria

†Corresponding author: O. J. Oyebode; oyebodedare@yahoo.com

Nat. Env. & Poll. Tech.
Website: www.neptjournal.com

Received: 09-12-2022

Revised: 23-01-2023

Accepted: 01-02-2023

Key Words:

Pollution abatement
Water resource planning
Engineering assessment
Flooding mitigation
Hydraulic structures

ABSTRACT

Pollution abatement and flood control activities require effective water resource planning, engineering assessment, sophisticated technology, and appropriate hydraulic structure designs. This paper x-rays flood mitigation and pollution abatement strategies that can be adopted in the Kaduna metropolis in Nigeria. Analytical hierarchy process of design, questionnaires, engineering assessment approach, and standard method for estimation of the runoff discharge was adopted for this research. Estimating water balance components and QSWAT Hydrological Model can be used with the QGIS interface for a greener environment. Suitable hydraulic systems were designed for long-term flood control in the River Kaduna catchment area through an analytic hierarchy Process. Statistical analysis, manning equations, and rational methods were utilized for adequate assessment and planning. The hydraulic discharge capacity of culverts, open channels, and other hydraulic structures was carefully checked. Flooding greatly impacts infrastructural development, and inadequate drainage systems contribute to it. Mitigation strategies, adequate water resource planning, and management will greatly benefit from addressing flood-related issues in the study area. This research provides information on the flood vulnerability of infrastructures and mitigation strategies that can be adopted in the study area. Viable policies and management strategies can be utilized to avert losses traceable to floods in developing and developed countries.

INTRODUCTION

Environmental pollution and flooding-related issues must be avoided in developing and developing nations. Since rivers provided a consistent, even though not always reliable, flow of water for household, agricultural, industrial, and nautical purposes, numerous cities grew independently along many river valleys around the world. These cities include New York along the Hudson River, Cairo along the Nile River, and Kaduna, the capital of Kaduna State in Nigeria, which is situated along the River Kaduna. It is vital to reduce shortages caused by the water demands of irrigation systems in a variety of climatic and environmental settings. Even though the ideal scenario would satisfy all water needs, the best results would indicate otherwise. To preserve the effectiveness, maintenance, and sustainability of the aquifer, the groundwater level drawdown can be decreased (Rezaei & Safavi 2022). Governments, the general public, and all other participants in the water sector are all impacted by the serious issue of water stress. Groundwater must be utilized

for industrial purposes, effective irrigation systems, and the production of drinking water in the majority of countries globally (Felisa et al. 2022). Flood control, efficient use of water resources, and catastrophe mitigation must all be prioritized by those in charge of managing river basins and water projects. By acting quickly and correctly forecasting floods, flood damages can be decreased (Oyebode et al. 2022). Pollution abatement refers to technology applied, or measures taken to reduce pollution and its environmental impacts. The most commonly used technologies are scrubbers, noise mufflers, filters, incinerators, wastewater treatment facilities, and composting of wastes. It promotes more efficient use of raw materials, staff resources, equipment, energy, and water. It improves worker health and safety through improved air quality, decreased use of toxic substances, and fewer personnel protective equipment requirements. Groundwater contamination is an international issue affecting both ecological services and human health. The water sector will benefit from strategic management, which will also address issues relating to human health threats (Oyebode & Otoko 2022, Oyebode 2022, Ogarekpe et al. 2023). Natural disasters are unavoidable, necessitating careful observation and implementing mitigation strategies to

ORCID details of the authors:

O. J. Oyebode: <https://orcid.org/0000-0003-2792-146X>

lower vulnerability and risk. The main goal of vulnerability index creation, a crucial instrument in flood management, is pinpointing the region most susceptible to floods. Flood risk is examined and divided into three categories: exposure, susceptibility, and flood hazard. Malaysia's average annual flood damage costs around \$100 million (Chan 2015, Bahar et al. 2022). Overuse of environmental resources degrades the watershed's ecosystem, and poor agricultural households are blamed for this degeneration (Sunaedi et al. 2022). Watershed improvements have been made due to the implementation of the Payment for Environmental Services (PES) program, particularly regarding water services (Redondo-Brenes & Welsh 2006, Pissarra et al. 2021).

On several occasions, these rivers overflow their banks and flood the adjoining properties on their floodplains. There are cases of flooding, such as River Kaduna in 2003, Elbe River in 2003, 2005, and 2007, River Sokoto in 2006, River Ogun in 2007, and many others. Consequently, flooding, an associated natural hazard with floodplain developments, is a major problem these cities had to contend with and develop policy, legislative and technical measures to control (Proverbs & Lamond 2017). Flooding is when a lot of water covers a normally dry area. It could be brought on by prolonged periods of heavy rain or a river overflow. Flooding is a catastrophe that needs to be reduced to prevent endangering lives (Oyeboade 2018). Around the world, natural disasters frequently result in physical (such as injuries, casualties, and property damages) and non-physical (psychological and mental) disruptions. The most common natural hazard, flooding, is not an exception. Over the past few decades, it has significantly harmed the environment and caused social harm in various parts of the world (Adjei-Darko 2017, Parsian et al. 2021).

Several unresolved problems and environmental dangers in rural areas and important settlements in Nigeria can be linked to floods and erosion (Oyeboade 2021). Environmental damage was caused by migration and industrial development (Oyeboade 2022a). The best materials and most recent structural engineering developments must ensure that water-retaining structures are adequately protected from sliding, earth pressures, hydrostatic forces, and overturning moments (Oyeboade 2022b). There is a need for adequate policy, maintenance of road networks, and weather station for effective planning, construction, and management of floods in developed nations of the world (Oyeboade 2021). In Nigeria, the flooding of urban settlements has become an annual occurrence. This usually becomes obvious at the peak of the rainy season. The resultant damage caused by the flooding calls for a more pragmatic approach to flood management and control. There are a lot of bridges and

collapse of buildings and flooding scenarios. Marketplaces and farmlands have also been submerged for weeks and sometimes washed away. As a result, flooding in Kaduna must be assessed.

Innovative stormwater management techniques, which depart from traditional "end of pipe" strategies, have attracted increasing attention over the past ten years (based on conveying water offsite to centralized detention facilities). By evacuating people and property from danger zones, nonstructural techniques lessen the damage. Elevated structures, property buyouts, long-term moves, zoning, subdivision, and building codes are some of them. New approaches that promote managing runoff as close to its source as possible, such as sustainable urban drainage systems, low-impact construction, or green infrastructures, have thus become quite popular among practitioners and public authorities (Sage 2015).

Measures performed to reduce, halt, and eradicate pollution from the environment are referred to as pollution abatement. Using catalytic converters in cars to reduce air pollution is an example of a technological solution. Equipment upgrading and installation of more effective equipment to cut waste production and raw material usage are very important. The decrease in environmental degradation and economic growth are mutually beneficial objectives. As the effort to reduce pollution increases, its effectiveness may rise as well. Even if environmental policies remain unchanged, pollution can be reduced because efficiency improvements make abatement less expensive (Managi 2006).

AREA OF THE STUDY

River Kaduna can be found upstream of the Shiroro Reservoir. Geographically, River Kaduna is located between latitudes 9°52'38"N and 10°39'07"N and between longitudes 6°52'33"E and 8°28'50"E (Fig. 1). Air masses, atmospheric pressure, and other climatic conditions control rainfall in the study area. (Butu et al. 2020). Fig. 2 presented flood-prone areas and hazard assessment of some Areas in Kaduna State.

PAST STUDIES

There were records of flood incidences in Kaduna state in Nigeria, according to George & Abdulkadir (2019), floods affect human activities, lives, and properties (Adelekan & Asiyambi 2016, Ibrahim & Abdullahi 2016). The technology used, or actions performed to reduce pollution and its environmental effects are referred to as pollution reduction. Scrubbers, noise mufflers, filters, incinerators, wastewater treatment facilities, and waste composting are the most frequently utilized technologies. Table 1 presented

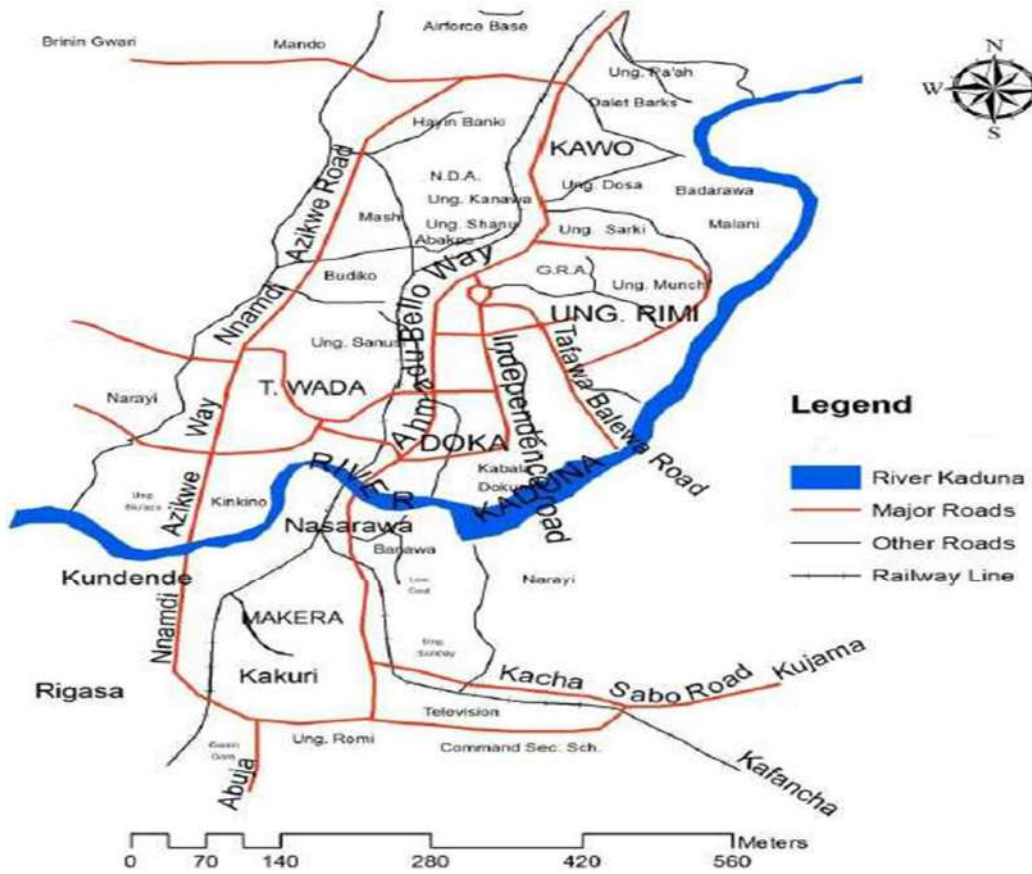
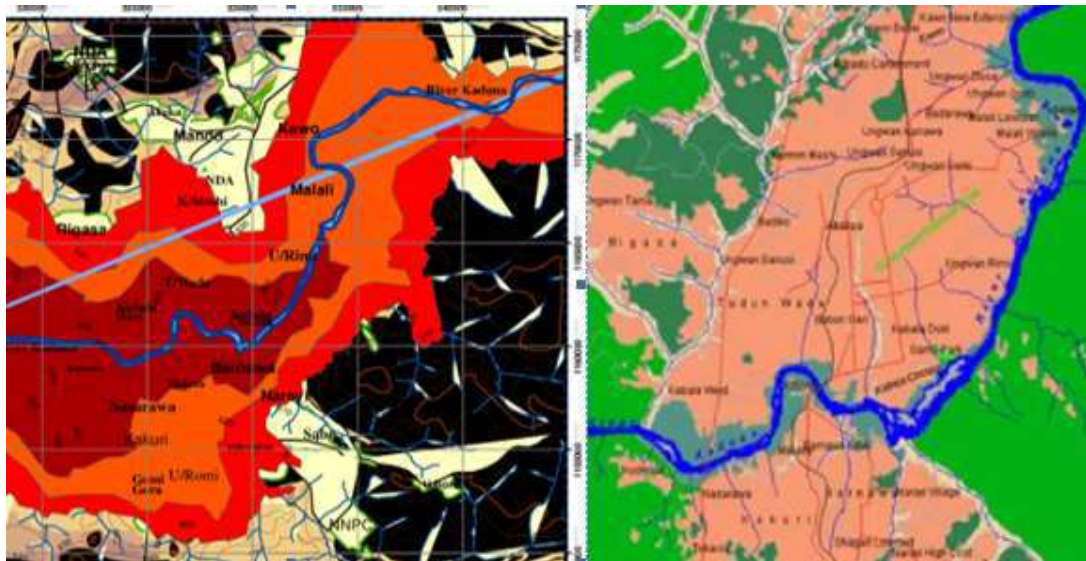


Fig. 1: Map of Kaduna Metropolis indicating major roads and the river.



Source: (Sule et al. 2016).

Fig. 2: Flood hazard assessment of some areas in Kaduna State.

Table 1: Continuous Occupation Floodable areas of Kaduna metropolis.

Consequence	Respondents (n=196)	Respondents [%]
Houses affected by flooding	127	64.29
Collapse Structure through floods	50	25.51
People restricted from movement	81	41.32
Polluted water origin	44	22.44
Heath Hazards traceable to floods	49	25

percentages of the flooded areas from a questionnaire survey. Table 2 presented flooding in 65% of the houses occupied by the respondents. There are cases of collapse for 26% of houses due to flooding. Besides harming personal belongings, every respondent stated how flooding impacted public infrastructures. These included flooded highways, downed telephone and electric lines, flooded marketplaces,

flooded schools, and blocked drainage systems.

MAJOR CAUSES OF FLOODING IN KADUNA METROPOLIS

Table 2 gives a summary of the scenario. Most tropical flood events, which are partly or entirely climatologically in nature, are thought to be primarily caused by rainfall intensity, duration, and amount (Johnson et al. 2016, Ibrahim & Abdullahi 2016).

EFFECTS OF FLOODS

Flood risks and disasters can be traced to blocked drainages, uncoordinated human activities, erratic electricity, and poor communication networks. Many farmlands, surface water, and accommodation were affected (Wahab & Falola 2018, Wamugi 2016).

Table 2: Main reasons for floods in Kaduna State.

Major reasons	Strongly agree	Agree	Neutral	Disagree	Strongly agree
Heavy rainfall	127(64.79%)	44(22.44%)	19(9.69%)	6(3.06%)	0(0%)
Overflowing of River Kaduna bank	105(53.57%)	60(30.61%)	6(3.06%)	22(11.22%)	3(1.58%)
Topography	114(58.16%)	61(31.12%)	0%	10(5.10%)	11(5.61%)
Infiltration	84(42.85%)	73(37.24%)	12(6.12%)	11(5.61%)	16(8.16%)
Lack of drainage network	160(81.63%)	31(15.82%)	0%	3(1.53%)	1(0.51%)
Poor drainage network	147(75%)	39(19.90%)	0%	4(2.04%)	6(3.06%)
Building on the water channel	96(48.90%)	52(26.53)	2(1.02%)	22(11.22%)	24(12.24%)
Dumping of waste on channels	122(62.24)	34(17.34%)	2(1.02%)	10(5.10%)	28(14.28%)
Climate change	27(13.77%)	73(37.24%)	1(0.51%)	34(17.34%)	61(31.12%)

Source: (Fieldwork 2015)

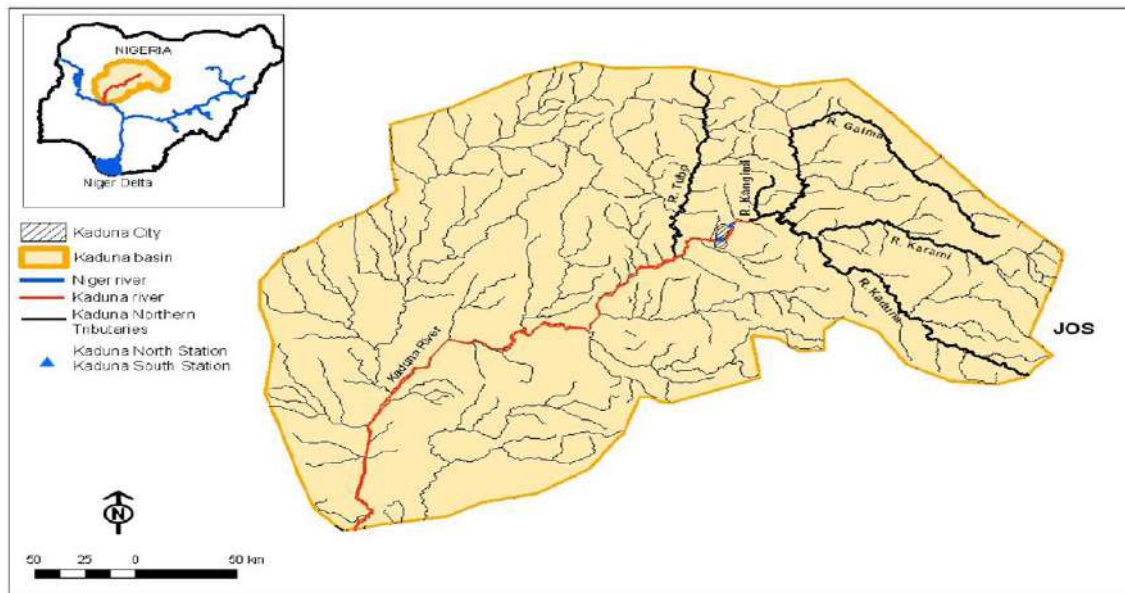


Fig. 3: Kaduna River basin.

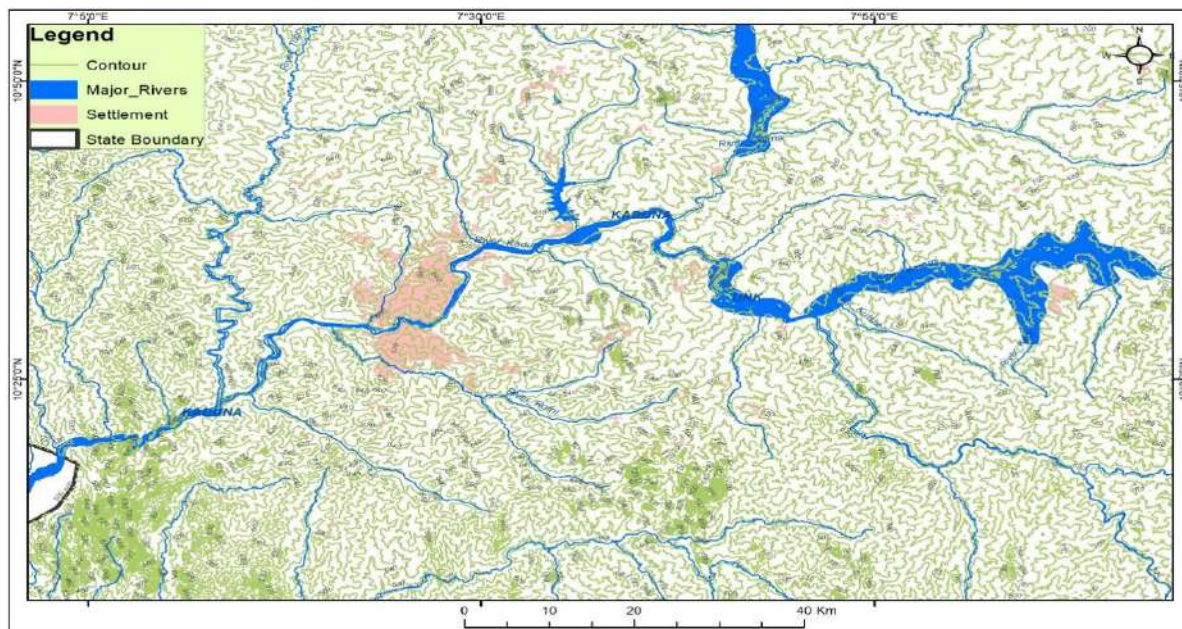


Fig. 4: Catchment area of River Kaduna.



Source: (Field survey 2021)

Fig. 5: Flooding in the Kaduna.



Fig. 6: Flooding in Nigeria.

MATERIALS AND METHODS

The study area considered was Kaduna State. Analytical hierarchy Process of design, questionnaires, and standard method for estimation of the runoff discharge was adopted for this research. The Analytic Hierarchy Process is a way of decision-making that evaluates several options, each with many of criteria to help choose the best option. It is frequently employed for choosing and prioritizing projects. Suitable hydraulic systems were designed for long-term flood control in the River Kaduna catchment area through an analytic hierarchy Process. Fig. 3 presents Kaduna River Basin, Fig. 4 gives the catchment Area of the River Kaduna, and Fig. 5

and Fig. 6 present a case study of flooding in Nigeria.

Velocities of flows were high in some communities (Ferguson et al. 2017). Commonly accepted values for Manning's roughness coefficient, n , are based on materials and workmanship required in the Standard Specifications (Hashim 2018).

Culverts

Culverts are designed for transportation and easy disposal of storm runoff from highways. Fig. 7 shows a typical culvert under a roadway. SWAT simulates different hydrological processes was presented in Fig. 8.



Fig. 7: Culvert under a roadway.

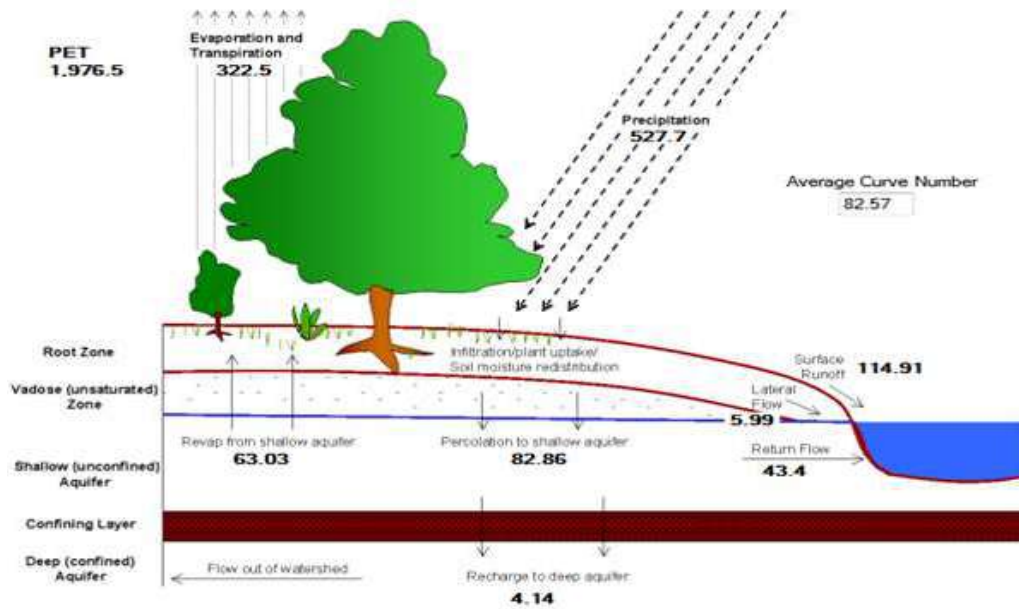


Fig. 8: Schematic representation of hydrologic components by SWAT output.

Hydrological Components and Processes in the SWAT Model

The SWAT enables the simulation of various physical processes in a watershed (Neitsch et al. 2011). Surface runoff, infiltration, evapotranspiration (ET), lateral flow, percolation to shallow and deep aquifers, and channel routing are simulated processes (Arnold et al. 1998). All of

these hydrological processes are simulated in shallow and deep aquifers as well as the surface, soil, and intermediate (vadose) zone. The stream flow in the main channel was influenced by the hydrological processes of surface runoff, subsurface or lateral flow, return flow, and base flow. The water balance equation is the foundation for SWAT’s simulation of the hydrologic cycle. The water balance equation is the foundation for the SWAT model’s simulation

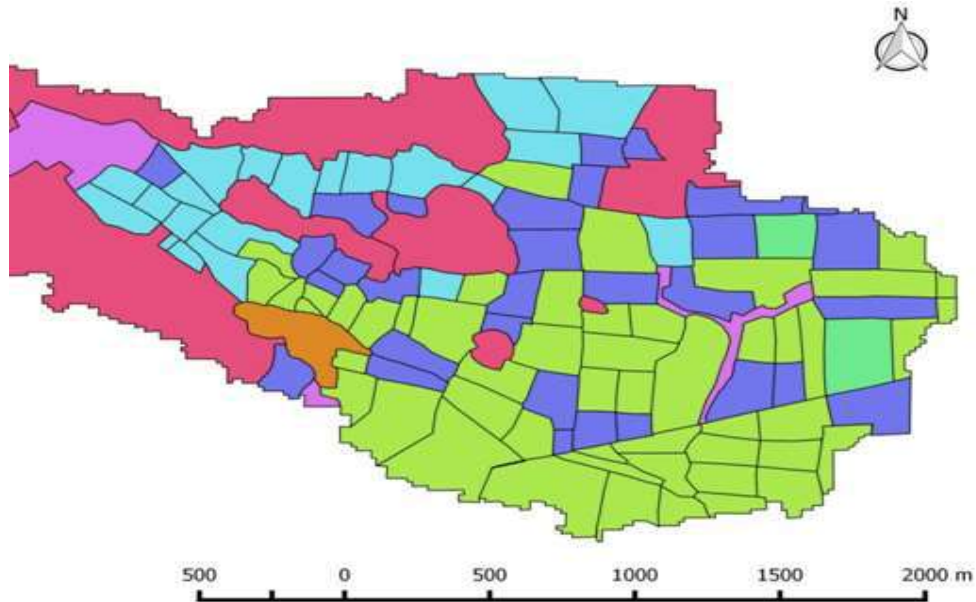


Fig. 9: The land-use map of the watershed.

of hydrological processes. Fig. 9 presented the land-use map of the watershed. The hydrologic cycle simulated by SWAT is based on the water balance equation. The simulation of hydrological processes in the SWAT model is based on the water balance equation.

$$SW_t = SW_o + \sum_{t=1}^t (R_{day} - Q_{surf} - E_a - w_{seep} - Q_{gw}) \quad \dots (1)$$

Design of Rectangular Culverts

The intake (also known as the inlet or fan), the barrel (or throat), and the diffuser are the three components of a culvert (also called the outlet or expansion fan). An accurate calculation of the discharge-frequency relationships is necessary for the construction of road drainage systems. While some facilities need a runoff hydrograph that estimates runoff quantities, others need a momentary peak flow rate. Based on projected design floods, methods for constructing road-crossing drainage culverts should account for essential storm duration. They should also use a hydraulic design methodology to maximize the culverts' size and hydraulic variables (Kang et al., 2009). A bridge is a substantial structure that spans a significant body of water or other physical barriers to allow traffic and people to cross. A box culvert is a structure resembling a tunnel that is erected beneath railroad tracks or roads to facilitate cross drainage from one side to the other. Culverts often have small spans and are buried in the ground. The roadway and the vehicles utilizing it are supported by the soil surrounding the culvert. A bridge contains support structures underneath it, however, there are open spaces between the supports that typically span more than 6 meters. It is crucial to be able to predict the load for projects with heavy backfill and similar tunnels. Designers must take several important aspects into account to appropriately obtain the earth pressure (Li et al., 2020). Fig. 10 indicates Culvert's elements.

$$\text{For } 0 < \frac{H_1}{D} \leq 1.2 \quad \dots(2)$$

$$Q = \frac{2}{3} C_B B H_1 \sqrt{g H_1 \frac{2}{3}} \quad \dots(3)$$

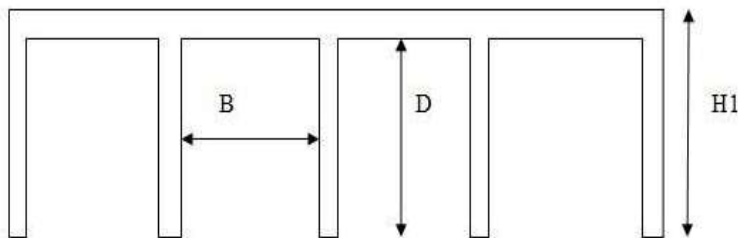


Fig. 10: Culvert's elements.

Table 3: Increment and reduction pattern of annual rainfall.

Period	R _i	R _m	R _i -R _m	% Change
1980-1990	112	111.5	0.5	0.45 %
1991-2001	111	111.5	-0.5	-0.45%
2002-2012	112	111.5	0.5	0.45%

Table 4: Data of statistics for discharge in the study area.

Month	Mean	Runs test
January	244.32	0.11
February	248.46	0.21
March	251.74	0.01
April	227.52	0.217
May	211.33	0.75
June	238.73	0.03
July	340.00	0.22
August	357.64	0.11
September	349.88	0.05
October	348.30	0.07
November	279.01	0.28
December	247.68	0.80

Source: (Abaje et al. 2012, Okafor & Ogbu 2018)

$$\text{For } \frac{H_1}{D} > 1.2 \quad \dots(4)$$

$$Q = C_h B D \sqrt{2g(H_1 - C_h D)} \quad \dots(5)$$

The rational formula is given by:

$$Q = \frac{CIA}{Z} \quad \dots(6)$$

Where: C is the runoff coefficient, Q is the maximum rate of runoff (m³.sec⁻¹.)

I = average rainfall intensity (mm.hr⁻¹.), A = drainage area (in ha), Z = conversion factor, 1 for English, and 360 for metric.

RESULTS AND DISCUSSION

Estimation of Peak Runoff Discharge

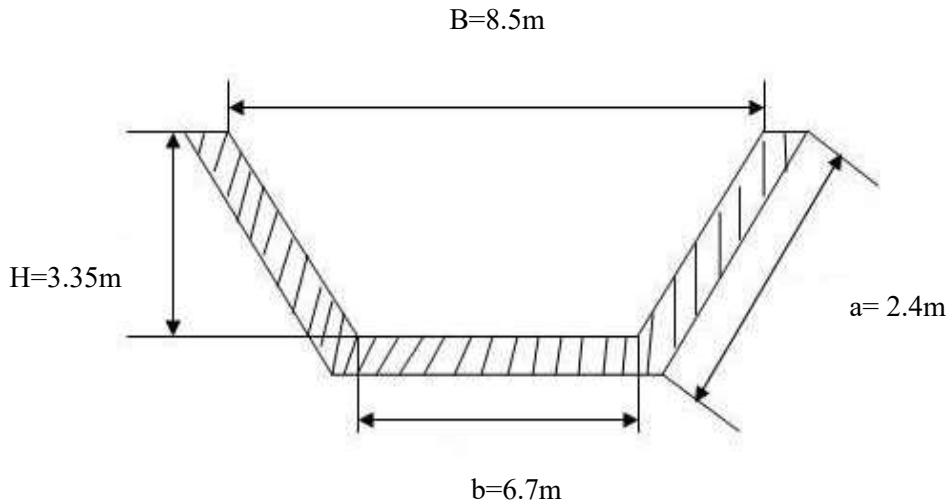


Fig. 11: Cross-section of an open channel.

The rainfall intensity has got to be calculated by using the common rainfall intensity method. The rainfall records of 1980-1990, 1991-2001 and 2002-2012 have a typical rainfall of 111.5 mm, as presented in Table 3.

However, in this research work, the predicted discharge was obtained from (Abayomi et al. 2015), as described in Table 4

The table above shows the mean average discharge determined using the rational method. It is noted that August has the highest discharge of 357.64 m³.s⁻¹, and January has the least discharge of 244.32 m³.s⁻¹. Fig. 11 presented the cross section of an open channel in the existing channel discharge capacity.

The determination of the discharge capacity of an open channel using the mining equation has taken into consideration the calculation of the following parameters:

$$\text{The area} = (8.5 + 6.7) \times \frac{3.35}{2} = 25.46 \text{ m}^2$$

$$\text{The injected parameter} = (2 \times 2.4) + 6.7 = 11.5\text{m}$$

$$\text{The hydraulic radius } R = \frac{A}{P} = \frac{25.46}{11.5} = 2.21\text{m} \dots(7)$$

$$\text{Estimated discharge } Q = AV = \frac{AR^{2/3}S^{1/2}}{n} \dots(8)$$

$$\text{The main channel slope } S = 0.032$$

Manning’s coefficient n = 0.03 because the channel is constructed in stone masonry.

Hydraulic Discharge Capacity

$$= \frac{1}{0.03} \times (25.46) \times (2.21)^{2/3} \times (0.032)^{1/2} = 258.25\text{m}^3/\text{s}$$

The hydraulic discharge capacity of the existing channel at its construction time was 258.25 m³.s⁻¹. For the open

channel, it was assumed that the channel is exposed to various use like solid waste dumped and sedimentation of considerable; it was assumed the height of the channel was reduced by 0.30. Therefore, calculating the discharge capacity of the open channel has to be considered the current situation where the channel height becomes 3.05 m.

The area after sedimentation can also be calculated as follows:

$$A = (8.5 + 6.7) \times \frac{3.08}{2} = 23.18\text{m}^2$$

$$P = (2 \times 2.4) + 6.7 = 11.5\text{m}$$

$$R = \frac{23.18}{11.5} = 2.01\text{m}$$

The discharge capacity of the channel has been again calculated by using the formula (Liu et al.);

$$Q = A \times V = \frac{1}{n} \times A \times R^{2/3} \times S^{1/2} \dots(9)$$

Hydraulic Discharge Capacity

$$= \frac{1}{0.03} \times (23.18) \times (2.01)^{2/3} \times (0.032)^{1/2} = 220.65\text{m}^3/\text{s}$$

The hydraulic discharge capacity of the existing open channel during heavy rain with high sedimentation is 220.65m³/s.

Design of the New Channel

The maximum predicted discharge is 357.64 m³.s⁻¹. Use n=1.5

$$\text{Chezy constant } c = 65, \quad Q = 357.64 \text{ m}^3.\text{s}^{-1}$$

$$\text{Hydraulic radius } R = \frac{y}{2}$$

$$\text{Area of flow, } A = \frac{Q}{V} = \frac{357.64}{23.18} = 15.43\text{m}^2$$

$$\text{Wetted parameter } p = b + 2y\sqrt{n^2 + 1} \quad (4.14)$$

$$R = \frac{A}{P} = \frac{15.43}{b+2y\sqrt{n^2+1}} = \frac{y}{2}$$

$$\text{i.e. } R = \frac{y}{2}$$

$$46.36 = y[b + 2y\sqrt{1.5^2 + 1}] = y(b+3.6)$$

$$46.36=by+3.6$$

$$A= (b + ny) y$$

$$S= (b+1.5y) y$$

$$by = 1.543 - 1.5y^2$$

$$y = \left(\frac{15.43}{2.1}\right)^{1/2} = 2.712\text{m}$$

By Substituting the value of (y = 2.712m) in the equation, we get

$$46.36 = b \times 2.712 + 3.6 \times (2.712)^2$$

$$46.36 = 2.712b + 26.478$$

$$\text{Bottom width, } b = \frac{46.36-26.478}{2.712} = 7.33\text{m}$$

$$\text{Top width, } V = C\sqrt{RS}$$

$$23.18 = \sqrt{\frac{y}{2}} S = 0.60 = 65 \sqrt{\frac{2.712}{2}} \times S = 75.69\sqrt{S}$$

$$S = \left(\frac{0.6}{75.69}\right)^2 = 6.284 \times 10^{-5}$$

$$B = b + 2ny$$

$$B = 7.33 + 2 + 1.5 \times 2.712 = 13.39 \text{ m}$$

The channel is assumed to be exposed to different use like solid waste, sedimentation, and dumps of considerable quantities. Thus it was assumed that the height of the channel was reduced by 0.30m

$$\text{i.e. } Q = AV = \frac{AR^{2/3}S^{1/2}}{n}$$

$$h = 3 - 0.3 = 2.7\text{m, } B = 13.4\text{m, } b = 7.33\text{m}$$

$$\text{The area} = (13.4 + 7.33) \times \frac{2.7}{2} = 27.98 \text{ m}^2$$

$$\text{The wetted parameter} = (2 \times 2.4) + 7.33 = 12.13\text{m}$$

$$\text{The hydraulic radius } R = \frac{A}{P} = \frac{27.98}{12.13} = 2.31\text{m}$$

$$\text{Estimated discharge } Q = AV = \frac{AR^{2/3}S^{1/2}}{n}$$

$$\text{The main channel slope } S = 0.032$$

$$Q = \frac{1}{0.03} \times (27.98) \times (2.31)^{2/3} \times (0.032)^{1/2} = 291.54\text{m}^3/\text{s}$$

The hydraulic discharge capacity of the channel after it was reduced by 0.30 due to the exposure to different use like solid waste, sedimentation, and dumps of considerable quantities $291.54 \text{ m}^3.\text{s}^{-1}$.

Existing Culvert Discharge Capacity

Fig. 12 presented the cross-section of the culvert. The discharge capacity of this ditch has been calculated by also considering its shape, parameters, and relation $\frac{H_1}{D}$.

$$\text{Dimensions: } B=7.2\text{m, } D=3.2 \text{ m, } H_1 = 4\text{m}$$

$$\frac{H_1}{D} = \frac{4}{3.2} = 1.25\text{m} > 1.2$$

$$Q = C_h BD \sqrt{2g(H_1 - C_h D)}$$

Where:

With: $C_h=0.6$ for square inlets

$$g = 9.81 \text{ m.s}^{-2}$$

Where: D = The inside Height (in m), B = The inside width (in m)

H_1 = The upstream energy Level, relative to the invert level (m)

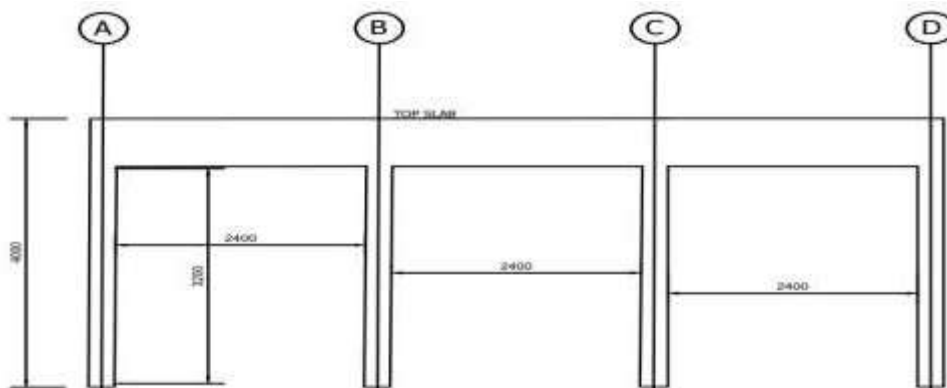


Fig. 12: Cross section of culvert.

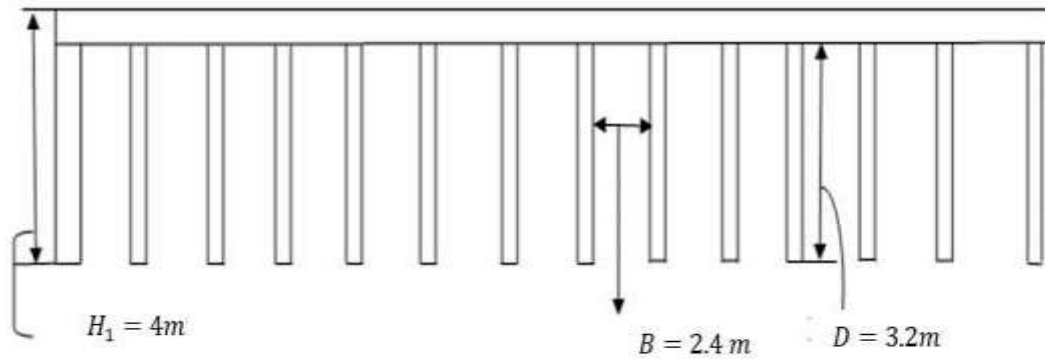


Fig. 13: Designed culverts under the bridge on the Kaduna.

$$Q = 0.6 \times 7.2 \times 3.2 \sqrt{2 \times 9.81 \times (4 - 0.6 \times 3.2)}$$

$$= 88.13 \text{m}^3/\text{s}.$$

The reduction of its discharge capacity.

$$Q = 0.6 \times 7.2 \times 3.2 \sqrt{2 \times 9.81 \times (3.7 - 0.6 \times 3.2)}$$

$$= 81.69 \text{m}^3/\text{s}$$

Dimension: D = 3.2m, and H₁ = 4m.

$$\frac{H_1}{D} = \frac{4}{3.2} = 1.25\text{m}$$

Since $\frac{H_1}{D} > 1.25\text{m}$ then, the following equation has been used

$$C_h B D \sqrt{2g(H_1 - C_h D)}$$

$$C_h = 0.6 \qquad g = 9.81 \text{m/s}^2$$

$$357.64 = 0.6 \times B \times 3.2 \sqrt{2 \times 9.81 \times (4 - 0.6 \times 1.92 \times 3.2)}$$

$$= 12.26B$$

$$B = \frac{357.64}{12.26} = 29.17\text{m}$$

Thus, this culvert’s design has been considered for the widening of the existing culvert. The widening had taken reference on the existing opening, which has a 2.4 m width; hence, for an opening of 2.4 widths:

$$b = \frac{29.17}{2.4} = 12.15 \text{ openings} \cong 13 \text{ openings}$$

$$b = 13 \text{ openings.}$$

In conclusion, the culvert under the bridge has to be with 13 openings with the inside width (D = 3.2) and the upstream energy level relative to the inlet level (H₁ = 4m) for each. Fig. 13 presented the designed culverts under the bridge on the Kaduna.

Levees, floodgates, floodwalls, and evacuation routes are all examples of flood mitigation techniques. Installation of rock beams, rock rip-raps, and sandbags, preserving normal slopes with vegetation or applying soil and cement on steeper slopes, and building or enlargement of drainage systems are also some of the common flood control strategies. Pollution may be abated by adhering to rules created to safeguard the environment. Practices like material substitution, switching to less dangerous materials, process modification, and modifying the production process to increase efficiency can all help to reduce pollution.

CONCLUSIONS

Pollution of the environment can be traced to flooding, climate change, blocking of drainages by illegal solid waste disposal, and lack of enforcement of flood management techniques. There is a great need for optimal evaluation and modification of the current drainage network of the state. It has been discovered that the Kaduna River is a tributary river of the River Niger that flows for 550 km through Nigeria. Data on daily rainfall were collected. Satellite-based remote technology is an effective tool for analyzing drainage networks, studying surface morphological features, and their correlation with groundwater management prospects at the basin level. The peak runoff discharge was 357.64 m³.s⁻¹. The hydraulic discharge capacity of the existing open channel was 258.25 m³.s⁻¹, where the channel had a section of top width (B) = 8.5 m, bottom width(b) = 6.7 m, and height(H) = 3.35 m which would be less when the hydraulic discharge capacity rises to 357.64 m³.s⁻¹ in August from the result obtained. Therefore, a new open channel was designed with a dimension of top width(B) = 13.39 m, bottom width(b) = 7.33 m, and height(H) = 3m. Adequate water resource planning and management will greatly benefit from addressing flood issues in the study area. The existing culverts have a dimension of B (width of culvert) = 7.2 m, D

(height of culvert) = 3.2 m, the width of culvert = 2.4m, and H1 (height of culvert to top slab) = 4.2m, which was estimated to carry $88.3 \text{ m}^3 \cdot \text{s}^{-1}$ of hydraulic discharge. Still, with the flooding of the study area, the dimension of the trench had to be increased to B (length of culvert) = 29.17m, D (height of culvert) = 3.2 m, the width of culvert = 2.4 m, and H1 (height of culvert to top slab) = 4 m. It was also noted that solid waste in the hydraulic structures also leads to clogging, reducing the capacity to be accommodated by the hydraulic structure. This research provides information on the flood vulnerability of infrastructures and mitigation strategies that can be adopted in the study area. The construction of these hydraulic structures in strategic locations will assist in flood control and the environmental health of Kaduna Metropolis. The open-source geospatial techniques were utilized to create different thematic maps of the study area that influence land use, soil, drainage, and slope used as input for the QSWAT model. QSWAT model proves a powerful tool in simulating the hydrology at the micro watershed scale. Estimating water balance components of a micro watershed by employing an efficient, calibrated, and validated SWAT model helps to understand each water balance component. Levees, dams, seawalls, and tide gates are flood control infrastructures that can be used as physical barriers to stop flooding caused by rising or rushing water. Pumping stations and canals, among other strategies, lessen floods.

RECOMMENDATIONS

Suggested recommendations that will contribute to flooding control in Kaduna include:

- i. Adequate measures such as mitigation and adaptation programs should be put in place to arrest flooding issues
- ii. Multidisciplinary platforms for generating effective strategic policies, adequate funding, and efficient operational mechanisms for flood management should be adopted.
- iii. Satellite-based remote technology should be embraced as an effective tool in analyzing drainage networks and studying surface morphological features and their correlation with groundwater management prospects at the basin level.
- iv. Routine maintenance should be carried out to determine the condition of the hydraulic structures.
- v. Multidisciplinary research on flood control should be adequately funded by appropriate authorities and policy makers. The outcome of such research should be implemented by engineers and other allied professionals.

- vi. Larger main drainage channels should be constructed to transport a large volume of water. Regular hydraulic structure cleaning should be done to remove all forms of silt and solid waste that would hinder water transportation to a safe location.
- vii. Regulating bodies should discourage building on the floodplain and control the release of potential solid waste into the drainages.
- viii. River re-channelization, raising home foundations, land use planning and management, and public education are among recommended flood remedial and management measures to stop activities that contribute to flooding in Kaduna's capital city.

REFERENCES

- Abaje, I.B., Ishaya, S. and Usman, S.U. 2010. An analysis of rainfall trends in Kafanchan, Kaduna State, Nigeria. *Research Journal of Environmental and Earth Sciences*, 2(2): 89-96.
- Adelekan, I.O. And Asiyambi, A.P. 2016. Flood risk perception in flood-affected communities in Lagos, Nigeria. *Natural Hazards*, 80: 445-469.
- Adjei-Darko, P. 2017. Remote Sensing and Geographic Information Systems for Flood Risk Mapping and Near Real-time Flooding Extent Assessment in the Greater Accra Metropolitan Area. Master's Thesis, KTH, Stockholm, Sweden, pp. 1-74.
- Bahar, A.M.A., Muhammad, M., Ali Khan, M.M. and Anees, M.T. 2022. Development of flood vulnerability and risk indices for Kelantan District, Peninsular Malaysia. *Nature Environ. Pollut. Technol.*, 61: 1158.
- Butu, A.W., Emeribe, C.N., Columbus, D., Leke, M.S.J. and Ananya, B.J. 2020. Effect of urbanization on channel platforms of River Kaduna from 1962-2017, Kaduna State, Nigeria. *J. Geogr. Trop. Environ.*, 4: 2.
- Chan, N.W. 2015. Impacts of Disasters and Disaster Risk Management in Malaysia: The Case of Floods. In Aldrige, D.P., Oum, S. and Sawada, Y. (eds), *Resilience and Recovery in Asian Disasters, Risks, Governance, and Society*. Springer, Cham, pp. 239-265.
- Felisa, G., Panini, G., Pedrazzoli, P. and Di Federico, V. 2022. Combined management of groundwater resources and water supply systems at basin scale under climate change. *Water Resour. Manag.*, 5: 1-16.
- Ferguson, R., Sharma, B., Hardy, R., Hodge, R. and Warburton, J. 2017. Flow resistance and hydraulic geometry in contrasting reaches of a bedrock channel. *Water Resour. Res.*, 53: 2278-2293.
- George, U. and Abdulkadir, A. 2019. An investigation of the 2017 flooding event in Nasarawa Hayi in Niger State, Nigeria. *Af. Sch. J. Environ. Design Constr. Manag.*, 15(4): 131-145.
- Hashim, N.A.E.K. 2018. Evaluation of the Impact of Rains and Floods on the Drainage System of Asphalt Pavement of Roads Case Study of Upper Atbara and Setit Dam Complex Project. Sudan University of Science and Technology, Sudan.
- Ibrahim, A.H. and Abdullahi, S.Z. 2016. Flood menace in Kaduna Metropolis: Impacts, remedial and management strategies. *Sci. World J.*, 11: 16-22.
- Johnson, F., White, C.J., Van Dijk, A., Ekstrom, M., Evans, J.P., Jakob, D., Kiem, A.S., Leonard, M., Rouillard, A. and Westra, S. 2016. Natural hazards in Australia: Floods. *Clim. Change*, 139: 21-35.
- Kang, M.S., Koo, J.H., Chun, J.A., Her, Y.G., Park, S.W. and Yoo, K. 2009. Design of drainage culverts considering critical storm duration. *biosystems engineering*, 104(3): 425-434.
- Li, S., Jianie, Y., Ho, I.H., Ma, L., Wang, Q. and Yu, B. 2020. Experimental

- and numerical analyses for earth pressure distribution on high-filled cut-and-cover tunnels. *KSCE Journal of Civil Engineering*, 24: 1903-1913.
- Managi, S. 2006. Are there increasing returns to pollution abatement? Empirical analytics of the Environmental Kuznets Curve in pesticides. *Ecological Economics*, 58(3): 617-636.
- Neitsch, S.L., Arnold, J.G., Kiniry, J.R. and Williams, J.R. 2011. Soil and Water Assessment Tool Theoretical Documentation Version 2009. Texas Water Resources Institute, USA.
- Ogarekpe, N.M., Nnaji, C.C., Oyeboode, O.J., Ekpenyong, M.G., Ofem, O.I., Tenebe, I.T. and Asitok, A.D. 2023. Groundwater quality index and potential human health risk assessment of heavy metals in water: A case study of Calabar metropolis, Nigeria. *Environ. Nanotechnol. Monit. Manag.*, 75: 100780.
- Okafor, G.C. and Ogbu, K.N. 2018. Assessment of the impact of climate change on the freshwater availability of Kaduna River basin, Nigeria. *Journal of Water and Land Development*.
- Oyeboode, O.J. 2018. Strategy for tackling flood and water scarcity for adequate water supply and public health in Nigeria. *Europ. J. Adv. Eng. Technol.*, 5(8): 656-664.
- Oyeboode, O.J. 2021. Hazard assessment and implementation strategies for mitigating flood and erosion in Nigeria. *IOP Conf. Ser. Mater. Sci. Eng.*, 1036: 012066.
- Oyeboode, O.J. 2022a. Sustainable waste management towards circular economy in Nigerian context: challenges, prospects, and way forward. In: Ayeni, O., Oladokun, O. and Orodu, O.D. (eds), *Advanced Manufacturing in Biological, Petroleum, and Nanotechnology Processing*. Springer International Publishing, Cham, pp. 237-248.
- Oyeboode, O.J. 2022b. Design of water retaining structures and application of environmental engineering for sustainable environment. In: Ayeni, O., Oladokun, O. and Orodu, O.D. (eds), *Advanced Manufacturing in Biological, Petroleum, and Nanotechnology Processing*. Springer, Cham, pp. 287-299.
- Oyeboode, O.J., and Otoko, J.A. 2022. Medical waste management and design of a low-cost incinerator for reduction of environmental pollution in a multi-system hospital. *Nature Environ. Pollut. Technol.*, 21(4): 1933-1942
- Parsian, S., Amani, M., Moghimi, A., Ghorbanian, A. and Mahdavi, S. 2021. Flood hazard mapping using fuzzy logic, analytical hierarchy process, and multi-source geospatial datasets. *Remote Sens.*, 13(23): 4761.
- Pissarra, T.C.T., Fernandes, L.F.F. and Pacheco, F.A.L. 2001. Production of clean water in agriculture headwater catchments: A model based on the payment for environmental services. *Sci. Total Environ.*, 785: 147331.
- Proverbs, D. and Lamond, J. 2017. Flood resilient construction and adaptation of buildings. In Cutter, S. (ed.), *Oxford Research Encyclopedia of Natural Hazard Science*, Oxford University Press, Oxford, pp. 64-96.
- Redondo-Brenes, A. and Welsh, K. 2006. Payment for hydrological, environmental services in Costa Rica: The provencal case study. *Trop. Resour. Bull.*, 25: 1925.
- Rezaei, F., and Safavi, H.R. 2022. Sustainable conjunctive water use modelling using dual fitness particle swarm optimization algorithm. *Water Resour. Manag.*, 15: 1-18.
- Sage, J., Berthier, E. and Gromaire, M.C. 2015. Stormwater management criteria for on-site pollution control: A comparative assessment of international practices. *Environmental management*, 56, pp.66-80.
- Sunaedi, N., Hadi, S.P. and Bambang, A.N. 2022. Payment for environmental services in Indonesia: Mutually beneficial watershed environmental management model. *Nature Environ. Pollut. Technol.*, 21(4): 615.
- Wahab, B. and Falola, O. 2018. Vulnerable households and communities' responses to flooding disasters in the Ibadan Metropolis, Nigeria. *Ibadan J. Sociol.*, 7: 46-75.
- Wamugi, S.M.A. 2016. Effects of climate change and adaptation strategies of smallholder farmers in Kilifi, Embu, and Budalangi. *Pwani University. J. Environ. Earth Sci.*, 8(7): 40-70.



Comparative Advanced Oxidation Decolorization of the Triphenylmethane Dye with Dimethyl Dioxirane and Hydrogen Peroxide

S. Vinotha*† and A. Leema Rose*

*PG and Research Department of Chemistry, Holy Cross College (Autonomous), Affiliated to Bharathidasan University, Trichy-620002, Tamilnadu, India

†Corresponding author: S. Vinotha; vinoyoga61805@gmail.com

Nat. Env. & Poll. Tech.
Website: www.neptjournal.com

Received: 22-09-2022

Revised: 06-12-2022

Accepted: 20-12-2022

Key Words:

Methyl violet
Dimethyl dioxirane
Hydrogen peroxide
Pseudo-first-order
Oxidant dosage

ABSTRACT

Methyl Violet (MV), a triphenylmethane dye, has been subjected to comparative studies with hydrogen peroxide and dimethyl dioxirane under optimum situations. When employing hydrogen peroxide, the photolysis process becomes slower, but the dye solutions are entirely decolorized and mineralized. The decolorization rate exhibits pseudo-first-order kinetics. The effect of pH, oxidant dosage, and methyl violet concentration on the degradation is also examined. Generated *o*-leucoaniline, 1,3-diphenylurea, 2-hydroxy benzoic acid, phenol, acetone, water, carbon dioxide, and carbon monoxide are identified and measured by GC-MS analysis. These substances remain in the dye solution along with dimethyl dioxirane, which is released faster during the last stages of degradation. The degradation rates of methyl violet reached 97.9% and 65.8% within 30 mins and 180 min of reaction time using dimethyl dioxirane and hydrogen peroxide.

INTRODUCTION

The textile sector uses many chemical dyes, and the effluents produced by these industries contain a significant portion of the dye that is not used, raising concerns about environmental health. Commercial dyestuffs are sometimes difficult for wastewater treatment facilities to remove from contaminated wastewater. Even minute concentrations of dyes have an impact on aesthetic appeal, gas solubility, and water transparency. Methyl violet, also known as crystal violet or N,N,N',N',N'',N''-hexamethyl pararosaniline, is a triphenylmethane dye that is widely used in the textile industry to dye nylon, silk, wool, and cotton as well as for biological stains and paper printing (Bumpus & Brock 1988). It is utilized as an antifungal drug for dermatological infections in both human and veterinary medicine and in oral medications to treat pinworms and other tropical disorders (Casas et al. 2009).

Additionally, methyl violet is frequently used in microbiological labs as a bactericidal and antiallergenic agent and in the analysis of Gram's stain for the primary classification of bacteria and Flemming triple stain with iodine (Mittal et al. 2008). According to toxicology data, methyl violet may cause skin and eye damage, irritation, and redness with pain or swelling, whereas it may be dangerous if inhaled, eaten, or absorbed via the skin (Mittal et al. 2008, Hameed 2008). So, while methyl violet can impact

the gastrointestinal tract when consumed, it can irritate the respiratory tract when inhaled (Mittal et al. 2008).

Methyl violet exhibits poor biodegradation and is labeled as a hazardous recalcitrant. The ineffective removal of methyl violet from wastewater by conventional effluent treatment systems causes it to disperse into the environment (Nelson & Hites 1980). Methyl violet and several triphenyl methane dyes are reportedly strong carcinogens, another delicate issue (Diachenko 1979). Many methods have been researched to remove methyl violet from wastewater, including chemical oxidation and reduction, physical precipitation and flocculation, photolysis, adsorption, electrochemical treatment, and reverse osmosis (Azmi et al. 1998). However, these methods are expensive, very loosely applicable to various dye wastewater, and only partially effective in removing the dye, which causes waterways (Fu & Viraraghavan 2001, Selvam et al. 2003). Compared to physical and biological treatment procedures, chemical processes are less costly and environmentally friendly, produce less sludge, and are therefore seen as promising and receiving more attention.

This paper highlights research on the decolorization of Methyl violet (Fig. 1) solutions by an advanced oxidation process. The efficiency of this AOP was evaluated by using dimethyl dioxirane and hydrogen peroxide as oxidants under

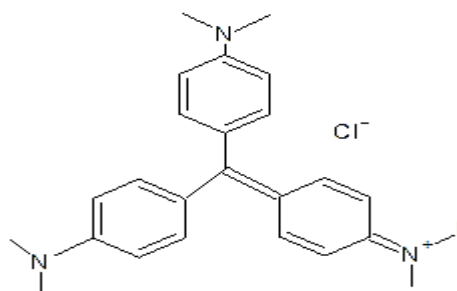


Fig. 1: Chemical structure of methyl violet.

similar situations. The effect of pH, dye concentration on the decolorization, rate of decolorization, and oxidants dosage were observed.

MATERIALS AND METHODS

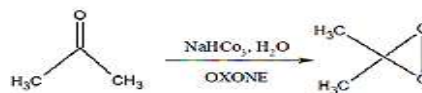
The potassium peroxy monosulfate was made available by TCI Chemicals (purity 99%). Acetone and sodium bicarbonate were supplied by Pure Chems and Merck, respectively. Hydrogen peroxide was purchased from ISOICHEM with 99% purity. Only analytical-grade substances were used for this experiment. None of the chemicals are further purified. Using an Elico Digital pH meter, the pH of the solution was determined. Because it is easily soluble in water, methyl violet dye (molecular formula $C_{24}H_{28}N_3Cl$, MW 393.95, $\lambda=561$ nm) is the dye used to symbolize organic dye. Therefore, this is made with distilled water and utilized in all studies. Due to its high water solubility, this dye is bought from S.D. fine chemicals. The decolorization of methyl violet was observed for all the optimized parameters using the instrument UV-Visible spectrophotometer (Hitachi U2910).

Preparation of an Oxidizing Agent

The solid potassium mono peroxy sulfate was added in one portion while stirring vigorously at room temperature to a 250 mL round-bottomed flask that was already filled with a mixture of water, acetone, sodium bicarbonate, and a magnetic stirring bar. This flask was also fitted with an additional funnel for solids containing this substance and was cooled using dry ice-acetone. The yellow dioxirane-acetone solution was made and deposited in the receiving flask.

Degradation Experiments

50 mL of methyl violet standard solutions (10 mg to 100 mg.L⁻¹) were prepared and used for each analysis. Every investigation was conducted at room temperature in a dark atmosphere. The dye solution's initial absorption peak was noted before the experiment began. Later the experiment was running for 30 min, 1 mL of the dye solution was taken



Equation.1. Preparation of dimethyl dioxirane.

out of the reaction mixture and diluted, and the amount of dye penetration was determined. The effects of pH were investigated by adjusting the pH of the solution with 0.1 N NaOH and 0.1 N HCl. As noted, the blank trials were carried out at room temperature and in the dark. The formula $(C_0 - C)/C_0 \times 100$ was used for the percentage decolorization. C_0 denotes the dye solution's starting concentration, and C represents the dye solution's concentration at time t . The same was repeated as mentioned above by using hydrogen peroxide as an oxidant under sunlight.

RESULTS AND DISCUSSION

Visual Observation of the Formation of an Oxidizing Agent

Dimethyl dioxirane was initially identified through visual examination. The reaction mixture's color change indicates the formation of dimethyl dioxirane. The aqueous solution of acetone and water first turn colorless, but when sodium



2(a)



2(b)

Fig. 2: (a) Sodium bicarbonate and acetone are combined in this solution. (b) The addition of potassium peroxy monosulfate forms dimethyl dioxirane.

bicarbonate and potassium peroxydisulfate are added, the color changes to pale yellow (Robert et al. 1985, Adam et al. 1987). Fig. 2a and 2b show the formation of dimethyl dioxirane.

Uv-Visible Spectroscopy

UV-visible (200-800 nm) examination of methyl violet dye supernatants at various period intervals revealed decolorization and a reduction in MV dye concentration. MV has a significant absorption peak at 561 nm in the UV-visible spectrum. The intensity of the primary peak dropped dramatically after oxidant treatment due to decolorization. After 30 min, the MV peak recorded at max 561 nm reduced without any change in the maximum until the full decolorization of the treated Methyl violet dye (Fig. 4). It has been reported that dye decolorization by dimethyl dioxirane may result from dye adsorption by the oxidant or chemical degradation. For example, in chemical degradation, the primary visible light absorption peak completely disappears, as seen in our investigation and illustrated in Fig. 3a.

Similarly, no reaction occurs while using hydrogen peroxide as an oxidizing agent at room temperature. The decolorization occurs in sunlight with hydrogen peroxide

as an oxidant under optimal conditions. The degradation process was monitored using UV-Visible spectroscopy at regular intervals of time. The characteristic peak slightly decreases after the completion of 3 h, which indicates that only 50% of degradation takes place at 3 h. Fig. 3b includes UV-Visible depictions of the degradation process.

A comparison of both oxidants revealed that the dimethyl dioxirane decolorized the dye solution within 30 mins. But hydrogen peroxide was not able to decolorize the dye solution completely. Only partial decolorization occurred at 3 h, which showed that dimethyl dioxirane was more powerful than hydrogen peroxide.

Fourier Transform Infrared Analysis

The FT-IR spectra of pure methyl violet (Fig. 4a) and the dye-decolorized sample (30 min) revealed a noticeable difference in the fingerprint wave number area of $1,500-500\text{ cm}^{-1}$, indicating methyl violet decolorization by dimethyl dioxirane. In the FT-IR spectrum of pure methyl violet, there are distinct peaks in the region of $1,500-500\text{ cm}^{-1}$ that correspond to the monosubstituted and para-disubstituted aromatic ring (Fig. 4a). However, the appearance of a wave number peak at 1583.29 cm^{-1} corresponds to the C=C stretching of the aromatic ring. At 1166.66 cm^{-1} , there

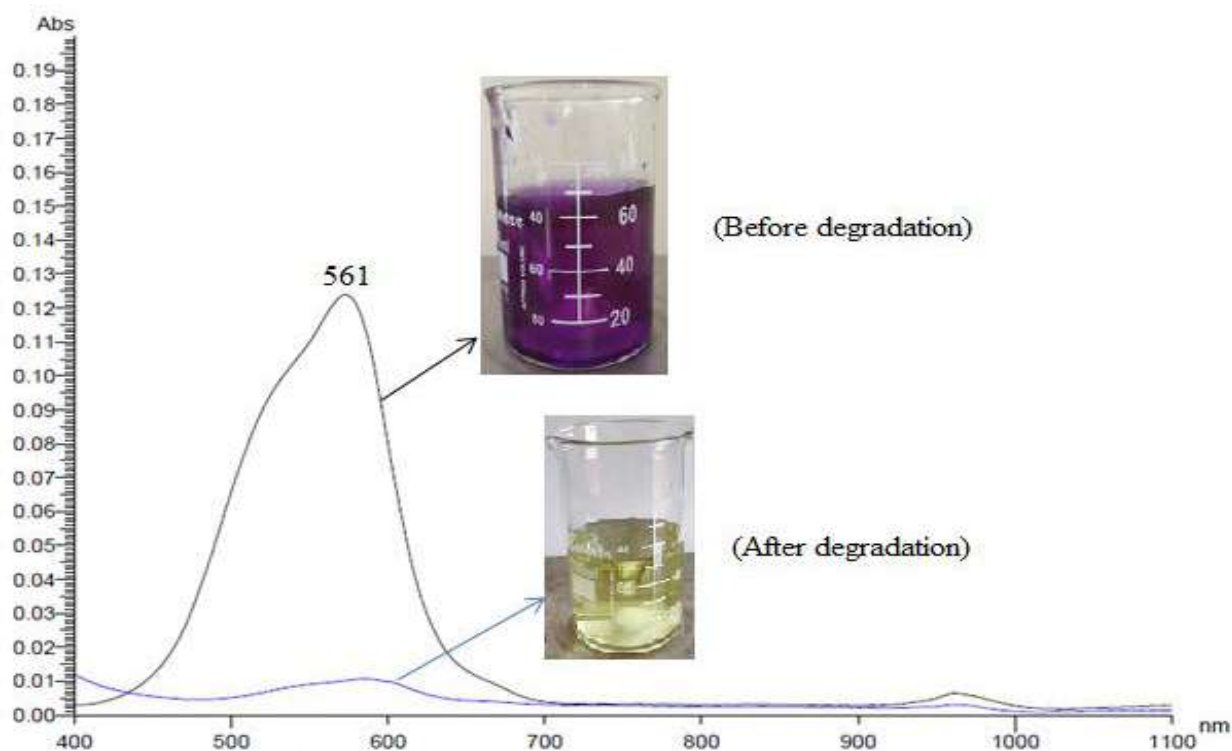


Fig. 3a: Depicts the methyl violet UV-visible spectrum under ideal conditions before and after degradation.

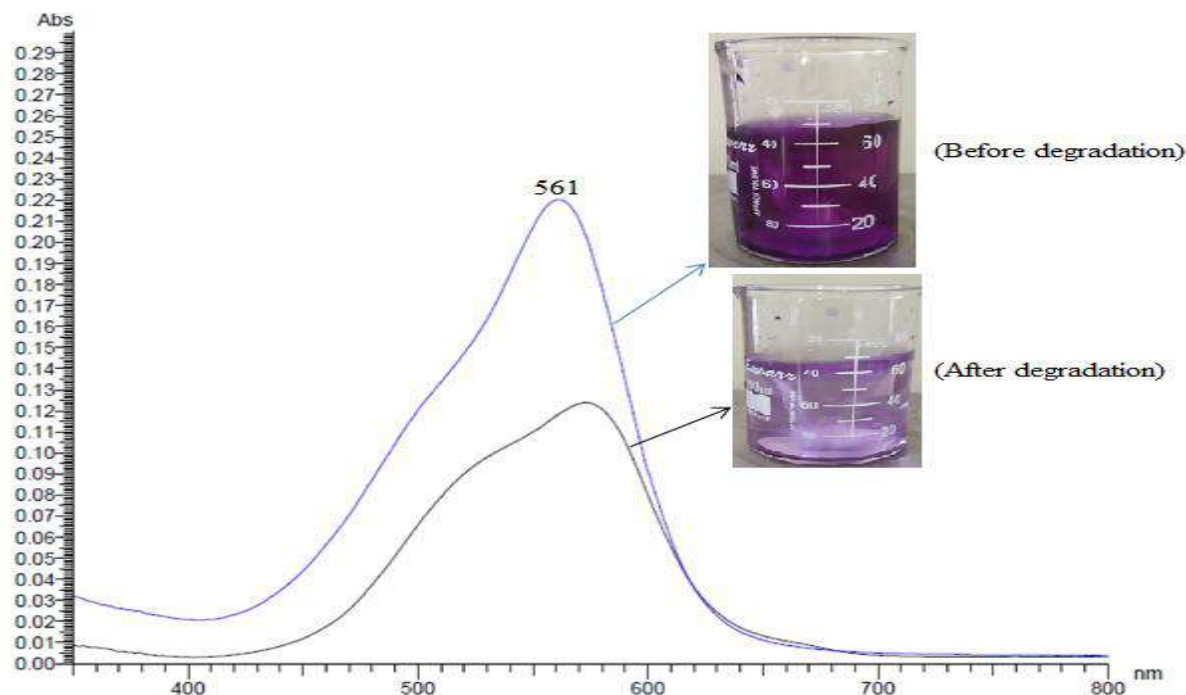


Fig. 3b: Demonstrates the UV-Visible spectra of methyl violet before and after their degradation in the presence of sunlight.

is also a peak for aromatic C-N stretching vibrations. At 2924.95 cm^{-1} , the C-H asymmetric stretching vibration was seen, while at 3160.93 cm^{-1} , the free -NH_2 group displayed an amide antisymmetric stretching vibration. The peak indicated a C=C stretching bend at 1666.28 cm^{-1} . Peaks at 1166.66 and 1113.70 cm^{-1} relate to the C-O stretch. The benzene ring bending is correlated with the peaks at 758.62 and 725.30 cm^{-1} . After degradation, the FT-IR spectrum of the decolorized MV products (Fig. 4b) showed characteristic peaks at 3435.88 cm^{-1} for hydrogen bonding, $2,074.66\text{ cm}^{-1}$, $1,633.49\text{ cm}^{-1}$ for -C-C- stretching, $1,116.65\text{ cm}^{-1}$ for -C-O- stretching. After decolorization, the IR spectra of methyl violet show various suppressed peaks.

Furthermore, the disappearance of many peaks at 758 , 725 , and 991 cm^{-1} shows that the ring has been lost. FT-IR spectrum analysis reveals different absorption bands for methyl violet dye before and after the advanced oxidation process. The findings demonstrated a considerable structural shift, which can be validated by comparing before and after degradation spectral images.

Similarly, The FT-IR spectra of pure methyl violet (Fig. 5a) and the dye-decolorized sample (3 h) revealed a noticeable difference in the fingerprint wave number of $1,500\text{-}500\text{ cm}^{-1}$, indicating methyl violet decolorization by hydrogen peroxide. The presence of specific peaks to the

fingerprint wave number region of $1,500\text{-}500\text{ cm}^{-1}$ represents the monosubstituted and para-disubstituted benzene rings in the FT-IR spectrum of pure methyl violet (Fig. 4a). In contrast, the presence of a wave number peak at 1583.29 cm^{-1} represents the C=C stretching of the benzene ring. There is also a peak for aromatic C-N stretching vibrations at 1166.66 cm^{-1} . C-H asymmetric stretching vibration was observed at 2924.95 cm^{-1} , while the free -NH_2 group showed amide antisymmetric stretching vibration at 3160.93 cm^{-1} . The peak at 1666.28 cm^{-1} indicated a C=C stretching bend. Peaks corresponding to the C-O stretch are located at 1166.66 and 1113.70 cm^{-1} . The peaks at 758.62 and 725.30 cm^{-1} correlate to benzene ring bending. After degradation, the FT-IR spectrum of the decolorized MV products (Fig. 5b) showed more same characteristic peaks at 3444.60 cm^{-1} corresponding to OH stretching, 2077.48 cm^{-1} and 1632.95 cm^{-1} for aromatic C-H bending, 1423.75 cm^{-1} for OH bending, 1279.80 cm^{-1} and 1216.54 cm^{-1} correspond to C-O stretching, 703 cm^{-1} for C=C stretching.

The major bands disappeared in FTIR spectra by using dimethyl dioxirane. Complete decolorization occurs in methyl violet using dimethyl dioxirane as an oxidant. Whereas using hydrogen peroxide as an oxidant, many peaks remain the same, and no complete decolorization occurs at reaction time. The result confirmed that dimethyl dioxirane is a more powerful oxidant than hydrogen peroxide.

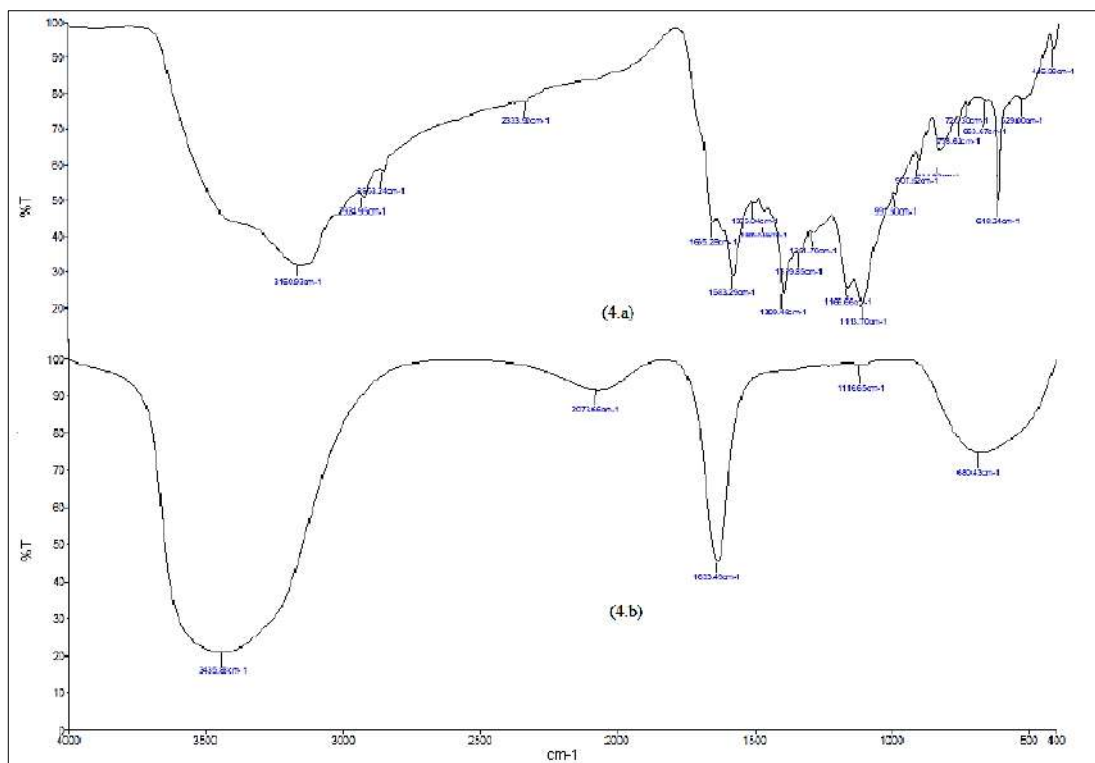


Fig. 4a: Shows the before-degradation FTIR spectra of pure methyl violet. 4b: Shows the after-degradation FTIR spectrum of methyl violet using dimethyl dioxirane.

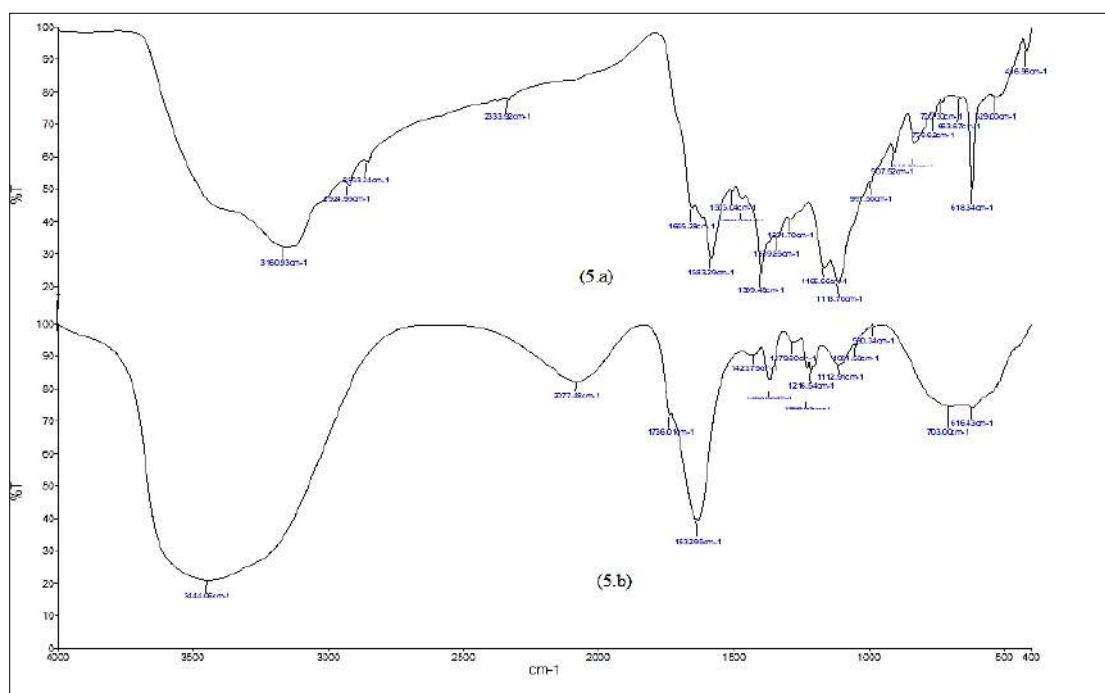
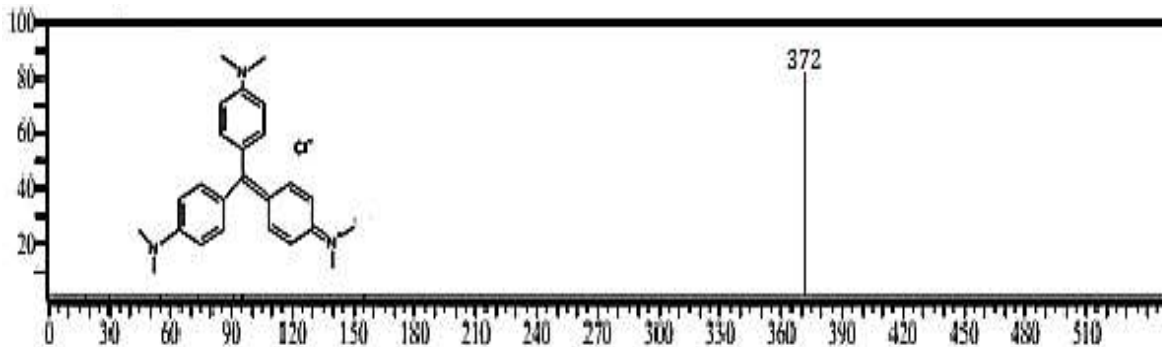
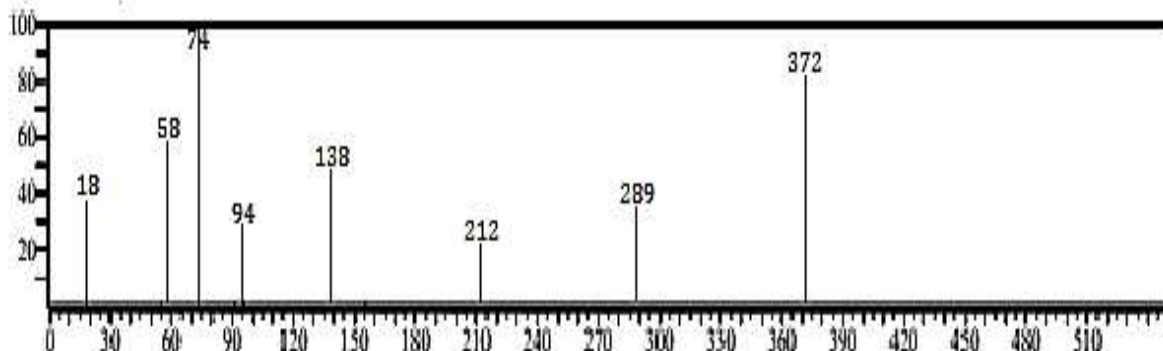


Fig. 5a: Shows the before-degradation FTIR spectra of pure methyl violet. 5b: Shows the after-degradation FTIR spectrum of methyl violet using hydrogen peroxide.



6a



6b

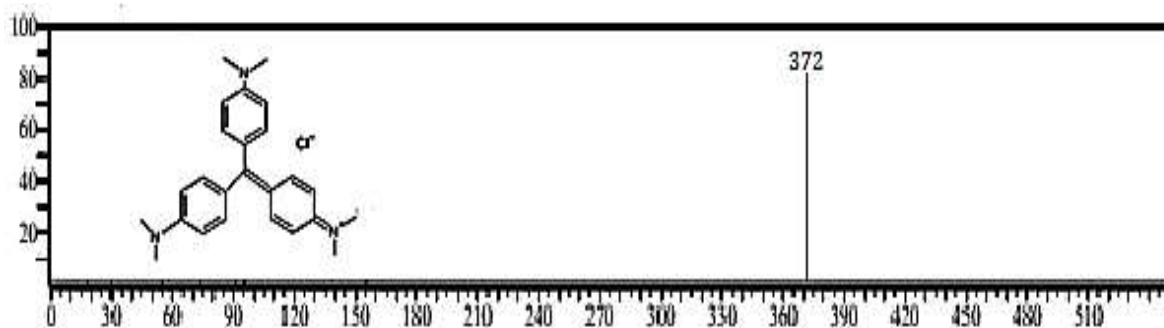
Fig. 6a & b: Shows the mass spectrum of before and after decolorization of methyl violet using dimethyl dioxirane as an oxidizing agent.

Mass Spectroscopy

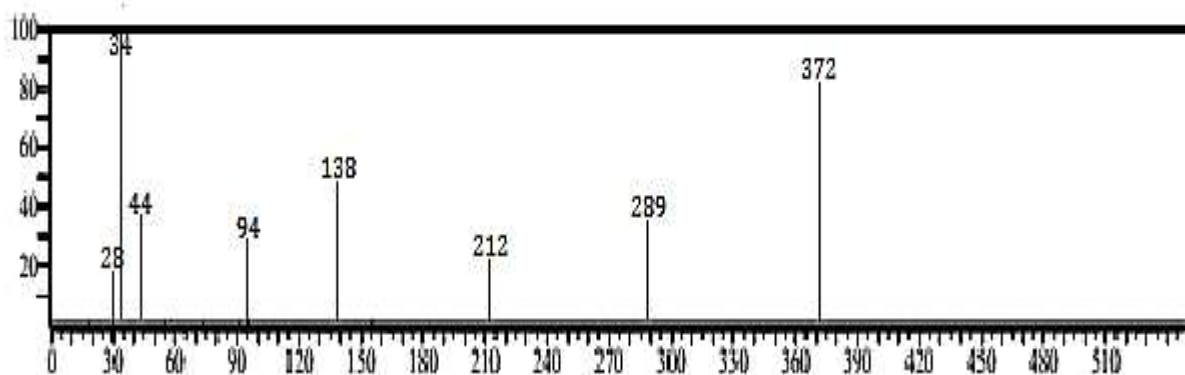
Fig. 6a depicts the mass spectra of the pure dye Methyl violet. Fig. 6e depicts the possible breakdown pathways of methyl violet dye using dimethyl dioxirane at room temperature. The MV dye's N-demethylation and the fragmentation of the chromospheric group as a result of the loss of heterocyclic conjugation and subsequent intermediate alkylation initially resulted in oxidative intermediate intermediates. In the second oxidation stage, heterocyclic species were added to the quinoid molecule, which caused the aromatic rings to open and carboxylic acids to be produced. The subsequent ring-opening processes may have produced $(\text{CH}_3)_2\text{CO}$ and H_2O as end products (Hunge et al. 2021, Ju et al. 2011). The corresponding spectra are determined by the molecular ions $M^+ = 372.2$ u. A progressive loss of C_nH_{2n} groups indicates the typical degradation of methyl violet with dimethyl dioxirane at normal temperature (Fig. 6b). MV detected seven degradation products with m/z values of 289.4 u, 212.2 u, 138.1 u, 94.1 u, 74.0 u, 58.0 u, and 18.0 u.

Fig. 6c depicts the mass spectra of the pure dye Methyl violet. Fig. 6f depicts the potential pathways for methyl violet dye degradation utilizing hydrogen peroxide in the presence of sunlight. The N-demethylation of the MV dye results in the production of oxidized intermediate products, which in turn causes the cleavage of the chromosphere structure due to the loss of aromatic conjugation and subsequent intermediate hydroxylation. The second process involved opening aromatic rings and forming carboxylic acids, while the first stage involved the degradation of hydroxylated species in producing the quinoid molecule. The ring-opening processes persisted, and CO_2 and CO may have been the final products of deterioration. The corresponding spectra are characterized by molecular ions, $M^+ = 372.2$ u. Under sunlight, the usual breakdown of methyl violet with hydrogen peroxide is characterized by a gradual loss of C_nH_{2n} groups (Fig. 6d). At $m/z = 289.4$ u, 212.2 u, 138.1 u, 94.1 u, 44.0 u, 34.0 u, and 28.0 u, MV produced seven degradation products.

The methyl violet dye reacts with dimethyl dioxirane, giving mineralization products such as acetone and water,

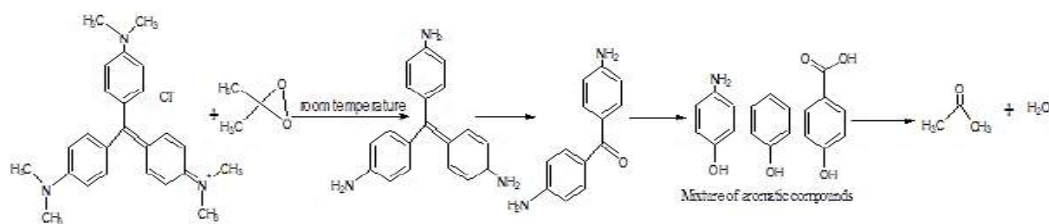


6.c

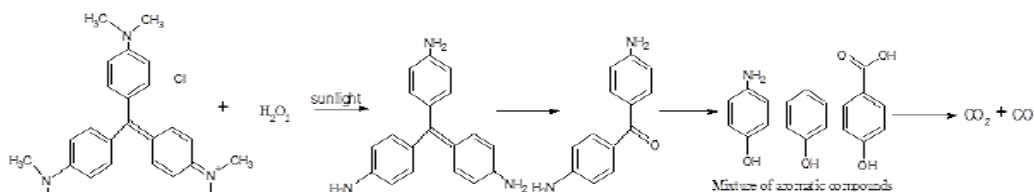


6.d

Fig. 6c & d: Shows the mass spectrum of before and after decolorization of methyl violet using hydrogen peroxide as an oxidizing agent.



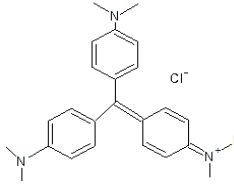
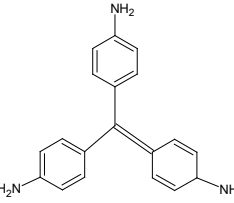
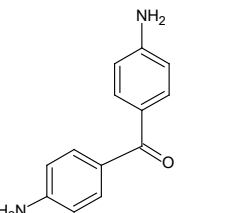
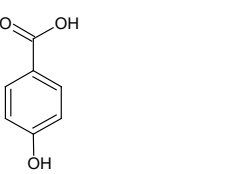
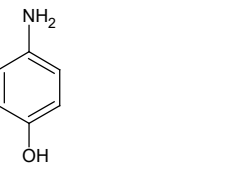
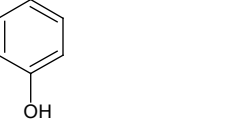
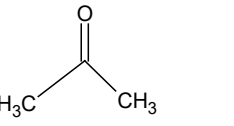
6.e



6.f

Fig. 6e & f: Possible pathways for degradation of methyl violet using dimethyl dioxirane and hydrogen peroxide as oxidizing agents.

Table 1: De-methylated intermediates of the methyl violet dye, including their chemical names, chemical structures, and m/z values.

Chemical name	Structure	m/z Value
[4-[bis[4-(dimethylamino) phenyl] methylidene]cyclohexa-2,5-dien-1-ylidene]-dimethyl azanium(Methyl violet dye)		372.52
o-Leucoaniline		289.37
1,3-Diphenylurea		212.24
2-Hydroxy benzoic acid		138.12
4-amino phenol		109.13
Phenol		94.11
Acetone		58.07
Water	H ₂ O	18.01
Carbon dioxide	CO ₂	44.00
Carbon monoxide	CO	28.01

which is harmless to humans and the environment. Similarly, methyl violet reacts with hydrogen peroxide, releasing harmful products like carbon dioxide and carbon monoxide. Compared to hydrogen peroxide, dimethyl dioxirane is more powerful and eco-friendly.

Effect of pH

Using dimethyl dioxirane, the impact of pH in the range of 3-9 is investigated for a 10 mg.L⁻¹ (50 mL) methyl violet dye solution. According to Fig. 7a, acidic pH=5 showed the highest decolorization efficacy. Good decolorization efficiency is attained at acidic and neutral pH levels because the anionic methyl violet dyes readily adsorb to the positively charged dimethyl dioxirane. Similarly, the impact of pH in the range of 3-9 is investigated using hydrogen peroxide and a 10 mg.L⁻¹ (50 mL) methyl violet dye solution. According to Fig. 7b, the acidic pH=7 environment had the highest decolorization efficacy. Hydrogen peroxide does not exhibit greater efficacy at the same pH; only a

small percentage of decolorization occurs over a period of time.

Effect of Oxidant

By varying the concentration of the oxidizing agent from 100 to 1000 μL for the 10 mg.L⁻¹ methyl violet dye solution illustrated in Fig. 8a, the appropriate amount of dimethyl dioxirane oxidant for effective methyl violet decolorization was found. Dyes continue to degrade up to a point at which the rate of decolorization starts to decline when the oxidizing agent concentration is raised to 500 μL . This is because adding 500 μL of dimethyl dioxirane to the dye solution caused the rate of decolorization to slow down, and the number of active sites needed for dye decolorization increased as the concentration of oxidizing agent increased. This is demonstrated by the fact that more active sites are needed for dye decolorization, which rises with an increase in the concentration of the oxidizing agent, and that the decolorization process gradually slows down after adding

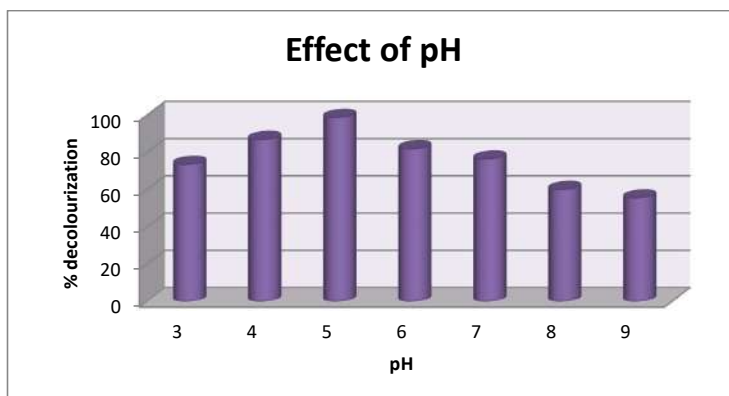


Fig. 7a: 10 mg.L⁻¹ methyl violet dye solution, 500 μL of dimethyl dioxirane, pH varied from 3 to 9, under room temperature.

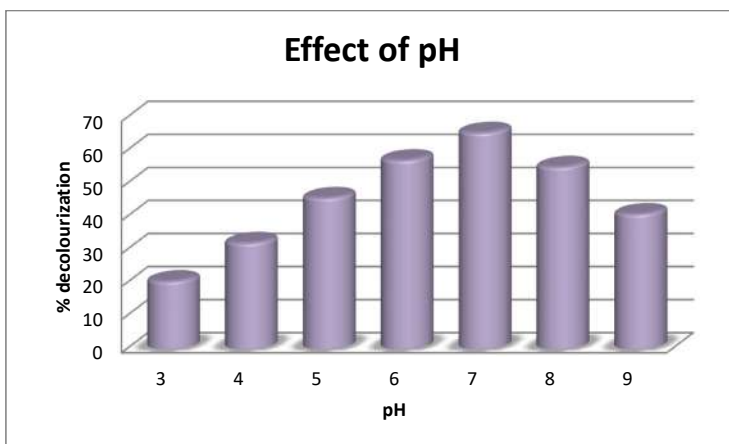


Fig. 7b: 10 mg.L⁻¹ methyl violet dye solution, 5mL of hydrogen peroxide, pH varied from 3 to 9, under sunlight.

500 μL of dimethyl dioxirane to the methyl violet dye solution. Approximately 98.42% of the dye is decolorized after 500 μL in 30 min.

Similarly, the optimum amount of hydrogen peroxide for efficient methyl violet decolorization was determined by adjusting the oxidant concentration from 1 to 10 mL for 10 mg.L^{-1} of methyl violet dye solution shown in Fig. 8b. With 5 mL of hydrogen peroxide. Methyl violet dye can be fully decolorized; beyond that, the decolorization rate starts to decline. As the oxidant concentration rises, the active sites needed for dye decolorization also increase. However, if too much oxidant has been added to the dye solution, the suspension becomes turbid, which reduces sunlight penetration. The photo decolorization process slows down due to the dye solution's decreased exposure to sunshine (Hu et al. 2003 & Soroosh et al. 2019). At the same time, just 12% of the dye was decolorized with hydrogen peroxide at

room temperature. This demonstrates that the dye is resistant to self-photolysis and that a supporting catalyst is required for effective methyl violet decolorization. With 5 mL, approximately 75.59% of the dye is decolorized in 180 min. To decolorize the dye solution in sunlight, more hydrogen peroxide is required.

Effect of Initial Dye Concentration

The maximum dye decolorization effectiveness is assessed using 500 μL of dimethyl dioxirane at an ideal pH of 5 by operating at room temperature to determine the best concentration of methyl violet dye. The dye concentration is varied between 10-100 mg.L^{-1} . Within 30 min, 10 mg.L^{-1} of the methyl violet dye had approximately 97.9% of its color removed. Without a supporting catalyst, dimethyl dioxirane can ably decolorize 10-100 mg.L^{-1} of methyl violet dye solution under room temperature. About 26.8% of 100 mg.L^{-1}

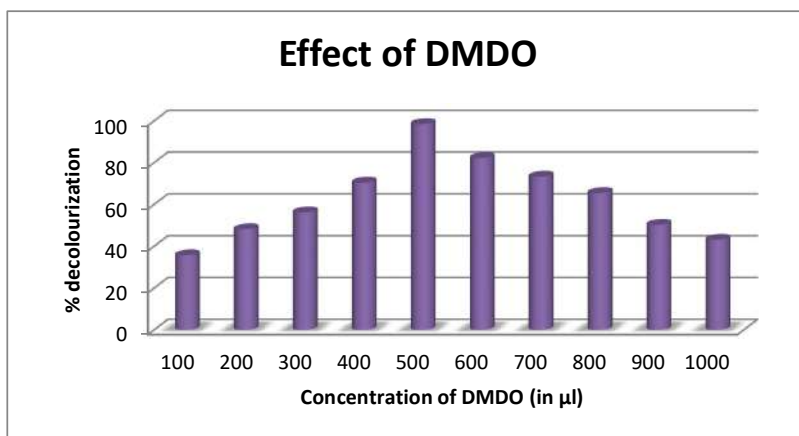


Fig. 8a: 10 mg.L^{-1} methyl violet dye solution, dimethyl dioxirane dosage varied from 500 μL to 1000 μL , pH = 5, under room temperature.

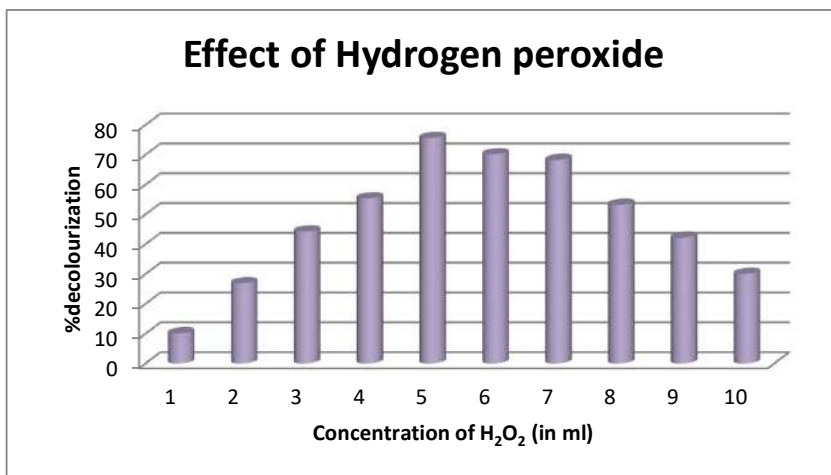


Fig. 8b: 10 mg.L^{-1} methyl violet dye solution, hydrogen peroxide dosage varied from 1mL to 10 mL, pH = 5, under sunlight temperature.

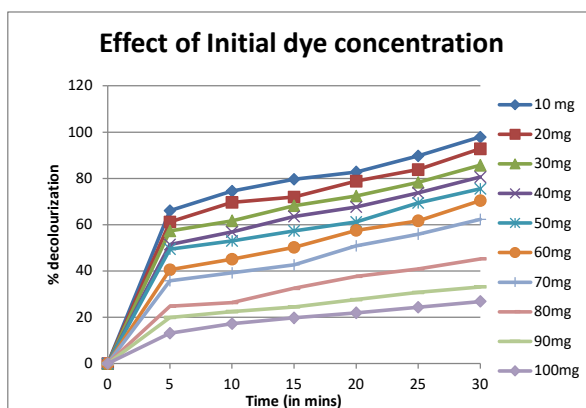


Fig. 9a: 500 µL of dimethyl dioxirane, pH=5, initial methyl violet dye concentration varied from 10 mg.L⁻¹ to 1000 mg.L⁻¹, under room temperature.

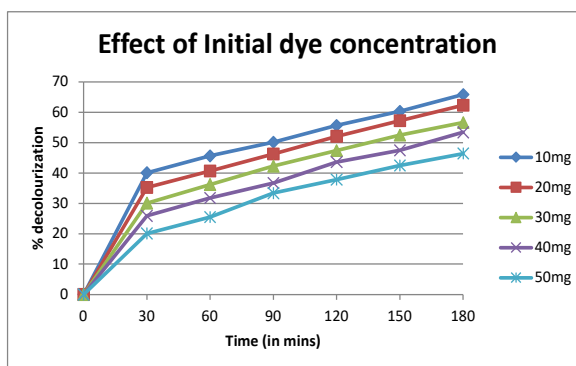


Fig. 9b: 5 mL of hydrogen peroxide, pH=7, initial methyl violet dye concentration varied from 10 mg.L⁻¹ to 50 mg.L⁻¹ under sunlight.

of methyl violet dye can be decolorized within 30mins as shown in Fig. 9a.

Similarly, only 65.8% of dye decolorization took place within 180 min using hydrogen peroxide under sunlight at pH 7, as shown in Fig. 9b. Whereas, under room temperature, only 12% of the dye decolorization took place with hydrogen peroxide. This demonstrates strongly that the dye is resistant to self-photolysis and needs a supporting catalyst for efficient decolorization of methyl violet. Hydrogen peroxide can be able to decolorize only 50 mg.L⁻¹ of dye solution within 180 min. It takes more time to decolorize the dye solution compare to dimethyl dioxirane.

Kinetic Studies

The graph of ln(C/C₀) vs. reaction time was plotted using the extinction plot. Fig. 10a and 10b show a 10 mg.L⁻¹ methyl violet dye solution with 500 µL of dimethyl dioxirane and 5 mL of hydrogen peroxide. The slope is employed to determine the reaction rate constant of the plot. The reaction's rate constant was determined using equation (2) (Yadav et al. 2019).

$$\ln \frac{C_0}{C} = k.t \quad (2)$$

C₀ denotes the initial dye concentration, C_t is the dye concentration at time t, and k denotes the constant reaction rate.

Studies from earlier work demonstrate that concerning pollutant concentration, most oxidation processes follow pseudo-first-order kinetics (Bhargav et al. 2007, Eftaxias et al. 2001, Garg et al. 2010, Santos et al. 2004). The dimethyl dioxirane and hydrogen peroxide rate constant are 0.0144, 0.003, and the R² value is 0.9896, 0.9733. All the data points arranged along a straight line confirmed the result.

CONCLUSION

In conclusion, we have presented the comparison study results between hydrogen peroxide and dimethyl dioxirane. Dimethyl dioxirane is produced via a standard chemical process. The removal percentage was the preferred outcome. This study optimized the decolorization of methyl violet

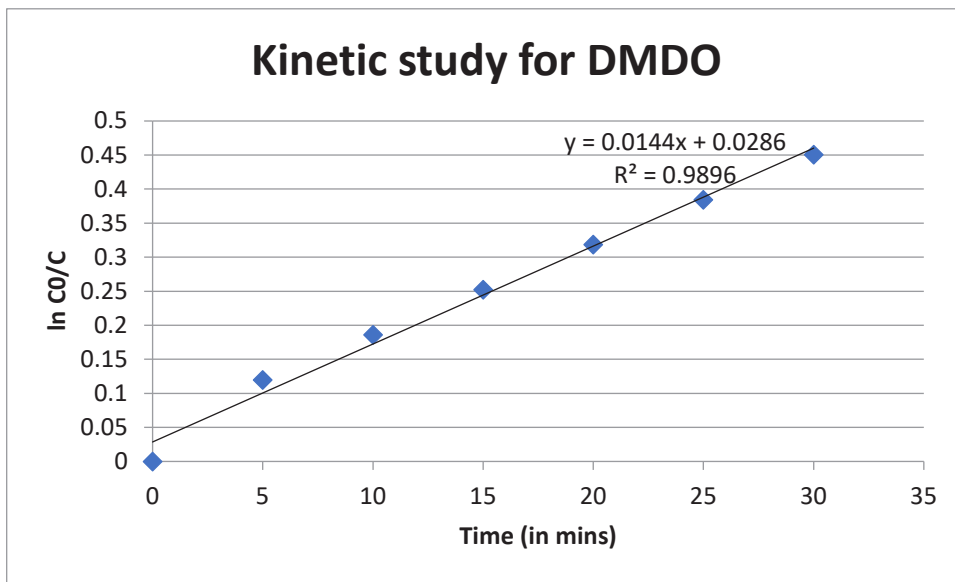


Fig. 10.a: The plot of $\ln C_0/C$ Vs. Time for 10 mg.L^{-1} of methyl violet dye solution.

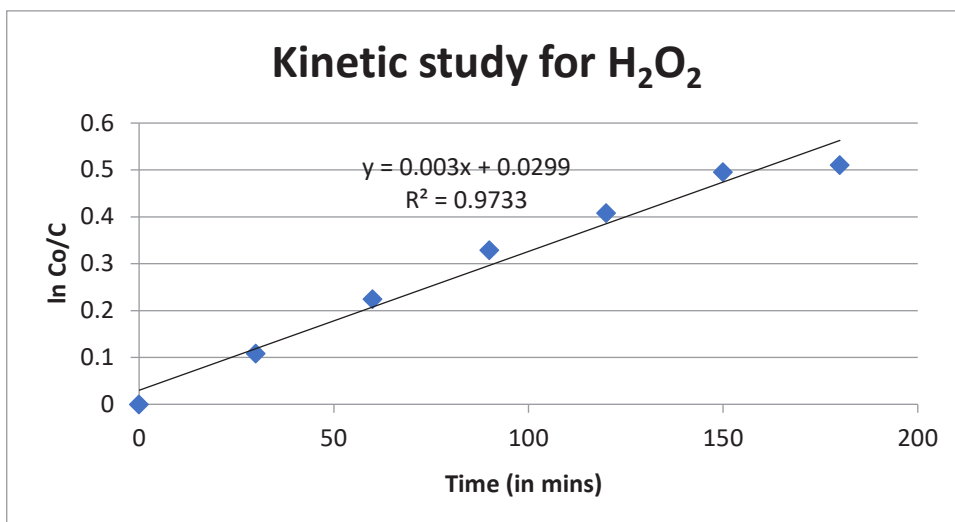


Fig. 10.b: The plot of $\ln C_0/C$ Vs. Time for 10 mg.L^{-1} of methyl violet dye solution.

dyes by efficient advanced oxidation using a dimethyl dioxirane and hydrogen peroxide system under ambient temperature and sunlight. Initial dye concentration, solution pH, and oxidant dosage were considered variant factors. Decolorization efficiencies of 97.9 % and 65.8% were achieved within 30 and 180 min of reaction time under optimum conditions for methyl violet. Results indicate that, when compared to hydrogen peroxide, the dimethyl dioxirane oxidation process is a viable and affordable method for dye removal from textile industry effluents. The end product, such as acetone and water, is produced by

employing dimethyl dioxirane as an oxidant to decolorize methyl violet. The dye decolorization process takes less than hydrogen peroxide as an oxidant. Compared to hydrogen peroxide, dimethyl dioxirane is a powerful, safe, affordable, and environmentally friendly oxidant.

ACKNOWLEDGEMENTS

The authors would like to express their heartfelt gratitude to Dr. S. Thennarasu, Senior Principal Scientist, Department of Organic and Bio-Organic Chemistry, Central Leather Research Institute, Chennai, for his insightful comments

that helped to complete the study effectively. We also acknowledge the invaluable assistance provided by Mrs. S. Vidhya and F. JaneetaPriya, assistant professors in the department of chemistry at Holy Cross College. We also appreciate Holy Cross College in Trichy's PG and Research Department of Chemistry for providing lab equipment.

REFERENCES

- Adam, W., Chan, Y.Y., Cremer, D., Gauss, J., Scheutzw, D. and Schindler, M. 1987. Spectral and chemical properties of dimethyl dioxirane as determined by experiment and ab initio calculations. *J. Org. Chem.*, 52: 2800-2803.
- Azmi, W., Sani, R.K. and Banerjee, U.C. 1998. Biodegradation of triphenylmethane dyes. *Enzyme Microbial. Tech.*, 22: 185-191.
- Bhargava, S.K., Tardio, J., Jani, H., Akolekar, D.B., Föger, K. and Hoang, M. 2007. Catalytic wet air oxidation of industrial aqueous streams. *Catal. Survey Asia*, 11(1-2): 70-86.
- Bumpus, J.A. and Brock, B.J. 1988. Biodegradation of crystal violet by the white rot fungus *Phanerochaete chrysosporium*. *Appl. Environ. Microbiol.*, 54: 1143-1150.
- Casas, N., Parella, T., Vincent, T., Caminal, G. and Sarrà, M. 2009. Metabolites from the biodegradation of triphenylmethane dyes by *Trametes versicolor* or laccase. *Chemosphere*, 75: 1344-1349.
- Diachenko, G.W. 1979. Determination of several industrial aromatic amines in fish. *Environ. Sci. Tech.*, 13: 329-333.
- Eftaxias, A., Font, J., Fortuny, A., Giralt, J., Fabregat, A. and Stüber, F., 2001. Kinetic modelling of catalytic wet air oxidation of phenol by simulated annealing. *Appl. Catal. B. Environ.*, 33(2): 175-190.
- Fu, Y. and Viraraghavan, T. 2001. Fungal decolorization of dye wastewaters: A review. *Bioresour. Tech.*, 79: 251-262.
- Garg, A., Mishra, I.M. and Chand, S. 2010. Oxidative phenol degradation using non-noble metal-based catalysts. *J. Clean. Prod.*, 38(1): 27-34.
- Hu, C., Yu, J.C., Hao, Z. and Wong, P.K. 2003. Effects of Acidity and Inorganic ions on the photocatalytic degradation of different azo dyes. *Appl. Catal. B Environ.*, 46: 35-47.
- Hunge, Y.M., Yadav, A.A., Khan, S., Takagi, K., Suzuki, N., Teshima, K., Terashima, C. and Fujishima, A. 2021. Photocatalytic degradation of bisphenol A using titanium dioxide @ nanodiamond composites under UV light illumination. *J. Colloid. Interface. Sci.*, 582: 1058-1066.
- Ju, Y., Fang, J., Liu, X., Xu, Z., Ren, X., Sun, C., Yang, S., Ren, Q., Ding, Y. and Yu, K. 2011. Photodegradation of crystal violet in TiO₂ suspensions using UV-vis irradiation from two microwave-powered electrodeless discharge lamps (EDL-2): products, mechanism, and feasibility. *J. Hazard. Mater.*, 185(2-3):1489-1498.
- Mittal, A., Gajbe, V. and Mittal, J. 2008. Removal and recovery of hazardous triphenylmethane dye: Methyl violet through adsorption over granulated waste materials. *J. Hazard. Mater.*, 150: 364.
- Nelson, C.R. and Hites, R.A. 1980. Aromatic amines in and near the buffalo river. *Environ. Sci. Tech.*, 14: 1147-1149.
- Robert W, Murray, R. and Ramasubbu, J. 1985. Dioxiranes: Synthesis and reactions of methyl dioxiranes. *J. Org. Chem.*, 50: 2847-2853.
- Santos, A., Yustos, P., Quintanilla, A. and García-Ochoa, F. 2004. Lower toxicity route in catalytic wet oxidation of phenol at basic pH by using bicarbonate media. *Appl. Catal. B*, 53(3): 181-194.
- Selvam, K., Swaminathan, K. and Chae, K.S. 2003. Decolorization of azo dyes and a dye industry effluent by a white rot fungus *Thelephora* sp. *Bioresour. Tech.*, 88: 115-119.
- Soroosh, M., Ali, S. and David James, E. 2019. Optimization of photocatalytic degradation of acid blue 113 and acid red 88 textile dyes in a UV-C/TiO₂ suspension system: Application of response surface methodology (RSM). *Catalysis*, 9: 360.
- Tan, I.A.W., Ahmad, A.L. and Hameed, B.H. 2008. Adsorption of basic dye on high-surface-area activated carbon prepared from coconut husk: Equilibrium, kinetic and thermodynamic studies. *J. Hazard. Mater.*, 154: 337-346.
- Yadav, A.A., Hunge, Y.M. and Kulkarni, S.B. 2019. Synthesis of multifunctional FeCO₂O₄ electrode using the ultrasonic treatment for photocatalysis and energy storage applications. *Ultrason. Sonochem.*, 104663 :58.



The Impact of High-Concentration Salt Solution on Morphological Changes in a Geosynthetic Clay Liner

N. P. Nisha* and J. Prakash Arul Jose*†

*Department of Civil Engineering, Noorul Islam Centre for Higher Education, Kumarakovil, Thuckalay, Kanyakumari District, Tamil Nadu, India

†Corresponding author: J. Prakash Arul Jose; joseprakash1430@gmail.com

Nat. Env. & Poll. Tech.
Website: www.neptjournal.com

Received: 24-08-2022

Revised: 20-10-2022

Accepted: 02-11-2022

Key Words:

Bentonite
Hydration
Swelling
Calcite
Permeability

ABSTRACT

Microscopic examination was used to begin investigating the changes in geosynthetic clay liner (GCL) specimens that had been hydrated with two separate solutions: pure water and a 50 percent concentration NaCl solution. After already being hydrated with NaCl aqueous solution, the GCL samples were examined under an electron microscope. Even though the treated GCL samples' surfaces mirrored those of the untreated GCL, a crystal deposit was found there. It was found that the bentonite particles in the GCL sample appeared more solid after being hydrated with distilled water as opposed to the NaCl solution using a scanning electron microscope (SEM). It seems that wetting the salt solution decreases the bentonite particles' tendency to swell. Additionally, it was demonstrated by the energy-dispersive X-ray spectrometer (EDS) data that distilled water hydration had no impact on the distribution of the elements identified in the GCL samples. On the other hand, the presence of bound chlorine demonstrated that the bentonite particles had absorbed the NaCl solution. The hydrated GCL sample's hydraulic conductivity showed some variation as well.

INTRODUCTION

The most popular way of disposing of solid waste around the world is still landfilling (Ludwig et al. 2002, Feng et al. 2004). Solid trash will begin to break down in landfills and produce leachate. (Justin 2000). Leachate is difficult to manage because it contains varying amounts of physiochemical components, pathogens, and heavy metals. (Daud et al. 2009, Mohajeri et al. 2010, Li et al. 2010, Foul et al. 2009, Palaniandy et al. 2010, Renou et al. 2008). If landfill effective organizational performance escapes and contaminates the environment, such as groundwater, there might be serious environmental and health consequences (Tian et al. 2016, Ruhl & Danirl 1997, Liu et al. 2015). The capability of landfills to serve as a hydraulic barrier to halt leaks or as an ideal place for leachate collecting (Hu et al. 2002, Jingjing 2014, Kalka 2012, Benfenati et al. 2002, Du et al. 2009, Chen et al. 2008). Leachate containment is therefore the most important purpose of landfill design and construction. (Yesiller Shackelford 2010) to lessen a landfill's negative effects on the environment and public health.

To minimize the environmental footprint of landfill leachate, landfills are fitted with just an impervious bottom liner to protect effluent from contamination located near

groundwater (Justin 2000, Alex et al. 2016). To prevent leachate intrusion, landfill firms typically install an impermeable soil layer at the bottom of a landfill, such as a compacted clay liner (CCL). In developed nations, besides that, geosynthetic liner (GCL) rather than clay-based liner has been used as a liquid waste barrier (CCL). Due to the GCL's superior advantages in terms of availability, transit, ability to handle, assembly, and affordability, it has eclipsed the CCL (Yesiller & Shackelford 2010). Once GCL is formed, it usually consists of two geosynthetic layers wedged together by bentonite, which, once hydrated, continues to expand and becomes impenetrable. The degree of hydration, temperature, and permeable liquid all have an impact on how permeable the geosynthetic layers are (Thammathiwat & Chim-oye 2010, Alex et al. 2022, Lake & Rowe 2000, Barclay & Rayhani 2013) as well as liner configuration, such as single or composite lines that contain geomembranes (Jingjing 2014, Bowders 2010).

The capacity of GCL to achieve maximal hydraulic performance depends on the saturation level. The liner system needs to be adequately hydrated for GCL to prevent liquid pollutant leaks (generally with water) (Bowders 2010). The flecks of bentonite in the GCL tend to expand and bind together as a result of hydration. The hydration process starts as soon as the GCL is placed over a subgrade,

such as damp soil. Because the subgrade is already moist, no water needs to be added to the GCL. When the GCL begins to hydrate, it collects water from the subgrade, grows in size, and eventually becomes moisture-resistant. As an effluent barrier, the GCL must interact with leachate, which may encompass organic substances, toxic substances, and inorganic materials (Kolstad et al. 2014, Petrov & Rowe 1997). Ionic species from acid and basic earth metals, such as Na^+ and Ca^{2+} ions, are present in large amounts in the leachate from landfills that store solidified or stabilized inorganic hazardous waste (SIHW). According to many flow-through leaching measurements, the Na^+ and Ca^{2+} ion content in this type of SIHW is typically somewhere between 1000 and 2000 mg.L^{-1} . for the first several pore quantities of flow (Poon et al. 2001, Chen et al. 2015). Several studies have been conducted to investigate the association between the hydraulic conductivity of GCL and the surface runoff of inorganic salt solutions (Kolstad et al. 2004, Petrov & Rowe 1997, Xue et al. 2012, Alex et al. 2022). It was discovered that the permeability of GCL changed whenever the solution contained a heavy amount of NaCl or a significant amount of ions. Furthermore, when the GCL was pervaded with small concentrations of NaCl solution, the hydraulic conductivity was noticed to be identical to the permeability of tap water or DI water (Lee & Shackelford 2005). Long-term permeation with a supersaturated NaCl aqueous solution produced a tremendous rise in the capillary pressure of the GCLs (Jo et al. 2005).

This investigation aimed to address the morphological alterations in GCLs as a continuation of earlier research findings. It does this by doing initial research from a microscopic perspective, therefore making it easier to understand how salt solution affects GCLs. In this study, the seepage fluid was a 50 percent concentrated NaCl solution.

MATERIALS AND METHODS

In this investigation, two different kinds of prepared GCL samples from two separate sources were examined. All of the samples contained sodium bentonite; the samples of bentonite powder were designated by the letter “P” on the label, while the samples of granular bentonite were designated by the letter “G.” Then, using distilled water and salt, solubilized NaCl solutions with a concentration of 50% were produced. The subscript on the sample labeling denoted the sample condition. The existing GCL specimens (dry) have been labeled with just an “O,” whereas the samples marked with “W” have been hydrated with distilled water and the samples marked with “N” have been hydrated with NaCl solution (Table 1). As previously mentioned, microscopic imaging was employed to study the GCL samples (Fig. 1), as

well as a scanning electron microscope (SEM) (Fig. 2), which was used to look at the bentonite particle size and sample morphology (JEOL-JSM-IT 200 with EDS). The samples were placed in a high vacuum chamber and subjected to a 15 kV analysis, followed by an XRD examination to identify the elements. The element composition was examined using XRD, and the resulting numbers are shown in Fig. 3.

RESULTS AND DISCUSSION

After hydration for two weeks, the GCL samples were baked to remove the moisture content. Any physical alterations were examined using optical microscopy both before and after hydration. The physical appearance of samples having IDs of P-O, G-O, P-W, and G-W shows no difference. It shows that hydration with distillate water had no impact on GCL samples after drying. Meanwhile, in P-N and G-N samples, some crystal particles were found on the top layer of bentonies; these are all the dried forms of NaCl crystals.

Morphology and Characterization of Samples

The GCL samples were again investigated for their shape and mineralogy using a scanning electron microscope (SEM). SEM images exhibit the liner member binding characteristics; they were used to absorb the physical changes due to inner particle interaction due to hydration. Fig. 2 shows the morphology of GCL samples, which illustrates the images of the sample particles when they are dry and later hydrated by distilled water and the NaCl solution. The sample P-O, and G-O in Fig. 2 shows bentonite before it has even been hydrated with any particular solution. The samples with P-O and G-O labels contain powder as well as granular bentonite, respectively. The particle clods inside the bentonite powder were larger and denser than those inside the granular bentonite particles, as shown in an analysis of the SEM image.

The distilled water hydrated samples of P-W and G-W show that the hydration process causes particle clods flocculation; it forms more solid bentonite particles, and the surface appearance shows that the particles have well-fitting

Table 1: GCL sample ID.

Sl.No	Sample code for microscopic examination	Bentonite type	Hydration condition
1.	P-O	Powder	Dry
2.	G-O	Granular	Dry
3.	P- W	Powder	Distillery water
4.	G- W	Granular	Distillery water
5.	P-N	Powder	NaCl
6.	G-N	Granular	NaCl

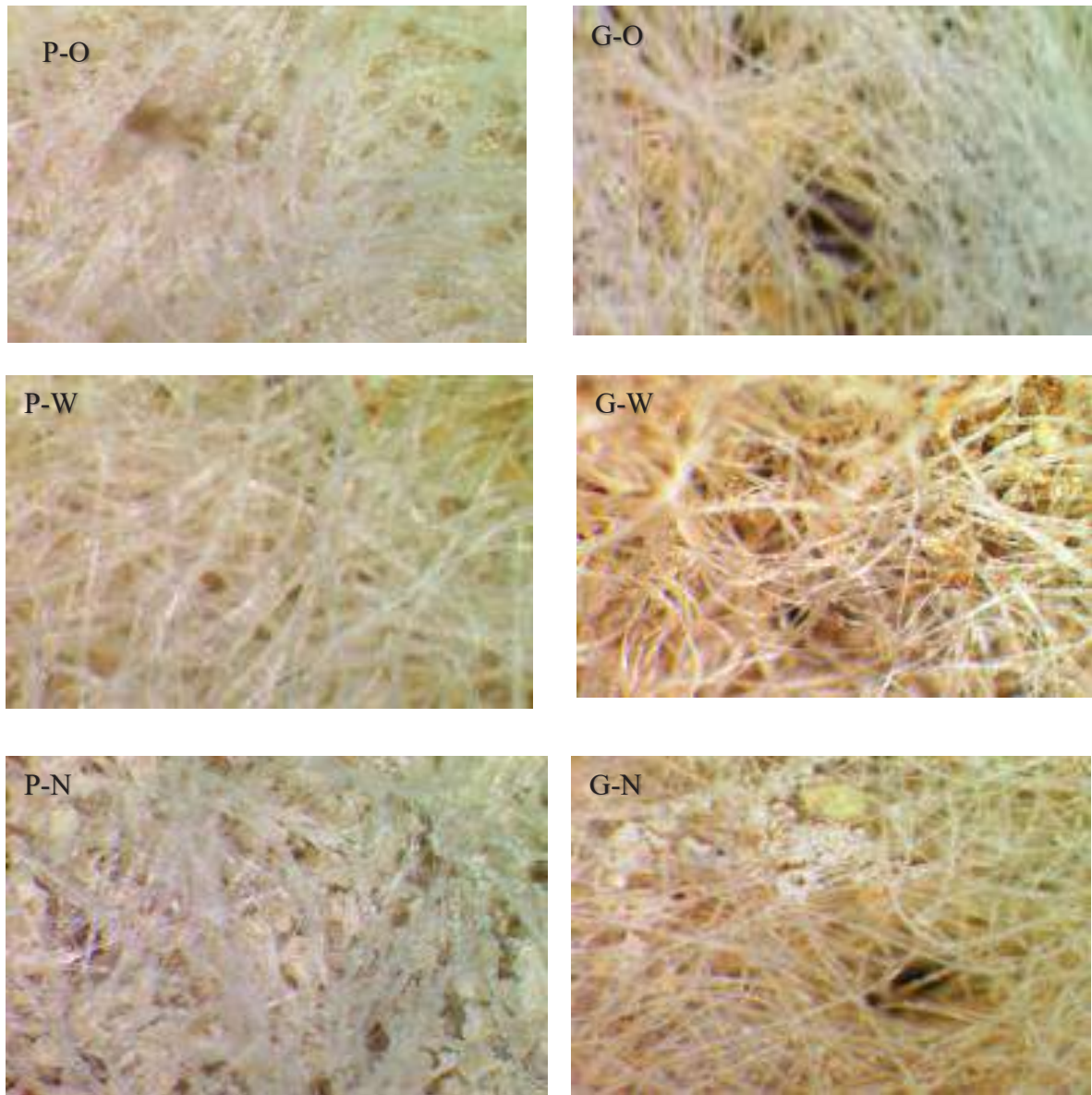


Fig. 1: P-O, G-O- preliminary state of the GCL; P-W, G-W - GCL samples hydration with distilled water; P-N, G-N- GCL specimens hydrated with NaCl solution.

attachments. As a result, hydrating bentonite with distilled water serves to decrease the voids between internal particles. Instead of the particles' structure and crystallography, the bentonite particles are significantly affected by the hydration of the material used in distilled water.

Fig. 2 depicts the morphology of hydrated bentonite molecules in a highly concentrated (50%) NaCl solution, labeled P-O and G-O, which exhibit blade-type crystal particles and crusted irregular particles, respectively. P-W and G-W both have crusted fungus-like structures with

high densities and irregular elliptical-shaped particles. Here we found that the arrangement of particles and interaction between the particles were observed, and it was found that they were entirely different from distilled water-hydrated specimens. The bentonite particles are more clustered and have high swelling. As a result, it is reasonable to believe that the highly concentrated concentration of solute can alter the reaction of bentonite particles. An X-ray diffraction spectrometer was used to quite successfully investigate the impact that hydration with alternative

approaches had on both types of bentonite particles (EDS). The distribution of elements within every sample was then calculated.

The existing chemical compositions of bentonite in the two distinct forms of powder and granular throughout GCL are shown in Fig. 3. When examined using XRD at a bearing angle of 2θ , it was noticed that bentonite contained silica (Si), aluminum (Al), and iron (Fe), as well as other elements of the

sum alkali group. The same minerals were discovered here, with quartz, mullite, and hematite being the three crystalline phases identified with different oxidation forms, silicates (SiO_2), aluminum oxide (Al_2O_3), ferric oxide (Fe_2O_3), and calcium oxide (CaO) being the major elements at 66.72%, 16.73%, 3.26%, and 1.46%, respectively, while minor alkali group elements such as magnesium (Mg), sodium (Na). Similarly, in this phase, after hydrating bentonite with distilled

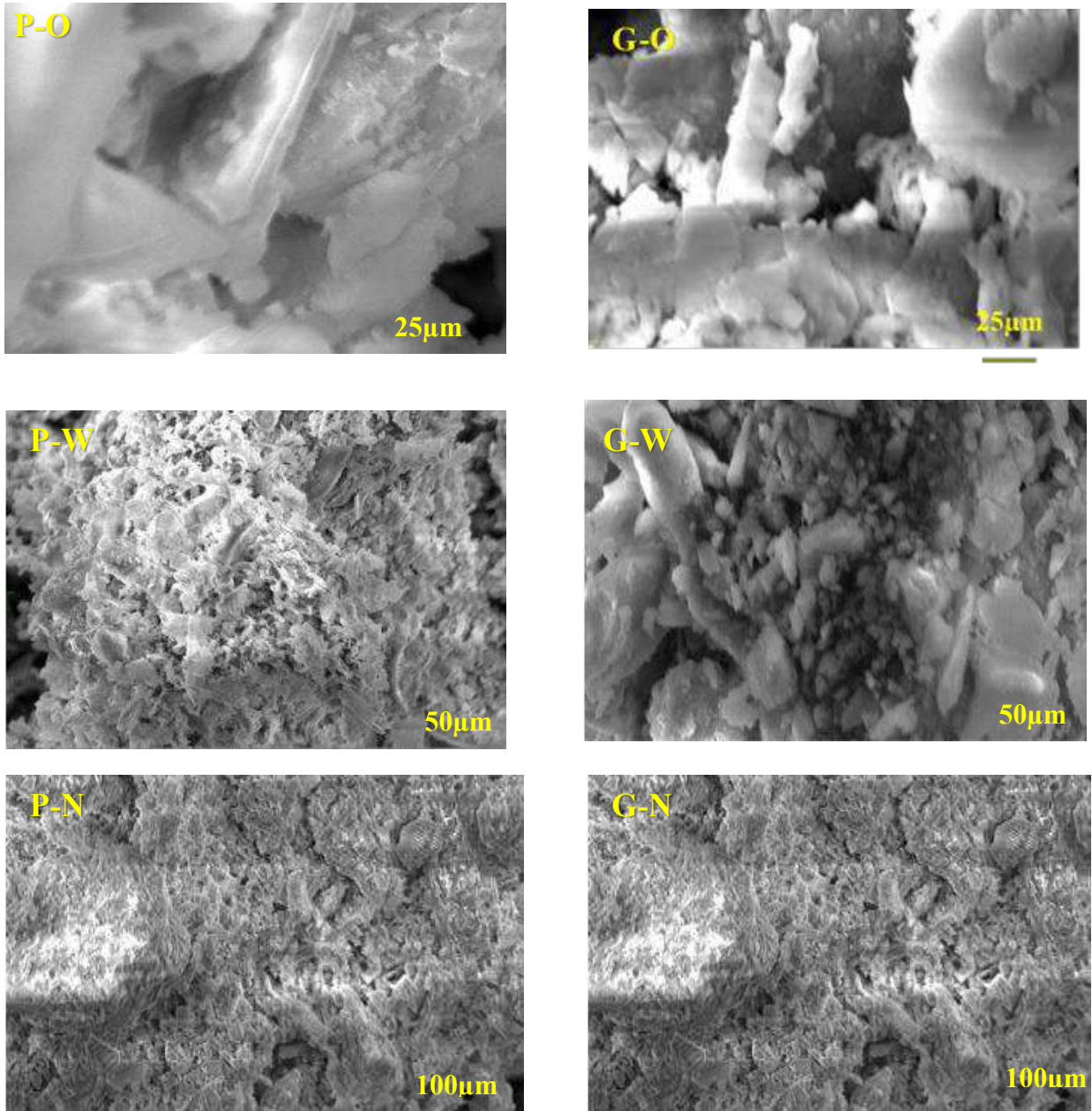


Fig. 2: SEM image of the bentonite particles: P-O, G-O: Before hydration; P-W, G-W hydrated with distilled water; P-N, G-N: hydrated with NaCl solution.

water, P-W and G-W specimens discovered the same element spreading. It should be demonstrated that no water content has been observed in any of the specimens upon oven drying, indicating that H₂O acted only as a supplement in all mixers.

The XRD humps of P-N and G-N show the element distribution of bentonite particles after the hydration of a highly concentrated (50%) NaCl solution. In this stage, the high amount of sodium chloride particles was absorbed, and

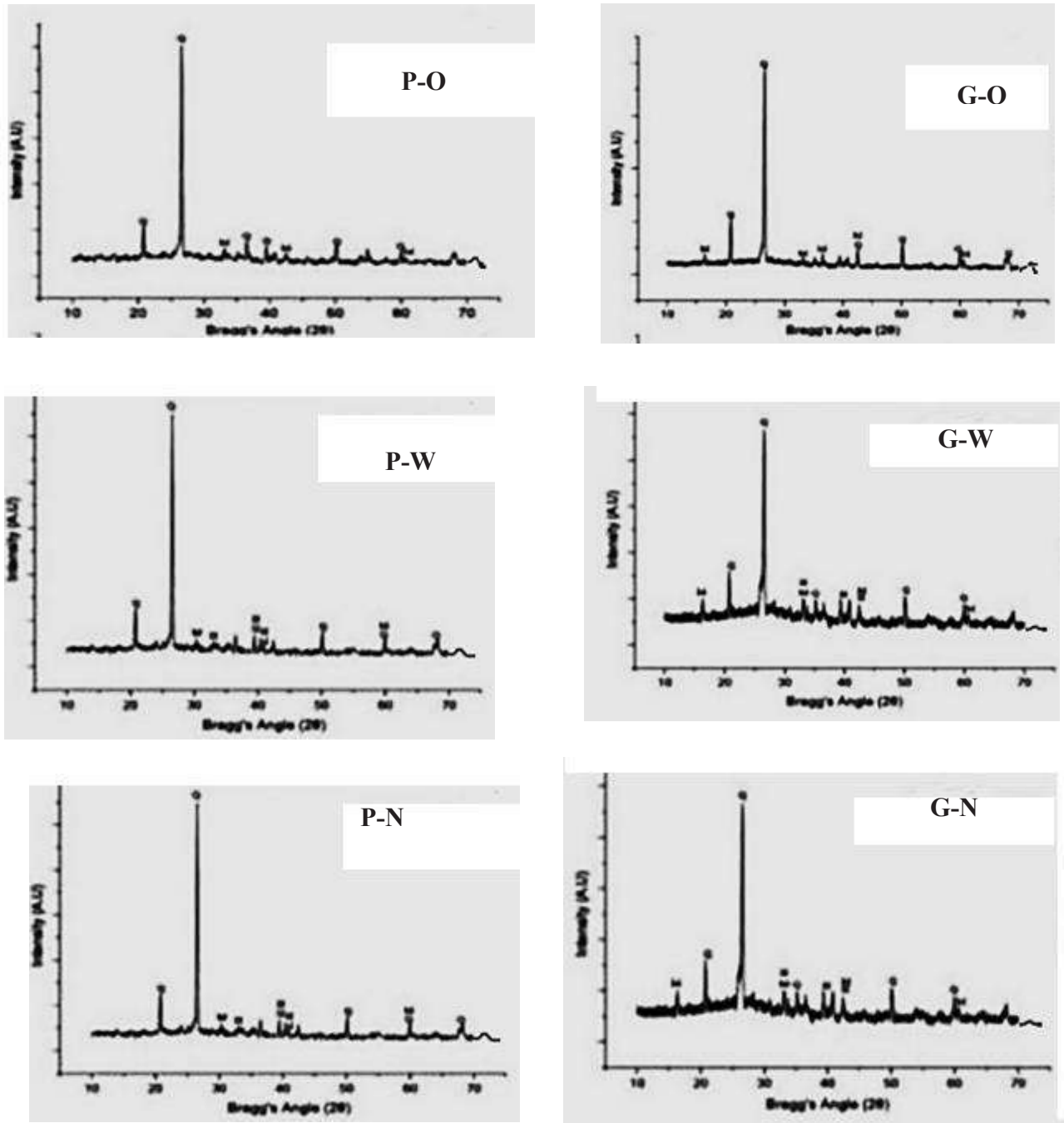


Fig. 3: XRD humps of the bentonite particles: P-O, G-O: Before hydration; P-W, G-W hydrated with distilled water; P-N, G-N: hydrated with NaCl solution.

it appeared with a brighter color in the SEM image, along with a small surface of bentonite. It was determined that only small modifications in the bonding structure of the bentonite particles had occurred; also, a highly concentrated NaCl solution significantly reduced the amount of CaO and MgO in the samples. Increased NaCl concentration can help carbonate minerals dissolve (Lee & Shackelford, 2005). This effect was observed in both granular and powder bentonites.

The Impact of Hydraulic Efficiency

The amount of water that is applied to the bentonite surface sandwiched between the two geotextiles determines its permeability (Lee & Shackelford 2005). The incompatibility of GCLs' permeability affects their performance since they are utilized as leachate barriers through landfill liners, and this is a significant issue during the landfill design phase. As a result, this study also evaluated the hydraulic performance of GCLs when they were hydrated with all these types of permanent solutions, distillate water, and NaCl. The outcomes are shown in Fig. 4. The current study, as previously stated, furthermore explored the effectiveness of using a GCL as an equitized protective layer in the presence of NaCl in the seeping solution to evaluate the influence of different types of effective alternatives on a moisturized GCL. Both GCL samples' hydraulic conductivities were determined to be 1.41×10^{11} m.sec⁻¹ and 7.64×10^{11} m.sec⁻¹, respectively. Meanwhile, the highly concentrated NaCl (50%) solution has very slightly modified the permeability of GCL and tends to increase the permeability because the addition of minerals and salts to water can weaken this same adhesion strength of bentonite while increasing

permeability. According to the majority of other researchers' findings, the hydraulic permeability of clay increases with increasing concentrations of inorganic sodium chloride (Lee & Shackelford 2005). Meanwhile, the mineral loss causes the bentonite skeleton to end up losing and weakening the connection between molecules so that high concentrations of NaCl help improve permeability behavior. The hydraulic conductivity of samples P-W and G-W, on the other hand, is 1.39×10^{-10} m.sec⁻¹ and 1.96×10^{-10} m.sec⁻¹, respectively.

CONCLUSION

The main aim of the study was to examine the morphological changes of a geosynthetic clay liner in a highly concentrated salt solution. The laboratory tests show that using bentonite in conjunction with a geosynthetic clay liner improved particle properties while decreasing hydraulic conductivity. The following conclusions should be drawn from this experiment:

- According to the optical microscope analysis, the GCL samples appear to have remained unchanged after being hydrated using distilled water and then dried. When highly concentrated NaCl (50%) was used as the hydration solution, crystal deposits were discovered on both the bentonite surface as well as the geosynthetic cover.
- The surface morphology of bentonite particulate demonstrates that hydration of GCL layers of distilled water and NaCl solution changes the particle arrangement, even though bentonite particles show more attachment to each other upon distilled water hydration.

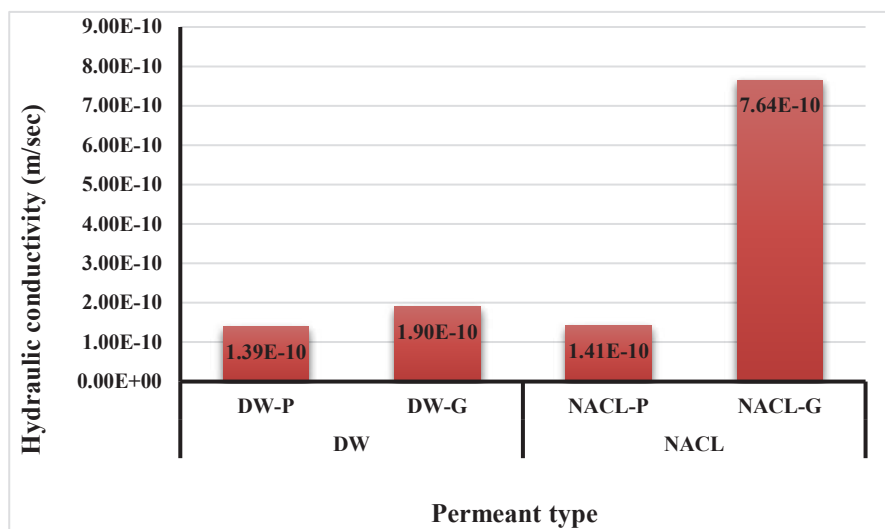


Fig. 4: Hydraulic conductivity of the GCL samples after hydration.

- The samples were hydrated with highly concentrated NaCl (50%) showing some small amounts of swelling in particles, while NaO particles were presented unevenly on the bentonite surface.
- The XRD humps show that the main elements of granular and powdered bentonite are silicon, aluminum, iron, and calcium. When GCL compounds containing granular bentonite or bentonite powder have been hydrated with NaCl solution, the flow rate of the GCL layer is enhanced because the salt impact amplifies the disintegration of calcite, leading to the loss of calcium cement and a softening of the structure of the bentonite samples. However, the bentonite powder particles effectively reduced the hydraulic conductivity rather than the granular particles.

REFERENCES

- Alex, A.G., Basker, R. and Chettyar, G. 2016. Effect of micro and nano particles in M-sand cement mortar. *International Journal for Civil and Structural Research*, 1(1): 67-76.
- Alex, A.G., Gebrehiwet Tewe, T., Kemal, Z. and Subramanian, R.B. 2022. Flexural behavior of low calcium fly ash based geopolymer reinforced concrete beam. *International Journal of Concrete Structures and Materials*, 16(1): 1-11.
- Alex, A.G., Gebrehiwet, T., Kemal, Z. and Subramanian R.B. 2022. Structural performance of low-calcium fly ash geo-polymer reinforced concrete beam. *Iranian Journal of Science and Technology, Transactions of Civil Engineering*, 1-12.
- Barclay, A. and Rayhani, M.T. 2013. Effect of temperature on hydration of geosynthetic clay liners in landfills. *Waste Management & Research*, 3(31): 265-272.
- Benfenati, E., Porazzi, E., Bagnati, R., Forner, F., Martinez, M.P., Mariani, G. and Fanelli, R. 2003. Organic tracers identification as a convenient strategy in industrial landfills monitoring. *Chemosphere*, 51(8): 677-683.
- Bouazza, A. and Bowders, J.J., (ed.) 2010. *Geosynthetic Clay Liners for Waste Containment Facilities*, Vol. 254. London: CRC Press.
- Chen, Y., Gao, D., Zhu, B. and Chen, R. 2008. Seismic stability and permanent displacement of landfill along liners. *Science in China Series E: Technological Sciences*, 51(4): 407-423.
- Chen, Y.G., Zhu, C.M., Ye, W.M., Cui, Y.J. and Wang, Q. 2015. Swelling pressure and hydraulic conductivity of compacted GMZ01 bentonite under salinization-desalinization cycle conditions. *Applied Clay Science*, 114: 454-460.
- Cossu, R. and Stegmann, R. (ed.) 2012. *Sanitary Landfilling: Process, Technology and Environmental Impact*. Academic Press.
- Das, B.M. ed. 2010. *Geotechnical Engineering Handbook*. J. Ross publishing.
- Daud, Z., Aziz, H.A., Adlan, M.N. and Hung, Y.T. 2009. Application of combined filtration and coagulation for semi-aerobic leachate treatment. *International Journal of Environment and Waste Management*, 4(3-4): 457-469.
- Du, Y.J., Shen, S.L., Liu, S.Y. and Hayashi, S. 2009. Contaminant mitigating performance of Chinese standard municipal solid waste landfill liner systems. *Geotextiles and Geomembranes*, 27(3): 232-239.
- Feng, X., Tang, S., Li, Z., Wang, S. and Liang, L. 2004. Landfill is an important atmospheric mercury emission source. *Chinese Science Bulletin*, 49(19): 2068-2072.
- Foul, A.A., Aziz, H.A., Isa, M.H. and Hung, Y.T. 2009. Primary treatment of anaerobic landfill leachate using activated carbon and limestone: batch and column studies. *International Journal of Environment and Waste Management*, 4(3-4): 282-298.
- Hu, T., Zeng, G. and Yuan, X. 2002. Decision-making mode of integrated disposal scheme for regional municipal solid waste. *Journal of Hunan University Natural Sciences*, 29(2): 79-87.
- Isidori, M., Lavorgna, M., Nardelli, A. and Parrella, A. 2003. Toxicity identification evaluation of leachates from municipal solid waste landfills: a multispecies approach. *Chemosphere*, 52(1): 85-94.
- Jingjing, F. ed. 2014. Leakage performance of the GM+ CCL liner system for the MSW landfill. *The Scientific World Journal*.
- Justin, M.Z. and Zupančič, M. 2009. Combined purification and reuse of landfill leachate by constructed wetland and irrigation of grass and willows. *Desalination*, 246(1-3): 157-168.
- Kalka, J. 2012. Landfill leachate toxicity removal in combined treatment with municipal wastewater. *The Scientific World Journal*.
- Kolstad, D.C., Benson, C.H. and Edil, T.B. 2004. Hydraulic conductivity and swell of nonprehydrated geosynthetic clay liners permeated with multispecies inorganic solutions. *Journal of Geotechnical and Geoenvironmental Engineering*, 130(12): 1236-1249.
- Lake, C.B. and Rowe, R.K. 2000. Swelling characteristics of needle punched, thermally treated geosynthetic clay liners. *Geotextiles and Geomembranes*, 18(2-4): 77-101.
- Lee, J.M. and Shackelford, C.D. 2005. Impact of bentonite quality on hydraulic conductivity of geosynthetic clay liners. *Journal of Geotechnical and Geoenvironmental Engineering*, 131(1): 64-77.
- Li, W., Zhou, Q. and Hua, T. 2010. Removal of organic matter from landfill leachate by advanced oxidation processes: a review. *International Journal of Chemical Engineering*.
- Liu, Y., Bouazza, A., Gates, W.P. and Rowe, R.K. 2015. Hydraulic performance of geosynthetic clay liners to sulfuric acid solutions. *Geotextiles and Geomembranes*, 43(1): 14-23.
- Ludwig, C., Hellweg, S. and Stucki, S. (eds.) 2012. *Municipal Solid Waste Management: Strategies and Technologies for Sustainable Solutions*. Springer Science & Business Media.
- Mohajeri, S., Aziz, H.A., Isa, M.H., Zahed, M.A. and Adlan, M.N. 2010. Statistical optimization of process parameters for landfill leachate treatment using electro-Fenton technique. *Journal of Hazardous Materials*, 176(1-3): 749-758.
- Palaniandy, P., Adlan, M.N., Aziz, H.A. and Murshed, M.F. 2010. Application of dissolved air flotation (DAF) in semi-aerobic leachate treatment. *Chemical Engineering Journal*, 157(2-3): 316-322.
- Petrov, R.J. and Rowe, R.K. 1997. Geosynthetic clay liner (GCL)-chemical compatibility by hydraulic conductivity testing and factors impacting its performance. *Canadian Geotechnical Journal*, 34(6): 863-885.
- Poon, C.S., Chen, Z.Q. and Wai, O.W. 2001. The effect of flow-through leaching on the diffusivity of heavy metals in stabilized/solidified wastes. *Journal of Hazardous Materials*, 81(1-2): 179-192.
- Renou, S., Givaudan, J.G., Poulain, S., Dirassouyan, F. and Moulin, P. 2008. Landfill leachate treatment: Review and opportunity. *Journal of Hazardous Materials*, 150(3): 468-493.
- Ruhl, J.L. and Daniel, D.E. 1999. Geosynthetic clay liners permeated with chemical solutions and leachates. *Journal of Geotechnical and Geoenvironmental Engineering*, 123(4): 369-381.
- Thammathiwat, A. and Chim-oye, W. 2010. Effect of permeant liquid on the swell volume and permeability of geosynthetic clay liners. *Electronic Journal of Geotechnical Engineering*, 15: 1183-1197.
- Tian, K., Benson, C.H. and Likos, W.J. 2016. Hydraulic conductivity of geosynthetic clay liners to low-level radioactive waste leachate. *Journal of Geotechnical and Geoenvironmental Engineering*, 142(8): 04016037.

Xue, Q., Zhang, Q. and Liu, L. 2012. Impact of high concentration solutions on hydraulic properties of geosynthetic clay liner materials. *Materials*, 5(11): 2326-2341.

Yesiller, N. and Shackelford, C.D. 2010. Chapter 13: Geo environmental engineering. In: *Geotechnical Engineering Handbook*, pp.13-52.

Young Jo, H., Benson, C.H. and Edil, T.B. 2004. Hydraulic conductivity and cation exchange in non-prehydrated and prehydrated bentonite permeated with weak inorganic salt solutions. *Clays and Clay Minerals*, 52(6): 661-679.



Protection of the Environment Under Trade and Investment Agreements: An Analysis Based on Existing Legal Frameworks

Kudrat-E-Khuda (Babu)*†, Nazia Afroz Ananna* and Arghyadeep Chakraborty**

*Daffodil International University, Department of Law, Dhaka, Bangladesh

**Sister Nivedita University, Department of Law, Kolkata, India

†Corresponding author: Kudrat-E-Khuda (Babu); kekbabu@gmail.com

Nat. Env. & Poll. Tech.

Website: www.neptjournal.com

Received: 03-01-2023

Revised: 06-02-2023

Accepted: 07-02-2023

Key Words:

Trade and Investment Agreement

Environment protocol

World Trade Organization

ABSTRACT

Free trade causes damage to the environment substantially as it puts pressure on natural resources in its venture to expand economic activities. On the other hand, there is also an argument that free trade has the potential to improve environmental quality by contributing to growth. Such growth enhancement may help individuals, organizations, or governments raise funds and spend more on environmental protection. This paper highlights the links between trade and the environment. Besides, it also shows how international trade and environmental protection are both essential to the well-being of humanity and, conversely, how they are mutually supportive. This paper also scrutinizes how the WTO plays a role in balancing trade and the environment, as many WTO agreements have environmental exceptions.

INTRODUCTION

The issues regarding the correlation between environmental policy and international trade have been one of the major talking points in public policy discussion in the current decade. These issues became more prominent in the ongoing coronavirus pandemic as huge concerns gained momentum regarding the impact of climate change. Especially global awareness of continuously rising temperatures, ozone depletion, and climate change are among the major concerns (Alam 2008). Apart from that, concerns raised about pollution, liberalization of trade, and capital flows have appeared as a threat to the environment. The growing campaigns against globalization argue that trade liberalization will expand the production, use, and sport of goods, increasing environmental damage.

Moreover, setting stricter environmental policies than other countries to protect the environment will make the government more concerned about surviving competitive business. In addition, there is now a major trade dispute over ensuring quality control of national products (Matsushita et al. 2006). Acknowledgments have been made for the increasing integration of economic and environmental issues of international legal frameworks. The issue of environmental protection is a fundamental part of the development of the Rio Declaration. To realize the goals of environment and development, the "Agenda 21" of the Rio Declaration

emphasized making trade and environment supportive of each other. It also buoys macroeconomic policies favoring the environment and development and encourages financial support to developing countries (Rio Declaration 1992). To achieve the objectives of environmental protection, Agenda 21 also helps the countries to mitigate international debts. There are some conflicting aspects of the relationship between trade and the environment. The agreements like GATT are being used to undermine environmental control. On the other hand, it is feared that GATT environmental regulation is being used to protect local trade and industries. Discussing the relationship between trade and the environment, many argue that trade promotes economic growth but, in that case, degrades the environment.

On the other hand, there is a justification that trade increases the funds to protect the environment. Another argument is that imposing various kinds of environmental restrictions on trade can harm the environment by slowing down economic growth. Besides, the current world trade patterns create differentiating effects on natural resources and environmental standards in developing countries. The third major link is that within the trade measures, a country's citizens can protect against another nation's environmental degradation. In particular, the trading system can effectively establish and implement environmental laws and frameworks. Environmental measures aimed at domestic activities - such as natural resource exploitation, product

quality, and certain processes - are relatively uninterrupted by current trade law systems. The state governments enjoy the freedom to control and manage the exploitation of natural resources within their territories. Another link between the environment and trade is that the steps taken to implement international environmental agreements are less likely to be challenged under existing trade rules. Agenda 21 specifies the need for harmonization of trade and environmental policy. The CSD emphasizes the need for an integrated approach to sustainability by such a type of trading system that would be more open and equitable and simultaneously provide improved market access for products from developing countries. It would also provide environmental protection and mutually supportive trade and environmental policies. Environmentalists blame the multilateral trading system for many reasons (Faruque 2021). They argue that trade could lead to environmental damage without environmental protection through measures aimed at economic growth by misusing natural resources and generating environmental waste. If the business system does not ensure adequate environmental protection, trade liberalization policies can supersede environmental regulations. They say the sanctions imposed on trade must be eased to ensure environmental protection, especially global or cross-border environmental issues, and to strengthen international environmental treaties. And even if a country or its trade system causes pollution, it does not spread to other countries. However, countries with no strong obligation to safeguard the environment get some extra advantage in global business as they constantly try to defy environmental requirements and standards.

MATERIALS AND METHODS

The current paper uses secondary data, *i.e.*, books, articles, national and international law reports, Acts, etc., besides the primary data. All the relevant data and information from the existing paper were collected and used from primary and secondary sources. The secondary data sources include books, articles, different national and international law reports, Acts, etc. The information from books, journals, booklets, proceedings, newsletters, souvenirs, and consultancy reports available in the library of Daffodil International University, Bangladesh, was compiled chronologically to complete it successfully. The necessary support and figures were taken from the Department of Environment (DoE), Bangladesh; The World Health Organization (WHO); the *Daily Star*; Springer. And the Financial Express. The selected data (collected from the selected stations between July 2020 and August 2021) reveals that the first debate about environment and trade was incepted in the 1920s when preparation was going on for formulating the "Convention for the Abolition of Import and Export Prohibitions and Restrictions 1927",

the first multilateral law. It is the first legal instrument that empowers the state to restrict any trade for the sake of humans, animals, and the environment from disease and 'extinction.' Subsequently, the General Agreement on Tariffs and Trade (GATT) 1948 contains an exception that empowers the parties to take measures to conserve fish and wild animals. Article XX refers to "applying the measures 'taken in pursuance of an inter-governmental agreement for the conservation of fisheries resources, migratory birds or wild animals.'" However, the debate over trade and the environment gained momentum in the early 1970s.

RESULTS AND DISCUSSION

Trade Measures in Environmental Agreements

It is important to include trade provisions in environmental laws to achieve sustainable development and reduce the negative effects of trade. The trade sanctions have already been integrated into some of the environmental agreements. Those agreements include; (i) agreements to protect wildlife; (ii) agreements to protect the environment of the importing state from harmful organisms and substances; (iii) agreements to protect the global commons. To prohibit trade in listed species, state parties have undertaken the 1973 Convention on International Trade in Endangered Species of Wilde Life and Flora (Esty 1994). The Bamako Convention in 1991 has empowered to impose a complete ban on all imports of hazardous wastes. The 1987 Montreal Protocol has empowered stakeholders to prohibit exporting and importing substances that deplete the ozone layer. The 1992 UNFCC and the 1992 Convention on Biological Diversity also work for both trade and the environment. With a view of the present situation, it is evident from the existing suggestions that if there is a conflict between the obligations under the Environmental and Trade Agreements, the obligations under the Environmental Agreement will prevail over those under the Free Trade Agreement.

It is argued that Biosecurity Protocol-2000 restricts cross-border transportation of living organisms developed by modern biotechnology, which may adversely affect biodiversity. Therefore, with these issues in mind, the parties to the protocol must take the necessary steps to protect human health.

Trade-Related Measures in CITES

The measures prescribed related to trade in CITES must be implemented to ensure that those agreements do not threaten wildlife and plant survival. Its provision regarding the trade of listed species restricts business with non-party states or stakeholders. It also has a provision for taking measures in case of any such violation. Based on a specific species list,

CITES plays a role as a regulator for the trade of specific wildlife and plant specimens by providing certificates and giving permission to the concerned stakeholders after scrutinizing their appeals (Sturm 2002). Thus, the strict rules that protect the “Appendix I” species, which are in danger of extinction, restrict their trade in exceptional circumstances and play a more supportive role in their survival. As per the specimens of “Appendix I” species, the import of those is prohibited for commercial purposes. An export permit is required for Appendix I species and will only be granted if the following conditions are met: (a) the exporting party has advised that the export will not be detrimental to the species’ survival; (b) the exporting party is satisfied that the species has been legally acquired; (c) the exporting party is satisfied that the method of shipment for the specimens will minimize risks of injury, damage to health, and cruel treatment; and (d) the exporting party is satisfied that the specimens will be transported in.

Appendix II and III species, which are not currently threatened with extinction, require just an export license with some of the above-mentioned features or, in the case of specific Appendix III species, a certificate of origin. CITES further stipulated that a party’s authorization and certification must be in accordance with the Convention. Every certificate or permission bears the title of the Convention, and the names of the authorities concerned (Sturm & Ulph 2002). The authority will also assign a control number with permission or certification. These initiatives will encourage a transparent and harmonious system avoiding any misconduct and play an effective compliance monitoring role. There are some exceptions to the role of CITES. For example, CITES, through its provision of exemptions and special procedures, facilitates certain kinds of trade that do not affect wild animals. However, under some special circumstances, CITES permits any Party to trade with others not a signatory of the Convention.

The Measures Prescribed in the Montreal Protocol

The Montreal Protocol was finalized in 1987 to stop the generation or import of substances affecting the ozone layer. It also contains some measures that control the storage and use of ozone-depleting substances. Article 4 is one of the trade-related provisions, which prohibits the trade of the ozone-depleting substance with any non-party to the protocol, and controls the international movement of products containing the substances. Article 4B of the protocol obliges parties to maintain due process for getting or taking a license for importing or exporting those substances and preventing illegal trade and ensuring the availability of the related data. Montreal Protocol can play a significant role in decreasing global emissions of ODS.¹⁰ as the Protocol has endorsed some necessary measures.

Measures in Basel Convention

Basel Convention is a multilateral environmental agreement among the state parties. This agreement has been signed to protect human health and the environment from the harm caused by hazardous wastes (Basel Convention 1989). Article-4 of the convention restricts the parties from importing any type of harmful waste for disposal. It also obliges state parties or the authorities concerned to restrict the export of the wastes to other parties. Under this Convention, parties can stop the export-import trade of hazardous wastes if they think it may be unable to manage the wastes and maintain environmentally friendly processes. Article 4 also restricts parties from permitting exporting and importing hazardous wastes to or from a non-party of the Convention. Any transborder movement of harmful wastes is not allowed as it is no longer subject to a bilateral, multilateral, or regional agreement as Basel Convention does not compromise with the policies of environment-friendly management of hazardous wastes. Finally, Article 4 of the Convention obliges the concerned parties that they will have to package the wastes and label those before their transboundary movement. Those wastes must be transported properly, maintaining the generally accepted and recognized international rules and standards. Besides, related necessary documents must be collected and carried out during the transboundary movement of hazardous wastes.

As per Article 6, parties must notify the about the hazardous wastes in writing to the intended country before shipment. The party will also inform other countries that need to be crossed to transit. The documents must include all the necessary details, such as reasons for the export, identities, and description of the wastes and the waste generalization country, exporter and carrier, and other necessary details. Besides, details on special handling requirements -- including emergency steps to be taken in case of any accidents and waste disposal method -- will have to be mentioned. On the other hand, the importer of the waste or the Party concerned with the destination of the waste must give feedback to the notifier in written form on whether it is being done with its consent or not. Finally, the party supposed to import the wastes will not commence any transboundary movement until the written consent and other detailed necessary information are accepted.

Measures in Bio-safety Protocol

Biosafety Protocol is an international framework that provides a uniform requirement for ensuring the safe international transport and use of products. Although this Protocol contains a broader objective, it mainly sheds light on the transboundary movements of LMOs. Most of the

provisions of the Protocol are related to the trade, which encompasses the ALA mechanism significantly referring to parties involved with the trade and the systems of handling, transport, identification, and packaging LMOs. As per Article 8 of the Protocol, the exchange of notifications between both parties of export and import and the proposed transboundary movement in writing has been made mandatory for the trade.

Stockholm Convention on Persistent Organic Pollutants (POPs)

The Stockholm Convention instructs the parties to ban the trade regarding POPs between countries that abide by the provisions of the Convention to ensure that all POPs are used and disposed of within the compass of the imposed restrictions (The Stockholm Convention 2004). According to Article 3, the import of the listed chemicals has been banned if it is not bought from another Party and the shipment of chemicals is not prepared in such a way that helps dispose of the product in an environmentally friendly system or if the chemical is not covered maintain a proper discharge method. It also empowers the state parties to restrict the export of chemicals if there is any concern about disposing of the chemicals and not maintaining the environment. However, the parties who are signatories of the convention can import or export among them. Besides, the parties can export the chemicals to non-parties who have certified compliance related to the concerned provisions of the Convention.

Environmental Obligations in Trade Agreements

The first debate about environment and trade was inception in the 1920s when preparation was going on for formulating the “Convention for the Abolition of Import and Export Prohibitions and Restrictions 1927”, the first multilateral law. It is the first legal instrument that empowers the state to restrict any trade for the sake of humans, animals, and the environment from disease and ‘extinction’ (Buckley 1993). Subsequently, the General Agreement on Tariffs and Trade (GATT) 1948 contains an exception that empowers the parties to take measures to conserve fish and wild animals. Article XX refers to “applying the measures ‘taken in pursuance of an inter-governmental agreement for the conservation of fisheries resources, migratory birds or wild animals.’” However, the trade and environment debate gained momentum in the early 1970s.

WTO’s Provisions on the Environment

The World Trade Organization (WTO) deals with international trade rules between the member state parties. The WTO was formed in 1994 through negotiation among several nations to ensure smooth trade. The agreement has

already been ratified by the parliaments of over 160 member countries. The WTO and its annexes were born through the Marakesh Agreement 1994 (Charnovitz 2007). WTO was established after the General Agreement on Tariffs and Trade (GATT) was incorporated into the 1994 Agreement. However, the trade and environment issues were adopted at the conference of the ministers of the WTO member states in Uruguay. At the conference, the member states were assigned to determine the relations between trade and environmental measures for sustainable growth. They were also asked to modify the international trading system keeping relations between trade and environmental measures. The introduction of the 1994 Agreement encompasses an environmental provision that states that trade relations should be based on the objective of sustainable development goals (Taubman & Watal 2022). There are many exceptions to the trade rules in the Article XX of GA. Article XX reads as follows:

“Subject to the requirement that such measures are not applied in a manner which would constitute a means of arbitrary or unjustifiable discrimination between countries where the same conditions prevail or a disguised restriction on international trade, nothing in this Agreement shall be construed to prevent the adoption or enforcement by any contracting party of measures.

- Necessary to protect the human, animal, or plant life or health.
- Relating to the conservation of exhaustible natural resources, if such measures are effective in conjunction with restriction on domestic production or consumption.

The chapeau: The exceptions elaborated under Article XX are qualified by an introductory clause called the chapeau. Thus, even if a measure otherwise falls within one of the exceptions in Article XX, it would be illegal under the chapeau if it constitutes (i) arbitrary or unjustifiable discrimination between the countries where the same conditions prevail or (ii) a disguised restriction on international trade.”

Though the word “environment” has not been mentioned in Article XX, it can be used to justify some environment-friendly rules to influence free trade. However, environmental measures should not be the result of camouflage protectionism. The Appellate Body states that it is ‘necessary’ to set a measure under paragraph XX (b) if there is no alternative to the GATT-compliant. However, there is a condition that it should not contradict GATT provisions. However, Article XX (g) can be considered a special provision to the GAAT. Article XX (g) instructs the member states of the WTO to take the necessary steps to conserve extractable natural resources. In 1994, the WTO intervened regarding shrimp import into the US and its

impact on turtles. The ruling was adopted on November 6, 1998 (Mohammed 2022). From then, it was known as the “Shrimp-Turtle” case. The Appellate body used the WTO Preamble as an example of general exceptions in Article XX of GATT. Since then, the member states and other concerned stakeholders have been given reference to the example for justification for a stronger environmental dimension to the WTO. However, the preface to the WTO Agreement emphasized the need to follow the sustainable development objectives for global trade. Following the US “Gasoline” and the “Shrimp-Turtle” related cases, it has been stated that for dealing with any case of any exception under Article XX (b) and (g), it will have to be considered so that it would not be arbitrary, discriminatory on trade. Therefore, environmental exceptions have appeared in many agreements with WTO.

Trade-Related Aspects of Intellectual Property Rights (TRIPS)

The TRIPS specifically addresses issues related to environmental protection. There are environmental exceptions to the agreement regarding patents. Under the TRIPS agreement, any member state may exclude an innovation from patentability if it thinks it works to safeguard the life and health of humans, animals, or plants and the overall environment in the region (TRIPS Agreement 1995). This treaty ensures the member states the right to revoke the innovation of any patents that could endanger the environment. WTO members can revoke patentability for inventions “the prevention of commercial exploitation of which is necessary within their territory to protect public order or morality, including to protect human, animal, or plant life or health, or to avoid serious prejudice to the environment, provided that such exclusion is not made solely because the exploitation is prohibited by their law,” according to Article 27.2. Article 27.3 states that member states may exempt (a) “diagnostic, therapeutic, and surgical methods for the treatment of humans or animals,” and (b) “plants and animals other than microorganisms, and essentially biological processes for the production of plants or animals other than non-biological and microbiological processes” from patentability. WTO members may also use patents, an “effective sui generis system,” or a combination of the two techniques to protect their plant varieties under subparagraph.

Technical Barriers to Trade (TBT) Agreement

TBT recognizes environmental protection, activities, and efforts to protect the environment as a legitimate objective. It assesses the quality of different products and their shape and performance of pro Moreover. It also deals with the technical quality of different products. Such quality and

other measurements of products can be used to hinder the trade of those products, and therefore, these measurements can be made only subject to certain requirements (TBT Agreement 1994). Therefore, these assessment measures of this article play a supportive role in materializing the goals of health or environmental protection. The TBT treaty emphasizes that no member state may impose such standards and technical rules, creating ‘unjust discrimination’ among the other countries where similar conditions exist. Under paragraph 2 of this Agreement, any member state cannot say anything or do anything that may appear as a barrier to any legitimate purpose. Apart from that, the agreement provides a list of legitimate objectives. It also takes measures for the protection of human and animal life as well as the environment.

Application of Sanitary and Phytosanitary Measures Agreement

The SPS provides some conditions for different issues, including the ‘ecology and environment, within its criteria, as a part of its effort to manage risks. It also obliges the member states to consider ecosystems as disease-free areas. This agreement insists the member states adopt sanitary and phytosanitary measures to protect animals and plants from diseases and ensure the supply of safe foods for consumers. The steps to ensure safety may vary based on the situations and topics. It may be related to the origination of the products, such as whether those are brought from a safe zone; processed or produced following a special procedure; contain only the permitted additives, or there has the maximum use of pesticide. By nature, they work to limit trade related to sanitary and phytosanitary systems. Adopting international standards also encourages harmonizing measures between the sanitary and phytosanitary. Apart from that, this agreement upholds the right of member states to adopt their higher standards in light of SPS. For initiating any measures, it should be aligned with the SPS, and it must be for the safeguarding of humans, animals, plants, or the environment. It should be based on scientific principles and evidence. Besides, the measures taken must not ‘arbitrarily or unjustifiably discriminate between Members’ or ‘constitute a disguised restriction at international trade. ‘Measures should be taken following the appropriate risk assessment based on the scientific evidence and following the related PPMs, economic and environmental situations.

The Agreement on Agriculture

This agreement was signed containing measures to safeguard the environment. It states that the member states must reform agriculture to protect the environment. It also states that the government of the member states will allocate budget

environment programs and have commitments for subsidy for the sake of the environment. According to Annex 2 of this agreement, the measures taken domestically with minimal impact on trade should be allowed and excluded from reduction commitments on the expenditures under environmental programs.

The General Agreement on Trade in Services, 1994

This agreement has a general exceptions clause asking the member states to adopt necessary policy measures to protect the environment. It is also an exception for taking necessary measures to protect human, animal, or plant health. However, this must not result in arbitrary or unjustifiable discrimination and must not constitute 1 protectionism in disguise.

Committee on Trade and Environment

Negotiators approved a decision on Trade and Environment at the WTO conference held in Uruguay in 1994 on formulating policies regarding international trade and the environment to support each other for multilateral trading. The WTO Committee on Trade and Environment (CTE) was formed in 1995. Here are the terms of reference mentioned in CTE in Marrakech:

- Identifying the relationship between trade and environmental measures to promote sustainable development;
- Preparing recommendations if there is a need for modifications of the provisions in the multilateral trading system aiming to make those compatible, equitable, and non-discriminatory to nature. However, the WTO committee has lessened the agenda of this broad mandate to 10 items for work, and the discussion for its framework is held based on this agenda. The 10 items on the agenda are:
 - The link between trade regulations and environmental trade measures, such as those found in MEAs.
 - The impact of trade on the link between trade rules and environmental policies.
 - a) The interplay between trade restrictions and environmental fees and taxes
 - b) The link between trade rules and environmental product requirements, such as packaging, labeling, and recycling restrictions and standards.
 - Trade standards governing the transparency (i.e., full and timely disclosure) of environmental trade measures and environmental policies with trade implications.
 - The link between the WTO's dispute-resolution systems and those of MEAs.

- The potential for environmental policies to obstruct developing country exports' access to markets, as well as the potential environmental advantages of eliminating trade restrictions and distortions.
- The issue of illegal items in the United States is exported.
- The environment and the TRIPS Agreement are inextricably linked.
- The connection between the environment and service trade.
- The World Trade Organization's (WTO) relationships with various organizations, both non-governmental and intergovernmental.
- Since establishing the Committee on Trade and Environment in 1994, it has been playing a vital role in bringing environmental issues to the agenda of WTO.

Environmental Dispute Settlement Under WTO

Though WTO has been playing a crucial role in protecting and preserving the environment while ensuring sustainable development, it has settled only a few environmental disputes. The cases --Tuna-Dolphin, US-Gasoline, US-Shrimp, and EC-Asbestos -- were dealt with in light of the GATT Article XX (general exceptions). In the 1991 Tuna-Dolphin case, the WTO panel dealt with an import ban on a certain type of tuna product from Mexico. The United States imposed a ban as yellowfin tuna were being caught for export using a method that also killed dolphins (Mexico etc., versus the US: 'tuna-dolphin,' 1991). Dolphins are considered an endangered species as per the Marine Mammal Protection Act of the US. In this case, the US argued that they had taken the decision of the ban for the sake of the lives of dolphins, and there was no other better option rather than imposing sanctions in that case. But, the ban on Tuna import violated Article XI (1) of GATT, which prohibits restrictions on imports or exports. However, a dispute settlement panel found that the reason behind the ban was not necessary for the US to protect dolphins as the panel did not find any evidence that the US had tried any other options, including negotiating international cooperative arrangements, before imposing the ban. The Tuna-Dolphin II case was filed on another incident of imposing a ban on tuna products from countries that processed tuna imported from the offending countries. But both panels in two Tuna-Dolphin cases reached the point that none of the Articles XX (b) and XX(g) of GATT can justify the ban.

However, both panels finally concluded that, per Article XX (b), the ban failed to conduct the 'necessary' test. They also explained that 'necessary' means no other reasonable

alternative exists. Later, the Appellate Body of WTO reviewed the decisions of the two panels on two Tuna-Dolphin cases and reached some decisions in light of the extra-territorial scope of Article XX(b) and (g). However, extra-territorial measures have been considered an important factor in these resources. In *Tuna-Dolphin* case-1, the appellate body concludes that the regional jurisdiction of a concerned country will be solely for its decision to protect living things and natural resources. GATT does not allow any measures regarding trade that goes against the environmental issues beyond the territory of a country. In detail, it can be stated that any nation can set environmental policies within its territory. Still, the state cannot take any measures regarding the environmental values outside its territory. Such a provision complies with standards or rules with the long-standing international legal principles of state sovereignty. So the Panel for Tuna-Dolphin case-1 decided that any nation can take measures to produce natural resources as this is under its territorial jurisdiction.

Meanwhile, the Panel of the Tuna-Dolphin Case 2 concluded that the government of a state party could impose restrictions in light of Article XX (g) in case of extra-territoriality only against a citizen or vessel in their own country. The decision of extraterritorial jurisdiction has been considered based on the concept of nationality on how a nation controls the activities of its citizens. However, in the Shrimp-Turtle case, some countries --India, Malaysia, Pakistan, and Thailand --jointly came up with objections in early 1997 against the US ban on importing certain shrimp and shrimp products.

The main purpose of the US ban was for the protection of sea turtles as the US had listed five species of sea turtles in the country's water bodies as endangered or threatened under the country's Endangered Species Act of 1973 (India etc. versus the US: 'shrimp-turtle,' 1998). The law also prohibited the harassment, hunting, capture, killing, or attempting to do any of these against the turtles within the US, in its territorial sea, and on the high seas. Under the law, US shrimp trawlers must use "turtle excluder devices" (TEDs) in their nets when fishing to protect the turtles. Section 609 of US Public Law 101-102 was ratified in 1989 to deal with import-related issues. It stated that the country would not import shrimps that are caught using the technology, which may affect sea turtles adversely if a nation's fishing environment does not appear to threaten the sea turtles. However, the appellate body stated that WTO member countries preserve the right to take any measures under the WTO rules to protect the environment for the sake of human, animal or plant and endangered species. It also stated that if any member states take measures to protect sea turtles, it would be legalized

under Section 20 of GAIT. Article 20 of GAIT deals with various exceptions to the trade rules of "O's" if certain criteria are met.

Although the lawsuit was filed to protect the environment, the United States lost the case only because of differences among WTO members. This is because the countries of the Western Hemisphere - mainly in the Caribbean - have not been able to take immediate steps to provide technical and financial assistance, as well as their fishermen to start using non-turtle devices. Thus, the United States unilateral measures to protect marine turtles violated Chapeau's standards against arbitrary and unreasonable discrimination. Besides, some evidence was found against the US as the authorities concerned of the state did not maintain due process in issuing the certificate for shrimp imports, following the basic standards and due process. The appellate body observed that GATT requires a strict adherence to the basic requirements of the proper process' complying with the exceptions to treaty obligations. Though the evidence of violations was found in the above two cases, it was determined that WTO would approve legal, environmental measures.

In the 1998 EC-Asbestos case, Canada stressed the need for discussion with the EC in response to the decree by France on 24 December 1996 regarding the ban on asbestos and products containing asbestos (Sander 2015). Canada said the measures taken by France violated Articles 2, 3, and 5 of the SPS Agreement, Article 2 of the TBT Agreement, and Articles III, XI, and XIII of GATT 1994. Later in 2000, the Panel found that: the part of the "embargo" of the Decree of 24 December 1996 was out of the purview of the TBT Agreement, but it's part of the "exception" in the decree fell under the TBT Agreement, and chrysotile asbestos fibers and other products substituted for them as per Article III:4 of GATT 1994. Besides, information regarding asbestos-cement and fibro-cement submitted to the Panel is similar to Article 111:4 of GATT 1994. On March 12, 2001, the Appellate Body ruled that the French Decree banning asbestos and asbestos-containing products had not been shown as contradictory to obligations under WTO agreements. Rather, it overturned the Panel's finding that the TBT Agreement does not allow such prohibitions. It also found that measures applied in light of the TBT Agreement were viewed as an integrated part of the whole. The Appellate Body determined that they could not scrutinize Canada's claims that the measure taken under the decree was not in light of the TBT Agreement. Then, the appellate body revised the Panel's findings concerning "like products," per Article 111:4 of the GATT 1994. In particular, the appellate body observed that the Panel did not take the

health risks associated with asbestos from its “similarity” test into account and excluded those issues. The appellate body, however, upheld the conclusion of the Panel, stating that the French Decree was “necessary to protect human life or health” in light of Article XX(b) of the GATT 1994. While ruling on the EC– Asbestos case, the appellate body said, “It is undisputed that WTO members have the right to determine the level of protection of health that they consider appropriate in a given situation.”

Investment Agreements

Moreover, many more multilateral and bilateral investment agreements have provisions for environmental protection. Notable among these agreements is a tripartite investment agreement of Canada, the United States, and Mexico, which is known as NAFTA.

NAFTA has provided that each treaty country will not encourage or allow foreign investment in providing low-quality health and safety or low environmental standards.

NAFTA also prioritizes obligations under certain environmental agreements, such as Montreal Protocol, CITES, and Basel Convention. In Article 1114(1) of the NAFTA, it has been stated that nothing in Chapter 11 shall be construed to prevent a Party from adopting, maintaining, or enforcing any measure that it considers appropriate to ensure that investment activity in its territory is undertaken in a manner sensitive to environmental concerns. Another agreement was signed as a subsidiary agreement to NAFTA, the North American Agreement on Environmental Cooperation. Significantly, both treaties were made effective from 1 January 1994. Although NAFTA’s environmental provisions have no legal obligations, the North American Agreement on Environmental Cooperation supports to environmental goals and objectives of NAFTA (Glick 1994). The general objectives of the agreement are to protect the environment, promote sustainable development, and increase compliance with environmental laws and regulations. Bilateral investment agreements (BITs) are gradually expanding for their consideration in terms of environmental law. In general, BITs encourage the flow of foreign investment and, at the same time, protect foreign investors in the host states against the nationalization or occupation of foreign investment. Most of the BITs which have been signed in recent times have provisions regarding environmental concerns.

CONCLUSION

Indeed, the issues regarding the correlation between environmental policy and international trade have been one of the major talking points in public policy discussion in

the current decade. These issues became more prominent in the ongoing coronavirus pandemic as huge concerns gained momentum regarding the impact of climate change. Especially global awareness of continuously rising temperatures, ozone depletion, and climate change issues are among the major concerns. Hence, an integrated approach through an open and equitable multilateral trading system is crucial for sustainable development. The concerned authorities, governments of different countries, environmental activists, business people, policymakers, trade organizations, and mass media should come together. At the same time, formulating and implementing trade and environment-friendly policies are vital to ensure environmental protection. Emerging trends in development and the environment suggest that environmental protection legislation is strongly integrated with multilateral trade-related instruments and investment agreements to facilitate sustainable development and minimize the negative effects of trade.

ACKNOWLEDGEMENTS

The authors are thankful to Mr. Akanda Muhammad Jahid, Staff Reporter at the Daily Star, and Dr. Md. Milan Khan, Honorable Librarian at Daffodil International University, Bangladesh, for their kind support and cooperation in this work.

REFERENCES

- Alam, S. 2008. Sustainable Development and Free Trade. Routledge, London, pp. 235.
- Basel Convention. 1989. Basel Convention–Controlling Transboundary Movements of Hazardous Waste and Their Disposal. <http://www.basel.int/> (Accessed 1 March 2022).
- Buckley, R. 1993. International trade, investment, and environmental regulation. *J. World Trade*, 27(4): 102-110.
- Charnovitz, S. 2007. The WTO’s environmental progress. *J. Environ. Law*, 10(3): 685-706.
- Esty, D.C. 1994. The Greening of the GATT. Institute for International Economics, Washington DC.
- Faruque, A.A. 2021. International Environmental Law: Global and Bangladesh Context. New Warsi Book Corporation, Dhaka.
- Glick, L. 1994. Understanding the North American Free Trade Agreement: Legal and Business Consequences of NAFTA. Springer, Berlin.
- India etc. versus the US: shrimp-turtle (1998) ‘DS58: United States-Import Prohibition of Certain Shrimp and Shrimp Products’. [Online] https://www.wto.org/english/tratop_e/dispu_e/cases_e/ds58_e.htm (Accessed 25 December 2021).
- Mexico etc. versus US: tuna-dolphin (1991) ‘Mexico etc. versus US: ‘tuna-dolphin.’ [Online] https://www.wto.org/english/tratop_e/envir_e/edis04_e.htm#:~:text=The%20panel%20reported%20to%20GATT,content%20of%20the%20tuna%20imported (Accessed 30 January 2022).
- Mohammed, A. 2022. Ngozi Okonjo-Iweala and WTO Leadership: Nigerian-American Economist & Director General of the World Trade Organization. WTO, Geneva
- Mutsushita, M., Schoenbaum, T.J. and Mavroidis, P.C. 2006. The World Trade Organization: Law, Practice, and Policy. Oxford University Press, Oxford.

- Rio Declaration. 1992. Rio Declaration on Environment and Development 1992. Retrieved from <https://www.jus.uio.no/lm/environmental.development.rio.declaration.1992/portrait.a4.pdf> (Accessed 23 February 2022).
- Sander, G.G. 2015. The EC–Asbestos Case. Retrieved from <https://opil.ouplaw.com/view/10.1093/law:epil/9780199231690/law-9780199231690-e2105> (Accessed 24 January 2022).
- Sturm, D. and Ulph, A. 2002. Environment and trade: The implication of imperfect information and political economy. *World Trade Rev.*, 1(3): 235-256.
- Taubman, A. and Watal, J. 2022. Trade in Knowledge: Intellectual Property, Trade, and Development in a Transformed Global Economy. Cambridge University Press, Cambridge.
- TBT Agreement. 1994. Agreement on Technical Barriers to Trade. Retrieved from https://www.wto.org/english/docs_e/legal_e/17-tbt_e.htm (Accessed 1 March 2022).
- The Stockholm Convention. 2004. Stockholm Convention-Protecting Human Health and the Environment from Persistent Organic Pollutants. Retrieved from <http://www.pops.int/TheConvention/Overview/tabid/3351/Default.aspx> (Accessed 11 January 2022).
- TRIPS Agreement. 1995. Overview: The TRIPS Agreement. Retrieved from https://www.wto.org/english/tratop_e/trips_e/intel2_e.htm (Accessed 25 February 2022).



Types and Distribution of Macroinvertebrates Stressed by Heavy Metals in Mangrove Forests

W. Budijastuti*†, R. Ambarwati*, N. Ducha*, F. Rachmadiarti*, L. Lisdiana* and K. Sahani*

*Department of Biology, Faculty of Mathematics and Natural Sciences, Universitas Negeri Surabaya, Ketintang street, Gayungan, Surabaya 60231, East Java, Indonesia

† Corresponding author: Widowati Budijastuti; widowatibudijastuti@unesa.ac.id

Nat. Env. & Poll. Tech.
Website: www.neptjournal.com

Received: 20-09-2022

Revised: 03-11-2022

Accepted: 11-11-2022

Key Words:

Macroinvertebrates
Heavy metals
Principal Component Analysis
Mangrove forests

ABSTRACT

Heavy metals can decrease the number of species in nature. This research aims to determine the relationship between the type of macroinvertebrates stressed by heavy metals in the Wonorejo Mangrove Area, Surabaya, East Java. This type of research is observational. The determination of stations was done using the purposive random sampling method. Tests for Pb and Cd content were carried out using the AAS method. Nutrient content testing was carried out using the AAS and Kjeldahl methods. Data analysis was presented descriptively, and multivariate analysis was done using Principal Component Analysis (PCA). Based on the present research, it can be concluded that there are variations in the type and distribution of macroinvertebrates stressed by heavy metals in the mangrove area of Surabaya. Station 1 is dominated by *Ocypode ryderi*, Station 2 by *Assimineae* sp., Station 3 by *Scylla paramamosain*, and Station 4 by *Cerithidea* sp. with the high presence of metals (Cd, Pb), and soil and water nutrients (Org-C, N) at Stations 1, 3, and 4. The Station 2 has only Pb. *Assimineae* sp. (Phylum Mollusca) can be the best candidate for metal bioindicators because it appears in all locations where soil and water have been contaminated with Pb and Cd metals without affecting their life.

INTRODUCTION

A mangrove forest area is an ecosystem located in a transitional area between land and ocean ecosystems that hold various important roles for life (Riry et al. 2020). In Surabaya, namely on the East Coast of Surabaya (Pamurbaya), there is a Wonorejo Mangrove Forest Area located in the eastern part of Surabaya City and directly adjacent to the Madura Strait. This area belongs to the estuary area, the estuary of various rivers in Surabaya, such as the Jagir River (DAS Brantas) and the Avour channel (artificial river), which flows from Rungkut District to the Madura Strait. These rivers are known to pass through industrial areas, so they have the potential to carry heavy metals to the Wonorejo Mangrove Forest Area (Wijaya & Sanjaya 2021).

Heavy metals are metallic elements with a density greater than 5 g.cm^{-3} , such as Pb and Cd (Syachroni 2017). Pb has a shiny grayish color, atomic number 82, an atomic weight of 207.20, and a melting point of 1740°C (Mauriza et al. 2020). Cd has an atomic number of 48, an atomic weight of 112.40, and a melting point of 321°C . In seawater, Cd is in the form of CdCl_2 , while in freshwater CdCO_3 and brackish water (river estuaries), the amount of both is balanced (Fatmawati Nur 2013). Based on previous research showed that silvofishery

pond water in the Wonorejo Mangrove Area in July 2018 contained Pb of 0.022 ppm and Cd of 0.087 ppm (Wijaya et al. 2019a) than in June 2019 found Pb of 0.304 ppm, and Cd of 0.047 ppm (Wijaya et al. 2019b) and in December 2021, found Pb of 0.045 ppm, and Cd of 0.005 ppm (Wijaya & Sanjaya 2021).

Heavy metal pollution can harm the environment because it is not decomposed, can accumulate in sediments and the water column, and is absorbed in living tissue. High concentrations of heavy metals can interfere with metabolic processes and morphological changes and cause the death of biota (Sari et al. 2017). The research conducted by Budijastuti (2016) shows that the presence of heavy metals Pb and Cr can affect the morphometric structure, including length, weight, body diameter, and the size of the male and female genital holes in earthworms through Principal Component Analysis (PCA) analysis.

Macroinvertebrates are a group of animals without a backbone, with a body size of more than 1 mm (Diantari et al. 2017), equipped with good adaptability in polluted environments. In the mangrove ecosystem, macroinvertebrates are important; they can help reduce water pollutants, become food for other biota, and be a bioindicator of water quality

(Riry et al. 2020). Two phyla belonging to macroinvertebrates, such as Arthropoda and Molluscs, are known to have the ability as metal bioindicators. Phylum Arthropoda can be an environmental cleaner and bioindicator of metal pollution because of its ability to accumulate Pb, Cd, and Zn (Rohyani & Farista 2013). In addition, Mollusc phyla, especially Gastropods, can be used as bioindicators of pollution because they have a wide tolerance level for water and can accumulate heavy metals (Wulansari & Kuntjoro 2018).

Information about the types of macroinvertebrates that are stressed by heavy metals in Indonesia, especially in the Wonorejo Mangrove Area, and their relationship with heavy metals is not yet known, so this study was conducted to analyze the relationship between the types of invertebrates that were stressed by heavy metals in the Wonorejo Mangrove Area.

MATERIALS AND METHODS

Study Area and Collection of Samples

This type of research is observational. The research was conducted in August 2021 in the Wonorejo Mangrove Area, Surabaya, at four stations (Fig. 1). determination of stations is done using the purposive random sampling method. Station 1 is located on the riverside jogging track at coordinates 7°18'26.9"S 112°49'31"E, station 2 is located in a riverside mangrove at coordinates 7°18'32"S 112°49'59"E, station 3 is located in the estuary at coordinates 7°18'25"S 112°49'35"E, station 4 is located in the pond at coordinates 7°18'32"S 112°49'42"E.

Macroinvertebrates were collected using the hand-collecting method and by digging to a depth of 5 cm

for macroinvertebrates in the substrate. Samples were documented and sorted, and each species was counted at the Taxonomy Laboratory of the Department of Biology, FMIPA, Universitas Negeri Surabaya.

Soil and water samples were taken from each station to analyze the content of heavy metals Pb and Cd, nutrient contents of organic C and N, and some environmental parameters. The heavy metal content of Pb and Cd was analyzed at the Chemistry Laboratory, FMIPA, State University of Surabaya, using the Atomic Absorption Spectrophotometer method. The organic C and N nutrient contents were analyzed at the Faculty of Public Health, Airlangga University. The analysis of the nutrient content of organic C used the Atomic Absorption Spectrophotometer method, while the analysis of the nutrient content of N used the Kjeldahl method. Environmental parameter measurements were carried out in situ, including soil moisture and soil pH using a soil tester, soil temperature using a soil thermometer, air temperature using a thermometer, CO₂ using a CO₂ meter, light intensity using a lux meter, and salinity using a refractometer.

Testing of Heavy Metals of Pb and Cd

Testing the content of heavy metals Pb and Cd in soil and water samples in the Wonorejo Mangrove Area, Surabaya was divided into 3 stages: sample preparation, calibration curve making, and sample analysis using Atomic Absorption Spectrophotometer (AAS) at a wavelength of 217.0 nm. The formula used to determine the metal content of Pb is as follows:

a. Soil

$$\text{Metal levels (mg.kg}^{-1}\text{)} = \frac{C_{\text{reg}} \times P \times V}{G}$$



Fig. 1: Sampling location.

b. Sea water

$$\text{Metal levels (mg.L}^{-1}\text{)} = \frac{\text{Creg} \times P \times V1}{V2}$$

Where:

Creg = Read concentration (mg.L⁻¹)

P = Dilution factor

G = Sample weight (kg)

V1 = Measured sample volume (L)

V2 = Volume of the dissolved sample (L)

V = Volume of sample solution (L)

Testing the Nutrient Contents of Organic C and N

Testing the Nutrient Contents of Organic C

Testing the nutrient organic C content in soil samples was divided into 3 stages: sample preparation, calibration curve creation, and sample analysis using the Atomic Absorption Spectrophotometer (AAS) method at a wavelength of 561 nm. The formula for calculating organic C content is as follows:

$$\text{C-organic (\%)} = \frac{(\text{abs sample value} - \text{blanko}) \times \text{vol sample volume}}{\text{sample weigh}} \times 10^{-4}$$

Testing the Nutrient Contents of N

Testing for total nitrogen content was made using the Kjeldahl method. First, sample preparation was carried out, then the solution obtained was titrated until pink. The titration volume of the sample (Vs) and the blank (Vb) was recorded and calculated using the following formula:

$$\text{N-total (\%)} = \frac{(V_a - V_b) \times N_{H2SO4} \times \text{atom nitrogen weigh}}{\text{sa mple weigh (mg)}} \times 100\%$$

Data Analysis

Data analysis was presented descriptively and multivariate analysis was done using Principal Component Analysis (PCA).

RESULTS

Types of Macroinvertebrates in the Wonorejo Mangrove Area

Based on the results of the research, it was found that 214 macroinvertebrates consisted of 2 Phyla, 6 Classes, 23 Families, and 34 species (Table 1).

Based on the results of PCA analysis related to the correlation of distribution of macroinvertebrates at each station based on Phylum, Class, Family, and species centered on 2 main axes with an eigenvalue of more than 1 with a total variance of 61.698%. At Station 1, macroinvertebrates by phylum were dominated by Arthropods but also small amounts of Mollusca (Fig. 2A); by class (Fig. 2B) dominated by Crustacea, Insecta, Arachnida, Gastropod; by Family

(Fig. 2C) dominated by Ocypodidae, Libellulidae, Chrysomelidae, Onchidiidae, and Potamididae; and by species (Fig. 2D) dominated by *Ocypode ryderi*, *Crocothemis selvilia*, *Leucauge* sp, *Aspidomorpha deusta*, *Paraonchidium* sp., and *Cerithidea obtusa* with the largest distribution in *Ocypode ryderi* Species (Table 1).

At Station 2 and Station 3, based on the phylum (Fig. 2A), the composition of macroinvertebrates is almost the same between Arthropoda and Mollusca; based on class (Fig. 2B), dominated by Crustacea, Arachnida, Gastropod, and Bivalves; by Family (Fig. 2C) dominated by Portunidae, Sesarmidae, Ocypodidae, Oxyopidae, Potamididae, Littorinidae, Assimineidae, and Mytilidae; and by species (Fig. 2D) dominated by *Scylla paramamosain*, *Pseudosarma moeschii*, *Ocypode mortoni*, *Oxyopes javanus*, *Telescopium telescopium*, *Echinolittorina* sp., *Assimineea* sp., and *Perna* sp. At Station 2, the distribution of *Assimineea* sp. was found the most, while at Station 3, *Scylla paramamosain* species were found the most (Table 1).

At Station 4, based on the species (Fig. 2A), the macroinvertebrates were dominated by Arthropods; based on class (Fig. 2B), dominated by Crustacea, Arachnida, Insecta, and Gastropod; by Family (Fig. 2C) dominated by Sesarmidae, Ocypodidae, Lycanidae, Nymphalidae, Araneidae, Vespidae, Erebididae, Pentatomoidae, Dinidoridae, Mantidae, Potamididae, and by species (Fig. 2D) dominated by *Episesarma singaporense*, *Tubuca*, *Zizina otis*, *Acraea violae*, *Argiope* sp, *Polistes* sp, *Amata huebneri*, *Euthyrhynchus* sp, *Cyclopelta obscura*, *Mantis religiosa*, and *Cerithidea*. At this station, the distribution of *Cerithidea* sp. was found the most (Table 1).

Measurement of Metals and Nutrient in Water and Soil of Wonorejo Mangrove Area

Based on the results of PCA analysis (Fig. 3), it can be seen that there is a negative correlation between levels of organic C(g.100g⁻¹) and Cd(mg.kg⁻¹), N(g.100g⁻¹) and Cd(mg.kg⁻¹), Cd(mg.L⁻¹) and Pb(mg.kg⁻¹) and positive correlation between organic C(g.100g⁻¹) and N(g.100g⁻¹)

In Fig. 3C, it can be seen that Stations 1, 3, and 4 have strong characteristics of mangrove soil and water metals and nutrients, namely Cd (mg.kg⁻¹), organic C (g.100g⁻¹), N (g.100g⁻¹), Pb (mg.L⁻¹), Cd (m.L⁻¹) while at Station 2 the prominent feature of metal and nutrients in mangrove soil and water is Pb (mg.kg⁻¹).

Measurement of Ecological Environment in Wonorejo Mangrove Area

Based on the results of PCA analysis (Fig. 4), it can be seen that there is a negative correlation between ecological

parameters, namely soil pH and soil moisture, air temperature and air humidity, CO₂ and air humidity, light intensity and air humidity, soil salinity and pH, and salinity and air humidity. While the correlation is positive between air temperature and soil temperature, CO₂ and air temperature, light intensity and soil pH, light intensity and soil temperature, light intensity

and air temperature, light intensity and CO₂, and salinity and air temperature.

In Fig. 4C, Station 1 has strong environmental ecology characteristics, including soil pH and salinity. Station 2 has prominent environmental and ecological characteristics: soil temperature, air humidity, air temperature, CO₂, light

Table 1: Types of Macroinvertebrates in the Wonorejo Mangrove Area.

Phylum	Class	Family	Species	Station				Σ		
				1	2	3	4			
Arthropoda	Crustacea	Grapsidae	<i>Metopograpsus frontalis</i>	1	1			2		
		Portunidae	<i>Scylla paramamosain</i>		2	3		5		
		Sesarmidae	<i>Pseudosesarma moeschii</i>		1	1	2	4		
			<i>Episesarma singaporense</i>	5	2	5		12		
		Camptandriidae	<i>Ilyogynnis microcherium</i>	1	1			2		
		Ocypodidae	<i>Tubuca Bellator</i>	6	8	2		16		
			<i>Ocypode mortoni</i>			2		2		
			<i>Tubuca rosea</i>	5	7	1		13		
			<i>Tubuca coarctata</i>	3	3	1		7		
			<i>Ocypode ryderi</i>	12	1			13		
			<i>Austruca triangularis</i>	3	3			6		
		Arachnida	Araneidae	<i>Argiope sp</i>	1	2		2	5	
				<i>Leucauge sp</i>		2		1	3	
			Oxyopidae	<i>Oxyopes javanus</i>			2		2	
	Insecta	Lycaenidae	<i>Zizina Otis</i>	4			5	9		
		Nymphalidae	<i>Acraea violae</i>	2			6	8		
		Libellulidae	<i>Crocothemis selvilia</i>	5			4	9		
		Chrysomelidae	<i>Aspidomorpha deusta</i>		2		1	3		
		Apidae	<i>Apis sp</i>	1	2		1	4		
		Vespidae	<i>Polistes sp</i>		1		1	2		
		Erebidae	<i>Amata huebneri</i>				1	1		
		Pentatomoidae	<i>Euthyrhynchus sp</i>		1		2	3		
		Dinidoridae	<i>Cyclopelta obscura</i>		1		2	3		
		Mantidae	<i>Mantis religiosa</i>	2	2		2	6		
		Mollusca	Gastropoda	Ellobiidae	<i>Ellobium sp1</i>	4				4
					<i>Ellobium sp2</i>	4				4
				Onchidiidae	<i>Paraonchidium sp1</i>	1				1
<i>Paraonchidium sp2</i>	5							5		
Potamididae	<i>Telescopium</i>			4	3			7		
	<i>Cerithidea obtuse</i>				5			5		
	<i>Cerithidea sp</i>					10	10			
Littorinidae	<i>Echinolittorina sp.</i>				1		1			
Assimineidae	<i>Assimineia sp.</i>		3	32			35			
Bivalvia	Mytilidae		<i>Perna sp</i>			2		2		
		Σ	72	82	20	40	214			

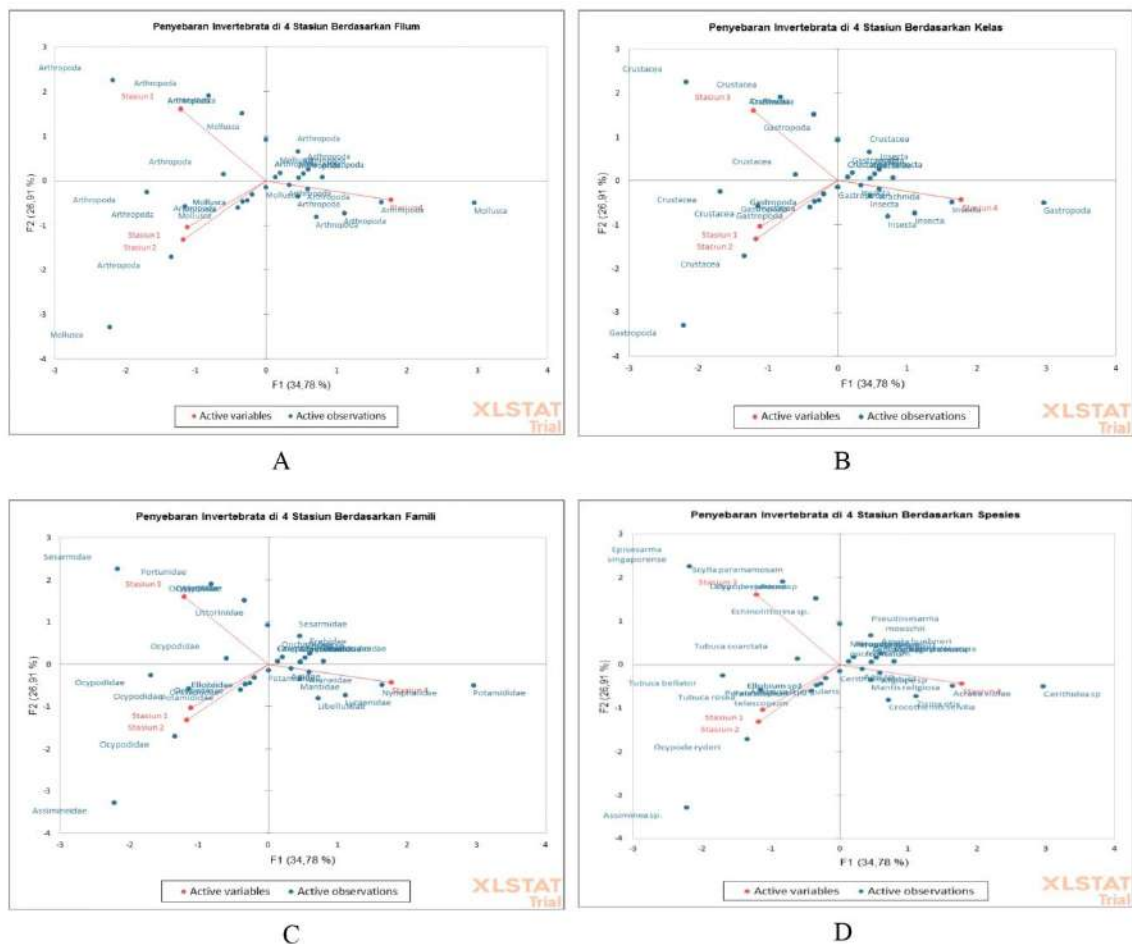


Fig. 2: Distribution of macroinvertebrates at 4 stations in the Wonorejo Mangrove Area based on: A. Phylum, B. Class, C. Family, D. Species.

Table 2: Average Metal and Nutrient Test Results in Water and Soil of Wonorejo Mangrove Area.

Station	Test Result of Soil Metal		Test Result of Nutrient		Test Result of Water Metal	
	Pb [mg.kg ⁻¹]	Cd [mg.kg ⁻¹]	Org-C [g.100g ⁻¹]	N [g.100g ⁻¹]	Pb [mg.L ⁻¹]	Cd [mg.L ⁻¹]
1	0.402±0.0169	0.220±0.0045	0.942±0.0979	0.071±0.0046	0.028±0.0056	0.008±0.0010
2	0.288±0.0298	0.194±0.0057	1,243±0.0766	0.080±0.0025	0.055±0.0133	0.005±0.0012
3	0.333±0.0059	0.109±0.0043	2,045±0.0787	0.116±0.0053	0.048±0.0137	0.006±0.0006
4	0.387±0.0129	0.170±0.0022	2.002±0.0299	0.129±0.0089	0.058±0.0025	0.003±0.0013

Note: Station 1 jogging track by the river; Station 2 riverside macroves; Station 3 estuary; Station 4 pond

Table 3: Average Ecological Data on Wonorejo Mangrove Area.

Station	Soil Moisture [%RH]	Soil pH	Soil Temperature [°C]	Air Humidity [%]	Air Temperature [°C]	CO ₂ [ppm]	Light Intensity (Lux)	Salinity [‰]
1	10	7	27,8	82%	31.15	472,2	310	10
2	10	7	29	75%	30	414	345	10
3	10	7,2	29	83%	29,6	413	617	27
4	10	7,2	30,2	78%	33	494	1800	10

Note: Station 1 jogging track by the river; Station 2 riverside macroves; Station 3 estuary; Station 4 pond

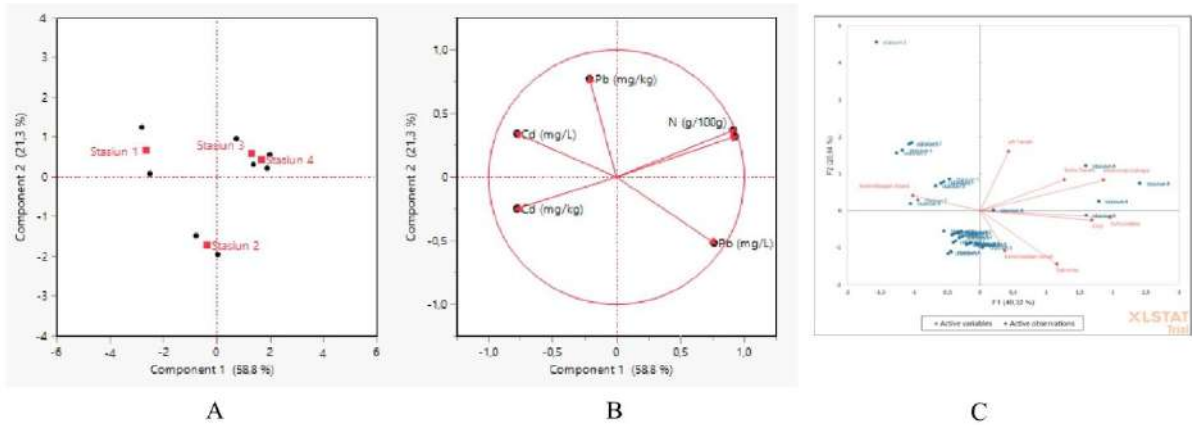


Fig. 3: PCA Graph of distribution of research station points based on metal and nutrient properties of soil and water mangrove: A. Projection of observation station points on the main component; B. Distribution of metal and nutrient soil and water mangrove properties in the main components; C. Classification of observation stations based on metal and nutrient properties of mangrove soil and water.

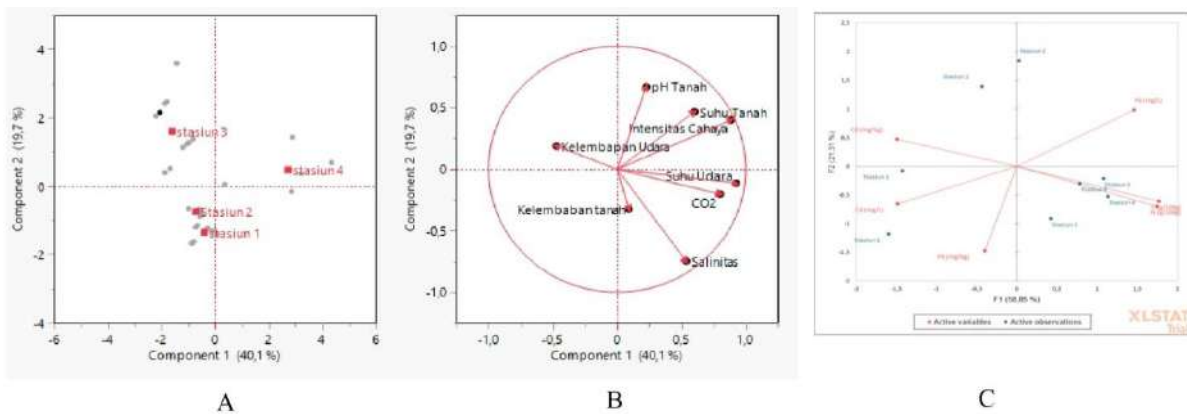


Fig. 4: PCA Graph distribution of research station points based on environmental ecological characteristics: A. Projection of observation station points on the main component; B. Distribution of environmental ecological characteristics in the main components; C. Observation station point classification based on environmental ecological characteristics.

intensity, soil pH, and salinity. Station 3 has environmental ecological characteristics such as soil pH, temperature, air temperature, CO₂, light intensity, and salinity. Meanwhile, Station 4 has environmental and ecological characteristics of soil temperature, air temperature, CO₂, light intensity, and air humidity.

DISCUSSION

The Wonorejo mangrove forest area in Surabaya is a wetland area dominated by mangrove forests and traditional ponds with high diversity potential (Akhadah et al. 2019). This area is not only managed for Mangrove Ecotourism, silvofishery ponds, and traditional ponds (Wijaya & Sanjaya 2021) but is also a spawning location, nursery, and a place for foraging, spawning, rearing, and sheltering for several species of macroinvertebrates.

Based on the study results, Station 1 was dominated by macroinvertebrates of the species *Ocypode ryderi*, *Crocothemis selvilia*, *Leucauge* sp, *Aspidomorpha deusta*, *Paraonchidium* sp2, and *Cerithidea obtuse* with the largest distribution in the species *Ocypode ryderi*. *Ocypode ryderi*, or Ghost Crab, is a nocturnal biota commonly found in tropical and subtropical regions. It has a carapace size ranging from 2.375-2.4 cm and lives by making burrows in the sand. These ghost crabs live in the highest tide areas, and when the sea water is high, they can control the water that enters their burrows (Elfandi et al. 2018).

The existence of this crab population is strongly influenced by the condition of the beach, which is its habitat. Unspoiled beaches usually have ghost crabs because the food chain process is still maintained. Polluted beaches will rarely find ghost crabs (Elfandi et al. 2018). The negative effects caused

by exposure to heavy metals in animals are in the form of disturbances in the rate of feeding, respiration, reproduction processes, morphological abnormalities, behavior, and functions of body organs, which will ultimately have an impact on the distribution of a species (Marbun et al. 2013).

Based on the results of the study, at the location where this species was found (Station 1), it has strong characteristics of Metals and Soil Nutrients and Mangrove Water, namely Cd (mg.kg^{-1}), organic C (g.100g^{-1}), N (g.100g^{-1}), Pb (mg.L^{-1}), Cd (mg.L^{-1}). However, the presence of these heavy metals did not affect the distribution of Ghost Crab (*Ocypode ryderi*) because the number was still abundant at this station, so it can be seen that this species can adapt to heavy metal stress and can be a bioindicator. This aligns with Stelling Wood's (2016) statement that Ghost Crab is widely used as an ecological indicator for the environment.

Based on the results of PCA analysis, Station 1 has strong environmental ecology characteristics, including soil pH and salinity, which are negatively correlated. This means that the higher the soil pH, the lower the salinity. The degree of acidity (pH) is a limiting factor that can affect the survival of macroinvertebrates if it is too acidic or alkaline. At this station, the soil pH value is 7 and is classified as a neutral pH suitable for macroinvertebrate life, including mollusks and arthropods. This is in accordance with Fatmala et al. (2017) statement that ground surface arthropods can live well and must be in a neutral pH range between 6-8 (Fatmala et al. 2017). In addition, this station has a salinity value of 10‰ which is considered good and in line with the statement of Riry et al. (2020) that the salinity level of mangrove waters is (0.5-35 ppt) so that it can support the survival of macroinvertebrates.

Stations 2 and 3 are dominated by the same species, namely *Scylla paramamosain*, *Pseudosesarma moeschii*, *Ocypode mortoni*, *Oxyopes javanus*, *Telescopium telescopium*, *Echinolittorina* sp., *Assiminea* sp., and *Perna* sp. However, Station 2 has the largest distribution of *Assiminea* sp. while Station 3 is *Scylla paramamosain*. *Assiminea* sp has the characteristics of a short upper shell with a blunt end of the shell, a round bottom, reddish body color, with a body size ranging from 0.5 cm (Achsana 2019). This species belongs to the mollusk phylum, which can be used as a bioindicator of the condition of the mangrove ecosystem (Sani et al. 2020). This is in accordance with the results of the study that the distribution of *Assiminea* sp was not affected by the presence of heavy metals in station 2, which was known at this station to have strong Metal and Nutrient characteristics of Soil and Mangrove Water, namely Pb (mg.kg^{-1}).

Scylla paramamosain, or the mud crab, has a brown carapace characteristic. The outer chela is orange. There are six sharp spines on the frontal margin, one spine is not sharp

on the carpus and two blunt spines on the right side of the chela. Mangrove crabs have a wide distribution area and can tolerate and adapt strongly to mangrove forests (Gita, 2016). Mangrove crabs can be a bioindicator because mangrove crabs have habitats in shallow coastal areas with mud substrate (Susilo et al. 2017). Based on research conducted by Noviani et al. (2020), mangrove crabs can accumulate Pb metal of $0-0.053 \text{ mg.kg}^{-1}$, so they have the potential to become metal pollution bioindicators. This is in accordance with the results of the study that the distribution of *Scylla paramamosain* at station 3 has the highest value even though, based on heavy metal testing, this station has strong Metal and Nutrient characteristics of Soil and Mangrove Water, including Cd (mg.kg^{-1}), organic C (g.100g^{-1}), N (g.100g^{-1}), Pb (mg.L^{-1}), Cd (mg.L^{-1}) but the presence of these metals did not affect the population of *Scylla paramamosain*.

Based on PCA analysis, it is known that stations 2 and 3 almost have similarities in the dominant environmental and ecological characteristics, including soil temperature, air humidity, air temperature, CO₂, light intensity, soil pH, and salinity. However, the characteristic of air humidity is only at station 2. This station's air humidity value is quite high, namely 75%RH. Fatmala et al. (2017) state that high humidity is better for soil animals than low humidity. However, ground surface arthropods may die or migrate to other places in very high humidity conditions. Low humidity will stimulate soil surface arthropods to move to a place with optimum humidity, thus allowing the formation of groups. In addition, air humidity has a negative correlation with air temperature and CO₂. The lower the temperature and CO₂, the higher the humidity, and vice versa. This is because low temperatures result in higher water activity in the air, so air humidity becomes high.

Station 4 is dominated by macroinvertebrates from *Episesarma singaporense*, *Tabuca*, *Zizina otis*, *Acraea violae*, *Argiope* sp, *Polistes* sp, *Amata huebneri*, *Euthyrhynchus* sp, *Cyclopelta obscura*, *Mantis religiosa*, and *Cerithidea* with the distribution of species *Cerithidea* sp. found to be more abundant than other species. *Cerithidea* sp. has a habitat in the tropics with moderately warm temperatures (28-30 °C), in shallow waters, and lives on the bottom of muddy substrates and estuarine environments. Based on research by Wahyudi et al. (2015), *Cerithidea* sp. can accumulate Pb of $1,900 \pm 0.393$ ppm and has the potential as a bioaccumulator and bioindicator. This is in accordance with the results of the study at the location where this species was found (Station 4) has strong characteristics of Metals and Soil Nutrients and Mangrove Water, namely Cd (mg.kg^{-1}), organic C (g.100g^{-1}), N (g.100g^{-1}), Pb (mg.L^{-1}), Cd (mg.L^{-1}). *Cerithidea* sp. will accumulate these metals along with the entry of food;

however, the presence of these heavy metals does not affect the distribution of *Cerithidea* sp. because their numbers are still abundant at this station and other stations; it can be seen that these species can adapt to heavy metal stress and can be a bioindicator of metal pollution.

Based on the research results, Station 4 has dominant environmental and ecological characteristics: soil temperature, air temperature, CO₂, light intensity, and humidity. All these characteristics, except humidity, are positively correlated with each other. This means that the higher the soil temperature, the higher the air temperature, and vice versa. The higher the CO₂, the higher the air temperature, and vice versa. The higher the light intensity, the higher the soil temperature, and vice versa. The higher the light intensity, the higher the air temperature, and vice versa., the higher the light intensity, the higher the CO₂, and vice versa.

Soil temperature can affect the sustainability of ecosystems. Soil animal life is also determined by soil temperature. Extremely high or low temperatures can kill ground animals. Soil temperature generally also affects soil animals' growth, reproduction, and metabolism. Each type of soil animal has an optimum temperature range. This activity is very limited at temperatures below 10°C. The optimum beneficial soil biota activity rate occurs at 18-30°C (Husamah et al. 2017). In addition, according to Burhanuddin et al. (2019), the temperature range of 26-31 °C is still within the tolerance limit of macroinvertebrate life. This is in accordance with the study's results that the average values of soil and air temperatures at the location were 29 °C and 30.9 °C, which is still quite good for biota.

This study's average carbon dioxide or CO₂ value was 448.3 ppm, which is still considered good and permissible. This is in accordance with the statement of Kurniawan (2019) the permissible CO₂ threshold value according to OSHA is 500 ppm. CO₂ does not cause harmful health effects if it is at a concentration above 550 ppm but if it is above 800 ppm, CO₂ can indicate a lack of fresh air.

The population of soil macrofauna will decrease with the increasing intensity of incoming light. The intensity of sunlight the ecosystem receives is a critical determinant of primary productivity, which can affect species diversity and nutrient cycles. The high and low intensity of sunlight is influenced by the density of the canopy and the location of the angle of incidence of sunlight. The higher the canopy density of a protective plant and the denser (density and large/wide) canopy, the lower the intensity of sunlight that can enter the soil surface (Qomariyah et al. 2021). This study's average light intensity value is 768Lux which is still classified as a good light intensity.

Based on this research, it can be seen that from all stations, *Assiminea* sp. (phylum mollusca) can be the best candidate for metal bioindicator because of its appearance in all locations where soil and water have been contaminated with Pb and Cd metals without affecting their life. This is in accordance with Marett et al. (2019) that mollusks can be used as bioindicators of heavy metals because of their slow mobility, the tendency to settle, and feeding methods that filter suspensions, making them easy to adapt and accept any environmental changes that occur.

CONCLUSION

Based on this research, it can conclude that there are variations in the type and distribution of macroinvertebrates stressed by Pb and Cd in the Mangrove Area of Surabaya. Station 1 is dominated by *Ocypode ryderi*, station 2 *Assiminea* sp., station 3 *Scylla paramamosain*, and Station 4 *Cerithidea* sp. with the characteristics of Metals and Soil and Water Nutrients at stations 1, 3, and 4, namely Cd (mg.kg⁻¹), organic C (g.100g⁻¹), N (g.100g⁻¹), Pb (mg.L⁻¹), Cd (mg.L⁻¹) while Station 2 only Pb (mg.kg⁻¹). *Assiminea* sp. (phylum Mollusca) can be the best metal bioindicator candidate because of its appearance in all locations where soil and water have been contaminated with Pb and Cd metals without affecting their life.

ACKNOWLEDGEMENT

Thank you to the head of the university and faculty from Universitas Negeri Surabaya for the financial support.

REFERENCES

- Achsan, N. 2019. Study of Macroinvertebrates Community Structure and Environmental Quality in the Mangrove Ecosystems of Sidoarjo Mud Island, East Java. Dissertation. Universitas Islam Negeri Sunan Ampel Surabaya
- Akhadah, N., Sanora, G.D., Nurlaili, R.A. and Ambarwati, R. 2019. Diversity and abundance of birds in the mangrove area of Wonorejo Surabaya. *Biol. Nat. Sem.*, 9: 237-242.
- Budijastuti, W. 2016. Candidate Types of Earthworms Potentially as Bioindicators of Heavy Metals Pb and Cr Based on Abundance, Morphometric Structure, and Cysteine Content. Retrieved from <http://lib.unair.ac.id> (Accessed on 23 July 2022).
- Burhanuddin, I.I., Setyobudiarso, H and Sudiro. 2019. Study of Macroinvertebrate Biomonitors and Lake Sentani Water Quality Status, Jayapura Regency. Proceedings of the National Seminar on Sustainable Infrastructure in the Industrial Revolution Era 4.0, Malang. 55-64. [Indonesian]
- Diantari, N.P.R., Ahyadi, H., Rohyani, I.S. and Suana, I.W. 2017. Diversity of Ephemeroptera, Plecoptera, and Trichoptera insects as bioindicators of water quality in the Jangkok River, West Nusa Tenggara. *J. Entomol., Indo.*, 14(3): 135-142.
- Elfandi, T., Adi, W. and Syari, I.A. 2018. The density of ghost crabs (*Ocypode*) at Batu Bedaun Beach and Air Anyir Beach of Bangka. *Akuatik J. Sumb. Pera.*, 12(1): 10-17.

- Fatmala, L., Kamal, S. and Agustina, E. 2017. Diversity of soil surface arthropods under pine (*Pinus merkusii*) vegetation stands Tahura Pocut Meurah Intan. Proceed. Nat. Bio. Sem., 63: 2115
- Gita, R.S.D. 2016. Mangrove crab diversity (*Scylla* spp.) in Alas Purwo national park. J. Biol. Pemb. Biol., 1(2): 146-161.
- Husamah, R., Sisti, A. and Hudha, A.M. 2017. Soil Animal Ecology (Theory and Practice). Penerbit Universitas Muhammadiyah, Malang.
- Kurniawan, A. 2019. Basics of Environmental Quality Analysis. Wineka Media, Malang.
- Marbun, L.R. and Widyorini, N. 2013. Diversity and abundance of macrozoobenthos substrates in based metal lead (Pb) in the coast of Jakarta bay. Journal of Management of Aquatic Resources. 2(2): 54-59.
- Maretta, L., Widiani, G.N. and Septiana, N.I. 2019. Mollusc diversity on the White Sand Beach, South Lampung. Biotropika: J. Trop. Biol., 7(3): 87-94.
- Mauriza, R., Ashari, M. and Yahya, H. 2020. Test the effectiveness of the shells of gold conch (*Pomacea canaliculata* L.) as a biosorbent in absorbing metal lead (Pb). J. Phi Pend. Fisik. Terap., 1(3): 25-32.
- Noviani, E., Sulistiono, K. and Samosir, A.M. 2020. Heavy metal (Pb, Hg) extent in mud crab (*Scylla serrata*) in Cengkong Coastal Waters, Banten Bay, Indonesia. Omni-Akuatika, 16(2): 108-115.
- Nur, Fatmawati 2013. Cadmium (Cd) heavy metal phytoremediation. Biogenesis, 1(1): 74-83.
- Qomariyah, N., Nugroho, A.S. and Hayat, M.S. 2021. Soil macrofauna in horticultural land, Losari Village, Sumowono District, Semarang Regency. Quagga: J. Pend. Biol., 13(1): 68-73.
- Riry, K.Z., Prihatmo, G. and Kisworo, M. 2020 Macroinvertebrate Diversity in the Mangrove Ecosystem in Lempong Pucung Hamlet, Kampung Laut District, Cilacap Regency. Proceedings of the National Biology Seminar in the Gowa COVID-19 Pandemic Era, 19 September 2020. [Indonesian]
- Rohyani, I.S and Farista, B. 2013. The diversity of soil arthropods at Kerandangan protected forest and natural park in West Lombok. J. Biol. Trop., 13(1): 39-44.
- Sani, L.H., Candri, D.A., Ahyadi, H. and Farista, B. 2020. Mollusk community structure in natural mangrove areas and south coastal rehabilitation of Lombok Island. J. Trop. Biol., 20(1): 139-147.
- Sari, S.H.J., Kirana, J.F.A. and Guntur. 2017. Analysis of dissolved heavy metals Hg and Cu in Wonorejo Coastal Waters, East Coast of Surabaya. J. Pend. Geogr., 22(1): 1-9.
- Stelling Wood T. 2016. Responses of Ghost Crabs and Other Scavengers to Habitat Modification Of Urban Sandy Beaches. Thesis. Master of Philosophy at The University of New South Wales School of Biological, Earth and Environmental Sciences. Sydney.
- Susilo, A., Setyawati, T.R. and Yanti, A.H. 2017. Morphometry of mangrove crab (*Scylla* spp.) in the Mutusan River Estuary mangrove forest area, Sambas Regency. Protobiont, 6(1): 53-58.
- Syachroni, S.H. 2017. Analysis of cadmium (Cd) heavy metal content in rice fields in Palembang City. SYLVA, 6(1): 23-29
- Wahyudi, R.A., Purnomo, T. and Ambarwati. R. 2015. The level of leads (Pb) and population density of *Cerithidea* sp. on the southern shores of Bangkalan Madura, East Java. LenteraBio, 4(3): 174-179.
- Wijaya, N.I, Sanjaya, R. and Nuhman. 2019a. Influence of Waters in Silvofishery Ponds on Wonorejo Mangroves That Contaminated by Heavy Metals Pb, Cd, and Cu toward Aquaculture Animals. Proceedings of the 7th- International Seminar on Ocean and Coastal Engineering, Environmental and Natural Disaster Management (ISOCEEN). December 2019, pp. 207-211.
- Wijaya, N.I. and Sanjaya, R.F. 2021. Mangrove density on Pb, Cu, and Cd metal content in milkfish meat (*Chanos chanos*) at Mangrove Wonorejo, Surabaya. J. Pert.Terp., 9(2): 150-161.
- Wijaya, N.I., Trisyani, N. and Sulestiani, A. 2019b. Potential development of mangrove crab silvofishery cultivation (*Scylla serrata*) in the Wonorejo Mangrove Area, Surabaya. J. Forest Res. Nature Conserv., 16(2): 173-189.
- Wulansari, D.F. and Kuntjoro, S. 2018. Gastropod diversity and its role as bioindicator of heavy metal lead (Pb) at Kenjeran Beach, Bulak District, Surabaya City. LenteraBio, 7(3): 241-247.



Assessment of Sodium Chloride (NaCl) Induced Salinity on the Growth and Yield Parameters of *Cichorium intybus* L.

A. Khan*† , A. A. Khan* , S. Samreen*  and M. Irfan** 

*Lab No. 41, Ecology and Environmental Botany Laboratory, Department of Botany, Aligarh Muslim University, Aligarh, U.P., India

**Department of Botany, Sanskriti University, Mathura, U.P., India

†Corresponding author: A. Khan; akhan9361@gmail.com

Nat. Env. & Poll. Tech.
Website: www.neptjournal.com

Received: 17-09-2022
Revised: 02-10-2022
Accepted: 04-11-2022

Key Words:

Cichorium intybus L.
Sodium chloride
Chlorophyll
Proline

ABSTRACT

The present study was done on the hypothesis that excess sodium chloride (NaCl) in the soil decreases the growth and yield of *Cichorium intybus* L. To investigate this hypothesis, a pot experiment was conducted in which chicory seeds were sown in garden soil-filled earthen pots and treated with three different doses of sodium chloride (45, 75, and 105 mM kg⁻¹ soil) except the control, and each treatment was replicated three times. The results revealed that all the saline treatments significantly ($p \leq 0.05$) reduced the vegetative (including root and shoot length, dry weight, number of leaves, leaf area, number of branches, and photosynthetic pigments) and reproductive (mean fruit number/plant, mean seed number/fruit, and total seed yield/plant) growth parameters of *Cichorium intybus*. On increasing NaCl concentration in the soil, chlorophyll content significantly ($p \leq 0.05$) decreased while proline content in the fresh leaves increased significantly ($p \leq 0.05$). From the results, it is concluded that *Cichorium intybus* L. can tolerate a moderate level of sodium chloride stress (45-75 mM NaCl kg⁻¹ soil) but is sensitive to high doses of sodium chloride stress (105 mM NaCl kg⁻¹ soil).

INTRODUCTION

Plants tolerate several biotic and abiotic stresses of the environment for their survival (Teshome et al. 2020). Drought, salinity, flood, and extreme cold are the major abiotic stresses that plants have to tolerate (Gidhay Adhanom 2019, Nazir et al. 2019). Climate change increases the intensity of these abiotic stresses, which affect the survival and yield of plants (Chaudhry & Sidhu 2021, Corwin 2021, Zandalinas et al. 2021). Among these abiotic stresses, salinity is rapidly increasing in the environment and affects the fertility of agricultural lands (Hassani 2021, Ullah et al. 2021).

Soil salinity is a measure of salt content in the soil that is commonly expressed as electrical conductivity (EC) and measured in deci Siemens (dS). However, to express salt concentrations, molarity units, such as millimoles per liter, are frequently used (mmol_c L⁻¹). Contrarily, sodicity is defined in terms of the sodium adsorption ratio (SAR)

or the exchangeable sodium percentage (ESP). Saline soil has an EC greater than or equal to 4 deci Siemens per meter (dS m⁻¹) at 25°C; A sodic soil has a SAR greater than 13 (mmol_c L⁻¹) or an ESP of 15 or more, and saline-sodic soils are those with EC greater than or equal to 4 dS m⁻¹ or 40 mM NaCl, and SAR > 13 (mmol_c L⁻¹) (Stavridou et al. 2017). Furthermore, few researchers considered soils with lower ESP values (6-8%) as sodic soils (Mohanavelu et al. 2021; Stavi et al. 2021). Soil salinization is the process through which salt concentration in the soil increases to levels that have an impact on environmental health, agricultural productivity, a farmer's financial stability, and quality of life (Kumar & Sharma 2020). Various anthropogenic activities, such as irrigation without proper drainage planning, increase saline areas around the world and reduce agricultural land available for crop production (Gidhay Adhanom 2019). Besides this, the domestic and industrial discharge, enriched with various kinds of salts, in freshwater bodies contaminated the water of these freshwater bodies, and when the water of these freshwater bodies is used in irrigation, it increases the salinity of agricultural soil and reduces its fertility, ultimately decreasing growth and yield of the crops (Petropoulos et al. 2017, Dietz et al. 2021).

ORCID details of the authors:

Adnan Khan: <https://orcid.org/0000-0002-8789-6617>

Athar Ali Khan: <https://orcid.org/0000-0002-1692-860X>

Sayma Samreen: <https://orcid.org/0000-0002-8992-7800>

Mohd Irfan: <https://orcid.org/0000-0002-1232-9650>

Plants affected by saline toxicity showed poor growth and reduced crop/seed yield by a significant amount (Egamberdieva et al. 2019, El-Sabagh et al. 2021). Scientists from various countries are attempting to find plants that can survive in moderate-to-high saline soil without compromising growth and yield to combat the food shortage caused by climate change (Petropoulos et al. 2017). In general, NaCl-induced toxicity reduces plant growth by damaging root cells, resulting in a lack of water uptake and osmotic stress, increasing the pH of the soil (alkalization), which causes poor uptake of essential nutrients that come with the water in the plants, resulting in an imbalance of mineral nutrition (excess Na^+ ions decrease absorption of K^+ , NH_4^+ , and Ca^{++} ions, and excess Cl^- ions decrease absorption of NO_3^- ions Na^+ induced salinity also reduced transpiration and photosynthesis in the plants by disturbing the stomatal conductance, altering the enzymatic activities of photosynthesis, CO_2 availability in mesophyll cells, and modifications in chloroplast structure (Arshi et al. 2010, Petropoulos et al. 2017).

Cichorium intybus L. (Chicory) plant is a member of the family Asteraceae commonly known as chicory. It is widely distributed in Asia, Africa, Europe, and South America (Abbas et al. 2015, Aisa et al. 2020, Mavrina et al. 2021). Chicory plant contains compounds like alkaloids, coumarins, flavonoids, inulin, unsaturated sterols, sesquiterpene lactones, and vitamins (Jangra & Madan 2018, Aisa et al. 2020, Das et al. 2020). Fresh chicory leaves have a laxative property, while dried chicory root powder mostly contains inulin, a polymer of fructose, and root powder is mainly used in the adulteration of coffee (Abbas et al. 2015, Street et al. 2013). Chicory leaves and seeds are used in traditional medicines for the treatment of fever, diarrhea, jaundice, renal problems, and gallstones due to their pharmacological properties (Aisa et al. 2020, Mavrina et al. 2021, Choudhary et al. 2021) as well as found useful in bio-monitoring of various heavy metals in the environment (Aksoy 2008). Chicory is also used as a forage crop due to its high nutritive value, and anti-helmentic and laxative properties. It improves the milk yield of dairy livestock (Street et al. 2013, Piluzza et al. 2014).

India is the home of more than 1.32 billion people and is projected to become the most populated country in the world. This population rise poses challenges related to food security in India (Sharma et al. 2020; Kumar & Sharma 2020). In India, approximately 6.727 million hectares of land are salt-affected and classified into two types: sodic soils and saline soils. In India, Uttar Pradesh and Gujarat State have the most saline soils (71.2%) and sodic soils (35.6%), respectively. Areas of the Indo-Gangetic region of India that are affected by sodic soils originated when groundwater containing high levels of carbonates and bicarbonates is irrigated. This, along with the execution of canal irrigation projects without sufficient

drainage, has resulted in widespread salinity in India, which is expected to worsen with time (Kumar & Sharma 2020).

As a result, India must select and cultivate crops that can grow in saline or sodic soil. Therefore, the present research focused on evaluating the dose-dependent response of chicory to NaCl stress in terms of growth, biochemical (chlorophyll and proline contents), and yield parameters and is also helpful to determine the level of NaCl in the soil below which chicory can easily grow and provide a good yield.

MATERIALS AND METHODS

Study Area

Before initiating the experiment, soil samples were taken from several field beds to analyze the soil characteristics. All soil samples were analyzed at the Government Agriculture Farm's Soil Testing Laboratory in Aligarh, India. Table 1 lists the physicochemical characteristics of the soil utilized in the experiment.

Experimental work has been done in the natural greenhouse of the botany department of Aligarh Muslim University, Aligarh, India. Aligarh (27.88°N latitude and 78.08°E longitude) has a semi-arid and sub-tropical climate with sandy loam and alkaline soil. Most of the rainfall is received from July through September.

Plant Material and Experimental Design

Chicory seeds (*Cichorium intybus* L.) were procured from the herbal garden of Jamia Hamdard, New Delhi, and cleaned

Table 1: Physico-chemical characteristics of garden soil used in the study.

Characteristics	Observation/value
Color	Light Brownish
Texture	Sandy loam
CEC (meq. 100 g ⁻¹ soil)	3.20
pH	7.1
EC ($\mu\text{mhos.cm}^{-1}$)	312
Total organic carbon (%)	0.800
Nitrate nitrogen(NO_3N) g kg ⁻¹ soil	0.320
Phosphorus (P) g kg ⁻¹ soil	0.130
Potassium (K^+) mg.L ⁻¹	24.10
Magnesium (Mg^{2+}) mg.L ⁻¹	30.34
Sodium (Na^+) mg.L ⁻¹	13.45
Calcium (Ca^{2+}) mg.L ⁻¹	23.00
Bicarbonate (HCO_3^-) mg.L ⁻¹	20.28
Carbonate (CO_3^{2-}) mg.L ⁻¹	93.04
Sulphate (SO_4^{2-}) mg.L ⁻¹	19.10
Chloride (Cl^-) mg.L ⁻¹	34.55

with a 0.01% HgCl_2 solution, then washed three times with double-distilled water (DDW). Earthen pots of 12-inch size were autoclaved for 30 minutes after being filled with 3 kg of soil. Five to eight seeds were sown with proper spacing in each pot. Three plants were kept in each pot, and after germination, those were almost the same height and leaf number.

Plants were treated with 45, 75, and 105 mM NaCl kg^{-1} soil and were applied in the form of a dilute aqueous solution of sodium chloride (NaCl) when plants were 3 weeks old. Each treatment/dose was replicated three times. Control pots received no sodium chloride. Irrigation was carried out using tap water as required. The experiment was conducted in a simple randomized block design (SRBD). The plants were harvested at full maturity (170 DAS). The sampling of plants was done at the vegetative stage, 80 days after sowing (80 DAS) and at maturity (170 DAS) to estimate different growth and biochemical parameters.

Estimation of Vegetative and Reproductive Growth Parameters

The sampling of growth parameters was done at 80, and 170 days after sowing (DAS). Quantitative data for the following parameters were gathered, (a) Root and Shoot length (in cm); (b) Root and shoot dry weight (in g); (c) Mean leaf number plant^{-1} ; (d) Mean leaf area (cm^2); (e) Mean number of branches plant^{-1} ; (f) Mean fruit number plant^{-1} ; (g) Mean seed number fruit^{-1} ; (h) Mean seed number plant^{-1} . Three replicates were used for all measurements. A decrease or increase in NaCl -treated plants was calculated in comparison to the control.

For sampling, plants were harvested at two growth stages, the root-shoot junction was cut with precision, and the lengths of their shoot and root were estimated on a metric scale and expressed in centimeters. For estimating plant dry mass, samples were dried in an oven at 65-70°C for 72 hours. The dry biomass of the shoot and root of each plant was recorded on an analytical balance (Wensar Weighing Scales Limited, Lucknow, India) and expressed in grams. The total number of fully expanded leaves counted from three replicates of each treatment was divided by the sample size to obtain the mean leaf number of plant^{-1} . The graph paper method (Pandey & Singh 2011) was used to calculate the leaf area of mature leaves. Data obtained from three replicates were summed and divided by three to obtain the mean value of each remaining vegetative and reproductive parameter.

Estimation of Chlorophyll and Proline Contents

Using Arnon's method (Arnon 1949), the chlorophyll content of fresh leaf samples was estimated. The absorbance of the

prepared sample was read on a spectrophotometer (2700, Analytical Technologies Ltd., Labtronics, India) at 645 and 663 nm for chlorophyll against the blank (80% acetone). The Bates et al. (1973) method was used to estimate the proline content of the fresh leaves. Finally, the prepared sample was transferred to the ice bath and the mixture was extracted with toluene and read at 520 nm on a spectrophotometer (2700, Analytical Technologies Ltd., Labtronics, India) using L-proline as a standard.

Statistical Analysis

One-way analysis of variance (ANOVA) of data was done by using statistical software R ver. x64-4.1.2 (package library, Agricolae). To determine the significance of the difference of means at $P \leq 0.05$, Duncan's multiple range test (DMRT) was performed with the same software.

RESULTS

Vegetative Growth Parameters

All treatments except control caused a significant reduction in root and shoot length, root and shoot dry weight, mean leaf number, mean leaf area, and mean number of branches at both sampling stages (80 and 170 DAS). 105 mM NaCl kg^{-1} soil treatment caused the highest reduction of 50% and 39% in root length, 56% and 40% in shoot length, 41% and 39% in root dry weight, and 48% and 43% in shoot dry weight, 50% and 28% in mean leaf number, 41% and 37% in mean leaf area, and 41% and 29% in the mean number of branches over control at 80 DAS and 170 DAS, respectively (Table 2).

Chlorophyll and Proline Content

All treatments except the control caused a significant decrease in the photosynthetic pigments (chlorophyll a, chlorophyll b, total chlorophyll) and a significant increase in proline content at both sampling stages (80 and 170 DAS). 105 mM NaCl kg^{-1} soil treatment caused the highest decrease of 41% and 23% in chlorophyll a, 42% and 29% in chlorophyll b, and 42% and 29% in total chlorophyll content over control at 80 DAS and 170 DAS respectively (Fig. 1a-f). The same treatment caused the highest increase of 114% and 136% in proline content over control at 80 DAS and 170 DAS respectively (Fig. 2a and b).

Reproductive Growth and Yield Parameters

Plants treated with 45, 75, and 105 mM NaCl kg^{-1} soil showed a significant ($P \leq 0.05$) reduction of 08%, 17%, and 25% in fruit yield per plant over control at the harvesting stage or 170 DAS. Plants treated with the same doses of NaCl resulted in a statistically significant ($P \leq 0.05$) reduction of 05%, 10%,

Table 2: Effects of different treatments of Sodium Chloride (45, 75 and 105 mM NaCl kg⁻¹ soil) on growth and biochemical parameters of chicory at 80 DAS and 170 DAS.

<i>Cichorium intybus</i> L.	Different treatments of NaCl mM kg ⁻¹ of soil (80 DAS)					Different treatments of NaCl mM kg ⁻¹ of soil (170 DAS)					
	CONTROL	45 mM	75 mM	105 mM	CONTROL	45 mM	75 mM	105 mM			
Parameters (80 DAS)											
Root Length (cm)	20.73±1.65a	16.30±1.67ab	13.63±1.40bc	10.27±1.07c	26.73±1.97a	23.33±1.76ab	19.50±1.61bc	16.30±1.57c			
Shoot Length (cm)	74.50±6.21a	55.07±5.90b	42.67±3.84bc	32.5±3.40c	140.60±12.11a	117.00±10.39ab	105.33±7.62bc	84.33±6.69c			
Root Dry Weight (g)	1.13±0.12a	0.86±0.07ab	0.75±0.07b	0.66±0.08b	4.95±0.41a	4.28±0.33ab	3.68±0.20bc	3.00±0.29c			
Shoot Dry Weight (g)	4.00±0.23a	2.92±0.24b	2.45±0.23bc	2.06±0.22c	15.57±1.37a	12.90±1.24ab	11.00±1.15bc	8.80±0.81c			
Number of branches	4.00±0.57a	3.33±0.33ab	3.00±0.57ab	2.33±0.33b	8.00±0.58a	7.00±0.58ab	6.33±0.33b	5.67±0.33b			
Number of Leaves	43.00±4.62a	34.33±4.63ab	28.00±4.61ab	21.33±4.09b	80.00±5.77a	71.67±6.06ab	63.00±7.0ab	57.33±5.21b			
Leaf area (cm ²)	45.42±5.13a	36.08±3.49ab	31.33±2.60b	26.50±2.45b	76.33±7.74a	65.00±5.51ab	58.00±6.43ab	48.00±3.46b			

Data represent the mean and standard error of three replicates. Different letters indicate significant differences between treatments at $p < 0.05$, ($n = 3$) through the DMRT test.

and 14% in seed yield per fruit over control. Plants treated with 45, 75, and 105 mM NaCl kg⁻¹ soil caused a maximum significant ($P \leq 0.05$) reduction of 13%, 26%, and 35% in seed yield per plant over control at the harvesting stage or 170 DAS (Table 3).

DISCUSSION

Along with sunlight, ample water and nutrient supply are required for proper plant growth (El-Ramady et al. 2014, Ahanger et al. 2016, Xu et al. 2021). The root is the first organ that has to face salt stress in the soil (Arshi et al. 2010, Bhatt et al. 2015, Chaudhry & Sidhu 2022). Excess sodium ion (Na⁺) in the soil affects the soil texture; it increased pH (alkalization), which is produced by the presence of HCO₃⁻ and CO₃⁻² and decreases the availability of organic matter and essential elements or ions to the roots, causing ion imbalances by inducing competition of Na⁺ with K⁺ and Ca⁺⁺ (nutrient deficiency) and Cl⁻ with NO₃⁻² (Stavi et al. 2021). Salinity also reduces nutrient availability to crops or ion toxicity (salt stress) by inducing Na⁺ accumulation in the cytoplasm, or a combination of these factors reduces cell division and cell expansion in root and shoots, resulting in a decrease in root and shoot growth and biomass (Arshi et al. 2010, Upadhyay et al. 2012, Bhatt et al. 2015, Hafez et al. 2021). It was earlier reported that excess NaCl reduced leaf expansion, cell division, and cell elongation by reducing water entrance in the cell, affecting water balance (osmotic stress) in the plants, resulting a decrease in vegetative and reproductive growth parameters. Same results are found in the present study (Table 2, Table 3, Fig. 1a-f, Fig. 2a and b) (Jaleel et al. 2008, Machado & Serralheiro 2017, Hafez et al. 2021).

The current study discovered that a decrease in photosynthetic parameters of chicory was associated with Na⁺ and Cl⁻ ions-induced phytotoxicity at both sampling stages and that it increases as NaCl concentration in the soil increases (Fig. 1a-f). NaCl stress decreases the CO₂ availability in the mesophyll cells by disturbing stomatal conductance, also producing reactive oxygen species (ROS) leading to oxidative stress which disrupts the activities of enzymes involved in photosynthesis like RuBP Carboxylase/oxygenase, damages chlorophyll structure by decreasing tocopherol content, protectant of chlorophyll in the cytoplasm (Machado & Serralheiro 2017, Hafez et al. 2021). Moreover, Na⁺ and Cl⁻ ions accumulation (ionic stress) in the cytoplasm of plant cells damaged the chloroplast structure, causing modifications in the composition of the thylakoid membrane and other pigments resulting in the inhibition of electron transport (Singh et al. 2020). NaCl stress also decreases the rate of photosynthesis by promoting

Table 3: Effects of different treatments of Sodium Chloride (45, 75 and 105 mM NaCl kg⁻¹ soil) on yield parameters of chicory at 170 DAS.

<i>Cichorium intybus</i> L.	Different treatments of NaCl mM kg ⁻¹ of soil (170 DAS)			
Parameters (170 DAS)	Control	45 mM	75 mM	105 mM
Number of fruits (heads)	75.00±5.51a	68.67±4.33ab	61.67±2.60ab	56.00±4.73b
Seeds per fruit (head)	40.33±2.03a	38±1.53ab	36±1.15ab	34.67±1.20b
Seeds per plant	3025.00±73.98a	2609.33±71.27b	2220.00±24.25c	1941.33±100.37d

Data represent the mean and standard error of three replicates. Different letters indicate significant differences between treatments at $p < 0.05$, ($n = 3$) through DMRT test.

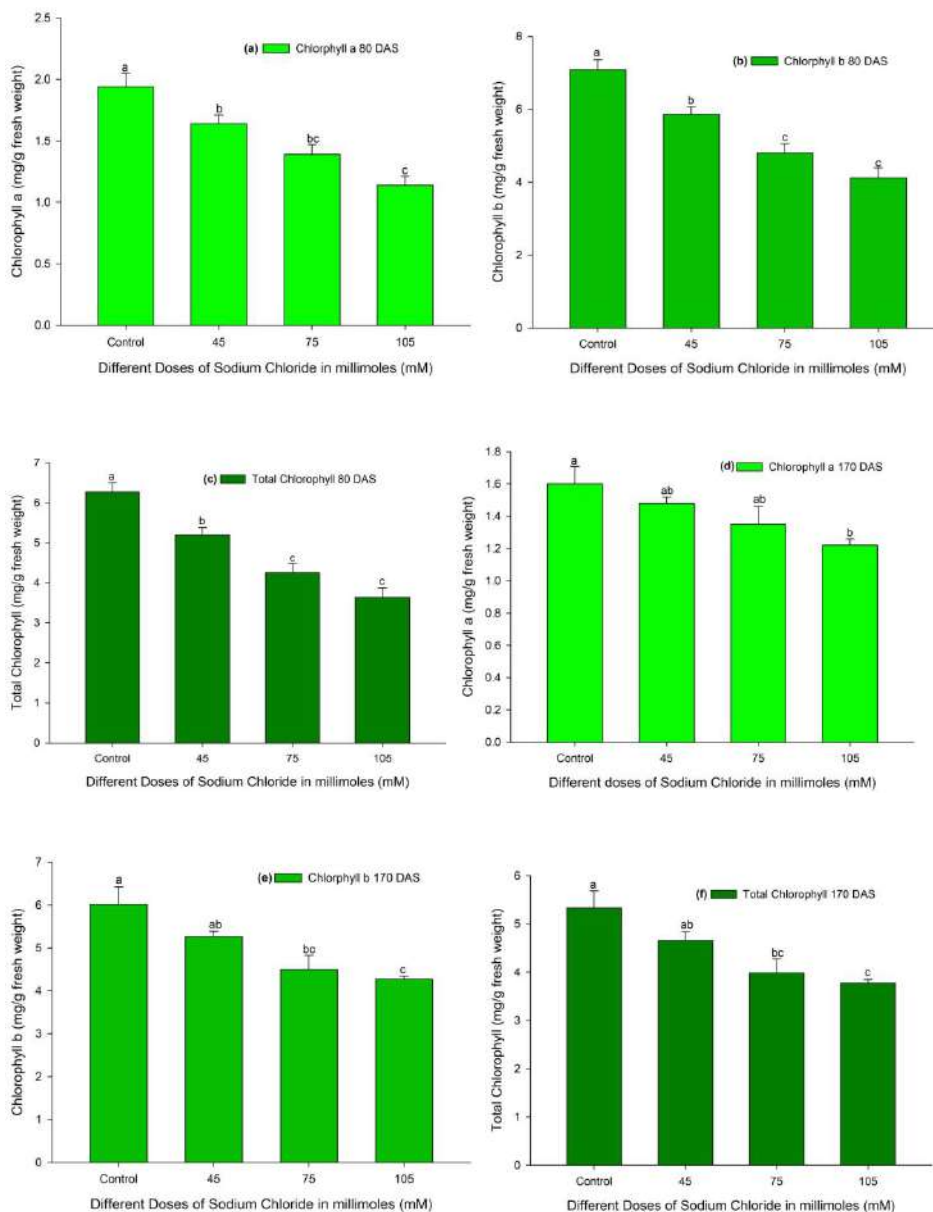


Fig. 1 a-f: Effects of different treatments of Sodium Chloride (45, 75 and 105 mM NaCl kg⁻¹ soil) on chlorophyll content (a, b and total) of chicory at 80 DAS and 170 DAS. Data represent the mean and standard error of three replicates. Different letters above the bars indicate the significant differences between treatments at $p < 0.05$, ($n = 3$) through the DMRT test.

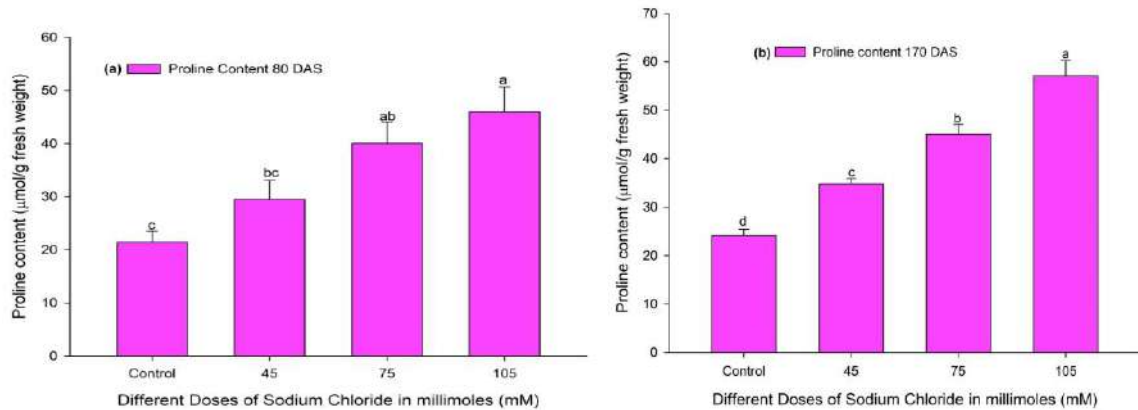


Fig. 2 a and b: Effects of different treatments of Sodium Chloride (45, 75 and 105 mM NaCl kg⁻¹ soil) on proline content in fresh leaves of chicory at 80 DAS and 170 DAS. Data represent the mean and standard error of three replicates. Different letters above the bars indicate the significant differences between treatments at $p < 0.05$, ($n = 3$) through the DMRT test.

stomatal closure by reducing K⁺ ions concentration in the cell. Scientists discovered similar results in plants such as Cassia, Senna, Catharanthus, Oats, Millets, and Maize at various salinity levels (Arshi et al. 2006, Jaleel et al. 2008, Bhatt et al. 2015, Hafez et al. 2021).

Plants accumulate a high amount of proline in their organs/tissues to maintain osmotic balance and prevent cell membrane leakage to survive in any abiotic stress condition, such as salinity (Monteoliva et al. 2014). A significant increase in proline content was recorded in chicory grown under different levels of NaCl stress (Fig. 2a and b) at both sampling stages, suggesting that NaCl stress has imbalanced the osmotic equilibrium in chicory leaves. Earlier studies on chicory like Arshi et al. (2010), Sergio et al. (2012) and Petropoulos et al. (2017) confirmed that increasing NaCl stress increased proline contents in the leaves of the chicory plants, which is the result of an increase in protein degradation of plant tissues (Monteoliva et al. 2014). Leaf area plays an important role in biomass accumulation in plants, and a decrease in leaf area reduces the rate of photosynthesis leading to a lesser amount of biomass production in plants (Weraduwege et al. 2015). In this experiment, the significant ($p \leq 0.05$) decrease (Table 2, Fig. 1a-f, Fig 2a and b) in vegetative growth, leaf area, branching, and biomass of chicory by the lowest to highest treatment treatment of NaCl stress, i.e., 45 to 105 mM NaCl Kg⁻¹ soil was due to a reduction in water balance, cell division and cell expansion, decrease in photosynthesis and photosynthetic pigments, increase in protein degradation, translocation, and assimilation of photosynthetic products (Arshi et al. 2010, Petropoulos et al. 2017, Hafez et al. 2021) and our results agree with findings of Sergio et al. 2012 which concluded that chicory plants can survive in mild salinity.

Crop/seed yield is an important parameter of productivity and a high level of salinity decreases the crop/seed yield of the plants (Munns & Gilliham 2015, Stavridou et al. 2017, Ullah et al. 2021). In this experiment, results (Table 3) showed that each level of salinity decreased the crop/seed yield of chicory considerably. Poor seed or grain yield of cultivated crops harms farmers' economies (Petropoulos et al. 2017, Stavridou et al. 2017, Zandalinas et al. 2021). Our findings suggested that chicory showed poor growth and yield at 105 mM NaCl kg⁻¹ soil treatments and the values of both parameters are directly correlated with a high concentration of NaCl in the soil.

CONCLUSION

The results of this study concluded that NaCl-induced toxicity inhibited the vegetative and reproductive growth of chicory plants in a concentration-dependent manner. At 105 mM NaCl kg⁻¹ soil causes a considerable loss of 35 percent in total seed output plant⁻¹ which is a considerable economic loss for farmers. Finally, it is concluded that chicory can be grown in moderate saline soil (45 mM and 75 mM NaCl kg⁻¹ soil) without compromising their growth and yield but at or beyond the level of salinity like 105 mM NaCl kg⁻¹ soil, chicory starts to show poor growth and yield, which is not suitable or recommended to the farmers for cultivation, to save them from economic loss.

ACKNOWLEDGEMENT

The authors are grateful to the Chairperson, Department of Botany, Aligarh Muslim University (A.M.U.), Aligarh for providing research experiment facilities and technical support for sample analysis. The authors would also like to

thank the University Grant Commission (UGC), New Delhi, for funding this research by providing a non-NET fellowship to the corresponding author (Adnan Khan) for Ph. D.

REFERENCES

- Abbas, Z.K., Saggi, S., Sakeran, M.I., Zidan, N., Rehman, H. and Ansari, A.A. 2015. Phytochemical, antioxidant and mineral composition of hydroalcoholic extract of chicory (*Cichorium intybus* L.) leaves. Saudi J. Biol. Sci., 22(3): 322-26. <https://doi.org/10.1016/j.sjbs.2014.11.015>
- Ahanger, M.A., Morad-Talab, N., Abd-Allah, E.F., Ahmad, P. and Hajiboland, R. 2016. Plant growth under drought stress: Significance of mineral nutrients. Water Stress and Crop Plants: A Sustainable Approach, 2: 649-668. <https://doi.org/10.1002/9781119054450.ch37>
- Aisa, H.A., Xin, X. and Tang, D. 2020. Chemical constituents and their pharmacological activities of plants from *Cichorium* genus. Chinese Herbal Medicines., 12(3): 224-236.
- Aksoy, A. 2008. Chicory (*Cichorium intybus* L.): a possible biomonitor of metal pollution. Pak. J Bot., 40(2): 791-797.
- Arnon, D.I. 1949. Copper enzyme in isolated chloroplasts polyphenol oxidase in *Beta vulgaris*. Plant Physiol., 24(1): 1-15. <https://doi.org/10.1104/2fpp.24.1.1>
- Arshi, A., Abidin, M.Z. and Iqbal, M. 2006. Effect of CaCl₂ on growth performance, photosynthetic efficiency and nitrogen assimilation of *Cichorium intybus* L. grown under NaCl stress. Acta Physiol. Plantarum., 28(2): 137-147. <https://doi.org/10.1007/s11738-006-0040-z>
- Arshi, A., Ahmad, A., Aref, I.M. and Iqbal, M. 2010. Effect of calcium against salinity-induced inhibition in growth, ion accumulation and proline contents in *Cichorium intybus* L. J. Environ. Biol., 31(6): 939-944.
- Bates, L.S., Waldren, R.P. and Teare, I.D. 1973 Rapid determination of free proline for water-stress studies. Plant and Soil., 39(1): 205-207. <https://doi.org/10.1007/BF00018060>
- Bhatt, R., Asopa, P.P., Sihag, S., Sharma, R., Kachhwaha, S. and Kothari, S.L. 2015. Comparative three-way analysis of biochemical responses in cereal and millet crops under salinity stress. J. Appl. Biology and Biotechnol., 3(06): 022-028. <https://doi.org/10.7324/JABB.2015.3604>
- Chaudhry, S. and Sidhu, G.P.S 2021. Climate change regulated abiotic stress mechanisms in plants: a comprehensive review. Plant Cell Reports., 41: 1-31. <https://doi.org/10.1007/s00299-021-02759-5>
- Choudhary, S., Kaurav, H. and Chaudhary, G. 2021. Kasani beej (*Cichorium intybus*): Ayurvedic view, folk view, phytochemistry and modern therapeutic uses. Int. J. Res. in Appl. Sci. and Biotechnol., 8(2): 114-125. <https://doi.org/10.31033/ijrasb.8.2.14>
- Corwin, D.L. 2021. Climate change impacts on soil salinity in agricultural areas. European J. Soil Sci., 72(2): 842-862. <https://doi.org/10.1111/ejss.13010>
- Das, S., Vasudeva, N. and Sharma, S. 2016. *Cichorium intybus*: A concise report on its ethnomedicinal, botanical, and phytopharmacological aspects. Drug Development and Therapeutics., 7(1): 1-12. <https://doi.org/10.4103/2394-6555.180157>
- Dietz, K.J., Zörb, C. and Geilfus, C.M., 2021. Drought and crop yield. Plant Biology, 23(6):881-893. <https://doi.org/10.1111/plb.13304>
- Egamberdieva, D., Wirth, S., Bellingrath-Kimura, S.D., Mishra, J. and Arora, N.K. 2019. Salt-tolerant plant growth promoting rhizobacteria for enhancing crop productivity of saline soils. Front. Microbiol., 10:2791. <https://doi.org/10.3389/fmicb.2019.02791>
- El Sabagh, A., Islam, M.S., Skalicky, M., Ali Raza, M., Singh, K., Anwar Hossain, M., Hossain, A., Mahboob, W., Iqbal, M.A., Ratnasekera, D., Singhal, R.K., Ahmed, S., Kumari, A., Wasaya, A., Sytar, O., Brestic, M. ÇIG F, Erman, M., Habib Ur Rahman, M., Ullah, N. and Arshad, A. 2021. Salinity stress in wheat (*Triticum aestivum* L.) in the changing climate: Adaptation and management strategies. Front. Agron., 3: 661932. <https://doi.org/10.3389/fagro.2021.661932>
- El-Ramady, H.R., Alshaal, T.A., Amer, M., Domokos-Szabolcsy, É., Elhawat, N., Prokisch, J. and Fári, M. 2014. Soil quality and plant nutrition. In: Sustainable Agriculture Reviews., 14: 345-447. Springer, Cham. https://doi.org/10.1007/978-3-319-06016-3_11
- Gidhay Adhanom, O. 2019. Salinity and sodicity hazard characterization in major irrigated areas and irrigation water sources, Northern Ethiopia. Cogent Food & Agric., 5(1): 1673110. <https://doi.org/10.1080/23311932.2019.1673110>
- Hafez, E.M., Osman, H.S., Gowayed, S.M., Okasha, S.A., Omara, A.E.-D., Sami, R., Abd El-Monem, A.M. and Abd El-Razek, U.A. 2021. Minimizing the adversely impacts of water deficit and soil salinity on maize growth and productivity in response to the application of plant growth-promoting rhizobacteria and silica nanoparticles. Agronomy, 11: 676. <https://doi.org/10.3390/agronomy11040676>
- Hassani, A., Azapagic, A. and Shokri, N. 2021. Global predictions of primary soil salinization under changing climate in the 21st century., Nature Communications, 12(1): 6663, 1-17. <https://doi.org/10.1038/s41467-021-26907-3>
- Jaleel, C.A., Sankar, B. Sridharan, R. and Panneerselvum, R. 2008. Soil salinity alters growth, chlorophyll content, and secondary metabolite accumulation in *Catharanthus roseus*. Turkish J. Biol., 32(2): 79-83.
- Jangra, S.S. and Madan, V.K. 2018. Proximate, mineral and chemical composition of different parts of chicory (*Cichorium intybus* L.). J. Pharmacog. and Phytochem., 7(5): 3311-3315.
- Kumar, P. and Sharma, P.K. 2020. Soil salinity and food security in India. Front. Sustain. Food Syst., 4:533781. <https://doi.org/10.3389/fsufs.2020.533781>
- Machado, R.M.A. and Serralheiro, R.P. 2017. Soil Salinity: Effect on vegetable crop growth. Management practices to prevent and mitigate soil salinization. Horticulturae., 3(2): 30. <https://doi.org/10.3390/horticulturae3020030>
- Mavrina, P.O., Saybel, O.L. and Malankina, E.L. 2021. Possibilities of using leaves cultivated chicory (*Cichorium intybus* L.) as a medicinal plant material (review). Vegetable crops of Russia., 2021(4): 105-110. <https://doi.org/10.18619/2072-9146-2021>
- Mohanavelu, A., Naganna, S.R. and Al-Ansari, N. 2021. Irrigation induced salinity and sodicity hazards on soil and groundwater: An overview of its causes, impacts and mitigation strategies. Agriculture., 11(10):983. <https://doi.org/10.3390/agriculture11100983>
- Monteoliva, M.I., Rizzi, Y.S., Cecchini, N.M., Hajirezaei, M.R. and Alvarez, M.E., 2014. Context of action of proline dehydrogenase (ProDH) in the hypersensitive response of Arabidopsis. BMC Plant Biol., 14(1): 1-11. <https://doi.org/10.1186/1471-2229-14-21>
- Munns, R. and Gilliland, M. 2015. Salinity tolerance of crops-what is the cost? New Phytologist., 208(3): 668-673. <https://doi.org/10.1111/nph.13519>
- Nazir, F., Hussain, A. and Fariduddin, Q. 2019. Hydrogen peroxide modulate photosynthesis and antioxidant systems in tomato (*Solanum lycopersicum* L.) plants under copper stress. Chemosphere., 230: 544-558. <https://doi.org/10.1016/j.chemosphere.2019.05.001>
- Pandey, S.K. and Singh, H. 2011. A simple, cost-effective method for leaf area estimation. J. Bot., 2011: 1-6. <https://doi.org/10.1155/2011/658240>
- Petropoulos, S.A., Levizou, E., Ntatsi, G., Fernandes, Â., Petrotos, K., Akoumianakis, K., Barros, L. and Ferreira, I.C. 2017. Salinity effect on nutritional value, chemical composition and bioactive compounds content of *Cichorium spinosum* L. Food Chemistry., 214: 129-136. <http://dx.doi.org/10.1016/j.foodchem.2016.07.080>
- Piluzza, G., Sulas, L. and Bullitta, S. 2014. Dry matter yield, feeding value, and antioxidant activity in Mediterranean chicory (*Cichorium intybus* L.) germplasm. Turkish Journal of Agricultural Forestry, 38(4): 506-514. <https://doi.org/10.3906/tar-1309-70>
- Sergio, L., Da Paola, A., Cantore, V., Peralice, M., Cascarano, N.A., Bianco, V.V. and Di Venere, D. 2012. Effect of salt stress on growth parameters, enzymatic antioxidant system and lipid peroxidation in wild

- chicory (*Cichorium intybus* L.). *Acta Physiologiae Plantarum*, 34(6): 2349-2358. <https://doi.org/10.1007/s11738-012-1038-3>
- Sharma, A., Monlai, S., Shi, Z., Manpoong, C., Raghavan, M., Linggi, B. and Wangsu, M. 2020. Current status of food security in India. *Ind. J. Pure App. Biosci.*, 8(1): 293-302. <http://dx.doi.org/10.18782/2582-2845.7980>
- Stavi, I., Thevs, N. and Priori, S. 2021. Soil salinity and sodicity in drylands: A review of causes, effects, monitoring, and restoration measures. *Front. Environ. Sci.*, 9: 712831. <https://doi.org/10.3389/fenvs.2021.712831>
- Stavridou, E., Hastings, A., Webster, R.J. and Robson, P.R.H. 2017. The impact of soil salinity on the yield, composition and physiology of the bioenergy grass *Miscanthus x giganteus*. *GCB Bioenergy*, 9(1): 92-104. <https://doi.org/10.1111/gcbb.12351>
- Street, R., Sidana, A. and Prinsloo, G. 2013. *Cichorium intybus*: Traditional uses, phytochemistry, pharmacology, and toxicology. *Evidence-Based Complementary and Alternative Medicine*, 579319. <http://dx.doi.org/10.1155/2013/579319>
- Teshome, D.T., Zharare, G.E. and Naidoo, S. 2020. The threat of the combined effect of biotic and abiotic stress factors in forestry under a changing climate. *Front. Plant Sci.*, 11:601009. <https://doi.org/10.3389/fpls.2020.601009>
- Ullah, A., Bano, A. and Khan, N. 2021. Climate change and salinity effects on crops and chemical communication between plants and plant growth-promoting microorganisms under stress. *Front. Sust. Food Sys.*, 5: 618092. <https://doi.org/10.3389/fsufs.2021.618092>
- Upadhyay, A., Tripathi, S. and Pandey, S.N. 2012. Effects of soil sodicity on growth, nutrient uptake and bio-chemical responses of *Ammi majus* L. *Research Journal of Soil Biology*, 4(3): 69-80. <https://doi.org/10.3923/rjsb.2012.69.80>
- Weraduwanage, S.M., Chen, J., Anozie, F.C., Morales, A., Weise, S.E. and Sharkey, T.D. 2015. The relationship between leaf area growth and biomass accumulation in *Arabidopsis thaliana*. *Front. Plant Sci.*, 6: 167. <https://doi.org/10.3389/fpls.2015.00167>
- Xu, J., Guo, Z., Jiang, X., Ahammed, G.J. and Zhou, Y. 2021. Light regulation of horticultural crop nutrient uptake and utilization. *Horticult. Plant J.*, 7(5): 367-379. <https://doi.org/10.1016/j.hpj.2021.01.005>
- Zandalinas, S.I., Fritschi, F.B. and Mittler, R. 2021. Global warming, climate change, and environmental pollution: Recipe for a multifactorial stress combination disaster. *Trends in Plant Science*, 26(6): 588-599. <https://doi.org/10.1016/j.tplants.2021.02.011>



Comparison of Machine Learning Models in the Prediction of Accumulation of Heavy Metals in the Tree Species in Kanchipuram, Tamilnadu

R. Sumathi*† and G. Sriram**

*Department of Civil and Structural Engineering, Sri Chandrasekharendra Saraswathi Viswa Mahavidyalaya, Enathur, Kanchipuram-631 561, Tamilnadu, India

**Department of Mechanical Engineering, Sri Chandrasekharendra Saraswathi Viswa Mahavidyalaya, Enathur, Kanchipuram-631 561, Tamilnadu, India

†Corresponding author: R. Sumathi; sumathiram72@gmail.com

Nat. Env. & Poll. Tech.
Website: www.neptjournal.com

Received: 14-09-2022

Revised: 03-11-2022

Accepted: 10-11-2022

Key Words:

Machine learning
Heavy metals
Accumulation
Plant species
Prediction

ABSTRACT

Arsenic, aluminum, iron, lead, chromium, copper, zinc, manganese, and cadmium are some of the heavy metal pollutants in the air that cause severe impacts on the biotic and abiotic environment. This study intended to find the accumulation capacity of the heavy metals on the leaves of tree species such as *Terminalia catappa*, *Syzygium cumini*, *Saraca asoca*, *Pongamia glabra*, and *Ficus religiosa* and predict their accuracy by comparing different machine learning (ML) models. The samples were collected at six different locations (likely Vellagate, Cancer Institute, CSI hospital area, Moongilmandapam, Collectorate, and Pallavarmedu) and distributed in a manner within Kanchipuram town, Tamil Nadu, in February and March of 2018 and 2019, respectively. Six ML methods were selected, such as KStar (K*), Lazy IKB, Logistic Regression Algorithm (LR), LogitBoost Classifier (LB), Meta Randomizable Filtered Classifier (MRFC), and Random Tree (RT), for prediction and to compare the efficiency of their predictions. Out of six models, Logistic functions perform well in terms of TP rate when compared to other classifiers (93.21%–99.81% TPR– 0.93–0.99) and Logitboost attained a low TP rate that ranged from 0.76 to 0.82. This study indicates the feasibility of different ML methods in the prediction of species capabilities toward the accumulation of heavy metals.

INTRODUCTION

Air pollution is one of the significant problems in the environment and causes serious health hazards to human beings and has a severe impact on non-living things. Industrialization, urbanization, and an increased number of vehicles lead to the emission of various gases, particulate matter, and heavy metals. Out of this, heavy metals pose complexity on human health, and sometimes losses are inexpressible, so it is essential to quantify them and also reduce their concentration in the atmosphere. Monitoring by equipment presented many challenges, including the high cost of establishing sampling stations, confined sampling, and extensive labor (Norouzi 2016, Gaza 2018). All these difficulties are overcome with biomonitoring techniques by using a variety of vegetation since plants are available and distributed in remote areas, which makes sampling and monitoring very easy and economical (Sharma et al. 2015). Bio-monitoring measures the pollutant levels in the atmosphere both quantitatively and qualitatively by analyzing the accumulation, deposition, and distribution

rates in the environment (Ozturk et al. 2017). Plants like mosses and lichens are perfect biomonitors, but due to their unavailability in industrial and urban areas, higher vascular plants are now used (Chang 2016, Ojiodu 2018, and Asawari Tak 2017). Heavy metals deposited on the leaves of the trees directly quantify the pollution level in the atmosphere (Maghakyan 2016). The percentage of dust deposited on the leaves of roadside trees is high compared with the trees away from roads (Ahmed 2016). Heavy metals deposited on the trees available in the local areas are an effective tool for measuring the air quality and developing these trees was used to maintain the greenbelt (Hajizadeh 2019).

The results obtained from the analysis were validated by using machine learning tools, which provided more accuracy (Akiladevi 2020). Particulate matters 2.5 in the air were effectively predicted by using auto-regression and logistic regression models (Aditya 2018). Machine learning models such as the linear support vector machine and boosted trees were used to predict the PM 2.5 level in the air based on six climatic factors (Deters 2017). In the ML approach, root

mean square error and mean absolute error were taken as the scales to compare the accuracy of the various regression models (Saba Ameer et al. 2017).

In this study, the heavy metals such as Al, As, Cd, Cr, Pb, Mn, Fe, Cu, and Zn deposited on the leaves of *Saraca asoca* (Ashoka), *Terminalia catappa* (Badam), *Ficus religiosa* (Pupil), *Pongamia glabra* (Pongam), and *Syzygium cumini* (Jamun) were experimentally analyzed. The accuracy of the results was predicted by a machine learning approach using various algorithms, namely KStar (K*), Lazy IKB, Logistic Regression Algorithm (LR), LogitBoost Classifier (LB), Meta Randomizable Filtered Classifier (MRFC), and Random Tree (RT).

MATERIALS AND METHODS

Sampling Species

In this present study, five trees, such as *S. asoca*, *T. catappa*, *F. religiosa*, *P. glabra*, and *S. cumini*, were selected based on their easy availability and generally found in all the selected sites. Out of these five trees *S. asoca* and *S. cumini* are evergreen trees, *T. catappa* and *P. glabra* are deciduous trees, and *F. religiosa* comes under both categories. Leaves from all six selected tree species were sampled in the early hours of the day, from 6 a.m. to 8 a.m., during February and March of 2018 and 2019. Samples were collected at two various heights, viz., less than 1.8 m and above 2.4 m, to identify the pollutants at any level from different sources. The

collected samples were stored carefully in zip-lock covers to prevent any addition or deletion of pollutants and brought to the laboratories for analysis. The experiment was carried out by using inductively coupled plasma mass spectrometry after the closed microwave digestion process.

Study Area

Kanchipuram is a district in the northeast of Tamil Nadu, adjacent to the Bay of Bengal. It is bounded in the west by Vellore and Thiruvannamalai districts, in the north by Thiruvallur District and Chennai District, and the south by Villupuram District. It lies between 11°00' and 12°00' north latitudes and 77°28' and 78°50' east longitudes. The district has a total geographical area of 4,432 km² and a coastline of 57 km. The town of Kanchipuram is the district headquarters. The maximum and minimum temperatures range from 28.0°C to 45.0°C and 14.0°C to 21.0°C, respectively. Fig. 1 shows the index map of Kanchipuram with the site location of the sample collection. Samples were collected at six different locations in the distributed way in Kanchipuram town, such as the residential area (Pallavarmedu), commercial area (Collectorate), sensitive area (CSI hospital), institutional area (Cancer Institute), industrial area (Vella gate), and traffic area (Moongil Mandapam).

Dataset Construction

The baseline factors were gathered from the actual dataset and each factor was converted to be convenient for the

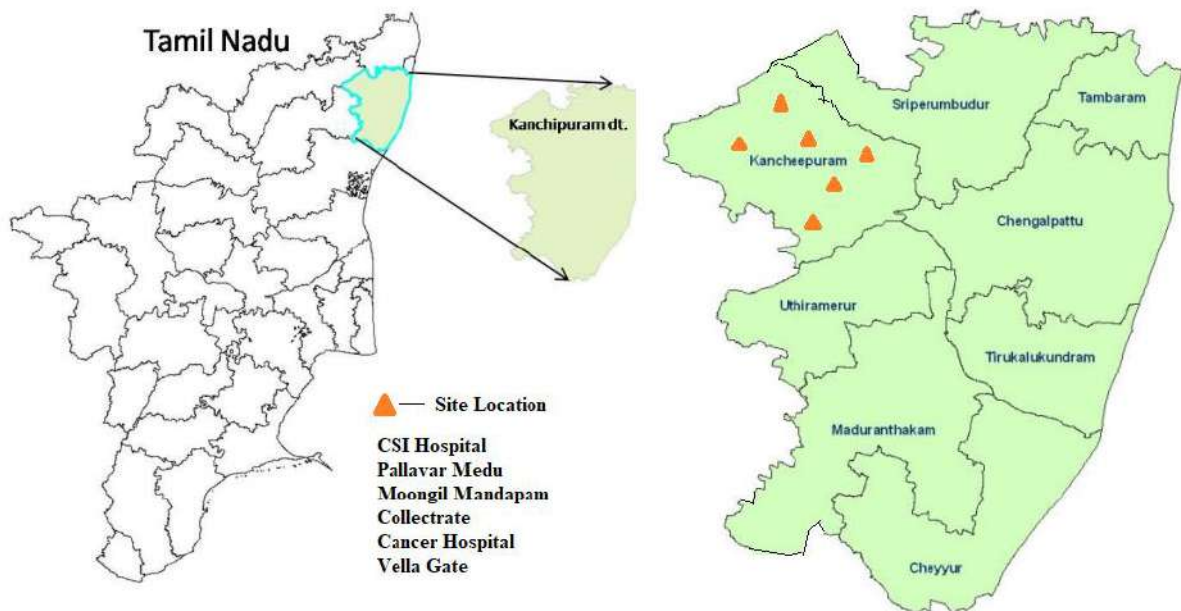


Fig. 1: Study Area – Kanchipuram.

cluster analysis to the scale between 0 and 1 and analyzed by weka.clusterers SimpleKMeans. After framing the dataset, the program code for reference was prepared. The factors that were fed as input data were latitude, longitude, nine heavy metals (Al, As, Fe, Cu, Cd, Cr, Pb, Zn and Mn), site, site name and sample name, totaling 14 attributes and 30 instances, such as five species at six sites.

RESULTS AND DISCUSSION

The results obtained from the experiments were taken

for statistical analysis. Mean, median and standard deviation were calculated for 2018 and 2019 (Tables 1 and 2).

Heavy metal deposition on the leaves of the tree species at both the high point and low point for the two consecutive years 2018 and 2019 were taken for the analysis, totaling thirty instances and fourteen attributes. The information or results obtained from the experiment were run by using Weka classifiers, including various classifiers such as KStar (K*), Lazy IKB, Logistic Regression Algorithm (LR), LogitBoost Classifier (LB), Meta Randomizable Filtered Classifier (MRFC) and Random Tree (RT). The time taken

Table 1: Statistical analysis of pollutants deposited at six sites on five species during 2018.

Parameters	Max	Min	Mean	Median	STD
<i>S. asoca- 2018</i>					
Fe	124.8	59.1	93.89	98	23.78
Cu	2.2	0	0.56	0	0.93
Zn	21.15	0	8.69	7.675	9.01
Al	75.65	26.05	48.15	44.45	18.35
As	1.15	0	0.19	0	0.47
Mn	9.8	0	4.45	3.875	4.92
<i>T. catappa</i>					
Fe	86.05	21.7	39.12	33.125	26.15
Cu	1.6	0	0.27	0	0.65
Zn	11.3	0	4.66	4.01	5.22
Al	54.25	5	21.42	15.875	18.07
As	0	0	0.00	0	0.00
Mn	10.1	0	4.47	4.125	4.93
<i>F. religiosa</i>					
Fe	44.5	15	27.61	28.38	11.26
Cu	1.35	0	0.41	0.00	0.64
Zn	8.05	5.95	6.46	6.18	0.79
Al	28.9	14.2	18.26	17.13	5.47
Mn	9.65	6.05	7.38	6.85	1.48
<i>P. glabra</i>					
Fe	130.2	17.5	50.95	31.90	45.40
Cu	2.75	0	0.82	0.00	1.28
Zn	14.45	1.15	6.88	6.15	6.80
Al	109.75	7.85	36.64	21.50	39.29
Mn	14.585	0	6.16	4.63	6.97
<i>S. cumini</i>					
Fe	69.15	7.85	34.27	23.40	25.50
Cu	1.05	0	0.18	0.00	0.43
Zn	10.35	0	3.66	2.63	4.35
Al	43.9	9.4	20.87	13.40	14.50
Mn	14.4	0	4.04	1.71	5.70

Table 2: Statistical analysis of pollutants deposited at six sites on five species during 2019.

Parameters	Max	Min	Mean	Median	STD
<i>S. asoca-2019</i>					
Fe	149.195	10.8	87.55	94.67	64.22
Zn	35.95	1.225	9.38	3.1775	13.55
Al	131.095	3.2365	35.43	14.8275	49.63
Cr	1.185	0	0.20	0	0.48
Mn	37.975	0	8.11	2.323	14.73
<i>T. catappa</i>					
Fe	41.84	5.995	20.46	16.7025	15.83
Zn	31.335	0	6.20	1.3525	12.34
Al	66.23	0	22.47	17.23	24.29
Mn	2.765	0	0.62	0	1.12
<i>F. religiosa</i>					
Fe	52.25	3.425	29.00	25.22	19.08
Zn	8.67	0	3.78	4.06	3.05
Al	61.25	3.985	23.43	15.14	21.32
Mn	5.43	0	1.14	0.00	2.18
<i>P. glabra</i>					
Fe	108.99	18.21	40.73	25.45	34.39
Zn	25.56	0	5.49	2.20	9.91
Al	94.58	4.09	37.99	34.72	34.69
Mn	4.37	0	1.45	0.96	1.79
<i>S. cumini</i>					
Fe	54.255	11.915	30.40	29.95	14.97
Zn	3.39	0	1.62	1.38	1.16
Al	47.68	4.535	24.99	25.23	13.82
Mn	3.23	0	1.52	1.46	1.04

to test the model on the training data was 0.01 seconds. From the evaluation of the training set, results such as correctly classified instances, incorrectly classified instances, mean absolute error, root mean squared error, relative absolute

error, and root relative squared error were obtained. The true positive rate is taken as the correctly classified instances. After completing the analysis, the correlation between the various classifiers was calculated, and the performance of the machine

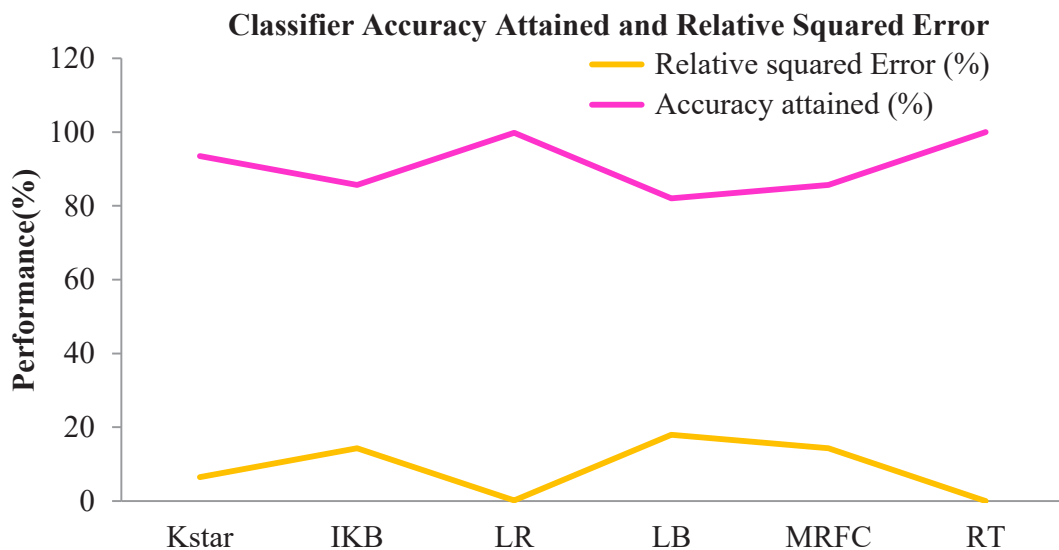


Fig. 2: Performance of the machine learning tools for the prediction of the pollutants at the high point during 2018 (Deposition).

learning tools for the prediction of the pollutants at the high point in 2018 and 2019 respectively is shown in Figs. 2 and 3.

Hyejin Park & Kim (2019) predicted the impact of heavy metals, namely cadmium, mercury, and lead, on hypercholesterolemia (HC) in the population and compared the accuracy of various five machine learning algorithms based on the data received from the Korea National Health Department. Vijayarani & Muthulakshmi (2013) analyzed the performance of two classifiers, namely Lazy and Bayesian, by considering various factors and proved

that the Bayesian classifier is less efficient than the Lazy classifier.

Figs. 4 and 5 show the performance of the machine learning tools for the prediction of the pollutants at the high point and low point during 2018 and 2019 respectively.

The accuracy measures of different classifiers for high and low points for the deposition during 2018 and 2019 were listed in Tables 3 and 4. and it is observed that logistic functions perform well in terms of TP rate when compared to other classifiers.

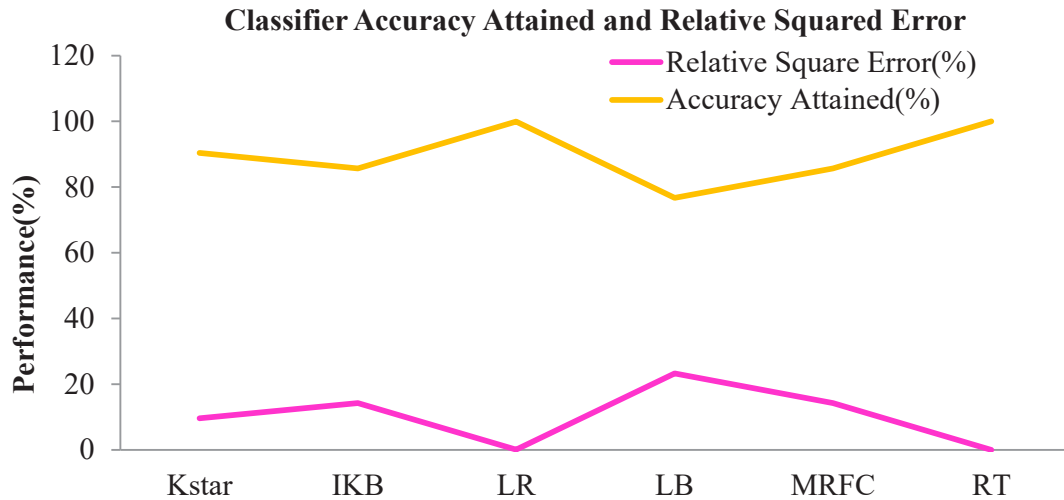


Fig. 3: Performance of the machine learning tools for the prediction of the pollutants at the low point during 2018 (Deposition).

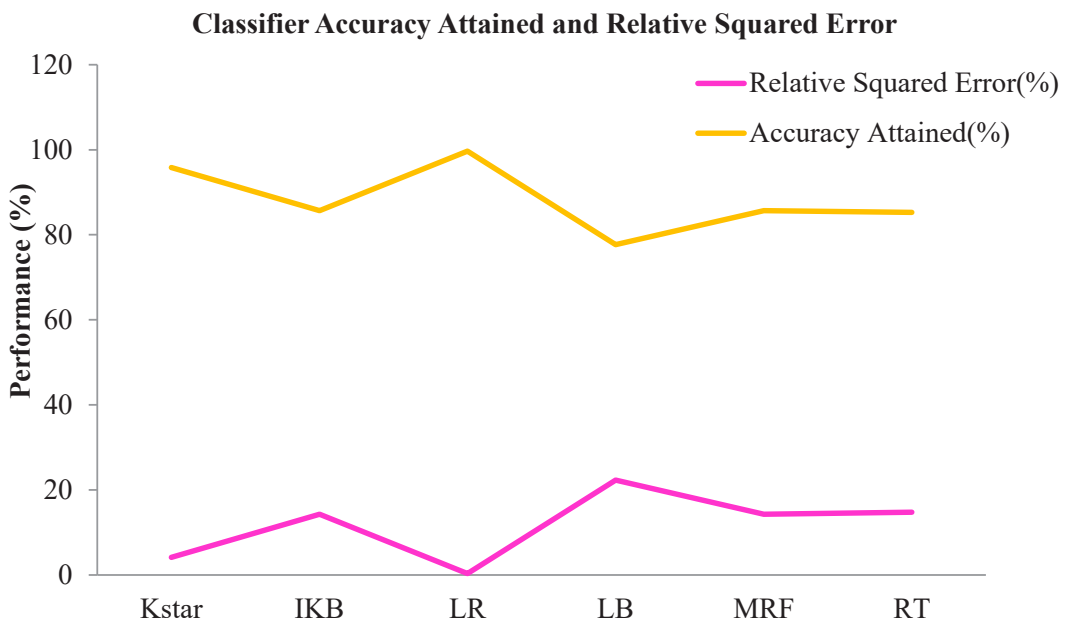


Fig. 4: Performance of the machine learning tools for the prediction of the pollutants at the high point during 2019 (Deposition).

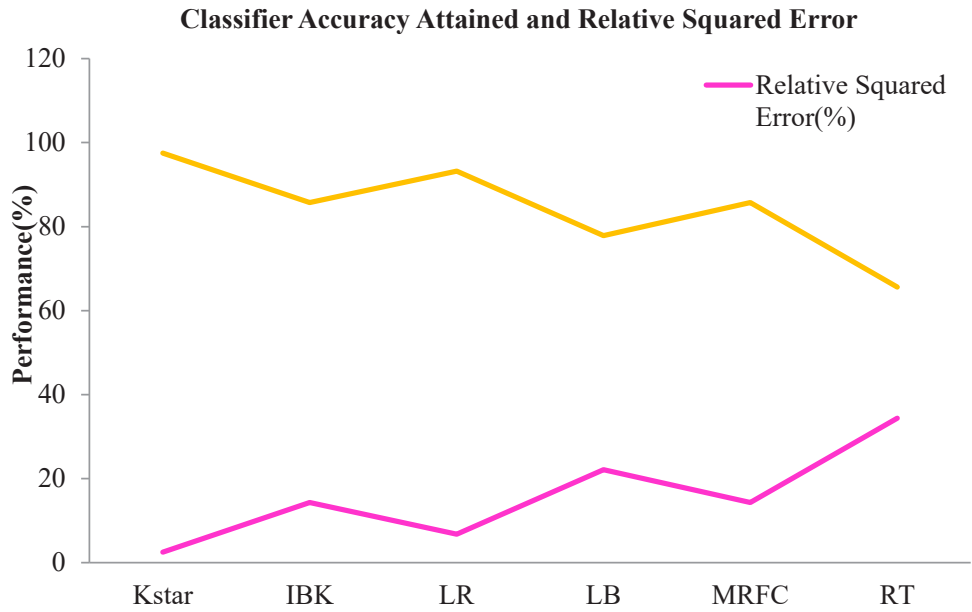


Fig. 5: Performance of the machine learning tools for the prediction of the pollutants at the low point during 2019 (Deposition).

Table 3: Efficiency analysis of each data classification model- High Point (Deposition).

Performance Error	Different Model Algorithms											
	Kstar		Lazy IKB		Functions-Logistic		Logit Boost		Meta Randomizable Filtered classifier		Trees-Random Tree	
Year	2018	2019	2018	2019	2018	2019	2018	2019	2018	2019	2018	2019
Number of Selected Attributes	14	14	14	14	14	14	14	14	14	14	14	14
Correctly Classified Instances(%)	93.52	95.84	85.71	85.71	99.81	99.67	82.04	77.69	85.71	85.71	100	85.27
Incorrectly Classified Instances(%)	6.48	4.16	14.29	14.29	0.19	0.33	17.96	22.31	14.29	14.29	0	14.73
TR Rate(True Positive Rate)	0.93	0.95	0.85	0.85	0.99	0.99	0.82	0.77	0.85	0.85	1	0.85

Table 4: Efficiency analysis of each data classification model- Low Point (Deposition).

Performance Error	Different Model Algorithms											
	Kstar		Lazy IKB		Functions-Logistic		Logit Boost		Meta Randomizable Filtered classifier		Trees-RandomTree	
Year	2018	2019	2018	2019	2018	2019	2018	2019	2018	2019	2018	2019
Number of Selected Attributes	14	14	14	14	14	14	14	14	14	14	14	14
Correctly Classified Instances(%)	90.41	97.50	85.71	85.71	99.80	93.21	76.72	77.84	85.71	85.71	100	65.61
Incorrectly Classified Instances(%)	9.59	2.50	14.29	14.29	0.20	6.79	23.28	22.16	14.29	14.29	0	34.39
TR Rate(True Positive Rate)	0.90	0.97	0.85	0.85	0.99	0.93	0.76	0.77	0.85	0.85	1	0.65

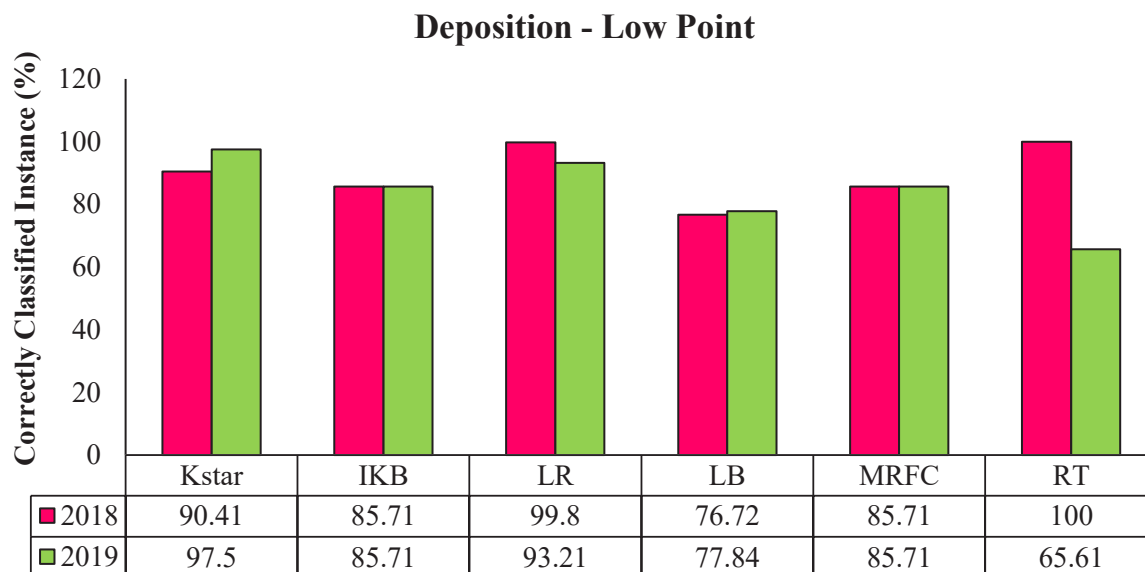


Fig. 6: Comparison between different classifier for predicting pollutants measured at low point of the tree (Deposition).

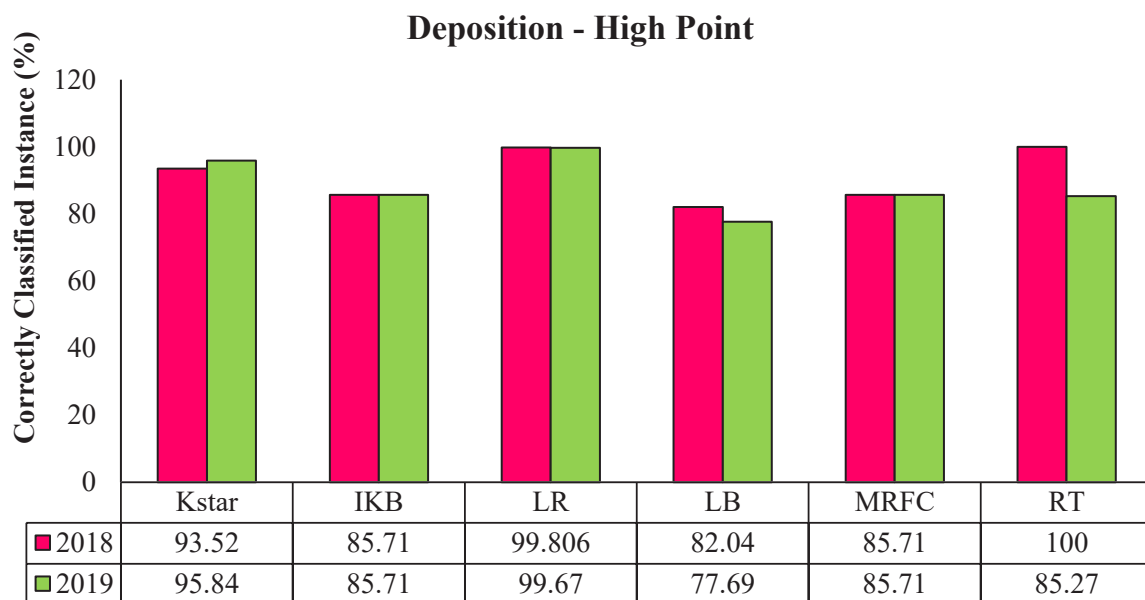


Fig. 7: Comparison between different classifier for predicting pollutants measured at high point of the tree (Deposition).

Figs. 6 and 7 show the comparison between the classifiers' correctly classified instances of a low point and high point during the deposition of heavy metals on the leaves from 2018 to 2019, respectively.

CONCLUSIONS

It is well known that machine learning techniques using various prediction models are widely used in various

applications and in different fields with strong abilities. In this research paper, the deposition of nine heavy metals on the leaves of five tree species was predicted using six ML classifiers and compared with each other. The results obtained from the study indicated that the performance of the machine learning tools for the prediction of the pollutants at the high point and low point during 2018 and 2019 was good. The deposition of heavy metals was analyzed both in 2018 and 2019 at high and low points, with logistic boost methods

showing lower performance and logistics functions showing better performance with higher accuracy and a true positive rate. Based on these findings, ML may serve as an alternate method for predicting the deposition of heavy metals from the atmosphere.

REFERENCES

- Aasawari Tak, A. and Umesh Kakde, B. 2017. Assessment of air pollution tolerance index of plants: A comparative study. *Inter. J. of Phar. and Pharma. Sci.*, 9(7): 83-89. <http://dx.doi.org/10.22159/ijpps.2017v9i7.18447>
- Aditya, C R. Chandana Deshmukh, R. Nayana, D K. and Praveen Gandhi Vidyavastu. 2018. Detection and prediction of air pollution using machine learning models. *Inter. J. of Engg. Trends and Tech.*, 59(4): 204-207.
- Ahmed, S.S. Jabeen, R. Johar, S. Hameed, M. and Irfan, S. 2016. Effects of roadside dust pollution on fruit trees of Miyyaghundi (Quetta) and Ghanjdori (Mastung), Pakistan. *Inter. J. of Basic and App. Sci.*, 5(1): 38-44. <http://dx.doi.org/10.14419/ijbas.v5i1.5477>
- Akiladevi, R. Nandhini Devi, B. Nivesh Karthick, V. and Nivetha, P. 2020. Prediction and Analysis of Pollutant using Supervised Machine Learning. *Inter. J. of Recent Tech. and Engg.*, 9(2): 50-54. <http://dx.doi.org/10.35940/ijrte.A2837.079220>
- Ameer, S., Shah, M.A., Khan, A., Song, H., Maple, C., Islam, S.U. and Asghar, M.N., 2019. Comparative analysis of machine learning techniques for predicting air quality in smart cities. *IEEE Access*, 7: 128325-128338.
- Chang, L., Peng, Z. and Yanming, F. 2016. Monitoring airborne heavy metal using mosses in the city of Xuzhou, China. *Bull. of Environ. Contamin. and Toxi.*, 96: 638-644.
- Deters, J.K. Zalakeviciute, R. MarioGonzalez, R. and Rybarczyk, Y. 2017. Modeling PM2.5 urban pollution using machine learning and selected meteorological parameters. *Hind. J. of Electri. and Comp. Engg.*, pp. 1-14. <https://doi.org/10.1155/2017/5106045>
- Etim, N.E.O. Anthony, O. E. Mbom-Obong, N.E. and Dodeye, O. 2015. Heavy metal levels in Pine (*Pinus caribaeae* Morelet) tree barks as indicators of atmospheric pollution Calabar Municipality, South Eastern Nigeria. *J. of Environ. and Earth Sci.*, 5(22): 30- 32.
- Gaza, T. and Kugara, J. 2018. Study of heavy metal air pollution, using a Moss (*Grimmia dissimulate*) biomonitoring technique. *Univer. J. of Chem.*, 6(1): 1-13. <https://doi.org/10.13189/ujc.2018.060101>
- Hajizadeh, Y. Mokhtari, M. Faraji, M. Abdolajnejad, A. and Mohammadi, A. 2019. Biomonitoring of airborne metals using tree leaves: Protocol for biomonitor selection and spatial trend. *MethodsX*. 6: 1694-1700. <https://doi.org/10.1016/j.mex.2019.07.019>
- Hyejin Park, H. and Kim, K. 2019. Comparisons among machine learning models for the prediction of hypercholesterolemia associated with exposure to lead, mercury, and cadmium. *Inter. J. of Environ. Res. and Pub. Health.*, 16: 1-8. <https://doi.org/10.3390/ijerph16152666>
- Maghakyan, N. Tepanosyan, G. Belyaeva, O. Sahakyan, L. and Saghatelian, A. 2016. Assessment of pollution levels and human health risk of heavy metals in dust deposited on Yerevan's tree leaves (Armenia). *Acta Geochimica.*, 36(1): 16- 26. <https://doi.org/10.1007/s11631-016-0122-6>
- Mohammad, B. Md. Venna, E.P.R. Pallepogu, C.P. and Madhu Babu Redapongala, B.M. 2020. Predictive modelling of air pollution using machine learning models and neural networks. *Inter. J. of Scien. & Tech. Res.*, 9(6): 623-631.
- Norouzi, S. Khademi, H. Cano, A.F. and Acosta, J.A. 2016. Biomagnetic monitoring of heavy metals contamination in deposited atmospheric dust, a case study from Isfahan, Iran *J. of Environ. Manage.*, 173: 55-64. <http://doi.org/10.1016/j.jenvman.2016.02.035>
- Ojiodu, C.C. Olumayede, E.G. and Okuo, J.M. 2018. The level of heavy metals in the atmosphere of a macro environment, Lagos State, Southwestern - Nigeria using Moss plant (*Dicranium scorparium*) as bioindicator. *Sci. World J.*, 13(4): 69-74.
- Ozturk, A. Yarci, C. and Ozyigit, I.I. 2017. Assessment of heavy metal pollution in Istanbul using plant (*Celtis australis* L.) and soil assays. *Biotech. & Biotechnological Equip.*, 31(5): 948- 954. <https://doi.org/10.1080/13102818.2017.1353922>
- Sharma, A. and Uniyal, S.K. 2015. Heavy metal accumulation in *Pyrrosia flocculosa* (D. Don) Ching growing in sites located along a vehicular disturbance gradient. *Environ. Moni. and Assess.*, 188(547): 1-12. <https://doi.org/10.1007/s10661-016-5561-3>
- Vijayarani, S. and Muthulakshmi, M. 2013. Comparative analysis of Bayes and Lazy classification algorithms. *Inter. J. of Advan. Res. in Comp. and Communi. Engg.* 2(8): 3118-3124.



Isolation and Screening of Probiotic Bacteria from the Gut of Polychaetes as a Probiotic Potential for Fish Aquaculture

S. Balasubramanian*, T. Bettin Thomas**, D. Mathavan*, R. Sathish Kumar*, G. Uma*, R. D. Stevens Jones** and T. Citarasu†* 

*Aquatic Animal Health Laboratory, Centre for Marine Science and Technology, Manonmaniam Sundaranar University, Rajakkamangalam-629502, Kanyakumari District, Tamil Nadu, India

**Department of Zoology, Scott Christian College, Nagercoil-629003, Kanyakumari District, Tamil Nadu, India, Affiliated to Manonmaniam Sundaranar University, Tirunelveli, India

†Corresponding author: T. Citarasu; citarasu@gmail.com

Nat. Env. & Poll. Tech.
Website: www.neptjournal.com

Received: 20-10-2022
Revised: 13-12-2022
Accepted: 24-12-2022

Key Words:

Polychaetes
Gut-associated bacteria
Probiotics
Antimicrobial activity
Aeromonas hydrophila

ABSTRACT

In the present study, a total of 17 morphologically different gut-associated bacteria were isolated from four species of estuarine polychaetes: polychaetes *Capitella capitata*, *Scalibregma inflatum*, *Dendronereis aesturiana*, and *Namalycastis abiuma*. The isolated strains were evaluated for their probiotic activities, such as digestive enzymes including protease, amylase, and lipase, and antimicrobial activities by the agar well diffusion method against fish pathogens. Based on their better enzymatic and antibacterial activities, two bacterial strains, CMST Poly1 and CMST Poly2, were selected for further probiotic studies. Based on the biochemical and morphological characterization, both probiotic strains were characterized as Gram-positive, rod-shaped, non-motile, non-spore-forming, homofermentative, absence of catalyzing enzymes and notable proteolytic activity, and susceptibility to various antibiotics. Further, these two strains were confirmed by 16S rRNA gene sequence analysis as *Bacillus subtilis* CMST Poly1 and *Priestia megaterium* CMST Poly2. Our results revealed that strains *Bacillus subtilis* CMST Poly1 and *Priestia megaterium* CMST Poly2 can potentially be used as probiotic strains in aquaculture applications.

INTRODUCTION

The aquaculture sector is a promising source of high-quality animal protein and food supply for the entire world. There is a growing need for seafood globally, and global aquaculture output has made a significant contribution to the world economy. Fish raised in modern intensive aquaculture systems experience a range of harmful environmental conditions, which weaken their immune systems and make them more susceptible to diseases (Lieke et al. 2019). One of the main factors contributing to significant economic losses in the production of freshwater fish is bacterial fish diseases (Silva et al. 2012). The infections caused by *Aeromonas* spp., *Pseudomonas fluorescens*, *Vibrio anguillarum*, *Flavobacterium columnare*, *Edwardsiella tarda*, *Streptococcus* spp., and *Enterococcus* sp. are the primary causes of mortality in fish (Plumb 1997). Gastrointestinal disease in humans can also be brought on by certain virulent

microorganisms (Igbiosa et al. 2012). Commonly used synthetic drugs, antibiotics, and chemotherapeutics for managing bacterial infections in aquaculture sectors may have unfavorable impacts such as bacterial resistance, drug resistance, and environmental contamination (Nya & Austin 2011, Wang et al. 2015). As a result, alternative methods of disease control must be developed, including eco-friendly disease prevention measures, to preserve the sustainability of aquaculture (Nawaz et al. 2018). According to many studies, probiotics are a viable alternative to antibiotics for treating bacterial infections because of their nutritional content and their ability to counteract the negative effects of antibiotics and other medications (Jinendiran et al. 2019, Chen et al. 2019). In aquaculture, probiotics are live microorganisms that provide health advantages to the host and are beneficial in disease prevention and encouraging growth through improving immunological response (Son et al. 2009, Abumourad et al. 2013), supplying nutrients, and enzymatic activities (Yang et al. 2015).

Almost all benthic marine and estuarine sediments contain polychaetes, which are frequently the dominant species and

ORCID details of the authors:

T. Citarasu: <https://orcid.org/0000-0001-6166-620X>

individuals in the macrobenthos (Fauchald 1977, Grassle & Maciolek, 1992, Ward & Hutchings 1996). In captivity, polychaetes are frequently added to shrimp brooders in addition to squid and oysters since they are the natural prey of wild penaeid shrimps. For the spawning effectiveness and reproductive success of brooders, the well-balanced food content of polychaetes is essential (Palmer et al. 2014). On this basis, the goal of this study was to examine the polychaete gut and evaluate its potential as a source of probiotics through *in vitro* testing of probiotic enzyme synthesis.

MATERIALS AND METHODS

Collection and Identification of Polychaetes

The samples of marine polychaetes were collected using a scoop from the estuarine sediments of Manakkudy (Lat. 8.08°N and Long. 77.48°E), Kanyakumari District, South West coast of India. The collected samples were immediately transported to the lab in sterile and live conditions in sterilized bottles. The morphological identification of samples depends on morphometric and meristic traits such as color patterns, the structure of wings and legs, the arrangement of head and mouth parts, and genitalia (Fauvel 1953, Day 1967).

Isolation of Probiotic Microbes

Samples were immediately brought to the lab for microbiological investigation in sterile polythene bags with sterile saltwater. Live polychaetes' body surfaces were cleaned with sterile water before being swabbed with 60-70% ethanol for surface sterilization. Using sterile forceps, the polychaetes' gut samples were extracted aseptically and homogenized in phosphate-buffered saline (10 mM PBS, pH 7.2). Following this, 100 microliters of the serially diluted sample was plated on Zobell marine agar medium supplemented with 1% peptone and incubated for 48-72 hours at 37°C. By repeatedly sub-culturing at least three times, the morphologically distinct colonies were chosen, purified, and then stored for future use at 4°C.

Agar Well Diffusion Assay

To verify the inhibitory activity, antagonistic strains were tested using an agar well diffusion assay against the aquaculture pathogen *Aeromonas hydrophila* (Cintas et al. 1995). ZMB broth was used to culture antagonistic microorganisms for 48-72 hours at 37°C. The bacterial suspension was separated by centrifugation after incubation, and cell-free culture supernatants were used for the antibacterial assay. A bacterial pathogen was cultured in a 15 mL glass test tube containing 5 mL of Muller Hinton (MH) broth and was then incubated aerobically at 37°C

for 24 hours. Then, 50 mL of sterile-filtered supernatants were poured into wells (6 mm in diameter) that had been aseptically pierced using the base tip of a 200 mL sterilized pipette. The plates were then incubated at 37°C for 24 hours, and clear zones indicated the presence of antibacterial activity, and the zone was measured. The control was the same sterile broth (ZMB).

Screening of Probiotic Enzymatic Activities

Bacteria that produce extracellular enzymes were examined for amylase, lipase, and protease, respectively, on starch, tributyrin, and skim milk agar plates. Amylolytic activities of the isolates were screened on starch agar plates containing (g.L⁻¹): starch 10.0, peptone 5.0, glucose 5.0, agar 30.0, and NaCl 30.0, pH 7. By flooding the plates with iodine solution after 24 hours of incubation at 37°C, the zone of the clearing was identified. By comparing the zone of clearance diameter to the colony diameter, promising amylase-producing strains were selected. Skim milk agar plates were used to test the isolated bacterial strains for protease activity. The isolate that showed a distinct zone forming surrounding the growing colony was identified as a protease producer. Tributyrin nutritional agar plates with 1% (v/v) of tributyrin were used to evaluate the isolate's capacity to produce lipase activity. Clear zones in bacterial colonies were considered to indicate the presence of bacteria that produce lipase.

Antibiotic Sensitivity and Hemolytic Test

By using a disc diffusion assay in nutrient agar, the isolates' antibiotic susceptibility was determined. The following antibiotic discs were used: Ampicillin (2 µg), Tetracycline (5 µg), Erythromycin-E (5 µg), Chloramphenicol (5 µg), and Gentamycin (10 µg) (Hi Media, Mumbai). Briefly, 0.1 mL of each antagonistic strain was inoculated into the ZMA, and then antibiotic discs were placed on the ZMA and incubated overnight at 37°C. The results of the clear zone were measured in diameters and denoted as Sensitive (S), Intermediate (I), and Resistance (R). On top of the blood agar medium, which contains 5% (v/v) human blood, strains were streaked. The plates were checked for the hemolytic reaction after 48 h of incubation at 37°C.

Identification of Probiotic Bacteria

Bergey's manual of determinative bacteriology (Garrity et al. 2001) was used to identify the potential probiotic strains based on their morphological, biochemical, and phenotypic properties. 16S rRNA gene sequencing was used to confirm the identification. The probiotic strains' genomic DNA was isolated using a modified method (Sharma & Singh 2005). Using universal primers

(FP: 5'-AGAGTTTGATCCTGGCTCAG-3' and RP: 5'-CGTTACCTTGTTACGACTT-3'), the 16S rRNA gene was amplified. The following PCR conditions were used: initial denaturation at 94°C for 5 min, then 35 cycles of denaturation at 94°C for 1 min, annealing at 60°C for 1 min, extension at 72°C for 1 min, and a final extension

at 72°C for 10 min. Following purification, an automated DNA sequencer immediately began sequencing the PCR products. The CLUSTAL X program was used to examine the homology of gene sequences in GenBank. The neighbor-joining method (MEGA 6.0) was used to build the phylogenetic tree (Saitou & Nei 1987).

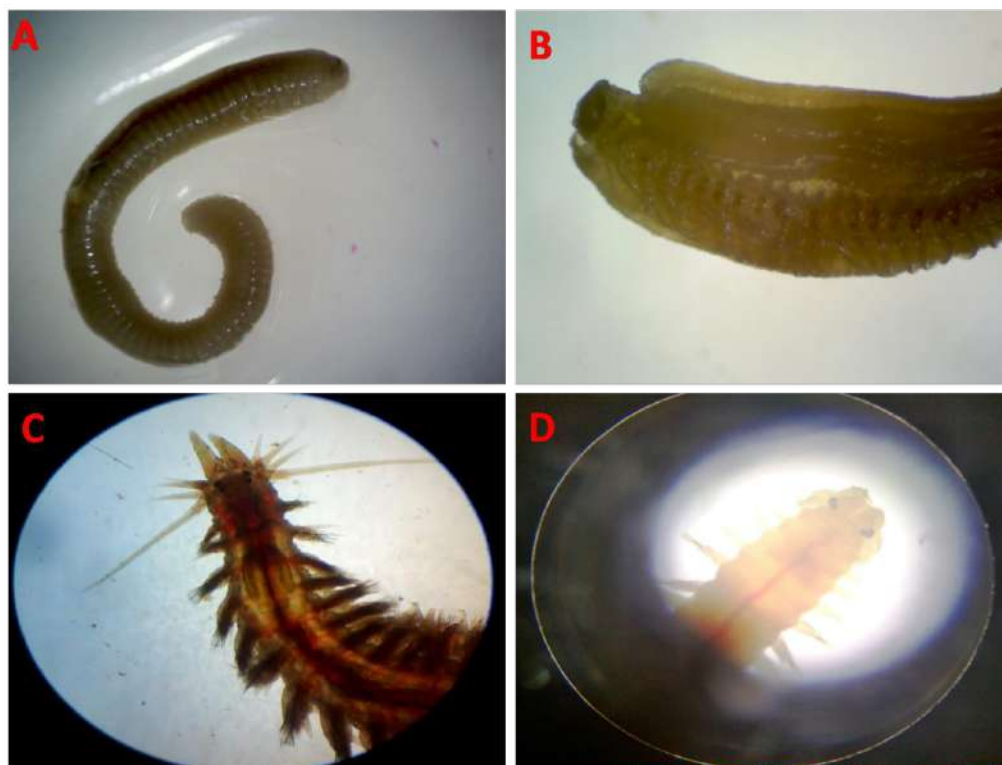


Fig. 1: Polychaetes collected from estuarine sediments of Manakkudy, Kanyakumari District, Southwest coast of India. A. *Capitella capitata*; B. *Scalibregma inflatum*; C. *Dendronereis aesturiana*; D. *Namalycastis abiuma*.

Table 1: The important key characters of the collected polychaetes.

S. No.	Family	Species Name	Key character	Reference
1.	Capitellidae	<i>Capitella capitata</i>	<ul style="list-style-type: none"> Abdominal segments without branchiae Peristomium and the next six segments with winged capillaries Prostomium conical with a pair of ventro-lateral eyes. 	Fauvel, (1953); Day (1967)
2.	Scalibregmatidae	<i>Scalibregma inflatum</i>	<ul style="list-style-type: none"> Body rusty brown, swollen anteriorly but narrowed posteriorly. Length up to 60 mm, with 60 segments. Skin tessellated. Prostomium pale with divergent processes forming a stout T. 	Fauvel, (1953); Day (1967)
3.	Nereidae	<i>Dendronereis aesturiana</i>	<ul style="list-style-type: none"> Body about 50 mm in length and only 1 mm wide, belongs to the genus <i>Dendronereis</i> this species and other mud-dwelling polychaetes. Most members of this family have four pairs of tendril-like appendages. In <i>Dendronereis</i> the gills are the most developed and resemble a well-branched tree. 	Fauvel, (1953); Day (1967)
4.	Nereidae	<i>Namalycastis abiuma</i>	<ul style="list-style-type: none"> Brown epidermal pigment dorsally and on pygidium; prostomium with shallowly cleft anteriorly, antennae extending short of tip of palpophore. <i>N. abiuma</i> species group except body uniform in width anteriorly, tapering gradually posteriorly. Eyes, 2 pairs, black. 	Fauvel, (1953); Day (1967)

RESULTS AND DISCUSSION

Totalling four species of polychaetes *Capitella capitata*, *Scalibregma inflatum*, *Dendronereis aesturiana* and *Namalycastis abiuma* (Fig. 1) were identified and their key important characters were presented in Table 1.

Over the past few decades, aquaculture production has significantly increased around the world. One of the most dynamic and promising economic sectors for global food supply is sustainable shrimp and fish production (Jinendiran et al. 2019). Probiotics have positive impacts on aquaculture, including increased growth performance (Merrifield et al. 2010), pathogen reduction, and the prevention of infectious illnesses by enhancing innate and acquired immunity (Qi et al. 2009, Nayak 2010). The greatest sources to screen beneficial bacteria based on their effective combative impact against infectious disease in aquaculture are the symbiotic associations of microbes within the host or with the aquatic environment (inter-intra-specific interactions) (Verschuere et al. 2000). *Bacillus subtilis*, *B. licheniformis*, *B. pumilus*, *B. megaterium*, and *B. halotolerans* were among the additional gut-associated bacteria that were identified and described from several polychaetes (Priscilla et al. 2022). In this work, a total of 17 types of distinguishable bacterial strains were

isolated from four different polychaetes species - *Capitella capitata*, *Scalibregma inflatum*, *Dendronereis aesturiana*, and *Namalycastis abiuma* - and evaluated for probiotic activity.

The five isolates were given the names Poly1, Poly2, Poly3, Poly4, and Poly5. Of the five isolates, three produced only lipase and protease, but only two isolates (Poly1 and Poly2) had activity for all three enzymes, such as protease, lipase and amylase (Fig. 2 and Table 2). Of the five isolates, two isolates, Poly1 and Poly2, produce antimicrobial activity against the fish pathogen *Aeromonas hydrophila* (Table 3) and produce a clear zone greater than 10 mm.

Probiotic microorganisms reportedly produce digestive enzymes to enhance the host's digestibility, according to Mohapatra et al. (2012). Additionally, the protease enzyme enhances functional qualities by creating antimicrobial peptide (AMP)-mediated defensive mechanisms against encroaching pathogens by cleaving their receptors in the intestinal epithelial cell wall (Hosoi & Kiuchi 2003). In this study, it was discovered that the probiotic bacteria *Priestia megaterium* CMST Poly2 and *Bacillus subtilis* CMST Poly1 have protease, amylase, and lipase activities. These enzymes may help the host's GI tract to digest

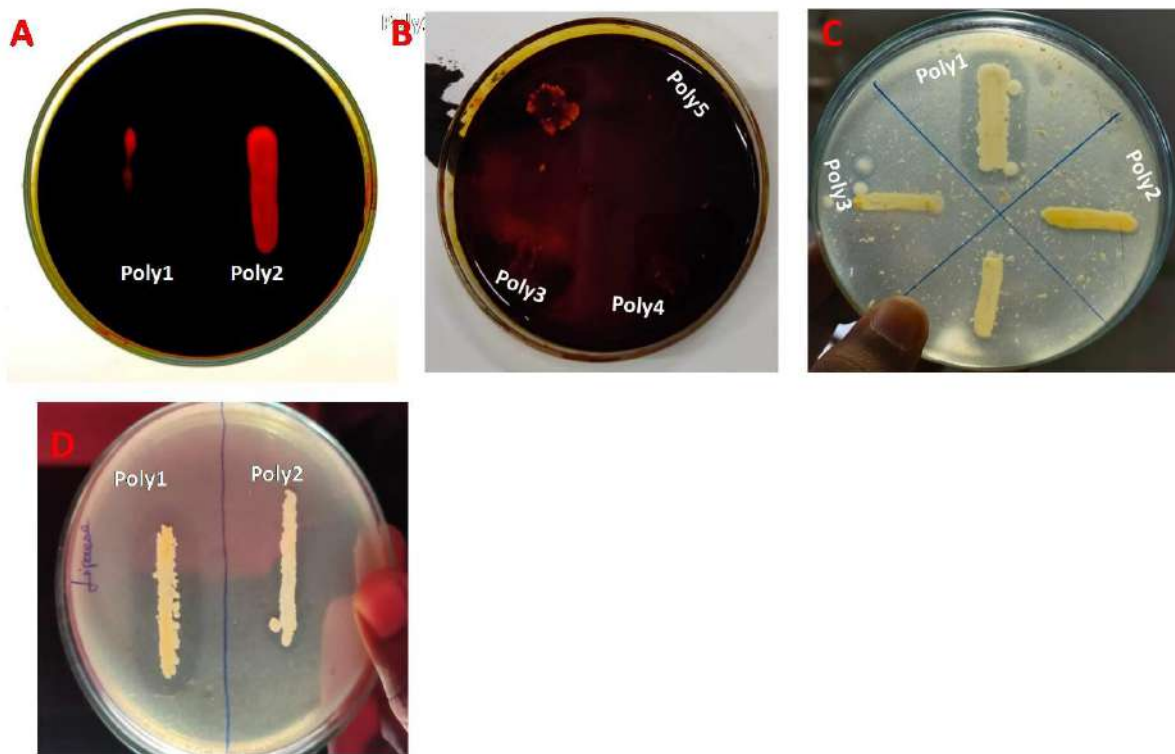


Fig. 2: Screening of extracellular enzyme activities. A. Amylase activity, B. Protease activity, C. Lipolytic activity (clear zone indicating positive results; Absence of zone indicating negative results for the enzyme activities).

Table 2: Screening of enzymatic activities for the probiotics bacteria.

S. No.	Strains Name	Extracellular enzymes activity		
		Protease	Amylase	Lipase
1.	Poly1	+	+	+
2.	Poly2	+	+	+
3.	Poly3	-	-	+
4.	Poly4	+	-	+
5.	Poly5	+	-	+

'+' : Positive Activity; '-' : Negative activity

Table 3: The screening of antimicrobial activity against fish pathogen *Aeromonas hydrophila* using the agar well diffusion assay.

Sl. No	Strains Name	Fish pathogen <i>Aeromonas hydrophila</i>
		Zone of inhibition (mm)
1.	Poly1	+
2.	Poly2	+
3.	Poly3	-
4.	Poly4	-
5.	Poly5	-

'+' : Positive Activity; '-' : Negative activity

proteins, lipids, and carbohydrates. Similar findings were made by Dawood et al. (2016) and Priscilla et al. (2022) on the production of hydrolytic enzymes amylase, lipase, and proteinase by Gram-positive *Bacillus* spp., isolated from the intestines of polychaetes. The hydrolytic enzymes enhance the host's enzyme activity and cause the creation of digestive enzymes, which improve feed utilization, survival, and immune response in the host. The ability of *Bacillus* spp. to create extracellular enzymes, such as amylolytic, proteolytic, cellulolytic, and lipolytic in the GI tracts of

tropical freshwater fish, was also the subject of numerous research studies (Bairagi et al. 2002, Kar & Ghosh, 2008, Mondal et al. 2010, Ray et al. 2012, Banerjee et al. 2013).

The probiotic strains Poly1 and Ploy 2 produce no holozone on the blood agar, which indicates that they did not produce any hemolytic activity and are harmless to cultured animals. The results of the antimicrobial disc diffusion susceptibility tests on two strains for five antibiotics are summarized in Table 4. The probiotic bacterial strains Poly1 and Ploy2 showed no resistance to the majority of tested antibiotics such as ampicillin, penicillin, tetracycline, and kanamycin (Fig. 3). Further screenings for the probiotic candidates can be done by examining the antibiotic susceptibility test results of isolates. The present results clearly showed that candidate bacterial strains had no antagonistic effect against tested commercial antibiotics. Similar to Thankappan et al. (2015), they reported that *Bacillus* spp. was susceptible to the various antibiotics amoxicillin, cephalexin, streptomycin, penicillin-G, gentamycin, and erythromycin. Likewise, Sorokulova et al. (2008) have described the commercial probiotics *B. subtilis* and *B. licheniformis* as being susceptible to common antibiotics.

Bacillus, *Lactobacillus*, *Lactococcus*, *Leuconostoc*, *Shewanella*, *Aeromonas*, *Clostridium*, and *Saccharomyces* species are among the probiotic bacteria frequently utilized in aquaculture (Nayak 2010). The immune systems and health advantages of Japanese flounder, black tiger prawns, white leg prawns, and western king prawns can all be improved by probiotics (Rengpipat et al. 1998; Chiu et al. 2007). In Nile tilapia, *Bacillus pumilus* may improve health and reduce illness (Aly et al. 2008). Infection with *Aeromonas hydrophila* was prevented by the probiotic bacteria *Bacillus*

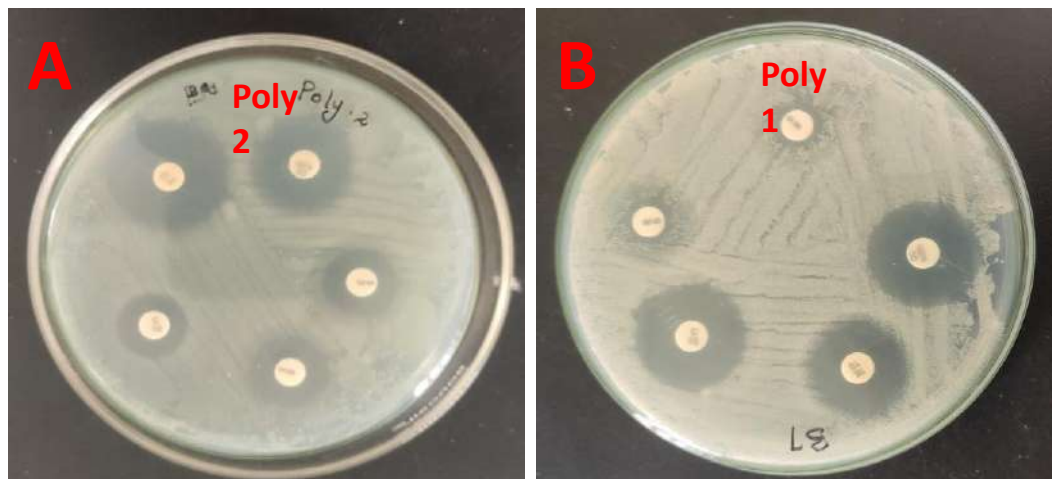


Fig. 3: Antibiotic susceptibility profile of the probiotics strains. A: *Priestia megaterium* CMST Poly2, B: *Bacillus subtilis* CMST Poly1.

Table 4: Morphological and biochemical characters of probiotic bacteria.

Characters	Probiotic bacterial strains	
	CMST Poly1	CMST Poly2
Gram's staining	+	+
Shape	Rod	Rod
Capsule staining	-	-
Spore formation	+	+
Motility	+	+
Glucose	+	+
Mannitol	-	+
Sucrose	-	+
Indole	-	-
Methyl red	+	+
Voges Proskauer	+	+
Citrate	+	+
Urease	-	-
Casein hydrolysis	+	+
Oxidase	+	+

licheniformis and *Bacillus pumilus*, as previously described by Ramesh et al. (2015). The isolated probiotic strains Poly 1 and Poly 2 were identified using biochemical traits (Table 4) and 16S rRNA gene sequencing, and the accession number was then submitted to GenBank. Both isolates are gram-positive, rod-shaped microorganisms that can use glucose, galactose, methyl red, Voges Proskauer, and catalase negatively. It was determined to be from the genus *Bacillus* spp. Our morphological and biochemical findings were found to be consistent with those of previous reports (Chu et al. 2010, Rajashekhar et al. 2017, Lee et al. 2017). The isolated strain belongs to the Firmicutes, Bacillaceae, according to phylogenetic analyses. The phylogenetic tree produced using the neighbor-joining approach explains the strain's evolutionary relationship to other genera and species (Fig. 4). The isolate's 16S rRNA gene sequence was uploaded to GenBank as *Bacillus subtilis* CMST Poly1 and *Priestia megaterium* CMST Poly2, respectively (Accession number: OP435726). Probiotic bacterial strains *Bacillus subtilis*, *Bacillus cereus*, and *Bacillus amyloliquefaciens* were discovered using morphological and biochemical testing,

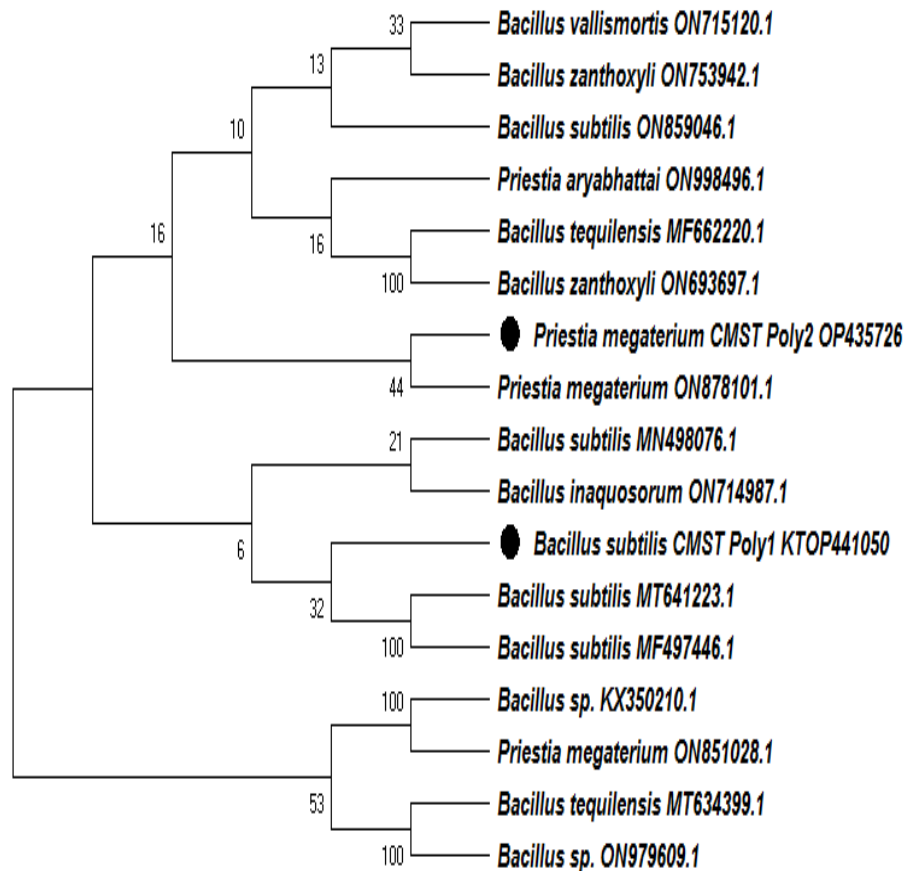


Fig. 4: Neighbor-joining phylogram based on comparative analysis of 16S ribosomal RNA gene sequences of two probiotic bacterial strains CMST Poly1 and CMST Poly2 and the closest related type strains. Percentage bootstrap values are shown at the branching points of 1000 replicates.

and their identification was further confirmed using 16S rRNA gene sequencing. Similar discoveries have also been published by Kavitha et al. (2018) and Shah et al. (2010). Several authors have reported that *B. subtilis*, *Bacillus* sp., and *B. amyloliquefaciens* are safe to use as probiotics for aquaculture use based on current investigations (Banerjee et al. 2017, Nandi et al. 2017a, & Nandi et al. 2017b).

CONCLUSION

Our findings concluded that two bacteria, *Bacillus subtilis* CMST Poly1 and *Priestia megaterium* CMST Poly2, were isolated and identified as potential probiotic candidates from polychaetes. These bacteria demonstrated good hydrolytic enzyme activity, were susceptible to common antibiotics, and exhibited no hemolytic activity *in vitro*. Additionally, the antimicrobial assay screening revealed that two prospective probiotic bacteria have inhibitory effects against the fish disease *Aeromonas hydrophila*, although more research is required to identify the antimicrobial metabolites. To screen and develop the prospective use of probiotics in fish aquaculture, this baseline study should be used as a reference.

REFERENCES

- Abumourad, I. M.K., Abbas, W.T., Awaad, E.S., Authman, M. M.N., El-Shafei, K. and Sharaf, O. M. 2013. Evaluation of *Lactobacillus plantarum* as a probiotic in aquaculture: emphasis on growth performance and innate immunity. *J. Appl. Sci. Res.*, 9: 572-582.
- Aly, S.M., Ahmed, Y.A., Ghareeb, A.A. and Mohamed, M.F., 2008. Studies on *Bacillus subtilis* and *Lactobacillus acidophilus*, as potential probiotics, on the immune response and resistance of *Tilapia nilotica* (*Oreochromis niloticus*) to challenge infections. *Fish Shellfish Immunol.*, 25: 128-136. <https://doi.org/10.1016/j.fsi.2008.03.013>
- Bairagi, A., Ghosh, K.S., Sen, S.K. and Ray, A.K. 2002. Enzyme producing bacterial flora isolated from fish digestive tracts. *Aquacult. Int.*, 10: 109-121. <https://doi.org/10.1023/A:1021355406412>
- Banerjee, G., Ray, A.K., Askarian, F. and Ringø, E., 2013. Characterization and identification of enzyme-producing autochthonous bacteria from the gastrointestinal tract of two Indian air-breathing fish. *Benef. Microbes.*, 4: 277-284. <https://doi.org/10.3920/bm2012.0051>
- Banerjee, G., Nandi, A. and Ray, A.K. 2017. Assessment of hemolytic activity, enzyme production and bacteriocin characterization of *Bacillus subtilis* LR1 isolated from the gastrointestinal tract of fish. *Arch. Microbiol.*, 199: 115-124. <https://doi.org/10.1007/s00203-016-1283-8>
- Cintas, L. M., Rodriguez, J. M., Fernandez, M.F., Sletten, K., Nes, I. F., Hernandez, P.E. and Holo, H. 1995. Isolation and characterization of pediocin L50, a new bacteriocin from *Pediococcus acidilactici* with a broad inhibitory spectrum. *Appl. Environ. Microbiol.*, 61(7): 2643-2648. <https://doi.org/10.1128/AEM.61.7.2643-2648.1995>
- Chen, N. Z. and Wang, W. 2019. Effects of *Lactobacillus pentosus* on the growth performance, digestive enzyme and disease resistance of white shrimp, *Litopenaeus vannamei* (Boone, 1931). *Aquacult. Res.*, 48:2767-2777. <https://doi.org/10.1111/are.13110>
- Chiu, C. H., Guu, Y. K., Liu, C. H., Pan, T. M. and Cheng, W. 2007. Immune responses and gene expression in white shrimp, *Litopenaeus vannamei*, induced by *Lactobacillus plantarum*. *Fish & Shellfish Immunology.*, 23(2): 364-377. <https://doi.org/10.1016/j.fsi.2006.11.010>
- Chu, W., Lu, F., Zhu, W. and Kang, C. 2010. Isolation and characterization of new Potential probiotic bacteria based on quorum-sensing system. *J. Appl. Microbiol.*, 110: 202-208. <https://doi.org/10.1111/j.1365-2672.2010.04872.x>
- Day, J. H. 1967. A monograph on the polychaeta of Southern Africa. Trustees of the British Museum (Natural History). Publication No., 656.
- Dawood, M.A.O., Koshio, S. Ishikawa, M. and Yokoyama, S. 2016. Effects of dietary inactivated *Pediococcus pentosaceus* on growth performance, feed utilization and blood characteristics of red sea bream, *Pagrus major* juvenile. *Aquac. Nutr.*, 22: 923-932. <https://doi.org/10.1111/anu.12314>
- Fauchald, K. 1977. The polychaete worms, definitions and keys to the orders, families and genera. *Nat. Hist. Mus. LA County Mus. Sci. Ser.*, 28: 1-190.
- Fauvel, P. 1953. Annelida Polychaeta. The Fauna of India Including Pakistan, Ceylon, Burma and Malaya. 507.
- Grassle, J.F. and Maciolek, N.J. 1992. Deep-sea species richness; regional and local diversity estimates from quantitative bottom-sampling. *Am. Nat.*, 139: 313-41.
- Garrity, G. M, Boone, D. R. and Castenholz, R. W. 2001. *Bergey's Manual of Systematic Bacteriology*, 2nd ed., Springer, New York.
- Hosoi, T. and Kiuchi, K. 2003. *Handbook of Fermented Functional Foods*. CRC Press, pp. 227-245.
- Igbinsosa, I.H., Igumbor, E.U., Aghdasi, F., Tom, M. and Okoh. A. I. 2012. Emerging *Aeromonas* species infections and their significance in public health, *Sci. World J.*, 625023: 1-13. <https://doi.org/10.1100/2012/625023>
- Jinendiran S., Boopathi, S., Sivakumar, N. and Selvakumar, G. 2019. Functional characterization of probiotic potential of novel pigmented bacterial strains for aquaculture applications. *Probiotics Antimicrob Proteins.*, 11: 186-197. <https://doi.org/10.1007/s12602-017-9353-z>
- Kar, N., Roy, R.N., Sen, S.K. and Ghosh, K. 2008. Isolation and characterization of extra-cellular enzyme-producing bacilli in the digestive tracts of rohu, *Labeo rohita* (Hamilton) and murrel, *Channa punctatus* (Bloch). *Asian Fish. Sci.*, 21 (4): 421-434. <http://dx.doi.org/10.33997/j.afs.2008.21.4.006>
- Kavitha, M., Raja, M. and Perumal, P. 2018. Evaluation of probiotic potential of *Bacillus* spp. isolated from the digestive tract of freshwater fish *Labeo calbasu* (Hamilton, 1822). *Aquaculture Reports*, 11: 59-69. <https://doi.org/10.1016/j.aqrep.2018.07.001>
- Lieke, T., Meinelt, T., Hoseinifar, S.H., Pan, B., Straus, D. L. and Steinberg, C.E.W. 2019. Sustainable aquaculture requires environmental-friendly treatment strategies for fish diseases. *Rev. Aquac.*, 12(2): 943-965. <https://doi.org/10.1111/raq.12365>
- Lee, A., Cheng, K.C. and Liu, J.R. 2017. Isolation and characterization of a *Bacillus amyloliquefaciens* strain with zearalenone removal ability and its probiotic potential. *PLoS One*, 12(8): e0182220. <https://doi.org/10.1371/journal.pone.0182220>
- Mohapatra, S., Chakraborty, T., Prusty, A. K., Das, P., Paniprasad, K. and Mohanta K.N. 2012. Use different microbial probiotic in the diet of rohu, *Labeo rohita* fingerlings: effect on growth, nutrient digestibility and retention, digestive enzyme activities and intestinal microflora. *Aquacult Nutr.*, 18(1): 1-11. <https://doi.org/10.1111/j.1365-2095.2011.00866.x>
- Mondal, S., Roy, T. and Ray, A.K. 2010. Characterization and identification of enzyme-producing bacteria isolated from the digestive tract of *Labeo bata*. *J. World Aquacult. Soc.*, 41: 369-377. <https://doi.org/10.1111/j.1749-7345.2010.00378.x>
- Merrifield, D. L., Harper, G. M., Dimitroglou, A., Ringø, E. and Davies, S. J. 2020. Possible influence of probiotic adhesion to intestinal mucosa on the activity and morphology of rainbow trout (*Oncorhynchus mykiss*) enterocytes. *Aquacult. Res.*, 41: 1268-1272. <https://doi.org/10.1111/j.1365-2109.2009.02397.x>
- Nya, E.J. and Austin, B. 2011. Development of immunity in rainbow trout (*Oncorhynchus mykiss*, Walbaum) to *Aeromonas hydrophila* after the

- dietary application of garlic. *Fish Shellfish Immunol.*, 30: 845-850. <https://doi.org/10.1016/j.fsi.2011.01.008>
- Nawaz, A., Javaid, A. B., Irshad, S., Hoseinifar, S. H. and Xiong, H. G. 2018. The functionality of prebiotics as immunostimulant: Evidences from trials on terrestrial and aquatic animals., *Fish Shellfish Immunol.*, 76: 272-278. <https://doi.org/10.1016/j.fsi.2018.03.004>
- Nayak, S. K. 2010. Probiotics and immunity: a fish perspective. *Fish Shellfish Immunol.*, 29: 2-14. <https://doi.org/10.1016/j.fsi.2010.02.017>
- Nandi, A., Dan, S.K., Banerjee, G., Ghosh, P., Ghosh, K. Ringø, E. and Ray, A.K. 2017a. Probiotic potential of Autochthonous bacteria isolated from the gastrointestinal tract of four freshwater teleost's. *Probiotics Antimicrob. Proteins.*, 9: 12-21. <https://doi.org/10.1007/s12602-016-9228-8>
- Nandi, A., Banerjee, G., Dan, S.K., Ghosh, P., Ghosh, K. and Ray, A.K. 2017b. Screening of autochthonous intestinal microbiota as candidate probiotics isolated from four freshwater teleosts. *Curr. Sci.*, 113(4): 25.
- Plumb, J. A., Infectious diseases of tilapias, In: Costa-Pierce, B. A. and Rakocy, J.E. (Eds.). 1997. *Tilapia aquaculture in the Americas*. J. World Aquac Soc., 1: 212-228.
- Palmer, P.J., Wang, S., Houlihan, A. and Brock, I., 2014. Nutritional status of a nereidid polychaete cultured in sand filters of mariculture wastewater. *Aquac. Nutr.*, 20: 675-691. <https://doi.org/10.1111/anu.12129>
- Priscilla, L., Rajeev, M. and Pandian, S. K. 2022. Gut associated culturable bacterial community in intertidal polychaete worms (Annelida: Polychaeta), their characterization and implications in captive shrimp aquaculture. *Regional Studies in Marine Science*, 52: 102274. <https://doi.org/10.1016/j.rsma.2022.102274>
- Qi, Z., Zhang, X.H., Boon, N. and Bossier, P. 2009. Probiotics in aquaculture of China current state, problems and prospect. *Aquaculture*, 290: 15-21. <https://doi.org/10.1016/j.aquaculture.2009.02.012>
- Ray, A.K., Ghosh, K. and Ringø, E. 2012. Enzyme-producing bacteria isolated from fish gut: a review. *Aquacult. Nutr.*, 18: 465-492. <https://doi.org/10.1111/j.1365-2095.2012.00943.x>
- Rengpipat, S., Rukpratanporn, S., Piyatiratitivorakul, S. and Menasveta, P. 1998. Probiotics in aquaculture: a case study of probiotics for larvae of the black tiger shrimp (*Penaeus monodon*). In: Flegel, T.W. (Ed.), *Advances in Shrimp Biotechnology*. National Center for Genetic Engineering and Biotechnology, Bangkok.
- Ramesh, D., Vinothkanna, A., Rai, A.K. and Venkada Subramanian, V. 2015. Isolation of potential probiotic *Bacillus* spp. and assessment of their sub cellular components to induce immune responses in *Labeo rohita* against *Aeromonas hydrophila*. *Fish Shellfish Immunol.*, 45: 268-276. <https://doi.org/10.1016/j.fsi.2015.04.018>
- Rajashekhar, M. Shahanaaz, E. and Vinay, K. 2017. Biochemical and molecular characterization of *Bacillus* spp. isolated from insects. *J. Entomol. Zool. Stud.*, 5(5): 581-588.
- Silva, B.C., Mouriño, J.L.P., Vieira, F.N., Jatoba, A., Seifert, W. Q. and Martins, M. L. 2012. *Haemorrhagic septicaemia* in the hybrid surubim (*Pseudoplatystom acoruscans* and *Pseudoplatystom afasciatum*) caused by *Aeromonas hydrophila*. *Aquacult. Res.*, 43: 908-916. <https://doi.org/10.1111/j.1365-2109.2011.02905.x>
- Son, V.M., Changa, C. C., Wu, M. C., Guu, Y. K., Chiu, C. H. and Cheng, W. 2009. Dietary administration of the probiotic, *Lactobacillus plantarum*, enhanced the growth, innate immune responses, and disease resistance of the grouper *Epinephelus coioides*. *Fish Shellfish Immunol.*, 26: 691-698. <https://doi.org/10.1016/j.fsi.2009.02.018>
- Saitou, N. and Nei, M. 1987. The neighbor-joining method: a new method for reconstructing phylogenetic trees. *Mol. Biol. Evol.*, 4: 406-425. <https://doi.org/10.1093/oxfordjournals.molbev.a040454>
- Sorokulova, B., Pinchuk, V., Denayrolles, M., Osipova, G., Huang, J. M., Cutting, S. M. and Urdaci, M. C. 2008. The safety of two *Bacillus* probiotic strains for human use. *Dig Dis Sci.*, 53(4): 954. <https://doi.org/10.1007/s10620-007-9959-1>
- Sharma, A. D. and Singh, J. 2005. A nonenzymatic method to isolate genomic DNA from bacteria and Actinomycete. *Anal. Biochem.*, 337: 354-356. <https://doi.org/10.1016/j.ab.2004.11.029>
- Shah, K., Mody, K., Keshri, J. and Jha, B. 2010. Purification and characterization of a solvent, detergent and oxidizing agent tolerant protease from *Bacillus cereus* isolated from the Gulf of Khambhat. *J. Mol. Catal. B: Enzym.*, 67: 85-91. <https://doi.org/10.1016/j.molcatb.2010.07.010>
- Thankappan, B., Ramesh, D., Ramkumar, S., Natarajaseenivasan, K. and Anbarasu, K. 2015. Characterization of *Bacillus* spp. from the gastrointestinal tract of *Labeo rohita* towards to identify novel probiotics against fish pathogens. *Applied biochemistry and biotechnology.*, 175(1): 340-353. <https://doi.org/10.1007/s12010-014-1270-y>
- Verschuere, L., Rombaut, G., Sorgeloos, P. and Verstraete W. 2000. Probiotic bacteria as biological agents in aquaculture. *Microbiol. Mol. Biol. Rev.*, 64(4): 655-671. <https://doi.org/10.1128%2Fmmbr.64.4.655-671.2000>
- Wang, J.L., Meng, X. L. Lu, R.H. Wu, C. Luo, Y. T. and Yan, X. 2015. Effects of *Rehmannia glutinosa* on growth performance, immunological parameters and disease resistance to *Aeromonas hydrophila* in common carp (*Cyprinus carpio* L.). *Aquaculture*. 435: 293-300. <https://doi.org/10.1016/j.aquaculture.2014.10.004>
- Ward, T. and Hutchings, P. A. 1996. Effects of trace metals on in faunal species composition in polluted intertidal and subtidal marine sediments near a lead smelter, Spencer Gulf, South Australia. *Mar. Ecol. Progr. Ser.*, 135: 123-35.
- Yang, F., Wang, A., Zeng, X., Hou, C., Liu, H. and Qiao, S. 2015. *Lactobacillus reuteri* I5007 modulates tight junction protein expression in IPEC-J2 cells with LPS stimulation and in newborn piglets under normal conditions. *BMC Microbiology.*, 15(1): 1-11. <https://doi.org/10.1186/s12866-015-0372-1>



Analyses of Polycyclic Aromatic Hydrocarbons (PAHs) in the Ganga River Water in Uttar Pradesh, India

Poonam Sonwani¹ and Sandhya Bharti[†]

Fish Physiology and Ecotoxicology Laboratory, Department of Zoology, Babasaheb Bhimrao Ambedkar University, Lucknow, Uttar Pradesh, India

[†]Corresponding author: Sandhya Bharti; sandhyabharti54@gmail.com

Nat. Env. & Poll. Tech.
Website: www.neptjournal.com

Received: 29-10-2022
Revised: 06-01-2023
Accepted: 17-01-2023

Key Words:

Ganga river
PAHs analysis
Carcinogenic compounds
Benzo(a)pyrene

ABSTRACT

Polycyclic aromatic hydrocarbons (PAHs) were analyzed in the Ganga River water samples collected from three cities. Jajmau (Kanpur), Dala Khera (Fatehpur), and Kara Kachar (Kaushambi) of Uttar Pradesh, India. At Jajmau (Kanpur), out of sixteen PAHs, eight were found in the Ganga river water in concentration ($\mu\text{g.L}^{-1}$) order: acenaphthylene (3.8356) > pyrene (0.5878) > fluorene (0.5752) > anthracene (0.2806) > benzo(b)fluoranthene (0.1960) > phenanthrene (0.0526) > benzo(a)pyrene (0.0234) > naphthalene (0.006). In contrast, in Dala Khera (Fatehpur), two PAHs: anthracene (0.2806) and fluorene (0.07894), were observed. In Kara Kachar (Kaushambi), only single phenanthrene (0.04507) was detected. It was noticed that the three-ring types of PAHs occur commonly in all three sites. It is concerning because the river water sampled had PAH concentrations, namely Acy, Flu, Phe, and Pyr, that were relatively higher than those recommended ($0.05 \mu\text{g.L}^{-1}$) by WHO (1998) in surface water. In contrast, the amounts of Nap, Ant, BbF, and Bap were recorded within the safe levels in Kanpur, while in the other two cities (Fatehpur and Kaushambi), Phe and Ant were detected lower than their permissible limit. Flu was measured as higher than its recommended value by WHO (1998). Similarly, the concentration of Acy, Ant, Pyr, BbF and BaP in river water samples at Jajmau, Kanpur were higher than their safe limits suggested by RIVM report 607711007/2012 for inland surface water while Nap, Flu, and Phe were lower than their recommended values. However, at, Dala Khera and Kara Kachar (Fatehpur and Kaushambi respectively), the concentrations of Ant, Flu and Phe were lower than their prescribed limits given by RIVM 607711007/2012.

INTRODUCTION

Polycyclic aromatic hydrocarbons (PAHs) are the priority pollutants that have imposed severe ecological and human health risks due to their non-biodegradable and lipophilic nature (Kafilzadeh et al. 2011, Wolska et al. 2012, Duttagupta et al. 2020a). Chemically, they bear two to six fused aromatic rings of carbon and hydrogen atoms. They enter into the environment via anthropogenic activities or natural sources such as industrial emissions, automobiles fuel burning, incomplete combustion of fossils fuels like petroleum and coal, domestic, agricultural, and urban waste-water discharges or volcanic eruption, forest fires, and natural oil seepage respectively (Agarwal et al. 2006, Farooq et al. 2011, Li & Ran 2012, Awe et al. 2020, Ofori et al. 2020). Though more than hundreds of PAHs have been identified in water,

soil, and air, sixteen of them, namely Naphthalene (Nap), Acenaphthylene (Acy), Acenaphthene (Ace), Fluorene (Flu), Phenanthrene (Phe), Anthracene (Ant), Fluoranthene (Flu), Pyrene (Py), Benzo(a)anthracene (BaA), Chrycene (Chy), Benzo(b)fluoranthene (BbF), Benzo(k)fluoranthene (BkF), Benzo(a)pyrene (BaP), Dibenzo(a,h)anthracene (DbA), Benzo(ghi)perylene (Bper), and Indeno(1,2,3-cd) pyrene (IP) were reported to exhibit carcinogenic effects (USEPA 2013). Despite being toxic, they are extensively utilized in the market to manufacture various industrial and commercial goods. They are preferred because PAHs containing raw materials are readily available, cost-effective, and have peculiar characteristics that endow waterproofing, abrasion resistance, binding ability, moisture and UV radiation protection, flexibility, elasticity, adhesiveness, tensile strength to the products that increase their shelf lives (USEPA 2013, Purr et al. 2016). Consequently, vast amounts of effluents containing PAHs from these industrial types get released into the aquatic ecosystem directly or indirectly

ORCID details of the authors:

Poonam Sonwani: <https://orcid.org/0000-0003-3264-3046>

Sandhya Bharti: <https://orcid.org/0000-0001-7883-4572>

(Sogbanmu et al. 2019, Duttgupta et al. 2020b). However, most of the studies were confined to the analysis of PAHs concentrations in the sediments of the aquatic ecosystem such as Hooghly river estuary (Zanardi-Lamardo et al. 2019), Cochin estuary (Ramzi et al. 2017), Adyar river, Cooum river, Ennore estuary, and Pulicat lake (Goswami et al. 2016), Yamuna river (Agarwal et al. 2006, Kumar et al. 2014) and Hooghly and Brahmaputra river (Khuman et al. 2018). Only few workers have measured it in surface freshwater resources (Kafilzadeh et al. 2011, Hussain et al. 2014, Singare 2016, Srivastava et al. 2017). Some researchers also demonstrated PAHs' detrimental effects on aquatic fauna. For instance, physiological malfunctions such as muscles atrophy in fish (Olayinka et al. 2019), CAT and LPO in *Mya arenaria* (Frouin et al. 2007), GST and CAT *Mytilus trossulus* and *Neries* (Pempkowiak et al. 2006). Since humans directly consume fish as one of the primary proteinaceous sources, it could be dangerous to their lives. Hence, PAH analysis in the aquatic ecosystem should be monitored regularly (Incardona et al. 2015, Wu et al. 2011, Patel et al. 2020). For the current purpose, the concentration of sixteen toxic PAHs was analyzed in the Ganga river water samples collected from three major cities of Uttar Pradesh, India: Kanpur, Fatehpur, and Kaushambi. River water sampling was conducted from the Ganga in Uttar Pradesh (UP), India, because the Ganga traverses a maximum (of 1000 km) in UP,

and several industrial estates drain their waste directly into the river leading to its contamination. Since Ganga is globally worshipped as "Ganga Ma" and is extensively used by millions of people for ritual activities, drinking, bathing, and domestic purposes. Therefore, it becomes imperative to analyze PAHs in the Ganga river water (Haritash et al. 2016, Nagpure et al. 2017).

MATERIALS AND METHODS

Chemicals

Sixteen mix PAHs external standard ($2000 \mu\text{g.mL}^{-1}$) was purchased from Chem Service Inc. Germany. Dichloromethane (CAS No. 75-09-2), Acetonitrile (CAS No. 75-05-8), and n-hexane (CAS No. 110-54-3) were procured from Merk Life Sciences. Silica gel (CAS No. 112926-00-8) was bought from Sigma-Aldrich, high purity grade (7734), pore size 60\AA , 70-230 mesh.

Instrumentation

An Agilent 1220 Infinity HPLC was equipped with a UV detector (254nm). Operating conditions were: flow rate- 0.9 mL.min^{-1} , sample volume - $20 \mu\text{L}$, run time- 45 min, column: ZORBAX Eclipse C18 (250mm long \times $5\mu\text{m}$ ID), mobile phase was water and acetonitrile as ratio of 60:40, programme was set same as APHA AWWA (2008).

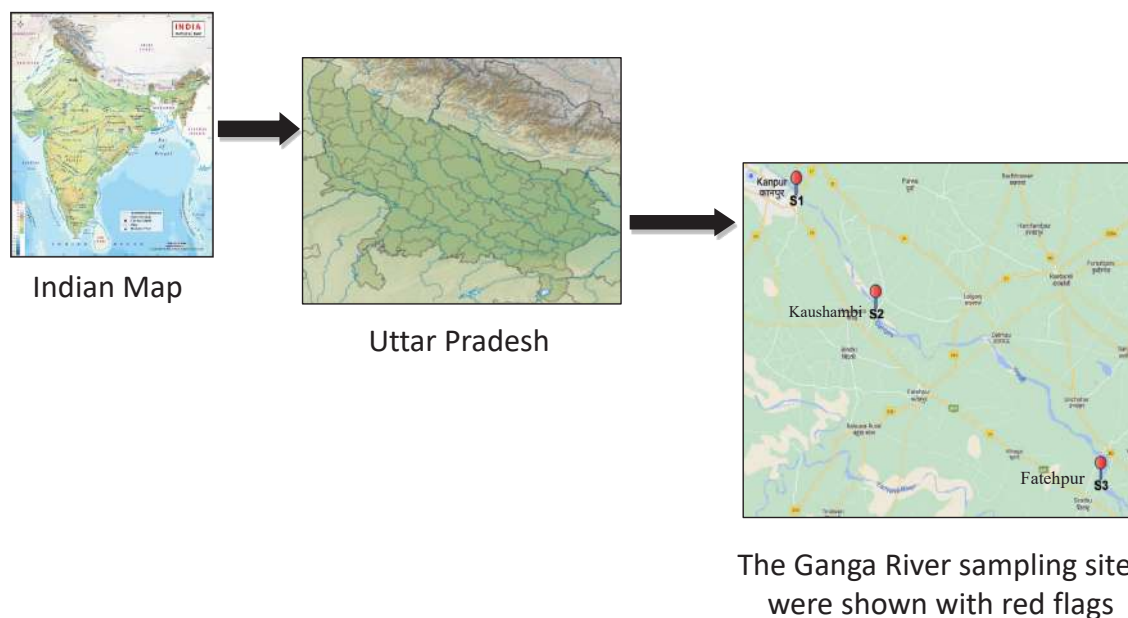


Fig. 1: Map of the Ganga River showing the sampling sites.

Study Area

The present study was carried out about the stretch of 183 km from Kanpur to Kaushambhi, lying in the basin of Ganga (Fig. 1). The sampling sites were Jajmau (Kanpur, Latitude 26.435391° and Longitude 80.408684°), Dala Khera (Fatehpur, Latitude (26.103616° and Longitude 80.66689°), and Kara Kachar (Kaushambi, Latitude 25.706076° and Longitude 81.366626°). Approximately 200 large and small industries are located in Kanpur along the Ganga river bank, having significant sludge sources generated by industries. Kanpur poured 18 drains (domestic and industrial waste) directly into River Ganga. A common effluent treatment plant (CETP) is located at Jajmau, but it is insufficient for treating industrial, tannery, and domestic effluent. Fatehpur, which is the meeting point of the Pandu River to the Ganga, drifts most of the domestic effluents of rural and urban areas. River Pandu joins seven drains named Panki TTP drain, ICI drain, Ganda Nalla, COD Nalla, Halwakhanda Nalla, Ratanpur Nalla, and Panki thermal power by passing through Kanpur. Almost 210,000 tons of fly ash coal-based power plant was discarded in Pandu River in Kanpur. Pandu receives domestic wastes from villages/towns (Sultanpur, Kaindepur, Matinpur, Pure Dayal, Saurajpur, Kotla, Khalispur, Baghauri, Lahangi Aht) located at Fatehpur (UPPCB 2015), and these effluents ultimately dump into river Ganga. District Kaushambi is rich in many historical places in which most of the area is covered by agricultural land. A few famous temples, such as Karadham, Sheetla Maa, and the Jain, are the primary source of tourist fascination. Kara Kachar is the spot of the present study, obtaining agricultural and ritual waste.

Water Sampling

The present study is conducted in the rainy season from 25-08-2021 to 30-10-2021. We collected river samples to the midstream of the Ganga River below 30 cm of the surface in 1-liter amber glass bottles for PAHs analysis by following APHA-AWWA (2008) and immediately transferred to the ice box and brought them to the laboratory for further extraction and cleanup.

Extraction and Cleanup of the Sample

First, by adding Acetonitrile to the stock solution, we prepared calibration standards solution at four concentration levels, 1%, 3%, 5%, and 7%. We extracted the sample within seven days of collection and thoroughly analyzed it within forty days of extraction according to EPA method 610. The samples were extracted with the liquid-phase extraction method of APHA AWWA (2008) The extraction procedure involved a 1 L water sample in a 2 L beaker added 80ml of dichloromethane. After adding DCM, shake the sample for 15 min.

Furthermore, pour it into 2 L of the separatory funnel and hold it for 5 min to separate aqueous and non- aqueous phase. After the separation, the nonaqueous extract was collected in another conical flask and repeated this process thrice. The pooled extract was filtered with Whatman 42 filter paper. After extraction, a sample cleanup was performed by making the slurry of 10 g activated silica gel in n-hexane and placed in a 50 mL and 10 mm internal diameter (ID) chromatographic glass column and placing 1-2 cm anhydrous sodium sulfate to the top of the column for demoiurized the sample. Before loading the sample, wash the column by DCM three to four times. PAHs were eluted by applying the mixture (50 mL) of n-hexane and dichloromethane in the ratio (30:20, v/v). The extracted sample was concentrated in a rotatory evaporator till the sample remained at 0.5 μ L and made up the sample 1 mL by adding 0.5 μ L Acetonitrile.

RESULTS

Table 1 represents the concentration of various PAHs found in the Ganga river water samples at all three different sampling cities, namely Jajmau (Kanpur), Dalakhera (Fatehpur), and Kara Kachar (Kaushambi) of Uttar Pradesh, India. Results represent the triplicate analysis of the samples as the mean value. It was noted that Ace, Fl_n, BaA, Chy, Bk_f, DbA, BPer, and IP PAHs were not present in the Ganga river water samples at any of the three cities. However, the rest eight PAHs, namely Nap (two-rings), Acy, Flu, Phe, Ant (three-rings), Pyr (four-rings), and BbF, BaP (five-rings), were found in Kanpur. Flu and Ant were present in the Ganga river water samples at Fatehpur, and only Phe was detected in Kaushambi (Table 1). The concentrations (μ g.L⁻¹) of eight PAHs in Kanpur followed the order: Nap (0.006) < BaP (0.0234) < Phe (0.0526) < BbF (0.1960) < Ant (0.2806) < Flu (0.5752) < Pyr (0.5878) < Acy (3.8356) (Table 1). The results conclude that PAH concentration exceeds at the urban site than in semi-urban and rural areas. Kanpur is known for anthropogenic pollution due to local vehicle combustion, industrial coal combustion, and biomass burning. Therefore, surface run-off, vehicle emissions, or industries may contaminate rivers primary with PAHs. The amounts (μ g.L⁻¹) of Flu and Ant were 0.07894 and 0.0017, respectively, at Fatehpur, while the quantity of Phe was 0.04507 μ g.L⁻¹ in Kaushambi (Table 1). The finding of high variation in PAH distribution at all three cities can be due to the resuspension of road dust by wind and vehicles. Further, Ganga river water samples at Kanpur were noticed to be contaminated with both low molecular weight (LMW) and high molecular weight (HMW) PAHs having rings ranging from one to five. It was observed that 3-ringed PAHs were commonly present at all three sites (Table 1). According to Ravindra et al. (2008), three PAH rings correspond to

Table 1: Concentration ($\mu\text{g.L}^{-1}$) of PAHs in the Ganga River water samples in the three different studied sites.

S. No.	Polycyclic aromatic hydrocarbons	Jajmou (Kanpur)	Dala Khera (Fatehpur)	Kara Kachar (Kaushambi)
1.	Naphthalene	0.006 \pm 0.00072	ND	ND
2.	Acenaphthylene	3.8356 \pm 0.3009	ND	ND
3.	Acenaphthene	ND	ND	ND
4.	Fluorene	0.5752 \pm 0.0462	0.07894 \pm 0.009	ND
5.	Phenanthrene	0.0526 \pm 0.01163	ND	0.04507 \pm 0.015
6.	Anthracene	0.2806 \pm 0.0288	0.0017 \pm 0.003	ND
7.	Fluoranthene	ND	ND	ND
8.	Pyrene	0.5878 \pm 0.097	ND	ND
9.	Benzo(a)anthracene	ND	ND	ND
10.	Chrysene	ND	ND	ND
11.	Benzo(b)fluoranthene	0.1960 \pm 0.0237	ND	ND
12.	Benzo(k)fluoranthene	ND	ND	ND
13.	Benzo(a)pyrene	0.0234 \pm 0.0017	ND	ND
14.	Dibenzo(a,h)anthracene	ND	ND	ND
15.	Benzo(ghi)perylene	ND	ND	ND
16.	Indeno(1,2,3-cd)pyrene	ND	ND	ND

ND = Not detected

pyrogenic sources such as diesel, creosote, and coal tar pitch used for transportation. All three studied cities are suggested to contribute to PAH contamination by pyrogenic sources. The concentration of Acy, Flu, Phe, and Pyr in river water samples was comparatively higher than their levels recommended ($0.05 \mu\text{g.L}^{-1}$) by WHO (1998) in surface water. Although on the contrary, the amounts of Nap, Ant, BbF, and Bap were recorded within the safe levels of WHO

(1998). In the other two cities (Fatehpur and Kaushambi), Phe and Ant were detected lower than their permissible limit, while Flu was measured at higher levels compared to their recommended values at Dala Khera (Fatehpur) than WHO (1998) limits. Similarly, the concentration of Acy, Ant, Pyr, BbF, and BaP in a river water sample at Kanpur (Fig. 2) was higher than their safe limit suggested by the RIVM report (607711007/2012) in inland surface water while Nap,

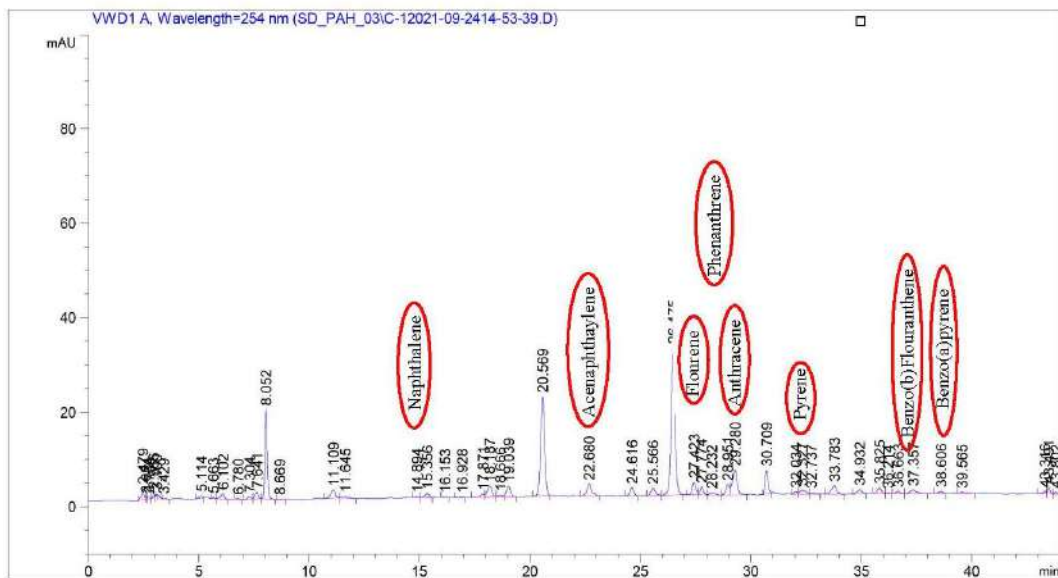


Fig. 2: Graph showing identified PAHs at Jajmou (Kanpur), UP, India.

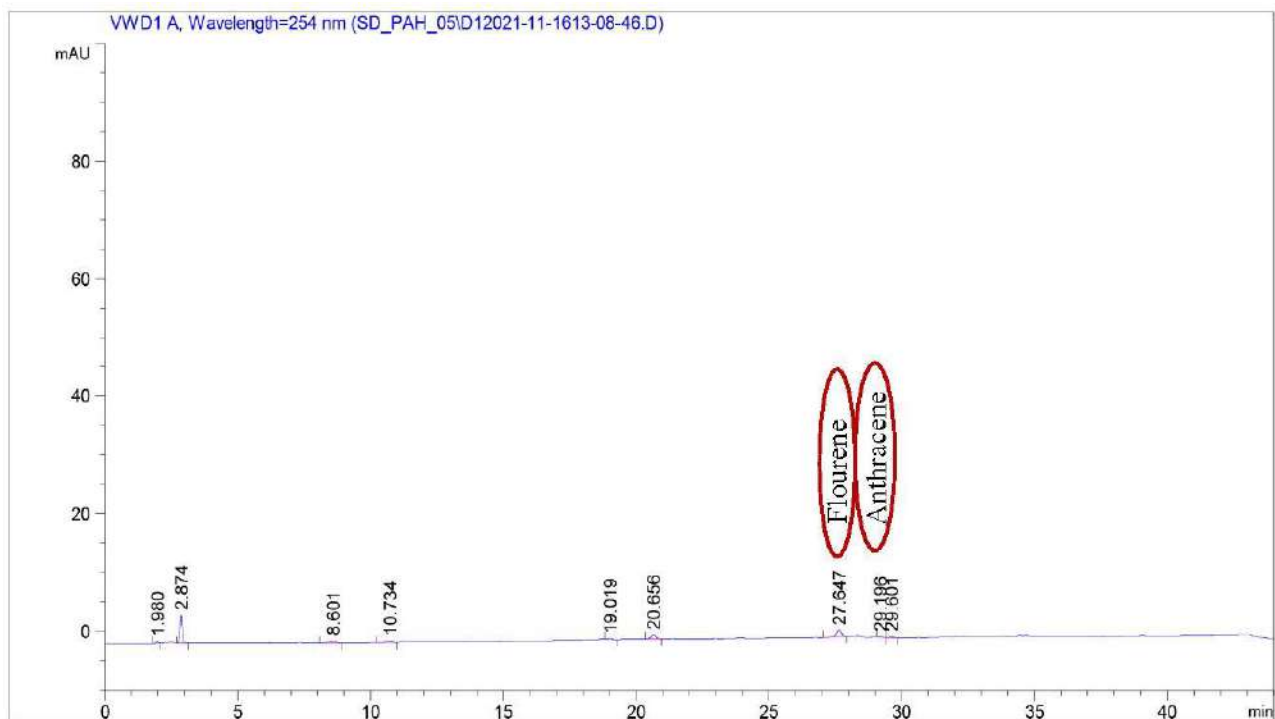


Fig. 3: Graph showing identified PAHs at Dala Khera (Fatehpur), UP, India.

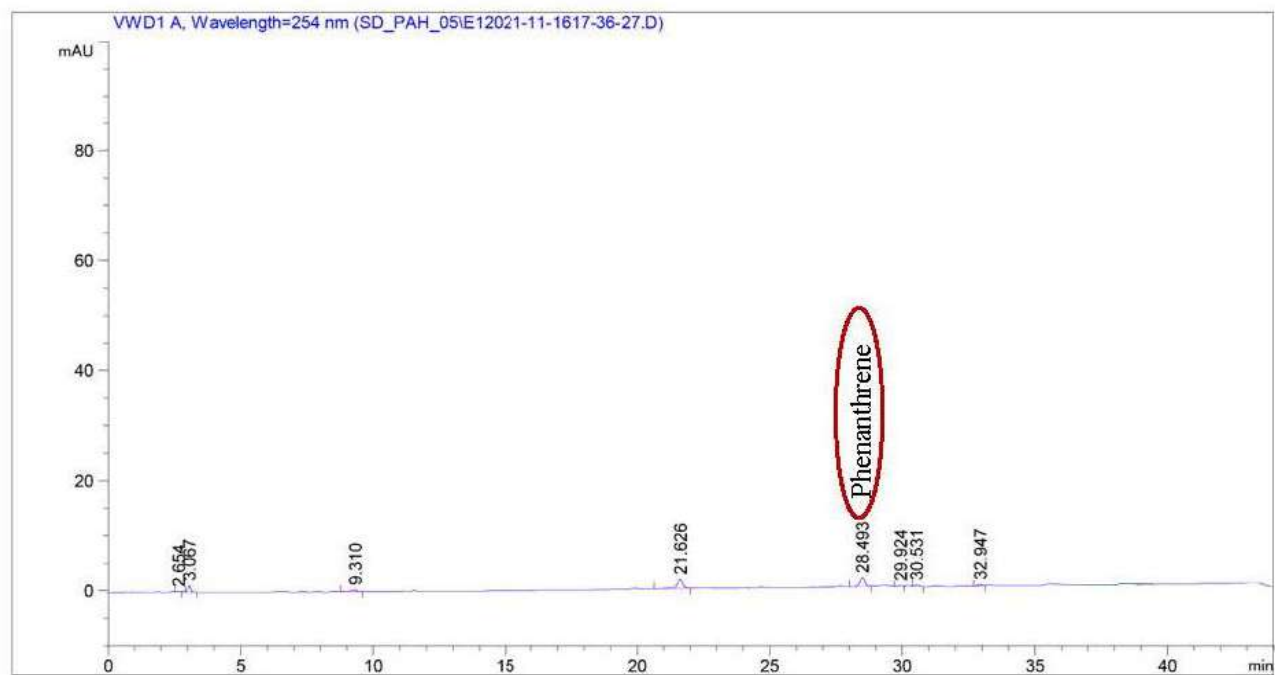


Fig. 4: Graph showing identified PAHs at Kara dham (Kaushambi), UP, India.

Table 2: Sixteen studied PAHs and their retention time.

S. No.	Polycyclic aromatic hydrocarbons (PAHs)	Retention time (min)
1.	Nap	14.698
2.	Ace	22.13
3.	Acy	24.020
4.	Flu	27.156
5.	Phe	28.385
6.	Ant	29.292
7.	Fln	31.182
8.	Pyr	32.240
9.	BaA	34.552
10.	Chy	34.744
11.	BbF	37.428
12.	BkF	37.777
13.	BaP	38.586
14.	DbA	39.601
15.	Bper	41.078
16.	IP	41.430

PAHs, while individual PAHs are less studied (Table 3). The observed PAH concentration in the present study was compared with the other river of the world, including India. The PAH concentration was comparable with the Vall River, Klip River, Chenab River, and Nile River. In India, some authors have previously revealed different types of PAHs in the Ganges River water ranging from 0.001 to 10.6 $\mu\text{g.L}^{-1}$ (Srivastava et al. 2017, Sharma & Singh 2018; Duttagupta 2020a). The Nap and Phe concentrations in Ganga River at Jajmau (Kanpur) and Kara Kachar (Kaushambi) were lower than the concentration 4.9–10.6 $\mu\text{g.L}^{-1}$ and 3.32–6.61 $\mu\text{g.L}^{-1}$ noticed by Duttagupta et al. (2020b) in the Ganga River, Western Bengal Basin, India.

Further, the concentration of BaP (0.0234 $\mu\text{g.L}^{-1}$) was comparatively higher than BaP in the Nile River of Egypt (Refai et al. 2022). BaP was investigated in Jajmau, Kanpur, which has been described as the most potent carcinogenic and used as a standard indicator for all PAHs (Masih et al. 2019). BaP measures the potential toxicity of the other priority PAH congeners by multiplying the PAH concentration by its corresponding toxic equivalent factor

Table 3: Occurrence of PAHs in rivers globally.

S.No.	PAHs	River	Concentration	Reference
PAHs concentration in the Indian River				
1.	Σ PAHs	Mithi river (Mumbai, India)	157.96±18.99 $\mu\text{g.L}^{-1}$	Singare (2016)
2.	Σ PAHs	Ganga river (India)	0.05-65.9 ng.L^{-1}	Sharma & Singh (2018)
3.	Σ PAHs	Sea water, Mumbai Harbour (India)	83.3-377.5 ng.L^{-1}	Pandit et al. (2006)
5.	Naphthalene Phenanthrene	Ganga river basin (India)	4.9-10.6 $\mu\text{g.L}^{-1}$ 3.32-6.61 $\mu\text{g.L}^{-1}$	Duttagupta et al. (2020a, 2020b)
6.	Acenaphthylene, Fluorene, Phenanthrene, Anthracene, Pyrene, Benzo(a)anthracene, Chrycene, Benzo(b)fluoranthene, Benzo(a)pyrene, Dibenzo(a,h)anthracene, Indeno(1,2,3-ed)pyrene, Benzo (g,h,i) perylene	Ganga river (India)	0.001-1.78 $\mu\text{g.L}^{-1}$	Srivastava et al. (2017)
7.	Σ PAHs	Ganga river (India)	0.06-84.21 $\mu\text{g.L}^{-1}$	Malik et al. (2011)
8.	Σ PAHs	Municipal drain water Delhi, (India)	2.5-300 ppb	Kumar et al. (2020)
Globally, PAHs concentration in river water				
9.	Σ PAHs	Densu river basin (Ghana)	37.1 $\mu\text{g.mL}^{-1}$	Amoako et al. (2011)
	Σ PAHs	Luan river (China)	99.4 ng.L^{-1}	Cao et al. (2018)

Flu, and Phe were measured lower than its recommended value. However, the concentration of Ant, Flu, and Phe was lower than their recommended safe limit by RIVM (607711007/2012). Table 2 shows the retention time of the 16 PAH studied.

DISCUSSION

Literature studies revealed that generally, PAH levels contamination occurred in rivers of the world (Table 3). Most of the research has been done as the sum of the sixteen

S.No.	PAHs	River	Concentration	Reference
10.	Acenaphthalene	Vall river (South Africa)	0.00815-0.0828 mg.L ⁻¹	Moja et al. (2013)
	Phenanthrene		0.0214-0.0263 mg.L ⁻¹	
	Anthracene	Klip river (South Africa)	0.0073-0.0092 mg.L ⁻¹	
	Fluoranthene		0.098-0.1205 mg.L ⁻¹	
	Naphthalene		0.0339-0.0382 mg.L ⁻¹	
	Acenaphthalene		0.001-0.0073 mg.L ⁻¹	
	Phenanthrene		0.0487-0.0521 mg.L ⁻¹	
	Anthracene		0.03582-0.4072 mg.L ⁻¹	
Fluoranthene	0.0552-0.0593 mg.L ⁻¹			
11.	Nap	Chinab river (Pakistan)	192.6 ng.L ⁻¹	Farooq et al. (2011)
	Acy		53.78 ng.L ⁻¹	
	Ace		47.23 ng.L ⁻¹	
	Flu		92.22 ng.L ⁻¹	
	Phe		158.3 ng.L ⁻¹	
	Anth		32.23 ng.L ⁻¹	
	Fluo		35.65 ng.L ⁻¹	
	Pyr		63.45 ng.L ⁻¹	
	BaA		1.21 ng.L ⁻¹	
	Chr		3.08 ng.L ⁻¹	
	BbF		1.75 ng.L ⁻¹	
	BkF		2.34 ng.L ⁻¹	
	BaF		1.32 ng.L ⁻¹	
	Ind		0.25 ng.L ⁻¹	
	dBahAn		0.02 ng.L ⁻¹	
BghiP	1.38 ng.L ⁻¹			
∑PAHs	686.92 ng.L ⁻¹			
12.	∑PAHs	Raba river (Hungary)	41-437 ng.L ⁻¹	Nagy et al. (2013)
13.	Banzo(a)pyrene	Nile river (Egypt)	0.07 µg.L ⁻¹	Refai et al. (2022)
	∑PAHs		0.87 µg.L ⁻¹	
	Fluoranthene		0.14±0.14 µg.L ⁻¹	
14.	∑PAHs	Kor river (Iran)	51.42-291.4 ng.L ⁻¹	Kafilzadeh et. al (2011)
15.	∑PAHs	Danube river (Europe)	25-357 ng.L ⁻¹	Nagy et al. (2012)
16.	∑PAHs	Warri river (Nigeria)	34 ng.L ⁻¹	Asagbra et al. (2015)
17.	∑PAHs	Luanhe river (China)	309.75 ng.L ⁻¹	Li et al. (2010)

(TEF). The concentration ($\mu\text{g.L}^{-1}$) of Nap (0.006), Acy (3.8356), Phe (0.0526), and Ant (0.2806) in our reports were lower than Vall river (South Africa) (Table 3). The concentration ($\mu\text{g.L}^{-1}$) of Acy, Flu, Ant, Pyr, and BbF in our result was higher than in the Chenab river noted by Farooq et al. 2011 (Table 3). However, the level of PAHs studied in the Ganga River is considerably lower than in other rivers investigated globally (Table 3). The lowest amount of PAHs was detected at Kaushambi, located in wide-open areas with low levels of human impact. There is almost no traffic, combustion activities, or direct discharges of industrial effluents. Globally, LMW PAHs are most studies usually formed from low-temperature processes. HMW PAHs are nonvolatile and non-biodegradable, originating from high-temperature processes. The overall assessment showed that PAHs in the Ganga River water samples in all three studied sites at different cities might be due to their emission from diverse sources but more predominantly have pyrogenic origin than petrogenic.

CONCLUSION

The present study revealed that the Ganga River was contaminated with several kinds of PAHs at Jajmau, Dala Khera and Kara Kachar studied sites at Kanpur, Fatehpur, and Kaushambi. Further, the three-ringed PAHs were comparatively more than five and six-ringed PAHs. According to Jinadasa et al. (2020), three-ringed PAHs are highly damaging for fish in the early life stage; therefore, it may lead to an imbalance in the ecosystem. Hence, it is imperative to investigate PAHs distribution and sources in the Ganga River water from urban or rural areas. The findings of this study provide a new dimension of PAHs distribution in the river Ganga.

REFERENCES

- Agarwal, T., Khillare, P.S. and Shridhar, V. 2006. PAHs contamination in Bank sediment of the Yamuna River, Delhi, India. *Environ. Monit. Assess.*, 123(1-3): 151-166. doi:10.1007/s10661-006-9189-6

- American Public Health Association, American Water Works Association (APHA AWWA) 2008. Standard Methods for the Examination of water and wastewater, Water Environment Federation.
- Amoako, J., Ansa-Asare, O.D., Karikari, A.Y. and Dartey, G. 2011. Levels of polycyclic aromatic hydrocarbons (PAHs) in the Densu River Basin of Ghana. *Environ. Monit. Assess.*, 174(1-4): 471-480. doi:10.1007/s10661-010-1471-y
- Asagbra, M.C., Adebayo, A.S., Anumudu, C.I., Ugwumba, O.A. and Ugwumba, A.A.A. 2015. Polycyclic aromatic hydrocarbons in water, sediment, and fish from the Warri River at Ubeji, Niger Delta, Nigeria. *Afr. J. Aquat. Sci.*, 40(2): 193-199. doi:10.2989/16085914.2015.1035223
- Awe, A.A., Opeolu, B.O., Olatunji, O.S., Fatoki, O.S., Jackson, V.A. and Snyman, R. 2020. Occurrence and probabilistic risk assessment of PAHs in water and sediment samples of the Diep River, South Africa. *Heliyon*, 6(6): e04306. doi:10.1016/j.heliyon.2020.e04306
- Cao, Z., Shen, M., Chen, Q., Liu, J., Yan, G., Wang, M. and Zhao, X. 2018. Multimedia and spatial distribution, internal accumulation, and source diagnostics of polycyclic aromatic hydrocarbons (PAHs) of the Luan River Basin, China. *Polycycl. Aromat. Compd.*, 38(1): 1-12. doi:10.1080/104006638.2016.1138972
- Duttagupta, S., Mukherjee, A., Bhattacharya, A. and Bhattacharya, J. 2020a. Wide exposure of persistent organic pollutants (PoPs) in natural waters and sediments of the densely populated Western Bengal basin, India. *Sci. Total Environ.*, 717: 137187. doi:10.1016/j.scitotenv.2020.137187
- Duttagupta, S., Mukherjee, A., Routh, J., Devi, L.G., Bhattacharya, A. and Bhattacharya, J. 2020b. Role of aquifer media in determining the fate of polycyclic aromatic hydrocarbons in the natural water and sediments along the lower Ganges river basin. *J. Environ. Sci. Health Part A Toxic Hazard. Subst. Environ. Eng.*, 55(4): 354-373. doi:10.1080/10934529.2019.1696617
- Farooq, S., Eqani, S.A., Malik, R.N., Katsoyiannis, A., Zhang, G., Zhang, Y., Li, J., Xiang, L., Jones, K.C., Shinwari, Z.K., Shinwari, Z.K. and Ali-Mushtajab, A.S. 2011. Occurrence, fingerprinting, and ecological risk assessment of polycyclic aromatic hydrocarbons (PAHs) in the Chenab River, Pakistan. *J. Environ. Monit.*, 13(11): 3207-3215. doi:10.1039/c1em10421g
- Frouin, H., Pellerin, J., Fournier, M., Pelletier, E., Richard, P., Pichaud, N., Rouleau, C. and Garnerot, F. 2007. Physiological effects of polycyclic aromatic hydrocarbons on soft-shell clam *Mya arenaria*. *Aquat. Toxicol.*, 82(2): 120-134. doi:10.1016/j.aquatox.2007.02.005
- Goswami, P., Ohura, T., Guruge, K.S., Yoshioka, M., Yamanaka, N., Akiba, M. and Munuswamy, N. 2016. Spatio-temporal distribution, source, and genotoxic potential of polycyclic aromatic hydrocarbons in estuarine and riverine sediments from southern India. *Ecotoxicol. Environ. Saf.*, 130: 113-123. doi:10.1016/j.ecoenv.2016.04.016
- Haritash, A.K., Gaur, S. and Garg, S. 2016. Assessment of water quality and suitability analysis of River Ganga in Rishikesh, India. *Appl. Water Sci.*, 6(4): 383-392. doi:10.1007/s13201-014-0235-1
- Hussain, K., Rajbangshi, R. and Hoque, R.R. 2014. Understanding levels and sources of PAHs in the water of Bharalu tributary of the Brahmaputra river. *Asian J. Water, Environ. Pollut.*, 11(2): 89-98.
- Incardona, J.P., Carls, M.G., Holland, L., Linbo, T.L., Baldwin, D.H., Myers, M.S., Peck, K.A., Tagal, M., Rice, S.D. and Scholz, N.L. 2015. Very low embryonic crude oil exposures cause lasting cardiac defects in salmon and herring. *Sci. Rep.*, 5: 1-13. doi:10.1038/srep13499
- Kafilzadeh, F., Shiva, A.H. and Malekpour, R. 2011. Determination of polycyclic aromatic hydrocarbons (PAHs) in water and sediments of the Kor River, Iran. *Middle-East Journal of Scientific Research*, 10(1): 01-07.
- Khuman, S.N., Chakraborty, P., Cincinelli, A., Snow, D. and Kumar, B. 2018. Polycyclic aromatic hydrocarbons in surface waters and riverine sediments of the Hooghly and Brahmaputra Rivers in Eastern and Northeastern India. *Sci. Total Environ.*, 636: 751-760. doi:10.1016/j.scitotenv.2018.04.109
- Kumar, B., Verma, V.K., Gaur, R., Kumar, S., Sharma, C.S. and Akolkar, A.B. 2014. Validation of HPLC method for determination of priority polycyclic aromatic hydrocarbons (PAHs) in waste water and sediments. *Pelagia Res. Libr. Adv. Appl. Sci. Res.*, 5(1): 201-209.
- Kumar, B., Verma, V.K., Kumar, S., Sharma, C.S. and Akolkar, A.B. 2020. Benzo(a)Pyrene Equivalency and Source Identification of Priority Polycyclic Aromatic Hydrocarbons in Surface Sediments from Yamuna River. *Polycycl. Aromat. Compd.*, 40(2): 396-411. doi:10.1080/10406638.2018.1441878
- Li, H. and Ran, Y. 2012. Distribution and bioconcentration of polycyclic aromatic hydrocarbons in surface water and fishes. *Sci. World J.*, 12: 2910. doi:10.1100/2012/6/32910
- Li, Y., Liu, J., Cao, Z., Lin, C. and Yang, Z. 2010. Spatial distribution and health risk of heavy metals and polycyclic aromatic hydrocarbons (PAHs) in the water of the Luanhe River Basin, China. *Environ. Monit. Assess.*, 163(1-4): 1-13. doi:10.1007/s10661-009-0811-2
- Malik, A., Verma, P., Singh, A.K. and Singh, K.P. 2011. Distribution of polycyclic aromatic hydrocarbons in water and bed sediments of the Gomti River, India. *Environ. Monit. Assess.*, 172(1-4): 529-545. doi:10.1007/s10661-010-1352-4
- Masih, J., Dyavarchetty, S., Nair, A., Taneja, A. and Singhvi, R. 2019. Concentration and sources of fine particulate associated polycyclic aromatic hydrocarbons at two locations on the western coast of India. *Environ. Technol. Innov.*, 13: 179-188. doi:10.1016/j.eti.2018.10.012
- Moja, S.J., Mtunzi, F. and Madlanga, X. 2013. Determination of polycyclic aromatic hydrocarbons (PAHs) in river water samples from the Vaal Triangle area in South Africa. *J. Environ. Sci. Health Part A Toxic Hazard. Subst. Environ. Eng.*, 48(8): 847-854. doi:10.1080/10934529.2013.761477
- Nagpure, N.S., Srivastava, R., Kumar, R., Dabas, A., Kushwaha, B. and Kumar, P. 2017. Mutagenic, genotoxic and bioaccumulative potentials of tannery effluents in freshwater fishes of River Ganga. *Hum. Ecol. Risk Assess.*, 23(1): 98-111. doi:10.1080/10807039.2016.1229116
- Nagy, A.S., Simon, G. and Vass, I. 2012. Monitoring of polycyclic aromatic hydrocarbons (PAHs) in surface water of the Hungarian upper section of the Danube River. *Nov. Biotechnol. Chim.*, 11(1): 27-36. doi:10.2478/v10296-012-0003-2
- Nagy, A.S., Szabó, J. and Vass, I. 2013. Occurrence and distribution of polycyclic aromatic hydrocarbons in surface water of the Raba River, Hungary. *J. Environ. Sci. Health Part A Toxic Hazard. Subst. Environ. Eng.*, 48(10): 1190-1200. doi:10.1080/10934529.2013.776455
- Ofori, S.A., Cobbina, S.J. and Doko, D.A. 2020. The occurrence and levels of polycyclic aromatic hydrocarbons (PAHs) in African environments—a systematic review. *Environ. Sci. Pollut. Res.*, 27(26): 32389-32431. doi:10.1007/s11356-020-09428-2
- Olayinka, O.O., Adewusi, A.A., Olujimi, O.O. and Aladesida, A.A. 2019. Polycyclic aromatic hydrocarbons in sediment and health risk of fish, crab, and shrimp around Atlas Cove, Nigeria. *J. Health Pollut.*, 9(24): 204. doi:10.5696/2156-9614-9.24.191204
- Pandit, G.G., Sahu, S.K., Puranik, V.D. and Raj, V.V. 2006. Exchange of polycyclic aromatic hydrocarbons across the air-water interface at the creek adjoining Mumbai harbour, India. *Environ. Int.*, 32(2): 259-264. doi:10.1016/j.envint.2005.08.021
- Patel, A.B., Shaikh, S., Jain, K.R., Desai, C. and Madamwar, D. 2020. Polycyclic aromatic hydrocarbons: Sources, toxicity, and remediation approaches. *Front. Microbiol.*, 11: 813. doi:10.3389/fmicb.2020.562813
- Pempkowiak, J., Pazdro, K., Kopecka, J., Perez, E. and Sole, M. 2006. Toxicants accumulation rates and effects in *Mytilus trossulus* and *Nereis diversicolor* exposed separately or together to cadmium and PAHs. *J. Environ. Sci. Health Part A Toxic Hazard. Subst. Environ. Eng.*, 41(11): 2571-2586. doi:10.1080/10934520600927963
- Purr K, Osiek D, Lange M, Adlunger K, Burger A, Hain B, Kuhnhenh K, Klaus T, Lehmann H, Monch L. Integration of Power to Gas/Power to

- Liquids into the ongoing transformation process. German Environment Agency, Dessau-Roßlau. 2016.
- Ramzi, A., Habib Rahman, K., Gireeshkumar, T.R., Balachandran, K.K., Jacob, C. and Chandramohanakumar, N. 2017. Dynamics of polycyclic aromatic hydrocarbons (PAHs) in surface sediments of Cochin estuary, India. *Mar. Pollut. Bull.*, 114(2): 1081-1087. doi:10.1016/j.marpolbul.2016.10.015
- Ravindra, K., Sokhi, R. and Vangrieken, R. 2008. Atmospheric polycyclic aromatic hydrocarbons: Source attribution, emission factors, and regulation. *Atmos. Environ.*, 42(13): 2895-2921. doi:10.1016/j.atmosenv.2007.12.010
- Refai, H.M., Helmy, A.M. and Ghuniem, M.M. 2022. Exposure and cancer risk assessment of polycyclic aromatic hydrocarbons (PAHs) in River Nile of Egypt. *Int. J. Environ. Anal. Chem.*, 1: 1-14. doi:10.1080/03067319.2021.2022656
- Sharma, V. and Singh, P. 2018. Correlation study on physicochemical parameters of river Ganga during different seasons in Haridwar. *Int. J. Res. Advent. Technol.*, 6(9): 181.
- Singare, P.U. 2016. Carcinogenic and endocrine-disrupting PAHs in the aquatic ecosystem of India. *Environ. Monit. Assess.*, 188(10): 5597. doi:10.1007/s10661-016-5597-4
- Sogbanmu, T. O., Osibona, A.O. and Otitoloju, A.A. 2019. Specific polycyclic aromatic hydrocarbons identified as ecological risk factors in the Lagos lagoon, Nigeria. *Environ Pollut.*, 255: 113295. doi:10.1016/j.envpol.2019.113295
- Srivastava, P., Sreekrishnan, T.R. and Nema, A.K. 2017. Human health risk assessment and PAHs in a stretch of river Ganges near Kanpur. *Environ. Monit. Assess.*, 189(9): 661. doi:10.1007/s10661-017-6146-5
- USEPA 2013 U. S. Environmental Protection Agency (EPA) international decontamination research and development conference. US Environ Prot Agency. 2014;2(EPA/600/R-14/210):1-779.
- Uttar Pradesh Pollution Control Board (UPPCB). 2015. Action Plan for Restoration of Polluted Stretch of River Hindon From District Saharanpur to District Ghaziabad. <http://www.uppcb.com/pdf/RIVER-HINDON.pdf>
- Wolska, L., Mechlińska, A., Rogowska, J. and Namieśnik, J. 2012. Sources and fate of PAHs and PCBs in the marine environment. *Crit. Rev. Environ. Sci. Technol.*, 42(11): 1172-1189. doi:10.1080/10643389.2011.556546
- World Health Organization (WHO). 1998. Polynuclear aromatic hydrocarbons in Drinking-water Background document for development of WHO Guidelines for Drinking-water Quality. WHO/SDE/WSH/03.04/59. 2.
- Wu, B., Zhang, R., Cheng, S.P., Ford, T., Li, A.M. and Zhang, X.X. 2011. Risk assessment of polycyclic aromatic hydrocarbons in aquatic ecosystems. *Ecotoxicology*, 20(5): 1124-1130. doi:10.1007/s10646-011-0653-x
- Zanardi-Lamardo, E., Mitra, S. and Vieira-Campos, A.A. 2019. Distribution and sources of organic contaminants in surface sediments of Hooghly river estuary and Sundarban mangrove, the eastern coast of India. *Mar. Pollut. Bull.*, 146: 39-49. doi:10.1016/j.marpolbul.2019.05.043



Effects of Flex Fuel in Light Duty Power Generators on the Environment and Circular Bio-Economy

S. Padmanabhan*†, C. Joel**, S. Mahalingam***, J. R. Deepak****, S. Baskar***** and M. Ruban*****

*School of Mechanical and Construction, Vel Tech Rangarajan Dr. Sagunthala R&D Institute of Science and Technology, Chennai, India

**Department of Mechanical Engineering, Easwari Engineering College, Chennai, India

***Department of Mechanical Engineering, Sona College of Technology, Salem, India

****School of Mechanical Engineering, Sathyabama Institute of Science and Technology, Chennai, India

*****Department of Automobile Engineering, Vels Institute of Science, Technology & Advanced Studies (VISTAS), Chennai, India

†Corresponding author: S. Padmanabhan; padmanabhan.ks@gmail.com

Nat. Env. & Poll. Tech.
Website: www.neptjournal.com

Received: 09-10-2022

Revised: 06-12-2022

Accepted: 20-12-2022

Key Words:

Flex-fuel engine

Light duty power generator

Ethanol

Circular bio-economy

Emission characteristics

ABSTRACT

Environmental sustainability encompasses various problems, including clean air, renewable energy, climate change, safe environments, and the capacity to live in a healthy community. One possible strategy for addressing these global problems is the circular bio-economy. Cleaner and lower-carbon environments may be fostered via the production of bioenergy and biomaterials, which can also help to maintain the energy-environment connection. To improve sustainability and the state of the planet, scientists are looking at renewable energy sources like ethanol. Compared to gasoline, ethanol has a reduced carbon footprint and a greater energy density, making it a viable alternative fuel. This study gives an overview of ethanol as a possible alternative fuel for flex-powered power generators in India to meet the goals of the circular bio-economy. This paper details the results of flex-fuel testing conducted on a light-duty power generator using an ethanol-gasoline mix. The findings reveal improved thermal efficiency and lower fuel consumption rates than basic fuel. The emissions of both carbon monoxide and unburned hydrocarbons were shown to be reduced.

INTRODUCTION

A flexible-fuel or dual-fuel vehicle is one whose internal combustion engine can operate on multiple fuel types. It may use regular gasoline in combination with an alcohol or ethanol-based fuel. Fuel injection and spark timing in modern flex-fuel engines may be automatically modified based on the actual blend detected by a fuel composition sensor, allowing for the combustion of any percentage of the resultant blend in the combustion chamber. About 60 million cars, motorbikes, and light-duty trucks have been produced and sold across the globe that can run on ethanol, making it the most popular commercially accessible flex fuel. Vehicles with a flexible fuel engine may run on either pure gasoline or a mixture of gasoline and ethanol up to 83% by volume (Stein et al. 2013, Thamilarasan et al. 2022).

The term “circular economy” refers to an economic model intended to be restorative and regenerative. Its primary objective is to maintain the highest possible level of utility and value for all products, components, and materials at all times, distinguishing between technical and biological cycles. The circular economy primarily emphasizes the effective use of limited resources. It ensures that those resources are recycled and utilized for as long as it is economically viable. To close loops of raw biomass materials, minerals, water, and carbon, bio-refining is one of the most important fundamentals enabling methods of the circular economy. As a result, bio-refining is the most effective technique for the bio-economy’s large-scale, environmentally responsible use of biomass. It will result in the cost-competitive co-production of food and feed components, bio-based products, and bioenergy, along with optimum societal, economic, and environmental consequences (Venkatesh et al. 2018, Venkatesh 2022, Ranjbari et al. 2022).

The researcher’s investigation focused on how ethanol was burned in a flex fuel engine. An investigation was

ORCID details of the authors:

Padmanabhan, S: <https://orcid.org/0000-0003-4813-975X>

conducted into applying high-compression hydrous ethanol reforming and supercharging lean-burn situations to improve performance and thermal efficiency. Adding ethanol to gasoline increased the emissions of nitrogen oxides (Gravalos 2011). Hydrocarbon and carbon monoxide emissions are brought down to their overall lowest levels. Under a wide range of loading situations, it was discovered that changing the percentage of ethanol to gasoline in the fuel mix led to significantly different levels of energy efficiency as well as pollution. According to the data, the emissions concentrations increased as the engine load grew but decreased as the ethanol level increased (Jesus et al. 2021).

Analytically analyzed steady-state engines were used in the study to investigate the effect that a combination of ethanol and gasoline would have on power, torque, amount of fuel consumed, and emissions. The vast bulk of the research that has been done so far on gasoline-ethanol blends in engines has focused on ethanol mix ratios up to twenty percent, with varying degrees of effectiveness (Doğan et al. 2017). The findings of multiple trials indicated little or no reaction to ethanol concentration up to 10% by volume, which suggests that engine operating circumstances have a more substantial impact on the engine's characteristics and the pollutants it produces at low ethanol blend levels. The performance of spark-ignition (SI) engines operating on ethanol-gasoline blends while maintaining a constant fuel-air ratio has recently garnered much attention (Stein et al. 2013).

When the speed of the engine is increased, as well as when the quantity of ethanol in the fuel mix is decreased, there is a tendency for the volumetric efficiency to drop. This is something that can be observed. There is a discernible reduction in the quantity of exhaust gas emissions produced whenever there is an increase in the ratio of ethanol to gasoline fuel that is used (Tibaquirá et al. 2018) increasing gasoline octane rating and reducing dependence on petroleum products. However, recently environmental authorities in large urban centers have expressed their concerns on the true effect of using ethanol blends of up to 20% v/v in in-use vehicles without any modification in the setup of the engine control unit (ECU). When the amount of ethanol in the fuel mix was increased to a level greater than 20%, there was a concomitant increase in saturated hydrocarbon emissions. The emission of more aromatic compounds and unburned ethanol was caused by higher concentrations of ethanol in the fuel mixture than when ethanol was present in lower concentrations. A general reduction in the emissions produced accompanied the vehicle's acceleration. This is because one ethanol molecule has a significantly higher number of oxygen atoms than molecules of other alcohol. The gasoline will take more oxygen to catch fire, so plan accordingly (Koten et al. 2020).

The mixtures that contain between 10 and 15% ethanol have proven to be the most popular, which is likely because they can completely cut emissions. Those fuels that contained a greater proportion of ethanol in their overall makeup had much fewer emissions when compared to the traditional alternatives. When dual fuels were utilized, there was a discernible reduction in the amounts of carbon monoxide, hydrocarbons, and smoke produced. On the other hand, an increase in both the oxidation of the combustion process and the temperatures at which the combustion took place led to a rise in the amount of carbon dioxide and nitrogen oxides released into the atmosphere (Ramadhas et al. 2016, Sambandam et al. 2022).

The quantity of energy required to make ethanol is impacted by the volume of water combined with the ethanol throughout the manufacturing process. Hydrous ethanol had a positive effect on the flame's growth and the time it took for the flame to propagate, but it did not affect the flame's stability. After combining gasoline, methanol, and ethanol, it was examined to see if the resulting mixture was consistent and homogenous (Bielaczyc et al. 2013) but increase others. Ethanol is rarely used neat as an automotive fuel; blends with standard gasoline are much more common. Low (5%–15%). Under every and all conditions of operation, a mixture that contains even a small amount of methanol produces more power than gasoline on its own. Because of the unique qualities exhibited by mixtures of methanol and gasoline, ethanol and gasoline, and their respective combinations, the combustion system has been adapted to accommodate these new fuels. Because of the aforementioned factors, it is challenging to pinpoint the principles of how ethanol or methanol affects emissions. This is because of the complexity of the relationship between these factors. When low-ethanol mixes comprising less than 20% ethanol were utilized, there was no noticeable change in engine efficiency or torque.

On the other hand, there was a reduction in the engine performance when the proportion of blending was increased (Koç et al. 2009, Mohammed et al. 2021, Padmanabhan et al. 2022). This study gives an overview of ethanol as a possible alternative fuel for a flex-powered power generator to meet the goals of the circular bio-economy. This paper details the results of flex-fuel testing conducted on a light-duty power generator using an ethanol-gasoline with an incremental blend.

MATERIALS AND METHODS

Ethanol is an eco-friendly, ecological-made fuel that outperforms gasoline thanks to its higher octane rating. Jobs in ethanol production are especially welcome in rural areas that lack other economic opportunities. Ethanol, a

bio-organic fuel, has the potential to displace fossil fuels in vehicles. Potentially helpful in reducing transportation-related carbon emissions and enhancing environmental outcomes (Ramadhass et al. 2016). Blending ethanol with gasoline and its influence on fuel qualities are discussed. In this case study, we use real-world data to demonstrate how adding ethanol to gasoline significantly improves knock resistance and full-load performance. The basic impacts of ethanol combustion and the decreased enrichment need under high speed/high load situations are discussed, along with the potential for downsizing and slowing down that is made possible by higher ethanol concentration (Stein et al. 2013).

For spark-ignition engines, ethanol may be used either alone as a fuel source or blended with gasoline. In 2013, India's BIS Specification 2796: 2013 allowed for a 10% ethanol mix in gasoline, and that number might rise in the future. Studying the effects of using ethanol-blended fuel in a modern gasoline engine is extremely desired. To reduce oil imports, the Indian government previously mandated a 10% ethanol component in gasoline (Ramadhass et al. 2016).

In India, light duty power generator engines are still widely used for power generators that produce greater pollution levels. However, various modifications will be necessary to improve the combustion rate and thermal efficiency of these engines because renewable energy sources are not always accessible in all parts of India and during all seasons. Ethanol is a fuel derived mostly from agricultural resources such as sugarcane and maize. Because of this, ethanol is an enticing replacement for gasoline to decrease dependency on fossil fuels and lower carbon net emissions into the environment. Adding OH components to gasoline improved full combustion and reduced hazardous emissions. This reduction in hazardous emissions affected the combustion potentiality or capacity to burn for a shorter amount of time, which was the shortcoming that the gasoline engine was trying to overcome (Sambandam et al., 2022). The properties of gasoline and ethanol were tabulated in Table 1 (Sambandam et al. 2022).

An investigational experiment was conducted on a low-duty power-generating engine capable of running on Flex Fuel (FF). It was determined to carry out this experiment

Table 1: Properties of flex fuel.

Sl.No	Property	Unit	Ethanol	Gasoline
1.	Lower Heating Value	[MJ.kg ⁻¹]	26.9	44.0
2.	Kinematic Viscosity, at 20°C	cSt	1.5	0.5
3.	Density, at 15°C	[kg.m ⁻³]	785	737
4.	Flash Point	[°C]	14	-40
5.	Research Octane Number	RON	115	90
6.	Motor Octane Number	MON	100	82
7.	Oxygen (%)	-	35	0
8.	Stoichiometric Air/Fuel Ratio	-	8.9	14.5

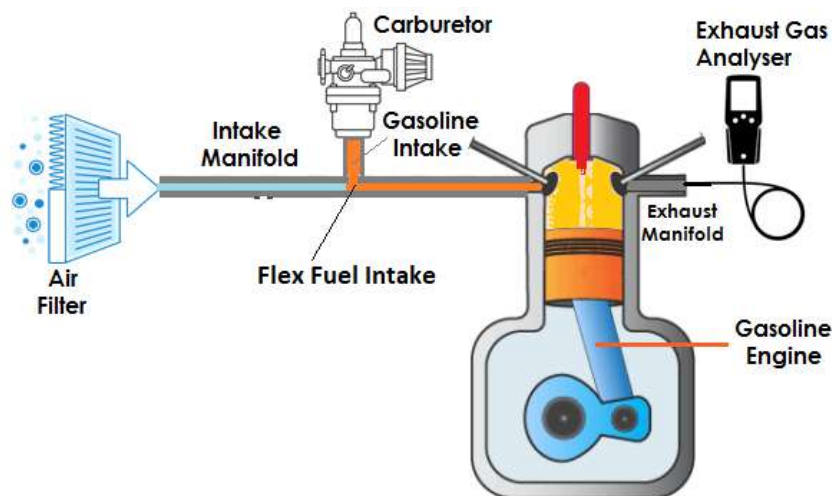


Fig. 1: Schematic diagram of the Flex Fuel setup.

using a spark ignition engine with a compression ratio of 4.5:1 and a peak output of 2.89 kW at an engine speed of 3200 rpm. This engine was a single-cylinder, four-stroke air-cooled engine with 180 cc of work capacity. To guarantee the best possible performance and the fewest amount of harmful emissions, the required test runs, both with and without an ethanol blend, were carried out under four distinct load circumstances, ranging from 25% to 100% capacity. An air-cooled, spark-ignition, single-cylinder, four-stroke engine with an incremental load was employed in this study work to investigate the effects of ethanol blends as flex fuel on the performance and emission characteristics of the engine. The mechanical loading resulted in a change to the incremental load. Fig. 1 presents a diagrammatic representation of the utilization of a light-duty power generation engine (Sambandam et al. 2022).

RESULTS AND DISCUSSION

Impact on Brake Thermal Efficiency

Fig. 2 depicts the variation in thermal brake efficiency as a function of load, and, as was previously said, adding ethanol led to improved combustion. Maximum thermal efficiency of ethanol rises to 9.3%, 16.3%, and 26%, respectively, demonstrating a notable performance boost at full load.

Ethanol speeds up combustion, allowing for more efficient use of energy. It is more efficient and displays characteristics that bring the cycle closer to the goal of constant volume combustion.

Higher hydrogen flame velocities and a wider variety of flames contribute to this improvement, making the flex fuel engine more potent. Testing an engine without ethanol under varying loads slows down the combustion process. On the other hand, ethanol greatly increased the combustion rate, leading to greater thermal efficiency. The stoichiometric ratio between ethanol and gasoline is also lower. The increased fuel mass may now be burned with the same air volume. More fuel is used because the lean mixture fills the remaining space.

Impact on Specific Fuel Consumption

The specific fuel consumption of the brakes under four different loads is shown in Fig. 3 for both ethanol-mixed and regular gasoline. Even if the engine load was initially decreased, it was proven that fuel consumption would increase regardless of the mix condition. In addition, ethanol's smaller heating valve than gasoline means that temperature swings will depend on loads. When ethanol is added to the mixture, the engine's specific fuel consumption drops by 6% to 28% across the blends. The results showed

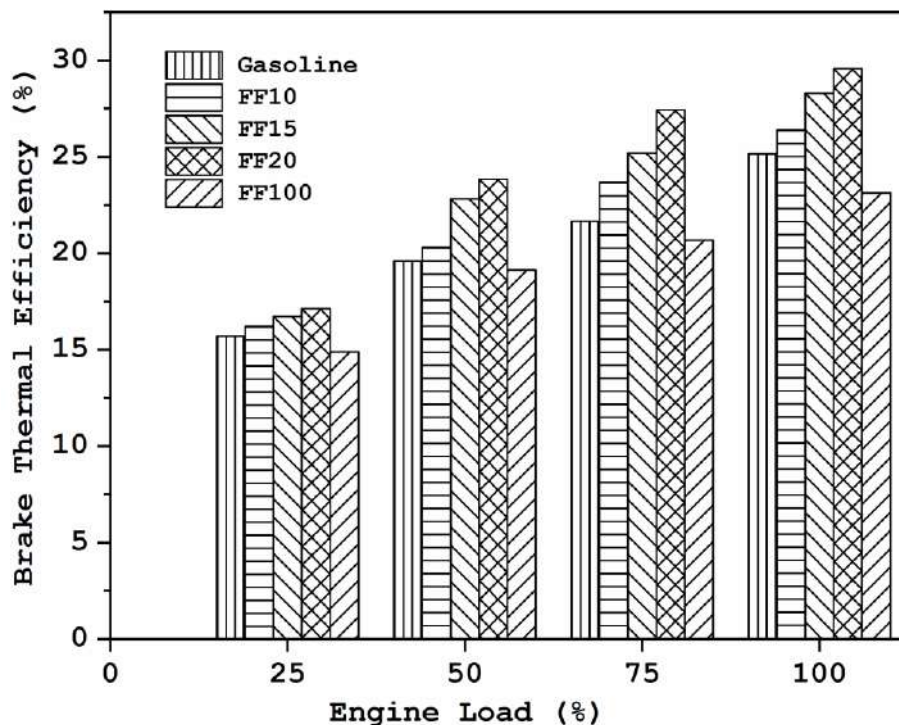


Fig. 2: Impact of flex fuel on brake thermal efficiency.

that using 20% ethanol reduced fuel consumption by 28% compared to gasoline. Adding hydrogen and oxygen to gasoline created a more turbulent mixture of air and fuel, leading to more efficient combustion and a larger flame thrust, and higher calorific values than could have been achieved with gasoline alone.

Impact on Carbon Monoxide Emission

Fig. 4 depicts the CO emission rate versus engine load. Combustion efficiency and the ratio of air to fuel are the primary factors in determining CO emissions. The engine was run at its optimum midrange speed to lower carbon

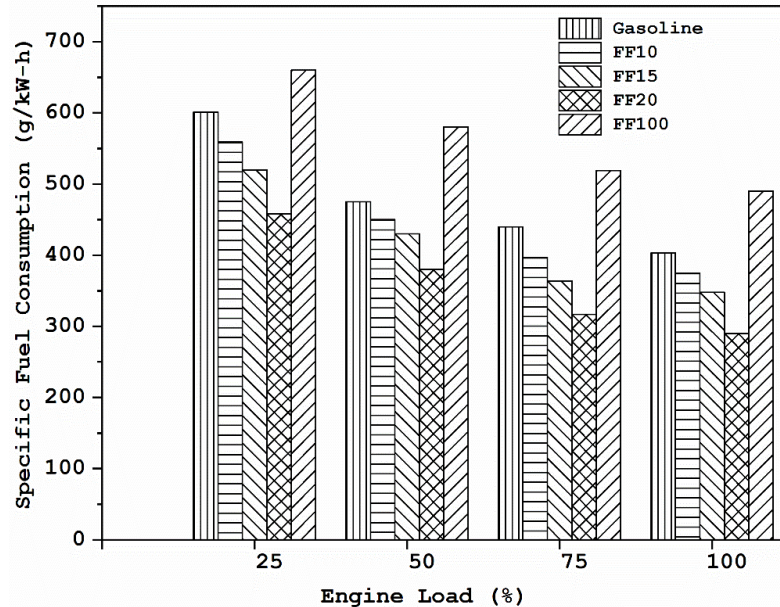


Fig. 3: Impact of flex fuel on specific fuel consumption.

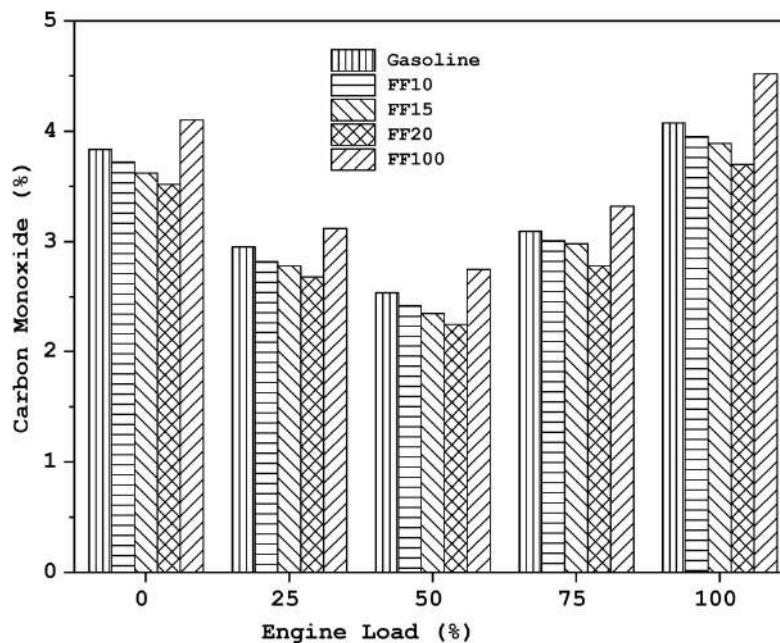


Fig. 4: Impact of flex fuel on carbon monoxide.

monoxide emissions. Combining ethanol and oxygen improved the combustion process, and CO emissions were reduced. It is possible that the introduction of oxygenated compounds that improve CO combustion in the cylinder or post-combustion activities led to a reduction in emissions. However, lowering CO emissions might involve more than watering the gas. Ethanol blends that increase combustion and improve lean-running engine performance can reduce CO by 6% to 23% ethanol percentages, respectively. The chemical properties of ethanol are superior, as it has a wider spectrum of combustibility and a faster flame speed. The rapid and complete combustion of an ethanol-gasoline combination destroys pure gasoline.

Impact on Unburned Hydrocarbon Emission

It can be seen in Fig. 5 that when ethanol was present, the amount of unburned hydrocarbons emitted into the exhaust dropped for all loads. For all loads studied, it was found that the combination of ethanol and HC resulted in a substantial decrease in HC content. Ethanol improved engine performance and led to complete combustion. Since the volumetric flow rates of ethanol differed, the percentage reductions in unburned hydrocarbon volume ranged from 3% to 11%. Compared to gasoline, hydrogen has a shorter quenching time, which reduces hydrocarbon emissions. Ethanol blends decreased hydrocarbon emissions because of the ethanol's low flammability and the relatively high

in-cylinder pressure and temperature produced by the rapid flame velocity. Complete combustion occurs due to the additional oxygen provided by the ethanol combination, resulting in less HC emissions.

Impact on Circular Bio-Economy and Environmental

Because of worldwide environmental and health concerns about fossil fuel usage, investment in biofuels as sustainable alternatives has gained steam over the past decade. Therefore, to successfully make the shift to a low-carbon and circular economy, it is essential to properly manage the various components of the biofuel supply chain, such as the production of biomass feedstock, the logistics of transporting biomass, the biofuel production in bio-refineries, and the biofuel distribution to consumers (Ranjbari et al. 2022).

Bio-waste must be converted into high-value energy and resources to achieve a circular bio-economy. Recycling and bioconversion integration for increased process performance is also evaluated. This endeavor aims to reduce barriers to bio-waste recycling in the circular economy. More study, market analysis, and finance are needed to commercialize alternative commodities and encourage their use. To maximize bio-waste usage, utilize a holistic, rigorous strategy that draws on various disciplines and uses data to improve and establish new methods (Xu et al. 2022). The circular bio-economy can help solve global issues. Bioenergy and biomaterials production could lessen environmental impact

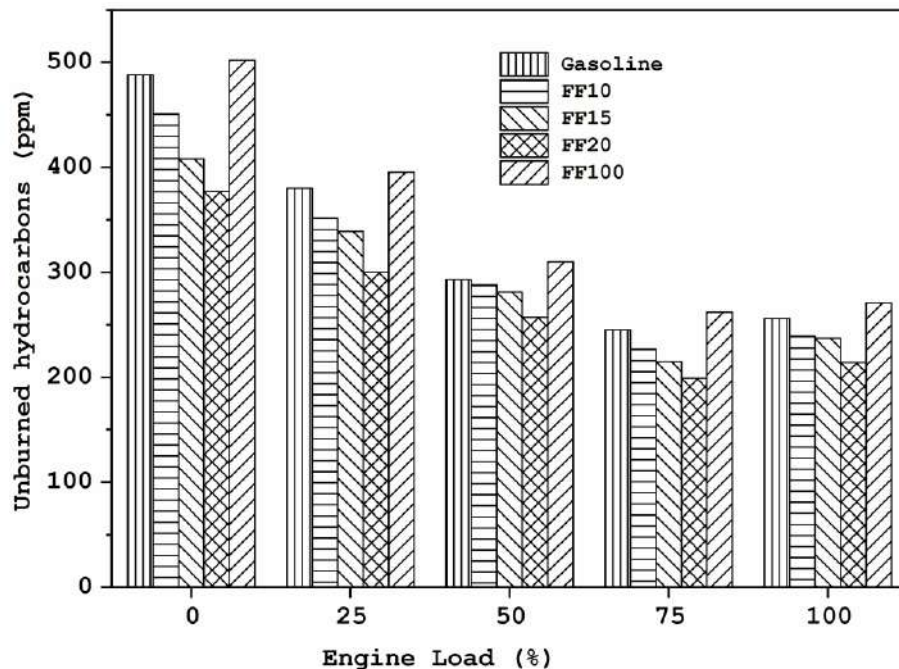


Fig. 5: Impact of flex fuel on unburned hydrocarbon.

by substituting petroleum as an industrial feedstock. The waste bio-refinery linked to the circular bio-economy may help with carbon management and greenhouse gas emissions. Implementing a waste bio-refinery circular bio-economy method exemplifies a low carbon economy by reducing greenhouse gas emissions (Leong et al. 2021).

Ethanol may have certain benefits over fossil fuels in terms of safety because it is water-soluble, biodegradable, and easily evaporated. Ethanol fuel is the most cost-effective alternative to other forms of energy since it can be manufactured in virtually any country. Ethanol is a fuel that may be produced from several plants, including maize. There are several distinct kinds of ethanol, but the one that is most frequently used is E10, and the proportion of E10 to other ingredients in blends can range anywhere from 10 to 15 percent worldwide. In several countries, including the United States and Brazil, it is possible to utilize a high-level ethanol fuel mix that includes between 50 and 85% of ethanol (Jesus et al. 2021, Butt et al. 2021). Ethanol has lower production costs than fossil fuels due to its ease of production. Burning ethanol as fuel produces only carbon dioxide and water as by-products. The released carbon dioxide does not significantly contribute to the problem of pollution.

On the other hand, it is believed that the combustion of ethanol generated from biomass such as maize and sugarcane results in “atmospheric carbon neutrality.” This is because as the biomass grows, it takes in carbon dioxide, which has the potential to counteract the amount of carbon dioxide that is emitted when ethanol is burned. The three primary areas of concentration in the circular economy are the feedstock, the manufacturing process, and the distribution of the end product. The product’s afterlife never received the consideration it deserved from the company. It has not been considered how the product will be maintained once it has reached the end of its useful service life (Leong et al. 2021, Venkatesh et al. 2018, Xu et al. 2022).

The percentage of ethanol mixed with gasoline in India reached 10.16 percent in 2022, significantly higher than the country’s goal. Additionally, the nation has committed to reaching a blending rate of twenty percent by the year 2025. The successful E20 ethanol blending project in India may save the government \$4 billion each year in 2020-21 when the country’s net petroleum imports will be 185 Mt at \$551 billion (Doğan et al. 2017, Stein et al. 2013) ethanol which has high octane rating, low exhaust emission, and which is easily obtained from agricultural products has been used in fuels prepared by blending it with gasoline in various ratios (E0, E10, E20, and E30. Traditional fuels tend to be more expensive, but ethanol is more environmentally friendly since it generates less pollution. This type of mixed fuel is both a

requirement and an opportunity due to the large amount of cropland that is now accessible, the expanding production of food grain and sugarcane, and the technological prowess to convert vehicles to operate on E20. Compared to four-wheeled cars, two-wheeled vehicles showed a reduction in CO emissions of up to half, while four-wheeled vehicles saw a reduction of up to thirty percent. In addition, the combination of ethanol and gasoline can cut hydrocarbon emissions by around 20% (Tibaquirá et al. 2018) increasing gasoline octane rating and reducing dependence on petroleum products. However, recently environmental authorities in large urban centers have expressed their concerns on the true effect of using ethanol blends of up to 20% v/v in in-use vehicles without any modification in the setup of the engine control unit (ECU).

The primary goal of this study is to reduce harmful emissions from a small gasoline-powered generator. Carbon monoxide is hazardous to human health because it affects the blood’s capacity to deliver oxygen to and from tissues. Specifically, hemoglobin is rapidly oxidized to carboxyhemoglobin upon contact with carbon monoxide in the blood. When carbon monoxide is found in the lungs, hemoglobin does not achieve a saturation level of 100% oxygen. This hydrocarbon has also been demonstrated to decrease the synthesis of white blood cells, suppress the immune system, and make white blood cells more susceptible to infection. Another consideration is that pollutant phototoxicity changes as plants progress through their life cycles (Sambandam et al. 2022, Padmanabhan et al. 2022).

CONCLUSION

Much of the energy used today, especially in transportation, comes from the fossil fuel sector. Experts’ focus has shifted to renewable energy sources like ethanol on flex-fuel due to the depletion of fossil fuels and the discharge of harmful pollutants. To increase the engine’s performance, minimize harmful emissions on environmental sustainability, and fulfill circular bio-economy standards, an experimental inquiry was undertaken on a light-duty power generator fueled by an ethanol-gasoline blend. When ethanol is added to the mixture, the engine’s specific fuel consumption drops by 6% to 28% across the blends. The maximum thermal efficiency of ethanol rises to 26% at full load. The percentage reductions in unburned hydrocarbon volume ranged from 3% to 11%. Ethanol blends that increase combustion and improve lean-running engine performance can reduce carbon monoxide by 6% to 23%. This study gives an overview of ethanol as a possible alternative fuel for flex-powered power generators to meet the goals of the circular bio-economy.

REFERENCES

- Bielaczyc, P., Woodburn, J., Klimkiewicz, D., Pajdowski, P. and Szczotka, A. 2013. An examination of the effect of ethanol-gasoline blends' physicochemical properties on emissions from a light-duty spark ignition engine. *Fuel Process. Technol.*, 107: 50-63.
- Butt, O.M., Ahmad, M.S., Che, H.S. and Rahim, N.A. 2021. Usage of on-demand oxyhydrogen gas as clean/renewable fuel for combustion applications: A review. *Int. J. Green Energy*, 18(13): 1405-1429.
- Doğan, B., Erol, D., Yaman, H. and Kodanli, E. 2017. The effect of ethanol-gasoline blends on performance and exhaust emissions of a spark ignition engine through exergy analysis. *Appl. Therm. Eng.*, 120: 433-443.
- Gravalos, I. 2011. Performance and emission characteristics of spark ignition engine fuelled with ethanol and methanol gasoline blended fuels. *Intech Open*, 7: 176. doi:10.5772/23176.
- Jesus, G.M.K., Jugend, D., Paes, L.A.B., Siqueira, R.M. and Leandro, M.A. 2021. Barriers to the adoption of the circular economy in the Brazilian sugarcane ethanol sector. *Clean Technol. Environ. Policy*, 21: 921 doi:10.1007/s10098-021-02129-5.
- Koç, M., Sekmen, Y., Topgül, T. and Yücesu, H.S. 2009. The effects of ethanol-unleaded gasoline blends on engine performance and exhaust emissions in a spark-ignition engine. *Renew. Energy*, 34(10): 2101-2106.
- Köten, H., Karagöz, Y. and Balci, Ö. 2020. Effect of different levels of ethanol addition on performance, emission, and combustion characteristics of a gasoline engine. *Adv. Mech. Eng.*, 12(7): 1-13.
- Leong, H.Y., Chang, C.K., Khoo, K.S., Chew, K.W., Chia, S.R., Lim, J.W., Chang, J. and Show, P.L. 2021. Waste biorefinery towards a sustainable circular bioeconomy: A solution to global issues. *Biotechnol. Biofuels*, 14(1): 87.
- Mohammed, M.K., Balla, H.H., Al-Dulaimi, Z.M.H., Kareem, Z.S. and Al-Zuhairy, M.S. 2021. Effect of ethanol-gasoline blends on SI engine performance and emissions. *Case Stud. Therm. Eng.*, 25: 100891.
- Padmanabhan, S., Giridharan, K. and Stalin, B. 2022. Energy recovery of waste plastics into diesel fuel with ethanol and ethoxy ethyl acetate additives on circular economy strategy. *Sci. Rep.*, 12(1): 5330.
- Ramadhas, A.S., Singh, P.K., Sakthivel, P., Mathai, R. and Sehgal, A.K. 2016. Effect of ethanol-gasoline blends on combustion and emissions of a passenger car engine at part load operations. *SAE Tech. Pap.*, 2: 152. doi:10.4271/2016-28-0152
- Ranjbari, M., Shams, E.Z. and Ferraris, A. 2022. Biofuel supply chain management in the circular economy transition: An inclusive knowledge map of the field. *Chemosphere*, 296: 133968.
- Sambandam, P., Giridharan, K. and Stalin, B. 2022. Sustainability and environmental impact of ethanol and oxyhydrogen addition on a nanocoated gasoline engine. *Bioinorg. Chem. Appl.*, 19: 415.
- Sambandam, P., Murugesan, P., Shajahan, M.I., Sethuraman, B. and Abdelmoneam Hussein, H.M. 2022. Sustainability and environmental impact of hydroxy addition on a light-duty generator powered with an ethanol-gasoline blend. *J. Renew. Energy Environ.*, 9(2): 82-92.
- Stein, R.A., Anderson, J.E. and Wallington, T.J. 2013. An overview of the effects of ethanol-gasoline blends on SI engine performance, fuel efficiency, and emissions. *SAE Int. J. Eng.*, 6(1): 470-487.
- Thamilarasan, J., Ravikumar, V. and Yadav, S.P.R. 2022. Sustainability improvement of ethanol-blended gasoline fuelled spark ignition engine by nanoparticles. *Nanomater. J.*, 22: 3947.
- Tibaquirá, J.E., Huertas, J.I., Ospina, S., Quirama, L.F. and Niño, J.E. 2018. The effect of using ethanol-gasoline blends on the mechanical, energy, and environmental performance of in-use vehicles. *Energies*, 11(1): 1-17.
- Venkata Mohan, S., Chiranjeevi, P., Dahiya, S. and Naresh Kumar, A. 2018. Waste derived bioeconomy in India: A perspective. *New Biotechnol.*, 40: 60-69.
- Venkatesh, G. 2022. Circular bio-economy-paradigm for the future: Systematic review of scientific journal publications from 2015 to 2021. *Circ. Econ. Sustain.*, 2(1): 231-279.
- Xu, M., Yang, M., Sun, H., Gao, M., Wang, Q. and Wu, C. 2022. Bioconversion of biowaste into renewable energy and resources: A sustainable strategy. *Environ. Res.*, 214: 113929.



Effects of Traffic on Particulate Matter (PM_{2.5}) in Different Built Environments

Naina Gupta† and Sewa Ram

*School of Planning and Architecture, New Delhi, India

†Corresponding author: Naina Gupta; nainagupta9793@gmail.com

Nat. Env. & Poll. Tech.
Website: www.neptjournal.com

Received: 15-10-2022

Revised: 06-12-2022

Accepted: 20-12-2022

Key Words:

Environment
Pollution modeling
Vehicular pollution
Particulate matter
Neural network

ABSTRACT

Globally, vehicular pollution is one of the greatest concerns in urban areas. Several studies on air pollution have been conducted using deterministic, statistical, and soft computing methods. However, there has been little research on how soft-computing methods like Artificial Neural Networks (ANN) can help us comprehend vehicular pollution's non-linear and highly complex dispersion. This study uses an ANN-based vehicular pollution model to investigate the effect of vehicular traffic on PM_{2.5} concentrations in built-up and open terrain-surrounding environments. Five distinct pollution models were developed for two locations in Delhi, considering PM_{2.5} pollutants, meteorological variables, traffic flow, and traffic composition into account. The results concluded that under open terrain conditions, the significance of the traffic variable in its association with PM_{2.5} is almost half the significance observed under built-up conditions. Also, in terms of PM_{2.5} reductions, the maximum reduction observed at Location-1 (built-up environment), and Location-2 (open terrain environment) is 1.85 and 2.44 times the percent reduction in traffic during peak hours, respectively. The study's findings have significant ramifications for the current practices of ignoring the contribution of traffic and the built environment to pollution and adopting measures like an odd-even rule and high fuel and parking prices to combat pollution.

INTRODUCTION

The World Health Organization (WHO 1980) defines air pollution as “contamination of the indoor or outdoor environment by any chemical, physical, or biological agent that modifies the natural characteristics of the atmosphere.” India is the fifth country in the world in terms of worst air quality and the fourth-largest emitter of greenhouse gases (UNEP 2019). A recent study analyzed pollution and global health effects for more than 7,000 cities worldwide between 2010 and 2019 (Health Effects Institute 2022). Delhi ranked first in the list of the top 10 most polluted cities when PM_{2.5} levels were compared.

According to a recent study (Health Effects Institute 2022) that analyzed pollution and global health effects for over 7,000 cities worldwide between 2010 and 2019, Delhi ranked first among the top 10 most polluted cities in terms of PM_{2.5} contributions. In 2019, Delhi's average annual PM_{2.5} concentration was 110 µg.m⁻³, nearly three times the regulatory threshold of 40 µg.m⁻³.

Several pollution studies have been conducted over the past two decades; however, developing a reliable vehicular pollution model is still a challenge due to a large number of dynamic and influencing variables (such as wind speed, direction, vehicle wake, etc.) that have a significant impact

on the pollution. This demonstrates the clear need for a better understanding of the sources and dispersion of pollution or a reliable model for pollution prediction. This paper discusses the results of an ANN-based vehicular pollution model and the contribution of traffic to PM_{2.5} under two distinct boundary conditions.

OVERVIEW OF VEHICULAR POLLUTION MODELLING

Modeling approaches for vehicular pollution modeling are broadly categorized as a deterministic, statistical, hybrid of statistical and deterministic approaches, and soft-computing (Nagendra & Khare 2004). Deterministic models estimate pollutant concentration from datasets related to emission inventory and meteorological variables, whereas statistical/empirical models predict pollutant concentration by establishing statistical relationships between the dependent (pollutant concentrations) and independent variables (meteorological, traffic). Several researchers have concluded that deterministic models are relatively accurate at predicting air pollution and valuable for long-term planning choices. However, they do not adequately model vehicular pollution (Khare & Nagendra 2007). The accuracy of deterministic models is contingent on whether their underlying assumptions are satisfied. Similarly, statistical

Table 1: Review of Indian case studies related to pollution modeling.

Reference	Approach	Variables
(Gupta et al. 2023)	CALINE	1,2,3,5
(Dass et al. 2021)	Fuzzy	1, 2
(Dutta & Jinsart 2021)	Comparison of Multi Linear Regression (MLR) and ANN	1,2
(Kaur & Mandal 2020)	ANN	1,2
(Agarwal et al. 2020)	ANN	1,2
(Yadav & Nath 2018)	Comparison of Principal Component Analysis, MLR, and ANN)	1,2
(Dhyani et al. 2017)	CALINE-based Gaussian plume dispersion model	1,2,3
(Mishra et al. 2015)	Comparison of MLR, Neuro-Fuzzy, and ANN	1,2
(Kumar et al. 2015)	CALINE	1,2,4,5,6
(Singh et al. 2013)	Statistical (Decision Tree)	1,2
(Prakash et al. 2011)	Soft Computing (Recurrent Neural Network)	1,2

Note: 1- Pollutant; 2- Meteorological; 3- Traffic and road characteristics; 4- Land use; 5- Surface characteristics; 6- Source emission data

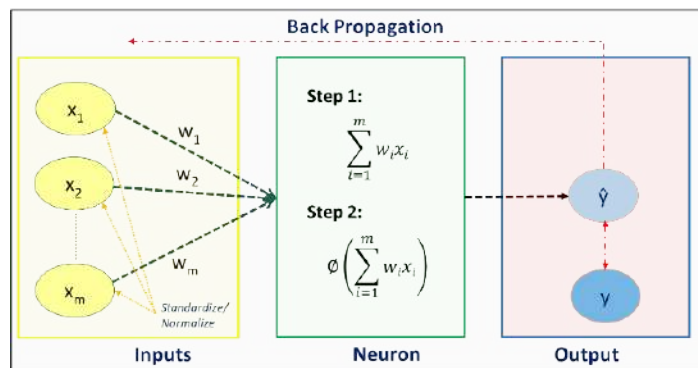


Fig. 1: ANN architecture.

models yield superior results for site-specific analyses but subpar results for nonlinear data sets.

In the recent past, numerous modeling studies have been conducted using multi-layer neural networks to forecast PM, NO₂, O₃, and SO₂ concentrations, whereas the application of neural networks to model vehicular pollution is limited (Batterman et al. 2014, Heydari et al. 2021, Kumar 2016, Rahimi 2017, Shams et al. 2021, Sofuoglu et al. 2006).

Table 1 above summarizes several Indian case studies relating to air pollution/vehicle pollution modeling over the years. Considering the non-linear and complex relationships in the environment, these research papers suggest neural networks and other soft computing techniques for modeling air pollution. In terms of vehicular pollution modeling, however, deterministic or statistical approaches predominate. In addition, the results predicted by deterministic models are more reliable than those predicted by statistical approaches if the plume model's boundary conditions are precisely defined.

VEHICULAR POLLUTION MODELLING USING ANN

ANN is an offshoot of artificial intelligence developed in the 1950s to mimic the architecture of the biological brain. It has since become an indispensable tool for modeling nonlinear dynamic processes. The neural network approach is a promising alternative to conventional models due to its self-correcting, self-learning, and similar processing characteristics (Khare & Nagendra 2007). The fundamental architecture of ANN is depicted in Fig. 1.

It consists of input layers, hidden layers, and output layers. The number of input layers matches the number of independent variables. Hyper-parameters refer to the number of neurons in the hidden layers, the number of layers, and various other neural network parameters, such as the learning rate, activation function, learning algorithm, number of epochs, batch size, etc. These hyper-parameters are optimized to improve the model's performance.

In ANN, the multi-layer neural network has been widely used in air pollution research due to its ability to model highly nonlinear relationships and generalize accurately when treated with new, unseen data (Abiodun et al. 2018, Gardner & Dorling 1998). To obtain good model results, it is essential to avoid overtraining neural networks, in which the model learns insignificant details in the training data, resulting in poor generalization when tested with new, unseen data (Bilbao & Bilbao 2017).

To avoid overtraining neural networks, models are typically trained on a subset of inputs and outputs to determine weights and then validated on the remaining data to determine the accuracy of model predictions. The dataset is separated into training, test, and validation datasets. The training dataset is used to evaluate the model's generalization performance during training. Training is complete when the model's performance on the test dataset reaches its maximum. The test dataset is not utilized during the modeling process but at the conclusion to evaluate the model's predictability beyond the training dataset. The final neural network model and hyper-parameter tuning are evaluated by utilizing the validation dataset.

The following six sequential steps have been followed to model vehicular pollution using ANN:

1. Selecting Optimal ANN-based Vehicular Pollution Model Architecture
2. Selecting the Best Activation/Transfer Function
3. Selecting Optimum Learning Parameters
4. Initializing Network Weights and Bias
5. Model Training and Generalization
6. Model Evaluation

INTRODUCTION TO SURVEY LOCATIONS

In this study, a vehicular pollution model was developed for two locations, Location-1: Bahadur Shah Zafar Road (28.63°, 77.24°), one of the busiest corridors in Delhi, the National Capital of India, and Location-2: Near Millenium Depot (28.59°, 77.26°). The right of way for Location-1 is 40 m, and for Location-2 is 70 m. The locations have a kerbside air quality sampling station (approximately 3 meters above the ground) monitored by the Central Pollution Control Board (CPCB). The source apportionment study (CPCB 2016) for Delhi also revealed that nearly 30 percent of the observed pollution at Location-1 is caused by vehicular traffic. The predominant land uses surrounding Location-1 are commercial and institutional, and predominantly urban green and blue spaces surrounding Location-2.

MATERIALS AND METHODS

Pollutant Data

The CPCB provided the hourly pollutant data set (PM_{2.5} concentrations, g.m⁻³) for January 2019 that was used for training, validating, and testing the predictive ability of the ANN model at both locations.

Meteorological Data

The hourly meteorological data set for January 2019 was collected for the closest weather station at Safdarjung (approximately 10 km from these locations). The input variables in the study are temperature in °C, dew point temperature in °C, relative humidity in %, precipitation in mm, wind direction in degrees, wind speed in Km.h⁻¹, mixing height in meters, and atmospheric pressure in hPa.

Traffic Data

Using videography surveys, 16 hours of traffic data were collected on one weekday (Monday) and one weekend day (Sunday) in January 2019 for both locations. The data have been extrapolated to a 24 h count, and an adjustment factor for daily variation has been assumed based on fuel sales data from the station closest to the sites (less than 1 km). The average daily volume at Location-1 is 1,45,356 Passenger Car Units (PCU). Peak-hour traffic is observed between 10:30 and 11:30 a.m. The percentage composition of weekday and weekend traffic is nearly identical, with two- and four-wheeler vehicles accounting for 77 percent of the total.

The average daily volume at Location-2 is 1,39,108 Passenger Car Units (PCU). Peak-hour traffic is observed between 04:40 and 05:45 p.m. The percentage composition of weekday and weekend traffic is nearly identical, with two- and four-wheeler vehicles accounting for 68 percent of the total.

Model Development

The modeling procedure begins with the pre-processing of the data, which begins with data cleansing and input selection. As the ANN model can learn the pattern and assign weights accordingly, it is not necessary to eliminate the insignificant variables. A genetic algorithm (GA) is used to incorporate the most pertinent characteristics of the dataset into the neural network. This feature selection technique outperforms conventional methods and efficiently manages large data sets with numerous features.

One monthly dataset for January 2019 has been used for model training. The selected dataset is divided into training,

validation, and test sets. The entire data set is separated into a training and test set with a 70:30 ratio. The test set is not utilized during the modeling procedure, but after the modeling, the procedure evaluates the model's ability to predict beyond the training dataset. The validation set is carved out from the training set at a ratio of 70:30 for hyper-parameter tuning.

This is followed by feature scaling of the dataset, and in this study, the 'Mean, and Standard Deviation Scaling Method' was chosen for feature scaling of input data using Eq. 1:

$$z = \frac{x - u}{s} \quad \dots(1)$$

where 'x' is the observation, 'u' is the mean value, and 's' is the standard deviation. The 'sci-kit learn' package in python libraries was used for the feature scaling of the input data.

The list of meteorological and traffic characteristic variables parameters considered input variables include Temperature, Dew Point Temperature, Relative Humidity, Precipitation, Wind Direction, Wind Speed, Atmospheric Pressure, Mixing Height, Pasquill stability category, vehicular flow, vehicular composition. Five models with varying combinations of independent input variables and optimization algorithms were developed to determine the most accurate model. The most significant model for Location-1 is discussed in detail, and a summary of the remaining models for both locations is provided in Table 3.

Model-1

This model was created using the Python library's 'Keras' package. Temperature (temp), wind speed (wspd), traffic flow (tf), mixing height (mh), and atmospheric pressure (pa) were considered input variables (pres). On the input and output layers, the activation function is the identity function, while the activation function on the hidden layer is a hyperbolic tangent. The total number of hidden layers

was identified so that the predicted hidden neurons on the test data set would yield the lowest prediction error. Several computational runs with random values of the number of neurons in hidden layers were performed for the model, and the combination yielding the minimum Mean Square Error after the network stabilizes and having satisfactory statistical performance (in terms of 'd' and RMSE) is considered to be the optimal number of neurons in the hidden layers. The trained ANN-based model network is saved at frequent intervals of training epochs, and its applicability is evaluated. The process continues until the performance of the trained model on the test dataset is optimal. After modeling with the selected hyper-parameters and plotting the mean absolute error of the training and test datasets, the number of epochs was determined. Early stopping was utilized to determine the optimal number of epochs. In this study, only a few hyper-parameters are optimized, while the rest are chosen theoretically. The activation function, learning rule, and batch size hyper-parameters were selected manually. The remaining hyper-parameters were optimized using the 'random search' algorithm in the 'Keras tuner' package from the Python libraries.

Table 2 depicts the interconnections between input, output, and hidden layers based on synaptic weights.

Table 3 displays the summary of model results indicating the significance of the model on the training dataset and its effectiveness on the testing dataset. Fig. 2 depicts a graph comparing observed and predicted values.

Tables 4 and 5 summarize the five distinct pollution models developed for this study.

The results of the modeling indicate that the combination of temperature, wind speed, mixing height, traffic flow, and atmospheric pressure produces the best model results for Location 1 and that the combination of temperature, wind speed, wind direction, relative humidity, mixing height, traffic flow, and atmospheric pressure produces the best

Table 2: Parameter estimates (Bias & Synaptic weights).

Predictor		Input layer						Output Layer
		(Bias)	temp	Wspd	tf	mh	pres	PM _{2.5}
Hidden Layer 1	H(1:1)	-0.27	-0.42	-0.17	-1.47	-1.22	0.41	0.03
	H(1:2)	4.77	0.17	1.00	0.88	1.50	-0.60	-2.13
	H(1:3)	3.85	-0.53	1.36	0.22	-0.11	-2.22	-1.57
	H(1:4)	2.14	0.40	0.52	0.28	-0.75	0.78	-1.39
	H(1:5)	0.07	-0.04	-0.30	0.86	-0.77	0.29	0.35
	H(1:6)	0.24	-0.05	-0.05	-0.29	0.22	-0.17	0.22
	H(1:7)	0.21	-0.39	-0.20	0.46	0.05	-0.35	-0.09
	(Bias)							4.59

Table 3: Model summary.

Model Significance			Independent & Normalized Variable Importance		
Training	Sum of Squares Error	71.20	temp	0.15	35.60%
	MSE	0.33	wspd	0.22	51.20%
	RMSE	0.57	tf	0.09	21.70%
	Relative Error	0.28	mh	0.12	28.60%
	Stopping Rule Used	100 consecutive step(s) with no error decrease ^b		pres	0.42
Testing	Sum of Squares Error	28.12			
	MSE	0.13			
	RMSE	0.36			
	Relative Error	0.23			

b. Error computations are based on the testing sample.

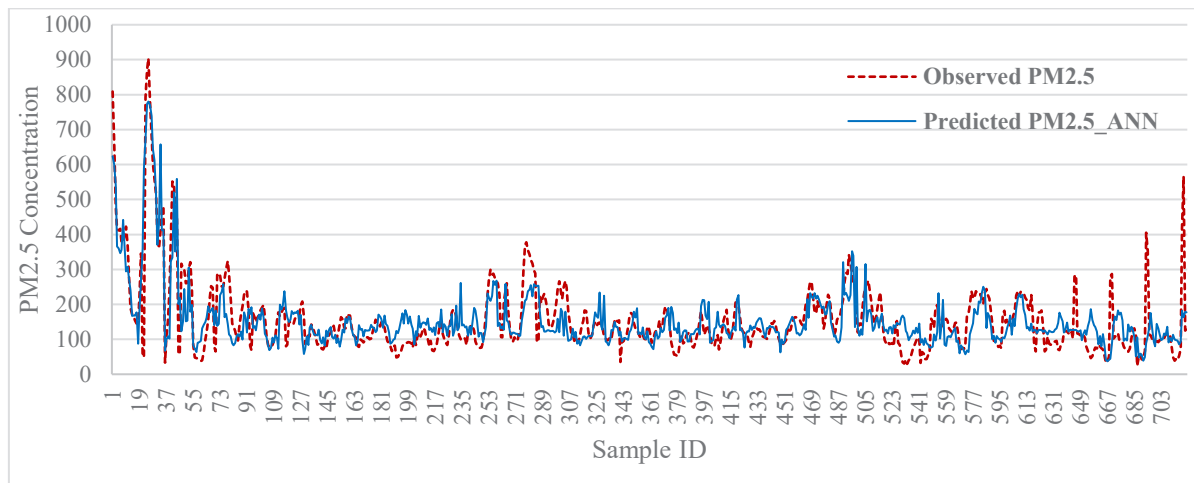


Fig. 2: Observed vs. Predicted PM_{2.5}.

model results for Location 2. In addition to the previous models, an ANN model was developed considering only traffic composition (Model 5). Still, the model predicted very poor results for both locations, indicating the inability of ANN models to account for the ‘lag effect’ in the absence of meteorological variables. Nevertheless, when considering traffic and meteorological variables, ANN can predict pollutant concentrations satisfactorily.

RESULTS AND DISCUSSION

Sensitivity Analysis

In addition, the model’s sensitivity to reductions in traffic flow ranging from -5 percent to -20 percent was evaluated for both locations. Fig. 3 (Location-1) and Fig. 4 (Location-2) demonstrate that as traffic volume decreases, the pollutant concentration decreases as well increases, indicating that as traffic volume decreases beyond a certain threshold, the significance of the traffic variable in pollution prediction diminishes. Although pollution is predicted to increase as

volume decreases, the predicted value of PM_{2.5} is always less than or equal to the observed value.

The results concluded that a more than 20% reduction during peak hours would diminish the significance of the traffic variable, while the significance of background pollution would predominate at Location-1. Further, by decreasing traffic at the site by 20% during rush hour (10:30 am-11:30 am), the concentration of PM_{2.5} pollutants could be reduced by 37%. Similarly, the results concluded that with a 9% reduction in traffic, the pollutant concentration could be reduced to 22% in the peak hours (16:45-17:45) at Location-2.

However, to achieve the PM_{2.5} concentration specified by air quality standards, the predicted concentration must be reduced by an average of 88 percent during the peak hours for location-1 and 63 percent at Location 2. As a result, we can conclude that the contribution of background pollution is greater after a reduction in traffic volume of 20 percent for Location-1 and greater after a reduction in traffic volume of 10 percent for Location-2.

Table 4: Summary of model outputs for Location-1.

Input Layer		Model 1	Model 2	Model 3	Model 4	Model 5
		temp, wspd, t_flow, mixh, pres	temp, dwpt, rhum, wspd, pres, t_flow	temp, rhum, wspd, pres, t_flow	Mixh, temp, wdir, wspd, pres, rhum, t_flow	2w, 3w,4w, Goods, Bus, temp, wspd, mixh
Hidden Neurons		7	4	5	7	8
Transfer function		Hyperbolic tangent	Logistic	Hyperbolic tangent	Hyperbolic tangent	Logistic
Learning		Levenberg-Marquardt	Stochastic Gradient	Stochastic Gradient	Levenberg-Marquardt	Stochastic Gradient
Training	MSE	0.32	0.42	0.36	0.02	0.73
	RMSE	0.57	0.65	0.6	0.14	0.86
	Relative Error	0.28	0.37	0.32	0.31	0.64
Testing	MSE	0.13	0.12	0.19	0.01	0.59
	RMSE	0.36	0.35	0.43	0.11	0.77
	Relative Error	0.23	0.45	0.39	0.28	0.55
	d	0.82	0.76	0.78	0.75	0.61
	R ²	0.74	0.62	0.66	0.56	0.42

Table 5: Summary of Model Outputs for Location-2.

Input Layer		Model 1	Model 2	Model 3	Model 4	Model 5
		temp, wspd, t_flow, mixh,pres	temp, dwpt, rhum, wspd, pres, t_flow	temp, rhum, wspd, pres, t_flow	Mixh, temp, wdir, wspd, pres, rhum, t_flow	2w, 3w,4w, Goods, Bus, temp, wspd, mixh
Hidden Neurons		6	6	5	9	11
Transfer function		Hyperbolic tangent	Logistic	Hyperbolic tangent	Hyperbolic tangent	Logistic
Learning		Levenberg-Marquardt	Stochastic Gradient	Stochastic Gradient	Levenberg-Marquardt	Stochastic Gradient
Training	MSE	0.08	0.28	0.45	0.13	0.35
	RMSE	0.29	0.53	0.67	0.37	0.59
	Relative Error	0.19	0.42	0.45	0.24	0.31
Testing	MSE	0.1	0.42	0.67	0.05	0.12
	RMSE	0.31	0.65	0.82	0.22	0.34
	Relative Error	0.2	0.36	0.42	0.19	0.49
	d	0.89	0.75	0.71	0.91	0.66
	R ²	0.8	0.65	0.62	0.81	0.59

The results concluded that under open terrain conditions, i.e., Location-2, the significance of the traffic variable in its association with PM_{2.5} is almost half the significance observed under built-up conditions for Location-1. Also, in terms of PM_{2.5} reduction, the maximum reduction observed at Location-1 (surrounding built-up environment), and Location-2 (open terrain surrounding environment) is 1.85 and 2.44 times the percent reduction in traffic during peak hours, respectively. Hence, it can be concluded that the surrounding built environment has a significant role in influencing pollution dispersion, and appropriate actions must be taken to reduce the overall amount of background pollution (Gupta et al. 2020).

CONCLUSIONS

Most of the research carried out in the previous decade related to vehicular pollution modeling was based on deterministic (particularly plume-based dispersion model) and statistical approaches. These methods do not fully reflect the complex and non-linear relationships between the variables. As a result, the ANN approach ought to be investigated further to investigate the intricate interrelationships between urban traffic, climatological factors, and other types of pollutants. In addition, the creation of a dependable vehicular pollution model could assist local authorities in the development of effective strategies for the management of air quality.

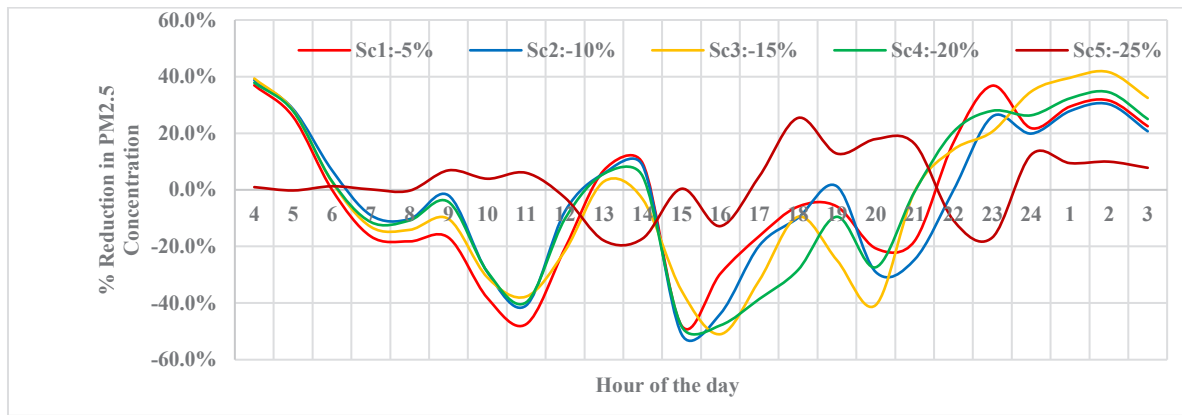


Fig. 3: % Reduction in PM_{2.5} concentration with reduction in traffic volume for Location-1.

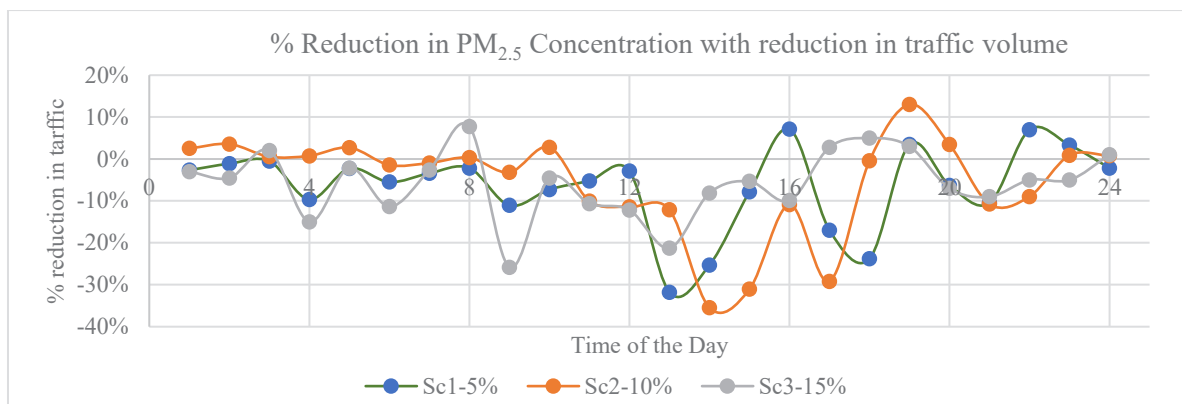


Fig. 4: % Reduction in PM_{2.5} concentration with reduction in traffic volume for Location-2.

The ANN approach has predicted satisfactory results for vehicular pollution modeling in this study. Nevertheless, additional traffic variables, such as composition, speed, fuel type, and so on, seasonal variations, and the impact of the physical environment, need to be investigated further.

REFERENCES

Abiodun, O.I., Jantan, A., Omolara, A.E., Dada, K.V., Mohamed, N.A. and Arshad, H. 2018. State-of-the-art in artificial neural network applications: A survey. *Heliyon*, 4(11): e00938, ISSN 2405-8440.

Agarwal, S., Sharma, S., Rahman, M.H., Vranckx, S., Maiheu, B., Blyth, L., Janssen, S., Gargava, P., Shukla, V.K. and Batra, S. 2020. Air quality forecasting using artificial neural networks with real-time dynamic error correction in highly polluted regions. *Sci. Tot. Environ.*, 735: 139454. <https://doi.org/10.1016/j.scitotenv.2020.139454>

Batterman, S., Ganguly, R., Isakov, V., Burke, J., Arunachalam, S., Snyder, M., Robins, T. and Lewis, T. 2014. Dispersion modeling of traffic-related air pollutant exposures and health effects among children with asthma in Detroit, Michigan. *Transp. Res. Rec.*, 2452: 105-112. <https://doi.org/10.3141/2452-13>

Bilbao, I. and Bilbao, J. 2017. Overfitting Problem and the Over-Training in the Era of Data: Particularly for Artificial Neural Networks.

2017 Eighth International Conference on Intelligent Computing and Information Systems (ICICIS), 5-7 December 2017, Cairo, Egypt, IEEE, Piscataway, NJ, USA, pp. 1165-1174.

Central Pollution Control Board (CPCB). 2016. Air Quality Monitoring, Emission Inventory and Source Apportionment Studies –Delhi. Available at: <https://cpcb.nic.in/displaypdf.php>

Central Pollution Control Board (CPCB). 2020. Monitoring Network. Available at: <https://www.cpcb.nic.in/automatic-monitoring-data>.

Dass, A., Srivastava, S. and Chaudhary, G. 2021. Air pollution: A review and analysis using fuzzy techniques in Indian scenario. *Environ. Technol. Innov.*, 22: 101441.

Dhyani, R., Sharma, N. and Maity, A.K. 2017. Prediction of PM_{2.5} along urban highway corridor under mixed traffic conditions using Caline4 model. *J. Environ. Manag.*, 198: 24-32.

Dutta, A. and Jinsart, W. 2021. Air pollution in Indian cities and comparison of MLR, ANN, and CART models for predicting PM₁₀ concentrations in Guwahati, India. *Asian J. Atmos. Environ.*, 15(1): 68-93.

Gardner, M.W. and Dorling, S.R. 1998. Artificial Neural Networks (the multilayer perceptron): A review of applications in the atmospheric sciences. *Atmos. Environ.*, 32(14-15): 2627-2636.

Gupta, N., Ram, S. and Sudagani, B.G. 2020. Statistical Approach for Modelling Exposure to Background Air Pollution. *Urban India, NIUA New Delhi*, pp. 51-60.

Gupta, N., Ram, S. and Sudagani, B.G. 2023. Environmental Capacity of Roads Under Mixed Traffic Conditions. In: Devi, L., Errampalli, M., Maji, A. and Ramadurai, G. (eds), *Proceedings of the Sixth International*

- Conference of Transportation Research Group of India, Springer, Singapore, pp. 416-436. https://doi.org/10.1007/978-981-19-4204-4_6
- Health Effects Institute. 2022. Air Quality and Health in Cities: A State of Global Air Report 2022. Health Effects Institute, Boston, MA.
- Heydari, A., Majidi, N.M., Astiaso, G.D., Keynia, F. and Santoli, L. 2021. Air pollution forecasting application based on deep learning model and optimization algorithm. *Clean Technol. Environ. Policy*, 24: 607-621.
- Kaur, M. and Mandal, A. 2020. PM_{2.5} Concentration Forecasting Using Neural Networks for Hotspots of Delhi. 2020 International Conference on Contemporary Computing and Applications (IC3A), 5-7 Feb 2020, Lucknow, India, IEEE, Piscataway, USA, pp. 19-28.
- Khare, M. and Nagendra, S.M.S. 2007. Artificial Neural Networks in Vehicular Pollution Modeling, Springer, Berlin.
- Kumar, A. 2016. Modeling for vehicular pollution in the urban region; A review. *Pollution*, 6: 5-12.
- Kumar, A., Dikshit, A., Fatima, S. and Patil, R. 2015. Application of WRF model for vehicular pollution modeling using AERMOD. *Atmos. Clim. Sci.*, 5: 57-62. <https://doi.org/10.4236/acs.2015.52004>.
- Mishra, D., Goyal, P. and Upadhyay, A. 2015. Artificial intelligence based approach to forecast PM_{2.5} during haze episodes: A case study of Delhi, India. *Atmos. Environ.*, 102: 239-248.
- Nagendra, S.M. and Khare, M. 2004. Artificial neural network-based line source models for vehicular exhaust emission predictions of an urban roadway. *Transp. Res. Part F Transp. Environ.*, 9(3): 199-208.
- Prakash, A., Kumar, U., Kumar, K. and Jain, V.K. 2011. A wavelet-based neural network model to predict ambient air pollutants' concentration. *Environ. Model. Assess.*, 16: 503-517.
- Rahimi, A. 2017. Short-term prediction of NO₂ and NO_x concentrations using multilayer perceptron neural network: A case study of Tabriz, Iran. *Ecol. Process.*, 6: 359.
- Shams, S.R., Jahani, A., Kalantary, S., Moeinaddini, M. and Khorasani, N., 2021. Artificial intelligence accuracy assessment in NO₂ concentration forecasting of metropolises air. *Sci. Rep.*, 11: 1805.
- Singh, K.P., Gupta, S. and Rai, P. 2013. Identifying pollution sources and predicting urban air quality using ensemble learning methods. *Atmos. Environ.*, 80: 426-437.
- Sofuoglu, S.C., Sofuoglu, A., Birgili, S. and Tayfur, G. 2006. Forecasting ambient air SO₂ concentrations using artificial neural networks. *Energy Sources B: Econ. Plan. Policy*, 1-2: 127-136. <https://doi.org/10.1080/009083190881526>
- UN Environment Programme (UNEP). 2019. Emissions Gap Report. UNEP. Available at: <https://www.unep.org/resources/emissions-gap-report-2019>.
- World Health Organization (WHO) 1980. Glossary on Air Pollution. Available at: https://www.euro.who.int/__data/assets/pdf_file/0008/155717/WA15.pdf.
- Yadav, S., 2020. Weight Initialization Techniques in Neural Networks Medium. Available at: <https://towardsdatascience.com/weight-initialization-techniques-in-neural-networks-26c649eb3b78>.
- Yadav, V. and Nath, S. 2018. Novel hybrid model for daily prediction of PM₁₀ using principal component analysis and Artificial Neural Network. *Int. J. Environ. Sci. Technol.*, 16(6): 2839-2848.



Effects of Corn Straw Biochar, Soil Bulk Density and Soil Water Content on Thermal Properties of a Light Sierozem Soil

Y. Q. Li^(**), L. J. Li^{*}, B. W. Zhao^{*†}, Y. Zhao^{*}, X. Zhang^{*} and X. Dong^{**(***)}

^{*}School of Environmental and Municipal Engineering, Lanzhou Jiaotong University, Lanzhou 730070, China

^{**}Gansu Dust Suppression for Transportation and Storage Engineering Research Center, Lanzhou 730070, China

^{***}Lanzhou Tianji Environmental Protection Limited Company, Lanzhou 730070, China

[†]Corresponding author: B. W. Zhao; zhbw2001@sina.com

Nat. Env. & Poll. Tech.
Website: www.neptjournal.com

Received: 02-12-2022

Revised: 02-01-2023

Accepted: 05-01-2023

Key Words:

Biochar
Thermal conductivity
Heat capacity
Thermal diffusivity
Light sierozem

ABSTRACT

This research aimed to quantify the effects of biochar derived from corn straw on soil thermal conductivity, capacity, and diffusivity. Firstly, the amount of biochar application (w/w) added to light sierozem soil was 0% to 5%, and the mixtures were packed into soil columns at a consistent bulk density (1.20 g.cm^{-3}). Secondly, soil columns with a consistent biochar addition rate (5%) were packed to different bulk densities of 1.30, 1.25, 1.20, 1.15, and 1.10 g.cm^{-3} . Soil thermal characteristics were measured under the control of soil moisture content from 0% to 40%. Under consistent bulk-density conditions, biochar could significantly reduce soil thermal conductivity and diffusivity. Still, there wasn't a significant influence on soil heat capacity in most soil moisture content levels. With the decrease of soil bulk density, soil thermal conductivity, capacity, and diffusion coefficient reduced significantly. As soil water content increased, all the indexes of thermal properties largely improved, and the effects were much more significant than those of biochar amendment and bulk density change on soil thermal performances. This research could supply an implication to evaluate the influence of biochar amendment on soil thermal performances.

INTRODUCTION

Soil thermal properties, including soil thermal conductivity, heat capacity, and diffusivity, are important parameters affecting the soil profile's energy distribution and heat transfer (Liu et al. 2018b). Many studies have shown that soil temperature changes have important effects on soil physicochemical properties and biochemical processes, such as soil hydrothermal coupling transmission (Zhao & Si 2019), soil organic matter decomposition and mineralization (Nieves et al. 2021, Semenov et al. 2022), plant growth (Yang et al. 2022), and greenhouse gas emission (Nsalambi & Stephanie 2018). Precise information on soil thermal properties are widely used in meteorological and industrial applications (Tong et al. 2021), agricultural management (Mendis et al. 2022), soil physical process simulation (Bayat et al. 2020), and many other fields.

Biochar is a carbon-rich material produced through biomass pyrolysis (such as crop residues and wood wastes) in an anoxic environment (Moreira & Feijoo 2017). Biochar application is a new technology, which has been recognized increasingly because of its potential role in carbon sequestration (Papageorgiou et al. 2021), greenhouse gas mitigation (Khan et al. 2022), soil improvement (Shi et

al. 2022, Geng et al. 2022), crop productivity enhancement (Melo et al. 2022, Singh et al. 2022). Recently, the physical effects of biochar amendment on surface albedo and soil temperature have attracted extensive attention. The porous black biochar applied to the soil inevitably makes the soil darker and reduces the soil albedo and solar radiation intensity, thus affecting the soil temperature. Oguntunde et al. (2008) detected that the soil color near a charcoal kiln in Ghana is darker than in the distance. This is attributed to the deposition of the escaping charcoal particles, which reduces the surface reflectance by 37.0% and increases the average surface temperature by 4°C . Ding et al. (2019) showed that soil temperature was more sensitive to external temperature changes after the application of biochar. Liu et al. (2018a) showed that applying biochar significantly reduced soil temperature at 5 cm depth and regulated diurnal temperature fluctuations.

Moreover, Zhang et al. (2017) studied seasonal changes in albedo after biochar application on planted and unplanted farmland. It was found that the influence of biochar on the albedo mainly occurred in winter and was related to crop coverage. Therefore, biochar application in soil plays an important role in soil energy balance and temperature distribution.

Soil thermal properties depend on the soil composition of gas, liquid, and solid in a porous medium (Liu et al. 2018b). In contrast, due to its large surface area and low bulk density, biochar can cause changes in soil structure and composition, which in turn can affect the thermal properties of the soil (Usowicz et al. 2016). However, researches on the influences of biochar on soil heat characteristics are particularly scarce (Usowicz et al. 2016), which limits our knowledge to understand the mechanisms of soil temperature change in the presence of biochar. In addition, soil thermal properties are often closely related to atmospheric temperature (Camilo et al. 2022), especially in the arid and semi-arid regions of the Loess Plateau, which are extremely sensitive to climate change, and land-atmosphere interactions in these regions play an important role in the regional climate (Lu et al. 2022). Therefore, considering the effects of changes in soil bulk density and water content on soil thermal properties during biochar application may be important for the potential of biochar to mitigate climate change. We investigated the effects of corn stover biochar, soil bulk density, and water content on soil thermal properties in the loess region's typical light sierozem soil. This study aims to provide a reference for understanding biochar's contribution to soil thermal properties and objectively evaluate biochar's potential role in soil temperature change.

MATERIALS AND METHODS

Materials

The tested soil was sampled from the 0-20 cm soil layer on a hill at Lanzhou Jiaotong University, China, and was classified as light sierozem soil. The soil specimen was naturally dried and sieved with a 2-mm sieve. And the soil belonged to silty loam. The proportions of sand, silt, and clay particles were 78.85%, 19.25%, and 1.9%, respectively. The soil bulk density was 1.35 g.cm^{-3} . The organic matter content of the soil was 20 g.kg^{-1} .

The corn straw was obtained from Longnan City, Gansu Province, China. The straw was cleaned with running water, stoved at 80°C for 12 h in a drying oven (101-2A, Cangzhou Sansi times equipment Co., Ltd, Cangzhou, China), then triturated with a lapping machine (JM-F50, Jiangsu Banderi Stainless Steel Co., Ltd, Yancheng, China). The fragments were placed in a muffle roaster (XL-2018, Hebi Wanbo Instrument Co., Ltd, Hebi, China) and pyrolyzed at 500°C for 6 h by oxygen-limiting and temperature-controlling methods. The biochar prepared by the above method had 74.5% C, 18.2% O, 2.5% H, and 0.2% N. The BET- N_2 absorption method determined the specific surface area was $60.87 \text{ m}^2\text{.g}^{-1}$ and the average intraparticle pore size was 3.74 nm. The particle density of biochar was determined to be 1.18

g.cm^{-3} using the pycnometer method. The biochar bulk density was 0.709 g.cm^{-3} .

Experimental Design

The experiments consist of two parts. In the first part, biochar was evenly added to the soil according to certain mass ratios (w/w) 0%, 1%, 2%, 3%, 4%, and 5%. Then, 120 g dry soil-biochar mixtures were weighed and put into 6 plastic columns with the same specifications (inner diameter 5cm, volume 100 cm^3). By this means, the bulk density of soil could be calculated as 1.20 g.cm^{-3} . In the second part, the biochar application rate was 5%. The soil-biochar mixtures were packed into plastic columns at bulk densities of 1.10, 1.15, 1.20, 1.25, and 1.30 g.cm^{-3} (110, 115, 120, 125, 130 g dry soil-biochar mixtures were weighed and added to 6 plastic columns with the same specifications). There was a movable cover on top of each plastic column. When it was opened, a sensor could be inserted into the soil from the top to measure the thermal properties of the soil. The soil volumetric moisture content was regulated using a syringe to inject different amounts of water into soil-biochar mixtures from the top of the plastic column. Then, those columns were closed and stored at ambient temperature (20°C) for 72 h to obtain a balance for soil thermal property measurements. The volumetric soil water contents were programmed as 0%, 10%, 20%, 30%, and 40%.

Soil Thermal Properties Determination

The soil thermal characteristics, including thermal conductivity, diffusivity, and capacity, were measured by a KD2Pro man-pack soil thermal characteristics analysis meter which is equipped with an SH-1 double-point sensing element (7% accuracy, 1.3 mm diameter, 3 cm long, and 60 mm spacing, Decagon Devices Inc., Pullman, USA).

Data Analysis

The significance of biochar application's influence on soil thermal characteristics was tested by one-way ANOVA analysis (ANOVA). A least significant difference (LSD) test was used in the multiple comparison tests to study the differences between biochar treatments. Statistical analysis was completed with SPSS 22.0 software (IBM, New York, USA), and the significance level was set as 0.05. Origin 8.0 (OriginLab, Northampton, Massachusetts, USA) was used for the data regression and graphing.

RESULTS AND DISCUSSION

Influences of Biochar Addition on Soil Thermal Characteristics

The soil thermal conductivity at constant bulk density with different soil moisture content levels is revealed in Fig. 1.

The values of soil thermal conductivity reduced with the increase of biochar amendment rate. When the amendment rate is 5%, and the soil moisture content is 0%, 10%, 20%, 30%, and 40%, the values of thermal conductivity are 0.154, 0.446, 0.681, 0.841 and 1.09 $\text{W}\cdot\text{m}^{-1}\cdot\text{K}^{-1}$, which decrease by 15.4%, 24.5%, 15.9%, 24.2%, and 5.2%, respectively, compared with those values of the control sample. Biochar amendment showed remarkable impacts ($p > 0.05$) on thermal conductivity at all kinds of soil water content. The biochar thermal conductivity was determined as 0.055 $\text{W}\cdot\text{m}^{-1}\cdot\text{K}^{-1}$, which is far below those of water at 20°C (0.594 $\text{W}\cdot\text{m}^{-1}\cdot\text{K}^{-1}$) and quartz (7.7 $\text{W}\cdot\text{m}^{-1}\cdot\text{K}^{-1}$) (Lu et al. 2007). Therefore, biochar application was expected to reduce soil thermal conductivity. In addition, biochar application could increase soil organic matter content (Ondrasek et al. 2019). Soil thermal conductivity is inversely associated with soil organic matter content (Mustamo et al. 2019). Therefore, the reduction of soil thermal conductivity may be due to the increase of soil organic matter content from biochar application.

Fig. 2 shows that soil thermal capacity under diverse biochar application rates hadn't marked a difference in most soil water moisture levels. The volumetric heat capacity of biochar particles is 2.9 $\text{J}\cdot\text{cm}^{-3}\cdot\text{K}^{-1}$, which is higher than that of mineral particles (1.9 $\text{J}\cdot\text{cm}^{-3}\cdot\text{K}^{-1}$) and soil organic matter (2.5 $\text{J}\cdot\text{cm}^{-3}\cdot\text{K}^{-1}$) (Liu et al. 2018b). Therefore, biochar application was expected to increase soil thermal capacity.

However, Fig. 2 shows that biochar application in this study mostly had no significant effect on soil thermal capacity. Still, Shang et al. (2015) reported that biochar application increased soil thermal capacity when applied at 40-60 $\text{t}\cdot\text{hm}^{-1}$. The lack of a significant increase in heat capacity in this study may be due to the large thermal capacity of soil moisture and the small percentage of biochar, and the small amount of biochar was not enough to change the thermal capacity of the soil.

Fig. 3 shows that the values of soil thermal diffusivity decrease with the biochar amendment rate increasing. When the rate is 5%, and the soil moisture content is 0%, 10%, 20%, 30%, and 40%, the values of soil thermal diffusivity are 0.160, 0.339, 0.374, 0.371, and 0.420 $\text{mm}^2\cdot\text{s}^{-1}$, which decrease by 3.6%, 15.3%, 14.0%, 24.0%, and 15.7%, respectively, compared with those values of the control sample. The thermal diffusivity of biochar was 0.165 $\text{mm}^2\cdot\text{s}^{-1}$, which was approximately equal to that of soil at 0.166 $\text{mm}^2\cdot\text{s}^{-1}$ (dry soil with a soil density of 1.20 $\text{g}\cdot\text{cm}^{-3}$). Still, in most cases in this study, the soil thermal diffusivity decreased with increasing biochar application, which may be related to the alteration of soil porosity by biochar (Hardie et al. 2014, Herath et al. 2013). Although the total porosity of the soil didn't significantly change, biochar application can change the pore size distribution of soil and then lead to the enhancement of soil microbial activity and community, which has been indicated in a lot of research (Zhang & Shen

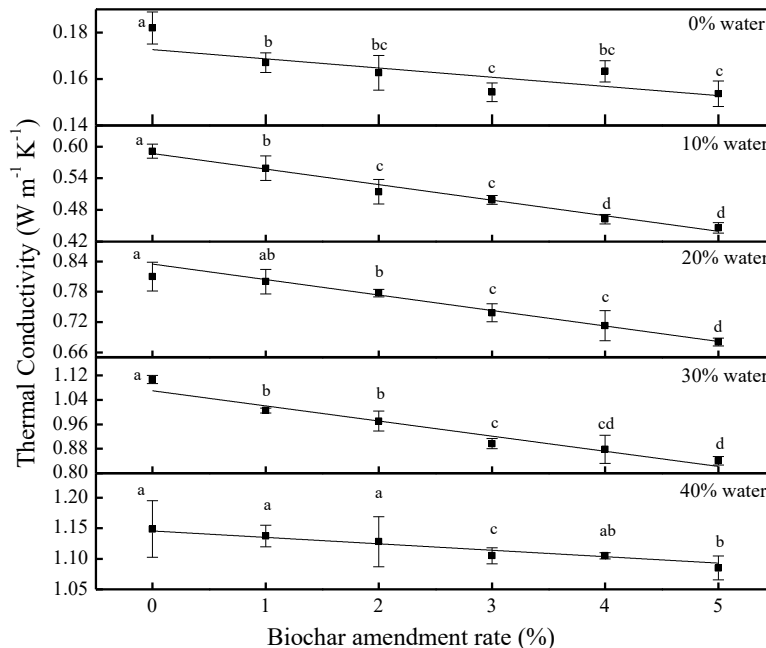


Fig. 1: Influences of biochar addition on thermal conductivity of the soil.

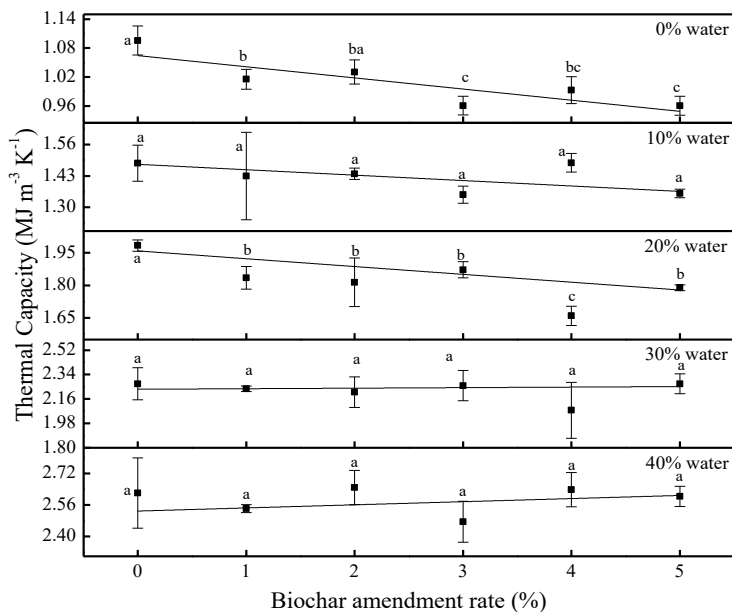


Fig. 2: Influences of biochar addition on soil heat capacity.

2022, Yan et al. 2021). In addition, considering that thermal diffusivity is the ratio of thermal conductivity to thermal capacity when thermal conductivity decreases while thermal capacity remains constant, soil thermal diffusivity inevitably decreases, which is consistent with the values measured in this study.

Influences of Bulk Density on Soil Thermal Characteristics

With soil bulk density reduction, soil thermal conductivity showed the same trend and gradually decreased (Fig. 4). When the water content was kept at 0%, 10%, 20%, 30%, and 40%, soil thermal conductivity decreased from 0.277 to 0.159, 0.555 to 0.480, 0.791 to 0.643, 0.971 to 0.837, and 1.08 to 0.990 $\text{W}\cdot\text{m}^{-1}\cdot\text{K}^{-1}$ with soil bulk density decreasing from 1.30 to 1.10 $\text{g}\cdot\text{cm}^{-3}$. Except for the 40% soil water content level, the diverse bulk density gradients in the soil columns had remarkable effects ($p < 0.05$) on soil thermal conductivity. At the same soil water content level, reducing soil bulk density could inevitably lead to increased aerated soil porosity and solid particle reduction. The contact between solid soil particles and water is somewhat isolated, which hinders the heat conduction of the solid and liquid phases. This results in soil thermal conductivity decreasing with soil bulk density reduction. In addition, the air thermal conductivity is only 1% of those of the solid phase and liquid phase in soil, which further hinders heat transfer. Toková et al. (2020) found that the application of biochar significantly reduced soil bulk density (12% reduction) and increased soil

porosity (12% increase), while the reduction in soil thermal conductivity was mainly attributed to the biochar-induced reduction in soil bulk density and increase in total porosity (Zhao et al. 2016).

Fig. 5 shows that when the water content was kept at 0%, 10%, 20%, and 30%, the values of soil thermal capacity decreased from 1.22 to 0.948, 1.55 to 1.42, 1.97 to 1.80, and 2.43 to 2.14 $\text{MJ}\cdot\text{m}^{-3}\cdot\text{K}^{-1}$ with soil bulk density decreasing from 1.30 to 1.10 $\text{g}\cdot\text{cm}^{-3}$. However, when the soil moisture content is 40%, thermal capacity increases with decreasing bulk density, mainly because when the moisture content is too high, water will be abundantly present in the soil pore space, and the lower the bulk density, the higher the soil moisture content, and the greater contribution of moisture to thermal capacity.

Fig. 6 shows that soil bulk density reduction leads to a decrease in soil thermal diffusivity at large. When the water content was kept at 0%, 10%, 20%, 30%, and 40%, the thermal diffusivity of soil decreased from 0.227 to 0.168, 0.343 to 0.328, 0.404 to 0.357, 0.419 to 0.391, and 0.449 to 0.362 $\text{mm}^2\cdot\text{s}^{-1}$ with soil bulk density decreasing from 1.30 to 1.10 $\text{g}\cdot\text{cm}^{-3}$.

Influences of Soil Moisture Content on Thermal Characteristics

Soil water content is the most effective and dynamic element, which could affect soil thermal properties (Mengistu et al. 2017, Usowicz et al. 2017). As revealed in Fig. 7,

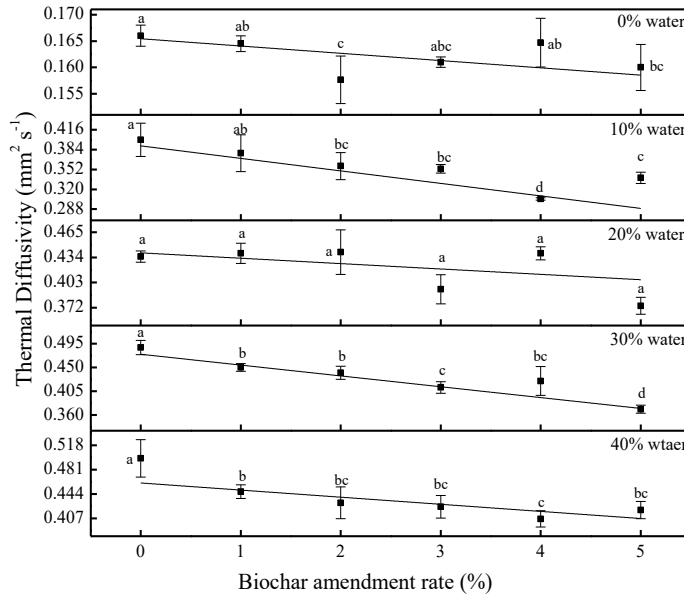


Fig. 3: Influences of biochar addition on soil thermal diffusivity.

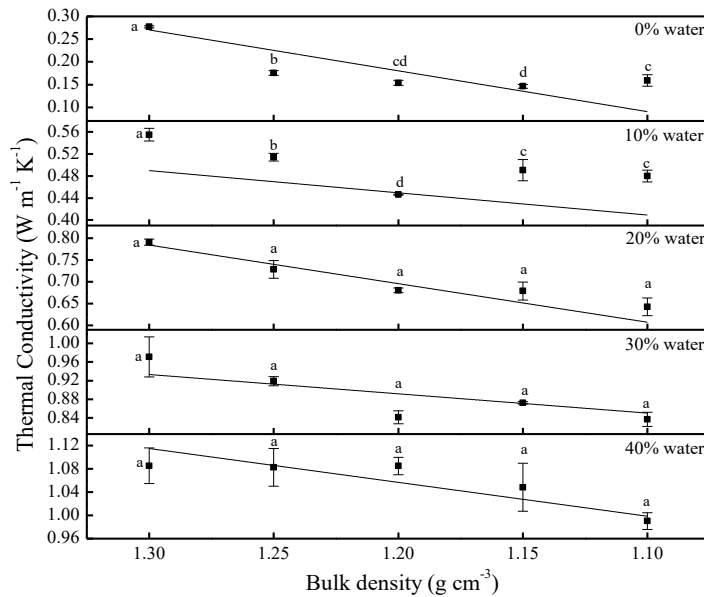


Fig. 4: Effects of biochar addition on thermal diffusivity of the soil.

the influence of soil moisture content on soil thermal characteristics is extremely more significant than those of biochar application and soil bulk density change.

Fig. 7a and Fig. 7b show that soil thermal conductivity increases rapidly with soil moisture content increasing under constant or changing bulk density. Still, with soil water content further increasing, the increasing trend of soil thermal conductivity slows down. When the soil moisture

content is 40%, the thermal conductivity values are as high as those of samples with no water amendment. At low soil water content levels, soil thermal conductivity is mainly achieved through the contact between solids. As the water film thickness on the soil particles' surface increases, the contact between soil particles changes from point to surface, and soil thermal conductivity increases instantly. When soil moisture content increases to a certain value (approximately

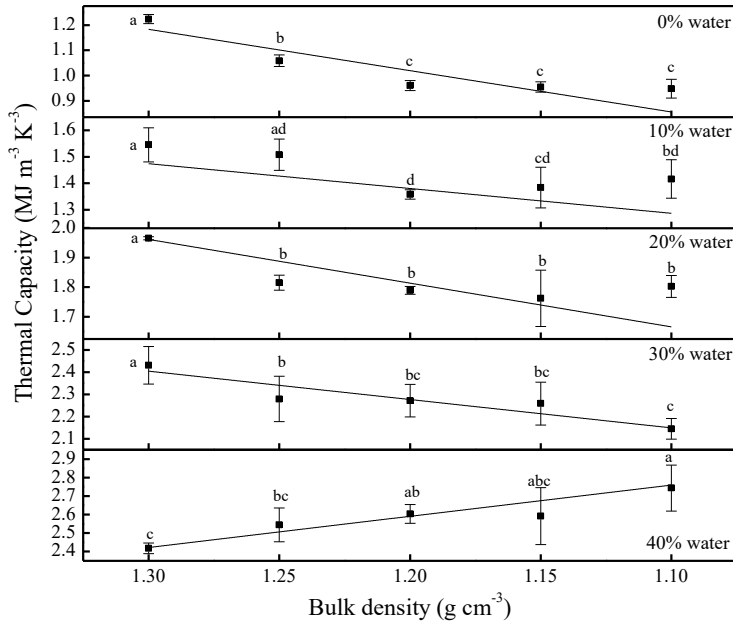


Fig. 5: Effects of bulk density on soil thermal capacity.

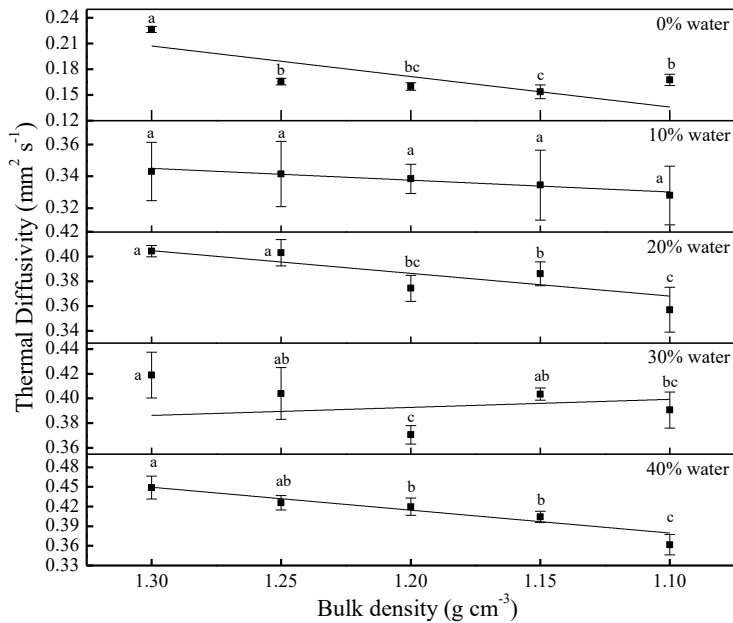


Fig. 6: Effects of bulk density on soil thermal diffusivity.

0.03 cm³.cm⁻³), the continued increase in moisture mainly exists in capillary water and gravity water. The thermal conductivity increase mainly depends on the volume of water rather than that of air, so the rate of increase is slowed (Fu et al. 2014). The equations reflecting the relation between thermal conductivity and moisture content were obtained by regression with high R² values, listed in Table 1.

The soil thermal capacity enhances linearly with soil water content increasing (Fig. 7c and Fig. 7d), mainly because the soil thermal capacity is the sum of the thermal capacities of gas, liquid, and solid phases in soil. The thermal capacity of the water phase in soil increases with soil water content increasing. Although the air content in soil decreases with soil water content increasing, water has a higher heat

capacity than air, which makes the decrease in soil thermal capacity caused by the decrease in air content not obvious.

The linear equations were obtained and listed in Table 1 with R^2 values more than 0.94.

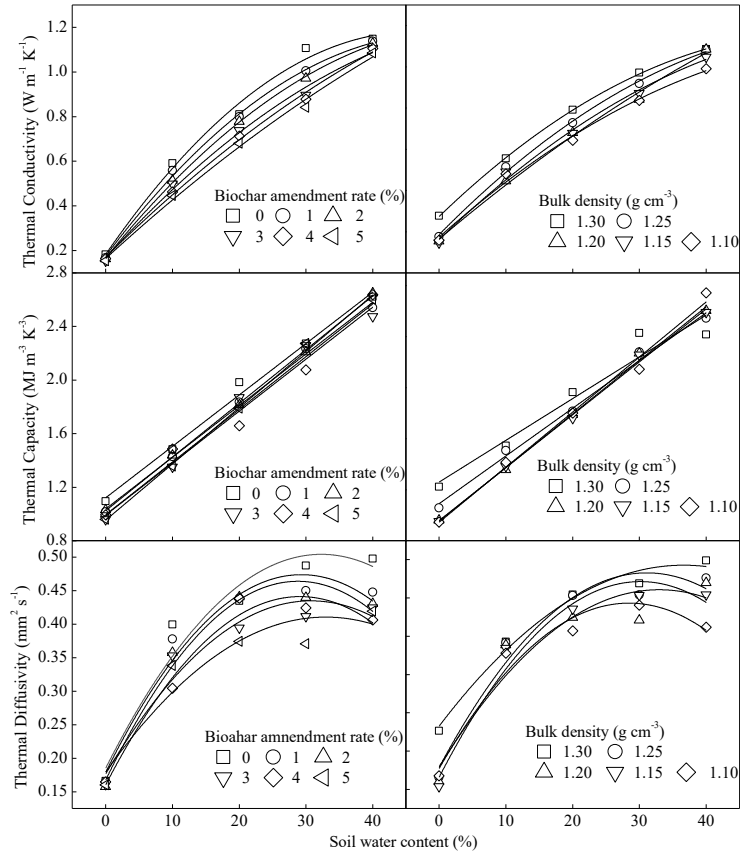


Fig. 7: Influences of soil water content on thermal properties of the soil.

Table 1: Regression results of the relation between the thermal property (y) and moisture content (x).

Runs	Fitting equation											
	Thermal conductivity				Thermal capacity				Thermal diffusivity			
	$y = -ax^2 + bx + c$				$y = ax + b$				$y = -ax^2 + bx + c$			
	a	b	c	R^2	a	b	R^2	a	b	c	R^2	
Biochar application rates [%]	0	4.69	0.0432	0.184	0.99	0.0384	1.12	0.99	0.00031	0.0198	0.186	0.95
	1	3.97	0.0397	0.177	0.99	0.0386	1.04	0.99	0.00034	0.0202	0.179	0.97
	2	3.28	0.0370	0.168	0.99	0.0401	1.03	0.99	0.00036	0.0206	0.168	0.98
	3	2.53	0.0293	0.168	0.99	0.0394	0.997	0.98	0.00027	0.0168	0.177	0.95
	4	1.64	0.0295	0.172	0.99	0.0388	0.994	0.98	0.00033	0.0193	0.161	0.98
	5	1.22	0.0275	0.165	0.99	0.0420	0.956	0.99	0.00021	0.0140	0.180	0.91
Bulk density [g.cm ³]	1.30	0.00027	0.0323	0.275	0.99	0.0327	1.26	0.94	1.57	0.0115	0.233	0.98
	1.25	0.00027	0.0329	0.187	0.99	0.0374	1.09	0.99	2.63	0.0164	0.179	0.96
	1.20	0.00012	0.0275	0.165	0.99	0.0420	0.956	0.99	2.13	0.0140	0.1800	0.91
	1.15	0.00024	0.0313	0.163	0.99	0.0415	0.960	0.99	2.81	0.0170	0.167	0.97
	1.10	0.00022	0.0289	0.175	0.99	0.0432	0.947	0.99	2.67	0.0152	0.177	0.97

The relation between thermal diffusivity and moisture content is not a simple linear relationship (Fig. 7e and Fig. 7f). The ratio of thermal conductivity to thermal capacity is thermal diffusivity. Under conditions of low water content, thermal diffusivity rises with moisture content increasing. However, when water content exceeds a certain value (30% v/v), the thermal diffusivity decreases with the moisture content increasing. This occurs because when the soil water content is further increased (the volume ratio is greater than 30%), although the thermal conductivity (numerator) increases, the heat capacity (denominator) increases faster, resulting in the decrease of thermal diffusivity, this is consistent with the study of Liu et al. (2018b). The regression results were also obtained and listed in Table 1 with R^2 values more than 0.91.

CONCLUSIONS

Under constant bulk density conditions, soil thermal diffusivity and conductivity reduced with the increase of biochar application amount. Biochar amendment hadn't an obvious effect on soil thermal capacity. Soil thermal conductivity, capacity, and diffusivity diminished obviously with soil bulk density decrease. However, the influence of water content on soil thermal performances is much more significant than those of biochar application and bulk density change. All soil thermal performance indexes were largely enhanced with soil water content increase.

ACKNOWLEDGMENT

This work was supported by the [National Natural Science Foundation of China] under Grant [51766008, 21467013, 21167007].

REFERENCES

- Bayat, H., Mazaheri, B. and Mohanty, B. P. 2020. Estimating soil water characteristic curve using landscape features and soil thermal properties. *Soil Till. Res.*, 203: 104688.
- Camilo, M.A., Fidel, G.R., Norman, J.S., Hugo, B., Francisco, J.V., Almudena, G.G., Felix, G.P., Elena, G.B., Pedro, J.R., Thomas, S. and Jorge, N. 2022. Near-surface soil thermal regime and land-air temperature coupling: A case study over Spain. *Int. J. Climatol.*, First published: 29 April 2022.
- Ding, Y., Gao, X., Qu, Z., Jia, Y., Hu, M. and Li, C. 2019. Effects of biochar application and irrigation methods on soil temperature in farmland. *Water*, 11(3): 499.
- Fu, Y., Lu, Y. and Ren, T. 2014. Influences of finite probe property on soil thermal property estimated by heat pulse technique. *Trans. Chin. Soc. Agric. Eng.*, 30(19): 71-77.
- Geng, N., Kang, X., Yan, X., Yin, N., Wang, H., Pan, H., Yang, Q., Lou, Y. and Zhuge, Y. 2022. Biochar mitigation of soil acidification and carbon sequestration is influenced by materials and temperature. *Ecotox. Environ. Safe.*, 232: 113241.
- Hardie, M., Clothier, B., Bound, S., Oliver, G. and Close, D. 2014. Does biochar influence soil physical properties and soil water availability? *Plant Soil*, 376: 347-361.
- Herath, H., Camps-Arbestain, M. and Hedley, M. 2013. Effect of biochar on soil physical properties in two contrasting soils: An Alfisol and an Andisol. *Geoderma*, 209-210: 188-197.
- Khan, M.N., Li, D., Shah, Asad., Huang, Jing., Zhang, L., Avelino, N. D., Han, T., Du, J., Ali, S., Sial, T. A., Lan, Z., Hayat, S., Song, Yi., Bai, Y. and Zhang, H. 2022. The impact of pristine and modified rice straw biochar on the emission of greenhouse gases from red acidic soil. *Environ. Res.*, 208: 112676.
- Liu, Y., Yang, S., Lu, H. and Wang, Y. 2018a. Effects of biochar on spatial and temporal changes in soil temperature in cold waterlogged rice paddies. *Soil Till. Res.*, 181: 102-109.
- Liu, Z., Xu, J., Li, X. and Wang, J. 2018b. Mechanisms of biochar effects on thermal properties of red soil in south China. *Geoderma*, 323: 41-51.
- Liu, Z., Xu, J., She, D., Li, X. and Wang, J. 2018c. Effects of biochar addition on thermal properties of loamy soil. *Acta Pedol. Sin.*, 55(4): 933-944.
- Lu, S., Guo, W., Ge, J. and Zhang, Y. 2022. Impacts of land surface parameterizations on simulations over the arid and semiarid regions: the case of the loess plateau in China. *J. Hydrometeorol.*, 23(16): 891-907.
- Lu, S., Ren, T., Gong, Y. and Horton, R. 2007. An improved model for predicting soil thermal conductivity from water content at room temperature. *Soil Sci. Soc. Am. J.*, 71(1): 8-14.
- Melo, L.C.A., Lehmann, J., Carneiro, J.S. and Arbestain, M. C. 2022. Biochar-based fertilizer effects on crop productivity: a meta-analysis. *Plant and Soil*, 472: 45-58.
- Mendis, S.S., Udawatta, R., Anderson, S.H., Ansari, J. and Salceda, M. 2022. Effects of cover crops on soil thermal properties of a corn cropping system. *Soil Sci. Soc. Am. J.*, 86(5): 1194-1205.
- Mengistu, A.G., van Rensburg, L.D. and Mavimbela, S.S.W. 2017. The effect of soil water and temperature on thermal properties of two soils developed from aeolian sands in South Africa. *Catena*, 158: 184-193.
- Moreira, M.T. and Feijoo, I.N.G. The prospective use of biochar as adsorption matrix – A review from a lifecycle perspective. *Bioresour. Technol.*, 246: 135-141.
- Mustamo, P., Ronkanen, A.K., Berglund, Ö., Berglund, K. and Kløve, B. 2019. Thermal conductivity of unfrozen and partially frozen managed peat soils. *Soil Till. Res.*, 191: 245-255.
- Nieves, B., José, A.R.A., Jorge, P. and César P. C. 2021. The effect of extreme temperatures on soil organic matter decomposition from Atlantic oak forest ecosystems, *iScience*, 24(12): 103527.
- Nsalambi, V.N. and Stephanie, S. 2018. Monitoring soil thermal properties and CO₂, CH₄ and NO₂ emissions in a corn field in central Missouri. *Discov. Agric.*, 4: 75-84.
- Oguntunde, P. G., Abiodun, B. J., Ajayi, A. E. and van de Giesen, N. 2008. Effects of charcoal production on soil physical properties in Ghana. *J. Plant Nutr. Soil Sci.*, 171: 591-596.
- Ondrasek, G., Begić, H.B., Zovko, M., Filipović, L., Meriño-Gergichevich, C., Savić, R. and Rengel, Z. 2019. Biogeochemistry of soil organic matter in agroecosystems & environmental implications. *Sci. Total Environ.*, 658: 1559-1573.
- Papageorgiou, A., Azzi, E. S., Enell, A. and Sundberg, C. 2021. Biochar produced from wood waste for soil remediation in Sweden: Carbon sequestration and other environmental impacts. *Sci. Total Environ.*, 776: 145953.
- Semenov, V. M., Lebedeva, T. N., Zinyakova, N. B., Khromyckina, D. P., Sokolov, D. A., Lopes de Gerenyu, V. O., Kravchenko, I. K., Li, H. and Semenov, M. V. 2022. Dependence of soil organic matter and plant residue decomposition on temperature and moisture in the long-term incubation experiments. *Eurasian Soil Sci.*, 55: 926-939.
- Shang, J., Geng, Z., Zhao, J., Geng, R. and Zhao, Y. 2015. Effects of biochar on water thermal properties and aggregate stability of Lou soil. *Chin. J. Appl. Ecol.*, 26: 1969-1976.

- Shi, G., Wu, Y., Li, T., Fu, Q. and Wei, Y. 2022. Mid- and long-term effects of biochar on soil improvement and soil erosion control of sloping farmland in a black soil region, China. *J. Environ. Manage.*, 320: 115902.
- Singh, H., Northup, B. K., Rice, C. W. and Prasad, P. V. V. 2022. Biochar applications influence soil physical of biochar application and re-application on soil bulk density, porosity, saturated hydraulic conductivity, water content, and soil water availability in a silty loam and chemical properties, microbial diversity, and crop productivity: A meta-analysis. *Biochar*, 4: 8.
- Toková, L., Lgaz, D., Horák, J. and Aydin, E. 2020. Effect of biochar application and re-application on soil bulk density, porosity, saturated hydraulic conductivity, water content, and soil water availability in a silty loam Haplic Luvisol. *Agronomy*, 10(7): 1005.
- Tong, C., Li, X., Lin, D. and Wang, H. 2021. Prediction of the temperature profiles for shallow ground in a cold region and cold winter hot summer region of China. *Energy Build.*, 242: 110946.
- Usovicz, B., Lipiec, J., Łukowski, M., Marczewski, W. and Usovicz, J. 2016. The effect of biochar application on thermal properties and albedo of loess soil under grassland and fallow. *Soil Till. Res.*, 164: 45-51.
- Usovicz, B., Łukowski, M.I., Rüdiger, C., Walker, J.P. and Marczewski, W. 2017. Thermal properties of soil in the Murrumbidgee River Catchment (Australia). *Int. J. Heat Mass Tran.*, 115: 604-614.
- Yan, T., Xue, J., Zhou, Z. and Wu, Y. 2021. Biochar-based fertilizer amendments improve the soil microbial community structure in a karst mountainous area. *Sci. Total Environ.*, 794: 148757.
- Yang, W., Parsons, D. and Mao, X. 2022. Exploring limiting factors for maize growth in Northeast China and potential coping strategies. *Irrig. Sci.*, 1: 22.
- Zhao, J., Ren, T., Zhang, Q., Du, Z. and Wang, Y. 2016. Effects of biochar amendment on soil thermal properties in the North China Plain. *Soil Sci. Soc. Am. J.*, 80: 1157-1166.
- Zhao, Y. and Si, B. 2019. Thermal properties of sandy and peat soils under unfrozen and frozen conditions. *Soil Till. Res.*, 189: 64-72.
- Zhang, J. and Shen, J. 2022. Effects of biochar on soil microbial diversity and community structure in clay soil. *Ann. Microbiol.*, 72: 35.
- Zhang, Y., Hu, X., Zou, J., Zhang, D., Chen, W., Wang, X., Chen, Y. and Liu, Y. 2017. Effects of biochar on soil surface albedo, temperature and moisture in agricultural soil. *Environ. Sci.*, 28(8): 1234-1239.



Efficient Copper Adsorption from Aqueous Solution by *Dictyuchus sterile* Pellets

Rana Hadi Hameed Al-Shammari*†, Shaimaa Satae M. Ali** and Moayad Salih Hussin*

* Department of Biology, College of Science, Mustansiriyah of University, Baghdad, Iraq

**Environmental Studies and Research Center, University of Babylon, Iraq

†Corresponding author: Rana Hadi Hameed Al-Shammari; dr.rana@uomustansiriyah.edu.iq

Nat. Env. & Poll. Tech.
Website: www.neptjournal.com

Received: 28-08-2022

Revised: 18-10-2022

Accepted: 01-11-2022

Key Words:

Bio-adsorption
Fungal pellets
Trace metals
Water molds

ABSTRACT

A common heavy metal pollutant of water resources, copper (II), can cause serious health problems or even death. Over the past few years, several filamentous fungi strains have been isolated, identified, and tested for their ability to bio-adsorb heavy metals for potential use in the bio-remediation of copper from wastewater. In this study, variables, including the dosage of fungal pellets, temperature, pH, time, initial copper concentration, and agitation rate, were assessed to select the best conditions for the adsorption of copper by *Dictyuchus sterile* pellets. To identify the active groups responsible for metal adsorption, microscopic observations were made using a light microscope and scanning electron microscope. The copper adsorbent was then analyzed before and after adsorption using an atomic adsorption spectrophotometer and Fourier transform infrared spectroscopy. The ideal adsorption conditions were: fungal pellets with a wet weight of 1 g.L⁻¹ at a temperature of 25°C, pH 5.5, the initial copper concentration of 100 ppm, and shaking at a speed of about 250 rpm for 72 h to achieve a removal efficiency rate of 95%. Copper adsorbed with the biomass of the fungal pellets was 57 mg.g⁻¹. The use of fungal pellets would be a method that can be used to increase the surface area of adsorption and also is thought to be one of the most cost-effective ways to remove trace metals from polluted water.

INTRODUCTION

Clean water is a significant concern because the world's population is growing, and needs are becoming increasingly urgent (Boretti & Rosa 2019). Industrialization and civilization have significantly advanced, undoubtedly improving living standards and comforts for people, but accidentally upsetting the critical environmental balance that nature had created over a millennium (EPA 2002). These human activities and industrial discharges are contaminating the water. Organic, inorganic, and biological particles comprise these pollutants' three main categories. The primary pollutant in water is heavy metals, which are produced as waste in various industries, including textile, pharmaceutical, and leather (Barakat 2011). Heavy metal removal is essential because they are hazardous, carcinogenic compounds that shouldn't be released into the environment directly (Gautam et al. 2014, Burakov et al. 2018). Trace metals are generally eliminated through chemical and physical processes such as

adsorption to inorganic materials, electro dialysis, chemical precipitation, crystallization, coagulation, flocculation, reduction, and ion exchange (Gupta et al. 2011, 2012a, 2012b). However, the removal of metals requires a lot of chemicals and energy and produces byproducts.

On the other hand, biological remediation using microorganisms (algae, bacteria, fungi) has been investigated for their capacity for metal adsorption from polluted waters, with fungi beneficial for this aim due to their accessibility, low cost, and capacity to ingest significant amounts of heavy metals (Bayramoğlu & Arica 2008, Dhankhar & Hooda 2011, Maznah et al. 2012, Kumar et al. 2019). Many fungal genera, *Aspergillus*, *Fusarium*, *Mucor*, *Penicillium*, and *Saccharomyces* biomass, have been considerable attention because of their large capacity for metal removal (Çeribası & Yetis 2001, Kiran et al. 2005, Parvathi et al. 2007, Bayramoğlu & Arica 2008). Since a great deal of work has been done in this field. By adhering to their mycelium from the freshwater shrimp cultivation pond, fungi such as *Pythium* sp., *Dictyuchus sterile*, and *Scytalidium lignicola* were shown to accumulate zinc, lead, and cadmium (Duddridge & Wainwright 1980). The adsorption efficiency

ORCID details of the authors:

Rana Hadi Hameed Al-Shammari: <https://orcid.org/0000-0001-8195-9368>

Shaimaa Satae M. Ali: <https://orcid.org/0000-00031588-7882>

of trace metals by terrestrial filamentous fungi has been confirmed by researchers (Damodaran et al. 2013, Dixit et al. 2015, Dusengemungu et al. 2020). Consequently, numerous studies have examined the effectiveness of various fungal species in removing heavy metals from wastewater. Recently, fungi have been among the classes of microorganisms that have received the most attention in the biological remediation of contaminants (Shakya et al. 2016). These heterotrophic microbes can biotransform metal contaminants through chemical alteration or metabolic mechanisms. They are a good option for bioremediation of pollution because they can grow on contaminants and establish extended mycelial networks (Harms et al. 2011). The cell wall of water molds (Oomycetes) is composed mainly of glucan and cellulose (4-20%), the amino acid hydroxyproline, which is considered the site of the dominance of metal binding sites, such as the chemical groups acetamido, amide, phosphate, amino, amine, sulfhydryl, carboxyl, and hydroxyl groups (Anbia & Alvand 2012, Bulgariu & Bulgariu 2012). This research aims to develop an efficient method for copper ion uptake from aqueous solutions employing *Dictyuchus* and growth parameter optimization to maximize heavy metal adsorption.

MATERIALS AND METHODS

Isolation and Preparation of Fungal Pellets

The previously described technique was used to isolate *Dictyuchus sterile* isolates (Dick 1969). As in the previous study, the baiting technique was employed for sample isolation where sesame seeds *Sesamum indicum* L were used as baits (Dick 1969, Al-Rekabi & 1996). In separate sterile polyethylene bags, samples of decaying plant leaves obtained from the Al-Jaish channel were brought to the mycology laboratory. After gently mixing the sample, 1 mL of river water was added to 10 cm Petri dishes containing 10 mL of sterile distilled water and 3 sterile sesame seeds and boiled for 15 min to kill bacteria. After 7 days of incubation, fungal growth appears on the seeds, which have been cleaned with sterile distilled water and purified by utilizing Czapek-Dox broth for liquid cultivation (NaNO_3 , K_2HPO_4 , KCl, MgSO_4 , FeSO_4 , 10 g glucose), at 25°C and pH 5.5, with a shaking speed of 150 rpm for five days (1×10^4 spores.mL⁻¹ in 500 mL of suspension) (Alrubaie & Al-Shammari 2018).

Incubation Conditions Affecting Removal Efficiency and Mass Adsorption

Adsorption Dosage of Fungal Pellets Biomass and Initial Metal Concentration

The adsorbent dose was optimized using (0.2, 0.4, 0.6, 0.8, 1.0, and 1.2 g) while holding all other variables constant.

Initial copper concentration, pH, and agitation speed, copper were absorbed and removed from the environment by fungal pellets. Initial concentration tests of aqueous copper nitrate were conducted with concentrations of 20, 40, 60, 80, and 100 ppm in a volume of 100 ml. To modify the pH, 1 HCL and 1 NaOH were applied. pH readings were measured with a digital pH meter (3, 5, 7, 9, 11). By adding 1g of fungal pellets to 100 mL of 100 ppm copper solutions and agitating the mixture for 24 h at a speed ranging from 50 to 250 rpm at pH 5.5 at 25 °C, it was possible to study the effect of agitation speed variation on equilibrium (Al-Mamoori et al. 2020).

Optimization of Contact Time and Temperature

The pH, temperature, and rpm were optimized using data from previous batches, and the mass in grams of fungal biomass was maintained in 100 mL copper ions solutions while being shaken. Samples were analyzed at predetermined intervals after 15, 30, 45, 60, and 75 h. pH and contact time constant and increasing temperature, we investigated how pH affects adsorption studies (20, 25, 30, 35, 40 °C).

Fourier Transform Infrared Spectroscopy (FTIR) Characterization and SEM Morphological Examination

The Fourier transform infrared spectra of fungal pellets exposed to copper (at initial metal concentrations of each metal 100 mg.L⁻¹, exposure time 75 h and those non-exposed to copper were obtained using an FTIR spectrophotometer. The samples were then dried in an oven at 50°C. the FTIR spectra were recorded at 25°C in the range of 400–4000 cm⁻¹. The light microscope was generally used in the morphological identification of fungi under low power objectives (10X, 40X) and SEM (Bruker, Japan). After adsorption, fungal pellets were collected, washed with distilled water five times, and dried at 70°C to examine their morphology. A surface elemental analysis of the fungal pellets was carried out using SEM after they were fixed in 3% glutaraldehyde in distilled water at 4°C for 3 h. (Zhang et al. 1998).

Trace Metals Concentration Measurement and Statistical Analysis

Atomic adsorption spectroscopy (AAS) was used in these investigations to quantify the concentration of copper. The holo cathode device (Analytikjena AG instrumentation) was used to correct and standardize the wavelength. After being removed from the flask by Whatman No. 1 filter paper that had been dried overnight in an oven at 50 °C fungal, the amount of copper absorbed by the fungal pellets was determined using the equation below (Zhang et al. 1998).

$$M = \frac{C_i - C_e}{F} * V$$

M: Mass of adsorbed metal on the weight of fungal biomass adsorbent (mg.g^{-1})

C_e : Residual metal concentration Residue in solution in equilibrium after Adsorption (ppm)

C_i : Initial metal concentration before adsorption (ppm)

V: volume of solution (L)

F: adsorbent mass of fungal pellets (g)

The equation below was used to calculate the effectiveness of removing trace metals (Anbia and Alvand, 2012).

$$RE \% = \frac{(C_i - C_f) \times 100}{C_i}$$

C_i : Initial metal ion concentration (mg.L^{-1}) before adding the fungal pellets

C_f : Residual metal ion concentration (mg.L^{-1}) after adding the fungal pellets

Statistical Analysis

The significant difference between various values of the incubation conditions was determined statistically using a two-way ANOVA followed by a student t-test. Each factor was attained with three replicates.

RESULTS AND DISCUSSION

Characteristics and Pellets Formation of *Dictyuchus sterile*

Fungus *Dictyuchus sterile* was isolated from contemned water from the Al-Jaish channel in Baghdad and classified depending on morphological features of colonies and



Fig. 1: Morphological features of fungus *Dictyuchus sterile*. A) dictyoid discharge mode of zoospores 7 days after inoculation in water culture; B) globular, terminal gemma. Magnification power 40X. scale bar =50 μm .

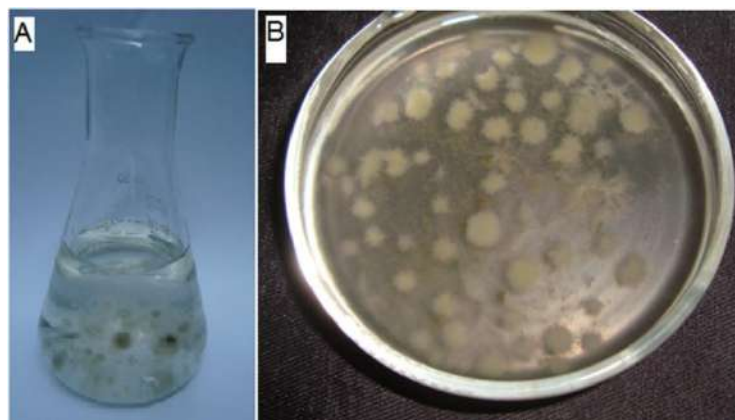


Fig. 2: Fungal pellets after 5 days of incubation and shaking incubation with 180 rpm 25°C.

Table 1: Incubation factors affect removal efficiency percentage and mass of adsorbed copper on the weight of fungal biomass adsorbent represented as the mean of three replicates \pm standard deviation. Deferent letters within the column represent the significant differences ($p \leq 0.05$).

Factors		RE%	M [mg.g ⁻¹]
Adsorption dosage of fungal pellets biomass [mg]	200	16	17.12 \pm 1.4c
	400	23	18.82 \pm 1.9c
	600	61	20.33 \pm 0.3b
	800	91	55.90 \pm 0.8a
	1000	92	59.98 \pm 1.8 a
Contact time (mins)	15	11	\pm 0.22c12
	30	13	\pm 0.5c14
	45	67	\pm 0.3b32
	60	88	\pm 0.04a54
	75	91	\pm 0.12a56
The initial concentration of copper ions [ppm]	20	94	\pm 0.2a18
	40	91	\pm 0.5b33
	60	92	\pm 0.4b51
	80	90	\pm 0.024b 74
	100	93	\pm 0.25a88
Shaking rate [rpm]	50	55	\pm 3.37c 13
	100	54	\pm 0.061c11
	150	76	\pm 0.011c 43
	200	88	57 \pm 0.06b
	250	93	\pm 0.04a 59
pH	3	43	\pm 0.10c 32
	5	92	57 \pm 0.2a
	7	66	41 \pm 0.1b
	9	21	11 \pm 0.2d
	11	13	9 \pm 0.3e
Temperature [°C]	20	32	31.55 \pm 0.10c
	25	95	72.18 \pm 1.02a
	30	88	54.56 \pm 2.6b
	35	79	49.34 \pm 3.37b
	40	34	18.55 \pm 0.10c

vegetative structures, which are non-septate hypha. In Fig. 1 A, B, dictyoid and achlyoid zoospores are abundant in a fusiform and spherical shape, while the sporangia are abundant in branches, and sexual reproduction is absent (Fig. 2).

Incubation Conditions Affecting Copper Adsorption

Adsorption Dosage of Fungal Pellets

As shown in (Table 1), copper ions adsorption exhibits a clear relationship with the amount of fungal pellets biomass; as biomass quantity increases, copper ions adsorption increases

(Bulgariu & Bulgariu 2012). An equilibrium has been formed, and ions-saturated connections are present since further increase has no discernible effect.

Initial Concentration of Copper Ions and Temperature

Due to easy access to binding sites, fungal biomass is overloaded; as the concentration of metal ions increases, the removal percentage decreases. The ratio of copper ions adsorption and equilibrium rises when copper ion concentration increases to 120 mg.L⁻¹ because of the higher concentration gradient's force to startle. This demonstrates that copper ions have a better removal by keeping optimized parameters constant, such as 25°C, 1 gm.100 mL⁻¹ dose for copper for 75 h, 180 rpm, pH 5.5, initial ion concentrations range from 20 to 120 mg.L⁻¹. Table 1 shows the dosage of fungal biomass effect on copper ion removal; at 120 ppm, the initial Cu concentration removal efficiency was 95%. In this investigation, the elimination present as biomass grows is directly associated with biomass dosage. As the concentration of copper ions in the solution grew, increasing removal percentages were seen until all of the adsorbent's binding sites were covered (Mathew et al. 2016). Once equilibrium is attained, the adsorbent's ability to remove metal ions decreases due to a lack of binding sites. It was discovered that the initial copper ion concentrations and clearance percentages were 95 percent at 120 ppm. Large amounts of fungal biomass can help clean up polluted aqueous solutions and restore polluted ecosystems. According to research, fungi can survive in temperatures as high as 40°C while feeding on various carbon sources, including fatty acids and oils. According to earlier research (Iskandar et al. 2011, Li et al. 2014), excellent efficiency is only seen at temperatures above 40°C. Therefore, fungi's ability to remove heavy metals in cold regions is insufficient.

Effect of pH on Adsorption

The most crucial component in ions adsorption is water pH, which also impacts the solubility of metal ions, the chemistry of metals in water, and the charge on the surface of cells (Bulgariu & Bulgariu 2012). According to Table 1, the pH range was between 3-11. The findings demonstrated that the chemical characteristics of an aqueous solution with a low pH and surface locations for metal adsorption on fungal biomass influence copper adsorption. Impact on the pH of the dissolved ions on the fungal cell wall's H₃O⁺ bonding. Additionally, ions at low pH do not provide a positive metal to biomass due to the repulsive forces produced. In other words, the amount of negative load on these sites is decreased due to the high proton concentration and the associated shortage of protons in related sites. Therefore, it lessens or stops ions from bonding. When the units are released, the metal adsorbs to the surface due to the units' negative

charge. The chemical characteristics of each metal determine the pH of the cell.

Due to enhanced copper absorption, the ideal pH for the adsorption process in this investigation was chosen to be 5.5. These outcomes, which are displayed in (Fig. 4), came from the investigation of the adsorption. The study's findings about the morphologies of Oomycota indicated a consistent ability to adsorb trace metals from aqueous solutions (Kaczmarek & Boguś 2021). According to a report, the wall of filamentous fungal cells contains chitin, which is involved in the metal adsorption process (Shakya et al. 2016). Compared to chitin, which is a powerful N-poly adsorbent, chitosan (di acetate Acetyl glucosamine) it's thought to take traces of metal out of aqueous solutions. The amino group's nitrogenous location should cause this. The maximal adsorption capacity of the fungus is related to the amount of chitosan it contains because chitosan causes adsorption. The primary components of filamentous fungi's cell walls are chitosan, chitin, and phosphorous. However, a sizable portion of the filaments' wall is composed of chitin and chitin, and its quantity is higher than that of yeast (Hall 2002, Bellion et al. 2006). The increased capacity of the heads to absorb metal solution pH increase can be due to other components, such as galactose and lipids, which are present in equal concentrations. The adsorption of hydrogen ions might cause it from the aqueous solution that was either neutralized, or H^+ liberated from fungal biomass (Sen 2012).

Effect of Shaking Speed

With more incredible shaking speeds, metal ion adsorption rises. After examining several shaking rates, 250 rpm was determined to be the ideal speed, as shown in (Table 1). The largest amount of copper ions was found to be adsorbed at 210 rpm. In contrast, all other parameters, including temperature (25°C), dosage (1.0 gm.50 mL⁻¹ for 75 h), rpm (100, 130, 160, 190, 210), pH (5.5), and starting concentration (100 mg.L⁻¹), were held constant.

Incubation Time

For copper and biomass from fungal pellets, the adsorption process was examined for contact times ranging from 15 to 75 h. According to investigations and the findings in Table 1, the total time needed for this part was 75 h. The amount exceeds the highest percentage of adsorption, and after the specified period, copper metal typically responds in 50 min. The proportion of adsorption with the adsorbent does not change significantly with time, nor does the amount of adsorption. Calculated at that moment was 73.38 percent. Due to the enormous number of vacant sites in the early days, it is possible to keep the other variables constant. *Aspergillus niger* was used in earlier experiments to remove copper. Its

highest maximum removal capability was observed in 18 h with 25.2 mg.g⁻¹ Cu (Tsekova & Todorova, 2002). After 6 h of incubation, *Rhizopus oligosporus* absorbed mercury at a rate of 33.33 mg.g⁻¹ (Ozsoy 2010).

Analysis of Active Compounds By FTIR Spectra and SEM Imaging

To examine the active groups in the cell wall, either the blank adsorbent (fungal pellets only) or the fungal pellets plus copper ion, both of which are shown in (Fig. 3). The fungus is typically present in samples that were collected both before and after IR spectrum adsorption. Copper adsorption peaks were visible in the FTIR spectrum of fungal biomass pellets before copper adsorption at 3425, 3138, 1745, 1456.3, 1016, 1058, 960, and 819 cm⁻¹. These peaks were moderate before and after adsorption and showed a reduction in peak intensity. The peak in the fungal biomass sample before copper adsorption at 3425 cm⁻¹ is assigned to O-H. It can be attributed to the C-H group containing lipids and phospholipids. The band at 1635 cm⁻¹ is assigned to C=O. The band at 1456 cm⁻¹ is related to carbonate carboxylate or methyl. The characteristic adsorption peak at 1078 cm⁻¹ represents C-OH stretching. Si-OH and S-O are assigned to the bands at 960 and 819, respectively. Before copper adsorption, the sample's FTIR spectrum showed that the previously mentioned characteristic adsorption peaks were shifted to new positions: 3425, 2926, 1635, 1456.3, 1078, 1024, 960 and 819 cm⁻¹ after copper adsorption by the fungal pellets' biomass. These results show the association of these functional groups in the adsorption of copper ions. The peak at 2926 cm⁻¹ representing C-H stretching vibrations shifted to 3425 cm⁻¹, which was assigned to the stretching vibration of N-H. The carboxylic acid (C = O) band at 1635 cm⁻¹ is moved to a lower wavelength at 1624 cm⁻¹. The variation in the wave number reveals the involvement of the carboxylic acid in the ion exchange process. The peak at 1456 cm⁻¹ representing C-H stretching vibrations shifted to the peak at 1422 cm⁻¹ which is assigned to the stretching vibration of C = O. In addition, a peak at 819 cm⁻¹ shifted to 602 cm⁻¹ might be associated with the bending modes of alcoholic hydroxyl (-OH). The band moved from 1024 cm⁻¹ representing C-OH stretching vibrations to 1078 cm⁻¹, corresponding to C-O stretching vibrations.

In conclusion, FITR confirms that copper ions are adsorbed mainly by carboxylic, phenolic, and amide groups copper ions and the functional groups on the fungal pellets biomass complexed together, resulting in changes in wave numbers and intensities. The results of the spectra before the adsorption of copper metal in the normal state show that carboxyl functional groups- COOH, amide (NH₂),

3-phosphate PO_4 , and a hydroxyl group (OH) play an essential role in adsorption. Accumulation of copper on fungal surface morphology was examined by using SEM, extracellular aggregation of copper in the mycelial surface as in (Fig. 4), components of fungal cell walls as cellulose,

melanin, and phenols represent sites for adsorption to occur, which provide oxygen-rich metal-binding (Garcia-Rubio et al. 2020). These cell wall components (exopolysaccharides) could be most possibly responsible for the adsorption of heavy metals (Liu et al.2001).

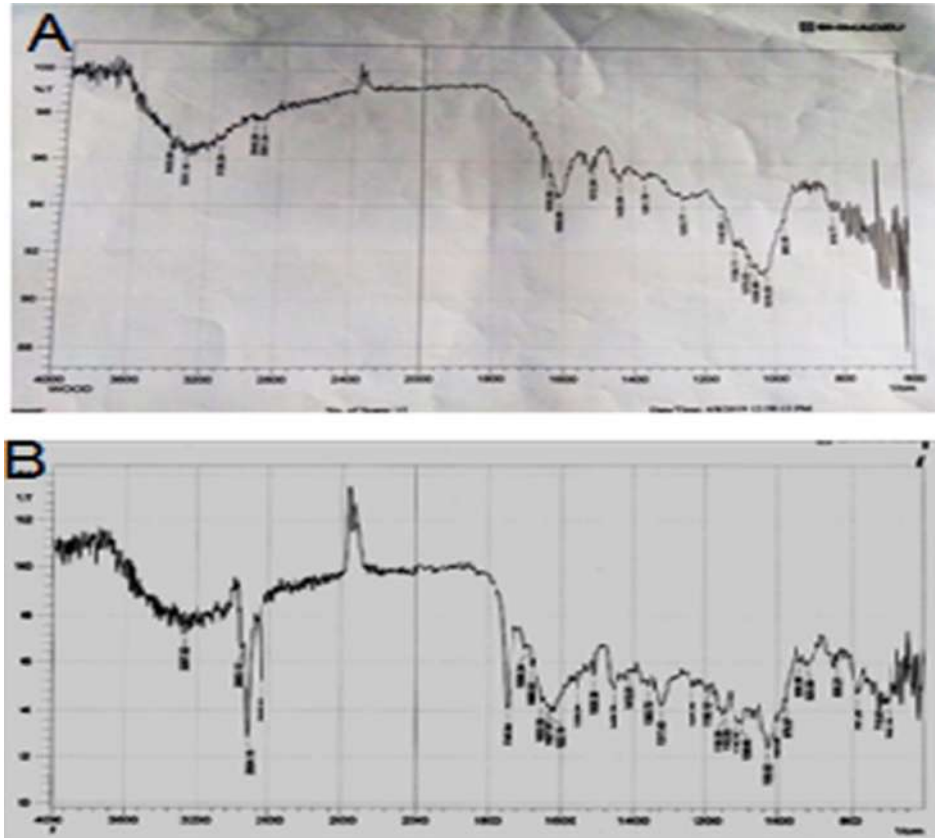


Fig. 3: Fourier transforms infrared spectroscopy(FT-IR) spectra of fungal pellets. A) before copper adsorption and B) after copper adsorption.

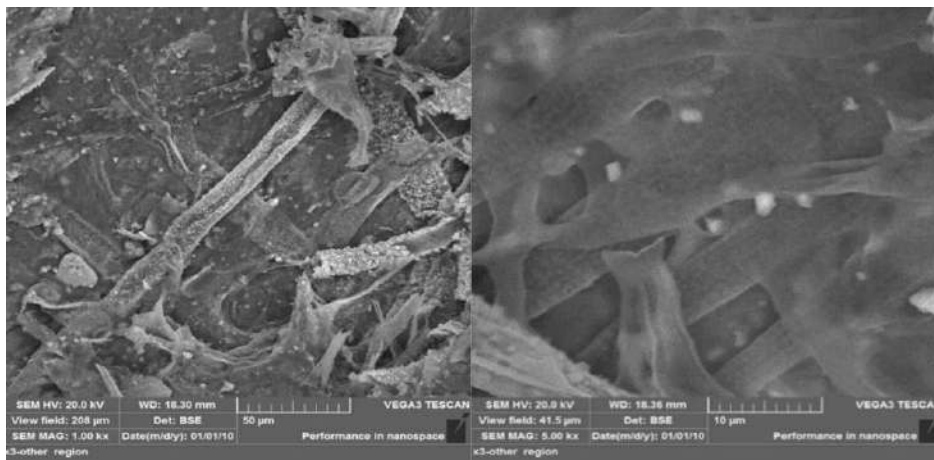


Fig. 4: SEM micrograph of the fungal pellets grown at 100 ppm copper.

CONCLUSION

Fungal biomass pellets of *Dictyuchus sterile* were used to remove copper metal from the aqueous solution. The highest removal percentage of copper was 95 %, and fungal pellets adsorbed copper. Fungal biomass pellets of *D. sterile* (M) was 57 mg.g⁻¹ were established at optimized conditions: pH 5.5 with 75 h of contact time during the experiment, one biomass dose of fungus pellets was used, a 100 ppm concentration was used, 250 rpm was used, and the temperature was 25 °C. According to this study, removing heavy metals like copper from contaminated water using the intended method is a more environmentally friendly option. According to FTIR spectrum analysis and SEM images, the principal adsorbents for copper ions on the adsorbent surface are active groups in the fungal cell wall like carbonate, hydroxyl, carboxyl, phosphate, and ammonium nitrate.

ACKNOWLEDGEMENT

The author would like to acknowledge the Biology Department, College of Science, Mustansiriyah University, Baghdad province, Iraq, for supporting this research.

REFERENCES

- Al-Mamoori, A.M.J, Al-Shammari, R.H.H.J.Y., Al-Amari, J. and Al-Juboori, M. 2020. Removal of *Anabaena* sp. Bloom and microcystin-LR by coculturing with *Mucor rouxii* pellets. *Aqua. Ecosyst. Health Manag.*, 23(3): 267-273. <https://doi.org/10.1080/14634988.2020.1816002>
- Al-Rekabi, S. and An, N.R.B. 1996. Specificity of baits in isolating Saprolegniaceae. *AL-Mustansiriya J. Sci.*, 7(1): 16-35.
- Alrubaie, G. and Al-Shammari, R.H. 2018. Microalgae *Chlorella vulgaris* harvesting via co-pelletization with filamentous fungus. *Bagh. Sci. J.*, 15(1): 31-36.
- Anbia, M. and Alvand, M. 2012. Fast and efficient removal of orthophenanthroline and 2, 20-bipyridine from aqueous solutions by adsorption on modified nanoporous carbon. *Sci. Iran.*, 19(6): 1573-1579.
- Barakat, M. 2011. New trends in removing heavy metals from industrial wastewater. *Arab. J. Chem.*, 4(4): 361-377.
- Bayramoğlu, G. and Arica, M.Y. 2008. Removal of heavy mercury (II), cadmium (II), and zinc (II) metal ions by live and heat-inactivated *Lentinus edodes* pellets. *Chem. Eng. J.*, 143(1-3): 133-140.
- Bellion, M., Courbot, M., Jacob, C., Blaudez, D. and Chalot, M. 2006. Extracellular and cellular mechanisms sustaining metal tolerance in ectomycorrhizal fungi. *FEMS Microbiol. Lett.*, 254(2): 173-181.
- Boretti, A. and Rosa, L. 2019. Reassessing the projections of the world water development report. *NPJ Clean Water*, 2(1): 1-6.
- Bulgariu, D. and Bulgariu, L. 2012. Equilibrium and kinetics studies of heavy metal ions biosorption on green algae waste biomass. *Bioresour. Technol.*, 103(1): 489-493.
- Burakov, A.E., Galunin, E.V., Burakova, I.V., Kucherova, A.E., Agarwal, S., Tkachev, A.G. and Gupta, V.K. 2018. Adsorption of heavy metals on conventional and nanostructured materials for wastewater treatment purposes: A review. *Ecotoxicol. Environ. Safety*, 148: 702-712.
- Çeribasi, I.H. and Yetis, U. 2001. Biosorption of Ni (II) and Pb (II) by *Phanerochaete chrysosporium* from a binary metal system-kinetics. *Water*, 27(1): 15-20.
- Damodaran, D., Balakrishnan, R.M. and Shetty, V. K. 2013. The uptake mechanism of Cd (II), Cr (VI), Cu (II), Pb (II), and Zn (II) by mycelia and fruiting bodies of *Galerina vittiformis*. *BioMed Res. Int.*, 7: 012
- Dhankhar, R. and Hooda, A. 2011. Fungal biosorption—an alternative to meet the challenges of heavy metal pollution in aqueous solutions. *Environ. Technol.*, 32(5): 467-491.
- Dick, M. 1969. Morphology and taxonomy of the oomycetes, with special reference to Saprolegniaceae, Leptomitaceae, and Pythiaceae: I. Sexual reproduction. *New Phytol.*, 68(3): 751-775.
- Dixit, R., Malaviya, D., Pandiyan, K., Singh, U.B., Sahu, A., Shukla, R. and Lade, H. 2015. Bioremediation of heavy metals from soil and aquatic environment: an overview of principles and criteria of fundamental processes. *Sustainability*, 7(2): 2189-2212.
- Duddridge, J. and Wainwright, M. 1980. Heavy metal accumulation by aquatic fungi and reduction in viability of *Gammarus pulex* fed Cd²⁺ contaminated mycelium. *Water Res.*, 14(11): 1605-1611.
- Dusengemungu, L., Kasali, G., Gwanama, C. and Ouma, K. O. 2020. Recent advances in biosorption of copper and cobalt by filamentous fungi. *Front. Microbiol.*, 11: 3285.
- Garcia-Rubio R., de Oliveira, H.C., Rivera, J. and Trevijano-Contador N. 2020. The fungal cell wall: *Candida*, *Cryptococcus*, and *Aspergillus* species. *Front. Microbiol.*, 9(10): 2993. doi: 10.3389/fmicb.2019.02993.
- Gautam, R.K., Mudhoo, A., Lofrano, G. and Chattopadhyaya, M.C. 2014. Biomass-derived biosorbents for metal ions sequestration: Adsorbent modification and activation methods and adsorbent regeneration. *J. Environ. Chem. Eng.*, 2(1): 239-259.
- Gupta, V. K., Ali, I., Saleh, T. A., Nayak, A. and Agarwal, S. 2012a. Chemical treatment technologies for wastewater recycling. An overview. *RSC Adv.*, 2(16): 6380-6388.
- Gupta, V.K., Jain, R., Mittal, A., Saleh, T.A., Nayak, A., Agarwal, S. and Sikarwar, S. 2012b. Photo-catalytic degradation of toxic dye amaranth on TiO₂/UV in aqueous suspensions. *Mater. Sci. Eng.*, 32(1): 12-17.
- Gupta, V.K., Jain, R., Saleh, T., Nayak, A., Malathi, S. and Agarwal, S. 2011. Equilibrium and thermodynamic studies on the removal and recovery of safranin-T dye from industrial effluents. *Sep. Sci. Technol.*, 46(5): 839-846.
- Hall, J.A. 2002. Cellular mechanisms for heavy metal detoxification and tolerance. *J. Exp. Bot.*, 53(366): 1-11.
- Harms, H., Schlosser, D. and Wick, L. Y. 2011. Untapped potential: Exploiting fungi in bioremediation of hazardous chemicals. *Nature Rev. Microbiol.*, 9(3): 177-192.
- Iskandar, N.L., Zainudin, N.A.I.M. and Tan, S.G. 2011. Tolerance and biosorption of copper (Cu) and lead (Pb) by filamentous fungi isolated from a freshwater ecosystem. *J. Environ. Sci.*, 23(5): 824-830.
- Kaczmarek, A. and Boguś, M. I. 2021. Fungi of entomopathogenic potential in Chytridiomycota and Blastocladiomycota, and fungal allies of the Oomycota and Microsporidia. *IMA Fungus*, 12(1): 1-13.
- Kiran, I., Akar, T. and Tunalı, S. 2005. Biosorption of Pb (II) and Cu (II) from aqueous solutions by pretreated biomass of *Neurospora crassa*. *Process Biochem.*, 40(11): 3550-3558.
- Kumar, A., Kumar, V. and Singh, J. 2019. Role of fungi in the removal of heavy metals and dyes from wastewater by biosorption processes. In Yadav, A.N., Mishra, S., Singh, S. and Gupta, A. (eds), *Recent Advancement in White Biotechnology Through Fungi*, Springer, Cham, pp. 397-418.
- Li, F., Gao, Z., Li, X. and Fang, L. 2014. The effect of environmental factors on the uptake of 60Co by *Paecilomyces catenellannulatus*. *J. Radioanal. Nucl. Chem.*, 299(3): 1281-1286.
- Liu, Y., Lam, M. and Fang, H. 2001. Adsorption of heavy metals by EPS of activated sludge. *Water Sci. Technol.*, 43(6): 59-66.
- Mathew, B.B., Jaishankar, M., Biju, V.G. and Beeregowda, K.N. 2016. Role of bioadsorbents in reducing toxic metals. *J. Toxicol.*, 11: 201.
- Maznah, W.W., Al-Fawwaz, A. and Surif, M. 2012. Biosorption of copper and zinc by immobilised and free algal biomass, and the effects of

- metal biosorption on the growth and cellular structure of *Chlorella* sp. and *Chlamydomonas* sp. isolated from rivers in Penang, Malaysia. *J. Environ. Sci.*, 24(8): 1386-1393.
- Ozsoy, H.D. 2010. Biosorptive removal of Hg (II) ions by *Rhizopus oligosporus* produced from corn-processing wastewater. *Afr. J. Biotechnol.*, 9(51): 8783-8790.
- Parvathi, K., Naresh Kumar, R. and Nagendran, R. 2007. Biosorption of manganese by *Aspergillus niger* and *Saccharomyces cerevisiae*. *World J. Microbiol. Biotechnol.*, 23(5): 671-676.
- Sen, M. 2012. A comparative study on biosorption of Cr (VI) by *Fusarium solani* under different growth conditions. *Open J. Appl. Sci.*, 2(03): 146.
- Shakya, M., Sharma, P., Meryem, S.S., Mahmood, Q. and Kumar, A. 2016. Heavy metal removal from industrial wastewater using fungi: uptake mechanism and biochemical aspects. *J. Environ. Eng.*, 142(9): C6015001.
- The United States Environmental Protection Agency (EPA). 2002. The National Water Quality Inventory: Report to Congress for the 2002 Reporting Cycle: A Profile. The United States Environmental Protection Agency (EPA), Washington, DC.
- Tsekova, K. and Todorova, D. 2002. Copper (II) accumulation and superoxide dismutase activity during growth of *Aspergillus niger* B-77. *Zeitschr. Naturforsch.*, 57(3-4): 319-322.
- Zhang, L., Zhao, L., Yu, Y. and Chen, C. 1998. Removal of lead from aqueous solution by non-living *Rhizopus nigricans*. *Water Res.*, 32(5): 1437-1444.



Comparative Assessment and Monitoring Changes in NDVI of Achanakmar Tiger Reserve (ATR) and its Buffer Zone, India

Anupama Mahato*†

*Department of Forestry, Wildlife and Environmental Sciences, Guru Ghasidas Vishwavidyalaya, Bilaspur, C.G., India

†Corresponding author: Anupama Mahato; anupamamahato4@gmail.com

Nat. Env. & Poll. Tech.
Website: www.neptjournal.com

Received: 27-08-2022

Revised: 24-10-2022

Accepted: 03-11-2022

Key Words:

Achanakmar tiger reserve
Buffer zone
Normalized difference vegetation index
Vegetation mapping

ABSTRACT

Achanakmar Tiger Reserve (ATR), endowed with rich biological diversity and lush green vegetation in and around, makes it more unique. It is also an integral part of the Achanakmar Amarkantak Biosphere Reserve (AABR) and has been identified as one of the important tiger reserves of the Central Indian landscape due to its connectivity with other protected areas and tiger reserves in neighboring landscapes. Vegetation mapping and monitoring are important to understand changes in ecosystem processes and associated temporal and spatial impacts. Pre- and post-monsoon IRS, LISS III, and AWiFS satellite data from 2000, 2004, 2008, 2010, and 2013 were used for the present study. This paper is an attempt to examine the variation in the normalized difference vegetation index (NDVI) of ATR and its buffer zone on a seasonal and temporal basis. Climate conditions such as temperature, precipitation, relative humidity, etc. play an important role in the growth and development of healthy vegetation. The NDVI value of ATR has shown fluctuation and recorded positive growth over the past 14 years with few exceptions. The post-monsoon season recorded a higher NDVI value as compared to the pre-monsoon months. The maximum NDVI value was recorded in 2004 (+0.539) for the entire ATR and its buffer zone.

INTRODUCTION

Since the early 1970s, the Normalized Difference Vegetation Index (NDVI) has been the most widely used vegetation index for studying vegetation and phenology. This term was first used by Rouse et al. (1973) and is directly related to the photosynthetic capacity and thus the energy absorption of plant canopies (Sellers 1985, Myneni et al. 1995).

NDVI is a sensitive parameter of surface vegetation and vegetation growth that reflects the difference between the radiation absorption in the red spectral region caused by chlorophyll and the reflectivity of canopy structure caused by the near-infrared spectral region, which can effectively characterize the vegetation environment, its changes, and effects (Leon-Tavares et al. 2021, Morawitz 2006, Pu et al. 2022). NDVI is associated with biomass, carbon sequestration, plant water stress, and biodiversity (Nagendra et al. 2013, Gillespie et al. 2019).

Multispectral satellite data collected at regular intervals with a Geographical Information System (GIS) provides a suitable platform for vegetation data analysis (Muhati et al. 2018). This technique and data are more appropriate than traditional ground surveys because it takes less time to detect the changes that have preceded the area, is less expensive,

and provides a nearly real picture of larger and physically inaccessible areas (Nad et al. 2022).

Achanakmar was officially established as a wildlife sanctuary in the year 1975 under the Wildlife (Protection) Act, 1972. Later, it was declared a tiger reserve in 2009 due to the presence of endangered tiger species. Tigers and leopards are the biggest predators in this area. It is a habitat for more than 50 species of mammals, including bison, spotted deer, sambhar, nilgai, mouse deer, striped hyena, etc. The Maniyari River, which originates in the core zone of ATR, is its lifeline. Many seasonal and perennial tributaries feed into the Maniyari River. This area is home to a few indigenous tribal groups such as the Baiga, Kol, Munda, and others. The ATR connects many different tiger reserves and protected areas of the Central Indian landscape through corridors.

Champion & Seth (1968) categorized ATR's forest vegetation into northern tropical moist deciduous and southern dry mixed deciduous forests (Roychoudhury 2013). Sal (*Shorea robusta*) is the dominant tree species, followed by Sal mixed forest, which includes tree species such as *Terminalia tomentosa*, *Diospyros melanoxylum*, *Adina cordifolia*, *Pterocarpus marsupium*, *Madhuca indica*, *Anogeissus latifolia*, and *Tectona grandis* (plantation). Bamboo (*Dendrocalamus strictus*) is also found on higher

and lower slopes with various tree species (Mandal et al. 2017). More than 50 tree species and over 600 medicinal plant species were found here. Twenty-five threatened floral species under various threat levels as enlisted by the IUCN Red List are found in ATR. It includes one critically endangered species (*Rauwolfia serpentina*), five endangered species (*Adiantum capillus veneris* L., *Lygodium flexuosum* (L.) Sw, *Clerodendrum serratum* (Linn.) Moon, *Acorus calamus* L., *Eulophia herbacea* Linds.), and 19 vulnerable species (Roychoudhury et al. 2012).

Numerous studies have been carried out in the ATR to assess floral diversity (Sahu 2011, Singh & Sharma 2017, Sandey & Sharma 2016, Singh et al. 2005, Shukla & Singh 2009) and faunal biodiversity (Roychoudhury et al. 2019, Mandal et al. 2017). However, little is known about the use of geospatial technology in monitoring the vegetation of the Achanakmar Tiger Reserve.

Today, remote sensing and GIS have emerged as useful tools to monitor ecological impacts and changes in green corridors, offering capabilities to detect and interpret floral

and faunal habitat quality (Nad et al. 2022). There have been an increasing number of studies that have used NDVI to study ecosystem dynamics and disturbances in protected areas (Prasai 2022, Gillipsie et al. 2019, Nemani et al. 2009).

The present study aims to assess and monitor the seasonal and annual NDVI trends of ATR between 2000 and 2013. Emphasis has also been placed on examining the same NDVI trends for its buffer zone (excluding the core zone), as more than 30% of the ATR consists of the buffer zone, which is more vulnerable to anthropogenic influence, and therefore fluctuations in the NDVI value of this area may impact the overall NDVI trend of the entire reserve area.

MATERIALS AND METHODS

Study Area

The geographical extent of the Achanakmar Tiger Reserve (ATR) is between 22°17' and 22°38' North latitudes and 81°31' and 81°57' East longitude. It covers an area of 914.017 km², of which 626.195 km² belongs to the core

Table 1: Area details of the core and buffer zone of ATR.

Area	Area (km ²)	Status	Legal Status	Total Forest Area (km ²)
Core Area (Critical tiger Habitat)	551.552	Achanakmar Wildlife Sanctuary	Reserve Forest	626.195
	74.643	Non Protected area of Bilaspur and Marwahi Forest Division	Reserve Forest	
Buffer Area	248.902	-	Reserve Forest	287.822
	38.920	-		
Total Tiger Reserve Area = 914.017 km ²				

(Source: Forest Dept., Govt. of Chhattisgarh)

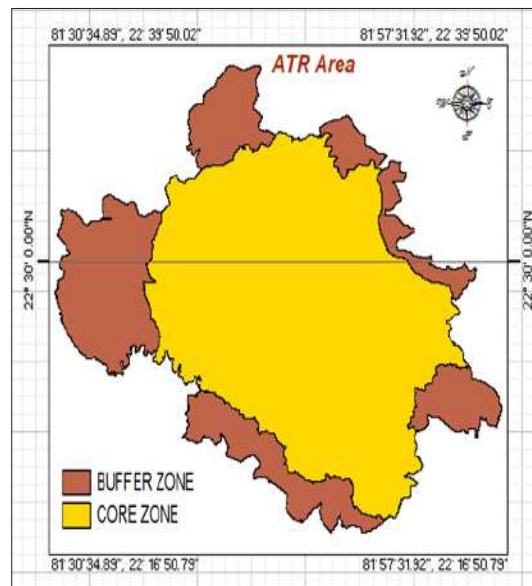


Fig. 1: Map of Achanakmar Tiger Reserve (ATR) illustrating its core and buffer zones.

zone (critical tiger habitat) and 287.822 km² to the buffer zone (Fig. 1, Table 1). It is located in the Mungeli district of Chhattisgarh state.

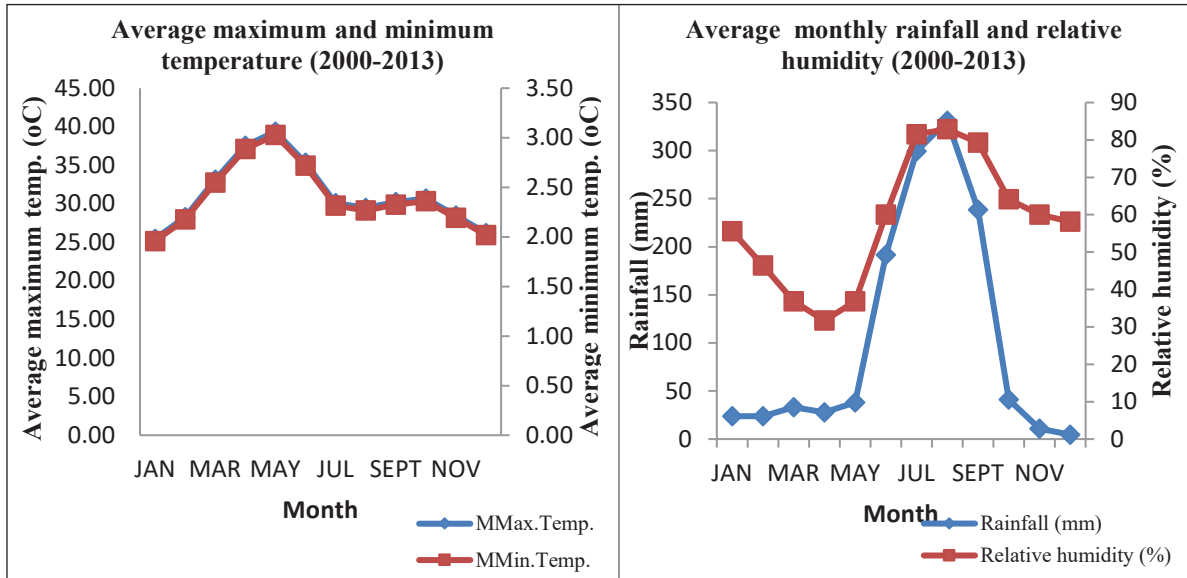
Climate

The study area is characterized by a tropical climate. The average annual precipitation of the study area is more than 1200 mm (Fig. 3), and most of the precipitation falls from July to October. The average annual temperature of the region ranges from 2°C to 46.7°C (Fig. 2). The meteorological data

has been obtained from the Indian Meteorological Division (IMD, Pune) of ATR’s nearest meteorological station, Pendra Road station.

Data Used

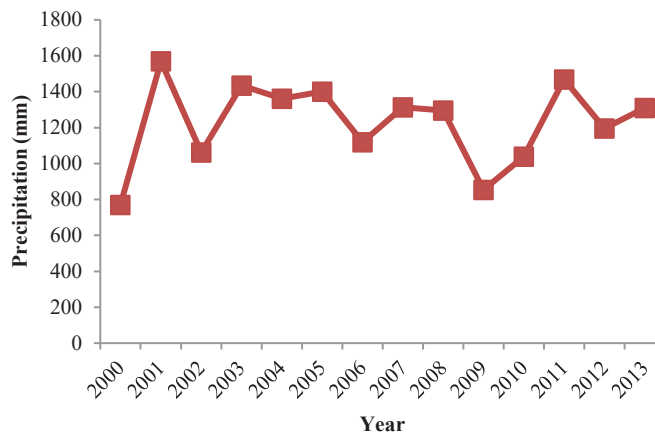
Multitemporal and multispectral satellite data from Indian Remote Sensing (IRS) satellites was used to assess and monitor NDVI for the entire ATR and its buffer zone. For the current study, cloud-free data from pre-monsoon and post-monsoon have been used (Table 2). IRS-1 D LISS-



(Source: IMD, Pune)

Fig. 2: Average maximum and minimum temperature (a) and average monthly rainfall and relative humidity (b) of ATR during 2000-2013.

Average annual precipitation of ATR (2000-2013)



(Source: IMD, Pune)

Fig. 3: Average annual precipitation of ATR during the time frame (2000-2013).

Table 2: Detailed description of satellite data.

Satellite and Sensor	Path/row	Date and year of image acquisition
IRS 1D, LISS 3	102/56	28 th Feb 2000
		10 th Oct 2000
IRS P6, LISS 3	102/56	29 th Feb 2004
		19 th Nov 2004
IRS P6, LISS 3	102/56	3 rd March 2008
		29 th Oct 2008
IRS P6, AWiFS	99/58	6 th Feb 2010
		28 th Oct 2010
IRS P6, LISS 3	102/56	5 th Feb 2013
		14 th Dec 2013

LISS - Linear Imaging and Self Scanning, AWiFS - Advanced Wide Field Sensor

III satellite data from 2000 and IRS-P6 LISS-III satellite data from 2004, 2008, and 2013 covering the Achanakmar Tiger Reserve area have been procured from the National Data Centre, National Remote Sensing Centre (NRSC), Hyderabad. IRS P6 and AWiFS satellite imagery for 2010 was downloaded from the website (<http://bhuvan.nrsc.gov.in/>). The satellite data for the year 2000 was geo-corrected using the ground control points from the 2004 geo-referenced satellite imagery. The entire tiger reserve area and its buffer zones are delineated based on the map provided by the state forest department.

Methodology

The obtained images were registered in the Universal

Transverse Mercator (UTM) map projection with the datum WGS-84. The study area is located in zone 43 (N) of UTM. IGIS software version 1.0 has been used for image processing. Image pre-processing includes layer stacking, mosaicking, and image enhancement. The geo-referenced satellite images were clipped (an image subset) using the Achanakmar Tiger Reserve (ATR) area boundary. The ATR shape file was obtained from the Forest Department, Government of Chhattisgarh. The image transformation tool of IGIS software has been used to extract NDVI information. The pre and post-monsoon satellite images of the years 2000, 2004, 2008, 2010, and 2013 were used for the present study. NDVI analysis and monitoring were performed separately for the entire ATR area and its buffer zone.

RESULTS

The analysis of spatiotemporal NDVI of ATR was performed during pre- and post-monsoon months for ATR and its buffer zone (excluding the core zone), as illustrated in Fig. 4.

NDVI Dynamics of ATR During Pre-Monsoon Months

The data reveals that during 2000, the NDVI value ranged between -0.129 and +0.405 for the entire ATR. NDVI values in the buffer zone decreased slightly (-0.122 and +0.344) during the same time period. The maximum NDVI value for both ATR and its buffer zone was recorded in 2004 at +0.414. In 2008, the recorded NDVI value ranged from -0.022 to +0.281. During 2010, the NDVI value ranged between -0.118 and +0.360 for ATR, whereas its buffer zone recorded a lesser NDVI value of +0.318. In 2013, the maximum

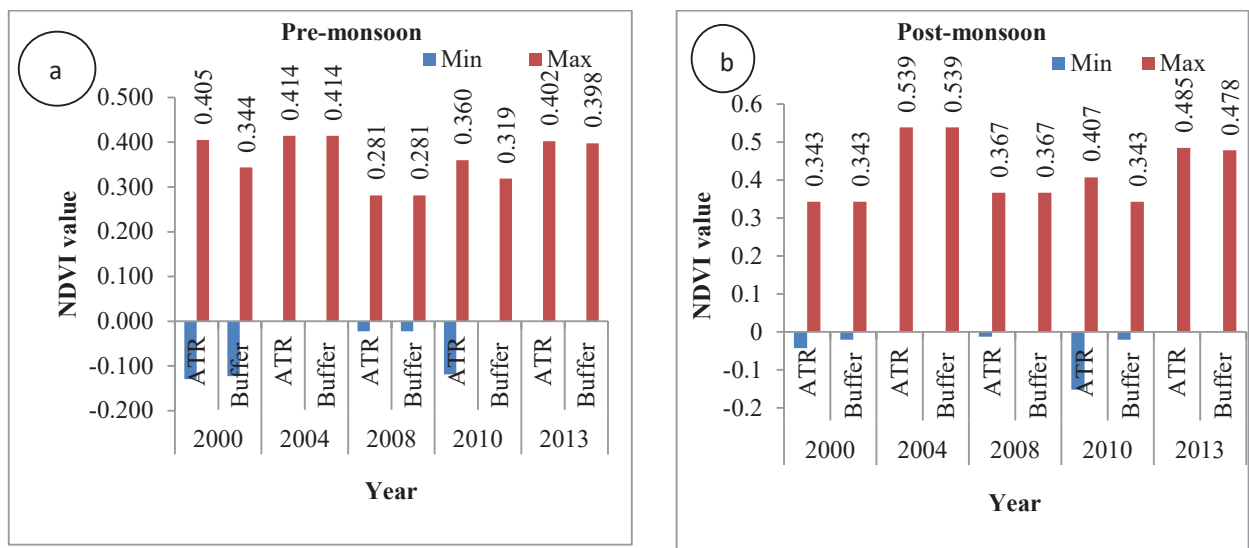


Fig. 4: Spatial patterns and seasonal differentiation of NDVI change for ATR and its buffer zone a) Minimum and maximum NDVI values during pre-monsoon and b) post-monsoon season.

NDVI value recorded was +0.402 for the entire ATR, while the buffer zone recorded a decline in NDVI value of +0.397.

NDVI Dynamics of ATR For the Post-Monsoon Months

The variation of NDVI values of ATR and its buffer zone during post-monsoon months is depicted in Fig. 4. The positive values represent different types of vegetation classes, while near zero and negative values indicate non-vegetation classes, such as water and barren land. The data reveals that in 2000, the NDVI value ranged between -0.042 and +0.343 for the entire ATR. In 2004, the maximum NDVI value for ATR and its buffer zone was +0.539. In 2008, the minimum and maximum values ranged from -0.012 to +0.367. During the same year, the buffer zone recorded a maximum NDVI value of +0.367. For 2010, the NDVI value ranged from -0.152 to +0.407 and -0.020 to +0.343 for ATR and its buffer zone, respectively. The year 2013 recorded a maximum NDVI value of +0.485 for the entire ATR and its buffer zone of +0.478. The higher NDVI values may be due to the development of ground flora, crops in agricultural fields, and a healthier tree canopy (Fig. 5).

Table 3: Mean NDVI values of ATR and its buffer zone (2000, 2004, 2008, 2010 and 2013).

Year	Pre-monsoon		Post-monsoon	
	ATR	Buffer	ATR	Buffer
2000	0.0883	0.0268	0.1205	0.0393
2004	0.1431	0.0451	0.1956	0.0633
2008	0.0656	0.0203	0.1292	0.0419
2010	0.0644	0.0282	0.1233	0.0393
2013	0.1527	0.0484	0.1763	0.0563

Analysis of NDVI Trends

The ATR area recorded the highest mean NDVI value of 0.1956 (standard deviation of 0.2022) in 2004, followed by 2013 (mean NDVI of 0.1763 and standard deviation of 0.1825 during the post-monsoon month for the entire ATR area) (Table 3). The temporal and seasonal variation in NDVI values is due to fluctuations in greenness in the entire tiger reserve area and its buffer zone.

The variation in maximum NDVI values for the entire ATR and its buffer zone was recorded at its highest for the years 2000 (0.0612), 2010 (0.0412), and 2013 (0.0043)

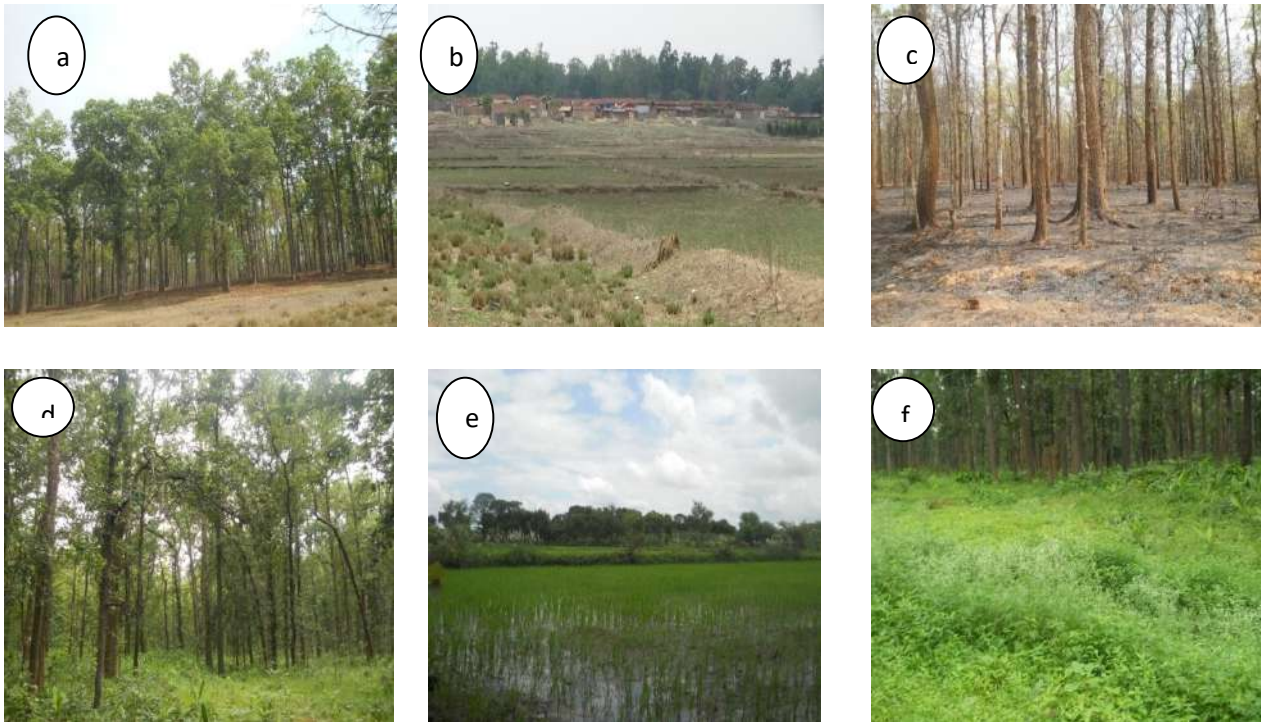


(Photo courtesy: Author)

Fig. 5: Field photographs showing forest and ground flora of ATR, during pre-monsoon (a- Sal forest, b- fallow agricultural land, c- post fire occurrence) and post-monsoon season (d- mix forest with ground regeneration, e- cultivated agricultural fields, f- parthenium weed growth beside the roadside of the core zone).

during the pre-monsoon months. Both the ATR area and its buffer area recorded similar NDVI values. In contrast, variation in NDVI values for ATR and its buffer zone was observed in the post-monsoon months of 2010 (0.0647) and 2013 (0.0065). As a result, the variation in NDVI values of ATR and its core zone was greater during pre-monsoon months than during post-monsoon months.

DISCUSSION

The Achanakmar Tiger Reserve recorded the highest NDVI value during the post-monsoon month of 2004 (+0.539) and the lowest NDVI value (+0.281) in 2008 during pre-monsoon. The higher NDVI coincides with the good rainfall during this period, which is responsible for the formation of a healthy canopy. The maximum variation in NDVI value for the entire ATR and its buffer zone was observed during the post-monsoon season in 2010. This may be due to the growth of ground vegetation and the natural regeneration of forest tree species. Agricultural fields and weed growth, in addition to the fragmented landscape such as roads, etc., also lead to an increasing greening of the area.

Pu et al. (2022) used MODIS NDVI data from 2000 to 2020 for spatiotemporal vegetation monitoring of China Panda National Park. The study stipulated that there is a strong correlation between precipitation and NDVI and that this is the most important controlling factor in vegetation structure, composition, and distribution (Bolstad 1998). The annual temperature and variability of a region also regulate photosynthesis (Liu et al. 2010), influencing the NDVI value.

On the other hand, the pre-monsoon season experiences dry summer months and occasional forest fires, leading to a reduction in vegetation canopy, reducing reflectance, and therefore NDVI values. Thus, water availability and other climatic factors such as temperature and solar radiation affect the NDVI values of the ATR area. NDVI decreased significantly in protected areas of southern California during the summer, according to Gillespie et al. (2018). Weil & Xinfeng (2015) have shown a positive correlation of NDVI with precipitation and average air temperature in the Yarlung Zangbo river basin, Tibet. Similar results were recorded for ATR; the years with relatively good rainfall had higher NDVI values compared to years with prolonged dry summer months and less rain.

Studying the mechanism of climate change response to NDVI changes is of great importance for predicting vegetation dynamics (He et al. 2021). A similar study was carried out by Prasai et al. (2022) to analyze the annual and seasonal variation of the NDVI of Chitwan National Park in Nepal, and a positive trend of the NDVI was observed between 1988 and 2000. Much advance study has been done by Matas et al.

(2022), in which long-term monitoring of NDVI was used to assess the vulnerability of threatened plants in the protected areas of southern Europe.

A similar study has been done by Mallegowda et al. (2015), who analyzed the NDVI of the Biligiri Rangaswamy Temple Tiger Reserve, South India. The studies illustrate the drastic changes in the protected areas' LULC and NDVI between 1973 and 2014, and higher NDVI values were recorded in 1973 compared to 2014. Reddy & Reddy (2013) used the NDVI to measure the vigor of vegetation and assess LULC in the Kaddam watershed of the Godavari river basin, India. The study illustrates the seasonal relationship between NDVI values for all LULC classes in the same year, observing the dynamic behavior of vegetation vigor with respect to the season.

Similar studies were carried out by Biswal et al. (2013), and the study reported that the NDVI class >0.4 of the buffer zone excluding the core zone of Simlipal Biosphere Reserve increased by 20,000 hectares. The result of this study showed that less dense vegetation has undergone deforestation compared to very dense vegetation. The protected areas, which are less affected by human activities, can be used to track the effect of climate change on vegetation and the functioning of natural ecosystems.

CONCLUSION

The current study focuses on the spatiotemporal NDVI trends of ATR and its buffer zone between 2000 and 2013. The year 2004 recorded higher NDVI values during the pre-monsoon season (+0.414) and the post-monsoon season (+0.538) for ATR as well as for its buffer zone. The variation in maximum NDVI values occurs during the post-monsoon months. The declines in NDVI values during pre-monsoon months have also been recorded.

Therefore, water availability and other climatic factors such as temperature and solar radiation affect the NDVI values. While the lowest NDVI peak was recorded during March 2008 for both the ATR area and its buffer zone, the current year and previous years recorded longer periods of higher temperatures and less precipitation.

Long-term monitoring and analysis of ATR's NDVI can help study the impact of climate change and other climatic factors on floral and faunal diversity. There is a need to develop and provide scientifically credible information on the current status and long-term changes in the composition and vegetation of protected areas. The study can also help shape policies and other conservation measures and in addressing issues such as climate change, habitat degradation, and biodiversity loss.

ACKNOWLEDGEMENT

The author is grateful to the University Grand Commission (UGC) for providing a fellowship for this research work. The author also thanks the forest department and the government of Chhattisgarh for providing constant help and support.

REFERENCES

- Biswal, A., Jeyaram, A., Mukherjee, S. and Kumar, U. 2013. Ecological significance of core, buffer and transition boundaries in biosphere reserve: A remote sensing study in Similipal, Odisha, India. *Computational Ecology and Software*, 3(4): 126-137.
- Bolstad, P. V., Swank, W. and Vose, J. 1998. Predicting Southern Appalachian overstory vegetation with digital terrain data. *Landsc. Ecol.*, 13: 271-283.
- Champion, H.G. and Seth, S.K. (ed). 1968. *A Revised Survey of the Forest Types of India*. Government of India Publication. New Delhi.
- Gillespie, T. W., Madson, A., Cusack, C. F. and Xue, Y. 2019. Changes in NDVI and human population in protected areas on the Tibetan Plateau. *Arctic, Antarctic, and Alpine Research*, 51(1): 428-439.
- Gillespie, T. W., Ostermann-Kelm, S., Dong, C., Willis, K. S., Okin, G. S. and MacDonald, G. M. 2018. Monitoring changes of NDVI in protected areas of Southern California. *Ecological Indicators*, 88: 485-494.
- He, P., Xu, L., Liu, Z., Jing, Y. and Zhu, W. 2021. Dynamics of NDVI and its influencing factors in the Chinese Loess Plateau during 2002-2018. *Reg. Sustain.*, 2(1): 36-46.
- Leon-Tavares, J., Roujean, J. L., Smets, B., Wolters, E., Tote, C. and Swinnen, E. 2021. Correlation of directional effects in vegetation NDVI time-series. *Remote Sens.*, 13(6): 1130.
- Liu, Y., Liu, R. and Ge, Q. 2010. Evaluating the vegetation destruction and recovery of Wenchuan earthquake using MODIS data. *Nat. Hazards.*, 54(3): 851-862.
- Mallegowda, P., Rengaiyan, G., Krishnan, J. and Niphadkar, M. 2015. Assessing habitat quality of forest-corridors through NDVI analysis in dry tropical forests of south India: implications for conservation. *Remote Sensing*, 7(2): 1619-1639.
- Mandal, D., Basak, K., Mishra, R. P., Kaul, R. and Mondal, K. 2017. Status of leopard *Panthera pardus* and striped hyena *Hyaena hyaena* and their prey in Achanakmar Tiger Reserve, Central India. *The Journal of Zoology Studies*, 4: 34-41.
- Matas-Granados, L., Pizarro, M., Cayuela, L., Domingo, D., Gomez, D. and Garcia, M. B. 2022. Long-term monitoring of NDVI changes by remote sensing to assess the vulnerability of threatened plants. *Biological Conservation*, 265. 109428. <https://doi.org/10.1016/j.biocon.2021.109428>.
- Morawitz, D.F., Blewett, T.M., Cohen, A. and Alberti, M. 2006. Using NDVI to assess vegetative land cover change in central Puget Sound. *Environ. Monit. and Assess.*, 114(1): 85-106.
- Muhati, G.L., Olago, D. and Olaka, L. 2018. Land use and land cover changes in a sub-humid montane forest in an arid setting: a case study of the Marsabit forest reserve in northern Kenya. *Glob. Ecol. and Conserv.*, 16(e00512). <https://doi.org/10.1016/j.gecco.2018.00512>.
- Myneni, R. B., Hall, F. G., Sellers, P. J. and Marshak, A. L. 1995. The interpretation of spectral vegetation indexes. *IEEE Transactions on Geoscience and Remote Sensing*, 33(2): 481-486.
- Nad, C., Roy, R. and Roy T.B. 2022. Human elephant conflict in changing land-use land cover scenario in and adjoining region of Buxa tiger reserve, India. *Environmental Challenges*, 7: 100384. <https://doi.org/10.1016/j.envc.2021.100384>
- Nagendra, H., Lucas, R., Honrado, J. P., Jongman, R. H., Tarantino, C., Adamo, M. and Mairota, P. 2013. Remote sensing for conservation monitoring: Assessing protected areas, habitat extent, habitat condition, species diversity, and threats. *Ecological Indicators*, 33: 45-59.
- Nemani, R., Hashimoto, H., Votava, P., Melton, F., Wang, W., Michaelis, A. and White, M. 2009. Monitoring and forecasting ecosystem dynamics using the terrestrial observation and prediction system (TOPS). *Remote Sensing of Environment*, 113(7): 1497-1509.
- Prasai, R. 2022. Using google earth engine for the complete pipeline of temporal analysis of NDVI in Chitwan National Park of Nepal. *Research Square*, <https://doi.org/10.21203/rs.3.rs-1633994/v1>
- Pu., M., Zhao, Y., Ni., Z., Huang, Z., Peng, W., Zhou, Y., Liu, J. and Gong 2022. Spatio-temporal evolution and driving forces of NDVI in China's Giant Panda National Park. *International Journal of Environmental Research & Public Health*, 19(11): 6722. <https://doi.org/10.3390/ijerph19116722>.
- Reddy, A. S. and Reddy, M. J. 2013. NDVI based assessment of land use land cover dynamics in a rainfed watershed using remote sensing and GIS. *International Journal of Scientific & Engineering Research*, 4(12): 87-93.
- Rouse, J.W., Jr., R.H. Haas, J.A. Schell and D.W. Deering. 1973. Monitoring vegetation systems in the Great Plains with ERTS (eds.). In: *Proc. Earth Res. Tech. Satellite-1 Symposium*, Goddard. Space Flight Cent., Washington, DC, pp. 309-317.
- Roychoudhary, N. 2013. Project Completion Report of Lead institution for Achanakmar-Amarkantak Biosphere Reserve, Chhattisgarh. Tropical forest Research Institute. Jabalpur: 1-94.
- Roychoudhury, N., Sharma, R. and Mishra, R.K. 2019. Scope and challenges of biodiversity conservation and management in Achanakmar-Amarkantak Biosphere Reserve. *Plants and Environment*, 1(1): 46-54.
- Roychoudhury, N., Sharma, R., Yadav, D. K. and Kushwaha, D. K. 2012. Achanakmar Amarkantak biosphere reserve: A paradise of biodiversity. *Vaniki Sandesh*, 2(4): 27-37.
- Sahu, P. K. 2011. Plants used by Gond and Baiga wome in ethnogynaecological disorders in Achanakmar wild life sanctuary, Bilaspur, C.G. *Int. J. of Pharm. & Life Sci.*, 2(2): 559-561.
- Sandey, H. and Sharma, A. 2016. Study on ethnomedicinal plants of Achanakmar-Amarkantak Tiger Reserve of Chhattisgarh. *Journal of Scientific Letters*, 1(3): 216-222.
- Sellers, P. J. 1985. Canopy reflectance, photosynthesis and transpiration. *International Journal of Remote Sensing*, 6(8): 1335-1372.
- Shukla, A. N. and Singh K. P. 2009. Pteridophytes flora of Achanakmar Amarkantak biosphere Reserve, Central India. *Indian Forester*, 135(2): 271-280.
- Singh, A. and Sharma, A. 2017. Studies on threatened flora in Achanakmar-Amarkantak Biosphere Reserve, Bilaspur (CG). *Journal of Scientific Letters*, 2(2): 71-74.
- Singh, L., Sharma, B., Agrawal, R. and Puri, S. 2005. Diversity and dominance of a tropical moist deciduous forest in Achanakmar Wildlife Sanctuary. *Bulletin of the National Institute of Ecology*, 15: 1-9
- Weil, Z. and Xinfeng, F. 2015. Analysis and Evaluation of principal climatic factors of NDVI in the Yarlung Zangbo River Basin. *Journal of Physics: Conference Series*, 622(1): 012048.



Comparative Study on the Indoor Air Quality in Critical Areas of Hospitals in Malaysia

Kerk Teck Seng, Lee Chia Shen, Ngo Sin Ling, Sim Pei Chin, Tan Jia Xin, Tan Kai En, Adnaan Ahmed Jama, Azian Hariri and Nurul Fitriah Nasir† 

Faculty of Mechanical and Manufacturing Engineering, Universiti Tun Hussein Onn Malaysia, Parit Raja, Batu Pahat, Johor, 86400, Malaysia

†Corresponding author: Nurul Fitriah Nasir; fitriah@uthm.edu.my

Nat. Env. & Poll. Tech.
Website: www.neptjournal.com

Received: 09-06-2022
Revised: 15-10-2022
Accepted: 16-10-2022

Key Words:

Indoor air quality (IAQ)
Air pollutants
Hospitals
DOSH
ASHRAE

ABSTRACT

Indoor Air Quality (IAQ) is the air quality within and around buildings and structures, particularly regarding building occupants' health and comfort. IAQ assessments were performed using an objective measurement of molecular gaseous pollutants to determine the IAQ profile in the hospital's critical areas. It also analyses the effects on patients in different environments and the sources that result in deviations from approved criteria. This comparative study is aimed to investigate the concentration of different compounds in different critical departments in the hospital and propose solutions to the related problem as an improvement in indoor air quality. The data was compared with the standards and regulations. It was found that the TVOC level in the CCU department, specifically in the fluoroscopy room, has exceeded the allowable limit. A few suggestions have been raised to lower the exceeded value. The risks and symptoms held by the occupants in the hospital buildings if they face poor indoor air quality were discussed. Further study can be conducted to relate the short and long-term health issues among medical staff to poor indoor air quality.

INTRODUCTION

The air quality within and around buildings and structures is called indoor air quality (IAQ). The primary form of concern for indoor air quality is most likely an undesired component that affects the comfort of the occupants (Kumar 2010). ASHRAE has released a report on the indoor air quality (IAQ) of Sierra Leone and Liberia's healthcare facilities. Research carried out based on the IAQ of the healthcare facilities is limited. In tropical climate countries, the study found that most people did not experience dissatisfaction with their health conditions. Indoor air quality and heat exposure are significant workplace occupational health and safety concerns. Indoor air contaminants can potentially induce temporary illness, impairment, disease, and, in extreme situations, death.

Formaldehyde (HCHO), carbon dioxide (CO₂), carbon monoxide (CO), and total volatile organic compounds (TVOCs) are the most common contaminants that are assessed for indoor air quality in buildings. There are no regulations for TVOC and microbiological contaminants

among the abovementioned pollutants. Acute low-level carbon monoxide exposure may result in several neuropsychological symptoms. Without additional sources, human CO₂ emissions form a significant component of indoor carbon dioxide pollution, such as burning fuel, gases exposed from transport, and electricity (Asadi et al. 2013). The carbon dioxide exposed to people may cause various health effects, such as headaches, dizziness, and restlessness. Total volatile organic compounds are gases emitted from products or processes. VOCs in the air can irritate the eyes, nose, and throat, cause difficulties in breathing and nausea, and it may harm the central nervous system and other organs.

This comparative study aimed to analyze the sources of problems in the indoor air quality of hospitals in Malaysia. The impacts of poor indoor air quality in the healthcare building will affect the occupant's health as well as the daily activities of the workers there. Thus, the method of measurement of the compounds and the solution to control the concentration level of the compounds are also discussed in this study.

IAQ AUDIT

Indoor air quality (IAQ) in the building would be evaluated

ORCID details of the authors:

Nurul Fitriah Nasir: <https://orcid.org/0000-0003-0467-5593>

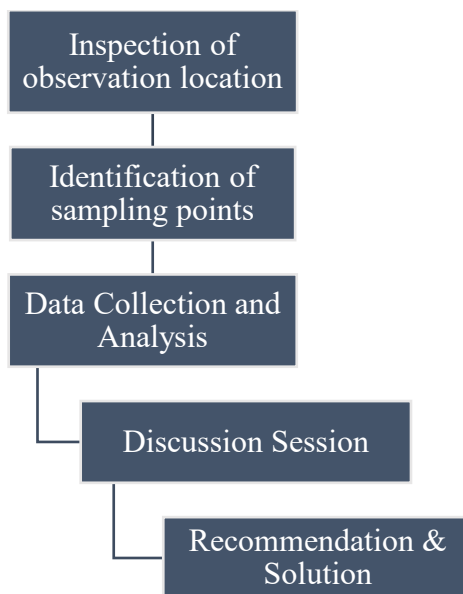


Fig. 1: IAQ audit methodology.

by following the standard of IAQ audit, which involved the physical parameters, concentration of contaminants in the air, and the measurement of biological indicators. Referring to Fig. 1, the IAQ audit methodology is distributed into five stages: the determination of sampling points, inspection of observation location, data collection, data analysis, and giving out the solutions (Sun 2012).

Inspection of Observation Location

The first stage of the IAQ assessment is to investigate the observation location, the critical area in the hospital. At the initial stage, much information should be collected before identifying the sampling points, such as occupants' conditions, feedback, layout and architectural information of the target buildings, locations stored or placed of the potential sources, and the HVAC system in the buildings. At the same time, the possible location where suspected as the possible bad air quality room is investigated. Some potential sampling points which have bad indoor air quality are critical areas like the Intensive Care Unit (ICU), Coronary Care Unit (CCU), and Operating Theatres (OPT) is investigated. The primary information like working area (m^2) and location information (hygiene, air intake location, source of contaminants) of the critical area are recorded to ensure high accuracy of IAQ assessment results.

Identifications of Sampling Points

The sampling points in the critical area of the hospital are determined after an investigation of the location. The sampling points are distributed to the points suspected of bad

air quality by considering the HVAC system of the location and the potential source of material used in that area. Based on the standard developed by the department of occupational safety and health (DOSH), the sampling positions should be measured for at least 8 h. The testing period should occur at four intervals or in different situations. For example, day shift, night shift, high peak situation, and loosened situation. Based on the standard industry code of practice on indoor air quality developed by DOSH, the minimum number of sampling points depends on the area of the building area (Table 1). There are some criteria considered when choosing the sampling points. For example, the sampling points should be located at a primary workstation and should not disturb the daily work activities in the study area. Next, the sampling points should not be set directly in front of the HVAC system and direct sunlight. The sampling points are also not suggested in hallways or passageways. The sampling points should not directly attach to the corner, windows, walls, and other vertical surfaces (minimum 0.5-meter distances). The

Table 1: Minimum Number of Sampling Points.

Total Floor Area (served by MVAC) [m^2]	Minimum Number of Sampling
< 3,000	1 per 500 m^2
3,000 - < 5,000	8
5,000 - < 10,000	12
10,000 - < 15,000	15
15,000 - < 20,000	15
20,000 - < 30,000	21
$\geq 30,000$	1 per 1,200 m^2

Table 2: Results of measurement for critical areas in Malaysia's hospitals.

Sampling Location Information			Chemical Gaseous Pollutants				
Department	Room	Sampling Location	TVOC [ppm]	CO [ppm]	CO ₂ [ppm]	HCOH [ppm]	
Threshold Limit			3	0.2	1000	0.1	
CCU	Cubicle 5	A1	0.2	0.0	422	0.00	
	Isolation Room 1	A2	0.5	0.0	490	0.09	
	Fluoroscopy	A3	9.3	0.2	389	0.05	
ICU	Isolation Room 1	B1	1.2	0.0	361	0.00	
	Isolation Room 2	B2	2.8	0.0	350	0.08	
	In front of Bay 5	B3	0.1	0.0	304	0.00	
Operating Theatre	Pre-Op Holding 2	C1	0.8	0.0	472	0.00	
	Post-Anaesthesia Recovery 3	C2	0.0	0.0	385	0.00	
	In front of Anaes. Work Room	C3	1.3	0.0	498	0.00	
	To OT's Corridor	C4	1.8	0.0	472	0.00	
	Operating Room 1 (General)		C5	0.0	0.0	418	0.00
			C6	0.0	0.0	390	0.00
	Operating Room 2 (General)		C7	0.1	0.0	413	0.00
			C8	0.0	0.0	338	0.00
	Operating Room 3 (Neurology)		C9	0.0	0.0	444	0.00
			C10	0.0	0.0	471	0.00
	Operating Room 4 (General)		C11	0.5	0.0	399	0.00
			C12	0.2	0.0	422	0.00
	Operating Room 5 (Cardiac)		C13	0.0	0.0	442	0.00
			C14	0.0	0.0	414	0.00
	Operating Room 6 (Orthopaedic)		C15	0.0	0.0	364	0.00
			C16	0.1	0.0	371	0.00

sampling positions should not prevent the staff from leaving the study area. Lastly, the inlet of samplers should be placed between 75 and 120 cm, preferably 110 cm from the floor.

Data Collection and Analysis (Chemical Indicator)

Different types of indicators are used to obtain the concentration of different compounds. The chemical indicators measure the concentration of carbon dioxide, carbon monoxide, formaldehyde, and total volatile organic compounds (TVOC). After that, the concentration of the chemical compounds is compared with the standards of the American Society of Heating, Refrigerating and Air-Conditioning Engineers (ASHRAE) and DOSH. The solution is proposed when certain chemical compounds' concentration exceeds the threshold limit listed in the standard. The measurement tools used for the related chemical compounds and the hospital's potential sources are ANLOR Compu Flow IAQ Meters Model CF930, PPM Formal Demeter htv and the-M, and Mini RAE 2000 Portable VOC Monitor (model PGM 7600).

IAQ DATA FOR CRITICAL AREAS IN THE HOSPITAL

In this study, the results for measuring the chemical gaseous pollutants are illustrated and thus compared with the threshold limit, which refers to the standard DOSH (2005), ASHRAE (2019), and Guidelines for Good Indoor Air Quality in Office Premises Singapore, ENV (1996). Then, the action to reduce the chemical pollutants is discussed. The measurements for critical areas are illustrated in Table 2, while the threshold limit of each chemical gaseous pollutant is summarized as well.

Once the source of VOC is found indoors, the VOC level could be increased significantly to ten times higher than the outdoor VOC level and can result in chronic diseases. The TVOC level should not be exceeded 3ppm, which refers to DOSH and ENV. All the sampling locations are within the threshold limit except in CCU, A3, and the Fluoroscopy room, which contains an exceeded value of 9.3 ppm. VOC can be found in several sources, including paints, furniture,

cleaning agents, fire suppression coatings, and other solvents. Since there is a close space without any air-conditioning system, it has caused poor ventilation conditions while there is not contain any office equipment. Fresh air is encouraged to introduce to improve ventilation, and the TVOC level could be reduced. After completing the renovation work and design development, the measurement was conducted repeatedly since the fresh air was recirculated, and 0.8 ppm was achieved, which is not exceeded the threshold limit.

According to ASHRAE, a substantial amount of carbon monoxide can cause symptoms like nausea and unconsciousness or, in extreme circumstances, even fatal. The standard has a threshold limit of 10 ppm. The carbon monoxide level in the critical area is within the threshold limit, ranging from 0 to 0.2 ppm. The possible source of 0.2 ppm of carbon monoxide probably comes from the operating medical instrument in the fluoroscopy room in CCU.

The respiration of occupants in critical areas is the possible primary source of carbon dioxide. By referring to the ASHRAE Standard and Malaysian Code of Practice on Indoor Air Quality, the threshold limit of carbon dioxide is 1000 ppm, while the carbon dioxide level measured in the critical area in the hospital is within the range of 304 to 498 ppm, which is not exceeded the threshold limit of the standard mentioned above. Therefore, there is no need to renovate to improve indoor air quality based on carbon dioxide levels in this critical area. According to the ASHRAE Standard, formaldehyde is a colorless, pungent gas that serves as a preservative in healthcare facilities, such as mortuaries and medical laboratories. Some possible sources of formaldehyde are paper product coating, fiberboards, glue, and others. Individuals exposed to formaldehyde should not exceed the limit of 0.1 ppm for 8 h ENV (1996). The measured formaldehyde level for all sampling locations in the hospital's critical area is 0 to 0.09 ppm.

POTENTIAL SOURCES FOR DIFFERENT KINDS OF COMPOUNDS

Total Volatile Organic Compounds

TVOC was adopted to measure the overall VOCs in a given hospital space. By referring to Table 2, all the locations are within the threshold limit by ASHRAE Standard except for one location, the fluoroscopy room. VOCs' concentration levels, such as aromatic and halogenated hydrocarbons, ketones, aldehydes, and limonene, were widely variable between hospitals due to building age and product type used according to health activities conducted in each department. High temporal variability was observed in concentrations of alcohol, probably due to the intensive use of alcohol-based

hand rubs in all hospital places. In addition, some specificity of hospital activities, such as the healthcare of patients and staff, may be exposed to a wide range of VOCs emitted from the products of disinfectants and sterilants (Bessonneau et al. 2013). Most studies have assessed that hospital activities and healthcare workers are only exposed to a few compounds, such as anesthetic gases, primarily found in operating rooms, glutaraldehyde, and ethylene oxide, usually found in disinfection units. In other sites, such as operating rooms investigated in other studies, indoor air was contaminated mainly by anesthetic gases, aldehydes, oxides, and alcohols (Glumbakaité et al. 2003). The highest VOC concentrations were observed in rooms with natural ventilation, while the HVAC system will significantly decrease the VOC concentration levels (Sidheswaran et al. 2013).

Carbon Monoxide

From the data obtained, the carbon monoxide concentration in the hospital is very close to zero and only showed an insignificant value in the Fluoroscopy department. Therefore, the emission of carbon dioxide exposure in the indoor environment of the hospital is minimal. Carbon monoxide is produced from the incomplete combustion of hydrocarbons containing fuels such as wood, gasoline, coal, natural gas, and oil. The fluoroscopy department may release very little carbon monoxide during x-ray radiation. In addition, other sources of carbon monoxide in the hospitals are from the vehicles' exhausts, including cars, motors, and ambulances outdoors in hospitals. The department near the drop-off or parking area is exposed to vehicle carbon monoxide emissions. Various fuel-burning appliances will produce certain concentration levels of carbon monoxide. However, these appliances should handle or use in an open area to avoid excess inhaling of carbon monoxide.

Carbon Dioxide

All humans, animals, plants, fungi, and microorganisms can produce carbon dioxide gas. From Table 2, the CO₂ concentration of hospitals is within the standard or guideline established by ASHRAE or DOSH. Many factors, such as human behavior, patient and staff density, and the performance of ventilation systems, influence the indoor concentration of carbon monoxide in hospitals. The occupant density in hospitals is the primary source of carbon dioxide because, through respiration or breathing, the human body uses inhaled oxygen and produces carbon dioxide. The air that humans exhale has a much higher carbon dioxide concentration than the surrounding air. During human exhalations, the carbon dioxide will mix with the air in a closed room, and the overall carbon dioxide concentration

will rise. Therefore, carbon dioxide concentration will increase in a small room with multiple occupants for a long time. This situation will occur in the isolation room for patients, which is enclosed. In addition, improper heating, ventilation, and air conditioning system (HVAC) can cause a rise in the concentration of carbon dioxide levels. The air-conditioning, which is not functioning, will elevate the level of carbon dioxide in the hospital. Smoking also can release smoke and chemicals into the air as smoking involves a complete combustion reaction. This will also produce a small amount of carbon dioxide. However, in a small, closed space, smoking can reduce the oxygen concentration level of the air around. Alongside this process, releasing carbon dioxide will further change the air's composition and make occupant challenging to breathe.

Formaldehyde

The formaldehyde concentration is relatively low in the hospital. Some potential sources cause the emission of formaldehyde. Air cleaning is broadly applied to reduce contaminant concentrations in many buildings. The HVAC systems usually have filters to remove airborne particles from incoming outdoor air and recirculated indoor air. A study showed that some filters release specific amounts of formaldehyde by increasing the humidity. In addition, formaldehyde-based product such as personal care and consumer items is commonly used by people. The products usually contain formaldehyde emission elements. They act like a preservative to kill bacteria or microorganisms and prevent the growth of viruses or pathogens, extending the product storage life. This kind of product is commonly used in hospitals for cleaning purposes.

Furthermore, the surface coatings such as latex paint will contain low formaldehyde emissions. Many studies have been conducted previously, showing that cigarette smoking significantly contributes to the high formaldehyde concentrations indoors. Although the hospital area is prohibited smoking, some smokers may have their cigarettes in the staircase area.

TYPICAL SYMPTOMS AND RISKS OF EXPOSURE

Total Volatile Organic Compounds

Total volatile organic compounds are the primary sources that cause poor indoor air quality and harm human health. Some key symptoms are linked with total volatile organic compounds exposure, for instance, nose and throat discomfort, headache, dizziness, tiredness, vomiting, allergic skin reaction, shortness of breath, and also impact

on the nasal cavity. The early signs or immediate symptoms of people after exposure to volatile organic compounds are irritation of the eyes and nose, dizziness, headache, amnesia, and blurred vision (Rumchev et al. 2007, Alford & Kumar 2021). Long-term exposure to volatile organic compounds or exposure to a high concentration and large quantity of total volatile organic compounds can trigger adverse health concerns such as irritation of the eyes, nose, and throat, dull headaches, or nausea, as well as permanent damage to the body organ including liver, kidney, lungs, and central nervous system in extreme cases. Furthermore, some volatile organic compounds are suspected of leading to cancer. Volatile Organic compounds exposure could be very harmful to young children, older adults, people with respiratory problems, and people hypersensitive to the chemical compounds.

Carbon Monoxide

A large amount of carbon monoxide is hazardous to the human body as the inhaled carbon monoxide would displace oxygen in the body cells and result in a shortage of oxygen in the body organ, including the heart, lungs, brain, and other crucial body organs. Exposure to a high concentration of carbon monoxide or continued exposure to carbon monoxide can lead to permanent brain and heart damage and even death. Common signs of carbon monoxide poisoning include dizziness, blurred vision, confusion, dull headache, muscle weakness, breathing difficulty, confusion, vomiting, and heart irregularity (Harper & Croft-Baker 2004). Carbon monoxide poisoning could be very harmful to unborn babies, children, older adults, and people with coronary heart disease. Properly controlling the amount and concentration of carbon monoxide is crucial to preserve high indoor air quality in the hospital, as many patients and staff have different age levels and health conditions. For pregnant patients or staff, carbon monoxide exposure might cause miscarriage, premature birth, congenital disability, fetal brain damage, and fetal death, as fetal hemoglobin is more likely to absorb carbon monoxide than adult hemoglobin.

Moreover, children usually take more breaths per minute than adults. They tend to inhale more carbon monoxide in the air, which causes them as one of the high-risk groups for carbon monoxide toxicity. Lastly, exposure to carbon monoxide may increase the risk of developing brain damage in the elderly, who are more prone to become ill in those with health concerns, such as respiratory problems and memory impairment.

Carbon Dioxide

Carbon dioxide does not show any toxic effect at lower

dosages. At the same time, it may cause a rapid respiratory rate, irregular heart rate, drowsiness, dizziness, and impaired consciousness as the concentration of carbon dioxides increases. In severe cases, exposure to an extremely high concentration of carbon dioxide may lead to convulsions, coma, permanent brain and organ damage, and even death (Langford 2005, Bierwirth 2017). Maintaining a low and minimum amount of indoor air in the hospital is crucial for the psychomotor performance of staff, especially nurses and doctors in critical areas such as CCU, ICU, and operating theatre. This is because a high level of carbon dioxide above 1000 ppm has significant adverse influences on people's cognitive performance, such as decision-making, problem-solving, and speed of individual movement (Azuma et al. 2018). In addition, carbon dioxide poisoning would lead to confusion or unusual thinking, panic attack, and the ability of the individual to communicate effectively with others. The medical team in the hospital needs to deliver effective patient care and perform well in their task to avoid misdiagnosis and wrong judgments, which might result in negative patient outcomes.

Formaldehyde

High levels of formaldehyde significantly affect human health, commonly correlated to eye, nose, and throat complaints and fatigue (Asare-Donkor et al. 2020). Negative health effects from exposure to formaldehyde may happen from inhalation or direct contact with formaldehyde, such as eyes, mouth, and skin. The main hazardous effects of acute formaldehyde inhalation are irritation of the eyes, nose, throat, and lungs and the adverse impact on the nasal cavity. Coughing, sneezing, muscle aches, and bronchitis are other side effects of formaldehyde exposure in the human body. These health effects could have occurred in people of different ages and health conditions. However, these health effects are more common in young children, the elderly, and people with breathing problems. The low level of formaldehyde exposure could result in an itchy and burning sensation in the eyes, nose, and skin, sore throat, and respiratory problems (Zain et al. 2019).

Nevertheless, hypersensitive people might have a severe allergic reaction when exposed to a low dose of formaldehyde. People exposed to chronic formaldehyde are more liable to become hypersensitive to formaldehyde and have a high risk of developing cancer. Statistics show an increase in cases of female workers handling formaldehyde resins for long periods having menstrual disorders. However, no evidence suggests any correlation between formaldehyde and miscarriage and a congenital disability.

CONCLUSION

This study aims to investigate the concentration of different compounds in the different critical departments in the hospital. The study was conducted before and after the renovation. From the comparison made at all sampling locations in the critical area of the hospital, the data was under the threshold limit after completing the renovation to reduce the chemical gaseous pollutants. Indoor air quality is vital to improving indoor air pollution. Indoor air pollution contributes to various respiratory and cardiovascular health effects, from simple symptoms to severe illnesses. Due to its high-level chemical contaminant, formaldehyde is not feasible to remove or isolate. Therefore, the building must be clean and sterile well based on the guideline in Malaysia so that the contaminant can be reduced. The source of formaldehyde could be sealed well or enclosed to reduce the emission of formaldehyde. Moreover, outdoor air is crucial to promote good air quality through natural ventilation, such as opening windows and doors. Future research can be conducted to investigate the short and long-term health risks of medical staff and their relation with IAQ.

ACKNOWLEDGEMENT

Communication of this research is made possible through monetary assistance from Universiti Tun Hussein Onn Malaysia and the UTHM Publisher's Office via Publication Fund E15216.

REFERENCES

- Alford, K.L. and Kumar, N. 2021. Pulmonary health effects of indoor volatile organic compounds-a meta-analysis. *Int. J. Environ. Res. Pub. Health*, 18(4): 65-73.
- Asadi, E., da Silva, M.C. and Costa, J.J. 2013. A systematic indoor air quality audit approach for public buildings. *Environ. Monit. Assess.*, 185(1): 865-875.
- Asare-Donkor, N.K., Kusi, J., Appiah, V., Torve, R.B. Voegborlo, M. and Adimado, A.A. 2020. Formaldehyde exposure and its potential health risk in some beauty salons in Kumasi Metropolis. *J. Toxicol.*, 88: 75167.
- ASHRAE 2019. Ventilation for Acceptable Indoor Air Quality. ANSI/ASHRAE Standard 62.1.
- Azuma, K., Kagi, N., Yanagi, U. and Osawa, H. 2018. Effects of low-level inhalation exposure to carbon dioxide in indoor environments: A short review on human health and psychomotor performance. *Environ. Int.*, 121: 51-56.
- Bessonneau, V., Mosqueron, L., Berrubé, A., Mukensturm, G., Buffet-Bataillon, S., Gangneux, J.P. and Thomas, O. 2013. VOC contamination in hospitals, from a stationary sampling of a large panel of compounds, in view of healthcare workers and patients exposure assessment. *PLoS One* 8(2): e55535.
- Bierwirth, P.N. 2017. Carbon Dioxide Toxicity and Climate Change: A Major Unapprehended Risk for Human Health. Doctoral Thesis. Australian University, Sydney, pp. 1-25.
- DOSH. 2005. Code of Practice on Indoor Air Quality. Malaysia, Department of Occupational Safety and Health, Ministry of Human Resources, Malaysia.

- ENV. 1996. Singapore Guidelines for Good Indoor Air Quality In Office Premises. Singapore, Institute of Environmental Epidemiology, Ministry of the Environment, Singapore.
- Glumbakaitė, E., Žymantienė, Z., Šeškauskas, V., Smolianskienė, G. and Jurkuvėnas, V. 2003. Quality of the air and health assessment of the medical staff handling disinfection chemicals in Lithuanian hospitals. *Indoor Built Environ.*, 12(1-2): 105-111.
- Harper, A. and Croft-Baker, J. 2004. Carbon monoxide poisoning: Undetected by both patients and their doctors. *Age Ageing*, 33(2): 105-109.
- Kumar, A. 2010. *Air Quality*. IntechOpen, London.
- Langford, N.J. 2005. Carbon dioxide poisoning. *Toxicol. Rev.*, 24(4): 229-235.
- Rumchev, K., Brown, H. and Spickett, J. 2007. Volatile organic compounds: Do they present a risk to our health? *Rev. Environ. Health*, 22(1): 39-55.
- Sidheswaran, M., Chen, W., Chang, A., Miller, R., Cohn, S., Sullivan, D., Fisk, W.J., Kumagai, K. and Destailats, H. 2013. Formaldehyde emissions from ventilation filters under different relative humidity conditions. *Environ. Sci. Technol.*, 47(10): 5336-5343.
- Sun, P.K. 2012. Case Study of Indoor Air Quality of Health Care Facilities and Hospitals in Malaysia. Master's Degree, University of Malaya.
- Zain, S.M., Azmi, Y., Veloo, M. and Shaharudin, R. 2019. Formaldehyde exposure, health symptoms, and risk assessment among hospital workers in Malaysia. *J. Environ. Prot.*, 10: 861-879.



Visitors Perceptions of the Climate Comfort at the Padang Coastal Tourism Area, Indonesia

N. Y. Sudiar*^(***)†  and M. I. Gautama**^(***) 

*Physics Department, Universitas Negeri, Padang, West Sumatra, Indonesia

**Sociology Department, Universitas Negeri, Padang, West Sumatra, Indonesia

***Research Center for Climate Change, Universitas Negeri, Padang, West Sumatra, Indonesia

†Corresponding author: N. Y. Sudiar; nysudiar@fmipa.unp.ac.id

Nat. Env. & Poll. Tech.
Website: www.neptjournal.com

Received: 28-08-2022

Revised: 18-10-2022

Accepted: 28-10-2022

Key Words:

Visitors perceptions
Climate comfort
Coastal tourism

ABSTRACT

This study explains visitors' perceptions of climate comfort in the Padang coastal tourism area, including Air Manis Beach, Padang Beach, Nirwana Beach, and Pasir Jambak Beach. Climate comfort index calculation using the Holiday Climate Index (HCI) and survey methods are used to take data. The survey is conducted to collect data on climate comfort perception and the role of weather on that comfort. There are 409 respondents in this study. Most visitors state that weather affects climate comfort during their trip (99%) and need weather information for outdoor tourism (98.5%). However, only 27.1% are looking for weather information before traveling outdoors. This coastal tourism area's perceived level of climate comfort is comfortable (64%). The thermal sensation is neutral (66%). Meanwhile, the average score of the comfort index in Padang is neutral throughout the year. The temperature interval indicates the comfortable category is between 26°C-28°C.

INTRODUCTION

As a strategic industry, the tourism sector must be managed professionally by considering various factors such as climate. Climate suitability has an impact on tourism destinations (Olya & Alipour 2015). The tourism industry is very sensitive to weather and climate (Li et al. 2016, Roshan et al. 2016) because these factors determine where tourists travel. Weather and climate are critical external factors influencing tourists' decision to visit an area (Priego et al. 2015, Ruty & Scott 2016). Therefore, climatic and weather conditions are important for tourism activities.

Moreover, some methods can be used to express comfort level, such as Tourism Climate Index (TCI), first introduced by Mieczkowski (1985). This method uses 5 weather parameters; air temperature, humidity, rainfall, sunshine, and wind speed (Ramazanipour & Behzadmoghaddam 2013). However, TCI has some weaknesses. It does not include the effects of longwave and shortwave radiation flux (Freitas & Scott 2007), subjective assessment, weighting system for climate variables, and low data resolution using monthly data (Scott et al. 2016). Thus, to cover the shortfall in TCI,

Holiday Climate Index (HCI) method is introduced. The advantage of HCI compared to TCI lies in the rating scale of each climate component and the weight of each parameter (Scott et al. 2016).

Further, studies related to climate comfort for tourism areas in Indonesia are still very rare. Haryadi et al. (2019) used TCI to calculate the climate comfort index in Samosir Regency, North Sumatra. While Noor et al. (2018) used HCI to identify tourist comfort in the Banjarmasin area, South Kalimantan. Furthermore, Sudiar et al. (2019a) combined the two methods to determine the level of climate comfort in Ancol Eco-Park, Bogor Botanical Gardens, and Cibodas Botanical Gardens; in addition, using a special HCI method in tropical areas for the thermal aspect is underrated. According to the suggestion from our previous study, the use of the HCI method needs to be modified on the thermal aspect (Sudiar et al. 2019b). This study modified the thermal aspect rating to the highest scale (10 out of 10). The effective temperature was 25°C-28°C (Sudiar 2020), and the highest thermal rating for the HCI method was 23°C-25°C (Scott et al. 2016). For this reason, this study used the HCI method by modifying the thermal aspect so that a climate comfort level is suitable for tropical skin.

Furthermore, the determination of the comfort index based on climate variables was initiated by Mieczkowski

ORCID details of the authors:

N. Y. Sudiar: <https://orcid.org/0000-0003-3921-4586>

M. I. Gautama: <https://orcid.org/0009-0003-1529-5526>

(1985), known as the Tourism Climate Index (TCI), and it changed into the Holiday Climate Index (HCI) (Scott et al. 2016). HCI and TCI were consistently higher in Barcelona, Istanbul, Rome, London, Paris, and Stockholm (Scott et al. 2016). The results of using TCI in Northern Cyprus showed that precipitation harmed tourist comfort (Olya & Alipour 2015). The results of TCI use in North America showed that TCI could be widely used for determining the comfort of the tourism climate. However, the monthly period used needs to be replaced with a period more closely resembling the length of the general holiday period, such as 7-10 days (Scott & McBoyle 2001). On the other hand, TCI in Australia was used as a tool for optimal vacation spot identification and not as a predictor of travel (Amelung & Nicholls 2014).

However, studies on using TCI and HCI for tourism climate comfort are rarely done in Indonesia. Of the few studies, some of the studies are in Citeko West Java, Jatim Park 2, Karangates, Samosir North Sumatra, Banjarmasin South Kalimantan, and our previous research in three natural tourism areas Eco-Park Ancol, Bogor Botanical Gardens, and Cibodas Botanical Gardens. The TCI score in Citeko, West Java, showed that the tourist area is more comfortable in the dry season than in the rainy season (Iftah 2015). The TCI and HCI score in Jatim Park 2 and Karangates showed that HCI is better to use than TCI in tropical areas with relatively high rainfall and temperature (Kurnia 2016). The right time to visit Samosir based on TCI is February (Haryadi et al. 2019). This result is in contrast to that in Citeko, where the comfortable time is the dry season (June-July-August), while the best time to visit Samosir is in the rainy season (February). The HCI score in Banjarmasin is the dry season (Noor et al. 2018). The results of research at Eco-Park Ancol, Bogor Botanical Gardens, and Cibodas Botanical Gardens showed that HCI is more sensitive to use in tropical areas than TCI (Sudiar 2020). Furthermore, HCI needs to be modified in terms of thermal aspects because temperature variations in Indonesia throughout the year are very small (Sudiar et al. 2019a).

MATERIALS AND METHODS

The study area of this research was located in the coastal area of Padang City, West Sumatra, Indonesia, such as Air Manis Beach, Padang Beach, Nirwana Beach, and Pasir Jambak Beach. These areas were chosen because the four areas were always crowded with tourists. The method used was climate comfort index calculation using HCI and surveys. The survey conducted at tourist sites aimed to avoid bias because the observation stations for measuring weather parameters were not located at tourist sites.

The data calculation was taken from two Meteorology, Climatology, and Geophysics Agency (BMKG) observation

Table 1: Component of Holiday Climate Index (HCI).

Aspect	Climate Variable	Index Weighting [%]	
		Urban	Beach
Thermal	Maximum temperature [°C]	40	30
	Mean Relative humidity [%]		
Aesthetic	Cloud Cover [%]	20	35
Physics	Daily rainfall (mm)	30	25
	Wind Velocity (km/hour)	10	10

stations, the Minangkabau International Airport (BIM) and the Maritime Meteorology, Teluk Bayur. The climate data used was air temperature, humidity, rainfall, sunshine, and wind speed during 10 years (2011-2020). The data used for the survey was direct measurements of air temperature, humidity, and wind speed at tourist sites using an anemometer with the type of Lutron model ABH-4224 which complied with ISO 9001 standard.

The HCI weighting was designed based on the survey results, and the largest score did not emphasize temperature (Table 1).

The HCI score was then calculated based on the climate variables score used with the following equation:

$$\text{HCI urban} = (\text{TC} \times 4) + (\text{A} \times 2) + [(\text{P} \times 3) + (\text{W} \times 1)] \quad \dots(1)$$

$$\text{HCI beach} = (\text{TC} \times 3) + (\text{A} \times 3.5) + [(\text{P} \times 2.5) + (\text{W} \times 1)] \quad \dots(2)$$

TC is thermal comfort with the weather parameters temperature and humidity. A is aesthetic with cloud cover weather parameters, and P is physical weather parameters with rainfall (P) and wind speed (W). Since the objects of research were coastal areas, equation (2) was used to calculate the climate comfort index.

Then, interviews with 409 respondents were conducted to measure weather parameters. The survey was conducted from August-September 2021 using simple random sampling. The number of visitors at Air Manis Beach, Padang Beach, Nirwana Beach, and Pasir Jambak Beach was considered to be more than 100 thousand people per month (Maswar 2017), so the Slovin formula was used to determine the sample size as follows:

$$n = N / (1 + Ne^2) \quad \dots(3)$$

n was the minimum sample size, N was the population size, and e was the margin of error. Based on equation (3), the minimum sample for an error of 5% was 385 people.

Next, convert the temperature measurement to the effective temperature using the following equation (Blazejczyk et al. 2012):

$$\text{ET} = 37 - \frac{37 - T}{0,68 - 0,0014 \cdot RH + \frac{1}{1,76 + 1,4 \cdot v^{0,75}}} - 0,29 \cdot T \cdot (1 - 0,01 \cdot RH) \quad \dots(4)$$

ET was the effective temperature, T was the measurement temperature, RH was the relative humidity, and v was the wind velocity.

The resulting comfort level gained from calculating historical data was verified through survey results. The data transformation method was used from ordinal to interval, Method of Successive Intervals (MSI). MSI is the process of converting ordinal data (very uncomfortable, uncomfortable, neutral, comfortable, and very comfortable) into interval data (Ningsih et al. 2019). Since the statistical process required quantitative data, qualitative data (ordinal data) must be changed into quantitative (interval).

RESULTS AND DISCUSSION

Visitor Profile

In this study, the sample of visitors was slightly more dominated by men (50.6%) than women (49.4%). Most of the visitors were late teens (17-25 years) and early adults (26-35 years) (Al Amin & Dwi 2017), with 50.4% and 31.5%, respectively. The visitors with high school education or equivalent were dominant (58.4%) and undergraduate education (29.8%). Most visitors to this beach tourism area were local tourists who lived in Padang (62.8%) (Fig. 1). 409 visitors were willing to be interviewed, most of whom were young. It means that young people were more concerned about climate comfort than older people.

Visitor Perceptions of Comfort

Through closed questions, the respondents were asked several things about tourist comfort at tourist sites related

to weather parameters such as air temperature, humidity, wind speed, and sunlight. The first question was whether the clothes worn when visiting tourist sites were decided after taking into account the weather factor. Most visitors answered that they only considered the air temperature (58.9%) and sunshine (60.6%). There were 34% who did not consider the weather factor at all. In fact, as a form of body adaptation to temperature, choosing clothes that suit the environment was important. By choosing suitable clothes, visitors would still feel comfortable at the tourist location. Furthermore, they were asked while visiting tourist sites did they consider the weather factor. Most visitors answered that they only considered the air temperature (65.3%) and wind (66.7%). Meanwhile, 26.4% said they did not consider the weather factor.

The next question was whether the weather was an important factor they consider when doing outdoor tours. The majority (98.8%) answered "Yes." The next question was whether the weather affected comfort. The majority (99%) answered "Yes." Furthermore, they were asked whether every outdoor tourism location needed to add climate comfort information. The majority (98.5%) answered Yes. Surprisingly, when they were asked whether they first look for weather information before visiting tourist sites or not, a total of 72.9% answered, "No" (Fig. 2). Based on the answers given by the visitors, it can be concluded that weather parameters were an important factor in terms of travel comfort, especially outdoor tourism. But unfortunately, the majority of them still did not take advantage of weather information in making decisions to travel. One of the reasons was that the tourist area did not prioritize weather information, which resulted in a high volume of tourists.

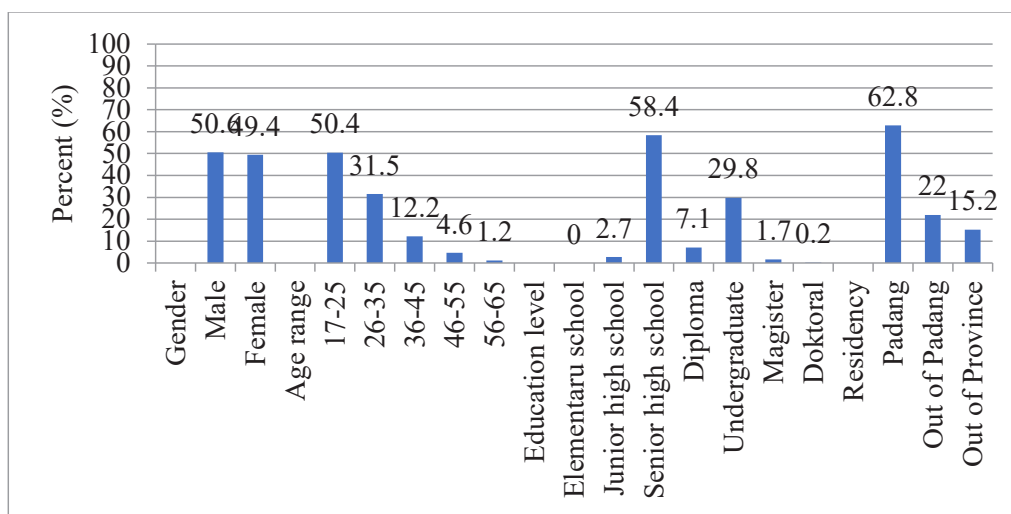


Fig. 1: Profile of visitors in the coastal tourism area of Padang.

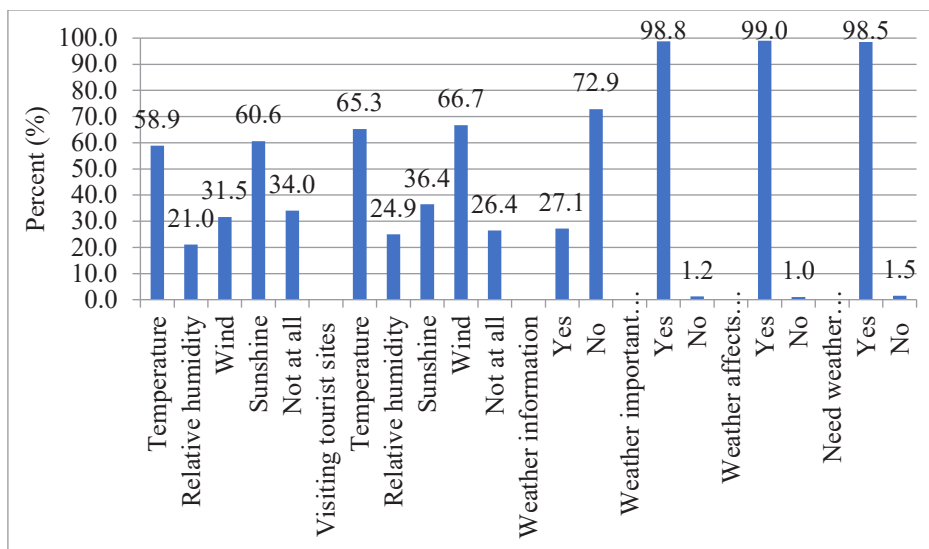


Fig. 2: Visitors' perceptions of tourist comfort based on climate parameters.

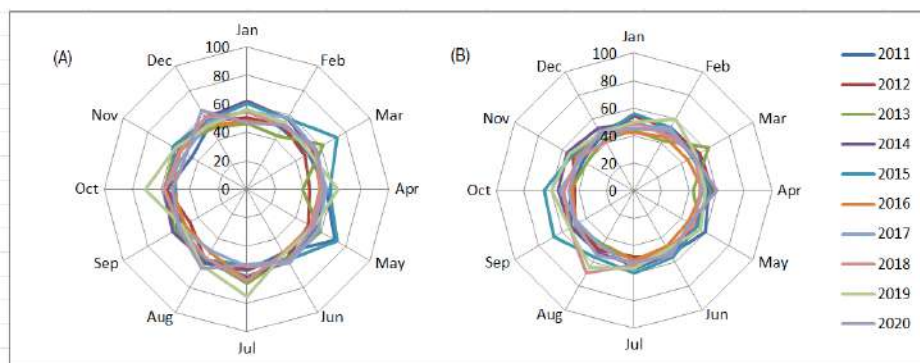


Fig. 3: Climate comfort score for 10 years (A) BIM Station and (B) Teluk Bayur Station.

Climate Comfort Score

The climate comfort score was calculated using equation (2). The optimal effective temperature (comfortable) in the thermal aspect of the HCI method was 23°C-25°C (Scott et al. 2016). This thermal aspect needed to be modified because the temperature variations throughout the year in the tropical area were not the same as in the sub-tropical and temperate areas. Research conducted in Dhaka, which has a tropical hot-humid climate, showed that the range of comfortable outdoor conditions using the PET method was 29.5°C-32.5°C (Sharmin et al. 2019). Meanwhile, research conducted in Kuala Lumpur showed that comfortable outdoor conditions also using the PET method obtained 25.6°C (Aghamohammadi et al. 2021). Our previous research found that the highest thermal rating was an effective temperature of 25°C-28°C (Sudiar 2020). These results were used to modify

the thermal aspect to calculate the climate comfort score in the coastal tourism area of Padang.

To determine the climate comfort score in Padang, we used historical data from 2011-2020 (10 years) from two BMKG stations. We did this because there were no weather stations at tourist sites. The results of these calculations can be seen in Fig. 3 that the average year-round climate comfort score in Padang was neutral (Table 2). A comfortable climate was an HCI score of ≥ 60 , a neutral score of 40 to 59, and an uncomfortable score of < 40 (Ramazanipour & Behzadmoghaddam 2013, Scott et al. 2016). These results provided an overview of the general conditions of climate comfort in Padang that was not specifically for coastal tourism areas. Calculation of comfort scores in coastal tourist areas must be done by directly measuring weather parameters such as air temperature, humidity, and wind velocity.

Table 2: HCI score.

ttScore	Category	Information
100-90	Ideal	Very Comfortable
89-80	Excellent	
79-70	Very Good	Comfortable
69-60	Good	
59-50	Acceptable	Neutral
49-40	Marginal	
39-30	Unfavorable	Uncomfortable
29-20	Very unfavorable	
19-10	Extremely Unfavorable	Very Uncomfortable
9-0	Impossible	

Visitor Comfort Level

Visitors were given closed-ended questions to obtain information about the range of comfort levels they felt based on weather parameters. The answer categories were very uncomfortable, uncomfortable, neutral, and comfortable. The comfort level calculation was carried out using MSI. The results of the interviews showed that the overall level of comfort in the coastal tourism area of Padang was comfortable (64%) (Fig. 4).

In addition to asking about the comfort level, this study also asked about the thermal sensation visitors feel. Thermal comfort was measured by involving air temperature, radiation temperature, air humidity, and airflow velocity (Mayer & Hoppe 1987). Thus, we can interpret the thermal sensation as a sensation the skin feels using weather parameters. The

answer categories were 7 categories; very hot, hot, slightly hot, neutral, slightly cold, cold, and very cold. The results of interviews showed that the coastal tourism area of Padang had a neutral thermal sensation (66%) (Fig. 5). A study conducted in Kuala Lumpur found that 62% (n=243) stated a neutral thermal sensation at 25.6°C PET (Aghamohammadi et al. 2021).

When conducting interviews with respondents, air temperature, humidity, and wind speed measurements at tourist sites were also carried out. The measurements at tourist sites showed that the air temperature interval was from 26.5°C-33.8°C. The air humidity interval was 58.9% - 81.2%, and the wind speed interval was 0.1 m/s-6.3 m.s⁻¹. The measurement results were converted to effective temperature because the temperature felt by the skin was the effective temperature. The average effective temperature was 27.5°C (306 people). Furthermore, the average effective temperature in the neutral category was 28.2°C (68 people). Next, the effective temperatures for uncomfortable, very comfortable, and very uncomfortable conditions were 28.9°C (28 people), 26.8°C (6 people), and 28.3°C (1 person) (Fig. 5). To get the level of climate comfort in the coastal tourism area, the effective temperature was carried out by linear regression:

$$Y = -0,4299x + 29,234 \dots(5)$$

With R² = 0.7201. From equation (5), the comfortable interval was the effective temperature between 26°C - 28°C. Interestingly, when the effective temperature was 28°C, the sensation felt by visitors was a bit hot (Fig. 5). Although

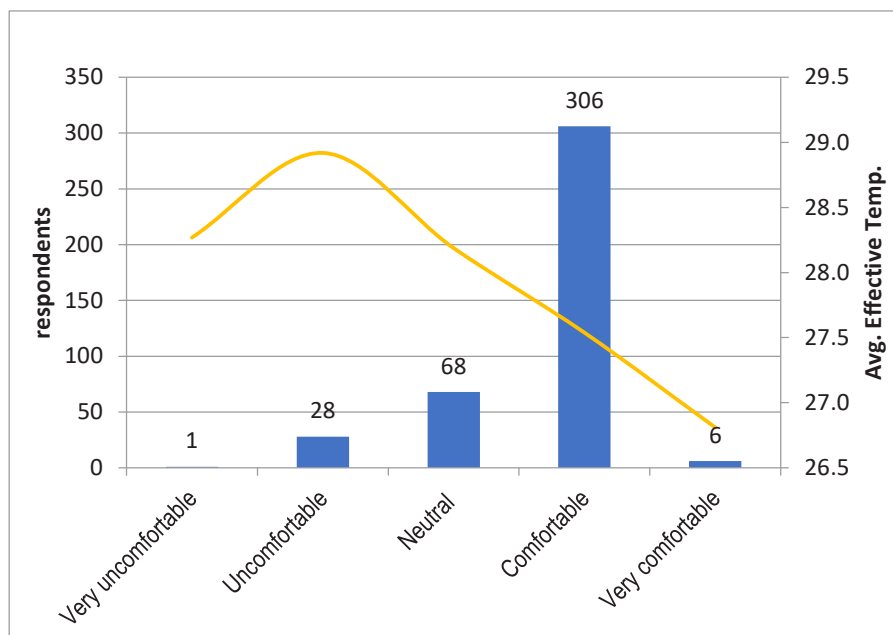


Fig. 4: The level of comfort felt by visitors in the coastal tourism area of Padang City.

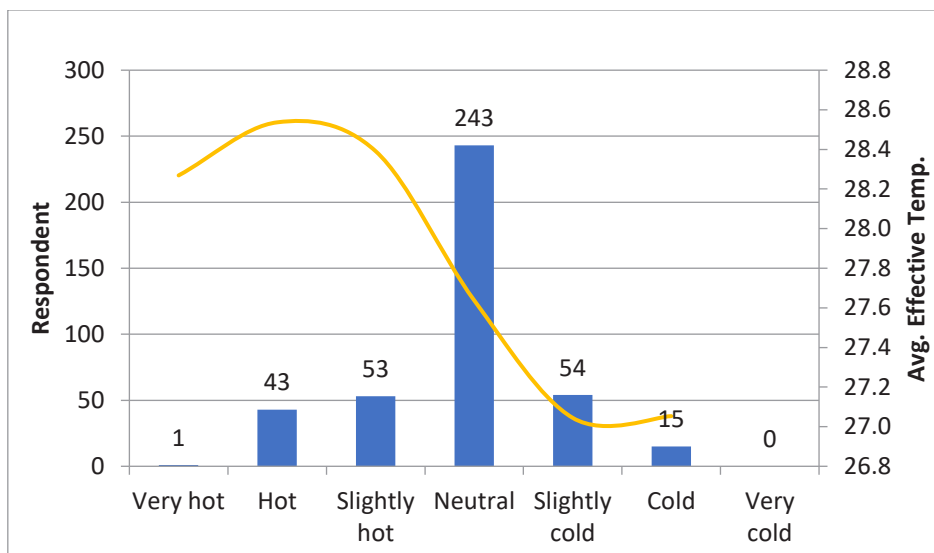


Fig. 5: Thermal sensation felt by visitors in the coastal area of Padang.

they felt a slightly hot sensation, they still categorized the condition as comfortable. This indicated that although the air temperature in the coastal area was high, the sensation felt by the body remained comfortable because the wind was blowing quite hard.

The results of the effective temperature obtained in this study were slightly different from the previous results. Previous research was conducted in three locations with diverse topography, from coastal to mountainous. On the contrary, this research specialized in the coastal area. This difference further confirmed that climate comfort also depended on the variable of residence. In Dhaka and Kuala Lumpur, the neutral thermal sensation is 29.5°C-32.5°C and 25.6°C, respectively (Sharmin et al. 2019, Aghamohammadi et al. 2021). Singapore's acceptable operating temperature interval was 26.3°C-31.7°C (Yang et al. 2013). In determining the operating temperature, it was important to consider how air temperature, average radiation temperature, and wind speed affected a person's thermal comfort (Hwang et al. 2010). Most visitors who lived in the coastal area, of course, had adapted to these environmental conditions.

CONCLUSION

The visitors considered that the weather was an important factor to consider for outdoor tourism activities. Young people (late teens and early adults) were more concerned with climate comfort for outdoor tourism than older people. The HCI method found that Padang's average year-round climate comfort score was neutral. The interviews with visitors showed that the overall level of comfort in the coastal tourism area of Padang was comfortable. Furthermore,

the comfortable interval felt by visitors was the effective temperature between 26°C-28°C, and the perceived thermal sensation was neutral.

ACKNOWLEDGMENTS

The authors would like to thank Lembaga Penelitian dan Pengabdian Masyarakat Universitas Negeri Padang for funding this work with contract number: 874/UN35.13/LT/2021.

REFERENCES

- Aghamohammadi, N., Saun, F.C., Mohd Idrus, M.H., Ramakreshnan, L., Haque, U. and Haque, U. 2021. Outdoor thermal comfort and somatic symptoms among students in a tropical city. *Sustain. Cities Soc.*, 72: 103015. <https://doi.org/10.1016/j.scs.2021.103015>.
- Al Amin, A.N. and Dwi, J. 2017. Classification of human age based on box-counting fractal dimensional analysis of facial images with canny edge detection. *Sci. J. Math.*, 2(6): 33-42.
- Amelung, B. and Nicholls, S. 2014. Implications of climate change for tourism in Australia. *Tour. Manag.*, 41: 228-244. <http://doi.org/10.1016/j.tourman.2013.10.002>.
- Blazejczyk, K., Epstein, Y., Jendritzky, G., Staiger, H. and Tinz, B. 2012. Comparison of UTCI to selected thermal indices. *Int. J. Biometeorol.*, 56: 515-535. Doi: 10.1007/s00484-011-0453-2.
- Freitas, C.R.D. and Scott, D. 2007. Assessment method for climate and tourism based on daily. *Tourism*, 11: 52-58.
- Haryadi, A., Kusratmoko, E. and Karsidi, A. 2019. Climate comfort analysis for tourism in Samosir district. *E3S Web Conf.*, 94: 5001. <https://doi.org/10.1051/e3sconf/20199405001>.
- Hwang, R.L., Lin, T.P., Cheng, M.J. and Lo, J.H. 2010. Adaptive comfort model for tree-shaded outdoors in Taiwan. *Build. Environ.*, 45(8): 1873-1879. doi:10.1016/j.buildenv.2010.02.021
- Iftah, V.R. 2015. Analysis of the climate index of the tourism sector in Citeko, West Java. Thesis. IPB University, Bogor.
- Kurnia, R.F.A. 2016. Analysis of Climate Comfort Index: Case Study:

- Taman Wisata Jatim Park 2 and Karangates. Thesis. IPB University, Bogor.
- Li, H., Song, H. and Li, L. 2016. A Dynamic panel data analysis of climate and tourism demand: Additional Evidence. *J. Travel Res.*, 56: 158-171. <https://doi.org/10.1177/0047287515626304>.
- Maswar, D. 2017. Investment opportunities for the Development of the Padang beach area. DPMPTSP, West Sumatra.
- Mayer, H. and Hoppe, P. 1987. Thermal comfort of man in different urban environments. *Theor. Appl. Climatol.*, 38: 43-49.
- Mieczkowski, Z. 1985. The tourism climatic index: a method of evaluating world climates for tourism. *Canadian Geographer/Le Géographe Canadien*, 29(3): 220-233.
- Noor, A.B.S., Rakhmat, D.I., Khasanah, S.N. and Kurniawan, W. 2018. Utilization of holiday climate index (HCI) information in the tourism sector: Case study: Banjarmasin City. *Appl. Res.*, 54: 616-628
- Olya, H.G.T. and Alipour, H. 2015. Risk assessment of precipitation and the tourism climate index. *Tour. Manag.*, 50: 73-80. <http://doi.org/10.1016/j.tourman.2015.01.010>.
- Priego, F.J., Rosselló, J. and Santana-Gallego, M. 2015. The impact of climate change on domestic tourism: A gravity model for Spain. *Reg. Environ. Change*, 15: 291-300. <https://doi.org/10.1007/s10113-014-0645-5>.
- Ramazanipour, M. and Behzadmoghaddam, E. 2013. Analysis of tourism climate index of Chalooos city. *Int. J. Human. Manag. Sci.*, 1(5): 2320-2324.
- Roshan, G., Yousefi, R. and Fitchett, J.M. 2016. Long-term trends in tourism climate index scores for 40 stations across Iran: The role of climate change and influence on tourism sustainability. *Int. J. Biometeorol.*, 60: 33-52. <https://doi.org/10.1007/s00484-015-1003-0>.
- Rutty, M. and Scott, D. 2016. Comparison of climate preferences for domestic and international beach holidays: A case study of Canadian travelers. *Atmosphere*, 7: 230. <https://doi.org/10.3390/atmos7020030>.
- Scott, D. and McBoyle, G. 2001. Using a 'tourism climate index' to examine the implications of climate change for climate as a tourism resource. *Int. Soc. Biometeorol.*, 11: 69-88.
- Scott, D., Rutty, M., Amelung, B. and Tang, M. 2016. An inter-comparison of the holiday climate index (HCI) and the tourism climate index (TCI) in Europe. *Atmosphere*, 17: 25-36. [Doi:10.3390/atmos7060080](https://doi.org/10.3390/atmos7060080).
- Setia, N. and Hendra, D. 2019. Application of interval successive method in multiple linear analysis. *Jambura J. Math.*, 1: 43-53.
- Sharmin, T., Steemers, K. and Humphreys, M. 2019. Outdoor thermal comfort and summer PET range: A field study in tropical city Dhaka. *Energy Build.*, 198: 149-159. <https://doi.org/10.1016/j.enbuild.2019.05.064>.
- Sudiar, N.Y. 2020. Climatological Comfort of Natural Tourism Areas in Indonesia. Dissertation. IPB University, Bogor.
- Sudiar, N.Y., Koesmaryono, Y., Perdinan, P. and Arifin, H.S. 2019a. Characteristics and climate comfort of nature-based tourist sites in Ancol Eco-Park, Bogor Botanical Gardens, and Cibodas Botanical Gardens. *Environ. Sci.*, 15: 240. <https://doi.org/10.20527/es.v15i2.6967>.
- Sudiar, N.Y., Koesmaryono, Y., Perdinan, P. and Arifin, H.S. 2019b. Studies of thermal comfort in the Jakarta north coast tourism region of Indonesia. *Int. J. Adv. Res.*, 7(9): 476-483.
- Yang, W., Wong, N.H. and Jusuf, S.K. 2013. Thermal comfort in outdoor urban spaces in Singapore. *Build. Environ.*, 59: 426-435. [doi:10.1016/j.buildenv.2012.09.008](https://doi.org/10.1016/j.buildenv.2012.09.008).



Anaerobic Biodegradability Potential of RCF-Based Kraft Paper Mill Effluent

Abhishek Tyagi^{*(**)}†, Amitabh Raj Tripathi^{**}, Pratibha Naithani^{*} and M. K. Gupta^{**}

^{*}Graphic Era (Deemed to be University), Dehradun, Uttarakhand, India

^{**}Central Pulp and Paper Research Institute, Saharanpur, U.P., India

†Corresponding author: Abhishek Tyagi; abhishektyagi34@gmail.com

Nat. Env. & Poll. Tech.
Website: www.neptjournal.com

Received: 17-08-2022

Revised: 01-11-2022

Accepted: 04-11-2022

Key Words:

Anaerobic biodegradability
Kraft paper mill effluent
Methanogenic sludge activity
Biochemical methane potential
SEM

ABSTRACT

The present study collected anaerobic sludge from a paper mill operating a UASB reactor on agro-based raw material (wheat straw) washings for biogas production. After determining the sludge profile and methanogenic activity of anaerobic sludge, it was further used to determine the anaerobic biodegradability of RCF-based kraft paper mill effluent. The sludge profile of collected anaerobic sludge was found w.r.t. Suspended Solids (SS) 60 g.L⁻¹, Volatile Suspended Solids (VSS) 23 g.L⁻¹, Inorganic content 62% & Organic content 38%. The presence of effective microbes in anaerobic sludge was confirmed by SEM (Scanning Electron Microscope). Degradation of organic matter present in effluent by anaerobic digestion leads to the production of biogas (methane & CO₂), a renewable energy source. The sludge profile and methanogenic activity findings supported the anaerobic treatment of kraft paper mill effluent and were positive. The methanogenic activity of anaerobic sludge was determined as 0.832 gCOD.gVSS⁻¹×Day, and the average anaerobic biodegradability of RCF-based kraft paper mill effluent was found to be 71.5%.

INTRODUCTION

RCF-based paper mills use waste paper as fibrous raw material for manufacturing paper and paper boards. In India, Recycled Fiber (RCF) based paper mills use indigenous (Fig. 1) and imported waste paper (Fig. 2) in different ratios as per product quality on market demand. RCF-based kraft paper-making process includes waste paper slushing, pulp cleaning & screening, pulp refining, stock preparation, and sheet formation.

Most water requirement is met by reusing and recycling backwaters in a closed loop. Fresh water is used only in sections like paper machine showers, steam generation, chemical preparation, etc. The schematic flow diagram of the process (Fig. 3).

Most wastewater generated by paper industries is rich in various biopolymers like starch, cellulose, hemicelluloses, glucose, lignocelluloses, etc. These biopolymers can be converted into sustainable biofuels, i.e., ethanol, butanol, biodiesel, biogas, hydrogen, methane, biohythane, etc., through its bioremediation by anaerobic digestion (Bhatia et al. 2020). To accomplish both of these obligations, the utilization of wastewater should be done in such a manner so that the process used would treat the wastewater along with the production of some cherished products which

can be reutilized further (Reungsang et al. 2016, Ijaz et al. 2016). Using effluent/ wastewater for energy generation is economical, as this does not require expensive processes. While several emerging technologies contribute to the wastewater resource recovery challenge, biological approaches give the greatest promise to recover essential resources from effluent efficiently (Bhatia et al. 2020). Moreover, fossil sources are very limited and may deplete in the future, so alternative energy sources must be developed. Therefore, the best approaches include using wastewater to produce energy products like bioethanol, biogas, biodiesel, etc., which can be transformed into electricity (Kassongo & Togo 2011).

BMP, anaerobic biodegradability, and digestibility are similar. They all deal with the degradation of organic matter by microorganisms in anaerobic conditions. At high gas production, less organic matter remains after digestion, indicating higher biodegradability (Lesteur et al. 2010). The BMP value can be used as an index of the anaerobic biodegradation potential. The BMP is the experimental value of the maximum quantity of methane produced per gram of volatile solids (VS). The BMP is measured with the BMP test, which consists of a respirometric test, i.e., measuring the methane or biogas produced by a known quantity of waste in a batch in anaerobic conditions (Hansen et al. 2003).



Fig. 1: Indigenous fibrous raw material.

Fig. 2: Imported fibrous raw material.

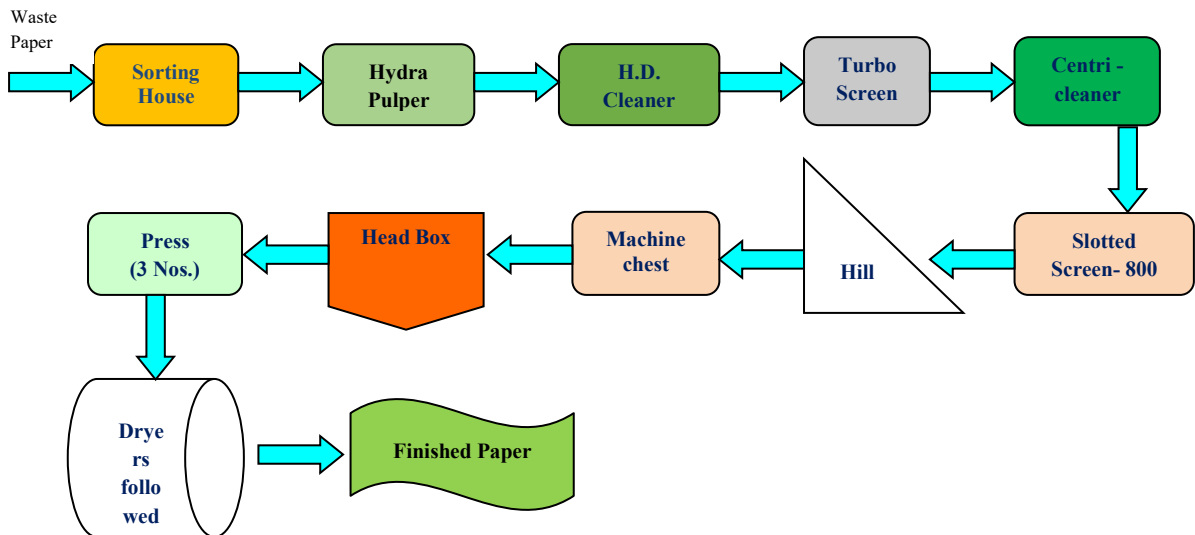


Fig. 3: Layout of the manufacturing process for kraft paper.

Overall Objective of the Study

Anaerobic biodegradability potential of effluent generated in RCF-based kraft paper mills.

Specific Objectives of the Study

(1) Characterization of effluent collected from RCF-based kraft paper mills.

(2) Determination of sludge profile of anaerobic sludge.

(3) Determination of the methanogenic activity of anaerobic sludge.

MATERIALS AND METHODS

The RCF-based kraft paper mills visited to manufacture unbleached kraft paper from waste paper (indigenous &

imported) and chemical additives like starch as sizing chemical, Poly Aluminium Chloride (PAC) as retention aid, etc. The paper-making process is water intensive; water requirement depends on pulp and stock consistency to be maintained in different unit operations. As the mills manufacture unbleached kraft paper and board, almost all unit operations are usually completed with backwater circulating in a closed loop. Grab effluent samples were collected from the mills for physical-chemical analysis per BIS/APHA standards.

Anaerobic Sludge Profile

Sludge profile is the determination of suspended solids, volatile suspended solids, and organic & inorganic constituents in the anaerobic sludge. As given in BIS and APHA (2017) standards, the gravimetric method determined the suspended and volatile solids. The anaerobic sludge collected was first washed with tap water and siphoned the supernatant water after settling the sludge (Fig. 4 & Fig. 5).

Methanogenic Activity of Anaerobic Sludge and Biodegradability of the Effluent

A sludge activity test is usually carried out in batch experiments where a fixed amount of substrate serves as feed for a predetermined amount of sludge. The specific sludge activity is estimated from the methane production rate or the substrate depletion rate and the amount of sludge present. It is usually expressed in $\text{g COD.gVSS}^{-1}\times\text{day}$. Therefore,

Sludge activity ($\text{g COD.gVSS}^{-1}\times\text{day}$) =

$$\frac{\text{maximum methane production rate (L/day)}}{\text{Amount of sludge (in g VSS)}} \times 2.6$$

$$= \frac{y/x \times 24 \times 2.6}{\text{Amount of sludge (in g VSS)}}$$

Where,

y/x is the maximum gas production rate where the curve is steepest.

2.6 is the factor, i.e., 1 L of methane produced corresponds with 2.6 g of COD removed

The assay is performed to determine the specific methanogenic activity of anaerobic sludge and the biodegradability of the effluent. It measures the potential in anaerobic sludge to convert the organic matter into biogas (methane). Where biodegradability is the measure of total methane production and COD removal efficiency from certain wastewater. In the biodegradability test, COD reduction is determined via gas production, so one or more blanks should always be

incubated. For blank, sludge with all chemicals added, but with tap water instead of wastewater. The gas produced by the blank (from COD present in the sludge and deterioration of the sludge) should be subtracted from the samples with an equal amount of sludge. The anaerobic biodegradability of wastewater is calculated as follows:

$$\text{Biodegradability (\%)} = \frac{(\text{Gas}_x - \text{Gas}_B)}{\text{COD}_x} \times 260$$

Where,

Gas_x is the amount of CH_4 produced by wastewater at the end of the test, L

Gas_B is the amount of CH_4 produced by blank at the end of the test, L



Fig. 4: Collected anaerobic sludge.



Fig. 5: Washed sludge dewatering by siphoning.

COD_X is the amount of total COD added to perform the experiment.

260, is the conversion factor CH₄ produced by COD

The methanogenic activity of sludge and biodegradability is dependent on many factors. The real activity potential of sludge can be measured when ideal conditions are provided. The factors affecting are as under:

Temperature

The temperature plays an important role in the activity of sludge. Normally 30°C is recommended to measure the activity of sludge. The sludge activity can be measured at the same temperature we expect in practice.

The Concentration of Substrate and Sludge

The concentration of substrate in the micro-environment of the methanogenic bacteria is critical. The ranges of concentration of substrate & sludge are given below (Table 1).

Activity Period

The activity period is the time period when the methane gas production rate is the highest during the feeding. The period should at least cover about 50% substrate used and should not be short.

It has been realized that the sludge content and activity are subject to many changes during the reactor operation. After the stable operation, the activity will remain constant, but sludge content will increase steadily. The experiments for methanogenic sludge activity were carried out with glucose, and anaerobic biodegradability was performed with RCF-based kraft paper mill effluent and calculated successfully. The experiments were conducted with a 500 mL serum bottle with a septum. The test procedure is described below:

Anaerobic sludge 130 mL (3g VSS), glucose 4 g as feed, and nutrients NaHCO₃ (5 g), K₂HPO₄ (2g), and NH₄Cl (0.5 g) were mixed and made up to 1 L with tap water. The pH of the assay was maintained at 7.2. From this 1 L solution, 500 mL was taken in a serum bottle to calculate the methanogenic activity. The air in the headspace was replaced by Nitrogen gas. The bottle was placed in a water bath at 30°C temperature, and the hose was connected to another bottle containing alkaline (KOH solution). The alkaline solution bottle was connected to a measuring cylinder to record the level of liquid displaced by biogas generated during the experiment. The experimental setup is the same for biodegradability as sludge activity, except wastewater (COD) is taken as feed instead of glucose, and nutrients are added as follows, NaHCO₃, g (amount of COD added

g × L), K₂HPO₄, mg (amount of COD added g × 54) and NH₄Cl, mg (amount of COD added g × 16). The experimental setup is shown below (Fig. 6).

RESULTS AND DISCUSSION

The effluent was analyzed as per the standard test method of BIS and APHA. The results of the analysis of effluent samples for various pollution parameters are given below (Table 2). The analysis results show that the mills operate at low freshwater consumption, and effluent generated has COD & BOD on the higher side. The higher COD and BOD show that effluent carried the more organic load and is good for bio methanation to produce biogas.

By characterization of anaerobic sludge, the sludge profile was determined. The results of the analysis are given below (Table 3). The results were encouraging, with 23 g.L⁻¹ VSS and 37.78% organic content.

The experiment performed to determine sludge activity with glucose was performed successfully, and calculations are shown below:

Maximum methane production rate (l/day) or y/x (Fig. 7) = (0.630–0.480)/28 – 20 = 0.02

Amount of sludge (g VSS) = 1.5

Sludge activity (g COD.gVSS⁻¹ × day) =

$$\frac{y/x \times 24 \times 2.6}{\text{Amount of sludge (in g VSS)}} \\ = 0.02 \times 24 \times 2.6/1.5 = 0.832$$

The cumulative gas production to calculate the y/x value is in Fig. 7. The results were satisfactory. The methanogenic activity of sludge was found to be 0.832 gCOD.gVSS⁻¹×Day. This shows that the microbes present in sludge were healthy and active.

SEM Study of Granules

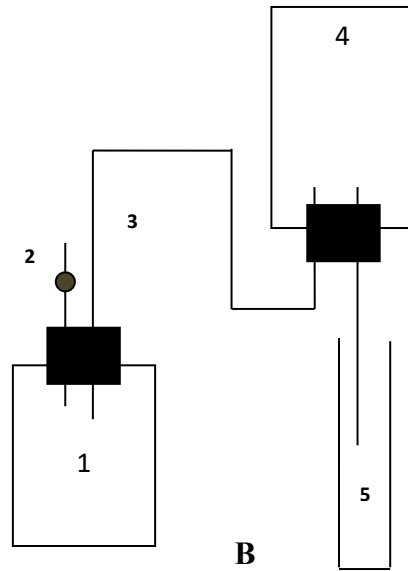
Visual examination of granular biomass shows a spherical shape and black. On the surface of granules, some irregular projects were also seen. SEM images of granules showed that the surface of granules was rough and uneven. The size of granules was 1 to 5 μm and exhibited a good settling tendency. The morphology of the granules demonstrated

Table 1: Sludge and substrate concentration for methanogenic activity assay.

S. No.	Experimental Set-Up	Sludge g VSS.L ⁻¹	VFA/Sucrose g COD.L ⁻¹
1.	Stirred	2.0 – 5.0	2.0 – 4.0
2.	Unstirred	1.0 – 1.5	3.5 – 4.5



A



- 1 Serum bottle with culture medium in a water bath
- 2 Sample Point
- 3 Biogas Circuit
- 4 Serum bottles contain the alkaline solution
- 5 Measuring cylinder

Fig. 6: Experimental setup with serum bottle to determine anaerobic sludge activity & biodegradability (A), Flow diagram with details (B).

the presence of a heterogeneous bacterial population on the surface of the granules (Fig. 8).

The biodegradability results of effluent are shown below:

The total amount of COD (COD_x) added to the bottle was = 2 g

The amount of gas produced by a bottle containing effluent was (Gas_x) = 0.66 & 0.68 L

The amount of gas produced by blank bottles containing sludge & tap water was (Gas_B) = 0.12

$$\begin{aligned} \text{Biodegradability (\%)} &= \frac{(\text{Gas}_x - \text{Gas}_B)}{\text{COD}_x} \times 260 \\ &= (0.66 - 0.12) \times 260 / 2 = 70.2 \\ &= (0.68 - 0.12) \times 260 / 2 = 72.8 \end{aligned}$$

The average biodegradability (%) was found to be about 71.5. The results show that the effluent collected from RCF-based kraft paper mills contains a high organic load, easily biodegradable with anaerobic bacteria by anaerobic digestion.

Table 2: Analysis results of the effluent of RCF-based kraft paper mills.

S. No.	Parameters	Method Followed	Mill – A	Mill – B	Mill – C
1.	pH	IS: 3025; P- 11	6.37	6.27	6.87
2.	TS, mg.L ⁻¹	IS: 3025; P- 15	14,873	13,481	13,677
3.	TSS, mg.L ⁻¹	IS: 3025; P- 16	3,171	2,786	3,688
4.	TDS, mg.L ⁻¹	IS: 3025; P- 17	10,862	10,389	9,664
5.	COD (As Such), mg.L ⁻¹	IS: 3025; P- 58	8,412	8,058	7,596
6.	COD (Soluble), mg.L ⁻¹	IS: 3025; P- 58	8,028	7,639	7,073
7.	BOD (As Such), mg.L ⁻¹	IS: 3025; P- 44	3,216	3,029	2,158
8.	BOD (Soluble), mg.L ⁻¹	IS: 3025; P- 44	3,052	2,844	2,019
9.	Inorganic Solids, %	IS: 3025; P- 18	52.35	55.81	57.36
10.	Organic Solids, %	IS: 3025; P- 18	47.65	44.19	42.64

Table 3: Sludge profile results.

S. No.	Parameters	Unit	Method Followed	Results
1.	Total Solids (TS)	g.L^{-1}	IS: 3025; P- 15	61.83
2.	Suspended Solids (SS)	g.L^{-1}	IS: 3025; P- 16	60.00
3.	Volatile Suspended Solids (VSS)	g.L^{-1}	IS: 3025; P- 18	23.00
4.	Inorganic Solids	%	IS: 3025; P- 18	62.22
5.	Organic Solids	%	IS: 3025; P- 18	37.78

CONCLUSIONS

The findings of the mill visit indicate that the RCF-based kraft paper mills increased the reuse & recycling of backwater into the process, which extremely reduced their freshwater consumption & wastewater discharge. The characterization results of effluent collected show a high organic load in the effluent and have good potential to generate methane by anaerobic digestion. Sludge profile & activity results show that the anaerobic sludge used in the experiment was healthy & active. The methanogenic activity was found at about $0.832 \text{ gCOD.gVSS}^{-1} \times \text{day}$, which proves the above statement. The visual examination of granular sludge with SEM also confirms the presence of anaerobic biomass. The biodegradability results were encouraging, with an average biodegradability of 71.5%. It indicates the effluent contains organic load, which can be easily treated with anaerobic digestion. The process generates methane, a value-added product from wastewater that can be used as an energy source.

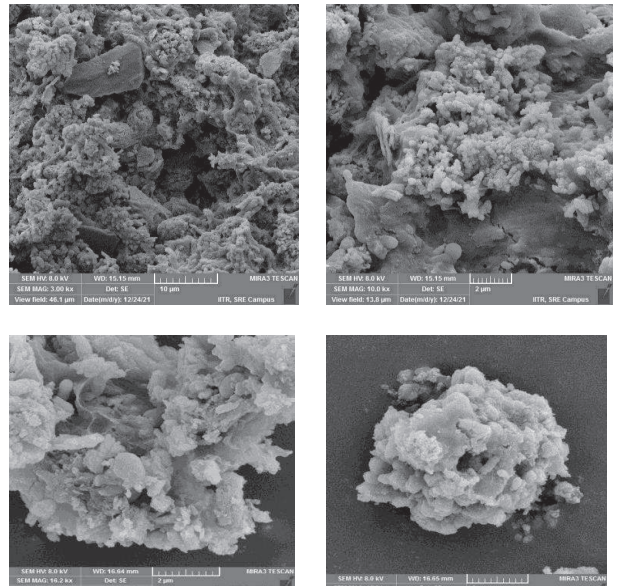


Fig. 8: SEM images of the heterogeneous bacterial population on the surface of the granules.

REFERENCES

- APHA. 2017. Standard Methods for the Examination of Water and Wastewater. Twenty-Third edition. American Public Health Association/American Water Works Association/Water Environment Federation, Washington, DC, USA.
- Bhatia, R.K, Ramadoss, G., Jain, A.K., Dhiman, R.K, Bhatia, S.K. and Bhatt, A.K. 2020. Conversion of waste biomass into gaseous fuel: Present status and challenges in India. *Bio Energy Res.*, 4: 137. <https://doi.org/10.1007/s12155-020-10137-4>

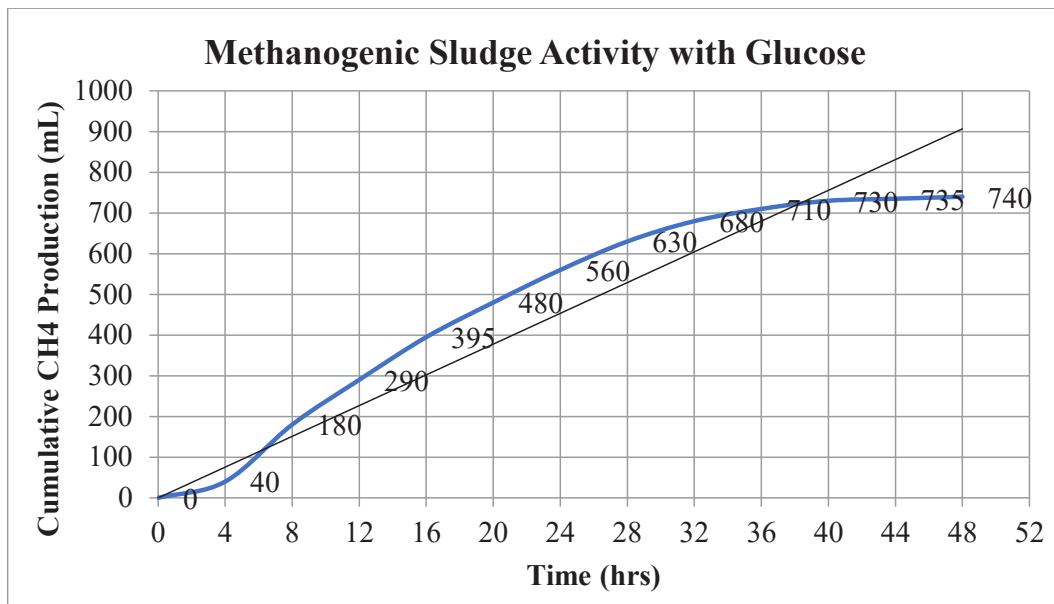


Fig. 7: Cumulative methane production from glucose.

- BIS (Bureau of Indian Standards), IS: 3025 (Part 1), 1987. Methods of Sampling and Test (Physical and Chemical) For Water and Wastewater. Manak Bhavan, Bahadur Shah Zafar Marg, New Delhi 110002.
- Hansen, T.L., Schmidt, J.E., Angelidaki, I., Marca, E., Jansen, J.C., Mosbaek, H. and Christensen, T.H. 2003. Method for determination of methane potentials of solid organic waste. *Waste Manag.*, 24: 393-400. [https://doi: 10.1016/j.wasman.2003.09.009](https://doi:10.1016/j.wasman.2003.09.009). <https://doi:10.1016/j.procbio.2009.11.018>
- Ijaz, A., Iqbal, Z. and Afzal, M. 2016. Remediation of sewage and industrial effluent using bacterially assisted floating treatment wetlands vegetated with *Typha domingensis*. *Water Sci. Technol.*, 74: 9. <https://doi:10.2166/wst.2016.405>
- Kassongo, J. and Togo, C.A. 2011. Evaluation of full-strength paper mill effluent for electricity generation in mediator-less microbial fuel cells. *Afr. J. Biotechnol.*, 10(69): 15564–15570. [https://doi: 10.5897/AJB11.146](https://doi:10.5897/AJB11.146)
- Lesteur, M., Bellon-Maurel, V., Gonzalez, C., Latrille, E., Roger, J.M., Junqua, G. and Steyer, J.P. 2010. Alternative methods for determining anaerobic biodegradability: A review. *Process Biochem.*, 45: 431-440.
- Reungsang, A., Sittijunda, S. and Sreela, C. 2016. Methane production from acidic effluent discharged after the hydrogen fermentation of sugarcane juice using batch fermentation and a UASB reactor. *Renew. Energy*, 86: 1224-1231. <http://doi.org/10.1016/j.renene.2015.09.051>



Tests for Evaluating the Efficacy of Phosphoric Acid Activated Charcoals from Two Biomasses

Abhijit S. Jadhav*† and Ravindra Nalawade**

*Department of Chemical Engineering, AISSMS College of Engineering, Kennedy Road, Pune 411001, Maharashtra, India

**Department of Civil Engineering, AISSMS College of Engineering, Kennedy Road, Pune-411001, Maharashtra, India

†Corresponding author: Abhijit S. Jadhav; asj.paper@gmail.com

Nat. Env. & Poll. Tech.
Website: www.neptjournal.com

Received: 23-08-2022

Revised: 03-11-2022

Accepted: 10-11-2022

Key Words:

Activated charcoal
Areca nutshell
Coconut shell
Phosphoric acid activation
Methylene blue adsorption
Caramel adsorption
Acetic acid number

ABSTRACT

Good quality activated charcoals were prepared from areca nutshell and coconut shell using phosphoric acid as a chemical activating agent at 400°C. Physico-chemical properties like iodine number, methylene blue number, and surface area of two activated charcoals were measured to assess the porous nature. A special test called acetic acid number was devised to understand the quality of functional groups on charcoal surfaces. Proximate analysis and physical properties of the two activated charcoals closely matched those of a commercial sample, confirming the good quality of samples prepared in the laboratory. Adsorption of isolated caramel from waste stream obeyed Freundlich isotherm, and the data could be explained based on the physisorption of large size molecules on the walls of mesoporous solid surface. Adsorption of methylene blue involving Coulombic attraction towards the areca nut shell-derived activated charcoal could be predicted and confirmed based on the acetic acid number for the first time.

INTRODUCTION

With the rapid advancement in science and technology, the standard of living of humankind has reached new high horizons. At the same time, water, air, and land pollution has also reached intolerable limits exposing humankind to the hazards of ecological calamities. The major problem faced by people of all nations, especially developing countries, is water pollution. Alcohol distilleries and dyestuff-based industries are the major polluters of water because their effluent streams are highly colored. Distilleries produce colored effluent called spent wash to 7-12 liters per liter of alcohol produced. The spent wash is highly toxic and contains high BOD (55×10^3) and COD (approximately $110-140 \times 10^3$) ppm. High BOD and COD associated with spent wash are due to bio-refractory components, like melanoidin, caramels, anthocyanins, tannins, lignins, and different xenobiotic compounds (Pandey et al. 2003, Tiwari et al. 2007).

The textile industry is the major consumer of dyes, and about 10-15% of the dyes used come out through effluent streams (Zolliger 1987, Hai et al. 2007, Hussain 2006). In addition to the textile industry, dye manufacturing, paper and

pulp, tannery, and paint industries produce large quantities of effluent-containing dyes. These effluents are considered objectionable because they cause carcinogenic skin irritation (Christe 2007). Dyestuffs are difficult to decompose biologically because they are highly structured polymeric (Namasivayam et al. 2001). In the case of distillery effluent, even after initial biological treatment, coloring compounds are not removed even though BOD and COD are reduced to a certain extent. Thus, removing coloring material is the major problem in both effluents. Many methods are popular for the color removal of this wastewater, viz. floatation, chemical coagulation, chemical oxidation, and adsorption (Gupta et al. 2000). Among these, adsorption has been very popular for color removal from wastewater because of its many advantages. These are: it is simple in design, comparatively inexpensive, easy to handle, and offers sludge-free cleaning operation. Commercial activated charcoal has been popular for color removal by adsorption. The cost factor has been the major stumbling block for its use on an industrial scale. Hence, low-cost alternative adsorbents derived from industrial and agricultural wastes are becoming popular nowadays (Crini 2006, Gupta 2009, Ong et al. 2014, Antal et al. 2003). However, the efficiency of these wastes for

color removal is low, which can be improved by conversion of the selected lignocellulosic materials (Hassler 1967, Silva et al. 2001) and industrial as well as municipal wastes (Cazetta et al. 2016, Dias et al. 2015) into activated charcoal by the physical and chemical activation process. These processes reduce activated charcoal with a large surface area, which can attract various molecules in water on its surface (Hassler 1967). The nature of these attractive forces mainly depends on the size of the pores and the molecules attracted. These forces are called physical, or Van der Waal's forces and the adsorption involved is termed physical adsorption.

Sometimes in adsorption behavior, chemical change seems to be involved, which is called chemisorption. It is very specific and depends on the chemical nature of both adsorbate and adsorbent. Determining which kind of adsorption is predominant requires a lot of tests, physical and chemical, as well as the use of sophisticated instruments.

In our present study, we have used two biomasses, viz. areca nutshell, and coconut shell, to prepare activated charcoal with phosphoric acid as activating agent in the ratio phosphoric acid: biomass 3:1. Simple physical and chemical tests have been used to predict which kind of activated charcoal (AC) is effective for the color removal of entirely different kind of colored bodies from wastewaters. This has practical significance indeed. Few simple tests have been able to a priori predict or explain the uptake of natural plant-based dyes caramel (isolated from distillery spent wash) and a basic dye methylene blue from simulated wastewaters for the first time

MATERIALS AND METHODS

Precursor for Activated Charcoals (AC)

Dry areca nut shell samples were procured from coastal Karnataka, India. The fibrous portion of the shell was cut into small (10 mm × 10 mm) pieces and stored. Similarly, coconut shell was procured from a local dealer. It was crushed into small pieces of 10 mm size and stored

Preparation of AC

About 300 g of areca nut shell pieces were taken in a 2.0 L beaker. To this, about 627 cm³ of ortho-phosphoric acid [at H₃PO₄: Biomass:: 3:1, H₃PO₄ required is (300 × 3 × 1/(0.85 × 1.69)) = 627 cm³] dissolved in a small quantity of deionized water was added slowly along with deionized water, till the surface of the precursor was completely immersed in the acid solution. The mixture was kept soaked in the acid for 24 h with occasional stirring with a glass rod to improve the efficiency of the soaking of the biomass by the acid. After this

incipient wetting, the water content in the acid solution in the beaker was evaporated on a low flame. The dry mass in the beaker was transferred to a stainless steel (SS) container of size 30 cm × 9 cm × 9 cm. The SS container with acid-loaded biomass was placed in a muffle furnace with the lid partially open. A small flow of nitrogen gas was introduced into the furnace to maintain an oxygen-free atmosphere. The furnace was heated slowly to attain 400°C in 30 min and maintained at this temperature for 90 min. The heating was stopped immediately, and the material was allowed to cool under nitrogen flow. The cooled sample was removed from the furnace the next day to obtain acid-laden activated charcoal. This mass was washed several times with distilled water to remove the free phosphoric acid completely and then dried in an oven at 110°C for 6 h. The dried sample was crushed and sieved through a 100 mesh sieve to obtain areca nut shell activated charcoal (ASAC). Activated charcoal from coconut shell (CSAC) was prepared using a similar procedure. The results have been tabulated in Table 1.

Characterization

The characterization of both activated charcoal samples CSAC and ASAC was carried out to obtain the methylene blue, iodine, and specially devised acetic acid numbers.

Methylene blue number: The Methylene blue number of both CSAC and ASAC samples was determined as per the Indian Standard Specification IS 2230-1962 (Gokarn et al. 2005)

Iodine number: The iodine number of both CSAC and ASAC samples was determined according to D-4607-94 (Meshtram & Lataye 2014).

Acetic acid number: This novel concept was perceived and devised for the first time to quantitatively determine functional groups on activated charcoal surfaces (approximate). Grams of glacial acetic acid is adsorbed by 10 g of activated charcoal. The procedure consists of dissolving 50 cm³ of glacial acetic acid in water and making it up to a volume of 500 cm³ in a volumetric flask. Initially, blank reading is taken by titrating 10 cm³ of this solution against 1 N sodium hydroxide solution. One gram of activated charcoal sample is accurately weighed, mixed with 50 cm³ of the acetic acid solution in a 100 cm³ conical flask, and stirred slowly for 15 min using a magnetic stirrer. The solution is allowed to stand still for the active charcoal to settle. 10 cm³ of the supernatant solution is then titrated against 1 N sodium hydroxide solution. The amount in grams of acetic acid captured by 10 g of activated charcoal samples is calculated by material balance calculations. The acetic acid number of two activated charcoal samples, CSAC and ASAC, are tabulated in Table 1.

Table 1: Properties of activated charcoals.

	Areca nutshell (ASAC)	Coconutshell (CSAC)	Commercial E. Merck
Proximate Analysis:			
Moisture %	15.4	11.9	9.7
Ash %	6.5	4.9	4.9
Fixed carbon %	71.6	78.2	85.4*
Volatile matter %	6.5	5.0	
Physico-Chemical Properties:			
Surface area, m ² .g ⁻¹	1813	744	--
Iodine no.	906	901	--
Methylene blue no.	15	15	180
Acetic acid no.	3	6	--
Coloring Matter Adsorption/Removal Capacity, V_{C0} cm³/g			
Caramel	148.7	121.3	--
Methylene blue	514.0	--	--
Freundlich Constant (1/n)			
Caramel	1.1444	2.2939	
Methylene blue	0.4534	--	

Batch Adsorption Studies

Adsorbate Caramel

Almost pure caramel was isolated from distillery spent-wash procured from Ugar Sugar Works Ltd., Ugarkhurd, Karnataka, India. One liter of spent wash (COD29600) was mixed with equal water in a beaker. It was treated with inorganic coagulants to precipitate color bodies like melanoidin and lignin, which are bio-refractory and negatively charged. The treated sample was allowed for 12 h for the sludge to settle and subsequently filtered. The filtrate was treated with lime to precipitate excess coagulants and some coloring matter. This solution was again filtered to obtain a dark yellow-colored filtrate. A few drops of dilute hydrochloric acid were added to the filtrate to adjust the pH to 5. This is pure caramel solution in water and is pale yellow (Jagtoyen & Derbyshire 1991). The COD of this solution was 1280 ppm.

Adsorbate Methylene Blue

1.0 g of AR grade methylene blue sample was accurately weighed and dissolved in 1 liter of deionized water. The pH of the solution was found to be 5.3 and was used as such, without any pH adjustment, since the adsorption of methylene blue on activated charcoal is reported to be maximum at pH between 4 and 12 (Guo & Rockstraw 2006).

Adsorption Equilibrium Studies

Adsorption of Caramel on CSAC and ASAC

30 cm³ of caramel solution was stirred with 100 mg (m) of CSAC for 30 min using a magnetic stirrer. It was filtered,

and the optical density of the filtrate was measured using a UV-Vis spectrophotometer at 420 nm. The difference (x) in optical density (OD) of the original solution and filtrate measured the amount of caramel adsorbed by 100 mg of CSAC. Experiments were repeated with 100 mg increments of CSAC, and the corresponding OD was measured. The value of x/m corresponding to the OD was calculated. Preliminary studies indicated that 30 min of stirring was sufficient to reach equilibrium. Similar experiments were conducted using different weights of ASAC, and from the OD, the x/m was determined.

Adsorption of Methylene Blue on CSAC and ASAC

Adsorption experiments were conducted using 1000 ppm of solution of methylene blue as above with ASAC. The corresponding data with respect to OD and x/m were collected, as reported in the previous section. In this case, the time required to reach equilibrium was 60 min. However, when experiments were initiated using CSAC, the difference in OD after adsorption was negligible; this indicated that coconut shell-derived activated charcoal did not participate effectively in decolorizing methylene blue solution in the present case.

RESULTS AND DISCUSSION

Proximate Analysis and Yield of Activated Charcoals

The proximate analysis and yields of activated charcoals are presented in Table 1. Interestingly, the proximate

analysis of CSAC and ASAC are almost identical and closely resemble that of the commercially popular activated charcoal of E Merck (Personal communication, Merck Life Sciences Pvt. Ltd., 2017). It also justifies the experimental conditions selected for the preparation of activated charcoal. Sufficiently high ratio of impregnate to the precursor (phosphoric acid biomass:: 3: 1) in the present case coupled with the carbonization temperature of 400°C (90 min) must be responsible for obtaining good quality activated charcoal (Zuo et al. 1995). Another significant observation in the present study is that the nature and composition of precursors, particularly cellulose and lignin content (having measured values of 58%, 36% cellulose, and 16%, 48% lignin in areca nutshell and coconut shell, respectively) did not make much difference with respect to the composition of activated charcoal as revealed by the nearly identical values of proximate analysis parameters. It is reported that lignocellulosic materials undergo two processes during phosphoric acid activation: impregnation and heat treatment. During impregnation, phosphoric acid and lignocellulosic macromolecule composite is formed, and during subsequent heat treatment, modification of morphology and dimensions of cellular units existing before impregnation takes place (Molino et al. 1995, Savova et al. 2001, Tseng et al. 2003). Impregnated phosphorous is also responsible for the creation of a large number of micropores (Ying et al. 2006). The yields of active charcoal from areca nut shells and coconut shells were 27.7% and 22.1%, respectively. This yield value is higher than that of active charcoal obtained by one-step activation of biomass at 800°C (Savova et al. 2001).

Characterization of Activated Charcoals

Nature of Pores and Porous Surface

Activation of biomass produces activated charcoal, which comprises small holes and crevices providing a large surface area. These crevices are called pores, and pore size distribution depends on the biomass's nature and activation type. Depending on the incremental nature and size, these pores are classified as micropores (< 2 nm), mesopores (2-50 nm), and macropores (> 50 nm) (Boehm 1966). Iodine numbers that mainly characterize micropores contributing to the surface area were 906 mg.g⁻¹ and 901 mg.g⁻¹ for ASAC and CSAC, respectively. The measured surface area of the two activated charcoal samples, ASAC and CSAC, was 813 m².g⁻¹ and 744 m².g⁻¹, respectively. The high values of iodine numbers indicate the high surface area of activated charcoals, confirmed by surface area measurement (Table 1). The Methylene blue number of ASAC and CSAC were both 15 mg.g⁻¹, which is very low compared to the methylene blue number 180 mg.g⁻¹ of the commercial sample of E. Merck (Jagtoyen 1991). It is worth noting that the methylene blue

number signifies the number of mesopores in the activated charcoal (Leon et al. 1994). The role of mesopores will be discussed later.

Chemical Nature of the Porous Surface

Activated charcoal prepared in this study originates from the chemical activation of biomass using phosphoric acid. Hence, porous surfaces must necessarily be developed involving chemical functional groups. In most cases, the surface of the activated charcoals is known to possess oxygen functional groups, which are mainly acidic in nature. These are characterized by titration with an alkali called Boehm titration (Al-Degs et al. 2000). The acidic functional groups are responsible for the attraction of basic molecules leading to their chemisorption. In addition, basic groups are also developed on the carbon surface during its activation and/or further treatment with various chemicals and gas streams (Savova et al. 2000). Thus, activated charcoal can have on its surface both acidic and basic groups (Tseng et al. 2003, Al-Degs et al. 2000). Basic groups can also be estimated by Boehm titration using mild acids (Boehm 1966).

Simple Method for Characterizing the Nature of Chemical Functional Groups on Activated Charcoal

Activated charcoal contains many surface groups, such as carboxylic, lactonic, phenolic, carbonyl, and etheric (Leon et al. 1994). Determination of these groups by Boehm titration (Boehm 1966) involves using many chemicals and consuming more than 24 h (Li et al. 2009). The present method uses excess acetic acid to neutralize basic chemical functional groups on activated charcoal surfaces. On back titration of the unreacted acid, determination of the exact quantity of acetic acid adsorbed/absorbed by 10 g of activated charcoal is easily possible. It is named acetic acid number, and the details of the estimation of this number are already described in section 2.3.3. As seen in Table 1, the acetic acid number for ASAC was 3, while that for CSAC was 6. Its implication is discussed in the next section.

Adsorption of Coloring Matter on Two Activated Charcoal Samples

Following the adsorption equilibrium studies described in section 2.4.3, the nature of adsorption of coloring matter (caramel and methylene blue) by ASAC and CSAC was determined using Freundlich adsorption isotherm (Chermisinoff & Allerbusch 1983). This isotherm shows the distribution of adsorbate (coloring matter) between the adsorbent (activated charcoal) and solution phase at equilibrium. Empirical Freundlich equation, which relates the amount of adsorbate in the solution phase to that of adsorbent (activated charcoal) by the expression:

$$x/m = k C^{1/n} \quad \dots(1)$$

where x is the amount of adsorbate adsorbed, m is the weight of activated charcoal, C is the equilibrium concentration of adsorbate in solution after adsorption, and 1/n is the Freundlich constant, also called surface heterogeneity factor (dimensionless). Taking logarithm of both sides,

$$\ln(x/m) = \ln k + (1/n) \ln C \quad \dots(2)$$

A plot of ln(x/m) against ln C should yield a straight line from which x/m corresponding to the initial adsorbate concentration C₀ can be obtained. Here C corresponds

to the measured optical density or OD, as the change in OD has been directly proportional to the change in C in the concentration range studied. The adsorption capacity of activated charcoal can be estimated by using the relation:

$$V_{C_0} = (x/m)_{C_0} (V/C_0) \quad \dots(3)$$

V_{C₀} is the theoretical volume of colored solution (in cm³), which can be treated per gram of activated charcoal to completely remove the coloring body in the solution (or adsorption capacity).

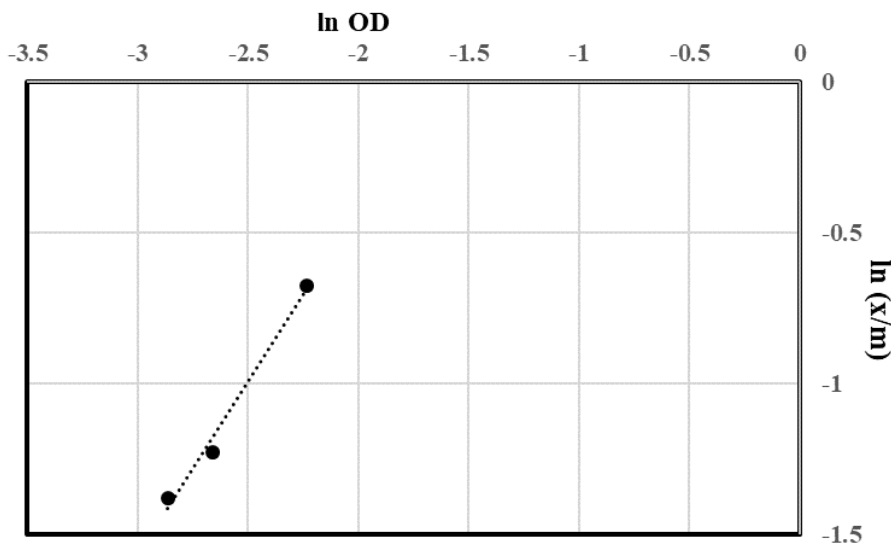


Fig. 1: Ln(x/m) versus ln OD plot for the adsorption of caramel (initial concentration of caramel: 1280 ppm, volume of caramel solution: 30 cm³, room temperature, pH: 5.0) on ASAC.

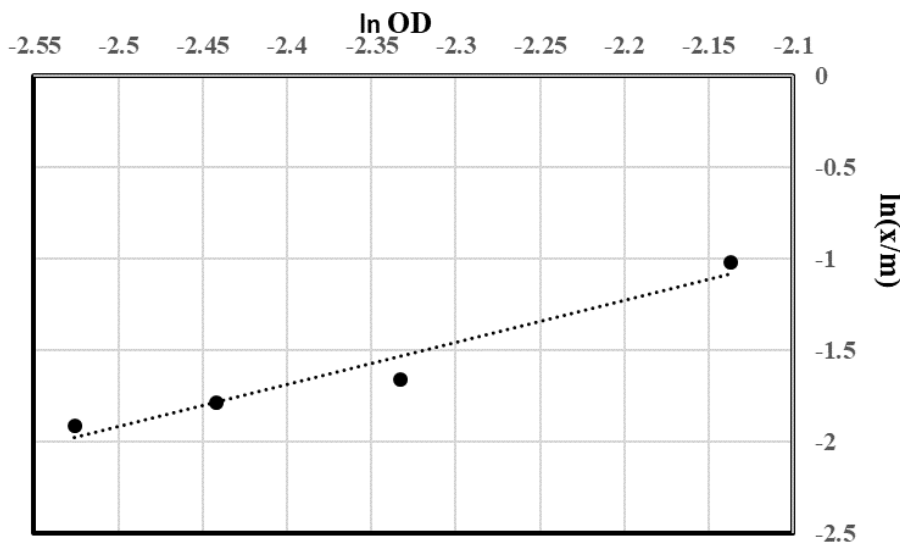


Fig. 2: Ln(x/m) versus ln OD plot for the adsorption of caramel (initial concentration of caramel: 1280 ppm, volume of caramel solution: 30 cm³, room temperature, pH: 5.0) on CSAC.

Adsorption of Caramel on ASAC and CSAC

The adsorption data of caramel on ASAC and CSAC (section 2.4.3.1) were used to obtain a plot of $\ln(x/m)$ against $\ln C_0$. These plots are presented in Fig. 1 (ASAC) and 2 (CSAC). Both the plots show straight lines indicating the applicability of Freundlich isotherm in both cases. The straight line plot was used to obtain values of $(x/m)_{C_0}$ and V_{C_0} for both the activated charcoal samples and are tabulated in Table 1. V_{C_0} or capacity of ASAC and CSAC for the capture of caramel was found to be $148.7 \text{ cm}^3 \cdot \text{g}^{-1}$ and $121.3 \text{ cm}^3 \cdot \text{g}^{-1}$ respectively. It is also quite evident that the capacity of activated charcoals in both cases was low. The value of constant $1/n$ of Figs 1 and 2 further confirms this fact. $1/n$ values were 1.1444 and 2.2939 for ASAC and CSAC, respectively. The value of $1/n$, greater than unity, also points to unfavorable adsorption for caramel on both ASAC and CSAC (Sogut & Caliskan 2017). Caramel, a sugar degradation product, is a high molecular weight compound. Caramel has a very small charge (Davis 2001). Hence it is clear that the adsorption of caramel on activated charcoals must be governed by physical adsorption. The mesopores formed during phosphoric acid activation are conducive to transport and adsorption on both ASAC and CSAC. The methylene blue numbers for ASAC and CSAC are similar and small, paving the way for similar capacity for the adsorption of caramel.

Adsorption of Methylene Blue on ASAC and CSAC

As seen in section 2.4.3.2, adsorption of methylene blue was possible only with respect to ASAC. The adsorption data of methylene blue was used to obtain a plot of x/m against

C_0 . The straight line plot shown in Fig. 3 again indicates the applicability of Freundlich isotherm in this case also. From the plot, $(x/m)_{C_0}$ was obtained, which was used to obtain the value of V_{C_0} , the capacity of ASAC as $514 \text{ cm}^3 \cdot \text{g}^{-1}$. The slope of the Freundlich isotherm plot, $1/n$, has a value of 0.4539, indicating highly favorable methylene blue adsorption on ASAC (Sogut & Caliskan 2017). Methylene blue is known to be a basic dye (Meshtram & Lataye 2014), and the Coulombic attraction between its positively charged ions and the negative surface of activated charcoal (ASAC) seems to be responsible for their efficient binding. Our studies on acetic acid numbers have indicated that ASAC has a lower value of the acetic acid number of 3 than 6 for CSAC. This confirms that ASAC has more acidic groups than CSAC, and CSAC must have a good number of basic groups on its surface, as indicated by a higher acetic acid number. The highly basic nature of CSAC is the reason for its negligible affinity for the basic dye methylene blue, as seen in section 2.4.3.2.

Our studies on acetic acid numbers have indicated that ASAC has a lower value of the acetic acid number of 3 than 6 for CSAC. This confirms that ASAC has more acidic groups than CSAC, and CSAC must have a good number of basic groups on its surface, as indicated by the higher acetic acid number. The highly basic nature of CSAC is the reason for its negligible affinity for the basic dye methylene blue, as seen in section 2.4.3.2.

CONCLUSIONS

Two types of activated charcoals were prepared using areca nutshell and coconut shell by chemical activation. The

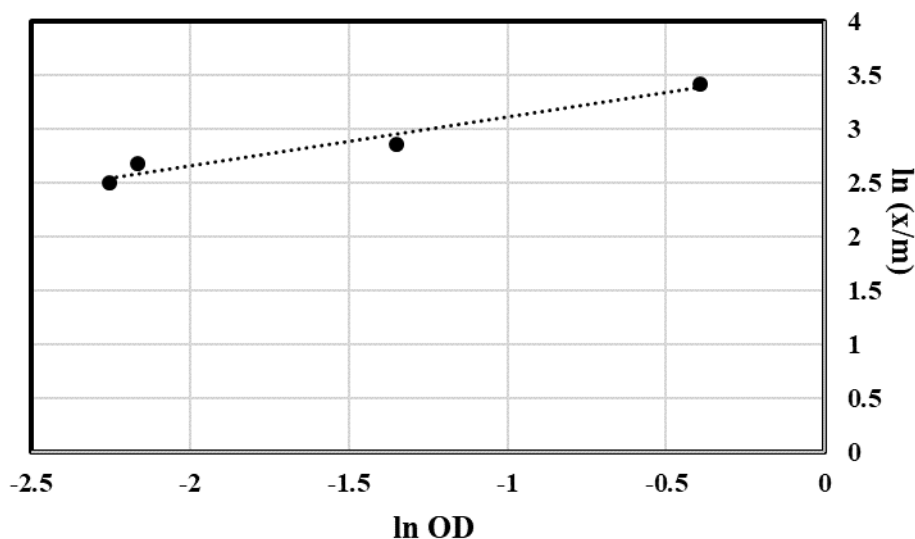


Fig. 3: $\ln(x/m)$ versus $\ln OD$ plot for the adsorption of methylene blue (initial concentration of methylene blue: 1000 ppm, volume of methylene blue solution: 30 cm^3 , room temperature, pH: 5.3) on ASAC.

preparation conditions have proven conducive to obtaining good quality active charcoals with highly developed pore structures. The proximate analysis parameters of these samples were comparable to those of commercial activated charcoal of E. Merck. The adsorption data of caramel solution on ASAC and CSAC and that of methylene blue solution on ASAC fitted well with Freundlich isotherm. The acetic acid number of activated charcoal, devised and estimated for the first time, could explain the surface groups' basic/acidic nature, influencing the adsorption/absorption of chemically charged coloring matter.

ACKNOWLEDGMENTS

The authors are thankful to the authorities of AISSMS College of Engineering, Pune, India. Deccan Sugar Technology Association (DSTA), Pune, India. National Chemical Laboratory, Pune, India, and Birla Institute of Technology, Ranchi, India, for their help and encouragement.

REFERENCES

- Agtoyen, M.J. and Derbyshire, T. 1991. Some considerations of the origins of porosity on carbons from chemically activated wood. *Carbon*, 31: 1185-1192. [https://doi.org/10.1016/0008-6223\(93\)90071-H](https://doi.org/10.1016/0008-6223(93)90071-H)
- Al-Degs, Y., Khraishah, A.M., Allen, S.J. and Ahmad, M.N. 2000. Effect of carbon surface chemistry on the removal of reactive dyes from textile effluent. *Water Res.*, 34(1): 927-935. [https://doi.org/10.1016/S0043-1354\(99\)00200-6](https://doi.org/10.1016/S0043-1354(99)00200-6)
- Antal, M.J. and Grønli, M. 2003. The art, science, and technology of charcoal production. *Industrial & Engineering Chemistry Research*, 42(8): 1619-1640.
- Boehm, H.P. 1966. Chemical identification of surface groups. *Adv. Catal.*, 16: 179-274. [https://doi.org/10.1016/S0360-0564\(08\)60354-5](https://doi.org/10.1016/S0360-0564(08)60354-5)
- Chermisinoff, P.N. and Allerbusch, F. 1983. *Carbon Handbook*. Ann Arbor Science Publishers, Ann Arbor, Michigan. <https://doi.org/10.1002/ahch.19830110106>
- Christe, R.M. 2007. *Environmental Aspects of Textile Dyeing*. Woodhead Publishers, Boca Raton, Florida.
- Crini, G. 2006. Non-conventional low-cost adsorbents for dye removal: A review. *Bioresour. Technol.*, 97: 1061-1085. <https://doi.org/10.1016/j.biortech.2005.05.001>
- Davis, S.W. 2001. The chemistry of color removal; A processing perspective. *Proc. S.Afr. Sugar Technol. Assoc.*, 75: 328-336.
- Dias, J.M., Alvim-Ferraz, M.C.M., Almeida, M.J., Rivera, J. and Sanchez-Polo, M. 2007. Waste materials for activated carbon preparation and its use in aqueous-phase treatment: A review. *J. Environ. Manag.*, 85: 833-846. <https://doi.org/10.1016/j.jenvman.2007.07.031>
- Gokarn, A.N., Sankpal, N.V. and Dongare, M. K. 2005. An improved process for the treatment of distillery effluent. *Indian Pat.*, 19: 3284
- Guo, Y. and Rockstraw, D.A. 2006. Physical and chemical properties of carbon synthesized from xylan, cellulose, and kraft lignin by H₃PO₄ activation. *Carbon*, 44: 1464-1475. <https://doi.org/10.1016/J.CARBON.2005.12.002>
- Gupta, V.K. 2009. Application of low-cost adsorbents for dye removal A review. *J. Environ. Manag.*, 90: 2313- 2342, <https://doi.org/10.1016/j.jenvman.2008.11.017>
- Gupta, V.K., Mohan, D., Sharma, S. and Sharma, M. 2000. Removal of basic dyes (rhodamine and methylene blue) from aqueous solutions using bagasse fly ash. *Sep. Sci. Technol.*, 35: 2097-2113. <https://doi.org/10.1081/SS-100102091>
- Hai, F.I., Yamamoto, K. and Fukushi, K. 2007. Hybrid treatment systems for dye wastewater. *Crit. Rev. Eng. Sci. Technol.*, 37: 315-377. <https://doi.org/10.1080/10643380601174723>
- Hassler, S.W. 1967. *Activated Carbon*. Leonard Hill, London.
- Hussain, Q. 2006. Potential applications of the oxidoreductive enzymes in the decolorization and detoxification of textile and other synthetic dyes from polluted water: A review. *Crit. Rev. Biotechnol.*, 26: 201-221. <https://doi.org/10.1080/07388550600969936>
- Leon, Y., Leon, C.A. and Rodovic I.R. 1994. *Chemistry and Physics of Carbon*. Marcel Dekker, New York, <https://www.researchgate.net/publication/284299367>
- Li, B., Lei, Z. and Huang, Z. 2009. Surface treated activated carbon for removal of aromatic compounds from water. *Chem. Engg. Technol.*, 32: 63-70, <https://doi.org/10.1002/ceat.200800535>
- Meshtram, M.L. and Lataye, D.H. 2014. Adsorption of methylene blue dye onto activated carbon prepared from pongamia pinnata seed. *Inter. J. Eng. Res. Technol.*, 3: 1216-1220.
- Molino, M.F., Rodriguez, F. and Caturla, M.J. 1995. Porosity granular carbon activated with phosphoric acid. *Carbon*, 33: 1105-1113, [https://doi.org/10.1016/0008-6223\(95\)00059-M](https://doi.org/10.1016/0008-6223(95)00059-M)
- Namasivayam, C., Dinesh Kumar, M., Selvi, K., Ashruffunnisa Begam, R., Vasanthi, T. and Yamuna, R.T. 2001. Waste coir pith: A potential biomass for the treatment of dyeing wastewaters. *Biomass Bioener.*, 21: 477- 483. [https://doi.org/10.1016/S0961-9534\(01\)00052-6](https://doi.org/10.1016/S0961-9534(01)00052-6)
- Ong, S.T., Keng, P.S., Lee, S.L. and Hung, Y.T. 2014. Low-cost adsorbents for sustainable dye-containing wastewater treatment. *Asian J. Chem.*, 26: 1873-1881.
- Pande, R.A., Melhotra, A., Tankiwale, S., Pande, S., Palke, P.P. and Kaul, S.N. 2003. Treatment of biologically treated distillery effluent: A case study. *Int. J. Environ. Stud.*, 60: 263-275.
- Savova, D., Apak, E., Ekinci, E., Yardim, F., Petrov, N., Budhinova, T., Razvigorova, M. and Minkova V. 2001. Biomass conversion to carbon adsorbents and gas. *Biomass Bioener.*, 21: 133-142. [https://doi.org/10.1016/S0961-9534\(01\)00027-7](https://doi.org/10.1016/S0961-9534(01)00027-7)
- Silva, T.S., Ronix, A.O., Pizoti, L.S., Souza, P.K.T., Leandro, K.C., Bedin, K.K., Beltrame, A.L., Cazetta, V.C. and Almeida, R. 2016. Mesoporous activated carbon from industrial laundry sewage sludge: Adsorption studies of reactive dye Remazol Brilliant Blue R. *Chem. Eng., J.* 303: 467-476. <https://doi.org/10.1016/j.cej.2016.06.009>
- Sogut, E.G. and Caliskan, N. 2017. Isothermal and kinetic studies of Pb(II) adsorption on raw and modified dolomite using a non-linear regression method. *Fresenius Env. Bull.*, 26: 2721-2729.
- Tiwari, P.K., Batra, V.S. and Balakrishnan, M. 2007. Water management initiatives in sugarcane molasses-based distilleries in India. *Res. Conserv. Recycle.*, 52: 351-367.
- Tseng, R.L., Wu, F.C. and Juang, R.S. 2003. Liquid phase adsorption of dyes and phenols using pine wood-based activated carbons. *Carbon*, 41: 487-495. [https://doi.org/10.1016/S0008-6223\(02\)00367-6](https://doi.org/10.1016/S0008-6223(02)00367-6)
- Ying, W.Z., Qi-Gang, C., Wen-Xin, J. and Guang-Hua, L. 2006. Improved methods for carbon adsorption studies for water and wastewater treatment 25: 110 -120. <https://doi.org/10.1002/ep.10122>
- Zolliger, H. 1987. Color chemistry: Synthesis, properties, and applications of organic dyes and pigments. *Chemie*, 43(40): 5291-5292. <https://doi.org/10.1002/anie.200385122>
- Zuo, S., Yang, J. and Liu, J. 2010. Effects of heating history of impregnated lignocellulosic material on pore development during phosphoric acid activation. *Carbon*, 48: 3293-3311. <https://doi.org/10.1016/j.carbon.2010.04.042>



Purification Efficiency of Eutrophic Water by Three Submerged Plants

Y. Hu*, D. X. Qian*, H. Zhu**, L. F. Wang**†, B. Wang*, Q. F. Ling** and X. D. Xiao*

*Gold Mantis School of Architecture, Soochow University, Suzhou, 215123, China

**School of Biology and Basic Medical Science, Soochow University, Suzhou, 215123, China

†Corresponding author: Lifen Wang; wanglf@suda.edu.cn

Nat. Env. & Poll. Tech.
Website: www.neptjournal.com

Received: 21-09-2022

Revised: 03-11-2022

Accepted: 13-12-2022

Key Words:

Submerged plants
Purification
N & P removal
Eutrophic water

ABSTRACT

The increase of nitrogen and phosphorus causes eutrophication in water bodies. Using submerged plants to decrease the pollution from water bodies is an effective way. In this research, three common submerged plants (*Vallisneria natans*, *Hydrilla verticillata*, and *Ceratophyllum demersum*) and their combinations were used to purify eutrophic water. The control treatment did not contain any plants. The removal effects and dynamic regulations of the three plants with their combinations of nutrients (such as nitrogen and phosphorus) in water were analyzed. All three species and their combinations above could grow in the eutrophic water and efficiently remove aquatic nutrients. All the treatment groups had a higher pollutant removal rate for total nitrogen (TN) and total phosphorus (TP) than that of the blank control. In these treatment groups, treatment F (50 g *Vallisneria natans* plus 50 g *Ceratophyllum demersum*) had the highest removal rate of TP at 57.53%; treatment B (100 g *Vallisneria natans*) had the best removal rate of TN at 92.04 %. Among these plants and their combinations, *Vallisneria natans* and *Ceratophyllum demersum* showed better purification ability; the combination of these two submerged plants and the combination of three submerged plants were more applicable for the restoration of eutrophic water.

INTRODUCTION

Under the dual influence of the rapid development of modern society and human activities, water environmental problems caused by eutrophication are becoming more and more serious (Feng et al. 2020). In 2007, massive algal blooms occurred in Taihu Lake, Wuxi, causing drinking water problems for hundreds of thousands of people there and serious social impact and economic losses (Zhao et al. 2004). Therefore, there is an urgent need for a solution to the eutrophication of lake water. Besides that, most rivers, lakes, and partial landscape waters in China have experienced pollution from organic pesticides and algal blooms.

As the primary producers of a freshwater ecosystem, submerged plants can provide many kinds of food, habitat, and breeding sites for various aquatic organisms (Zhou et al. 2012). At the same time, submerged plants can improve the dissolved oxygen and light conditions of the water body, increase the spatial ecological niche of the water body, and play an important role in the matter and energy cycles in the water ecosystem (Li et al. 2010). The results show that submerged plants can improve the content of nutrient salts and planktonic algae in eutrophication water, thus improving the water quality (Wang et al. 2014). Therefore, submerged vegetation is often used for the ecological restoration of eutrophic lake water.

Submerged plant restoration is an effective means to improve the water quality and ecological environment of urban eutrophic lakes (Huang et al. 2018). Without dredging, submerged plant restoration can still effectively control the endogenous load, reduce the content of nitrogen and phosphorus in lake water, inhibit the growth of algae, and reduce the level of water eutrophication. Through the absorption of nutrients, submerged plants slow down the increase of nutrient content in the water body, conduct photosynthesis at the same time, increase the dissolved oxygen in the water body, and provide oxygen for the respiration of animals and aerobic microorganisms in the water body (Fan et al. 2007). The physiological and biochemical reactions of submerged plants absorb nitrogen and phosphorus in the water as nutrients and form nucleic acids in their own structure, so as to effectively reduce the possibility of eutrophication and control the outbreak of algal blooms (Zhang et al. 2012). The growth cycle of submerged plants is also longer, which can more effectively improve the oxidation degree of a water body than floating plants and significantly affect the content of dissolved oxygen, pH, and inorganic carbon in the water body (Zhang et al. 2009). The oxygen released from submerged plants in eutrophic waters will be rapidly consumed. The formation of the rhizosphere oxidation zone reduces the diffusion of phosphorus in sediment from sediment to the water body by

the forming iron-phosphorus complex, so as to reduce the efflux of phosphorus to a certain extent and purify the water quality (Wang et al. 2019). Different submerged plants have different removal rates of total nitrogen, ammonia nitrogen, nitrate nitrogen, and total phosphorus.

China has relatively abundant natural resources. Suzhou, located in east China, is one of the most important central cities in the Yangtze River Delta and a scenic tourist city. It has a complex water system and abundant rainfall. Meanwhile, during the industrial process, some river and lake waters have been polluted, which destroys the ecological structure and leads to the loss of the original function of the water ecosystem. Therefore, considering the characteristics of the climate and environment in Suzhou, three submerged plants (*Vallisneria natans*, *Hydrilla verticillata*, and *Ceratophyllum demersum*) and their combinations were adopted to study their effects on the purification of eutrophic water. In this study, the purification effect of them in eutrophication water was explored through controlled experiments, providing a certain theoretical basis for improving the water environment by submerged plants.

MATERIALS AND METHODS

Plant material: Seedlings of *Vallisneria natans*, *Hydrilla verticillata*, and *Ceratophyllum demersum* were bought from the flowers and seedlings base in Suzhou. The selected aquatic plants were common species in Jiangsu Province. The bought seedlings were cultured indoors for 14 days to adapt to the experimental environment, and seedlings of similar growth in each species were chosen for the experiment.

Water of treatment and experimental location: The water was tap water from the laboratory after exposure to the sun to remove chlorine. Compared with *Environmental Quality Standards for Surface Water (GB 3838-2002)*, the pH of treatment water was 7.80, and TN and TP were 5.50 and 0.45 mg·L⁻¹, respectively. The experimental location was on the platform of the second floor of the Gold Mantis School of Architecture at Soochow University. The plants were exposed to the natural sunlight fully, and there was no effect of precipitation.

Experimental method: The experiment period was July–August 2021. The temperature during the experiment was maintained at 30 ± 2°C. The plants were planted in 60-liter plastic barrels with a radius of 37 cm and a water depth of 40 cm. And the control planting barrels contained no plants. Before the experiment, seedlings of the same species and sizes were selected, and the bodies were washed carefully using tap water to avoid the adhesion of soil and other factors. The quartz sand at the bottom of the plastic barrels used to fix the plants in place was rinsed with water after purchase. The

plant combinations follow: A was the blank control with no plants; B was 100 g *Vallisneria natans*; C was 100 g *Hydrilla verticillata*; D was 100 g *Ceratophyllum demersum*; E was 50 g *Vallisneria natans* plus 50 g *Hydrilla verticillata*; F was 50 g *Vallisneria natans* plus 50 g *Ceratophyllum demersum*; G was 50 g *Hydrilla verticillata* plus 50 g *Ceratophyllum demersum* and H consisted of 33.3 g of each of the three plants mentioned above. Except for the blank control, the same initial fresh plant weight was guaranteed in each barrel. Each treatment had three repetitions.

Each water sample was taken at 7 a.m. (GMT +8) from 20 cm below the water surface in the control and treatment barrels. PH, TP, TN, NH₄⁺-N and NO₃⁻-N were analyzed each time. After the last sampling, the fresh weight and dry weight of the plant would be counted. Water lost through evaporation was added back to its original state over time.

Chemical analysis: The pH of water samples was measured with a pH meter FE20 (Mettler-Toledo, Shanghai, China). The TN was measured with the potassium persulfate digestion UV spectrophotometric method (*HJ 636-2012*), and the TP was measured with the ammonium molybdate spectrophotometric method (*GB11893-89*). The NH₄⁺-N and NO₃⁻-N were analyzed by Nessler's reagent spectrophotometry (*HJ 535-2009*) and the spectrophotometric method with phenol disulfonic acid (*GB 7480-87*).

Data processing: The removal rate was calculated using the method of Lei et al. (2015):

$$\text{Removal rate} = (C_0 - C_i) / C_0 \times 100\% \quad \dots(1)$$

C₀ and C_i are pollutant concentrations at the beginning of the experiment and on the day i, respectively.

RESULTS

Plant growth and development: The three species of submerged plants grew well during the experiment period. The water in the blank barrels remained clear and odorless. Plants all survived in the treatment environment and developed normally. They grew appreciably in length, width, and weight. Among the three species, *Vallisneria natans* grew the most in fresh weight and *Ceratophyllum demersum* in length and branch number (Fig. 1). *Ceratophyllum demersum* changed the least in its dry weight (Fig. 2). During the treatment period, the changes in fresh weight, dry weight, and moisture content of three submerged plants showed statistically significant differences. In this process, the moisture content of all three plants decreased, and the most was *Hydrilla verticillata*, from 96.73% to 95.26%. *Vallisneria natans* and *Ceratophyllum demersum* were from 96.23% to 94.02% and 96.84 % to 96.66%, respectively.

Changes in pH: The initial pH of the treatment water was

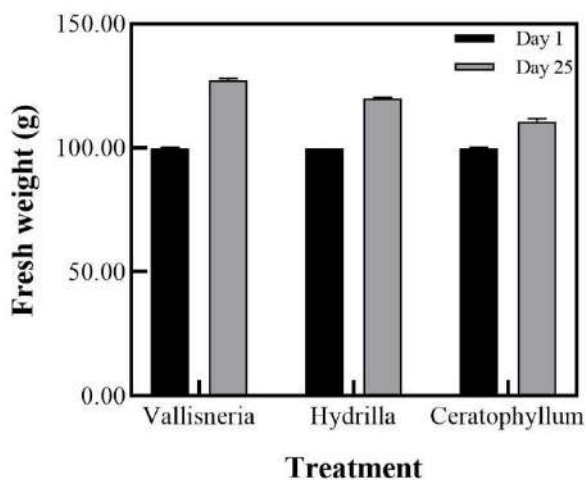


Fig. 1: Fresh weight changes of the three submerged plants on the 1st and 25th day.

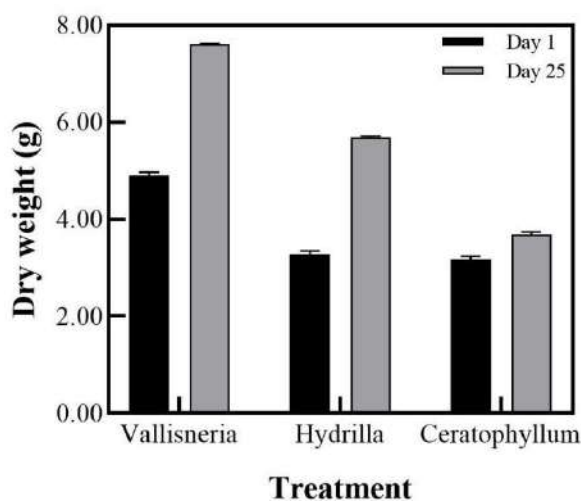


Fig. 2: Dry weight changes of the three submerged plants on the 1st and 25th day.

7.80, and there were differences in the changes in pH among the different treatments (Fig. 3). The differences between the pH of the blank control and the pH of different treatments, including three submerged plants and their combinations, were used to analyze the pH changes of eutrophic water. At the beginning of the five days, the differences between the pH of the blank control and that of all treatments increased slightly between 0.00 and 0.60. From the 5th to the 15th, the differences between the pH of the blank control and that of treatments B, C, and H continued to decrease; the differences between the pH of the blank control and that of treatments D and F increased after the first decrease, while the other two treatments decreased after the first increase. After the 15th, except for C and D, other treatments all increased slightly. And during the experiment period, the

pH in all the samples remained slightly alkaline. At the beginning of the experiment, there were no statistically significant differences between the different treatments ($p < 0.05$). On the 5th, treatments B and C had significant differences from the control groups, respectively. Over the period, only treatments E and F had significantly different results from each other on the last sampling day. The pH differences between the blank control and the other treatments varied greatly at first but eventually became stable.

TP concentration reduction and removal rate: The TP content in each treatment decreased with treatment time. Comprehensive analysis showed that the TP content of the water decreased during the sampling days. After 25 days of treatment, the removal rates of TP content in eutrophic water

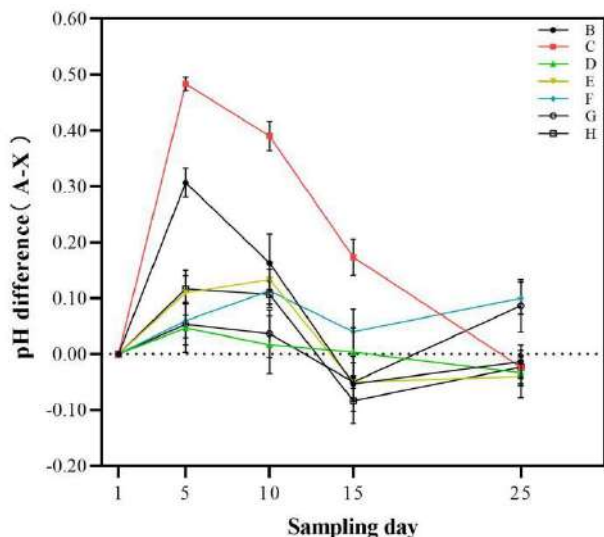


Fig. 3: Effects of different treatments on pH of eutrophic water.

by different submerged plant combinations were analyzed (Figs. 4 and 5).

The average TP content in the blank control decreased from $0.45 \text{ mg}\cdot\text{L}^{-1}$ to $0.32 \text{ mg}\cdot\text{L}^{-1}$. And corresponding values for treatment B were from $0.45 \text{ mg}\cdot\text{L}^{-1}$ to $0.22 \text{ mg}\cdot\text{L}^{-1}$; for treatment, C were from $0.45 \text{ mg}\cdot\text{L}^{-1}$ to $0.26 \text{ mg}\cdot\text{L}^{-1}$; for treatment D were from $0.45 \text{ mg}\cdot\text{L}^{-1}$ to $0.23 \text{ mg}\cdot\text{L}^{-1}$; for treatment, E were from $0.45 \text{ mg}\cdot\text{L}^{-1}$ to $0.21 \text{ mg}\cdot\text{L}^{-1}$; for treatment F were from $0.45 \text{ mg}\cdot\text{L}^{-1}$ to $0.19 \text{ mg}\cdot\text{L}^{-1}$; for treatment, G were from $0.45 \text{ mg}\cdot\text{L}^{-1}$ to $0.24 \text{ mg}\cdot\text{L}^{-1}$; and for treatment H were from $0.45 \text{ mg}\cdot\text{L}^{-1}$ to $0.20 \text{ mg}\cdot\text{L}^{-1}$.

At the end of the experiment, the differences between them and the blank control were significant ($P < 0.05$). On the 25th day, the removal rate of the blank control was 28.46%. Among all the treatments, treatment F had the highest removal rate at 57.53%, which was slightly higher than that of treatment H (55.41%). The removal rates of TP by treatments E, B, D, and G were 54.2%, 52.08%, 49.36%, and 46.93%, respectively. Treatment C had the lowest removal rate of TP at 42.7%. During the experiment, the variation trends of TP residues within treatments in water were similar. In the first 5 days of the experiment, the concentration decreased in a wide range and the removal rates were high, but they slowed down in the later period. After 25 days of treatments, treatment F showed only $0.19 \text{ mg}\cdot\text{L}^{-1}$. In this experiment, the TP contents were removed from the water by 42.70-57.53% in the plant treatments compared with the blank control.

TN concentration reduction and removal rate: In general, the TN content of water showed a decreasing trend over time,

and the control group was no exception. The TN removal rates of plant treatments were higher than those of the blank control (Figs. 6 and 7).

The TN content of each treatment decreased with the extension of treatment time to different degrees. The average TN content in the blank control decreased from $5.50 \text{ mg}\cdot\text{L}^{-1}$ to $1.69 \text{ mg}\cdot\text{L}^{-1}$. And corresponding values for treatment B were from $5.50 \text{ mg}\cdot\text{L}^{-1}$ to $0.44 \text{ mg}\cdot\text{L}^{-1}$; for treatment C, from $5.50 \text{ mg}\cdot\text{L}^{-1}$ to $1.06 \text{ mg}\cdot\text{L}^{-1}$; for treatment D, from $5.50 \text{ mg}\cdot\text{L}^{-1}$ to $0.54 \text{ mg}\cdot\text{L}^{-1}$; for treatment E, from $5.50 \text{ mg}\cdot\text{L}^{-1}$ to $0.61 \text{ mg}\cdot\text{L}^{-1}$; for treatment F, from $5.50 \text{ mg}\cdot\text{L}^{-1}$ to $0.51 \text{ mg}\cdot\text{L}^{-1}$;

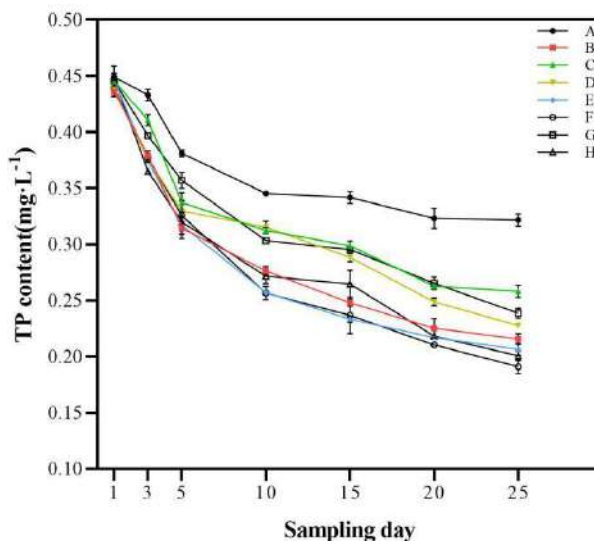
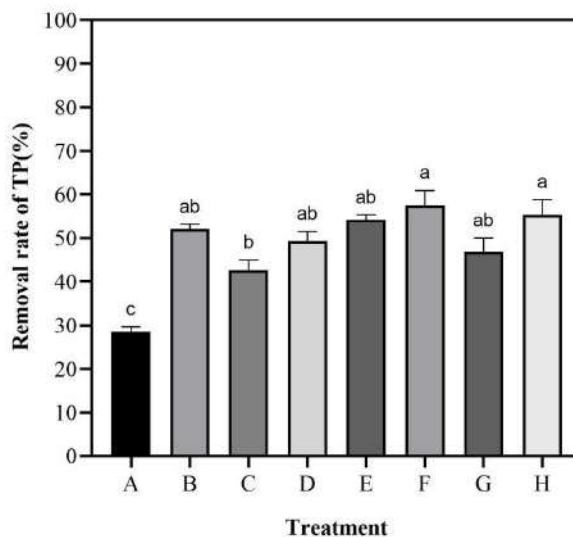


Fig. 4: Effects of different treatments on TP content of eutrophic water.



*Different low case letters above columns indicate statistical differences at $P < 0.05$.

Fig. 5: Removal rate of TP by different treatments.

for treatment G, from $5.50 \text{ mg}\cdot\text{L}^{-1}$ to $1.02 \text{ mg}\cdot\text{L}^{-1}$; and for treatment H, from $5.50 \text{ mg}\cdot\text{L}^{-1}$ to $0.47 \text{ mg}\cdot\text{L}^{-1}$.

The TN removal rates varied with plant combinations and treatment time. In our study, the TN removal rates of the treatment group containing plants were higher than those of the blank control, and the differences between them and the control group were significant ($P < 0.05$). On the 25th day, the removal rate of the blank control was 69.31%. Treatment B had the best removal rate of TN at 92.04%. The removal rates of TP by treatments H, F, D, and E were 91.38%, 90.76%, 90.24%, and 88.90%, respectively. Treatment C

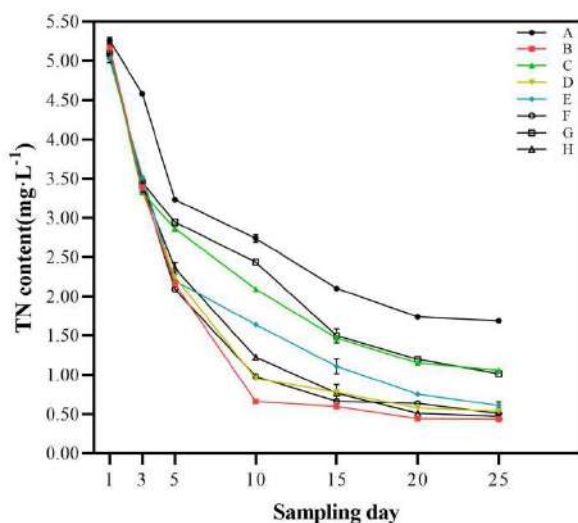
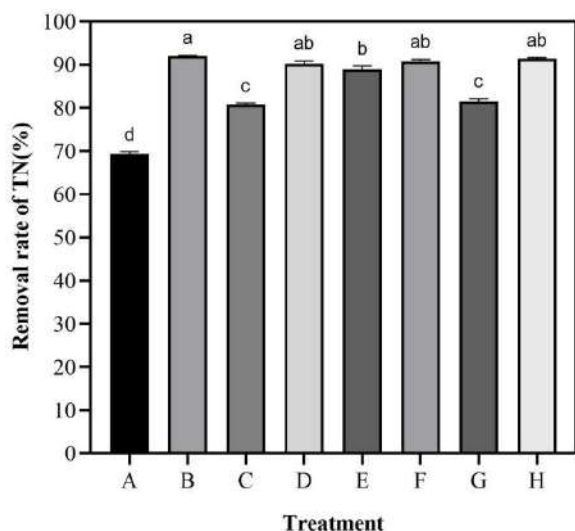


Fig. 6: Effects of different treatments on TN content of eutrophic water.



*Different low case letters above columns indicate statistical differences at $P < 0.05$.

Fig. 7: Removal rate of TN by different treatments.

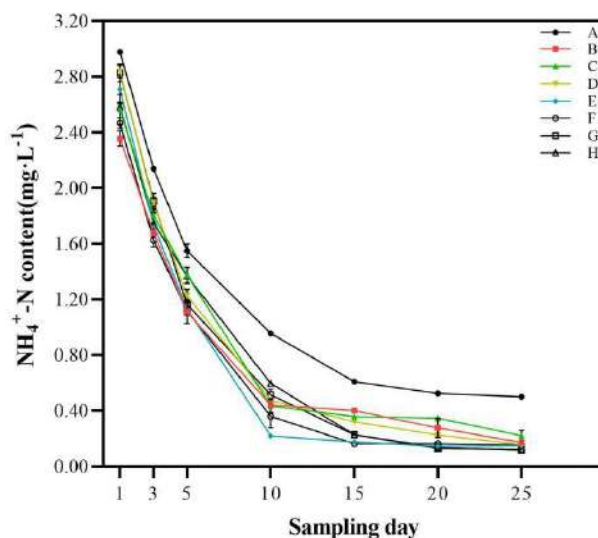


Fig. 8: Effects of different treatments on NH_4^+ -N content of eutrophic water.

had the lowest removal rate at 80.74%, a little lower than that of treatment G (81.53%).

NH_4^+ -N concentration reduction and removal rate:

During the experiment, all treatment groups had a certain removal effect on NH_4^+ -N in water, and the removal trends were almost the same (Fig. 8). At the end of day 25, the content of the blank control was $0.50 \text{ mg}\cdot\text{L}^{-1}$, and the final contents of all treatments were lower than $0.23 \text{ mg}\cdot\text{L}^{-1}$. There was little difference in the removal effect of NH_4^+ -N in different treatment groups. Among them, treatment G had the best effect, and the content of NH_4^+ -N in the final water was only $0.12 \text{ mg}\cdot\text{L}^{-1}$, and the removal rate was slightly higher than treatment H. Treatment B had the lowest removal effect, which was $0.22 \text{ mg}\cdot\text{L}^{-1}$.

NO_3^- -N concentration reduction and removal rate:

At the first five days of the experiment, the NO_3^- -N content in each treatment decreased rapidly, then the trend became gentle (Fig. 9). At the end of day 25, the content of the blank control was $1.13 \text{ mg}\cdot\text{L}^{-1}$, and the final contents of all treatments were lower than $0.55 \text{ mg}\cdot\text{L}^{-1}$. Treatment C had the best removal effect, with a final water content of less than $0.12 \text{ mg}\cdot\text{L}^{-1}$, followed by treatment B. In the process of detecting the content of this substance in water by submerged plants, the following conclusions were drawn by analyzing the experimental data. The removal effects of these three submerged plant monomers were better than those of the combined plant combinations under the same fresh weight.

DISCUSSION

Water eutrophication is one key cause of water pollution

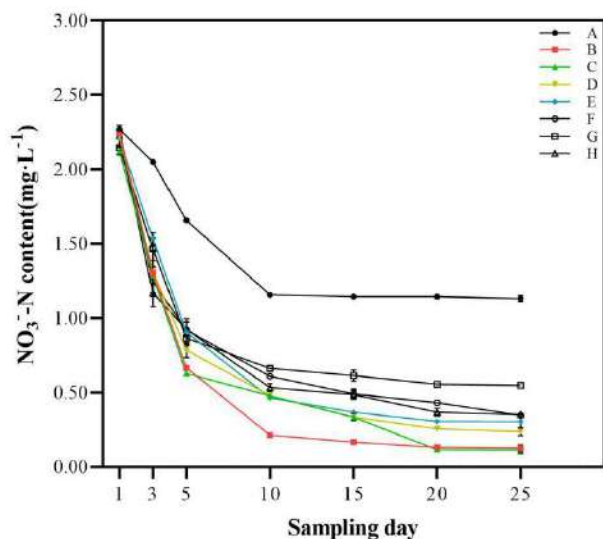


Fig. 9: Effects of different treatments on NO₃⁻-N content of eutrophic water.

(Dai et al. 2016) and a difficult problem of environmental pollution control (Quan et al. 2003). At present, there are many management methods for eutrophic water bodies, both at home and abroad. Whether it is to reduce the source of exogenous nutrients or take various measures to eliminate algae, existing methods cannot achieve a lasting and ideal effect (Gu et al. 2019). Effective control of nutrient elements in water bodies is considered to be the basic step in the management of water eutrophication and its impact on the environment (Rezania et al. 2021). Phytoremediation is a potentially suitable technology method to absorb large amounts of nitrogen, phosphorus, and plant substances during plant growth so as to avoid water eutrophication (Su et al. 2019). Submerged plants also have good ecological effects on water restoration.

The results showed that three submerged plants and their four combinations had played a significant role in purifying eutrophic water within 25 days. Generally speaking, the biomass of the studied plants increased with time during the test period, indicating that they all grew normally in the test environment and had strong ecological adaptability to nitrogen and phosphorus (Su et al. 2019). The pH differences between each treatment group and the blank control also changed from large to small, and the pH changes gradually tended to be stable. In this regard, the intervention of submerged plants also had a certain balancing effect on the pH of the water. With the change in treatment time, the pH of each group had been kept slightly alkaline, which was consistent with other results (Wang et al. 2019). After 25 days of the experiment, the concentration of total nitrogen, total phosphorus, ammonia nitrogen, and nitrate nitrogen in

each group showed a downward trend, which was also the same as some previous research results (Yang et al. 2018).

However, this research also had limitations. Many studies have used artificial sewage (Yu et al. 2019) with different initial concentrations of nitrogen and phosphorus. This research only used one concentration combination in water. This led to a lack of comprehensive analysis of the purification capacity of three submerged plants. This experiment did not simulate the living environment of submerged plants under natural conditions and had no impact from natural precipitation. The biological experiment amount was on a small scale, which would also lead to the deviation of the research results.

Although there were some limitations in this experiment, three common submerged plants in Jiangsu Province were selected for this research. The experimental results applied to the ecological environment of this region and could provide a theoretical basis and practical experience for the ecological protection of this region. Moreover, in the current research on the role of aquatic plants in the remediation of water eutrophication, more researchers have studied emergent plants and floating plants, as well as their combinations. Therefore, this experiment provided new ideas and experience for further study of submerged plants and their combinations for aquatic ecological restoration.

CONCLUSIONS

The results of this experiment showed that, compared with the blank control without submerged plants, the submerged plants and their combinations could improve the removal effect of nitrogen and phosphorus in eutrophic water and reduce the degree of eutrophication in the water. Among the three submerged plants and four combinations selected in this experiment, each treatment had a purification effect. Both *Vallisneria natans* and *Ceratophyllum demersum* had a higher capacity for monomer purification in submerged plants. Their removal rates of TP and TN from water were 92.04%, 52.08%, and 90.24%, 49.36%, respectively. *Vallisneria natans* showed better purification ability, which was consistent with many existing research results. From the aspect of combinations of submerged plants, treatments F (50 g *Vallisneria natans* plus 50 g *Ceratophyllum demersum*) and H (33.3 g of each of the three plants) were better. These two combinations removed more nitrogen and phosphorus from eutrophic water. Meanwhile, *Hydrilla verticillata* had a poorer purification capacity than others.

In this experiment, the same initial biomass of submerged plants in each treatment was used as a unified standard. The microbial community is often studied as an important part of the water ecosystem, which is of great significance

to water restoration. However, no differences in microbial communities in water before and after the experiment were found in this study. In addition, photosynthetic indexes in submerged plants were not detected in this experiment, so more comprehensive discussions and comparisons could not be carried out. The interaction between submerged plants will be carried out in future experiments.

ACKNOWLEDGMENTS

This work was financially supported by Soochow University & Suzhou Yuanke Collaborative innovation Center Project (No. SY2022006); National Natural Science Foundation of China: General Program (No. 52178046); Major university-enterprise cooperation project of Soochow University (No. P113403020).

REFERENCES

- Dai, S. and Li Q.W. 2016. Removal efficiency of eight plants in two different ecological water. *Journal of Northeast Forestry University*, 44(7): 80-83.
- Du, S.T., Shentu, J.L., Luo, B.F., Shamsi, I.H., Lin, X.Y., Zhang, Y.S. and Jin, C.W. 2011. Facilitation of phosphorus adsorption onto sediment by aquatic plant debris. *Journal of Hazardous Materials*, 191(1-3): 212-218.
- Fan, Y.Y. 2007. The research on the effect of the growth of submerged plants and physiological of eutrophication of nitrogen and phosphorus. Wuhan: Central China Normal University
- Feng, Q., Yi, J., Liu, S.M., Zhao, F.B., Zhang, J. and Chai, X.L. 2020. The pollution situation, treatment techniques and countermeasures of urban black and odors water in China. *Environmental Engineering*, 38(08): 82-88.
- Gao, G. 1996. Effectives of purification of aquaculture wastewater by *Ele alga* and *Helicobacter vulgaris*. *Journal of Lake Sciences*, 8(2): 184-188.
- Gu, C., Li, F., Xiao, J., Chu, S., Song, S. and Wong, M.H. 2019. A novel submerged *Rotala rotundifolia*, its growth characteristics and remediation potential for eutrophic waters. *Scientific Reports*, 9(1): 14855-9.
- Huang, X.L., Guo, Y.M., Wan, B., Hu, H.J., Tong, L. and Li, X.P. 2018. Effects of submerged plant restoration on ecological environment of urban eutrophic lakes. *Environmental Engineering*, 36(07): 17-21.
- Lei, T.W., Wei, X.F., Dai, Y.L., Guo, Y.H. and Xu, J.X. 2015. Research on water purification of 6 common submerged Macrophytes. *Journal of Anhui Agricultural Sciences*, 43(36): 160-161+196.
- Li, L.Y. and Du, G.S. 2010. Study on allelopathic inhibition of algae by aquatic higher plants. *World Sci. Tech. R & D*, 32(04): 505-508.
- Quan, W.M., Shen, X.Q. and Yan, L.J. 2003. Advances in research of biological purification of European water body. *Chinese Journal of Applied Ecology*, 14 (11): 2057-2061.
- Rezania, S., Kamyab, H., Rupani, P.F., Park, J., Nawrot, N., Wojciechowska, E., Yadav, K.K., Lotfi Ghahroudi, M., Mohammadi, A.A., Thirugnana, S.T., Chelliapan, S. and Cabral-Pinto, M.M.S. 2021. Recent advances on the removal of phosphorus in aquatic plant-based systems. *Environmental Technology & Innovation*, 24: 101933.
- Rice, P.J., Anderson, T.A. and Coats, J.R. 1997. Phytoremediation of herbicide-contaminated surface water with aquatic plants. *Phytoremediation of Soil and Water Contaminants*, 664: 133-151.
- Shao, J.H., Wu, Z.X., Yu, G.L., Peng, X. and Li, R.H. 2009. Allelopathic mechanism of pyrogallol to *Microcystis aeruginosa* PCC7806 (Cyanobacteria): From views of gene expression and antioxidant system. *Chemosphere*, 75: 924-928.
- Su, F., Li, Z., Li, Y., Xu, L., Li, Y., Li, S., Chen, H., Zhuang, P. and Wang, F. 2019. Removal of total nitrogen and phosphorus using single or combinations of aquatic plants. *International Journal of Environmental Research and Public Health*, 16(23): 4663.
- Wang, L. 2014. Genetic variation of aquatic macrophytes in diverse environments and their phenotypic adaptation to interference. Wuhan: Central China Normal University.
- Wang, L.F., Yang, Y., Guo, G.L., Luo, K.D., Mao, J.P. and Wang, B. 2019. Purification efficiency of eutrophic water by different aquatic plant combinations. *Nature Environment and Pollution Technology*, 18(2): 479-483.
- Yang, J., Qi, Y., Li, H. and Xu, G. 2018. Comparison of nitrogen and phosphorus purification effects of different wetland plants on eutrophic water. IOP conference series. *Earth and Environmental Science*, 113(1): 12042.
- Yu, S., Miao, C., Song, H., Huang, Y., Chen, W. and He, X. 2019. Efficiency of nitrogen and phosphorus removal by six macrophytes from eutrophic water. *International Journal of Phytoremediation*, 21(7): 643-51.
- Zhang, Y., Wang, S.R., Li, C.X., Wang, C.M. and Wu, E. 2009. Restoration effects of submerged plants on eutrophic water bodies and their research prospects. *Inner Mongolia Prataculture*, 21(04): 17-21.
- Zhang, Y.J., Liu, X.P., Jin, J., Dong, Y., Duan, T., Zhang, M.M., Zhang, L.T. and Li, Z. 2012. Research progress on water purification by submerged plants. *Ecological Mode*, 30(27): 72-79.
- Zhao, T., Guan, X.M. and Yang, C.S. 2004. The types, sources and harm of water pollutants to human body. *Heilongjiang Science and Technology of Water Conservancy*, 31(02): 99.
- Zhou, J., Liu, Y., Liu, Y.F., Chen, S.H., Gao, J.Q. and Zhang, R.Q. 2012. Removal of fluoride from water by five submerged Plants. *Bulletin of Environmental Contamination and Toxicology*, 89(2): 395-399.



Experimental Aeration Investigations on Supersaturated Total Dissolved Gas Dissipation

Yuanbo Yao , Huixia Yang[†], Yunyun Wang, Jiajia Liang and Ling Yang

College of Civil Engineering, Guizhou University, Guiyang 550025, Guizhou, China

[†]Corresponding author: Huixia Yang; bt-yanghuixia@163.com

Nat. Env. & Poll. Tech.
Website: www.neptjournal.com

Received: 27-10-2022

Revised: 08-12-2022

Accepted: 02-01-2023

Key Words:

Aeration
Supersaturated TDG dissipation
Aeration rate
Aeration depth
Aeration aperture

ABSTRACT

Supersaturation of total dissolved gas (TDG) is mainly produced by high dam discharge, excess oxygen production by plant photosynthesis, and a sharp increase in water temperature, which may directly lead to fish and aquatic organisms suffering from “gas bubble disease” (GBD) or death. Aeration was one of the methods used to solve the dissipation of supersaturated TDG. In this paper, aeration had an obvious promotion effect on the dissipation of supersaturated TDG. For the calculation and analysis of supersaturated TDG dissipation coefficient, the aeration rate was proportional to TDG dissipation coefficient and had a promoting effect on it, while the aeration depth and aeration aperture were inversely proportional to TDG dissipation coefficient and played an inhibitory effect on it. The supersaturated TDG dissipation coefficient was affected by a factor of $K_{TDG,Q} > K_{TDG,D} > K_{TDG,H}$. A quantitative relationship between the supersaturated TDG dissipation coefficient and aeration rate, aeration depth, and aeration aperture was obtained, respectively, as well as important expressions with comprehensive effect factors; their margins of error average within 10%. This research method has an important guiding significance for improving the living environment of fish and other aquatic organisms, alleviating the adverse effects of supersaturated TDG.

INTRODUCTION

In recent decades, hydroelectric power generation had become one of the main new energy sources, which not only saved the exploitation of fossil energy and avoided air pollution but also improved people’s living environments (Cai 2016, Zuo 2005). However, some researchers found that many fish died in the dam watershed (Tan et al. 2006); they believed that when the high dam discharged, the gas was drawn into the water and the strong turbulence in the water cushion pond caused the surface of the water to inhale, the two methods might lead to a large number of air bubbles in the water, resulting in a significant increase in the dissolved gas content (Cheng et al. 2005), this formed supersaturated total dissolved gas (TDG) (Weitkamp et al. 1980, Harvey 1967), which may directly lead to “gas bubble disease” (GBD) and even death of fish and organisms in water (Wu et al. 2021, Yuan et al. 2017). In addition, excess oxygen production in plant photosynthesis and a rapid increase in water temperature might also lead to total dissolved gas supersaturation in water (Agarwal et al. 2001, Boyd et al.

1994). Among them, the dissipation of supersaturated TDG belonged to the dissipation at the interface of the air-water and water, and both dissipation processes were affected by factors such as water turbulence, temperature, bubble size, and concentration variation (Wang et al. 2019).

So far, many researchers have proposed their own mitigation measures for reducing the generation of supersaturated TDG and accelerating its release. They set up deflectors in the spillway, optimized the way of water discharge, and adjusted cascade reservoirs (Monk et al. 2011, Fu et al. 2010, Politano et al. 2012), and Colt et al. (1984) used siphon devices and packed columns to reduce the supersaturated TDG concentration in the culture pond. Feng et al. (2012, 2014, 2017) also found that the design of a water-blocking medium with different arrangement forms, densities, and surface roughness was conducive to the dissipation of supersaturated TDG under the action of the column as a water-blocking medium; this method was also conducive to the release of supersaturated TDG under certain conditions of sand content and turbulent intensity. Huang et al. (2017) added adsorbent substances (activated carbon) into supersaturated water, which significantly promoted the dissipation of supersaturated TDG, and the

ORCID details of the authors:

Yuanbo Yao: <https://orcid.org/0000-0003-1395-8130>

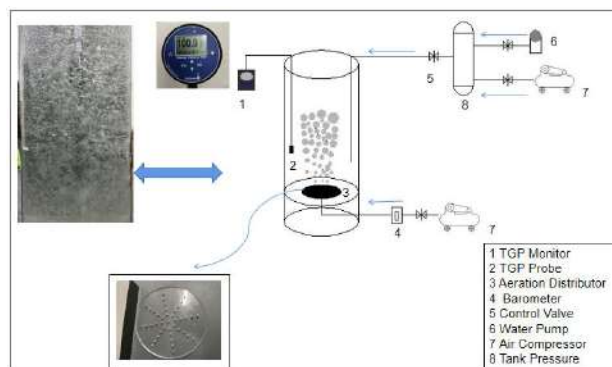


Fig. 1: Experiments and sketches.

effect of substances with a large surface area was more obvious. Du et al. (2017) designed a submersible pump, and different pump numbers, powers, placement methods, and drainage directions were conducive to the dissipation of supersaturated dissolved oxygen. Liu et al. (2015) found that a certain wind speed can promote the dissipation of supersaturated TDG under different wind speeds and fit their relational expressions. Based on the gas-liquid mass transfer theory, Huang et al. (2016) used the aeration method to have a significant effect on the dissipation of dissolved oxygen (DO) and obtained the relationship between its dissipation coefficient (release rate) and aeration conditions. Microporous aeration can increase dissolved oxygen. Cheng et al. (2013) found a relationship between oxygen dissipation and microporous conditions. Li et al. (2007) summarized the theory of the optimal bubble group for microporous aeration and obtained the regular changes of oxygen mass transfer rate, bubble size, and aeration performance.

Under experimental aeration conditions, the effect of aeration on the dissipation of supersaturated TDG and the expression of its dissipation coefficient and aeration conditions (aeration rate, aeration depth, and aeration aperture) were studied to provide new methods and research directions for alleviating the adverse effects of supersaturated TDG.

MATERIALS AND METHODS

Laboratory instrumentations: the supersaturated TDG generation device in Fig. 1 was modified and designed with reference to Li et al. (2010). The experimental device mainly includes an aeration distributor ($D = 0.6, 0.9, \text{ and } 1.2 \text{ mm}$), tank pressure ($D = 0.6 \text{ m}$, $h = 1.2 \text{ m}$), barometer ($Q = 0.5\text{--}5.0 \text{ m}^3 \cdot \text{h}^{-1}$), release tank ($D = 0.4 \text{ m}$, $H = 1.8 \text{ m}$), measuring instrument TGP ($0 - 600 \%$, $\pm 0.1\%$), air compressor ($90 \text{ L} \cdot \text{min}^{-1}$).

Experimental steps: During the experiment, the water pumped water, the air compressor input gas, which

was mixed in the venturi tube, then entered the autoclave together to form supersaturated water, and we put the supersaturated water into a square water tank equipped with an aeration distributor. When the water depth reached the predetermined depth, the set aeration rate was mobilized, and the TGP started to continuously measure the supersaturated TDG concentration in the water and stopped recording when the concentration reached about 100%. Table 1 was the experimental aeration condition. There were 36 groups of experiments.

EXPERIMENTAL RESULTS ANALYSIS AND LINEAR FITTING

Analysis of Experimental Results

Fig. 2 shows the experimental aeration conditions with aeration aperture $D = (0.6, 0.9, 1.2) \text{ mm}$, aeration depth $H = (0.4, 0.8, 1.2) \text{ m}$, and aeration rate $Q = (0.5, 1.0, 1.5, 2.0) \text{ m}^3 \cdot \text{h}^{-1}$. It can be seen from this that the initial concentration of supersaturated TDG is about 140%, which belongs to the supersaturated state, and then gradually reaches the saturated state (Colt 1983). Moreover, under the same aeration depth and aeration aperture, the increase in the aeration rate causes the dissipation time to decrease, but under other same conditions, the increase in aeration depth and aeration aperture leads to an increase in the dissipation time. The reason analysis shows that: (1) the increase in aeration rate enhances the turbulence intensity of the water body, increases the number of bubbles in the water, and also strengthens the mass transfer between the bubble interface and the water surface (Witt et al. 2018, Chanson 2004). (2) The increase of water depth leads to the weakening of the turbulence

Table 1: Experimental aeration conditions.

Aeration depth (H/m)	Aeration aperture (D/mm)	Aeration rate ($Q/\text{m}^3 \cdot \text{h}^{-1}$)
0.4, 0.8, 1.2	0.6, 0.9, 1.2	0.5, 1.0, 1.5, 2.0

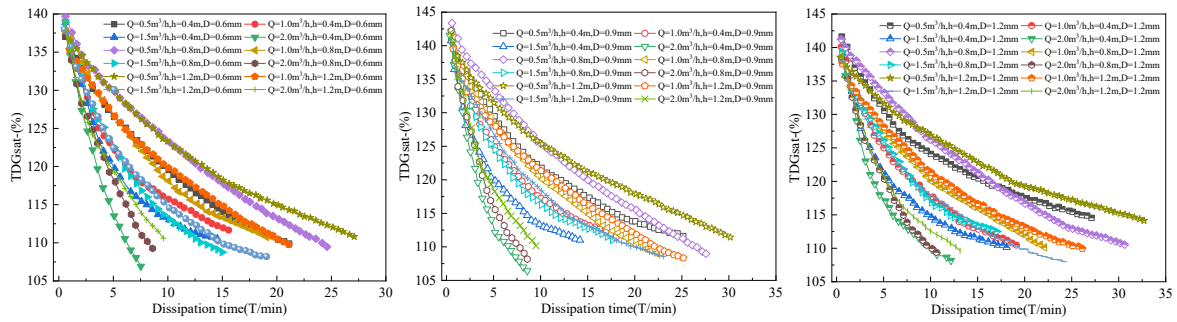


Fig. 2: The dissipation process of supersaturated TDG.

intensity caused by the bubbles in water, and the increase of the aeration aperture causes the bubble diameter to become larger, so that the number of bubbles at the same aeration rate decrease, and the two factors lead to the mass transfer at the bubble interface and water surface mass transfer being weakened (Cao et al. 2019, Huang et al. 2010).

Supersaturated TDG Linear Fitting

To further analyze the effect of aeration on the release of

supersaturated TDG, a first-order kinetic equation was introduced to change the saturation of supersaturated TDG with time as equation (1) (U.S. Army Corps of Engineers 2005), with the fitting of results shown in Table 2.

$$\frac{d(G - G_{eq})}{dt} = k_{TDG}(G - G_{eq}) \quad \dots(1)$$

Where G is the TDG saturation (%), G_{eq} is the equilibrium saturation of TDG (usually 100%), k_{TDG} is the dissipation

Table 2: Dissipation coefficient k_{TDG}

Number	Aeration aperture (D/mm)	Aeration depth (H/m)	Aeration rate (Q/m ³ •h)	k_{TDG}	R^2
1.	0.6	0.4	0.5	0.063 ± 0.00	0.999
2.	0.6	0.4	1.0	0.073 ± 0.00	0.968
3.	0.6	0.4	1.5	0.092 ± 0.00	0.949
4.	0.6	0.4	2.0	0.245 ± 0.00	0.998
5.	0.6	0.8	0.5	0.056 ± 0.00	0.997
6.	0.6	0.8	1.0	0.067 ± 0.00	0.990
7.	0.6	0.8	1.5	0.102 ± 0.00	0.993
8.	0.6	0.8	2.0	0.172 ± 0.00	0.996
9.	0.6	1.2	0.5	0.046 ± 0.00	0.998
10.	0.6	1.2	1.0	0.062 ± 0.00	0.998
11.	0.6	1.2	1.5	0.083 ± 0.00	0.990
12.	0.6	1.2	2.0	0.136 ± 0.00	0.993
13.	0.9	0.4	0.5	0.050 ± 0.00	0.987
14.	0.9	0.4	1.0	0.067 ± 0.00	0.977
15.	0.9	0.4	1.5	0.088 ± 0.00	0.951
16.	0.9	0.4	2.0	0.226 ± 0.00	0.995
17.	0.9	0.8	0.5	0.054 ± 0.00	0.997
18.	0.9	0.8	1.0	0.067 ± 0.00	0.998
19.	0.9	0.8	1.5	0.072 ± 0.00	0.969
20.	0.9	0.8	2.0	0.198 ± 0.00	0.997
21.	0.9	1.2	0.5	0.039± 0.00	0.996
22.	0.9	1.2	1.0	0.060 ± 0.00	0.996
23.	0.9	1.2	1.5	0.067 ± 0.00	0.991
24.	0.9	1.2	2.0	0.151 ± 0.00	0.990

Number	Aeration aperture (D/mm)	Aeration depth (H/m)	Aeration rate (Q/m ³ ·h)	k_{TDG}	R^2
25.	1.2	0.4	0.5	0.036 ± 0.00	0.970
26.	1.2	0.4	1.0	0.069 ± 0.00	0.985
27.	1.2	0.4	1.5	0.071 ± 0.00	0.946
28.	1.2	0.4	2.0	0.133± 0.00	0.968
29.	1.2	0.8	0.5	0.047 ± 0.00	0.999
30.	1.2	0.8	1.0	0.057 ± 0.00	0.997
31.	1.2	0.8	1.5	0.070 ± 0.00	0.976
32.	1.2	0.8	2.0	0.141 ± 0.00	0.999
33.	1.2	1.2	0.5	0.030 ± 0.00	0.992
34.	1.2	1.2	1.0	0.051 ± 0.00	0.997
35.	1.2	1.2	1.5	0.064± 0.00	0.994
36.	1.2	1.2	2.0	0.107 ± 0.00	0.983

coefficient (release rate) (h⁻¹), and T is the dissipation time(h).

It can be seen from Table 2 that the error values of the supersaturated TDG dissipation coefficient are relatively small, and the average correlation coefficient exceeds 0.99, which has certain practical significance. Among them, when the aeration rate increases from 0.5 m³.h⁻¹ to 2.0 m³.h⁻¹, the average increment of the supersaturated TDG dissipation coefficient is 245.62%; when the aeration depth increases from 0.4 m to 1.2 m, the average reduction of the supersaturated TDG dissipation coefficient is 24.74%; and when the aeration aperture increases from 0.6 mm to 1.2 mm, the average reduction of the supersaturated TDG

dissipation coefficient is 31.75%, which shows that effect on the supersaturated TDG is $K_{TDG,Q} > K_{TDG,D} > K_{TDG,H}$. Therefore, it is shown that the aeration rate can promote the release of supersaturated TDG, while the aeration depth and aeration aperture inhibit its dissipation.

Relationship Between $K_{TDG,Q}$ and Aeration Rate

According to the relevant research results of the effect of aeration on the re-oxygenation dissipation coefficient, the relationship between the re-oxygenation dissipation coefficient and aeration did not increase linearly (Mavinic et al. 1974, Cheng et al. 2013). The aeration rate is the first important factor, the reason analysis shows that the increasing

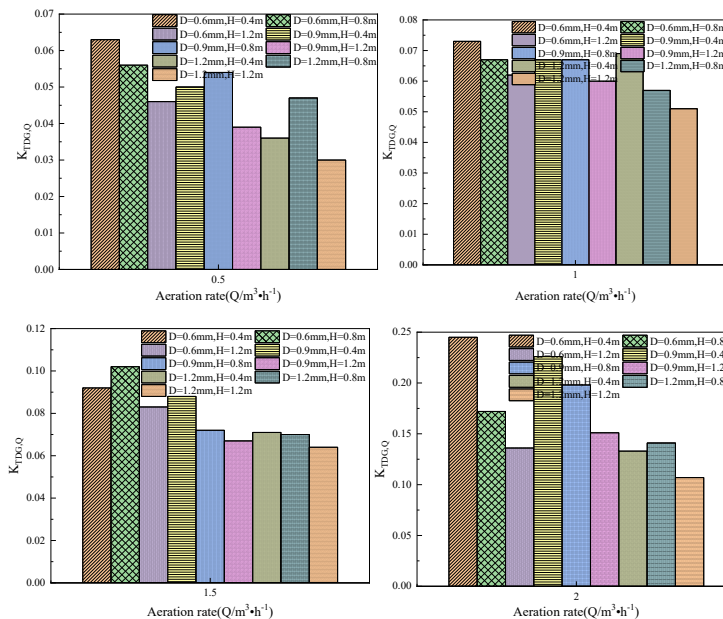


Fig. 3: Relationship between aeration rate and dissipation coefficient.

water depth leads to the weakening of the turbulent intensity of the water induced by bubbles, thus weakening the mass transfer effect of TDG at the water-air interface (Cheng et al. 2005, Huang et al. 2010). The aeration rate and dissipation coefficient are brought into the ORIGIN software to obtain Fig. 3 and the multivariate nonlinear regression analysis of SPSS to obtain the proportional relationship between the two as equation (2).

$$K_{TDG,Q} = 0.153\left(\frac{Q}{2.0}\right)^{1.296} \dots(2)$$

where $K_{TDG,Q}$ is the dissipation coefficient (release rate) (h^{-1}), Q is the aeration rate (m^3/h).

Relationship Between $K_{TDG,D}$ and Aeration Aperture

Aeration aperture is the second important factor, the reason analysis shows that the increasing aeration aperture decreases the density of the bubble group in the water tank, which weakens the turbulence intensity of the water and the transfer effect of the gas-liquid interface (Cheng et al. 2014, 2015). The aeration aperture and dissipation coefficient are brought into the ORIGIN software to obtain Fig. 4, and the inverse relationship between the two is obtained in the multivariate nonlinear regression analysis of SPSS as equation (3).

$$K_{TDG,D} = 0.102\left(\frac{0.6}{D}\right)^{0.395} \dots(3)$$

where $K_{TDG,D}$ is the dissipation coefficient (release rate) (h^{-1}), D is the aeration aperture(mm).

Relationship Between $K_{TDG,H}$ and Aeration Depth

Aeration depth is the third important factor; the reason for this is that the analysis shows that the increasing water depth leads to the weakening of the turbulent intensity of the water induced by bubbles, thus weakening the mass transfer effect of TDG at the water-air interface (Cheng et al. 2005, Huang et al. 2010). The aeration depth and dissipation coefficient are brought into the ORIGIN software to obtain Fig. 5 and the inverse relationship between the two is obtained in the multivariate nonlinear regression analysis of SPSS as equation (4).

$$K_{TDG,H} = 0.103\left(\frac{0.4}{H}\right)^{0.249} \dots(4)$$

where $K_{TDG,H}$ is the dissipation coefficient (release rate) (h^{-1}), H is the aeration depth (m).

Relationship Between K_{TDG} and Q, D and H

In the process of an aeration experiment, the supersaturated

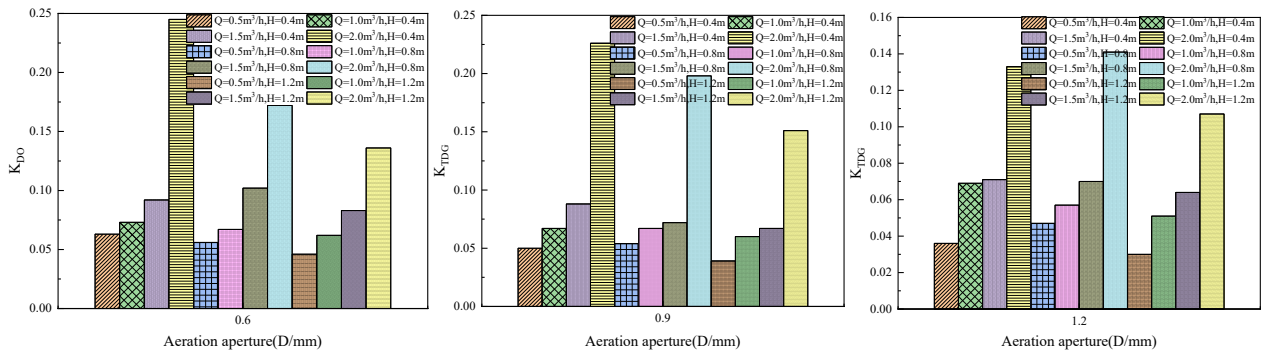


Fig. 4: Relationship between aeration aperture and dissipation coefficient.

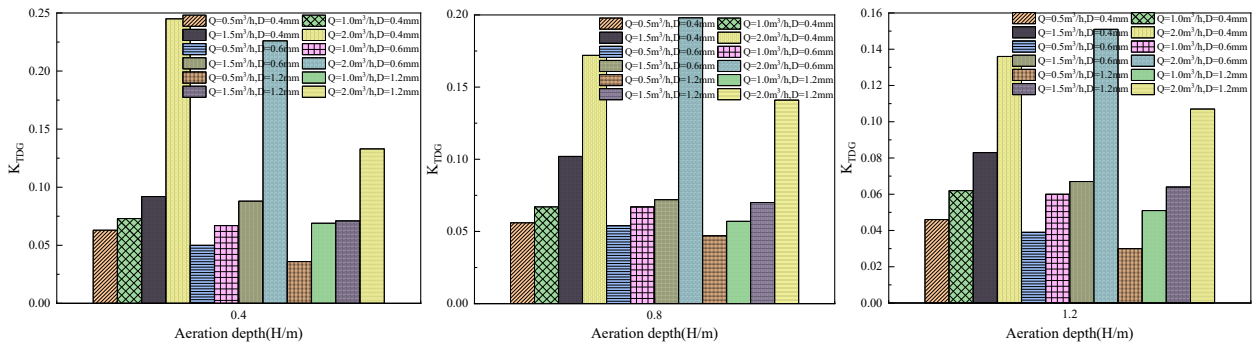


Fig. 5: Relationship between aeration depth and dissipation coefficient.

Table 3: Ranges of dissipation coefficients in the quantitative relationship.

Q_0	D_0	H_0	α	β_1	β_2	β_3
2.0	0.6	0.4	0.211	1.322	0.420	0.294

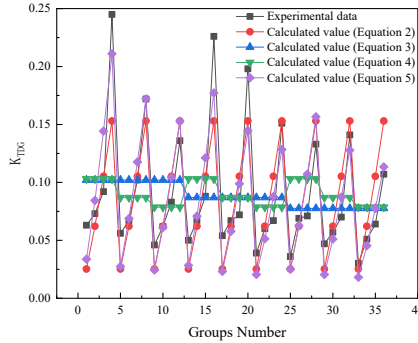


Fig. 6: Error between experimental data and calculated value

TDG release coefficient is mainly affected by the aeration rate, aeration aperture, and aeration depth. According to the specific tank size and experimental data, all the experimental values are brought into the multivariate nonlinear regression analysis of SPSS, and the quantitative relationship between TDG dissipation coefficient and initial value is shown in Table 3, and their relationship is obtained as equation (5).

$$K_{TDG} = \alpha \left(\frac{Q}{Q_0}\right)^{\beta_1} \left(\frac{D}{D_0}\right)^{\beta_2} \left(\frac{H}{H_0}\right)^{\beta_3} \rightarrow K_{TDG} = (0.211) \left(\frac{Q}{2.0}\right)^{1.322} \left(\frac{0.6}{D}\right)^{0.420} \left(\frac{0.4}{H}\right)^{0.294} \dots(5)$$

where K_{TDG} is the dissipation coefficient (release rate) (h^{-1}), Q is the aeration rate ($m^3 \cdot h^{-1}$), D is the aeration aperture (mm), H is the aeration aperture (m).

Errors Between Experimental Date and Calculated Values

Drawing on the former error analysis method (Cheng et al. 2015), the root mean square error (6) and the absolute average error (7) were used for error analysis to judge the availability of the equation. The error is obtained as shown in Fig. 6.

$$RMSE = \sqrt{\frac{\sum_{i=1}^n (a_i - b_i)^2}{n}} \dots(6)$$

$$AME = \frac{\sum_{i=1}^n |a_i - b_i|}{n} \dots(7)$$

For equation 2, the error of RMSE is 2.99% and AME is 2.25%, the error of RMSE is 5.12% and AME is 3.91% for equation 3, the error of RMSE is 5.12% and AME is 4.04% for equation 4 and the error of RMSE is 2.40% and AME is 1.97% for equation 5. Their errors are all within 10%. This shows that the quantitative relationship between the supersaturated TDG release coefficient and aeration rate,

aeration aperture and aeration depth can reflect the effect of aeration on the release of supersaturated TDG, and has strong applicability in practical environmental application engineering.

DISCUSSION

- (1) TDG dissipation is related to many factors, such as bubble area, turbulence intensity of the water body, temperature, and so on. Due to limited experimental conditions, the influence of these factors on TDG dissipation needs to be further studied in the next step.
- (2) At present, aeration plays an obvious role in promoting the TDG dissipation process, and the influence relationship between aeration rate, aeration depth, and aeration aperture on release coefficient is preliminarily obtained as equation (5). However, the application of this equation requires further systematic experimental research and theoretical analysis, summarizes the evolution law of TDG dissipation, and establishes a more generally applicable quantitative relationship between the dissipation process and the aeration conditions.
- (3) A natural water body is affected by water velocity, seasonal hydrological conditions, and complex geological structures. If the actual supersaturated TDG river basin is aerated, this will be disturbed by unknown problems. Aeration in local river basins may effectively mitigate the harm of supersaturated TDG.

CONCLUSION

Under aeration conditions, aeration can promote the dissipation of supersaturated TDG. The aeration rate is

proportional to the dissipation coefficient of supersaturated TDG and promotes its release, while the aeration depth and aeration aperture are related to the dissipation coefficient of supersaturated TDG in an inversely proportional relationship and inhibit its dissipation, as well as affect the size of the dissipation coefficient of supersaturated TDG as $K_{TDG,Q} > K_{TDG,D} > K_{TDG,H}$. A quantitative relationship between the supersaturated TDG dissipation coefficient and the aeration rate, aeration aperture, and aeration depth, respectively, is obtained: $K_{TDG,Q} = 0.153(\frac{Q}{2.0})^{1.296}$,

$$K_{TDG,D} = 0.102(\frac{0.6}{D})^{0.395}, \quad K_{TDG,H} = 0.103(\frac{0.4}{H})^{0.249} \quad \text{and the}$$

important expressions of the comprehensive effect factors:

$$K_{TDG} = (0.211)(\frac{Q}{2.0})^{1.322}(\frac{0.6}{D})^{0.420}(\frac{0.4}{H})^{0.294}. \quad \text{Their errors are all within}$$

10%.

Aeration is one of the important methods to mitigate the adverse effects of supersaturated TDG, and it has important guiding significance for exploring and mitigating the harm of supersaturated TDG.

ACKNOWLEDGEMENTS

The article is supported by: National Natural Science Foundation of China (Grant No.51709053) and the Science and Technology Fund of Guizhou Province [No.QKHJ-2019-1117].

REFERENCES

- Agarwal, A., Ng, W.J. and Liu, Y. 2011. Principle and applications of microbubble and nanobubble technology for water treatment. *Chemosphere*, 84(9): 1175-1180.
- Boyd, C.E., Watten, B.J. and Goubier, V. 1994. Gas supersaturation in surface waters of aquaculture ponds. *Aquacultural Engineering*, 13(1): 31-39.
- Cai, X.Q. 2021. Analysis on comparative advantages of hydroelectric power generation. *Science and Technology Innovation and Application*, (2016-18): 193-193. (In Chinese)
- Cao, L., Li, Y. and An, R. 2019. Effects of water depth on GBD associated with total dissolved gas supersaturation in Chinese sucker (*Myxocyprinus asiaticus*) in upper Yangtze River. *Scientific Reports*, 9(1): 1-8.
- Chanson, H. 2004. Air-water flows in water engineering and hydraulic structures. Basic processes and metrology. *Hydraulics of Dams and River Structures*, 3-16.
- Cheng, X.J., Chen, Y.C., Gao, Q.H. and Chen, Y. 2005. Analysis on supersaturated reoxygenation of dam body discharge of Three Gorges Reservoir. *Journal of Hydropower*, 6: 62-67. (In Chinese)
- Cheng, X.J., Xie, J., Yu, D.G. and Zeng, Y.X. 2013. Calculation and analysis of oxygen mass transfer at aerated oxygen-enriched micro-bubble-water interface and water surface. *Journal of Agricultural Engineering*, 29(13): 190-199. (In Chinese)
- Cheng, X.J., Zeng, Y.X., Xie, J. and Gong W.B. 2014. Effect of microporous aeration flow rate and aeration pipe length on water oxygenation performance. *Journal of Agricultural Engineering*, 30(22): 209-217. (In Chinese)
- Cheng, X.J., Zeng, Y.X. and Xie, Y.N. 2015. Microporous aeration oxygen enrichment test and analysis at the bottom of pond. *Journal of Chinese Academy of Water Resources and Hydropower Sciences*, 13(05): 339-343. (In Chinese)
- Colt, J. and Bouck, G. 1984. Design of packed columns for degassing. *Aquacultural Engineering*, 3(4): 251-273.
- Colt, J. E. 1983. The computation and reporting of dissolved gas levels. *Water Research*, 17(8): 841-849.
- Du, K.K., Li, Y.F., Liu, L., Ru, H.J., Wu, X.X., Zhang, Y., Liu, X.J. and Ni, C.H. 2017. Preliminary study on the influence of turbulence on the release of supersaturated dissolved oxygen in water body. *Freshwater Fisheries*, 47(5): 21-25. (In Chinese)
- Feng, J., Li, R., Liang, R. and Shen, X. 2014. Eco-environmentally friendly operational regulation: an effective strategy to diminish the TDG supersaturation of reservoirs. *Hydrology and Earth System Sciences*, 18(3): 1213-1223.
- Feng, J.J., Li, R., Shi, C.H. and Zuo, J.C. 2017. Experimental study on the influence of water-resisting media on the release process of supersaturated total dissolved gas. *Journal of Southwest University for Nationalities (Natural Science Edition)*, 43(1): 89-94. (In Chinese)
- Feng, J.J., Li, R., Tang, C.Y. and Yong, X.D. 2012. Impact of sediment concentration on release process of supersaturated total dissolved gas. *Progress in Water Science*, 23(5): 702-708. (In Chinese)
- Fu, X., Dan, L.I. and Zhang, X. 2010. Simulations of the three-dimensional total dissolved gas saturation downstream of spillways under unsteady conditions. *Journal of Hydrodynamics, Ser. B*, 22(4): 598-604.
- Harvey, H.H. 1967. Supersaturation of lake water with a precaution to hatchery usage. *Transactions of the American Fisheries Society*, 96(2): 194-201.
- Huang, R.H., Li, R., Feng, J.J., Qu, L. and Niu, J.L. 2016. Experimental study on recovery of dissolved oxygen supersaturated water by aeration. *Journal of Hydropower*, 35(6): 80-86. (In Chinese)
- Huang, X., Li, K. and Du, J. 2010. Effects of gas supersaturation on lethality and avoidance responses in juvenile rock carp (*Procypris rabaudi* Tchang). *Journal of Zhejiang University Science B*, 11(10): 806-811.
- Huang, Y.N., Li, R., Li, J.L. and Huang, Y.H. 2017. Experimental study on promoting supersaturated dissolved oxygen release from water by specific surface area. *Hydroelectric Energy Science*, 35(4): 45-48. (In Chinese)
- Li, E., Zeng, X.Y. and Fan, Y.H. 2007. Method for determining the optimal bubble group for microporous aeration. *Water treatment technology*, 7: 21-24. (In Chinese)
- Li, R., Huang, X., Li, K.F., Yi, W.M., Li, J., Deng, Y., Feng, J.J., Qu, L. and Liang, R.F. 2010. Device for the Study of Oversaturation of Total Dissolved Gas in Water and Its Impact on Fishes. <https://patents.google.com/patent/CN201479739U/zh>
- Liu, Q., Wang, L.L., Zou, X., Hu, Z.H. and Zeng, Z.G. 2015. Effect of wind speed on release rate of supersaturated total dissolved gas. *Scientific and technological progress of water conservancy and hydropower*, 35(4): 28-31. (In Chinese)
- Mavinic, D.S. and Bewtra, J.K. 1974. Mass transfer of oxygen in diffused aeration systems. *Canadian Journal of Civil Engineering*, 1(1): 71-84.
- Monk, B.H., Long, C.W. and Dawley, E.M. 1980. Feasibility of siphons for degassing water. *Transactions of the American Fisheries Society*, 109(6): 765-768.
- Niu, J., Li, R. and Shen, X. 2015. Experimental research on the promotion of supersaturated total dissolved gas dissipation by the use of activated carbon. *Nature Environment & Pollution Technology*, 14(2): 367.
- Politano, M., Amado, A.A. and Bickford, S. 2012. Evaluation of operational strategies to minimize gas supersaturation downstream of a dam. *Computers & Fluids*, 68: 168-185.

- Tan, D.C., Ni C.H., Zheng, Y.H., Li, L.Y. and Li, Y.F. 2006. River gas supersaturation caused by high dam and its effect on fish. *Freshwater Fisheries*, 3: 56-59. (In Chinese)
- U.S Army Corps of Engineers. 2005. Technical analysis of TDG processes. U.S. Army Corps of Engineers–Northwest Division, Environmental Resources, and Fish Planning Offices.
- Wang, Y., Politano, M. and Weber, L. 2019. Spillway jet regime and total dissolved gas prediction with a multiphase flow model. *Journal of Hydraulic Research*, 57(1): 26-38.
- Weitkamp D.E. and Katz M. 1980. A review of dissolved gas supersaturation literature. *Transactions of the American Fisheries Society*, 109(6): 659-702.
- Witt, A., Gulliver, J.S. and Shen, L. 2018. Numerical investigation of vorticity and bubble clustering in an air entraining hydraulic jump. *Computers & Fluids*, 172: 162-180.
- Wu, X.X., Li, Y.F., Yang, C.S., Du, K.K., Ru, H.J., Zhang, Y., Liu, L. and Ni, C.H. 2021. Effects of total dissolved gas (TDG) supersaturation stress on blood physiological indexes of *Spinibarbus sinensis*. *Freshwater Fisheries*, 51(3): 102-107. (In Chinese)
- Yuan, L., Yuan, Y., Wang, Y.M., An, R.D. and Li, K.F. 2017. Acute and chronic lethal effects of total dissolved gas supersaturation on loaches. *Engineering Science and Technology*, 49(S2): 56-61. (In Chinese)
- Zuo, D.Q. 2005. *Hydropower and Environmental Ecology*. Scientific and Technological Progress of Water Resources and Hydropower, 2: 1-7. (In Chinese)



The Potential of Phytoremediation to Treat Different Types of Wastewater - A Review

Vijayant Panday†  and Ananda Babu K. 

Department of Civil Engineering, Shri Vaishnav Institute of Technology and Science, SVVV, Indore, India

†Correspondence author: Vijayant Panday; vijayantcivil@gmail.com

Nat. Env. & Poll. Tech.
Website: www.neptjournal.com

Received: 12-09-2022

Revised: 06-12-2022

Accepted: 22-12-2022

Key Words:

Phytoremediation
Wastewater treatment
BOD
COD
Nutrients
Heavy metals

ABSTRACT

Globally, with an increase in population, water demand is also increasing, but on the other hand, water availability is continuously decreasing due to various factors. Contamination of existing water bodies is the main factor for the freshwater shortage. Conventional methods are there to treat polluted water, but their construction and operational cost are very high. Phytoremediation is an economical, solar-driven, green plants (macrophytes) based, environment-friendly technology being researched worldwide. Many researchers contributed to identifying the potential of phytoremediation to treat different types of wastewater. Along the same line, an attempt has been made with this literature survey to contribute to technological advancement. The study results showed that water hyacinth plants could potentially treat almost all types of wastewater. Still, their use with other plants like *Phragmites australis*, *Azolla filiculoides*, *Lemna minor*, *Typha latifolia*, etc., as polyculture (mixed culture) could perform way better than the individual. It not only improves the efficiency of phytoremediation but also helps some plants to grow and perform for a long duration when used in mixed culture.

INTRODUCTION

Urban India generates around 73 billion liters of sewage on daily basis (Barco & Borin 2017). The installed operational treatment capacity is only about 37% to treat this huge sewage. Remaining untreated sewage is mainly responsible for surface and groundwater quality degradation in India. This situation worsens when this sewage is mixed with other types of wastewater, like industrial effluent. An increase in domestic and industrial wastewater treatment plants can be a solution, but economic feasibility is the main obstacle to its application (Roy et al. 2014). In addition, these conventional treatment plants require a centralized collection network for the effluents, which again puts a question mark on their feasibility in rural areas with low population density. Phytoremediation is an alternative wastewater treatment technology that is being researched all over the world. It offers great potential to treat wastewater, compared to conventional methods like trickling filters, sequential batch reactors, up-flow anaerobic sludge blankets, activated sludge processes, etc. (Ajibade & Adewumi 2017).

Phytoremediation is a technique in which green plants (Macrophytes) convert pollutants into harmless forms (Abbasi & Abbasi 2010). The phytoremediation system uses natural plants, making this technique eco-friendly and economical. It is a solar-dependent, in situ treatment technology (Kinidi & Salleh 2017).

Plants are the key component of this system. The function of the different parts of the plant is depicted in Table 1. Microorganism lives and grow on and around the plant's root. Oxygen supplied by the roots help microorganisms decompose organic matter, uptake of nutrient and heavy metals, and other biological processes (Amarea et al. 2018). Phytoremediation technology is generally used in the form of constructed wetlands (Chavan & Dhulap 2012a, 2012b). It can treat almost all types of wastewater, including domestic, municipal, industrial, etc. (Agarry et al. 2018). For effective phytoremediation, it is very necessary to select an appropriate plant with high uptake of pollutants that can survive and grow well in wastewater (Magar et al. 2017).

Various studies conducted by many researchers to treat different types of wastewater using diverse plant species like *Phragmites australis*, *Eichhornia crassipes*, *Azolla filiculoides*, *Typha latifolia*, *Salvinia molesta*, *Pistia*

ORCID details of the authors:

Vijayant Panday: <https://orcid.org/0000-0002-4427-1094>

Ananda Babu K.: <https://orcid.org/0000-0001-8808-2116>

Table 1: Summarises the role played by different parts of the plant. (Source: Abbasi & Abbasi 2010)

Plant Parts	Function
Roots and/or Stems (within the water column)	Provide surface to grow bacteria Provide media for adsorption and filtration of solids Source of natural polymers to help in Sedimentation and Flocculation.
Stems and/or leaves (on or above the water surface)	Attenuate sunlight hence curtails the growth of algae Reduce the effect of wind on water Worked as a facilitator for gases and heat transfer between water and atmosphere

Table 2: Studies on phytoremediation of different types of wastewater.

Types of wastewaters	Plant species	Concentration reduction (in %)	Reference
Greywater	<i>Canna indica</i> , <i>Colocasia</i> , <i>Hymenocallis littoralis</i> , and <i>Phragmites australis</i>	TN:34.54, NH ₄ -N:53.06, PO ₄ -P: 37.49 COD: 58.26	Nema et al. (2020)
Municipal Wastewater	<i>Phragmites australis</i> , <i>Iris pseudacorus</i>	TN:74.3, NH ₄ -N: 62.1, NO ₃ -N: 77.7, TP: 29.6, PO ₄ -P: 37.4, COD:46.7	Barco and Borin (2017)
	<i>Iris pseudacorus (IP) and Phragmites australis (PA)</i> , <i>Lemna minor (LM)</i> , <i>Azolla filiculoides (AF) and Pistia stratiotes (PS)</i>	NO ₃ -N: 69, NH ₄ -N: 76, PO ₄ -P: 53, TP: 63, COD: 45.6 - 76.8, BOD: 37.7- 62.3	Ali et al. (2017)
	<i>Phragmites australis</i> , <i>Azolla filiculoides</i> , <i>Pistia stratiotes</i> , <i>Lemna minor</i> , <i>Lactuca sativa</i>	NH ₄ -N:70, TN: 59	Prajapati et al. (2017)
	<i>Commelina cyanea</i> , <i>Phragmites australis</i> , and water hyacinth	NO ₃ -N: 92, NO ₂ -N: 91, PO ₄ -P: 85%, COD:69, BOD: 74	Ajibade and Adewumi (2017)
Domestic wastewater	water hyacinth	NH ₃ -N: 64, BOD: 61, COD: 41	Rezania et al. (2016)
	<i>Phragmites karka</i>	NO ₃ -N: 84, NO ₂ -N: 76, PO ₄ -P- 68	Khare and Jain (2019)
	Green algae (<i>Chlorella vulgaris</i>), duckweed, and water hyacinth	COD:43, BOD:42	El-din and Aziz (2018)
	<i>Monochoria vaginalis</i> , <i>Typha angustifolia</i> , <i>Limnocharis flava</i> , <i>Lepironia articulata</i> , <i>Pistia stratiotes</i> and <i>Eichhornia crassipes</i>	BOD:79.4	Syukor et al. (2014)
	<i>Typha latifolia</i> , <i>Phragmites australis</i> , <i>Colocasia esculenta</i> , <i>Polygonum hydropiper</i> , <i>Alternanthera sessilis</i> and <i>Pistia stratoites</i>	NO ₃ -N: 84, PO ₄ -P: 76, NH ₄ -N: 86, BOD: 90	Rai et al. (2013)
	<i>Phragmites karka</i>	NH ₄ -N: 45–55, NO ₃ -N: 33–45, TN: 45–50, BOD: 40–50	Prashant et al. (2013)
	<i>Pennisetum pedicellatum</i> and <i>Cyperus rotundus</i>	NH ₄ -N: 84.47; NO ₃ - N: 69, PO ₄ -P: 90, BOD: 83, COD: 65	Thalla et al. (2019)
Sewage	<i>Azolla filiculoides</i>	NH ₄ -N:54.8, NO ₂ -N: 71.4, P-68.65, TP:80.52	Soman and Arora (2018)
	<i>Cana indica</i>	NO ₃ : 73.13, PO ₄ : 56.02, BOD: 73.77, COD: 75.19,	Chavan and Dulap (2012)
	<i>Eichhornia crassipes</i>	NO ₃ -N: 86.63, BOD: 48.69, COD: 54.38, Co: 78.78, Cu: 28.90, Fe: 23.42	Chavan and Dulap (2012)
Industrial Wastewater	<i>Eichhornia crassipes</i> , <i>Salvinia molesta</i> and <i>Pistia stratiotes</i>	Zn: 36, Fe: 26.6, Cu: 32.6, Cr: 58.6, Ni: 26.9, Cd: 27.1, Pb: 42.4	Kodituwakku et al. (2020)
	<i>Lemna minor</i>	Cd: 44.93, Cr :32.26, Ni :74.48, Pb :79.1	Al-Khafaji et al. (2017)
Petroleum refinery wastewater	<i>Azolla filiculoides</i>	N: 33, P: 40.5, COD: 98.8	Golzary et al. (2017)
Petroleum refinery secondary wastewater	<i>Eichhornia crassipes</i>	NO ₃ -N: 72.8, BOD ₅ : 94.6, COD: 80.2, Cd: 94, Pb: 92.5, Cr: 93, Fe : 94.8, Ni : 92.2, Zn: 87	Agarry et al. (2018)

Table Cont....

Types of wastewaters	Plant species	Concentration reduction (in %)	Reference
The mixture of textile, distillery, and domestic sources	<i>Lemna minor</i> and <i>Azolla filiculoides</i>	TN: 94.6, P: 98, COD: 96, BOD: 92, Co: 72, Cd: 66, Zn: 91, Cr:26, Ni: 50, Cu: 91, Fe: 83, Mn: 89	Amarea et al. (2018)
Industrial mines wastewater	Water hyacinth (<i>Eichhornia crassipes</i>)	BOD: 50, COD: 34, Cr (VI): 99.5	Saha et al. (2017)
Textile effluent	<i>Chara vulgaris</i>	COD: 78, BOD: 82	Daud et al. (2018)
	<i>Eichhornia crassipes</i> , <i>Pistia stratiotes</i> and <i>Salvinia molesta</i>	NO ₃ -N: 79.5, PO ₄ -P: 81.9, COD: 74, Cd: 47.4, Zn: 99, Ni: 59.3	Wickramasinghe et al. (2018)
	<i>Pistia stratiotes</i> , <i>Eichhornia crassipes</i> and <i>Oedogonium</i> sp.	Pb: 98.1, Fe: 94.4, Cd: 89.74, Cu: 98.64	Tabinda et al. (2019)
Landfill leachate	Duckweed (<i>Lemna minor</i>)	COD: 39, BOD: 47, Cu: 91, Zn: 86, Pb: 81, Ni: 76, Fe: 78	Daud et al. (2018)
	<i>Phragmites australis</i> , Vetiver grass	NO ₃ -N: 83, PO ₄ -P: 82, BOD: 68, COD: 60	Koupai et al. (2019)
Laundry Wastewater	Kiapu and water hyacinth	PO ₄ -P: 54.3, COD: 77.5	Siswoyo et al. (2019)
Dairy wastewater	Water hyacinth	TN: 66, TP: 89, BOD: 85.59, COD: 85.86	Trivedy and Pattanshetty (2002)

Units in mg.L⁻¹, TN: Total nitrogen, NO₃-N: Nitrate nitrogen, NO₂-N: Nitrite nitrogen, NH₄-N: Ammonia nitrogen, TP: Total phosphorus, PO₄-P: Orthophosphate, N: Nitrogen, P: Phosphorus, Cd: Cadmium, Pb: lead, Cr: Chromium, Fe: Iron, Ni: nickel, Zn: Zinc, Co: Cobalt, Cu: copper

stratiotes, Vetiver grass, etc., have been reviewed and depicted in Table 2.

The aim of the present study was to investigate the potential of phytoremediation to decrease oxygen demand (BOD, COD), nutrients, and heavy metals for different types of wastewater.

PHYTOREMEDIATION POTENTIAL

Potential to Abate Oxygen Demand (COD, BOD)

Biochemical oxygen demand (BOD) and chemical oxygen demand (COD) are generally used to indicate the organic strength of different types of wastewater. BOD (BOD₅) and COD are the two important parameters to analyze the treatment efficiency of any technology to treat the organic pollution of wastewater. These two parameters are used globally. The higher percentage of removal of BOD and COD indicates the potential of technology to treat the organic contamination of polluted water.

Fatmawati & Azizah (2018) performed a Comparative experimental study on sewer water with three samples. In Set-1, Set-2, and Set -3 the percentage of the *Kiapu* plant used were 0%, 50%, and 100%. Samples were analyzed before and after the treatment to determine BOD reduction. In the Results Set, -3 performed well compared to the other two sets, showing the *kiapu* plant's phytoremediation ability.

Panday (2005) studied the effect of phytoremediation if the two plants *Lemna minor* and *E.crassipes* were used in monoculture (use of single plant) and polyculture (use of multiple plants). Four experimental sets were used to treat polluted river water. Set 1 with no aquatic plants(control), set -2 with 100% *E. Crassipes* plant, set-3 with 100% *Lemna minor* plant, and Set-4 with 50% each of both the plants. Samples were analyzed for COD and BOD reduction. Set-4 showed a significant reduction in COD and BOD compared to other sets. It was clear from the results (Table 3) that the combined use of *Lemna minor* and *E.crassipes* is favorable for phytoremediation.

El-Din & Aziz (2018) evaluated the wastewater treatment efficiency of three aquatic plants, water hyacinth, duckweed, and green algae, with laboratory-scale experiments. COD and BOD reduction were determined after 21 days of detention time. *Duckweed* showed higher removal efficiency for BOD and COD than water hyacinth and green algae.

Textile effluent not only pollutes water but also imparts color to the water body. Due to this, the color penetration of sunlight is interrupted and affects the aquatic ecosystem. It also causes skin irritation, allergies, etc., because of the various dyes in the textile effluent. Mahajan et al. (2019) studied the treatment potential of *Chara vulgaris* to treat textile effluent. To check the adaptability of selected macrophytes, dilution of different percentage concentrations (10, 25, 50 and 75) of textile effluent was prepared.

After 120 hours of treatment, *Chara vulgaris* showed a maximum reduction of BOD (82%) and COD (78%) in 10% concentrated textile effluent. Due to the toxic effect of effluent, no significant reduction was observed in 50% and 75% concentrated effluent. This study revealed that dilution of highly concentrated effluent is necessary for effective phytoremediation.

Similarly, Adelodun et al. (2021) used water hyacinth to purify textile effluents and monitored changes in the physicochemical properties weekly to estimate the removal rate of contaminants. Removal of COD and other nutrients was observed, and water hyacinth is very effective in treating textile effluent. Still, results were continuously altered due to the decomposition of dead elements of the plant (because of the high strength of textile effluent). So, dilution of the effluent is suggested before the phytoremediation.

Siswoyo et al. (2019) investigated the ability of phytoremediation combined with sludge as an absorbent to treat laundry waste. Water hyacinth and kiapu plant were used, sludge obtained from a water treatment plant (WTP) was used, and concentration reduction of COD was analyzed. Results of the study showed that this combination of phytoremediation and absorption could remove 77.5% of COD from laundry wastewater.

Potential to Abate Nutrients

Excessive nutrients (like nitrogen and phosphorus) in any water body result in eutrophication. Due to eutrophication, excessive growth and decay of plants and algae have caused water quality degradation. It also disturbs the penetration of sunlight-induced degradation of water quality. It also depletes dissolved oxygen in the water body (Kinidi & Salleh 2017). The phosphorus removal capacity of plants depends on various factors like their growth rate, water depth, season, per unit area biomass, etc. (Amarea et al. 2018). Nitrogen removal involves nitrification and denitrification, nitrogen uptake by plants, ammonia volatilization, etc. (Amarea et al. 2018). Many researchers have studied the potential of various aquatic macrophytes to abate nutrients. Even after treatment, these plants can be used for animal feeding,

compost production, high protein source, biogas production, etc. (Pandey 2015).

Nema et al. (2020) conducted a study to identify the treatment potential of four macrophytes (*Phragmites australis*, *Canna indica*, *Hymenocallis littoralis*, and *Colocasia*) to treat greywater. Two reactors, R-1 (monoculture) and R-2 (mixed culture), were prepared and operated for 90 days with a 10 mL/min flow rate. The removal efficiency of ammonia and phosphate was higher in R-2, with significant differences of 13% and 10%, respectively. It was also discovered that *Phragmites australis* survived in R-2, while in R-1, it deteriorated during the experiment.

Ali et al. (2017) investigated the treatment potential of various floating treatment wetlands (FTWs) to treat domestic wastewater. A total of six pairs of wetlands (five with plants and one without plants as control) were used. Samples were collected and analyzed weekly for three months. Results of the study showed that as compared to *A. filiculoides*, *P. stratiotes*, and *L. minor*, Emergent macrophytes (*P. australis* and *I. pseudacorus*) performed better in low as well as in high influent concentration.

Similarly, Prajapati et al. (2017) conducted an experimental study to identify the treatment efficiency of different plants in FTWs. The study results showed that *P. stratiotes* were best in removing total nitrogen and ammonia with 59% and 70% efficiency, respectively. Removal of phosphate was found to be high for *P. stratiotes* with 29.5% efficiency, followed by *L. sativa* with 24.1%.

Rai et al. (2013) developed a constructed wetland with six macrophytes (*Polygonum hydropiper*, *Phragmites australis*, *Typha latifolia*, *Pistia stratiotes*, *Colocasia esculenta*, and *Alternanthera sessilis*) to evaluate the treatment potential in sewage water. For the full establishment of constructed wetland, six months were provided. After that, the monitoring of CW started. Samples were collected from the outlet with a retention time of 36 hours and compared with inlet samples. Results showed a reduction of PO_4 -P, NO_3 -N, and NH_4 -N between 75% and 86%.

Koupai et al. (2019) conducted a pilot study to improve the leachate quality using Reed and vetiver plants. Phosphate

Table 3: Comparative results for monoculture and polyculture.

Plant Species	Type of Culture	Average concentration reduction [%]	Reference
P1	Monoculture	BOD: 67, COD: 62, Nitrate: 55, Phosphate: 82	Pandey (2015)
P2	Monoculture	BOD: 54, COD: 56, Nitrate: 44, Phosphate: 76	
P1+P2	Polyculture	BOD: 73, COD: 74, Nitrate: 65, Phosphate: 86	Nema et al. (2020)
P3, P4, P5, P6	Monoculture	COD: 51, Ammonia: 41, Phosphate: 28	
P3+P4+P5+P6	Polyculture	COD: 58, Ammonia: 54, Phosphate: 38	

P1: Water hyacinth, P2: *Lemna minor*, P3: *Canna indica*, P4: *Colocasia*, P5: *Hymenocallis littoralis*, P6: *Phragmites australis*

and nitrate reduction after 3, 7, 14, and 21 days was analyzed. Results of the study showed that vetiver grass reduced 82-83% of phosphate and nitrate while the reed plant reduced 60-63% in 21 days.

Wickramasinghe and Jayawardana (2018) examined the pollutant removal efficiency of *Eichhornia crassipes* (water hyacinth), water lettuce, and *Salvinia molesta* (water fern) to treat textile wastewater. The reduction efficiencies of nitrates and phosphates by each aquatic plant were estimated. All three species observed significant reductions in nitrates and phosphates. Among all three plants, *Eichhornia crassipes* showed the highest percentage reduction (81.9%) for phosphate, whereas *S. molesta* showed the highest percentage reduction (79.5%) for nitrate reduction.

Ajibade & Adewumi (2017) performed an experimental study on municipal wastewater with a Laboratory-scale constructed wetland to evaluate the phytoremediation potential of Water hyacinth in addition to *Phragmites australis* and *Commelina cyanea*, before and after treatment samples were collected and analyzed for nutrients removal. Results showed that all the plants effectively abate nutrients. *Phragmites australis* obtained the highest removal efficiency for Nitrite, Nitrate, and phosphate.

Potential to Abate Metals

Contamination of the environment with metal ions is increasing and has become a major concern worldwide. With rapid industrialization and urbanization, sources of metals are also increasing (Rana & Maiti 2020). Some anthropogenic sources are depicted in Table 4.

Metals in the contaminated aquatic environment can enter the food chain through their consumption by a living organism. The presence of metals in the food chain could create serious hazards (Rana & Maiti 2020). Some plants

have extraordinary power to accumulate metals in their body. Such types of plants are called hyperaccumulating plants (Mahajan & Kaushal 2018). They can tolerate and even grow in high metal concentrations. While screening these plants, food crops should be avoided (Panday et al. 2019).

Agarry et al. (2018) studied the potential of constructed wetlands vegetated with *Eichhornia crassipes* to treat petroleum refinery secondary wastewater. A total of five constructed wetlands were prepared, out of which three were planted with *Eichhornia crassipes*, and the remaining two served as the unvegetated control. The vegetated constructed wetland significantly performed better than the unvegetated control. The study showed 90 to 95% iron, nickel, chromium, lead, and cadmium removal efficiency in 10 days. Similarly, Saha et al. (2017) also examined the phytoremediation potential of Water hyacinth to treat toxic hexavalent chromium (Cr VI) contamination from wastewater of chromite mines. It was found that Water hyacinth removed 99.5% Cr (VI) of processed water in just 15 days. Similar efficiency was achieved in a large-scale experiment using 100 liters of the same wastewater.

Panday et al. (2019) Conducted a pot experiment to identify the best lemon grass varieties to treat sites contaminated through tannery effluent. Of nine selected varieties of lemon grass, Suwarna showed the highest removal efficiency of about 70 to 85% for lead, chromium, and cadmium.

Sukumaran (2013) assessed the efficiency of *Eichhornia crassipes*, *Typha latifolia*, *Pistia stratiotes*, and *Salvinia molesta* in treating effluent. Constructed wetlands based on *Typha latifolia* and *Eichhornia crassipes* were found viable options for effluent treatment. *Eichhornia crassipes* observed a significant reduction in the lead than *Typha latifolia* (emergent plant), whereas *Typha latifolia* prominently removed metals like cadmium and copper.

Table 4: Anthropogenic sources of common metals found in wastewater.

Metal	Anthropogenic sources
As	Tannery, electroplating, pesticides, fertilizers, smelting, landfilling paints/chemicals, and mining
Cd	Manufacturing of cadmium–nickel batteries, phosphate fertilizers, pigments, stabilizers, alloys, and electroplating industries
Cu	Electroplating, agricultural run-off, mining, electrical and electronics, iron and steel production, nonferrous metal industry, printing and photographic industries, and metalworking and finishing processes
Hg	Solid waste incineration, coal and oil combustion, and pyrometallurgical processes
Ni	Nickel plating, colored ceramics, electroplating, batteries manufacturing, mining, and metal finishing and forging
Cr	Electroplating, leather tanning, metal finishing, nuclear power plant, textile industries, and chromate preparation
Pb	Combustion of coal, processing, and manufacturing of lead products, manufacturing of lead additives such as tetraethyllead (TEL) for gasoline
Zn	Mining, smelting, steel making, fossil fuel combustion, phosphate fertilizer, manure, sewage sludge, pesticides, motor vehicles, and galvanized metal

Source: Rana & Maitii (2020)

Kodituwakku & Yatawara (2020) experimented on a pilot-scale constructed wetland (free flow) to treat industrial sewage sludge with the help of *Eichhornia crassipes*, *Salvinia molesta*, and *Pistia stratiotes*. Among these three macrophytes, *S. molesta* showed the highest percentage decreases in Fe, Cu, Zn, Cr, and Ni, whereas the highest % reduction in Cd and Pb was shown by *P. stratiotes* and *E. crassipes*, respectively.

CONCLUSION

In the present literature, numerous studies conducted for the phytoremediation of various types of wastewater using diverse plant species have been reviewed. It can be concluded that phytoremediation can potentially treat wastewater from different sources. It has been found in the present literature that limited literature is available based on the comparative study with the use of monoculture and polyculture (mixed culture) of plants. Results showed higher treatment efficiency could be obtained using mixed culture plants. It not only improves the efficiency of phytoremediation but also helps some plants to grow and perform for a long duration when used in mixed culture. It is also observed that in the case of strong industrial effluent, dilution of the sample can increase the overall efficiency.

REFERENCES

- Abbasi, T. and Abbasi, S.A. 2010. Factors that facilitate wastewater treatment by aquatic weeds – the mechanism of the weeds' purifying action. *Int. J. Environ., Stud.*, 67(3): 349-371. DOI: 10.1080/00207230902978380
- Adelodun, A.A., Olajire, T., Afolabi, N.O., Akinwumiju, A.S., Akinbobola, E. and Hassan, U. O. 2021. Phytoremediation potentials of *Eichhornia crassipes* for nutrients and organic pollutants from textile wastewater. *Int. J. Phytoremed.*, 3: 1-9.
- Agarry, S.E., Oghenejoboh, K.M., Latinwo, G.K. and Owabor, C.N. 2018. Bioremediation of petroleum refinery wastewater in vertical surface-flow constructed wetland vegetated with *Eichhornia crassipes*: lab-scale experimental and kinetic modeling. *Environ. Technol.*, 41(14):1793-1813. <https://doi.org/10.1080/09593330.2018.1549106>
- Ajibade, F.O. and Adewumi, J. R. 2017. Performance evaluation of aquatic macrophytes in a constructed wetland for municipal wastewater treatment. *FUTAJEET*, 11(1):01-11.
- Ali, S.A., Lens, P. and Bruggen, H.V. 2017. Purifying municipal wastewater using floating treatment wetlands: free-floating and emergent macrophytes. *Adv. Recycl. Waste Manag.*, 2(30): 138. DOI: 10.4172/2475-7675.1000138
- Al-Khafaji, M.S., Al-Ani, F.H. and Ibrahim, A.F. 2017. Removal of some heavy metals from industrial wastewater by *lemna minor*. *KSCE J. Civ. Eng.*, 11: 1-6. DOI 10.1007/s12205-017-1112-x
- Amarea, E., Kebedeb, F. and Mulat, W. 2018. Wastewater treatment by *Lemna minor* and *Azolla filiculoides* in tropical semiarid regions of Ethiopia. *Ecol. Eng.*, 120: 464-473. <https://doi.org/10.1016/j.ecoleng.2018.07.005>
- Barco, A. and Borin, M. 2017. Treatment performance and macrophytes growth in a restored hybrid constructed wetland for municipal wastewater treatment. *Ecol. Eng.*, 107: 160-171. <http://dx.doi.org/10.1016/j.ecoleng.2017.07.004>
- Chavan, B. L. and Dhulap, V. P. 2012a. Optimization of pollutant concentration in sewage treatment using construction wetland through phytoremediation. *Int. J. Adv. Res. Eng. Appl. Sci.*, 1(6): 01-16.
- Chavan, B.L. and Dhulap, V.P. 2012b. Treatment of sewage through phytotechnological studies with constructed wetland using *Eichhornia crassipes*. *J. Environ. Res. Dev.*, 7 (2): 660-667.
- Daud, M.K., Ali, S., Abbas, Z., Zaheer, I.E., Riaz, M.A., Malik, A., Hussain, A. and Rizwan, M. 2018. Potential of duckweed (*Lemna minor*) for the phytoremediation of landfill leachate. *J. Chem.*, 15: 540. <https://doi.org/10.1155/2018/3951540>
- El-Din, S.B. and Aziz, R.A.A. 2018. Potential uses of aquatic plants for wastewater treatment. *J Microbiol Biotechnol. Rep.*, 2: 47-48.
- Fatmawati, D. and Azizah, R. 2018. Effectiveness of using crape plants (*Pistia stratiotes*) in decreasing BOD level of surface water in West Pagutan of Mataram City. *Dama Int. J. Res.*, 3(7):40-44.
- Golzary, A., Tavakoli, O., Rezaei, Y. and Karbassi, A.R. 2018. Wastewater treatment by *Azolla filiculoides*: A study on color, odor, cod, nitrate, and phosphate removal. *Pollution*, 4(1): 69-76. DOI: 10.22059/poll.2017.236692.290
- Khare, P. and Jain, N.K. 2019. Phytoremediation of wastewater by constructed wetland system in government new law college, Indore. *J. Pharmacog. Phytochem.*, 8(2): 1192-1195.
- Kinidi, L. and Salleh, S. 2017. Phytoremediation of nitrogen as green chemistry for wastewater treatment system. *Int. J. Chem. Eng.*, 12: 205. <https://doi.org/10.1155/2017/1961205>
- Kodituwakku, K.A.R.K. and Yatawara, M. 2020. Phytoremediation of industrial sewage sludge with *Eichhornia crassipes*, *Salvinia molesta*, and *Pistia stratiotes* in batch-fed free water flow constructed wetlands. *Bull. Environ. Contam. Toxicol.*, 20: 805. <https://doi.org/10.1007/s00128-020-02805-0>
- Koupai, J.A., Jamalain, M. A. and Dorafshan, M. M. 2019. Improving Isfahan landfill leachate quality by phytoremediation using Vetiver and Phragmites plants for using in green space irrigation. *J. Water Wastewater*, 16: 2867. Doi:10.22093/wwj.2019.186145.2867.
- Magar, R., Khan, A. and Honnutagi, A. 2017. Wastewater treatment using water hyacinth. *Int. Eng. Cong.*, 32: 546.
- Mahajan, P. and Kaushal, J. 2018. Role of Phytoremediation in reducing cadmium toxicity in soil and water. *J. Toxicol.*, 36: 4365. <https://doi.org/10.1155/2018/4864365>
- Mahajan, P., Kaushal, J., Upmanyu, A. and Bhatt, J. 2019. Assessment of phytoremediation potential of *Chara vulgaris* to treat toxic pollutants of textile effluent. *J. Toxicol.*, 56: 738. <https://doi.org/10.1155/2019/8351272>
- Nema, A., Yadav, K. and Christian, R. 2020. A small-scale study of plant orientation in treatment performance of vertical flow constructed wetland in a continuous flow. *International Journal of Phytoremediation*. 11: 201. <https://doi.org/10.1080/15226514.2020.1715918>
- Pandey, A.K. 2015. Waste water management through aquatic macrophytes. *Int.Sci. Cong. Assoc.*, 4(3): 41-46.
- Pandey, J., Verma, R.K. and Singh, S. 2019. Screening of most potential candidates among lemongrass varieties for phytoremediation of tannery sludge contaminated sites. *Int. J. Phytoremed.*, 16: 538. DOI:10.1080/15226514.2018.1540538
- Prajapati, M., Bruggen, J.J.A., Dalu, T. and Malla, R. 2017. Assessing the effectiveness of pollutant removal by macrophytes in a floating wetland for wastewater treatment. *Appl. Water Sci.*, 101: 4801-4809. <https://doi.org/10.1007/s13201-017-0625-2>
- Prashant, B.S.K., Sharma, J.K., Singh, N. and Ram. 2013. Treatment performance of artificial floating reed beds in an experimental mesocosm to improve the water quality of river Kshipra. *Water Sci. Technol.*, 56: 401. doi: 10.2166/wst.2013.401
- Rai, U.N., Tripathi, R.D., Singh, N.K., Upadhyay, A.K., Dwivedi, S.,

- Shukla, M.K., Mallick, S., Singh, S.N. and Nautiyal, C.S. 2013. Constructed wetland as an ecotechnological tool for pollution treatment for the conservation of the Ganga River. *Bioresour. Technol.*, 148: 535-541. <http://dx.doi.org/10.1016/j.biortech.2013.09.005>
- Rana, V. and Maiti, S.K. 2020. *Municipal and Industrial Wastewater Treatment Using Constructed Wetlands*. Springer, Cham, pp. 329-367.
- Rehman, K., Ijaz, A., Arslan, M. and Afzal, M. 2019. Floating treatment wetlands as biological buoyant filters for wastewater reclamation. *Int. J. Phytoremed.*, 16: 546 DOI:10.1080/15226514.2019.1633253
- Rezania, S., Md Din, M.F., Shazwin., Taib, M., Dahalan, F., Songip, A. R., Singh, L. and Kamyab, H. 2016. The efficient role of an aquatic plant (water hyacinth) in treating domestic wastewater in continuous system. *Int. J. Phytoremed.*, 18(7): 679-685. <http://dx.doi.org/10.1080/15226514.2015.1130018>
- Roy, S., Biswas, J. K. and Kumar, S. 2014. Nutrient removal from wastewater by macrophytes – an eco-friendly approach to wastewater treatment and management. *Energy Environ. Res.*, 4(2): 55-63. <http://dx.doi.org/10.5539/eer.v4n2p55>
- Saha, P., Shinde, O. and Sarkar, S. 2017. Phytoremediation of industrial mines wastewater using water hyacinth. *Int. J. Phytoremed.*, 19(1): 87-96. <http://dx.doi.org/10.1080/15226514.2016.1216078>
- Siswoyo, E., Utari, A. W. and Mungkari, L. G. 2019. Adsorption combined phytoremediation system for treatment of laundry wastewater. *MATEC Web Conf.*, 280: 05002 <https://doi.org/10.1051/mateconf/201928005002>
- Soman, D.A.V. and Arora, A. 2018. Bioremediation of municipal sewage water with *Azolla microphylla*. *Int. J. Adv. Res.*, 6(5): 101-108. <http://dx.doi.org/10.21474/IJAR01/7012>
- Sukumaran, D. 2013. Phytoremediation of heavy metals from industrial effluent using constructed wetland technology. *Appl. Ecol. Environ. Sci.*, 1(5):92-97. DOI:10.12691/aees-1-5-4
- Syukor, A.R., Zularisam, A. W., Ideris, Z., Mohd Ismid, M. S., Nakmal, H. M., Sulaiman, S., Hasmanie, A. H., Siti Norsita, M. R. and Nasrullah, M. 2014. Performance of phytogreen zone for BOD5 and SS removal for refurbishment of conventional oxidation pond in an integrated phytogreen system. *Int. J. Agri. Biosyst. Eng.*, 8(3):164-169.
- Tabinda, A.B., Arif, R.A., Yasar, A., Baqir, M., Rasheed, R., Mahmood, A. and Iqbal, A. 2019. Treatment of textile effluents with *Pistia stratiotes*, *Eichhornia crassipes* and *Oedogonium* sp. *Int. J. Phytoremed.*, 51: 1522. DOI:10.1080/15226514.2019.1577354.
- Thalla, A.K., Devatha, C.P., Anagh, K. and Sony, E. 2019. Performance evaluation of horizontal and vertical flow constructed wetlands as tertiary treatment options for secondary effluents. *Appl. Water Sci.*, (9): 147. <https://doi.org/10.1007/s13201-019-1014-9>
- Trivedy, R.K. and Pattanshetty, S.M. 2002. Treatment of dairy waste by using water hyacinth. *Water Sci. Technol.*, 45(12): 329-334.
- Wickramasinghe, S. and Jayawardana, C.K. 2018. The potential of aquatic macrophytes *Eichhornia crassipes*, *Pistia stratiotes*, and *Salvinia molesta* in phytoremediation of textile wastewater. *J. Water Sec.*, 11: 4. DOI: <https://doi.org/10.15544/jws.2018.001>



Extreme Flood Calibration and Simulation Using a 2D Hydrodynamic Model Under a Multipurpose Reservoir

Chinar Garg†  and Ananda Babu K. 

Department of Civil Engineering, SVITS, SVVV, Indore, India

†Corresponding author: Chinar Garg; chinargrawal@gmail.com

Nat. Env. & Poll. Tech.
Website: www.neptjournal.com

Received: 16-07-2022
Revised: 08-12-2022
Accepted: 22-12-2022

Key Words:

Hydrodynamic model
Calibration
Simulation
Flood hydrograph
Validation
HEC-RAS

ABSTRACT

Extreme floods have become common in Asian cities, with recent increases in urbanization and extreme rainfall driving increasingly severe and frequent events. Understanding the flood dynamic is essential for developing strategies to reduce risk and damage, thus ensuring the city's protection. Channel roughness is a sensitive parameter in developing a hydraulic model for flood forecasting and flood inundation mapping. A High-resolution 2D HEC-RAS model was used to simulate the flood events of 1994, 1998, 2002, 2006, and 2015. The calibrated model, in terms of channel roughness, has been used to simulate the flood for the year 2006 in the river. The performance of the calibrated HEC-RAS-based model has been assessed by capturing the flood peaks of observed and simulated floods and computation of root mean squared error (RMSE) for the intermediated gauging stations on the lower Tapi River. Results revealed that there is good agreement between simulated and observed floods.

INTRODUCTION

India has witnessed rapid growth in its population in the past 50 years, which has put pressure on the country's water resources (Ahmed et al. 2013, Liu et al. 2019). This stress is further increased by global warming impacts, including increased precipitation, storm intensity, and rising seawater levels in coastal and low-lying areas, which are responsible for pluvial and urban flooding (Rangari et al. 2019). Because of changing climatic conditions, the chances of flooding in the cities on the river's banks and in coastal areas have increased dramatically. Floods are one of the primary reasons for the loss of life and property due to their devastating effects. It affects the emotional, social as well as economic life of the people who are affected by it. Flooding is a natural disaster, but its behavior changes due to human intervention in flood plains and catchments, such as the construction of bridges, roads, and houses, consequently increasing the risk and losses to properties and life (Timbadiya et al. 2011). Thus, there is an urgent need to predict the water level along the river accurately. Hence, reliable hydraulic models are required for the same.

ORCID details of the authors:

Chinar Garg: <https://orcid.org/0000-0001-7161-047X>

Ananda Babu K.: <https://orcid.org/0000-0001-8808-2116>

A simulation is a primary tool for proper reservoir planning and management by assessing various scenarios for different operating conditions (Koutsoyiannis & Economou 2003). Simulation modeling is often used to examine and evaluate the performance of complex water resource systems. Simulation models may be deterministic or stochastic. The simulation model may be time-sequenced or event-sequenced. In a time-sequenced model, the properties of the system, such as inflow, storage, releases, deficits, and surplus, are examined at a fixed time interval, viz. seasonally, monthly, ten-daily, weekly, daily, or hourly basis. In event-sequenced simulation models, the event is fixed, viz., the number of times droughts or floods occurred. Wurbs (1993) presented various computer models developed for evaluating reservoir operations and emphasized that the model selection and analysis approach for a particular application depends on the characteristics of the application, the extent of ease provided by alternate models, and the preference of the analyst. With advancements in computer technology, various hydraulic models (1D and 2D) have been developed for flood forecasting and flood inundation mapping.

Predicting stage and discharge in the river is considered the flood warning parameter in any river across the globe (Quiroga et al. 2016). Generally, levels are predicted along the river, and inflows are predicted for reservoirs.

Apart from that, insurance studies and the development of risk map predictions of water levels are essential for effectively managing future flooding. Thus, estimating water levels in flood plains is of prime importance. Stages in the stream and their corresponding value of discharges and several other parameters are reliant on the roughness of the channel. Hence, the prediction of channel roughness also plays a significant role in studying open channel flow, especially in hydraulic modeling (Bhandari et al. 2017). The channel roughness is not a constant parameter, and it varies along the river depending upon variation in channel characteristics.

For example, the flood in 2006 alone caused direct damage to the nation's US \$ 4200 million, and the whole city remained submerged for more than two days (Thakar 2007). Thus, there is an urgent requirement for a hydrodynamic model which should predict the flood levels considering the release from the Ukai dam in the lower part of the Tapi River for flood forecasting and planning safety measures in and around Surat city. Accordingly, channel roughness for the lower Tapi River (Ukai dam to Hope Bridge) has been calibrated using stream flow data of the past floods, i.e., 1994, 1998, 2002, 2006, and 2015 flood data.

MATERIALS AND METHODS

The Study Area

The Tapi River flows east to west in central India, between the Godavari and Narmada rivers. It is one of the major rivers of peninsular India, having a length of about 725 km. Tapi River originates at a place known as Multai in the Betul district of Madhya Pradesh state, having an elevation of about 753 m. For the initial 282 km, the river flows through Madhya Pradesh, in which the path of 54 km is the borderline

area next to Maharashtra State. It rises in the eastern Satpura Range of Southern Madhya Pradesh and flows westward to the Nimar region of Madhya Pradesh, having historical importance. Tapi River flows in Maharashtra before entering Gujarat. After traveling the length of 214 km in Gujarat, the Tapi river finally joins the Arabian Sea in the Gulf of Cambay after crossing Surat city.

The Tapi River basin has a total area of 65,145 km². The basin lies in the states of Maharashtra (51,504 km²), Madhya Pradesh (9,804 km²), and Gujarat (3,837 km²). The entire Tapi Basin can be divided into three sub-basins: Upper Tapi Basin from the origin up to Hathnur, having an area of 29 430 km², the Middle Tapi Basin from Hathnur to Sarangkhedha gauging site, having an area of 31861 km² and the Lower Tapi Basin from Ukai Dam up to the Arabian Sea having an area of 3854 km².

Surat city is in the Lower Tapi basin. Low banks and many rapids characterize the Tapi River after the Kakrapar Weir. The Tapi passes through small towns like Kathor and Mandvi. There are large chances of occurrence of flood due to the low banks beyond the Kakrapar Weir. The Tapi River is braided in some portions, and the river has very rocky strata at places like Veratha Village, Khanjroli, and Bodhan. Lower Tapi, as the study area, is shown below in Fig 1. There are 14 major tributaries to the Tapi River, having a length of more than 50 km. On the left bank are ten important tributaries, and on the right bank are four tributaries.

Data Sources for the Present Study

The required data is collected from various agencies to carry out the present study, as described below.

Landsat Images

Earth-Explorer (<http://earthexplorer.usgs.gov>) provides

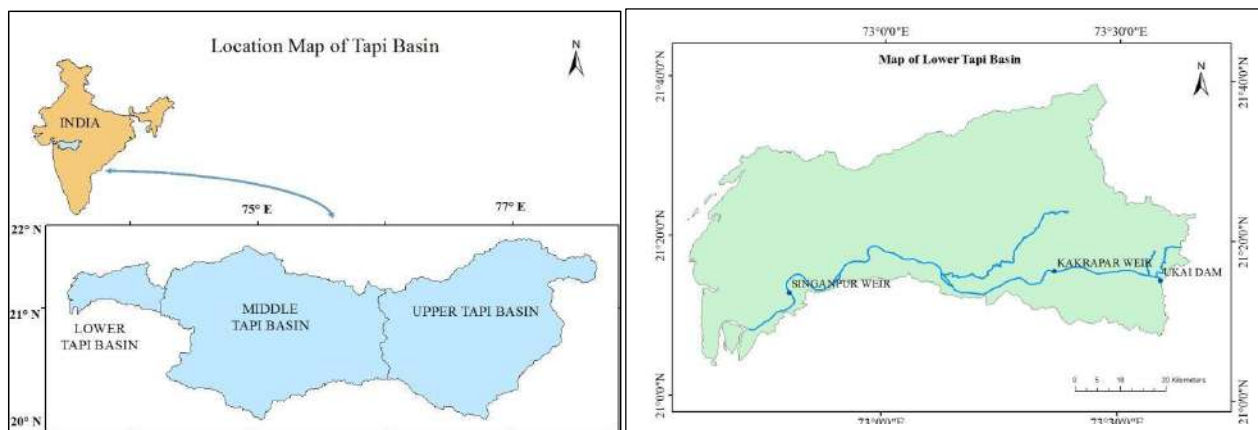


Fig 1: Index map of lower Tapi Basin.

online search, display browsing, data export, and downloading data from the U.S. Geological Survey (USGS) archives. And Landsat 8 images for the study period were obtained from the above-mentioned website.

Digital Elevation Model

The present study downloaded DEMs from USGS Earth Explorer (<http://earthexplorer.usgs.gov>). Among the available DEM in USGS, the most accurate one is SRTM (Shuttle Radar Topography Mission) 1 arc second (30m), and hence it is used.

Hydraulic Data

Hourly outflow data from Ukai Dam and the consecutive levels from the Kakrapar weir and Causeway weir were collected from the flood control cell, Surat Irrigation Circle, Surat, and hourly levels of the Ghala gauging stations were collected from CWC for 1994, 1998, 2002, 2006 and 2015 flood data.

Methodology

The present study demonstrates the calibration of Manning's roughness coefficient, 'n.' It uses the same in the simulation of future floods in the lower Tapi River from the Ukai dam to the Hope bridge using 2D hydrologic modeling. 2D hydrodynamic modeling of rivers becomes easy due to readily available software such as HEC-RAS, Flow 3D, etc.

The 2D hydrodynamic model was developed by using a 30 m resolution DEM. For all the cross-sections, Manning's n value was assigned. A Weir of a height of 4.75 m was created at the causeway location. Flow hydrograph was given as the boundary condition from the upstream, and the model was simulated. For different n values model was calibrated.

RESULTS AND DISCUSSION

Hydro-Dynamic Model Calibration

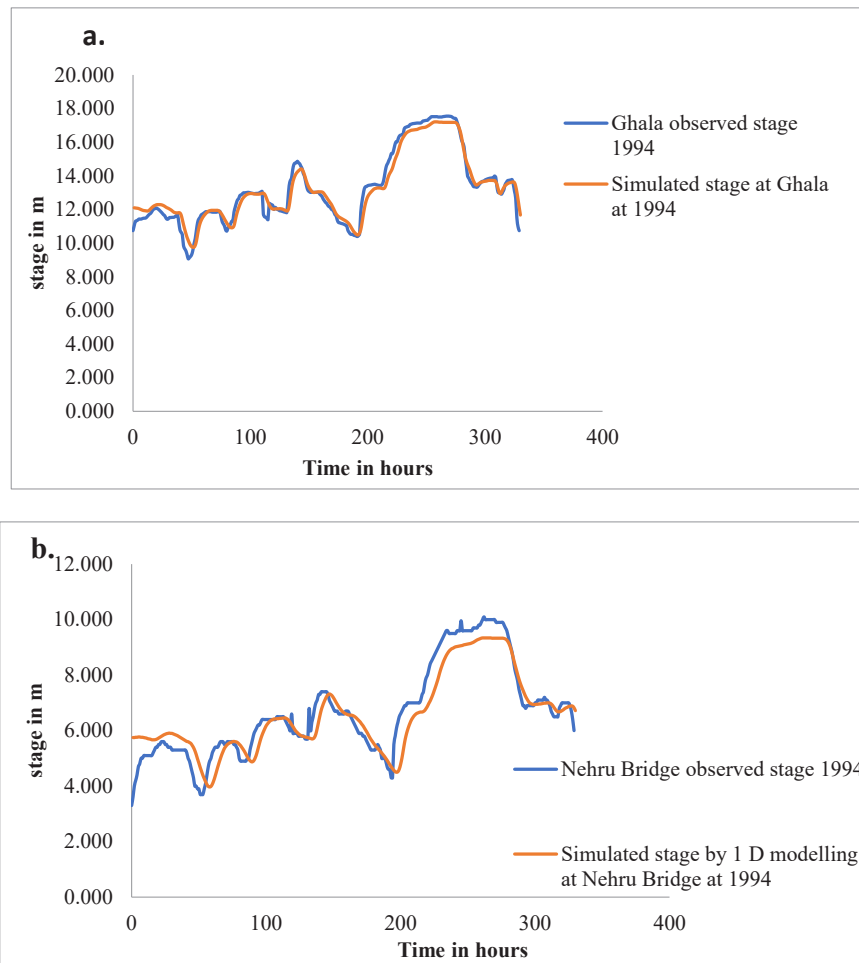


Fig. 2: Observed and simulated stages hydrograph of 1994 using HEC-RAS 2D modeling at a) Ghala; b) Nehru Bridge.

Table 1 (a): Calibration table for the 2 D model for the year 1994 flood.

Manning's 'n' value	RMSE		
	Kakrapar weir	Nehru Bridge	Ghala
0.015	2.9	1.1	1.8
0.02	0.29	0.71	1.6
0.025	0.27	0.9	1.78
0.03	0.21	1.2	2.4
0.035	0.20	0.7	1.9

Table 1 (b): Calibration table for the 2 D model for the year 1998 flood.

2 D Model performance table for 1994 flood with n = 0.035			
Parameters	R ²	RMSE	SE
Ghala	0.9741	0.017631	4.524833
Nehru Bridge	0.8897	0.586411	0.111394

Using the measured water surface elevation data, the HEC-RAS model is calibrated against Manning's roughness coefficient (n-value). An n-value is first estimated based on the previous Studies on the Tapi River (Timbadiya et al. 2011) and in consultation with textbook guidelines. Using this as a starting point, the n-value progressively changes until an optimization parameter. The model was calibrated based on the coefficient of correlation and RMSE. The

Table 2: Model performance for 1998 and 2002 at Ghala and Nehru Bridge.

Model Performance Table		
Parameters	Coefficient of Correlation r ²	
	2 D Modeling	
Ghala	1998	0.8967
	2002	0.9591
Nehru	1998	0.9607
	2002	0.8952

correlation coefficient was maximized to optimize the results and get the best n value. Fig. 2 a & b show the calibration and stage results of the HEC-RAS 2D model for the Ghala and Nehru Bridge, respectively. From Fig 2 a & b, it can be seen that there is a good prediction from the model for Manning's value of 0.027 on banks and 0.035 in the river. Table 1 (a and b) shows the calibration results for the 2D model for the year 1994 and 1998 flood events, respectively.

Table 1 (a and b) shows that the calibrated Manning's n value of 0.035 for the flood plain is in good agreement with the observed stage at both gauging sites.

HEC RAS 2D models were simulated for three years at two gauging sites. From the figures, it can be seen that there is a very close simulation obtained from 2D hydrodynamic

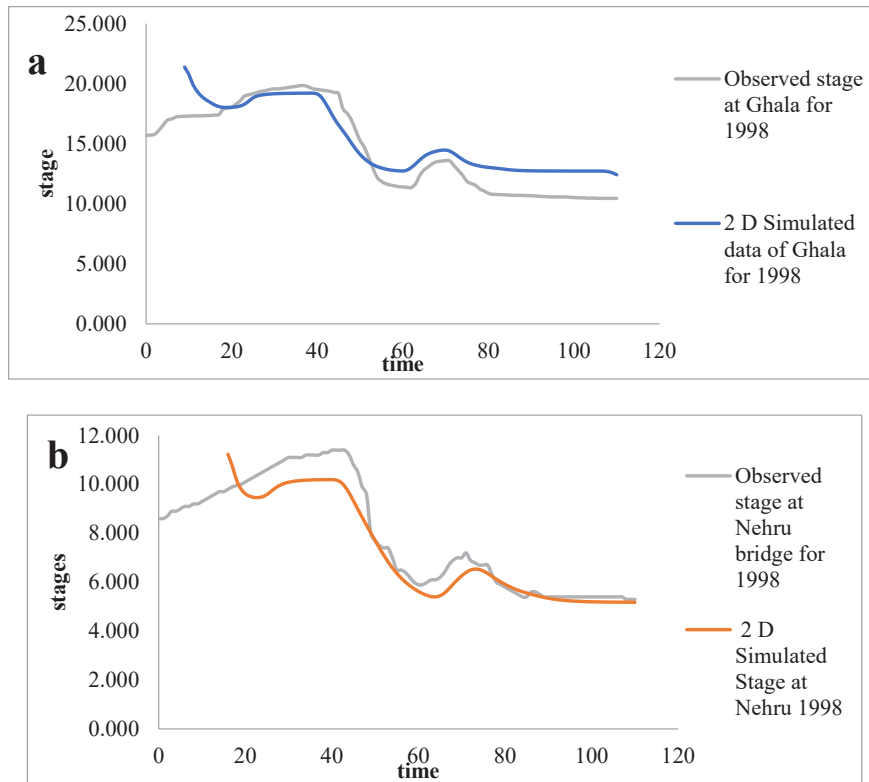


Fig. 3: Observed and simulated Stage of 2D for 1998 at a) Ghala; b) Nehru Bridge.

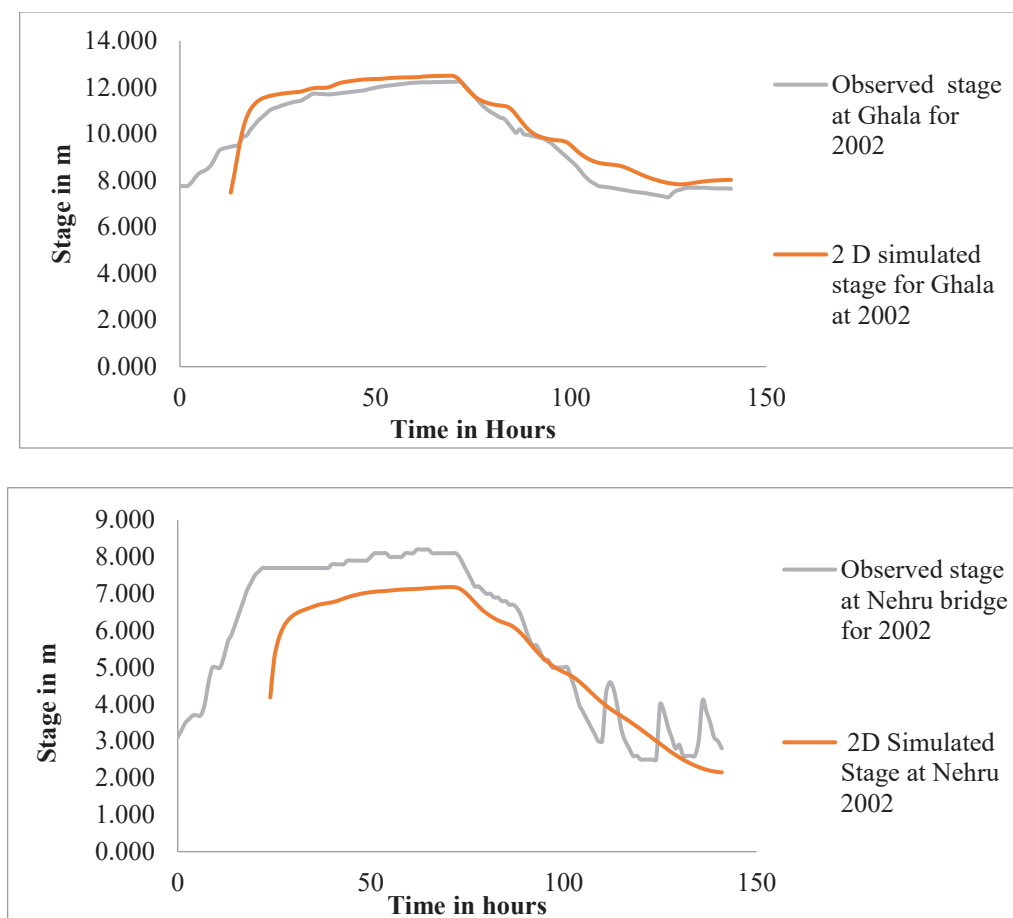


Fig. 4: Observed and simulated Stage for 2D for 2002 at a) Ghala b); Nehru Bridge.

models. The 2D model prediction always has a better correlation coefficient between observed and predicted stages for all the gauging sites, as shown in Table 2.

Fig. 3 (a & b) and Fig. 4 (a & b) show the predicted and observed stages for the two different years for 2D models at Ghala and Nehru Station for 1998 and 2002, respectively. From Fig. 3 (a & b) and Fig. 4 (a & b), there is a good prediction of stages at both the gauging sites for 1998 and 2002, respectively.

Calibration Result OF HEC-RAS 2D Model for Extreme Flood

The maximum water level obtained for different locations, known as the distributed water level outside the river, is obtained with the help of surveys. These levels are compared with the simulated levels with the help of HEC-RAS 2D. The model was calibrated for the year 2006. Around 15 to 20 levels are taken from each zone of the city, and the city is divided into 7 zones. Initially, the model was made with the help of 12 m × 12 m mesh, and the stability condition was

satisfied by giving the time step of 30 seconds. The initial values of manning’s roughness value were assumed to be 0.2, 0.03, 0.035, 0.04, and 0.1 for Urban, Agriculture, water, barren land, and forest, respectively. After simulation, levels obtained at different locations are shown in Table 3. Fig. 5 shows the flood inundation map for the study area under the year 2006 flood event. In this case Coefficient of correlation between observed and predicted levels was 0.62, as shown in Fig. 6. From Fig. 6, it can be seen that the entire Surat

Table 3: Simulated and measured levels for the year 2006 flood.

Location	Measured Level	Simulated Level
Akruthi Bungalow	1.850	1.244
Valentine cinemas	1.246	1.515
Sarojini Naidu Udhyan	2.121	1.87
Bakipark Society	2.345	3.0
Rambay Palace	3.600	3.855
Raghkul Palace	3.600	3.655
Silk Plaza	2.750	1.3

city was under flood. And almost all the roads were flooded except in the southwest area, where some roads can be seen as not flooded.

Table 3 shows that simulated levels are close to the observed levels for the flood that happened in the year 2006. For Rambay Palace and Raghukul Palace, the levels simulated were very close.

From Fig. 6, it can be seen that there is a good correlation between observed and simulated water levels for the selected locations.

Validation Result of HEC-RAS 2D Model

HEC-RAS 2D model is calibrated by changing Manning's roughness coefficient (n) for different classes to observe the water levels. When the simulated and observed water

levels matched, those values of Manning's n for the five land use classes were fixed. By considering the calibrated Manning's roughness coefficient, the 2015 extreme event was considered for validation. In addition, the hydrologic response of the catchment for release from the Ukai Dam was considered. Inlet boundary condition was defined as the discharge obtained from the extreme event and routed hydrograph of the release at the Ghala gauging station. The downstream boundary condition was defined as the causeway water level. The obtained flood map for 2015 is shown below in Fig 7.

It is evident from Fig. 8 that for 2015, the area of inundation is found to be less, and the nearer portion of the Lower Tapi underwent flooding to a lesser extent. The level obtained at the Causeway, Nehru Bridge, and Ghala gauging stations were 1.7 m, 6.05 m, and 6.8 m, respectively.

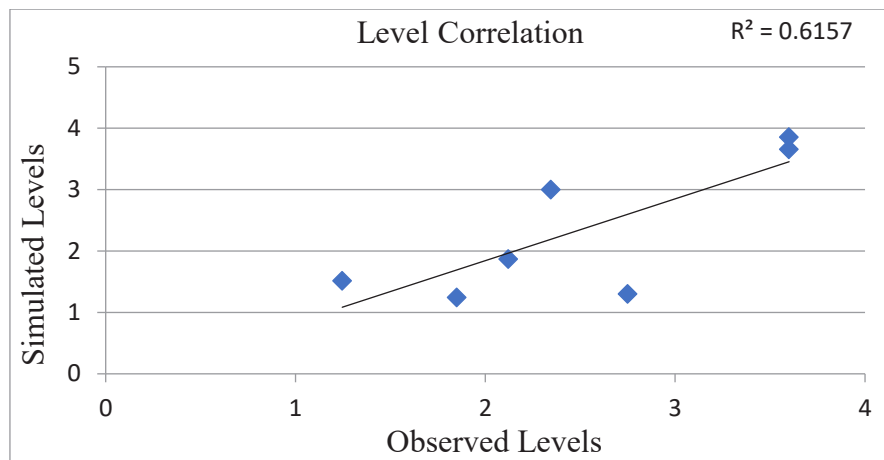


Fig 6: Correlation between observed and simulated water levels for the flood of the year 2006.

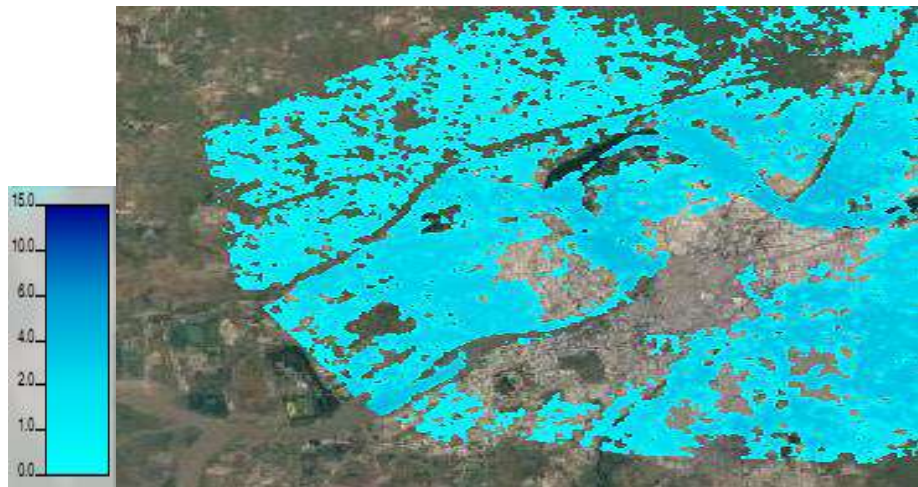


Fig 7: Flood Inundation map for predicted image for the year 2015.

Measured levels at the Causeway, Nehru Bridge, and Ghala gauging station were 1.8 m, 5.95 m, and 6.6 m, respectively. The obtained results show close agreement between observed and simulated water levels. This shows the satisfactory model performance for the given set of conditions.

CONCLUSIONS

The developed HEC-RAS 2D model is calibrated for the extreme event of the 2006 flood, and the water levels obtained are compared with the measured water levels. The Manning's roughness coefficient (n) obtained from the HEC-RAS 2D model during the calibration period as the flood period of 2006 estimated the values as 0.025 for urban, 0.035 for water and barren land, 0.1 for agriculture and 0.12 for the forest, which may be useful in estimating the future flood peaks. The correlation between observed and simulated water levels for the selected locations is found to be 0.61, which indicates that the model is performing well. HEC-RAS 2D model is validated using the releases from the Ukai Dam for 2015 and validated for the same year. Simulated levels at Causeway, Nehru Bridge, and Ghala gauging station are 1.7 m, 6.05 m, and 6.8 m, respectively. Measured levels at the Causeway, Nehru Bridge, and Ghala gauging station are 1.8 m, 5.905 m, and 6.6 m, respectively.

This shows the model is performing well for the given set of conditions.

REFERENCES

- Ahmed, Z., Rao, D.R.M., Reddy, K.R.M. and Raj, Y.E. 2013. Urban flooding—a case study of Hyderabad. *Glob. J. Eng. Des. Technol.*, 2(4): 63-66.
- Bhandari, M., Nyaupane, N., Mote, S.R., Kalra, A. and Ahmad, S. 2017. 2D unsteady flow routing and flood inundation mapping for lower region of the Brazos River watershed. *World Environ. Water Resour. Congr.*, 16: 292-303.
- Koutsoyiannis, D. and Economou, A. 2003. Evaluation of the parameterization simulation optimization approach for the control of reservoir systems. *Water Resour. Res.*, 39(6): 1170.
- Liu, Y., Wang, C., Yu, Y., Chen, Y., Du, L., Qu, X. and Gui, C. 2019. Effect of urban stormwater road runoff of different land-use types on an urban river in Shenzhen, China. *Water*, 11(12): 2545.
- Quirogaa, V.M., Kurea, S., Udoa, K. and Manoa, A. 2016. Application of 2D numerical simulation for the analysis of the February 2014 Bolivian Amazonia flood: Application of the new HEC-RAS version 5. *Ribagua*, 3(1): 25-33.
- Rangari, V.A., Umamahesh, N.V. and Bhatt, C.M. 2019. Assessment of inundation risk in urban floods using HEC RAS 2D. *Model. Earth Syst. Environ.*, 5(4): 1839-1851.
- Thakar, G. 2007. People's Committee on Gujarat Floods 2006: A report. Unique Offset, Ahmedabad.
- Timbadiya, P.V., Patel, P.L. and Porey, P.D. 2011. Calibration of HEC-RAS model on prediction of flood for lower Tapi River, India. *J. Water Resour. Prot.*, 3(11): 805.
- Wurbs, R.A. 1993. Reservoir-system simulation and optimization models. *J. Water Resour. Plan. Manag.*, 119(4): 455-472.



Study on the Temporal and Spatial Distribution of Air Pollutants in Typical Cities of China

He Tao† and Tihao Hou

College of Civil Engineering and Architecture, Zhengzhou University of Aeronautics, Zhengzhou 450046, Henan, China

†Corresponding author: Tao He: 54757050@qq.com

Nat. Env. & Poll. Tech.
Website: www.neptjournal.com

Received: 07-09-2022

Revised: 06-12-2022

Accepted: 07-12-2022

Key Words:

Air pollutants

Air quality

Yellow river basin

Space-time distribution law

ABSTRACT

The present study selects cities such as Zhengzhou, Kaifeng, Anyang, Hebi, Xinxiang, Jiaozuo, and Puyang along the Yellow River Basin in Henan Province. The data of six pollutants, such as PM_{2.5}, PM₁₀, SO₂, CO, NO₂, and O₃, in various cities from 2019 to 2021, and the monthly primary pollutant data of seven cities in the past five years were collected through various channels. The air quality of the above seven cities was analyzed with the spatial-temporal distribution of pollutants as the research objective and geographic information system as the research tool. The results show that affected by the distribution of key pollution sources and meteorological conditions in the urban area, the PM_{2.5} concentration generally shows a zonal feature of decreasing from northwest to Southeast. The high-value area is located in the north and west of the integrated area of the seven cities, and the low-value area is located in the Southeast of the seven cities.

INTRODUCTION

In recent years, the problem of air pollution in China has become more serious with the continuous improvement of social and economic levels, while accelerating the process of urbanization and industrialization. The form of air pollution has undergone significant changes, and pollutants will be transported and transformed between cities and regions, transforming from point source pollution and single pollution to non-point source pollution and composite pollution, seriously damaging the ecological environment.

China has proposed the concept of coordinated air pollution control, taking typical regions as pilot areas and adopting multiple measures to build a “regional” scale governance system. This is of great significance for controlling the scope of pollution, reducing the degree of air pollution, and building an environmentally friendly society. In this paper, the data of typical regions in recent years were compared to analyze the effectiveness of governance.

MATERIALS AND METHODS

Geographical Position

The Yellow River enters Henan Province from Tongguan City, Shanxi Province, and flows through 31 counties in 9 cities under the jurisdiction of Henan Province. The total length of rivers in Henan is 711km, and the drainage area

is 36200 km², accounting for 21.7% of the total area of Henan Province. This paper takes seven cities of Zhengzhou, Xinxiang, Puyang, Kaifeng, Jiaozuo, Anyang, and Hebi as research areas, studies and evaluates the atmospheric environmental quality of the Yellow River Basin in the province, and analyzes the changes and reasons for the ecological environment in the seven cities in the past five years.

Climatic Conditions

The climate of the seven cities in Henan Province in the Yellow River Basin belongs to the temperate continental monsoon region. The annual average temperature is not lower than 0°C, and the annual accumulated temperature is between 3200°C and 4500°C. It is a transitional climate between subtropical and temperate regions with high temperatures and rain in summer, cold and dry in winter, and four distinct seasons. The terrain is mostly plain, and the population is relatively dense.

Social Development

In recent years, with the rapid economic development, the Yellow River Basin has become one of the areas where high energy consumption and high pollution enterprises are concentrated in Henan Province due to the continuous impact of human activities, industrial agglomeration, and other factors. At the same time, the rich water and soil

resources brought by the Yellow River make agriculture more developed, the overall economic benefits are higher, and the population is relatively dense.

RESULTS AND DISCUSSION

Annual Variation of Air Pollutants in Typical Cities

CO Concentration in seven cities in 2019-2021: For excellent days, take Zhengzhou as an example, 203 days in 2019, 231 days in 2020, and 237 days in 2021. It can be seen that the number of excellent days has basically maintained a year-on-year growth trend in the past three years, and the air quality has gradually improved (Bai et al. 2020, 2021, Chen et al. 2019).

It can be seen from the above Fig. 1, 2, & 3 that the high value of the monthly average concentration of CO is in January, February, November, and December. The concentration in the other eight months is relatively stable

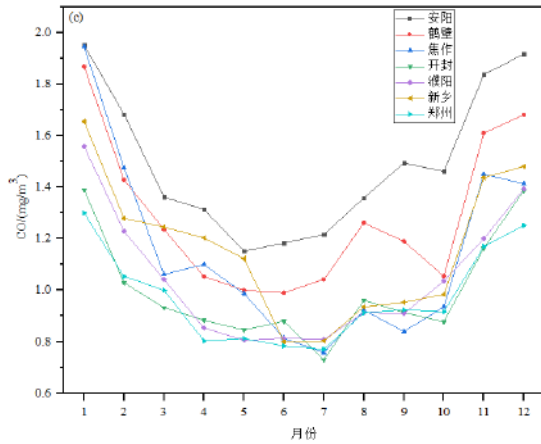


Fig. 1: CO concentration monthly changes in seven cities in 2019.

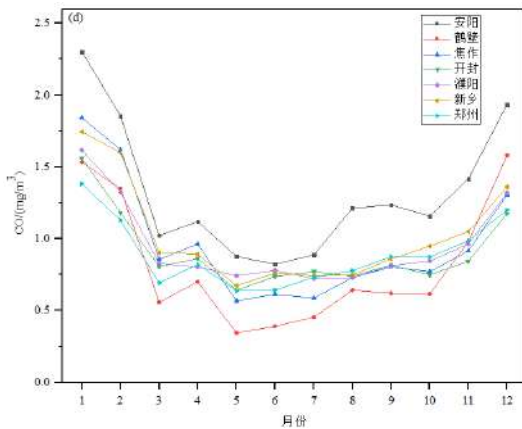


Fig. 2: CO concentration monthly changes in seven cities in 2020.

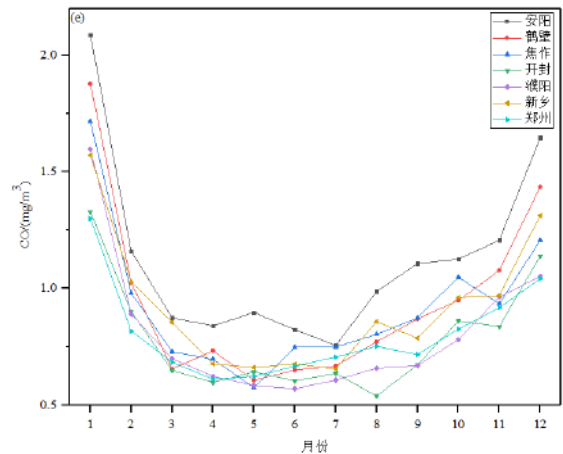


Fig. 3: CO concentration monthly changes in seven cities in 2021.

at a low value, generally showing a U-shaped change trend (Cohen et al. 2017, Deng et al. 2020, Duan et al. 2020).

NO₂ concentration in seven cities in 2019-2021: It shows that the monthly concentration of NO₂ in January, November, and December is the highest, decreasing month by month from January to July and increasing month by month from July to December (Fig. 4 to Fig. 6). The overall trend of change is U-shaped, and the annual change is relatively smooth. The abnormal change curve of NO₂ in February and March 2020 is because of the pandemic. Travel was greatly reduced, and the concentration changes were in a low range (Fan et al. 2020a, 2020b).

SO₂ concentration in seven cities in 2019-2021: The monthly concentration of NO₂ in January, November, and December is the highest, decreasing month by month from January to July and increasing month by month from July to December (Fig. 7 to Fig. 9). The overall trend of change is U-shaped, and the annual change is relatively smooth.

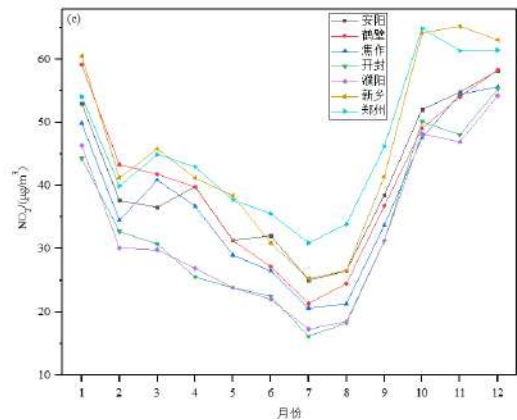


Fig. 4: NO₂ concentration monthly changes in seven cities in 2019.

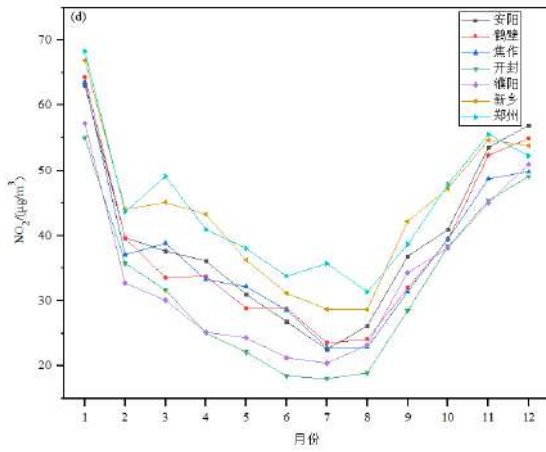


Fig. 5: NO₂ concentration monthly changes in seven cities in 2020.

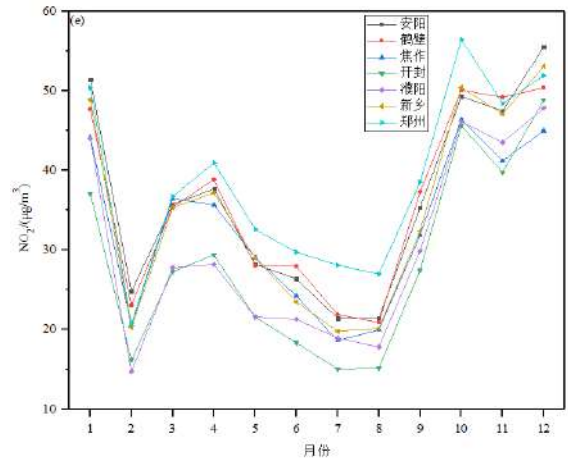


Fig. 6: NO₂ concentration monthly changes in seven cities in 2021.

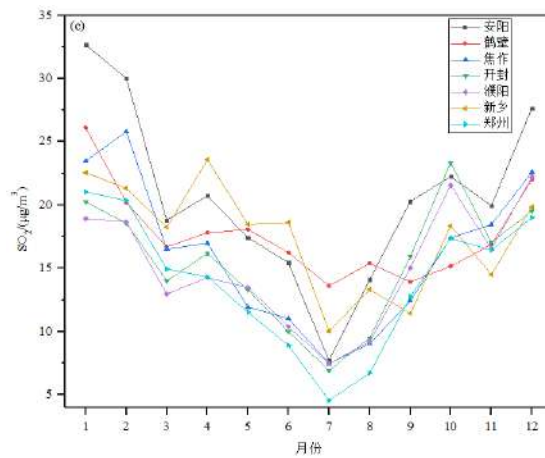


Fig. 7: SO₂ concentration monthly changes in seven cities in 2019.

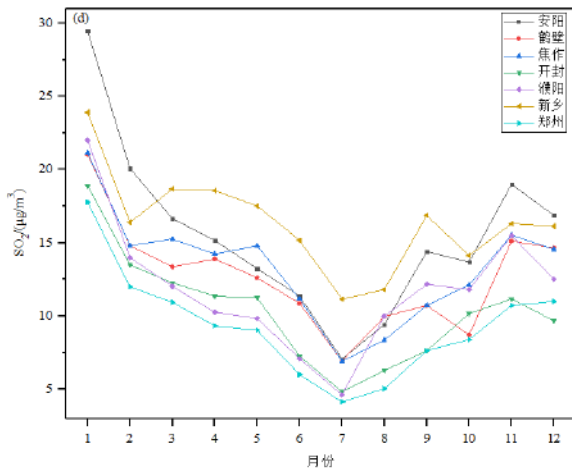


Fig. 8: SO₂ concentration monthly changes in seven cities in 2020.

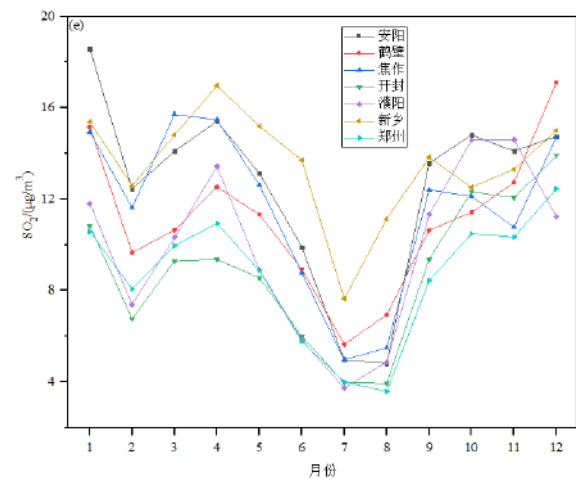
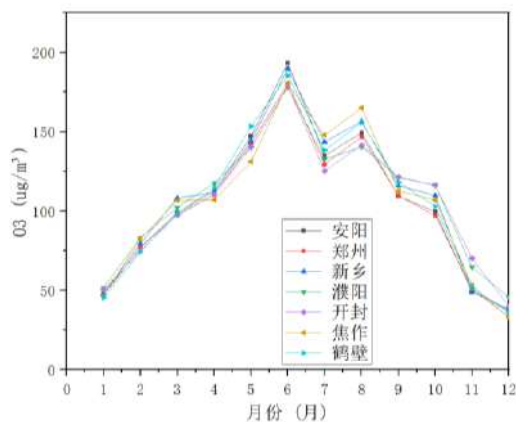
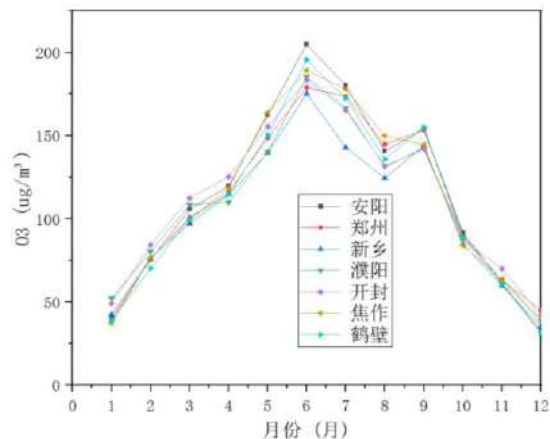
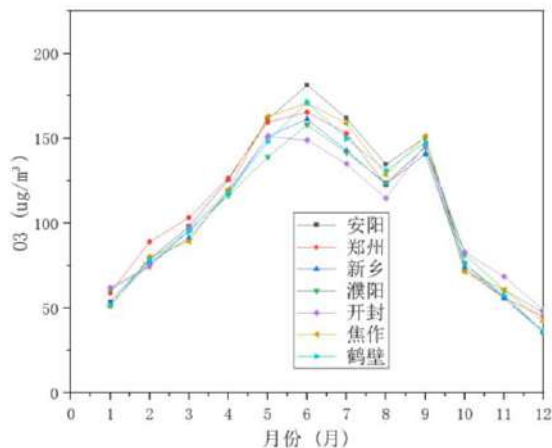


Fig. 9: SO₂ concentration monthly changes in seven cities in 2021.

Fig. 10: O₃ concentration monthly changes in seven cities in 2019.Fig. 11: O₃ concentration monthly changes in seven cities in 2020.Fig. 12: O₃ concentration monthly changes in seven cities in 2021.

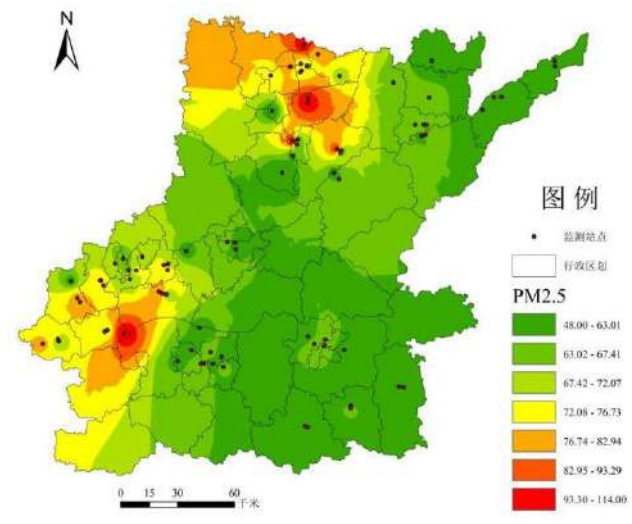
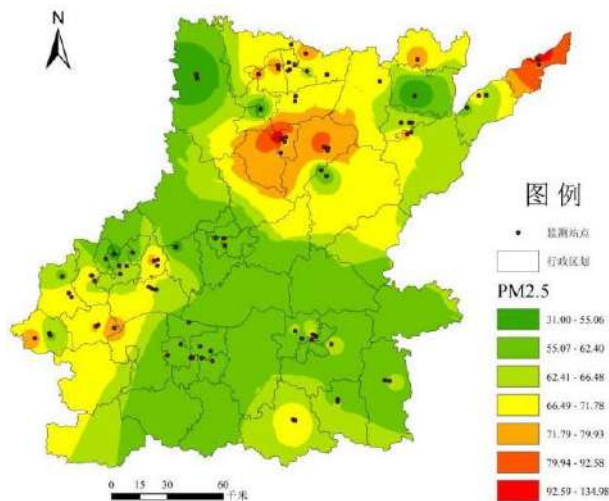
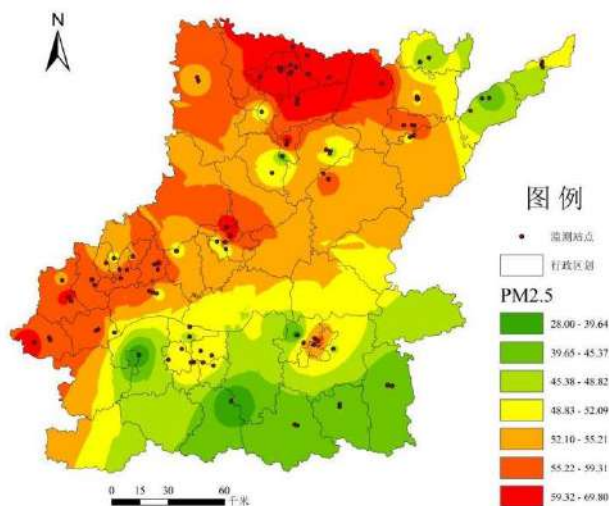
The abnormal change curve of NO₂ in February and March 2020 is due to the pandemic. Travel was greatly reduced, and the concentration changes were low. The monthly average concentration of SO₂ is not obvious. It is on the high side in January, February, and December, and the overall change also shows a U-shaped trend. It is worth mentioning that the change in SO₂ in 2020 was relatively disordered. Because of the pandemic, people living in isolation in winter used a large amount of coal for heating, resulting in an abnormal surge in February and March. The high concentration continued to decline slowly until June and July and then rose sharply due to the rebound of the pandemic.

O₃ concentration in seven cities in 2019-2021: The change curves of ozone in the past five years are the same, showing a convex change trend (Fig. 10 to Fig. 12). This is because the volatile organic compounds and nitrogen oxides mentioned above have a series of photochemical chain reactions under

strong ultraviolet radiation in summer, which improves atmospheric oxidation and leads to a sharp increase in surface ozone concentration. In summer, the ozone concentration was at a high level in May, June, and August. In January, February, November, and December, when the concentration of other pollutants was higher, the ozone concentration remained at a low level.

Evaluation Method

Take the average concentration of PM_{2.5} in Zhengzhou in 2020 as an example. ArcGIS software was used to sort out the obtained GIS data through coordinate system transformation, distortion correction, screening, and other steps, and then obtain the parts related to Zhengzhou municipal area. All monitoring stations in the seven cities are marked in Fig. 12 to Fig. 14, with a total of more than ten points (Jiang et al. 2020, Kong et al. 2020, Kuerban et al. 2020).

Fig. 12: Spatial distribution of PM_{2.5} in seven cities in 2019.Fig. 13: Spatial distribution of PM_{2.5} in seven cities in 2020.Fig. 14: Spatial distribution of PM_{2.5} in seven cities in 2021.

In the spatial scale analysis, after the annual average of pollutants at each monitoring station is linked to the location information of each monitoring point, Kriging interpolation analysis is carried out using the module in Arc GIS to present the spatial distribution of PM_{2.5} pollutants intuitively.

It can be seen from the data in Figs. 12, 13, & 14 that the regional atmospheric PM_{2.5} concentration data had a relatively downward trend in the past five years. Overall, the PM_{2.5} index of Jiaozuo, Xinxiang, and Anyang in the northwest is higher than that of Zhengzhou and Kaifeng in the Southeast. In the winter and spring seasons, with a high

incidence of PM_{2.5} pollution in the seven cities, the wind direction is mainly northwest wind, and the pollutants mainly spread from northwest to Southeast.

It also can be seen, in the past three years, the months with a high monthly average concentration of PM_{2.5} in the seven cities are in January and February and November to December. The concentration is generally lower from March to September than 90 $\mu\text{g}\cdot\text{m}^{-3}$. In the past five years, the average concentration of PM_{2.5} showed a downward trend year-on-year, but the downward trend was not obvious. Supervision and management should be strengthened during cold weather and less rainfall in winter.

CONCLUSION

This paper takes Zhengzhou, Kaifeng, Anyang, Hebi, Xinxiang, Jiaozuo, and Puyang in the Henan section of the Yellow River Basin as the research objects. It analyzes the data of six pollutants in the past three years. Various methods are used to determine the concentration of pollutants in various cities and analyze their spatial and temporal distribution. It provides a scientific reference and basis for the related research of air pollution prevention and control in cities in the future. The main conclusions of this paper are as follows:

- (1) Each year's winter and spring seasons, i.e., January and February, November and December, are the peak periods of air pollution of PM_{2.5}, PM₁₀, and other pollutants except O₃. It is difficult for pollutants to be diffused or adsorbed for purification due to low temperatures, little winter rain, and low wind speed. In addition, coal resources are mainly used for heating and power generation in winter, and coal combustion emits more sulfur oxides, nitrogen oxides, and fine particles into the air.
- (2) The seven cities in Henan in the statistics belong to the cities in northern China, which are vulnerable to sand and dust in spring. By analyzing the monthly variation curve of the ratio of PM_{2.5} to PM₁₀, it can be seen that the impact of spring dust weather on PM₁₀ is greater than that of PM_{2.5}; The winter heating period has a greater impact on PM_{2.5} than on PM₁₀.

ACKNOWLEDGMENT

This work was supported by the Foundation of Science and Technology Research Project of Henan Province

(222102320273), and the Project of Henan Provincial Department of Education (23A610012).

REFERENCES

- Bai, L., Lu, X. and Yin, S.S. 2020. A recent emission inventory of multiple air pollutants, PM_{2.5} chemical species, and its spatial-temporal characteristics in central China. *J. Clean. Prod.*, 269: 122114
- Bai, X.X., Tian, H.Z. and Liu, X.Y. 2021. Spatial-temporal variation characteristics of air pollution and apportionment of contributions by different sources in Shanxi province of China. *Atmos. Environ.*, 244: 117926
- Chen, L., Zhu, J. and Liao, H. 2019. Assessing the formation and evolution mechanisms of severe haze pollution in the Beijing-Tianjin-Hebei region using process analysis. *Atmos. Chem., Phys.*, 19(16): 10845-10864.
- Cohen, A.J., Brauer, M. and Burnett, R. 2017. Estimates and 25-year trends of the global burden of disease attributable to ambient air pollution: An analysis of data from the global burden of diseases study 2015. *The Lancet*, 391(10130): 1576-1576.
- Deng, F., Lv, Z. and Qi, L. 2020. A big data approach to improving the vehicle emission inventory in China. *Nature Commun.*, 11(1): 2801.
- Duan, J., Huang, R.J. and Li, Y. J. 2020. Summertime and wintertime atmospheric processes of secondary aerosol in Beijing. *Atmos. Chem. Phys.*, 20(6): 3793-3807.
- Fan, H., Zhao, C. and Yang, Y. 2020a. A comprehensive analysis of the spatio-temporal variation of urban air pollution in China during 2014-2018. *Atmos. Environ.* 220(12): 17066.
- Fan, Y. B., Liu, C.Q. and Li, L.J. 2020b. Large contributions of biogenic and anthropogenic sources to fine organic aerosols in Tianjin, North China. *J. Atmos. Chem. Phys.*, 20(1): 117-137.
- Jiang, P.Y., Zhong, X. and Li, L.Z. 2020. On-road vehicle emission inventory and its spatio-temporal variations in North China Plain. *Environ. Pollut.*, 267: 115639.
- Kong, L.W., Feng, M. and Liu, Y.F. 2020. Elucidating the pollution characteristics of nitrate, sulfate, and ammonium in PM_{2.5} in Chengdu, Southwest China, based on long-term observations. *Atmos. Chem. Phys.*, 20(19): 11181-11199.
- Kurban, M., Waili, Y. and Fan, F. 2020. Spatio-temporal patterns of air pollution in China from 2015 to 2018 and implications for health risks. *J. Environ. Pollut.*, 258(12): 113659.



Investigation of Adsorption of Nd(III) on Boron Nitride Nanosheets in Water

C. Fu*, Y. He*, C. Yang*, J. He*, L. Sun*, K. Du*, X. Zhang**, G. Sheng*, L. Li*, L. Wang*† and W. Linghu*

*Department of Chemistry and Chemical Engineering, Shaoxing University, Zhejiang 312000, P. R. China

**Department of International Education, Beijing University of Chemical Technology, Beijing 100029, P. R. China

†Corresponding authors: Linxia Wang; wlxsyx@163.com

Nat. Env. & Poll. Tech.
Website: www.neptjournal.com

Received: 08-11-2022

Revised: 25-01-2023

Accepted: 03-02-2023

Key Words:

Boron nitride nanosheets
Adsorption
Neodymium Nd(III)
Environmental remediation

ABSTRACT

In this paper, boron nitride materials were prepared by a two-step synthesis method, and this material's adsorption property for neodymium ions was explored. The experimental results show that the adsorption capacity of boron nitride is closely related to pH. When the pH is 6.0, the adsorption performance of the material is the best; the kinetic data show that the adsorption equilibrium can be reached in about 150 min, and the adsorption capacity at equilibrium is 207.3 mg.g⁻¹. In addition, the Freundlich and Langmuir models were used to fitting the thermodynamic results. It was found that the adsorption process of boron nitride on Nd(III) involved both monolayer adsorption and multi-layer adsorption. These data indicate that boron nitride has a good adsorption effect on Nd(III) in water and is a promising material for environmental remediation.

INTRODUCTION

In recent years, with the rapid development of science and technology, the demand for rare earth elements continues to increase. Neodymium is a rare earth element often used to prepare Nd-Fe-B permanent magnet materials (Kamimoto et al. 2017) for energy storage and constant magnetic field generation. In addition, neodymium is also commonly used in the doping modification of materials (Wojcieszak et al. 2012) and in tracking isotopic elements (Wilson et al. 2012). Although Nd(III) plays a key role in many fields, such as permanent magnet materials, we must face the harm caused by Nd(III) pollution. Industrial sewage containing rare earth elements has caused serious environmental pollution (Zhao et al. 2021). Rare earth elements can induce human respiratory, cardiovascular, and nervous diseases (Shin et al. 2019). Therefore, how to remove neodymium from the environment has caused extensive research. At present, methods for removing Nd from wastewater have been widely reported. Among these methods, adsorption is feasible due to its high removal rate and simple operation. The core of the adsorption method lies in the adsorbent. The common materials used for adsorption are carbon, zeolite, clay, polymeric materials, etc. At the same time, new adsorption materials are constantly being developed and applied.

Boron nitride (BN) has great development potential because of its excellent properties, such as high mechanical strength, good electrical insulation, oxidation resistance,

etc. (Kim et al. 2018). Due to its special properties, the application field of BN has gradually expanded in recent years. Researchers such as Lale have explored the hydrogen storage capacity of BN (Lale et al. 2018). An's research group prepared graphene/boron nitride composite aerogels (An et al. 2017), and BN is even used as a nanocarrier for anticancer drugs (Emanet et al. 2017). BN is also often used in adsorption and to adsorb heavy metal ions and organic dyes (Yu et al. 2017). Song studied the removal performance of BN materials for antibiotic pollutants in water (Song et al. 2017). Li et al. used BN materials to study the adsorption of metal ions such as Cr³⁺, Co²⁺, and Ni²⁺ and organic pollutants such as tetracycline, methyl orange, and Congo red (Li et al. 2013). In summary, this paper uses BN materials to conduct adsorption experiments on Nd to explore the effect of different adsorption conditions on the adsorption performance of BN.

This paper investigated the adsorption capacity of BN on Nd(III) ions in wastewater. SEM, TEM, XRD, and FT-IR analyzed the morphology and structure of BN material. Subsequently, the kinetic and thermodynamic experimental data were fitted to propose a possible adsorption mechanism.

MATERIALS AND METHODS

Experimental Materials and Preparation of BN

The chemical reagents used in this experiment were all

analytical reagent grade without further purification. This experiment used a two-step synthesis method to prepare BN adsorbents (Li et al. 2020). The melamine and boric acid are mixed uniformly according to the molar ratio of 1:2 and calcined in a muffle furnace for 1 hour, the temperature is constant at 1373K, and the product is obtained by natural cooling. All reagents used in the experiments were prepared with deionized water.

Characterization

In this study, the scanning electron microscope (SEM) of Japan Electronics (JEOL) and JSM-6360LV were used to characterize the surface morphology of BN materials. Transmission electron microscopy (TEM) can be used to observe the finer structure of the sample and the microstructure inside the material. After uniformly dispersing the samples, our team used the JEM-101 transmission electron microscope of Japan Electronics Corporation for TEM characterization. The X-ray energy dispersive spectrometer (XRD), manufactured in Panaco, Netherlands, with the model Empyrean, is used to determine the crystal form of BN materials. The Fourier infrared spectrometer (NICOLET6700) of ThermoElectric Technology Company of the United States determined the molecular structure and chemical composition of BN samples, such as functional groups. The spectra ranged from 400 to 4000 cm^{-1} , and the resolution was better than 4 cm^{-1} .

Batch Adsorption Experiments

Herein, neodymium nitrate hexahydrate was used as Nd(III) source to prepare Nd(III) stock solution. Test solutions of different concentrations needed to be obtained by diluting the stock solution. To adjust the acidity and alkalinity of the solution and explore the effect of the best acidity and alkalinity environment on the adsorbent's performance, it is necessary to add a small amount of HCl and NaOH to adjust the pH of the solution. After adjusting the pH of the solution, a certain amount of BN adsorbent was added, and it was fully shaken at 303.0 K for 12 h to ensure that the adsorption equilibrium was reached. Finally, the solution was separated through a 0.22- μm polyethersulfone membrane filter. In the adsorption kinetics of BN on Nd(III), the pH of the solution was adjusted to 6, and the test solution was taken out at certain intervals. To obtain the adsorption isotherm, the temperature was set at 303.0 K and 313.0 K in the experiment, the solution was obtained by subsequent separation, and the concentration of neodymium ions was determined by spectrophotometry at 632 nm. The performance of BN is reflected by the amount of Nd(III) adsorbed on the adsorbent per unit weight (adsorption capacity, q). The adsorption capacity at any time t and the adsorption capacity at equilibrium are denoted by q_t and

q_e ($\text{mg}\cdot\text{g}^{-1}$), respectively. C_0 is the initial concentration of the solution, the concentration at time t and the concentration at equilibrium time are C_t and C_e , respectively, V (L) is the volume of the solution, and m (g) is the amount of adsorbent. The calculation formula for the relevant parameters is as follows:

$$q_t = \frac{C_0 - C_t}{m} V \quad \dots(1)$$

$$q_e = \frac{C_0 - C_e}{m} V \quad \dots(2)$$

RESULTS AND DISCUSSION

Adsorption

To explore the effect of the initial pH of the neodymium stock solution on the BN adsorption performance, we adopted a batch experiment, adding 10 mg BN adsorbent to 100 ml of 50 $\text{mg}\cdot\text{L}^{-1}$ Nd(III) solutions with different initial pH. The results are shown in the figure. Fig. 1A shows that as the pH of the solution increases, the adsorption effect is significantly improved. Still, Fig. 1B shows that, without adding adsorbent, when the pH is greater than 7, the solution's residual Nd(III) content will also be greatly reduced. This is because when the hydrogen ion concentration in the solution is low, Nd(III) will form precipitation, which greatly interferes with the adsorption. Considering the above two situations, we believe that pH 6 is the most suitable, and we set the initial pH of the subsequent experiments to 6.

Fig. 2A shows the change curve of the adsorption amount of BN on Nd(III) with contact time. It can be seen that the adsorption amount of BN increases rapidly before 60 min, and the adsorption amount increases more rapidly in the range of 60-150 min. Slowly, the adsorption equilibrium was reached at about 150 min, and the maximum adsorption capacity was 207.3 $\text{mg}\cdot\text{g}^{-1}$. Through the adsorption process, the adsorption results can be predicted and verified according to the change of the adsorption amount with contact time. Herein, pseudo-first-order, pseudo-second-order, and intraparticle diffusion models are used to fit the experimental data. They can be expressed as linearized formulas (3-5) (Ho & McKay 1999, Ho 2006).

$$\ln(q_e - q_t) = \ln q_e - k_1 t \quad \dots(3)$$

$$\frac{t}{q_t} = \frac{1}{k_2 q_e^2} + \frac{t}{q_e} \quad \dots(4)$$

$$q_t = K_d \times t^{1/2} + I \quad \dots(5)$$

Herein, K_1 (min^{-1}) and K_2 ($\text{g}\cdot\text{mg}^{-1}\cdot\text{min}^{-1}$) are the rates of first, and second-order adsorption constants and K_d ($\text{g}\cdot\text{mg}^{-1}\cdot\text{min}^{-1/2}$) is the rate constant of intraparticle

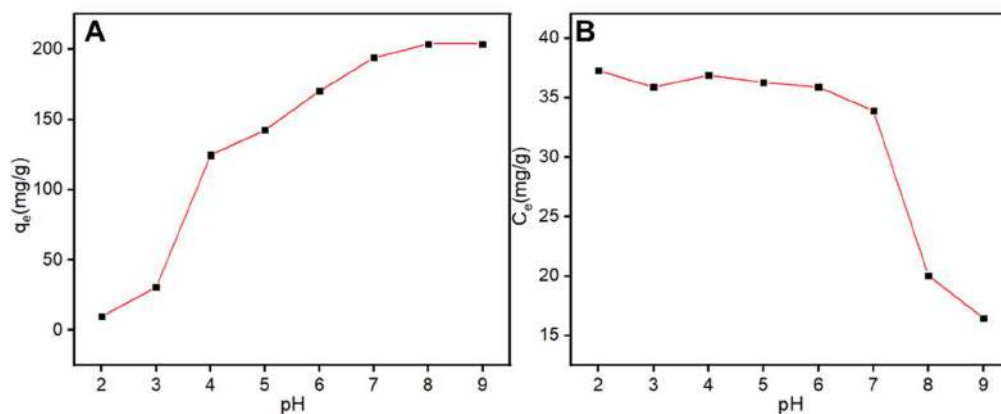


Fig. 1: Effect of initial pH value on BN adsorption capacity (q_e) (A), the residual concentration (C_e) of Nd(III) solution under different pH conditions (B).

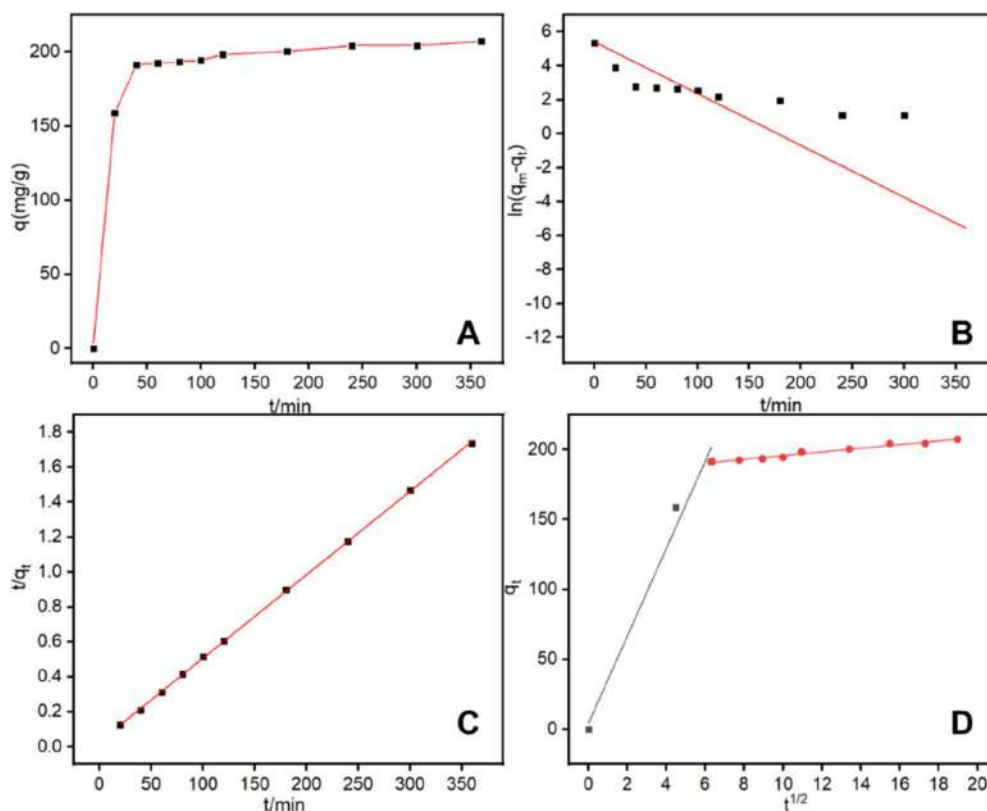


Fig. 2: Adsorption time curve of BN on Nd(III) solution (A), pseudo first order model (B), pseudo Second Order Model (C), intraparticle Diffusion Model (D), experimental conditions: initial pH is 6, $C=40 \text{ mg L}^{-1}$, $m=20 \text{ mg}$, $V=100 \text{ mL}$.

diffusion. I is the rate constant with the boundary Layer thickness-related parameters; the greater the thickness of the boundary layer, the greater the value of I will be. The relevant parameters of kinetic fitting are shown in Table 1. By comparing the experimental data of pseudo-first-order fitting and pseudo-second-order fitting, it is found that the

pseudo-second-order model best describes the adsorption of neodymium ions by BN. Among them, chemisorption is dominant (Shan et al. 2020). To further explore the adsorption mechanism of BN on neodymium ions, an intraparticle diffusion model was used for fitting. The result is shown in Fig. 2D. It can be seen that the adsorption process

Table 1: Adsorption kinetic model parameters.

Nd(III)/BN	Model							
	Pseudo first order		Pseudo second order		Intra-particle diffusion			
Parameters	q_e [mg.g ⁻¹]	224.856	q_e [mg.g ⁻¹]	209.643	I_1	4.320	I_2	182.544
	K_1	0.031	K_2 [g.mg ⁻¹ .min ⁻¹]	7.58×10^{-4}	K_{d1}	31.239	K_{d2}	1.316
	R^2	0.560	R^2	0.999	R^2	0.967	R^2	0.967

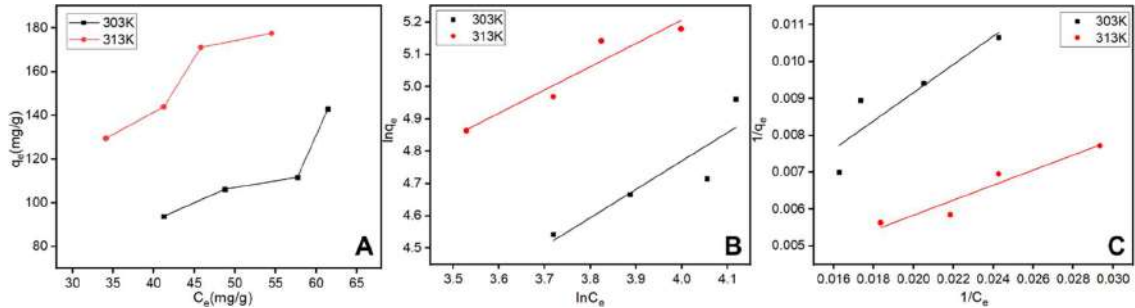


Fig. 3: Adsorption isotherms of BN on Nd(III) at T=303K and 313 (A), Freundlich model (B), Langmuir model(C), experimental conditions: initial pH is 6, m=20 mg, V=100 mL.

of BN is mainly divided into two stages. The first stage has a large slope and a short duration, indicating that the main adsorption process in this stage is the diffusion of neodymium ions to the material’s surface to complete the adsorption. In the second stage, the slope is small, and the adsorption equilibrium is reached.

The adsorption isotherm describes the relationship between the adsorption capacity (q_e) and the adsorbent’s equilibrium concentration (C_e) at equilibrium, which is very important for analyzing the adsorption process. Further, speculating on the adsorption mechanism (Li et al. 2014), Fig. 3 A shows the adsorption isotherms of BN for Nd(III) at 303K and 313K. It can be seen from the figure that with the increase of the remaining concentration, the adsorption capacity of the adsorbent is improved, which means that the higher concentration is favorable for the adsorption of BN. In addition, the increase in temperature also significantly improved the adsorption performance of the material, indicating that high temperature is beneficial to adsorption.

Table 2: Adsorption isotherm model parameters.

Nd(III)/BN	Model			
	Freundlich		Langmuir	
303K	1/n	1.138	q_m	666.667
	K_F	3.507	K_L	0.00392
	R^2	0.800	R^2	0.823
313K	1/n	1.388	q_m	568.182
	K_F	10.222	K_L	0.00864
	R^2	0.911	R^2	0.925

To gain a deeper understanding of the adsorption mechanism of BN, we adopted the Freundlich model and the Langmuir model, and the results are shown in Fig. 3B and Fig.3C. The linearization formulas of these two models are as follows (6-7) :

$$\ln q_e = \ln K_F + n \ln C_e \quad \dots(6)$$

$$\frac{1}{q_e} = \frac{1}{q_m} + \frac{1}{K_L \times q_m} \cdot \frac{1}{C_e} \quad \dots(7)$$

$K_F((\text{mg}^{1-n} \cdot \text{L}^n)/\text{g})$ and n are constants of the Freundlich model, K_F reacts to the adsorption capacity, and n is a nonlinear factor corresponding to the heterogeneous energy of the adsorption surface. $q_m(\text{mg g}^{-1})$ is the maximum adsorption capacity of the adsorbent, and $K_L(\text{L.mg}^{-1})$ is a constant of the Langmuir model, which is related to the stability of the binding site. Fig. 3B and Fig. 3C are the fitting results of the isotherm model, and the relevant parameters are shown in Table 2. The fitting of the two models is not in good agreement with the experimental results. The main reason is that the adsorption mechanism of BN on Nd(III) is complex, including both monolayer adsorption and multi-layer adsorption.

Characterization

To determine the morphology and structure of BN material, it was characterized by SEM and TEM. Fig. 4A and B are SEM characterization images of BN. It can be seen from the figure that BN material is overall flaky, with some defects and protrusions on the surface. These characteristics are conducive to improving the adsorption capacity of materials.

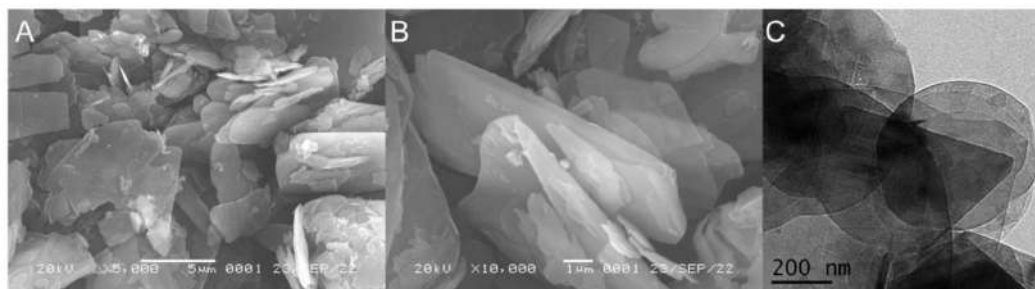


Fig. 4: SEM image (A, B) and TEM image (C) of BN.

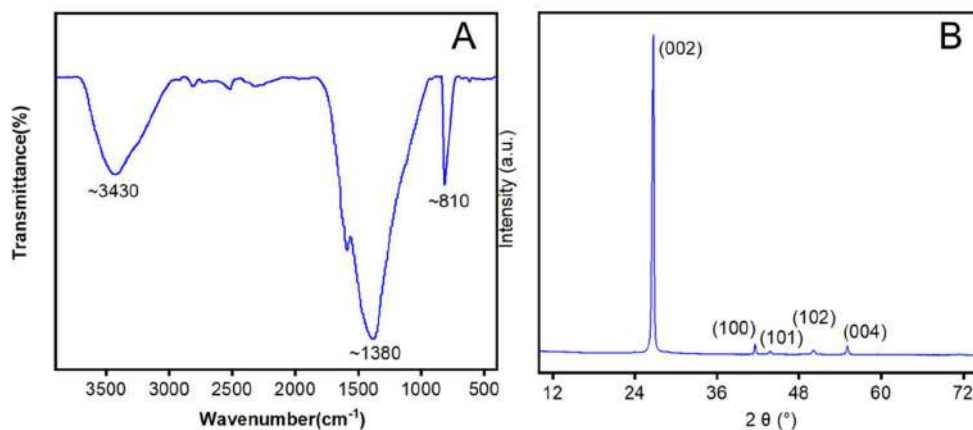


Fig. 5: FTIR spectra (A) and XRD pattern (B) of BN.

It can be seen from Fig. 4C that BN is an elliptical or circular sheet material, and the darker part in the figure is due to the overlapping of multi-layer sheet materials.

To determine the molecular structure and chemical composition of BN materials, such as functional groups, FT-IR was used to characterize them. The result is shown in Fig. 5A. Two characteristic absorption peaks were found at ~ 1380 and $\sim 810\text{cm}^{-1}$. According to the literature, the peaks were generated by B-N-B and B-N bending vibrations (Zhang et al. 2021). At $\sim 3430\text{cm}^{-1}$, a prominent broad peak may be because BN contains more -OH groups (Hou et al. 2019). Figure 5B is the XRD of BN material. The crystal plane diffraction peaks of BN appear at 26.7° , 41.5° , 43.8° , 50.1° , and 55.0° and correspond to the 002, 100, 101, 102, and 004 crystal planes of BN, respectively, which is consistent with the standard card 00-045-0893 (Matović et al. 2016).

CONCLUSION

Based on the above experiments and analysis, the BN material was prepared by a two-step synthesis method. The adsorption performance and mechanism of BN material for Nd (III) ions were investigated. The experimental results

showed that the adsorption capacity of BN was closely related to pH, and when pH was 6, the adsorption capacity of BN was the best; The kinetic data showed that the adsorption rate of BN was very fast in the first 50 min, and gradually decreased in the following 50 min. The adsorption balance could be reached in about 150 min. The adsorption amount in equilibrium was $207.3\text{mg}\cdot\text{g}^{-1}$.

Moreover, the kinetic data of BN well fitted the pseudo-second-order model, indicating that the adsorption process was dominated by chemical adsorption. In addition, the Freundlich and Langmuir models were used to fit and analyze the thermodynamic results. It was found that the adsorption process of BN on Nd (III) involves both monolayer adsorption and multilayer adsorption. SEM, TEM, FT-IR, and XRD also show that the surface morphology and functional groups of BN materials are conducive to improving their adsorption performance. In conclusion, BN is a low-cost material and a simple preparation method. It has a good adsorption effect for Nd (III) ions and has certain application prospects.

ACKNOWLEDGEMENT

The Zhejiang Basic Public Welfare Research project

supported the work in 2018 (LGG18B070002) and the Project of Shaoxing University (No. 2022LG003). We also sincerely thank the young and middle-aged academic cadres from Shaoxing University.

REFERENCES

- An, F., Li, X.F., Min, P., Li, H.F., Dai, Z. and Yu, Z.Z. 2017. Highly anisotropic graphene/boron nitride hybrid aerogels with long-range ordered architecture and moderate density for highly thermally conductive composites. *Carbon*, 126: 119-127.
- Emanet, M., Şen, Ö. and Çulha, M. 2017. Evaluating boron nitride nanotubes and hexagonal boron nitrides as nanocarriers for cancer drugs. *Nanomedicine*, 12(7): 797-810.
- Ho, Y.S. 2006. Review of second-order models for adsorption systems. *J. Hazard. Mater.*, 37: 681-689.
- Ho, Y.S. and McKay, G. 1999. Pseudo-second order model for sorption processes. *Process Biochem.*, 34: 451-465.
- Hou, Y., Yang, W., Zhong, C., Wu, S., Wu, Y., Liu, F., Huang, X. and Wen, G. 2019. Thermostable SiCO@ BN sheets with enhanced electromagnetic wave absorption. *Chem. Eng. J.*, 378: 122239.
- Kamimoto, Y., Itoh, T., Kuroda, K. and Ichino, R. 2017. Recovery of rare-earth elements from neodymium magnets using molten salt electrolysis. *J. Mater. Cycles Waste. Manag.*, 19(3): 1017-1021.
- Kim J.H., Pham, T.V., Hwang, J.H., Kim, C.S. and Kim, M.J. 2018. Boron nitride nanotubes: Synthesis and applications. *Nano Converg.*, 5(1): 1-13.
- Lale, A., Bernard, S. and Demirci, U.B. 2018. Boron nitride for hydrogen storage. *Chem PlusChem*, 83(10): 893-903.
- Li, J., Jin, P. and Tang, C. 2014. Cr(III) adsorption by fluorinated activated boron nitride: a combined experimental and theoretical investigation. *RSC Adv.*, 4: 14815-14821
- Li, J., Xiao, X., Xu, X., Lin, J., Huang, Y., Xue, Y., Jin, P., Zou, J. and Tang, C. 2013. Activated boron nitride is an effective adsorbent for metal ions and organic pollutants. *Sci. Rep.*, 3(1): 1-7.
- Li, L., Chang, K.K., Fang, P., Du, K., Chen, C.G., Zhou, S.D., Shen, C., Linghu, W.S., Sheng, G.D., Hayat, T. and Guo, X.J. 2020. Highly efficient Ni(II) scavenging by porous hexagonal boron nitride: Kinetics, thermodynamics and mechanism aspects. *Appl. Surf. Sci.*, 521: 146373.
- Matović, B., Luković, J., Nikolić, M., Babić, B., Stanković, N., Jokić, B. and Jelenković, B. 2016. Synthesis and characterization of nanocrystalline hexagonal boron nitride powders: XRD and luminescence properties. *Ceram. Int.*, 42(15): 16655-16658.
- Shan, R., Shi, Y., Gu, J., Bi, J., Yuan, H., Luo, B. and Chen, Y. 2020. Aqueous Cr (VI) removal by biochar derived from waste mangosteen shells: Role of pyrolysis and modification on its absorption process. *J. Environ. Chem. Eng.*, 8(4): 103885.
- Shin, S.H., Kim, H.O. and Rim, K.T. 2019. Worker safety in the rare earth elements recycling process from the review of toxicity and issues. *J. Environ. Chem. Eng.*, 10(4): 409-419.
- Song, Q., Fang, Y., Liu, Z., Li, L., Wang, Y., Liang, J., Huang, Y., Lin, J., Hu, L., Zhang, J. and Tang, C. 2017. The performance of porous hexagonal BN in high adsorption capacity towards antibiotics pollutants from aqueous solution. *Chem. Eng. J.*, 325: 71-79.
- Wilson, D.J., Piotrowski, A.M., Galy, A. and Nicholas, M.I. 2012. A boundary exchange influences deglacial neodymium isotope records from the deep western Indian Ocean. *Earth Planet. Sci. Lett.*, 341: 35-47.
- Wojcieszak, D., Kaczmarek, D., Domaradzki, J., Mazur, M., Morawski, A.W., Janus, M., Prociów, E. and Gemmellaro, P. 2012. Photocatalytic properties of transparent TiO₂ coatings doped with neodymium. *Pol. J. Chem. Tech.*, 14(3): 1-7.
- Yu, S.J., Wang, X.X., Pang, H.W., Zhang, R., Song, W.C., Fu, D., Hayat, T. and Wang, X.K. 2017. Boron nitride-based materials for removing pollutants from aqueous solutions: a review. *Chem. Eng. J.*, 333: 343-360.
- Zhang, Y., Si, H., Liu, S., Jiang, Z., Zhang, J. and Gong, C. 2021. Facile synthesis of BN/Ni nanocomposites for effective regulation of microwave absorption performance. *J. Alloys Compd.*, 850: 156680.
- Zhao, Q., Wang, Y., Xu, Z. and Yu, Z.S. 2021. Using straw-derived biochar as the adsorbent for La (III) and Nd (III) removal in aqueous solutions. *Environ. Sci. Pollut. Res.*, 28(34): 47024-47034.



Microbial Consortia Preparation for Amylase, Protease, Gelatinase and Lipase Production from Isolates Obtained from Organic Kitchen Waste

Snehal Masurkar[†] and Girish R. Pathade

Krishna Institute of Allied Sciences, Krishna Institute of Medical Sciences (Deemed to be University), Malkapur, Karad-415110, Maharashtra, India

[†]Corresponding author: Snehal Masurkar; snehalmasurkar2882@gmail.com

Nat. Env. & Poll. Tech.
Website: www.neptjournal.com

Received: 29-09-2022

Revised: 02-11-2022

Accepted: 12-11-2022

Key Words:

Amylase
Protease
Lipase
Gelatinase
Kitchen waste
Microbial consortium

ABSTRACT

Households, restaurants, canteens, and hotel wastes constitute kitchen waste. Every day our growing cities generate more and more waste, which is overloading our municipal systems. The main aim of the present work was to prepare a microbial consortium that can effectively and rapidly bring about the degradation of kitchen wastes that can be used in agricultural soils. More than 100 different bacterial isolates were obtained from various kitchen waste dumping areas. The bacterial isolates were studied to produce enzymes like amylase, gelatinase, lipase, and protease on respective media plates. The best 20 isolates were subjected to enzyme quantification. The isolates showing maximum production for all four enzymes were selected for consortia preparation. The consortia of isolates were prepared by permutation combinations. Amongst all consortia prepared consortium No. 7 showed maximum enzymatic potential. The bacterial isolates in the best consortium (No. 7) were further characterized and identified as KW104 *Serratia marcescens*, KW37 *Micrococcus luteus*, KW128 *Brevindimonas mediterranea*, KW91 *Bacillus tequilensis*, and KW97 *Exiguobacterium mexicanum*. This consortium showed rapid degradation of waste as compared to others in 15 days duration of time showing good potential for compost formation when applied to plant growth.

INTRODUCTION

Organic kitchen waste comprises to be a major proportion of the waste generated, causing pollution. These wastes are collected and dumped into landfills, causing major pollution (Bouallagui et al. 2004). The traditional composting method takes a relatively long time, several days to months. Recently, rapid or fast methods have been developed and are quite attractive and eco-friendly. Also, one of the limitations of these methods is that 100% degradation does not occur at the end of the process and some biodegradation process continues even after the end product (fertilizer) is applied to the soil. The period required for degradation is still too prolonged. Composting is one of the methods that can be followed for the degradation of kitchen waste, wherein microbes degrade the waste (Sarkar et al. 2011). A consortium of effective microorganisms contains many species of microorganisms capable of coexisting and bringing out the effective degradation of organic waste (Higa 1996). The biological treatment of kitchen waste appears to be the most cost-effective and carries less negative environmental impact (Coker 2006). Kitchen waste contains a high

proportion of biodegradable organic material and therefore, microorganisms can play important role in its degradation (Pan et al. 2012). The increase in the efficacy of the process is therefore desirable. Composting at home can be used as a sound method of kitchen waste management, and the waste can be managed at the source itself and thereby recycled.

MATERIAL AND METHODS

Food Waste Samples

Food waste samples were obtained from houses, canteens, and cafeterias nearby Karad and preserved in the laboratory until further use.

Isolation of Bacteria from Food Waste Samples

Microorganisms are isolated from kitchen food wastes in liquid enrichment culture, followed by isolation on solid media. Representative pure isolates were characterized based on their biochemical and morphological properties and preserved at 40°C till further use.

Primary Screening of Bacteria for Amylase, Protease, Lipase and Gelatinase Production

The selected bacteria from enrichment were grown on milk agar and gelatin agar plates. The colonies showing zones of hydrolysis were further selected for production and characterization.

The Gelatinase Estimation

The good strain selection was made by secondary screening method. The best bacterial strain obtained was inoculated in 100 mL gelatin broth and incubated for 48 h at 30°C. The Aliquot of culture broth was centrifuged at 7000 rpm for 20 min, and pellet supernatant was separately obtained. The pellet was added to the buffer and suspended andsonicated for one min and the remaining broth was used without centrifugation.

Estimation of Gelatinase Enzyme

The Tran & Nagano (2002) method was used for the gelatinase assay. The gelatinase units are expressed as expressed mol of leucine equivalent per min.mL⁻¹ of the culture filtrate

Estimation of Protease

The enzyme protease was estimated by using the Begetal method. The unit of protease activity was defined as the enzyme required to release 1 micro -gm of tyrosine per mL per min.

The Amylase Estimation

The amylase assay was done by the DNSA method. The one unit of enzyme activity was measured as the amount of enzyme that releases 1µmole of reducing sugar (glucose) per minute under assay conditions (U.mL⁻¹.min⁻¹).

The Estimation of Lipase

For the quantitative estimation of lipase titrimetric method was used. The unit of enzyme is defined as the amount of enzyme that releases 1 µmole of fatty acid per minute under assay conditions and calculated as

Lipase activity =

$$\frac{(\text{Volume of titrant alkali, mL}) \times (\text{Normality of NaOH})}{(\text{Time of incubation}) \times (\text{Volume of enzyme solution, mL})}$$

Preparation of Bacterial Consortium

The best 20 isolates were selected for consortia by permutation and combination. The ten different combinations were prepared. The antagonism assays and maximum enzyme production of the bacterial isolates at certain intervals. (24 h, 48 h, 72 h, 4 days, 5 days) was studied.

Characterization of Bacterial Isolates Obtained from the Best Consortium

16srRNA gene sequencing studies identified the members from the best consortium.

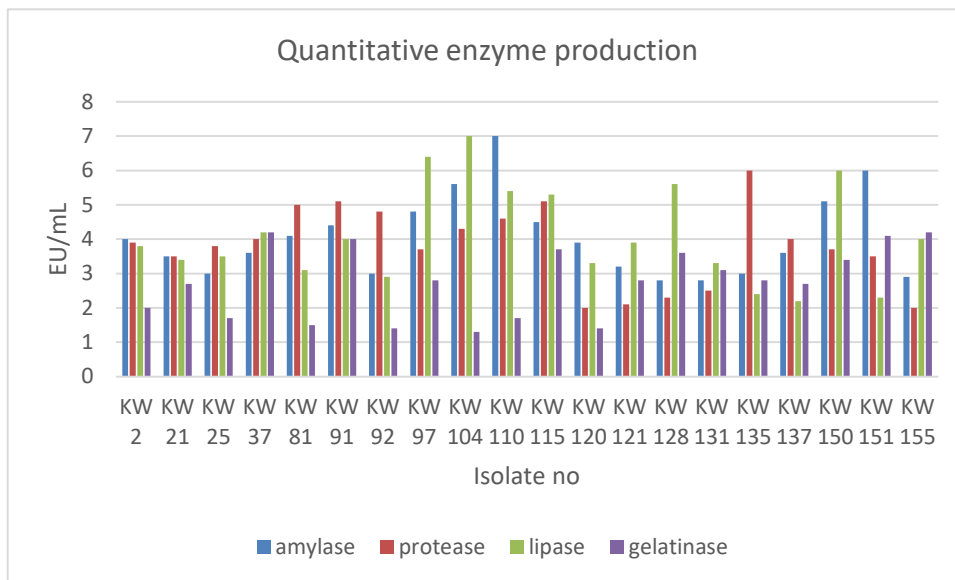


Fig. 1: Quantitative enzyme production.

Table 1: Quantitative enzyme assays for 20 promising isolates.

Sr. No.	Quantitative enzyme production by obtaining the best isolates expressed in EU.mL ⁻¹				
	Isolate No.	Amylase	Protease	Lipase	Gelatinase
1.	KW 2	4	3.9	3.8	2
2.	KW 21	3.5	3.5	3.4	2.7
3.	KW 25	3	3.8	3.5	1.7
4.	KW 37	3.6	4	4.2	4.2
5.	KW 81	4.1	5	3.1	1.5
6.	KW 91	4.4	5.1	4	4
7.	KW 92	3	4.8	2.9	1.4
8.	KW 97	4.8	3.7	6.4	2.8
9.	KW 104	5.6	4.3	7.0	1.3
10.	KW 110	7	4.6	5.4	1.7
11.	KW 115	4.5	5.1	5.3	3.7
12.	KW 120	3.9	2	3.3	1.4
13.	KW 121	3.2	2.1	3.9	2.8
14.	KW 128	2.8	2.3	5.6	3.6
15.	KW 131	2.8	2.5	3.3	3.1
16.	KW 135	3	6	2.4	2.8
17.	KW 137	3.6	4	2.2	2.7
18.	KW 150	5.1	3.7	6	3.4
19.	KW 151	6	3.5	2.3	4.1
20.	KW 155	2.9	2	4	4.2

RESULTS AND DISCUSSION

Identification of Bacteria

Out of 157 isolates, 20 best isolates were selected for further study based on the larger zones of hydrolysis. They were designated as KW-2, KW-21, KW25, KW37, KW81, KW81,

KW91, KW92, KW97, KW104, KW110, KW115, KW120, KW121, KW128, KW131, KW155, KW135, KW137, KW150, KW15. All these isolates were subjected to enzyme production quantitatively (Table 1 and Fig. 1).

All these 20 were selected for preparing 10 consortia using permutation combination with five isolates in each consortium (Table 2).

After this, all these consortia were subjected to compatibility tests. From the compatibility studies, it was

Table 2: Types of consortia.

Consortia	Isolate Composition/combination				
1	KW2	KW81	KW110	KW131	KW155
2	KW21	KW115	KW135	KW151	KW25
3	KW37	KW97	KW121	KW150	KW91
4	KW92	KW104	KW120	KW128	KW137
5	KW2	KW115	KW110	KW151	KW155
6	KW21	KW97	KW135	KW150	KW25
7	KW37	KW104	KW97	KW128	KW91
8	KW92	KW115	KW120	KW151	KW137
9	KW2	KW97	KW110	KW150	KW155
10	KW21	KW104	KW135	KW128	KW25

Table 3: Quantitative enzyme production from six consortia.

Sr. No.	Consortia No.	Quantitative enzyme production by consortia EU.mL ⁻¹			
		Amylase	Protease	Lipase	Gelatinase
1	1	10	15	15	11
2	3	12	20	18	13
3	6	9	10	16	15
4	7	18	22	18	19
5	9	10	15	13	16
6	10	13	16	12	12

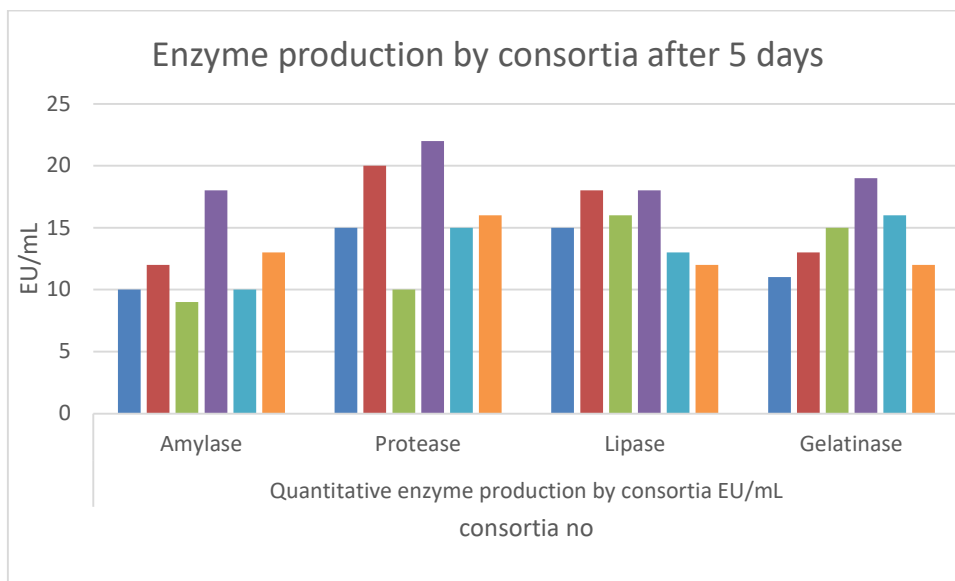


Fig. 2: Enzyme production by consortia after 5 days.

Table 4: Colony properties of members of the best consortium.

No.	Size	Shape	Color	Margin	Elevation	Opacity	Consistency
KW-37	2mm	Circular	Red	Entire	Low convex	Opaque	Moist
KW-128	1mm	Circular	White	irregular	Flat	translucent	Dry
KW-91	2mm	Circular	white	irregular	Flat	translucent	Moist
KW-97	1mm	Circular	white	irregular	Flat	translucent	Moist
KW-104	2mm	Circular	orange	Entire	Convex	Opaque	Moist

clearly understood that 6 consortia were compatible with each other for all enzyme production (Table 3).

The above results indicate that consortium No. 7 was more effective for the production of respective enzymes (Fig. 2). 16SrRNA Sequencing identified the isolates of consortium No. 7.

Cultural, Morphological and Biochemical Characteristics of the Isolates from Consortium No. 7

Table 5: Gram nature and motility property of the promising isolates from consortium No. 7.

Sr. No.	Isolate No.	Gram Nature	Motility
1.	KW-37	Gram-positive, cocci shaped.	Motile
2.	KW-128	Gram Positive, rod-shaped	Motile
3.	KW-91	Gram-positive rods	Motile
4.	KW-97	Gram-positive rods	Motile
5.	KW-104	Gram negative, coccobacilli/ short rods	Motile

The cultural, morphological, and biochemical characteristics of the obtained isolates are shown in Tables 4, 5, 6 & 7 respectively. The colony properties of members of all the bacteria present in best consortia are presented in Table 4.

Table 5 shows the gram nature and motility of the promising isolates from consortium No. 7.

The detailed biochemical characterization of the obtained promising isolates from consortium 7 is given in Table 6.

The promising isolates from consortium No. 7 were identified by 16 S rRNA Gene sequencing. The results of gene sequence identification and obtained gene accession numbers are given in Table 7.

A total of 157 bacterial isolates were obtained. In the secondary screening, 20 were found promising and were used to prepare different consortia. Out of 10 consortia, consortia No. (7) was the best consortium. Out of the promising isolates, one was cocci, three were rods and one was coccobacillus in nature. The 16 -SrRNA gene sequencing studies identified them as *Micrococcus luteus*,

Table 6: Biochemical Characteristics of the promising isolates from Consortium No. 7.

Test	KW-37	KW-128	KW-91	KW-97	KW-104
Sugars :-(fermentation) Glucose	-ve	+ve	+ve	+ve	+ve
Sucrose	+ve	+ve	+ve	+ve	+ve
Fructose	-ve	+ve	+ve	+ve	+ve
Arabinose	-ve	+ve	+ve	+ve	+ve
Lactose	+ve	+ve	+ve	+ve	+ve
Mannitol	+ve	-ve	-ve	-ve	-ve
L-Tryptophan (indole production)	-ve	+ve	+ve	+ve	+ve
Sodium pyruvate (vogesproskauer)	-ve	+ve	+ve	+ve	+ve
Methyl red	+ve	+ve	+ve	+ve	+ve
Urease	+ve	-ve	-ve	-ve	-ve
Catalase	-ve	+ve	+ve	+ve	+ve
Citrate	+ve	+ve	+ve	+ve	+ve
Gelatin hydrolysis	+ve	+ve	+ve	+ve	+ve
Starch hydrolysis	+ve	+ve	+ve	+ve	+ve

Bacillus tequilensis, *Exiguobacterium mexicanum*, and *Serratia marcescent*. Consortium No. (7) was found to be an effective consortium that can be used for faster degradation of organic kitchen waste as compared with the reports of Anuradha *et. al*(Anuradha.S.Tanksali Sridevi.S.Angadi Asha.Arwikar2014).

It can be used as an effective and fast method for deleting kitchen waste and forming compost. Fang *et al.* (2001) prepared a consortium of three organisms. Results and therefore present the maiden report.

In contrast, Karnchanawong & Nissaikla (2014), based on their extensive studies, concluded that adding inoculants to facilitate composting household organic waste was not necessary; instead and mature compost can be used as a seed starter to improve composting. Anwar *et al.* (2017) reported optimum biodegradation of kitchen waste by a consortium of *Serratia s*, *Pseudomonas aeruginosa*, *Bacillus cereus*, *Bacillus subtilis*, and *Bacillus megaterium* at 7.0 pH and 45°C temperature. In view of previous reports, our results

Table 7: Summary of the closest neighbour(s) for promising isolates in consortium No. 7:

Strain No.	ClosestNeighbour*	
	TaxonomicDesignation	Accession No. (NCBI)
KW-37	<i>Micrococcus luteus</i> NCTC2665(T)	OP482489
KW-128	<i>Brevundimonas mediterranea</i> V4. BO.10(T)	OP482496
KW-91	<i>Bacillus tequilensis</i> KCTC13622(T)	OP482499
KW-97	<i>Exiguobacterium mexicanum</i> 8N(T)	OP482500
KW-104	<i>Serratia marcescens</i> ATCC13880(T)	OP482501

are better as we used seven different enzymatic potentials by best consortia.

CONCLUSION

These promising isolates obtained in the present study have the potential to be used in a consortium of fast degradation of kitchen waste samples.

ACKNOWLEDGEMENTS

The authors of this study are thankful to Hon. Chairman Dr. Suresh J. Bhosale, Krishna Charitable Trust, and the Research Fund Allocation Committee of KIMSDU for the facilitation of the Ph. D. work.

REFERENCES

Anuradha, S., Tanksali, S., Angadi, S. and Asha, A. 2014. Treatment of kitchen waste by microbial culture. *Int. J. Res. Eng. Technol.*, 3: 115.

Anwar, H., Ashraf, M., Saqib, M., Ashraf, M.A. and Ishfaq, K. 2017. Isolation and screening of biodegrading bacteria from kitchen waste and optimization of physiochemical conditions to enhance degradation. *Int. J. Sci. & Eng. Res.*, 8(4): 2229-5518.

Bouallagui, H., Hamdi, M., Cheikh, R.B., Touhami, Y., Delgenes, J.P. and Hamdi M. 2004. Two-phase anaerobic digestion of fruit and vegetable wastes: Bioreactor performance. *Biochem. Eng. J.*, 21(2): 193-197.

Coker, B. 2006. Environmental remediation by composting. *Biocycle*, 47: 18-23.

Fang, M., Wong, M.H. and Wong, J.W.C. 2001. Digestion activity of thermophilic bacteria isolated from ash-amended sewage sludge compost. *Water, Air, and Soil Pollution*, 126: 1-12.

Higa, T. 1990. Composting and composting of solid animal manure. *Norsk Land Bruks Forsking*, 4 : 245-256.

Karnchanawong, S. and Nissaikla, S. 2014. Effects of microbial inoculation on composting of household organic waste using passive aeration bin.

- International Journal of Recycling of Organic Waste in Agriculture, 3: 113-119.
- Pan, I., Bomba, D. and Sen, S.K. 2012, Composting of common organic wastes using microbial inoculants. *Biotech.*, 2(2): 127-134.
- Sarkar, P., Meghvanshi, M. and Singh, R. 2011. Microbial consortium: A new approach to ineffective degradation of organic kitchen wastes. *Int. J. Environ. Sci. Dev.*, 62: 326-332.
- Tran, L.H. and Nagano, H. 2002. Isolation and characteristics of *Bacillus subtilis* CN2 and its collagenase production. *J. Food Sci.*, 67(3): 1184-87.
- Yoon, S., Ha, S., Kwon, S., Lim, J., Kim, Y., Seo, H. and Chun, J. 2017. Introducing EzBioCloud: A taxonomically united database of 16-SrRNA and whole-genome assemblies. *Int. J. Syst. Evol. Microbiol.*, 67: 1613-1617.



Denaturing Gradient Gel Electrophoresis (DGGE) Analysis Indicating Increased Microbial Diversity in Landfill Area Near Conserved Wetland

M. B. Chakraborty[†], S. R. Patgiri, A. S. Rahman, A. Dasgupta and G. Pegu

Department of Botany, Cotton University, Guwahati-781001, Assam, India

[†]Corresponding author: M. B. Chakraborty; moitrayeebchakraborty@cottonuniversity.ac.in

Nat. Env. & Poll. Tech.
Website: www.neptjournal.com

Received: 17-06-2022

Revised: 06-10-2022

Accepted: 15-10-2022

Key Words:

Anthropogenic disturbance
Landfill
Leachate
Microbial diversity
DGGE

ABSTRACT

The ecological balance of an ecosystem has a relation to its biodiversity. Although it has been established that biodiversity and ecological stability are related, generalization about the exact nature of this relation remains elusive and more so in microbial diversity. A growing volume of studies has indicated that anthropogenic activities impact biodiversity, but it is difficult to generalize the impact of anthropogenic activities on microbial diversity. Landfilling by municipal solid waste is one such activity where microbes play a major role, and leachates are released from the landfill, altering the soil's physical and chemical nature. Change in factors like carbon source, pH, and toxicity of the soil is most likely to affect the indigenous microflora of the soil. The present study was undertaken to compare the microbial diversity of soil receiving landfill leachate with that of the soil not receiving any landfill leachate to assess the impact of the landfilling activity on microbial diversity. The landfill site selected for the study was that of Kamrup Metro District of Assam, located at Boragaon, near the Ramsar wetland called Deeporbeel. By using the Denaturing Gradient Gel Electrophoresis (DGGE) method, it has been found that the microbial diversity of the soil receiving leachate was higher than that of the soil not receiving any leachate from the landfill.

INTRODUCTION

Most biodiversity studies have focused mostly on plants and animals. Ecological theories have been developed by studying aboveground ecosystems but have neglected the below-ground systems, despite the latter's importance to global nutrient cycling and life on the Earth (Lynch et al. 2004). The study of microbial diversity by culture-dependent methods had been limited earlier because only 1% of the total microflora can be cultured under lab conditions. Recent use of culture-independent methods like DGGE and metagenomics has brought newer insights into microbial ecology. Despite these advances, the link between microbial diversity and soil functions is still a major challenge. Several field studies have examined how disturbance affects microbial diversity, but the findings of different studies contradict each other. The lack of consensus on how disturbance affects microbial diversity highlights the need for more studies in this field.

In general ecology, Wilhm (1967) observed that benthic diversity was depressed in the Oklahoma stream, receiving inadequately treated municipal wastes. Increased exposure to mercury in the field decreased the sequence diversity of bacteria (Muller et al. 2001). No difference in bacterial diversity between operational and non-operational landfill

was observed (Jayanthi et al. 2016). Song et al. (2015) investigated the bacterial communities of ten landfill leachate samples from five landfill sites in China and found that the bacterial community function (e.g., cellulolytic bacteria, sulfate-reducing bacteria (SRB), sulfate-oxidizing bacteria, and xenobiotic organic compound (XOC)-degrading bacteria) was diverse, but the pattern is unclear. The stored waste's conductivity, organic matter, and moisture content strongly correlate with microbial diversity (Wang et al. 2016). Pérez-Leblic et al. (2012) observed low diversity of microorganisms and decreased enzymatic activity with an increase in the concentration of hydrocarbons. Contradictory findings make generalizing the relationship between microbial diversity and ecological disturbance difficult. The dynamics of the biotic and abiotic components of the landfills remain far from being fully understood. According to Themelis and Ulloa (2007), it is inevitable to gain further knowledge about the microbially mediated processes in landfills since landfilling is still the major way of depositing waste at a global scale.

MATERIALS AND METHODS

Collection of Soil Samples

For this study, soil samples were collected from two different

sites, one adjacent to the landfill site and receiving leachate from it and the other situated away from the landfill site towards wetland Deepor Beel and not receiving any leachate from the landfill. A composite sample of the soil receiving leachate from the landfill was collected from five different sites within the inactive landfill site of Paschim Boragaon area (26°06.872'' N and 91°40.896'' E Site Elevation: 46.9m above sea level), and another composite soil sample that did not receive any landfill leachate was collected from five different sites near the Ramsar wetland of Deeporbeel (located between latitude 26°03'26''-26°09'26''N and longitude 90°36'39''-90°41'25''E) were transported to the laboratory in ice-pack at 4°C. Soil samples were collected from a depth of 7.5 cm using a sterile spatula and transferred to a sterile container. Soil samples were labeled broadly as polluted (P₁ P₂) receiving leachate and non-polluted (N₁, N₂) not receiving any leachate. Each sample was a composite sample of 5 subsamples collected from 5 different sites.

Extraction of DNA from Soil

0.25 g of each sample was used to isolate the DNA. DNA was directly extracted from the soil samples using *PowerSoil*® *DNA Isolation Kit* (Mo Bio Laboratories Inc.), and nano reading was noted.

Gel Electrophoresis

0.8% Agarose gel is prepared in TAE buffer. The gel was poured into the gel cast, and a 1mm thick comb was put in to make wells. After about 30 minutes at room temperature,

the comb was removed carefully, and DNA samples of each soil sample were loaded. The gel was then run in the electrophoretic unit to separate the DNA.

PCR Amplification

This study used the PCR technique to amplify DNA for 16S rRNA. Primers for PCR were designed to be specific for 16S rRNA. A forward primer designated as F-968 and a reverse primer situated at position 1401 were used to amplify bacterial 16S rRNA gene fragments. The PCR amplified the V6-V8 region of the DNA.

Denaturing Gradient Gel Electrophoresis (DGGE)

A 30% polyacrylamide gel with a 35-55% denaturant gradient was prepared. The comb of 1mm thickness was inserted to produce wells. The gel was allowed to cool for an hour. After the gel had cooled down, the wells were loaded roughly with an equal amount of DNA sample (50µl) with 5µl loading dye. Electrophoresis was carried out 1x TAE buffer at 100V for 16-17 hrs at 60°C. The gel was stained in 0.5µg/ml ethidium bromide for 15-20 mins. The gel was then destained in water, observed under a UV transilluminator at 256 nm, and photographed.

RESULTS AND DISCUSSION

DNA Concentration from Soil Sample

The DNA concentration in the samples N₁, N₂, P₁, and P₂ were studied using Nanodrop software (Table 1).

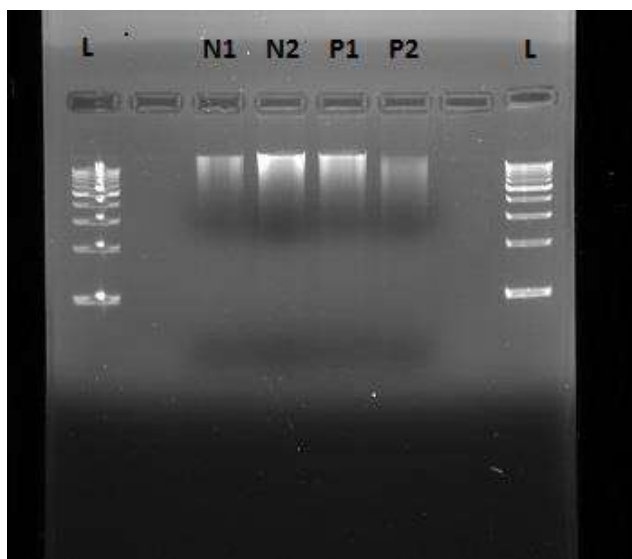


Fig. 1: Result of Gel Electrophoresis. L = Ladder DNA, N₁ = DNA Sample of N₁ Site, N₂ = DNA Sample of N₂ Site, P₁ = DNA Sample of P₁ Site, P₂ = DNA Sample of P₂ Site.

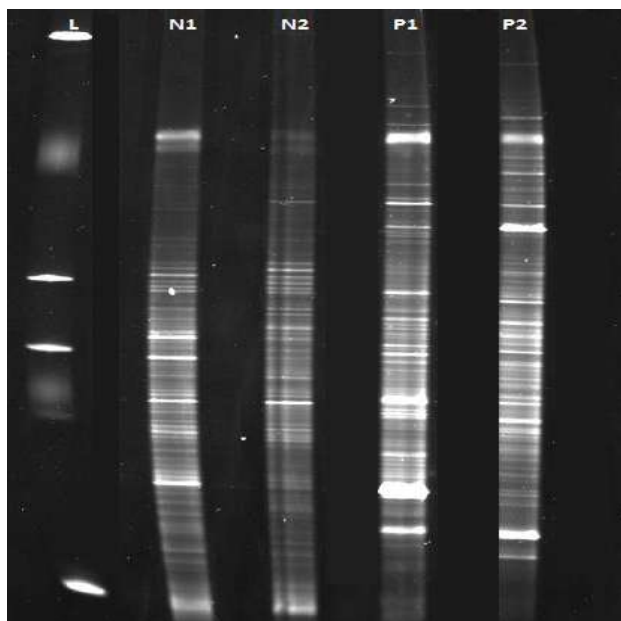


Fig. 2: Result of DGGE (Density Gradient Gel Electrophoresis) analysis. L = Ladder DNA, N1 = Bacterial Diversity of N1 Site, N2 = Bacterial Diversity of N2 Site, P1 = Bacterial Diversity of P1 Site, P2 = Bacterial Diversity of P2 Site.

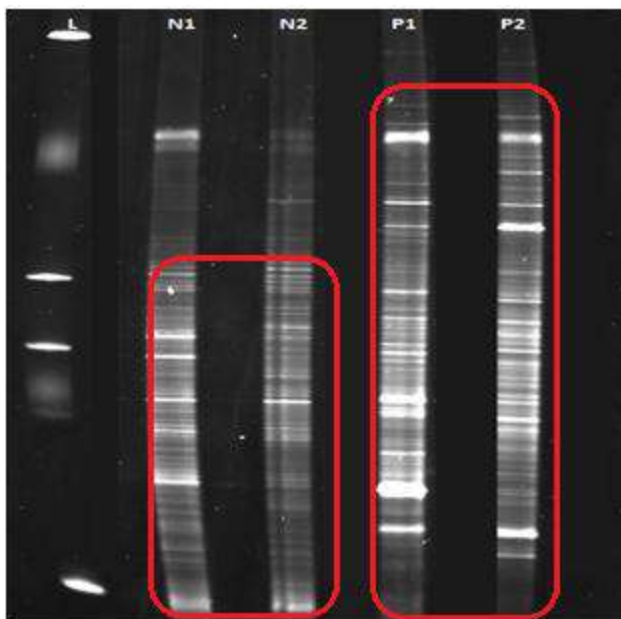


Fig. 3: Comparison of DNA bands separated by Density Gradient Gel Electrophoresis (DGGE). Polluted soil samples show more bands corresponding to higher bacterial diversity.

The nucleic acid concentration given by nanodrop reading gives an idea about the purity of the genomic DNA content extracted from the soil samples. The ratio of absorbance at 260 nm and 280 nm is used to assess the purity of DNA and RNA extracted from the sample (Fig. 1). A ratio of ~ 1.8 is accepted as pure for DNA, and a ratio of ~ 2.0 for RNA (Page

2010). In our samples, though the nucleic acid concentration in N1 is quite high, i.e., $50.4 \text{ ng} \cdot \mu\text{l}^{-1}$, the A260/A280 ratio is appreciably less, which may indicate the presence of protein or other contaminants that also absorb strongly at 280 nm. The 260/280 ratio of the N2, P1, and P2 samples is ~ 2.0 , which may indicate RNA contamination. Sometimes

Table 1: The DNA concentration in the samples N1, N2, P1, and P2 using Nanodrop software.

SL.	Sample	Nucliec Acid Conc.($\mu\text{g.ml}^{-1}$)	A260	A280	260/280	260/230	Sample Type
1.	BLANK	0.0	0.001	-0.043	-0.02	0.01	DNA
2.	N1	50.4	1.007	2.066	0.49	0.48	DNA
3.	N2	26.1	0.522	0.266	1.96	23.51	DNA
4.	P1	22.6	0.453	0.277	2.00	-55.31	DNA
5.	P2	12.7	0.254	0.127	2.00	-3.89	DNA

variation in the ratio might also occur due to changes in sample pH (Wilfinger et al. 1997). The A260/A230 ratio is a secondary measure of nucleic acid purity. The A260/A230 ratio values for pure samples should be more than the respective A260/A280 values. In our samples, we got an appreciably low value indicating greater salt in the extract (Smith et al. 2010). Urea, carbohydrates, and phenolate ions also have absorbances near 230 nm, which might hinder the absorbance of nucleic acid.

Agarose gel electrophoresis of the purified DNA compliments the data obtained from absorbance readings. The concentration of DNA is determined after the gel electrophoresis is completed. The DNA in the agarose gel is visualized by staining with intercalating agents like ethidium bromide. This method is useful in cases where the contaminants absorbing at 260nm make accurate quantification impossible.

DGGE (Denaturing Gradient Gel Electrophoresis) of the amplified 16S rDNA is a culture-independent technique frequently used for bacterial community analysis in microbial ecosystems. DGGE separates the bacterial DNA of different species depending on their GC content. The different bands obtained after the DGGE indicate the diversity of bacterial species in the sample. The separated DNA from DGGE is visualized after staining with ethidium bromide. Each prominent band indicates a bacterial species. We can see a difference between the bacterial diversity of the non-polluted soil sample (N1 & N2) and the polluted soil sample (P1 & P2). A few species are also common to both sites. The polluted site is seen to be more diversified than the non-polluted site, as indicated by the DGGE bands.

Findings from DGGE analysis (Fig. 2) show that the number bands indicating different bacteria are more in the soil receiving leachate. In Fig. 3, it can be seen that some bacteria are common to both the polluted soil samples (box a, b, and e), while some bacteria are common to non-polluted soil samples (box c). Some bacteria have been found in all the soil samples (box d). Many ecological studies have indicated that high species diversity positively correlates with a system's ecological stability and that anthropogenic disturbances reduce species diversity. But

findings from the present study indicate higher bacterial diversity in the disturbed soil receiving leachate from landfill. The findings may be interpreted in the light of the intermediate disturbance hypothesis, which suggests that at low disturbance frequency, species diversity is low because competitively dominant species exclude competitively inferior species, while at high disturbance frequency, species diversity is low because only species that quickly colonize and reach maturity can survive. Only at intermediate levels of disturbance do a mix of colonizers and competitors co-exist (Hughes 2010).

CONCLUSION

The study shows that the microbial diversity of the soil receiving landfill leachate differs from that of the indigenous microflora of the soil not receiving any leachate. Contradictory to the expectation of lower microbial diversity in the polluted soil, it has been found that the microbial diversity of the soil receiving landfill leachate was higher than that of the soil not receiving any leachate. The increase in diversity can be interpreted in the light of Such a shift in microbial community structure can have some serious implications in the long run and affect other ecosystems. The ecological balance of the adjacent Ramsar wetland of Deepor beel seems to be under threat due to the landfilling activity.

ACKNOWLEDGEMENT

We express gratitude to Dr. Madhusmita Dehingia and Dr. Manasi Das of the Institute of Advanced Study in Science & Technology (IASST), Gorchuk, Paschim Boragaon, Guwahati-35, Assam, for extending technical support.

REFERENCES

- Hughes, A. 2010. Disturbance and diversity: An ecological chicken and egg problem. *Nature Educ. Knowl.*, 3(10): 48.
- Jayanthi, B., Emenike, C.U., Agamuthu, P., Simarani, K., Mohamad, S. and Fauziah, S.H. 2016. Selected microbial diversity of contaminated landfill soil of Peninsular Malaysia and the behavior towards heavy metal exposure. *J. Catena*, 147: 25-31.

- Lynch, J.M., Benedetti, A., Insam, H., Nuti, M.P., Torsvik, K.V. and Nannipieri, P. 2004. Microbial diversity in soil: Ecological theories, the contribution of molecular techniques and the impact of transgenic plants and transgenic microorganisms. *Biol. Fertil. Soils*, 36(3): 385.
- Muller, A.K., Rasmussen, L.D. and Sorensen, S.J. 2001. Adaptation of bacterial community to mercury contamination. *FEMS Microbiol. Lett.*, 204: 49-53. Doi. 10.1016/S0378-1097(01)00376-7.
- Page, A.F. 2010. *The MIQE Guidelines and Assessment of Nucleic Acids Prior to qPCR and RT-qPCR*. Thermo Fischer Scientific, Wilmington, Delaware, USA, pp. 1-3.
- Pérez-Leblic, M.I., Turmero, A., Hernández, M., Hernández, A.J., Pastor, J., Ball, A.S., Rodríguez, J. and Arias, M.E. 2012. Influence of xenobiotic contaminants on landfill soil microbial activity and diversity. *J. Environ. Manag.*, 95: S285-S290. <https://doi.org/10.1016/j.jenvman.2010.07.017>
- Smith, H.L., Hickey, J., Jablin, M.S., Trujillo, A., Freyer, J.P. and Majewski, J. 2010. Mouse fibroblast cell adhesion was studied by neutron reflectometry. *Biophys. J.*, 98(5): 793-799. <https://doi.org/10.1016/j.bpj.2009.11.019>
- Song, L., Wang, Y. and Tang, W. 2015. Bacterial community diversity in municipal waste landfill sites. *Appl. Microbiol. Biotechnol.*, 99: 7745. <https://doi.org/10.1007/s00253-015-6633>
- Themelis, N.J. and Ulloa, P.A. 2007. Methane generation in landfills. *Renew. Energy*, 32: 1243-1257
- Wang, X., Cao, A., Zhao, G., Zhou, C. and Xu, R. 2016. Microbial community structure and diversity in a municipal solid waste landfill. *Waste Manag.*, 66: 79-87. DOI: 10.1016/j.wasman.2017.04.023.
- Wilfinger, W.W., Mackey, K. and Chomczynski, P. 1997. Effect of pH and ionic strength on the spectrophotometric assessment of nucleic acid purity. *Biotechniques*, 22(3): 474-481. Doi: 10.2144/97223st01.
- Wilhm, J.L. 1967. Comparison of some diversity indices applied to populations of benthic macroinvertebrates in a stream receiving organic wastes. *J. Water Pollut. Control Fed.*, 39: 1673.



Biodegradation and Kinetic Study of Hazardous Metribuzin Herbicide Using a Novel Soil Bacterial Isolate *Olivibacter oleidegradans* Strain SP01 in Aqueous Solution

Sulbha R. Kadam and Madhuri K. Pejaver

Department of Environmental Science, B. N. Bhandarkar College of Science, Thane, 400601, India

†Corresponding author: Sulbha Ramchandra Kadam; sulbha.kadam86@gmail.com

Nat. Env. & Poll. Tech.
Website: www.neptjournal.com

Received: 05-11-2022

Revised: 10-12-2022

Accepted: 24-12-2022

Key Words:

Metribuzin

Olivibacter oleidegradans

Pesticide degradation

Soil isolate

Bioremediation

ABSTRACT

In the present work, degradation of the herbicide metribuzin ($C_8H_{14}N_4OS$) has been performed. A novel metribuzin-degrading bacterium, *Olivibacter oleidegradans* strain SP01, was isolated from the metribuzin-contaminated soil by an enrichment technique. To investigate the effect of various parameters on metribuzin degradation, various experiments were performed at an initial concentration in the range of 20-100 $mg.L^{-1}$, a pH of 5-9, and a temperature of 25-40°C. Around 85% of the highest percentage degradation of metribuzin was obtained at a concentration of 20 $mg.L^{-1}$ in 120 h under optimized conditions. The current work for the Metribuzin degradation study fits well with first-order reactions. Also, at higher concentrations, i.e., 100 $mg.L^{-1}$, only 40.3% degradation of metribuzin was observed. The *Olivibacter oleidegradans* strain SP01 has the potential to be extremely beneficial in the removal of Metribuzin from the environment.

INTRODUCTION

Pesticides are used to kill or prevent the growth of pests that cause damage to crops, shrubs, trees, timber, and other desirable vegetation. Pesticides are classified into various groups based on their application, such as insecticides, herbicides, fungicides, nematicides, rodenticides, micro biocides, and so on. Worldwide, various pesticides of different chemical formulas are widely used for both agricultural and non-agricultural practices. Currently, in Asia, India is the leading pesticide manufacturing and utilizing country and has acquired the 12th rank in the global market (Mathur 1999). India is the world's second-most populous country, and its economy is mainly based on agriculture. Hence, a large number of pesticides are used to increase agricultural yield and meet the food demand of the population. Pesticides enter the environment through different routes: (i) agricultural water runoff; (ii) effluent discharge from pesticide manufacturing industries; (iii) formulating industries; and (iv) chemical spills (Sakkas et al. 2005). Once it enters the water stream, it causes severe threats to human beings and the environment.

Metribuzin is a herbicide of the triazinone class. It inhibits the process of photosynthesis in various broadleaf weeds and grasses (Arsenault & Ivany 2001). Hence, it is widely applied as a pre and post-emergence herbicide in the fields of crops

such as sugarcane, tomato, potato, and maize. Furthermore, it is lethal to aquatic plants and has long-term effects on aquatic organisms (Fairchild & Sappington 2002). Inhalation of metribuzin by mammals affects the central nervous system, kidney, thyroid, and liver. The half-life of metribuzin is recorded as between 5 and 50 days (Quesada-Molina et al. 2007). Its water solubility is recorded as 1.05 $g.L^{-1}$ (Yahiaoui et al. 2011). Metribuzin's liquid solubility and weak sorption to soil cause surface and groundwater pollution by its residue. Many researchers have reported on surface and groundwater contamination by metribuzin. Metribuzin also disrupts the endocrine system in higher animals and leads to physiological disorders (Maumbe & Swinton 2003). Due to this, many countries have incorporated metribuzin into their list of endocrine disruptors. Also, metribuzin residue affects the establishment of subsequent crops and disrupts the crop rotation system (Huang et al. 2018). Apart from this, metribuzin residue also affects soil microflora and its activities (Lone et al. 2014). Hence, to tackle environmental pollution by metribuzin, it attracts attention to the need to develop effective eco-friendly bioremediation strategies at point sources to protect water bodies and the environment. So far, different remediation strategies have been used to clean up pesticide pollution (Arora et al. 2012). Microorganisms can convert toxic pollutants into less toxic or inactive compounds (Abatenh et al. 2017). As of today, only a few

bioremediation techniques have been reported so far by various authors in the literature for metribuzin removal (Tamilselvan et al. 2014, Myresiotis et al. 2012). Zhang et al. (2014) have reported about 73.5% degradation of metribuzin using *Bacillus* sp. (N1) at an initial concentration of 20 mg.L⁻¹ in 5 days, at optimum pH 7 and temperature of 30°C. Furthermore, (Gopal et al. 2011) reported about 86% of metribuzin degradation by using the *Burkholderia cepacia* strain within 20 days. Apart from this, Wahla et al. (2018) observed about 98.63% of metribuzin degradation at an initial concentration of 45 mg.L⁻¹, optimum pH 7, and temperature of 30 °C with an inoculum density of 5 x 10⁵ CFU.mL⁻¹ using bacterial consortia such as *Rhodococcus rhodochrous*, *Bacillus aryabhatai*, *Bacillus tequilensis*, and *Bacillus safensis*. Also, Tamilselvan et al. (2014) studied metribuzin degradation by bacterial isolates such as *Pseudomonas aeruginosa*, *Staphylococcus aureus*, *Bacillus subtilis*, etc.

For successful bioremediation of metribuzin, efficient inocula, optimization of media components and various environmental factors such as incubation temperature, pH, pesticide concentrations and inoculum size plays a major role (Varjani & Upasani 2017, Annadurai et al. 2008, Jabeen et al. 2015). Hence, the optimization of various parameters for metribuzin degradation is carried out in the present work by using a novel soil isolate. Also, it is evident from the previous literature that an isolated bacterial strain has not been studied earlier for metribuzin degradation. Therefore, enrichment methods have been used for the isolation of bacterial strains from the metribuzin-contaminated soil. A novel bacterial strain is effective and efficient for the removal of metribuzin and showed good removal of metribuzin.

MATERIALS AND METHODS

Materials

Commercial grade metribuzin having an MW of 214.2 g.mol⁻¹ (88.55% w/w) was purchased from a local shop, Bhavani Krushi Seva Kendra, Hingangaon Bk., Sangli, Maharashtra, India. All other required chemicals and Agar-agar were purchased from Hi-Media Laboratories Pvt.Ltd., Mumbai. Also, the AR-grade sodium hydroxide (NaOH) and sulfuric acid (HCL) chemicals were obtained from S. D. Fine Chemicals Ltd., Mumbai, India.

Enrichment and Isolation of Metribuzin Degrading Bacteria

For the enrichment, soil samples were collected from the sugarcane vegetated agricultural field at Hingangaon Bk, Sangli, Maharashtra, India, where a large amount of

metribuzin was used repeatedly. The sampling farm is situated at a latitude of 17.3914°N, a longitude of 74.3419°E, and an altitude of 669 meters above sea level. At the time of sampling, the sugarcane crop was 4 months old. Soil samples were collected at random depths ranging from 0 to 15 cm below the soil surface. The soil samples were collected in the sterilized polythene bag and immediately stored and maintained at 4 °C temperature (Mishra 2015). In the laboratory, the soil samples were sieved through 2 mm sieves to remove gravel and debris. 1 gm. of soil was mixed into 250 mL Erlenmeyer flasks (A) containing 100 mL of Minimal Salt Medium (MSM) with a metribuzin concentration of 100 mg.L⁻¹ and incubated for the next 12 days at 150 rpm. 1 mL of sample from the incubated flask (A) was transferred into a 250-mL Erlenmeyer flask (B) containing fresh 100 mL MSM broth with a 100 mg.L⁻¹ concentration of metribuzin and incubated for 72 hours at 150 rpm. 0.1 mL of the sample from the flask (B) was spread on MSM agar plates having a 100 mg.L⁻¹ concentration of metribuzin and incubated at 30 °C temperature for 48-72 hrs. After 48-72 h of incubation, morphologically distinct colonies were picked up and restreaks on MSM agar plates until purified colonies were obtained. Ten pure cultures were isolated, grown on nutrient agar slant, and stored in the refrigerators at 4°C until required in subsequent experiments.

Identification of the Bacterial Isolates

For the identification of the novel metribuzin-degrading bacterial isolates, 16S rRNA gene sequence analysis was conducted at a professional molecular biology laboratory (Geneom Biotech Pvt. Ltd., Pune, India), and the universal primers 8F (5' AGAGTTTGATCCTGGCTCAG-3'), 806R (5' GGACTACHVGGGTWTCTAAT-3'), 515F (5' CCATCTCATCCCTGCGTGTCTC-3'), and 13B (5' AGGCCCGGGAACGTATTAC-3'), were used for the amplification of the 16S rRNA gene (Turner et al. 1999). The gene sequence was deposited in the NCBI GenBank with an accession number of OM527185.1. The blast analysis of nucleotide sequences was performed at the National Center for Biotechnology Information (NCBI) for phylogenetic analysis. The 16 S r RNA sequence of the strain *Olivibacter* shared 99% identity with *Olivibacter oleidegradans* and *Olivibacter jilunii* (Fig 1). A phylogenetic tree has been constructed by using the neighbor-joining technique by MEGA6 software.

Culture Maintenance and Media

The isolated strain was maintained on Minimal Salt Medium (MSM) Agar having a composition of- Minimal Salt Medium containing: 5 g glucose, 3 g K₂HPO₄, 6 g Na₂HPO₄, 0.1 g

MgSO₄·7 H₂O, 2 g NH₄Cl, and 5 g NaCl dissolved in 1 L of DW. A metribuzin biodegradation experiment was performed in MSM broth.

Experimental Methodology

Metribuzin Degradation Capacity of the Isolated Strain

To check the degradation capacity of an isolated strain, experiments were performed in the laboratory. A 24-hour old grown culture of *Olivibacter oleidegradans* strain SP01 was added to 100 mL of MSM medium in a 500 mL flask with metribuzin as the sole carbon and energy source and incubated at 30°C., at 150 rpm in a rotary shaker. The uninoculated flask is considered as a control. The experiments lasted 5 days, and samples were collected every 24 hours and centrifuged for 15 minutes at 10000 rpm at 4°C temperature, with the supernatant filtered through a 0.45 mm membrane filter to remove any other particles. The supernatant was analyzed for the residual concentration of metribuzin using a UV-visible spectrophotometer at 293 nm. All the experiments were performed in triplicate. To test the effect of metribuzin concentration, a concentration of (20-100 mg.L⁻¹) and an operating pH of (5-9) were maintained using HCl and NaOH. Further, the effect of temperature on metribuzin degradation was studied in the range of 25-40°C respectively.

Analytical Methods

In the present study, to obtain cell-free medium, a sample was centrifuged at 10,000 rpm for 15 min., and the supernatant was filtered using a membrane filter (0.45 mm) to remove any other particles (Anwar et al. 2009). The absorption was measured using a UV-visible spectrophotometer at 293 nm. The concentration of Metribuzin was calculated by analyzing the absorbance of the metribuzin solution.

RESULTS AND DISCUSSION

Isolation and Screening of Metribuzin Degrading Bacteria

Initially, the isolation of metribuzin-degrading bacteria was carried out by the enrichment method, and morphologically different ten pure cultures were isolated by streak plate methods. To check the metribuzin resistance capacity of these isolates, pure cultures were streaked on MSM agar plates having various metribuzin concentrations of 20, 40, 60, 100, 200, 250, 300, 400, and 500 mg.L⁻¹. The resistance capacity of isolates was studied using MSM agar plates with metribuzin as the sole 'C' and energy source. Furthermore, for the identification of metribuzin-degrading bacteria, isolated strains were cultured individually in MSM broth

with a 20 mg.L⁻¹ concentration of metribuzin as the sole 'C' and energy source, and after one week of incubation, the residual concentration of the metribuzin was measured and the degradation percentage was calculated. The isolate (B2), later identified as *Olivibacter oleidegradans* strain SP01, tolerated metribuzin up to 400 ppm and had a higher efficiency of metribuzin degradation than all other isolates, so it was chosen for further study.

Microorganism used, Molecular Sequence and Evolutionary Studies

The degrading bacteria is isolated from a metribuzin-contaminated farm field using an enrichment technique. The identification of the isolates was done using 16S rRNA gene sequencing. The identified nucleotide sequence is very close to that of the *Olivibacter* genus; hence, the strain was designated as *Olivibacter oleidegradans* strain SP01 sp.

The sequence of *Olivibacter* was submitted to the NCBI GeneBank, and they have given it the accession number OM 527185.1. Fig. 1 shows the phylogenetic relationship of *Olivibacter* sp. with species of the identical genus of the GenBank database. The accession numbers of other species are presented in parentheses. In the phylogenetic branch, the homology relationship results showed that *Olivibacter* sp. has a maximum of 99% similarity with other species such as the *Olivibacter oleidegradans* strain and the *Olivibacter jilunii* strain. Many authors have reported the functions of *Olivibacter*. Szabo et al. (2011) reported the oil (hydrocarbon) degradative properties of the *Olivibacter oleidegradans* strain. Also, Chen et al. (2013) isolated *Olivibacter jilunii* from DDT-contaminated soil. However, to our knowledge, no study has been performed to date on the degradation of metribuzin using the *Olivibacter* strain.

Pesticide Degradation Kinetics

Bacteria utilize pesticides as the sole carbon and energy source for their growth and hence degradation of pesticide occurs. The rate constant for the degradation process was calculated by using the following equation.

$$\ln \left[\frac{C_0}{C} \right] = k't \quad \dots(1)$$

Where C represents the concentration of pesticide in mol.L⁻¹ and is the initial concentration. k' represents a rate constant (hr⁻¹) and degradation time is denoted as t. As shown in Fig. 2, the plot of ln v/s time (t) is a straight line passing through the origin. This confirms that the degradation of metribuzin by bacteria is showing a first-order reaction kinetics.

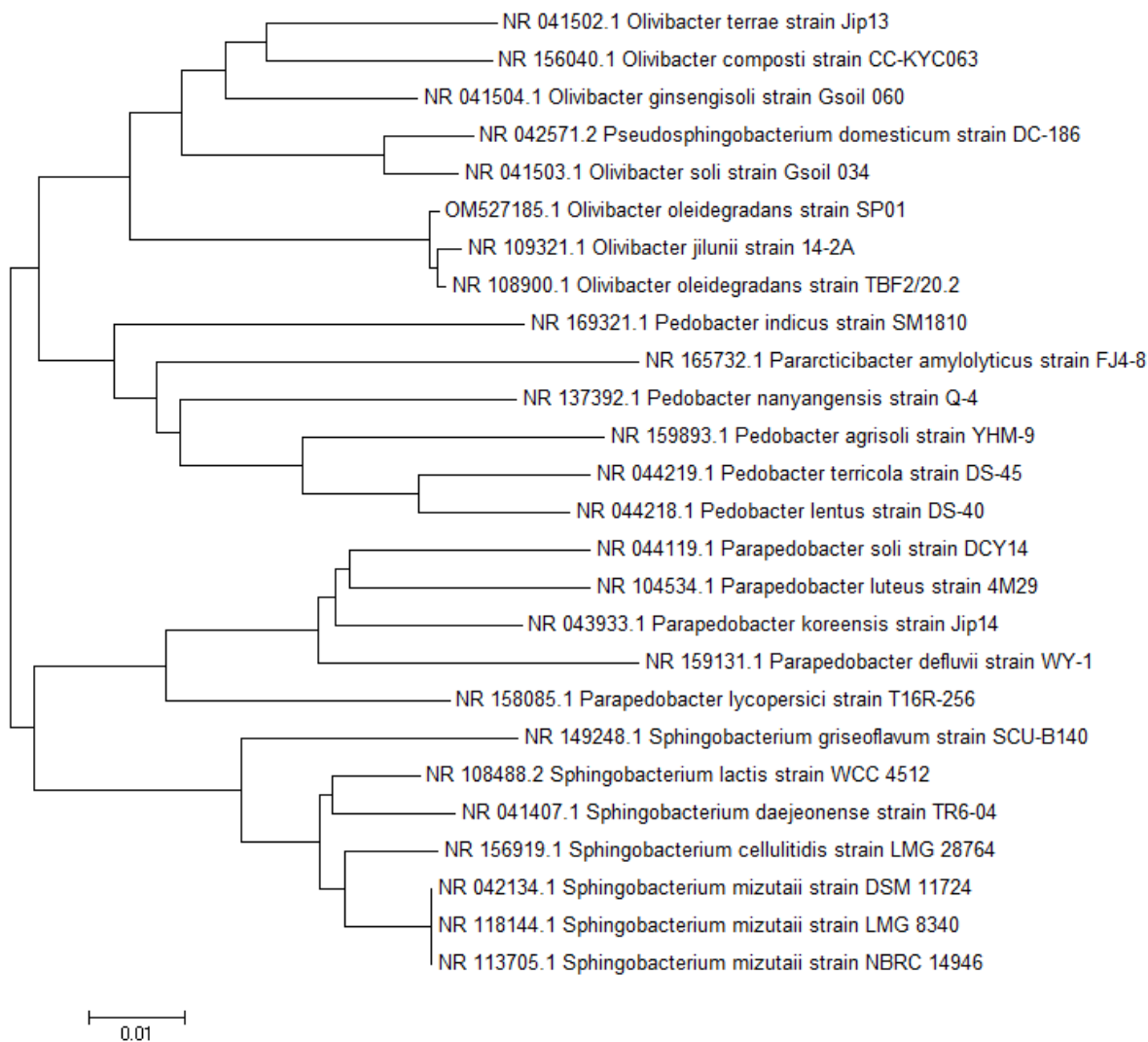


Fig.1: Phylogenetic tree constructed by using neighbor-joining analysis of 16S rRNA sequences from 25 bacteria. GeneBank accession numbers are given with species names.

Effect of Initial Concentration

To study the effect of various concentrations, experiments were performed at initial concentrations such as 20, 40, 60, and 100 mg.L⁻¹ at constant pH 7, inoculation of 4%, and a temperature of 30°C. Table 1 shows that metribuzin degradation decreased from 80.38% to 40.3% with an increase in the concentration of Metribuzin from 20 mg.L⁻¹ to 100 mg.L⁻¹. Furthermore, the rate constants were observed in decreasing order from 14.1 10⁻³ hr⁻¹ to 4.10 10⁻³ hr⁻¹.

A maximum metribuzin degradation rate of 80.38% was observed at the 20 mg.L⁻¹ concentration. Fig. 2 shows that at lower metribuzin concentrations, i.e., 20 mg.L⁻¹, the metribuzin degradation rate was higher. Toxicity to

bacteria occurs at higher concentrations, which may affect the organism's growth. Hence, at higher concentrations, very little metribuzin degradation was observed. According to the literature, similar findings were made for the organic

Table 1: Metribuzin degradation and kinetic rate constant with respect to various concentrations. (pH-7, Temp. 30°C, Inoculations 4%, capacity-100 mL).

Concentration (mg.L ⁻¹)	Degradation (%)	Rate constant (k'×10 ³ hr ⁻¹)	R ²
20	80.38	14.1	0.98
40	68.26	9.20	0.98
60	64.16	7.80	0.97
100	40.3	4.10	0.98

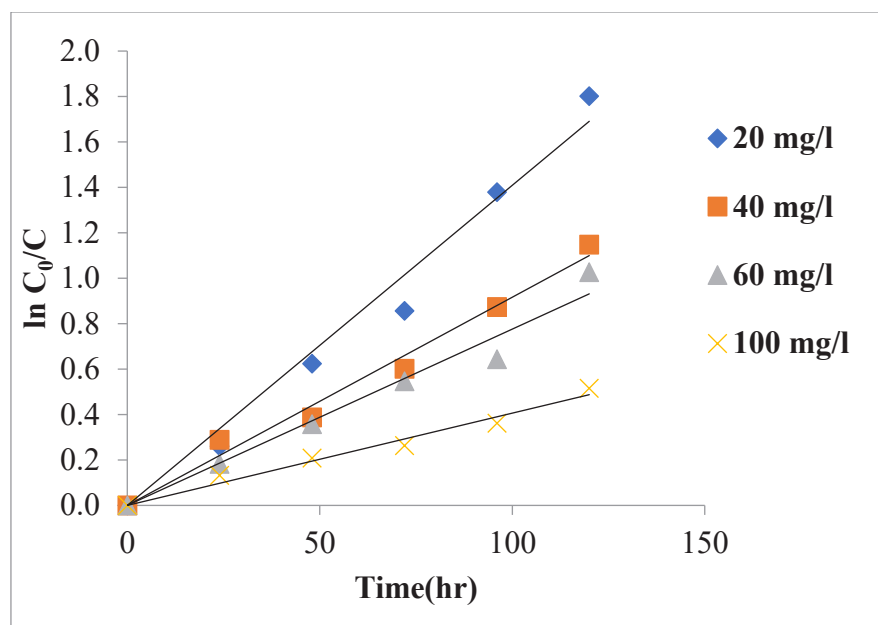


Fig. 2: Effect of various concentrations on metribuzin degradation (pH -7, Temp. 30°C, Inoculations 4%, capacity-100 mL).

pollutants degradation study. Zhang et al. (2014) have stated that the biodegradation rate of metribuzin decreased with an increase in its concentration when *Bacillus* sp. was used. Also, Wahla et al. (2018) have reported the highest degradation of metribuzin at lower concentrations by using a bacterial consortium.

Effect of Initial pH

Several experiments were carried out at pH ranges of (5, 6, 7, 8, & 9) to investigate the effect of pH on Metribuzin degradation. The obtained results were represented in Fig. 3 It shows that maximum degradation rates of 83.38 % were observed at pH 7, i.e., at neutral pH. It is concluded from Table 2 that at acidic conditions, i.e., at pH 5, and basic conditions, i.e., at pH 8 and 9, the decreased rate constant was observed.

The obtained results indicate that bacteria are adaptable to neutral pH and that pH has a direct impact on bacterial

Table 2: Percentage of degradation and kinetic rate constant with respect to various pH (concentration of 20 mg.L⁻¹, Temp. 30°C, Inoculations 4%, capacity-100 mL).

pH	Degradation (%)	Rate constant (k' 10 ³ hr ⁻¹)	R ²
5	31	3.30	0.98
6	58	7.50	1
7	80.38	14.1	0.98
8	33	3.60	0.99
9	23	2.20	0.98

growth. Another reason is that pH also affects the metabolic activities of bacteria, and hence, maximum degradation was observed at an optimum neutral pH. Zhang et al. (2014) observed maximum degradation of metribuzin at pH 7 by using *Bacillus* sp. In addition, Phugare & Jadhav (2014) reported a similar pH trend for the biodegradation study of Acetamiprid using a *Rhodococcus* sp.

Effect of Temperature

In the present study, to examine the effect of temperature on metribuzin degradation, various experiments were performed at temperatures in the range of 25 to 40°C. The percent degradation with respect to its temperature has been represented in Table 3. It can be concluded from Fig. 4 that maximum degradation of 84.46% was observed at 35°C. The observed percent degradation at 25°C and 45°C was 42% and 64%, respectively. It can be concluded that temperature plays an important role in bacterial degradation activity.

Table 3: Percentage of degradation and kinetic rate constant at various Temperatures. (concentration of 20 mg.L⁻¹, pH-7, Inoculations 4%, capacity-100 mL).

Temperatures (°C)	Degradation (%)	Rate constant (k' 10 ³ hr ⁻¹)	R ²
25	42	4.80	0.99
30	80.38	14.1	0.98
35	84.46	14.3	0.98
40	64	8.50	1

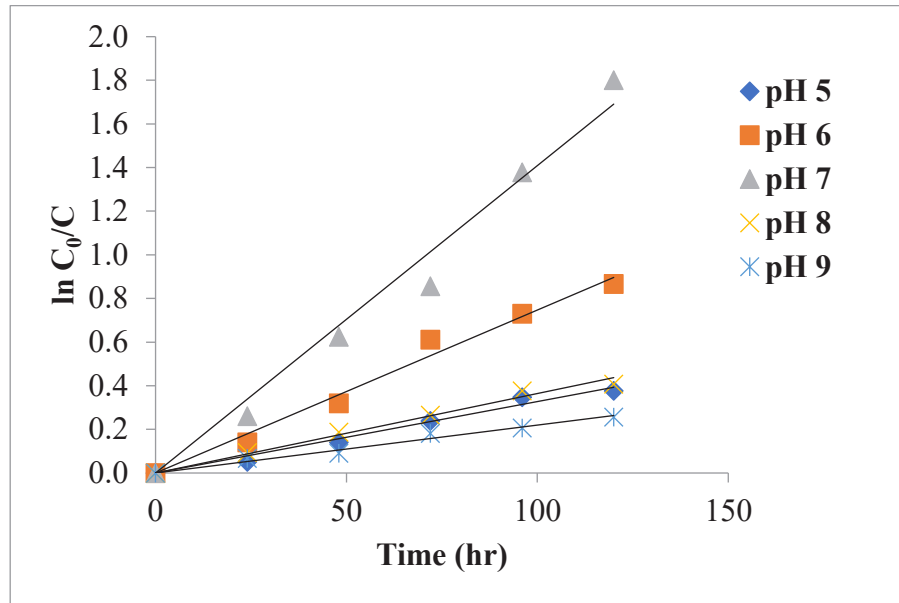


Fig. 3: Metribuzin degradation with respect to various pH (concentration 20 mg.L⁻¹, Temp. 30°C, Inoculations 4%, capacity-100 mL).

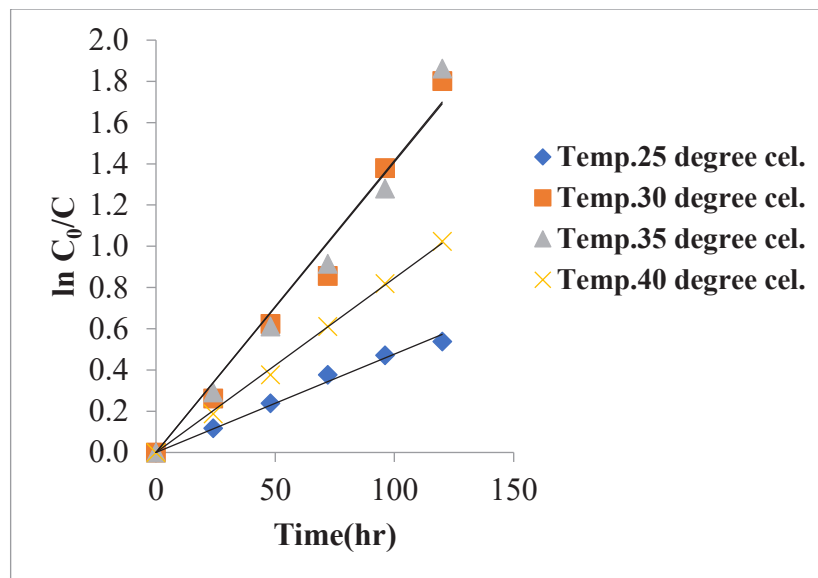


Fig. 4: Metribuzin degradation with respect to various temperatures (initial concentration 20 mg.L⁻¹, pH 7, Inoculations 4%, capacity-100 mL).

Higher or lower temperatures may affect the metabolic and enzymatic activity of the bacteria, resulting in significantly less degradation when compared to the optimum temperature of 35°C. Also, lower or extreme temperatures inhibit the growth rate of the bacteria, and hence, the degradation rate was observed to be lower than the optimum temperature. Also, Wahla et al. (2018) reported the highest degradation of metribuzin at 35°C temperature by using bacterial consortium. Furthermore, Phugare &

Jadhav (2014) also reported a similar trend of the temperature for the biodegradation study of Acetamiprid by using a *Rhodococcus* sp.

CONCLUSION

Metribuzin biodegradation was accomplished in the current study under a variety of operating conditions, including initial concentration, pH, and temperature. Lower concentration favors the degradation of metribuzin. The maximum

degradation of metribuzin was observed at a neutral pH of 7 and a temperature of 35°C. Metribuzin-degrading *Olivibacter oleidegradans* strain SP01 is successfully identified in the present study. *Olivibacter oleidegradans* strain SP01 is highly efficient for the removal of metribuzin and can be used for the bioremediation of this herbicide. In addition, the kinetic parameters of metribuzin degradation were also studied. A 1st order fitted well for the biodegradation study of metribuzin by using *Olivibacter oleidegradans* strain SP01.

ACKNOWLEDGMENT

Sulbha R. Kadam would like to acknowledge Sadguru Gadage Maharaj College of Karad, and the Microbiology Department for providing the research and other infrastructural facilities.

REFERENCES

- Abatenh, E., Gizaw, B., Tsegaye, Z. and Wassie, M. 2017. Application of microorganisms in bioremediation- a review. *J. Environ. Microbiol.*, 1: 2-9.
- Annadurai, G., Ling, L.Y. and Lee, J.F. 2008. Statistical optimization of medium components and growth conditions by response surface methodology to enhance phenol degradation by *Pseudomonas putida*. *J. Hazard. Mater.*, 151: 171-178.
- Anwar, S., Liaquat, F., Khan, Q.M., Khalid, Z.M. and Iqbal, S. 2009. Biodegradation of chlorpyrifos and its hydrolysis product 3, 5, 6-trichloro-2-pyridinol by *Bacillus pumilus* strain C2A1. *J. Hazard. Mater.*, 168: 400-405.
- Arora, P. K., Sasikala, C. and Ramana, C.V. 2012. Degradation of chlorinated nitroaromatic compounds. *J. Appl. Microbiol. Biotechnol.*, 93: 2265-2277.
- Arsenault, W. J. and Ivany, J. A. 2001. Response of several potato cultivars to metribuzin and diquat. *J. Crop. Prot.*, 20: 547-552.
- Chen, K., Tang, S., Wang, G., Xing Nie, G., Fen Li, Q., Dong Zhang, J., Jun Li, W. and Peng Li, S. 2013. *Olivibacter jilunii* sp. nov., isolated from DDT-contaminated soil. *International Journal of Systematic and Evolutionary Microbiology*, 63: 1083-1088.
- Fairchild, J.F. and Sappington, L.C. 2002. Fate and effects of the triazinone herbicide Metribuzin in experimental pond mesocosms. *J. Arch. Environ. Contam. Toxicol.*, 43: 198-202. doi: 10.1007/s00244-002-1208-1.
- Gopal, M., Dutta, D., Jha, S., Kalra, S., Bandyopadhyay, S. and Das, S. 2011. Biodegradation of imidacloprid and metribuzin by *Burkholderia cepacia* strain CH9. *J. Pestic. Res.*, 23: 36-40.
- Huang, X., Zhang, H., Chen, F. and Song, M. 2018. Colonization of *Paracoccus* sp. QCT6 and enhancement of metribuzin degradation in maize rhizosphere soil. *J. Curr. Microbiol.*, 75: 156-162.
- Jabeen, H., Iqbal, S., Anwar, S. and Parales, R.E. 2015. Optimization of profenofos degradation by a novel bacterial consortium PBAC using response surface methodology. *J. Int. Biodeterior. Biodegrad.*, 100: 89-97.
- Lone, A.H., Raverkar, K.P., Pareek, N. and Chandra, R. 2014. Response of soil microbial communities to the selective herbicides: a microcosm approach. *J. Pure. Appl. Microbiol.*, 8: 1559-1567.
- Mathur, S. C. 1999. Future of Indian pesticides industry in next millennium. *Pesticide Information*, 24 (4): 9-23.
- Maumbe, B. M. and Swinton, S. M. 2003. Hidden health costs of pesticide use in Zimbabwe's small holder cotton growers. *J. Soc. Sci. Med.*, 57: 1559-1571.
- Mishra, A. 2015. Microbial degradation of methyl parathion by soil bacterial isolate and consortium. *International Journal of Research Studies in Biosciences (IJRSB)*, 15-19.
- Myresiotis, C.K., Vryzas, Z. and Papadopoulou-Mourkidou, E. 2012. Biodegradation of soil-applied pesticides by selected strains of plant growth-promoting rhizobacteria (PGPR) and their effects on bacterial growth. *J. Biodegradation*, 23: 297-310.
- Phugare, S. S. and Jadhav, J. P. 2014. Biodegradation of acetamidiprid by isolated bacterial strain *Rhodococcus* sp. BCH2 and toxicological analysis of its metabolites in silkworm (*Bombax mori*). *J. of Clean-Soil, Air, Water*, 41: 1-9.
- Quesada-Molina, C., Garcia-Campana, A.M., Del Olmo-Iruela, L. and Del Olmo, M. 2007. Large volume sample stacking in capillary zone electrophoresis for the monitoring of the degradation products of metribuzin in environmental samples. *J. Chromatogr.*, 1164: 320-328. doi:10.1016/j.chroma.2007.06.076.
- Sakkas, V. A., Dimou, A., Pitarakis, K., Mantis, G. and Albanis, T. 2005. TiO₂ photocatalyzed degradation of diazinon in an aqueous medium. *Environ. Chem. Lett.*, 3: 57-61. Doi: 10.1007/s10311-004-0091-6.
- Szabo, I., Szoboszlai, S., Kriszt, B., Ha' hn, J., Harkai, Baka, P. E., Ncsics, A., Kaszab, E., Privler, Z. and Kukolya, J. 2011. *Olivibacter oleidegradans* sp. nov., a hydrocarbon degrading bacterium isolated from a biofilter cleanup facility on a hydrocarbon-contaminated site. *International Journal of Systematic and Evolutionary Microbiology*, 61: 2861-2865.
- Tamilselvan, C., Joseph, S.J., Mugunthan, G., Kumar, A. S. and Ahamed, S. S. M. 2014. Biological degradation of metribuzin and profenofos by some efficient bacterial isolates. *ILNS.*, 9: 2300-9675.
- Turner, S., Pryer, K.M., Miao, V.P.W. and Palmer, J. D. 1999. Investigating deep phylogenetic relationships among cyanobacteria and plastid by small subunit rRNA sequence analysis. *J. Eukaryot Microbiol.*, 46(4): 327-338.
- Varjani, S.J. and Upasani, V.N., 2017. A new look on factors affecting microbial degradation of petroleum hydrocarbon pollutants. *Int.J. Biodeterior. Biodegrad.*, 120: 71-83.
- Wahla, A.Q., Iqbal, S., Anwar, S., Firdous, S. and Mueller, J. A. 2018. Optimizing the metribuzin degrading potential of a novel bacterial consortium based on Taguchi design of experiment. *Journal of Hazardous Materials*, 366: 1-9.
- Yahiaoui, O., Aizel, L., Lounici, H., Drouiche, N., Goosen, M. F. A., Pauss, A. and Mameri, N. 2011. Evaluating removal of metribuzin pesticide from contaminated groundwater using an electrochemical reactor combined with ultraviolet oxidation. *J. Desalination*, 270: 84-89. doi: 10.1016/j.desal.2010.11.025.
- Zhang, H., Zhang, Y., Hou, Z., Wu, X., Gao, H., Sun, F. and Pan, H. 2014. Biodegradation of triazine herbicide metribuzin by the strain *Bacillus* sp. N1. *J. Environ. Sci. Health B*, 49: 79-86.



The Impact of Climate Change, Economic Growth, and Population Growth on Food Security in Central Java Indonesia

Suryanto Suryanto* , Irwan Trinugroho*, Fitri Susilowati**, Jean Baptiste Aboyitungiye***
and Yuaninda Hapsari*

*Center for Environmental Research (PPLH) and FEB Universitas Sebelas Maret, Jalan Ir. Sutami 36A Surakarta, Indonesia

**Universitas PGRI Yogyakarta, Jalan IKIP PGRI 1 No. 117, Yogyakarta, Indonesia

***Bank of the Republic of Burundi, J967+M2V, Ave De La Revolution, Bujumbura, Burundi

†Corresponding author: Suryanto Suryanto; Suryanto_feb@staff.uns.ac.id

Nat. Env. & Poll. Tech.
Website: www.neptjournal.com

Received: 26-11-2022

Revised: 04-01-2023

Accepted: 14-01-2023

Key Words:

Food security
Climate change
Economic growth
Population growth

ABSTRACT

As climate change continues to cause more frequent weather shocks such as droughts and floods and increasingly erratic rainfall, people in developing regions are threatened by crop failures and hunger. In this study, the researchers describe how climate change influences food security in Central Java, seen from the frequency of floods, rainfall, and rainy days. This study also added another variable, i.e., economic growth, reviewed through GRDP and the amount of rice production. Using the Common effect model, the study results revealed that rainy days and population were the variables significantly influencing food security in cities/regencies in Central Java Province. Meanwhile, two other variables, i.e., rainfall and GRDP, had no significant effect on food security in cities/regencies in Central Java Province.

INTRODUCTION

In its latest report on food insecurity, the Global Hunger Index indicates that in 2019, 8.4% of the world's population was undernourished; in 2020, we reached 9.9% (Grebmer et al. 2021). About a third of the world's population (2.37 billion) lacked year-round access to adequate food in 2020, an increase of 320 million in one year; between 2019 and 2020, this indicator increased as much as in the previous five years combined (FAO 1983). Although it is still too early to attribute these phenomena to anthropogenic climate change, significant changes in temperature and precipitation due to the increase in the concentration of greenhouse gases could seriously disrupt agricultural production systems and jeopardize global food security.

The FAO (1983) focused on access to food to define food security as ensuring that people have physical and economic access to the food they need. The increased frequency and number of extreme events such as drought or floods would seriously threaten this stability, whether the effects are felt at

the national level or through the global food market. Aiming for food security makes it possible to: improve the health and well-being of citizens and progress toward collective well-being (Clapp et al. 2022 and Ani et al. 2021).

The Indonesian government has made the issue of food security one of its development priorities by including it in the Medium-Term Development Plan (RPJM). However, accomplishing good food security is still challenging for Indonesia. It can be seen from the calculation results of the Global Food Security Index (GFSI), which reported that Indonesia in 2020 had a score of 59.5, down 3.1 points compared to the previous year. The decline in Indonesia's GFSI number caused Indonesia 2020 to be ranked 65th out of 113 countries after being ranked 62 in 2019. Indonesia's position was below Thailand, Vietnam, the Philippines, and Singapore compared to other countries in ASEAN.

Despite impressive economic growth and poverty reduction, Indonesia's food security still faces significant challenges. According to (Rozaki 2021 and Suryanto Kumalasari et al. 2021), Indonesia is one of the countries with food security most vulnerable to climate change in Southeast Asia. It is caused by climate change, which significantly affects the agricultural sector, one of the crucial sectors

ORCID details of the authors:

Suryanto Suryanto: <https://orcid.org/0000-0002-3763-9639>

in Indonesia as an agricultural country. Climate change, especially rainfall, can influence the productivity of the agricultural sector. Lobell et al. (2008) argued that climate change would affect systems related to production, storage, access, to food price stability, which will impact the condition of food security.

Another factor that also affects food security is economic growth. The Food and Agriculture Organization (FAO) states that economic growth is needed for sustainable solutions to food security. High economic growth will impact increasing the income and welfare of the poor. This condition will increase people's access to food and reduce their vulnerability to economic pressures. In line with the opinion of Manap & Ismail (2019), efficient economic growth will reduce poverty, hunger, and malnutrition to achieve food security, especially in developing countries such as Indonesia.

In addition, Rozaki (2021) also asserts that food security has three aspects: availability, affordability, and utilization. The aspect of food availability is related to the availability of food commodities to meet the community's food needs. In this case, Indonesia has its indicators to assess the condition of food security nationally and regionally. The indicator is the Food Security Index (IKP) based on three aspects of food security.

On the other side, the need for food will always increase along with the increase in population. This statement is consistent with the opinion of Thomas Malthus (1798) in (Pham et al. 2020) and (Montano & García-López 2020) that population growth will increase exponentially while the growth of food availability will increase arithmetically. The theory can be interpreted that along with the increasing population, the problem of food availability will also be more complex.

Indonesia is one of the countries with the largest population in the world. Based on data from the Central Statistics Agency (2018), the population in Indonesia reached 267 million people. The large population impacts other problems, including the increasing conversion of agricultural land amid growing food needs.

Specifically, Central Java is one of the provinces in Indonesia as a national food buffer. The level of rice production in Central Java itself still fluctuates every year. Based on data from the Central Statistics Agency (2021), rice production in Central Java in 2018 was 10,499,588.23 tons and continued to decline in 2019 and 2020, 9,655,653.98 tons and 9,489,164.62 tons, respectively.

The decline in rice production in Central Java is influenced by the condition of the rice harvest area, which

is increasingly threatened due to natural disasters that often occur in Central Java, especially floods because of climate change. From 2018 to 2020, there were 254 flood events in Central Java. Based on data from the flood event recap of the Water Resources and Spatial Planning Public Works Agency (2020), flood events in Central Java throughout 2020 damaged rice fields up to 3,465 ha.

Research by Oskorouchi & Sousa-Poza, (2021) described the impact of climate change on food security in Afghanistan. Using the 2SLS analysis method, they found that the flood disaster significantly impacted food security long-term, related to decreasing calorie consumption and fulfilling community nutrition. Kinda & Badolo (2019)) also elucidated the impact of climate change in terms of rainfall on food security in developing countries from 1960 to 2016. The Fixed Effect analysis results uncovered that rainfall had caused a decrease in food security in developing countries.

Further, limited literature has examined the impact of climate change on food security. It mainly used the HCVI (Hunger and Climate Vulnerability Index) indicator as a new measure developed to assess an area's food security level by combining related information to climate events (Krishnamurthy et al. 2014, Rosalia et al. 2021, Suryanto et al. 2021).

Because of the lack of literature related to the topic of the effect of climate change on food security using HCVI as a new measure of food security, this study added an economic growth variable, measured through Gross Regional Domestic Product (GRDP) and the population in Central Java as a national food buffer area, which prone to disasters due to climate change.

MATERIALS AND METHODS

Research Methods

Empirical model: This study aimed to analyze the effect of climate change in terms of rainfall and rainy days, economic growth from GDP, and population on food security in Central Java. Employing the panel data regression analysis method, this study used data from 22 cities/regencies in Central Java from 2018 to 2020. The following equation is utilized in this study:

$$\text{Foodsecurity}_{it} = \beta_0 + \beta_1 \text{rain_fall}_{it} + \beta_2 \text{rainy_days}_{it} + \beta_3 \text{loggrdp}_{it} + \beta_4 \text{log_population}_{it} + e_{it}$$

rain_fall is the rainfall variable (log) in city/regency *i* at period *t*; rainy_days is the rainy-day variable (log) in city/regency *i* at period *t*; loggrdp is the GRDP variable (log) in city/regency *i* at period *t*; lpend is a variable of the population (log) in city/regency *i* at period *t*

Three estimators were used: ordinary least squares (OLS), fixed effects (FE), and random effects (RE). However, the OLS estimator is biased since it does not consider the heterogeneity of entities (cities/regencies) that simultaneously affect the variables. Therefore, the FE or RE estimators were the ones employed.

Variable Description

Food security: According to the FAO (2012), food security is a condition in which all people at all times, both physically and economically, have access to sufficient, safe, and nutritious food to meet their daily nutritional needs. The food security indicator in this study used the HCVI (Hunger and Climate Vulnerability Index), which is a measure to assess the food security level by combining information related to climate events and relevant measures of sensitivity and adaptive capacity of food security (Krishnamurthy et al. 2014).

Climate change: Based on the IPCC (2014), climate change is defined as human intervention to reduce or increase the absorption of greenhouse gases. This change refers to an identifiable change in climatic conditions, such as using statistical tests with an average change and/or variability of its properties and persisting over a prolonged period. Climate change in this study employed the variables of flood frequency, rainfall, and rainy days.

Rainfall is the height of rainwater influenced by climatic conditions, topography, rotation, and the confluence of air currents that collect in a flat place, do not evaporate, do not seep, and do not flow in millimeters (mm) (Badan Pusat Statistik, 2018 or Central Statistics Agency of Semarang Regency 2018). Meanwhile, rainy days are the number of rainy days with an average intensity above 1, 20, 50, and 100 mm/day in a year. Climate change data in this study were obtained from the publications of the Central Statistics Agency per city/regency in Central Java.

Economic growth: Economic growth in this study used annual Gross Regional Domestic Product (GRDP) data based on constant prices in 2010 to determine how much production increased without calculating the amount of inflation. GRDP also can provide an overview of the ability of a region to create added value in a specific period. GRDP data in this study were obtained from the publications of the Central Statistics Agency per city/regency in Central Java.

Total Population

The population is all people who occupy a specific area within six months or more or all who occupy a particular area for less than six months but intend to settle there (Badan Pusat Statistik 2019). The population data in this study

was obtained from the publication of the Central Statistics Agency per city/regency in Central Java.

RESULTS

Based on the test results for selecting the best model, the Hausman, and the Chow tests, it was found that the common effect of the best model to be used in this study, with each $prob > chi^2$ of 0.28 more than 0.05 and $prob > F$ of 0.15 more than 0.05. Thus, this study used the common effect model (CEM).

From the classical assumption test in this study, it was uncovered that the model used was free from multicollinearity problems, with a value of $VIF\ 1.21 < 10$, and heteroscedasticity and autocorrelation problems, with $prob > chi^2$ of 0.33 and 0.16 more than 0.05, respectively. Hence, the model in this study was BLUE (Best Linear Unbiased Estimator).

Following are the regression results with the common effect model:

Table 1 presents the estimation of results using the common effect model. We found that two variables had a significant effect on food security in cities/regencies in Central Java Province, with a significance level of 0.005 and 0.003, respectively. The two variables were rainy days and population. Meanwhile, two other variables, i.e., rainfall and GRDP, had no significant effect on food security in cities/regencies in Central Java Province.

The coefficient of the rainy_days variable of 0.19 indicates that the frequency of rainy days significantly positively affected food security in cities/regencies. It means an increase in the number of rainy days pretends to farmers to cultivate their land

But, the impact of rainy days differs from rainfall in Central Province. Although the impact of rainfall is not

Table 1: Common effect model.

rain_fall	-0.12 (0.722)
rainy_days	0.19 (0.005)
log_gdrp	0.064 (0.114)
log_population	-0.1 (0.003)
Cons	-0.24 (0.805)
R-sq	0.52
Prob > F	0.000

Source: processing data

significant on food security, the signs of this variable are negative. The volume of rain may increase the risk of flood. It aligns with research by (Oskorouchi & Sousa-Poza 2021), describing that floods significantly and negatively affected food security in Afghanistan.

It suggests that the flood events that hit cities/regencies in Central Java caused food insecurity. This considerable influence can be caused by floods that often afflict Central Java Province. There were 254 flood events reported in Central Java from 2018 to 2020, in which the flood damaged 3,465 ha of rice fields.

Thobei et al. (2014) stated that climate variability has little effect on crop production. According to the National Disaster Management Authority of Indonesia, the average rainfall in cities/ regencies in Central Java Province was 2378 mm, with an average of 122 rainy days, which is still within the limits of the expected average rainfall ranging from 2000 to 3000 mm per year and the expected average rainy day of 144 per year.

Moreover, the economic growth variable using the GRDP indicator revealed a significant positive effect with a coefficient of 8.53, so an increase in GRDP in the cities/regencies in Central Java Province would lead to an increase in food security. Following research conducted by Manap & Ismail (2019) using the Generalized Method of Moments (GMM) method, it was found that economic growth positively affected food security. This positive effect is because a higher economic growth level will reduce the poverty rate, increase life expectancy, and increase the number of workers.

Higher economic income leads to the other macroeconomic indicators that make up the food security level, thus affecting the increase in food security. To reduce poverty and hunger, it is essential that growth reaches the poor and can meet the increased needs for income to create demand for the assets controlled by these populations. Poor households should be able to use the additional economic assets to improve their diets in quantity and quality.

DISCUSSION

Concerning food and nutritional security, the impacts of climate change will be reductions in food availability following declines in agricultural and animal production, increases in the prices of agricultural products, and malnutrition (Godde et al. 2021). For many Africans, the ability to access sufficient, nutritious, and safe food capable of meeting their dietary needs has been increased by a succession of natural disasters and epidemics (Ahmed 2020).

Many studies have demonstrated that changing climate variability directly affects food security systems. Using semi-structured interviews and special reports from International Non-governmental organizations, Ani et al. (2021) revealed that climate change has negatively affected food security in Nigeria. Moreover, the significant negative effect of floods on food security has been described by (Oskorouchi & Sousa-Poza 2021) in their research related to the impact of climate change, particularly floods, on food security in Afghanistan. Using the 2SLS analysis method, the results showed that the flood disaster significantly impacted food security in the long term, related to decreasing calorie consumption and fulfilling community nutrition. These results are supported by the research results by (Akukwe et al. 2020) with the regression method, revealing that flood disasters had a negative and significant effect on food security in Southeast Nigeria by increasing the number of households vulnerable to food security by 92.8% (Abia et al. n.d; Ani et al. 2021). In Asian continent also showed the impact of climate change harms humanity. Based on the research of Abdelfattah & Abdelfattah (2021) found that climate change has impacted water availability. The scarcity of water would affect crop production and the daily consumption of the population.

Kinda & Badolo (2019) have also elucidated the impact of climate change concerning rainfall on food security in developing countries from 1960 to 2016. The results of the fixed effect analysis method demonstrated that rainfall had caused a decrease in food security in developing countries. In addition, a study by (Gladys 2017) using the Pearson correlation method explained consistent results, where climate change, especially rainfall and rainfall frequency, negatively affected food production, affecting food security conditions in Kitui, Kenya. Besides, some researchers, such as Case et al. (2007) and Nugroho et al. (2022), noted that recurring environmental disasters in parts of Indonesia have worsened food availability.

Economic growth is also one factor that can affect a region's food security condition. The relationship between the level of economic growth and the state of food security demonstrated by Świetlik (2018) showed a significant territorial difference between GDP and food security levels. Research by Manap & Ismail (2019) using the Generalized Method of Moments (GMM) method found that economic growth positively affected food security.

Meanwhile, a study on the effect of rice production on food security was conducted (Martadona & Elhakim 2020) with confirmatory factor analysis techniques and exposed that the amount of agricultural production had a significant positive effect on food security.

The growth of the world population and the rise in living standards are challenges for tomorrow's food security (van Dijk et al. 2021), (Nepal et al. 2021), (Abdelfattah & Abdelfattah 2021). With no land area expansion, population growth will threaten food production in developing countries. Studies have confirmed that population growth affects household food security (Hall et al. 2017). In his study using the VAR approach, Ceesay & Ben Omar Ndiaye (2022) showed that population significantly affects food security in the short run and is insignificant in the long run.

CONCLUSION

Based on the data analysis results using the common effect method in this study, rainy days and population variables have significantly affected food security in cities/regencies in Central Java Province. Meanwhile, two other variables, i.e., rainfall and GRDP, had no significant effect on food security in cities/regencies in Central Java Province.

From the results of statistical testing, we noticed that rainfall harms food security, although it is not significant. The implication for the government to anticipate is to control the variability of climate change. Managing climate change, including rainfall variations, requires several mitigation policies.

The government has implemented several policies to overcome the food security problem. In this case, intervention from the government is needed to reduce the risk of climate change. The government can implement effective climate change mitigation strategies. Investments related to agricultural research should also be increased, accompanied by extending methods to farmers in mitigating climate change risks. Investments in mitigation, i.e., clean energy technologies and land-use changes, particularly the switch to bioenergy production, will prevent or reduce agricultural production losses caused by climate change.

In addition, the government is expected to increase social protection for the community to stabilize economic growth and minimize the impact of the economic crisis on food security. Besides that, the government should still be concerned about managing the population's growth to decrease the demand for food.

ACKNOWLEDGEMENT

The authors express gratitude to Prof Irwan Trinugroho for his assistance. This research has been supported and funded by MAIPARK Reinsurance Company in Indonesia.

REFERENCES

- Abdelfattah, M.A. and Abdelfattah, M. A. 2021. Climate change impact on water resources and food security in Egypt and possible adaptive measures. *Emerging Challenges to Food Production and Security in Asia, Middle East, and Africa*. https://doi.org/10.1007/978-3-030-72987-5_10
- Abia, W.A., Onya, C.A., Shum, C. E., Amba, W. E., Niba, K. L. and Abia, E. A. 2019. Food Security Concerns, Climate Change and Sea Level Rise in Coastal Cameroon. *Afr. Clim. Hand. Coast. Asp.*, 8: 1-21 https://doi.org/10.1007/978-3-030-42091-8_21-1
- Ahmed, S.M. 2020. Impacts of drought, food security policy and climate change on the performance of irrigation schemes in Sub-saharan Africa : The case of Sudan. *Agric. Water Manag.*, 232: 106064. <https://doi.org/10.1016/j.agwat.2020.106064>
- Akukwe, T.I., Oluoko-Odingo, A.A. and Krhoda, G.O. 2020. Do floods affect food security? A before-and-after comparative study of flood-affected households' food security status in South-Eastern Nigeria. *Bull. Geogr. Socio Eco. Ser.*, 47: 115-131. <https://doi.org/10.2478/BOG-2020-0007>
- Ani, K.J., Anyika, V.O. and Mutambara, E. 2021. The impact of climate change on food and human security in Nigeria. *Int. J. Clim. Change Strat. Manag.*, 11: 119. <https://doi.org/10.1108/ijccsm-11-2020-0119>
- Badan Pusat Statistik 2018. BPS Provinsi Jawa Tengah Dalam Angka. In: Badan Pusat Statistik.
- Badan Pusat Statistik 2019. Provinsi Jawa Tengah Dalam Angka. In: Provinsi Jawa Tengah Dalam Angka.
- Busnita, S.S., Oktaviani, R. and Novianti, T. 2017. How far climate change affects Indonesian paddy production and rice price volatility. *Int. J. Agric.*, 11: 201.. <https://doi.org/10.25077/ijasc.1.1.1-11.2017>
- Case, M., Ardiansyah, F. and Spector, E. 2007. Climate Change in Indonesia has implications for humans and nature. *Energy*, 01: 13.
- Ceesay, E.K. and Ben Omar Ndiaye, M. 2022. Climate change, food security and economic growth nexus in the Gambia: Evidence from an econometrics analysis. *Res. Glob.*, 5: 100089. <https://doi.org/10.1016/j.resglo.2022.100089>
- Clapp, J., Moseley, W.G., Burlingame, B. and Termine, P. 2022. Viewpoint: The case for a six-dimensional food security framework. *Food Policy*, 106: 102164. <https://doi.org/10.1016/j.foodpol.2021.102164>
- FAO. 1983. The State of Food and Agriculture. *World Review: The Situation in Sub-Saharan Africa Women In Developing Agriculture*. FAO, Geneva
- FAO. 2012. Climate Change Adaptation and Mitigation. <http://www.fao.org/3/i2855e/i2855e.pdf>
- Gladys, K. V. 2017. Rainfall and temperature variability and its effect on food security in Kitui County. *International Journal of Development and Sustainability*, 6(8): 924-939.
- Godde, C.M., Mason-D'Croz, D., Mayberry, D.E., Thornton, P.K. and Herrero, M. 2021. Impacts of climate change on the livestock food supply chain: A review of the evidence. *Glob. Food Sec.*, 28: 100488. <https://doi.org/10.1016/j.gfs.2020.100488>
- Grebner, K., Bernst, J., Wiemers, M., Schiffer, T., Hanano, A., Towey, O., Chéilleachair, Ní, R., Foley, C., Gitter, S., Ekstrom, K. and Fritschel, H. 2021. *Glob. Hung. Indx.*, 54: 646.
- Hall, C., Dawson, T.P., Macdiarmid, J.I., Matthews, R.B. and Smith, P. 2017. The impact of population growth and climate change on food security in Africa: looking ahead to 2050. *Int. J. Agric. Sustain.*, 15(2): 124-135. <https://doi.org/10.1080/14735903.2017.1293929>
- IPCC. 2014. Climate Change 2014: Climate Change, Adaptation, and Vulnerability In Organization & Environment.
- Kinda, S. R. and Badolo, F. 2019. Does rainfall variability matter for food security in developing countries ? *Cogent Economics & Finance*, 7(1): 1640098. <https://doi.org/10.1080/23322039.2019.1640098>

- Krishnamurthy, P. K., Lewis, K. and Choularton, R. J. 2014. A methodological framework for rapidly assessing the impacts of climate risk on national-level food security through a vulnerability index. *Global Environmental Change*, 25(1): 121-132. <https://doi.org/10.1016/j.gloenvcha.2013.11.004>
- Lobell, D. B., Burke, M., Tebaldi, C., Mastrandrea, M. D., Falcon, W. P. and Naylor, R. L. 2008. Prioritizing climate change adaptation needs for food security in 2030. *Science*, pp. 319. <https://doi.org/10.1126/science.1152339>
- Manap, N.M.A. and Ismail, N.W. 2019. Food security and economic growth. *Int. J. Mod. Trends iSoc. Sci.*, 11: 108-118. <https://doi.org/10.35631/ijmtss.280011>
- Martadona, I. and Elhakim, S.K. 2020. Factors that affect the participation of farmers in the success of the implementation of rice farming insurance program (AUTP) in Padang City : SEM-PLS Analysis. *Hexagro*, 4(2), 97-107. <https://doi.org/10.36423/hexagro.v4i2.489>
- Montano, B. and García-López, M. 2020. Malthusianism of the 21st century. *Environmental and Sustainability Indicators*, 6: 100032. <https://doi.org/10.1016/J.INDIC.2020.100032>
- Nepal, R., Musibau, H. O. and Jamasb, T. 2021. Energy consumption as an indicator of energy efficiency and emissions in the European Union : A GMM based quantile regression approach. *Energy Policy*, 158(August): 1-10. <https://doi.org/10.1016/j.enpol.2021.112572>
- Nugroho, H.Y.S.H., Indrawati, D.R., Wahyuningrum, N., Adi, R.N., Supangat, A.B., Indrajaya, Y., Putra, P.B., Cahyono, S.A., Nugroho, A.W., Basuki, T.M., Savitri, E., Yuwati, T. W., Narendra, B.H., Sallata, M.K., Allo, M.K., Bisjoe, A.R., Muin, N., Isnain, W., Ansari, F. and Hani, A. 2022. Toward water, energy, and food security in rural Indonesia. *Rev. Water*, 14(10): 1-25. <https://doi.org/10.3390/w14101645>
- Oskorouchi, H. R. and Sousa-Poza, A. 2021. Floods, food security, and coping strategies: Evidence from Afghanistan. *Agricultural Economics (United Kingdom)*, 52(1): 123-140. <https://doi.org/10.1111/agec.12610>
- Pham, N. M., Huynh, T. L. D. and Nasir, M. A. 2020. Environmental consequences of population, affluence and technological progress for European countries: A Malthusian view. *Journal of Environmental Management*, 260: 110143. <https://doi.org/10.1016/J.JENVMAN.2020.110143>
- Rosalia, A. C. T. and Hakim, L. 2021. Spatial analysis of the impact of flood and drought on food security index. *Nature Environment and Pollution Technology*, 20(2). <https://doi.org/10.46488/NEPT.2021.v20i02.031>
- Rozaki, Z. 2021. Food security challenges and opportunities in Indonesia post COVID-19. In: *Advances in Food Security and Sustainability*, 6: 119-168. <https://doi.org/10.1016/bs.af2s.2021.07.002>
- Suryanto, Kumalasari, R., Guritno, D. C., Saputro, N. and Marniyati, S. 2021. Do social-economy vulnerability index and poverty index have correlation? Study in Begawan solo watershed. *International Journal of Business and Society*, 22(2): 985-1003. <https://doi.org/10.33736/ijbs.3777.2021>
- Suryanto, S. and Rahman, A. 2019. Application of livelihood vulnerability index to assess risks for farmers in the Sukoharjo Regency and Klaten Regency, Indonesia. *Jamba J. Disas. Risk Stud.*, 11(1): <https://doi.org/10.4102/jamba.v11i1.739>
- Suryanto, Utomowati, R., Gravitiani, E. and Rosalia, A. C. T. 2021. Hunger climate vulnerability index (HCVI) and macroeconomic indicators downstream of Bengawan Solo Watershed. *IOP Conference Series: Earth and Environmental Science*, 824(1). <https://doi.org/10.1088/1755-1315/824/1/012113>
- Świetlik, K. 2018. Economic Growth Versus the Issue of Food Security in Selected Regions and Countries Worldwide. *Problems of Agricultural Economics*, 356(3): 127-149. <https://doi.org/10.30858/zer/94481>
- Thobei, T., Sutarno, S. and Komariah, K. 2014. Effects of climate change on crop production in Thaba-Tseka and Mokhotlong districts Lesotho Highlands. *IOSR J. Agric. Veter. Sci.*, 7(1): 37-44. <https://doi.org/10.9790/2380-07143744>
- van Dijk, M., Morley, T., Rau, M.L. and Saghai, Y. 2021. A meta-analysis of projected global food demand and the population at risk of hunger for 2010–2050. *Nature Food*, 2(7): 494-501. <https://doi.org/10.1038/s43016-021-00322-9>



Molecular Docking Analysis of *Embelia ribes* for Selected Constituents as *Spodoptera frugiperda* (Fall Armyworm) Beta Glycosidase and Caspase-1 Inhibitors

Srinivasan Kumaraswamy*, Vasantha-Srinivasan Prabhakaran**  and Radhakrishnan Narayanaswamy***† 

*Department of Biochemistry, St. Peter's Institute of Higher Education and Research (SPIHER), Avadi, Chennai-600 054, Tamilnadu, India

**Department of Bioinformatics, Saveetha School of Engineering, SIMATS (Deemed to be University), Thandalam, Chennai-602 105, Tamilnadu, India

***Department of Biochemistry, Saveetha Medical College and Hospital, SIMATS (Deemed to be University), Thandalam, Chennai-602 105, Tamilnadu, India

†Corresponding author: Radhakrishnan Narayanaswamy; kishnanbio07@gmail.com

Nat. Env. & Poll. Tech.
Website: www.neptjournal.com

Received: 25-10-2022

Revised: 08-12-2022

Accepted: 24-12-2022

Key Words:

Molecular docking

Spodoptera frugiperda

Embelia ribes

Embelin

Vilangin

ABSTRACT

Insect pest control is one of the major issues facing the agriculture sector because of the need for new agrochemicals and biocontrol agents that are environmentally friendly, economically affordable, and safe for human health. *Spodoptera frugiperda* (fall armyworm) is one of the insect pests that causes huge damage to various crops around the globe due to its generalist nature. In the present study, three selected *Embelia ribes* Burm F (Myrsinaceae) constituents, which include embelin, 5-O-methylembelin, and vilangin; one semi-synthetic compound (potassium embelate); three synthetic compounds, namely coenzyme Q₁₀, dopaquinone, and idebenone; and two reference compounds (azadirachtin and amitraz) were assessed on the docking behavior of *S. frugiperda* (beta glycosidase and caspase-1). The docking studies showed that coenzyme Q₁₀ exhibited the highest binding energies (-130.61 and -434.56 kcal. mol⁻¹) for the target enzymes *S. frugiperda* (beta glycosidase and caspase-1, respectively). Thus, the present investigation provides new knowledge in understanding *Embelia ribes* Burm F (Myrsinaceae) constituents as possible inhibitors against *S. frugiperda* (beta glycosidase and caspase-1) enzyme activities. Furthermore, the present work can help to develop new insecticides and pesticides against *S. frugiperda* and other related insect pests.

INTRODUCTION

The long-term usage of synthetic fertilizers and pesticides contaminates soil and surface water, and they are also reported to cause ill effects in animals (fish) and humans (Patel & Gajar 2001). Moreover, the use of synthetic pesticides leads to environmental issues like bioaccumulation and biomagnification, which cause huge losses to our biological wealth and resources. Similarly, overuse of chemical fertilizers (like nitrogenous, phosphoric, and potassium) has negatively affected the soil texture and altered the pH value of the soil, causing an imbalance in nutrient absorption for crops, fruits, plants, and vegetables (Dhar 2020). The increasing awareness about the ill effects

of synthetic fertilizers and pesticides has forced us to look for alternative ways (organic farming) and technologies (like traditional hydroponics and aquaponics). Moreover, there is a huge rise in demand for the use of plant-based (botanical) pesticides, especially for crop protection (Nas 2004). Now, worldwide agricultural scientists are investigating and developing botanical pesticides (using indigenous plant materials) to protect against insect infestations (Pavunraj et al. 2011). Moreover, the use of indigenously available plants or herbs in the control and management of pests is a traditional, adopted, and practiced agricultural technology in many countries, including India (Roy et al. 2005). The advantage of using botanical pesticides is that they are non-selective toxins or poisons that are active against a wide range of agricultural pests (Pavunraj et al. 2011). Several phytochemicals have been reported to be potent alternatives to chemical pesticides (Leatemia & Isman 2004). The mechanism of action of phytochemicals has been reported by

ORCID details of the authors:

Vasantha-Srinivasan Prabhakaran: <https://orcid.org/0000-0003-3415-3315>

Radhakrishnan Narayanaswamy: <https://orcid.org/0000-0001-5259-761X>

many researchers. For instance, the antifeedant (Raja et al. 2005), larvicidal (Kabaru & Gichia 2001), ovicidal (Pavunraj et al. 2006), repellent (Paredes-Sanchez et al. 2021), etc. are the few reported mechanisms of action employed by the phytochemicals for the control and management of pests. In the present study, we focus on *Spodoptera frugiperda* (Fall Armyworm), which is one of the major pests and has the following crops like cotton, maize, millet, rice, sorghum, soybean, and sugarcane (Deshmukh et al. 2021).

Embelia ribes Burm. f., a dense shrub of the family Myrsinaceae, has been reported to possess numerous medicinal uses. *E. ribes* has been known to possess phytoconstituents, namely, christembine, daucosterol, 5-*O*-methylembelin, embelinol, embeliol, embeliaribyl ester, embelin, embolic acid, rapanone, sitosterol, and vilangin, etc. (Mhaskar et al. 2011). *Brassica juncea* and *E. ribes* have been reported to safeguard the seeds from several fungal diseases and pests. In addition, treatment with these plant extracts also stimulates disease resistance after the germination of the seeds (Dhar 2020). Moreover, embelin (a bioactive constituent of *E. ribes*) has been reported to be effective against stored grain pests (Dhar 2020). Thus, the background mentioned above prompts us to carry out the present work on three selected constituents of *E. ribes*, namely, embelin, 5-*O*-methylembelin, and vilangin; one semi-synthetic compound (potassium embelate); three synthetic compounds, namely coenzyme Q10, dopaquinone, and idebenone; and two reference compounds (azadirachtin and amitraz), which were assessed on the docking behavior of *S. frugiperda* (beta glycosidase and caspase-1) by using the PatchDock method.

MATERIALS AND METHODS

Ligand Preparation

Chemical structures of three ligands (constituents of *E. ribes*) namely 1) embelin (CID no: 3218); 2) 5-*O*-methylembelin (CID no:171489); 3) vilangin (CID no:417182); one semi-synthetic compound 4) potassium embelate (CID no: 23677950); three synthetic compounds namely, 5) coenzyme Q10 (CID no: 5281915); 6) dopaquinone (CID no: 439316); 7) idebenone (CID no: 3686); two reference compounds namely, 8) azadirachtin (CID no: 5281303); and 9) amitraz (CID no: 36324) were downloaded from PubMed database. These selected ligands were prepared according to the earlier report (Mohan et al. 2022). These prepared structures were used for further study (PatchDock).

Identification and Preparation of Target Protein

The three-dimensional (3D) structure of the *Spodoptera*

frugiperda beta glycosidase (PDB ID: 5CG0 with a resolution of 2.09 Å) and caspase-1 (PDB ID: 1M72 with a resolution of 2.30 Å) were obtained from Protein Data Bank (PDB). A chain of both proteins was processed individually by removing other chains, ligands, and crystallographically observed water (H₂O) molecules (i.e., water without hydrogen bonds) by using UCSF Chimera software.

Molecular Docking Study

A docking study was performed for the selected (three *E. ribes* constituents; one semi-synthetic; three synthetic, and two reference compounds) ligands using the PatchDock online server. Finally, the binding site analysis was carried out for the best-docked pose using the PyMOL software (Mohan et al. 2022).

RESULTS AND DISCUSSION

Spodoptera frugiperda has gained much attention worldwide due to its outbreaks in Africa (since 2016) and Asia (since mid-year 2018). In 2018, *S. frugiperda* has been reported for the first time in India, and that too in South India (Shivamogga and Davanagere districts of Karnataka State) on the maize crop (Deshmukh et al. 2021). *S. frugiperda* has been reported to cause primarily huge damage to maize crops, followed by other host crops like millets, vegetables, and sorghum (Day et al. 2018).

In general, beta glycosidases have been involved in hydrolyzing glycosides to release carbohydrates (Marana et al. 2000). *Spodoptera frugiperda* beta glycosidase (Sfβgly) is a secreted digestive enzyme present in midgut epithelial cells. *Spodoptera frugiperda* beta glycosidase (Sfβgly) has been previously reported in relation to its i) catalysis, ii) substrate recognition, and iii) thermal stability (Otsuka et al. 2020). Thus, in the present study, *Spodoptera frugiperda* beta glycosidase (Sfβgly) was selected as one of the target enzymes.

Caspases have been involved in the carrying out of the apoptosis process, and the apoptotic pathway is highly conserved in the metazoans. Thus, caspases serve as a fascinating target for medical treatment. *Spodoptera frugiperda* caspase-1 (Sf-caspase 1) is the chief effector caspase of *S. frugiperda* (Forsyth et al. 2004). Therefore, in the present study, *Spodoptera frugiperda* caspase-1 (Sf-caspase 1) was selected as the second target enzyme.

Table 1 shows the chemical nature and botanical source of nine selected ligands. Out of nine ligands, seven ligands belong to the quinone (55.6%). Similarly, alpha amino acid (11.1%), tertiary amino compound (11.1%), and triterpenoid (11.1%) are three other classes of selected ligands.

Table 1: Nature of chemical class and source of nine selected ligands.

S.No.	Ligand name	Nature of chemical class	Source
1.	Coenzyme Q ₁₀	Quinone	<i>Arachis hypogaea</i> , <i>Brassica oleracea</i> , <i>Brassica rapa</i> , <i>Citrus clementina</i> , <i>Daucus carota</i> , <i>Glycine max</i> , <i>Malus domestica</i> , <i>Petroselinum crispum</i> , <i>Pisum sativum</i> , <i>Solanum lycopersicum</i> and <i>Solanum tuberosum</i>
2.	Dopaquinone	Alpha amino acid	Present in the human skin and feces
3.	Embelin	Quinone	<i>Embelia ribes</i> , <i>Ardisia humilis</i> , <i>Connarus ritchiei</i> , <i>Embelia barbeyana</i> , <i>Embelia kilimandscharica</i> , <i>Embelia robusta</i> , <i>Embelia tsjersium-cottam</i> , <i>Myrsine africana</i> , <i>Myrsine capitellata</i> , <i>Myrsine semiserrata</i> and <i>Rapanea umbellata</i>
4.	Idebenone	Quinone	Synthetic one
5.	5- <i>O</i> -Methylembelin	Quinone	<i>Embelia ribes</i>
6.	Potassium embelate	Quinone	Synthetic one
7.	Vilangin	Quinone	<i>Embelia ribes</i>
8.	Azadirachtin	Triterpenoid	<i>Azadirachta indica</i>
9.	Amitraz	Tertiary amino compound	Synthetic one

Table 2: The interaction energy analysis of nine selected ligands with the *Spodoptera frugiperda* beta glycosidase using the PatchDock method

S.No.	Ligand names	-ACE* (-kcal.mol ⁻¹)	Interaction of amino acid residue	Bond distance (Å)
1.	Coenzyme Q 10	130.61	Arg189 Asn249 Glu271	2.9 2.8 2.8
2.	Dopaquinone	+271.02	Gln39 Ser247 Asn249 Tyr331 Glu451 Trp452	3.5 2.9 2.9 3.3 2.4 3.1
3.	Embelin	+40.45	His142 Glu187 Glu451 Trp452	3.6 2.5 2.9 3.2
4.	Idebenone	34.07	Gln39 His142 Arg267 Glu271	2.1 2.6 3.0 3.5
5.	5- <i>O</i> -Methylembelin	+52.22	Glu187 Glu399	1.6, 2.3 and 2.5 2.4
6.	Potassium embelate	+22.46	His142 Glu187	3.3 1.8 and 3.3
7.	Vilangin	83.22	No interactions	-
8.	Azadirachtin	+5.95	Arg189	3.2 and 3.4
9.	Amitraz	+53.98	No interactions	-

Note: ACE*- Atomic contact energy

The docking studies revealed that coenzyme Q₁₀ exhibited the highest (ACE) atomic contact energy (-130.61 kcal.mol⁻¹) with the *Spodoptera frugiperda* beta glycosidase enzyme. In contrast, idebenone showed the lowest binding energy (-34.07 kcal.mol⁻¹) with the target enzyme *Spodoptera frugiperda* beta glycosidase (Table 2).

In the present study, six ligands namely, dopaquinone (+271.02 kcal.mol⁻¹); amitraz (+53.98 kcal.mol⁻¹);

5-*O*-Methylembelin (+52.22 kcal.mol⁻¹); embelin (+40.45 kcal.mol⁻¹); potassium embelate (+22.46 kcal.mol⁻¹) and azadirachtin (+5.95 kcal.mol⁻¹) have shown poor (ACE) atomic contact energy values (Table 2).

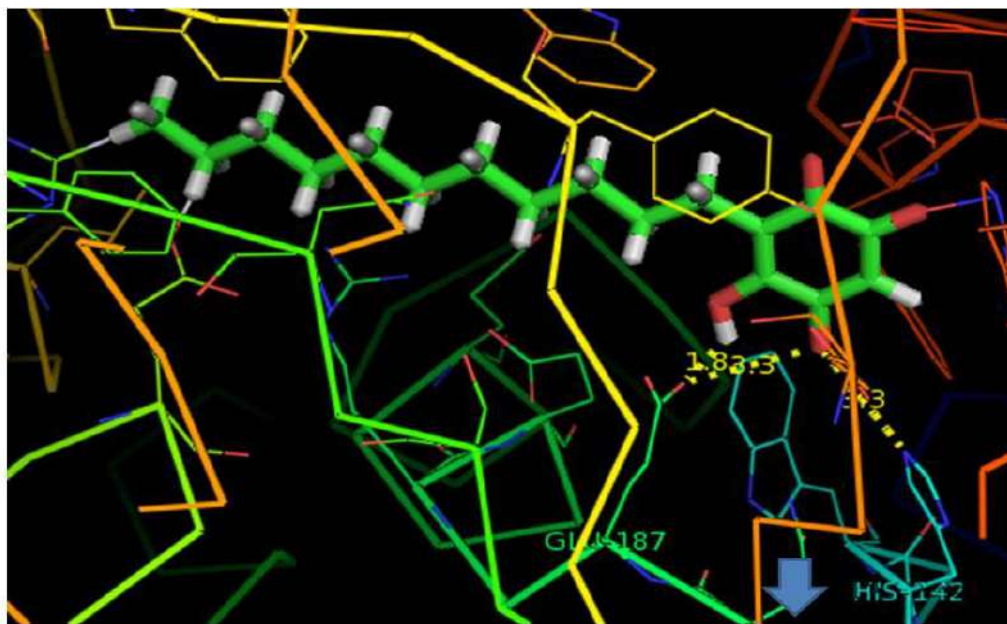
Three ligands such as embelin, 5-*O*-Methylembelin, and potassium embelate were shown to interact with the Glu 187 amino acid residue of the *Spodoptera frugiperda* beta glycosidase enzyme (as shown in Table 2). Similarly,

Tamaki et al. (2016) reported that the mutation in Glu 187 amino acid position results in the worst effect on *Spodoptera frugiperda* beta glycosidase hydrolytic activity. In the present study, three ligands such as embelin, idebenone, and potassium embelate (Fig. 1) are shown to interact with the His 142 amino acid residue of the *Spodoptera frugiperda* beta glycosidase enzyme. Similarly, Tamaki et al. (2016) reported that the His 142 amino acid residue is present in the glycone binding site of the *Spodoptera frugiperda* beta glycosidase enzyme.

The docking studies showed that azadirachtin exhibited the highest (ACE) atomic contact energy (-504.85 kcal.

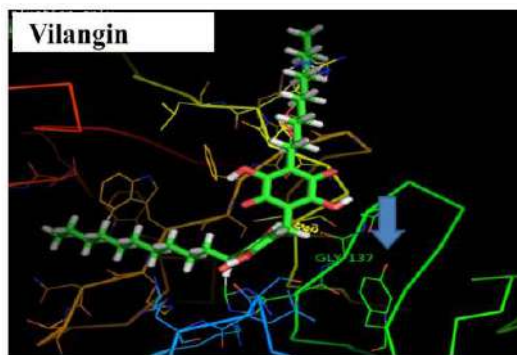
mol⁻¹) with the *Spodoptera frugiperda* caspase-1 enzyme. In contrast, vilangin showed the lowest binding energy (-155.16 kcal.mol⁻¹) with the target enzyme *Spodoptera frugiperda* caspase-1 (Table 3).

The binding energy results showed the following order: azadirachtin (-504.85 kcal.mol⁻¹), < coenzyme Q₁₀ (-434.56 kcal.mol⁻¹), < idebenone (-292.08 kcal.mol⁻¹), < 5-O-Methylembelin (-258.03 kcal.mol⁻¹), < potassium embelate (-246.62 kcal.mol⁻¹), < amitraz (-236.96 kcal.mol⁻¹), < embelin (-210.73 kcal.mol⁻¹), < vilangin (-155.16 kcal.mol⁻¹).



Note: ↓ Down arrow mark represents the Histidine (His) amino acid at position 142 of the *Spodoptera frugiperda* beta glycosidase enzyme interacting with the ligand (potassium embelate). The dotted lines represent the hydrogen bonds.

Fig. 1: Interaction of potassium embelate with the target enzyme *Spodoptera frugiperda* beta glycosidase.



Note: ↓ Down arrow mark represents the Glycine (Gly) amino acid at position 137 of the *Spodoptera frugiperda* caspase-1 enzyme interacting with the ligand (vilangin). The dotted lines represent the hydrogen bonds.

Fig. 2: An interaction of potassium embelate with the target enzyme *Spodoptera frugiperda* caspase-1.

Table 3: The interaction energy analysis of nine selected ligands with the *Spodoptera frugiperda* caspase-1 using the PatchDock method.

S.No.	Ligand names	-ACE* (-kcal.mol ⁻¹)	Interaction of amino acid residue	Bond distance (Å)
1.	Coenzyme Q 10	434.56	No interactions	-
2.	Dopaquinone	187.98	Arg40 Tyr202 Ile204	3.5 1.6 and 3.3 2.5
3.	Embelin	210.73	Arg203	2.3, 2.4 and 3.2
4.	Idebenone	292.08	Ile204	3.1 and 3.4
5.	5-O-Methylembelin	258.03	No interactions	-
6.	Potassium embelate	246.62	Arg203 Ile204	3.2 3.1, 3.1 and 3.4
7.	Vilangin	155.16	Gly137	2.6 and 3.3
8.	Azadirachtin	504.85	Arg203	2.5
9.	Amitraz	236.96	No interactions	-

Note; -ACE*- Atomic contact energy

In the present study, three ligands such as embelin, potassium embelate, and azadirachtin were shown to interact with the Arg 203 amino acid residue of the *Spodoptera frugiperda* caspase-1 enzyme. Interestingly one ligand (vilangin) was shown to interact with the Gly 137 amino acid residue (Fig. 2) of the *Spodoptera frugiperda* caspase-1 enzyme. This result is on par with the previous report (Forsyth et al. 2004 and Wang et al. 2021).

Secondly, metabolites from *Azadirachta indica* have been known to possess antifeedant and repellent activity against *Spodoptera frugiperda* (Paredes-Sanchez et al. 2021). *Embelia ribes* has been reported as one of the plants used in crop disease management practices in ancient medieval and premodern India (Nene 2003). Similarly, *E. ribes* leaf extracts have shown to possess growth inhibition and feeding deterrence on *Spodoptera litura* (Noosidum & Chandrapatya 2015). To the best of our knowledge, no docking reports are available for the *S. frugiperda* enzymes (beta glycosidase and caspase-1) till date.

CONCLUSION

In the present study, all the nine selected ligands have been shown to dock with both the target enzymes. To our understanding, we are the first to describe the docking behavior of *S. frugiperda* enzymes (beta glycosidase and caspase-1) with that of nine selected ligands even though *E. ribes* crude extract has been known to possess antifeedant activity. These results provide new insight into understanding their inhibitory activities and pave way for further *in vitro* investigation of these 9 selected ligands as possible inhibitors against both the *Spodoptera frugiperda* enzymes (beta glycosidase and caspase-1).

REFERENCES

- Day, R., Abrahams, P., Bateman, M., Beale, T., Clotley, V., Cock, M., Colmenarez, Y., Corniani, N., Early, R., Godwin, J. and Gomez, J. 2017. Fall armyworm: impacts and implications for Africa. *Outlooks Pest Manag.*, 28(5): 196-201.
- Deshmukh, S.S., Prasanna, B.M., Kallelshwaraswamy, C.M., Jaba, J. and Choudhary, B. 2021. Fall armyworm (*Spodoptera frugiperda*). In: *Polyphagous Pests of Crops*, Springer, Singapore., pp. 349-372.
- Dhar, A. 2020. Plant protection practices by using botanicals for sustainable agriculture. *Plant Arch.*, 20(2): 3741-3746.
- Forsyth, C.M., Lemongello, D., LaCount, D.J., Friesen, P.D. and Fisher, A.J. 2004. Crystal structure of an invertebrate caspase. *J. Biol. Chem.*, 279(8): 7001-7008.
- Kabaru, J.M. and Gichia, L. 2001. Insecticidal activity of extracts derived from different parts of the mangrove tree *Rhizophora mucronata* (Rhizophoraceae) Lam. against three arthropods. *African Journal of Science and Technology*, 2(2).
- Leatemia, J.A. and Isman, M.B. 2004. Insecticidal activity of crude seed extracts of *Annona* spp., *Lansium domesticum* and *Sandoricum koetjape* against lepidopteran larvae. *Phytoparasitica*, 32(1): 30-37.
- Marana, S.R., Terra, W.R. and Ferreira, C. 2000. Purification and properties of a β -glycosidase purified from midgut cells of *Spodoptera frugiperda* (Lepidoptera) larvae. *Insect Biochemistry and Molecular Biology*, 30(12): 1139-1146.
- Mhaskar, M., Joshi, S., Chavan, B., Joglekar, A., Barve, N. and Patwardhan, A. 2011. Status of *Embelia ribes* Burm f.(Vidanga), an important medicinal species of commerce from northern Western Ghats of India. *Curr. Sci.*, 100(4): 547-552.
- Mohan, S., Prabhakaran, V.S. and Narayanaswamy, R. 2022. *In silico* analysis of *Cissus rotundifolia* constituents as human neutrophil elastase (HNE), matrix metalloproteinases (MMP 2 and MMP 9), and tyrosinase inhibitors. *Appl. Biochem. Biotechnol.*, 194(1): 232-245.
- Nas, M.N. 2004. *In vitro* studies on some natural beverages as botanical pesticides against *Erwinia amylovora* and *Curtobacterium flaccumfaciensis* subsp. *poinsettiae*. *Turk. J. Agric. For.*, 28(1): 57-61.
- Nene, Y.L. 2003. Crop disease management practices in ancient medieval and pre-modern India. *Asian Agri-Hist.*, 7(3): 185-201.
- Noosidum, A. and Chandrapatya, A. 2015. Growth inhibition and feeding deterrence from leaf extracts of *Embelia ribes* Burm. f. on *Spodoptera litura* (F.) (Lepidoptera: Noctuidae). *Khon Kaen Agr. J.*, 43(4): 773-780.

- Otsuka, F.A., Chagas, R.S., Almeida, V.M. and Marana, S.R. 2020. Homodimerization of a glycoside hydrolase family GH1 β -glucosidase suggests distinct activity of enzyme different states. *Protein Sci.*, 29(9): 1879-1889.
- Paredes-Sánchez, F.A., Rivera, G., Bocanegra-García, V., Martínez-Padrón, H.Y., Berrones-Morales, M., Niño-García, N. and Herrera-Mayorga, V. 2021. Advances in control strategies against *Spodoptera frugiperda*. A review. *Molecules*, 26(18): 5587.
- Patel, M.B. and Gajjar, S.N. 2001. Bioefficacy of various plant leaf extracts against *Spodoptera litura* (Fabricius) (Noctuidae: Lepidoptera). *Indian J. Appl. Entomol.*, 15(2): 32-34.
- Pavunraj, M., Muthu, C., Ignacimuthu, S., Janarthanan, S., Durairamdiyan, V., Raja, N. and Vimalraj, S. 2011. Antifeedant activity of a novel 6-(4, 7-hydroxy-heptyl) quinone from the leaves of the milkweed *Pergularia daemia* on the cotton bollworm *Helicoverpa armigera* (Hub.) and the tobacco armyworm *Spodoptera litura* (Fab.). *Phytoparasitica*, 39(2): 145-150.
- Pavunraj, M., Subramanian, K., Muthu, C., Seenivasan, S.P., Durairamdiyan, V., Packiam, S.M. and Ignacimuthu, S. 2006. Bioefficacy of *Excoecaria agallocha* (L.) leaf extract against the armyworm *Spodoptera litura* (Fab.) (Lepidoptera: Noctuidae). *Entomol.*, 31(1): 37.
- Raja, N., Jeyasankar, A., Venkatesan, S.J. and Ignacimuthu, S. 2005. Efficacy of *Hyptis suaveolens* against lepidopteran pests. *Curr. Sci.*, 88(2): 220-222.
- Roy, B., Amin, R., Uddin, M.N., Islam, A.T.M.S., Islam, M.J. and Halder, B.C. 2005. Leaf extracts of *Shiyalmutra* (*Blumea lacera* Dc.) as botanical pesticides against lesser grain borer and rice weevil. *J. Biol. Sci.*, 5(2): 201-204.
- Tamaki, F.K., Souza, D.P., Souza, V.P., Ikegami, C.M., Farah, C.S. and Marana, S.R. 2016. Using the amino acid network to modulate the hydrolytic activity of β -glycosidases. *PLoS One*, 11(12): e0167978.
- Wang, Y., Goodman, C.L., Ringbauer Jr, J., Li, Y. and Stanley, D. 2021. Prostaglandin A2 induces apoptosis in three cell lines derived from the fall armyworm, *Spodoptera frugiperda*. *Arch. Insect Biochem. Physiol.*, 108(3): e21844.



Effect of Compliance with Environmental Regulations in the Construction of Public Civil Works, Cajamarca, Peru

D. Quinto* , D. Sanchez* , M. Milla*† , M. Torres* , B. Cayatopa* , D. Jara**  and E. Morales*** 

*Facultad de Ingeniería, Universidad Nacional de Jaén, Ciudad de Jaén, Cajamarca, Perú. C.P. 06801, Perú

**Facultad de Ciencias de la Salud, Universidad Nacional de Jaén, Ciudad de Jaén, Cajamarca/Perú. C.P. 06801, Perú

***Facultad de Ciencias Naturales y Aplicadas, Universidad Nacional Intercultural Fabiola Salazar Leguía de Bagua (UNIFSLB), Bagua 01721, Perú

†Corresponding author: M. Milla; manuel.milla@unj.edu.pe

Nat. Env. & Poll. Tech.

Website: www.neptjournal.com

Received: 06-11-2022

Revised: 09-12-2022

Accepted: 02-01-2023

Key Words:

Environmental standards
Environmental regulations
Public civil works

ABSTRACT

Construction activities produce considerable environmental effects and have resulted in a growing demand to implement favorable environmental practices. In this sense, this research aimed to evaluate the effect of the level of compliance with environmental regulations in public civil works in the San Ignacio, Cajamarca, Peru district. Data were obtained through direct observation and structured interviews in 7 selected construction sites. The deductive and analytical method was used. As a result, the level of compliance was obtained. Work 4 had the highest rank, and works 2 and 5 had the lowest. Currently, all the works are in a similar range of compliance. The degree of association between the level of compliance with environmental regulations and the current state of the civil works indicates a probability of 0.0190, which shows that the low level of compliance with environmental regulations in the construction of public civil works in the district of San Ignacio generates a deterioration in the quality of the environment and increases the possibility of administrative sanctions.

INTRODUCTION

Worldwide, the ongoing trends of population growth and urbanization generate a constant increase in construction work (Asare 2022). In Peru, there are a large number of public civil works that are executed in different areas of the country to improve the living conditions of the population (Casavielles et al. 2011), these works may be directed by regional and local governments, which are responsible for hiring those in charge of the execution, depending on the magnitude of the work (Indahningrum et al. 2020). De La O Muñoz (2020) states that, in the construction process, the company or contractor must comply with the activities inherent to its competence according to the costs established in the Environmental Management and Management Plan.

It is also important to identify the main problems that affect the environment of the works (Enshassi et al. 2014) to

establish management measures based on the incorporation of programs and guidelines that include prevention strategies and control and mitigation measures of the environmental impacts generated around the works (Corazi 2017). Dust generation, noise pollution, operations with vegetation removal, and air pollution are the most significant environmental impacts of construction projects (Enshassi et al. 2014). Civil construction works impact flora and fauna depending on their nature and extent (Hashemkhani et al. 2018).

In this sense, this study posed the question: what will be the effect of the level of compliance with environmental regulations? In relation to this, it was evaluated with criteria such as the Environmental Management Plan, Environmental Surveillance Plan, Contingency Plan, Solid Waste Minimization and Management Plan (PMMRS), and the Community Relations and Environmental Compensation Plan (Plan de Relaciones Comunitarias y Compensación Ambiental).

Based on the above, the objective of this research was to evaluate the effect of the level of compliance with environmental regulations in the construction of public civil works in the district of San Ignacio in the Cajamarca region,

ORCID details of the authors:

D. Quinto: <https://orcid.org/0000-0002-6092-0971>

D. Sanchez: <https://orcid.org/0000-0002-7829-0269>

M. Milla: <https://orcid.org/0000-0003-3931-9804>

M. Torres: <https://orcid.org/0000-0002-0892-0341>

B. Cayatopa: <https://orcid.org/0000-0002-8640-7754>

D. Jara: <https://orcid.org/0000-0002-9177-5578>

E. Morales: <https://orcid.org/0000-0002-8623-3192>

2021, to ensure environmental viability and counteract the negative effects generated by the execution of public civil works.

MATERIALS AND METHODS

Scope of the Study

The research was conducted in San Ignacio's district, department of Cajamarca - Peru. Seven public civil works were chosen, taking as criteria that all of them were in the process of execution (Work 1: San Ignacio, Work 2: San Ignacio, Work 3: San Ignacio, Work 4: San Ignacio, Work 5: Caserío Los Lirios, Work 6: Caserío Atapaca, Work 7: Caserío Ihuamaca, Work 8: Caserío Ihuamaca, Work 8: Caserío Ihuamaca).

The method used was the analytical deductive method (McKibben et al. 2020). The characterization of environmental regulations was determined by reviewing national legal bodies, such as norms, regulations, and guidelines related to compliance with environmental criteria in the construction of public civil works of educational, transportation, hydraulic, and urban infrastructure. The level of compliance with environmental regulations was obtained through frequency distribution and percentage analysis of data using the Non-Parametric Bidimensional Friedman Test. The data were collected by identifying the public civil works under construction (execution) in the district of San Ignacio through the Infrastructure and Territorial Development Management of the Provincial Municipality of San Ignacio.

The interviews were based on 5 criteria (Environmental Management Plan, Environmental Monitoring Plan, Contingency Plan, Solid Waste Minimization and Management Plan (PMMRS), and Community Relations and Environmental Compensation Plan). The application group was the resident, supervisor, or environmental specialist of the designated works, with the purpose of knowing the level of compliance with environmental regulations in the construction of public civil works. Likewise, to perceive the current state in situ of the works, a tour was made through each of them, where direct observation was made, taking into

Table 1: Variables Measurement Scale.

Compliance Level	Current State of Public Civil Works
1 = Very bad	0 - 20 = Very por
2 = Malo	20 - 40 = Deficient
3 = Regular	40 - 60 = Regular
4 = Good	60 - 80 = Good
5 = Very Good	80 - 100 = Excellent

account the 5 criteria applied in the interview. Spearman's rank correlation coefficient was used to analyze the effect of the level of compliance with environmental regulations based on the data obtained from the scales for measuring the variables established (Table 1).

The data were processed with the Statistics V 8.0 statistical package (Análisis et al. 2012), and contingency tables were prepared to characterize the environmental regulations in the execution of public civil works. Frequency distribution tables were constructed, and a percentage data analysis was performed to identify compliance with environmental regulations in the construction of public civil works. Spearman's ordinal rank correlation coefficient was calculated to estimate the degree of association between the variables' level of compliance with environmental regulations and the current state of construction of public civil works, as well as Friedman's test to detect differences between the works with respect to the level of compliance with environmental regulations and the criteria defined for the evaluation.

RESULTS

The characterization of environmental regulations was based on three categories: 6 laws, 5 regulations, and a guide for preparing the Environmental Management Strategy (Table 2).

The level of compliance with environmental regulations shows that Works 4 has the highest level of compliance, while Works 2 and 5 have the lowest level of compliance. On the other hand, Criterion 4 has the highest level of compliance. Criterion 3 has the lowest level of compliance (Table 3).

According to the two-dimensional Friedman Test for the current status, there is no significant difference, so all works are at the same level of compliance. At the same time, Criterion 1 has the highest level of compliance for the current status, and Criterion 4 has the lowest level of compliance for the current status (Table 4).

The degree of association between the variables' level of compliance with environmental regulations and the current state of the civil works was significant, which translates into a tendency to a directly proportional behavior between the variables, i.e., the higher the level of compliance with environmental regulations, the better the current state of the civil works, and vice versa (Table 5). The probability of 0.0190 shows a significant difference between the two variables.

DISCUSSION

Strict laws should be enacted where institutions conduct

Table 2: Characterization of Environmental Regulations.

Laws	Regulations	Guides
Law N°28611 - General Environmental Law.	Supreme Decree N°019-2009-MINAM - Regulation of the National System of Environmental Impact Assessment.	Environmental Management Strategy in the Framework of the National Environmental Impact Assessment System - Ministerial Resolution N°019-2020-MINAM
Law No. 28245 - Framework Law of the National Environmental Management System.	Supreme Decree N°008-2005-PCM - Regulation of the National Environmental Management System Framework Law.	
Law N°27446 - National Environmental Impact Assessment System Law.	Supreme Decree N°057-2004-PCM - Regulation of the General Law on Solid Waste.	
Law N°29968 - Law of the National Environmental Certification Service for Sustainable Investments.	Supreme Decree N°003-2013-VIVIENDA - Regulations for the Management and Handling of Waste from Construction and Demolition Activities - Supreme Decree N°019-2016-VIVIENDA amending the regulations.	
Law No. 29325 - Law of the National Environmental Assessment and Control System.	Peruvian Technical Standard NTP 900.058 2019.	
Legislative Decree N°1278 - Law on Integral Solid Waste Management, Legislative Decree 1501, which amends the Law on Integral Solid Waste Management.		

Table 3: Level of Compliance with Environmental Regulations.

Statistical Test for the Construction Site	
Chi-square, corrected for ties	20.77
Degree of freedom	6
Probability	0.0020 (**)
Construction work	Meaning of Rank
1	3.20
2	2.00
3	4.80
4	6.40
5	2.00
6	5.30
7	4.30
Statistical Test for Criterion	
Chi-square, corrected for ties	10.70
Degree of freedom	4
Probability	0.0301 (*)
Criteria	Meaning of Rank
1	3.71
2	3.29
3	1.93
4	3.79
5	2.29

NS: Not Significant; P < 0.05; S: Significant; P > 0.05 (*); AS: Highly Significant; P > 0.01 (**)

Environmental Impact Assessments (EIA) in the early stages of civil works construction to reduce the negative impacts they may generate (Enshassi et al. 2014). EIAs should be evaluated objectively, implemented well, and

Table 4: Current Status of Public Civil Works.

Statistical Test for Construction Site	
Chi-square, corrected for ties	12.47
Degree of freedom	6
Probability	0.0522
Construction Work	Meaning of Rank
1	3.20
2	2.40
3	4.20
4	6.00
5	3.00
6	4.70
7	4.50
Statistical Test for Criterion	
Chi-square, corrected for ties	12.80
Degree of freedom	4
Probability	0.0123 (*)
Criteria	Meaning of Rank
1	4.29
2	3.43
3	2.57
4	2.00
5	2.71

NS: No Significant; P < 0.05; S: Significant P > 0.05 (*); AS: Highly Significant P > 0.01 (**).

Table 5: Effect of the Level of Compliance on Public Civil Works in the District of San Ignacio.

Compliance Level	
Current Status	0.8829
Probability	0.0190 (*)

NS: No Significant; P < 0.05; S: Significant; P > 0.05 (*); AS: Highly Significant; P > 0.01 (**)

avoided personal interests (Crawley & Aho 1999, Wu et al. 2011).

Therefore, in this research, through the characterization of environmental regulations, it is confirmed that in Peru, environmental laws regulate the construction sector through compliance with environmental management instruments and should be interpreted correctly to avoid biases in decision-making. Likewise, public and effective participation must be guaranteed (Badr 2009).

The execution of the various works has caused a large part of the environmental components, such as soil, air, and biota of the areas of affluence, to be altered (Çelik et al. 2017, Xue et al. 2015). Therefore it recommends implementing and complying with environmental monitoring programs to control possible negative impacts on the physical, biotic environment and the environment of human interest (Opoku 2019). However, these present a compliance deficit, as shown in the results obtained based on the Score for Work in Compliance Level, where a probability of 0.0020 was obtained, indicating a highly significant difference between the 7 works compared, in which points to work 4 with the highest level of compliance and works 2 and 5 with the lowest level of compliance, resulting in the environmental impacts being negative or positive according to their compliance range.

Dust generation, noise pollution, operations with vegetation removal, and air pollution are the most significant environmental impacts of construction projects (Mok et al. 2015). There are various origins for producing environmental impacts (Mohammed et al. 2022). Such impacts originated from excavation, earth movement, and mobilization of machinery and equipment (Asare 2022, Shehadeh et al. 2022). With the 7 projects evaluated, it could be evidenced by many authors.

On the other hand, a very important factor to consider is the management of Construction and Demolition Waste (CDW) within the construction sites causes serious pollution on a global scale (Rondinel-Oviedo 2021, Wang et al. 2020). The government and the parties involved in the management and handling of CDW are in the adaptation process, so the current management is still very incipient (Chen et al. 2019). We agreed that criterion 4 is related to the Solid Waste Minimization and Management Plan, which has the lowest level for the current state of the construction site. In other words, it points to inadequate CDW management in the construction sites of our study.

Finally, the degree of association between the level of compliance with environmental regulations and the current state of the civil works indicates a probability of 0.0190, showing a significant difference between both variables.

In other words, the higher the level of compliance with environmental regulations, the better the current state of the work, and vice versa. Therefore, implementing appropriate business practices in environmental management related to infrastructure works contributes to the sustainability of the environment.

CONCLUSION

When the level of compliance with environmental regulations is higher, there are low rates of environmental impacts in the construction of such works. On the other hand, if the level of compliance with environmental regulations is lower, there is the possibility of finding greater environmental aspects altered by the works, generating additional administrative sanctions.

The public civil works in the district of San Ignacio, according to the level of compliance, work 4 presented the highest level of compliance and works 2 and 5 the lowest, criterion 4 the highest level of compliance, and criterion 3 the lowest. On the other hand, for the current status of the work, it was verified that all the works are at a similar level of compliance. Criterion 1 has the highest level, and criterion 4 has the lowest.

The degree of association between the variables' level of compliance with environmental regulations and the current state of the civil works was significant, which translates into a tendency to a directly proportional behavior between the variables, i.e., the higher the level of compliance with environmental regulations, the better the current state of the civil works, and vice versa.

ACKNOWLEDGMENTS

We want to thank the works office of the Provincial Municipality of San Ignacio for permitting us to visit the works in situ.

REFERENCES

- Análisis, P., Statistix, E. and Statistix, E. 2012. Índice 2 Introducción Edit: Statistics, pp. 1-14.
- Asare, T. J. 2022. Safe use of road construction tools, machinery, and equipment on site. *Central Europ. Manag. J.*, 30: 798-808.
- Badr, E.S.A. 2009. Evaluation of the environmental impact assessment system in Egypt. *Impact Assess. Proj. Appr.*, 27(3): 193-203. <https://doi.org/10.3152/146155109X465959>
- Casavieles, R N.R., Aguilera, O.L.B., Calzadilla, C.G., Ediltrudis, I., Sierra, S., Rojas Verdecia, I., Lorenzo, R. and Vi, M. 2011. Sustainable improvement of the population's quality of life-based on community-wide work. *Rev. Cub. Salud Púb.*, 37(3): 219-229. <http://scielo.sld.cu>
- Çelik, T., Kamali, S. and Arayici, Y. 2017. Social cost in construction projects. *Environ. Impact Assess. Rev.*, 86-77 :64. <https://doi.org/10.1016/j.eiar.2017.03.001>
- Chen, J., Hua, C. and Liu, C. 2019. Considerations for better construction

- and demolition waste management: Identifying the decision behaviors of contractors and government departments through a game theory decision-making model. *J. Clean. Prod.*, 212: 190-199. <https://doi.org/10.1016/j.jclepro.2018.11.262>
- Corazi, M. 2017. Environmental Management and Occupational Health in Sanitation Rehabilitation Works in the South-Tacna Region. Retrieved from <http://www.upt.edu.pe/upt/web/home/contenido/100000000/65519409>
- Crawley, D. and Aho, I. 1999. Building environmental assessment methods: Applications and development trends. *Build. Res. Inform.*, 27(4-5): 300-308. <https://doi.org/10.1080/096132199369417>
- De La O Muñoz, E. 2020. Environmental Impact in the Construction Process of the Water and Sanitation Service in the Zootechnics Faculty of the National University of Huancavelica. Retrieved from [http://repositorio.upecen.edu.pe/bitstream/UPECEN/84/1/Informe Final 2014.pdf](http://repositorio.upecen.edu.pe/bitstream/UPECEN/84/1/Informe%20Final%202014.pdf)
- Enshassi, A., Kochendoerfer, B. and Rizq, E. 2014. An evaluation of environmental impacts of construction projects. *Rev. Ingen. Constr.*, 29(3): 234-254. <https://doi.org/10.4067/s0718-50732014000300002>
- Hemkhani, Z.S., Pourhossein, M., Yazdani, M. and Zavadskas, E.K. 2018. Evaluating construction projects of hotels based on environmental sustainability with the MCDM framework. *Alex. Eng. J.*, 57(1): 357-365. <https://doi.org/10.1016/j.aej.2016.11.002>
- Indahningrum, R.P., Naranjo, J., Hernández, N.J., Peccato, L. and Hernández, O. 2020. The technical verification process and its influence on the quality of the constructions of the District of Chiclayo. *Appl. Microbiol. Biotechnol.*, 2507(1): 1-9.
- McKibben, W.B., Cade, R., Purgason, L.L. and Wahesh, E. 2020. How to conduct a deductive content analysis in counseling research. *Counsel. Outcome Res. Eval.*, 2: 1-13.
- Mohammed, M., Shafiq, N., Al-Mekhlafi, A.B.A., Rashed, E.F., Khalil, M.H., Zawawi, N.A., Muhammad, A. and Sadis, A.M. 2022. The mediating role of policy-related factors in the relationship between the practice of waste generation and sustainable construction waste minimisation: PLS-SEM. *Sustainability (Switzerland)*, 14(2):2056. <https://doi.org/10.3390/su14020656>
- Mok, K.Y., Shen, G.Q. and Yang, J. 2015. Stakeholder management studies in mega construction projects: A review and future directions. *Int. J. Proj. Manag.*, 33(2): 446-457. <https://doi.org/10.1016/j.ijproman.2014.08.007>
- Opoku, A. 2019. Biodiversity and the built environment: Implications for the sustainable development goals (SDGs). *Resour. Conserv. Recycl.*, 141: 1-7. <https://doi.org/10.1016/j.resconrec.2018.10.011>
- Rondinel-Oviedo, D.R. 2021. Construction and demolition waste management in developing countries: A diagnosis from 265 construction sites in the Lima metropolitan area. *Int. J. Construct. Manag.*, 6: 1-12. <https://doi.org/10.1080/15623599.2021.1874677>
- Shehadeh, A., Alshboul, O., Tatari, O., Alzubaidi, M.A. and Hamed El-Sayed Salama, A. 2022. Selection of heavy machinery for earthwork activities: A multi-objective optimization approach using a genetic algorithm. *Alex. Eng. J.*, 61(10): 7555-7569. <https://doi.org/10.1016/j.aej.2022.01.010>
- Wang, Z., Li, H. and Yang, X. 2020. Vision-based robotic system for on-site construction and demolition waste sorting and recycling. *J. Buil. Eng.*, 32: 101769. <https://doi.org/10.1016/j.jobte.2020.101769>
- Wu, J., Chang, I.S., Bina, O., Lam, K.C. and Xu, H. 2011. Strategic environmental assessment implementation in China: Five-year review and prospects. *Environ. Impact Assess. Rev.*, 31(1): 77-84. <https://doi.org/10.1016/j.eiar.2010.04.010>
- Xue, X., Zhang, R., Zhang, X., Yang, R.J. and Li, H. 2015. Environmental and social challenges for urban subway construction: An empirical study in China. *Int. J. Proj. Manag.*, 33(3): 576-588. <https://doi.org/10.1016/j.ijproman.2014.09.003>



Large Scale Cultivation and Pretreatment Optimization of Freshwater Microalgae Biomass for Bioethanol Production by Yeast Fermentation

S. Karthikeyan[†]

Department of Biotechnology, Faculty of Engineering, Karpagam Academy of Higher Education, Coimbatore-641 021, Tamil Nadu, India

[†]Corresponding author: S. Karthikeyan; karthik.gene@gmail.com

Nat. Env. & Poll. Tech.
Website: www.neptjournal.com

Received: 11-11-2021
Revised: 07-01-2022
Accepted: 08-02-2022

Key Words:

Bioethanol
Microalgae
Carbohydrate
Pretreatment
Fermentation

ABSTRACT

The rapid depletion of the world's fossil fuel reserves and global warming issues have promoted the search for sustainable alternative energy resources. In the present investigation, large-scale cultivation of naturally isolated freshwater microalgae *Asterarcys quadricellulare* strain was carried out using tertiary treated municipal wastewater as a growth medium in an open HRP pond for bioethanol production. A total of 12.091 kg of dry biomass was obtained at the end of the study. The lipid extracted carbohydrate rich spent microalgae biomass was converted to bioethanol by ethanolic fermentation. The biomass was first pre-treated with different concentrations of H₂SO₄ and HCL hydrolysis with different temperatures and reaction times. The biomass treated with a 2.0% concentration of H₂SO₄, showed maximum yields of glucose 308.38 mg.g⁻¹ at 100°C with 180 min reaction time. The hydrolysates derived from the hydrolysis of microalgae biomass were used as a substrate for fermentation by using *S. cerevisiae*. The obtained bioethanol was analyzed using HPLC and the purity of ethanol was 90%.

INTRODUCTION

The rapid depletion of the world's fossil fuel reserves increasing the energy demand. Fossil fuel is not a renewable energy source and is going to be inadequate due to the rapid growth in population, industrial development, and excessive energy consumption. Energy consumption could increase between 17% and 50% by 2040 relative to 2012 (IEA 2014). The available fossil fuel resources may get exhausted in less than the coming 50 years at the current rate of utilization (Abou-Shanab et al. 2011). The current levels of usage of coal, oil, and gas as a primary energy consumption account for 82% in 2012 and is to be expected to cause an increase in global atmospheric temperature above 3.6°C by 2100 (IEA 2014). On the other hand, fossil fuels are the largest contributor of greenhouse gases emitting more than 6 billion tons of CO₂ annually to the biosphere. For a sustainable energy future, the search for an alternative energy source is an important prerequisite that is renewable, economical, and environmentally friendly.

Biofuels are classified depending on the type of biomass used for their production. First-generation biofuels are primarily produced from edible food biomass resources corn and soybeans (Naik et al. 2010, Mohr & Raman 2013), and race with land and water usage for the production of food

(Ho et al. 2014). The second generation of biofuels can be produced from a wide collection of different feedstocks, ranging from lignocellulosic plant biomass to municipal solid wastes, which do not battle with food resources. The major problem with this generation is developing cost-effective biomass conversion technology. Biofuels produced from algae and cyanobacteria are classified as third-generation biofuels. Biofuel based on microalgae systems is an attractive source and is a high-potential fossil fuel replacement.

Microalgal biofuel systems have the potential advantages of having higher photosynthetic efficiency, the ability to synthesize and accumulate large quantities of neutral lipids, and higher biomass productivity and multiplication rate. The microalgae are also able to grow in saline/brackish water/coastal seawater, utilize nutrients from a variety of wastewaters with the added benefit of wastewater bioremediation, produce valuable by-products (proteins, polysaccharides, pigments, hydrogen and biopolymers), and grow in culture vessels successfully throughout the year as compared to other energy crops (Sangapillai & Marimuthu 2019). Selection of the suitable microalgae strain is a crucial factor in successful biofuel production from microalgae strain. The selected strain should have rapid biomass productivity, high lipid productivity, able to survive in stressful conditions, have high CO₂ sinking

capacity, have limited nutritional requirements, and provide valuable co-products.

Microalgae can grow well in domestic, municipal, and agricultural wastewater. Growing microalgae in wastewater offers several economic and environmental merits, providing the most promising approach for sustainable ways of biofuel production. Wastewater can serve as a natural growth media rich in organic nutrients such as N, P, K, and other minor nutrients for algal cultivation which would ensure sustainability in terms of nutrient removal and wastewater remediation (Mahapatra & Ramachandra 2013). Wastewater usage for microalgae cultivation eliminates competition for freshwater, saves the cost of nutrients supplement, and reduces CO₂ emissions coupled with simultaneous nutrient removal and lipid production with wastewater treatment (Chinnasamy et al. 2010). The major drawback of growing microalgae in treated wastewater is the low amount of biomass due to the depletion of essential nutrients. This can be adjusted by the supplementation of essential nutrients to the wastewater in order to enhance microalgae growth (Abou-Shanab et al. 2013). In the present study *A. quadricellulare* (KT280061) lipid-extracted biomass was used as a substrate for bioethanol production.

MATERIALS AND METHODS

Microalgae Cultivation in HRP Pond

The green microalgae, *Asterarcys quadricellulare* strain (KT280061) isolated from freshwater were used in this study. The species was characterized morphologically and phylogenetically in a previous study (Karthikeyan & Thirumarimurugan 2017). Large-scale cultivation of *A. quadricellulare* was carried out in two high-rate production ponds (HRP) of the same size in this study. The HRP pond was 8.5 m in length, 3.0 m in width, and 0.30 m in height. The ponds were built with tarpaulin sheets also for the flexibility for pond shifting after completion of work. Five liters of optimally grown *A. quadricellulare* culture was inoculated in 45 L of modified bold basal medium (BBM) in a 100 L capacity transparent plastic tank. The tank was kept under controlled laboratory conditions for 5 days to avoid initial contamination. Later, the culture was exposed to direct sunlight for 5 days. The culture grown in transparent plastic tanks was inoculated in 450 L of modified BBM medium in a small open pond having a capacity of 750 L. The culture was allowed to grow under direct sunlight for 7 days and it was used as inoculum for the HRP pond cultivation. The total inoculum was transferred to an HRP pond containing 4500 L of 60% MTTSW-containing medium. The loss of evaporation was compensated by adding tap water every day and the culture volume was maintained at a depth of 20 cm

throughout the experiment. The paddle wheels were used for mixing at a speed of 20 rpm and turned off at night. The pH of the culture medium was monitored using an automatic pH meter. The microalgae grown in a modified BBM medium served as a control. This study was conducted for 30 days.

Harvesting of Microalgae

For harvesting microalgae biomass, 500 L of grown culture pumped from the experimental pond into the storage tank was subjected to an electro-clarification process. The volume of the chamber was 100 L with one MS electrode placed at the center. The retention time inside the reaction chamber was 0.25 min. The reaction was carried out at voltage 8.0 (eV) along with continuous agitation at 100 rpm. The treated cells in the culture were stored in an inverted cone-shaped tank and allowed to settle at the bottom of the clarifier and slurry was collected for drying. The harvested thick microalgae slurry was dried directly under sunlight for 4 days on a tarpaulin sheet and the dried biomass was collected, stored in an airtight container, and stored under refrigeration conditions for further studies.

Extraction of Total Lipids from Microalgae Biomass

The total lipids were extracted according to Folch et al. (1956) method using chloroform and methanol (2:1 (v/v)). After lipid extraction, the residual spent biomass was dried at room temperature overnight. The spent dried biomass was ground into powder using a pestle and mortar and used for bioethanol production.

Optimization of Acid Pre-treatment Conditions

The spent residual algal biomass of *A. quadricellulare* was subjected to acid pretreatments to produce sugar hydrolysates for ethanol fermentation. Two different acids such as H₂SO₄ and HCL acid were used at various concentrations viz., 0.5, 1.0, 1.5 and 2.0 in the ratio of 1:10 (w/v) for pretreatments. Both acid-treated samples were subjected to different temperatures viz., 30, 40, 60, 80 and 100°C and different time durations viz., 30, 60, 90, 120 and 150 min separately in a shaking condition. After centrifugation, the sugar content in the supernatant was estimated by using the Dubois et al. (1956) method.

Extraction of Sugars from Microalgal Biomass

About 100 g of spent residual biomass powder was treated with the optimized concentration of 500 mL of 2% (v/v) sulphuric acid at 100°C for 3 h with intermittent shaking. The pretreated biomass hydrolysate was centrifuged at 10000 rpm for 15 min. The supernatant containing the sugar content was estimated using Dubois et al. (1956) method.

The sugar filtrate was adjusted to pH 4.8 and autoclaved at 121 °C for 15 min.

Bioethanol Production by *Saccharomyces cerevisiae*

Saccharomyces cerevisiae was used for ethanologenic fermentation of *A. quadricellulare* hydrolysates. The commercial yeast cells of *S. cerevisiae* were obtained from the local market and one gram of yeast was resuspended aseptically in 9 mL of warmed distilled water and left for 15 min with proper mixing. Yeast *S. cerevisiae* pre-culture was grown in YPD (1% yeast extract, 2% peptone, and 2% D-glucose) medium at pH 4.8, 30 °C for 24 h at 200 rpm. After the aerobically 10% of overnight grown pre-cultured yeast cells were transferred to the liquid fraction of pretreated algal biomass hydrolysate. The airtight fermentation flasks were kept under anaerobic conditions at 30 °C for 3 days. The fermentation mixture was distilled and the distillate was analyzed by HPLC for the presence of bioethanol.

RESULTS AND DISCUSSION

Large Scale Cultivation and Harvesting of Microalgae

Large-scale cultivation of *A. quadricellulare* was performed

in an open HRP pond system. The maximum accumulation of biomass (total dry weight) was recorded as 1.21 g.L⁻¹ on the 25th day. The average pH and TDS values were 8.2 and 1.55 ppm respectively. Electro-clarification is a new technology used for removing solid particles from water in the wastewater treatment process (Phalakornkule et al. 2009). The obtained mass-cultured *A. quadricellulare* biomass from open HRP was subjected to electro-clarification to concentrate the microalgae biomass. About 100 L of algal culture was transferred into the electro-clarification chamber from the open pond and the cells get aggregated under the optimum electrical current. The aggregated microalgae biomass was then transferred into the clarifier with 1.0 ppm of polyacrylamide. The biomass was left overnight. On the next day, a clear supernatant was discarded and the remaining 10 L of concentrated wet algal biomass was recovered from the outlet. *Nannochloropsis sp.* and *Chaetoceros calcitrans* were cultured and electro-flocculated with a harvesting efficiency of 95 and 92% respectively observed under the optimum voltage and current (Raut et al. 2017). This technique facilitates the removal of 90% water from the algal culture. The concentrated wet biomass was exposed to direct sunlight for 4 days. A total of 12.091 kg of dry biomass was obtained at the end of the study.

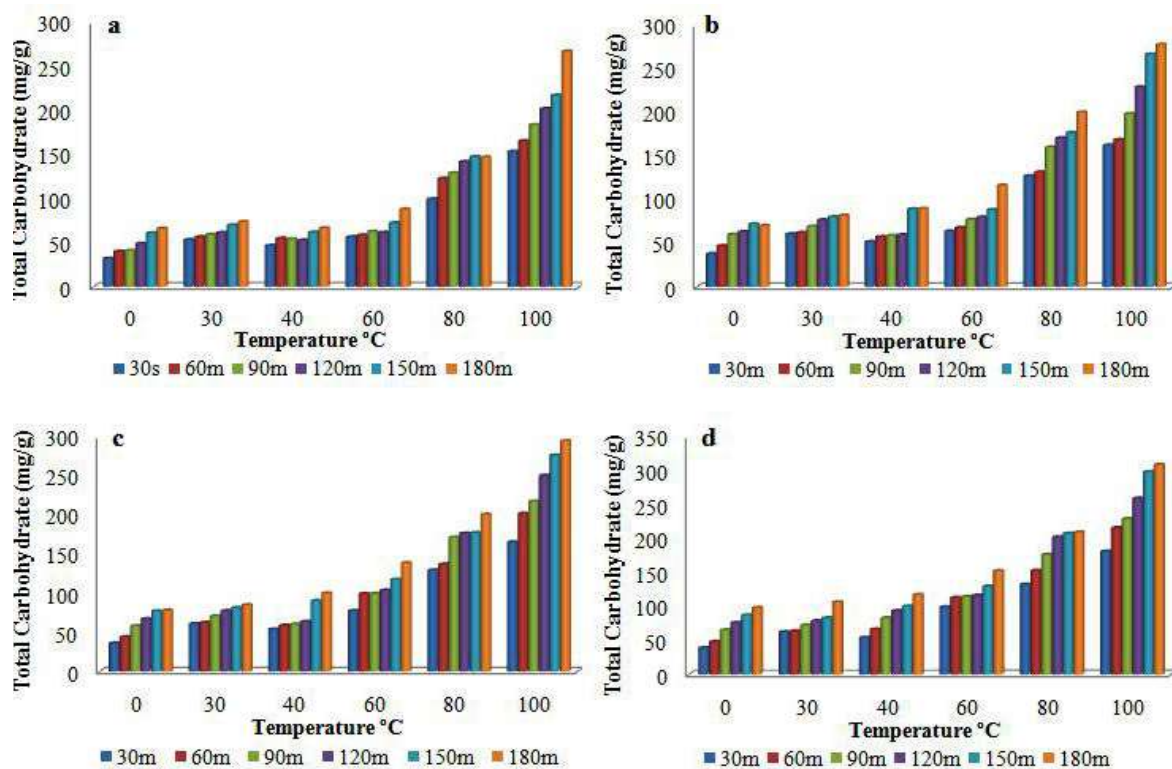


Fig. 1: Effect of Different concentrations of H₂SO₄ on carbohydrate yield (a) 0.5% H₂SO₄ (b) 1.0% H₂SO₄ (c) 1.5% H₂SO₄ (d) 2.0% H₂SO₄.

Optimization of Biomass Pretreatment

Acid hydrolysis is one of the best methods for disturbing the cell wall material and releasing the total carbohydrate content from microalgae biomass to perform fermentation. For the hydrolysis of lipid-extracted microalgae biomass, sulfuric acid (H_2SO_4) and hydrochloric (HCL) acid were used in different concentrations viz., 0.5%, 1.0%, 1.5% and 2.0%. The hydrolysis reaction for each concentration was performed at five different temperatures (30, 40, 60, 80 and 100°C) at different time intervals (30, 60, 90, 120, 150 and 180 min). The effect of H_2SO_4 and HCL acid hydrolysis on carbohydrate extraction was investigated. Among the four different concentrations of H_2SO_4 , 2.0% showed the maximum yield of glucose (308.38 mg.g⁻¹) at 100°C with 180 min reaction time (Fig. 1). For all the pretreatment time intervals increasing the acid concentration from 0.5% to 2%, accompanied with the enhancement of glucose yield. The lowest amount of glucose yield (266.7 mg/g) was obtained from 0.5% H_2SO_4 pretreated microalgae biomass at 100°C with 180 min reaction time. In the case of HCL acid, among the four different concentrations of HCL, 2.0% showed the maximum yield of glucose (288.15 mg.g⁻¹) at 100°C with 180 min reaction time (Fig. 2).

For all the pretreatment time intervals increasing the hydrochloric acid concentration from 0.5% to 2%, accompanied by the enhancement of glucose yield. The lowest amount of glucose yield (143.1 mg.g⁻¹) was obtained from 0.5% HCL pretreated microalgae biomass at 100°C with 180 min reaction time. When compared to hydrochloric acid, the 2.0% sulfuric acid pretreated lipid spent microalgae biomass showed a maximum yield of 308.38 mg/g of carbohydrate at 100°C with 180 min reaction time. Acid quantity and strength for a specified amount of microalgae biomass directly influence the hydrolysis reaction and the yield of fermentable sugar (Ho et al. 2013, Khan et al. 2017). High acid strength leads to the degradation of monomeric sugars and conversion to other side products (Miranda et al. 2012). Acid hydrolysis at high temperatures might be more productive. Previous studies reported, the temperature range of 100-200°C required for the pretreatment of microalgae biomass depending on the acid concentration and reaction time to release the monomeric fermentable sugars for fermentation (Harun & Danquah 2011, Khan et al. 2017). This optimized concentration was used for the fermentation of spent microalgae biomass.

Bioethanol Production

Saccharomyces cerevisiae is usually used in fermentations

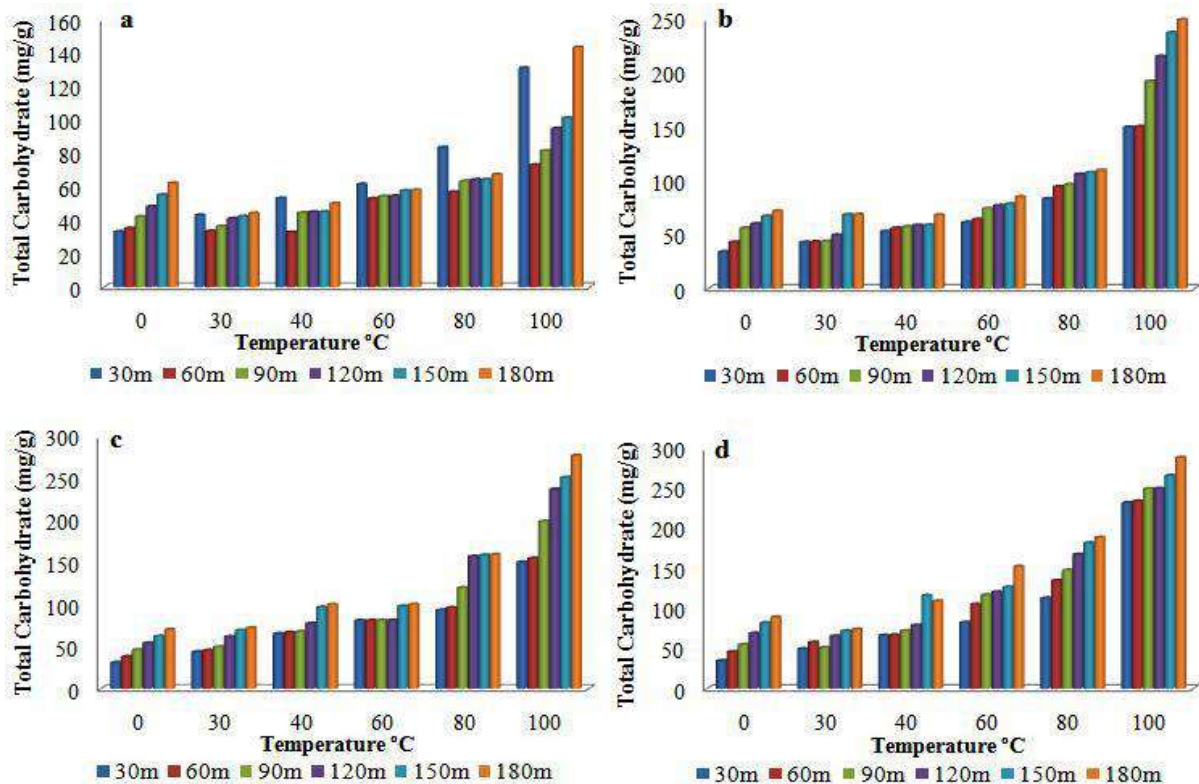


Fig. 2: Effect of different concentrations of HCL on carbohydrate yield (a) 0.5% HCL (b) 1.0% HCL (c) 1.5% HCL (d) 2.0% HCL.

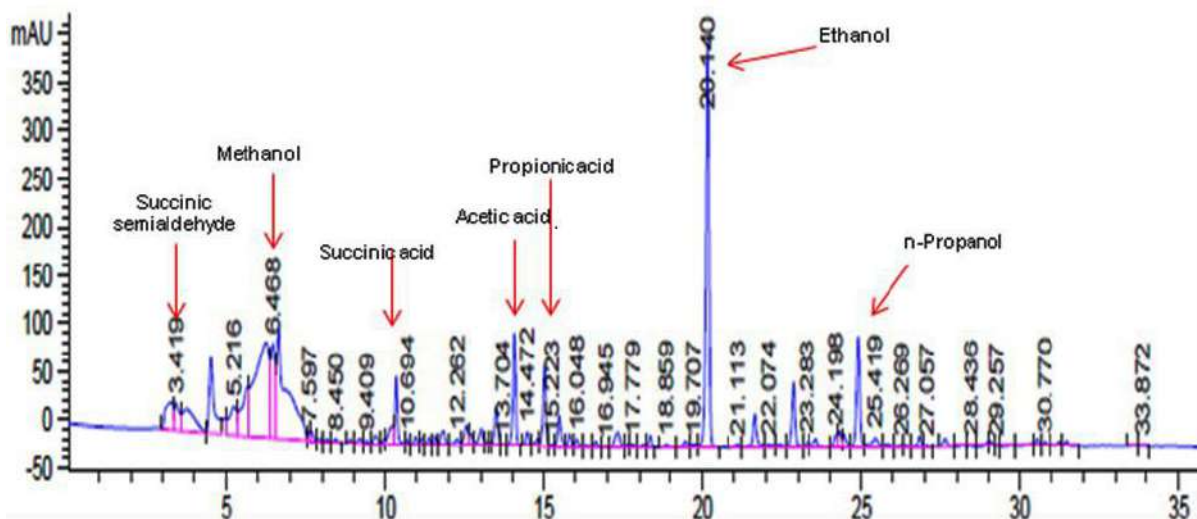


Fig. 3: HPLC analysis of bioethanol obtained from residual biomass of *Asterarcys quadricellulare*.

for the commercial production of bioethanol (Zhou et al 2011). Based on the acid-pretreated studies, for the ethanolic fermentation experiments using *S. cerevisiae*, the hydrolysates derived from the hydrolysis of 100 g of microalgae biomass at 100°C using 2.0% H₂SO₄ with reaction time 180 min was used as substrate. The utilization of acid for the disruption of cell walls was very efficient when compared to other physical methods. These acids pretreatment comparatively yield higher sugar, as well as a lesser amount of inhibitors, was produced (Miranda et al. 2012). The pre-cultured *S. cerevisiae* was inoculated with the microalgae pretreated hydrolysate and kept under anaerobic conditions at 30°C for 3 days. After fermentation, the mixture was filtered and the filtrate was distilled at 70°C. The yield of bioethanol was estimated at 0.192 g ethanol.g⁻¹ of biomass. The bioethanol was analyzed using HPLC and the purity of ethanol was 90% (Fig. 3). Choi et al. (2010) reported in general the typical ethanol fermentation yields from microalgae biomass using yeast *S. cerevisiae* do not exceed 0.3 g ethanol.g⁻¹ of dry algae biomass.

CONCLUSION

Due to increasing global oil demand and climate change, algal biofuels have gained more attention as an alternative renewable energy source. In this present study, the native microalgae *A. quadricellulare* isolated from freshwater were cultivated in an open pond system with 60% municipal tertiary treated sewage wastewater and 40% modified BBM-containing medium. The microalgae biomass was harvested by electro-clarification method and the total lipid content was extracted from the microalgae biomass. The lipid-extracted carbohydrate-rich biomass was then pretreated with

2.0% sulfuric acid and it showed a maximum yield of 308.38 mg.g⁻¹ of carbohydrate at 100°C with 180 min reaction time. The hydrolyzed biomass was fermented with *Saccharomyces cerevisiae* for bioethanol production. The yield of bioethanol obtained was estimated at 0.192 g ethanol.g⁻¹ of biomass. The cultivation of these freshwater microalgae offers new opportunities in biofuel production. In the future, the cultivation of microalgae strain KT280061 in wastewater appears to be a low-cost, eco-friendly sustainable, feasible, and scalable approach for large-scale biofuel applications.

REFERENCES

- Abou-Shanab, R. A., Hwang, J. H., Cho, Y., Min, B. and Jeon, B. H. 2011. Characterization of microalgal species isolated from freshwater bodies as a potential source for biodiesel production. *Applied Energy*, 88(10): 3300-3306.
- Abou-Shanab, R. A., Ji, M. K., Kim, H. C., Paeng, K. J. and Jeon, B. H. 2013. Microalgal species growing on piggery wastewater as a valuable candidate for nutrient removal and biodiesel production. *Journal of Environmental Management*, 115: 257-264.
- Chinnasamy, S., Bhatnagar, A., Hunt, R. W. and Das, K. C. 2010. Microalgae cultivation in a wastewater dominated by carpet mill effluents for biofuel applications. *Bioresource Technology*, 101(9): 3097-3105.
- Choi, S.P., Nguyen, M.T. and Sim, S.J. 2010. Enzymatic pretreatment of *Chlamydomonas reinhardtii* biomass for ethanol production. *Bioresource Technology*, 101(14): 5330-5336.
- Dubois, M., Gilles, K. A., Hamilton, J. K., Rebers, P. T. and Smith, F. 1956. Colorimetric method for determination of sugars and related substances. *Analytical Chemistry*, 28(3): 350-356.
- Folch, J., Lees, M and Sloane-Stanley, G. H. 1957. A simple method for the isolation and purification of total lipids from animal tissues. *Journal of Biological Chemistry*, 226 (1): 497-509.
- Harun, R. and Danquah, M. K. 2011. Influence of acid pre-treatment on microalgal biomass for bioethanol production. *Process Biochemistry*, 46(1): 304-309.

- Ho, D. P., Ngo, H. H. and Guo, W. 2014. A mini review on renewable sources for biofuel. *Bioresource Technology*, 169: 742-749.
- Ho, S. H., Huang, S. W., Chen, C. Y., Hasunuma, T., Kondo, A. and Chang, J. S. 2013. Bioethanol production using carbohydrate-rich microalgae biomass as feedstock. *Bioresource Technology*, 135: 191-198.
- IEA. World Energy Outlook 2014. Paris, France: IEA Publications; 2014.
- Karthikeyan, S. and Thirumarimurugan, M. 2017. Isolation and growth optimisation of freshwater microalgae *Asterarcys quadricellulare*. *International Journal of Materials and Product Technology*, 55(1-3): 254-271.
- Khan, M. I., Lee, M. G., Shin, J. H. and Kim, J. D. 2017. Pretreatment optimization of the biomass of *Microcystis aeruginosa* for efficient bioethanol production. *AMB Express*, 7(1): 1-9.
- Mahapatra, D. M. and Ramachandra, T. V. 2013. Algal biofuel: bountiful lipid from *Chlorococcum* sp. proliferating in municipal wastewater. *Current Science*, 105: 47-55.
- Miranda, J. R., Passarinho, P. C. and Gouveia, L. 2012. Pre-treatment optimization of *Scenedesmus obliquus* microalga for bioethanol production. *Bioresource Technology*, 104: 342-348.
- Mohr, A. and Raman, S. 2013. Lessons from first generation biofuels and implications for the sustainability appraisal of second generation biofuels. *Energy Policy*, 63: 114-122.
- Naik, S. N., Goud, V. V., Rout, P. K. and Dalai, A. K. 2010. Production of first and second generation biofuels: a comprehensive review. *Renewable and Sustainable Energy Reviews*, 14(2): 578-597.
- Phalakornkule, C., Polgumhang, S. and Tongdaung, W. 2009. Performance of an electrocoagulation process in treating direct dye: batch and continuous upflow processes. *World Academy of Science, Engineering and Technology*, 57: 277-282.
- Raut, N., Saini, D. K. and Vaidya, R. 2017. Harvesting *Chaetoceros Calcitrans* and *Nannochloropsis* sp. via electroflocculation. *American Journal of Applied Sciences*, 14(9): 852-861.
- Sangapillai, K. and Marimuthu, T. 2019. Isolation and selection of growth medium for freshwater microalgae *Asterarcys quadricellulare* for maximum biomass production. *Water Science and Technology*, 80(11): 2027-2036.
- Zhou, N., Zhang, Y., Wu, X., Gong, X. and Wang, Q. 2011. Hydrolysis of *Chlorella* biomass for fermentable sugars in the presence of HCl and MgCl₂. *Bioresource Technology*, 102(21): 10158-10161.



Stabilisation of Spent Wash by Polyhydroxybutyrate (PHB) Producing Microorganisms Isolated from Karad Region, Maharashtra

G. V. Patil*† and G. R. Pathade*

*Krishna Institute of Allied Sciences, Krishna Institute of Medical Sciences (Deemed University), Karad, Maharashtra, India

†Corresponding author: G. V. Patil; gayatri25patil.gp@gmail.com

Nat. Env. & Poll. Tech.
Website: www.neptjournal.com

Received: 07-10-2022

Revised: 01-11-2022

Accepted: 14-11-2022

Key Words:

PHB producers
Spent wash
COD
Stabilization

ABSTRACT

In recent years, there has been a significant increase in the needs of the overgrowing population. Naturally, industrial belts increased worldwide to satisfy the variety and quantity of needs. While producing the products, a huge quantity of waste is generated and added continuously to the environment, causing hazardous effects on the flora and fauna. Spent wash is one of the most important types of industrial waste since it is the liquid waste that is left over after making alcohol and it pollutes the environment. Despite effluent quality standards, untreated or partially treated sewage frequently enters water courses or soils. It is always overloaded with organic and inorganic substances. The stabilization of the effluent by microorganisms is reflected in the form of COD reduction. The present study attempted to isolate the PHB-producing organisms and use them to stabilize the spent wash.

The locally isolated, characterized, and identified 11 PHB-producing microorganisms from the Karad region of Maharashtra were used to stabilize spent wash. They include *Candida orthopsilosis*, *Bacillus subtilis*, *Bacillus cereus*, *Bacillus megaterium*, *Klebsiella grimontii*, *Citrobacter freundii*, and members of *Staphylococcus* and *Rhodococcus*. All potential organisms were reported to stabilize the spent wash. The degree of stabilization was measured in terms of the percent reduction of COD and BOD. The % reduction was reported at 95.31% and 81.39% of COD and BOD, respectively, by *Klebsiella grimontii*, followed by 92.18% and 80.46% reductions of COD and BOD, respectively, by *Staphylococcus*. These organisms are promising in the treatment of spent wash.

INTRODUCTION

Interest in low-carbon and more sustainable energy production has grown in several nations worldwide due to worries about climate change, energy security, and the depletion of fossil fuels (Chooyok et al. 2013). Bioenergy is a carbon-neutral, renewable energy source that may be used to create any fuel. The need for sustainable and renewable biofuels, particularly bioethanol, is increasing globally, and ethanol distillery businesses are expanding quickly to meet this demand (David et al. 2015).

Molasses waste wash is the term for the high volume of strong wastewater produced by the ethanol distillery industry. The world's water quality and soil quality are seriously threatened by the ever-increasing output of molasses waste wash, which produces undesired residual liquid waste (Mohana et al. 2009). Distillery waste wash is a caramelized and recalcitrant waste with extremely high COD, BOD, SS, inorganic solids, color, and low pH. Melanoidins, which make up 2% of the total wasted wash by mass, are primarily responsible for the spent wash's deep, dark brown color (Naik

et al. 2010). For melanoidin, including distillery effluent, color removal is difficult. Typically, 10-15 L of wastewater is produced for every liter of alcohol (Biradar 2003).

If distillery waste is disposed of improperly, it poses a major risk to the nearby land and water bodies because it blocks sunlight from penetrating the aquatic environment, depleting the dissolved oxygen concentration. This happened due to the melanoidin pigment, a dark brown pigment produced by the Maillard reaction between sugar and amino compounds (Pandey et al. 2003, Satyawali & Balkrishnan 2007, Khandegar & Saroha 2012). Investigations into how to decolorize it physically or chemically were unsuccessful. Utilizing microbial activity to decolorize the spent wash has received more attention recently. Environmentalists and academics face challenges in distillery waste wash's economical and environmentally responsible management. Distillery waste wash can be treated using various physical, chemical, and biological techniques, particularly for decolorization and COD removal. The method most frequently used to treat distillery waste wash is bio-methanation, followed by aerobic treatment (Yadav 2012). Chemical oxygen demand

(COD) and biological oxygen demand are reduced by aerobic treatment by up to 50-70%. (Shruti et al. 2013). Since biological treatment with bacterial cultures has a reduced operating cost, it might be a useful alternative to reduce COD in wastewater. In the current investigation, isolated PHB producers were utilized locally to reduce COD and BOD to stabilize the organic matter and make it easier to dispose of without endangering the local flora and fauna.

MATERIALS AND METHODS

Physicochemical Characterization of Distillery Spent Wash Sample

The effluent was analyzed in triplicate, before and after the addition of potential organisms, for its color, odor, pH, Chemical Oxygen Demand (COD) by Dichromate reflux method, and Biochemical Oxygen Demand (BOD) by Winkler's modified Alkali-Azide method (Greenberg et al. 1998).

Use of Potential Isolates for Stabilization of Effluent

Out of 75 locally isolated microorganisms with PHB production ability, 11 isolates with excellent PHB production potential (Table 1) were identified and used to test their abilities to stabilize the spent wash in terms of reduction in COD and BOD.

The COD Determination

The extent of organic matter degradation was determined mainly by the reduction in COD values. To determine the COD, 100 mL of mineral salt medium supplemented with 10% spent wash was inoculated with 1 % inoculum containing 1×10^8 CFU.mL⁻¹ potential PHB producers separately and incubated for 96 h at 30°C. After incubation, it was diluted

Table 1: Potential PHB-producing microorganisms.

Sr. No.	Isolate No.	Isolate identified as	Accession Number
1.	1	<i>Candida orthopsilosis</i>	OP393929
2.	10	<i>Bacillus subtilis</i>	OP415431
3.	20	<i>Bacillus cereus</i>	OP430573
4.	24	Member of <i>Bacillus</i>	-
5.	33	Member of <i>Rhodococcus</i>	-
6.	37	<i>Klebsiella grimontii</i>	OP458827
7.	38	Member of <i>Bacillus</i>	-
8.	41	<i>Citrobacter freundii</i>	OP434597
9.	45	Member of <i>Staphylococcus</i>	-
10.	46	Member of <i>Staphylococcus</i>	-
11.	72	<i>Bacillus megaterium</i>	OP435363

to 1:1500, and samples were used to determine COD values by the dichromate reflux method (Hu & Grasso 2005). These values were then used to calculate the % reduction of COD, which directly revealed the extent of stabilization of effluent. The controls were without inoculum added.

The BOD Determination

The reduction in BOD values determined the extent of organic matter degradation. To determine the BOD, 100 mL of mineral salt medium supplemented with 10% spent wash was inoculated with 1 % inoculum containing 1×10^8 CFU.mL⁻¹ potential PHB producers separately and incubated for 96 h. After incubation, it was diluted, and samples were used to determine BOD values by modifying Winkler's alkali azide method (Sawyer & McCarty 1978, Greenberg et al. 1998) calculates the amount of oxygen absorbed by bacteria during organic matter breakdown. Five days at 20°C are used to measure the change in DO concentration. The BOD is determined by subtracting the starting DO from the final DO. These values were then used to calculate the % reduction of BOD, which directly revealed the extent of stabilization of effluent. The controls were without inoculums added.

RESULTS AND DISCUSSION

Physicochemical analysis of raw spent wash (Table 2) reflects its heavy organic load in terms of high values of COD and BOD. The color of the spent wash was observed as deep dark brown with an unpleasant odor and acidic pH.

The high values of COD and BOD in raw spent wash warn of the danger caused to the environment and make more attention to proper treatment to stabilize the organic load. This can be achieved effectively by the use of microbial treatment. In the present study, 11 potential PHB producers attempted to degrade the organic contents and reduce the COD and BOD.

Use of Potential Isolates for Stabilization of Spent Wash

The results of stabilization of spent wash in terms of COD value and % reduction are summarized in Table 3;

Table 2: Physicochemical analysis of spent wash sample.

Sr. No.	Parameter	Results
1.	Color	Deep dark brown
2.	Odor	Unpleasant burn
3.	pH	5.5
4.	COD	128000 mg.L ⁻¹
5.	BOD	43000 mg.L ⁻¹

Table 3: COD value and % COD reduction of effluent after treatment with potential isolates. (Initial COD at 0 hr was 1,28,000 mg.L⁻¹).

Sr.No.	Isolate No.	COD value (after h)				% COD reduction (after h)				
		24	48	72	96	24	48	72	96	120
1.	1	1,20,000	90,000	48,000	18,000	6.25	29.68	62.5	85.93	86.98
2.	10	36,000	36,000	18,000	12,000	71.87	71.87	85.93	90.62	92.12
3.	20	60,000	30,000	18,000	11,000	53.12	76.56	85.93	91.40	93.20
4.	24	1,20,000	18,000	18,000	18,000	6.25	85.93	85.93	85.93	87.43
5.	33	96,000	24,000	12,000	12,000	25	81.25	90.62	90.62	92.62
6.	37	24,000	18,000	12,000	6,000	81.25	85.93	90.62	95.31	97.31
7.	38	90,000	84,000	36,000	18,000	29.68	34.37	71.87	85.93	86.98
8.	41	66,000	36,000	24,000	12,000	48.43	71.87	81.25	90.62	92.50
9.	45	66,000	60,000	42,000	18,000	48.43	53.12	67.18	85.93	87.20
10.	46	1,20,000	60,000	24,000	10,000	6.250	53.12	81.25	92.18	93.20
11.	72	60,000	36,000	24,000	18,000	53.12	71.87	81.25	85.93	87.10

From Table 3, it can be noticed that COD values decreased as the time of reaction increased. It is evident from the table that the % COD reduction for the isolate was maximum after 96 hrs. of incubation, while after 120 hrs. of incubation, the % COD reduction was meagerly increased up to 1-2%, and hence 96 hrs. of incubation was taken as values as after the period of reduction. Hence COD values due to remaining isolates were determined and considered only up to 96 hrs. The range of COD values at the end of 96 hrs was recorded between 18000 to 6000. When these values were compared with values of COD from the original sample, i.e., 128000, a tremendous decrease in COD was noticed. The range of % reduction in COD for all these 12 isolates was found to be 84.37% to 95.31%, which indicates the excellent efficiency of isolates for stabilization of spent wash in terms of % COD reduction. A maximum % reduction of COD, i.e., 95.31, was reported using isolate 37, identified as *Klebsiella grimontii*. As Mohana et al. (2009) noted, the considerable potential for pollution makes the release of untreated wasted wash effluent into the environment hazardous to the ecosystem. Because of this, the stability of spent wash that shows a decrease in COD is considerably more important.

Ramachandra (1993) noticed COD reduction by *Pseudomonas stutzeri*, *P. acidovorans*, and *Enterbacter* sp. *Alcaligenes eutrophus* growing in the spent wash. Kumar et al. (1997) reported 41% and 39% COD reduction by LA-1 and D-2 isolates under optimized conditions in eight days. Sharma et al. (2000) measured 60 % COD reduction by several lactic acid bacteria from anaerobically digested molasses spent wash (ADMSW). Sudarshan et al. (2012) utilized *Azotobacter vinelandii* ATCC 12837 and ATCC 13705 to reduce COD levels (1100 mg.L⁻¹) of DSW to 200 mg.L⁻¹ after fermentation was completed. Thus they successfully reduced the COD value to the permitted level.

In the present study, we have also achieved these two purposes of obtaining higher PHB quantity, and maximum COD reduction in distillery spent wash. Thus present results are on the same track of research giving suitable solutions for disposing of spent wash after proper treatment and sustaining the environment. The results of the stabilization of spent wash in terms of BOD value and % reduction are summarized in Table 4.

From Table 4, it is observed that values of BOD were recorded between 14200 to 8000. When these values were compared with values of BOD from the original sample, i.e., 43000, a large extent decrease in BOD was noticed. The range of % reduction in BOD for all these 11 isolates was found to be 66.98% to 81.39%, which indicated the excellent efficiency of isolates for stabilization of spent wash in terms of % BOD reduction. The maximum % reduction of BOD, i.e. 81.39 was reported using isolate number 37, identified as *Klebsiella grimontii* (Table 5).

Table 4: BOD value and % BOD reduction of effluent after treatment with potential isolates BOD value at 0 hrs was 43000 mg.L⁻¹.

Sr.No.	Isolate Number	BOD Value mg.L ⁻¹ after 5 days	% Reduction of BOD
1.	1	11400	73.48
2.	10	9200	78.60
3.	20	14200	66.98
4.	24	10200	76.28
5.	33	9200	78.60
6.	37	8000	81.39
7.	38	11400	73.48
8.	41	8800	79.53
9.	45	13800	67.90
10.	46	8400	80.46
11.	72	12800	70.23

Table 5: Physicochemical analysis of spent wash treated with *Klebsiella grimontii*.

Sr. No.	Parameter	Results
1.	Color	Faint brown
2	Odor	Unpleasant burn
3.	pH	5.7
4.	COD reduction	95.31%
5.	BOD reduction	81.39%

The pioneering research on bacterial wasted wash decolorization was carried out by (Kumar et al. 1997). They found that under ideal conditions, two aerobic bacterial isolates, LA-1 and D-2, achieved the highest levels of decolorization (36.5% and 32.5%) and COD reduction (41% and 39%) in just eight days. Ramachandra (1993) named four bacterial species as *Pseudomonas stutzeri*, *P. acidovorans*, *Enterbacter* sp., and *Alcaligenes eutrophus*, which were primarily found thriving in the wasted wash. They saw a significant reduction in BOD and COD and a decolorization of up to 60%. Sharma et al. (2000) isolated numerous lactic acid bacteria (ADMSW) from anaerobically digested molasses wasted wash.

Some isolates lowered COD by 60% and decolorized ADMSW (25% v/v) by 70%. The viability of utilizing *Pseudomonas putida* for decolorizing used wash was discussed by Ghosh et al. (2003). The organism exhibited the capacity to extracellularly transform glucose into gluconic acid and hydrogen peroxide using glucose oxidase. The hydrogen peroxide created by this enzymatic oxidation removed the color from the used wash by oxidizing melanoidins. According to Sirianuntapiboon et al. (1988), Mycelia sterile D90 was the most effective strain, decolorizing molasses pigment by nearly 93% after eight days. When nutrients such as glucose (2.5%), NaNO₃ (0.2%), KH₂PO₄ (0.1%), and MgSO₄.7H₂O (0.05%) were added to molasses wastewater, this strain also induced a BOD drop of nearly 80%. However, when these nutrients were absent, the decolorization yield was only 17.5%.

Our present results of COD reduction are on the same line of research as that of Kumar et al. (1997), Ramachandra (1993), Sharma et al. (2000) and Ghosh et al. (2003). On the other hand, the results of BOD reduction are similar to the results of Sirianuntapiboon et al. (1988).

A high % reduction in COD and BOD reflects these isolates' abilities to degrade the effluent's organic content. Thus converting the original hazardous effluent, such as a form of effluent that is safe to discharge into public water bodies by a suitable division nearby Karad city and safeguarding flora and fauna of the ecosystem.

CONCLUSIONS

The isolated 11 PHB producers efficiently degrade the organic content and stabilize the spent wash. The *Klebsiella grimontii* has the potential to stabilize the spent wash to a maximum degree by achieving a 95.31% reduction in COD and an 81.39% reduction in BOD. Thus biological treatment using *Klebsiella grimontii* culture may be a good alternative to stabilize the spent wash to a good extent.

ACKNOWLEDGMENT

We are very much thankful to the management of the Krishna Institute for inspiration and for providing all necessary laboratory facilities for the present research work

REFERENCES

- Biradar, A. 2003. Physico-chemical and Biological Methods for the Treatment of Post Anaerobic Distillery Spent Wash. Ph.D. thesis. Centre for Environmental Science and Engineering Indian Institute of Technology, Mumbai.
- Choyok, P., Pumijumng, N. and Ussawarujikulchai, A. 2013. The water footprint assessment of ethanol production from molasses in Kanchanaburi and Suphanburi province of Thailand. APCBEE Procedia, 5: 283-287.
- David, C., Arivazhagan, M. and Tuvakara, F. 2015. Decolorization of distillery spent wash effluent by electrooxidation (EC and EF) and Fenton processes: a comparative study. Ecotoxicol. Environ. Safety, 121: 142-148.
- Ghosh, M., Ganguli, A. and Tripathi, A.K. 2003. Treatment of anaerobically digested distillery spent wash in a two-stage bioreactor using *Pseudomonas putida* and *Aeromonas* sp. Process Biochem., 7: 857-862.
- Greenberg, A.E., Eaton, A.D., Clesceri, L.S. and Franson, M.A.H. (eds). 1998. Standard Methods for the Examination of Water and Wastewater. Twentieth Edition. American Public Health Association (APHA), American water works association (AWWA), Water Environment Federation (WEF), Washington, DC.
- Hu, Z. and Grasso, D. 2005. Water analysis: Chemical oxygen demand. Encycl. Anal. Sci., 14: 325-330.
- Khandegar, V. and Saroha, A.K. 2012. Electrochemical treatment of distillery spent wash using aluminum and iron electrodes. Chin. J. Chem. Eng., 20(3): 439-443.
- Kumar, V., Wati, L., Nigam, P., Banat, I.M., McMullan, G., Singh, D. and Marchant, R. 1997. Microbial decolorization and bioremediation of anaerobically digested molasses spent wash effluent by aerobic bacterial cultures. Microbios, 89: 81-90.
- Mohana, S., Acharya, B.K. and Madamwar, D. 2009. Distillery spent wash: Treatment technologies and potential applications. J. Hazard. Mater., 163: 12-22.
- Naik, N., Jagadeesh, K.S. and Noolvi, M.N. 2010. Enhanced degradation of melanoidin and caramel in bio methanated distillery spent wash by microorganisms isolated from mangroves. Iran. J. Energy. Environ., 14: 47-35.
- Pandey, R.A., Malhotra, S., Tankhiwale, R. and Pande, S. 2003. Treatment of biologically treated distillery effluent: A case study. J. Clean Energy Technol., 14: 133.
- Ramachandra, M. 1993. Development of Indigenous Technology (Microbial Strains) for Removing Sulfur Compounds and Color from Distillery Effluent. Annual Progress Report, Industrial Toxicology Research Centre, Lucknow.

- Satyawali, Y. and Balakrishnan, M. 2007. Removal of color from bio-methanated distillery spent wash by treatment with activated carbons. *Bioresour. Technol.*, 98: 2629-2635.
- Sawyer, C.N. and McCarty, P.L. 1978. *Chemistry for Environmental Engineering*. Third Edition. McGraw-Hill, NY.
- Sharma, N., Wati, L. and Singh, D. 2000. Bioremediation of Anaerobically Digested Molasses Spent Wash By Lactic Acid Bacteria. Abstract Presented in AMI Conference, Birla Institute of Scientific Research, Jaipur, November, 25-27, pp. 175.
- Shruti, M., Krishna, B., Usha, M. and Murthy, N. 2013. Colour removal from bio-digester effluent by electrochemical treatment with and without fenton reagent. *Int. J. Curr, Eng. Technol.*, 6: 115-117.
- Sirianuntapiboon, S., Somachai, P., Ohmomo, S and Atthasampunna, P. 1988. Screening of filamentous fungi having the ability to decolorize molasses pigments. *Agric. Bio. Chem.*, 52: 387-392.
- Sudarshan, S., Lakhawat, S., Amrendra, N., Pathak, M.V., Kulkarni, K. and Garikipati, V. 2012. Production of poly D-hydroxy butyrate from distillery spent wash using mutant *Azotobacter vinelandii*. *Int. J. Adv. Biotechnol. Res.*, 3(2): 596-604.
- Yadav, S. 2012. Degradation and decolorization of post-methanated distillery effluent in biphasic treatment system of bacteria and wetland plant for environmental safety. Ph.D. thesis. School of Life Science, Pandit Ravi Shankar Shukla University.



A Review of Research on Materials for the Separation of Oil/water Mixtures

Xu Meng^{*(**)} (***) (****), Chengzhi Song^{**}, Junfeng Yan^{**}, Yanyan Dong^{**}, Aiqin Hou^{*}, Kongliang Xie^{*} and Liping Liang^{*(**)} †

*College of Chemistry, Chemical Engineering and Biotechnology, Donghua University, Shanghai 201620, China

**College of Textile and Garment, College of Life Science, Shaoxing University, Shaoxing, 312000, China

***Key Laboratory of Clean Dyeing and Finishing Technology of Zhejiang Province, Shaoxing University, Shaoxing, 312000, China

****Zhejiang Sub-center of National Carbon Fiber Engineering Technology Research Center, Shaoxing, 312000, China

†Corresponding author: Liping Liang; liangliping0702@163.com

Nat. Env. & Poll. Tech.
Website: www.neptjournal.com

Received: 04-12-2022

Revised: 23-01-2023

Accepted: 01-02-2023

Key Words:

Oil/water separation

Textile materials

Metal mesh

Environmental protection

ABSTRACT

Water pollution caused by oil spills at sea and industrial and daily wastewater discharges are causing serious damage to the ecological environment, not only in terms of economic losses but also in terms of human health and survival, a problem that needs to be addressed urgently. Oil/water separation is a global challenge, and while these problems are frequent, various oil/water separation strategies have been extensively investigated in recent years. The efficiency of the materials prepared is a key factor, as are the environmental friendliness and low cost of the methods and raw materials used in the experiments. This work reviews methods and materials applied in oil/water separation in recent years, including natural textile materials, metal meshes, synthetic membranes, particulate adsorbent materials, foams, sponges, aerogels, smart controllable special wettability separation materials.

INTRODUCTION

With rapid industrialization, oil spills in the food (Zhong et al. 2003), metal manufacturing (Rubio et al. 2002), petroleum (Pendashteh et al. 2011), pharmaceutical (Yu et al. 2017), weaving (Cheryan & Rajagopalan 1998) and other industries have led to mixed oil and water pollution of water resources (Wang et al. 2015). In addition to offshore oil spills, all areas of human life are subject to varying degrees of oil and water pollution. In addition to offshore oil spills, all areas of human life are subject to varying degrees of oil and water pollution. Oily wastewater has many compounds that are difficult to decompose, which causes serious damage to the ecological environment and endangers human health. It causes serious damage to the ecological environment and endangers the economy and health of human beings, and water pollution treatment is a global concern (Borges et al. 2016, Kang et al. 2020). Many studies have been carried out in recent years on efficient oil/water separation materials, with adsorption and filtration being the main means of treating oil/water mixtures (Dunderdale et al. 2015).

In addition to separation efficiency, environmental and cost issues and good recycling are key challenges for oil/water separation materials (Wang et al. 2009). This work describes

the various methods and materials used in recent years for oil/water separation, including natural textile fibers (Lahiri et al. 2019), synthetic membranes (Lin et al. 2017), adsorbent particles or powders (Wang et al. 2018b), aerogels (Zhou et al. 2018a), sponges, and foams (Feng & Yao 2018, Zhou et al. 2018b), filtering metal meshes and intelligently controlled wettability separation specialties. The various modification methods and oil/water separation materials have advantages, disadvantages, and limitations. Adsorbent substances are commonly used for their simplicity, high absorption rate, recyclability, and environmental friendliness (Lü et al. 2016). Commercial sponges can be used as substrates in the oil/water separation field due to their low price, high specific surface area, low density, and high porosity. Still, they can't be used directly for oil/water separation (Ke et al. 2014). High lipophilicity can be achieved by roughly structuring the sponge surface or modifying it with low surface energy materials (Chen et al. 2008). Aerogels have the advantage of ultra-low density and high specific surface area for oil absorption and are commonly used to treat oil slick materials (Reynolds et al. 2001). Natural cellulose-based materials are widely developed due to their comprehensive source, good biocompatibility, and low cost. Fabric surfaces generally modify them to reduce free energy and construct rough

structures (Gui et al. 2013, Zhu et al. 2009). Finally, the outlook for the application of these materials is presented.

OIL/WATER SEPARATION MATERIALS

Textile Materials

Natural textile materials can be used as good substrates for oil/water separation due to their low cost, high yield, stability, non-toxic, and environmentally friendly nature when handled properly (Mao et al. 2023, Xue et al. 2014). It is well known that the hydroxyl groups on the surface of natural fiber fabrics make them adsorb both oil and water, and they will not be used directly in the field of oil/water separation. The oleophilic and hydrophobic or hydrophilic properties are generally achieved by modifying the fabric's surface with chemicals to reduce the surface free energy and create a rough surface structure (Zhao et al. 2021). Various synthetic fibers are also attracting increasing interest (Gao et al. 2019b, Peng et al. 2020). These fabrics have good oil absorption properties and oil retention capacity under external forces and have promising applications in oil spill remediation (Lin et al. 2012).

Su et al. (2018) reported a magnetic field manipulation method for preparing bifunctional superhydrophobic

textiles with asymmetric rolling/fixed states. Iron oxide (F-Fe₃O₄) nanoparticles were modified by fluorosilanes and fabricated along the magnetic direction in the presence of polydimethylsiloxane (PDMS), forming surfaces with different levels and roughness on both sides of the fabric. The prepared textiles have superhydrophobicity, magnetic responsiveness, good chemical stability, adjustable surface morphology, and controllable adhesion. A schematic diagram of the fabrication of a bifunctional superhydrophobic fabric is shown in Fig. 1. Han et al. (2018) prepared a superhydrophobic cotton fabric by depositing polydimethylsiloxane (PDMS) coated SiO₂ nanoparticles on the surface of the cotton fabric using a hot gas deposition. It was found that the samples could only repel surfactant solutions and pure water when the PDMS/SiO₂ content deposited on the surface was further increased and the nanoparticles completely covered the surface gaps. The separation efficiency was stable in solutions with poor chemical conditions. Zhou et al. (2017) introduced phytate metal complexes on the fabric's surface to generate a rough hierarchical structure, followed by PDMS modification. A superhydrophobic cotton fabric was prepared. It has excellent resistance to UV radiation, high temperature, organic solvent impregnation, and good mechanical wear properties. The superhydrophobic/superhydrophilic fabric successfully separated oil/water

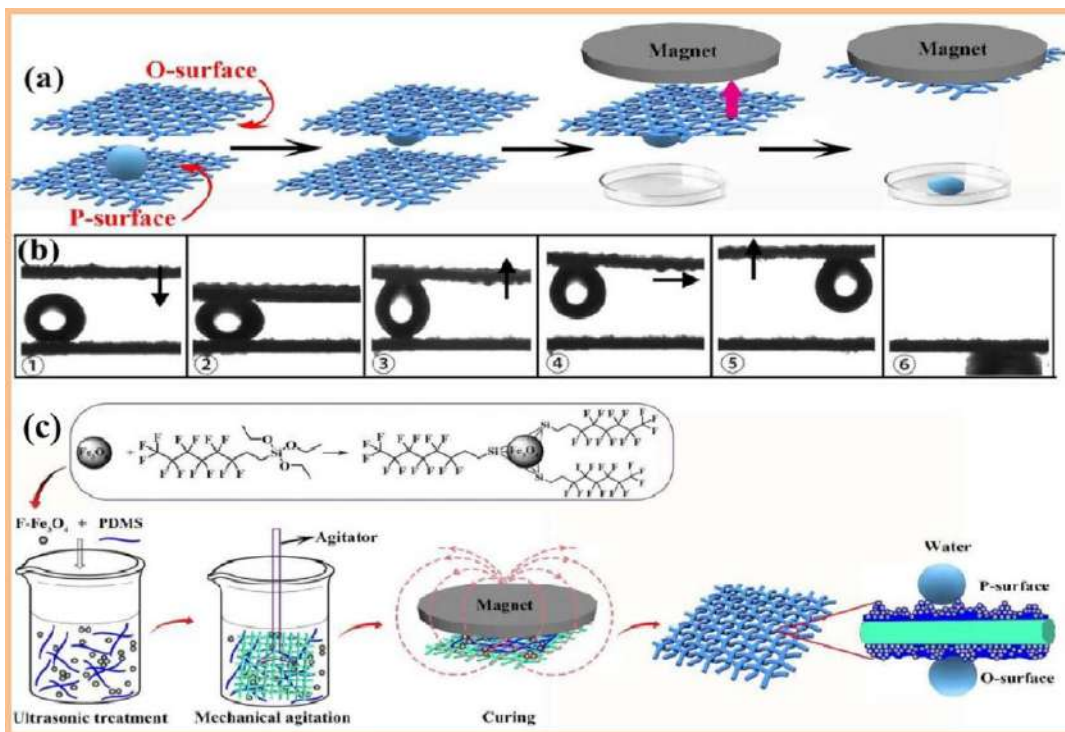


Fig. 1: (a) Schematic process and (b) detailed process of water droplet transportation, (c) schematic illustration for fabricating dual-functional superhydrophobic textile with roll-down/pinned states.

mixtures with a separation efficiency of 99.5 %. These super-resistant fabrics with phytate-metal complexes and polydimethylsiloxane (PDMS) are environmentally friendly, cost-effective, sustainable, and easily scalable.

The sol-gel method is the hydrolytic polymerization or hydrolytic condensation of raw materials in solution into porous spatially structured solids in a certain way (Antonelli & Ying 1995). Currently, nanoparticles such as silica are mainly used to build superhydrophobic surfaces on the surface of substrates, and this method is simple, effective, and product-controlled. Xie et al. (2019) used tetraethyl orthosilicate and hexadecyltrimethoxysilane, and cetyltrimethoxysilane to chemically modify cellulose membranes to prepare sustainable superhydrophobic cellulose membrane, which is a simple and efficient method that is environmentally friendly and durable, with an oil/water separation efficiency of up to 98 % even under harsh conditions. A schematic diagram of the separation mechanism, the separation efficiency of various oil/water

mixtures, and the SEM diagram are shown in Fig. 2.

Wang et al. (2016) prepared silylated cellulose using the sol-gel reaction of biodegradable microcrystalline cellulose and hexadecyltrimethoxysilane. The separation efficiency reached 99.93%. The modified silylated cellulose is a porous structure material, and its special hydrophobic properties give it good separation performance. Fig. 3 (a) shows the experimental silylated synthesis route.

Previous superhydrophobic cotton fabrics were not robust enough, so Cheng et al. (2019) prepared durable superhydrophobic cotton fabrics by a one-step solvothermal method. They were resistant to abrasion and sonication and maintained high efficiency in hydrophobic separation after treatment with high-temperature liquid nitrogen. Unlike other methods that use toxic fluorinated reagents to reduce surface-free energy, the team used divinylbenzene to form surface deposits on the cotton fabric under thermal polymerization of the solution, which is non-toxic and

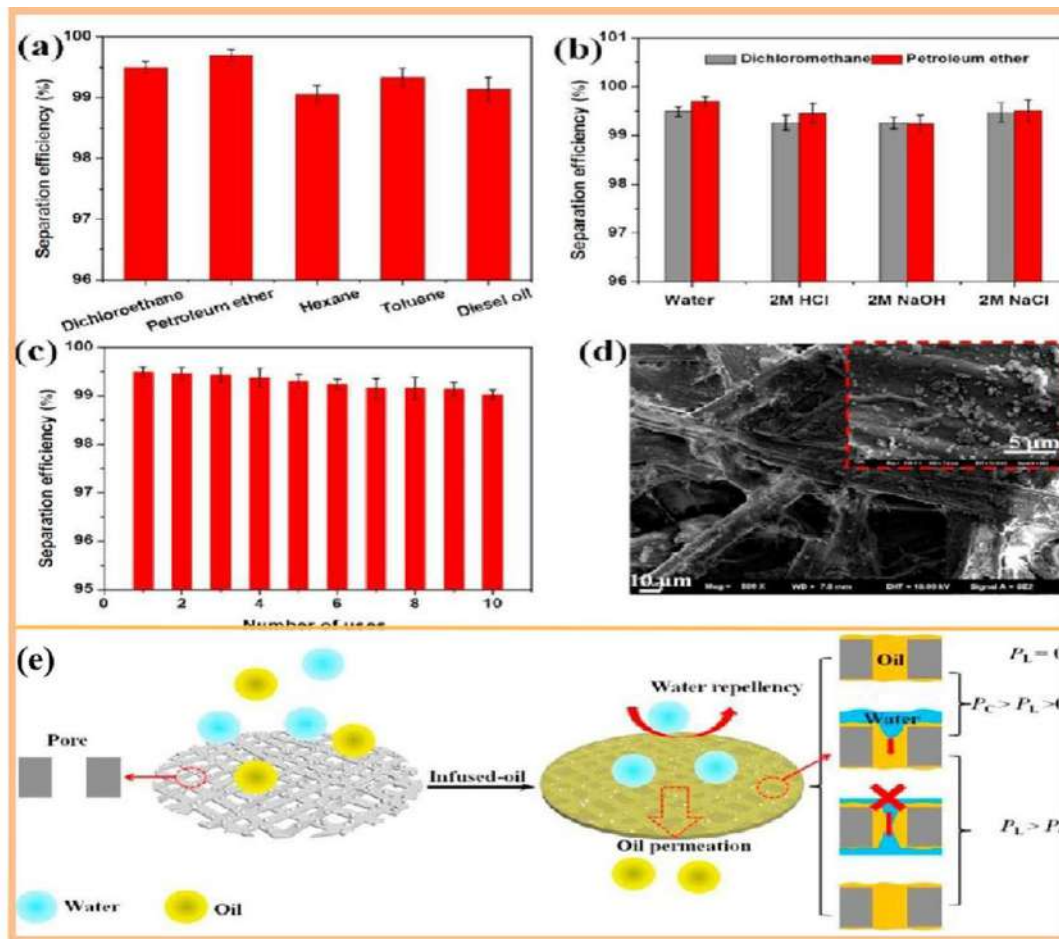


Fig. 2: (a) Separation efficiency for various oil/water mixtures, (b) and oils/corrosive liquids (2 M of acid, alkali, and salt solution), (c) separation efficiency for recycled separation, (d) SEM images of SOCM after 10 recycles, (e) schematic diagram of separation mechanism of SOCM.

reduces production costs, with separation efficiencies of up to 98 %. Fig. 3 (b) shows a schematic diagram of the one-step solvent and thermal polymerization method for preparing PDVB@CF.

Hu et al. (2020) synthesized an asymmetric wettability and Janus composite fabric by combining surface hydrophobic, oxidative, and chemical bath deposition treatments. The asymmetric wettability means that the composite fabric is partly silanized to obtain the hydrophobic side and partly oxidized at the interface to obtain the hydrophilic side. Based on this, the material can transport water in one direction and is more permeable than untreated fabrics. The method also combines gravity-driven effects to improve oil/water separation, which can be applied to other substrates and has potential applications. Fig. 3 (c) shows a schematic representation of the preparation process of the composite fabric. The process includes surface hydrophobization, oxidation treatment, and chemical bath deposition. Zhang et al. (2016) prepared a superhydrophobic and superoleophilic fabric by forming a certain roughness on the surface of the polyester fabric through the etching effect of alkali on the fibers and then dipping it in a mixture of intrinsic microporous polymer (PIM-1) and fluorinated alkyl silane (PTES) to reduce the surface free energy.

The main route to self-cleaning oil/water-separating cotton fabrics is using TiO_2 and its nanocomposites, which can achieve self-cleaning by decomposing pollutants due to their photocatalytic activity and hydrophilicity after light induction. The materials are inexpensive, environmentally friendly, and efficient (Montazer et al. 2011, Tung & Daoud 2013). Shaheen et al. (2019) used a sol-gel method to combine and condense titanium dioxide nanosol and silica nanosol on the surface of cotton fabrics. Unlike the traditional immobilized particle method, they used in situ deposition to improve the durability of the modified fabrics and combined with the photocatalytic effect of TiO_2 to produce superhydrophobic fabrics with certain self-cleaning ability, anti-bacterial and UV protection, and also have the prospect of mass production. Fig. 3 (d) shows a schematic diagram of the in-situ preparation of nanosol on cotton fabric and its surface modification. Yang et al. (2018a) deposited silica nanoparticles encapsulated by polydimethylsiloxane on the surface of the non-woven fabric by impregnation vapor phase deposition to obtain hydrophobic cotton samples that remained stable under harsh chemical conditions such as acidic, alkaline, and NaCl solutions.

Layer-by-layer is a top-down method for preparing environmentally friendly, inexpensive, multifunctional solid coatings. It allows control of the thickness and shape of the coating compared to other methods (Li et al. 2014).

The driving forces (Borges & Mano 2014) for layer-by-layer assembly include electrostatic interactions (Decher & Hong 1991), hydrogen bonding (Kim et al. 2008), and coordination (Wang et al. 2012). Yang et al. (2017) prepared superhydrophobic paper by assembling and depositing cationic starch and sodium alginate on the paper surface and silylating the surface with non-fluorosilane and trichloromethylsilane. They showed excellent resistance to moisture, self-cleaning ability, and higher tensile strength compared to the original paper.

Joung & Buie (2015) used electrostatic self-assembly techniques to deposit silica nanoparticles in a homogeneous dispersion on the surface of polyester fabrics to obtain a superhydrophobic surface by this rapid modification. In their previous work (Xu et al. 2013), superhydrophobic surfaces were also prepared using electrophoretic deposition (EPD) combined with polydimethylsiloxane (PDMS) modified SiO_2 nanoparticles (PDMS- SiO_2), which is not only fast, but can be controlled by electric field and time during the experimental reaction to control the thickness and shape of the coating, largely improving the durability of the modified fabric, and the combination of hybrid techniques defeats the combination of hybrid techniques eliminates the problem of not being able to control the deposition thickness through electrophoretic deposition methods.

Cellulose-based film materials can be used as candidate substrates for achieving superhydrophobic and superoleophilic surfaces by impregnation, spin coating, or spraying. Kollarigowda et al. (2017) prepared an oil/water separation material using cellulose membranes (CM) as a substrate through a simple chemical modification. Environmentally friendly anti-pollution membranes for oil/water separation, litter particle filtration, and thiol odor barrier were prepared by modifying the superhydrophilic nature of CM with silane and lauryl monomer block copolymers via reversible addition-transition transfer (RAFT) polymerization. The CM surface was modified from its original superhydrophilic nature to superhydrophobic, establishing efficient oil/water separation and thiol filtration. The film is environmentally friendly, biodegradable, and can effectively adsorb particles in complex water-oil particulate systems. Yong et al. (2018) reported the preparation of underwater oil sheets by a simple mechanical drilling process after forming microporous arrays on the surface of wood sheets. Composed of hydrophilic cellulose nanofibres, lignin, and hemicellulose, the wood was hydrophilic, and its inherent porous structure gave the surface excellent underwater superoleophobic properties. The synthetic flakes were successfully applied to separate oil/water mixtures and showed good separation capabilities. This separation method was green and cost-effective.

Metal Mesh

Metal mesh materials have a large surface area and porous structure with a controllable structure. They can also selectively adsorb oil/water mixtures under the influence of gravity, so gravity drive is a factor to be considered in preparing metal mesh separation materials. However, such meshes are sensitive to acid, alkali, or salt solutions and are only suitable under mild conditions. Usually, by treating the metal mesh with high surface energy and surface roughness underwater with hydrophobicity, water penetrates and forms a water film which forms a repellent effect on the oil in the mixture, thus achieving oil/water separation (Kollari Gowda et al. 2017, Xu et al. 2013). Commonly prepared by etching a modified metal surface and then by coating the particles (Yong et al. 2018).

Such special wettable materials can be effective for oil/water separation but are also susceptible to oil contamination or blockage, as their lipophilicity affects the separation efficiency. Dai et al. (2020) prepared polytetrafluoroethylene (PTFE) nanofibre coatings by molecular self-assembly. Thermally aged PTFE nanoparticles could undergo molecular rearrangement to obtain ultrathin PTFE nanofibre coatings with high homogeneity and excellent chemical stability by using electrostatic interactions as the driving force for self-assembly. The fiber is superhydrophobic and superlipophilic, effectively separates various oil/water mixtures, has good reusability, and has proven highly resistant to strong acids,

bases, and salt solutions. A schematic diagram of the PTFE nanofibre coating preparation process is shown in Fig. 4 (a).

The anchoring ability and accessibility of plant polyphenols inspire them. Chen et al. (2018) prepared an underwater super-oil repellent coating based on metal sheets using TA modified by dip-coating method to obtain a TA-coated copper surface with excellent underwater super-oil repellent properties. The anchoring effect of TA molecules with the metal surface resulted in a tantalum-plated copper surface with excellent underwater superhydrophobicity and ultra-low adhesion, easy processing, and low cost. The design of Du et al. (2018) was inspired by the superhydrophobicity of the lotus leaf surface. The stainless-steel mesh was etched with hydrofluoric acid, coated with silver nanoparticles, and modified with stearic acid (STA) to construct a superhydrophobic oleophilic structure with micro/nanostructures. The treated stainless-steel mesh is superhydrophobic and lipophilic, showing up to 98 % separation efficiency in oil/water separation experiments and maintaining a high separation efficiency after multiple cycles. In addition, the mesh shows good chemical resistance under harsh mixed solution conditions and good wear resistance in hot water. A schematic diagram of the fabrication of a superhydrophobic/superoleophilic stainless-steel mesh is shown in Fig. 4 (b). Inspired by superhydrophobic stainless-steel filters, Zeng et al. (2017) produced a superhydrophobic/superoleophilic stainless-steel

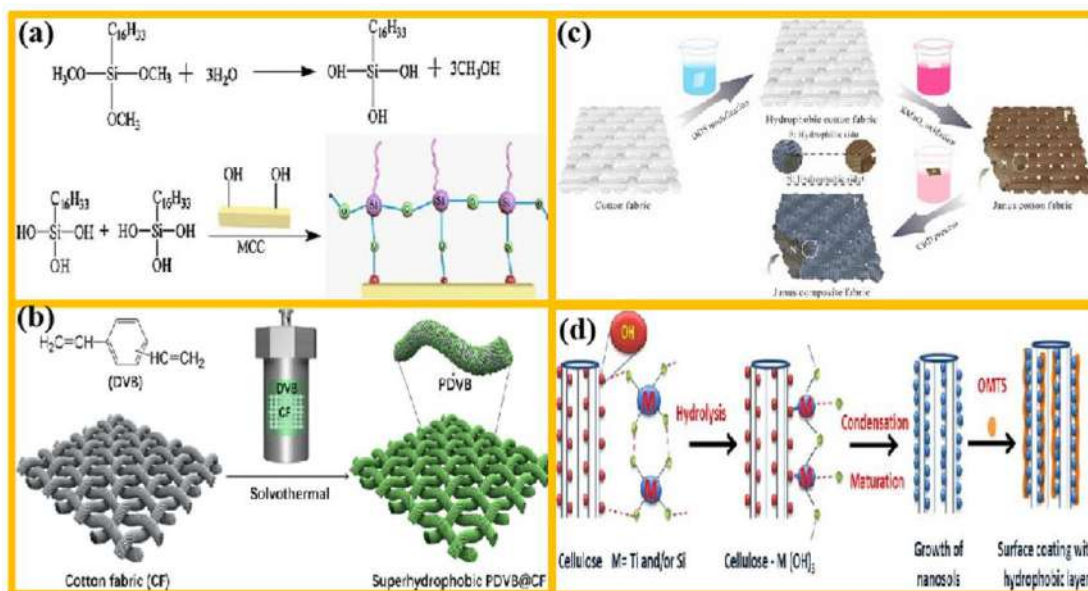


Fig. 3: (a) Synthetic route for silanization of MCC, (b) schematic illustration of the fabrication of PDVB@CF via a one-step solvothermal polymerization, (c) schematic illustration of the preparation process of a Janus composite fabric. The process includes surface hydrophobization, oxidation treatment, and chemical bath deposition, (d) diagram illustration of the in situ preparation of nano sols onto cotton fabrics, and their surface modification with OMTS.

mesh (SBS-SSM) filter. The hydrophilic silica particles were assembled on the stainless-steel mesh by electrostatic self-assembly. Then a fluoropolymer/SiO₂ nanoparticle solution was coated on the substrate, allowing the stainless-steel mesh surface to mimic beetle water back and obtain oil/water separation, which is simple and environmentally friendly compared to other superhydrophobic/superoleophilic surface preparation methods. The principle diagram of the SBS-SSM preparation is shown in Fig. 4 (c). Wang et al. (2018a) prepared TA/PVP coated stainless steel mesh using natural water-soluble polyphenols (TA) and highly biocompatible polymers (PVP). The materials are superhydrophilic and submerged superhydrophobic and can effectively separate oil/water mixtures. TA is a biocompatible, low toxicity, and superwet material. In addition, the TA/PVP coated stainless steel mesh exhibits good anti-fouling properties and is made into a funnel shape. Underwater oil collection units with TA/PVP coated stainless steel mesh in combination with underwater oil/water separation systems provide continuous collection and removal of oil contaminants from the underwater environment.

Zhou et al. (2021) used a fast, low-cost electrodeposition method to attach a metal-organic framework consisting of Co²⁺ ions and 2-methylimidazole to the copper mesh, which can be prepared in less than ten minutes. The difference in the action of Co²⁺ with specific groups (carboxyl or sulfhydryl) produces adsorption properties on mixed oil and water solutions with a long-lasting and stable separation capacity. After ten cycles, it still has 98 % separation efficiency.

Cao and Liu (2021) first ultrasonically pretreated the copper mesh and then prepared an underwater superoleophobic copper mesh by layer-by-layer self-assembly of inorganic sodium silicate and alumina powder (SSA) on copper (Cu) mesh. The modified copper mesh achieved an oil/water separation efficiency of 95 % even after heat treatment in a 700°C solution and maintained an efficiency of over 96 % after thirty cycles. Moreover, this experimental preparation required a short time and low raw material costs.

Gao et al. (2021) prepared a stainless steel mesh film with switchable wettability by in situ generation of ZnO nanowire arrays of ZnO-NAs on the surface of the stainless steel mesh, modified with hydrophobic properties. The preparation process also utilizes electro-wetting-induced oil/water separation, using ZnO-NAs to coat the SSM and a silane coupling agent as a bridging agent to improve the adhesion between the film and the metal mesh. Applying a low electric field controls this intelligent switchable wettability, and the response time is very fast. This method is extremely effective in treating wastewater and has good practicality. The modified material is not only durable but also has some antifouling ability.

Zhang et al. (2021) constructed by etching and in situ growth of a Prussian blue analog on a nickel grid with a coarse micro- and nano-scale grid structure. The composite grid exhibits strong superhydrophilicity and submerged

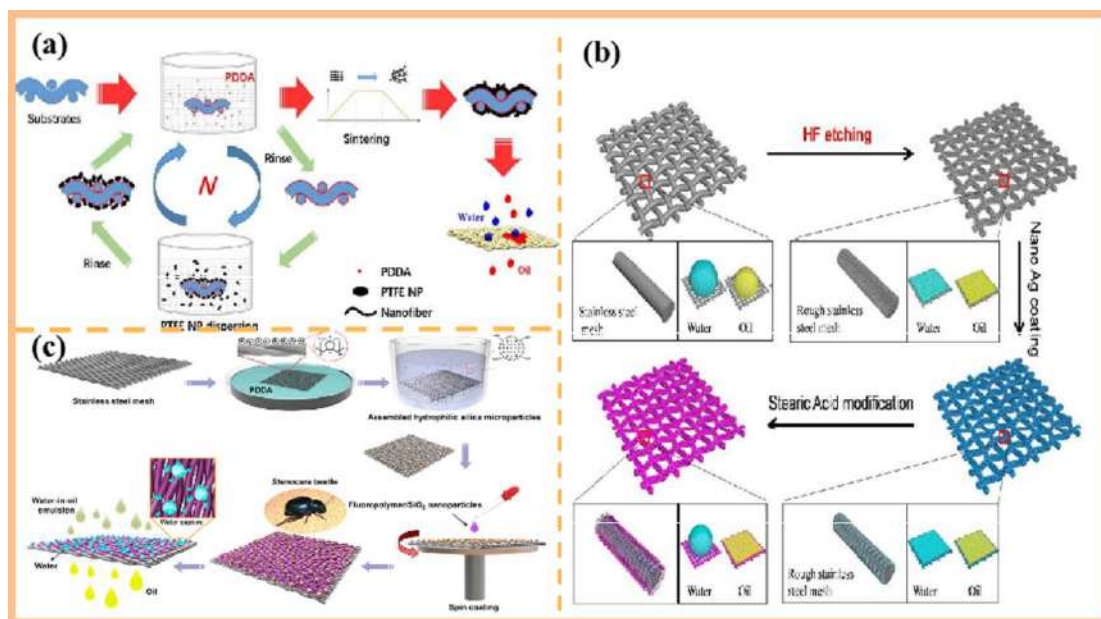


Fig. 4: (a) Schematic diagrams of the preparation process of PTFE nanofibrous coatings, (b) schematic illustration of the fabrication of the superhydrophobic/superoleophilic stainless-steel mesh, (c) schematic illustration of the fabrication of the superhydrophobic/superoleophilic stainless-steel mesh (SBS-SSM) filter.

superoleophobicity, and its stable separation efficiency and resistance to acids and bases make it a promising material for wastewater separation.

It is well known that separation materials are contaminated by crude oil as the surface free energy of contact with crude oil decreases in the dry state. Hence, materials must be pre-hydrated before oil/water separation (Peng et al. 2018, Yang et al. 2019). Filter membrane materials are commonly used in wastewater treatment, but their lack of pre-hydration is a major challenge (Zhao et al. 2019). Wang et al. (2021) used chitosan (CS)-cellulose nanocrystals (CNCs) in this way, the modified metal mesh has better hydration ability in both air and wastewater, reducing the risk of oil contamination while providing excellent oil/water separation performance. The raw material of this experiment, chitosan, is inexpensive and environmentally compatible, and the material prepared from cellulose is economical and environmentally friendly (Ma et al. 2021).

Synthetic Membrane Materials

Membrane separation technology is widely used in wastewater treatment due to its low energy (Lee & Park 2013), simple operation, and lack of secondary contaminants (Shi et al. 2019). However, conventional separation materials tend to have low efficiency, stability, and selectivity (Matsubayashi et al. 2017), limiting their application in oil/water separation (Wang et al. 2022).

Shi et al. (2018) used mussel adhesion protein to stimulate dopamine-modified poly (lactic acid) (PLA) nonwovens to obtain polydopamine (PDA)/PLA nonwovens. As a hygroscopic and oil separation material, it has high adsorption performance and selectivity and excellent photocatalytic degradation ability for various soluble organic pollutants under UV irradiation. The controlled wetting performance of the nonwoven was achieved by controlling the relative ratio of butyl titanate ($\text{Ti}(\text{OBU})_4$) to heptadecanoic acid (HFA) during the preparation process. Wu et al. (2018) coated dopamine on polyvinylidene fluoride (PVDF) membranes and then modified the superhydrophobic PVDF membranes by adding glutathione (GSH) through a simple reaction, reducing the serous membrane contamination caused by oil/water separation. The membrane was modified by adding glutathione (GSH) to the superhydrophobic PVDF membrane in a simple reaction, reducing the serous membrane contamination caused by oil/water separation and improving the reusability of the material. The PVDF membrane with high pure water permeability, good anti-fouling properties, and reusability, making it suitable for long-term efficient membrane separation. Fig. 5 shows FE-SEM images of PVDF (a, d), PVDF@PDA (b, e), and PVDF@PDA-GSH (c, f) surfaces. The PVDF@PDA-GSH membranes were prepared schematically, as shown in Fig. 5 (g).

Gupta and Kandasubramanian (2017) polymerized non-ionic surfactant-soaked nano tetrafluoroethylene

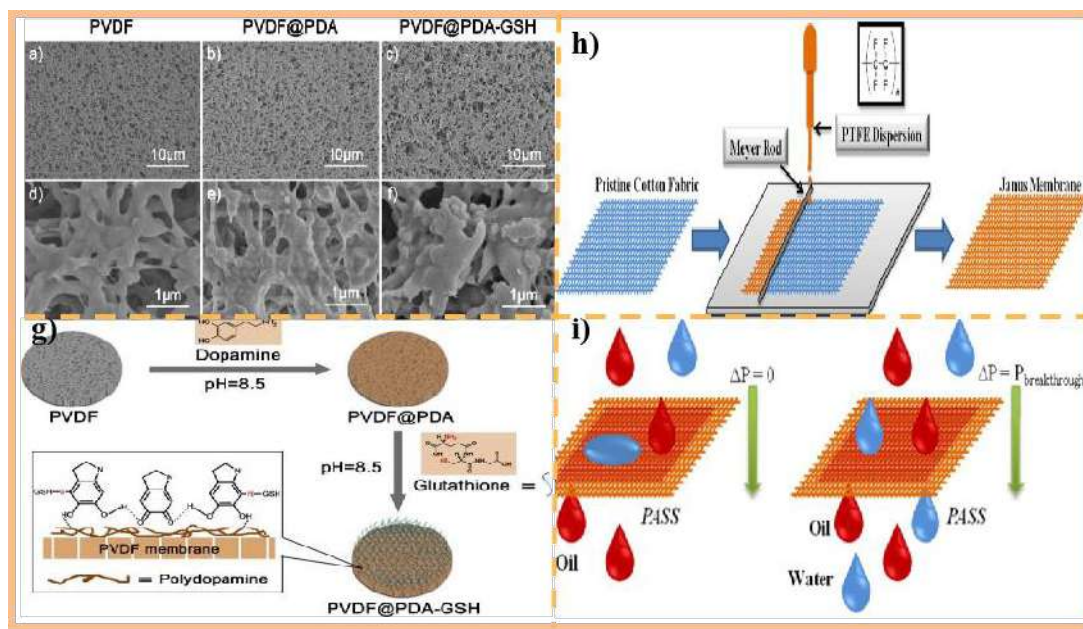


Fig. 5: (a-f) FE-SEM images of the surface of (a, d) PVDF, (b, e) PVDF@PDA, and (c, f) PVDF@PDA-GSH. The time of PDA and GSH treatment was 4 and 2 h, respectively, (g) schematic illustration for the fabrication of PVDF@PDA-GSH membrane, (h) schematic of the fabrication of Janus membrane, (i) Janus membrane as a directional fluid diode.

(PTFE) dispersions into modified superhydrophobic/superhydrophilic oil Janus films using the Meyer rod coating technique. This Janus film has excellent non-homogeneous wettability and anti-icing properties. We can still perform very good oil/water separation in some extreme environments and also have some flame retardancy and recyclability. An et al. (2018) prepared charged Janus membranes (CNTs) and hydrophobic microfiltration membranes using vacuum filtration. Hydrophilicity regulates the thickness of the carbon nanotube coating by controlling the number of carbon nanotubes deposited on the substrate membrane. This is because Janus films use the charge shielding effect to emulsify and separate heavy and light oils in emulsions. This team solved the problem that the normal Janus film preparation method couldn't control the thickness of the hydrophilic emulsion breaking layer. Fig. 5 (h) shows a schematic diagram of the fabrication of the double mask, and Fig. 5 (i) shows a schematic diagram of the double mask as a directional fluid diode.

Granular or Powdered Materials

Granular or powdered oil absorbent materials have excellent oil absorption properties (Zhang et al. 2020) and have been the star material in oil and water separation, which is particularly effective in the face of large areas of contamination, which has also received attention. Common metal oxides include TiO_2 , SiO_2 , Fe_3O_4 , ZnO , Al_2O_3 , and others, generally used as hydrophobic agents to modify other substrates (Eskandari et al. 2021). However, they must often

be modified with hydrophobic polymers to obtain better oil absorption or improve hydrophobicity. High cost, low efficiency, and environmental pollution, the performance of the material is prone to rapid degradation due to surface corrosion damage by the external environment (Ishchenko et al. 2021, Tabrizian & Amoozadeh 2016), the mechanical durability of the surface structure, chemical resistance remains a challenge, which makes the large-scale use of granular oil absorption materials limited.

Qu et al. (2018) produced a superwetted material based on kaolinite nanoparticles, exhibiting good oil removal properties in the air and underwater. The addition of perfluorooctanoic acid to form long chains under alkaline conditions greatly reduced the surface energy of the kaolin, giving the modified kaolin material good oil removal properties, and further improved the durability and chemical resistance of the modified kaolin material by binding tightly to the substrate in the presence of bis(3-trimethoxysilylpropyl)amine. Unlike previous materials, this material is suitable for almost any substrate and exhibits good hydrophilicity in air and water. Compared to conventional functional materials, the coating is stain-resistant, energy efficient, and easily recyclable. Fig. 6 (a) shows the wetting behavior and oil/water separation of modified superhydrophilic/superoleophobic kaolin materials. Wang et al. (2018b) prepared superhydrophobic particles by modifying TiO_2 , infiltrated the modified particle suspension into the material, and prepared 3D materials with superhydrophobic and superhydrophilic properties by simple impregnation and coating. By adding a certain

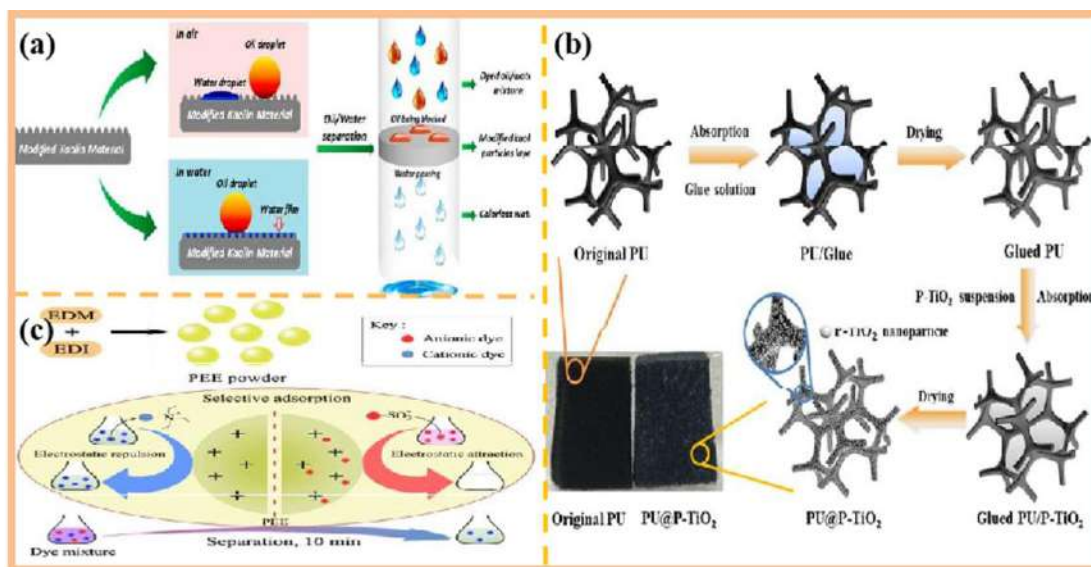


Fig. 6: (a) Schematics of the wetting behavior and oil/water separation of the modified superhydrophilic/superoleophobic kaolin materials, (b) schematic illustration of the fabrication process for PU@P-TiO₂ composite, (c) schematic of selective adsorption and separation process of dyes.

amount of TiO₂ nanoparticles to the hydrolyzed PTES solution, the hydroxyl groups on the TiO₂ surface condensed with water, and hydrophobic groups grafted onto the TiO₂ nanoparticle surface. And due to the glue's stability and the material's environmentally friendly nature, the oil removal function is efficient and long-lasting by means of good reuse and recyclability. A schematic diagram of the preparation process of PU@P-TiO₂ composites is shown in Fig. 6 (b).

Li et al. (2017) prepared quaternary ammonium salt hydrogels by a simple one-step copolymerization method as an effective adsorbent for removing dyes and insoluble oils and fats from water. It is an organic cationic adsorbent with large R₄N⁺ groups and has a much higher selective adsorption efficiency for anionic dyes than other commonly used adsorbents. The poor adsorption capacity of cationic dyes can be used for efficient and rapid adsorption on hybrid solutions. In addition, the adsorbent is reusable, efficient, and durable, making it a simple, inexpensive, and truly efficient adsorbent. The principle diagram of the dye-selective adsorption separation process is shown in Fig. 6 (c).

Aerogels

Aerogels are wet gels filled with air pores, usually obtained from dried organic or hydrogels (García-González et al. 2012, Pierre & Pajonk 2002). Using the properties of the porous structure, lightweight materials such as carbon nanotubes, graphene, silica, and alumina can be prepared, which are characterized by a large specific surface area and low density and have a wide range of applications (Liebner et al. 2008, Mohanan et al. 2005). However, aerogels are expensive, complex, and non-biodegradable, limiting their applications. Zhang et al. (2018) inspired cancellous bone. They successfully prepared many HAP nanopores with three-dimensional interconnection, porous mesh structure, special structure with high porosity and interconnection, and better adsorption of oil and organic solvents by using HAP nanowires freeze-drying method without using organic solvents. Compared to organic aerogels, HAP nanowire aerogels have good, environmentally friendly, and low-cost biocompatibility. The hydrophobic HAP nanowire aerogels have good PM 2.5 filtration efficiency, low airflow resistance, and high adsorption capacity for different oil and organic solvents. In addition, the hydrophobic HAP nanowire aerogels have excellent elastic properties, high reusability, and good recycling capacity (Hou et al. 2020, Liu et al. 2014). Fig. 7 shows (a) a schematic diagram of the cancellous bone microstructure, (b) digital images and SEM micrographs of cancellous bone, and (c) digital images and SEM micrographs of the prepared HAP nanowire aerogel.

Gao et al. (2018) used a mussel adhesive as an inspiration and a polydopamine interlayer as a medium. The polydopamine (PDA) coating prepared from the mussel adhesive was uniformly spun on nano-fibrillated cellulose (NFC) scaffold, linking the hydrophilic NFC with the desired hydrophobic octadecyl amine (ODA) molecules to give nano-fibrillated NFC surface hydrophobicity. With a high contact angle, the new superhydrophobic NFC aerogel allows the NFC scaffold to come into complete contact with the modifier, generating a structurally homogeneous aerogel that maintains its original porous structure intact and can absorb various oils and solvents in aqueous solutions. In nature, mussels have strong adhesion to almost all types of substrates through the secretion of adhesion proteins. The composite aerogel has excellent superhydrophobicity, ultra-low density, and high porosity. It has good oil/water absorption selectivity and can adsorb various organic solvents.

Yang et al. (2018b) successfully synthesized peptidoglycan aerogels using short peptides and polysaccharides by molecular self-assembly and freeze-drying. The microporous peptidoglycan aerogel was prepared by freeze-drying a hydrogel co-assembled with a simple dipeptide and the polysaccharide konjac dextran (KGM), which had good separation properties for various oils and fats. The peptide consists of a base methoxy attached to the C-terminus of a diphenylalanine peptide (Fmoc, FF), which self-assembles in water into a hydrogel composed of one-dimensional nanofibres. KGM is a functional polysaccharide with good hydrophilicity and gelation properties. The microstructure of the aerogel can be controlled by varying the mass ratio of Fmoc, FF, and KGM. KGM solution is rapidly freeze-dried in liquid nitrogen to form an aerogel with relatively weak mechanical strength compared to other inorganic aerogels. Still, the synthesized composite aerogel has good biocompatibility with peptide materials in oil/water separation.

Zhou et al. (2018a) successfully constructed superhydrophobic aerogels using silylated cellulose nanofibres and silica nanoparticles by a simple freeze-drying method. The prepared aerogel has high porosity, low density, good hydrophobicity, and a large water contact angle. It can be used for the filtration separation of surfactant-stabilized oil-in-water emulsions. The aerogel has a porous gradient structure with high roughness and low surface energy. The hydrophobic modifier reduces the surface energy of cellulose nanofibres and silica nanoparticles. The modified aerogel's density and specific surface area are increased by adding silica nanoparticles. By adding silica nanoparticles to improve the surface roughness and porosity of the material, the rough laminar structure and the lower surface can make the

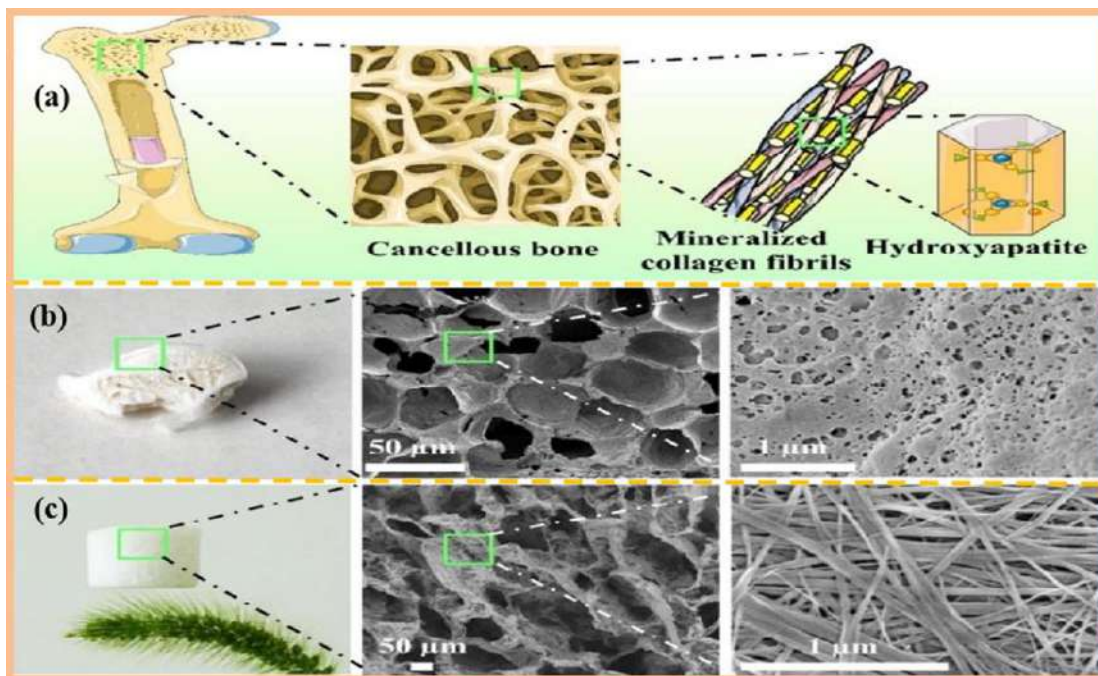


Fig. 7: (a) Schematic illustration of the microstructure of the cancellous bone, (b) digital image and SEM micrographs of the cancellous bone, (c) digital image and SEM micrographs of the as-prepared HAP nanowire aerogel.

aerogel superhydrophobic and highly efficient in separating oil/water emulsions without external pressure. It also has good anti-fouling properties and recyclability with long service life.

Sponge Materials

Common sponge materials include polyurethane and melamine sponges (Liu et al. 2017, Lou et al. 2004). Due to their low price, high specific surface area, low density, and high porosity, they can be used as oil/water separation substrates. Still, they can't be used directly for oil/water separation. High lipophilicity can be achieved by constructing the sponge surface structure more roughly or modifying it with low surface energy materials (Matsubayashi et al. 2017). Peng et al. (2018) reported superhydrophobic polydimethylsiloxane (PDMS) via UV-assisted thiol and prepared superhydrophobic and lipophilic melamine sponges from sponge materials by membrane functionalization. Due to the special strip microstructure and the hydrophobicity of the silicone, the new material has a high contact angle. First, the polymercapto cross-linker polymethyl vinyl silicone (PMVS) is soaked onto the melamine sponge, and UV-assisted curing is carried out. The resulting material has self-cleaning properties and different adsorption capacities for different oils and solvents. The prepared sponges had a convenient pore and

regular strip structure with superhydrophobic and lipophilic properties.

Feng & Yao (2018) reported that hydrophilic melamine sponges (MS) can be prepared into sponges with hydrophobic properties through modification by several methods: 1. Direct charring of MS can yield hydrophobic foam carbon, and the charred MS obtained has different adsorption properties at different temperatures. 2. Introduce hydrophobic functional group modification on the surface of MS, wrap the functional group monomer on the surface of MS, and then gel or polymerize to obtain the MS with a hydrophobic surface. 3. Treatment in HCl solution to obtain protonated mass spectra. The protonated mass spectra have excellent oil/water separation performance, usage stability, and anti-pollution performance. 4. MS or carbonic acid MS was used as a carrier, and the sponge surface was coated with graphene oxide (GO), metal-organic backbone (MOF), or other nanomaterials. Feng & Yoa (2018) coated the MS by furfuryl alcohol immersion and acid solution polymerization to modify the original MS. Furfuraldehyde reacted and polymerized on the surface of the MS, making the modified MS hydrophobic. Fig. 8 shows a schematic diagram of the preparation process (a) and SEM images at different magnifications (b-d) of the melamine filament-coated NiCo_2S_4 composite. Schematic diagram of the synthesis of alginate sponge and its application in copper (II) adsorption (e).

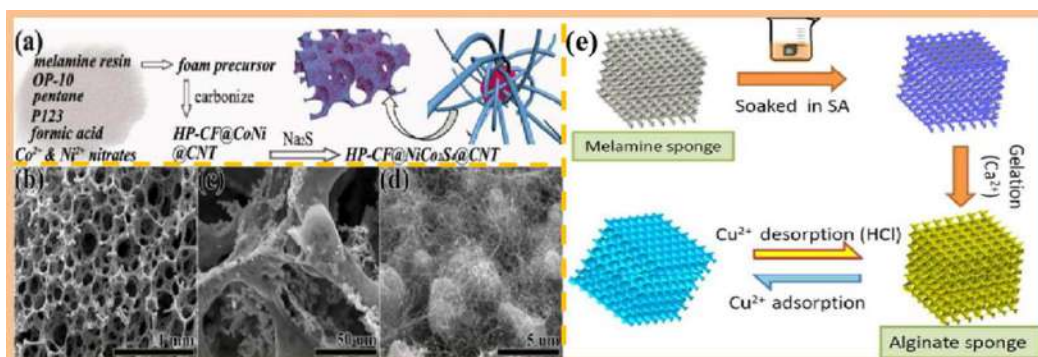


Fig. 8: Illustration of the fabrication process (a) and SEM images with different magnifications of melamine wires wrapped NiCo₂S₄ composites (b-d), (e) schematic illustration of the synthesis of alginate-MS and its application for Cu(II) adsorption.

Foam Materials

Unlike sponge materials, foam materials are inherently hydrophobic. They can be used directly for oil/water separation (Pan et al. 2015), and the roughness of the surface structure after construction can further obtain superhydrophobicity (Yu et al. 2015). Metal foam materials are also common, with very good flexibility and high mechanical strength, which can be called good oil/water separation materials after proper modification. Zhou et al. (2018b) dipped copper foam (CFs) into an aqueous hydrochloric acid solution, roughened the surface by solution etching, and then put them into TD nanorods synthesized by heating in an aqueous solution. After coating the TD nanorods, the CFs were superhydrophilic and superlipophilic. Modified TD-CF has a WCA value of approximately 0°, exhibits superhydrophobicity at a WCA value of 160°, and superhydrophobicity at an OCA value of 159°. In addition, TD is an excellent photocatalyst, and the water absorbed by the TD-CF material will return to its original state after evaporation. The absorbed oil decomposes into non-toxic substances such as carbon dioxide and water under UV irradiation, indicating that the material is efficient and durable with good recovery rates. The metal skeleton provides a high-strength material to cope with the external stresses encountered and resists wear and tear during use. The nanorods form a stable composite three-phase interface for oil/water separation through laminar pores and millions of conical micropores, eliminating the need for complex chemical modification processes to achieve high/low surface energy (Fujishima et al. 2008, Wang & Zhang 2012)87-89. Fig. 9 shows the general preparation route and use of TD-CFs for efficient continuous oil/water separation processes.

Smart Controllable Special Wetttable Separation Materials

In recent years, stimuli-responsive polymers have received much attention and development due to their great potential for research and application in manufacturing smart controllable materials (Zhang et al. 2020, Zheng et al. 2020). Oil/water mixtures are usually highly acidic and alkaline, which tends to corrode the separation material, thus affecting the stability of the separation efficiency. It is also easy to cause oil contamination to clog the material voids, resulting in a reduction in separation efficiency or even the outright failure of the separator. Compared to other oil/water separation materials, intelligent and controllable separation materials reduce consumption and speed up the separation process (Ren et al. 2020). However, only a few studies have reported on smart controllable separation materials.

Cao et al. (2014) prepared temperature and pH-responsive oil/water separation materials using stainless steel as a substrate for free radical polymerization triggered under UV light. The modified meshes have superhydrophilic and submerged superoleophobic properties with excellent separation efficiency. The method is novel and effective and opens up a new field of oil/water separation by selectively collecting oil or water from wastewater under temperature or pH regulation using dimethylaminoethyl methacrylate (DMAEMA), a raw material with excellent biocompatibility. A schematic diagram of the preparation of the hydrogel-coated mesh and the relative wettability of the mesh when in contact with oil is shown in Fig. 10 (a).

Cheng et al. (2015) reported the formation of smart controllable separation membranes by assembling responsive thiol molecules on the surface of copper mesh by an assembly technique. The modified material was extremely oleophobic under alkaline conditions and superhydrophobic under non-alkaline conditions and suggested that nanostructure and proper pore size on the substrate were keys to controllable separation.

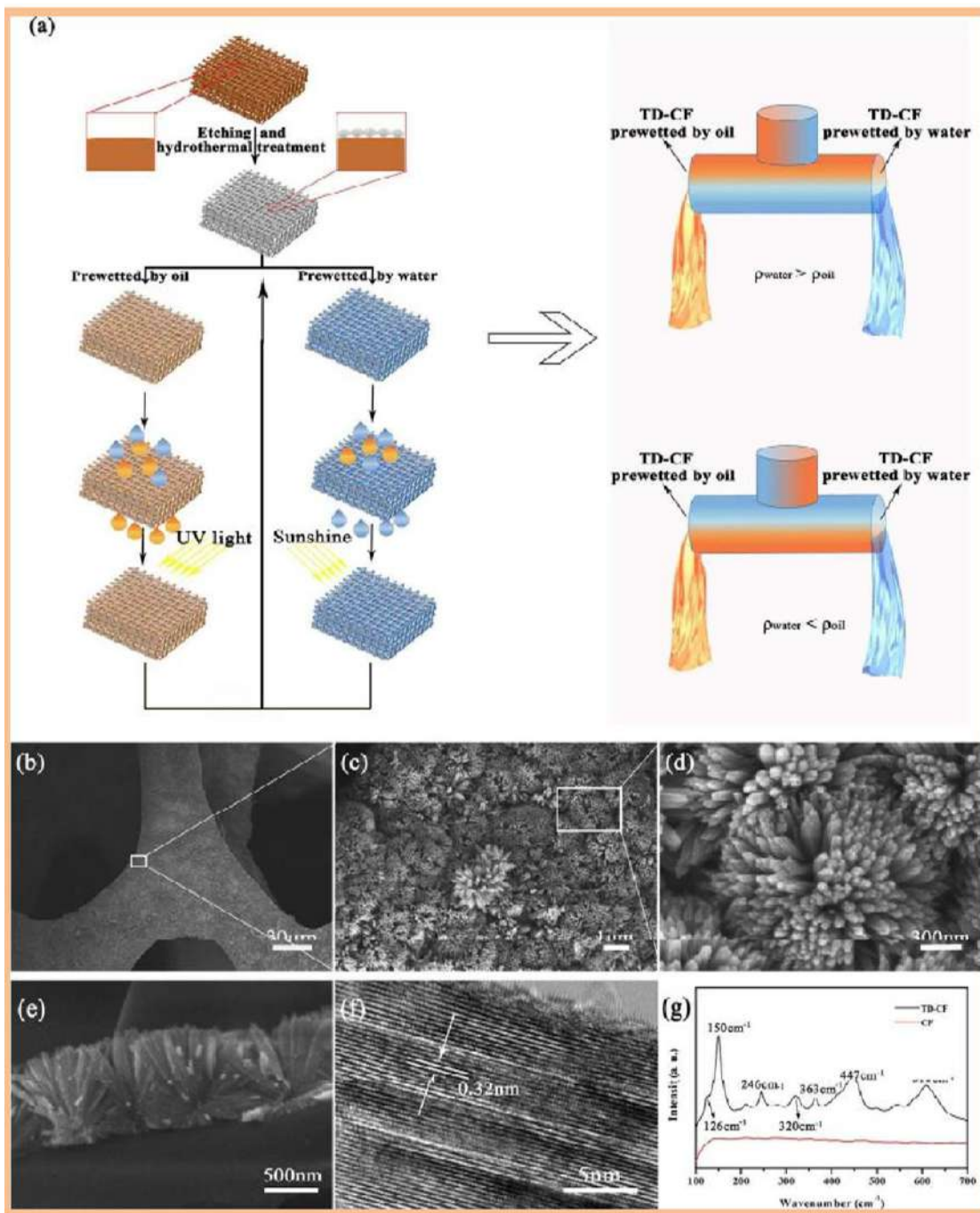


Fig. 9: (a) Illustration of the overall preparation route and usage of TD-CFs for high-efficiency and continuous oil-water separation process, (b-d) FESEM images on TD-CFs surface morphology with different magnification, (e) a cross-section FESEM image of TD coating, (f) HRTEM image of TD nanorods, (g) Raman spectra of TD-CF and commercial CF.

Xu et al. (2020) prepared the first visible light-responsive photocatalytic and pH-responsive super-wet melamine sponge (MS) with a porous elastic structure, providing a larger specific surface area and photocatalytic sites with

a greater ability to adsorb contaminants, showing high oil absorption and photocatalytic effects. The excellent and stable separation efficiency is expected to be a multifunctional wastewater treatment material.

Fu et al. (2017) reported a superhydrophobic antibacterial fabric prepared by cross-linking reaction of nanoparticles with adipic diisocyanate using cotton fabric as the base material. The modified cotton fabric had underwater lipophilic and hydrophobic properties and was more effective in separating oil and water in acidic emulsions. The cotton fabric substrate is low in environmental protection, has a long service life, and has a certain self-cleaning ability after oil and water contamination.

Li et al. (2019) first prepared cellulose nanofibers (CNFs) aerogels by surface-initiated atomic technology, grafting poly(N, N-dimethylamine-diethyl methacrylate), the modified aerogel surface hydrophobic can be converted to hydrophilic by the concentration of carbon dioxide, when carbon dioxide is dissolved by other gases materials transformed into hydrophobic crude oil. The intelligent switchable separation properties effectively prevent the separation material from being contaminated with oil. The cellulose feedstock makes the aerogel very environmentally friendly and shows good separation efficiency even when dealing with surfactant-stabilized emulsion-modified materials, which has great potential for development. The CO₂-responsive cellulose nanofibre aerogel reaction mechanism is shown in Fig. 10 (b).

Gao et al. (2019a) prepared wettability switchable biomimetic TiO₂-titanium meshes (BTMMs) using a one-step

dip coating method with polyvinylidene fluoride and modified TiO₂ suspensions. The modified metal mesh can be wettability switched intelligently by the action of surface hydroxyl groups and can self-healing and self-cleaning in addition to the effective separation of wastewater, which improves the material's recyclability and reduces energy loss. These properties increase the recyclability of the material and reduce energy losses. The preparation method is inexpensive and simple and has many applications. A schematic representation of the preparation is shown in Fig. 10 (c).

CONCLUSIONS

This work has reviewed the preparation and application of oil/water separation materials in recent years, granular or powdered materials, metal meshes, natural textile or synthetic film materials, aerogels, sponges, foams, and intelligent, controllable humidification separation materials. Special attention is paid to cellulose-based superlipophilic/superhydrophobic, superhydrophilic/superoleophobic, and smart, responsive oil/water separation materials. Cellulose is a widespread and inexpensive biomass material that exhibits unique oil absorption properties due to its inherent porous structure and is applied in oil/water separation. To improve oil/water selectivity, oil/water separation materials are prepared by modified graft copolymerization, surface

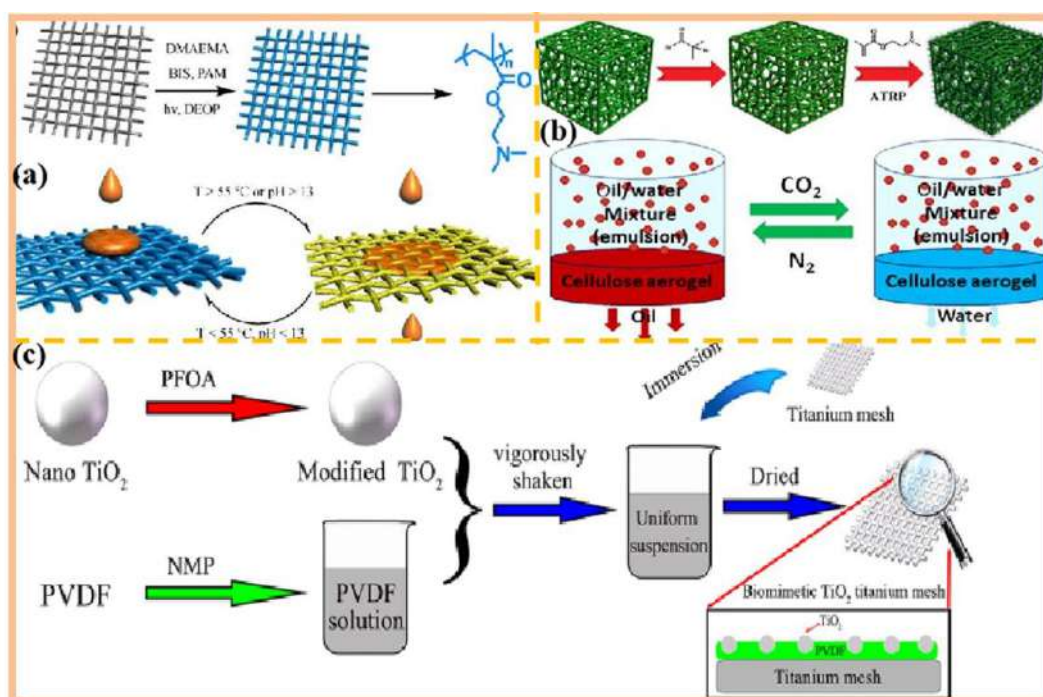


Fig. 10: (a) Schematic description of the preparation of PDMAEMA hydrogel coated mesh and the opposite wettability of the mesh when contacted with oil, (b) schematic illustration of the preparation of CNF-g-PDMAEMA Aerogel, (c) schematic illustration of the preparation process.

coating, particle adsorption, and construction of material surfaces or internal structures.

The durability and recyclability of the materials are still to be solved, and attention needs to be paid to the problem of separation materials being easily blocked by oil molecules. Without improving the anti-fouling properties of the materials, this will seriously affect the separation efficiency. There are also some key technical defects, such as the complexity of the synthesis process, the high cost, whether the environment is friendly, etc. Because of the complexity of the process, many successfully prepared materials are still limited to the laboratory research range; it is difficult to mass production applications. Therefore, low-cost, simple to prepare, self-cleaning, and durable oil and water separation materials should be vigorously developed.

ACKNOWLEDGMENTS

The authors gratefully acknowledge the financial support of the International Science and Technology Cooperation Project of Shaoxing University (Grant No. 2019LGGH1004).

REFERENCES

- An, Y., Yang, J., Yang, H.C., Wu, M.B. and Xu, Z.K. 2018. Janus membranes with charged carbon nanotube coatings for demulsification and separation of oil-in-water emulsions. *ACS Appl. Mater. Interfaces*, 10: 9832-9840.
- Antonelli, D.M. and Ying, J.Y. 1995. Synthesis of hexagonally packed mesoporous TiO₂ by a modified sol-gel method. *Angew. Chem. Int. Ed.*, 34: 2014-2017.
- Borges, J. and Mano, J.F. 2014. Molecular interactions driving the layer-by-layer assembly of multilayers. *Chem. Rev.*, 114: 8883-8942.
- Borges, M.E., Sierra, M., Méndez-Ramos, J., Acosta-Mora, P., Ruiz-Morales, J.C. and Esparza, P. 2016. Solar degradation of contaminants in water: TiO₂ solar photocatalysis assisted by up-conversion luminescent materials. *Sol. Energy Mater. Sol. Cells*, 155: 194-201.
- Cao, H. and Liu, Y., 2021. Facile design of a stable and inorganic underwater superoleophobic copper mesh modified by self-assembly sodium silicate and aluminum oxide for oil/water separation with high flux. *J. Colloid Interface Sci.*, 598: 483-491.
- Cao, Y., Liu, N., Fu, C., Li, K., Tao, L., Feng, L. and Wei, Y. 2014. Thermo and pH dual-responsive materials for controllable oil/water separation. *ACS Appl. Mater. Interfaces*, 6: 2026-2030.
- Chen, M., Qu, Y., Yang, L. and Gao, H. 2008. Structures and antifouling properties of low surface energy non-toxic antifouling coatings modified by nano-SiO₂ powder. *Sci China Chem.*, 51: 848-852.
- Chen, Y., Meng, J., Zhu, Z., Zhang, F., Wang, L., Gu, Z. and Wang, S. 2018. Bio-inspired underwater super oil-repellent coatings for anti-oil pollution. *Langmuir*, 34: 6063-6069.
- Cheng, Q.Y., Guan, C.S., Li, Y.D., Zhu, J. and Zeng, J.B. 2019. Robust and durable superhydrophobic cotton fabrics via a one-step solvothermal method for efficient oil/water separation. *Cellulose*, 26: 2861-2872.
- Cheng, Z., Wang, J., Lai, H., Du, Y., Hou, R., Li, C., Zhang, N. and Sun, K. 2015. pH-controllable on-demand oil/water separation on the switchable superhydrophobic/superhydrophilic and underwater low-adhesive superoleophobic copper mesh film. *Langmuir*, 31: 1393-1399.
- Cheryan, M. and Rajagopalan, N. 1998. Membrane processing of oily streams. Wastewater treatment and waste reduction. *J. Membr. Sci.*, 151: 13-28.
- Dai, J., Wang, L., Wang, Y., Tian, S., Tian, X., Xie, A., Zhang, R., Yan, Y. and Pan, J. 2020. Robust nacrelike graphene oxide-calcium carbonate hybrid mesh with underwater superoleophobic property for highly efficient oil/water separation. *ACS Appl. Mater. Interfaces*, 12: 4482-4493.
- Decher, G. and Hong, J.D. 1991. Buildup of ultrathin multilayer films by a self-assembly process. I consecutive adsorption of anionic and cationic bipolar amphiphiles on charged surfaces, *Makromolekulare Chemie. Macromolecular Symposia*. Wiley Online Library, pp. 321-327.
- Du, Z., Ding, P., Tai, X., Pan, Z. and Yang, H. 2018. Facile preparation of Ag-coated superhydrophobic/superoleophilic mesh for efficient oil/water separation with excellent corrosion resistance. *Langmuir*, 34: 6922-6929.
- Dunderdale, G. J., Urata, C., Sato, T., England, M. W. and Hozumi, A. 2015. Continuous, high-speed, and efficient oil/water separation using meshes with antagonistic wetting properties. *ACS Appl. Mater. Interfaces*, 7: 18915-18919.
- Eskandari, M., Shanaghi, A., Kamani, M. and Niari, M.A. 2021. Effect of nano-metal oxides (ZnO, Al₂O₃, CuO, and TiO₂) on the corrosion behavior of a nano-metal oxide/epoxy coating applied on the copper substrate in the acidic environment. *Appl. Nanosci.*, 11: 1605-1615.
- Feng, Y. and Yao, J. 2018. Design of melamine sponge-based three-dimensional porous materials toward applications. *Ind. Eng. Chem. Res.*, 57: 7322-7330.
- Fu, Y., Jin, B., Zhang, Q., Zhan, X. and Chen, F. 2017. pH-induced switchable superwettability of efficient antibacterial fabrics for durable selective oil/water separation. *ACS Appl. Mater. Interfaces*, 9: 30161-30170.
- Fujishima, A., Zhang, X. and Tryk, D. A. 2008. TiO₂ photocatalysis and related surface phenomena. *Surf. Sci. Rep.*, 63: 515-582.
- Gao, H., Liu, Y., Wang, G., Li, S., Han, Z. and Ren, L. 2019a. Switchable wettability surface with chemical stability and antifouling properties for controllable oil-water separation. *Langmuir*, 35: 4498-4508.
- Gao, M.L., Zhao, S.Y., Chen, Z.Y., Liu, L. and Han, Z.B. 2019b. Superhydrophobic/superoleophilic MOF composites for oil-water separation. *Inorg. Chem.*, 58: 2261-2264.
- Gao, Q., Zhao, J., Hu, J. and Wang, M. 2021. Applying a switchable superhydrophobic and hydrophilic ZnO nanorod array-coated stainless-steel mesh to electrically-induced oil/water separation. *Coll. Surf. A*, 628: 127231.
- Gao, R., Xiao, S., Gan, W., Liu, Q., Amer, H., Rosenau, T., Li, J. and Lu, Y. 2018. Mussel adhesive-inspired design of superhydrophobic nanofibrillated cellulose aerogels for oil/water separation. *ACS Sustain. Chem. Eng.*, 6: 9047-9055.
- García-González, C. A., Camino-Rey, M. C., Alnaief, M., Zetzl, C. and Smirnova, I. 2012. Supercritical drying of aerogels using CO₂: Effect of extraction time on the end material textural properties. *J. Supercrit. Fluids*, 66: 297-306.
- Gui, Z., Zhu, H., Gillette, E., Han, X., Rubloff, G.W., Hu, L. and Lee, S.B. 2013. Natural cellulose fiber as substrate for supercapacitor. *ACS Nano*, 7: 6037-6046.
- Gupta, P. and Kandasubramanian, B. 2017. Directional fluid gating by Janus membranes with heterogeneous wetting properties for selective oil-water separation. *ACS Appl. Mater. Interfaces*, 9: 19102-19113.
- Han, S.W., Kim, H.J., Woo, T.G., Jeong, J.H., Cha, B.J. and Kim, Y.D. 2018. Superhydrophobic fabric resistant to an aqueous surfactant solution as well as pure water for the selective removal of spill oil. *ACS Appl. Nano Mater.*, 1: 5158-5168.
- Hou, S., Wu, X., Lv, Y., Jia, W., Guo, J., Wang, L., Tong, F. and Jia, D. 2020. Ultralight, highly elastic and bioinspired capillary-driven

- graphene aerogels for highly efficient organic pollutants absorption. *Appl. Surf. Sci.*, 509: 1448-18.
- Hu, L., Liu, Y., Wang, Z., Zhou, Y., Zhang, Y., Liu, Y. and Li, B. 2020. A general in situ deposition strategy for synthesis of Janus composite fabrics with Co (CO₃) 0.5 OH⁻ 0.11 H₂O nanoneedles for oil-water separation. *ACS Appl. Nano Mater.*, 3: 3779-3786.
- Ishchenko, O., Rogé, V., Lamblin, G., Lenoble, D. and Fechete, I. 2021. TiO₂, ZnO, and SnO₂-based metal oxides for photocatalytic applications: principles and development. *C. R. Chim.*, 24: 103-124.
- Joung, Y.S. and Buie, C.R., 2015. Antiwetting fabric produced by a combination of layer-by-layer assembly and electrophoretic deposition of hydrophobic nanoparticles. *ACS Appl. Mater. Interfaces*, 7: 20100-20110.
- Kang, L., Wang, B., Zeng, J., Cheng, Z., Li, J., Xu, J., Gao, W. and Chen, K., 2020. Degradable dual superhydrophobic lignocellulosic fibers for high-efficiency oil/water separation. *Green Chem.*, 22: 504-512.
- Ke, Q., Jin, Y., Jiang, P. and Yu, J., 2014. Oil/water separation performances of superhydrophobic and superoleophilic sponges. *Langmuir*, 30: 13137-13142.
- Kim, B. S., Park, S. W. and Hammond, P. T. 2008. Hydrogen-bonding layer-by-layer-assembled biodegradable polymeric micelles as drug delivery vehicles from surfaces. *ACS Nano.*, 2: 386-392.
- Kollarigowda, R.H., Abraham, S. and Montemagno, C.D. 2017. Antifouling cellulose hybrid biomembrane for effective oil/water separation. *ACS Appl. Mater. Interfaces*, 9: 29812-29819.
- Lahiri, S. K., Zhang, P., Zhang, C. and Liu, L. 2019. Robust fluorine-free and self-healing superhydrophobic coatings by H₃BO₃ incorporation with SiO₂-Alkyl-Silane@ PDMS on cotton fabric. *ACS Appl. Mater. Interfaces*, 11: 10262-10275.
- Lee, S.Y. and Park, S.J. 2013. TiO₂ photocatalyst for water treatment applications. *J Ind Eng Chem.*, 19: 1761-1769.
- Li, D., Li, Q., Bai, N., Dong, H. and Mao, D. 2017. One-step synthesis of cationic hydrogel for efficient dye adsorption and its second use for emulsified oil separation. *ACS Sustain. Chem. Eng.*, 5: 5598-5607.
- Li, X., Hu, D., Huang, K. and Yang, C. 2014. Hierarchical rough surfaces formed by LBL self-assembly for oil-water separation. *J. Mater. Chem. A*, 2: 11830-11838.
- Li, Y., Zhu, L., Grishkewich, N., Tam, K. C., Yuan, J., Mao, Z. and Sui, X. 2019. CO₂-responsive cellulose nanofibers aerogels for switchable oil-water separation. *ACS Appl. Mater. Interfaces*, 11: 9367-9373.
- Liebner, F., Potthast, A., Rosenau, T., Haimer, E. and Wendland, M. 2008. Cellulose aerogels: Highly porous, ultra-lightweight materials. *ACS Appl. Mater. Interfaces*, 62: 129-135.
- Lin, H., Wang, Z.J., Wang, H., Xue, Q.Y. and Zhu, Y.J. 2012. The study of oil absorption of natural biomass materials. *J. Funct. Biomater.*, 43: 2412-2415.
- Liu, L., Lei, J., Li, L., Zhang, R., Mi, N., Chen, H., Huang, D. and Li, N. 2017. Cobweb-inspired superhydrophobic multiscaled gating membrane with embedded network structure for robust water-in-oil emulsion separation. *ACS Sustain. Chem. Eng.*, 5: 3448-3455.
- Liu, L., Lei, J., Li, L., Zhang, R., Mi, N., Chen, H., Huang, D. and Li, N. 2017. A facile method to fabricate the superhydrophobic magnetic sponge for oil-water separation. *Mater. Lett.*, 195: 66-70.
- Liu, Y., Ai, K. and Lu, L. 2014. Polydopamine and its derivative materials: synthesis and promising applications in energy, environmental, and biomedical fields. *Chem. Rev.*, 114: 5057-5115.
- Lou, X., Munro, S. and Wang, S. 2004. Drug release characteristics of phase separation pHEMA sponge materials. *Biomaterials*, 25: 5071-5080.
- Lü, X., Cui, Z., Wei, W., Xie, J., Jiang, L., Huang, J. and Liu, J. 2016. Constructing polyurethane sponge modified with silica/graphene oxide nanohybrids as a ternary sorbent. *Chem. Eng. J.*, 284: 478-486.
- Ma, W., Ding, Y., Li, Y., Gao, S., Jiang, Z., Cui, J., Huang, C. and Fu, G. 2021. Durable, self-healing superhydrophobic nanofibrous membrane with self-cleaning ability for highly-efficient oily wastewater purification. *J. Membr. Sci.*, 634: 119402.
- Mao, X., Wang, Y., Yan, X., Huang, Z., Gao, Z., Wang, Y., Huang, L., Kipper, M. J. and Tang, J. 2023. A review of superwetting membranes and nanofibers for efficient oil/water separation. *J. Mater. Sci.*, 1-31.
- Matsubayashi, T., Tenjimbayashi, M., Komine, M., Manabe, K. and Shiratori, S. 2017. Bioinspired hydrogel-coated mesh with superhydrophilicity and underwater superoleophobicity for efficient and ultrafast oil/water separation in harsh environments. *Ind. Eng. Chem. Res.*, 56: 7080-7085.
- Mohanan, J.L., Arachhige, I.U. and Brock, S.L. 2005. Porous semiconductor chalcogenide aerogels. *Science*, 307: 397-400.
- Montazer, M., Pakdel, E. and Moghadam, M.B. 2011. The role of nano colloid of TiO₂ and butane tetra carboxylic acid on the alkali solubility and hydrophilicity of proteinous fibers. *Coll. Surf. A.*, 375: 1-11.
- Pan, Y., Zhan, J., Pan, H., Yuan, B., Wang, W., Song, L. and Hu, Y. 2015. A facile method to fabricate superoleophilic and hydrophobic polyurethane foam for oil-water separation. *Mater. Lett.*, 159: 345-348.
- Pendashteh, A. R., Fakhru'R-Razi, A., Madaeni, S.S., Abdullah, L.C., Abidin, Z.Z. and Biak, D.R.A. 2011. Membrane foulants characterization in a membrane bioreactor (MBR) treating hypersaline oily wastewater. *Chem. Eng. J.*, 168: 140-150.
- Peng, B., Yao, Z., Wang, X., Crombeen, M., Sweeney, D.G. and Tam, K.C. 2020. Cellulose-based materials in wastewater treatment of petroleum industry. *Green Energy Environ.*, 5: 37-49.
- Peng, J., Deng, J., Quan, Y., Yu, C., Wang, H., Gong, Y., Liu, Y. and Deng, W. 2018. Superhydrophobic melamine sponge coated with striped polydimethylsiloxane by thiolene click reaction for efficient oil/water separation. *ACS Omega*, 3: 5222-5228.
- Pierre, A.C. and Pajonk, G.M. 2002. Chemistry of aerogels and their applications. *Chem. Rev.*, 102: 4243-4266.
- Qu, M., Ma, L., Zhou, Y., Zhao, Y., Wang, J., Zhang, Y., Zhu, X., Liu, X. and He, J. 2018. Durable and recyclable superhydrophilic-superoleophobic materials for efficient oil/water separation and water-soluble dyes removal. *ACS Appl. Nano Mater.*, 1: 5197-5209.
- Ren, J., Tao, F., Liu, L., Wang, X. and Cui, Y. 2020. A novel TiO₂@ stearic acid/chitosan coating with reversible wettability for controllable oil/water and emulsions separation. *Carbohydr. Polym.*, 232: 115807.
- Reynolds, J.G., Coronado, P.R. and Hrubesh, L.W. 2001. Hydrophobic aerogels for oil-spill clean up-synthesis and characterization. *J. Non-Cryst. Solids*, 292: 127-137.
- Rubio, J., Souza, M.L. and Smith, R.W. 2002. Overview of flotation as a wastewater treatment technique. *Miner. Eng.*, 15: 139-155.
- Shaheen, T. I., Salem, S. S. and Zaghoul, S. 2019. A new facile strategy for multifunctional textiles development through in situ deposition of SiO₂/TiO₂ nanosols hybrid. *Ind. Eng. Chem. Res.*, 58: 20203-20212.
- Shi, J., Zhang, L., Xiao, P., Huang, Y., Chen, P., Wang, X., Gu, J., Zhang, J. and Chen, T. 2018. Biodegradable PLA nonwoven fabric with controllable wettability for efficient water purification and photocatalysis degradation. *ACS Sustain. Chem. Eng.*, 6: 2445-2452.
- Shi, S., Xu, J., Zeng, Q., Liu, J., Hou, Y. and Jiang, B. 2019. Impacts of applied voltage on EMBR treating phenol wastewater: Performance and membrane antifouling mechanism. *Bioresour. Technol.*, 282: 56-62.
- Su, X., Li, H., Lai, X., Zhang, L., Liao, X., Wang, J., Chen, Z., He, J. and Zeng, X. 2018. Dual-functional superhydrophobic textiles with asymmetric roll-down/pinned states for water droplet transportation and oil-water separation. *ACS Appl. Mater. Interfaces*, 10: 4213-4221.
- Tabrizian, E. and Amoozadeh, A. 2016. A unique approach to magnetization of metal oxides: nano-Fe₃O₄@ TDI@ TiO₂ as a highly efficient, magnetically separable and recyclable heterogeneous nanocatalyst. *Catal. Sci. Technol.*, 6: 6267-6276.
- Tung, W.S. and Daoud, W.A. 2013. Self-Cleaning Fibers and Fabrics, In: Daoud, W.A. (Ed.), *Self-cleaning materials and surfaces*. John Wiley & Sons Inc., Chichester, West Sussex, United Kingdom, pp. 129-147.

- Wang, B., Liang, W., Guo, Z. and Liu, W. 2015. Biomimetic superlyophobic and superlyophilic materials applied for oil/water separation: a new strategy beyond nature. *Chem. Soc. Rev.*, 44: 336-361.
- Wang, C.F., Wang, W.N., Kuo, S.W., Chiang, Y.W., Hung, J.H. and Lee, K.J. 2018a. Biocompatible meshes with appropriate wettabilities for underwater oil transportation/collecting and highly effective oil/water separation. *Langmuir*, 34: 11442-11448.
- Wang, C., Yao, T., Wu, J., Ma, C., Fan, Z., Wang, Z., Cheng, Y., Lin, Q. and Yang, B. 2009. Facile approach in fabricating superhydrophobic and superoleophilic surface for water and oil mixture separation. *ACS Appl. Mater. Interfaces*, 1: 2613-2617.
- Wang, G. and Zhang, T. Y. 2012. Easy route to the wettability cycling of copper surface between superhydrophobicity and superhydrophilicity. *ACS Appl. Mater. Interfaces*, 4: 273-279.
- Wang, H., Bi, X., Zhao, Y., Yang, Z., Wang, Z. and Wu, M. 2022. Cu₃N nanoparticles with both (100) and (111) facets for enhancing the selectivity and activity of CO₂ electroreduction to ethylene. *New J. Chem.*, 46: 12523-12529.
- Wang, X., Jiang, Z., Shi, J., Liang, Y., Zhang, C. and Wu, H. 2012. Metal-organic coordination-enabled layer-by-layer self-assembly to prepare hybrid microcapsules for efficient enzyme immobilization. *ACS Appl. Mater. Interfaces*, 4: 3476-3483.
- Wang, X., Xu, S., Du Tan, Y., Du, J. and Wang, J. 2016. Synthesis and characterization of a porous and hydrophobic cellulose-based composite for efficient and fast oil-water separation. *Carbohydr. Polym.*, 140: 188-194.
- Wang, Y., He, Y., Li, H., Yu, J., Zhang, L., Chen, L. and Bai, Y. 2021. Layer-by-layer construction of CS-CNCs multilayer modified mesh with robust anti-crude-oil-fouling performance for efficient oil/water separation. *J. Membr. Sci.*, 639: 119776.
- Wang, Y., Zhu, Y., Yang, C., Liu, J., Jiang, W. and Liang, B. 2018b. Facile two-step strategy for the construction of a mechanically stable three-dimensional superhydrophobic structure for continuous oil-water separation. *ACS Appl. Mater. Interfaces*, 10: 24149-24156.
- Wu, W., Huang, R., Qi, W., Su, R. and He, Z. 2018. Bioinspired peptide-coated superhydrophilic poly(vinylidene fluoride) membrane for oil/water emulsion separation. *Langmuir*, 34: 6621-6627.
- Xie, A., Cui, J., Chen, Y., Lang, J., Li, C., Yan, Y. and Dai, J. 2019. One-step facile fabrication of sustainable cellulose membrane with superhydrophobicity via a sol-gel strategy for efficient oil/water separation. *Surf. Coat. Technol.*, 361: 19-26.
- Xu, L. P., Peng, J., Liu, Y., Wen, Y., Zhang, X., Jiang, L. and Wang, S. 2013. Nacre-inspired design of mechanical stable coating with underwater superoleophobicity. *ACS Nano*, 7: 5077-5083.
- Xu, X., Li, M., Li, X. and Zhang, L. 2020. Fabricated smart sponge with switchable wettability and photocatalytic response for controllable oil-water separation and pollutants removal. *J. Ind. Eng. Chem.*, 92: 278-286.
- Xue, Z., Cao, Y., Liu, N., Feng, L. and Jiang, L. 2014. Special wettable materials for oil/water separation. *J. Mater. Chem. A*, 2: 2445-2460.
- Yang, J., Li, H., Lan, T., Peng, L., Cui, R. and Yang, H. 2017. Preparation, characterization, and properties of fluorine-free superhydrophobic paper based on layer-by-layer assembly. *Carbohydr. Polym.*, 178: 228-237.
- Yang, M., Liu, W., Jiang, C., He, S., Xie, Y. and Wang, Z. 2018a. Fabrication of superhydrophobic cotton fabric with fluorinated TiO₂ sol by a green and one-step sol-gel process. *Carbohydr. Polym.*, 197: 75-82.
- Yang, M., Liu, W., Jiang, C., Liu, C., He, S., Xie, Y. and Wang, Z. 2019. Robust fabrication of superhydrophobic and photocatalytic self-cleaning cotton textile based on TiO₂ and fluoroalkylsilane. *J. Mater. Sci.*, 54: 2079-2092.
- Yang, X., Xie, Y., Wang, Y., Qi, W., Huang, R., Su, R. and He, Z. 2018b. Self-assembled microporous peptide-polysaccharide aerogels for oil-water separation. *Langmuir*, 34: 10732-10738.
- Yong, J., Chen, F., Huo, J., Fang, Y., Yang, Q., Bian, H., Li, W., Wei, Y., Dai, Y. and Hou, X. 2018. Green, biodegradable, underwater superoleophobic wood sheet for efficient oil/water separation. *ACS Omega*, 3: 1395-1402.
- Yu, L., Han, M. and He, F. 2017. A review of treating oily wastewater. *Arab. J. Chem.*, 10: S1913-S1922.
- Yu, S., Tan, H., Wang, J., Liu, X. and Zhou, K. 2015. High porosity supermacroporous polystyrene materials with excellent oil-water separation and gas permeability properties. *ACS Appl. Mater. Interfaces*, 7: 6745-6753.
- Zeng, X., Qian, L., Yuan, X., Zhou, C., Li, Z., Cheng, J., Xu, S., Wang, S., Pi, P. and Wen, X. 2017. Inspired by stenocara beetles: from water collection to high-efficiency water-in-oil emulsion separation. *ACS Nano*, 11: 760-769.
- Zhang, C., Li, P. and Cao, B. 2016. Fabrication of superhydrophobic-superoleophilic fabrics by an etching and dip-coating two-step method for oil-water separation. *Ind. Eng. Chem. Res.*, 55: 5030-5035.
- Zhang, N., Qi, Y., Zhang, Y., Luo, J., Cui, P. and Jiang, W. 2020. A review on oil/water mixture separation material. *Ind. Eng. Chem. Res.*, 59: 14546-14568.
- Zhang, R., Zhou, Z., Chang, Z., Dai, X., Chen, L. and Dai, J. 2021. Superhydrophilic, underwater superoleophobic and self-cleaning nickel composite mesh via simultaneous acid etching and in-situ growth of Prussian blue analogue for oil-water separation. *Coll. Surf. A Physicochem. Eng. Asp.*, 627: 127140.
- Zhang, Y. G., Zhu, Y. J., Xiong, Z. C., Wu, J. and Chen, F. 2018. Bioinspired ultralight inorganic aerogel for highly efficient air filtration and oil-water separation. *ACS Appl. Mater. Interfaces*, 10: 13019-13027.
- Zhao, J., Chen, H., Ye, H., Zhang, B. and Xu, L. 2019. Poly(dimethylsiloxane)/graphene oxide composite sponge: a robust and reusable adsorbent for efficient oil/water separation. *Soft Matter*, 15: 9224-9232.
- Zhao, X. Q., Wahid, F., Cui, J. X., Wang, Y. Y. and Zhong, C. 2021. Cellulose-based special wetting materials for oil/water separation: A review. *Int. J. Biol. Macromol.*, 185: 890-906.
- Zheng, W., Huang, J., Li, S., Ge, M., Teng, L., Chen, Z. and Lai, Y. 2020. Advanced materials with special wettability toward intelligent oily wastewater remediation. *ACS Appl. Mater. Interfaces*, 13: 67-87.
- Zhong, J., Sun, X. and Wang, C. 2003. Treatment of oily wastewater produced from refinery processes using flocculation and ceramic membrane filtration. *Sep. Purif. Technol.*, 32: 93-98.
- Zhou, P., Cheng, J., Yan, Y., Xu, S. and Zhou, C. 2017. Nature-inspired strategy toward superhydrophobic fabrics for versatile oil/water separation. *ACS Appl. Mater. Interfaces*, 9: 9184-9194.
- Zhou, P., Cheng, J., Yan, Y., Xu, S. and Zhou, C. 2021. Ultrafast preparation of hydrophobic ZIF-67/copper mesh via electrodeposition and hydrophobization for oil/water separation and dye adsorption. *Sep. Purif. Technol.*, 272: 118871.
- Zhou, S., You, T., Zhang, X. and Xu, F. 2018a. Superhydrophobic cellulose nanofiber-assembled aerogels for highly efficient water-in-oil emulsions separation. *ACS Appl. Nano Mater.*, 1: 2095-2103.
- Zhou, W., Li, S., Liu, Y., Xu, Z., Wei, S., Wang, G., Lian, J. and Jiang, Q. 2018b. Dual superlyophobic copper foam with good durability and recyclability for high flux, high efficiency, and continuous oil-water separation. *ACS Appl. Mater. Interfaces*, 10: 9841-9848.
- Zhu, C., Xue, J. and He, J. 2009. Controlled in-situ synthesis of silver nanoparticles in natural cellulose fibers toward highly efficient antimicrobial materials. *J. Nanosci. Nanotechnol.*, 9: 3067-3074.



Environmental Flow Assessment (EFA) of Tawi River Discharge at the Jammu Location Using the Global Environmental Flow Calculator (GEFC)

Maharshi Yadav*[†] , Govind Pandey* and Pradeep Kumar**

*Department of Civil Engineering, Madan Mohan Malaviya University of Technology, Gorakhpur, Uttar Pradesh, India

**Environmental Hydrology Division, National Institute of Hydrology, Roorkee, India

†Corresponding author: Maharshi Yadav; maharshiyadav@outlook.com

Nat. Env. & Poll. Tech.
Website: www.neptjournal.com

Received: 20-07-2022

Revised: 06-10-2022

Accepted: 15-10-2022

Key Words:

Environmental flow assessment
Tawi river
Global environmental flow calculator
Environmental management class
Hydro-ecological assessment

ABSTRACT

The water, food, and energy demands are the basic requirements of society. These demands are increasing daily due to an increase in population or lifestyle changes. To fulfill these ever-increasing demands, several water resource projects have come up which require the storage or diversion of river water. These interventions have caused widespread degradation of aquatic ecosystems. Due to the degradation of the aquatic ecosystem, several programs all around the globe began. In this series, Brisbane Declaration (2007) provided a more holistic definition of Environmental Flows (EFs) as the quantity, timing, duration, frequency, and quality of flows required to sustain freshwater, estuarine and near-shore ecosystems and the human livelihoods and well-being that depend on them. The present study was envisaged to assess for environmental flows of the Tawi river with a major objective of assessing the environmental flows of the Tawi river using the Global Environmental Flow Calculator developed by IWMI. The method provides E-Flows for different Environmental Management Classes. For the western Himalayan region, the river stretches in Environmental Management Class 'B' and 'C'. The assessment provides E-Flows in two ways: (i) the percentage of Mean Annual Runoff and (ii) average monthly environmental flows. E-Flows were estimated as 42.34% to 56.96% of Mean Annual Runoff and varied from 5.73 cumecs during November to 68.23 during August.

INTRODUCTION

The name of India itself can find the importance of rivers in India. India's name comes from a holy Himalayan River name Indus (Agoramoorthy 2015). This country is a land of rivers, and respect for great rivers such as Ganga, Godavari, Cauvery, Narmada Brahmaputra, etc., from east to west and north to south, can be found in daily life and cultural activities. Despite Rivers in India being respected as a mother, the conditions of major rivers are not very good. Pollution and alteration in Indian rivers cause damage to their habitat and imbalance in the ecological system of the riverine system. Gomati, Dikrong, Hindon, Subarnarekha, Ganga, Ghaggar, Kasardi, Kabini, Beas river, etc., are polluted with contaminants such as metals (Cr, Cu, Fe, Mn, Ni, Pb, etc.), pathogens, pesticides, carcinogens, etc. (Chakravarty & Patgiri 2009, Giri & Singh 2014, Jain et al. 2005, Kaushik et al. 2010, Kumar et al. 2018, Paul 2017, Taghinia et al. 2011,

Yadav et al. 2022a, 2022b). Not only industrial and sewage discharge in surface water bodies polluting and threatening the ecology of rivers/lakes but the alteration in flow patterns of rivers caused by various water resource development such as dams, canals, etc. (Operacz et al. 2018, Yadav et al. 2021a, 2021b, 2022a, 2022b, 2022c). Also causing adverse impacts on river quality and habitat. Assessment of ecological imbalances and habitat degradation need to address to prevent the ecological structure of the riverine system. Due to the very high hydropower capacity of Himalayan rivers, alterations in natural flow patterns rivers are highly disturbed. India produces 12% of its total electric power via hydroelectricity. Globally India ranks 5th concerning hydroelectric power capacity. Tehri, Tapovan Vishnugadh, Vishnugadh Pipalkoti, Singoli Bhatwari, Phata Bhuyang, Madhyamaheshwar, etc., are various hydropower projects installed on Himalayan rivers that have a high socio-economical impact. Despite electricity generation by hydropower projects, many adverse impacts occur due to alterations in the flow pattern of rivers. Finding a river in natural condition along its entire stretch is nowadays a fairy-tales. Restoring rivers in their natural conditions or recovering them sustainably is very important.

ORCID details of the authors:

Maharshi Yadav : <https://orcid.org/0000-0002-6503-2340>

Govind Pandey: <https://orcid.org/0000-0003-3520-4188>

An ecosystem is a natural unit consisting of biotic factors (all animals, plants, bacteria, viruses, and other microorganisms) in an area functioning with all of the environment's non-living (abiotic) factors. A river reach may be considered an aquatic ecosystem, and its catchment is a terrestrial ecosystem. These two ecosystems support distinct ecologies.

Increasing recognition of protection worldwide is a prerequisite for ecosystems where human beings are supplied with water (Dugan et al. 2002, Dyson et al. 2003).

Maintaining the ecosystem of the riverine system is a very cost-effective and valuable path to deliver services despite delivering manmade high technologies and monstrous structures (Emerton & Bos 2004). Identifying the full value and significance of the benefits of ecological systems, their investigation thoroughly can work as a potential protective tool for humans and animals in future profits. Recognition

and investigation of ecosystem benefits can save their values and provide help for their sustainable development. Big efforts and technological advancement fail seriously without considering the ecological balance.

For identifying the health of the river system, parameters like quality and quantity of water, sediments and their transport, food chain and its supply, and interaction between biotic and abiotic factors are very important parameters, but the most important parameter for the riverine ecosystem and its complex ecosystem structure is its flow regime (Dyson et al. 2003). Identification and significance of the flow become the key concept in the evolution of environmental flow for the riverine system (Hairan et al. 2021, Poff et al. 2009).

Study Area

The present study selected Tawi River, a left-bank tributary of Chenab River, for the low flow frequency analysis (Vinod

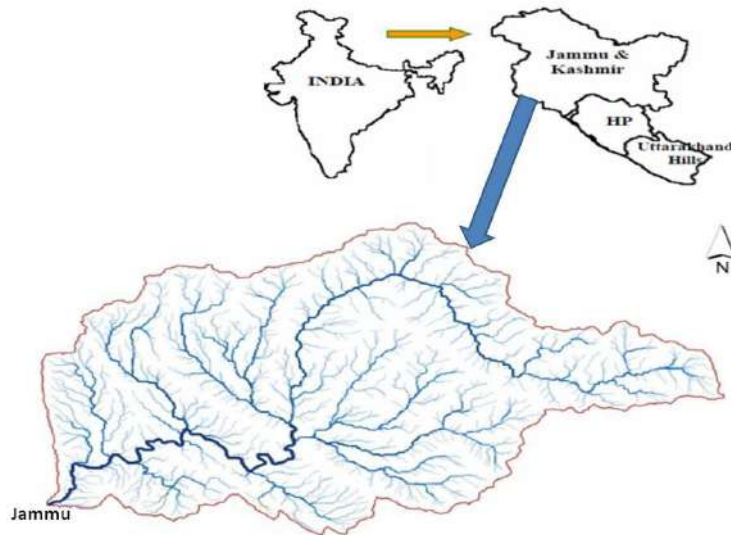


Fig. 1: Tawi river catchment area.

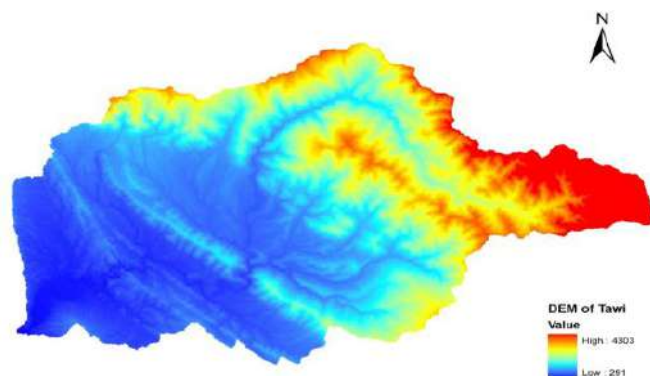


Fig. 2: Digital elevation mode (DEM) of Tawi catchment.

et al. 2016, Sharma & Chowdhary 2011, Sun et al. 2018, Goyal et al. 2005, Verma et al. 2012). From the Western Himalayan region, two riverine systems, the first Ganga riverine system, and the dual Indus river system are forming a great agricultural potential, hydroelectric generation potential, and other ecological systems for India. Tawi River, a major tributary of the Chenab River, originates from the Himalayan Glacame Kalikundi and its adjoining areas (Fig. 1). The shape of the basin is elongated in the upper part and broad in the lower part. The catchment area of the Tawi river up to Jammu is 2165 sq. km. After crossing the Jammu Ranbir canal, Tawi is divided into Nikki Tawi (flows towards the left) and Waddi Tawi (flows towards the right). The catchment area peaks at 6000msl in the glacier region and the lowest at 300 msl in the planer areas. Fig. 2 shows the digital elevation model of the Tawi River.

Mountainous Rivers have several sub-tributaries. Tawi River also has more than 2000 numbers of tributaries and sub-tributaries. Among the nine important tributaries of Tawi are Kali Kundi, Pitch, Margi, Chenani, Dhak Nalla, Naddal

Khund, Calari, Pharos, and Gamhi. The length of Kali Kundi is about 4 km, and its elevation varies from 4000 m to 3200 m. The pitch length is 2.0km with an elevation variation of 3600 m to 3200 m. Margi has two breaks profile, the first at 3200 m and the second at 2600 m, and the length is about 9.5 km. Chenani has a 7.5km length with elevation variation from 1700 m to 1100 m. Dhak Nalla has 2.5 km, and Naddal Kund has a 15 km length. Gamhi is 19 km long with small breaks at different places with elevation variations of 700 m to 400 m.

The Climatic Condition and Hydrology of the Tawi Catchment Area

This region experiences a hot summer season and a very cold winter season. Temperatures fall below 5°C in winter. The temperature reaches to peak in the May-June months. Bhadarwah and adjoining areas are tropical mountain-type climatic areas. The middle part, mainly the area of the Udhampur district, is a mountainous climate with the effect of the southwestern monsoon. Southwestern part is influenced

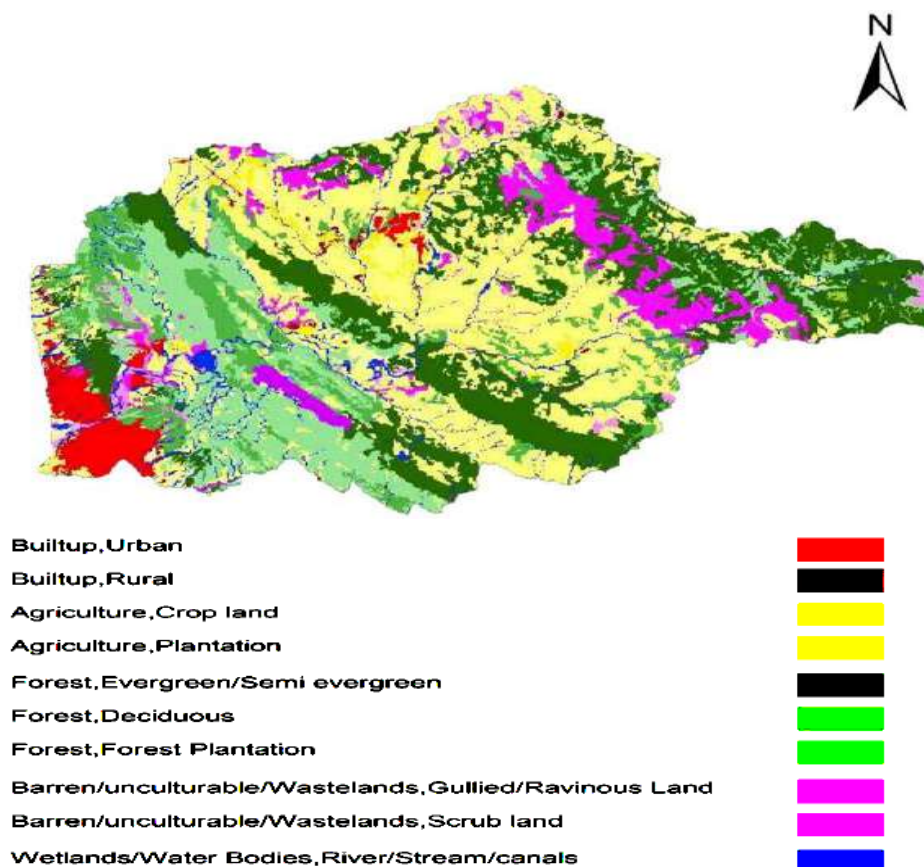


Fig. 3: Land use/Land cover in the Tawi river basin.

by monsoons and categorized as a subtropical wet and dry climate (Aqualogus 2018, Goyal et al. 2005, Jain et al. 2007, Sharma 2012).

55% of the total annual rainfall occurs from the end of June to the end of September. The average rainfall of Jammu district varies from 900 mm to 1000 mm. At higher altitudes, heavy snowfall occurs from December to February. According to the groundwater information booklet of CGWB (Aqualogus 2018), Jammu and Kashmir's rainfall is a major groundwater source in the Jammu district.

Groundwater quality is generally good for irrigation and domestic purposes, monitoring groundwater quality by CGWB. Considering the soil aspects of the Tawi river catchment area, the Doda district has alluvial soil. In midlands or foothills, the soil is generally sandy loam to silty clay loam due to the process of colluviation. At the Chenani location, due to the steep gradient in elevation potential of hydropower generation is utilized by various hydroelectric projects. Chenani I was commissioned in 1971 with three units (Unit I, Unit II, Unit III) and two more units in 1975 (Unit IV and Unit V) with a rated capacity of 17MW and a canal length of 18.64km. Chenani II was commissioned in 1996 with an installed capacity of 2MW in the Udhampur district, and Chenani III was commissioned in 2001 with an installed capacity of $3 \times 2.5 = 7.5$ MW. Tawi lift irrigation

canal with coverage of 28.8km starts from Bahu fort, opposite Jammu city. Udhampur canal is 26.5 km long and used for 2400 acres of irrigation and power generation of 8000KW. Subsidiary Lift Scheme on Tawi Canal at Raya, A subsidiary lift scheme to irrigate 1100 hectares of the fertile tract of land: uphill of the Tawi canal in the village of Raya has been envisaged. Major land cover is given in Fig. 3.

MATERIALS AND METHODS

Smakhtin & Anputhas (2006) reviewed various hydrology-based environmental flow assessment methodologies and their applicability in the Indian context. Based on the study, they combined the FDC approach and connected it with the EMCs.

The IWMI approach of EFA includes various steps and is built on a period record basis. FDC calculation is considered the first step for the environmental water requirement (EWR) for the selected sites. The sites with observed flow data are called 'source' sites. The sites where reference FDC and time series are required for the EF estimation are called 'destination' sites. The destination site is more significant because alteration in upstream causes influences downstream. Calculating unregulated stream flow variability and monthly flow time series provides information on the flow variability in unaltered conditions.

Table 1: EMCs Classes.

EMC	Ecological description	Management perspective
A: Natural	Original state or least alteration in river stream and riparian territory.	Applied for safeguarded rivers and basins, Natural reserves, and parks. No new water projects such as dams, canals, and deviations are allowed.
B: Slightly modified	Mostly unbroken biodiversity & altered habitats despite water resources expansion and basin amendments.	Agricultural development and water supply structures are present or tolerable.
C: Moderately modified	The environments and dynamics of the changed biota have been a concern, but basic ecosystem functions are still integral. Some sensitive species are lost and reduced in extent. Alien species present	Several problems and complexities belong with the requirement of socio-economic development projects (Dams and decline in water quality)
D: Largely modified	Big alterations and modifications in basic natural ecosystems/habitats have occurred. Species and their population were found to be less than expected. Species that have low tolerance levels are found in much lower numbers. Alien species prevail	Potential and observable problems attached to various water supply and resource development programs (including dams, diversions, transfers, habitat modification, and water quality degradation)
E: Seriously modified	Diversity in habitat was found to be declined extensively, species richness at minimum, intolerant species vanished, and only tolerable species were found. Indigenous species of ecosystems are not able to breed. Alien species have almost overtaken the ecosystem	Very high human population density and extreme exploitation of water resources.
F: Critically modified	Modifications have reached a critically modified level, and the ecosystem has been completely modified with almost total loss of natural habitat and biota. In the worst case, the basic ecosystem functions have been destroyed, and the changes are irreversible	This status is not acceptable from the management's perspective. Management interventions are necessary to restore flow patterns, river habitats, etc. (if still possible/feasible) – to 'move' a river to a higher management category.

Source: Smakhtin & Anputhas (2006)

In all the FDCs approaches, table flow values with respect to the .01, 0.1, 1, 5, 10, 20, 30, 40, 50, 60, 70, 80, 90, 95, 99, 99.9, 99.99 percentages are calculated based on available flow data. These points (i), by measuring 0.01 to 99.99 percent, ensure the variability of the whole range (ii) makes it simple for further steps. FDCs are designed straight from the observed record or form part of the record that could be considered 'unregulated.' Normally the earlier part of each record - preceding major dams' construction - is used to ensure that monthly flow variability, captured by the period-of-record FDC, is not seriously impacted. An FDC table is calculated for each destination site using a source FDC table from either the nearest or the only available observation flow station upstream.

EFs aim to maintain an ecosystem or upgrade it to, some prescribed or negotiated condition/status, also called environmental management class (EMC). The concept of EMCs is used in the IWMI approach. According to the EMC, class superiority signifies more water associated with maintaining the ecology and health of the riverine system. Natural flow amount needed naturally pristine condition of the river without alteration. EMCs A, B, C, D, E and F. are six EWR values described in Table 1.

By lateral shifting the original reference FDC to the left with the probability axis, a new FDC is obtained, and for the last tail values of shifted curve, linear extrapolation techniques are used. To determine the EMC A class original reference, FDC is shifted a single step left to the probability

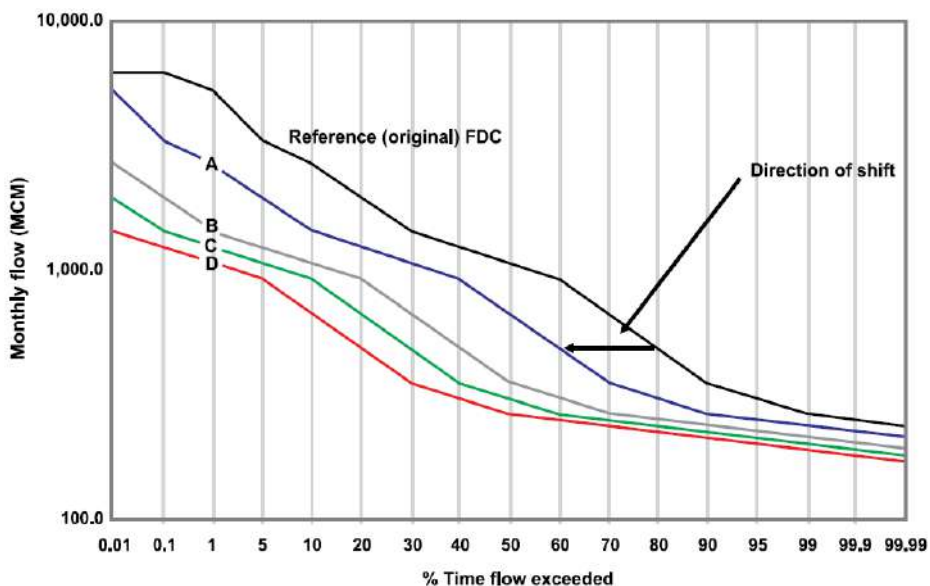
axis. For EMC B, shifting is done for two steps left to the probability axis. For the EMC C, shifting is done in three steps left and so on for further EMCs (Fig. 4).

FDC made for an EMC summarizes the EF regime, which suits this EMC. The curve, however, does not reflect the actual flow sequence. At the same time, once such environmental FDC is determined, this can be converted into average monthly flow time series. Hughes & Smakhtin (1996) described a spatial interpolation process in detail for the FDC and EMC.

RESULTS AND DISCUSSION

Open to access software named The Global Environmental Flow Calculator (GEFC), which is designed and developed by the scientist and engineers of the International Water Management Institute (IWMI). Flow duration curves are the basis of this methodology. Flow duration curves are improved and established as Environmental Management Classes (EMCs) using FDCs as the basic approach. Open access freely offered GEFC software needs an average of monthly discharge data of rivers for a significant amount of time to assess environment flows (Shaeri Karimi et al. 2012, Sood et al. 2017, Uday Kumar & Jayakumar 2021).

The present study utilized the daily hydrological data of the Tawi River to evaluate the environmental flows. There are six EMCs (A, B, C, D, E, F) are presented in GEFC, mutable from Unmodified to Critically modified. Each EMC is ex-



(Source: Smakhtin & Anputhas 2006)

Fig. 4: Illustration of estimation procedure of environmental FDCs for different EMCs.

pressed by its exclusive FDC. In this methodology, seventeen fixed percentage points considered representative of the flow regime is taken for the computation of flow duration curves for different EMCs. The FDC for each EMC is estimated by the oblique shift of the original reference FDC to the left along the percentage exceedance probability (X-Axis) by one percentage point.

The FDCs for different EMCs of the Tawi River have been presented in Fig. 5. From this figure. It may be concluded that discharges generally decrease from EMC A to

EMC F and tend to be approximately similar during the lean season.

The average monthly environmental flow series for different EMCs are shown in Fig. 6 and Table 2. The figure shows that the deviations in the discharges from the reference/natural flow are lower in the case of EMC 'A' and higher as we go from EMC 'A' to EMC 'F.' The lean season in the study area is from December to February, and the flows start increasing due to more snowmelt contribution. This reflects the flow values for different EMCs, as the

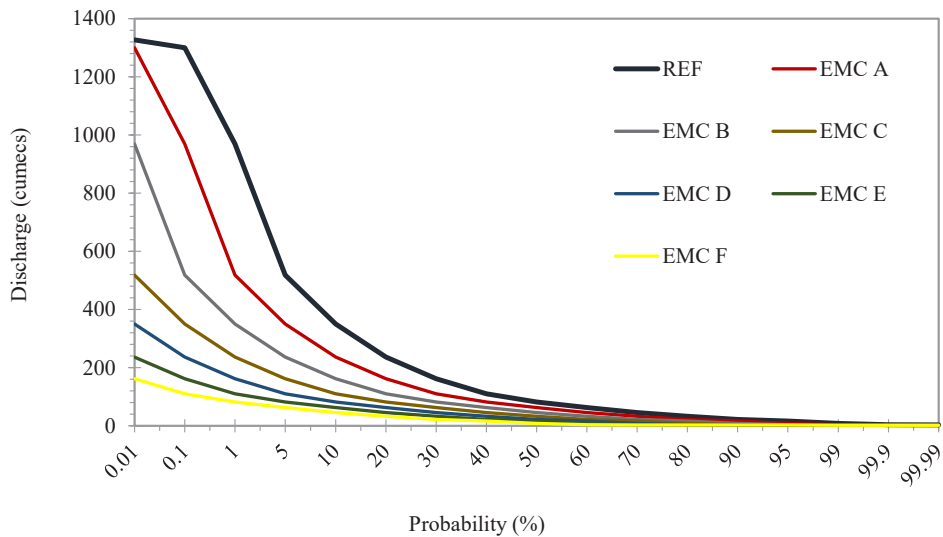


Fig. 5: Flow duration curves of Tawi River for different EMCs.

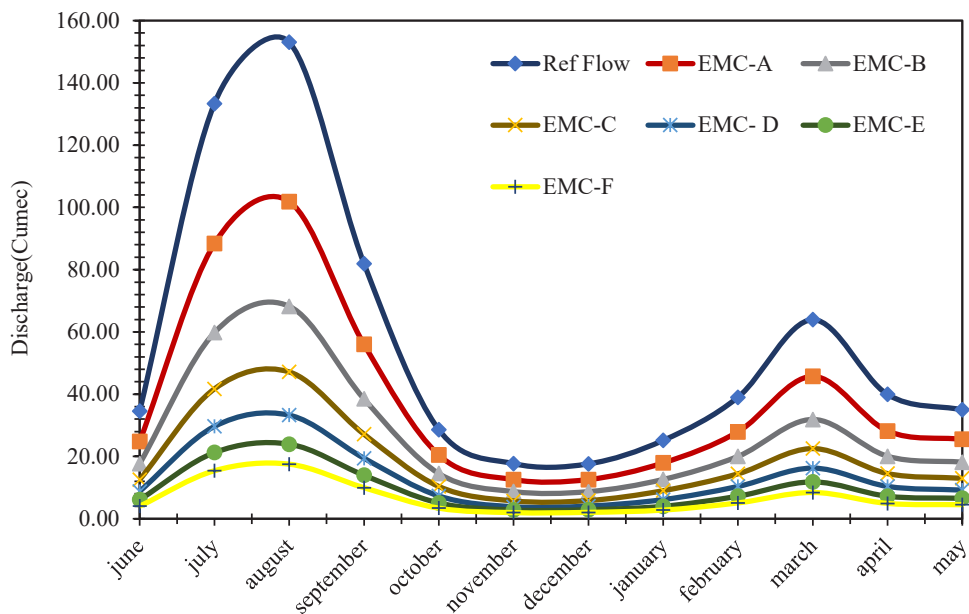


Fig. 6: Environmental flows of Tawi River for different EMCs.

Table 2: Environmental flows for different EMCs of Tawi River.

Month	Natural flows	Environmental flow (cumecs)					
		A	B	C	D	E	F
Jun	34.57	24.78	17.66	12.54	8.81	6.12	4.03
Jul	133.36	88.37	59.77	41.72	29.65	21.26	15.42
Aug	153.03	101.88	68.23	47.14	33.26	23.95	17.53
Sep	81.94	55.99	38.48	27.15	19.44	13.96	9.97
Oct	28.61	20.49	14.52	10.37	7.31	5.06	3.40
Nov	17.71	12.56	8.72	5.73	3.84	2.79	1.97
Dec	17.62	12.59	8.70	5.84	4.07	2.90	2.04
Jan	25.16	17.93	12.62	9.00	6.14	3.99	2.78
Feb	39.01	27.92	20.01	14.42	10.36	7.23	5.08
Mar	63.93	45.73	31.89	22.54	16.26	11.83	8.44
Apr	39.93	28.20	20.07	14.51	10.39	7.23	4.92
May	34.98	25.50	18.17	12.99	9.20	6.56	4.51
MAR (MCM)	1776	1362.01	1011.60	751.95	574.71	466.37	398.35
% of MAR	100.00	76.69	56.96	42.34	32.36	26.26	22.43

discharges for all the EMCs during the lean season are very close. Table 2 presents the environmental flows for different EMCs in two manners, i.e., the percentage of Mean Annual Runoff (MAR) and average monthly discharges. The table clearly shows that the percentage of Mean Annual Runoff (MAR) is higher to lower for EMCs from ‘A’ to ‘F’ (76.69% for EMC A and 22.43% for EMC F). The natural, as well as environmental flows are lowest in December.

Recommendations on the E-flows of the Tawi River

The status of the Ecological conditions of a river is subject

to the Environmental management class. The definition of the EMC depends on the empirical relationship between flow variations and ecological conditions. The methodology given by IWMI requires various ecological parameters and their ratings to assess the class of EMC. Without hydro-ecological depth information and ecological condition, EMC-B and EMC-C can be considered for maintaining the river’s health (Fig. 7).

December and November, with 17.62 cumecs and 17.71 cumecs values, are the lowest discharge value months in the Tawi River EFA analysis. Monsoon season months July and

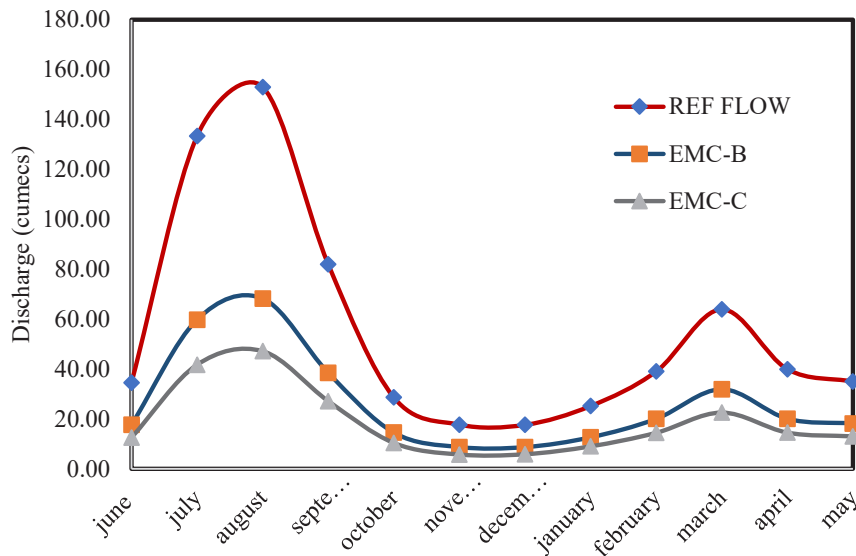


Fig. 7: Environmental flows of Tawi river for EMC ‘B’ and EMC ‘C’.

Table 3: Environmental flow of Tawi river for EMC-B and EMC-C.

Month	Natural Flows (cumec)	Environmental Flows (cumec)	
		EMC-B	EMC-C
June	34.57	17.66	12.5421
July	133.36	59.77	41.7154
August	153.03	68.23	47.1427
September	81.94	38.48	27.1456
October	28.61	14.52	10.3683
November	17.71	8.72	5.72713
December	17.62	8.70	5.83923
January	25.16	12.62	9.0013
February	39.01	20.01	14.4194
March	63.93	31.89	22.5367
April	39.93	20.07	14.5075
May	34.98	18.17	12.9899

August have 133.36 and 153.03 cumecs discharge values. EFA analysis suggests a minimum of 5.72 cumecs discharge require to maintain the well-functioning ecological system of the river. Environmental flows for the various months for EMC-B and EMC-C are given in Table 3.

Hydro-Ecological assessment of Krishna River at five different locations De sugar, Yadgir, Agraharam, NSP and Vijayawada, 69.2%, 70.5%, 68.4%, 72%, and 71.31% of MAR value was measured for respective locations. Researchers estimated that 43% of the time river was not maintained to the required EF due to Socioeconomic projects (Uday Kumar & Jayakumar 2021). Environmental flow assessment of Shahr Chai River in Iran conducted by Karimi et al. reveals that 68.8%, 44.1%, 28.2%, 18.9%, 13.4%, and 10.0%, respectively, for EMC A to EMC F. Karimi et al. analyze GEFC, desktop reserve model (DRM) and low flow frequency analysis for Shahr Chai River and found that minimum 1.2 m³.s⁻¹ which is 23% of natural MAR required for downstream for Urmia lake (Shaeri Karimi et al. 2012). EFA analysis of the Sone river was performed by Global Environmental Flow Calculator Software and estimated that a minimum of 18.9% of MAR is mandatory to uphold the reasonable condition of the sone river (Joshi et al. 2014). Environmental flows of the Tungabhadra River basin studied by the Priya et al. using GEFC reveals that Tungabhadra River basin by seeing the various discharge stations, which are Balehonur, Haralahalli, Hosaritti, Shivamogga, Honalli, Rattihalli, and Tungabhadra Dam, with a mean annual flow (MAF) of 36%, 24.8%, 27.2%, 16.2%, 23.3%, 21.1%, and 12.2%, correspondingly, to preserve the ecological situations of the river (Chandi Priya et al. 2022). Several other researchers studied the Environmental assessment of Rivers (Omo-

Gibe basin, Ethiopia , Selangor River, Zab River, Yangtze, Yellow and Lancang Rivers), using GEFC and analysed the EMCs and impact of various alterations in natural streams of rivers (Abdi & Yasi 2015, Hairan et al. 2021, Mahmood et al. 2020, Tesfaye et al. 2020).

CONCLUSIONS

FDCs were similar for a lean season (December to February) of river discharge, generally decreasing EMC A to EMC F, which was found to be the minimum for EMC F compared to reference flow. Environmental flow assessment of Tawi river discharge data was estimated using The Global Environmental Flow Calculator (GEFC), which reveals statistics for EMC A to EMC F. Mean annual runoff using original discharge data was calculated and compared with data obtained from GEFC for different classes of EMCs. EMC A was estimated at 1362 cumecs which are 76.69% of MAR. This indicates that 76.69% of MAR is required to maintain the natural condition of the river with the least alteration in flow or no alteration. It is suitable for protecting rivers from building projects such as dams and diversions. Tawi river is the Himalayan River which contains a high potential for hydropower projects for maintaining river ecological condition to the optimum level, and hydropower projects possibilities EMC B and EMC C are recommended. This study reveals 42 to 57 % of MARs fall under EMC B and EMC C. Minor irrigation expansion projects and Water supply structures are allowable in the EMC B category. For maintaining the ecological health of the Tawi river, it is recommended to maintain at least 42 to 57% of MAR during any socio-economic, irrigation, and water supply projects. Special attention requires in lean seasons in which discharge falls to very low values. Minimum discharge was found in November and December, 17.71 and 17.62 cumecs, respectively. Comparing EMC B and EMC C values for November and December, which vary between 8.7 to 12.59 cumecs to the original 17.71 to 17.62 needs special attention during the development of any projects of stream diversions to maintain ecological conditions with minimum impact. Further investigation requires discharge data using GEFC for different EMCs before and after the impact of various hydropower and diversions projects at various locations to understand the impact of such projects on the eco-hydrology of the Tawi river.

REFERENCES

- Abdi, R. and Yasi, M. 2015. Evaluation of environmental flow requirements using eco-hydrologic-hydraulic methods in perennial rivers. *Water Sci. Technol.*, 72(3): 354-363. doi: 10.2166/wst.2015.200
- Agoramoorthy, G. 2015. Sacred rivers: Their spiritual significance in Hindu Religion. *J. Relig. Health* 54(3): 1080-1090. doi: 10.1007/s10943-014-9934-z

- Aqualogus. 2018. Preliminary Morphology Report Text: Feasibility and Detailed Project Report for Flood Mitigation and Comprehensive River Management Measures for Tawi Basin. Technical Report. Aqualogus, pp. 1-44.
- Chakravarty, M. and Patgiri, A.D. 2009. Metal pollution assessment in sediments of the Dikrong River, N.E. India. *J. Hum. Ecol.*, 27(1): 63-67. doi: 10.1080/09709274.2009.11906193
- Chandi Priya, P.N., Shaik, R. and Singh, R.K. 2022. Assessment of Environmental Flows of Tungbhadra River Using Global Environmental Flow Calculator. In Dikshit, A.K., Narasimhan, B., Kumar, B. and Patel, A.K. (eds), *Innovative Trends in Hydrological and Environmental Systems*, Springer, Germany, pp. 727-42.
- Dugan, P.J., Baran, E., Tharme, R., Prein, M.A., Amerasinghe, R., Bueno, P., Dey, C., Jayasinghe, M., Niasse, G., Nieland, M., Tinh, V., Viswanathan, N., Welcomme, K., Brown, R.P. and Smakhtin, A. 2002. The Contribution of Aquatic Ecosystems and Fisheries to Food Security and Livelihoods: A Research Agenda. In Swallow, B. (ed), *Challenge Program on Water and Food, Background Papers, CGIAR, IWMI*, pp. 86-113
- Dyson, M., Bergkamp, G. and Scanlon, J. 2003. *Flow: The Essentials of Environmental Flows*. IUCN, Gland, Switzerland
- Emerton, L. and Bos, E. 2004. *Value : Counting Ecosystems as Water Infrastructure*. IUCN, Gland, Switzerland.
- Giri, S. and Singh, A.K. 2014. Assessment of surface water quality using heavy metal pollution index in Subarnarekha River, India. *Water Qual., Expo. Health* 5(4): 173-182. doi: 10.1007/s12403-013-0106-2
- Goyal, V.C., Jain, S.K. and Pareek, N. 2005. Water logging and drainage assessment in Ravi-Tawi irrigation command (J&K) using remote sensing approach. *J. Indian Soc. Remote Sens.*, 33(1): 7-15. doi: 10.1007/BF02989986
- Hairan, M.H., Jamil, N.R., Azmai, M.N.A., Looi, L.J. and Camara, M. 2021. Environmental flow assessment of a tropical river system using hydrological index methods. *Water*, 13(18): 2477. doi: 10.3390/w13182477
- Hughes, D.A. and Smakhtin, V. 1996. Daily flow time series patching or extension: a spatial interpolation approach based on flow duration curves. *Hydrological Sciences Journal*, 41(6): 851-871.
- Jain, C.K., Singhal, D.C. and Sharma, M.K. 2005. Metal pollution assessment of sediment and water in the river Hindon, India. *Environ. Monit. Assess.*, 105(1-3): 193-207. doi: 10.1007/s10661-005-3498-z
- Jain, S.K., Agarwal, P.K. and Singh, V.P. 2007. *Hydrology and Water Resources of India*. Springer Netherlands, Dordrecht, pp. 473-511.
- Joshi, K.D., Jha, D.N., Alam, A., Srivastava, S.K., Kumar, V. and Sharma, A.P. 2014. Environmental flow requirements of river Sone: Impacts of low discharge on fisheries. *Curr. Sci.*, 107(3): 478-488.
- Kaushik, A., Sharma, H.R., Jain, S., Dawra, J. and Kaushik, C.P. 2010. Pesticide pollution of River Ghaggar in Haryana, India. *Environ. Monit. Assess.*, 160(1-4): 61-69. doi: 10.1007/s10661-008-0657-z
- Kumar, V., Sharma, A., Bhardwaj, R. and Thukral, A.K. 2018. Temporal distribution, source apportionment, and pollution assessment of metals in the sediments of Beas River, India. *Hum. Ecol. Risk Assess. Int. J.*, 24(8): 2162-2181. doi: 10.1080/10807039.2018.1440529
- Mahmood, R., Jia, S., Lv, A. and Zhu, W. 2020. A preliminary assessment of environmental flow in the three rivers' source region, Qinghai Tibetan Plateau, China. *Ecol. Eng.*, 144: 105709. doi: 10.1016/j.ecoleng.2019.105709
- Operacz, A., Wałęga, A., Cupak, A. and Tomaszewska, B. 2018. The comparison of environmental flow assessment: The barrier for investment in Poland or river protection? *J. Clean. Prod.*, 193: 575-592. doi: 10.1016/j.jclepro.2018.05.098
- Paul, D. 2017. Research on heavy metal pollution of River Ganga: A review. *Ann. Agrar. Sci.*, 15(2): 278-286. doi: 10.1016/j.aasci.2017.04.001
- Poff, N.L., Richter, B.D., Arthington, A.H., Bunn, S.E., Naiman, R.J., Kendy, E., Acreman, M., Apse, C., Bledsoe, B.P., Freeman, M.C., Henriksen, J., Jacobson, R.B., Kennen, J. G., Merritt, D.M., Olden, J.D., Rogers, K., Tharme, R.E. and Warner, A. 2009. A new framework for developing regional environmental flow standards. *Freshwater Biol.*, 55(1): 147-70. doi: 10.1111/j.1365-2427.2009.02204.x
- Vinod, S., Singh, K.P., Tatiwal, J. and Kanwar, P. 2016. Report on Aquifer Mapping Outer Plains of Jammu Province, Jammu Kashmir. Technical Report. Central Ground Water, Jammu, pp. 1-105.
- Shaeri Karimi, S., Yasi, M. and Eslamian, S. 2012. Use of hydrological methods for assessment of environmental flow in a river Reach. *Int. J. Environ. Sci. Technol.*, 9(3): 549-58. doi: 10.1007/s13762-012-0062-6
- Sharma, K.K., and Chowdhary, S. 2011. Macroinvertebrate assemblages as biological indicators of pollution in a central Himalayan River, Tawi (J&K). *Int. J. Biodiv. Conserv.*, 3: 167-714.
- Sharma, R.R. 2012. Impact of climate change on river discharge: A case study of Birhun Khad, Tawi Basin, Jammu. *J. Indian Geomorphol.*, 1: 26-31.
- Smakhtin, V.U. and Anputhas M. 2006. An assessment of EF requirements of Indian river basins. Colombo. International Water Management Institute, Research Report, pp. 107.
- Sood, A., Smakhtin, V., Eriyagama, N., Villholth, K., Liyanage, N., Wada, Y., Ebrahim, G. Yimer, N. and Dickens, C. 2017. *Glob. Environ. Flow Inform. Sustain. Dev. Goals*, 16: 545-563.
- Sun, P., Zhang, Q., Yao, R., Singh, V.P. and Song, C. 2018. Low flow regimes of the Tarim river basin, China: Probabilistic behavior, causes and implications. *Water (Switzerland)*, 10(4): 1-18. doi: 10.3390/w10040470
- Taghinia Hejabi, A., Basavarajappa, H.T., Karbassi, A.R. and Monavari, S.M. 2011. Heavy metal pollution in water and sediments in the Kabini River, Karnataka, India. *Environ. Monit. Assess.*, 182(1-4): 1-13. doi: 10.1007/s10661-010-1854-0
- Tesfaye, T.W., Dhanya, C.T. and Gosain, A.K. 2020. Modeling the impact of climate change on the environmental flow indicators over Omo-Gibe Basin, Ethiopia. *Model. Earth Syst. Environ.*, 6(4): 2063-2089. doi: 10.1007/s40808-020-00813-x
- Uday Kumar, A. and Jayakumar, K.V. 2021. Modelling of environmental flow requirements using hydraulic and habitation models. *Ecol. Indic.*, 121: 107046. doi: 10.1016/j.ecolind.2020.107046
- Verma, M., Singh, B.P., Srivastava, A. and Mishra, M. 2012. Chemical behavior of suspended sediments in a small river draining out of the Himalaya, Tawi River, Northern India: Implications on provenance and weathering. *Himal. Geol.*, 33(1): 1-14.
- Yadav, M., Gole, V. L., Sharma, J. and Pandey, G. 2022a. Downstream microbial and physicochemical assessment of Aami river and analysis of sewage and industrial discharge. *J. Instit. Eng. India Ser. E*, 22: 4003. doi: 10.1007/s40034-022-00240-w
- Yadav, M., Gole, V.L., Sharma, J. and Yadav, R.K. 2021a. Biologically treated industrial wastewater disinfection using the synergy of US, LED-UVS, and oxidants. *Chem. Eng. Process.: Process Intensif.*, 169: 108646. doi: 10.1016/j.cep.2021.108646
- Yadav, M., Gole, V.L., Sharma, J. and Yadav, R.K. 2022b. Enhancing disinfection of contaminated natural water using a 40 KHz frequency cavitation reactor. *Environ. Eng. Sci.*, 39(4): 342-351. doi: 10.1089/ees.2020.0486
- Yadav, M., Gole, V.L., Sharma, J. and Yadav, R.K. 2021b. Sugar Industry Wastewater Treatment: Current Practices and Advances. In Shah, M. and Rodriguez-Couto, S. (eds), *Microbial Ecology of Wastewater Treatment Plants*, Elsevier, The Netherlands, pp. 151-74.
- Yadav, M., Pandey, G. and Kumar, P. 2022c. Low Flow Frequency Analysis of Tawi River Discharge at Jammu Location. *Int. J. Hydrol. Sci. Technol.*, 1(1): 1. doi: 10.1504/IJHST.2022.10045587



Identification and Characterization of Microplastics on the Surface Water in Laguna de Bay, Philippines

C. C. Deocaris*†, M. C. Fernandez*, A. R. Lee*, S. L. A. Miao* and J. B. P. Padolina**(***)

*Department of Physical Sciences, College of Science, Polytechnic University of the Philippines, Manila, Philippines

**Graduate School, University of the Philippines, Los Baños, Laguna, Philippines

***Pamantasan ng Lungsod ng Marikina, Marikina City, Metro Manila, Philippines

†Corresponding author: C. C. Deocaris; ccdeocaris@pup.edu.ph

Nat. Env. & Poll. Tech.
Website: www.neptjournal.com

Received: 24-09-2022

Revised: 29-11-2022

Accepted: 07-12-2022

Key Words:

Microplastics
Laguna de Bay
Surface water
Pollution

ABSTRACT

Laguna de Bay is the largest lake in the Philippines. It is surrounded by developing cities that pollute the lake with plastics from different industrial and domestic activities. In the study, microplastics were collected from the lake's surface water through three (3) collection points within the lake. The collection of microplastics was conducted from August 2018 to October 2018. About eight-hundred ninety (890) microplastics were collected and cataloged. Among the collection sites, 'Brgy. Sampiruhan' has the most microplastics, with a median of 15 ranging from 11-24 microplastics per 1000 L of lake water. On the other hand, 'Brgy. Napindan' has a median of 4 which ranges from 2-6 microplastics per 1000 L, and 'Brgy. San Isidro' has a median of 6 which ranges from 4-24 microplastics per 1000 L. Image analysis revealed that microplastics from this site were larger and angular. The color analysis shows signs of whitening and yellowing of the plastic materials, which suggests that the microplastics undergo photodegradation. Fourier-transform infrared spectroscopy (FTIR) found that most of the microplastics in the lake are made of polyethylene and its derivatives. Microplastics in Laguna de Bay show the continuous plastic pollution in the Philippines' largest lake.

INTRODUCTION

Microplastics are plastic materials smaller than 5 mm (Arthur et al. 2009, Bowmer & Kershaw 2010). Microplastics could be produced deliberately from plastic products such as plastic pellets, scrubbers, and microbeads (Browne et al. 2010, Arthur et al. 2009, Reddy et al. 2006), hence called primary microplastics. Secondary microplastics, on the other hand, are formed from large plastic debris through mechanical weathering, photo-oxidation, thermo-oxidation, and biological degradation (Thompson et al. 2004, Browne et al. 2007, Andrady 2011). Mechanical degradation happens when shearing forces are applied to the plastic material. This could form macro-radicals that react to oxygen-producing peroxy-radicals that initiate the degradation of the polymer chains in plastic materials (Potts 1991). The primary and secondary microplastics will roam in different bodies of water and continuously break into smaller fragments until they are invisible to the naked eye.

Microplastics are now present in oceans and shorelines worldwide (Barnes et al. 2009, Browne et al. 2011, Nelms et al. 2016). A wide range of organisms could ingest microplastics because of their size. Plastic products also

contain plasticizers and additives, which may leak into the water as the plastic material degrades. Plastic can also carry toxicants on its surface, causing more detrimental effects on marine life (Koelmans et al. 2016). Furthermore, the absorption of ultraviolet from sunlight induces photolytic, photooxidative, and thermo-oxidative reactions leading to the lysis of the polymer chains hence photodegradation (Ayako & Hirose 1999, Scott 2000, Valko et al. 2001). The absorption of ultraviolet light is facilitated by the light-absorbing functional groups (Chromophores) present in plastic polymers (Schnabel 1981). Photooxidative degradation of plastics polymers includes chain scission, crosslinking, and secondary oxidative reactions requiring the formation of free radicals (Ranby & Rabek 1981, Carlsson et al. 1976, Mc Kellar & Allen 1979, Ranby & Lucki 1980). Absorption of ultraviolet light (UV) at less than 290 nm induces the photo-Fries reaction of the chromophores of the plastic materials resulting in the yellowing of the microplastics or discoloration. UV at 330 nm can induce bleaching of the pigments added to the plastic products, which results in the fading of colors (Humphrey et al. 1973, Andrady et al. 1991). Pigments and stabilizers (i.e., chalk) protrude from the fractured polymer matrices producing

a scaly appearance and whitening the plastic surface. The prolonged mechanical stresses and photodegradation weather plastic and its byproducts (Yousif & Haddad 2013).

Laguna de Bay is the largest lake on the island of Luzon in the Philippines. The lake has an area of about 911 km² and a shoreline of 220 km. It has a shallow freshwater body. The lake is surrounded by urbanizing regions such as the National Capital Region (NCR), the Province of Rizal, and the Province of Laguna (LLDA 2015). Laguna de Bay has 21 tributaries, with the Marikina and Pagsanjan rivers as its main water source accounting for 80% of its water volume (Delos Reyes 1995). Laguna de Bay is the catch basin of waters from Metro Manila and nearby provinces. One of the rivers dumping waters in Laguna de Bay is the Pasig River (Gonzales 1987).

Furthermore, household and industrial waste from nearby provinces contributes to river pollution (Santos-Borja & Nepomuceno 2006). Plastics are included in the waste dumped in Laguna de Bay, which increases as urbanization and industrialization occur in Metro Manila and its nearby provinces (Regmi 2017). More so, the local governments surrounding the Laguna de Bay and the Laguna Lake Development Authority (LLDA) have implemented a policy to ban non-biodegradable plastic bags and promote biodegradable bags such as paper bags and eco-bags (LLDA 2011). The Philippines has a worsening problem with plastic pollution. In a survey in 2010, around 280-750 thousand metric tons of plastic debris in the ocean were traced from the country, making the Philippines one of the largest contributors of plastics in the ocean (Jambeck et al. 2015, Lebreton et al. 2017, Lebreton & Andrady 2019). Laguna

de Bay is connected to the Pacific Ocean through Manila Bay and the Pasig River in Metro Manila. In recent studies, microplastics were found and isolated in the Pasig River (Deocaris et al. 2019).

Furthermore, microplastics were also found in mussels harvested from Bacoor Bay (Argamino et al. 2016), an inlet southeast of Manila Bay. In this study, the occurrence and characteristics of microplastics collected in the south, west, and central parts of the Laguna de Bay were proven and defined. The collection was conducted in August and October of 2018. The main objective of this study is to show the abundance and identity of microplastic pollution in Laguna de Bay.

MATERIALS AND METHODS

Sample Collection and Processing

Three (3) sampling sites (Fig. 1) were assigned in this study, namely: (a) Brgy. Napindan, Taguig City (1426.87°30'' N 12120.61°05'' E); (b) Brgy. Sampiruhan, Calamba, Laguna (1430.92°12'' N, 12153.35°10'' E) and (c) P. Burgos St., Brgy. San Isidro, Tanay, Rizal (1435.46°29'' N, 12133.76°16'' E). The sampling site in Taguig city is in the western region of Laguna de Bay. In contrast, the sampling site in Calamba city is found in the southern region of Laguna de Bay, and the sampling site in the municipality of Tanay is found in the central region of the lake. Water samples were collected 5 to 10 m away from the shoreline. Three (3) sampling sites were selected because these are the sites close to urbanized cities around Laguna de Bay. Visits to the sampling sites were done in August and October 2018



Fig. 1: Laguna de Bay and the sampling sites. N – Brgy. Napindan, Taguig, Metro Manila; I – Brgy. San Isidro, Tanay, Rizal; S – Brgy. Sampiruhan, Calamba, Laguna.

because around this time is the wet season in the Philippines, where the inflow and outflow of water in the lake is more frequent, and the samples were collected from the surface water of the Laguna de Bay in triplicates.

The surface water was manually scooped using tared buckets, and the collected water was allowed to pass through a sieve stack setup consisting of 4,700 μm (4.7 mm) and 355 μm (0.35 mm) mesh sieves. Using this sieve stack, solid materials with sizes 0.35 to 4.7 mm will be trapped in between the stack. Around 500 and 2,000 liters of water were filtered during the first and second visits. Solids trapped in the 0.35 mm sieve mesh were washed with distilled water and transferred into glass containers. The collected solids were dried at 80-100°C overnight.

The dried materials were added to 20 mL of 2 M NaOH and heated around 100°C following the alkali digestion method described by Cole et al. (2014, 2015). Undigested solids were washed with distilled water, dried, and suspended in a saturated salt solution (density = 1.2 $\text{g}\cdot\text{mL}^{-1}$). Floating solids were manually picked, washed briefly in distilled water, and examined under the stereomicroscope. Photographs were taken to catalog each microplastic fragment collected. Alkali digestion was proffered over the wet-peroxide oxidation (WPO) method due to the availability of reagents and the simplicity of the procedure of the former. However, this digestion method could not isolate polyesters and nylon materials. Alkali digestion was conducted overnight for approximately 12 h.

Density Flootation Test

The collected microplastics were segregated based on their density. The microplastics were allowed to float on distilled water (1.00 $\text{g}\cdot\text{cm}^{-3}$), 50% isopropyl alcohol (0.95 $\text{g}\cdot\text{cm}^{-3}$), and vegetable oil (0.93 $\text{g}\cdot\text{cm}^{-3}$). A drop of dishwashing liquid was added to the liquid to lessen the surface tension of the microplastics on the liquid. The salt that was used for the technique was sodium chloride (NaCl) and was left overnight.

Microscopic Examination and Image Analysis

Photographs were taken for each fragment with illumination on top of the plastic fragments using a stereomicroscope with up to 40 \times Magnification. The length of each fragment was measured from the photomicrographs using ImageJ software version 1.8.0 (Schneider et al. 2012). The roundness scores of each microplastic fragment were calculated from the circularity and aspect ratios obtained from ImageJ using the formula of Takashimizu & Liyoshi (2016). The roundness score ranges from 0 (angular) to 1 (perfect circle). The color of each microplastic fragment was obtained by image

analysis. The color of the microplastics was expressed in CIE $L^* a^* b^*$ color space. And color values were obtained using the 'color distance' package in R (Weller 2019).

Identification of Microplastics Using ATR-FTIR

Attenuated Total Reflectance - Fourier-Transform Infrared Spectroscopy (ATR-FTIR) was conducted to identify the microplastics using Spectrum Two N FT-NIR Spectrometer (Perkin-Elmer, MA, USA). Thirty-two (32) representative samples were analyzed using ATR-FTIR. The FTIR spectra obtained from the samples were matched to the FTIR spectral libraries of known polymers using the SearchIt™ data toolbox of the KnowItAll® application (Biorad Informatics Division, PA, USA).

Data Analysis and Statistical Tests

Based on the Shapiro-Wilk for normality, occurrence, length, and roundness, the microplastics' CIELAB values L^* , a^* , and b^* were not normally distributed. Hence non-parametric tests such as the Kruskal-Wallis test was employed to test the effects of the location and the collection visits. The Wilcoxon Signed Test was used to determine the significant difference between the groups. All the measurements were expressed in the median and interquartile range (IQR). A Chi-square test was done to determine the dependence of the density of the microplastics distribution to the collections site. All statistical analyses were done in R 3.6.0 (R Core Team 2020).

RESULTS AND DISCUSSION

Occurrence of Microplastics in Laguna de Bay

Nine hundred twenty-seven (927) plastic fragments were isolated from the three (3) sampling sites (Table 1) collected in August 2018 and October 2018.

After conducting the density separation, microscopic examination, and image analysis, only 890 were microplastics, and the other 37 plastic fragments were too large to be classified as microplastics. Among the three (3) sampling sites, Brgy. Sampiruhan in Calamba, Laguna, has the highest occurrence of microplastics, having a median of 15 (IQR 11-21) fragments per 1000 L of water. Sampiruhan can be described as an urban and agricultural development zone by the municipality of Calamba, furthermore during the visits. Visible plastic waste is floating around the shore. On another site, Brgy. Napindan showed fewer microplastics than Sampiruhan due to the Pasig River that allows the dumping and draining of water in the Laguna de Bay, which allows the microplastic to be flushed in and out of the lake hence the minimal concentration of microplastics in Napindan.

Table 1: Characteristics of microplastics isolated in the three regions of Laguna de Bay.

Site	Brgy. Napindan	Brgy. San Isidro	Brgy. Sampiruhan
City/Municipality and Province	Taguig City, Metro Manila	Tanay, Rizal	Calamba, Laguna
Laguna Lake Region	West	Central	South
Median (IQR)			
Occurrence of Microplastics [number of microplastics per 1000 L]	4 (2-6) b	6 (4-24) ab	15 (11-24) a
Length [micrometers]	1,803 (1,306-3,521) ^a	1,676 (1,024-2,480) ^a	1,392 (983-1,862) ^b
Roundness	0.62 (0.37 - 0.74) ^a	0.54 (0.37-0.69) ^a	0.46 (0.32-0.63) ^b
CIELAB Luminance (L*)	66.8 (59.3-85.6) ^a	42.9 (38.9-65.1) ^b	47.5 (39.9-70.6) ^b
CIELAB blue-yellow (b*)	2.6 (-4.3-20.4) ^b	14.0 (6.2-23.7) ^a	17.2 (6.0-24.8) ^a

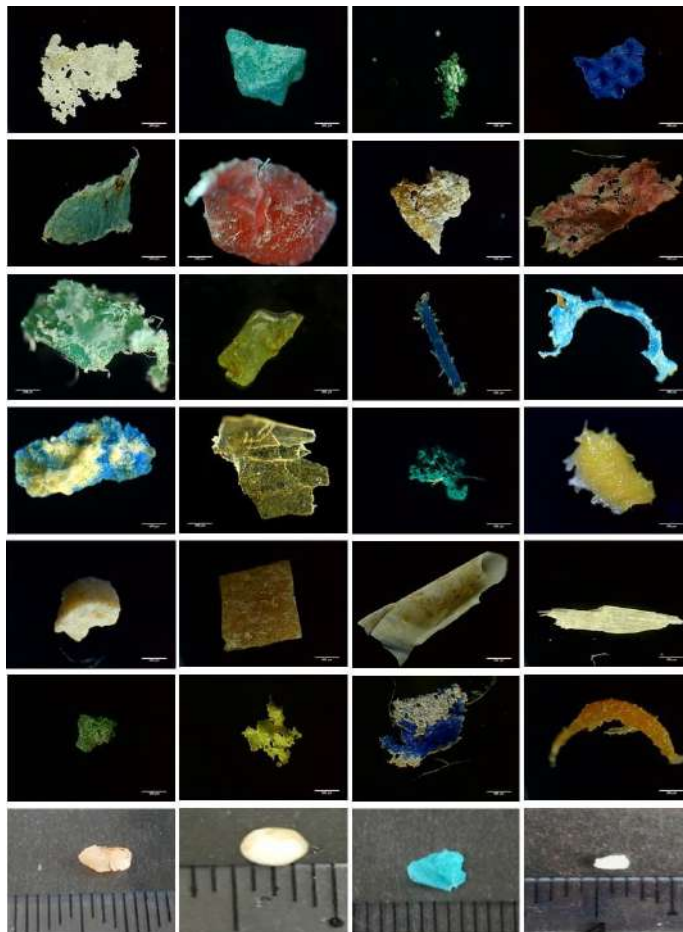


Fig. 2: Photographs of microplastics isolated from Laguna de Bay. Scale bars in the 1st to 6th rows are 355 micrometers. The graduations in the last row are 1 mm.

The occurrence of microplastics in the Pasig River (Deocaris et al. 2019) may also contribute to the concentration of microplastics in the Laguna de Bay. Napindan is an urbanized area with a thriving fishing community.

The occurrences of microplastics reported in this study were higher than in similar freshwater lakes in the

study by Dusaucy et al. (2021), wherein the occurrence of microplastics was studied in different lakes, the median microplastic occurrence is 1,442 microplastics per Liter ranging from 0.27 to 34,000 microplastics per Liter. The microplastic occurrences reported in this study are larger than the values obtained by Dusaucy in his microplastic studies.

Mechanical Weathering of Microplastics in Laguna de Bay

The length and roundness of microplastics in Laguna de Bay (see Table 1) appears to be different on each sampling site ($p < 0.05$). Microplastics from Sampiruhan were smaller and more angular compared to those collected from Napindan and San Isidro. The weathering effects that naturally happen on rocks and stones in a river also take place in large plastic materials, which results in small and round plastics until their sizes become microscopic; more so, microplastic may also collide with other materials that may contribute to the sheering forces that break the plastics more, this is comparable to small rocks in a river (Domokos et al. 2014). The same phenomenon was observed in the study conducted by Mearu (2020), wherein the polystyrene was exposed to agitating water, resulting in small and round plastic polystyrene fragments. In contrast with the angular plastics in Sampiruhan, the Napindan and San Isidro microplastics were round. This could be due to the rivers found in those sampling sites, wherein the Pasig River passes through Napindan. The Tanay River passes through San Isidro. Aside from the sheering forces that the rivers could contribute to breaking plastic materials into microplastics, the current within the different regions of Laguna de Bay may have contributed to the breaking of plastic fragments. The water at the center region of the Laguna de Bay flows southern, which rapidly converges with the water coming from the western region of the lake that flows eastern (Herrera et al. 2015). With continuous exposure to mechanical sheering forces that induce weathering, all microplastics will eventually become rounder over time; hence the angular microplastics in Sampiruhan will soon become round (Kowalski et al. 2016). More so, the rounding of microplastics will also result in loss of mass and, subsequently, the reduction of the particle density.

Photodegradation of Microplastics in Laguna de Bay

Apart from the Mechanical sheering forces from the rivers and the current within the Laguna de Bay, another factor that change the plastic material is photodegradation. Microplastics on the surface water are exposed to sunlight, an agent for photodegradation. The microplastics isolated

from Sampiruhan and San Isidro had more positive CIELAB b^* values, indicating the microplastics' yellowing due to photo-oxidation. The sunlight and heat induce the formation of free radicals due to the breakage of chemical bonds in the polymer structure, which alters the chromophores within the microplastic or polymer structure; hence the plastic changes its color (Andrady 2011, Barnes et al. 2009, Moore 2008). On the other hand, the microplastics collected from Napindan have the highest median CIELAB L^* values, which is the value for luminance. This suggests that the microplastics are whitening or turning to the color white, also an indication of discoloration, mainly through chalking, which is the formation of fine powders on the surface of the plastic or paint film due to weathering. Chalking occurs as increased amounts of polymer binder are removed from the surface of the microplastics causing pigments to protrude through the surface and produce a white and chalky appearance (McKeen 2019). More so, as the microplastics are exposed to photo-oxidation, the coloration of the microplastics turns more yellow.

Chemical Composition of Microplastics in Laguna de Bay

The microplastics isolated in Laguna de Bay are grouped into three density levels, as shown in Table 2. The distribution of microplastics within these density levels differs significantly by location ($p < 0.05$).

Around 40% of the microplastics collected in Sampiruhan have densities above the density of water (1.00 g.mL^{-1}), and plastic materials such as polystyrene, nylon, and polyethylene terephthalate are included in this density level (Kolb & Kolb 1991). Furthermore, microplastics with densities lower than 0.93 g.mL^{-1} are found in all three (3) sampling sites. Among the sampling sites, Sampiruhan has the highest number of microplastics with a density lower than 0.93 g.mL^{-1} . Several fish pens were observed in Sampiruhan, and these are commonly made of polypropylene and low-density polyethylene, and these plastics have a lower density than the water. Furthermore, these plastic polymers are less dense than water, are easily carried by currents, can stay afloat on the surface of the water, and are often exposed to sunlight, making way for more mechanical weather and photodegradation.

Table 2: Density profiles of the microplastics isolated in the three regions of Laguna de Bay.

Site	Density		
	$> 1.00 \text{ g.mL}^{-1}$	$0.93 - 1.00 \text{ g.mL}^{-1}$	$< 0.93 \text{ g.mL}^{-1}$
Brgy. Napindan	20 (19%)	66 (64%)	17 (17%)
Brgy. San Isidro	41 (22%)	124 (67%)	20 (11%)
Brgy. Sampiruhan	253 (40%)	323 (50%)	63 (10%)
Total	314 (34%)	513 (55%)	100 (11%)

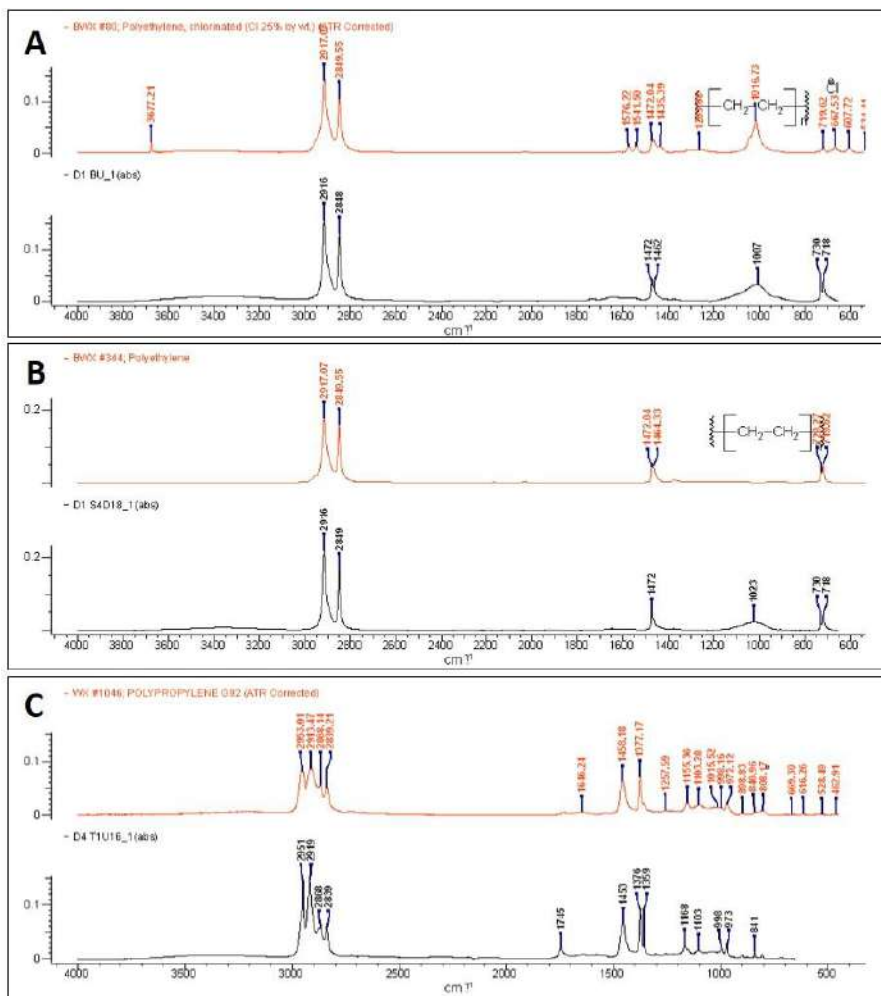


Fig. 3: FTIR spectra of selected microplastics from the surface water of Laguna de Bay. A. Chlorinated Polyethylene; B. Polyethylene; C. Polypropylene.

Attenuated total reflectance Fourier-transform infrared (ATR-FTIR) spectroscopy of selected microplastic fragments (Fig. 3) revealed the following plastic materials: polyethylene; polyethylene foam; medium-density polyethylene; high-density polyethylene; polyethylene ionomer; chlorinated polyethylene; polypropylene; maleic anhydride grafted polypropylene; styrene-butadiene isoprene rubber; styrene copolymer phosphonic diacid monomer; modified polyvinyl chloride with nitrile rubber; acrylonitrile butadiene copolymer. The ATR-FTIR configuration was set to 16 scans and 4 cm^{-1} resolution.

These polymer materials can be found in plastic products such as grocery bags, rubber tires, appliances, and plumbing products. Since Laguna de Bay is surrounded by various residential, commercial, and industrial establishments, it is difficult to avoid microplastic pollution, and it is polluted by microplastics as provided with the data of this study.

CONCLUSION

The study reports the microplastics' occurrence and profile isolated in Laguna de Bay. Fewer microplastics were isolated in Brgy. Napindan is compared to another sampling since it is located at the source of the Pasig River. The sites in Brgy. Sampiruhan and Brgy. San Isidro had higher microplastic occurrences, which could be attributed to the surrounding urbanized communities. The isolated microplastics had lengths ranging from 500 to 2,000 μm and appeared round, ranging from 0.2 to 0.8, and varied between sampling sites. The color coordinates of the microplastics suggest yellowing, an apparent sign of photodegradation of the plastic polymer and its additives. This study was also carried out to investigate the state of microplastics in Laguna de Bay, as there has been less focus on this area despite the obvious importance of the lake in agriculture.

RECOMMENDATIONS

Effective management programs for plastic pollution are recommended in the study sites and adjacent areas. In addition, it is suggested that pollutant accumulation in freshwater ecosystems in other provinces nearby should be further investigated to ensure environmental and human health safety conditions. It is also highly recommended that the agencies related to Laguna de Bay enforce policies that would reduce microplastic pollution and improve their management of the issue. Agencies such as Laguna Lake Development Authority (LLDA), Department of Energy and Natural Resources (DENR), Department of Trade and Industry (DTI), and National Water Resources Board may refer to this study on how to mitigate the growing problem of microplastics in Laguna de Bay.

ACKNOWLEDGEMENTS

Mr. A.K. Gallardo and Dr. J. Madrid of the Chemistry Division of the Philippine Nuclear Research Institute for their assistance in using the ATR-FTIR spectrometer.

SUPPLEMENTARY DATA

The data gathered and used in the study was uploaded in Mendeley Data (URL: https://data.mendeley.com/datasets/bxd3k2yntp/1?fbclid=IwAR3Z3IrSFjf_vIB_UDAH9MInzwYDD9UOkJszndgKgCaKi1D0GvhMykr6N8). The data in Mendeley is available to the public for academic purposes.

REFERENCES

- Andrady, A. L. 2011. Microplastics in the marine environment. *Marine Pollut. Bull.*, 62(8): 1596-1605
- Andrady, A., Fueki, K. and Torikai, A. 1991. Spectral sensitivity of polycarbonate to light-induced yellowing. *J. Appl. Polym. Sci.*, 42(7): 2105-2107.
- Argamino, C. and Janairo, J. 2016. Qualitative assessment and management of microplastic in Asian green mussels (*Perna viridis*) cultured in Bacoor Bay, Cavite, Philippines. *Environ. Asia*, 9(2): 48-54.
- Arthur, C., Baker, J. and Bamford, H. 2009. Proceedings of the international research workshop on the occurrence, effects, and fate of microplastic marine debris. Technical Memorandum NOS-OR&R-30, National Oceanic and Atmospheric Administration, NOAA Marine Debris Program and US Department of Commerce, Tacoma, WA, USA, pp. 1-49.
- Ayako, T. and Hirose, H. 1999. Polymer degradation stabilization. *Adv. Polym. Sci.*, 63(1):441.
- Barnes, D., Gsalgani, F., Thompson, R. and Barlaz, M. 2009. Accumulation and fragmentation of plastic debris in global environments. *Philos. Trans. R Soc. Lond. B Biol. Sci.*, 364(1526): 1985-1998.
- Bowmer, T. and Kershaw, P. 2010. Proceedings of the GESAMP International Workshop on Microplastic Particles as a Vector in Transporting Persistent, Bioaccumulating, and Toxic Substances in the Oceans, 28-30th June 2010, UNESCO-IOC, Paris, pp. 1-69
- Browne, M.A., Crump, P., Niven, S., Teuten, E., Tonkin, A., Galloway, T. and Thompson, R. 2011. Accumulation of microplastics on shorelines worldwide: Sources and sinks. *Environ. Sci. Technol.*, 45(1): 9175-9179.
- Browne, M.A., Galloway, T. and Thompson, R. 2007. Microplastic: An emerging contaminant of potential concern? *Integr. Environ. Assess. Manag.*, 3(4): 559-561.
- Browne, M.A., Galloway, T.S. and Thompson, R.C. 2010. Spatial patterns of plastic debris along estuarine shorelines. *Environ. Sci. Technol.*, 44(9): 3404-3409.
- Carlsson, D.J., Garton, A. and Wiles, D.M. 1976. Initiation of polypropylene photo-oxidation: 2. Potential processes and their relevance to stability. *Macromolecules*, 9(5): 695-701.
- Cole, M., Lindeque, T., Fileman, E., Halsband, C. and Galloway, T. 2015. The Impact of Polystyrene Microplastics on Feeding, Function, and Fecundity in the Marine Copepod *Calanus helgolandicus*. *Environmental Science & Technology*, 49(2): 1130-1137.
- Cole, M., Webb, H., Lindeque, P.K., Fileman, E.S., Halsband, C. and Galloway T.S. 2014. Isolation of microplastics in biota-rich seawater samples and marine organisms. *Sci. Rep.*, 4(1): 1-8.
- Delos Reyes, M.R. 1995. Geocology of Laguna de Bay, Philippines: Long-term Alternatives of a Tropical-Aquatic Ecosystem. 1820-1992, Ph. D. Dissertation. Hamburg University, Germany
- Deocaris, C.C., Allosada, J.O., Ardiente, L.T., Bitang, L.G.G., Dulohan, C.L., Lapuz, J.K. I., Padilla, L.M., Ramos, V.P. and Padolina J.B.P. 2019. Occurrence of microplastic fragments in the Pasig River. *H2 Open J.*, 2(1): 92-100.
- Domokos, G., Jerolmack, D.J., Sipos, A.Á. and Török Á. 2014. How river rocks round: resolving the shape-size paradox. *PLoS One* 9, e8865710.1371/journal.pone.0088657.
- Dusaucy, J., Gateuille, D., Perrette, Y. and Naffrechoux, E. 2021. Microplastic pollution of worldwide lakes. *Environ. Pollut.*, 284(117075): 1-13.
- Gonzales, E. 1987. A Socio-economics Geography (1961-85) of the Laguna lake resources and its Implications To Aquatic Resources Management and Development of the Philippine Islands. Dissertation. Cambridge University, England, United Kingdom.
- Herrera, E., Nadoka, K., Blanco, A. and Hernandez, E. 2015. Hydrodynamic investigation of a shallow tropical lake environment (Laguna Lake, Philippines) and associated implications for eutrophic vulnerability. *ASEAN J. Chem. Eng.*, C, 4(1): 48-62.
- Humphrey, J.S., Shultz, A.R. and Jaquiss, D.B.G. 1973. Flash photochemical studies of polycarbonate and related model compounds, photodegradation vs photo-Fries rearrangement. *Macromolecules*, 6(3): 305-314.
- Jambeck, J., Geyer, R., Wilcox, C., Siegler, T., Perryman, M., Andrady, A., Narayan, R. and Law, K.L. 2015. Plastic waste inputs from land into the ocean. *Science*, 347(6223): 768-771.
- Kellar, J.F. and Allen, N.S. 1979. Photochemistry of man-made polymers. *Appl. Sci.*, 54: 121-136.
- Koelmans, A., Bakir, A., Burton, G. and Janssen, C. 2016. Microplastics as a vector for chemicals in the aquatic environment: Critical review and model-supported reinterpretation of empirical studies. *Environ. Sci. Technol.*, 50(7): 3315-3326.
- Kolb, K.E. and Kolb, D.K. 1991. Method for separating or identifying plastics. *J. Chem. Edu.*, 68(4): 348.
- Kowalski, N., Reichardt, A.M. and Waniek, J.J. 2016. Sinking rates of microplastics and potential implications of their alteration by physical, biological, and chemical factors. *Marine Pollut. Bull.*, 109(1): 310-319.
- Laguna Lake Development Authority (LLDA) (2015) Laguna de Bay master plan: 2016 and beyond. Retrieved from <https://llda.gov.ph/wp-content/uploads/dox/ldbMP2016.pdf>
- Laguna Lake Development Authority (LLDA). 2011. Board Resolution No. 408. <https://llda.gov.ph/wp-content/uploads/dox/br/plasticban/br406s2011.pdf>

- Lebreton, L. and Andrady, A. 2019. Future scenarios of global plastic waste generation and disposal. *Pal. Commun.*, 5(6): 212. <https://doi.org/10.1057/s41599-018-0212-7>
- Lebreton, L.C.M., Zwet, J.V., Damsteeg, J., Slat, B., Andrady, A. and Reisser, J. 2017. River plastic emissions to the world's oceans. *Nature Commun.*, 8(15611): 1-10.
- McKeen, L.W. 2019. *Introduction to the Weathering of Plastics*. Wiley, NY.
- Mekaru, H. 2020. Effect of agitation method on the nanosized degradation of polystyrene microplastics dispersed in water. *ACS Omega*, 5(7): 3218-3227.
- Moore, C.J. 2008. Synthetic polymers in the marine environment: A rapidly increasing, long-term threat. *Environ. Res.*, 108(1): 131-139.
- Nelms, S., Duncan, E., Broderick, A., Galloway, T., Godfrey, M., Hamann, M., Lindeque, P. and Godley, B. 2015. Plastic and marine turtles. *ICES J. Marine Sci.*, 73(2):165-181.
- Potts, J.E. 1991. *Plastic Environmentally Degradation*. Wiley, NY.
- R Core Team. 2020. *R: A Language and Environment for Statistical Computing*. R Foundation for Statistical Computing, Vienna, Austria. URL <https://www.R-project.org/>.
- Ranby, B. and Lucki, J. 1980. New aspects of photodegradation and photo-oxidation of PS. *Pure Appl. Chem.*, 52(1): 295-303.
- Ranby, B. and Rabek, J.F. 1981. The effects of the hostile environment on coatings and plastics. *ACS Symp. Ser.*, 16: 291-301.
- Reddy, M.S., Basha, S., Adimurthy, S. and Ramachandraiah, G. 2006. Description of the small plastic fragments in marine sediments along the Alang-Sosiya ship-breaking yard, India. *Estuari. Coast. Shelf Sci.*, 68(3-4): 656-660.
- Regmi, R.K. 2017. Urbanization and related environmental issues of Metro Manila. *J. Adv. Coll. Eng. Manag.*, 3:79-92.
- Santos-Borja, A. and Nepomuceno, D.N. 2006. Laguna de Bay: Institutional development and charge for lake basin management. *Lakes Reserv. Sci., Policy Manag. Sustain. Use*, 11(4): 257-269.
- Schnabel, W. 1981. *Polymer Degradation: Principle and Practical Applications*. Wiley, NY, pp. 838-839.
- Schneider, C.A., Rasband, W.S. and Eliceiri, K.W. 2012. NIH Image to image: 25 years of image analysis. *Nature Methods*, 9(1): 671-675.
- Scott G. 2000. Green polymers. *Polym. Degrad. Stab.*, 68(1): 1-7.
- Takashimizu, Y. and Iiyoshi, M. 2016. New parameter of roundness R: circularity corrected by aspect ratio. *Prog. Earth Planet. Sci.*, 3(1): 1-16.
- Thompson, R.C., Olsen, Y., Mitchell, R.P., Davis, A., Rowland, S.J., John, A.W.G., McGonigle, D. and Russell, A.E. 2004. Lost at sea: where is all the plastic? *Science*, 304(1): 5672.
- Valko, L., Klein, E., Kovarik, P. and Simon, P. 2001. Kinetic study of thermal dehydrochlorination of poly(vinyl chloride) in the presence of oxygen: III. Statistical thermodynamic interpretation of the oxygen catalytic activity. *Europ. Polym. J.*, 37(1): 1123-1133.
- Weller, H. 2019. *Colordistance: Distance Metrics for Image Color Similarity*. R package version. 1.0. <https://CRAN.R-project.org/package=colordistance>
- Yousif, E. and Haddad, R. 2013. Photodegradation and photostabilization of polymers, especially polystyrene: *Rev. SpringerPlus*, 2(1): 398.

... Continued from inner front cover

- The text of the manuscript should run into **Abstract, Introduction, Materials & Methods, Results, Discussion, Acknowledgement** (if any) and **References** or other suitable headings in case of reviews and theoretically oriented papers. However, short communication can be submitted in running with **Abstract and References**. The references should be in full with the title of the paper.
- The figures should preferably be made on a computer with high resolution and should be capable of withstanding a reasonable reduction with the legends provided separately outside the figures. Photographs may be black and white or colour.
- Tables should be typed separately bearing a short title, preferably in vertical form. They should be of a size, which could easily be accommodated in the page of the Journal.
- References in the text should be cited by the authors' surname and year. In case of more than one reference of the same author in the same year, add suffix a,b,c,.... to the year. For example: (Thomas 1969, Mass 1973a, 1973b, Madony et al. 1990, Abasi & Soni 1991).

List of References

The references cited in the text should be arranged alphabetically by authors' surname in the following manner: (Note: The titles of the papers should be in running 'sentence case', while the titles of the books, reports, theses, journals, etc. should be in 'title case' with all words starting with CAPITAL letter.)

- Dutta, A. and Chaudhury, M. 1991. Removal of arsenic from groundwater by lime softening with powdered coal additive. *J. Water Supply Res. Techno. Aqua.*, 40(1) : 25-29.
- Hammer, D.A. (ed.) 1989. *Constructed Wetlands for Wastewater Treatment-Municipal, Industrial and Agricultural*. Lewis Publishers Inc., pp. 831.
- Haynes, R. J. 1986. Surface mining and wetland reclamation. In: Harper, J. and Plass, B. (eds.) *New Horizons for Mined Land Reclamation*. Proceedings of a National Meeting of the American Society for Surface Reclamation, Princeton, W.V.

Submission of Papers

- The paper can be submitted by e-mail as an attachment in a single WORD file at **contact@neptjournal.com**
- The paper can also be submitted online in a single WORD file through the **online submission portal** of journal's website: **www.neptjournal.com**

Attention

1. Any change in the authors' affiliation may please be notified at the earliest.
2. Please make all the correspondence by e-mail, and authors should always quote the manuscript number.

Note: In order to speed up the publication, authors are requested to correct the galley proof immediately after receipt. The galley proof must be checked with utmost care, as publishers owe no responsibility for mistakes. The papers will be put on priority for publication only after receiving the processing and publication charges.

Nature Environment and Pollution Technology

(Abbreviation: Nat. Env. Poll. Tech.)

(An International Quarterly Scientific Journal)

Published by



Technoscience Publications

A-504, Bliss Avenue, Opp. SKP Campus
Balewadi, Pune-411 045, Maharashtra, India

In association with

Technoscience Knowledge Communications

Mira Road, Mumbai, India

For further details of the Journal, please visit the website. All the papers published on a particular subject/topic or by any particular author in the journal can be searched and accessed by typing a keyword or name of the author in the 'Search' option on the Home page of the website. All the papers containing that keyword or author will be shown on the home page from where they can be directly downloaded.

www.neptjournal.com

©**Technoscience Publications:** The consent is hereby given that the copies of the articles published in this Journal can be made only for purely personal or internal use. The consent does not include copying for general distribution or sale of reprints.

Published for Proprietor, Printer and Publisher: Mrs. T. P. Goel, A-504, Bliss Avenue, Balewadi, Pune, Maharashtra, India; Editors: Dr. P. K. Goel (Chief Editor) and Prof. K. P. Sharma